frontiers | Research Topics

# Insights in virology 2021

**Edited by**
Chunfu Zheng and Douglas Paul Gladue

**Published in**
Frontiers in Microbiology

FRONTIERS EBOOK COPYRIGHT STATEMENT

The copyright in the text of individual articles in this ebook is the property of their respective authors or their respective institutions or funders. The copyright in graphics and images within each article may be subject to copyright of other parties. In both cases this is subject to a license granted to Frontiers.

The compilation of articles constituting this ebook is the property of Frontiers.

Each article within this ebook, and the ebook itself, are published under the most recent version of the Creative Commons CC-BY licence. The version current at the date of publication of this ebook is CC-BY 4.0. If the CC-BY licence is updated, the licence granted by Frontiers is automatically updated to the new version.

When exercising any right under the CC-BY licence, Frontiers must be attributed as the original publisher of the article or ebook, as applicable.

Authors have the responsibility of ensuring that any graphics or other materials which are the property of others may be included in the CC-BY licence, but this should be checked before relying on the CC-BY licence to reproduce those materials. Any copyright notices relating to those materials must be complied with.

Copyright and source acknowledgement notices may not be removed and must be displayed in any copy, derivative work or partial copy which includes the elements in question.

All copyright, and all rights therein, are protected by national and international copyright laws. The above represents a summary only. For further information please read Frontiers' Conditions for Website Use and Copyright Statement, and the applicable CC-BY licence.

ISSN 1664-8714
ISBN 978-2-8325-2276-9
DOI 10.3389/978-2-8325-2276-9

## About Frontiers

Frontiers is more than just an open access publisher of scholarly articles: it is a pioneering approach to the world of academia, radically improving the way scholarly research is managed. The grand vision of Frontiers is a world where all people have an equal opportunity to seek, share and generate knowledge. Frontiers provides immediate and permanent online open access to all its publications, but this alone is not enough to realize our grand goals.

## Frontiers journal series

The Frontiers journal series is a multi-tier and interdisciplinary set of open-access, online journals, promising a paradigm shift from the current review, selection and dissemination processes in academic publishing. All Frontiers journals are driven by researchers for researchers; therefore, they constitute a service to the scholarly community. At the same time, the *Frontiers journal series* operates on a revolutionary invention, the tiered publishing system, initially addressing specific communities of scholars, and gradually climbing up to broader public understanding, thus serving the interests of the lay society, too.

## Dedication to quality

Each Frontiers article is a landmark of the highest quality, thanks to genuinely collaborative interactions between authors and review editors, who include some of the world's best academicians. Research must be certified by peers before entering a stream of knowledge that may eventually reach the public - and shape society; therefore, Frontiers only applies the most rigorous and unbiased reviews. Frontiers revolutionizes research publishing by freely delivering the most outstanding research, evaluated with no bias from both the academic and social point of view. By applying the most advanced information technologies, Frontiers is catapulting scholarly publishing into a new generation.

## What are Frontiers Research Topics?

Frontiers Research Topics are very popular trademarks of the *Frontiers journals series*: they are collections of at least ten articles, all centered on a particular subject. With their unique mix of varied contributions from Original Research to Review Articles, Frontiers Research Topics unify the most influential researchers, the latest key findings and historical advances in a hot research area.

Find out more on how to host your own Frontiers Research Topic or contribute to one as an author by contacting the Frontiers editorial office: frontiersin.org/about/contact

# Insights in virology: 2021

**Topic editors**

Chunfu Zheng — University of Calgary, Canada

Douglas Paul Gladue — Plum Island Animal Disease Center, Agricultural Research Service (USDA), United States

**Citation**

Zheng, C., Gladue, D. P., eds. (2023). *Insights in virology: 2021*. Lausanne: Frontiers Media SA. doi: 10.3389/978-2-8325-2276-9

# Table of contents

06 Influenza A Virus–Host Specificity: An Ongoing Cross-Talk Between Viral and Host Factors
Miaomiao Zhang, Mingbin Liu, Shimeng Bai, Chen Zhao, Zejun Li, Jianqing Xu and Xiaoyan Zhang

15 DNA Engineering and Hepatitis B Virus Replication
Chun-yang Gan, Jing Cui, Wen-lu Zhang, Yu-wei Wang, Ai-long Huang and Jie-li Hu

35 Development of a Novel Avian Vaccine Vector Derived From the Emerging Fowl Adenovirus 4
Qing Pan, Yu Zhang, Aijing Liu, Hongyu Cui, Yulong Gao, Xiaole Qi, Changjun Liu, Yanping Zhang, Kai Li, Li Gao and Xiaomei Wang

45 Structural Analysis on the Severe Acute Respiratory Syndrome Coronavirus 2 Non-structural Protein 13 Mutants Revealed Altered Bonding Network With TANK Binding Kinase 1 to Evade Host Immune System
Farooq Rashid, Muhammad Suleman, Abdullah Shah, Emmanuel Enoch Dzakah, Shuyi Chen, Haiying Wang and Shixing Tang

55 The HBV Core Protein and Core Particle Both Bind to the PPiase Par14 and Par17 to Enhance Their Stabilities and HBV Replication
Umar Saeed, Zahra Zahid Piracha, Hyeonjoong Kwon, Jumi Kim, Fadia Kalsoom, Yong-Joon Chwae, Sun Park, Ho-Joon Shin, Hyun Woong Lee, Jin Hong Lim and Kyongmin Kim

75 Significantly Low Levels of IgG Antibodies Against Oncogenic Merkel Cell Polyomavirus in Sera From Females Affected by Spontaneous Abortion
Chiara Mazziotta, Giulia Pellielo, Mauro Tognon, Fernanda Martini and John Charles Rotondo

85 The Role of Unfolded Protein Response in Coronavirus Infection and Its Implications for Drug Design
Mei Xue and Li Feng

94 RNA Granules in Antiviral Innate Immunity: A Kaposi's Sarcoma-Associated Herpesvirus Journey
Nishi R. Sharma and Zhi-Ming Zheng

104 Hsp90 Inhibitors Inhibit the Entry of Herpes Simplex Virus 1 Into Neuron Cells by Regulating Cofilin-Mediated F-Actin Reorganization
Xiaowei Song, Yiliang Wang, Feng Li, Wenyan Cao, Qiongzhen Zeng, Shurong Qin, Zhaoyang Wang, Jiaoyan Jia, Ji Xiao, Xiao Hu, Kaisheng Liu, Yifei Wang and Zhe Ren

116 A Recombinant Porcine Reproductive and Respiratory Syndrome Virus Stably Expressing DsRed Protein Based on Bacterial Artificial Chromosome System
Na Li, Yiyi Zhang, Lunguang Yao, Yunpeng Shi, Qin Zhao, Baicheng Huang and Yani Sun

125 The Emerging Role of RNA Modifications in the Regulation of Antiviral Innate Immunity
Jie Tong, Wuchao Zhang, Yuran Chen, Qiaoling Yuan, Ning-Ning Qin and Guosheng Qu

138 Insights Into the Coinfections of Human Immunodeficiency Virus-Hepatitis B Virus, Human Immunodeficiency Virus-Hepatitis C Virus, and Hepatitis B Virus-Hepatitis C Virus: Prevalence, Risk Factors, Pathogenesis, Diagnosis, and Treatment
Sagarika Shahriar, Yusha Araf, Rasel Ahmad, Pravakar Kattel, Ganga Sagar Sah, Tanjim Ishraq Rahaman, Rahila Zannat Sadiea, Shahnaj Sultana, Md. Sayeedul Islam, Chunfu Zheng and Md. Golzar Hossain

154 The Hidden Enemy Within: Non-canonical Peptides in Virus-Induced Autoimmunity
Manivel Lodha, Florian Erhard, Lars Dölken and Bhupesh K. Prusty

164 What Should Be Learned From Repurposed Antivirals Against SARS-CoV-2?
Miguel Angel Martinez

169 The Role of Deubiquitinases in Virus Replication and Host Innate Immune Response
Qinglin Zhang, Qizhen Jia, Wenying Gao and Wenyan Zhang

183 Isolation and Genetic Characterization of Parvoviruses From Dogs, Cats, Minks, and Raccoon Dogs in the Eastern Region of Shandong Province, China
Jiakai Zhao, Hao Zhang, Lu Zhang, Qiang Zhang, Ning Zhou, Taofeng Du, Qin Zhao, En-Min Zhou, Yongkun Du and Yani Sun

194 The Construction and Immunogenicity Analyses of Recombinant Pseudorabies Virus With NADC30-Like Porcine Reproductive and Respiratory Syndrome Virus-Like Particles Co-expression
Jun Zhao, Ling Zhu, Lei Xu, Fengqing Li, Huidan Deng, Yao Huang, Sirui Gu, Xianggang Sun, Yuancheng Zhou and Zhiwen Xu

211 MiR-103a-3p Promotes Zika Virus Replication by Targeting OTU Deubiquitinase 4 to Activate p38 Mitogen-Activated Protein Kinase Signaling Pathway
Haiyan Ye, Lan Kang, Xipeng Yan, Shilin Li, Yike Huang, Rongrong Mu, Xiaoqiong Duan and Limin Chen

223 Innate Immune Evasion by Human Respiratory Syncytial Virus
Yan Ouyang, Hongqun Liao, Yan Hu, Kaiyuan Luo, Shaowen Hu and Huifang Zhu

232 Heat Shock Protein A6 Is Especially Involved in Enterovirus 71 Infection
Jiaoyan Jia, Ge Liu, Jianfeng Zhong, Ran Yan, Xun Song, Kai Zheng, Zhe Ren, Zhendan He and Qinchang Zhu

243 Multifunctional pMGF505-7R Is a Key Virulence-Related Factor of African Swine Fever Virus
Li Huang, Jiangnan Li, Jun Zheng, Dan Li and Changjiang Weng

247 Reactivation of Occult Hepatitis B Virus Infection During Long-Term Entecavir Antiviral Therapy
Chunyan Yuan, Jing Peng, Renxiang Xia, Jian He, Tianji Qiu and Yunqing Yao

252 Human Immunodeficiency Virus-1 Latency Reversal *via* the Induction of Early Growth Response Protein 1 to Bypass Protein Kinase C Agonist-Associated Immune Activation
Lilly M. Wong, Dajiang Li, Yuyang Tang, Gema Méndez-Lagares, George R. Thompson, Dennis J. Hartigan-O'Connor, Satya Dandekar and Guochun Jiang

265 Vitamin D3 Suppresses Human Cytomegalovirus-Induced Vascular Endothelial Apoptosis *via* Rectification of Paradoxical m6A Modification of Mitochondrial Calcium Uniporter mRNA, Which Is Regulated by METTL3 and YTHDF3
Wenbo Zhu, Hongbo Zhang and Shao Wang

283 Long-Term Expansion of Porcine Intestinal Organoids Serves as an *in vitro* Model for Swine Enteric Coronavirus Infection
Min Zhang, Lilei Lv, Hongming Cai, Yanhua Li, Fei Gao, Lingxue Yu, Yifeng Jiang, Wu Tong, Liwei Li, Guoxin Li, Guangzhi Tong and Changlong Liu

296 Genetic Characteristics of Porcine Hemagglutinating Encephalomyelitis Coronavirus: Identification of Naturally Occurring Mutations Between 1970 and 2015
Amina Nawal Bahoussi, Yan-Yan Guo, Rui-Zhu Shi, Pei-Hua Wang, Ya-Qian Li, Chang-Xin Wu and Li Xing

307 Genome-Wide Approaches to Unravel the Host Factors Involved in Chikungunya Virus Replication
Atsushi Tanaka and Youichi Suzuki

316 The Immunity Protection of Central Nervous System Induced by Pseudorabies Virus DelgI/gE/TK in Mice
Lei Xu, Jian-feng Wei, Jun Zhao, Si-yao Xu, Feng-qin Lee, Min-cai Nie, Zhi-wen Xu, Yuan-cheng Zhou and Ling Zhu

325 Pathogenicity and Immunogenicity of a Serially Passaged Attenuated Genotype 2c Porcine Epidemic Diarrhea Virus Cultured in Suspended Vero Cells
Fei-Fei Ge, Long-Shan Kang, Li-Ping Shen, Hai-Xiao Shen, De-Quan Yang, Xin Li, Hou-Bin Ju, Hong-jin Zhao and Jian Wang

335 Molecular Evidence of Orthomyxovirus Presence in Colombian Neotropical Bats
Manuel Uribe, Miguel E. Rodríguez-Posada and Gloria C. Ramirez-Nieto

344 Insights Into Persistent HIV-1 Infection and Functional Cure: Novel Capabilities and Strategies
Tram M. Ta, Sajjaf Malik, Elizabeth M. Anderson, Amber D. Jones, Jocelyn Perchik, Maryann Freylikh, Luca Sardo, Zackary A. Klase and Taisuke Izumi

frontiers in Microbiology

MINI REVIEW
published: 05 November 2021
doi: 10.3389/fmicb.2021.777885

# Influenza A Virus–Host Specificity: An Ongoing Cross-Talk Between Viral and Host Factors

*Miaomiao Zhang[1,2†], Mingbin Liu[1†], Shimeng Bai[1], Chen Zhao[1], Zejun Li[2]*, Jianqing Xu[1]* and Xiaoyan Zhang[1]**

[1]*Scientific Research Center, Shanghai Public Health Clinical Center & Institutes of Biomedical Sciences, Key Laboratory of Medical Molecular Virology of Ministry of Education/Health, Shanghai Medical College, Fudan University, Shanghai, China,* [2]*Shanghai Veterinary Research Institute, Chinese Academic of Agricultural Sciences & Animal Influenza Virus Evolution and Pathogenesis Innovation Team of the Agricultural Science and Technology Innovation Team, Shanghai, China*

OPEN ACCESS

**Edited by:**
*Chunfu Zheng,*
*University of Calgary, Canada*

**Reviewed by:**
*Zhenlong Liu,*
*McGill University, Canada*
*Yi-Quan Wu,*
*National Cancer Institute (NCI), United States*

***Correspondence:**
*Zejun Li*
*lizejun@shvri.ac.cn*
*Jianqing Xu*
*xujianqing@fudan.edu.cn*
*Xiaoyan Zhang*
*zhangxiaoyan@fudan.edu.cn*

*†These authors have contributed equally to this work*

**Specialty section:**
*This article was submitted to Virology, a section of the journal Frontiers in Microbiology*

**Received:** *16 September 2021*
**Accepted:** *19 October 2021*
**Published:** *05 November 2021*

**Citation:**
*Zhang M, Liu M, Bai S, Zhao C, Li Z, Xu J and Zhang X (2021) Influenza A Virus–Host Specificity: An Ongoing Cross-Talk Between Viral and Host Factors. Front. Microbiol. 12:777885. doi: 10.3389/fmicb.2021.777885*

One big threat from influenza A viruses (IAVs) is that novel viruses emerge from mutation alongside reassortment. Some of them have gained the capability to transmit into human from the avian reservoir. Understanding the molecular events and the involved factors in breaking the cross-species barrier holds important implication for the surveillance and prevention of potential influenza outbreaks. In this review, we summarize recent progresses, including several ground-breaking findings, in how the interaction between host and viral factors, exemplified by the PB2 subunit of the influenza virus RNA polymerase co-opting host ANP32 protein to facilitate transcription and replication of the viral genome, shapes the evolution of IAVs from host specificity to cross-species infection.

**Keywords: influenza A virus, host specificity, pathogenesis, host factors, PB2**

## INTRODUCTION

Influenza A virus (IAV) is a major pathogen that greatly impacts human health and the poultry industry with a broad host tropism, capable of infecting various hosts, including wildfowl, swine, bat, and humans being. IAV is a negative-stranded RNA virus comprising eight segments. Two major surface proteins of IAV are hemagglutinin (HA) and neuraminidase (NA), which are used for classifying IAV subtypes based on sequence similarity. Up to date, 18 HA and 11 NA subtypes have been discovered, with H17, H18, N10, and N11 being only found in bats (Tong et al., 2013). Besides HA and NA, the IAV genome encodes at least 16 additional viral proteins, among which PB2, PB1, PA, HA, NP, NA, M1, M2, NS1, and NS2 proteins have been extensively characterized with relatively clear function while PB2-S1, PB1-F2, PB1-N40, PA-X, PA-N155, PA-N182, M42, and NS3 protein represent more recently discovered proteins (Vasin et al., 2014) and their functions remain largely unknown.

Birds are the major, if not the only, natural reservoir of IAV. Avian influenza viruses (AIV) can be divided into low-pathogenic (LPAIV) and highly pathogenic (HPAIV) strains, as determined by the presence of different types of the proteolytic cleavage site in HA (Horimoto and Kawaoka, 2005). The genetic diversity of IAVs is driven by an error-prone replication machinery, in addition to genetic reassortment events where viruses co-infecting the same cell exchange segments. As a result, a cross-species spillover can occasionally occur as an AIV mutant acquires the ability to transmit into aquatic (dolphins, seals, whales) or terrestrial

mammals (pigs, horses, mink). Recent reports on human infection of AIV can be traced back to the year of 1997, when the contraction of H5N1 AIV killed 6 people in Hong Kong (Wong and Yuen, 2006). In 2003, an H7N7 AIV outbreak was reported in Netherlands, infecting 84 people with one death (Wong and Yuen, 2006). The threats of transmission of AIV to humans appear to continue growing: local outbreaks of highly pathogenic H5N1 AIV occurred in many Asia countries until 2004 (Stegeman et al., 2004); a total of 1,568 human infection H7N9 AIV has been reported, responsible for at least 617 deaths; the human spillover of H10N8 and H5N6 AIV were also observed (Chen et al., 2014; Yang et al., 2015). These indicate that, although breaking the cross-species barrier is difficult, there is always a likelihood of it happening with an expanding reservoir of AIV. Thus, exploring the molecular mechanisms underlying the host specificity of IAV and the events leading to their breach is an important step toward improving the preparedness of future influenza pandemics by instructing the development of enhanced surveillance of potential risk of avian-to-human transmission; identifying hidden virus–host interfaces as new targets for antivirals. This review will summarize recent advances that start to unfold the complexity of species-specific virus–host interactions underpinning the host range of IAVs.

## VIRAL DETERMINANTS OF IAV HOST SPECIFICITY

A clear announcement of host specificity of IAV is made because avian viruses generally show poor replication in mammalian cells, and vice versa. The host restriction of IAV has been linked to the difference between host of factors governing viral entry and multiple intracellular steps required for viral replication. Consequently, only AIVs with adaptive mutations, which account for a small portion of the virus pool that emerged from the natural reservoir, gain the ability to infect mammalian cells. These mutations are discussed in details per involved viral proteins.

### The Viral HA Protein

The entry of IAV into host cells, representing the first species barrier to overcome, is mediated by viral surface hemagglutinin (HA) glycoprotein. Although all HA proteins have a general cell receptor in sialic acids (SA), a diverse family of sugar units terminally attached to glycans decorating surface glycoproteins and glycolipids, they show an origin-dependent preference for sialic acid-galactose linkage. HAs from human influenza viruses preferably recognize α-2,6 linked SA (α-2,6 receptor) while those of avian origin showed a higher binding affinity with α-2,3-linked SA (α-2,3 receptor; Matrosovich et al., 1997, 2000). The correlation of this recognition pattern with SA distribution in human tissues explains why avian IAV normally cannot infect humans. In humans, α-2,6 receptors are mainly expressed on cells of the ciliated epithelium along the upper respiratory tract (URT), while α-2,3 receptors are primarily found in the lower respiratory tract (LRT; Shinya et al., 2006). In contrast, pig trachea presents both α-2,3 and α-2,6 receptors and is thus susceptible to infection of both human and avian virus, making pig a mixing vessel where new viruses can be generated through reassortment from parental virus of different origins.

Extensive structural studies have revealed the modes of interactions between HA and their corresponding SA receptor (Long et al., 2019). A wider receptor binding site (RBS) has been posited to form the basis of human-adapted HA accommodating α-2,6 SA linkage, which appears bulkier than the α-2,3 SA linkage. Several adaptive mutations in RBS of avian HAs have been shown to cause a switch of binding specificity, exemplified by E190D/G225D and A138S in H1 HA and Q226L/G228S in the HAs of H2 and H3 subtypes (Shi et al., 2014). These mutations increase binding affinity to the human receptor while reducing the binding to the avian receptor. The HA proteins of recently emerged H7N9 AIV that showed high pathogenicity in human infections appear to acquire some ability to bind to human receptor despite maintaining the preference for the avian receptor (Xu et al., 2013). This change was particularly exhibited by the Anhui-H7N9 virus, which harbors four mutations in RBS, namely S138A, G186V, T221P, and Q226L, accounting for the shift of receptor binding preference (Shi et al., 2013). As for the H5N1 virus, those causing human infections retain preference for avian receptor but such specificity can be skewed to human side by HA mutations in position 226 and 228, which are also required for airborne transmissibility (Stevens et al., 2008). Overall, typical AIV strains have not yet shown acquisition of transmissibility among humans until now. Despite the odds, the possibility of AIV breaking such a barrier cannot be ruled out, especially considering that multiple types of HA can attain airborne transmission ability in mammalian model systems (Kuchipudi et al., 2021).

### The Viral NA Protein

As another major viral surface protein alongside HA, NA possesses sialidase activity and is responsible for cleaving SA from the cell surface to facilitate the release of the progeny virus particle (Schrauwen et al., 2014). Strong evidence supporting the adaptation of NA to host came from the short-stalk NA favored by poultry IAV, which is speculated to match short length of glycan linked to SA receptor (Li et al., 2010). However, this type of NA does not support airborne transmission in ferrets, likely due to ineffective cleavage with longer glycan and the resultant virus clumping. Thus, it has been proposed that a functional balance between the SA binding of HA and NA sialidase activity is a critical element involved in the host fitness of IAV (Lakdawala et al., 2015). Interestingly, a second HA binding site was found on some NAs, contributing to their hemadsorption (Hd) activity. Such Hd site was originally thought to regulate the catalytic activity of NA positively, but the recent characterization of NA protein from the H7N9 virus indicated that its existence might allow enhanced receptor binding, particularly to human-like α2,6-linked sialic acid

(Benton et al., 2017). It remains to be determined whether the Hd site contributes to the ability of the H7N9 virus to infect humans infection.

## The Viral Polymerase Proteins

The transcription and replication of the viral genome, carried out by the viral RNA polymerase, are central to viral growth and consequently become a critical barrier to overcome during the adaptation of IAV to a new host. The tripartite RNA-dependent RNA polymerase (RdRp) of IAV consists of polymerase protein basic 1 (PB1), polymerase protein basic 2 (PB2), and polymerase acidic protein (PA). Inside the virus, all the eight viral RNA (vRNA) segments are coated by nucleoprotein (NP) with RdRp binding to the conserved 5′ and 3′ ends to form viral ribonucleoprotein (vRNP) complexes (Nilsson et al., 2017). Once transported into the nucleus in infected cells, RdRp first transcribes vRNA into mRNA for viral protein production, a process initiated by a cap snatching mechanism wherein a nucleotide sequence of 10–20 nt length is cleaved from the 5′ end of host mRNAs by a sequential action of PB2 and PA and subsequently serve as the primer for viral mRNA synthesis (Dias et al., 2009; Yuan et al., 2009). The replication of the viral genome ensues after accumulation and nuclear transport of newly synthesized RdRp proteins. In contrast to transcription, the RdRp-mediated replication is primer independent and involves cRNA as an intermediate product. Additionally, NP is required for replication while dispensable for transcription. Recent studies also suggest that the catalytic activity of RdRp in vRNA replication requires dimer formation between an RNA-bound RdRp and free RdRp, which acts as a relay station to synthesize vRNA from cRNA (Nilsson et al., 2017). The central domain of RdRp is composed of PB1, the C-terminal domain of PA, the N-terminal one-third of PB2 encompassing the N terminus, the lid domain, and the N1 and N2 linkers (Nilsson et al., 2017).

The host adaptation of IAV RdRp is best displayed on PB2, which is responsible for cap-binding and participates in NP binding *via* regions in its N- and C-terminals. Several mutations in PB2 have been identified to be important for promoting adaptation of avian IAV to mammalian, epitomized by Glu-to-Lys substitution at position 627 (E627K) and Asp-to-Asn substitution at position 701 (D701N; Gabriel and Fodor, 2014). Subbarao et al. first reported the identity of amino acid at position 627 as a dividing line between avian and human influenza virus with respective E and K dominance (Subbarao et al., 1993). Importantly, a single change of E to K at position 627 was sufficient for restoring the ability of a PB2 single gene reassortant to replicate effectively in canine (MDCK) cells (Subbarao et al., 1993). Further analysis revealed that PB2 E627K mutation could remarkably raise the RdRp activity in mammalian but not avian cells, leading to an increased virulence in mammalian hosts' pathogenicity (Subbarao et al., 1993; Hatta et al., 2001; Gabriel et al., 2005). Indeed, 627K is commonly shared by a wide spectrum of human pathogenic IAVs, including H5N1, H7N9, H10N8, and H5N6 subtypes (Gao et al., 2013; Garcia-Sastre and Schmolke, 2014; Yang et al., 2015). D701N as a mammalian-like signature was first identified by Li et al. through analyzing the genetic determinant underlying the ability of a duck H5N1 IAV to replicate in mice (Li et al., 2005). More recently, some H9N2 viruses isolated from minks were reported to contain the PB2 701N mutation and consequently showed enhanced virulence in mice compared to those without such mutation, supporting the potential of mink as a mixing vessel or intermediate host for H9N2 virus and possibly other IAVs (Xue et al., 2018).

Interestingly, other PB2 mutations, though less frequent than 627K or 701N, can also promote human adaption. For example, the 2009 pandemic H1N1 virus harbors neither PB2 627K nor PB2 701N signatures (Mehle and Doudna, 2009). Instead, its mammalian adaptation was supported by PB2 G590S/G591R polymorphisms, which also conveyed enhanced RdRp activity in human cells (Mehle and Doudna, 2009). PB2-Q591K and K526R are two other mutations shown in H9N2 virus and H7N9/H5N1 viruses capable of conferring effective replication in mammalian cells in the absence of 627K and 701N (Song et al., 2014; Wang et al., 2016). The combinatorial effects of different adaptive mutations have also been studied. H7N9 virus bearing both 627K and 526R replicates more efficiently in mammalian cells than those carrying the individual mutation, consistent with greater mortality in mice (Song et al., 2014). Mechanistically, the combination of 526R with 627K appeared to optimize the interaction between PB2 and nuclear export protein (NEP), thereby promoting higher polymerase activity. A similar synergistic effect between PB2-526R and 701N was also documented. In contrast, the co-existence of PB2 E627K and D701N mutations has not yet been detected in naturally occurring virus isolates, suggesting potential functional redundancy of the two mutations (Steel et al., 2009; Gabriel and Fodor, 2014).

Adaptive mutations of other components of IAV replication machinery were also identified, despite being less frequent than what was seen with PB2. A divergency at the position of PB1 protein of human influenza A/H1N1 viruses was recently identified: This position was predominantly occupied by the avian-associated serine residue before switching to mammalian-associated glycine residue near the onset of the 2009 pandemic (Lin et al., 2019). Subsequent studies showed that PB1-216G was a lower RdRp fidelity variant than PB1-216S, thereby allowing the H1N1 virus to yield adaptive mutations at higher rates and promoting viral epidemiological fitness (Lin et al., 2019). Multiple studies revealed the role of PA in the human adaptation of AIV. It was found that, in avian H9N2 background, a single replacement of PA segment from 2009 pandemic H1N1 virus resulted in enhanced viral polymerase activity, leading to a higher pathogenicity in infected mice (Sun et al., 2011). A systematic comparison of a panel of reassortant viruses between a duck-derived H5N1 and a highly transmissible human-infective H1N1 virus showed that PA and nonstructural gene are the major H1N1 determinants of droplet-mediated transmission between guinea pigs (Zhang et al., 2013). A couple of human adaptive PA mutations were identified, including E349G and PA 97I, with a positive impact on viral polymerase activity in mammalian cells (Song et al., 2009). Evidence

supports the concerted action between mutations of different RdRp subunits and NP protein in enhancing human adaptation. Gabriel et al. reported that mutations in PB2, PA, and NP, namely PB2 701N and 714R, PA 615N, and NP 319K, cooperatively enhance AIV SC35 (H7N7) polymerase activity and consequently enable an effective replication in mammalian cells (Gabriel et al., 2005). The coupling between PB2 D701N and NP D319K mutation was confirmed in other studies (Gabriel et al., 2011). The molecular mechanism(s) underpinning synergy between these mutations in enhancing mammalian fitness of AIV has yet to be fully delineated, though some studies, as described below, suggested the involvement of importin-α.

## NS1A and Other Viral Proteins

The interferon (IFN)-centered innate immune response represents the first-line defense against viral infection. Accordingly, IAV develops several viral countermeasures epitomized by nonstructural protein 1 (NS1). NS1 protein is produced by the co-linear transcript of RNA segment 8, which also encodes NS2 (NEP) through alternative splicing (Liu et al., 1997). NS1A comprises an RNA binding domain (RBD) and an effector domain (ED); both domains contribute to the ability of NS1A to use multiple rather than single tactics to evade the IFN antiviral response (Yin et al., 2007; Bornholdt and Prasad, 2008). Two main mechanisms have been proposed for the IFN countering the action of NS1A, namely blocking the activation of RIG-I, the major pattern recognition receptor responsible for sensing the incoming IAV genome, and inhibiting the activity of CPSF30 (Cleavage and polyadenylation specificity factor 30 kDa subunit) from suppressing the maturation and consequently the nuclear export of IFN mRNA (Cho et al., 2020; Rosário-Ferreira et al., 2020). The RNA-binding of NS1, once thought to sequester dsRNA produced by viral replication from host dsRNA sensor, was shown to primarily function as a competitor of 2′-5′-oligoadenylate synthetase (OAS) to suppress the RNaseL antiviral pathway (Min and Krug, 2006). NS1A is also engaged in interactions with various host factors without known roles in innate immune response, implicating additional regulatory roles in other aspects of the viral cycle (Rosário-Ferreira et al., 2020). The wide spectrum of host protein interactions by NS1A has been proposed as a result of the ready-for-exploitation nature of its ED (Cho et al., 2020) and/or a double-stranded RNA platform that strengthens the weak interactions NS1A with certain host factors (Chen et al., 2020).

Several naturally occurring mutations of NS1 have been linked to enhanced viral replication and pathogenicity, including D92E, P42S, and deletion of 80-84 residues (del80-84). As expected, these mutations were often associated with increased virus resistance to interferon (Seo et al., 2002). It is a bit of surprise that the CPSF30 binding site of NS1A is not conserved across IAVs: Although the majority of NS1A proteins bind to CPSF30, those from pandemic H1N1 2009 virus and human-infective H5N1 1997 virus cannot (Long et al., 2019), which leads to a hypothesis that gain or loss of CPSF binding of NS1A may be a viral means to balance between viral replication and interferon antagonism on the road toward mammalian adaptation. Sequence analyses also pinpoint several amino changes that could associate with the adaptation of AIV to mammalian host, such as the alteration of last amino acids from ESEV to RSKV (Zielecki et al., 2010), and the D125G substitution introducing an extra splice site into the NS gene (Selman et al., 2012). However, whether and how these changes may influence the host range of AIV remained to be determined. Overall, a link between NS1 mutations and cross-species transmission of AIVs is still elusive.

Apart from NS1A, the human adaptation of AIV may be facilitated by mutating viral accessory proteins that were recently discovered, such as PB1-F2 and PA-X. PB1-F2 is an 87-amino acid small protein produced from PB1 encoding sequence through +1 frameshift and has been shown to antagonize antiviral innate immunity possibly *via* interaction with components of the RIG-I/MAVS system, particularly the mitochondrial antiviral signaling (MAVS) protein (Mazur et al., 2008). Interaction between PB1-F2 and PB1 has also been documented and is in line with the enhancing effect of PB1-F2 on the RdRp activity (Mazur et al., 2008). The role of PB1-F2 in the viral pathogenesis was highlighted by the finding that a single amino acid substitution in PB1-F2, namely N66S, is associated with increased virulence of the 1997 human H5N1 virus is also conserved in the 1918 pandemic virus (Conenello et al., 2007). However, the ORF of PB1-F2 is often truncated or lost in swine or human IAVs, raising the speculation that PB1-F2 is not essential for IAV mammalian adaptation or a compensatory mechanism has been acquired (Long et al., 2019).

PA-X is the product of +1 ribosomal frameshifting during translation of PA protein, retaining the 191-aa long N-terminal endonuclease domain while acquiring a unique C-terminal region known as X-ORF, commonly encoding 61 aa (Jagger et al., 2012). PA-X is known to facilitate viral growth by coordinating the virus-mediated shutoff of host gene expression (Gaucherand et al., 2019). Interestingly, some IAV strains possess early stop codon in the X-ORF, resulting in a truncated PA-X protein 41 aa in length (Sun et al., 2020). Avian, equine, and human seasonal H3N2 and H1N1 influenza viruses generally encode full-length X-ORF while truncated X-ORF is characteristic of the 2009 pandemic H1N1, swine and canine viruses (Sun et al., 2020). In terms of swine influenza viruses (SIVs), the majority of early isolates were found to express a full-length PA-X until 1985, from when isolates featuring truncated PA-X gradually increased to become the dominant species, implicating a selection favoring truncated PA-X in pigs (Xu et al., 2016). Indeed, Xu et al. demonstrated that, in the background of a "triple-reassortment" H1N2 SIV, mutating X-ORF to express a full-length PA-X resulted in attenuated viral replication and transmission in pigs (Xu et al., 2017). By contrast, an investigation based on the 2009 pandemic H1N1 revealed that full-length PA-X protein supported increased virulence in mice relative to the truncated form (Gao et al., 2015). Thus, PA-X is a likely contributing factor to the host specificity of IAV. The notion was further strengthened by the finding that single human-specific amino acid substitutions in PA-X, particularly the R195K mutation, might underpin the animal-to-human jump of H7N9, H5N6, and H1N1/2009 viruses (Sun et al., 2020).

## INTRACELLULAR HOST FACTORS UNDERLYING THE HOST SPECIFICITY OF IAV: IMPORTIN-α AND ANP32A TAKE THE LEAD

A major recent advance in understanding the host specificity of IAV is identifying the related intracellular host factors, best represented by importin-α and ANP32 proteins.

### Importin-α

In uninfected cells, importin-α functions as an adaptor protein involved in the nuclear transportation of host proteins possessing nuclear localization signal (NLS; Stewart, 2007). IAV-infected cells are usurped by the virus to transport incoming vRNPs into the nucleus and are also responsible for nuclear importation of newly synthesized PB2 and NP proteins following primary transcription, which is a requisite for sustained viral replication (Stewart, 2007). Avian and human IAVs appear to engage different importin-α isoforms for effective viral replication as revealed using importin-α-silenced cells and importin-α-knockout mice: Avian virus depends on importin-α3, whereas human virus displays a switch to importin-α7 dependency; the 2009 H1N1 pandemic IAV instead showed a dual dependency of both importin-α3 and importin-α7, suggesting ongoing viral adaptation (Gabriel et al., 2011; Pumroy et al., 2015). Consistent with the viral replication data, avian- and human-like PB2 were found to bind preferentially to importin-α3 and importin-α7, respectively (Gabriel et al., 2011). Further evidence that differential importin-α recognition is a mechanism of IAV host specificity came from binding studies that D701N mutation enhances the interaction between PB2 and importin-α7, so does D319K for NP (Gabriel et al., 2011). Given the proximity of 701 to the NLS of PB2, it has been speculated that the D701N mutation might induce a conformation change that facilitates a stronger binding to importin-α (Tarendeau et al., 2007; Sediri et al., 2015). Interestingly, a most recent study identified a correlation between PB2-D701N/NP-D319K mutations and reduced expression of importin-α3 in the respiratory tract of IAV-infected humans and mice. As importin-α3 mediates the nuclear import of NF-κb and is thus required for induction of various antiviral genes in IAV-infected cells, its downregulation complements the virus's capability to access importin-α7 in ensuring that virus can gain replicative fitness in the human lung (Gabriel et al., 2008; Thiele et al., 2020).

### ANP32 Proteins

Once in the nucleus, the IAV viral polymerase needs to utilize host machinery for effective transcription and genome replication, and this represents another major barrier that AIV needs to surpass upon avian-mammalian adaptation. The original clue for this barrier came from the observation that the poor activity of avian IAV polymerase in mammalian cells could be rescued by fusion with avian cells to form heterokaryons, which can be explained by the absence of a supportive avian host factor in mammalian cells. Long et al. first discovered this longed-for host factor as chicken ANP32A. Surprisingly, there is a human homolog of chicken ANP32A (chANP32A); the major difference between chicken and human ANP32A is that the former possesses an additional 33 amino acids between the shared leucine-rich repeats and carboxy-terminal low-complexity acidic region domains owing to exon duplication (Long et al., 2016; **Figure 1**). Importantly, the 33-aa insertion was responsible for the superiority of chicken ANP32A over human ANP32A in supporting the activity of avian PB2-627E viral polymerase in mammalian cells (Long et al., 2016; Domingues and Hale, 2017). In this regard, the PB2 E627K mutation was selected to meet the viral need to co-opt the mammalian ANP32A for effective viral replication.

Subsequent studies further revealed deep connections between ANP32 family proteins and human adaption of IAV polymerase. The activity of ANP32A appears to be regulated by alternative splicing in avian cells, resulting in variants containing essential no (human-like), partial, or full 33aa-insertion (Baker et al., 2018). More interestingly, the usage of ANP32A splicing sites varies across different bird species, and some species predominantly express human-like ANP32A, most pronounced in swan goose (>70%) and ostrich (close to 100%; Domingues et al., 2019). It is thus proposed that the differential ANP32A splicing inherent to natural avian hosts may provide a pre-adaptation mechanism that shapes the evolution of PB2 to facilitate cross-species transmission (Domingues et al., 2019). A recent finding further strengthened the view of ANP32A as a facilitator of IAV evolution. Swine ANP32A is capable

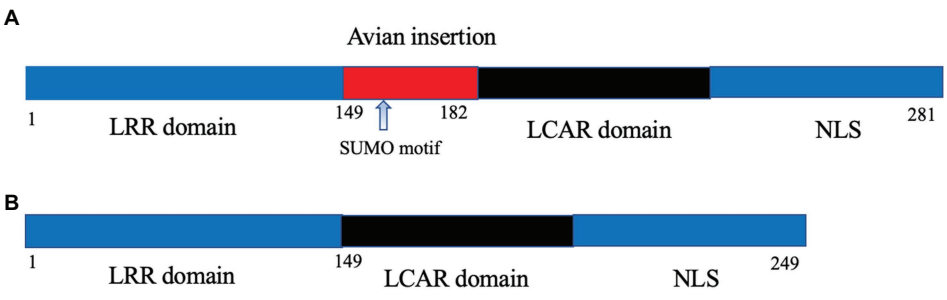


**FIGURE 1 |** Schematic illustration of chicken **(A)** and human ANP32A **(B)**. The avian-specific 33-amino acid insertion is highlighted in red with the containing SUMO binding motif being indicated by an arrow.

of supporting avian-type IAV polymerase activity, although to a less extent as compared with avian ANP32A, consistent with the pig as an important intermediate host for zoonotic IAVs (Zhang et al., 2020a). This unique feature of swine ANP32A was attributed to 106V, which exhibits positive epistasis with 156S and has not been found in other studied vertebrate species (Zhang et al., 2020a). Recent studies also revealed another member of ANP32 family, ANP32B, in regulating IAV polymerase activity. This revelation was made using human ANP32A and ANP32B single- and double-knockout cells as only in the latter cells was the viral polymerase activity abrogated (Zhang et al., 2019). The analysis also indicated that human ANP32B is a more potent pro-viral factor than human ANP32A. In contrast, the viral polymerase supporting activity was lost in chicken ANP32B, and further dissection pinpointed residue 129 and 130 as the critical determinant of ANP32B activity: Avian ANP32B possesses isoleucine and asparagine at the two positions, whereas in human ANP32A and ANP32B, as well as avian ANP32A, they are filled with asparagine and aspartate (Zhang et al., 2019).

The precise mechanism by which ANP32 regulates the activity of IAV RNA polymerase remains unclear. ANP32A or ANP32B was associated with the trimeric viral polymerase in infected cells or when they were simultaneously expressed by co-transfection (Zhang et al., 2019). The failure of ANP32A to bind to free PB2 in co-expressed cells indicated that such association requires the formation of a viral polymerase complex. On the other hand, *in vitro* binding assay employing purified protein revealed a direct interaction between ANP32A and the 627 domain of PB2. However, the binding of human or chicken ANP32A to viral polymerase appears to be independent of PB2-627 identity (Domingues and Hale, 2017). Following the finding that chicken ANP32A binds to PB2 stronger than human ANP32A, Domingues et al. discovered a sumo interaction motif (SIM) in the first four residues of the avian-specific 33-aa insertion and suggested it might account for increased binding of chicken ANP32A to PB2 (Domingues and Hale, 2017). However, a natural splicing variant of chicken ANP32A with SIM deletion can support viral polymerase activity, though less effective than that with a complete 33-aa insertion (Domingues and Hale, 2017). Recently, Baker et al. provided experimental evidences linking ANP32A to a specific form of the viral polymerase (Baker et al., 2018). The binding of ANP32A to viral polymerase in co-transfected cells was enhanced in the presence of viral genomic RNA. It was known that the low activity of PB2 627E viral polymerase can be trans-complemented by mutations at positions 3 and 5 of 3′ vRNA promoter. When assayed on reporter bearing such mutant vRNA promoter, chANP32A showed a little enhancing effect, implying the same or similar mechanism shared by a mutant promoter and chANP32A (Baker et al., 2018). These results are consistent with the hypothesis that ANP32A facilitates the assembly of either cRNP, vRNP, or both.

Structural approaches have also searched the molecular basis for recognition of ANP32A by PB2. Using a combination of NMR and quantitative ensemble analysis, Camacho-Zarco et al. conducted a comparative analysis of complex formed between human ANP32A and human-adapted PB2-627-NLS domain (K627 form) versus that comprising avian ANP32A and avian adapted PB2-627-NLS domain (Camacho-Zarco et al., 2020). Although both complexes were highly dynamic, they were found to display two different modes of interaction: Human ANP32A utilizes a track of positively charged residues including K627 to maximize interaction with highly acidic IDD domain (alternative name of LCAR to highlight its low complexity); with such positive charged surface being interrupted by E627, avian ANP32A can compensate this loss by broadening the sampling of IDD domain to exploit more expanded interaction surface, particularly involving a hexapeptide motif present in the avian-specific 33-aa insertion (Camacho-Zarco et al., 2020). Despite providing the first structural insight into host-specific ANP32A-PB2 interaction, the study from Camacho-Zarco et al. could not interpret the previous observation that chicken ANP32A binds to PB2 more strongly than its human ortholog. Instead, it would predict a higher binding affinity between human ANP32A and 627K type PB2. More recently, Carrique et al. reported cryo-EM structures of influenza C virus polymerase (FluPolC) in complex with human or avian ANP32A (Carrique et al., 2020). In both structures, two FluPolC molecules, one bound to a 47-nt long vRNA and one staying free, formed an asymmetric dimer that ANP32A bridges through its LRR domain (Carrique et al., 2020). The LCAR domain of ANP32A further stabilizes the complex formation in the FluPolC-chicken ANP32A structure with the avian-specific 33-aa insertion directly interacting with the two juxtaposed 627 domains of PB2 (Carrique et al., 2020). The authors thus proposed that ANP32A-FluPol dimer functions as a platform for viral genome replication, where a vRNA-bound $FluPol_R$ and a free $FluPol_E$ act sequentially in cRNA synthesis and the ensued vRNP assembly (Carrique et al., 2020). However, chicken ANP32A, unlike human ANP32A/B, has limited ability to support the viral polymerase of the influenza B virus (Zhang et al., 2020b), whether such platform is shared by IAV viral polymerase remains to be determined.

## CONCLUSION

The host specificity of the IAV is underpinned by complex interactions between viral proteins and host factors. This complexity is translated to the requirement of a constellation of mutations for the virus to adapt to a new host. Although recent studies begin to reveal the molecular basis of several human adaptive mutations, exemplified by PB2 627K, many questions remain to be addressed. For example, no clear consensus has been reached regarding the exact mechanism by which ANP32A is co-opted to enhance viral polymerase activity in a species-specific manner. To answer this, we might need a structure of ANP32A in complex with the matched viral polymerase of IAV. It is also unclear when the human adaptive mutations are selected in the human cells after transmission or preexisted in the animal side. In the case of

PB2 627K, the presence of human-like ANP32A in some bird species and the ability of swine ANP32B to support a certain degree of PB2 627K viral polymerase activity would suggest the second possibility. Identifying PB1–216G, which lowers the viral polymerase activity, reminds us that changing the intrinsic property of viral polymerase may lead to adaptive mutations.

Developing an effective countermeasure against innate immunity of new host is another essential stepstone for AIV to cross the species barrier. It is recognized that the outstanding ability of chicken cells to support AIV growth is at least partially ascribed to a compromised type I IFN system, i.e., lacking of a functional RIG-I homolog (Barber et al., 2010). In addition, the chicken version of Mx protein, which is a major IFN-induced anti-influenza effector molecule in mammal setting, is not capable of restricting influenza virus replication (Benfield et al., 2008). NS1A is the most likely viral candidate taking the assignment to cope with the challenge of more powerful innate immunity in mammal cells. Elucidating the relationship between the evolution of NS1A and adaptation of AIV to mammalian hosts and the underlying mechanism warrant future investigation.

It should also be noticed that environmental and physiological factors, which we have not discussed here, also play an important role in the host restriction of IAV, particularly the transmissibility, which adds more constraints to inter-species transmission. A critical hidden constraint is recently revealed by an elegant study of Soh et al., demonstrating that the architecture of genome code makes some potential human adaption mutations impossible because they are inaccessible to single nucleotide substitution (Soh et al., 2019). Extension of the comprehensive, active search for potential human adaption mutations to other viral proteins might provide us a map of risk spots on viral proteins that we need to be aware of when evaluating the cross-species transmission potential of avian viruses. Finally, further exploration of mechanisms underlying the host specificity and cross-species infection is expected to help dissect the complicated network of host factors usurped by IAVs, thus providing new targets for developing therapeutics and antiviral drugs.

## AUTHOR CONTRIBUTIONS

XZ, JX, and ZL contributed to conception and design of the study. MZ, ML, and SB organized the database and performed the statistical analysis. MZ and CZ wrote the manuscript. All authors contributed to manuscript revision and approved the submitted version.

## FUNDING

This work was supported by the National Natural Science Foundation of China (81771704, 82071788, 31902276), the Shanghai Pujiang Program (19PJ1409100), and the intramural Funding from Shanghai Public Health Clinical Center (to MZ).

## REFERENCES

Baker, S. F., Ledwith, M. P., and Mehle, A. (2018). Differential splicing of ANP32A in birds alters its ability to stimulate RNA synthesis by restricted influenza polymerase. *Cell Rep.* 24, 2581.e4–2588.e4. doi: 10.1016/j.celrep.2018.08.012

Barber, M. R., Aldridge, J. R. Jr., Webster, R. G., and Magor, K. E. (2010). Association of RIG-I with innate immunity of ducks to influenza. *Proc. Natl. Acad. Sci. U. S. A.* 107, 5913–5918. doi: 10.1073/pnas.1001755107

Benfield, C. T., Lyall, J. W., Kochs, G., and Tiley, L. S. (2008). Asparagine 631 variants of the chicken Mx protein do not inhibit influenza virus replication in primary chicken embryo fibroblasts or in vitro surrogate assays. *J. Virol.* 82, 7533–7539. doi: 10.1128/JVI.00185-08

Benton, D. J., Wharton, S. A., Martin, S. R., and McCauley, J. W. (2017). Role of neuraminidase in influenza A (H7N9) virus receptor binding. *J. Virol.* 91:e02293-16. doi: 10.1128/JVI.02293-16

Bornholdt, Z. A., and Prasad, B. V. (2008). X-ray structure of NS1 from a highly pathogenic H5N1 influenza virus. *Nature* 456, 985–988. doi: 10.1038/nature07444

Camacho-Zarco, A. R., Kalayil, S., Maurin, D., Salvi, N., Delaforge, E., Milles, S., et al. (2020). Molecular basis of host-adaptation interactions between influenza virus polymerase PB2 subunit and ANP32A. *Nat. Commun.* 11:3656. doi: 10.1038/s41467-020-17407-x

Carrique, L., Fan, H., Walker, A. P., Keown, J. R., Sharps, J., Staller, E., et al. (2020). Host ANP32A mediates the assembly of the influenza virus replicase. *Nature* 587, 638–643. doi: 10.1038/s41586-020-2927-z

Chen, G., Ma, L. C., Wang, S., Woltz, R. L., Grasso, E. M., Montelione, G. T., et al. (2020). A double-stranded RNA platform is required for the interaction between a host restriction factor and the NS1 protein of influenza A virus. *Nucleic Acids Res.* 48, 304–315. doi: 10.1093/nar/gkz1094

Chen, H., Yuan, H., Gao, R., Zhang, J., Wang, D., Xiong, Y., et al. (2014). Clinical and epidemiological characteristics of a fatal case of avian influenza A H10N8 virus infection: a descriptive study. *Lancet* 383, 714–721. doi: 10.1016/S0140-6736(14)60111-2

Cho, J. H., Zhao, B., Shi, J., Savage, N., Shen, Q., Byrnes, J., et al. (2020). Molecular recognition of a host protein by NS1 of pandemic and seasonal influenza A viruses. *Proc. Natl. Acad. Sci. U. S. A.* 117, 6550–6558. doi: 10.1073/pnas.1920582117

Conenello, G. M., Zamarin, D., Perrone, L. A., Tumpey, T., and Palese, P. (2007). A single mutation in the PB1-F2 of H5N1 (HK/97) and 1918 influenza A viruses contributes to increased virulence. *PLoS Pathog.* 3, 1414–1421. doi: 10.1371/journal.ppat.0030141

Dias, A., Bouvier, D., Crepin, T., McCarthy, A. A., Hart, D. J., Baudin, F., et al. (2009). The cap-snatching endonuclease of influenza virus polymerase resides in the PA subunit. *Nature* 458, 914–918. doi: 10.1038/nature07745

Domingues, P., Eletto, D., Magnus, C., Turkington, H. L., Schmutz, S., Zagordi, O., et al. (2019). Profiling host ANP32A splicing landscapes to predict influenza A virus polymerase adaptation. *Nat. Commun.* 10:3396. doi: 10.1038/s41467-019-11388-2

Domingues, P., and Hale, B. G. (2017). Functional insights into ANP32A-dependent influenza A virus polymerase host restriction. *Cell Rep.* 20, 2538–2546. doi: 10.1016/j.celrep.2017.08.061

Gabriel, G., Dauber, B., Wolff, T., Planz, O., Klenk, H. D., and Stech, J. (2005). The viral polymerase mediates adaptation of an avian influenza virus to a mammalian host. *Proc. Natl. Acad. Sci. U. S. A.* 102, 18590–18595. doi: 10.1073/pnas.0507415102

Gabriel, G., and Fodor, E. (2014). Molecular determinants of pathogenicity in the polymerase complex. *Curr. Top. Microbiol. Immunol.* 385, 35–60. doi: 10.1007/82_2014_386

Gabriel, G., Herwig, A., and Klenk, H. D. (2008). Interaction of polymerase subunit PB2 and NP with importin alpha1 is a determinant of host range of influenza A virus. *PLoS Pathog.* 4:e11. doi: 10.1371/journal.ppat.0040011

Gabriel, G., Klingel, K., Otte, A., Thiele, S., Hudjetz, B., Arman-Kalcek, G., et al. (2011). Differential use of importin-α isoforms governs cell tropism

and host adaptation of influenza virus. *Nat. Commun.* 2:156. doi: 10.1038/ncomms1158

Gao, R. B., Cao, B., Hu, Y. W., Feng, Z. J., Wang, D. Y., Hu, W. F., et al. (2013). Human infection with a novel avian-origin influenza A (H7N9) virus. *N. Engl. J. Med.* 368, 1888–1897. doi: 10.1056/NEJMoa1304459

Gao, H., Sun, H., Hu, J., Qi, L., Wang, J., Xiong, X., et al. (2015). Twenty amino acids at the C-terminus of PA-X are associated with increased influenza A virus replication and pathogenicity. *J. Gen. Virol.* 96, 2036–2049. doi: 10.1099/vir.0.000143

Garcia-Sastre, A., and Schmolke, M. (2014). Avian influenza A H10N8–a virus on the verge? *Lancet* 383, 676–677. doi: 10.1016/S0140-6736(14)60163-X

Gaucherand, L., Porter, B. K., Levene, R. E., Price, E. L., Schmaling, S. K., Rycroft, C. H., et al. (2019). The influenza A virus endoribonuclease PA-X usurps host mRNA processing machinery to limit host gene expression. *Cell Rep.* 27, 776.e7–792.e7. doi: 10.1016/j.celrep.2019.03.063

Hatta, M., Gao, P., Halfmann, P., and Kawaoka, Y. (2001). Molecular basis for high virulence of Hong Kong H5N1 influenza A viruses. *Science* 293, 1840–1842. doi: 10.1126/science.1062882

Horimoto, T., and Kawaoka, Y. (2005). Influenza: lessons from past pandemics, warnings from current incidents. *Nat. Rev. Microbiol.* 3, 591–600. doi: 10.1038/nrmicro1208

Jagger, B. W., Wise, H. M., Kash, J. C., Walters, K. A., Wills, N. M., Xiao, Y. L., et al. (2012). An overlapping protein-coding region in influenza A virus segment 3 modulates the host response. *Science* 337, 199–204. doi: 10.1126/science.1222213

Kuchipudi, S. V., Nelli, R. K., Gontu, A., Satyakumar, R., Surendran Nair, M., and Subbiah, M. (2021). Sialic acid receptors: the key to solving the enigma of zoonotic virus spillover. *Viruses* 13:262. doi: 10.3390/v13020262

Lakdawala, S. S., Jayaraman, A., Halpin, R. A., Lamirande, E. W., Shih, A. R., Stockwell, T. B., et al. (2015). The soft palate is an important site of adaptation for transmissible influenza viruses. *Nature* 526, 122–125. doi: 10.1038/nature15379

Li, Z., Chen, H., Jiao, P., Deng, G., Tian, G., Li, Y., et al. (2005). Molecular basis of replication of duck H5N1 influenza viruses in a mammalian mouse model. *J. Virol.* 79, 12058–12064. doi: 10.1128/JVI.79.18.12058-12064.2005

Li, Q., Qi, J., Zhang, W., Vavricka, C. J., Shi, Y., Wei, J., et al. (2010). The 2009 pandemic H1N1 neuraminidase N1 lacks the 150-cavity in its active site. *Nat. Struct. Mol. Biol.* 17, 1266–1268. doi: 10.1038/nsmb.1909

Lin, R. W., Chen, G. W., Sung, H. H., Lin, R. J., Yen, L. C., Tseng, Y. L., et al. (2019). Naturally occurring mutations in PB1 affect influenza A virus replication fidelity, virulence, and adaptability. *J. Biomed. Sci.* 26:55. doi: 10.1186/s12929-019-0547-4

Liu, J., Lynch, P. A., Chien, C. Y., Montelione, G. T., Krug, R. M., and Berman, H. M. (1997). Crystal structure of the unique RNA-binding domain of the influenza virus NS1 protein. *Nat. Struct. Biol.* 4, 896–899. doi: 10.1038/nsb1197-896

Long, J. S., Giotis, E. S., Moncorge, O., Frise, R., Mistry, B., James, J., et al. (2016). Species difference in ANP32A underlies influenza A virus polymerase host restriction. *Nature* 529, 101–104. doi: 10.1038/nature16474

Long, J. S., Mistry, B., Haslam, S. M., and Barclay, W. S. (2019). Host and viral determinants of influenza A virus species specificity. *Nat. Rev. Microbiol.* 17, 67–81. doi: 10.1038/s41579-018-0115-z

Matrosovich, M. N., Gambaryan, A. S., Teneberg, S., Piskarev, V. E., Yamnikova, S. S., Lvov, D. K., et al. (1997). Avian influenza A viruses differ from human viruses by recognition of sialyloligosaccharides and gangliosides and by a higher conservation of the HA receptor-binding site. *Virology* 233, 224–234. doi: 10.1006/viro.1997.8580

Matrosovich, M., Tuzikov, A., Bovin, N., Gambaryan, A., Klimov, A., Castrucci, M. R., et al. (2000). Early alterations of the receptor-binding properties of H1, H2, and H3 avian influenza virus hemagglutinins after their introduction into mammals. *J. Virol.* 74, 8502–8512. doi: 10.1128/JVI.74.18.8502-8512.2000

Mazur, I., Anhlan, D., Mitzner, D., Wixler, L., Schubert, U., and Ludwig, S. (2008). The proapoptotic influenza A virus protein PB1-F2 regulates viral polymerase activity by interaction with the PB1 protein. *Cell. Microbiol.* 10, 1140–1152. doi: 10.1111/j.1462-5822.2008.01116.x

Mehle, A., and Doudna, J. A. (2009). Adaptive strategies of the influenza virus polymerase for replication in humans. *Proc. Natl. Acad. Sci. U. S. A.* 106, 21312–21316. doi: 10.1073/pnas.0911915106

Min, J. Y., and Krug, R. M. (2006). The primary function of RNA binding by the influenza A virus NS1 protein in infected cells: inhibiting the 2′-5′ oligo (A) synthetase/RNase L pathway. *Proc. Natl. Acad. Sci. U. S. A.* 103, 7100–7105. doi: 10.1073/pnas.0602184103

Nilsson, B. E., Te Velthuis, A. J. W., and Fodor, E. (2017). Role of the PB2 627 domain in influenza A virus polymerase function. *J. Virol.* 91:e02467-16. doi: 10.1128/JVI.02467-16

Pumroy, R. A., Ke, S., Hart, D. J., Zachariae, U., and Cingolani, G. (2015). Molecular determinants for nuclear import of influenza A PB2 by importin α isoforms 3 and 7. *Structure* 23, 374–384. doi: 10.1016/j.str.2014.11.015

Rosário-Ferreira, N., Preto, A. J., Melo, R., Moreira, I. S., and Brito, R. M. M. (2020). The central role of non-structural protein 1 (NS1) in influenza biology and infection. *Int. J. Mol. Sci.* 21:1511. doi: 10.3390/ijms21041511

Schrauwen, E. J., de Graaf, M., Herfst, S., Rimmelzwaan, G. F., Osterhaus, A. D., and Fouchier, R. A. (2014). Determinants of virulence of influenza A virus. *Eur. J. Clin. Microbiol. Infect. Dis.* 33, 479–490. doi: 10.1007/s10096-013-1984-8

Sediri, H., Schwalm, F., Gabriel, G., and Klenk, H. D. (2015). Adaptive mutation PB2 D701N promotes nuclear import of influenza vRNPs in mammalian cells. *Eur. J. Cell Biol.* 94, 368–374. doi: 10.1016/j.ejcb.2015.05.012

Selman, M., Dankar, S. K., Forbes, N. E., Jia, J. J., and Brown, E. G. (2012). Adaptive mutation in influenza A virus non-structural gene is linked to host switching and induces a novel protein by alternative splicing. *Emerg. Microbes Infect.* 1:e42. doi: 10.1038/emi.2012.38

Seo, S. H., Hoffmann, E., and Webster, R. G. (2002). Lethal H5N1 influenza viruses escape host anti-viral cytokine responses. *Nat. Med.* 8, 950–954. doi: 10.1038/nm757

Shi, Y., Wu, Y., Zhang, W., Qi, J. X., and Gao, G. F. (2014). Enabling the 'host jump': structural determinants of receptor-binding specificity in influenza A viruses. *Nat. Rev. Microbiol.* 12, 822–831. doi: 10.1038/nrmicro3362

Shi, Y., Zhang, W., Wang, F., Qi, J., Wu, Y., Song, H., et al. (2013). Structures and receptor binding of hemagglutinins from human-infecting H7N9 influenza viruses. *Science* 342, 243–247. doi: 10.1126/science.1242917

Shinya, K., Ebina, M., Yamada, S., Ono, M., Kasai, N., and Kawaoka, Y. (2006). Avian flu: influenza virus receptors in the human airway. *Nature* 440, 435–436. doi: 10.1038/440435a

Soh, Y. S., Moncla, L. H., Eguia, R., Bedford, T., and Bloom, J. D. (2019). Comprehensive mapping of adaptation of the avian influenza polymerase protein PB2 to humans. *eLife* 8:e45079. doi: 10.7554/eLife.45079

Song, M. S., Pascua, P. N., Lee, J. H., Baek, Y. H., Lee, O. J., Kim, C. J., et al. (2009). The polymerase acidic protein gene of influenza A virus contributes to pathogenicity in a mouse model. *J. Virol.* 83, 12325–12335. doi: 10.1128/JVI.01373-09

Song, W., Wang, P., Mok, B. W., Lau, S. Y., Huang, X., Wu, W. L., et al. (2014). The K526R substitution in viral protein PB2 enhances the effects of E627K on influenza virus replication. *Nat. Commun.* 5:5509. doi: 10.1038/ncomms6509

Steel, J., Lowen, A. C., Mubareka, S., and Palese, P. (2009). Transmission of influenza virus in a mammalian host is increased by PB2 amino acids 627K or 627E/701N. *PLoS Pathog.* 5:e1000252. doi: 10.1371/journal.ppat.1000252

Stegeman, A., Bouma, A., Elbers, A. R., de Jong, M. C., Nodelijk, G., de Klerk, F., et al. (2004). Avian influenza A virus (H7N7) epidemic in The Netherlands in 2003: course of the epidemic and effectiveness of control measures. *J. Infect. Dis.* 190, 2088–2095. doi: 10.1086/425583

Stevens, J., Blixt, O., Chen, L. M., Donis, R. O., Paulson, J. C., and Wilson, I. A. (2008). Recent avian H5N1 viruses exhibit increased propensity for acquiring human receptor specificity. *J. Mol. Biol.* 381, 1382–1394. doi: 10.1016/j.jmb.2008.04.016

Stewart, M. (2007). Molecular mechanism of the nuclear protein import cycle. *Nat. Rev. Mol. Cell Biol.* 8, 195–208. doi: 10.1038/nrm2114

Subbarao, E. K., London, W., and Murphy, B. R. (1993). A single amino acid in the PB2 gene of influenza A virus is a determinant of host range. *J. Virol.* 67, 1761–1764. doi: 10.1128/jvi.67.4.1761-1764.1993

Sun, Y., Hu, Z., Zhang, X., Chen, M., Wang, Z., Xu, G., et al. (2020). An R195K mutation in the PA-X protein increases the virulence and transmission of influenza A virus in mammalian hosts. *J. Virol.* 94:e01817-19. doi: 10.1128/JVI.01817-19

Sun, Y., Qin, K., Wang, J., Pu, J., Tang, Q., Hu, Y., et al. (2011). High genetic compatibility and increased pathogenicity of reassortants derived from avian

H9N2 and pandemic H1N1/2009 influenza viruses. *Proc. Natl. Acad. Sci. U. S. A.* 108, 4164–4169. doi: 10.1073/pnas.1019109108

Tarendeau, F., Boudet, J., Guilligay, D., Mas, P. J., Bougault, C. M., Boulo, S., et al. (2007). Structure and nuclear import function of the C-terminal domain of influenza virus polymerase PB2 subunit. *Nat. Struct. Mol. Biol.* 14, 229–233. doi: 10.1038/nsmb1212

Thiele, S., Stanelle-Bertram, S., Beck, S., Kouassi, N. M., Zickler, M., Müller, M., et al. (2020). Cellular importin-α3 expression dynamics in the lung regulate antiviral response pathways against influenza A virus infection. *Cell Rep.* 31:107549. doi: 10.1016/j.celrep.2020.107549

Tong, S., Zhu, X., Li, Y., Shi, M., Zhang, J., Bourgeois, M., et al. (2013). New world bats harbor diverse influenza A viruses. *PLoS Pathog.* 9:e1003657. doi: 10.1371/journal.ppat.1003657

Vasin, A. V., Temkina, O. A., Egorov, V. V., Klotchenko, S. A., Plotnikova, M. A., and Kiselev, O. I. (2014). Molecular mechanisms enhancing the proteome of influenza A viruses: an overview of recently discovered proteins. *Virus Res.* 185, 53–63. doi: 10.1016/j.virusres.2014.03.015

Wang, C., Lee, H. H., Yang, Z. F., Mok, C. K., and Zhang, Z. (2016). PB2-Q591K mutation determines the pathogenicity of avian H9N2 influenza viruses for mammalian species. *PLoS One* 11:e0162163. doi: 10.1371/journal.pone.0169417

Wong, S. S., and Yuen, K. Y. (2006). Avian influenza virus infections in humans. *Chest* 129, 156–168. doi: 10.1378/chest.129.1.156

Xu, R., de Vries, R. P., Zhu, X. Y., Nycholat, C. M., McBride, R., Yu, W. L., et al. (2013). Preferential recognition of avian-like receptors in human influenza A H7N9 viruses. *Science* 342, 1230–1235. doi: 10.1126/science.1243761

Xu, G., Zhang, X., Liu, Q., Bing, G., Hu, Z., Sun, H., et al. (2017). PA-X protein contributes to virulence of triple-reassortant H1N2 influenza virus by suppressing early immune responses in swine. *Virology* 508, 45–53. doi: 10.1016/j.virol.2017.05.002

Xu, G., Zhang, X., Sun, Y., Liu, Q., Sun, H., Xiong, X., et al. (2016). Truncation of C-terminal 20 amino acids in PA-X contributes to adaptation of swine influenza virus in pigs. *Sci. Rep.* 6:21845. doi: 10.1038/srep21845

Xue, R., Tian, Y., Hou, T., Bao, D., Chen, H., Teng, Q., et al. (2018). H9N2 influenza virus isolated from minks has enhanced virulence in mice. *Transbound. Emerg. Dis.* 65, 904–910. doi: 10.1111/tbed.12805

Yang, Z. F., Mok, C. K., Peiris, J. S., and Zhong, N. S. (2015). Human infection with a novel avian influenza A (H5N6) virus. *N. Engl. J. Med.* 373, 487–489. doi: 10.1056/NEJMc1502983

Yin, C., Khan, J. A., Swapna, G. V., Ertekin, A., Krug, R. M., Tong, L., et al. (2007). Conserved surface features form the double-stranded RNA binding site of non-structural protein 1 (NS1) from influenza A and B viruses. *J. Biol. Chem.* 282, 20584–20592. doi: 10.1074/jbc.M611619200

Yuan, P. W., Bartlam, M., Lou, Z. Y., Chen, S. D., Zhou, J., He, X. J., et al. (2009). Crystal structure of an avian influenza polymerase PA(N) reveals an endonuclease active site. *Nature* 458, 909–912. doi: 10.1038/nature07720

Zhang, H., Li, H., Wang, W., Wang, Y., Han, G. Z., Chen, H., et al. (2020a). A unique feature of swine ANP32A provides susceptibility to avian influenza virus infection in pigs. *PLoS Pathog.* 16:e1008330. doi: 10.1371/journal.ppat.1008330

Zhang, Y., Zhang, Q., Kong, H., Jiang, Y., Gao, Y., Deng, G., et al. (2013). H5N1 hybrid viruses bearing 2009/H1N1 virus genes transmit in Guinea pigs by respiratory droplet. *Science* 340, 1459–1463. doi: 10.1126/science.1229455

Zhang, H., Zhang, Z., Wang, Y., Wang, M., Wang, X., Zhang, X., et al. (2019). Fundamental contribution and host range determination of ANP32A and ANP32B in influenza A virus polymerase activity. *J. Virol.* 93:e00174-19. doi: 10.1128/JVI.00174-19

Zhang, Z., Zhang, H., Xu, L., Guo, X., Wang, W., Ji, Y., et al. (2020b). Selective usage of ANP32 proteins by influenza B virus polymerase: implications in determination of host range. *PLoS Pathog.* 16:e1008989. doi: 10.1371/journal.ppat.1008989

Zielecki, F., Semmler, I., Kalthoff, D., Voss, D., Mauel, S., Gruber, A. D., et al. (2010). Virulence determinants of avian H5N1 influenza A virus in mammalian and avian hosts: role of the C-terminal ESEV motif in the viral NS1 protein. *J. Virol.* 84, 10708–10718. doi: 10.1128/JVI.00610-10

**Conflict of Interest:** The authors declare that the research was conducted in the absence of any commercial or financial relationships that could be construed as a potential conflict of interest.

**Publisher's Note:** All claims expressed in this article are solely those of the authors and do not necessarily represent those of their affiliated organizations, or those of the publisher, the editors and the reviewers. Any product that may be evaluated in this article, or claim that may be made by its manufacturer, is not guaranteed or endorsed by the publisher.

*Copyright © 2021 Zhang, Liu, Bai, Zhao, Li, Xu and Zhang. This is an open-access article distributed under the terms of the Creative Commons Attribution License (CC BY). The use, distribution or reproduction in other forums is permitted, provided the original author(s) and the copyright owner(s) are credited and that the original publication in this journal is cited, in accordance with accepted academic practice. No use, distribution or reproduction is permitted which does not comply with these terms.*

frontiers in Microbiology

ORIGINAL RESEARCH
published: 11 November 2021
doi: 10.3389/fmicb.2021.783040

# DNA Engineering and Hepatitis B Virus Replication

*Chun-yang Gan[1], Jing Cui[1], Wen-lu Zhang[1], Yu-wei Wang[2], Ai-long Huang[1]* and Jie-li Hu[1]**

[1] *Key Laboratory of Molecular Biology on Infectious Diseases, Ministry of Education, Chongqing Medical University, Chongqing, China,* [2] *Department of Laboratory Medicine, Chongqing Hospital of Traditional Chinese Medicine, Chongqing, China*

Recombinant DNA technology is a vital method in human hepatitis B virus (HBV), producing reporter viruses or vectors for gene transferring. Researchers have engineered several genes into the HBV genome for different purposes; however, a systematic analysis of recombinant strategy is lacking. Here, using a 500-bp deletion strategy, we scanned the HBV genome and identified two regions, region I (from nt 2,118 to 2,814) and region II (from nt 99 to 1,198), suitable for engineering. Ten exogenous genes, including puromycin N-acetyl transferase gene (*Pac*), blasticidin S deaminase gene (*BSD*), Neomycin-resistance gene (*Neo*), Gaussia luciferase (*Gluc*), NanoLuc (*Nluc*), *copGFP*, *mCherry*, *UnaG*, *eGFP*, and *tTA1*, were inserted into these two regions and fused into the open reading frames of hepatitis B core protein (HBC) and hepatitis B surface protein (HBS) via T2A peptide. Recombination of 9 of the 10 genes at region 99–1198 and 5 of the 10 genes at region 2118–2814 supported the formation of relaxed circular (RC) DNA. HBV DNA and HBV RNA assays implied that exogenous genes potentially abrogate RC DNA by inducing the formation of adverse secondary structures. This hypothesis was supported because sequence optimization of the UnaG gene based on HBC sequence rescued RC DNA formation. Findings from this study provide an informative basis and a valuable method for further constructing and optimizing recombinant HBV and imply that DNA sequence might be intrinsically a potential source of selective pressure in the evolution of HBV.

**Keywords: hepatitis B virus, recombination, replication, RNA splicing, DNA sequence optimization**

OPEN ACCESS

***Edited by:***
*Chunfu Zheng,*
*University of Calgary, Canada*

***Reviewed by:***
*Jiacheng Lin,*
*Fujian Medical University, China*
*Limin Chen,*
*Chinese Academy of Medical Sciences and Peking Union Medical College, China*

****Correspondence:***
*Ai-long Huang*
*ahuang1964@163.com*
*Jie-li Hu*
*102564@cqmu.edu.cn*

***Specialty section:***
*This article was submitted to Virology, a section of the journal Frontiers in Microbiology*

***Received:*** *25 September 2021*
***Accepted:*** *13 October 2021*
***Published:*** *11 November 2021*

***Citation:***
*Gan C-y, Cui J, Zhang W-l, Wang Y-w, Huang A-l and Hu J-l (2021) DNA Engineering and Hepatitis B Virus Replication. Front. Microbiol. 12:783040. doi: 10.3389/fmicb.2021.783040*

## INTRODUCTION

Infection with human hepatitis B virus (HBV) remains a public health problem around the world. More than 250 million people across the globe are estimated to be chronically infected with HBV (WHO, 2017; Polaris Observatory Collaborators, 2018; Schmit et al., 2020). Evidence shows that chronic HBV infection is a high-risk factor for the development of hepatocirrhosis and hepatocellular carcinoma.

HBV is a prototypical member of the Hepadnaviridae family, characterized by a relatively compact relaxed circular (RC) DNA genome and a special genomic replication mechanism via

reverse transcription of a redundant RNA intermediate (Summers and Mason, 1982). The RC DNA genome of HBV is repaired after infection, converted into covalently closed circular DNA (cccDNA) in the nucleus of hepatocyte, and transcribed to pregenomic mRNA (pgRNA), precore mRNA, preS1 mRNA, S mRNA, and X mRNA. PgRNA functions as a bicistronic mRNA directing the synthesis of hepatitis B core protein (HBC) and polymerase (Pol) and is the template for reverse transcription. HBV replication begins with the encapsidation of pgRNA, whereby Pol binds to the stem-loop structure, epsilon (ε), at the 5′ end of pgRNA, triggering the assembly of HBC and packaging of the ribonucleoprotein complex into an icosahedral nucleocapsid (Bartenschlager et al., 1990; Bartenschlager and Schaller, 1992; Pollack and Ganem, 1993; Shin et al., 2002). The host chaperone proteins mediate encapsidation, and the nucleocapsid provides a microenvironment for reverse transcription (Shin et al., 2002). Briefly, the minus-strand primer, estimated at 3 or 4 nucleotides (nt) long, is synthesized in a protein primed process with the bulge of epsilon as a template. The minus-strand primer links to the tyrosine residue at the 63rd amino acid of Pol (Pol 63Y) via a covalent bond (**Figure 1A**; Nassal and Rieger, 1996; Lanford et al., 1997) and translocates to the complementary region, DR1, at the 3′ end of pgRNA (**Figure 1B**; Rieger and Nassal, 1996), where the synthesis of minus-strand DNA resumes. Subsequently, pgRNA is reverse transcribed into minus-strand and simultaneously degraded by the RNase H domain of Pol, leaving the 11–16 oligonucleotides at 5′-terminal of pgRNA undigested (**Figure 1C**; Summers and Mason, 1982). These oligonucleotides function as primers for plus-strand synthesis. A fraction of plus-strand primers retained *in situ* extends to the 5′ end of the minus-strand DNA and forms duplex linear DNAs (DL DNAs) (**Figure 1D**). Most plus-strand primers translocate to DR2 and extend to the 5′ end of the minus-strand, copying a 10-nt redundant sequence named 5′r (**Figure 1E**; Haines and Loeb, 2007). Subsequently, the nascent 3′ end of plus-strand pairs with the 3′-proximal redundant region (3′r) of minus-strand, continuing elongation of plus-strand to form RC DNA (**Figures 1F,G**).

*cis*-Elements, including epsilon (ε), direct repeat sequences (DR1 and DR2), terminal redundancy (5′ r and 3′r), h5E, hM, h3E, and Φ, are essential in every step of HBV replication (**Figure 1H**). Epsilon (ε) is the encapsidation signal and the template for protein priming (Pollack and Ganem, 1993); DR2 (1588–1598) and DR1 (1822–1832) are essential for primer translocations; 5′ r and 3′r, located at 1816–1824 of the minus-strand, are essential for circularization; h5E (1511–1568), hM (2820–2868), and h3E (1833–1844) play a critical role in plus-strand primer translocation (Liu et al., 2004; Lewellyn and Loeb, 2007); Φ (1767–1793) is essential for minus-strand primer translocation (Tang and McLachlan, 2002; Abraham and Loeb, 2006).

Recombinant DNA technology is a powerful tool for research in the field of HBV. The last 30 years have seen attempts by researchers to reconstruct HBV for different purposes. Insertion of differently sized exogenous genes, including HIV Tat, ZeoR, fluorescent proteins (GFP, EGFP, hrGFP, RFP, DsRed), Renilla luciferase (Rluc), Guassia luciferase (Gluc), NanoLuc luciferase (Nluc), and blasticidin S deaminase (BSD), into HBV genome has allowed for the construction of associated recombinant viruses (Kimura et al., 1994; Chaisomchit et al., 1997; Protzer et al., 1999; Yoo et al., 2002; Untergasser and Protzer, 2004; Liu et al., 2009, 2013; Hong et al., 2013; Nishitsuji et al., 2015, 2018). However, some of these efforts were unsuccessful (Bai et al., 2016), and no systematic analysis of HBV's engineering strategy has been done.

In this view, we herein systematically analyzed the strategy of HBV engineering. First, a scan on the whole genome with a 500-bp deletion from position 1919 to position 1198 revealed two regions, nt 2,118–2,814 and nt 99–1,198, well-tolerable to deletion. Second, 10 exogenous genes, including puromycin N-acetyl transferase gene (*Pac*) (Lacalle et al., 1989), blasticidin S deaminase gene (*BSD*) (Kimura et al., 1994), Neomycin resistance gene (*Neo*) (Southern and Berg, 1982), Guassia luciferase (*Gluc*) (Verhaegent and Christopoulos, 2002), NanoLuc luciferase (*NLuc*) (England et al., 2016), *copGFP* (Shagin et al., 2004), *mCherry* (Shaner et al., 2004), *UnaG* (Kumagai et al., 2013), *eGFP* (Cormack et al., 1996), and *tTA1* (Baron et al., 1997), were inserted at position 2120 and position 155, respectively, via Thosea asigna virus 2A peptide (T2A) (Wang et al., 2015). Insertion of a majority of these genes supported RC DNA formation. We also systematically analyzed HBV RNA transcribed from different constructs to provide insight into how engineering affects the formation of RC DNA. The results showed that pgRNA splicing is common among those deletion variants and recombinants. However, this can hardly explain the failure of RC DNA formation of some recombinants. We thus provided a hypothesis that secondary structures induced by some of these exogenous genes might be potentially associated with abolishing RC DNA. This hypothesis was supported because sequence optimization of the UnaG gene based on HBC sequence, which is predicted to relieve the non-optimized UnaG on the structure of minus-strand DNA, rescued RC DNA formation.

# MATERIALS AND METHODS

## Constructs

HBV DNA was derived from HBV subtype ayw (GenBank accession number v01460) and numbered according to the only *Eco*RI site of the genome. The "C" of the *Eco*RI site (GAATTC) was designated as position 1. Pch9/3091, constructed by Nassal et al., transcribes pgRNA under the control of the cytomegalovirus immediate-early promoter (pCMV) (Nassal, 1992). All HBV variants were constructed based on Pch9/3091 using Golden Gate Assembly with a few modifications (Engler et al., 2009). Briefly, the Golden Gate Assembly system comprised the following components: 1 × NEB buffer 3.1 (NEB), 5 mM DTT, 1 mM ATP, 0.5 units/μL of *Bsm*BI, or *Bsm*BI-v2 (NEB), 150 units/μL of T7 DNA Ligase (NEB), and 3–5 ng/μL of each DNA fragment. The reaction was performed with 60 cycles of 37°C for 5 min and 16°C for 5 min, followed by a 5-min incubation at 60°C. Plasmid pch9-G2016T contains a G2016T mutation, which terminates HBC translation at the 40th amino acid (HBC 40E). Pch9-Δε has a deletion between nt 1,858 and 1,863 and two

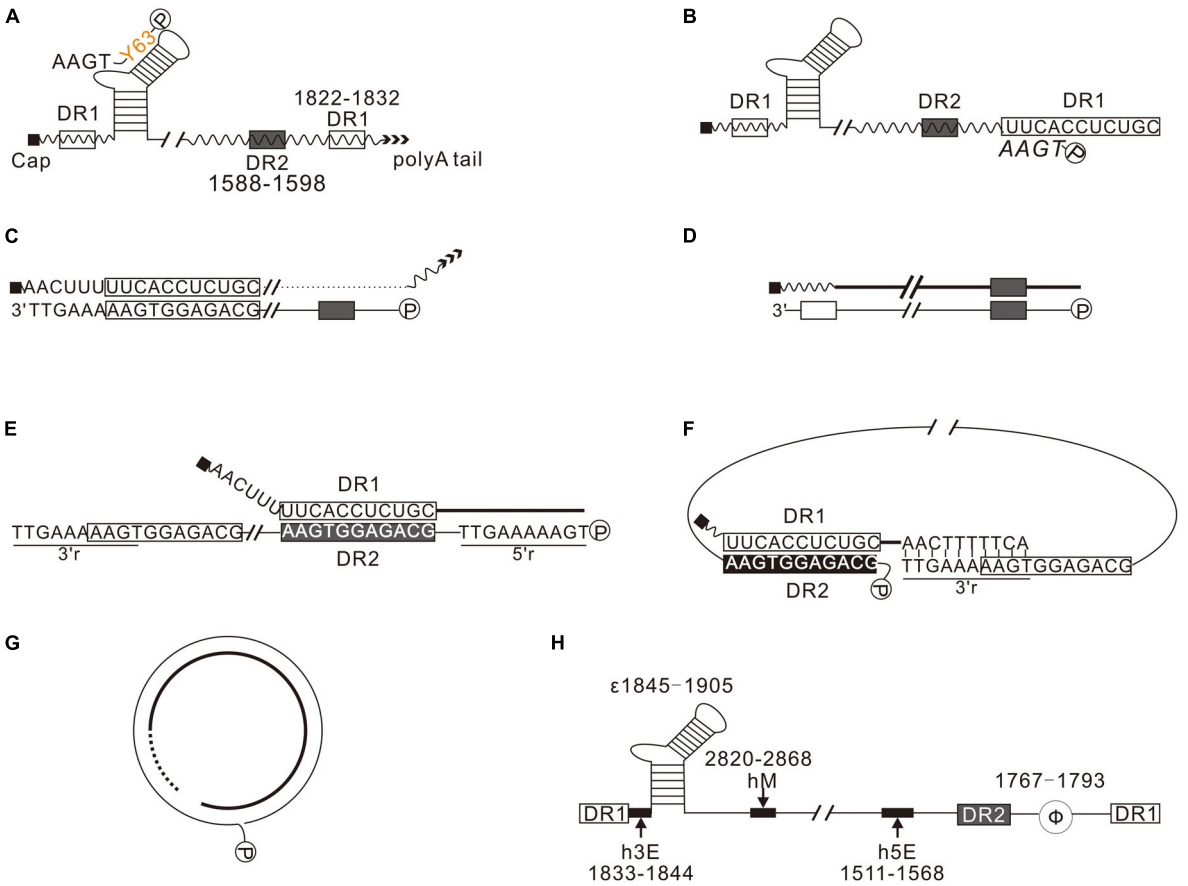


**FIGURE 1 |** Synthesis of HBV DNA. **(A)** Pol (P) binds to 5′-proximal epsilon, forming a ribonucleoprotein complex with pgRNA, encapsidated into nucleocapsid formed by HBC. In the nucleocapsid, using the bulge of epsilon as a template, Pol synthesizes the minus-strand primer. **(B)** The nascent minus-strand primer translocates to 3′-proximal DR1 of pgRNA via base pairing. **(C)** pgRNA was degraded by the RNase H domain of Pol during reverse transcription, leaving a 11–16 nt long oligonucleotides, which serves as the primer for plus-strand synthesis. **(D)** A few plus-strand primers are retained *in situ* and extend to the 5′-end of minus-strand DNA, forming duplex linear DNAs (DL DNAs). **(E)** Most plus-strand primers translocate to DR2. Here, the synthesis of plus-strand resumes and extends to the 5′-end of minus-strand. **(F)** The nascent plus-strand pairs with the 3′r of minus-strand to complete circularization. **(G)** The plus-strand is synthesized further to form RC DNA. **(H)** *cis*-Elements play a crucial role in HBV replication. h5E (1511–1568), hM (2820–2868), and h3E (1833–1844) are crucial for plus-strand primer translocation. Φ (1767–1793) is important for minus-strand primer translocation.

substitutions (G1877T and T1878A). PgRNA transcribed from this construct would not be encapsidated but be translated to both HBC and Pol.

## Cell Culture and Transfection

HepG2 was cultured in DMEM/F12 supplemented with 10% fetal bovine serum and 10 μg/mL ciprofloxacin, and the culture medium was refreshed every 3 days (25–50% confluence) or every day (100% confluence). HepG2 cells were seeded into 12-well plates 20 h before transfection. Transfection was performed with Lipo8000 (Beyotime, China), following the manufacturer's instructions.

## Core DNA Extraction and Southern Blotting

Plasmids were cotransfected, respectively, with pCH9-Δε, which expresses HBC and Pol *in trans*. Cells were harvested on day 5 posttransfection and washed once with phosphate-buffered saline (PBS). Core DNA was extracted as described previously (Abraham and Loeb, 2006). Briefly, cells in each well were lysed with 200 μL lysis buffer [50 mM Tris-HCl (pH 8.0), 1 mM EDTA, 0.2% NP40] and incubated at 37°C for 10 min. Lysed cells were centrifuged at 12,000 g for 5 min to remove the nuclei. The supernatant was supplemented with 5 mM $CaCl_2$ and 5,000 units/mL micrococcal nuclease (NEB) and incubated at 37°C for 1.5 h. Subsequently, the micrococcal nuclease was inactivated with 10 mM EDTA. The reaction systems were supplemented with 0.5% sodium dodecyl sulfate and 0.5 mg/mL pronase and incubated at 37°C for 1.5 h. Core DNA was extracted with phenol–chloroform precipitated with ethanol and dissolved into 20 μL 1 × *Eco*RI buffer. Core DNA (10 μL) was digested by *Eco*RI for 1 h and resolved with 10 μL undigested samples on 1.5% agarose gel at 4 V/cm for 1.5 h. Following electrophoresis, the gel was denatured by soaking into two volumes of 0.4 M NaOH for

15 min with gentle shaking and transferred onto a positively charged nylon membrane with 60 mL 0.2 M NaOH overnight. The membranes were neutralized by soaking into 100 mL neutralization buffer (2 × saline- sodium phosphate- EDTA (SSPE), 200 mM Tris-HCl, pH 7.5) for 15 min with shaking and then UV-crosslinked at 1,500 × 100 μJ/cm$^2$. Hybridization was performed via the DIG Easy Hyb (Roche, Germany) according to the manufacturer's protocol using a digoxin-labelled probe (nt 1,199–1,814) at 30 ng/mL and 46°C. Detection of digoxin was performed following the manufacturer's protocol (Roche, Germany), with some modifications according to a previously described method (Engler-Blum et al., 1993; McCabe et al., 1997). The NaCl concentration and the pH of the washing buffer were increased to 3 M and 8.0–9.0, respectively. In addition, 10 × blocking reagent was centrifuged at 13,000 g for 5 min, and the supernatant was added into washing buffer to reduce background.

## Total RNA Extraction and Northern Blotting

Total RNA was extracted using the TIANGEN RNA extraction reagent (TIANGEN, China) with some modifications. Briefly, cells were harvested on day 2 posttransfection and washed once with PBS. Next, cells were lysed in 500 μL/well Buffer RZ, and the lysate was supplemented with 1/5 volume of chloroform. The mixture was centrifuged at 13,000 g at 4°C for 10 min, and the supernatant was transferred into a new tube. Following phenol–chloroform extraction, total RNA was precipitated using ethanol and dissolved into 20 μL 1 × RNA loading buffer (60–73% formamide deioned, 1 × DNA loading buffer, and 10 μg/mL EtBr). RNA samples can be stored at -20°C for at least 1 month without degradation.

RNA samples were electrophoresed in TAE agarose gels according to a previously described method (Masek et al., 2005). The samples were first denatured at 65°C for 5 min and chilled on ice for 5 min before loading. Then, the samples were resolved on 1.2% 1 × TAE agarose gels at 4 V/cm and visualized under UV to examine the rRNAs. The gels were soaked into 120 mL 20 × saline sodium citrate (SSC) for at least 20 min. After that, RNA on the gels was transferred onto positively charged nylon membranes using 20 × SSC overnight. The membranes were UV-crosslinked directly on the next day. Hybridization and detection were performed by a similar method as the Southern blotting procedure except that the hybridization temperature was 60°C, and the low stringent washing temperature was 70°C.

## Reverse Transcription and Polymerase Chain Reaction

Reverse transcription was performed with TIANGEN FastKing RT Kit (TIANGEN, China) according to the manufacturer's instructions with modifications. The incubation time was extended to 10 min in the DNA removal step and 30 min in the reverse transcription step. The reverse transcription primers included R HBV 1370, R HBV 1547, R HBV 1680, and R HBV 1800. Polymerase chain reaction (PCR) was performed with PrimeStar Max Premix (Takara, Japan) according to the manufacturer's protocol.

## Sequence Optimization and DNA Structure Prediction

Sequence optimization of the exogenous genes was performed with DNAMAN version 8, using HBC sequence as the reference. Briefly, the DNA sequence of HBC was translated into protein, and the two most frequently used codons were used as the reference to optimize the sequence of selected genes. For DNA structure prediction, the secondary structure of DNA is predicted via DNAMAN version 8 as follows: load the sequences into the channel; select "sequence" > "secondary structure" > "current sequence."

## Luciferase Assay

Plasmids were transfected into HepG2 as described above. For the luciferase assay in medium, 10 μL culture medium was collected on day 2 posttransfection and added to 30 μL 1 × Gluc assay buffer [0.5 × coelenterazine (Promega) in PBS supplemented with 5 mM NaCl] (Tannous, 2009), or 30 μL 1 × Nluc assay buffer [0.25 × furimazine (Promega) in PBS supplemented with 0.1% bovine serum albumin] (Boute et al., 2016). Chemiluminescence was detected by using a GloMax® 20/20 Luminometer (Promega). For the luciferase assay in cell lysate, cells in each well were lysed with 200 μL lysis buffer (50 mM Tris-HCl (pH 8.0), 1 mM EDTA, 0.2% NP40) and incubated at 37°C for 10 min. Lysed cells were centrifuged at 12,000 g for 5 min to remove the debris. The supernatants (10 μL) were analyzed as described above.

## Blot Quantification and Statistical Analysis

According to the instructions on the website[1], Southern and Northern blots were quantified by ImageJ 1.53e. The relative intensity of RC DNA and that of pgRNA were analyzed via a two-tailed Student *t*-test. $p < 0.05$ was considered statistically significant. QQ PLOT was used to determine the frequency distribution of the data analyzed using GraphPad Prism 8 (GraphPad Software, United States).

# RESULTS

## Scanning of Hepatitis B Virus Genome for Desirable Recombination Sites

A series of deletion variants of the HBV genome was constructed based on Pch9/3091 to identify desirable regions for exogenous gene recombination (**Figure 2A**). Each variant had an approximated 500-bp deletion, spanning from 1919 to 1198 and skipping the *cis*-elements (**Table 1**). Pch9-Δε, in which the epsilon sequence was mutated to abort pgRNA encapsidation (**Figure 2C**), transcomplemented HBC and/or Pol for the damaged open reading frame (ORF) of HBC and/or Pol of some variants. The translation of HBC from Pch9-G2016T was

[1]https://imagej.nih.gov/ij/docs/menus/analyze.html#gels

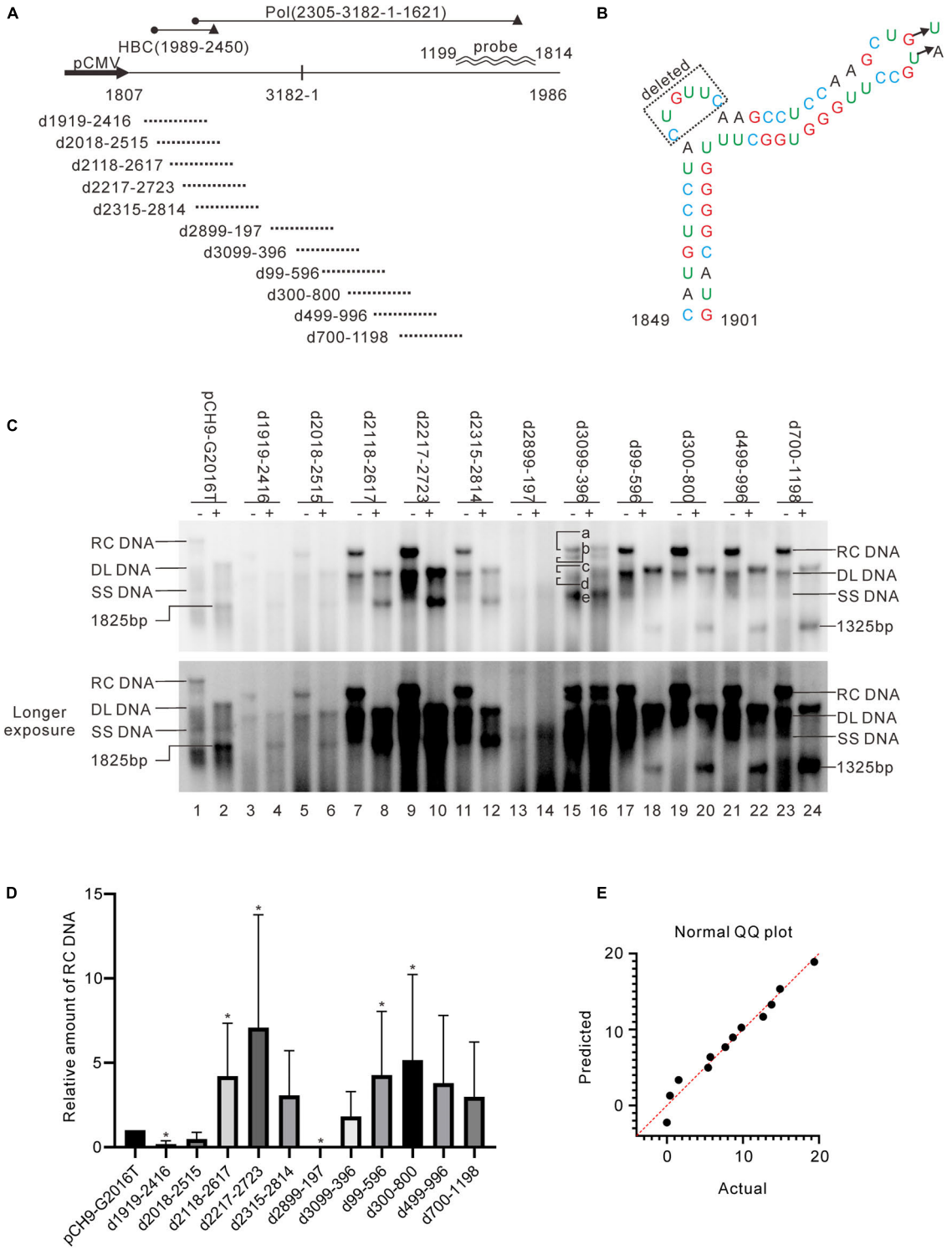


**FIGURE 2 |** Identification of two regions suitable for engineering. **(A)** Sequences that were deleted in different constructs. Deletion variants were named according to the sequences deleted. The black cycle and black triangle represent the start codon and the stop codon, respectively. The hybridization probe is shown (1199–1814). **(B)** The mutations of pCH9-Δε. Sequence from 1858 to 1863 was deleted, and two additional mutations, G1877T and T1878A, were introduced. **(C)** Representative Southern blotting of the deletion variants. The plus sign (+) denotes *Eco*RI digestion. RC, DL, SS DNA, and *Eco*RI digested fragments are indicated, respectively. **(D)** The relative intensity of RC DNA of deletion variants. The intensity of RC DNA of each sample was divided into the sum of RC DNA of all samples in the same membrane, respectively, to calculate the relative amount of RC DNA. $N = 5$. Asterisks (*) denote the difference between a deletion variant and pCH9-G2016T is statistically significant ($p < 0.05$). **(E)** Normal QQ plot of the relative amount of the RC DNAs.

**TABLE 1 |** Influence of deletion on the formation of RC DNA.

| Deletion region | Length of deletion (bp) | pgRNA splicing | Formation of RC DNA |
|---|---|---|---|
| 1919–2416 | 498 | Nearly 100% | +, 7.0% |
| 2018–2515 | 498 | Nearly 100% | +, 26.9% |
| 2118–2617 | 499 | 58% | +, 240.6% |
| 2217–2723 | 507 | 50% | +, 338.9% |
| 2315–2814 | 500 | 47% | +, 151.9% |
| 2899–197 | 481 | Nearly 100% | — |
| 3099–396 | 480 | 74% | +, 94.8% |
| 99–596 | 498 | 40% | +, 221.4% |
| 300–800 | 501 | 17% | +, 260.2% |
| 499–996 | 498 | 35% | +, 171.3% |
| 700–1198 | 499 | 45% | +, 134.4% |
| 2121–2819 | 699 | ND | +, 45.9% |

*ND, not determined.*

terminated at the 40th amino acid by introducing a stop codon. Cotransfection of Pch9-G2016T and Pch9-Δε served as the positive control. All the variants were cotransfected with Pch9-Δε into HepG2. Core DNA was extracted on day 5 posttransfection and subjected to Southern blotting.

Pch9-G2016T formed three major bands, including RC, DL, and single-stranded (SS) DNA (**Figure 2C**, lane 1). The smear below SS DNA was either uncompleted intermediates of SS DNA or spliced products reverse transcribed from spliced pgRNA (Abraham et al., 2008). As expected, the RC DNA was linearized via *Eco*RI digestion, migrating to the same position as the undigested DL DNA. DL DNA was cut into two smaller linear fragments by *Eco*RI, with expected lengths of 1,365 bp (1814–3178) and 1,825 bp (1–1825), respectively, as 1814 is the transcription starting site of pgRNA from Pch9/3091 (Liu et al., 2004). Notably, the 1,365-bp fragment was not detected because the probe hybridizes with region 1199–1814. The 1,825-bp fragment migrated faster than SS DNA (**Figure 2C**, lane 2).

RC and DL DNA were detectable for all the variants except D2899-197 and D3099-396, which electrophoresed faster than their counterparts from Pch9-G2016T ascribed to a 500-bp deletion (**Figure 2C**). SS DNAs of these variants were not detected. Following *Eco*RI digestion, the RC DNAs of these variants migrated to the same position as the undigested DL DNA, providing evidence of their circular configuration. DL DNAs of D1919-2416, D2018-2515, D2118-2617, D2217-2723, and D2315-2814 were cut into two fragments, including one with an expected length of 1,825 bp and the other of 865 bp (nt 1,814–3,178 with a 500-bp deletion, undetectable). DL DNAs of D99-596, D300-800, D499-996, and D700-1198 were cut into two fragments, including one with a length of 1,325 bp (nt 1–1,825 with a 500-bp deletion) and the other with 1,365 bp (1814–3178, undetectable) (**Figure 2C**).

D3099-396 produced five bands (**Figure 2C**, lanes 15 and 16, bands a–e), all of which were resistant to *Eco*RI digestion because the *Eco*RI site was deleted (**Figure 2A**). Plasmid D3099-397*Eco*RI, in which an *Eco*RI site (GAATTC) was introduced between 3098 and 398, was constructed to verify whether D3099-396 formed RC DNA. Like D3099-396, five bands, indicated as a, b, c, d, and e, were detected in D3099-397*Eco*RI (**Figure 3A**, lane 3). Band "a" moved to the same position as band "c" after *Eco*RI digestion, while bands "b," "d," and "e" remained unchanged (**Figure 3A**, lanes 3 and 4). These results demonstrated that band "a" is RC DNA, band "c" is DL DNA, band "e" is SS DNA, and bands "b" and "d" are likely to be spliced products. Thus, D2899-197 is the only variant that does not support the formation of RC DNA.

## Deletions Associated With Hepatitis B Virus RNA Splicing

It is intriguing that D2899-197 formed only weak SS DNA (**Figure 2C**, lanes 13 and 14) without impairing known *cis*-elements. One hypothesis is that the pgRNA expressed from this construct was spliced (Abraham et al., 2008). To address this question, we performed a systematic analysis of the influence of the deletions on HBV RNA splicing. Total RNA samples were assayed by Northern blotting and reverse transcribed into cDNA using primers R HBV 1370, R HBV 1547, R HBV 1680, and R HBV 1800, respectively, to identify whether the pgRNAs were spliced (**Figure 4A**). The cDNA was further amplified via PCR using primers F HBV 1821 or F HBV 1851 plus R HBV 1370, or R HBV 1547, or R HBV 1680, or R HBV 1800, respectively, and PCR products were gel-purified and sequenced.

Pch9-G2016T, as the positive control, is expected to transcribe pgRNA, preS1 mRNA, S mRNA, and X mRNA, regulated by cytomegalovirus immediate-early promoter (pCMV), S1 promoter, S2 promoter, and X promoter, respectively (**Figure 5A**; Panjaworayan et al., 2007). Notably, these RNAs presented as three major bands in Northern blotting (**Figure 5B**). Band "a" was pgRNA, and band "e" was X mRNA. Band "d," possibly comprised two close bands, was suggested to be preS1 and S mRNAs. Deletion variants D2118-2617, D2217-2723, D2315-2814, D3099-396, D99-596, D300-800, D499-996, and D700-1198 produced shorter pgRNAs than that of the control, owing to a 500-bp deletion for each (band "b," **Figure 5B**, lanes 7–12 and 15–24). However, variants D2899-197 showed no bands at position "b," but rather a smear at position "c." HBV RNA of this variant was reverse transcribed, and the corresponding DNA fragments were amplified and sequenced as described previously. Indeed, the sequencing results demonstrated that the pgRNA of D2899-197 was spliced with two patterns; one is 2065-487 (i.e., the sequence between nt 2065 and 487 is missing), and the other is spliced twice, from nt 2,445 to 280 and from nt 456 to 1,306 (**Figures 4E,F**).

Moreover, splicing was detected in other deletion variants. D1919-2416 showed one splicing pattern, from nt 2,445 to 487 (**Figure 4B**). D2018-2515 had two splicing patterns: one is from nt 2,983 to 487, and the other is spliced twice, from nt 2,983 to 280, and from nt 456 to 1,383 (**Figures 4C,D**). However, the splicing rates of pgRNAs of these two variants were not 100% because the two variants did support the formation of intact RC DNA (**Figure 2C**, lanes 3–6), which must be derived from complete pgRNA. Notably, the pgRNA of D3099-396 was spliced to a less extent but via a more complex mechanism. At least five splicing patterns, from nt 2,445 to 487, from nt 2,065 to 487, from nt 2,445 to 1,383, from nt 2,065 to 1,306, and from

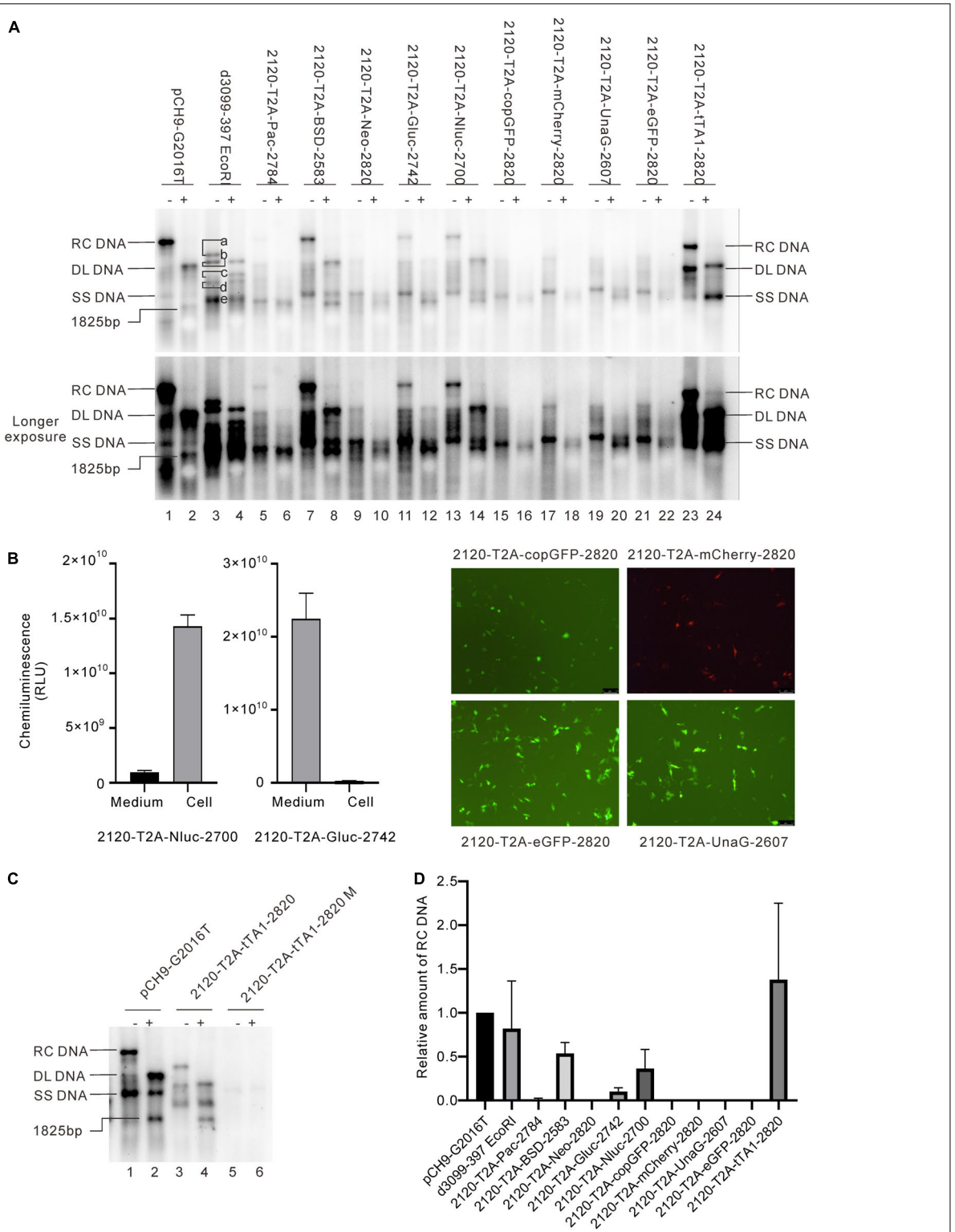


**FIGURE 3 |** Influence of the recombination at 2120 on HBV DNA replication. **(A)** Representative Southern blotting results of the recombinants. The plus sign (+) denotes *Eco*RI digestion. RC, DL, SS DNA, and *Eco*RI digested fragments are shown. **(B)** Expression of the exogenous genes from the recombinants. Luciferase activity (Gluc and Nluc) or fluorescence (copGFP, eGFP, mCherry, and UnaG) was detected. **(C)** Representative Southern blotting of 2120-T2A-tTA1-2820 M. Notably, M denotes a deletion from nt 2064 to 2072 and a mutation in tetR (A426G). **(D)** The relative intensity of RC DNA of the recombinants. The intensity of each RC DNA was divided into the sum of RC DNA of all samples in the same membrane, respectively, to calculate the relative intensity of RC DNA of each sample. $N = 4$.

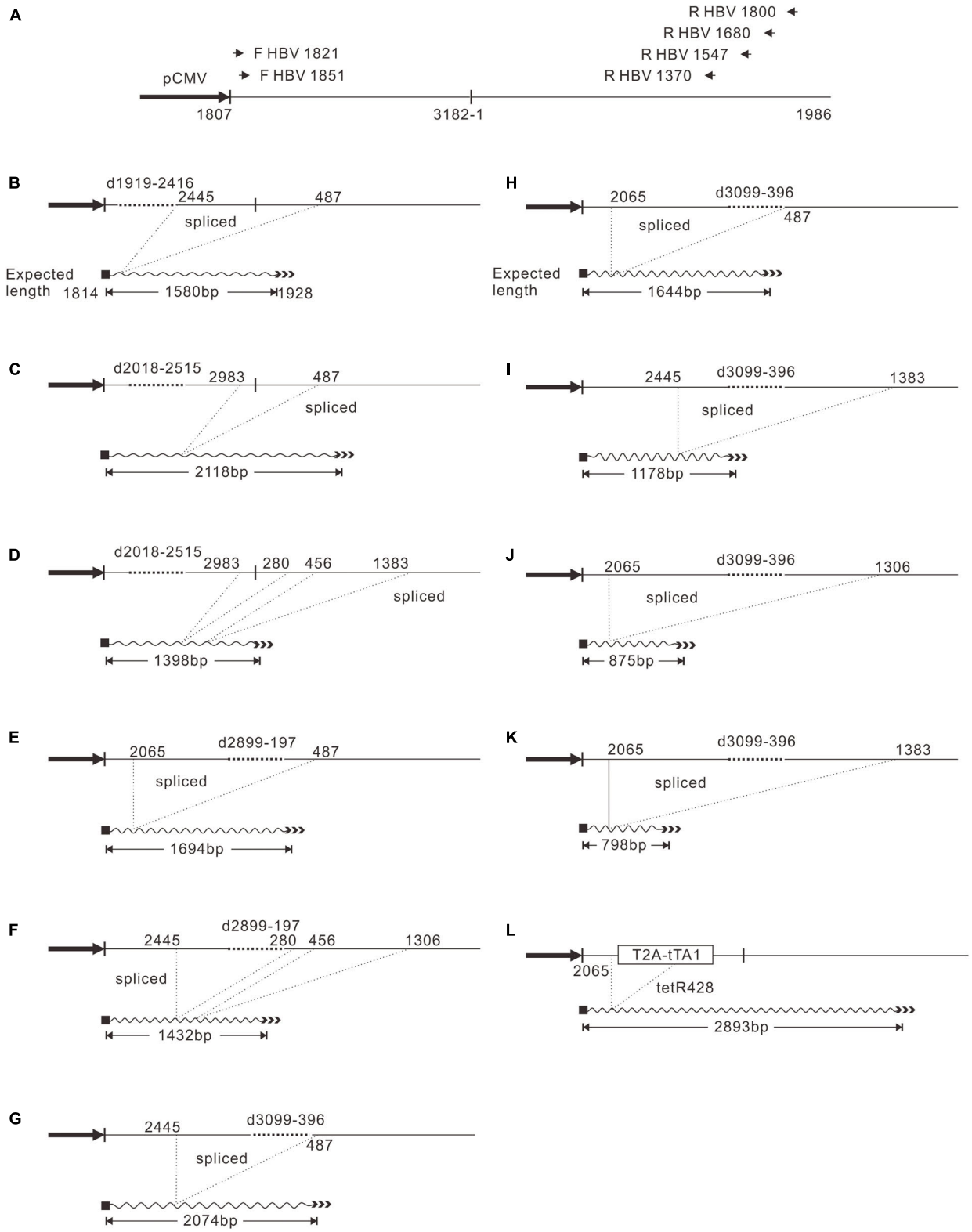


**FIGURE 4 |** PgRNA splicing pattern of D1919-2416, D2018-2515, D2899-197, D3099-396, and 2120-T2A-tTA1-2820. **(A)** Primers used for reverse transcription and PCR. Each primer was named by the position of 5′ end, respectively. PgRNA was reverse transcribed with reverse primers and subjected to PCR amplification using each forward primer combined with each reverse primer. The shortest bands were gel-purified and sequenced. **(B)** PgRNA splicing of D1919-2416. **(C,D)** PgRNA splicing of D2018-2515. **(E,F)** PgRNA splicing of D2899-197. **(G–K)** PgRNA splicing of D3099-396. **(L)** PgRNA splicing of 2120-T2A-tTA1-2820.

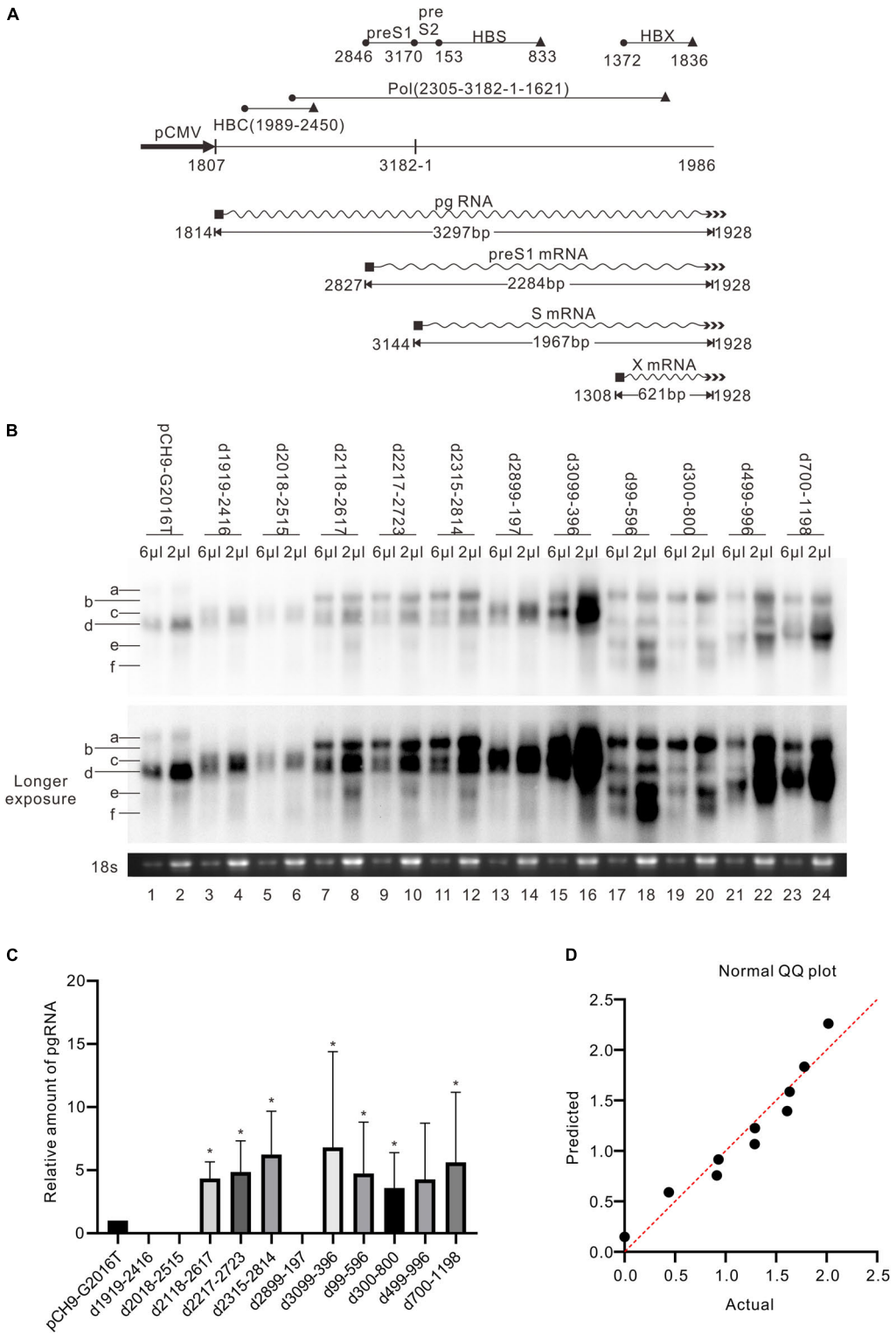


**FIGURE 5 |** RNA assay of the deletion variants. **(A)** The sequence of HBV transcripts. The wave lines represent RNA; the black rectangles represent 5′ cap; the multiple arrowheads represent the poly-A tail. The black cycles and black triangles represent the start codon and the stop codon, respectively. The length of each transcript is an estimation without a poly-A tail. **(B)** Representative Northern blotting results of the deletion variants. **(C)** The relative intensity of pgRNA of the deletion variants. The intensity of each pgRNA/18s rRNA was divided into the sum of pgRNA/18s rRNA of all samples in the same membrane, respectively, to calculate the relative intensity of pgRNA of each sample. $N = 4$. Asterisks (*) denote the difference between deletion variants and pCH9-G2016T is significant ($p < 0.05$). **(D)** Normal QQ plot of the relative amount of the pgRNAs.

**TABLE 2 |** Influence of exogenous gene engineering on the formation of RC DNA.

| Location | Exogenous gene | Length of gene (bp) | HBV region replaced | Expected change of pgRNA length (bp) | pgRNA splicing | Formation of RC DNA |
|---|---|---|---|---|---|---|
| Site 2120 (HBC and Pol region) | T2A-Pac | 663 | 2121–2783 | 0 | ++ | Weak, 1.3% |
| | T2A-BSD | 462 | 2121–2582 | 0 | + | +, 52.9% |
| | T2A-Neo | 858 | 2121–2819 | +159 | ++ | – |
| | T2A-Gluc | 621 | 2121–2741 | 0 | + | +, 10.2% |
| | T2A-Nluc | 579 | 2121–2699 | 0 | ++ | +, 33.8% |
| | T2A-copGFP | 723 | 2121–2819 | +24 | ++ | – |
| | T2A-mCherry | 774 | 2121–2819 | +75 | ++ | – |
| | T2A-UnaG | 486 | 2121–2606 | 0 | ++ | – |
| | T2A-eGFP | 784 | 2121–2819 | +83 | + | – |
| | T2A-tTA1 | 840 | 2121–2819 | +140 | ++++ | Spliced, 117.3% |
| Site 155 (HBS region) | T2A-Pac | 663 | 156–518 | 0 | + | Weak, 5.6% |
| | T2A-BSD | 462 | 156–617 | 0 | + | +, 64.4% |
| | T2A-Neo | 858 | 156–1013 | 0 | + | +, 33.8% |
| | T2A-Gluc | 621 | 156–776 | 0 | + | +, 76.2% |
| | T2A-Nluc | 579 | 156–734 | 0 | + | +, 79.7% |
| | T2A-copGFP | 723 | 156–878 | 0 | + | +, 18.9% |
| | T2A-mCherry | 774 | 156–929 | 0 | + | – |
| | T2A-UnaG | 486 | 156–641 | 0 | ++ | +, 33.9% |
| | T2A-eGFP | 784 | 156–938 | 0 | + | +, 25.0% |
| | T2A-tTA1 | 840 | 156–994 | 0 | + | +, 25.5% |

*++++, > 75%; +++, 50% – 75%; ++, 25% – 50%; +, 10% – 25%.*

nt 2,065 to 1,383, respectively, were revealed (**Figures 4G–K**). Some of these splicings are potential sources of the additional bands of D3099-396 detected via Southern blotting ("b" and "d" in **Figure 2C**, lane 15). Analysis of the splicing of pgRNA of D99-596, D300-800, D499-996, and D700-1198 is challenging because of the complicated bands.

In addition, the amount of pgRNA of deletion variants (except D1919-2416, D2018-2515, D2899-197, and D499-996) was significantly higher than Pch9-G2016T, respectively ($p < 0.05$) (**Figure 5C**). This observation provides evidence of these constructs' relatively higher amount of RC DNA (**Figures 2D**, **5C**).

## Deletions of 2,118–2,814 and 99–1,198 Produces More Relaxed Circular DNA Than Other Variants

Regions with the least impact on the formation of RC DNA were identified by comparing the relative amount of RC DNAs among these variants. Southern blotting was repeated five times, followed by analyzing the relative intensity of RC DNAs with ImageJ. Results demonstrated that the relative intensities of RC DNA of D2118-2617, D2217-2723, D99-596, and D300-800 were significantly higher than Pch9-G2016T (**Figure 2D**), whereas that of D1919-2416 and D2899-197 were significantly lower than Pch9-G2016T. Also, D2315-2814, D3099-396, D499-996, and D700-1198 produced a similar amount of RC DNA as Pch9-G2016T (**Figure 2D**). These results demonstrate that two regions are suitable for recombination, including 2,118–2,814 and 99–1,198.

## Influence of Recombination of Exogenous Genes at 2120 on Relaxed Circular DNA Formation

Given the data above, two positions, 2120 and 155, located in the ORF of HBC and HBS, respectively, were selected to insert foreign genes. First, three selection genes (Pac, BSD, and Neo), two luciferase genes (Gluc and Nluc), four fluorescent genes (copGFP, mCherry, UnaG, and eGFP), and one transactivating gene (tTA1) were inserted right after the valine residue at the 74th amino acid of HBC (HBC 74V, site 2120) (**Table 2**). Each gene was fused via a T2A peptide at the N-terminal to separate its expression from the HBV genome. The focus was on the formation of RC DNA as it is the precursor of functional cccDNA.

Results revealed that 2120-T2A-Pac-2784, 2120-T2A-BSD-2583, 2120-T2A-Gluc-2742, and 2120-T2A-Nluc-2700 formed RC DNA, migrating similarly to that of Pch9-G2016T (**Figure 3A**). RC DNAs were verified through *Eco*RI digestion, whereby the RC DNAs were linearized to the same position as the undigested DL DNAs (**Figure 3A**). The expression of exogenous genes was confirmed by the detection of chemiluminescence or fluorescence (**Figure 3B**). As for the amount of RC DNA, less of RC DNA of these constructs was reported than Pch9-G2016T. Insertion of BSD and Nluc maintained more RC DNAs than the insertion of Pac and Gluc (**Figure 3D**). 2120-T2A-tTA1-2820 formed an RC DNA band migrating faster than Pch9-G2016T, 2120-T2A-BSD-2583, 2120-T2A-Gluc-2742, and 2120-T2A-Nluc-2700 (**Figure 3A**, lanes 1, 2, 7, 8, 11–14, 23, and 24). It was speculated that the shorter product was potentially synthesized from spliced pgRNA.

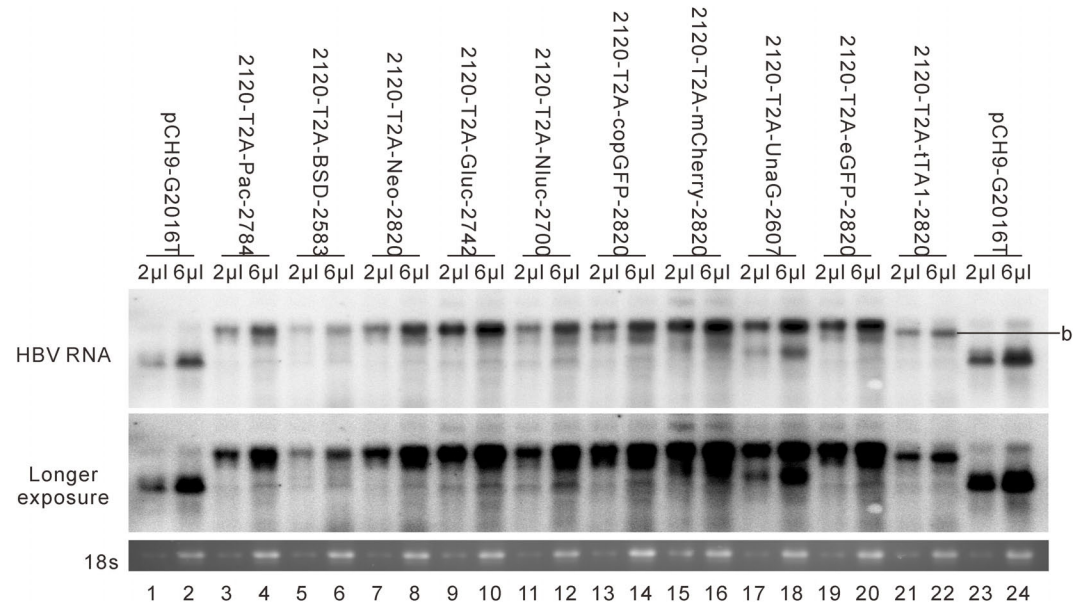


**FIGURE 6 |** RNA assay for the 2120 recombinants. Representative Northern blotting is shown.

A part of constructs formed only DL and SS DNA, including 2120-T2A-Neo-2820, 2120-T2A-copGFP-2820, 2120-T2A-mCherry-2820, 2120-T2A-UnaG-2607, and 2120-T2A-eGFP-2820 (**Figure 3A**). *Eco*RI digestion yielded 1,825-bp fragments, confirming the identity of DL DNAs. Notably, SS DNAs of 2120-T2A-copGFP-2820 and 2120-T2A-eGFP-2820 electrophoresed slightly faster than others (**Figure 3A**, lanes 15 and 21).

## Splicing of pgRNAs of the 2120 Recombinants

Different genes exert different effects on the formation of RC DNA. Therefore, to pursue the underlying reasons, we analyzed the RNAs from a part of the recombinants. All the recombinants tested, to some extent, showed pgRNA splicing (the bands right under pgRNA bands), although intact pgRNA was observed in all samples (**Figure 6** and **Table 2**). The spliced pgRNAs possibly explain the small RC DNAs of 2120-T2A-BSD-2583, 2120-T2A-Gluc-2742, and 2120-T2A-Nluc-2700 (**Figure 3A**). However, for 2120-T2A-tTA1-2820, the pgRNA was spliced approximately 80% (band "b" **Figure 6**, lanes 21 and 22). Sequencing results demonstrated that this RNA was spliced between HBV nt 2,065 and tetR nt 428 (sequence from HBV nt 2,065 to nt 428 of tetR was missing) (**Figure 4L**), providing potential evidence on why the RC DNA of 2120-T2A-tTA1-2820 electrophoresed faster than the RC DNA of Pch9-G2016T (**Figure 3A**, lanes 1 and 23). The splicing sites of 2120-T2A-tTA1-2820 were removed by deleting nt 2,064–2,072 and mutating A426 of tetR to G426. However, this manipulation did not rescue RC DNA formation (**Figure 3C**, lanes 5 and 6).

## Influence of Recombination of Exogenous Genes at 155 on Relaxed Circular DNA Formation

These 10 exogenous genes were also inserted right after the first methionine residue of HBS (site 155). Except for 155-T2A-mCherry-930, all of these insertions supported RC formation (**Figure 7A**). All the RC DNAs electrophoresed at the same position as that of Pch9-G2016T. Following *Eco*RI digestion, the RC DNAs shifted to undigested DL DNAs, and DL DNAs moved to 1,825-bp fragments. The expression of exogenous genes was confirmed by the detection of chemiluminescence or fluorescence (**Figure 7B**). Regarding the amount of RC DNA, constructs with BSD, Gluc, and Nluc were higher than those with Neo, copGFP, UnaG, eGFP, tTA1, and Pac (**Figure 7C**). 155-T2A-mCherry-930 only formed DL and SS DNA (**Figure 7A**, lanes 17 and 18). However, RNA assay demonstrated that 155-T2A-mCherry-930 produced normal pgRNA (**Figure 8**), supporting that RC DNA formation failure is attributed to obstacles in DNA synthesis steps. Shortened DL bands from 155-T2A-Pac-819, 155-T2A-BSD-618, 155-T2A-Neo-1014, 155-T2A-Gluc-777, 155-T2A-copGFP-879, 155-T2A-UnaG-642, and 155-T2A-eGFP-939 could be reverse transcribed from spliced RNA (compare **Figure 7A** with **Figure 8**).

## Sequence Optimization Improves Relaxed Circular DNA Formation for Some Recombinant Constructs

It was reported that insertion of UnaG aborted RC DNA formation at nt 2,120 but supported that at nt 155. Furthermore, recombination of UnaG maintained DL and SS DNA formation, suggesting the blockade of the translocation or circularization of

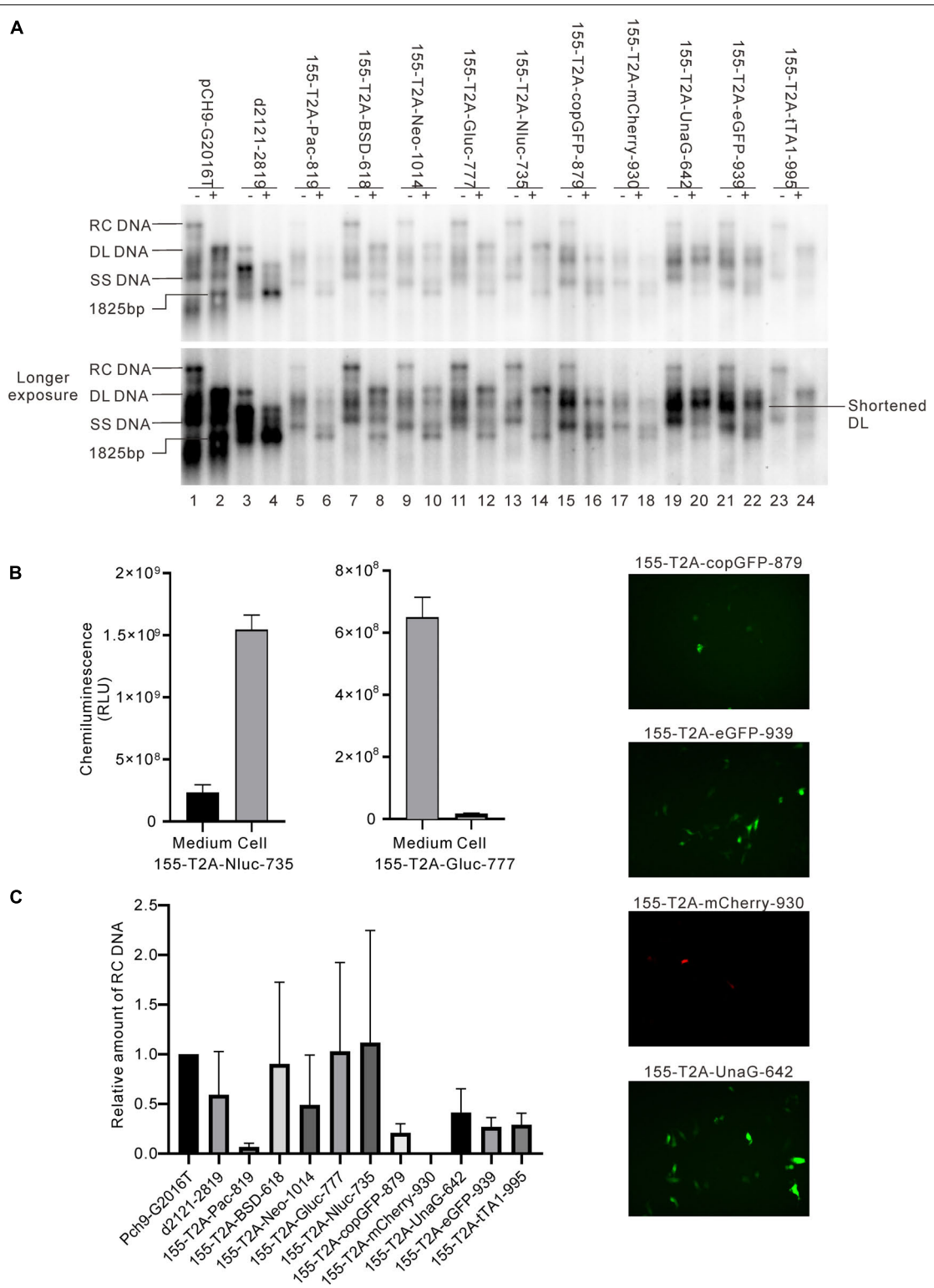


**FIGURE 7 |** Influence of the recombination at 155 on RC DNA formation. **(A)** A representative Southern blotting is shown. The plus sign (+) denotes *Eco*RI digestion. RC, DL, SS DNA, and *Eco*RI digested fragments are indicated. **(B)** Expression of the exogenous genes from the recombinants. Luciferase activity (Gluc and Nluc) or fluorescence (copGFP, eGFP, mCherry, and UnaG) was detected. **(C)** The relative intensity of RC DNA of the recombinants. The intensity of RC DNA of each sample was divided into the sum of RC DNA of all samples in the same membrane, respectively, to calculate the relative intensity of RC DNA of each sample. *N* = 4.

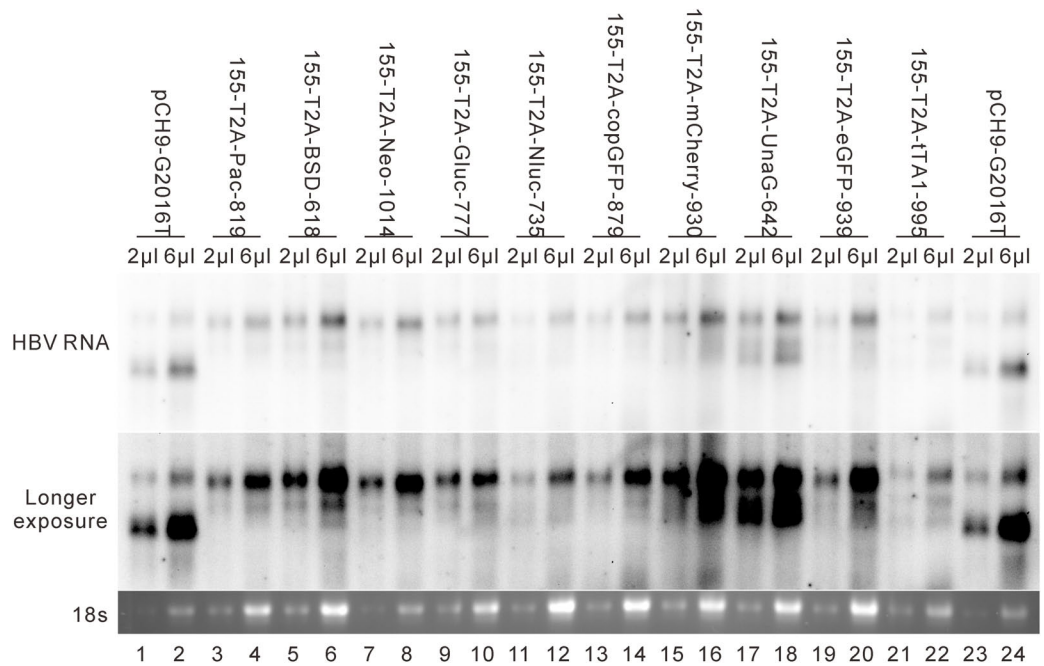


**FIGURE 8 |** RNA assay for the 155 recombinants. Representative Northern blotting is shown.

the plus-strand primer, which is dependent on where the foreign genes were inserted. These results implied that the insertion of UnaG at nt 2,120 might form the undesirable secondary or higher-order structure of minus-strand DNA, which possibly affects either the translocation of the plus-strand primer or the circularization step. Guided by this hypothesis, we optimized the sequence of genes inserted according to the DNA sequence of HBC, expecting that a DNA sequence resembling HBC would reduce the influence on replication. Five genes (*UnaG*, *Pac*, *Gluc*, *Nluc*, and *eGFP*) were optimized (**Table 3**) and inserted into the same positions as the unoptimized genes, respectively. Of note, the construct with optimized UnaG (UnaGco) formed RC DNA in a similar amount as that of the positive control (Pch9-G2016T). This band migrated to the same position as the RC DNA of Pch9-G2016T (**Figure 9A**, lanes 17 and 18). *Eco*RI digestion generated a fragment that electrophoresed faster than undigested DL DNA but slower than SS DNA of 2120-T2A-UnaGco-2607 (**Figure 9A**, lanes 17 and 18). These findings affirmed RC DNA identity because there is an *Eco*RI recognition site in UnaGco. *Eco*RI digestion is expected to produce a detectable band of 2,145 bp (the other should be 759 bp undetectable by our probe). In contrast, 2120-T2A-UnaG-2607 formed only DL and SS DNA (**Figure 9A**, lanes 15 and 16). The weak DL DNA could be revealed solely via *Eco*RI digestion, which cut DL DNA to a detectable 1,825-bp fragment. Northern blotting assay of HBV RNA demonstrated a significantly lower relative amount of intact pgRNA of 2120-T2A-UnaGco-2607 than that of 2120-T2A-UnaG-2607, whereas a part of pgRNA of both could be spliced (**Figures 10A,B**) indicating that the improvement in RC DNA formation by sequence optimization must be explained by improvement in the steps after pgRNA production. To address this, we analyzed the secondary structure of the sequence from the minus-strand DNAs by using DNAMAN 8. Three sequences corresponding to wild type HBV (nt 2,121–2,868), chimeric UnaG-HBV, and optimized UnaG-HBV (**Figure 11**) were predicted for secondary structure. Wild-type UnaG sequence profoundly impacts the overall structure of HBV (**Figures 11A,B**). Especially, the structure of *cis*-element hM is different between these two. On the contrary, optimized UnaG does not significantly influence the structure of HBV DNA fused (**Figure 11C**), with the hM showing a similar structure as that of wild-type HBV DNA. The influence of sequence optimization of Pac (Pacco) on HBV DNA replication seemed different. The SS DNA of 2120-T2A-Pac-2784 electrophoresed faster than the SS DNA of D3099-397 *Eco*RI (**Figure 3A**, lanes 3 and 5), demonstrating that the SS DNA of 2120-T2A-Pac-2784 was at least 487 bp shorter than the SS DNA of Pch9-G2016T. Evidence suggests that the shorter SS DNA is possibly an immature product paused by assumptive secondary RNA structures formed by the Pac gene, with a high content of "G and C" (72.8%). In line with this hypothesis, optimized Pac (Pacco, 2120-T2A-Pacco-2784) promoted SS DNA maturation (**Figure 9A**, lanes 3–6). The RC DNA intensity was only slightly enhanced without significance by Pac optimization ($p > 0.05$). 2120-T2A-Glucco-2742 and 2120-T2A-Nlucco-2700 formed RC, DL, and SS DNA (**Figure 9A**, lanes 7–14). At the same time, sequence optimization of Nluc and Gluc did not augment the amount of RC DNA further. Also, the pgRNA amount of 2120-T2A-Glucco-2742 and 2120-T2A-Nlucco-2700 were lower than the unoptimized counterparts (**Figure 10**).

Sequence optimization of eGFP (2120-T2A-eGFPco-2820) allowed for RC DNA formation, but with a shortened

**TABLE 3 |** The sequence of exogenous genes before and after optimization.

| Genes | | The sequence of exogenous genes before and after optimization | | | | | |
|---|---|---|---|---|---|---|---|
| Pac | 1 | ATGACCGAGT | ACAAGCCCAC | GGTGCGCCTC | GCCACCCGCG | ACGACGTCCC | CAGGGCCGTA |
| | 61 | CGCACCCTCG | CCGCCGCGTT | CGCCGACTAC | CCCGCCACGC | GCCACACCGT | CGATCCGGAC |
| | 121 | CGCCACATCG | AGCGGGTCAC | CGAGCTGCAA | GAACTCTTCC | TCACGCGCGT | CGGGCTCGAC |
| | 181 | ATCGGCAAGG | TGTGGGTCGC | GGACGACGGC | GCCGCGGTGG | CGGTCTGGAC | CACGCCGGAG |
| | 241 | AGCGTCGAAG | CGGGGGCGGT | GTTCGCCGAG | ATCGGCCCGC | GCATGGCCGA | GTTGAGCGGT |
| | 301 | TCCCGGCTGG | CCGCGCAGCA | ACAGATGGAA | GGCCTCCTGG | CGCCGCACCG | GCCCAAGGAG |
| | 361 | CCCGCGTGGT | TCCTGGCCAC | CGTCGGCGTC | TCGCCCGACC | ACCAGGGCAA | GGGTCTGGGC |
| | 421 | AGCGCCGTCG | TGCTCCCCGG | AGTGGAGGCG | GCCGAGCGCG | CCGGGGTGCC | CGCCTTCCTG |
| | 481 | GAGACCTCCG | CGCCCCACAA | CCTCCCCTTC | TACGAGCGGC | TCGGCTTCAC | CGTCACCGCC |
| | 541 | GACGTCGAGG | TGCCCGAAGG | ACCGCGCACC | TGGTGCATGA | CCCGCAAGCC | CGGTGCCTGA |
| Pacco (optimized) | 1 | ATGACTGAAT | ATAAACCTAC | CGTTAGACTA | GCTACACGAG | ATGATGTGCC | AAGGGCCGTA |
| | 61 | AGAACTCTCG | CTGCCGCTTT | TGCCGACTAC | CCTGCTACCC | GACATACAGT | CGATCCAGAC |
| | 121 | AGGCACATTG | AGAGAGTTAC | TGAATTGCAA | GAGCTATTCC | TCACCCGAGT | GGGATTGGAT |
| | 181 | ATCGGCAAGG | TATGGGTCGC | CGACGATGGA | GCTGCCGTTG | CTGTGTGGAC | AACTCCTGAA |
| | 241 | TCTGTAGAGG | CCGGCGCTGT | CTTTGCCGAA | ATTGGACCAA | GGATGGCTGA | GCTATCAGGC |
| | 301 | TCTAGACTCG | CCGCTCAGCA | ACAGATGGAA | GGATTGCTAG | CCCCTCATCG | ACCAAAAGAG |
| | 361 | CCTGCTTGGT | TCCTCGCCAC | CGTTGGCGTG | TCACCAGACC | ACCAAGGAAA | GGGCTTGGGA |
| | 421 | TCTGCTGTAG | TCCTACCTGG | CGTTGAAGCC | GCTGAGAGGG | CCGGAGTGCC | AGCTTTTCTC |
| | 481 | GAAACATCAG | CCCCTAGAAA | TTTGCCATTC | TATGAGCGAC | TAGGCTTTAC | TGTAACCGCT |
| | 541 | GATGTCGAAG | TTCCTGAGGG | ACCAAGGACA | TGGTGTATGA | CTAGAAAACC | TGGCGCCTGA |
| Gluc | 1 | ATGGGAGTCA | AAGTTCTGTT | TGCCCTGATC | TGCATCGCTG | TGGCCGAGGC | CAAGCCCACC |
| | 61 | GAGAACAACG | AAGACTTCAA | CATCGTGGCC | GTGGCCAGCA | ACTTCGCGAC | CACGGATCTC |
| | 121 | GATGCTGACC | GCGGGAAGTT | GCCCGGCAAG | AAGCTGCCGC | TGGAGGTGCT | CAAAGAGATG |
| | 181 | GAAGCCAATG | CCCGGAAAGC | TGGCTGCACC | AGGGGCTGTC | TGATCTGCCT | GTCCCACATC |
| | 241 | AAGTGCACGC | CCAAGATGAA | GAAGTTCATC | CCAGGACGCT | GCCACACCTA | CGAAGGCGAC |
| | 301 | AAAGAGTCCG | CACAGGGCGG | CATAGGCGAG | GCGATCGTCG | ACATTCCTGA | GATTCCTGGG |
| | 361 | TTCAAGGACT | TGGAGCCCAT | GGAGCAGTTC | ATCGCACAGG | TCGATCTGTG | TGTGGACTGC |
| | 421 | ACAACTGGCT | GCCTCAAAGG | GCTTGCCAAC | GTGCAGTGTT | CTGACCTGCT | CAAGAAGTGG |
| | 481 | CTGCCGCAAC | GCTGTGCGAC | CTTTGCCAGC | AAGATCCAGG | GCCAGGTGGA | CAAGATCAAG |
| | 541 | GGGGCCGGTG | GTGACTAA | | | | |
| Glucco (optimized) | 1 | ATGGGCGTGA | AAGTTCTCTT | CGCTCTCATC | TGCATCGCTG | TTGCCGAAGC | TAAGCCGACA |
| | 61 | GAGAATAATG | AAGATTTTAA | TATTGTTGCT | GTCGCCTCAA | ATTTCGCTAC | TACTGATCTA |
| | 121 | GACGCTGATA | GAGGTAAATT | GCCGGGCAAA | AAGCTTCCTC | TCGAGGTCCT | CAAAGAAATG |
| | 181 | GAGGCAAATG | CCAGGAAAGC | TGGCTGTACT | AGGGGATGTT | TGATATGTCT | ATCTCATATA |
| | 241 | AAATGCACTC | CAAAAATGAA | AAAGTTCATT | CCAGGTCGAT | GTCATACATA | TGAAGGAGAC |
| | 301 | AAAGAATCTG | CCCAAGGAGG | TATTGGAGAA | GCGATTGTGG | ACATACCAGA | AATTCCTGGA |
| | 361 | TTTAAGGATT | TGGAACCAAT | GGAACAATTT | ATTGCTCAAG | TAGATCTATG | TGTGGACTGT |
| | 421 | ACTACTGGAT | GTTTGAAGGG | CCTAGCCAAT | GTACAATGTA | GTGACCTCTT | AAAAAAATGG |
| | 481 | CTTCCTCAAA | GATGTGCTAC | TTTTGCATCA | AAAATTCAAG | GCCAAGTAGA | TAAAATTAAA |
| | 541 | GGCGCTGGCG | GTGACTAA | | | | |
| Nluc | 1 | ATGGTCTTCA | CACTCGAAGA | TTTCGTTGGG | GACTGGCGAC | AGACAGCCGG | CTACAACCTG |
| | 61 | GACCAAGTCC | TTGAACAGGG | AGGTGTGTCC | AGTTTGTTTC | AGAATCTCGG | GGTGTCCGTA |
| | 121 | ACTCCGATCC | AAAGGATTGT | CCTGAGCGGT | GAAAATGGGC | TGAAGATCGA | CATCCATGTC |
| | 181 | ATCATCCCGT | ATGAAGGTCT | GAGCGGCGAC | CAAATGGGCC | AGATCGAAAA | AATTTTTAAG |
| | 241 | GTGGTGTACC | CTGTGGATGA | TCATCACTTT | AAGGTGATCC | TGCACTATGG | CACACTGGTA |
| | 301 | ATCGACGGGG | TTACGCCGAA | CATGATCGAC | TATTTCGGAC | GGCCGTATGA | AGGCATCGCC |
| | 361 | GTGTTCGACG | GCAAAAAGAT | CACTGTAACA | GGGACCCTGT | GGAACGGCAA | CAAAATTATC |
| | 421 | GACGAGCGCC | TGATCAACCC | CGACGGCTCC | CTGCTGTTCC | GAGTAACCAT | CAACGGAGTG |
| | 481 | ACCGGCTGGC | GGCTGTGCGA | ACGCATTCTG | GCGTAA | | |
| Nlucco (optimized) | 1 | ATGGTTTTTA | CTCTCGAAGA | TTTTGTTGGT | GACTGGAGAC | AAACTGCTGG | ATATAATCTA |
| | 61 | GATCAAGTAT | TAGAACAAGG | AGGTGTATCA | TCTTTATTTC | AAAATTTAGG | AGTATCGGTA |
| | 121 | ACTCCTATTC | AAAGAATCGT | TCTTTCTGGC | GAAAATGGTT | TGAAAATCGA | CATTCATGTA |
| | 181 | ATCATTCCCT | ATGAAGGACT | CTCAGGAGAT | CAAATGGGAC | AAATTGAAAA | AATTTTTAAA |
| | 241 | GTGGTTTATC | CTGTAGATGA | TCACCATTTT | AAAGTCATCC | TACATTATGG | AACTTTAGTG |
| | 301 | ATAGATGGTG | TGACTCCTAA | TATGATCGAC | TATTTCGGAA | GACCTTATGA | AGGAATTGCT |
| | 361 | GTATTTGACG | GCAAGAAAAT | TACTGTTACT | GGTACTCTGT | GGAATGGAAA | TAAAATTATC |

*(Continued)*

**TABLE 3 |** (Continued)

| Genes | | The sequence of exogenous genes before and after optimization | | | | | |
|---|---|---|---|---|---|---|---|
| | 421 | GATGAGCGGT | TAATCAACCC | TGATGGATCA | CTACTTTTCC | GAGTTACCAT | TAATGGGGTT |
| | 481 | ACCGGTTGGA | GACTCTGTGA | ACGCATTCTA | GCGTAA | | |
| UnaG | 1 | ATGATCCTGG | AAAAATTCGT | CGGCACTTGG | AAGATCGCCG | ACAGCCACAA | CTTCGGCGAG |
| | 61 | TACCTGAAGG | CCATCGGCGC | CCCCAAGGAG | CTGTCTGACG | GCGGCGACGC | CACCACTCCC |
| | 121 | ACCCTGTATA | TCTCCCAGAA | AGACGGCGAC | AAGATGACCG | TGAAGATCGA | GAACGGCCCC |
| | 181 | CCCACTTTCC | TGGACACCCA | GGTAAAGTTC | AAGCTGGGCG | AGGAGTTCGA | CGAGTTCCCC |
| | 241 | AGCGACCGCC | GCAAGGGCGT | GAAGAGCGTC | GTGAACCTGG | TGGGGGAAAA | GCTGGTGTAT |
| | 301 | GTGCAAAAGT | GGGATGGGAA | GGAGACCACC | TACGTGCGCG | AGATCAAGGA | TGGCAAGCTG |
| | 361 | GTCGTGACCC | TCACCATGGG | CGACGTGGTG | GCCGTCCGCA | GCTACCGTCG | CGCCACCGAG |
| | 421 | TAA | | | | | |
| UnaGco (optimized) | 1 | ATGATTCTAG | AAAAATTTGT | TGGAACTTGG | AAGATCGCTG | ACTCTCATAA | TTTCGGCGAG |
| | 61 | TATCTCAAAG | CCATTGGAGC | TCCTAAGGAA | TTGTCAGATG | GCGGAGATGC | CACCACACCA |
| | 121 | ACTCTATACA | TCTCTCAAAA | AGATGGCGAC | AAGATGACCG | TGAAAATTGA | GAACGGACCT |
| | 181 | CCAACATTTC | TCGATACTCA | GGTAAAGTTC | AAATTGGGCG | AAGAGTTTGA | CGAATTCCCT |
| | 241 | TCAGATAGAC | GAAAGGGAGT | CAAATCTGTT | GTGAATCTAG | TAGGCGAGAA | GCTCGTCTAT |
| | 301 | GTTCAAAAAT | GGGACGGAAA | GGAAACCACA | TACGTGAGGG | AGATCAAAGA | TGGCAAGTTG |
| | 361 | GTAGTCACTC | TAACCATGGG | AGATGTTGTG | GCTGTAAGAT | CATATCGAAG | GGCCACAGAG |
| | 421 | TAA | | | | | |
| eGFP | 1 | ATGGTGAGCA | AGGGCGAGGA | GCTGTTCACC | GGGGTGGTGC | CCATCCTGGT | CGAGCTGGAC |
| | 61 | GGCGACGTAA | ACGGCCACAA | GTTCAGCGTG | TCCGGCGAGG | GCGAGGGCGA | TGCCACCTAC |
| | 121 | GGCAAGCTGA | CCCTGAAGTT | CATCTGCACC | ACCGGCAAGC | TGCCCGTGCC | CTGGCCCACC |
| | 181 | CTCGTGACCA | CCCTGACCTA | CGGCGTGCAG | TGCTTCAGCC | GCTACCCCGA | CCACATGAAG |
| | 241 | CAGCACGACT | TCTTCAAGTC | CGCCATGCCC | GAAGGCTACG | TCCAGGAGCG | CACCATCTTC |
| | 301 | TTCAAGGACG | ACGGCAACTA | CAAGACCCGC | GCCGAGGTGA | AGTTCGAGGG | CGACACCCTG |
| | 361 | GTGAACCGCA | TCGAGCTGAA | GGGCATCGAC | TTCAAGGAGG | ACGGCAACAT | CCTGGGGCAC |
| | 421 | AAGCTGGAGT | ACAACTACAA | CAGCCACAAC | GTCTATATCA | TGGCCGACAA | GCAGAAGAAC |
| | 481 | GGCATCAAGG | TGAACTTCAA | GATCCGCCAC | AACATCGAGG | ACGGCAGCGT | GCAGCTCGCC |
| | 541 | GACCACTACC | AGCAGAACAC | CCCCATCGGC | GACGGCCCCG | TGCTGCTGCC | CGACAACCAC |
| | 601 | TACCTGAGCA | CCCAGTCCGC | CCTGAGCAAA | GACCCCAACG | AGAAGCGCGA | TCACATGGTC |
| | 661 | CTGCTGGAGT | TCGTGACCGC | CGCCGGGATC | ACTCTCGGCA | TGGACGAGCT | GTACAAGTAG |
| EGFPco (optimized) | 1 | ATGGTTTCCA | AGGGGGAGGA | GCTATTTACA | GGTGTCGTCC | CTATTCTTGT | TGAATTGGAC |
| | 61 | GGAGATGTCA | ATGGACACAA | ATTTTCTGTC | TCCGGGGAGG | GAGAGGGAGA | CGCAACATAT |
| | 121 | GGCAAACTCA | CTCTCAAGTT | TATCTGCACC | ACTGGCAAGT | TACCTGTGCC | ATGGCCTACG |
| | 181 | CTTGTGACTA | CTCTAACATA | TGGTGTGCAA | TGTTTCTCTC | GCTATCCAGA | CCACATGAAA |
| | 241 | CAACACGATT | TTTTCAAATC | AGCTATGCCT | GAAGGGTATG | TTCAAGAGAG | GACTATCTTT |
| | 301 | TTCAAAGACG | ACGGAAATTA | TAAGACCAGA | GCAGAAGTCA | AATTCGAAGG | TGATACTCTG |
| | 361 | GTGAATCGAA | TCGAACTTAA | GGGTATTGAC | TTTAAGGAAG | ATGGTAATAT | TTTGGGCCAC |
| | 421 | AAATTAGAGT | ATAACTATAA | CTCTCATAAT | GTCTATATTA | TGGCAGACAA | ACAAAAAAAC |
| | 481 | GGGATAAAGG | TGAATTTTAA | AATTAGACAT | AACATCGAAG | ATGGGTCAGT | TCAACTCGCT |
| | 541 | GACCATTATC | AACAGAATAC | TCCTATCGGT | GATGGTCCTG | TTCTACTCCC | TGATAATCAC |
| | 601 | TATCTATCCA | CTCAATCAGC | TCTCTCAAAA | GACCCAAATG | AGAAAAGGGA | CCACATGGTG |
| | 661 | TTGCTAGAGT | TTGTTACTGC | GGCAGGAATT | ACACTAGGAA | TGGACGAGCT | ATATAAGTAG |

length. 2120-T2A-eGFPco-2820 formed a band, "f," which electrophoresed slightly faster than the RC DNA of Pch9-G2016T (**Figure 9A**, lane 21). Notably, this band disappeared after *Eco*RI digestion and was suggested to be a shortened RC DNA from a spliced RNA. However, we reported a substantial intact pgRNA in samples of 2120-T2A-eGFPco-2820 (**Figure 10A**, lane 22), demonstrating potential defects in DNA synthesis. It is possible that the band, "g," is the intact SS DNA, which is reverse transcribed from the intact pgRNA of 2120-T2A-eGFPco-2820 (**Figure 9A**, lanes 21 and 22).

## DISCUSSION

Previous studies indicate that HBV recombinant virus expressing foreign genes can be constructed successfully. However, a systematic exploration of the influence of different strategies of engineering on HBV replication is lacking. In the present study, the whole genome of HBV was scanned for regions suitable for engineering. "Suitable here" means supporting the formation of RC DNA, the precursor of functional cccDNA. This criterion allowed for the identification of two regions, 2118–2814 and 99–1198. Region 2118–2814 covers the C-terminal of

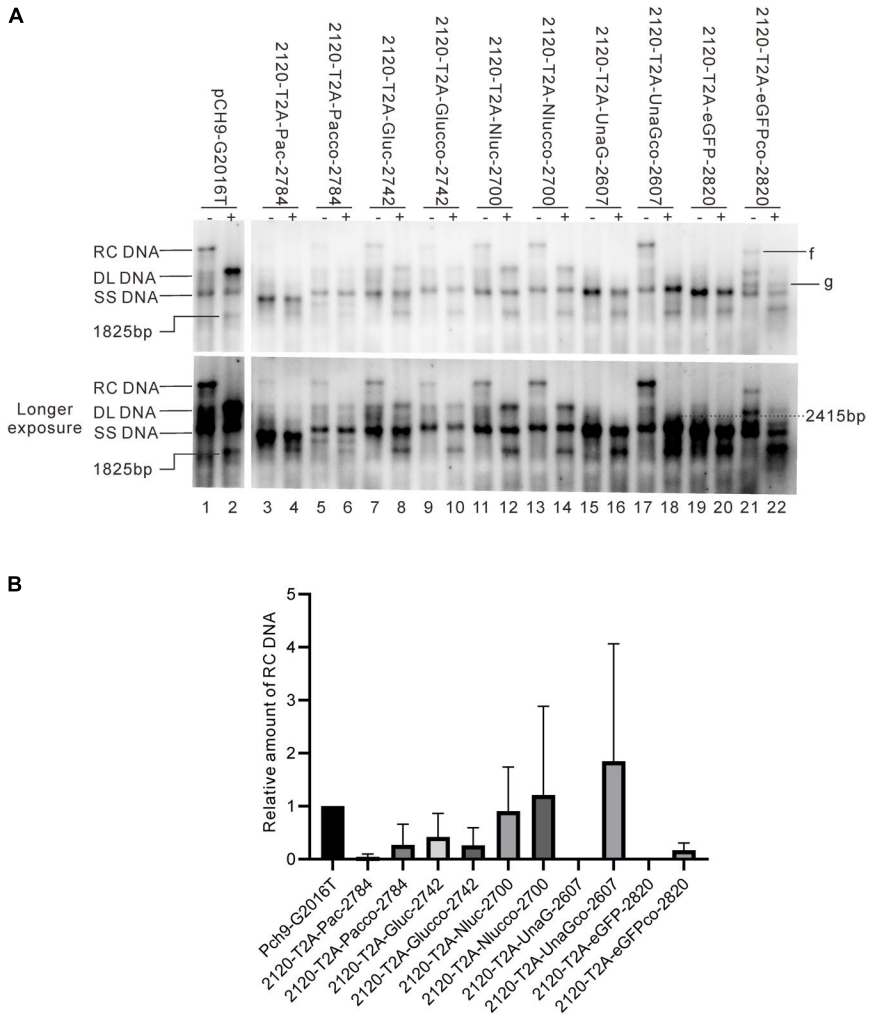


**FIGURE 9 |** Influence of sequence optimization of exogenous genes on HBV replication. **(A)** A comparison of HBV DNA from the recombinants before and after sequence optimization. The plus sign (+) denotes *Eco*RI digestion. RC, DL, SS DNA, and *Eco*RI digested fragments are indicated. **(B)** The relative intensity of RC DNA. The intensity of each RC DNA was divided into the sum of RC DNA of all samples in the same membrane to calculate the relative intensity of RC DNA of each sample. $N = 4$.

HBC and the N-terminal of TP domain of Pol, and its deletion efficiently supports RC DNA formation. Notably, this region partially overlaps the region (nt 2,124–2,712) previously utilized to recombine NanoLuc into an HBV of genotype C (accession number AB246345) (Nishitsuji et al., 2015). Region 2118–2814 can hardly extend further because the hM (2820–2868) region must be retained. Previously, researchers successfully inserted a 52-aa polypeptide into 1982–2312 (Wang et al., 2002, 2014; Deng et al., 2009). Even so, we think that extending the recombination region toward the N-terminal of HBC is undesirable. In the present analysis, deletion of 1919–2515 formed only weak RC and DL DNA, and the relatively lower level of core DNA was potentially associated with a low amount of intact pgRNA. Intriguingly, 1919–2515 deletion resulted in almost complete pgRNA splicing. A similar phenomenon was evident for D2899-197, which formed only weak SS DNA and showed a large part of pgRNA splicing. Elsewhere, a study revealed that 55% pgRNA of wild-type HBV suffered from splicing in HepG2 cells (Abraham et al., 2008). Taken together, significantly higher splicing of D1919-2515 and D2899-197 implies that the two regions are functional to protect authentic pgRNA from splicing. It is speculated that such protection is potentially associated with secondary or higher-order RNA structures that can hide the splicing sites.

Region 99-1198 covers the C-terminal of the spacer, RT, and RNaseH domains of Pol, overlapping preS2 and S ORF. In a previous study, BSD was inserted into the preS2 region, between *Xho*I (C^TCGAG, nt 125) and *Bsr*GI (T^GTACA, nt 766) (Liu et al., 2009). Moreover, Untergasser et al. inserted GFP between nt 1,446 and 2,347 (Untergasser and Protzer, 2004). This region contains h5E (nt 1511–1568), which has been reported to play a crucial role in RC DNA formation (Lewellyn and Loeb, 2007). The deletion of h5E (nt 1,511–1,568) was responsible for the poor RC DNA formation in this construction of HBV. Preserving h5E

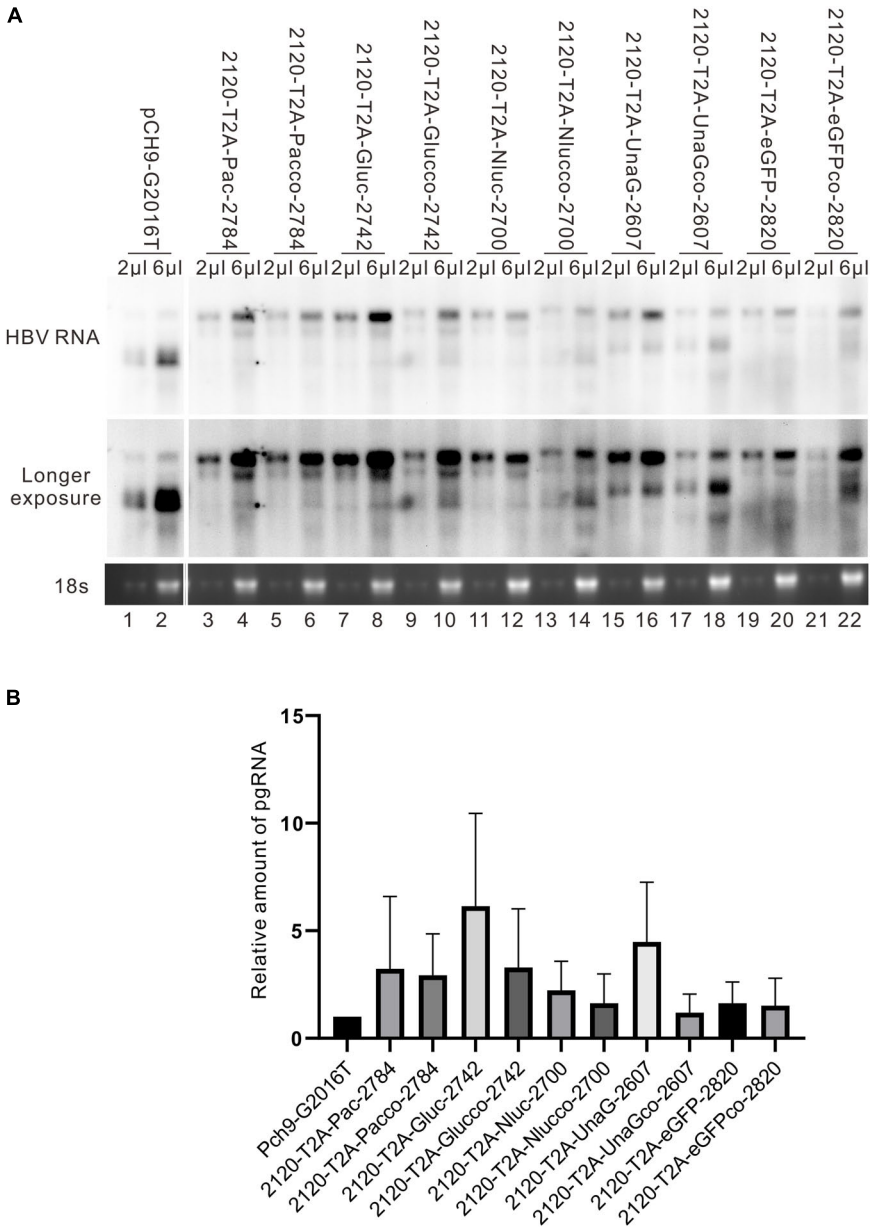


**FIGURE 10 |** HBV RNA assay of the recombinants before and after sequence optimization. **(A)** Representative Northern blotting of the recombinants before and after sequence optimization. **(B)** The relative intensity of pgRNA of the recombinants before and after sequence optimization. The ratio of each pgRNA/18s rRNA was calculated, and this ratio was then divided into the sum of pgRNA/18s rRNA of all samples in the same membrane to calculate the relative intensity of pgRNA of each sample. *N* = 3.

(nt 1,511–1,568), region 99–1198 is efficient for foreign genes recombination with a size < 1,000 bp.

Herein, in D3099-396, an additional band was detected between the RC and DL DNA. This band was likely pseudo-RC DNA, reverse transcribed from one of the spliced pgRNAs of D3099-396, because only spliced RC DNA could electrophorese faster than the unspliced RC DNA and slower than the unspliced DL DNA. Of note, all spliced pgRNAs of D3099-396 lacked hM (2820–2868), which was reported to be crucial for RC DNA formation (Lewellyn and Loeb, 2007).

Furthermore, we fused 10 foreign genes, via T2A peptides, into the ORF of HBC and HBS, at 2120 and 155, respectively. This in-frame arrangement allowed for the expression of foreign genes from two RNAs, preC RNA and pgRNA, or preS1 mRNA and S mRNA. T2A peptide fused at the N-terminal of the foreign genes reduced the potential impact of the fused HBV peptides on the function of foreign genes. The findings demonstrate that site 155 may be more tolerable to recombination than site 2120. Of the 10 genes, 9 were successfully inserted at site 155 without abolishing RC DNA formation, whereas 5 of the 10 genes inserted at site

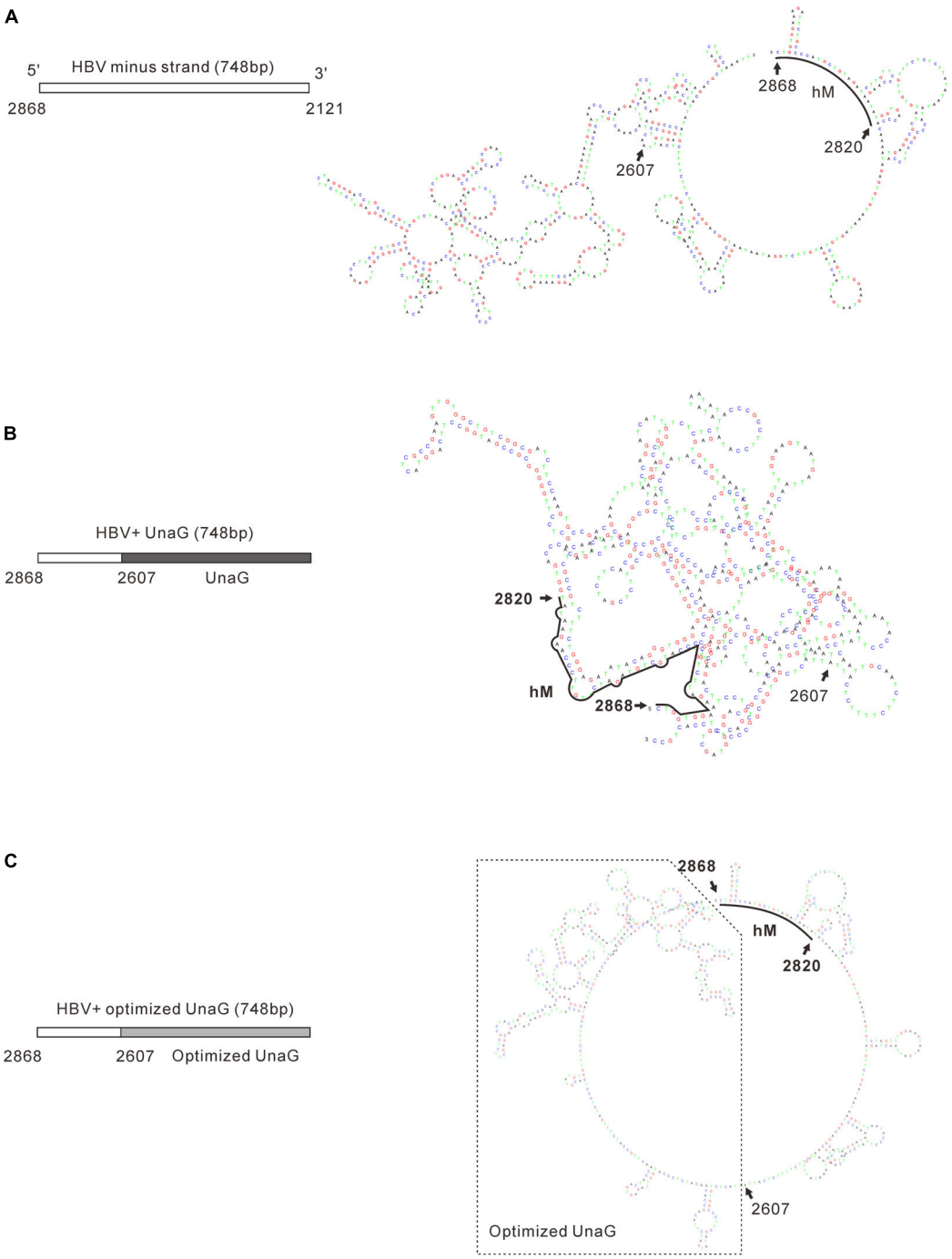


**FIGURE 11 |** Prediction of the secondary structure of minus-strand DNA of the recombinants. Secondary structures of the minus-strand DNA of wild-type HBV **(A)**, unoptimized UnaG recombinant **(B)**, and optimized UnaG **(C)** were predicated by using DNAMAN 8. The structure of *cis*-element hM (nt 2820–2868) is indicated. It is obvious that unoptimized UnaG profoundly affects the structure of HBV sequence, including hM. In contrast, optimized UnaG showed no significant impacts on the structure of the HBV sequence (nt 2607–2868).

2120 abrogated that. Besides, the deletion of HBV 2121-2819 did not abort RC DNA formation. Therefore, the failure of RC DNA formation of insertions of Neo, copGFP, mCherry, UnaG, and eGFP at 2120 was unlikely to be associated with deleting any *cis*-elements. Notably, the recombination of these genes still allowed for DL DNA formation. As such, the genes must interfere with the plus-strand primer translocation or the circulation step. Inserting the foreign genes close to hM (nt 2,820–2,868) implies that this arrangement could interfere with the base pairing between hM and h3E. These events are crucial for the translocation of

plus-strand primer (Lewellyn and Loeb, 2007), contributing to the abortion of RC DNA formation.

The most intriguing finding of this work is that optimization of the sequence of recombinant genes may improve RC DNA formation. Usually, codon optimization is used to improve the expression of proteins as this approach accommodates the codon bias of the host organism. However, we do not think the alteration in protein (UnaG) expression ameliorated RC DNA formation in the present case. First, the HBC and Pol were provided by transcomplementation. Second, the expression of UnaG or UnaGco was not essential for RC DNA formation. Third, 2120-T2A-UnaG-2607 produced a higher level of pgRNA and SS DNA than 2120-T2A-UnaGco-2607. These findings relay evidence that UnaG recombination has no adverse effects on the steps preliminary to synthesizing minus-strand DNA. However, it is plausible that UnaG impeded RC DNA formation by limiting the step of plus-strand synthesis or circularization at the DNA sequence level, for example, through the formation of some secondary structures. In line with this, structure prediction of the minus-strand DNA showed that wild-type UnaG sequence does disrupt the original structure of minus-strand DNA, whereas UnaGco profoundly ameliorates this impact (**Figure 11**). An interesting implication of our findings is that the primary sequence of minus-strand DNA intrinsically serves as a selection pressure during evolution. That is, mutations adversely impacting the secondary structure of minus-strand DNA would have less fitness and be weeded out.

## CONCLUSION

In conclusion, the current study provides an informative basis and a valuable method for constructing and optimizing recombinant HBV. Efforts are being taken to obtain and characterize reporter HBV based on the recombinants constructed in the study.

## DATA AVAILABILITY STATEMENT

The original contributions presented in the study are included in the article/supplementary material, further inquiries can be directed to the corresponding author/s.

## AUTHOR CONTRIBUTIONS

C-YG contributed to the implementation of the research. JC, W-LZ, Y-WW, A-LH, and J-LH contributed to the design of the research, the analysis of the results, and the writing of the manuscript. All authors contributed to the article and approved the submitted version.

## FUNDING

This work was supported by grants from the National Natural Science Foundation of China (81871635, 81671997, U20A20392, and 81902060), the Natural Science Foundation of Chongqing (cstc2020jcyj-msxmX0764 and cstc2020jscx-dxwtBX0022), the Science and Technology Commission of Yuzhong district, Chongqing (20180141), the 111 Project (No. D20028), and Key Laboratory of Molecular Biology on Infectious Diseases, Ministry of Education, Chongqing Medical University (No. 202104).

## REFERENCES

Abraham, T. M., and Loeb, D. D. (2006). Base Pairing between the 5′ Half of ε and a *cis*-Acting Sequence, F, Makes a Contribution to the Synthesis of Minus-Strand DNA for Human Hepatitis B Virus. *J. Virol.* 80, 4380–4387. doi: 10.1128/JVI.80.9.4380-4387.2006

Abraham, T. M., Lewellyn, E. B., Haines, K. M., and Loeb, D. D. (2008). Characterization of the contribution of spliced RNAs of hepatitis B virus to DNA synthesis in transfected cultures of Huh7 and HepG2 cells. *Virology* 379, 30–37. doi: 10.1016/j.virol.2008.06.021

Bai, W., Cui, X., Xie, Y., and Liu, J. (2016). Engineering Hepadnaviruses as reporter-expressing vectors: recent progress and future perspectives. *Viruses* 8:125. doi: 10.3390/v8050125

Baron, U., Gossen, M., and Bujard, H. (1997). Tetracycline-controlled transcription in eukaryotes: novel transactivators with graded transactivation potential. *Nucleic Acids Res.* 25, 2723–2729. doi: 10.1093/nar/25.14.2723

Bartenschlager, R., and Schaller, H. (1992). Hepadnaviral assembly is initiated by polymerase binding to the encapsidation signal in the viral RNA genome. *EMBO J.* 11, 3413–3420. doi: 10.1002/j.1460-2075.1992.tb05420.x

Bartenschlager, R., Junker-Niepmann, M., and Schaller, H. (1990). The P gene product of hepatitis B virus is required as a structural component for genomic RNA encapsidation. *J. Virol.* 64, 5324–5332. doi: 10.1128/JVI.64.11.5324-5332.1990

Boute, N., Lowe, P., Berger, S., Malissard, M., Robert, A., and Tesar, M. (2016). NanoLuc Luciferase - a multifunctional tool for high throughput antibody screening. *Front. Pharmacol.* 7:27. doi: 10.3389/fphar.2016.00027

Chaisomchit, S., Tyrrell, D. L., and Chang, L. J. (1997). Development of replicative and nonreplicative hepatitis B virus vectors. *Gene Ther.* 4, 1330–1340. doi: 10.1038/sj.gt.3300544

Cormack, B. P., Valdivia, R. H., and Falkow, S. (1996). FACS-optimized mutants of the green fluorescent protein (GFP). *Gene* 173, 33–38. doi: 10.1016/0378-1119(95)00685-0

Deng, Q., Mancini-Bourgine, M., Zhang, X., Cumont, M. C., Zhu, R., Lone, Y. C., et al. (2009). Hepatitis B virus as a gene delivery vector activating foreign antigenic T cell response that abrogates viral expression in mouse models. *Hepatology* 50, 1380–1391.

England, C. G., Ehlerding, E. B., and Cai, W. (2016). NanoLuc: a small luciferase is brightening up the field of bioluminescence. *Bioconjug. Chem.* 27, 1175–1187. doi: 10.1021/acs.bioconjchem.6b00112

Engler, C., Gruetzner, R., Kandzia, R., and Marillonnet, S. (2009). Golden gate shuffling: a one-pot DNA shuffling method based on type IIs restriction enzymes. *PLoS One* 4:e5553. doi: 10.1371/journal.pone.0005553

Engler-Blum, G., Meier, M., Frank, J., and Müller, G. A. (1993). Reduction of background problems in nonradioactive northern and Southern blot analyses enables higher sensitivity than 32P-based hybridizations. *Anal. Biochem.* 210, 235–244. doi: 10.1006/abio.1993.1189

Haines, K. M., and Loeb, D. D. (2007). The sequence of the RNA primer and the DNA template influence the initiation of plus-strand DNA synthesis in hepatitis B virus. *J. Mol. Biol.* 370, 471–480. doi: 10.1016/j.jmb.2007.04.057

Hong, R., Bai, W., Zhai, J., Liu, W., Li, X., Zhang, J., et al. (2013). Novel recombinant hepatitis B virus vectors efficiently deliver protein and RNA encoding genes into primary hepatocytes. *J. Virol.* 87, 6615–6624. doi: 10.1128/JVI.03328-12

Kimura, M., Takatsuki, A., and Yamaguchi, I. (1994). Blasticidin S deaminase gene from Aspergillus terreus (BSD): a new drug resistance gene for transfection of mammalian cells. *Biochim. Biophys. Acta* 1219, 653–659. doi: 10.1016/0167-4781(94)90224-0

Kumagai, A., Ando, R., Miyatake, H., Greimel, P., Kobayashi, T., Hirabayashi, Y., et al. (2013). A bilirubin-inducible fluorescent protein from eel muscle. *Cell* 153, 1602–1611. doi: 10.1016/j.cell.2013.05.038

Lacalle, R. A., Pulido, D., Vara, J., Zalacaín, M., and Jiménez, A. (1989). Molecular analysis of the pac gene encoding a puromycin N-acetyl transferase from Streptomyces alboniger. *Gene* 79, 375–380. doi: 10.1016/0378-1119(89)90220-5

Lanford, R. E., Notvall, L., Lee, H., and Beames, B. (1997). Transcomplementation of nucleotide priming and reverse transcription between independently expressed TP and RT domains of the hepatitis B virus reverse transcriptase. *J. Virol.* 71, 2996–3004. doi: 10.1128/jvi.71.4.2996-3004.1997

Lewellyn, E. B., and Loeb, D. D. (2007). Base pairing between cis-acting sequences contributes to template switching during plus-strand DNA synthesis in human hepatitis B virus. *J. Virol.* 81, 6207–6215.

Liu, J. X., Sun, D. X., and Cao, Z. C. (2009). [Stable cell line for secretion of replication-defective hepatitis B virus vector expressing blasticidin resistant gene]. *Zhonghua Shi Yan He Lin Chuang Bing Du Xue Za Zhi* 23, 316–318.

Liu, J., Cheng, X., Guo, Z., Wang, Z., Li, D., Kang, F., et al. (2013). Truncated active human matrix metalloproteinase-8 delivered by a chimeric adenovirus-hepatitis B virus vector ameliorates rat liver cirrhosis. *PLoS One* 8:e53392. doi: 10.1371/journal.pone.0053392

Liu, N., Ji, L., Maguire, M. L., and Loeb, D. D. (2004). cis-Acting sequences that contribute to the synthesis of relaxed-circular DNA of human hepatitis B virus. *J. Virol.* 78, 642–649. doi: 10.1128/jvi.78.2.642-649.2004

Masek, T., Vopalensky, V., Suchomelova, P., and Pospisek, M. (2005). Denaturing RNA electrophoresis in TAE agarose gels. *Anal. Biochem.* 336, 46–50. doi: 10.1016/j.ab.2004.09.010

McCabe, M. S., Power, J. B., de Laat, A. M., and Davey, M. R. (1997). Detection of single-copy genes in DNA from transgenic plants by nonradioactive Southern blot analysis. *Mol. Biotechnol.* 7, 79–84. doi: 10.1007/bf02821545

Nassal, M. (1992). The arginine-rich domain of the hepatitis B virus core protein is required for pregenome encapsidation and productive viral positive-strand DNA synthesis but not for virus assembly. *J. Virol.* 66, 4107–4116. doi: 10.1128/JVI.66.7.4107-4116.1992

Nassal, M., and Rieger, A. (1996). A bulged region of the hepatitis B virus RNA encapsidation signal contains the replication origin for discontinuous first-strand DNA synthesis. *J. Virol.* 70, 2764–2773. doi: 10.1128/JVI.70.5.2764-2773.1996

Nishitsuji, H., Harada, K., Ujino, S., Zhang, J., Kohara, M., Sugiyama, M., et al. (2018). Investigating the hepatitis B virus life cycle using engineered reporter hepatitis B viruses. *Cancer Sci.* 109, 241–249. doi: 10.1111/cas.13440

Nishitsuji, H., Ujino, S., Shimizu, Y., Harada, K., Zhang, J., Sugiyama, M., et al. (2015). Novel reporter system to monitor early stages of the hepatitis B virus life cycle. *Cancer Sci.* 106, 1616–1624. doi: 10.1111/cas.12799

Panjaworayan, N., Roessner, S. K., Firth, A. E., and Brown, C. M. (2007). HBVRegDB: annotation, comparison, detection and visualization of regulatory elements in hepatitis B virus sequences. *Virol. J.* 4:136. doi: 10.1186/1743-422X-4-136

Polaris Observatory Collaborators (2018). Global prevalence, treatment, and prevention of hepatitis B virus infection in 2016: a modelling study. *Lancet Gastroenterol. Hepatol.* 3, 383–403.

Pollack, J. R., and Ganem, D. (1993). An RNA stem-loop structure directs hepatitis B virus genomic RNA encapsidation. *J. Virol.* 67, 3254–3263. doi: 10.1128/jvi.67.6.3254-3263.1993

Protzer, U., Nassal, M., Chiang, P. W., Kirschfink, M., and Schaller, H. (1999). Interferon gene transfer by a hepatitis B virus vector efficiently suppresses wild-type virus infection. *Proc. Natl. Acad. Sci. U.S.A.* 96, 10818–10823. doi: 10.1073/pnas.96.19.10818

Rieger, A., and Nassal, M. (1996). Specific hepatitis B virus minus-strand DNA synthesis requires only the 5′ encapsidation signal and the 3′-proximal direct repeat DR1. *J. Virol.* 70, 585–589. doi: 10.1128/JVI.70.1.585-589.1996

Schmit, N., Nayagam, S., Thursz, M. R., and Hallett, T. B. (2020). The global burden of chronic hepatitis B virus infection: comparison of country-level prevalence estimates from four research groups. *Int. J. Epidemiol.* 50, 560–569. doi: 10.1093/ije/dyaa253

Shagin, D. A., Barsova, E. V., Yanushevich, Y. G., Fradkov, A. F., Lukyanov, K. A., Labas, Y. A., et al. (2004). GFP-like proteins as ubiquitous metazoan superfamily: evolution of functional features and structural complexity. *Mol. Biol. Evol.* 21, 841–850. doi: 10.1093/molbev/msh079

Shaner, N. C., Campbell, R. E., Steinbach, P. A., Giepmans, B. N., Palmer, A. E., and Tsien, R. Y. (2004). Improved monomeric red, orange and yellow fluorescent proteins derived from *Discosoma* sp. red fluorescent protein. *Nat. Biotechnol.* 22, 1567–1572. doi: 10.1038/nbt1037

Shin, H. J., Kim, S. S., Cho, Y. H., Lee, S. G., and Rho, H. M. (2002). Host cell proteins binding to the encapsidation signal epsilon in hepatitis B virus RNA. *Arch. Virol.* 147, 471–491. doi: 10.1007/s007050200001

Southern, P. J., and Berg, P. (1982). Transformation of mammalian cells to antibiotic resistance with a bacterial gene under control of the SV40 early region promoter. *J. Mol. Appl. Genet.* 1, 327–341.

Summers, J., and Mason, W. S. (1982). Replication of the genome of a hepatitis B–like virus by reverse transcription of an RNA intermediate. *Cell* 29, 403–415. doi: 10.1016/0092-8674(82)90157-x

Tang, H., and McLachlan, A. (2002). A pregenomic RNA sequence adjacent to DR1 and complementary to epsilon influences hepatitis B virus replication efficiency. *Virology* 303, 199–210. doi: 10.1006/viro.2002.1645

Tannous, B. A. (2009). Gaussia luciferase reporter assay for monitoring biological processes in culture and *in vivo*. *Nat. Protoc.* 4, 582–591. doi: 10.1038/nprot.2009.28

Untergasser, A., and Protzer, U. (2004). Hepatitis B virus-based vectors allow the elimination of viral gene expression and the insertion of foreign promoters. *Hum. Gene Ther.* 15, 203–210. doi: 10.1089/104303404772680001

Verhaegent, M., and Christopoulos, T. K. (2002). Recombinant Gaussia luciferase. Overexpression, purification, and analytical application of a bioluminescent reporter for DNA hybridization. *Anal. Chem.* 74, 4378–4385. doi: 10.1021/ac025742k

Wang, L., Kaneko, S., Honda, M., and Kobayashi, K. (2002). Approach to establishing a liver targeting gene therapeutic vector using naturally occurring defective hepatitis B viruses devoid of immunogenic T cell epitope. *Virus Res.* 85, 187–197. doi: 10.1016/s0168-1702(02)00043-6

Wang, Y., Wang, F., Wang, R., Zhao, P., and Xia, Q. (2015). 2A self-cleaving peptide-based multi-gene expression system in the silkworm Bombyx mori. *Sci. Rep.* 5:16273. doi: 10.1038/srep16273

Wang, Z., Zhu, K., Bai, W., Jia, B., Hu, H., Zhou, D., et al. (2014). Adenoviral delivery of recombinant hepatitis B virus expressing foreign antigenic epitopes for immunotherapy of persistent viral infection. *J. Virol.* 88, 3004–3015. doi: 10.1128/JVI.02756-13

WHO (2017). *Hepatitis B*. Available online at: https://www.who.int/news-room/fact-sheets/detail/hepatitis-b (accessed August, 2017).

Yoo, J., Rho, J., Lee, D., Shin, S., and Jung, G. (2002). Hepatitis B virus vector carries a foreign gene into liver cells *in vitro*. *Virus Genes* 24, 215–224. doi: 10.1023/a:1015320314201

**Conflict of Interest:** The authors declare that the research was conducted in the absence of any commercial or financial relationships that could be construed as a potential conflict of interest.

**Publisher's Note:** All claims expressed in this article are solely those of the authors and do not necessarily represent those of their affiliated organizations, or those of the publisher, the editors and the reviewers. Any product that may be evaluated in this article, or claim that may be made by its manufacturer, is not guaranteed or endorsed by the publisher.

*Copyright © 2021 Gan, Cui, Zhang, Wang, Huang and Hu. This is an open-access article distributed under the terms of the Creative Commons Attribution License (CC BY). The use, distribution or reproduction in other forums is permitted, provided the original author(s) and the copyright owner(s) are credited and that the original publication in this journal is cited, in accordance with accepted academic practice. No use, distribution or reproduction is permitted which does not comply with these terms.*

frontiers in Microbiology

ORIGINAL RESEARCH
published: 01 December 2021
doi: 10.3389/fmicb.2021.780978

# Development of a Novel Avian Vaccine Vector Derived From the Emerging Fowl Adenovirus 4

*Qing Pan[1], Yu Zhang[1], Aijing Liu[1], Hongyu Cui[1], Yulong Gao[1], Xiaole Qi[1], Changjun Liu[1], Yanping Zhang[1], Kai Li[1], Li Gao[1] and Xiaomei Wang[1,2]**

*[1] State Key Laboratory of Veterinary Biotechnology, Harbin Veterinary Research Institute, Chinese Academy of Agricultural Sciences, Harbin, China, [2] Jiangsu Co-innovation Centre for Prevention and Control of Important Animal Infectious Diseases and Zoonoses, Yangzhou University, Yangzhou, China*

Severe hepatitis-hydropericardium syndrome (HHS) associated with a novel viral genotype, fowl adenovirus 4 (FAdV-4), has emerged and widely spread in China since 2015, causing severe economic losses to the poultry industry. We previously reported that the hexon gene is responsible for pathogenicity and obtained a non-pathogenic hexon-replacement rHN20 strain; however, the lack of information about the non-essential regions for virus replication limits the development of a FAdV-4 vector. This study first established an enhanced green fluorescent protein (EGFP)-indicator virus based on the FAdV-4 reverse genetic technique, effective for batch operations in the virus genome. Based on this, 10 open reading frames (ORFs) at the left end and 13 ORFs at the right end of the novel FAdV-4 genome were deleted separately and identified as non-essential genes for viral replication, providing preliminary insertion sites for foreign genes. To further improve its feasibility as a vaccine vector, seven combinations of ORFs were successfully replaced with EGFP without affecting the immunogenicity of the vector backbone. Finally, a recombinant rHN20-vvIBDV-VP2 strain, expressing the VP2 protein of very virulent infectious bursa disease virus (vvIBDV), was rescued and showed complete protection against FAdV-4 and vvIBDV. Thus, the novel FAdV-4 vector could provide sufficient protection for HHS and efficient exogenous gene delivery. Overall, our findings systemically identified 23 non-essential ORFs for FAdV-4 replication and seven foreign gene insertion regions, providing valuable information for an in-depth understanding of the novel FAdV-4 pathogenesis and development of multivalent vaccines.

**Keywords: FAdV-4, vaccine vector, HHS, non-essential regions, IBDV**

OPEN ACCESS

***Edited by:***
*Chunfu Zheng,*
*University of Calgary, Canada*

***Reviewed by:***
*Manman Dai,*
*South China Agricultural University, China*
*Yi-Quan Wu,*
*National Cancer Institute (NCI), United States*

***Correspondence:**
*Xiaomei Wang*
*wangxiaomei@caas.cn*

***Specialty section:***
*This article was submitted to Virology, a section of the journal Frontiers in Microbiology*

***Received:*** *22 September 2021*
***Accepted:*** *29 October 2021*
***Published:*** *01 December 2021*

***Citation:***
*Pan Q, Zhang Y, Liu A, Cui H, Gao Y, Qi X, Liu C, Zhang Y, Li K, Gao L and Wang X (2021) Development of a Novel Avian Vaccine Vector Derived From the Emerging Fowl Adenovirus 4. Front. Microbiol. 12:780978. doi: 10.3389/fmicb.2021.780978*

## INTRODUCTION

Adenoviruses (family *Adenoviridae*) are non-enveloped, double-stranded DNA viruses that infect multiple vertebrates, including mammals, birds, fish, and reptiles (Greber, 2020). According to the International Committee on Taxonomy of Viruses (ICTV), the family *Adenoviridae* is classified into five genera: *Adenovirus, Aviadenovirus, Chadenovirus, Mastadenovirus,* and *Siadenovirus.* Fowl adenoviruses (FAdVs) belong to the genus *Aviadenovirus* and are defined as 5 species (A–E) and 12

serotypes (1–7, 8a–8b, 9–11) (Steer et al., 2009). Pathogenic FAdV strains infect chickens, causing inclusion body hepatitis (IBH), hepatitis-hydropericardium syndrome (HHS), and gizzard erosion (GE) (Liu et al., 2016; Li et al., 2018; Schachner et al., 2018; Wang et al., 2020). A severe outbreak of HHS by the novel FAdV-4 has occurred in China since 2015, causing severe economic losses to the poultry industry (Liu et al., 2016; Niu et al., 2016; Xia et al., 2017; Li et al., 2018).

With the development of gene editing and reverse genetic technology, various viruses have been successfully modified as viral vectors, such as poxvirus (Lévy et al., 2020), herpes virus (Herold et al., 2002), Newcastle disease virus (NDV) (Sun et al., 2020), and adenovirus (Wu et al., 2021). For instance, Fowlpox virus was used as a recombinant vaccine vector against mammalian and poultry viruses (Taylor et al., 1988; Boyle and Heine, 1993); Gallid herpesvirus 2 (GaHV-2), expressing the infectious bursal disease virus (IBDV) VP2 protein, was used for the prevention and control of Marek's disease virus (MDV) and IBDV (Li et al., 2016); whereas NDV was reported to be immunogenic and efficacious against avian influenza HA (Zhang X. et al., 2021). In addition, human adenovirus vectors have been widely used for gene therapy (Arnone et al., 2021) and vaccines against emergent viruses such as Ebola (Li et al., 2017) and SARS-Cov-2 (Tostanoski et al., 2021), however, non-human and non-mammalian adenoviruses, including FAdVs, are used less frequently as vectors.

The genome of human and mammalian adenoviruses (*Mastadenovirus*) is approximately 34–38 kb, including early transcription genes (E1, E2, E3, and E4) and late transcription genes (L1, L2, L3, L4, and L5). The genes located in E1 and E3 were identified as essential and non-essential genes, respectively, providing a theoretical basis for developing adenovirus vectors (Tatsis and Ertl, 2004). Nevertheless, FAdVs have the longest genome (43–36 kb) among adenoviruses without E1, E3, or E4 regions, whereas only the E2 and L1–L4 regions in the central part of the genome are conserved with mammalian adenoviruses. Previous studies on the chicken embryo lethal orphan (CELO) strain (non-pathogenic FAdV-1) showed that 16 of the 22 unassigned open reading frames (ORFs) are non-essential for virus replication and that the rightmost segment of the genome (containing ORF9, ORF10, and ORF11) can be replaced by an enhanced green fluorescent protein (EGFP) expression cassette (Michou et al., 1999; François et al., 2001). Nevertheless, the CELO-vectored vaccine could not protect chickens against HHS, and thus, a novel FAdV-4-based vaccine vector is urgently needed.

The inactivated FAdV-4 oil-emulsified vaccine can induce full protection (Pan et al., 2017b), whereas the live-vectored bivalent or multiple vaccines can further reduce the production cost and workload. Given the emergence, high pathogenicity, and lack of knowledge of the non-essential regions of the novel FAdV-4, limited progress has been achieved in vector development. We previously reported that the hexon gene played a critical role in FAdV-4 pathogenicity and obtained a non-pathogenic rHN20 strain (Zhang Y. et al., 2021). In this study, 10 ORFs at the left end and 13 ORFs at the right end of the novel FAdV-4 genome were separately deleted and identified as non-essential regions for virus replication based on an EGFP-indicator virus. Furthermore, seven combinations of ORFs were successfully replaced with EGFP without affecting the immunogenicity of the vector backbone. Finally, the FAdV-4 vector was used to deliver the VP2 protein of vvIBDV and provided complete protection against FAdV-4 and vvIBDV.

# MATERIALS AND METHODS

## Animals and Ethics Statement

Specific pathogen-free (SFP) chickens obtained from Harbin Veterinary Institute of Chinese Academy of Agricultural Sciences (HVRI, CAAS) were housed in a negative-pressure environment at the Experimental Animal Center of HVRI. The birds had *ad libitum* access to water and feed. The study was approved by the Ethical and Animal Welfare Committee of HVRI (approval No. HVRI-IACUC-2021-0426-5).

## Virus, Cell, and Antibody

The highly pathogenic FAdV-4 strain HLJFAd15 (GenBank accession number KU991797) was isolated in our laboratory (Pan et al., 2017a), and the non-pathogenic strain rHN20 was constructed as described previously (Zhang Y. et al., 2021). All FAdV-4 viruses propagated in chicken hepatocellular carcinoma (LMH) cells. The vvIBDV HLJ0504 strain was also isolated in our laboratory, and the cell-adapted IBDV rGtHLJVP2 strain, inducing cytopathic effects (CPE) in a continuous cell line of chicken embryo fibroblasts (DF-1), was constructed as described previously (Gao et al., 2011). LMH cells were cultured in DMEM/F12 (Sigma-Aldrich, St. Louis, MO, United States), whereas DF-1 in DMEM (Sigma-Aldrich). Both the mediums were supplemented with 10% fetal bovine serum (Sigma-Aldrich), 100 $\mu$ ml$^{-1}$ streptomycin, and 100 IU ml$^{-1}$ penicillin at 37°C and 5% $CO_2$. The anti-IBDV-VP2 monoclonal antibody was prepared in our laboratory.

## Construction of Recombinant Viruses

The FAdV-4 rHN20 fosmid was generated from the HLJFAd15 strain. Recombinant fosmids were engineered from rHN20 in *Escherichia coli* DH10B cells using the Counter-Selection BAC Modification kit (Gene Bridges, Heidelberg, Germany) as described previously (Zhang Y. et al., 2021). In brief, the rpsL-neo selection antibiotic cassette was inserted into the genome-expected sites, and rpsL-neo was replaced by a PCR-amplified product or single-stranded oligonucleotide with short homology arms.

The EGFP expression cassette from the pEGFP-N1 plasmid (Clontech, Mountain View, CA, United States) was inserted into the natural 1,966-bp deletion site (Pan et al., 2018) of rHN20 to construct the rHN20-EGFP recombinant fosmid. Next, each ORF was replaced with a single-stranded oligonucleotide to construct fosmids that individually deleted the 23 ORFs in the left and right ends of the FAdV-4 genome. Finally, the adjacent ORFs in the left and right ends of the FAdV-4 genome were divided factitiously into the L1, L2, L3, R1, R2, R3, and R4 regions. Every region was

first replaced with EGFP to construct fosmids, in which EGFP replaced several adjacent ORFs as described above.

VP2 from the vvIBDV strain HLJ0504 cDNA was cloned into the pEGFP-N1 plasmid, and the EGFP ORF was replaced to form the VP2-expressing cassette. The VP2 cassette was inserted into the natural1966-bp deletion site of rHN20 to obtain the rHN20-vvIBDV-VP2 fosmid.

All recombinant fosmids were transfected into LMH cells after digestion with *Fse*I (Thermo-Fisher Scientific, Waltham, MA, United States) for 120 h post-transfection. Cells transfected with fosmids should be frozen and thawed three times, and the cell supernatant was inoculated into fresh LMH cells. The cell supernatant was collected for amplification and identification when apparent cytopathic effect (CPE) and/or green fluorescence appeared. The accuracy of all the recombinant viruses was confirmed using PCR. The VP2 expression of rHN20-vvIBDV-VP2 was identified using an indirect fluorescence antibody (IFA) assay with the monoclonal anti-IBDV-VP2.

## Virus Growth Curve

FAdV-4 was inoculated into LMH cells at a multiplicity of infection (MOI) of 0.01. The viruses were harvested at 12, 24, 48, 72, 96, and 120 h post-infection for plaque assay to determine viral titers.

## Immunization and Challenge Test

For rHN20 recombinant viruses expressing EGFP, 2-week-old SPF chickens were randomized into five groups (n = 10): a healthy control, a challenge control, and three groups, each immunized with 200 μl of rHN20, rDL3-EGFP, or r HN20-EGFP. At 14 d post-immunization, the immunized and challenge control groups were challenged with 2,000 plaque-forming units (PFU) rWT-FAdV4, whereas the healthy control group was administered DMEM/F12. Data on the morbidity and mortality of chickens were collected daily for 14 days. Viral loads were determined by collecting heart, liver, spleen, lung, kidney, thymus, and bursa from deceased or euthanized chickens at the test endpoint. The liver and thymus were used for histopathological analysis.

In addition, 50 two-week-old SPF chickens were randomized into five groups ($n$ = 10): 2 groups were intramuscularly immunized with rHN20-vvIBDV-VP2, and the other 3 groups remained unimmunized. Neutralizing antibody titers in sera were determined at 7, 14, and 21 days post-immunization. At 21 days post-immunization, 10 immunized and 10 unimmunized chickens were challenged intramuscularly with 2,000 PFU virulent FAdV-4; the other 10 immunized and 10 unimmunized chickens were inoculated intranasally with $10^5$ $EID_{50}$ vvIBDV. The left 10 chickens were used as healthy control. The chickens were monitored daily, euthanized, and necropsied at 7 days post-challenge.

## Viral Load Detection

Total DNA from different tissues was extracted using the AxyPrep Body Fluid Viral DNA/RNA Miniprep kit (Corning, Corning, NY, United States). Virus genome copies and cellular copies were quantified using Premix Ex Taq (TaKaRa, Kusatsu, Shiga, Japan) as described previously (Baigent et al., 2005; Pan et al., 2017c). Real-time PCR was performed using QuantStudio5 (Applied Biosystems, Waltham, MA, United States). Viral loads were expressed as the number of viral genome copies per $10^6$ cells (copies $10^{-6}$ cells) (Zhang Y. et al., 2021).

## Histopathological Analysis

The tissues were fixed in 10% formalin and embedded in paraffin. The sections were stained with hematoxylin and eosin (H&E) and observed under a microscope.

## Virus-Neutralization Assay

After inactivation at 56°C for 30 min, each serum sample was filtered through a 0.22-μm pore size filter. A twofold serial dilution of the serum was mixed with 200 median tissue culture infectious dose ($TCID_{50}$) of the FAdV-4 rWT-EGFP strain or IBDV rGtHLJVP2 strain in a 96-well plate, incubated at 42°C for 1 h, and then added to the LMH or DF1 cells. After being cultured at 37°C for 72 h, IBDV CPEs were observed. After being cultured at 37°C for 6 day, the GFP expressed in FAdV-4 was visualized by fluorescence microscopy.

## Statistical Analysis

Two-way ANOVA with Tukey's multiple comparison test was used for identifying significant differences. Significance was set at $p < 0.05$. Statistical analysis was performed with GraphPad (GraphPad Software, San Diego, CA, United States).

# RESULTS

## Construction of rHN20-Enhanced Green Fluorescent Reporter Virus

To facilitate visualization of the virus on cells, we inserted an enhanced green fluorescent (EGFP) expression cassette on the natural 1,966 bp deletion between ORF42 and ORF43 of the FAdV-4 rHN20 strain (**Figure 1A**). The results showed that the rescued recombinant virus rHN20-EGFP strain could produce green fluorescence in LMH cells, whereas rHN20 could not (**Figure 1B**). PCR amplification of rHN20 and rHN20-EGFP genomic DNA revealed a 400-bp band for rHN20 and an approximately 2,000-bp band for rHN20-EGFP (**Figure 1C**). Comparing the replicative capacity of rHN20-EGFP with that of rHN20 on LMH cells, we found that rWT-EGFP replicated efficiently, despite its slightly reduced replicative capacity (**Figure 1D**). Thus, we successfully obtained an EGFP-expressing FAdV-4 reporter virus.

## Identification and Characterization of Open Reading Frames in Both Terminal Regions of FAdV-4 Genome

The ORFs at the left -and right-terminal regions of the FAdV genome are unique and not conserved within the *Adenoviridae* family (Davison et al., 2003). The FAdV-4 genome had 10 ORFs at the left end and 13 ORFs at the right end (**Figures 2A**, **3A**). To determine whether these

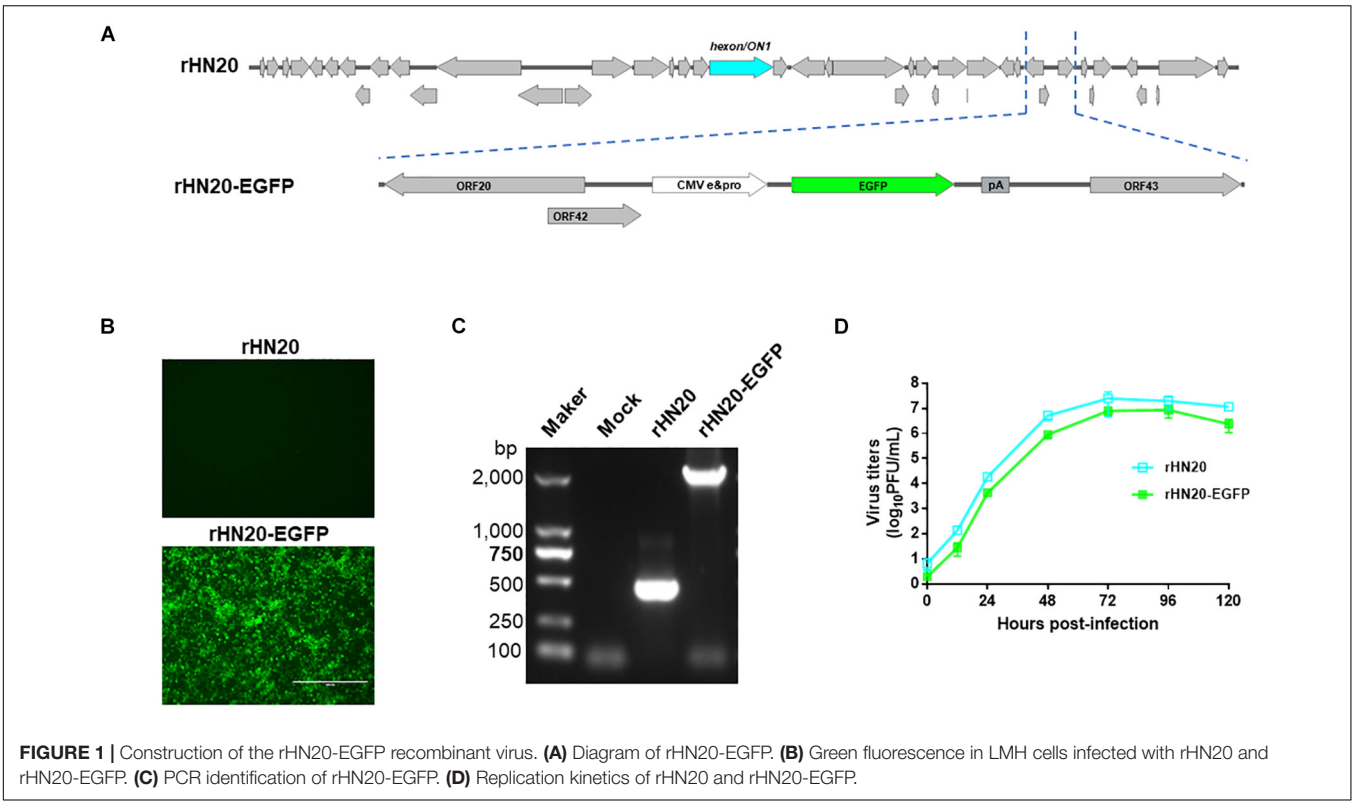


**FIGURE 1 |** Construction of the rHN20-EGFP recombinant virus. **(A)** Diagram of rHN20-EGFP. **(B)** Green fluorescence in LMH cells infected with rHN20 and rHN20-EGFP. **(C)** PCR identification of rHN20-EGFP. **(D)** Replication kinetics of rHN20 and rHN20-EGFP.

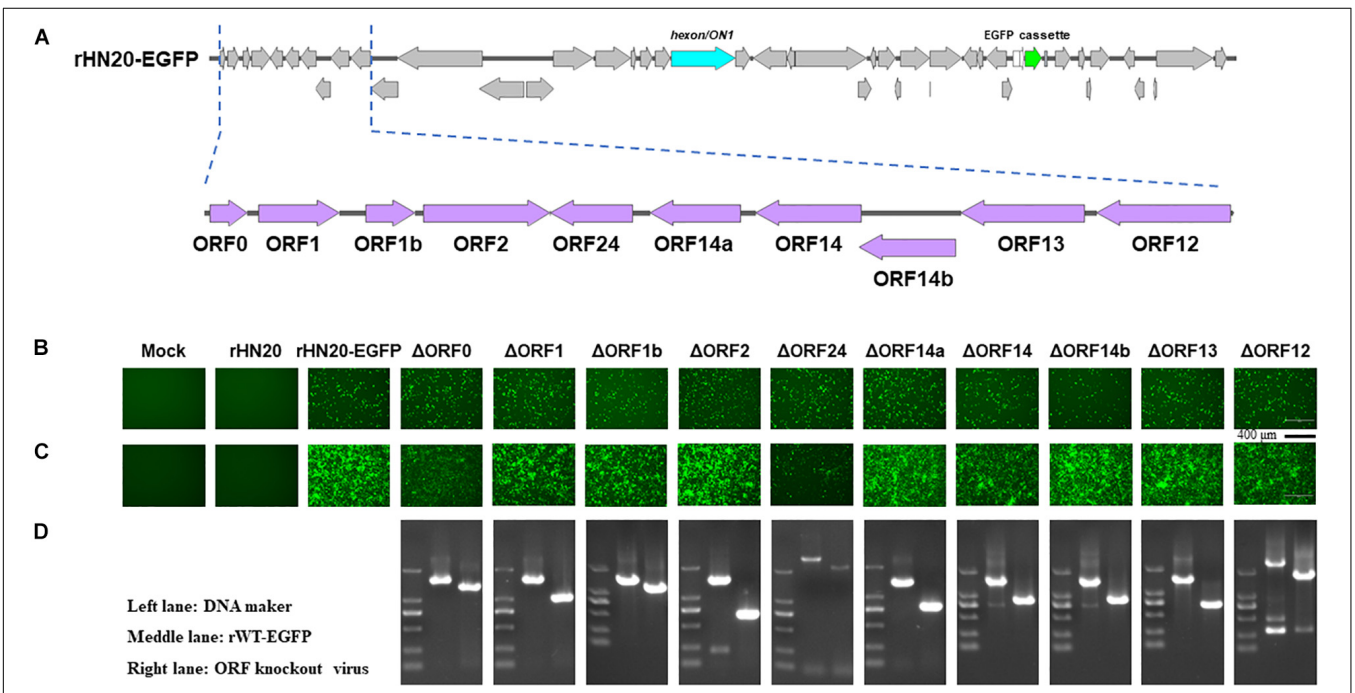


**FIGURE 2 |** Identification of non-essential open reading frames (ORFs) in the left of the FAdV-4 genome. **(A)** Diagram of the genomic structure of rHN20-EGFP. Focal amplifications in purple represent ORFs unique to fowl adenoviruses on the left. **(B)** Green fluorescence in LMH cells transfected with linearized ORF knockout recombinant fosmids at 48 h post-transfection. Scale bar, 200 μm. **(C)** Green fluorescence in LMH cells infected with ORF knockout recombinant viruses at 72 h post-infection. Scale bar, 200 μm. **(D)** PCR identification of ORF knockout recombinant virus. A fragment of each recombinant virus containing the knockout ORF was amplified, and rWT-EGFP was used as a control.

23 ORFs are essential genes, they were individually deleted in the rHN20-EGFP fosmid, linearized, and transfected into LMH cells to recure ORF-knockout viruses. EGFP served as a reporter gene to monitor transfection success and viral production. At 48 h post-transfection, cells transfected with all fosmids engineered from rHN20-EGFP exhibited apparent green fluorescence, whereas mock and rWT-FAdV4 control cells showed no fluorescence (**Figures 2B**, **3B**). Cell supernatants were harvested to infect new LMH cells, and all ORF-knockout recombinant viruses were successfully rescued (**Figures 2C**, **3C**). Furthermore, all ORF knockout viruses were identified by PCR amplifying the knockout site fragment, resulting in a smaller band than the control (**Figures 2D**, **3D**). Our data demonstrated that FAdV-4 could replicate after individual deletion of all 23 ORFs in both terminal regions of the viral genome.

## Construction of Recombinant Viruses With Enhanced Green Fluorescent Protein Substitutions of Several Open Reading Frames

To further confirm that the 23 ORFs in both terminal regions of the FAdV-4 genome were not essential for virus replication, the same ORFs in rHN20 were divided factitiously into L1, L2, L3, R1, R2, R3, and R4 regions that were each replaced by the EGFP cassette (**Figure 4A**). Seven recombinant viruses were generated, designated as rDL1-EGFP, rDL2-EGFP, rDL3-EGFP, rDR1-EGFP, rDR2-EGFP, rDR2-EGFP, and rDR3-EGFP. LMH cells infected with each of the seven recombinant viruses or rHN20-EGFP expressed green fluorescence (**Figure 4B**). All the eight EGFP-expressing recombinant viruses replicated efficiently in LMH cells (**Figure 4C**).

## Evaluation of Protective Efficacy of Live Recombinant Viruses Expressing Enhanced Green Fluorescent Protein

An immunization and challenge test was performed to evaluate whether the recombinant FAdV-4 viruses expressing EGFP could be used as live vaccines. Two-week-old SPF chickens were immunized with live rHN20, rDL3-EGFP, or rHN20-EGFP. At 14 d post-immunization, the chickens were challenged with a lethal dose of FAdV4 HLJFAd15. As described in **Figure 5A**, all live recombinant FAdV-4 showed 100% protection. No clinical signs or death were observed in chickens pre-inoculated with live rHN20, rDL3-EGFP, or rHN20-EGFP within 14 d post-challenge, whereas the mortality of challenge control chickens reached 80% at 4 d post-challenge (**Figure 5B**). Moreover, high viral loads were observed in the tissues, especially livers, of the challenge control group at 14 day post-challenge, whereas almost no viral load was detected in the tissues of the immunized groups (**Figure 5C**). In line with these findings, massive pathological lesions and vacuolar necrosis were observed in the liver and thymus of the challenge control group,

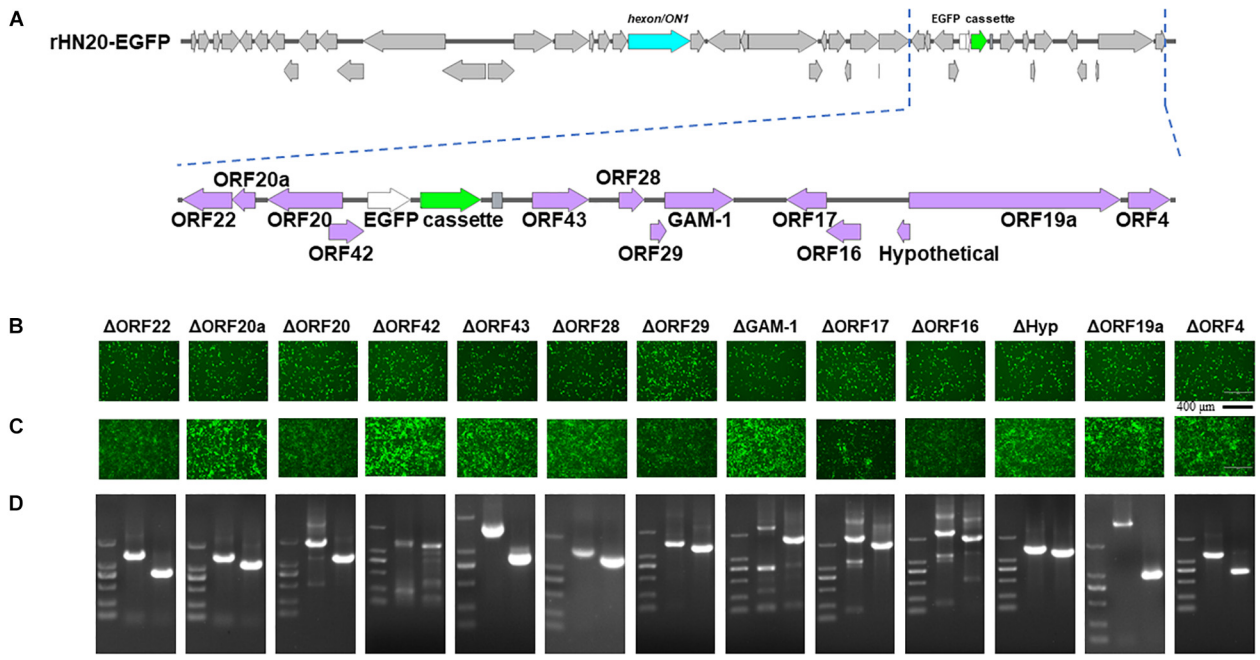


**FIGURE 3 |** Identification of non-essential open reading frames (ORFs) in the right of the FAdV-4 genome. **(A)** Diagram of the genomic structure of rHN20-EGFP. Focal amplifications in purple represent ORFs unique to fowl adenoviruses on the right. **(B)** Green fluorescence in LMH cells transfected with linearized ORF knockout recombinant fosmids at 48 h post-transfection. Scale bar, 200 μm. **(C)** Green fluorescence in LMH cells infected with ORF knockout recombinant viruses at 72 h post-infection. Scale bar, 200 μm. **(D)** PCR identification of ORF knockout recombinant virus. A fragment of each recombinant virus containing the knockout ORF flanked was amplified, and rWT-EGFP was used as a control.

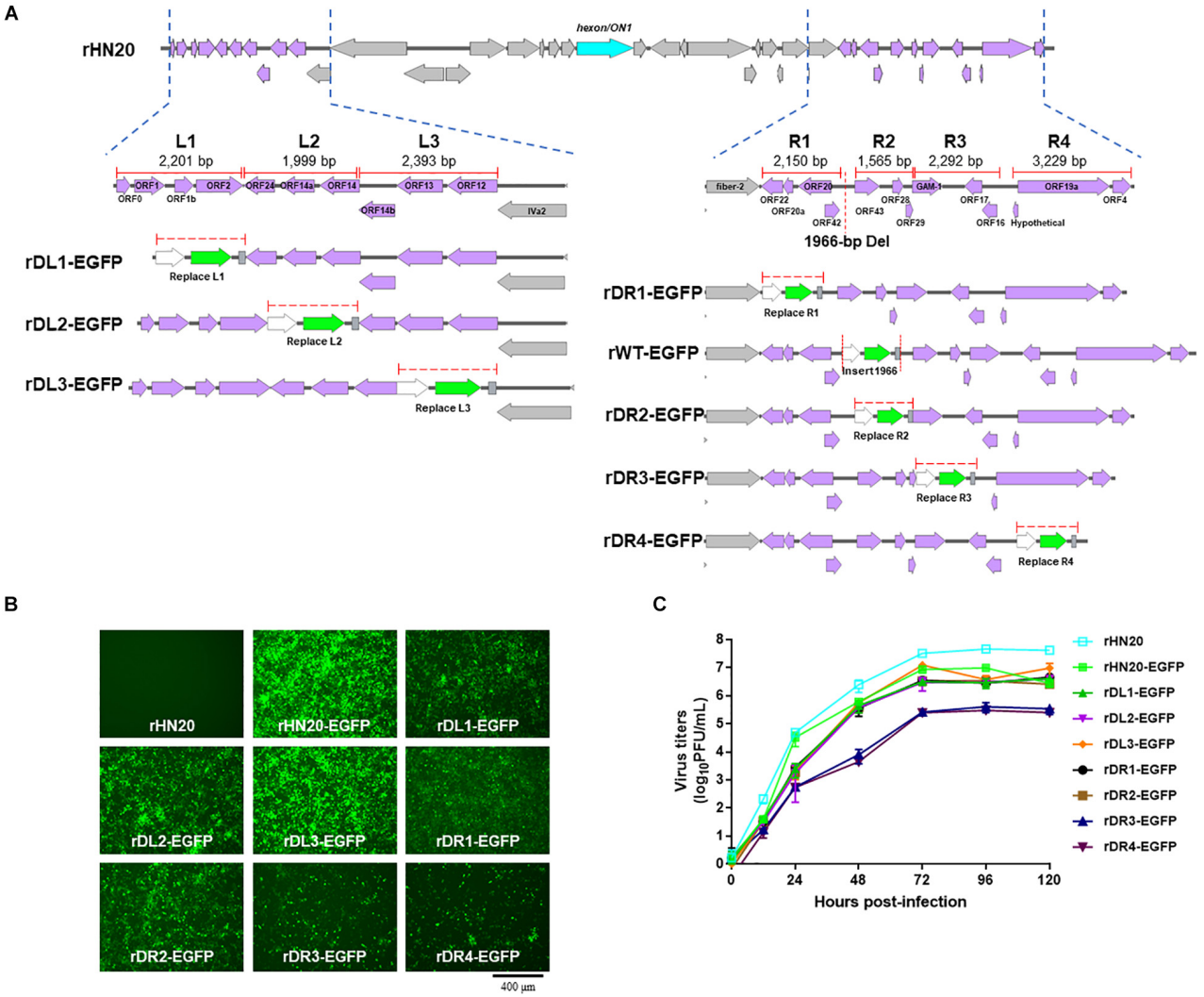


**FIGURE 4 |** FAdV-4 non-essential genes serve as insertion sites of foreign gene. **(A)** Construction of recombinant FAdV-4 expressing EGFP gene. The left ORFs of FAdV-4 are divided into the L1, L2, and L3 regions, and the right ORFs are divided into the R1, R2, R3, and R4 regions. The length of each region is indicated and each region is individually replaced by an EGFP expression cassette. **(B)** Green fluorescence in LMH cells infected with different recombinant fluorescent viruses. **(C)** Replication kinetics of different recombinant fluorescent viruses.

whereas no apparent pathological changes were found in any of the rHN20-, rDL3-EGFP, or rHN20-EGFP immunized groups (**Figure 5D**). Therefore, the insertion of EGFP did not impair the immunogenicity of FAdV-4.

## Construction of rHN20-vvIBDV-VP2 Recombinant Virus

The coding region of the vvIBDV VP2 gene was inserted into the rHN20 genome to assess whether rHN20 could deliver a protective antigen after adding a CMV promoter and poly-A to rescue the recombinant virus rHN20-vvIBDV-VP2 (**Figure 6A**). Using PCR and IFA, we found that the vvIBDV VP2 expression cassette was precisely inserted at the natural 1,966-bp deletion, and the vvIBDV VP2 protein could be expressed (**Figures 6B,C**). The growth kinetics of rHN20-vvIBDV-VP2 were delayed, and the virus titer was approximately a 1-log defect compared with rHN20 (**Figure 6D**).

## Protective Efficacy of Live rHN20-vvIBDV-VP2 Against FAdV-4 and vvIBDV

Chickens were vaccinated with rHN20-vvIBDV-VP2 to evaluate the protective efficacy of the rHN20-vvIBDV-VP2 recombinant virus, and serum neutralizing antibodies against FAdV-4 and vvIBDV were continuously detected. Next, they were challenged with FAdV-4 HLJFAd15 or vvIBDV HLJ0504 at 21 days post-vaccination. The virus neutralization assay showed that the immunized chicken serum had strong neutralizing activity against FAdV-4 (**Figure 7A**) and vvIBDV (**Figure 7B**). All immunized chickens did not

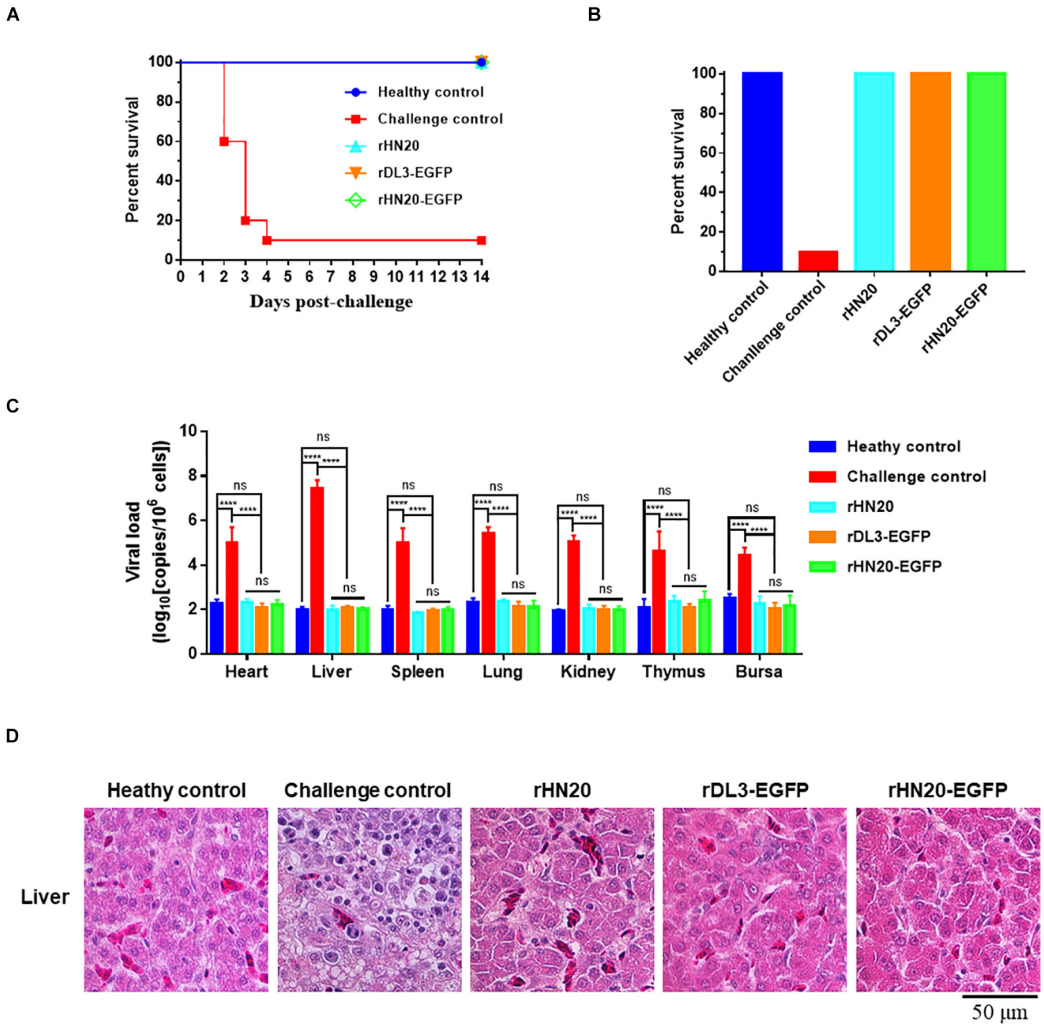


**FIGURE 5 |** Protection against FAdV-4 lethal challenge by live recombinant fluorescent viruses. Two-week-old SPF chickens ($n$ = 10) were injected with live rHN20, rDL3-EGFP, or rWT-EGFP and challenged with a lethal dose of FAdV-4 at 14 days post-injection. The healthy control was not treated. The challenge control was challenged but not immunized. **(A)** Survival curves of challenged chickens. **(B)** Survival rates of challenged chickens. **(C)** Viral loads in different tissues of challenged chickens. Heart, liver, spleen, lung, kidney, thymus, and bursa from dead or euthanized chickens were collected, and viral loads were determined using real-time PCR ($n$ = 3). ****Significance at $P < 0.0001$; ns, no significance. **(D)** Histological examination of liver from challenged chickens. Scale bar, 50 μm.

show any clinical signs or mortality after the challenge with FAdV-4 (**Figure 8A**) or vvIBDV (**Figure 8B**). In contrast, challenged chickens showed high mortality (100% for FAdV-4 and 70% for vvIBDV). In line with these findings, no histopathological changes were evident in the liver or bursa of immunized chickens; however, FAdV-4 challenge controls showed hepatocyte necrosis (**Figure 8C**), whereas vvIBDV challenge controls showed bursa cell necrosis and follicular atrophy (**Figure 8D**).

## DISCUSSION

Severe HHS associated with the novel genotype FAdV-4 has emerged and widely spread in China since 2015, resulting in severe economic losses to the poultry industry. Due to the high mortality in broilers (Wei et al., 2019), layers (Mei et al., 2020), and breeders (Mirzazadeh et al., 2021), it is necessary to develop an effective vaccine and therapeutic strategy to combat the novel FAdV-4. Previous studies showed that an inactivated FAdV-4 oil-emulsified vaccine (Pan et al., 2017b) and subunit vaccines based on fiber 2 and hexon (Ruan et al., 2018; Hu et al., 2021) could provide complete protection against FAdV-4. Recombinant *Lactococcus lactis* and *Enterococcus faecalis* expressing hexon (Jia et al., 2021) and Newcastle disease virus (NDV) expressing fiber 2 (Tian et al., 2020) were also constructed and evaluated. Given the emergence, high pathogenicity, and lack of knowledge of the non-essential regions of the novel FAdV-4, limited progress has been achieved on the development of the FAdV-4 vector. Live FAdV-4 vectored bivalent or multiple vaccines could further reduce the production cost and workload.

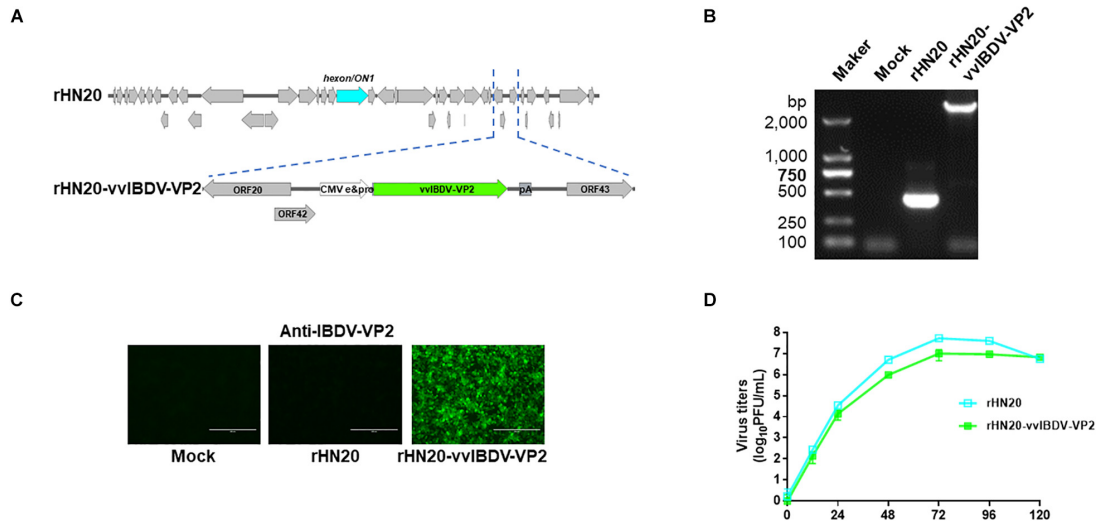


**FIGURE 6 |** Construction of rHN20-vvIBDV-VP2 recombinant virus. **(A)** Diagram of rHN20-vvIBDV-VP2. **(B)** PCR identification of rHN20-vvIBDV-VP2. **(C)** Indirect immunofluorescence (IFA) identification of rHN20-vvIBDV-VP2 with monoclonal anti-IBDV-VP2. **(D)** Replication kinetics of rHN20 and rHN20-vvIBDV-VP2.

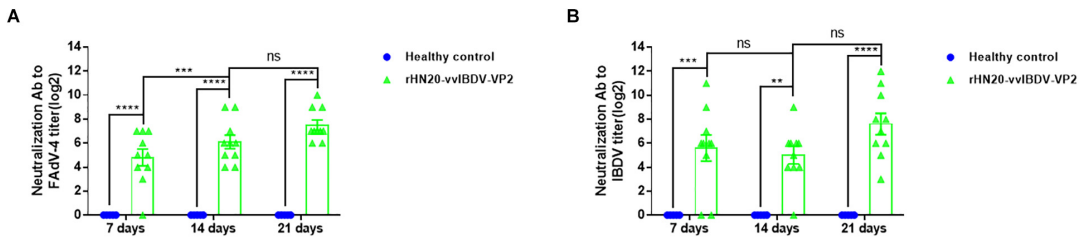


**FIGURE 7 |** Neutralizing antibody titers of live rHN20-vvIBDV-VP2. Neutralizing antibody titers to **(A)** FAdV-4 and **(B)** IBDV in two-week-old SPF chickens intramuscularly injected with live rHN20-vvIBDV-VP. **, ***, ****, significance at $P < 0.01$, $P < 0.001$, and $P < 0.0001$, respectively; ns, no significance.

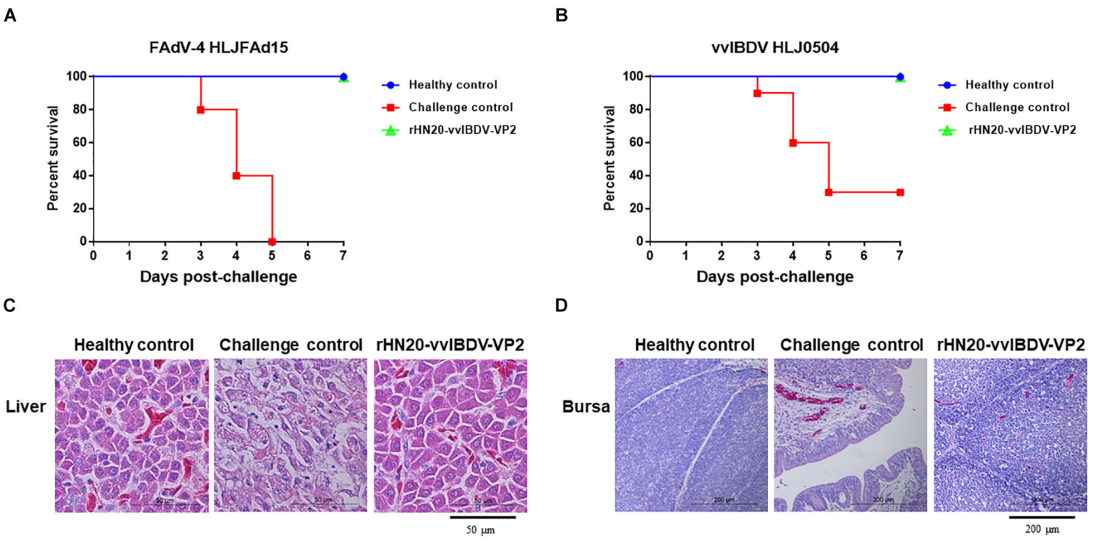


**FIGURE 8 |** Efficacy of live rHN20-vvIBDV-VP2 vaccine against FAdV-4 and vvIBDV. Immunized chickens were challenged with FAdV-4 or IBDV. Survival rates of chickens after **(A)** FAdV-4 or **(B)** IBDV challenge. **(C)** Pathological sections of liver from FAdV-4 challenged chickens. Scale bar, 50 μm. **(D)** Pathological sections of bursas from IBDV challenged chickens. Scale bar, 200 μm.

A fiber-2-edited live attenuated vaccine candidate was previously developed, providing efficient protection against lethal challenge with FAdV-4; however, the titer of the edited strain was significantly decreased (Xie et al., 2021), limiting the application of the vaccine. In our previous studies, the hexon gene was identified as critical for FAdV-4 pathogenicity, and a non-pathogenic hexon-replaced chimeric strain rHN20 was rescued, showing similar virus titers compared with the wild-type strain (Zhang Y. et al., 2021). Nevertheless, the unknown non-essential regions for replication have limited the FAdV-4 vector development. In the present study, 10 ORFs at the left end and 13 ORFs at the right end of the novel FAdV-4 genome were separately deleted and identified as non-essential regions for virus replication based on an EGFP-indicator virus, which is the first report to systemically identify the non-essential ORFs for FAdV-4 replication, providing preliminary insertion sites for exogenous genes and essential information for gene function studies. These results were consistent with investigations on other serotypes of FAdVs, which showed that 16 of the 22 terminal ORFs (ORF1–4, ORF7–18) can be knocked out by point mutation in FAdV-1 (François et al., 2001) and that six ORFs are dispensable for non-pathogenic FAdV-9 (Corredor and Nagy, 2010).

To further improve the efficiency and capacity of foreign gene insertion, we successfully replaced seven combinations of ORFs with EGFP without affecting the immunogenicity of the vector backbone. Moreover, the VP2 gene of vvIBDV was delivered by the FAdV-4 vector; the VP2 protein was successfully expressed, and the recombinant rHN20-vvIBDV-VP2 provided complete protection against the FAdV-4 and vvIBDV challenges. Evaluation of rHN20-vvIBDV-VP2 revealed the delivery capacity of the FAdV-4 vector and the immunogenicity of its backbone. Besides, the combination of rHN20 and vvIBDV-VP2 further increased the capacity and application availability of the vector. Meanwhile, the seven combinations provided more possibilities for inserting other exogenous antigen genes to develop multivalent vaccines. The FAdV-4 vector developed in the present study protected HHS and successfully delivered exogenous genes against the related diseases.

## CONCLUSION

In conclusion, we systematically identified all ORFs located at both ends of the emerging novel FAdV-4 genome as non-essential genes for virus replication. To further improve the feasibility of FAdV-4 as a vaccine vector, seven combinations of ORFs were successfully replaced with EGFP without affecting the immunogenicity of the vector backbone. Finally, a recombinant rHN20-vvIBDV-VP2 strain expressing the VP2 protein of vvIBDV provided complete protection against the FAdV-4 and vvIBDV challenges, highlighting that the FAdV-4 vector could sufficiently protect against HHS and efficiently deliver the exogenous gene. Overall, these findings systemically identified the non-essential ORFs for FAdV-4 replication and seven foreign gene insertion regions, providing valuable information for an in-depth understanding of virus pathogenesis and the development of multivalent vaccines.

## DATA AVAILABILITY STATEMENT

The original contributions presented in the study are included in the article/supplementary material, further inquiries can be directed to the corresponding author/s.

## ETHICS STATEMENT

The animal study was reviewed and approved by the Ethical and Animal Welfare Committee of HVRI.

## AUTHOR CONTRIBUTIONS

XW conceived and designed the experiments. QP, YuZ, and AL performed the experiments. QP and KL analyzed the data. HC, CL, YaZ, and LG contributed reagents, materials, and analysis tools. QP wrote the manuscript. YG and XQ were involved in the interpretation of the results and critically read the manuscript. All authors contributed to the article and approved the submitted version.

## FUNDING

This study was partly supported by the National Natural Science Foundation of China (32072879), the China Agriculture Research System (CARS-41-G15) and the Natural Science Foundation of Heilongjiang Province (TD2019C003).

## REFERENCES

Arnone, C. M., Polito, V. A., Mastronuzzi, A., Carai, A., Diomedi, F. C., Antonucci, L., et al. (2021). Oncolytic adenovirus and gene therapy with EphA2-BiTE for the treatment of pediatric high-grade gliomas. *J. Immunother. Cancer* 9:e001930.

Baigent, S. J., Petherbridge, L. J., Howes, K., Smith, L. P., Currie, R. J., and Nair, V. K. (2005). Absolute quantitation of Marek's disease virus genome copy number in chicken feather and lymphocyte samples using real-time PCR. *J. Virol. Methods* 123, 53–64. doi: 10.1016/j.jviromet.2004.08.019

Boyle, D. B., and Heine, H. G. (1993). Recombinant fowlpox virus vaccines for poultry. *Immunol. Cell Biol.* 71, 391–397. doi: 10.1038/icb.1993.45

Corredor, J. C., and Nagy, E. (2010). The non-essential left end region of the fowl adenovirus 9 genome is suitable for foreign gene insertion/replacement. *Virus Res.* 149, 167–174. doi: 10.1016/j.virusres.2010.01.014

Davison, A. J., Benkő, M., and Harrach, B. (2003). Genetic content and evolution of adenoviruses. *J. Gen. Virol.* 84, 2895–2908. doi: 10.1099/vir.0.19497-0

François, A., Eterradossi, N., Delmas, B., Payet, V., and Langlois, P. (2001). Construction of avian adenovirus CELO recombinants in cosmids. *J. Virol.* 75, 5288–5301. doi: 10.1128/jvi.75.11.5288-5301.2001

Gao, L., Qi, X., Li, K., Gao, H., Gao, Y., Qin, L., et al. (2011). Development of a tailored vaccine against challenge with very virulent infectious bursal disease virus of chickens using reverse genetics. *Vaccine* 29, 5550–5557. doi: 10.1016/j.vaccine.2011.04.106

Greber, U. F. (2020). Adenoviruses - Infection, pathogenesis and therapy. *FEBS Lett.* 594, 1818–1827. doi: 10.1002/1873-3468.13849

Herold, B. C., Marcellino, D., Marcelin, G., Wilson, P., Burrow, C., and Satlin, L. M. (2002). Herpes simplex virus as a model vector system for gene therapy in renal disease. *Kidney Int.* 61, S3–S8. doi: 10.1046/j.1523-1755.2002.0610s1003.x

Hu, J., Li, G., Xi, W., Cai, L., Rong, M., Li, H., et al. (2021). Development of a subunit vaccine based on fiber2 and hexon against fowl adenovirus serotype 4. *Virus Res.* 305:198552. doi: 10.1016/j.virusres.2021.198552

Jia, Z., Ma, C., Yang, X., Pan, X., Li, G., and Ma, D. (2021). Oral immunization of recombinant Lactococcus lactis and Enterococcus faecalis expressing dendritic cell targeting peptide and Hexon protein of fowl Adenovirus 4 induces protective immunity against homologous infection. *Front. Vet. Sci.* 8:632218. doi: 10.3389/fvets.2021.632218

Lévy, Y., Lacabaratz, C., Ellefsen-Lavoie, K., Stöhr, W., Lelièvre, J. D., Bart, P. A., et al. (2020). Optimal priming of poxvirus vector (NYVAC)-based HIV vaccine regimens for T cell responses requires three DNA injections. Results of the randomized multicentre EV03/ANRS VAC20 Phase I/II Trial. *PLoS Pathog.* 16:e1008522. doi: 10.1371/journal.ppat.1008522

Li, J. X., Hou, L. H., Meng, F. Y., Wu, S. P., Hu, Y. M., Liang, Q., et al. (2017). Immunity duration of a recombinant adenovirus type-5 vector-based Ebola vaccine and a homologous prime-boost immunisation in healthy adults in China: final report of a randomised, double-blind, placebo-controlled, phase 1 trial. *Lancet Glob. Health* 5, e324–e334. doi: 10.1016/s2214-109x(16)30367-9

Li, K., Liu, Y., Liu, C., Gao, L., Zhang, Y., Cui, H., et al. (2016). Recombinant Marek's disease virus type 1 provides full protection against very virulent Marek's and infectious bursal disease viruses in chickens. *Sci. Rep.* 6:39263. doi: 10.1038/srep39263

Li, L., Wang, J., Chen, P., Zhang, S., Sun, J., and Yuan, W. (2018). Pathogenicity and molecular characterization of a fowl adenovirus 4 isolated from chicken associated with IBH and HPS in China. *BMC Vet. Res.* 14:400. doi: 10.1186/s12917-018-1733-4

Liu, Y., Wan, W., Gao, D., Li, Y., Yang, X., Liu, H., et al. (2016). Genetic characterization of novel fowl aviadenovirus 4 isolates from outbreaks of hepatitis-hydropericardium syndrome in broiler chickens in China. *Emerg. Microbes Infect.* 5:e117. doi: 10.1038/emi.2016.115

Mei, C., Xian, H., Blackall, P. J., Hu, W., Zhang, X., and Wang, H. (2020). Concurrent infection of Avibacterium paragallinarum and fowl adenovirus in layer chickens. *Poult. Sci.* 99, 6525–6532. doi: 10.1016/j.psj.2020.09.033

Michou, A. I., Lehrmann, H., Saltik, M., and Cotten, M. (1999). Mutational analysis of the avian adenovirus CELO, which provides a basis for gene delivery vectors. *J. Virol.* 73, 1399–1410. doi: 10.1128/jvi.73.2.1399-1410.1999

Mirzazadeh, A., Grafl, B., Berger, E., Schachner, A., and Hess, M. (2021). Longitudinal serological monitoring of commercial broiler breeders for fowl adenoviruses (FAdVs)-presence of antibodies is linked with virus excretion. *Avian Dis.* 65, 177–187. doi: 10.1637/aviandiseases-D-20-00107

Niu, Y. J., Sun, W., Zhang, G. H., Qu, Y. J., Wang, P. F., Sun, H. L., et al. (2016). Hydropericardium syndrome outbreak caused by fowl adenovirus serotype 4 in China in 2015. *J. Gen. Virol.* 97, 2684–2690. doi: 10.1099/jgv.0.000567

Pan, Q., Liu, L., Gao, Y., Liu, C., Qi, X., Zhang, Y., et al. (2017a). Characterization of a hypervirulent fowl adenovirus 4 with the novel genotype newly prevalent in China and establishment of reproduction infection model of hydropericardium syndrome in chickens. *Poult. Sci.* 96, 1581–1588. doi: 10.3382/ps/pew431

Pan, Q., Yang, Y., Gao, Y., Qi, X., Liu, C., Zhang, Y., et al. (2017b). An inactivated novel genotype fowl adenovirus 4 protects chickens against the hydropericardium syndrome that recently emerged in China. *Viruses* 9:216.

Pan, Q., Yang, Y., Shi, Z., Liu, L., Gao, Y., Qi, X., et al. (2017c). Different dynamic distribution in chickens and ducks of the hypervirulent, novel genotype fowl adenovirus serotype 4 recently emerged in China. *Front. Microbiol.* 8:1005. doi: 10.3389/fmicb.2017.01005

Pan, Q., Wang, J., Gao, Y., Cui, H., Liu, C., Qi, X., et al. (2018). The Natural Large Genomic Deletion Is Unrelated to the Increased Virulence of the Novel Genotype Fowl Adenovirus 4 Recently Emerged in China. *Viruses* 10:494.

Ruan, S., Zhao, J., Yin, X., He, Z., and Zhang, G. (2018). A subunit vaccine based on fiber-2 protein provides full protection against fowl adenovirus serotype 4 and induces quicker and stronger immune responses than an inactivated oil-emulsion vaccine. *Infect. Genet. Evol.* 61, 145–150. doi: 10.1016/j.meegid.2018.03.031

Schachner, A., Matos, M., Grafl, B., and Hess, M. (2018). Fowl adenovirus-induced diseases and strategies for their control - a review on the current global situation. *Avian Pathol.* 47, 111–126. doi: 10.1080/03079457.2017.1385724

Steer, P. A., Kirkpatrick, N. C., O'Rourke, D., and Noormohammadi, A. H. (2009). Classification of fowl adenovirus serotypes by use of high-resolution melting-curve analysis of the hexon gene region. *J. Clin. Microbiol.* 47, 311–321. doi: 10.1128/jcm.01567-08

Sun, W., Leist, S. R., McCroskery, S., Liu, Y., Slamanig, S., Oliva, J., et al. (2020). Newcastle disease virus (NDV) expressing the spike protein of SARS-CoV-2 as a live virus vaccine candidate. *EBioMedicine* 62:103132. doi: 10.1016/j.ebiom.2020.103132

Tatsis, N., and Ertl, H. C. (2004). Adenoviruses as vaccine vectors. *Mol. Ther.* 10, 616–629. doi: 10.1016/j.ymthe.2004.07.013

Taylor, J., Weinberg, R., Languet, B., Desmettre, P., and Paoletti, E. (1988). Recombinant fowlpox virus inducing protective immunity in non-avian species. *Vaccine* 6, 497–503. doi: 10.1016/0264-410x(88)90100-4

Tian, K. Y., Guo, H. F., Li, N., Zhang, Y. H., Wang, Z., Wang, B., et al. (2020). Protection of chickens against hepatitis-hydropericardium syndrome and Newcastle disease with a recombinant Newcastle disease virus vaccine expressing the fowl adenovirus serotype 4 fiber-2 protein. *Vaccine* 38, 1989–1997. doi: 10.1016/j.vaccine.2020.01.006

Tostanoski, L. H., Gralinski, L. E., Martinez, D. R., Schaefer, A., Mahrokhian, S. H., Li, Z., et al. (2021). Protective efficacy of rhesus adenovirus COVID-19 vaccines against mouse-adapted SARS-CoV-2. *J. Virol.* [Epub Online ahead of print]. doi: 10.1128/jvi.00974-21

Wang, J., Zaheer, I., Saleemi, M. K., Qi, X., Gao, Y., Cui, H., et al. (2020). The first complete genome sequence and pathogenicity characterization of fowl adenovirus 11 from chickens with inclusion body hepatitis in Pakistan. *Vet. Microbiol.* 244:108670. doi: 10.1016/j.vetmic.2020.108670

Wei, Z., Liu, H., Diao, Y., Li, X., Zhang, S., Gao, B., et al. (2019). Pathogenicity of fowl adenovirus (FAdV) serotype 4 strain SDJN in Taizhou geese. *Avian Pathol.* 48, 477–485. doi: 10.1080/03079457.2019.1625305

Wu, S., Huang, J., Zhang, Z., Wu, J., Zhang, J., Hu, H., et al. (2021). Safety, tolerability, and immunogenicity of an aerosolised adenovirus type-5 vector-based COVID-19 vaccine (Ad5-nCoV) in adults: preliminary report of an open-label and randomised phase 1 clinical trial. *Lancet Infect. Dis.* [Epub Online ahead of Print]. doi: 10.1016/s1473-3099(21)00396-0

Xia, J., Yao, K. C., Liu, Y. Y., You, G. J., Li, S. Y., Liu, P., et al. (2017). Isolation and molecular characterization of prevalent Fowl adenovirus strains in southwestern China during 2015-2016 for the development of a control strategy. *Emerg. Microbes Infect.* 6:e103. doi: 10.1038/emi.2017.91

Xie, Q., Cao, S., Zhang, W., Wang, W., Li, L., Kan, Q., et al. (2021). A novel fiber-2-edited live attenuated vaccine candidate against the highly pathogenic serotype 4 fowl adenovirus. *Vet. Res.* 52:35. doi: 10.1186/s13567-021-00907-z

Zhang, X., Bo, Z., Meng, C., Chen, Y., Zhang, C., Cao, Y., et al. (2021). Generation and evaluation of recombinant Thermostable Newcastle Disease Virus Expressing the HA of H9N2 Avian Influenza Virus. *Viruses* 13:1606.

Zhang, Y., Liu, A., Wang, Y., Cui, H., Gao, Y., Qi, X., et al. (2021). A single amino acid at residue 188 of the hexon protein is responsible for the pathogenicity of the emerging novel virus fowl adenovirus 4. *J. Virol.* 95:e0060321. doi: 10.1128/jvi.00603-21

**Conflict of Interest:** The authors declare that the research was conducted in the absence of any commercial or financial relationships that could be construed as a potential conflict of interest.

**Publisher's Note:** All claims expressed in this article are solely those of the authors and do not necessarily represent those of their affiliated organizations, or those of the publisher, the editors and the reviewers. Any product that may be evaluated in this article, or claim that may be made by its manufacturer, is not guaranteed or endorsed by the publisher.

*Copyright © 2021 Pan, Zhang, Liu, Cui, Gao, Qi, Liu, Zhang, Li, Gao and Wang. This is an open-access article distributed under the terms of the Creative Commons Attribution License (CC BY). The use, distribution or reproduction in other forums is permitted, provided the original author(s) and the copyright owner(s) are credited and that the original publication in this journal is cited, in accordance with accepted academic practice. No use, distribution or reproduction is permitted which does not comply with these terms.*

frontiers in Microbiology

ORIGINAL RESEARCH
published: 01 December 2021
doi: 10.3389/fmicb.2021.789062

# Structural Analysis on the Severe Acute Respiratory Syndrome Coronavirus 2 Non-structural Protein 13 Mutants Revealed Altered Bonding Network With TANK Binding Kinase 1 to Evade Host Immune System

*Farooq Rashid[1], Muhammad Suleman[2], Abdullah Shah[3], Emmanuel Enoch Dzakah[4], Shuyi Chen[5], Haiying Wang[5] and Shixing Tang[1,5,6]**

*[1] Dermatology Hospital, Southern Medical University, Guangzhou, China, [2] Centre for Biotechnology and Microbiology, University of Swat, Mingora, Pakistan, [3] Department of Biotechnology, Shaheed Benazir Bhutto University, Sheringal, Dir, Pakistan, [4] Department of Molecular Biology and Biotechnology, School of Biological Sciences, College of Agriculture and Natural Sciences, University of Cape Coast, Cape Coast, Ghana, [5] Guangdong Provincial Key Laboratory of Tropical Disease Research, School of Public Health, Southern Medical University, Guangzhou, China, [6] Wenzhou Institute, University of Chinese Academy of Sciences, Wenzhou, China*

Mutations in severe acute respiratory syndrome coronavirus 2 (SARS-CoV-2) have made this virus more infectious. Previous studies have confirmed that non-structural protein 13 (NSP13) plays an important role in immune evasion by physically interacting with TANK binding kinase 1 (TBK1) to inhibit IFNβ production. Mutations have been reported in NSP13; hence, in the current study, biophysical and structural modeling methodologies were adapted to dissect the influence of major mutations in NSP13, i.e., P77L, Q88H, D260Y, E341D, and M429I, on its binding to the TBK1 and to escape the human immune system. The results revealed that these mutations significantly affected the binding of NSP13 and TBK1 by altering the hydrogen bonding network and dynamic structural features. The stability, flexibility, and compactness of these mutants displayed different dynamic features, which are the basis for immune evasion. Moreover, the binding was further validated using the MM/GBSA approach, revealing that these mutations have higher binding energies than the wild-type (WT) NSP13 protein. These findings thus justify the basis of stronger interactions and evasion for these NSP13 mutants. In conclusion, the current findings explored the key features of the NSP13 WT and its mutant complexes, which can be used to design structure-based inhibitors against the SARS-CoV-2 new variants to rescue the host immune system.

**Keywords: SARS-CoV-2, NSP13 mutants, TBK1, protein-protein docking, MD simulations**

OPEN ACCESS

***Edited by:***
*Chunfu Zheng,*
*University of Calgary, Canada*

***Reviewed by:***
*Haitao Hu,*
*University of Texas Medical Branch at Galveston, United States*
*Krishnakumar Devadas,*
*Center for Biologics Evaluation and Research (FDA), United States*

****Correspondence:***
*Shixing Tang*
*tamgshixing@smu.edu.cn*

***Specialty section:***
*This article was submitted to Virology, a section of the journal Frontiers in Microbiology*

***Received:*** *04 October 2021*
***Accepted:*** *29 October 2021*
***Published:*** *01 December 2021*

***Citation:***
*Rashid F, Suleman M, Shah A, Dzakah EE, Chen S, Wang H and Tang S (2021) Structural Analysis on the Severe Acute Respiratory Syndrome Coronavirus 2 Non-structural Protein 13 Mutants Revealed Altered Bonding Network With TANK Binding Kinase 1 to Evade Host Immune System. Front. Microbiol. 12:789062. doi: 10.3389/fmicb.2021.789062*

## INTRODUCTION

Severe acute respiratory syndrome coronavirus 2 (SARS-CoV-2) is the newly emerged virus that causes coronavirus disease 2019 (COVID-19). Its genome contains 5′untranslated region (UTR), 3′UTR, and ORF1a/b that encode 16 non-structural proteins (NSPs), four structural proteins, i.e., spike, envelop, membrane, and nucleocapsid, and nine accessory proteins, which include ORF3a, ORF3b, ORF6, ORF7a, ORF7b, ORF8, ORF9b, ORF9c, and ORF10 (Ribero et al., 2020).

Severe acute respiratory syndrome coronavirus 2 suppresses the immune response of the host during the early phase of infection (Chu et al., 2020). SARS-CoV-2 replicates more efficiently than severe acute respiratory syndrome coronavirus (SARS-CoV) in alveolar macrophages and pneumocytes (both type I and type II) in *ex vivo* lung tissues. Moreover, in the same model, SARS-CoV-2 also suppresses type I/II and III interferons (IFNs). However, more investigations are required on innate immune suppression by SARS-CoV-2, which is associated with viral pathogenesis.

The first line of defense against viral infections, including coronaviruses, is IFN production by the innate immune system. IFN-I production is initiated soon after recognizing pathogen-associated molecular patterns (PAMPs), such as viral mRNA. PAMPs are recognized by retinoic acid-inducible gene 1 (RIG-I) and melanoma differentiation-associated gene 5 (MDA5). When RIG-I and MDA5 are activated, they bind to the CARD domain of mitochondrial antiviral signaling protein (MAVs). When MAVs are activated, they recruit several downstream signaling components to the mitochondria to activate the inhibitors of k-B kinase ε (IKKε) and TANK binding kinase 1 (TBK1), which, in turn, phosphorylate IFN regulatory factor 3 (IRF3) and IRF7. The phosphorylation of IRF3 and IRF7 leads to dimerization and their translocation to the nucleus. Inside the nucleus, they trigger the expression of IFN-1 genes (Sharma et al., 2003; Kawai and Akira, 2007).

The individual protein of SARS-CoV-2 antagonizes IFNβ production by different mechanisms (Lei et al., 2020; Li et al., 2020; Xia et al., 2020; Yuen et al., 2020; Rashid et al., 2021a,b; Vazquez et al., 2021). Among these viral proteins, non-structural protein 13 (NSP13) was found to antagonize IFNβ production by binding to TBK1 to inhibit its phosphorylation and cause decreased activation of IRF3 and IFNβ (Xia et al., 2020; Yuen et al., 2020; Guo et al., 2021; Vazquez et al., 2021).

Severe acute respiratory syndrome coronavirus 2 has undergone various mutations. The mutations produced several variants in different countries. Some of the important variants are called variants of concern (VOCs), including Alpha, Beta, Gamma (P.1), and Delta (B.1.617.2), or variants of interest (VOIs), including Iota (B.1.526), Epsilon (B.1.429/427), Kappa (B.1.617.1), and Mu (Annavajhala et al., 2021; McCallum et al., 2021a,b; Nonaka et al., 2021; Planas et al., 2021). These mutations are responsible for enhanced dissemination, severe clinical outcomes, and increased infectivity of the variants (Chen et al., 2020). These mutations are reported in all viral proteins, including non-structural protein NSP13 (Cao et al., 2021). When compared to the reference strain, Wuhuan-Hu-1 (accession no. NC_045512), the mutations in NSP13 included P77L in Delta (B.1.617.2), Q88H in Iota (B.1.526), D260Y in Epsilon (B.1.429), E341D in Gamma (P.1.1), and M429I in Kappa (B.1.617.1) (Nagy et al., 2021). The mutations P504L and Y541C in NSP13 were important for different disease outcomes (Cao et al., 2021). The function of NSP13 has been reported in several studies to antagonize the production of IFNβ by physically binding to TBK1 and to evade immune response (Lei et al., 2020; Xia et al., 2020; Yuen et al., 2020; Guo et al., 2021; Vazquez et al., 2021). Since various VOIs and VOCs were emerging, we were interested in whether the pathogenesis of these variants might also be contributed by the mutations in NSP13 besides the spike protein in terms of its immune evasion. We were specifically interested in whether these mutations altered the binding efficiencies of NSP13 with TBK1 to antagonize IFNβ production and favor SARS-CoV-2 pathogenesis. In the current study, biophysical and comparative binding approaches were adapted to dissect the roles of NSP13 wild type (WT) and its mutants in the evasion of the immune system through its binding with TBK1. We explored that mutations in NSP13 had higher binding energies compared to the WT. These mutations may therefore justify the basis for stronger interactions with TBK1 and evasion from the immune system.

## METHODOLOGY

### Structural Modeling and Validation

A recently reported crystallized structure of NSP13 was retrieved from UniProt (Magrane and UniProt Consortium, 2011) and subjected to structural modeling of SARS-CoV-2 variants using Chimera v_ software (Goddard et al., 2005). Mutations, including P77L, Q88H, D260Y, E341D, and M429I, were introduced to model the mutant structures based on the structure of NSP13 WT. For structural comparison, each mutant was superimposed on the WT, and the root mean square deviation (RMSD) differences were recorded.

### Protein–Protein Docking

Protein–protein docking (NSP13 WT/ NSP13 mutants) was used to determine the efficiency of binding of NSP13 with the TBK1 human protein. For this purpose, the HDOCK algorithm was used. The docking interface was visualized by using Guru Interface (Xue et al., 2016).

### Molecular Dynamics Simulations

Dynamic behavior analysis of NSP13 WT and its mutants, P77L, Q88H, D260Y, E341D, and M429I, through molecular dynamics (MD) simulation was determined using AMBER20 (Salomon-Ferrer et al., 2013) using FF14SB force field. For system solvation, an OPC water box was used. For neutralization, Na+ ions were added to the system to balancing it (Price and Brooks, 2004). Energy minimization protocol was used to remove bad clashes from the system, and 3,000 cycles were used for conjugate algorithms (Watowich et al., 1988). For six thousand cycles, the steepest descent algorithm was used (Meza, 2010). The system was equilibrated at 1 atm pressure and heated at 300K. Molecular

dynamic simulations were run for 50 ns. Long-range electrostatic integrations, with a cutoff distance of 10.0Å, were treated by the Particle Mesh Ewald algorithm (Salomon-Ferrer et al., 2013). Covalent bonds were treated with the SHAKE algorithm (Kräutler et al., 2001). Amber20 CPPTRAJ package was used to analyze trajectories. Particle Mesh Ewald MD was used to carry out molecular dynamic simulations (Roe and Cheatham, 2013).

## Calculating Binding Free Energy

Actual binding energies were determined for NSP13 WT and NSP13 mutants with TBK1. MM/GBSA approach was used for this purpose, as it is the most acceptable approach for calculating the binding energies of molecular bindings (Khan et al., 2018, 2021b; Ali et al., 2019). GB, SA, vdW, and the electrostatic and free energy of NSP13 WT and NSP13 mutants were calculated (Hou et al., 2011). The equation used to calculate free energy is as follows

$$"\Delta G(\text{bind}) = \Delta G(\text{complex}) - [\Delta G(\text{receptor}) + \Delta G(\text{ligand})]". \text{(i)}$$

$$"G = \text{Gbond} + \text{Gele} + \text{GvdW} + \text{Gpol} + \text{Gnpol}". \quad \text{(ii)}$$

Gbond was bond, while Gele was electrostatic. DvdW means van der waals. Gpol was polarly solvated for free energy, and Gnpol was nonpolar solvated free energy. By using the generalized born (GB) solvent methods, the Gnpol and Gpol were analyzed.

# RESULTS

## Mutant Modeling of Non-structural Protein 13 and Its Superimposition on Non-structural Protein 13 Wild-Type

The accession number for the NSP13 WT sequence was NC_045512. To determine whether NSP13 mutants, compared to their WT counterpart, could affect their interaction with TBK1, mutants P77L, Q88H, D260Y, E341D, and M429I were generated by Chimera (**Figures 1A–F**). The superimposition of these generated mutants followed it on NSP13 WT, and RMSD values were observed. The RMSD differences were substantial for each superimposed structure. Due to mutations in NSP13 WT, the protein conformations and secondary structural elements were altered (**Figure 1G**). Therefore, it was necessary to analyze the binding efficiency of NSP13 mutants with TBK1. Hence, structural approaches, like biophysical simulations and protein–protein docking, were used to determine the impact of these variations on downstream immune evasion.

## Non-structural Protein 13 Wild-Type-TANK Binding Kinase 1 and Non-structural Protein 13 Mutant-TANK Binding Kinase 1 Docking

The role of NSP13 in immune evasion has been well established. NSP13 is physically bound to TBK1 to inhibit the phosphorylation of TBK1 and IRF3 and hence decrease IFNβ production (Xia et al., 2020). Under this scenario, it was indispensable to perform a binding analysis of NSP13 WT and NSP13 mutants with TBK1, and the proteins inside cells interact to regulate many biological processes (Khan et al., 2021a; Rashid et al., 2021b). The binding energies and structural determinants of these interactions are important steps to study the regulations of these processes. Binding affinity, which regulates molecular interactions, determines if the formation of complexes occurs under definite conditions (Smith and Sternberg, 2002). Protein–protein dockings of NSP13 WT and its various mutants were performed using HDOCK so that the level of pathogenicity of different mutants of SARS-CoV-2 could be determined.

The docking score predicted by HDOCK online server was −175 kcal/mol for the TBK1-NSP13 WT complex, and the PDBsum analysis showed that these structures formed three hydrogen bonds, two salt bridges, and 156 non-bonded contacts. The hydrogen bonds between TBK1-NSP13 WT included Arg191–Ser36, Gln17–Asp113, and Thr78–Gly170. However, the residues Arg191–Asp32 and Glu579–Lys584 formed salt bridges (**Figure 2A**).

Delta variant B.1.617.2 was first identified in India in December 2020 and spread to other countries. This variant harbor 10 mutations in spike protein. Since the NSP13 protein was responsible for antagonizing IFNβ production, we explored NSP13 mutations in the Delta variant. Indeed at amino acid position 77, NSP13 was mutated, i.e., P77L. Therefore, we were interested if this mutation could enhance the function of NSP13 in immune evasion and might help delta variants become more pathogenic. We, therefore, determined the docking score for this mutation and compared it to its WT counterpart.

The HDOCK docking score for P77L (TBK1-P77L) was −204 kcal/mol, the substitution of amino acid highly increased the interaction of NSP13 and TBK1, and 10 hydrogen bonds, one salt bridge, and 263 non-bonded contacts were formed (**Figure 2B**). The key residues to form hydrogen bonds were Tyr592–Asn51, Gln588–Gly17, Lys584–Arg22, Tyr406–Thr144, Arg405–Ala140, Arg405–His230, Glu178–Ser191, and Arg228–Lys192. Residues Arg573–Glu168 formed salt bridges. The P77L mutation was found to increase the function of the NSP13 protein by binding to TBK1 more strongly compared to WT. Therefore, it could be deduced that P77L might suppress IFNß production more stringently and make this virus more pathogenic.

The Iota variant (B.1.526) was first detected in the United States of America in November 2020. It has seven mutations in spike protein. Moreover, its NSP13 protein also harbored mutation at amino acid 88, i.e., Q88H. We, therefore, determined if this mutation could enhance the binding of NSP13 with TBK1 compared to WT. We first determined the docking score for this mutation and found that the HDOCK docking score for Q88H (TBK1-Q88H) was −210 kcal/mol. This analysis revealed that three salt bridges and three H-bonds were present. In addition, 210 non-bonded contacts were observed for this mutation. The Q88H mutation was observed to bind more stringently to TBK1 compared to WT. Residues Arg574–Asp483, Glu572–Arg155, and Glu572–His164 formed the salt

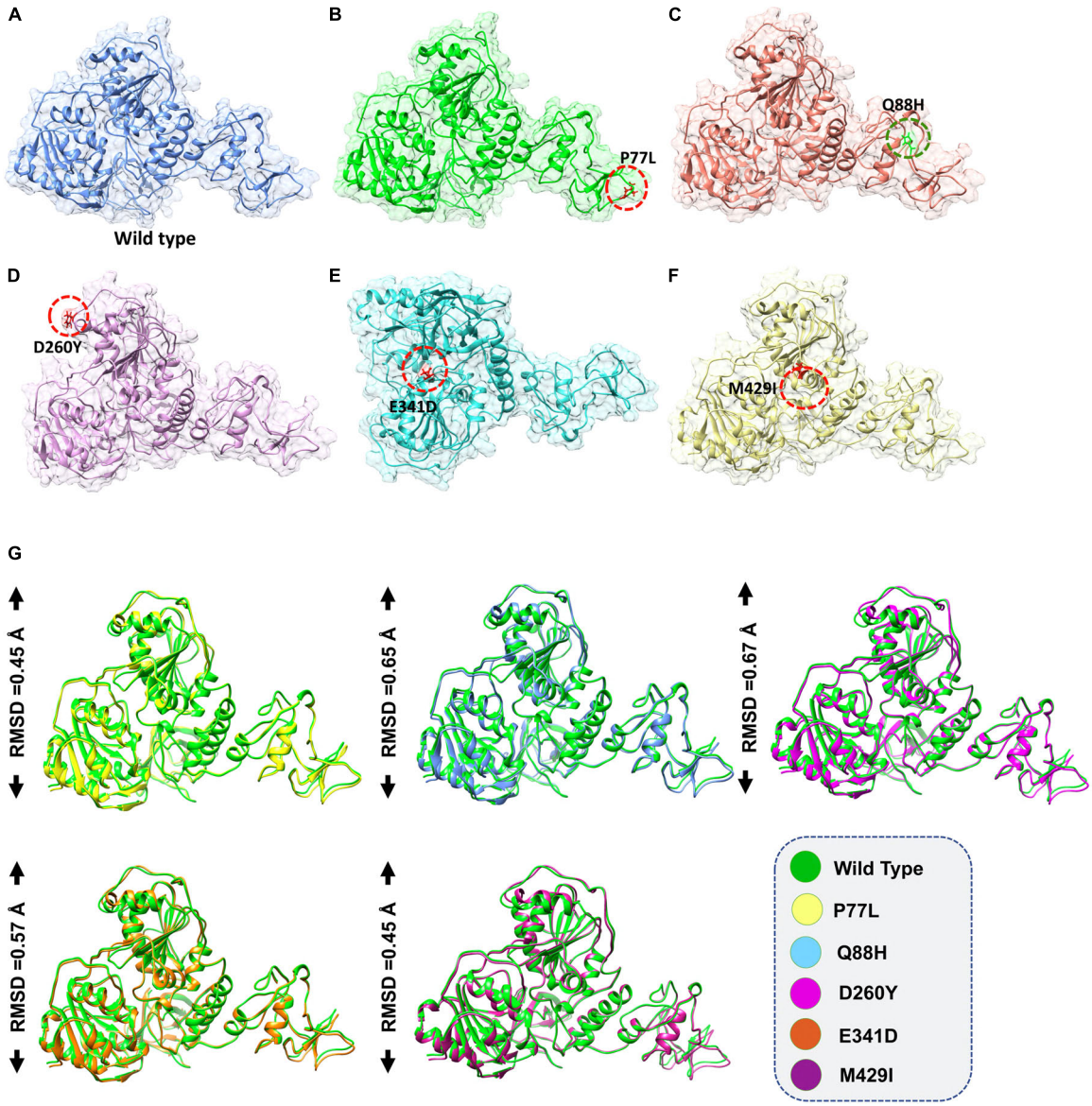


**FIGURE 1 |** Non-structural protein 13 (NSP13) mutant modeling and the superimposition of NSP 13 wild-type (WT) with NSP 13 mutants. **(A)** NSP13 WT, **(B)** P77L, **(C)** Q88H, **(D)** D260Y, **(E)** E341D, and **(F)** M429I. **(G)** Superimposed structure of NSP13 WT (green) with P77L (yellow), Q88H (cyan), D260Y (light magenta), E341D (orange), and M429I (dark magenta). The root mean square deviation (RMSD) values of each superimposition are shown.

bridges. Hydrogen bond-forming residues were Arg80–Arg22, Arg574–Asp483, and Glu572–Arg173 (**Figure 3A**).

In addition, the Epsilon variant (B.1.427/B.1.429) emerged in the United States in June 2020. This variant also has a mutation in NSP13 at position 260, i.e., D260Y. Therefore, we determined the docking score for this mutation and found that the HDOCK docking score for D260Y (TBK1-D260Y) was observed to be −227 kcal/mol. This analysis revealed that one salt bridge and eight H-bonds were present. In addition, 277 non-bonded contacts were observed for this mutation. D260Y mutation enhanced the binding with TBK1. The salt bridge was formed between Arg573-Glu168. The hydrogen bonds were formed between these residues Gln588–Gly17, Lys584–Arg22, Glu178–Ser191, Arg228–Lys192, Tyr406–Thr144, Arg405–His230, and Arg405–Ala140 (**Figure 3B**).

Gamma (P.1) was first identified in Brazil in December 2020. This variant also has a mutation in its NSP13 at amino acid position 341, i.e., E341D. We determined the docking score for this mutation and found that the predicted score of HDOCK for E341D (TBK1-E341D) was −245 kcal/mol. This analysis revealed the presence of five hydrogen bonds. In addition, 260 non-bonded contacts were observed for this mutation. Gln588–Gly17, Arg228–Lys192, Lys584–Arg22, Arg405–His230,

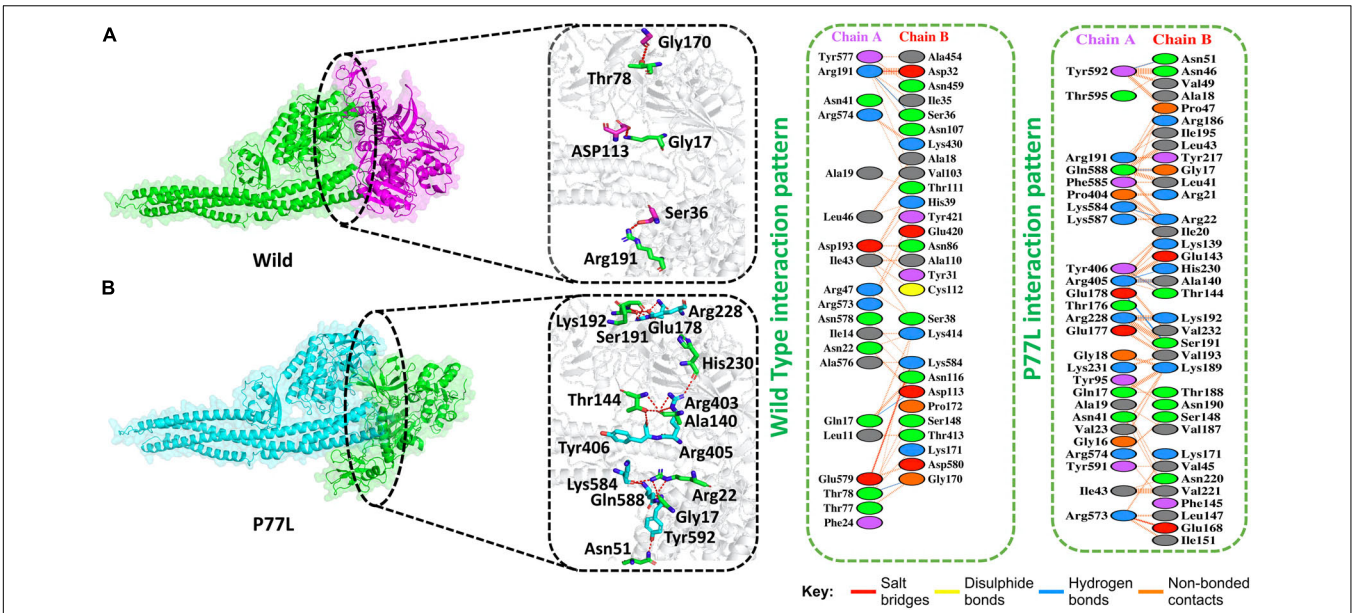


**FIGURE 2 |** Non-structural protein 13 WT and P77L mutant complex docking. **(A)** NSP13 WT and TANK binding kinase 1 (TBK1) key hydrogen bonding interactions with stick representations (left). Hydrogen bonds, non-bonded contacts, and salt bridges are shown by a 2D interaction (right). **(B)** P77L mutant and TBK1 key hydrogen bonding interactions along with their stick representation (left). Hydrogen bonds, non-bonded contacts, and salt bridges are shown by a 2D interaction (right).

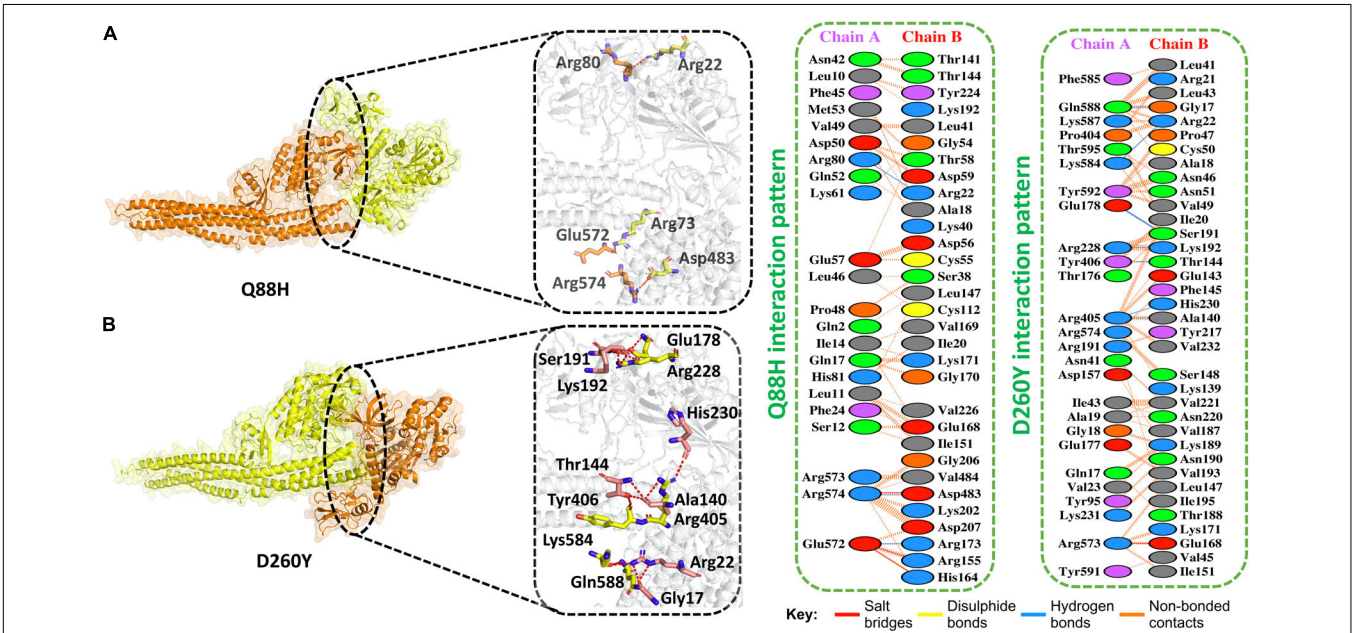


**FIGURE 3 |** Q88H and D260Y mutant complex docking. **(A)** Q88H mutant and TBK1 key hydrogen bonding interactions and representations of bonds by sticks (left). Hydrogen bonds, non-bonded contacts, and salt bridges are shown by a 2D interaction (right). **(B)** D260Y mutant and TBK1 key hydrogen bonding interactions and representations of bonds by sticks (left). Hydrogen bonds, non-bonded contacts, and salt bridges are shown by a 2D interaction (right).

and Tyr592–Asn51 formed hydrogen bonds between TBK1 and E341D mutant (**Figure 4A**).

The Kappa (B.1.617.1) variant was detected in India in December 2020. This variant also has a mutation in its NSP13 at amino acid position 429, i.e., M429I. We determined the docking score for this mutation and found that the HDOCK docking score for M429I (TBK1-M429I) was −229 kcal/M. The replaced amino acids increased the interactions of NSP13 to TBK1 compared to the WT complex. Five hydrogen bonds, one salt bridge, and 215 non-bonded contacts were reported (**Figure 4B**). Gln588–Gly17,

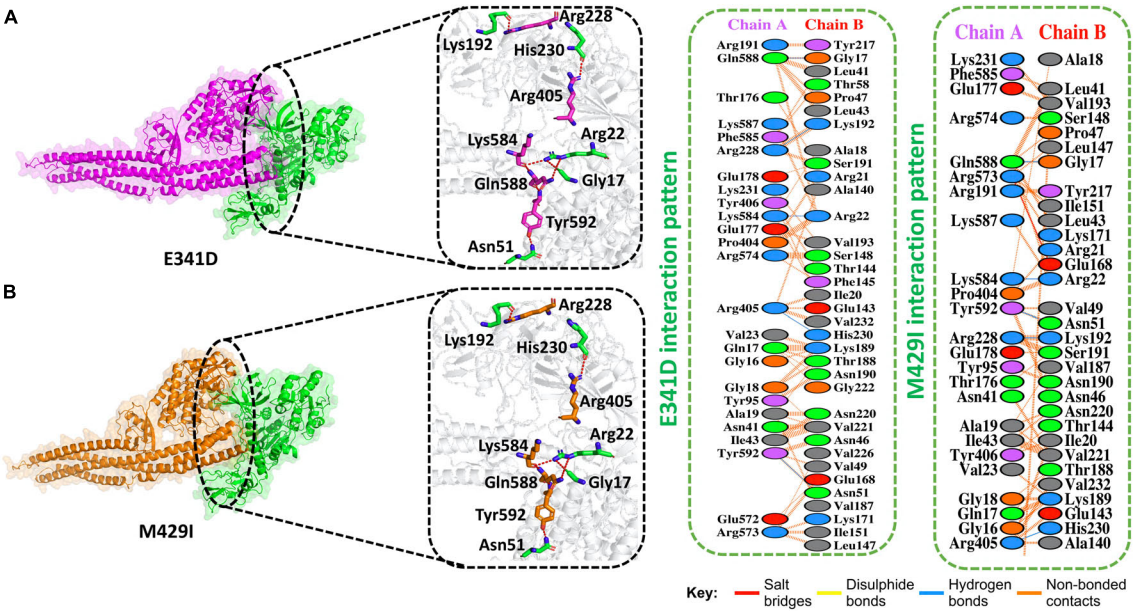


**FIGURE 4 |** E341D and M429I mutant complex docking. **(A)** E341D mutant and TBK1 key hydrogen bonding interactions and stick representations of bonds (left). Salt bridges, hydrogen bonding, and non-bonded interactions are shown by a 2D interaction (right). **(B)** M4291 mutant and TBK1 key hydrogen bonding interactions and stick representations of bonds (left). Salt bridges, hydrogen bonding, and non-bonded interactions are shown by a 2D interaction (right).

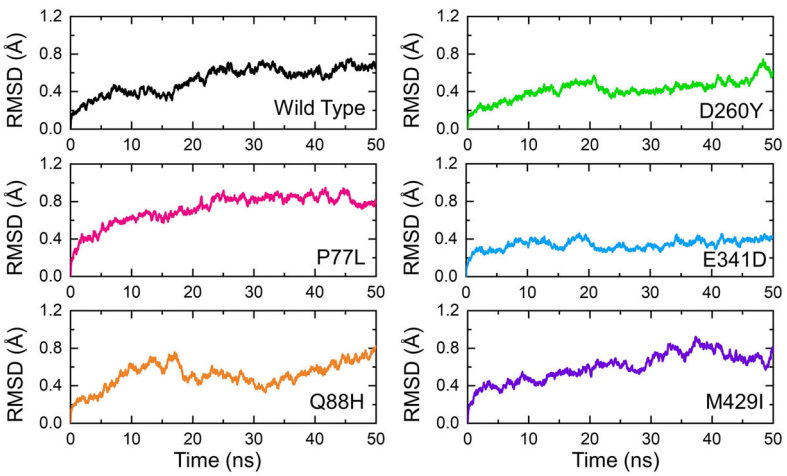


**FIGURE 5 |** Dynamic stability of the NSP13 WT and mutant complexes calculated as RMSD over the simulation time in nanoseconds. The RMSD of NSP13 WT is shown in black. For the mutants, the RMSDs are shown in different colors. RMSDs, root mean square deviations.

Lys584–Arg22, Tyr592–Asn51, Arg228–Lys192, and Arg405–His230 residues formed the hydrogen bonds. Arg573–Glu168 amino acids participated in the salt bridge formation.

## Structural–Dynamic Features of Non-structural Protein 13 Wild-Type and Its Mutant Complexes

Understanding the dynamic features of protein–protein complexes provides a better view of the regulation of different molecular mechanisms of the cell in a coordinated manner. The context of protein–protein interaction in the interpretation of host–pathogen interaction always aids in the comprehension of transmission and mechanism of the pathogenesis of the invader. Many previous studies used the dynamics of molecular machinery to demonstrate the exact mechanism of pathogenesis. In this regard, exploring the structural and dynamic stability of biological macromolecular association provides an understanding of the binding affinity. By employing the dynamic stability equation herein, we estimated the structural stability of each complex as RMSD (**Figure 5**). During the 50-ns simulation, the RMSD of the WT gradually increased over time.

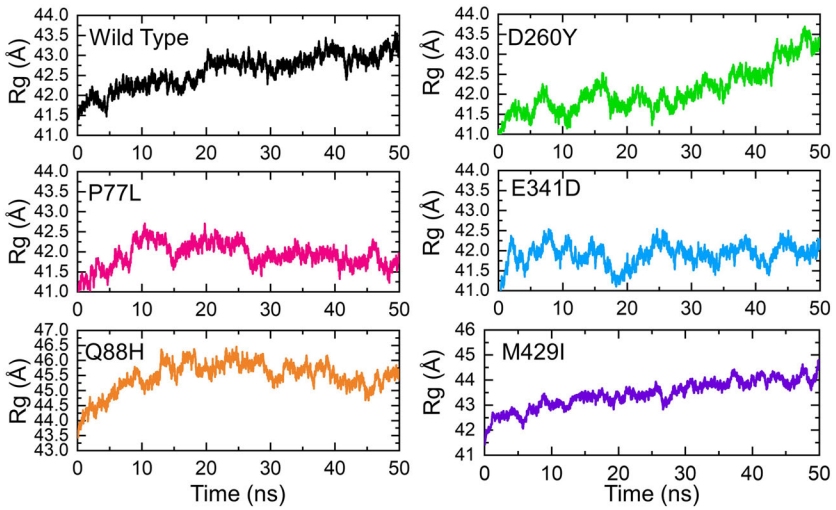


**FIGURE 6 |** Structural compactness of the NSP13 WT and mutant complexes calculated as radius of gyration (Rg) over the simulation time in nanoseconds. The Rg of WT is represented in black, while different colors are used for the mutants. Rg, radius of gyration.

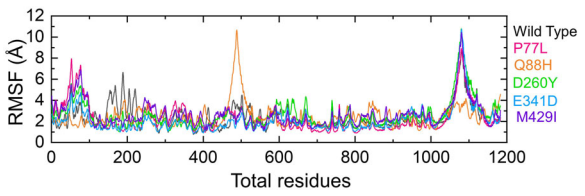


**FIGURE 7 |** Residual flexibility of the NSP13 WT and mutant complexes calculated as root mean square fluctuation (RMSF). The RMSFs of WT are represented in black, while different colors are used for mutants. RMSF, root mean square fluctuation.

The average RMSD observed was 0.3Å during the first 10 ns; however, the RMSD increased onward. During the last 35 ns, the RMSD value then increased further and reached 0.5Å. Minor structural deviations at 22, 28, 35–40, and 46 ns were reported.

On the other hand, the P77L mutant also exhibits a similar pattern of RMSD to the WT. The RMSD increased gradually over the simulation time; however, the structural deviation at different time intervals was minimal. The average root mean square fluctuation (RMSF) was reported to be 0.6Å. Unlike the WT and P77L, the Q88H complex demonstrated a higher structural instability. The RMSD gradually increased between 0 and 10 ns and then abruptly decreased for a short interval between 11 and 15 ns. More structural deviation was observed until 50 ns.

In contrast, D260Y and E341D displayed a more stable dynamic trend than the other complexes. Except for a minor deviation between 20–22 and 46–50 ns, the overall dynamics of the D260Y mutant revealed a very stable behavior, with an average RMSD of 0.3Å. Similarly, with few structural deviations between 15–20, 32–40, and 41–42 ns, the mean RMSD was also reported to be 0.3Å for E341D. Furthermore, the M429I mutant demonstrated similar deviations as the WT, P77L, and Q88H mutant. The average RMSD for M429I was 0.65Å; however, an increasing trend was reported – for instance, a previous study reported that mutations with increasing instability produce the function of radical protein, implying that these mutations have evolved with radical function and have increased infectivity (Hussain et al., 2020).

Next, we calculated the structural compactness of each complex as the radius of gyration (Rg) over the simulation time in nanoseconds. Structural compactness, in a dynamic environment, showed that binding and unbinding events of the interacting partners occurred during the simulation. Herein the Rg of each complex was calculated and shown (**Figure 6**). The WT gradually lost the compactness, and the Rg value increased with time. The average Rg value for the WT was recorded to be 42.5Å. The compactness of P77L was different from the WT. The structural compactness initially decreased during the first 10 ns; however, the Rg value then became flat. The Rg fluctuated between 41.5 and 42.0Å. The Rg increased between 15 and 20 ns and then decreased and remained persistent until 50 ns. The average value for the Q88H was reported to be higher; however, the Rg remained unchanged after 10 ns. The D260Y and M429I demonstrated a similar behavior. The Rg gradually increased, and many fluctuations were observed. The E341D mutant reported lower Rg with continuous increase or decrease in the Rg value during the simulation period. Consequently, this analysis showed that mutations had passed significant binding and unbinding events, which caused structural perturbations at different time intervals. Similar binding and unbinding events for other variants have previously been reported (Khan et al., 2021b).

The RMSF of residues was calculated to estimate the residual flexibility. Understanding the residual flexibility of the system is key to highlighting residues vital in holding the interacting ligand and overall stabilization of the complex. The residual flexibility demonstrated variations in different regions, i.e., 10–100 and 1,000–1,150, for all the complexes except Q88H at the position

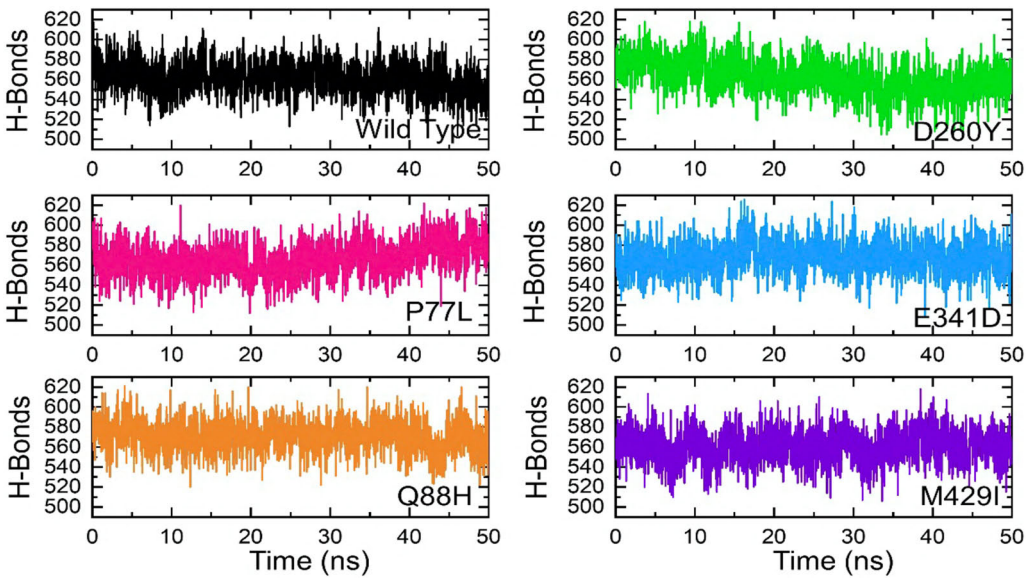


**FIGURE 8 |** Hydrogen bonding of the WT and mutant complexes calculated as a function of time. The H-bonds for WT are shown in black, while for mutants these are shown in different colors.

1,000–1,150. The WT demonstrated different flexibility patterns, in particular in the region between 150 and 200. Similarly, the Q88H exhibited more frequent fluctuations between 480 and 550. Moreover, no significant fluctuation was observed for other mutants except in the region of 1,400–1,500. These results confirmed that the difference in the dynamic flexibility resulted in variable conformational optimization and binding of the interacting proteins as indicated by the RMSF of each complex (**Figure 7**).

The binding variations were further explored through hydrogen bonding analysis as a function of time. The total number of hydrogen bonds was calculated, including the inter- and intra-molecules. The results from 2,500 structural frames revealed that the average number of hydrogen bonds in WT was 554, 583 in P77L, 579 in Q88H, 565 in D260Y, 585 in E341D, and 578 in M429I complex, respectively. The results indicated that significant hydrogen bonding reprogramming took place. The increased bonds in the mutant complexes delineated stronger affinity toward the interacting receptor, which resulted in higher affinity. The hydrogen bond graphs are shown (**Figure 8**).

The strength of a biomolecular association can be determined by estimating the binding affinity of the two interacting macromolecules. Computation of binding free energy using MM/GBSA methods is the most commonly used approach to re-rank docking conformations *via* calculations of structural–dynamic stability, the strength of interacting key hotspots, and total binding energies. The method mentioned above is computationally inexpensive than any other method, i.e., the alchemical free energy calculation method. The MM/GBSA technique is considered more accurate and comprehensive than the conventional scoring functions. Thus, to re-evaluate the binding scores of the WT and mutant complexes, we employed MM/GBSA approach using 2,500 structural frames

**TABLE 1 |** MM/GBSA analysis of the wild-type (WT) and mutant complexes.

| Complex | vdW | ELE | GB | SA | Total |
|---|---|---|---|---|---|
| WT | −139.00 | −280.54 | 361.48 | −16.66 | −74.72 |
| P77L | −190.54 | −211.66 | 340.29 | −22.73 | −84.64 |
| Q88H | −152.51 | −263.89 | 343.95 | −18.91 | −91.36 |
| D260Y | −194.07 | −218.37 | 345.16 | −23.52 | −90.80 |
| E341D | −192.69 | −243.29 | 374.08 | −23.27 | −85.17 |
| M429I | −185.02 | −199.99 | 325.25 | −22.22 | −81.98 |

*vdW, van der waal; ele, electrostatic; GB, polar solvation; and SA, surface area. All the energies are given in kcal/mol.*

(**Table 1**). The binding energies for NSP13 WT and mutant P77L, Q88H, D260Y, E341D, and M429I were −74.72, −84.64, −91.36, −90.80, −85.17, and −81.98 kcal/mol, respectively. The electrostatic interactions mainly guide the higher binding affinity. In conclusion, our findings showed that the mutant complex bound more robustly than WT, thus contributing toward higher infectivity and immune evasion.

## DISCUSSION

The SARS-COV-2 NSP13 protein is well known for its ability to evade the host immune system by binding to TBK1 and inhibiting the phosphorylation of TBK1 and IRF3 from suppressing IFNβ production and signaling. Since several mutations have been observed in NSP13 (Xia et al., 2020; Yuen et al., 2020; Guo et al., 2021; Vazquez et al., 2021), it was necessary to elucidate the effects of different NSP13 mutants on binding with TBK1. Using computational tools, understanding the impact of different mutations is an accurate and traditional approach (Hussain et al., 2020). Computational modeling and simulation approaches were

employed in the current study to dissect the binding of NSP13 mutants with TBK1.

The binding energies and structural determinants of these interactions are important steps to study regulations of protein–protein interactions. Dockings for protein–protein of NSP13 WT and its various mutants were performed using HDOCK. These docking results suggested that the scores for these mutants increased compared to those of WT, suggesting that the binding affinity with TBK1 may increase (**Figures 2–4**). An interaction analysis revealed that the number of hydrogen bonds and salt bridges (except E341D) also increased in these mutants compared to those in WT (**Figures 2–4**). Our results indicated that these mutants might favor a more efficient evasion of the host immune system than WT.

The structural instabilities from minor to large, as shown by RMSD values, were observed (**Figure 5**). However, mutations with increasing instability produced the function of the radical protein, thus implying that these mutations have evolved with radical function and may increase their infectivity (Hussain et al., 2020). Our findings revealed that the WT exhibited a different bonding network and dynamics than the mutants mentioned above. These mutations produced radical function by readjusting the protein topology. Previous mutations with radical functions and decreased stability were also reported to impact the binding and molecular function of the interacting molecules (Wang et al., 2021). These findings also revealed a substantial reprogramming of hydrogen and other bonds, consequently increasing the binding affinity. In addition, these findings were validated by estimating the binding free energy. It was observed that the mutations, in particular Q88H, have a higher binding affinity than WT and even other mutants (**Table 1**).

Similarly, the Q88H exhibited the least fluctuation among all the complexes, except in the region between 480 and 550 (**Figure 7**). However, experimental validations are required for these analyses in the future. It has been shown that NSP13 interacts with TBK1 and inhibits the phosphorylation of IRF3 and TBK1 (Xia et al., 2020). Therefore, it would be interesting to determine the binding of NSP13 mutants experimentally with TBK1 and whether the mutants bind more stringently to TBK1 than WT. Moreover, the differential effects on phosphorylation levels of TBK1 and IRF3 and inhibition of IFNβ production by NSP13 WT and its various mutants could be determined experimentally. Our biochemical data could infer that, compared to WT, various mutants of NSP13 may show more inhibitory effects on IFNβ production; however, experimental validations are indispensable. A mutational study of SARS-CoV-2 variants has revealed the basis for tighter binding and its correlation with infectivity. Moreover, immune evasion has also been revealed through extensive interaction and dynamics studies (Khan et al., 2021a). Therefore, continuous mutational analysis is highly required to determine the disease status and outcomes.

## DATA AVAILABILITY STATEMENT

The raw data supporting the conclusions of this article will be made available by the authors, without undue reservation.

## AUTHOR CONTRIBUTIONS

ST designed the project and edited the manuscript. FR did some analysis and wrote the manuscript. MS and AS did the biophysical and structural analysis. ED, HW, and SC edited the final manuscript. All authors contributed to the article and approved the submitted version.

## FUNDING

This funding was provided by the National Major Science and Technology Project, and the grant numbers are 2017ZX10202101-003, 2018ZX10302103-002, and 2017ZX10202102-003-004.

## REFERENCES

Ali, A., Khan, A., Kaushik, A. C., Wang, Y., Ali, S. S., Junaid, M., et al. (2019). Immunoinformatic and systems biology approaches to predict and validate peptide vaccines against Epstein-Barr virus (EBV). *Sci. Rep.* 9:720. doi: 10.1038/s41598-018-37070-z

Annavajhala, M. K., Mohri, H., Wang, P., Nair, M., Zucker, J. E., Sheng, Z., et al. (2021). Emergence and expansion of SARS-CoV-2 B.1.526 after identification in New York. *Nature* 597, 703–708. doi: 10.1038/s41586-021-03908-2

Cao, C., He, L., Tian, Y., Qin, Y., Sun, H., Ding, W., et al. (2021). Molecular epidemiology analysis of early variants of SARS-CoV-2 reveals the potential impact of mutations P504L and Y541C (NSP13) in the clinical COVID-19 outcomes. *Infect. Genet. Evol.* 92:104831. doi: 10.1016/j.meegid.2021.104831

Chen, J., Wang, R., Wang, M., and Wei, G.-W. (2020). Mutations strengthened SARS-CoV-2 Infectivity. *J. Mol. Biol.* 432, 5212–5226. doi: 10.1016/j.jmb.2020.07.009

Chu, H., Chan, J. F.-W., Wang, Y., Yuen, T. T.-T., Chai, Y., Hou, Y., et al. (2020). Comparative replication and immune activation profiles of SARS-CoV-2 and SARS-CoV in human lungs: an ex vivo study with implications for the pathogenesis of COVID-19. *Clin. Infect. Dis.* 71, 1400–1409. doi: 10.1093/cid/ciaa410

Goddard, T. D., Huang, C. C., and Ferrin, T. E. (2005). Software extensions to UCSF chimera for interactive visualization of large molecular assemblies. *Structure* 13, 473–482. doi: 10.1016/j.str.2005.01.006

Guo, G., Gao, M., Gao, X., Zhu, B., Huang, J., Luo, K., et al. (2021). SARS-CoV-2 non-structural protein 13 (nsp13) hijacks host deubiquitinase USP13 and counteracts host antiviral immune response. *Signal Transduct. Target. Ther.* 6, 2020–2022. doi: 10.1038/s41392-021-00509-3

Hou, T., Wang, J., Li, Y., and Wang, W. (2011). Assessing the performance of the MM/PBSA and MM/GBSA methods. 1. The accuracy of binding free energy calculations based on molecular dynamics simulations. *J. Chem. Inf. Model.* 51, 69–82. doi: 10.1021/ci100275a

Hussain, I., Pervaiz, N., Khan, A., Saleem, S., Shireen, H., Wei, D.-Q., et al. (2020). Evolutionary and structural analysis of SARS-CoV-2 specific evasion of host immunity. *Genes Immun.* 21, 409–419. doi: 10.1038/s41435-020-00120-6

Kawai, T., and Akira, S. (2007). Antiviral signaling through pattern recognition receptors. *J. Biochem.* 141, 137–145. doi: 10.1093/jb/mvm032

Khan, A., Gui, J., Ahmad, W., Haq, I., Shahid, M., Khan, A. A., et al. (2021a). The SARS-CoV-2 B.1.618 variant slightly alters the spike RBD–ACE2 binding affinity and is an antibody escaping variant: a computational structural perspective. *RSC Adv.* 11, 30132–30147. doi: 10.1039/D1RA04694B

Khan, A., Junaid, M., Kaushik, A. C., Ali, A., Ali, S. S., Mehmood, A., et al. (2018). Computational identification, characterization and validation of potential antigenic peptide vaccines from hrHPVs E6 proteins using immunoinformatics and computational systems biology approaches. *PLoS One* 13:e0196484. doi: 10.1371/journal.pone.0196484

Khan, A., Zia, T., Suleman, M., Khan, T., Ali, S. S., Abbasi, A. A., et al. (2021b). Higher infectivity of the SARS-CoV-2 new variants is associated with K417N/T, E484K, and N501Y mutants: an insight from structural data. *J. Cell. Physiol.* 236, 7045–7057. doi: 10.1002/jcp.30367

Kräutler, V., van Gunsteren, W. F., and Hünenberger, P. H. (2001). A fast SHAKE algorithm to solve distance constraint equations for small molecules in molecular dynamics simulations. *J. Comput. Chem.* 22, 501–508. doi: 10.1002/1096-987X(20010415)22:5<501::AID-JCC1021<3.0.CO;2-V

Lei, X., Dong, X., Ma, R., Wang, W., Xiao, X., Tian, Z., et al. (2020). Activation and evasion of type I interferon responses by SARS-CoV-2. *Nat. Commun.* 11:3810. doi: 10.1038/s41467-020-17665-9

Li, J.-Y., Liao, C.-H., Wang, Q., Tan, Y.-J., Luo, R., Qiu, Y., et al. (2020). The ORF6, ORF8 and nucleocapsid proteins of SARS-CoV-2 inhibit type I interferon signaling pathway. *Virus Res.* 286:198074. doi: 10.1016/j.virusres.2020.198074

Magrane, M., and UniProt Consortium (2011). UniProt knowledgebase: a hub of integrated protein data. *Database* 2011:bar009. doi: 10.1093/database/bar009

McCallum, M., Bassi, J., De Marco, A., Chen, A., Walls, A. C., Di Iulio, J., et al. (2021a). SARS-CoV-2 immune evasion by the B.1.427/B.1.429 variant of concern. *Science* 654, 648–654.

McCallum, M., Walls, A. C., Sprouse, K. R., Bowen, J. E., Rosen, L. E., Dang, H. V., et al. (2021b). Molecular basis of immune evasion by the Delta and Kappa SARS-CoV-2 variants. *Science* eabl8506. doi: 10.1101/2021.08.11.455956

Meza, J. C. (2010). Steepest descent. *WIREs Comput. Stat.* 2, 719–722. doi: 10.1002/wics.117

Nagy, Á, Pongor, S., and Gyõrffy, B. (2021). Different mutations in SARS-CoV-2 associate with severe and mild outcome. *Int. J. Antimicrob. Agents* 57:106272. doi: 10.1016/j.ijantimicag.2020.106272

Nonaka, C. K. V., Gräf, T., Barcia, C. A., de, L., Costa, V. F., de Oliveira, J. L., et al. (2021). SARS-CoV-2 variant of concern P.1 (Gamma) infection in young and middle-aged patients admitted to the intensive care units of a single hospital in Salvador, northeast Brazil, February 2021. *Int. J. Infect. Dis* 111, 47–54. doi: 10.1016/j.ijid.2021.08.003

Planas, D., Veyer, D., Baidaliuk, A., Staropoli, I., Guivel-Benhassine, F., Rajah, M. M., et al. (2021). Reduced sensitivity of SARS-CoV-2 variant delta to antibody neutralization. *Nature* 596, 276–280. doi: 10.1038/s41586-021-03777-9

Price, D. J., and Brooks, C. L. (2004). A modified TIP3P water potential for simulation with Ewald summation. *J. Chem. Phys.* 121, 10096–10103. doi: 10.1063/1.1808117

Rashid, F., Dzakah, E. E., Wang, H., and Tang, S. (2021a). The ORF8 protein of SARS-CoV-2 induced endoplasmic reticulum stress and mediated immune evasion by antagonizing production of interferon beta. *Virus Res.* 296:198350. doi: 10.1016/j.virusres.2021.198350

Rashid, F., Suleman, M., Shah, A., Dzakah, E. E., Wang, H., Chen, S., et al. (2021b). Mutations in SARS-CoV-2 ORF8 altered the bonding network with interferon regulatory factor 3 to evade host immune system. *Front. Microbiol.* 12:703145. doi: 10.3389/fmicb.2021.703145

Ribero, M. S., Jouvenet, N., Dreux, M., and Nisole, S. (2020). Interplay between SARS-CoV-2 and the type I interferon response. *PLoS Pathog.* 16:e1008737. doi: 10.1371/journal.ppat.1008737

Roe, D. R., and Cheatham, T. E. (2013). PTRAJ and CPPTRAJ: software for processing and analysis of molecular dynamics trajectory data. *J. Chem. Theory Comput.* 9, 3084–3095. doi: 10.1021/ct400341p

Salomon-Ferrer, R., Götz, A. W., Poole, D., Le Grand, S., and Walker, R. C. (2013). Routine microsecond molecular dynamics simulations with AMBER on GPUs. 2. explicit solvent particle mesh Ewald. *J. Chem. Theory Comput.* 9, 3878–3888. doi: 10.1021/ct400314y

Sharma, S., TenOever, B. R., Grandvaux, N., Zhou, G.-P., Lin, R., and Hiscott, J. (2003). Triggering the interferon antiviral response through an IKK-related pathway. *Science* 300, 1148–1151. doi: 10.1126/science.1081315

Smith, G. R., and Sternberg, M. J. E. (2002). Prediction of protein–protein interactions by docking methods. *Curr. Opin. Struct. Biol.* 12, 28–35. doi: 10.1016/S0959-440X(02)00285-3

Vazquez, C., Swanson, S. E., Negatu, S. G., Dittmar, M., Miller, J., Ramage, H. R., et al. (2021). SARS-CoV-2 viral proteins NSP1 and NSP13 inhibit interferon activation through distinct mechanisms. *PLoS One* 16:e0253089. doi: 10.1371/journal.pone.0253089

Wang, R., Chen, J., Gao, K., Hozumi, Y., Yin, C., and Wei, G.-W. (2021). Analysis of SARS-CoV-2 mutations in the United States suggests presence of four substrains and novel variants. *Commun. Biol.* 4:228. doi: 10.1038/s42003-021-01754-6

Watowich, S. J., Meyer, E. S., Hagstrom, R., and Josephs, R. (1988). A stable, rapidly converging conjugate gradient method for energy minimization. *J. Comput. Chem.* 9, 650–661. doi: 10.1002/jcc.540090611

Xia, H., Cao, Z., Xie, X., Zhang, X., Chen, J. Y. C., Wang, H., et al. (2020). Evasion of Type I interferon by SARS-CoV-2. *Cell Rep.* 33:108234. doi: 10.1016/j.celrep.2020.108234

Xue, L. C., Rodrigues, J. P., Kastritis, P. L., Bonvin, A. M., and Vangone, A. (2016). PRODIGY: a web server for predicting the binding affinity of protein-protein complexes. *Bioinformatics* 32, 3676–3678. doi: 10.1093/bioinformatics/btw514

Yuen, C. K., Lam, J. Y., Wong, W. M., Mak, L. F., Wang, X., Chu, H., et al. (2020). SARS-CoV-2 nsp13, nsp14, nsp15 and orf6 function as potent interferon antagonists. *Emerg. Microbes Infect.* 9, 1418–1428. doi: 10.1080/22221751.2020.1780953

**Conflict of Interest:** The authors declare that the research was conducted in the absence of any commercial or financial relationships that could be construed as a potential conflict of interest.

**Publisher's Note:** All claims expressed in this article are solely those of the authors and do not necessarily represent those of their affiliated organizations, or those of the publisher, the editors and the reviewers. Any product that may be evaluated in this article, or claim that may be made by its manufacturer, is not guaranteed or endorsed by the publisher.

*Copyright © 2021 Rashid, Suleman, Shah, Dzakah, Chen, Wang and Tang. This is an open-access article distributed under the terms of the Creative Commons Attribution License (CC BY). The use, distribution or reproduction in other forums is permitted, provided the original author(s) and the copyright owner(s) are credited and that the original publication in this journal is cited, in accordance with accepted academic practice. No use, distribution or reproduction is permitted which does not comply with these terms.*

frontiers in Microbiology

ORIGINAL RESEARCH
published: 14 December 2021
doi: 10.3389/fmicb.2021.795047

# The HBV Core Protein and Core Particle Both Bind to the PPIase Par14 and Par17 to Enhance Their Stabilities and HBV Replication

*Umar Saeed[1,2], Zahra Zahid Piracha[1,2], Hyeonjoong Kwon[1,2], Jumi Kim[1,2], Fadia Kalsoom[1,2], Yong-Joon Chwae[1,2], Sun Park[1,2], Ho-Joon Shin[1,2], Hyun Woong Lee[3], Jin Hong Lim[4] and Kyongmin Kim[1,2]**

[1]Department of Microbiology, Ajou University School of Medicine, Suwon, South Korea, [2]Department of Biomedical Science, Graduate School of Ajou University, Suwon, South Korea, [3]Department of Internal Medicine, Gangnam Severance Hospital, Yonsei University College of Medicine, Seoul, South Korea, [4]Department of General Surgery, Gangnam Severance Hospital, Yonsei University College of Medicine, Seoul, South Korea

OPEN ACCESS

**Edited by:**
*Douglas Paul Gladue, United States Department of Agriculture, United States*

**Reviewed by:**
*Xupeng Hong, The Pennsylvania State University, United States*
*Lin Deng, Kobe University, Japan*

***Correspondence:**
*Kyongmin Kim*
*kimkm@ajou.ac.kr*

**Specialty section:**
*This article was submitted to Virology, a section of the journal Frontiers in Microbiology*

**Received:** *14 October 2021*
**Accepted:** *17 November 2021*
**Published:** *14 December 2021*

**Citation:**
*Saeed U, Piracha ZZ, Kwon H, Kim J, Kalsoom F, Chwae Y-J, Park S, Shin H-J, Lee HW, Lim JH and Kim K (2021) The HBV Core Protein and Core Particle Both Bind to the PPIase Par14 and Par17 to Enhance Their Stabilities and HBV Replication. Front. Microbiol. 12:795047. doi: 10.3389/fmicb.2021.795047*

We recently reported that the PPIase Par14 and Par17 encoded by *PIN4* upregulate HBV replication in an HBx-dependent manner by binding to conserved arginine–proline (RP) motifs of HBx. HBV core protein (HBc) has a conserved $^{133}$RP$^{134}$ motif; therefore, we investigated whether Par14/Par17 bind to HBc and/or core particles. Native agarose gel electrophoresis (NAGE) and immunoblotting and co-immunoprecipitation were used. Chromatin immunoprecipitation from HBV-infected HepG2-hNTCP-C9 cells was performed. NAGE and immunoblotting revealed that Par14/Par17 bound to core particles and co-immunoprecipitation revealed that Par14/Par17 interacted with core particle assembly-defective, and dimer-positive HBc-Y132A. Thus, core particles and HBc interact with Par14/Par17. Par14/Par17 interacted with the HBc $^{133}$RP$^{134}$ motif possibly *via* substrate-binding E46/D74 and E71/D99 motifs. Although Par14/Par17 dissociated from core particles upon heat treatment, they were detected in 0.2 N NaOH-treated opened-up core particles, demonstrating that Par14/Par17 bind outside and inside core particles. Furthermore, these interactions enhanced the stabilities of HBc and core particles. Like HBc-Y132A, HBc-R133D and HBc-R133E were core particle assembly-defective and dimer-positive, demonstrating that a negatively charged residue at position 133 cannot be tolerated for particle assembly. Although positively charged R133 is solely important for Par14/17 interactions, the $^{133}$RP$^{134}$ motif is important for efficient HBV replication. Chromatin immunoprecipitation from HBV-infected cells revealed that the S19 and E46/D74 residues of Par14 and S44 and E71/D99 residues of Par17 were involved in recruitment of $^{133}$RP$^{134}$ motif-containing HBc into cccDNA. Our results demonstrate that interactions of HBc, Par14/Par17, and cccDNA in the nucleus and core particle–Par14/Par17 interactions in the cytoplasm are important for HBV replication.

**Keywords: Hepatitis B virus, HBV replication study, PPIase activity, parvulin 14, parvulin 17**

## INTRODUCTION

HBV is a prototype virus in the *Hepadnaviridae* family with a partially double-stranded, relaxed-circular (RC) DNA genome that shows exclusive tropism for hepatocytes (Seeger and Mason, 2015) HBV infection causes acute hepatitis, which can lead to chronic hepatitis B, liver fibrosis, cirrhosis, and hepatocellular carcinoma (Seeger and Mason, 2015). Currently available treatments cannot cure HBV infection (Cornberg and Manns, 2018; Revill et al., 2019). In total, 257 million people are living with chronic hepatitis B (World Health Organization Gobal Heptatitis report, 2017).

HBV infects hepatocytes by binding to heparan sulfate, followed by the sodium taurocholate cotransporting polypeptide (SLC10A1 or NTCP) receptor (Yan et al., 2012). Incoming core particle (capsid or nucleocapsid) moves to the nuclear pore complex and releases its genome into the nucleus. There, the polymerase-bound RC DNA genome is converted to covalently closed circular DNA (cccDNA) *via* several host proteins (Diab et al., 2018; Mohd-Ismail et al., 2019). The cccDNA minichromosome serves as a template for transcription of viral genes. The episomal cccDNA contains four overlapping open reading frames, which transcribe 3.5 kb pregenomic RNA (pgRNA) encoding HBc (core) and polymerase proteins, 2.4 and 2.1 kb S mRNAs producing large, middle, and small surface (HBs) proteins, and 0.7 kb X mRNA encoding HBx protein (Ganem, 2001; Hu and Seeger, 2015; Seeger and Mason, 2015).

The 21 KDa HBc protein consists of 183 and 185 amino acids in the ayw and adw subtypes, respectively, and has three domains, namely, the N-terminal domain (NTD) (Birnbaum and Nassal, 1990), linker domain (Watts et al., 2002), and C-terminal domain (CTD; Birnbaum and Nassal, 1990). The NTD (140 amino acids) is critical and sufficient for core particle assembly (Gallina et al., 1989; Birnbaum and Nassal, 1990). The linker domain (nine amino acids) performs critical roles during multiple stages of HBV replication (Liu et al., 2018). The CTD (34 [ayw] or 36 [adw] amino acids) is dispensable for capsid assembly, but plays important roles in pgRNA packaging and reverse transcription (Yu and Summers, 1991; Nassal, 1992; Köck et al., 2004; Jung et al., 2012). Through post-translational modifications of the CTD, HBc plays versatile roles in multiple stages of the HBV life cycle, including core particle assembly, reverse transcription, modulation of cccDNA transcription *via* epigenetic regulation (Jung et al., 2014; Zlotnick et al., 2015; Diab et al., 2018). HBc has reemerged as a promising anti-HBV target (Venkatakrishnan and Zlotnick, 2016; Xie et al., 2017; Diab et al., 2018).

Crystallography of C-terminally truncated HBc protein demonstrated that it contains five α-helices, among which helices 3 and 4 form an α-helical hairpin structure (Wynne et al., 1999). The α-helical hairpin further assembles into dimers and forms a four-helix bundle. Afterward, the trimers of dimers further assemble into hexamers to form HBV core particles (Birnbaum and Nassal, 1990). The HBV core particle is assembled *via* dimeric intermediates of HBc (Hatton et al., 1992; Bourne et al., 2009) and is thus composed of 90 or 120 HBc dimers depending on whether T = 3 or T = 4, respectively (Zlotnick et al., 1996).

The core particle incorporates pgRNA and polymerase containing reverse transcriptase and facilitates synthesis of DNA. The core particle with RC DNA is subsequently enveloped by HBs proteins as infectious virion (Hu and Seeger, 2015; Zlotnick et al., 2015; Venkatakrishnan and Zlotnick, 2016) or alternatively trafficked back to the nucleus and maintains the cccDNA pool (Ko et al., 2018).

Peptidyl-prolyl cis/trans isomerases (PPIases) regulate protein folding and functions by inducing cis/trans isomerization of target proteins (Göthel and Marahiel, 1999; Lu et al., 2007). There are four families of PPIases, namely, cyclophilins, FK506-binding proteins, parvulins, and protein Ser/Thr phosphatase 2A activator (Lu et al., 2007). Among parvulins, the *PIN1* gene encodes the PPIase NIMA-interacting 1 (Pin1) protein, while the *PIN4* gene encodes the Par14 and Par17 proteins (Lu et al., 1996; Rulten et al., 1999; Mueller et al., 2006). Par14/Par17 regulate cell cycle progression, chromatin remodeling, ribosomal RNA processing, and tubulin polymerization (Thiele et al., 2011; Saningong and Bayer, 2015; Matena et al., 2018).

We recently reported that Par14/Par17 are involved in the HBV life cycle. They are recruited to the HBV cccDNA and thereby augment HBV RNA transcription and DNA synthesis in an HBx-dependent manner (Saeed et al., 2019). Considering the importance of the RP motifs of HBx for Par14/Par17–HBx interactions in HBV replication (Saeed et al., 2019), we asked whether the RP motif of HBc is critical for its interaction with Par14/Par17 and HBV replication. Here, we found that Par14/Par17 are bona-fide binding partners of both HBc and the core particle. The Par14/Par17–HBc and/or –core particle interactions improved the stabilities of HBc and core particles. Similar to HBx–Par14/Par17–cccDNA interactions in the nucleus (Saeed et al., 2019), Par14/Par17 can directly bind to cccDNA, simultaneously associate with HBc, and promote HBV replication from cccDNA *via* transcriptional activation.

## MATERIALS AND METHODS

### Vector Construction

The human NTCP-C9 construct, pCDH-hNTCP-C9, was previously described (Piracha et al., 2018, 2020; Saeed et al., 2019) and generated by inserting hNTCP-C9 into pcDNA6.1 (a kind gift from Dr. Li W; Yan et al., 2012). The pCMV-3 × FLAG-tagged Par14 WT, -Par17 WT, -Par14-E46A/D74A, and -Par17-E71A/D99A constructs and short hairpin RNAs (shPIN4-#1, shPIN4-#5, and shControl) in pLK0.1 were described previously (Saeed et al., 2019). To construct Myc-tagged HBc WT, PCR-amplified HBc DNA (**Table 1**) was digested with *Msc*I and *Kpn*I and inserted into the

**Abbreviations:** HBV, hepatitis B virus; PPIase, peptidyl-prolyl cis/trans isomerases; Par14, parvulin 14; Par17, parvulin 17; NAGE, native agarose gel electrophoresis; cccDNA, covalently closed circular DNA; SDS-PAGE, sodium dodecyl sulfate polyacrylamide gel electrophoresis; ChIP, chromatin immunoprecipitation; NIRF, Np95/ICBP90-like RING finger protein; PRMT5, protein arginine methyltransferase 5; CREB, cAMP response element-binding protein.

**TABLE 1** | Primers used in this study.

| | Plasmid | | Sequence (5′-3′) |
|---|---|---|---|
| HBc | Myc-HBc | F | CTTATGGCCACGGACATTGACCCT |
| | | R | ATTGGTACCCTAACATTGAGATT |
| HBc mutants | HBc-Y132A | F | CTC CTC CAG CC*G C*TA GAC CAC CAA A |
| | | R | TTT GGT GGT CTA *GC*G GCT GGA GGA G |
| | HBc-R133A | F | ACT CCT CCA GCC TAT *GC*A CCA CCA AAT GCC CCT |
| | | R | AGG GGC ATT TGG TGG T*GC* ATAGGCTGGAGGAGT |
| | HBc-R133D | F | ACT CCT CCA GCC TAT *GAT* CCA CCA AAT GCC CCT |
| | | R | AGG GGC ATT TGG TGG *ATC* ATA GGC TGG AGG AGT |
| | HBc-R133E | F | ACT CCT CCA GCC TAT *GAA* CCA CCA AAT GCC CCT |
| | | R | AGG GGC ATT TGG TGG T*TC* ATA GGC TGG AGG AGT |
| | HBc-R133K | F | ACT CCT CCA GCC TAT *AA*A CCA CCA AAT GCC CCT |
| | | R | AGG GGC ATT TGG TGG T*TT* ATA GGC TGG AGG AGT |
| | HBc-R133L | F | CCT CCA GCC TAT *CT*A CCA CCA AAT GCC |
| | | R | GGC ATT TGG TGG T*AG* ATA GGC TGG AGG |
| | HBc-R133H | F | CCT CCA GCC TAT *CAT* CCA CCA AAT GCC |
| | | R | GGC ATT TGG TGG *ATG* ATA GGC TGG AGG |
| | HBc-P134A | F | CCA GCC TAT AGA *G*CA CCA AAT GCC CCT |
| | | R | AGG GGC ATT TGG TG*C* TCT ATA GGC TGG |
| | HBc-AAP | F | CCT CCA GCC TAT *GC*A *G*CA CCA AAT GCC |
| | | R | GGC ATT TGG TG*C* T*GC* ATA GGC TGG AGG |
| | HBc-RAA | F | CCA GCC TAT AGA *G*CA *G*CA AAT GCC CCT ATC |
| | | R | GAT AGG GGC ATT TG*C* TG*C* TCT ATA GGC TGG |
| | HBc-AAA | F | CCT CCA GCC TAT *GC*A *G*CA *G*CA AAT GCC CCT |
| | | R | AGG GGC ATT TG*C* TG*C* T*GC* ATA GGC TGG AGG |
| | pPB X def-1 | F | CAT CGT TTC C*T*T GGC TGC TAG GTT GTA CTG |
| | | R | CTA GCA GCC A*A*G GAA ACG ATG TAT AT |
| | pPB X def-2 | F | CTC TGC ACG TTG C*T*T GGA GAC CAC CGT G |
| HBc- and HBx- deficient HBV constructs | | R | CAC GGT GGT CTC CA*A* GCA ACG TGC AGA G |
| | pPB X def-3 | F | CTT GGA CTC CCA GCA *T*TG TCA ACG ACC GAC |
| | | R | GTC GGT CGT TGA CA*A* TGC TGG GAG TCC AAG |
| | HBc- and HBx- deficient | F | GAC CCT TAT AAA *T*AA TTT GGA GCT ACT GTG |
| HBV-HBc RP mutant | | R | GTA GCT CCA AAT T*A*T TTA TAA GGG TCA ATG TC |
| | HBV-HBc-AAP | F | CATCAAGTGTATCATATGCCAAGTACGC |
| | | R | CAAGAATATGGTGACCCGCAAAATGATG |
| | cccDNA | F | CTCCCCGTCTGTGCCTTCT |
| | | R | GCCCCAAAGCCACCCAAG |
| | Actin | F | CATGTACGTTGCTATCCAGGC |
| | | R | CTCCTTAATGTCACGCACGAT |

*1. F, forward; R, reverse.*

linearized pCMV-Myc vector (Addgene #631604), yielding Myc-HBc WT. Using the mutagenic primers listed in **Table 1**, the respective *Msc*I/*Kpn*I-digested PCR products were inserted into the pCMV-Myc vector, yielding pCMV-Myc-HBc-Y132A (TAT → GCT), -R133A (AGA → GCA), -R133D (AGA → GAT), −R133E (AGA → GAA), -R133K (AGA → AAA), −R133L (AGA → CTA), -R133H (AGA → CAT), -P134A (CCA → GCA), -AAP (AGACCA→ GCAGCA), −RAA (CCACCA→GCAGCA), and -AAA (AGACCACCA→GCAGCAGCA). The HBV WT subtype adwR9 in pcDNA3.1 (Invitrogen), designated pPB, in which pgRNA transcription is under the control of the CMV IE promoter, was previously described (Kim et al., 2004). The HBc-deficient HBV construct with a stop codon (TAA) at amino acid 8 of HBc (Jung et al., 2012) and the HBx-deficient HBV construct with three ATG codons changed to TTG were generated using the pPB construct and described previously (**Table 1**; Yoon et al., 2011). HBc-deficient mutant HBV was generated using the HBx-deficient mutant HBV construct (**Table 1**), yielding the double-deficient HBc-HBx-deficient HBV construct. To generate the HBV construct with HBc-AAP, PCR-amplified HBc-AAP DNA (**Table 1**) was digested with *Nde*I/*BsTe*II and ligated into the *Nde*I/*BsTe*II-digested pPB construct, yielding the HBV-HBc-AAP mutant. All constructs generated by site-directed mutagenic PCR were sequenced to confirm the presence of specific mutations and the absence of extraneous mutations.

## Cell Culture and DNA Transfection

Huh7, HepG2, HepG2-hNTCP-C9, HepAD38, and HEK293T cells were maintained in Dulbecco's modified Eagle's medium supplemented with 10% fetal bovine serum (Gibco BRL) and 1% penicillin–streptomycin in a humidified atmosphere (at 37°C in 5% $CO_2$), and passaged as described previously (Saeed et al., 2019). For transfection of Huh7 or HepG2 cells, 4 µg of the plasmid construct was mixed with 12 µg/µl polyethylenimine (PEI, Polysciences) and 200 µl of Opti-MEM (Gibco) and added to $2 \times 10^6$ cells in a 6 cm plate at 24 h after seeding. For co-transfection, 4 µg of 3×FLAG-Par14/Par17 WT or mutants plus 4 µg of Myc-HBc WT or mutants were mixed with 24 µg/µl PEI and 200 µl of Opti-MEM and the mixtures were added to cells as described above. For quadruple transfection, 3 µg of the HBc-HBx-deficient construct plus 3 µg of 3×FLAG-Par14/Par17 WT or mutants plus 3 µg of Myc-HBc WT or Myc-HBc-AAP plus 3 µg of Myc-HBx WT or Myc-HBx-AAAA were mixed with 24 µg/µl PEI and 200 µl of Opti-MEM and the mixtures were added to cells as described above. To ensure the same amount of DNA was transfected in each experimental setup, the amount of DNA was adjusted using the pCMV empty vector.

## Establishment of Stable Cell Lines

HepG2-hNTCP-C9 stable cells were generated as described previously (Nkongolo et al., 2014; Piracha et al., 2018, 2020; Saeed et al., 2019). The lentiviral vector system was used to generate Huh7, HepG2, and HepG2-hNTCP-C9-derived *PIN4* KD cells as described previously (Saeed et al., 2019). HepG2-hNTCP-C9 cells stably overexpressing Par14 or Par17 were described previously (Saeed et al., 2019).

## HBc Amino Acid Sequence Alignment

The following HBc amino acid sequences were randomly selected from the National Center for Biotechnology Information gene database: 10 (A–J) human HBV genotypes; other mammalian hepadnaviruses including chimpanzee HBV, ground squirrel hepatitis virus, orangutan HBV, woodchuck hepatitis virus, and woolly monkey HBV; and avian hepadnaviruses, such as duck HBV, heron HBV, ross goose HBV, snow goose HBV, and stork HBV. The HBc amino acid sequences were fed into the CLC Main Workbench 8 software (CLC Main Workbench 21.0 software, 2021) to generate representative consensus sequences and conservation graphs.

## Core Particle Immunoblotting, SDS-Page, and Western Blotting

Cells were lysed using 0.2% NP-40 (IGEPAL, Sigma-Aldrich)-TNE buffer (10 mM Tris–HCl [pH 8.0], 50 mM NaCl, and 1 mM EDTA) as described previously (Kim et al., 2004). Equal quantities of cell lysates measured by the Bradford assay were subjected to 13.5% SDS-PAGE. For reducing SDS-PAGE, sample buffer containing 125 mM Tris–HCl, pH 6.8, 20% glycerol, 4% SDS, 0.1% bromophenol blue, and 5% β-mercaptoethanol was used (Cold Spring Harbor Laboratory, 2015a). For non-reducing PAGE, sample buffer was as described above except that 5% β-mercaptoethanol was omitted (Cold Spring Harbor Laboratory, 2015b). To analyze core particles by immunoblotting, 4% of total lysates were electrophoresed in 1% native agarose gels. To analyze Par14/Par17 binding to core particles, lysates of Huh7 cells co-transfected with 3×FLAG-Par14/Par17 plus Myc-HBc were prepared at 72 h post-transfection. To detach Par14/Par17 binding outside the core particle, lysates were heated at 65°C for 2 h. Core particles were precipitated with 6% PEG (Kim et al., 2004), washed with 0.2% NP-40-TNE buffer to thoroughly remove Par14/Par17 detached from core particles. Thereafter, core particles were pelleted with 6% PEG, re-suspended in TNE buffer, and subjected to SDS-PAGE plus immunoblotting and NAGE plus immunoblotting. To detect Par14/Par17 proteins inside the core particle, core particles transferred to the PVDF membrane were treated with 0.2% NaOH for 40 s to open-up core particles and UV-crosslinked. By doing so, Par14/Par17 proteins inside the core particle could be detected by immunoblotting with mouse monoclonal anti-FLAG M2 (1:1,000, Sigma #F1804), rabbit monoclonal anti-PIN4 (1:1,000, Abcam #ab155283), and rabbit polyclonal anti-HBc (1:1,000, generated in-house) antibodies (Jung et al., 2012). Resolved proteins or core particles transferred to PVDF membranes were incubated overnight with primary antibodies (anti-FLAG, anti-PIN4, anti-HBc, and rabbit polyclonal anti-Myc [1:1,000, Santa Cruz Biotech #sc-789]; mouse monoclonal anti-GAPDH [1:5,000, Santa Cruz #sc-32233]; or rabbit polyclonal anti-H3 [1:5,000, Abcam #ab1791]), followed by an anti-rabbit or anti-mouse secondary antibody coupled to horseradish peroxidase (1:5,000, Thermo Fisher Scientific). The immunoblots were visualized by enhanced chemiluminescence (ECL Western blotting detection reagent, Amersham). Relative intensities were calculated using ImageJ v.1.46r.

## Co-immunoprecipitation

To examine Par14/Par17 and HBc interactions, lysates of $2 \times 10^6$ Huh7 cells were prepared at 72 h after transfection. Cell lysates were immunoprecipitated with a rabbit polyclonal anti-Myc antibody (1:1,000, Santa Cruz Biotechnology #sc-789) and immunoblotted with a mouse monoclonal anti-FLAG antibody (Sigma #F1804) or vice versa. Normal rabbit IgG (Merck Millipore #12-370) or normal mouse IgG (Merck Millipore #12-371) was used as a negative control for immunoprecipitation. The lysates were subjected to 16.5% SDS-PAGE and transferred to PVDF membranes for immunoblotting with a primary antibody (anti-Myc, anti-FLAG, or anti-GAPDH), followed by an anti-rabbit or anti-mouse secondary antibody coupled to horseradish peroxidase. The immunoblots were visualized by enhanced chemiluminescence.

## HBc Stability Analysis

*PIN4*-KD Huh7 cells ($2 \times 10^5$) grown on 6-well plates were transfected with 0.5 µg of respective constructs using 2 µg/ml PEI in 100 µl of Opti-MEM. At 24 h post-transfection, the medium was replaced with fresh medium containing 100 µg/ml cycloheximide (Sigma #C1988-1G) and harvested 0, 6, 12, or 24 h later.

## Northern and Southern Blotting

To analyze HBV RNA synthesis by Northern blotting, total RNA was extracted from HepG2-hNTCP-C9 cells using TRIzol reagent (Ambion, Invitrogen #15596026). Twenty micrograms of total RNA was denatured at 65°C for 10 min, electrophoresed on a 1.2% agarose gel (Ultrapure Agarose, Invitrogen #16500500) containing 1× MOPS buffer [10 mM EDTA, 200 mM MOPS, and 50 mM sodium acetate (pH 7.0)] and formaldehyde (Sigma-Aldrich #F8775), and transferred to a nylon membrane (Roche, Sigma-Aldrich #11417240001) as described previously (Kim et al., 2004; Saeed et al., 2019; Piracha et al., 2020). To analyze HBV DNA synthesis by Southern blotting, HBV DNA extracted from isolated core particles was separated by electrophoresis on a 1% native agarose gel and transferred to a nylon membrane (Whatman #10416296). HBV total RNAs or HBV DNAs were hybridized to a $^{32}$P-labeled random-primed probe specific for full-length HBV for 4 h at 68°C and then subjected to autoradiography as described previously (Kim et al., 2004). For Northern and Southern blotting of infected cells, total RNA and lysates were prepared at 5 and 9 days post-infection (p.i.), respectively.

## HBV Preparation and Infection

To infect hNTCP-C9-expressing HepG2 cells with HBV, HBV virions were prepared from HepAD38 cells, as described previously (Watashi et al., 2013; Nkongolo et al., 2014; Saeed et al., 2019; Piracha et al., 2020). For HBV infection, $2\times10^5$ HepG2-hNTCP-C9 and HepG2-hNTCP-C9-shControl, -shPIN4-#1, and -shPIN4-#5 cells on collagen-coated 6-well plates (Corning #354249) were infected with $1.7\times10^3$ GEq of HBV per cell in medium containing 4% PEG (Affymetrix #25322-68-3), as described previously (Ni et al., 2014; Saeed et al., 2019). To determine the effects of Par14/Par17 mutants on recruitment of HBc onto cccDNA, $2\times10^5$ HepG2, HepG2-hNTCP-C9, and HepG2-hNTCP-C9-shControl, -shPIN4-#1, and -shPIN4-#5 cells in collagen-coated 6-well plates were transfected with 0.5 μg of the respective Par14/Par17 WT or mutant constructs with 2 μg/ml PEI in 100 μl of Opti-MEM. At 24 h post-transfection, the medium was refreshed, and cells were infected with $1.7\times10^3$ GEq of HBV per cell. HBV WT or HBV-HBc-AAP mutant virions were prepared from HepG2 cells. Briefly, $5\times10^6$ HepG2 cells in collagen-coated 15 cm plates were transfected with 16 μg of the HBV WT or HBV-HBc-AAP construct using 64 μg/ml PEI in 400 μl of Opti-MEM. The cells were grown in Dulbecco's modified Eagle's medium supplemented with 10% fetal bovine serum, 1% penicillin–streptomycin, 5 μg/ml insulin, and 50 μM hydrocortisone hemisuccinate. The culture supernatants were collected every third day for 2 weeks, samples were pelleted using PEG, and HBV DNA was quantitated by Southern blotting as described previously (Saeed et al., 2019; Piracha et al., 2020). To recover the same amounts of virions for HBV-HBc-AAP compared with HBV WT, a 7-times larger volume of supernatant needed to be harvested for HBV-HBc-AAP. For infection, $2\times10^5$ HepG2-hNTCP-C9 cells, HepG2-hNTCP-C9 cells stably overexpressing Par14 or Par17, and HepG2-hNTCP-C9-shControl, -shPIN4-#1, and -shPIN4-#5 cells were plated as described above and infected with $1.7\times10^3$ GEq of HBV WT or HBV-HBc-AAP mutant virions per cell (Ni et al., 2014; Saeed et al., 2019; Piracha et al., 2020) Lysates were prepared at 9 days p.i. for SDS-PAGE and immunoblotting, core particle immunoblotting, cccDNA extraction, and ChIP analysis.

## cccDNA Extraction

HBV cccDNA was extracted using the Hirt protein-free DNA extraction procedure, as described previously (Cai et al., 2013) with minor modifications (Saeed et al., 2019). In brief, $2\times10^5$ HepG2-hNTCP-C9, *PIN4*-KD HepG2-hNTCP-C9, or Par14- or Par17-overexpressing stable HepG2-hNTCP-C9 cells were infected with HBV as described in the "HBV preparation and infection" sub-section. At 9 days p.i, when cells had reached 100% confluency, lysates were prepared to extract cccDNA and Southern blotting was performed as described in the "Northern and Southern blotting" sub-section.

## cccDNA Chip and PCR

HBV cccDNA ChIP analysis was performed (Belloni et al., 2009) with minor modifications as described previously (Saeed et al., 2019). Briefly, HBV-infected cells generated as described in the "HBV preparation and infection" sub-section were maintained for eight more days and lysed, and chromatin solutions were prepared as described previously (Belloni et al., 2009; Saeed et al., 2019). Crosslinked sonicated chromatin was subjected to immunoprecipitation with 3 μg of rabbit monoclonal anti-PIN4 (Abcam #ab155283), mouse monoclonal anti-FLAG M2 (Sigma #F1804), rabbit polyclonal anti-HBc (Jung et al., 2012), mouse monoclonal anti-RNA polymerase II (Abcam #ab817), rabbit polyclonal anti-AcH3 (Merck Millipore #06–599), and rabbit polyclonal anti-H3 (Abcam #ab1791) antibodies or normal mouse or rabbit IgG (negative controls) for 16 h at 4°C, incubated with protein A/G-plus agarose beads (Santa Cruz Biotechnology #sc-2003) overnight at 4°C, and centrifuged at 1,000 *g* for 5 min at 4°C to recover immunoprecipitated protein–DNA complexes. DNA was purified from the immunoprecipitated protein–DNA complexes as described previously (Belloni et al., 2009; Saeed et al., 2019). The DNA amount was adjusted to 50 ng after measurement of the $OD_{260}$. Actin levels (**Table 1**) were used to ensure equal loading of lysates. Immunoprecipitated chromatin was analyzed by semi-quantitative PCR (Applied Biosystems; GeneAmp PCR system 2700) or real-time quantitative PCR (Applied Biosystems by Thermo Fisher Scientific, QuantStudio 3 Real-Time PCR #A28131) using cccDNA-specific primers (Saeed et al., 2019; **Table 1**) according to the manufacturer's instruction (Merck Millipore, EZ ChIP 17-371).

## RNase Protection Assay

To examine encapsidated pgRNA, core particles were isolated from HepG2 cells transfected with HBc WT or HBc RP motif mutants plus HBc-deficient HBV, as described previously (Kim et al., 2004). Total RNA was extracted as described

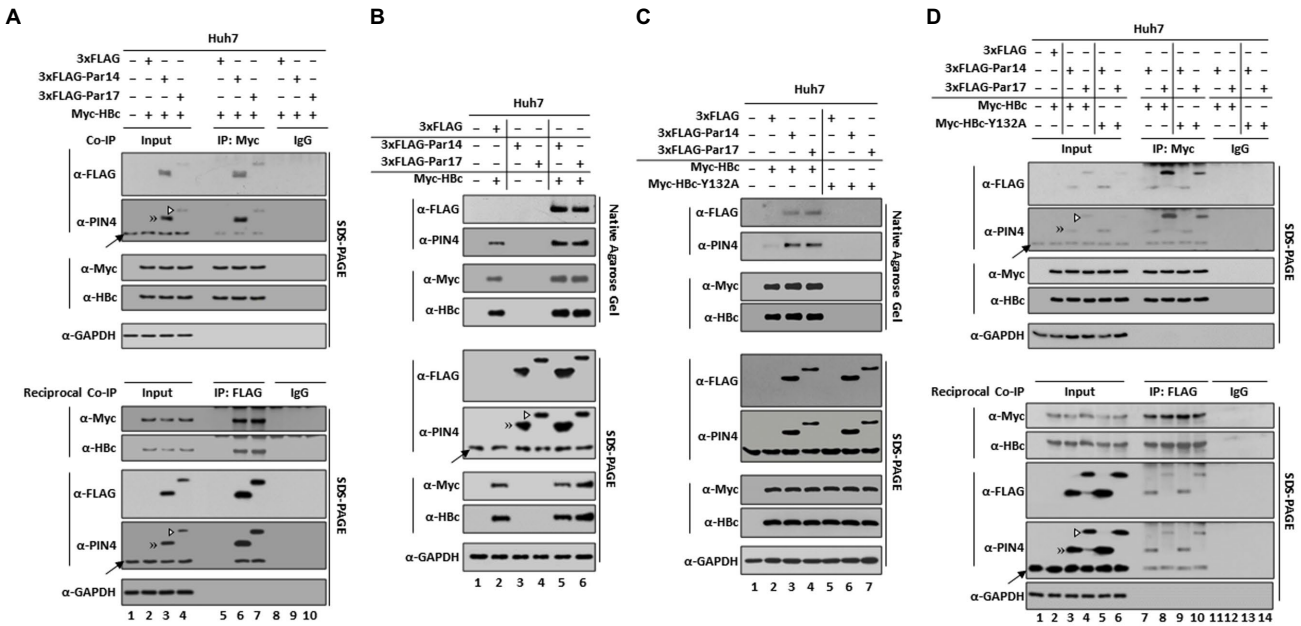


**FIGURE 1 |** Par14 and Par17 are novel binding partners of HBc and the core particle. **(A)** Co-immunoprecipitation reveals that Par14 and Par17 directly interact with the core particle and/or HBc of HBV. Huh7 cells in 6 cm plates were mock-transfected (lane 1) or co-transfected with 4 μg of Myc-HBc WT plus 3 × FLAG (lanes 2, 5, and 8), 3 × FLAG-Par14 WT (lanes 3, 6, and 9), or 3 × FLAG-Par17 WT (lanes 4, 7, and 10). At 72 h post-transfection, whole-cell lysates were prepared (lanes 1–4) and immunoprecipitated with an anti-Myc or anti-FLAG antibody (lanes 5–7). As a negative control, lysates were immunoprecipitated with normal rabbit IgG (Merck Millipore #12–370) or normal mouse IgG (Merck Millipore #12–371; lanes 8–10). SDS-PAGE and immunoblotting were performed. Resolved proteins were transferred to PVDF membranes and incubated overnight with mouse monoclonal anti-FLAG M2 (Sigma #F1804), rabbit monoclonal anti-PIN4 (1:1,000, Abcam #ab155283), rabbit polyclonal anti-Myc (Santa Cruz Biotech #sc-789), rabbit polyclonal anti-HBc (1:1,000, 17), and mouse monoclonal anti-GAPDH (1:5,000, Santa Cruz #sc-32,233) primary antibodies. GAPDH was used as a loading control. The blots were incubated with secondary antibodies (anti-mouse or anti-rabbit) coupled to horseradish peroxidase (1,5,000 dilution, Thermo Fisher Scientific). **(B)** NAGE and core particle immunoblotting reveal that the core particle of HBV interacts with Par14/Par17. Huh7 cells in 6 cm plates were mock-transfected (lane 1) or transfected with 3 × FLAG-Par14 WT (lane 3) or 3 × FLAG-Par17 WT (lane 4) or co-transfected with Myc-HBc WT plus 3 × FLAG (lane 2), 3 × FLAG-Par14 WT (lane 5), or 3 × FLAG-Par17 WT (lane 6). At 72 h post-transfection, cell lysates were prepared and subjected to 1% NAGE, transferred to a PVDF membrane, and immunoblotted with anti-FLAG, anti-PIN4, anti-Myc, and anti-HBc antibodies. **(C,D)** Both the HBV core particle and HBc interact with Par14/Par17. **(C)** NAGE and core particle immunoblotting demonstrate that HBc-Y132A is core particle assembly-defective, unlike HBc WT. Huh7 cells were mock-transfected (lane 1) or co-transfected with Myc-HBc WT or core particle assembly-defective Myc-HBc-Y132A plus 3 × FLAG (lanes 2 and 5), 3 × FLAG-Par14 WT (lanes 3 and 6), or 3 × FLAG-Par17 WT (lanes 4 and 7). **(D)** Co-immunoprecipitation reveals that Par14/Par17 directly interact with core particle assembly-defective HBc-Y132A. Lysates of transfected Huh7 cells were immunoprecipitated and subjected to SDS-PAGE as described above. The immunoblots were visualized by enhanced chemiluminescence (ECL Western blotting detection reagent, Amersham). Endogenous Par14 is marked with an arrow. Overexpressed Par14 and Par17 are marked with a double arrowhead and open arrowhead, respectively. A representative result from three independent experiments is shown.

above. The riboprobe was prepared as described previously (Kim et al., 2004; Piracha et al., 2020). Briefly, 446 nt of the digoxigenin (DIG)-UTP antisense probe was generated from the HBV sequence (nt 1,805–2,187) of the pGEM3Zf (+) plasmid (Kim et al., 2004) *in vitro* using SP6 RNA polymerase (Promega #P108B) with a kit (Roche #1363514). The RNase protection assay (RPA) procedure was conducted as described previously (Kim et al., 2004), except that labeling was performed with DIG (Piracha et al., 2020), according to the Roche protocol (Roche # 1363514, Roche #11585762001). Encapsidated and total RNAs (369 nt) following RNase digestion were electrophoresed on a 5% polyacrylamide-8 M urea gel and transferred to a nylon membrane (Roche, Sigma-Aldrich #11417240001). The membrane was incubated with an anti-DIG-AP antibody (1:1,000, Roche #11093274910) and visualized by the CSPD (Roche #11755633001) chemiluminescence reaction.

# RESULTS

## Par14 and Par17 Bind to Both HBc and the Core Particle of HBV

Par14 and Par17 bind to the RP motifs of HBx (Saeed et al., 2019); therefore, we reasoned that the single RP motif of HBc may serve as a binding site for Par14/Par17. To investigate whether HBc and/or the core particle can bind to Par14/Par17, co-immunoprecipitation and immunoblotting (**Figure 1A**) and NAGE and immunoblotting (**Figure 1B**) were performed. The anti-Myc and anti-FLAG antibodies immunoprecipitated Par14/Par17 and HBc, respectively (**Figure 1A**, lanes 6 and 7), demonstrating that HBc and/or the core particle can bind to Par14/Par17. NAGE and immunoblotting demonstrated that both Par14 and Par17 can physically interact with the core particle of HBV (**Figure 1B**, top and second panels, lanes 2, 5, and 6). Inhibition of

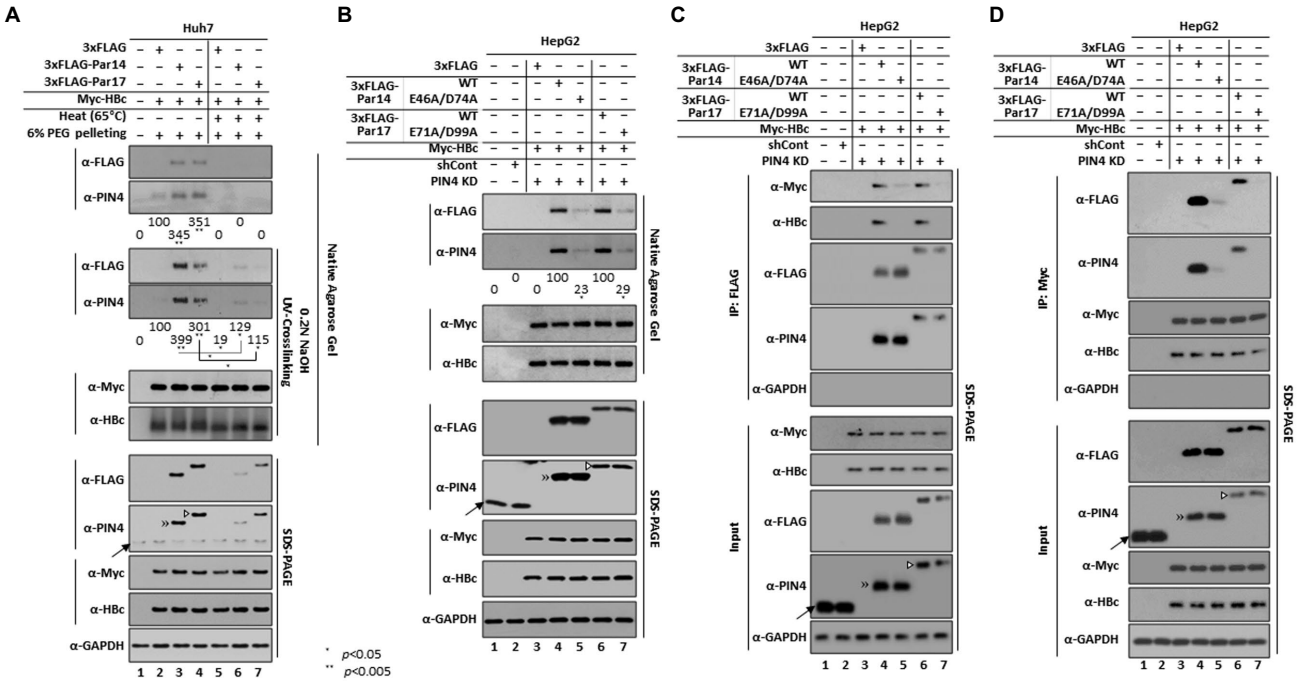


**FIGURE 2 |** Par14/Par17 bind both outside and inside the core particle, and the substrate-binding residues of Par14 (E46/D74) and Par17 (E71/D99) are critical for Par14/Par17–HBc and/or –core particle interactions. **(A)** Par14/Par17 bind both outside and inside HBV core particles. Huh7 cells were mock-transfected (lane 1) or co-transfected with Myc-HBc WT plus 3×FLAG (lanes 2 and 5), 3×FLAG-Par14 WT (lanes 3 and 6), or 3×FLAG-Par17 WT (lanes 4 and 7). At 72 h post-transfection, lysates were left untreated (lanes 1–4) or heated at 65°C for 2 h (lanes 5–7). These core particles were precipitated with 6% PEG, washed, and re-precipitated with 6% PEG. The pellet was suspended in TNE buffer and subjected to NAGE plus immunoblotting and SDS-PAGE plus immunoblotting as described in **Figure 1**. The PVDF membrane containing core particles was treated with 0.2 N NaOH for 40 s, crosslinked with UV, and immunoblotted with anti-FLAG, anti-PIN4, anti-Myc, and anti-HBc antibodies. **(B–D)** E46/D74 of Par14 and E71/D99 of Par17 are important for interactions with the core particle. Non-transduced and mock-transfected (lane 1) and control shRNA-transduced (lane 2) HepG2 cells were used as controls. shPIN4-#1–transduced *PIN4*-KD HepG2 cells in 6 cm plates were co-transfected with Myc-HBc WT plus 3×FLAG (lane 3), 3×FLAG-Par14 WT (lane 4), 3×FLAG-Par14-E46A/D74A (lane 5), 3×FLAG-Par17 WT (lane 6), or 3×FLAG-Par17-E71A/D99A (lane 7). **(C,D)** Lysates were immunoprecipitated with an anti-FLAG antibody and immunoblotted with an anti-Myc antibody **(C)** or vice versa **(D)**. At 72 h post-transfection, lysates were prepared. Lysates were subjected to NAGE and core particle immunoblotting as described **Figure 1B**. Input lysates and immunoprecipitants were also subjected to SDS-PAGE and immunoblotting as described in **Figures 1B–D**. Par14/Par17 bound to HBV core particles were measured using ImageJ v.1.46r. Representative results from three independent experiments are shown. Statistical significance was evaluated using Student's *t*-test. $^{*}p<0.05$; $^{**}p<0.005$ relative to the corresponding control (A and B).

parvulin with the competitive reversible inhibitor PiB (Uchida et al., 2003) or the competitive irreversible inhibitor juglone (Hennig et al., 1998; Chao et al., 2001) weakened the core particle–Par14/Par17 interactions (**Supplementary Figure S1**), suggesting they are dynamic on–off interactions. Consistently, heat treatment at 65°C weakened the core particle–Par14/Par17 interactions (**Supplementary Figure S2**).

This co-immunoprecipitation cannot discriminate Par14/Par17 binding to HBc, the core particle, or both; therefore, we examined the interactions of Par14/Par17 and HBc using a core particle assembly-defective dimer-positive HBc-Y132A mutant (Bourne et al., 2009). Consistent with a previous report, Myc-HBc-Y132A could not assemble into the core particle (**Figure 1C**, third and fourth panels, lanes 2–4 vs. 5–7; Bourne et al., 2009), although its expression was comparable with that of Myc-HBc WT (**Figure 1C**, seventh and eighth panels, lanes 2–4 vs. 5–7). Par14/Par17 were co-immunoprecipitated with HBc-Y132A (**Figure 1D**, lanes 9 and 10), demonstrating that HBc can bind to Par14/Par17. We conclude that both HBc and the core particle are binding partners of Par14/Par17.

## Par14/Par17 Bind Both Outside and Inside Core Particles

Although Par14/Par17 can bind to the core particle based on the finding that they dissociated from it upon heat treatment at 65°C (**Supplementary Figure S2**), we could not exclude the possibility that Par14/Par17 may be incorporated into the core particle. To investigate that, cytoplasmic lysates were mock-treated or heated at 65°C for 2 h. As expected, heat treatment dissociated Par14/Par17 from outside the core particle (**Figure 2A**, top and second panels, lanes 2–4 vs. 5–7). Then, this membrane was treated with 0.2 N NaOH for 40 s to open-up core particles (Kim et al., 2004, 2008; Jung et al., 2014), ultraviolet (UV)-crosslinked, and immunoblotted. Although Par14/Par17 were dissociated from core particles by heat treatment, they were still detected in opened-up core particles (**Figure 2A**, third and fourth panels, lanes 5–7)

without any changes on to the core particle level (**Figure 2A**, fifth and sixth panels, lanes 2–7), indicating that Par14/Par17 are associated inside the core particle. Par14/Par17 were still detected by SDS-PAGE and immunoblotting after heat treatment, further supporting the above conclusion (**Figure 2A**, seventh and eighth panels, lanes 5–7). These results demonstrate that Par14/Par17 can bind to and be incorporated into the core particle.

## The Substrate-Binding E46/71 and D74/99 Residues of Par14/Par17 Interact With HBc and/or the Core Particle

The negatively charged substrate-binding residues E46/71 and D74/99 of Par14/Par17 interact with the RP motifs of HBx (Saeed et al., 2019). Therefore, these residues of Par14/Par17 may also bind to the RP motif of HBc and/or the core particle. To exclude the effects of endogenous Par14/Par17, *PIN4* was knockdown (KD). NAGE and immunoblotting demonstrated that the substrate-binding-deficient Par14/Par17 mutants weakly interacted with the core particle (**Figure 2B**, top and second panels, lanes 4 vs. 5 and 6 vs. 7). The same lysates from **Figure 2B** were immunoprecipitated (**Figures 2C,D**). In accordance with **Figure 2B** (top and second panels), the E46A/D74A mutant of Par14 and E71A/D99A mutant of Par17 were not efficiently immunoprecipitated with HBc and/or the core particle (**Figures 2C,D**, top and second panels, lanes 4 vs. 5 and 6 vs. 7), indicating that the E46/71 and D74/99 of Par14/Par17 are important for the interactions with HBc and the core particle.

## The HBc RP Motif Is Conserved Among Human, Mammalian, and Avian Hepadnaviruses

Par14/Par17 interacted with HBc and the core particle (**Figures 1, 2**); therefore, we reasoned that the positively charged amino acid preceding proline in HBc may be the interaction site of Par14/Par17 similar to HBx (Saeed et al., 2019). Sequence analysis of HBc revealed a single $^{133}$RP$^{134}$ motif in its NTD (**Figure 3A**). Amino acid sequence alignments of human HBc proteins demonstrated that among 16 XaaPro motifs, the $^{133}$RP$^{134}$ motif is completely conserved among 30 isolates from 10 genotypes (**Figure 3A**), indicating that the conserved RP motif is important for the HBV life cycle and/or viral pathogenesis. Furthermore, HBc proteins of mammalian and avian hepadnaviruses have a completely conserved RP motif (**Figures 3B,C**). The avian hepadnavirus

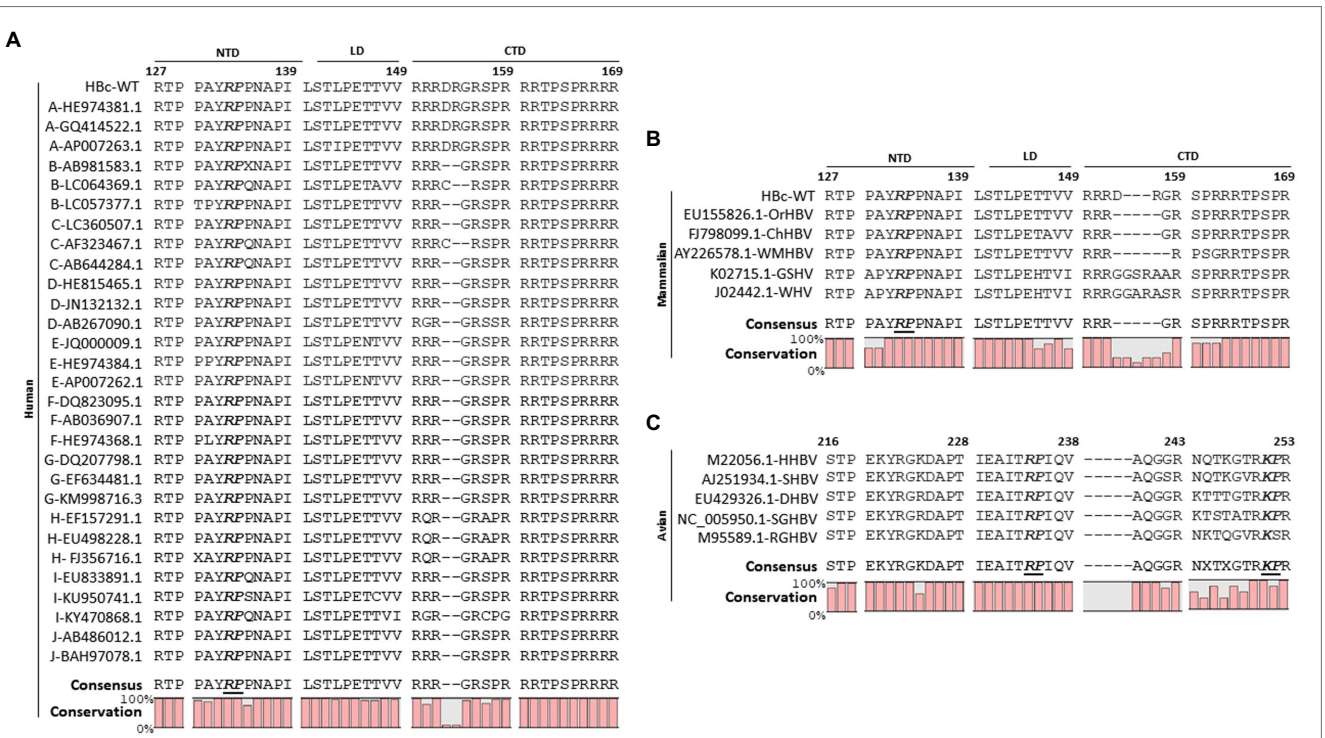


**FIGURE 3 |** The HBc $^{133}$RP$^{134}$ motif is conserved among human, mammalian, and avian hepadnaviruses. **(A)** The HBc $^{133}$RP$^{134}$ motif is completely conserved among isolates from 10 HBV genotypes including human HBV [adwR9 subtype (HBc WT)]. The partial NTD, linker, and partial CTD HBc amino acid sequences were aligned using CLC Main Workbench 8 software. The HBV genotype of each isolate is indicated in the left column, followed by accession numbers. **(B)** The mammalian HBc RP motif is completely conserved. The HBc amino acid sequences of orangutan HBV (OrHBV), chimpanzee HBV (ChHBV), woolly monkey HBV (WMHBV), ground squirrel hepatitis virus (GSHV), and woodchuck hepatitis virus (WHV) were aligned. **(C)** The avian HBc RP motif is completely conserved and an additional KP motif is also conserved. HBc amino acid sequences of heron HBV (HHBV), stork HBV (SHBV), duck HBV (DHBV), snow goose HBV (SGHBV), and ross goose HBV (RGHBV) were aligned. Accession numbers of mammalian and avian hepadnaviruses are presented. Conserved RP or KP motifs are shown in bold and italicized font. Consensus sequences and conservation percentages are shown at the bottom.

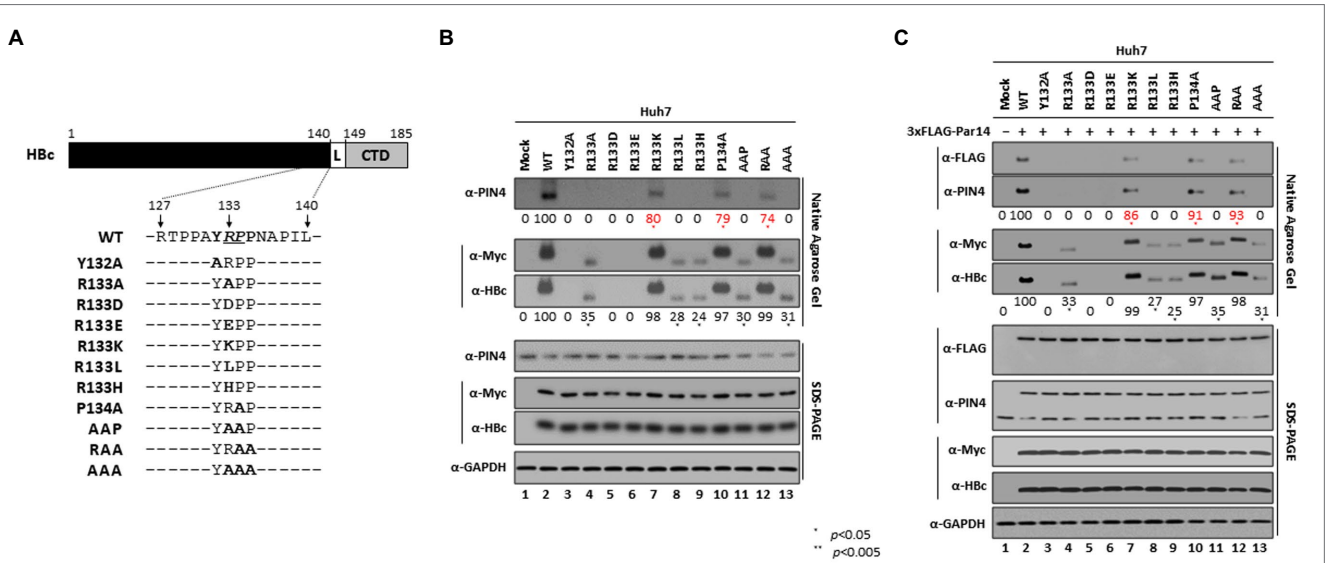


**FIGURE 4 |** The positively charged R133 residue in the conserved RP motif is critical for core particle assembly and interactions with Par14/Par17. **(A)** Schematic diagram of the HBc protein. The HBc $^{132}$YRPP$^{135}$ motif and single, double, and triple YRPP substitution mutants are indicated. **(B,C)** The positively charged R133 residue in the conserved RP motif is critical for core particle assembly and interactions with Par14/Par17. Huh7 cells in 6 cm plates were mock-transfected (lane 1) or transfected with Myc-HBc WT (lane 2), Myc-HBc-Y132A (lane 3), or Myc-HBc RP motif mutants (lanes 4–13) **(B)**. Huh7 cells were mock-transfected (lane 1) or co-transfected with 3 × FLAG-Par14 WT plus Myc-HBc WT (lane 2), Myc-HBc-Y132A (lane 3), or Myc-HBc RP motif mutants (lanes 4–13). At 72 h post-transfection, lysates were prepared and subjected to NAGE plus immunoblotting and SDS-PAGE plus immunoblotting, as described in **Figure 1**. Relative levels of Par14/Par17 bound to core particles and of core particles were calculated using ImageJ v.1.46r. Representative data from three independent experiments are shown. Statistical significance was evaluated using Student's *t*-test. $^{*}p < 0.05$ relative to the corresponding control.

HBc protein has an additionally conserved KP motif (**Figure 3C**).

## The Positively Charged R133 Residue in the Conserved RP Motif Is Critical for Core Particle Assembly and Interactions With Par14/Par17

To investigate the importance of the HBc RP motif, several RP motif mutants were constructed (**Figure 4A**) and core particle assembly was examined (**Figure 4B**, second and third panels). Expression of all HBc mutant proteins was comparable with that of HBc WT (**Figure 4B**, fifth and sixth panels). NAGE and immunoblotting revealed that a comparable level of core particles was assembled with the HBc-R133K, -P134A, and -RAA mutants as with HBc WT (**Figure 4B**, second and third panels, lanes 2 vs. 7, 10, and 12), indicating that a R or K residue at position 133 is critical for core particle assembly, but P134 and P135 are not. When R133 was changed to a D or E residue, the HBc mutant proteins showed an assembly-defective phenotype similar to HBc-Y132A (**Figure 4B**, second and third panels, lanes 3 vs. 5 and 6), suggesting that a negatively charged residue at position 133 interferes with core particle assembly, supposedly like HBc-Y132A (Bourne et al., 2009). Although other RP motif mutants (HBc-R133A, -R133L, -R133H, -AAP, and -AAA) were core particle assembly-positive with a reduced efficiency (**Figure 4B**, second and third panels, lanes 2 vs. 4, 8, 9, 11, and 13), endogenous Par14/Par17 could not bind to these mutant core particles (**Figure 4B**, top panel), indicating that a R or K at position 133 is critical for Par14/Par17 binding. Consistently, Par14/Par17 bound to core particles assembled by HBc-R133K, -P134A, and -RAA (**Figure 4B**, top panel, lanes 2 vs. 7, 10, and 12), further strengthening the above conclusion. Our results indicate that core particle–Par14/Par17 interactions stabilize the core particle or improve the efficiency of its assembly (**Figure 4B**, second and third panels, lanes 2, 7, 10, and 12 vs. 4, 8, 9, 11, and 13). Of note, core particles assembled by HBc-R133A, −R133L, -R133H, -AAP, and -AAA migrated rapidly in the agarose gel (**Figure 4B**, second and third panels, lanes 2 vs. 4, 8, 9, 11, and 13).

In Par14- or Par17-overexpressing cells, core particle assembly, core particle migration in the agarose gel, and core particle–Par14/Par17 interactions were all identical with **Figure 4B** (**Figure 4C** and **Supplementary Figure S3**). Core particles were not detected in the nucleus (**Supplementary Figure S4**), demonstrating that core particle–Par14/Par17 interactions must occur in the cytoplasm, not in the nucleus.

## Unlike Core Particle Assembly-Defective HBc-Y132A, Core Particle Assembly-Defective HBc-R133D and -R133E Cannot Interact With Par14/Par17

The HBc-R133D and -R133E mutants were core particle assembly-defective similar to HBc-Y132A (**Supplementary Figures 4B,C**, and **Figure 5A**, eighteenth and bottom panels, lanes 2 vs. 3, 4 and 5). Therefore, we examined HBc–Par14/Par17 interactions. Although HBc-Y132A interacted with Par14/

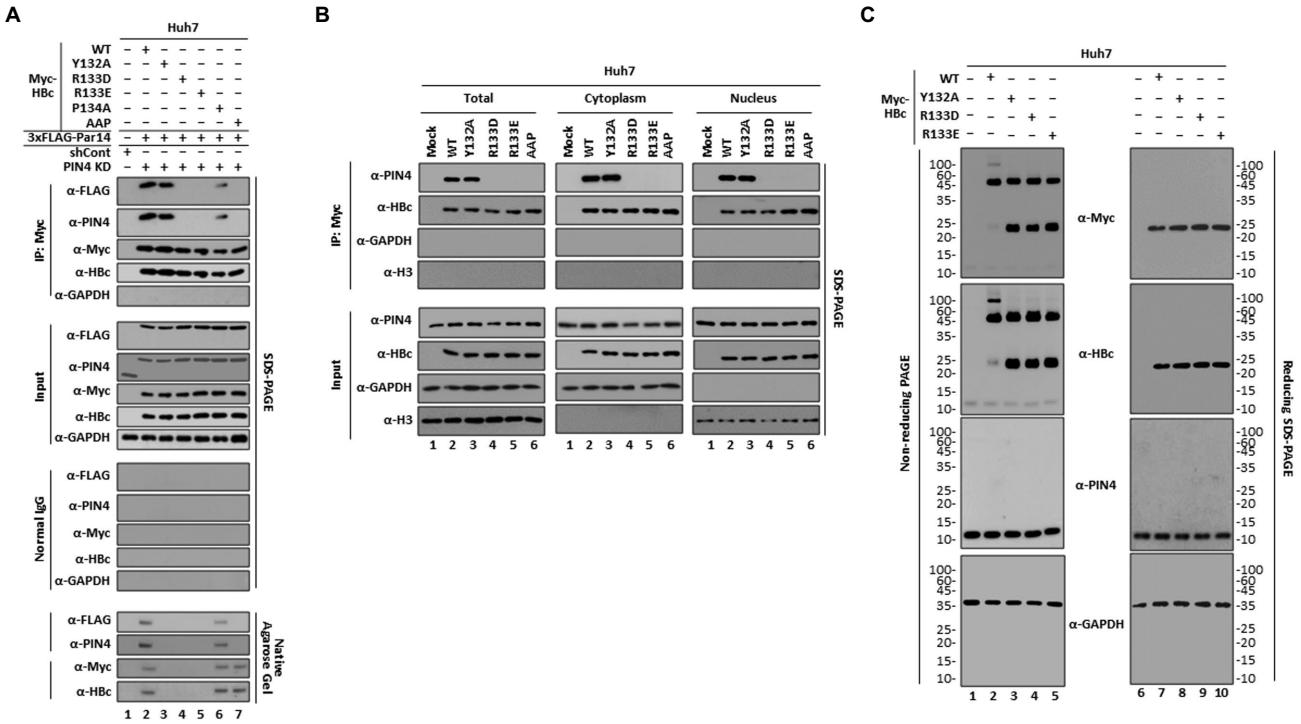


**FIGURE 5 |** Unlike core particle assembly-defective HBc-Y132A, core particle assembly-defective HBc-R133D and -R133E cannot interact with Par14/Par17. **(A)** The HBc $^{133}$RP$^{134}$ motif is important for binding to Par14. *PIN4*-KD Huh7 cells in 6 cm plates were co-transfected with 3 × FLAG-Par14 WT plus Myc-HBc WT (lane 2), -Y132A (lane 3), -R133D (lane 4), −R133E (lane 5), -P134A (lane 6), or -AAP (lane 7). Control shRNA-transduced and mock-transfected Huh7 cells were used as a negative control (lane 1). Lysates were immunoprecipitated with an anti-Myc antibody and immunoblotted with an anti-FLAG antibody. Lysates were subjected to NAGE and SDS-PAGE and then immunoblotted with anti-FLAG, anti-PIN4, anti-Myc, anti-HBc, and anti-GAPDH antibodies, as described in **Figure 1**. **(B)** Endogenous Par14/Par17 can interact with HBc WT and -Y132A in the nucleus and cytoplasm, unlike HBc-R133D, −R133E, and -AAP. Huh7 cells were mock-transfected (lane 1) or transfected with Myc-HBc WT (lane 2), -Y132A (lane 3), -R133D (lane 4), −R133E (lane 5), or -AAP (lane 6). At 72 h post-transfection, total cell lysates and cytoplasmic and nuclear fractions were prepared and analyzed by SDS-PAGE and immunoblotting [35]. **(C)** HBc-R133D and HBc-R133E may form dimers, similar to HBc-Y132A. Huh7 cells were mock-transfected (lanes 1 and 6) or transfected with Myc-HBc WT (lanes 2 and 7), -Y132A (lanes 3 and 8), -R133D (lanes 4 and 9), or -R133E (lanes 5 and 10). At 72 h post-transfection, whole-cell lysates were prepared and subjected to non-reducing PAGE or reducing SDS-PAGE as described in the "Materials and Methods" section, and then immunoblotted with anti-Myc, anti-HBc, anti-PIN4, and anti-GAPDH antibodies. Representative data from three independent experiments are shown.

Par17 similar to HBc WT (**Figures 1D**, **5A**, and **Supplementary Figure S5**, top and second panels, lane 2 vs. 3), the HBc-R133D, -R133E, and -AAP mutants did not interact with Par14/Par17 (**Figure 5A** and **Supplementary Figure S5**, top and second panels, lanes 2 and 3 vs. 4, 5, and 7) and HBc-P134A interacted with Par14/Par17 with a reduced efficiency (**Figure 5A** and **Supplementary Figure S5**, top and second panels, lanes 2 and 3 vs. 6). These results further demonstrate that R133 is critical for HBc–Par14/Par17 interactions.

Next, we investigated HBc–Par14/Par17 interactions in total, cytoplasmic, and nuclear fractions (**Figure 5B**). While HBc WT and -Y132A strongly interacted with endogenous Par14/Par17 in the total, cytoplasmic, and nuclear fractions, HBc-R133D, −R133E, and -AAP did not interact with Par14/Par17 at all (**Figure 5B**), further demonstrating the importance of R133 in $^{133}$RP$^{134}$ motif for Par14/Par17 binding.

Par14/Par17 facilitate the nuclear localization of HBx *via* its RP motifs (Saeed et al., 2019); therefore, we investigated whether binding of Par14/Par17 to HBc *via* the RP motif also affects its intracellular localization. Consistent with the previously reported localization of HBc *in vivo* (Diab et al., 2018),HBc WT and HBc RP motif mutants were detected both in the cytoplasm and nucleus (**Supplementary Figure S4**). However, we did not detect core particles in the nucleus by NAGE (**Supplementary Figure S4**). Unlike HBx (Saeed et al., 2019), Par14 WT did not affect the nuclear or cytoplasmic localization of HBc WT or mutants (**Supplementary Figure S6A**). The same results were obtained upon co-transfection of Par17 WT (**Supplementary Figure S6B**).

The dimer-positive HBc-Y132A mutant cannot assemble into core particles due to a deficiency of interdimeric interactions (Bourne et al., 2009). Therefore, we investigated whether core particle assembly-defective HBc-R133D or -R133E can form dimers similar to HBc-Y132A. Cytoplasmic lysates were subjected to non-reducing PAGE or conventional reducing SDS-PAGE and immunoblotting (**Figure 5C**). Consistent with the above results (**Figures 4B,C** and **5A,B**), expression levels of HBc proteins were comparable under reducing conditions (**Figure 5C**, lanes 7–10). Under non-reducing conditions, HBc WT formed a high molecular weight complex of HBc and dimeric HBc,

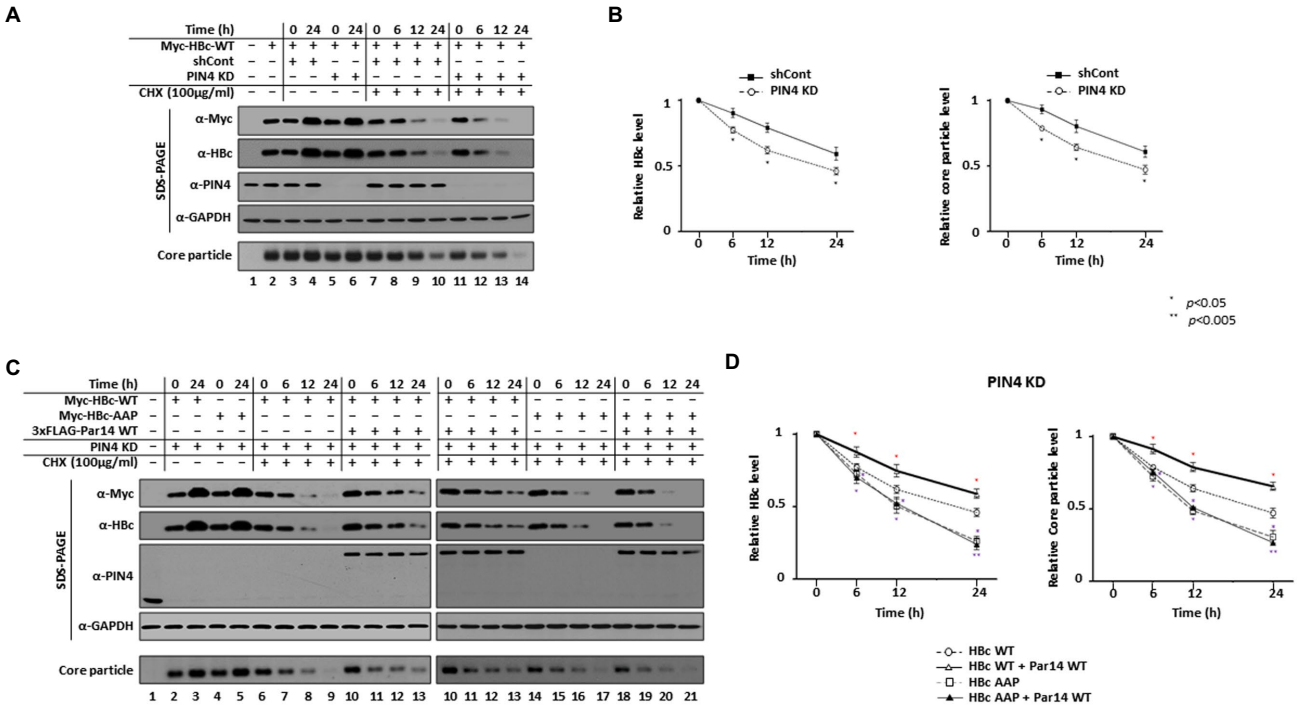


**FIGURE 6 |** Par14/Par17 can stabilize both HBc and the core particle through their interactions *via* the HBc RP motif. **(A,B)** The stabilities of HBc and the core particle are decreased in *PIN4*-KD Huh7 stable cells. Control shRNA-transduced (lanes 3, 4, and 7–10) and *PIN4*-KD (lanes 5, 6, and 11–14) Huh7 cells were transfected with Myc-HBc WT (lanes 2–14). As controls, Huh7 cells were mock-transfected (lane 1) or transfected with Myc-HBc WT (lane 2). At 24 h post-transfection, cells were treated with DMSO (lanes 2–6) or 100 μg/ml cycloheximide diluted in DMSO (lanes 7–14) and lysates were prepared at the indicated time points. **(C,D)** Par14 increases the stabilities of HBc and the core particle through the HBc $^{133}$RP$^{134}$ motif. *PIN4*-KD Huh7 cells (lanes 2–21) were transfected with Myc-HBc WT (lanes 2, 3, and 6–9) or Myc-HBc-AAP (lanes 4, 5, and 14–17) or co-transfected with 3 × FLAG-Par14 WT plus Myc-HBc WT (lanes 10–13) or Myc-HBc-AAP (lanes 18–21). Mock-transfected Huh7 cells were used as a negative control (lane 1). At 24 h post-transfection, cycloheximide-treated cells generated as described above were harvested at the indicated time points and subjected to SDS-PAGE and NAGE followed by immunoblotting with anti-Myc, anti-HBc, anti-PIN4, and anti-GAPDH antibodies. Representative results from three independent experiments are shown. Data are presented as mean HBc and core particle levels ± SD. Statistical significance was evaluated using Student's *t*-test. $^{*}p < 0.05$ relative to the corresponding control.

with a very low level of monomeric HBc (**Figure 5C**, lane 2). However, HBc-Y132A, -R133D, and -R133E formed a comparable level of dimeric HBc as HBc WT and much higher levels of monomeric HBc than HBc WT, and did not form a high molecular weight complex of HBc (**Figure 5C**, lanes 2 vs. 3, 4, and 5), suggesting that dimeric HBc-R133D and -R133E are defective in core particle assembly due to a deficiency of interdimeric interactions similar to HBc-Y132A.

## Par14/Par17 Stabilize Both HBc and the Core Particle Through Their Interactions *via* the HBc RP Motif

Par14 and Par17 interact with and thereby stabilize HBx (Saeed et al., 2019); therefore, we reasoned that they may also stabilize HBc and/or the core particle through their interactions even though HBc and/or the core particle are relatively stable. In *PIN4*-KD cells, the levels of HBc and core particles were decreased after 6 h and these decreases were enhanced after 12 h and peaked after 24 h compared with control cells (**Figure 6A**, top, second, and bottom panels, lanes 7–10 vs. 11–14). Accordingly, the half-lives of HBc (**Figure 6B** left) and the core particle (**Figure 6B** right) were decreased from >24 to 20 h and from >24to 21 h, respectively (**Figure 6B**).

When we exogenously expressed Par14 WT (**Figures 6C,D**) or Par17 WT (**Supplementary Figure S7**) in *PIN4*-KD cells, the half-lives of HBc and the core particle were increased from 20 to >24 h and from 21 to >24 h, respectively (**Figure 6D** left and Supplementary Figure S7), demonstrating that Par14 or Par17 increase the stabilities of HBc and the core particle (**Figures 6C** and **Supplementary Figure S7**, lanes 6–9 vs. 10–13). The half-life of HBc, which decreased from >24 to 20 h in *PIN4*-KD Huh7 cells, was further decreased from 20 to 12 h upon RP motif mutation (HBc-AAP). Likewise, the half-life of the core particle, which decreased from >24 to 21 h in *PIN4*-KD Huh7 cells, was further decreased to 13 h upon RP motif mutation (HBc-AAP), which clearly demonstrates the importance of the RP motif for stability of HBc. Unlike HBc WT, the presence or absence of Par14/Par17 did not affect the levels of HBc-AAP or core particles formed by HBc-AAP (**Figure 6C**, lanes 6–9 vs. 10–13 vs. 14–17 vs. 18–21, and **Supplementary Figure S7**). Furthermore, Par14 WT and Par 17 WT did not change the half-life of HBc-AAP or core particles formed by HBc-AAP (**Figure 6D**

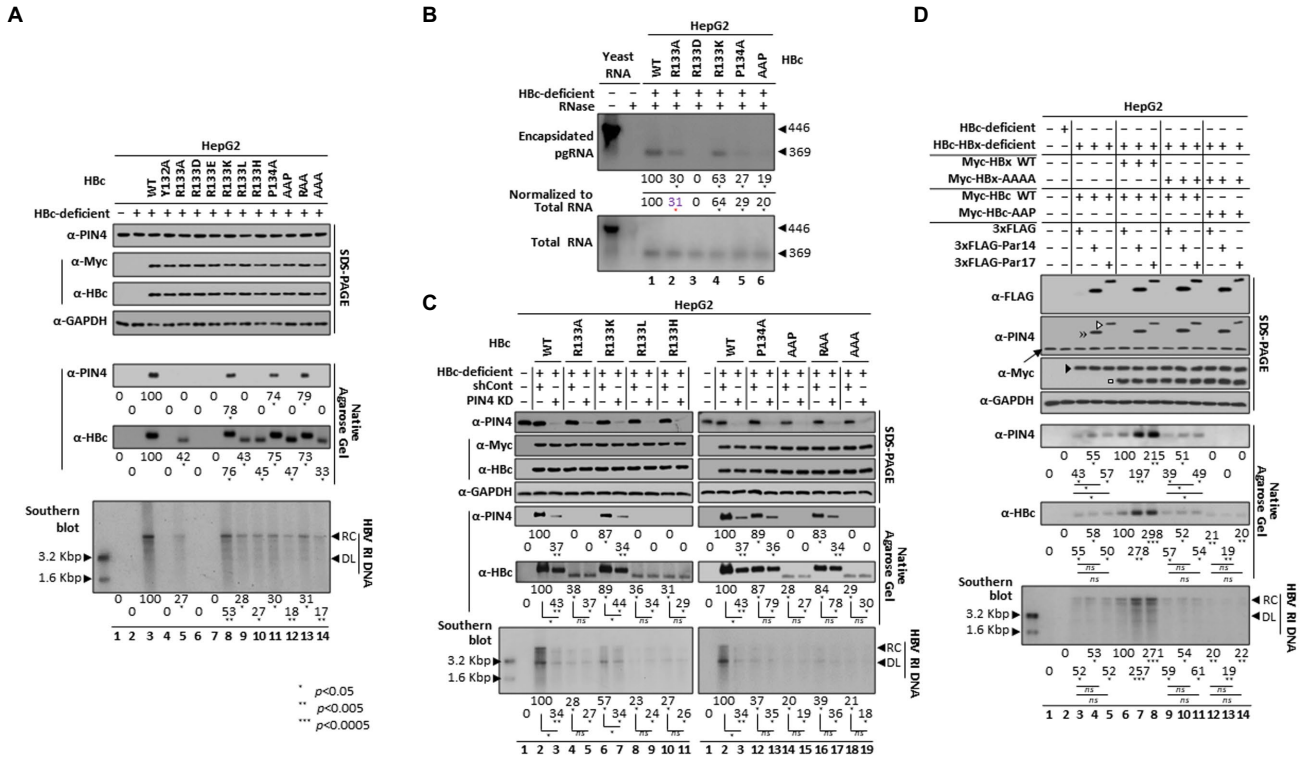


**FIGURE 7 |** The HBc RP motif is critical for Par14/Par17-mediated upregulation of HBV replication. **(A)** HBc RP motif mutants impair HBV replication. HepG2 cells in 6 cm plates were mock-transfected (lane 1), transfected with HBc-deficient HBV (lane 2), or co-transfected with HBc-deficient HBV plus Myc-HBc WT (lane 3), Myc-HBc-Y132A (lane 4), or Myc-HBc RP motif mutants (lanes 5–14). **(B)** The HBc RP motif is critical for pgRNA encapsidation. To examine encapsidated pgRNA and total RNA from HepG2 cells co-transfected with HBc-deficient HBV plus Myc-HBc WT or HBc RP motif mutants, an *in vitro*-transcribed DIG-UTP-labeled antisense RNA probe (446 nt) was hybridized overnight at 50°C with pgRNA from isolated core particles or 10 μg of total RNA. Protected RNA (369 nt) following RNase digestion was electrophoresed on a 5% polyacrylamide–8 M urea gel, transferred to a nylon membrane (Roche, Sigma-Aldrich #11417240001), immunoblotted with an anti-DIG-AP antibody, and visualized with CSPD. **(C)** The positively charged R133 or K133 residue in the RP motif facilitates core particle assembly, resulting in efficient HBV replication. Control shRNA-transduced (lanes 2, 4, 6, 8, 10, 12, 14, 16, and 18) and stable *PIN4*-KD (lanes 3, 5, 7, 9, 11, 13, 15, 17, and 19) cells were co-transfected with HBc-deficient HBV plus Myc-HBc WT (lanes 2 and 3) or Myc-HBc RP motif mutants (lanes 4–19). **(D)** Both HBx $^{19}$RP$^{20}$-$^{28}$RP$^{29}$ motifs and the HBc $^{133}$RP$^{134}$ motif are critical for Par14/Par17-mediated upregulation of HBV replication. HepG2 cells were mock-transfected (lane 1) or transfected with HBc-deficient HBV (lane 2). HepG2 cells were triple-transfected with HBc-HBx-deficient HBV plus Myc-HBc WT plus 3 × FLAG (lane 3), 3 × FLAG-Par14 WT (lane 4), or 3 × FLAG-Par17 WT (lane 5). HepG2 cells were quadruple-transfected with HBc-HBx-deficient HBV plus Myc-HBc WT plus Myc-HBx WT plus 3 × FLAG (lane 6), 3 × FLAG-Par14 WT (lane 7), or 3 × FLAG-Par17 WT (lane 8). HepG2 cells were quadruple-transfected with HBc-HBx-deficient HBV plus Myc-HBc WT plus Myc-HBx-AAAA plus 3 × FLAG (lane 9), 3 × FLAG-Par14 WT (lane 10), or 3 × FLAG-Par17 WT (lane 11). HepG2 cells were quadruple-transfected with HBc-HBx-deficient HBV plus Myc-HBc-AAP plus Myc-HBx-AAAA plus 3 × FLAG (lane 12), 3 × FLAG-Par14 WT (lane 13), or 3 × FLAG-Par17 WT (lane 14). The amount of transfected DNA was adjusted with the pCMV empty vector. Lysates were prepared at 72 h post-transfection and subjected to SDS-PAGE and NAGE, as described in **Figure 1**. Overexpressed Myc-tagged HBc and Myc-tagged HBx are marked by a closed arrowhead and open square, respectively (**D**, third panel). Southern blotting detected HBV replicative intermediate, partially double-stranded RC, and double-stranded linear DNAs, marked as HBV RI DNA, RC, and DL, respectively. The levels of the HBV core particle, Par14/Par17-binding to the core particle, and HBV DNA was measured using ImageJ v.1.46r. Representative results from three independent experiments are shown. Statistical significance was evaluated using Student's *t*-test. $^{*}p < 0.05$, $^{**}p < 0.005$, and $^{***}p < 0.0005$ relative to the corresponding control.

and **Supplementary Figure S7**). The overall levels of HBc-AAP and core particles formed by HBc-AAP were always less than in control cells (**Figure 6C**, lanes 6–9 vs. 10–13 vs. 14–17 vs. 18–21), indicating that HBc-AAP and core particles formed by HBc-AAP cannot be stabilized due to the lack of Par14/Par17 interactions. Of note, Par14/Par17 increased the stability of HBc-Y132A, but not of HBc-R133D (**Supplementary Figure S8**). Taken together, we reasoned that HBc and the core particle are stabilized through specific HBc– and/or core particle–Par14/Par17 interactions.

## The HBc RP Motif Is Crucial for Par14/Par17-Mediated Upregulation of HBV Replication

In light of our observation that the HBc $^{133}$RP$^{134}$ motif is important for HBc– and/or core particle–Par14/Par17 interactions (**Figures 4, 5**) and that Par14/Par17 upregulate HBV replication in an HBx-dependent manner (Saeed et al., 2019), we speculated that HBc– and/or core particle–Par14/Par17 interactions may also be involved in HBV replication. In accordance with **Figure 4**, the expression levels of proteins, core particle assemblies, core particle migration patterns, and core particle–Par14/Par17

interactions were presented (**Figure 7A**). As expected, HBc-Y132A, -R133D, and -R133E were replication-defective (**Figure 7A**, bottom panel, lanes 4, 6, and 7). HBc-R133A, -R133L, -R133H, -AAP, and -AAA supported HBV replication with a reduced efficiency (**Figure 7A**, bottom panel, lanes 5, 9, 10, 12, and 14) and were deficient in core particle–Par14/Par17 interactions (fifth panel). Although core particles formed by HBc-R133K, -P134A, and -RAA interacted with Par14/Par17 with similar efficiencies (**Figure 7A**, fifth and sixth panels, lanes 8, 11, and 13), HBV DNA synthesis was higher with HBc-R133K than with HBc-P134A and -RAA (**Figure 7A**, bottom panel, lanes 8 vs. 11 and 13). HBV DNA synthesis with HBc-P134A and -RAA was similar to that with HBc-R133A, -R133L, and -R133H (**Figure 7A**, bottom panel, lanes 11 and 13 vs. 5, 9, and 10), indicating that the RP motif itself is important for HBV replication. HBV replication with HBc-R133K was 53% of that with HBc WT, indicating that the RP motif is preferable to the KP motif for HBV replication (**Figure 7A**, bottom panel, lanes 3 vs. 8). HBV DNA synthesis was reduced more by HBc-AAP than by other core particle assembly-competent HBc RP mutants (**Figure 7A**, bottom panel, lanes 5, 8–11, and 13 vs. 12). HBV replication with HBc-AAA was comparable to that with HBc-AAP, demonstrating that P135 is not important for HBV replication (**Figure 7A**, bottom panel, lane 12 vs. 14).

Core particle assembly and HBV DNA synthesis were reduced by HBc RP motif mutants; therefore, pgRNA encapsidation from isolated core particles was examined by the RPA (**Figure 7B**). Except for the core particle assembly-defective HBc-R133D (**Figure 7B**, lane 3), the selected HBc RP mutants could encapsidate pgRNA with reduced efficiencies (**Figure 7B**, lanes 1 vs. 2 and 4–6). In accordance with HBV DNA synthesis (**Figure 7A**, bottom panel, lanes 3 vs. 8), pgRNA encapsidation by HBc-R133K was 63% of that by HBc WT (**Figure 7B**, lane 1 vs. 4). The decreased level of pgRNA encapsidated by HBc-AAP (**Figure 7B**, lane 1 vs. 6) was also comparable with the level of HBV DNA synthesis (**Figure 7A**, bottom panel, lanes 3 vs. 12), demonstrating that the RP motif is critical for pgRNA encapsidation.

Next, core particle assembly, core particle–Par14/Par17 interactions, and HBV DNA synthesis were compared between control and *PIN4*-KD HepG2 cells (**Figure 7C**). Core particle assembly by HBc WT and HBc-R133K was reduced in *PIN4*-KD cells (**Figure 7C**, sixth panel, lanes 2 vs. 3 and 6 vs. 7). However, core particle assembly by other HBc RP mutants was not reduced (**Figure 7D**, sixth panel), indicating that efficient core particle assembly is facilitated by a positively charged R or K residue in the RP motif. In accordance with the above results (**Figures 4B,C**, top panels, and **Figure 7A**, fifth panel), core particle–Par14/Par17 interactions with HBc WT, HBc-R133K, -P134A, and -RAA were presented (**Figure 7D**, fifth panel). As expected, core particle–Par14/Par17 interactions with these HBc proteins were decreased in *PIN4*-KD cells (**Figure 7D**, fifth panel). Consistent with core particle assembly by HBc WT and HBc-R133K (**Figure 7D**, sixth panel, lanes 2 vs. 3 and 6 vs. 7), HBV DNA synthesis was reduced in *PIN4*-KD cells (**Figure 7D**, bottom panel, lanes 2 vs. 3 and 6 vs. 7), in contrast with the other RP mutants. HBV DNA synthesis was decreased more with HBc WT than with HBc-R133K in *PIN4*-KD cells, indicating that RP is more preferred than KP for Par14/Par17 effects. When Par14 or Par17 was overexpressed, HBV replication was only enhanced with HBc WT and HBc-R133K (S10 and S11 Figs), further strengthening the importance of the RP or KP motif.

Par14/Par17 enhance HBV replication in an HBx-dependent manner by binding to the $^{19}$RP$^{20}$ and $^{28}$RP$^{29}$ motifs of HBx (Saeed et al., 2019). Therefore, Par14/Par17-mediated replication of HBc-HBx-double-deficient HBV was investigated. As expected, when HBc WT plus HBx WT were supplied to double-deficient HBV, Par14 WT and Par17 WT enhanced HBV replication (**Figure 7D**, sixth and bottom panels, lanes 6–8). When HBc WT was supplied to double-deficient HBV, neither Par14 WT nor Par17 WT enhanced HBV replication (**Figure 7D**, sixth and bottom panels, lanes 3–5), demonstrating the requirement for HBx (Saeed et al., 2019). When HBc WT plus HBx-AAAA were supplied, neither Par14 WT nor Par17 WT enhanced HBV replication, similar to cells that were only supplied HBc WT (**Figure 7D**, sixth and bottom panels, lanes 3–5 vs. 9–11). When HBc-AAP plus HBx-AAAA were supplied, HBV replication was not enhanced by Par14 WT or Par17 WT and was the lowest among the examined cells (**Figure 7D**, sixth and bottom panels, lanes 3–5, 6–8, 9–11, vs. 12–14), indicating that specific HBx–Par14/Par17 interactions and specific HBc– and/or core particle–Par14/Par17 interactions upregulate HBV replication.

## The HBc RP Motif Is Crucial for Par14/Par17-Mediated HBV Replication in an Infection System

To substantiate the aforementioned findings in an HBV infection system, virions of the full-length subtype adwR9 HBV WT (Kim et al., 2004) and the corresponding HBV-HBc-AAP mutant were prepared from transfected HepG2 cells. pgRNA transcription was controlled by the CMV IE promoter. To infect HepG2-hNTCP-C9 cells, the HBV WT or mutant HBV-HBc-AAP virion inoculum was adjusted to approximately $1.7 \times 10^3$ genome equivalents (GEq) per cell. Of note, while preparing HBV virions, mutant HBV-HBc-AAP produced 7 times less viruses than HBV WT ($0.55 \times 10^7$ GEq/ml vs. $3.87 \times 10^7$ GEq/ml), further indicating that the RP motif is crucial for viral replication. The levels of HBV RNAs, HBc protein, core particle assembly, core particle–Par14/Par17 interactions, and HBV DNA synthesis were lower in HBV-HBc-AAP-infected cells than in HBV WT-infected cells (**Figure 8A**, third, sixth, eighth, ninth, and bottom panels, lane 2 vs. 3). However, the level of cccDNA was comparable (**Figure 8A**, fifth panel, lane 2 vs. 3).

Next, shControl and *PIN4*-KD-HepG2-hNTCP-C9 cells were infected with HBV WT or mutant HBV-HBc-AAP. Consistent with **Figure 8A**, infection of shControl cells generated the same results (**Figure 8B**, third, fifth, sixth, ninth, and bottom panels, lane 2 vs. 3). As expected, the levels of HBV RNAs, HBc protein, core particle assembly, and HBV DNA synthesis

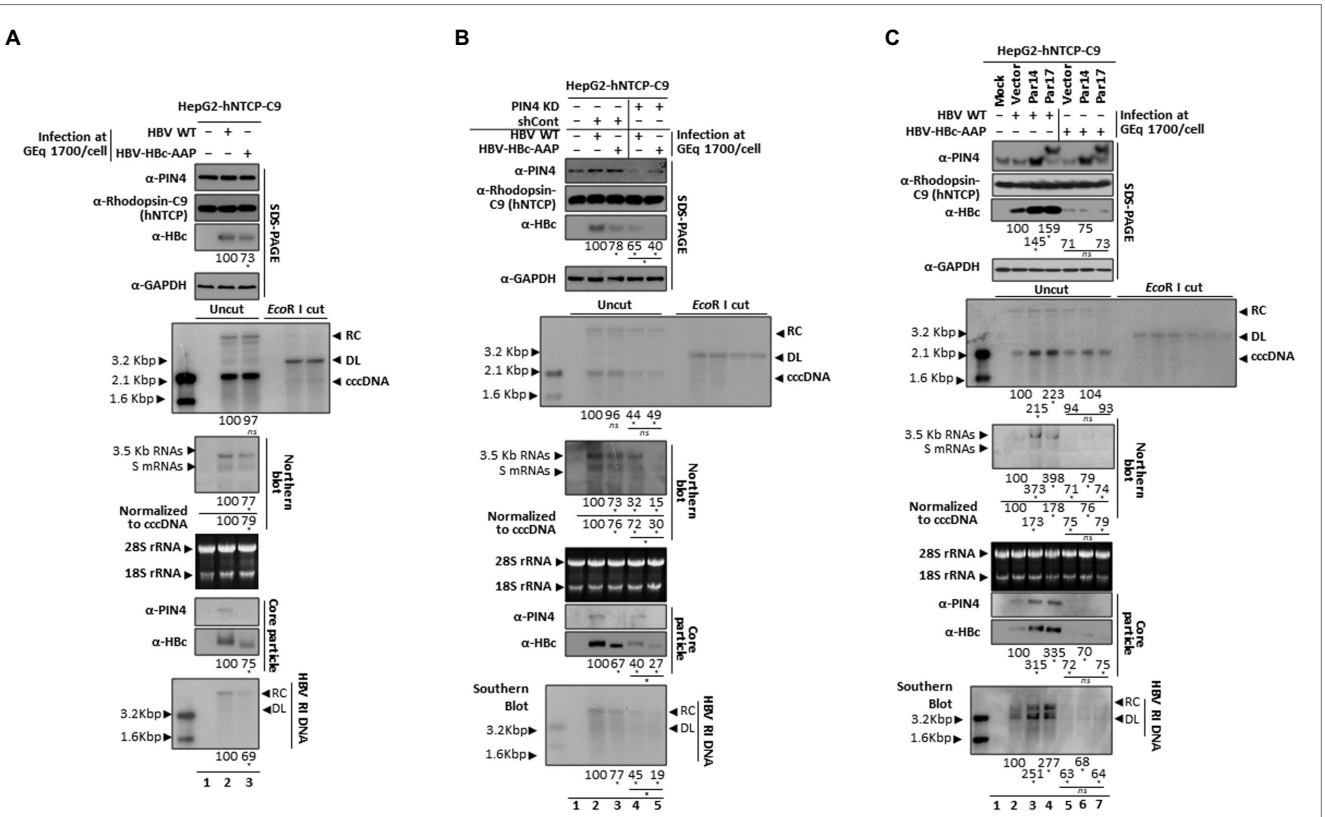


**FIGURE 8 |** The HBc RP motif is critical for Par14/Par17-mediated HBV replication in infected cells. **(A)** HBV replication was significantly decreased with HBV-HBc-AAP, demonstrating that the HBc $^{133}$RP$^{134}$ motif is important. A total of $2 \times 10^5$ HepG2-hNTCP-C9 cells were grown in collagen-coated 6-well plates, infected with $1.7 \times 10^3$ GEq of HBV WT (lane 2) or HBV-HBc-AAP mutant (lane 3) virions as described in the "Materials and Methods" section, and lysed at 9 days p.i. Lane 1 is a mock-infected control. **(B)** Decreased HBV replication in *PIN4* KD cells was further inhibited upon HBV-HBc-AAP infection. HepG2-hNTCP-C9-shControl (lanes 2 and 3) and HepG2-hNTCP-C9-shPIN4-#5 (lanes 4 and 5) cells were infected with HBV WT and HBV-HBc-AAP mutant virions, as described above. Lane 1 is mock-infected control HepG2-hNTCP-C9 cells. **(C)** Although Par14 and Par17 overexpression increased HBV replication in HBV WT-infected cells, it did not affect HBV replication in HBV-HBc-AAP-infected cells. Mock- (lane 1), empty vector- (lanes 2 and 5), Par14- (lanes 3 and 6), and Par17-transduced (lanes 4 and 7) HepG2-hNTCP-C9 cells were infected with $1.7 \times 10^3$ GEq of HBV WT (lane 2–4) or HBV-HBc-AAP mutant (lanes 5–7) virions and lysed at 5 (for total RNA) or 9 days p.i. HBV cccDNA was extracted and subjected to Southern blotting as described previously [35]. For Northern blotting, 20 μg of total RNA was loaded per lane. The 3.5 kb pgRNA, 2.1 and 2.4 kb S mRNAs, and 28S and 18S ribosomal RNAs are indicated. SDS-PAGE and immunoblotting, NAGE and immunoblotting of core particles, and Southern blotting were performed as described above. Relative levels of core particles, HBV RNAs, HBV cccDNA, and HBV RI DNAs were measured using ImageJ v.1.46r. Viral RNA levels were normalized to cccDNA levels. Data are presented as means from three independent experiments. Statistical significance was evaluated using Student's *t*-test. $^*p < 0.05$ relative to the corresponding control.

were lower in HBV-HBc-AAP-infected *PIN4*-KD cells than in HBV WT-infected *PIN4*-KD cells (**Figure 8B**, third, sixth, ninth, and bottom panels, lane 4 vs. 5). However, the ratio was more drastic in *PIN4*-KD cells (**Figure 8B**, lanes 2 vs. 3; lanes 4 vs. 5). The cccDNA level was comparable (**Figure 8B**, fifth panel, lane 4 vs. 5).

In HBV WT-infected, Par14/Par17-overexpressing cells, HBV cccDNA, HBV RNAs, HBc protein, core particle assembly, core particle–Par14/Par17 interactions, and HBV DNA synthesis were all significantly increased (**Figure 8C**, third, fifth, sixth, eighth, ninth, and bottom panels, lanes 2 vs. 3 and 4). However, HBV-HBc-AAP infection of Par14- or Par17-overexpressing HepG2-hNTCP-C9 cells did not affect HBV replication at all (**Figure 8C**, lanes 5 vs. 6 and 7), demonstrating that the RP motif of HBc is critical for Par14/Par17-mediated upregulation of HBV replication.

## Par14/Par17 Promote Recruitment of HBc Into HBV cccDNA in the Nucleus

HBV nuclear cccDNA is organized as a minichromosome in association with histone and non-histone cellular and viral proteins, including viral HBx and HBc proteins (Bock et al., 2001; Lucifora and Protzer, 2016; Piracha et al., 2020). We previously demonstrated HBx–Par14/Par17–cccDNA interactions in the nucleus (Saeed et al., 2019).

HBc associates with cccDNA as a non-histone protein (Bock et al., 2001; Guo et al., 2011; Lucifora and Protzer, 2016; Diab et al., 2018; Piracha et al., 2020) and HBc-Par14/Par17 interactions (**Figures 1, 2**, and **5A,B**) were also detected in the nucleus (**Figure 5B**). Therefore, recruitment of HBc onto cccDNA in the presence or absence of Par14/Par17 was examined by ChIP. Consistent with the previous report, Par14/Par17 overexpression enhanced recruitment of RNA polymerase II and acetylated

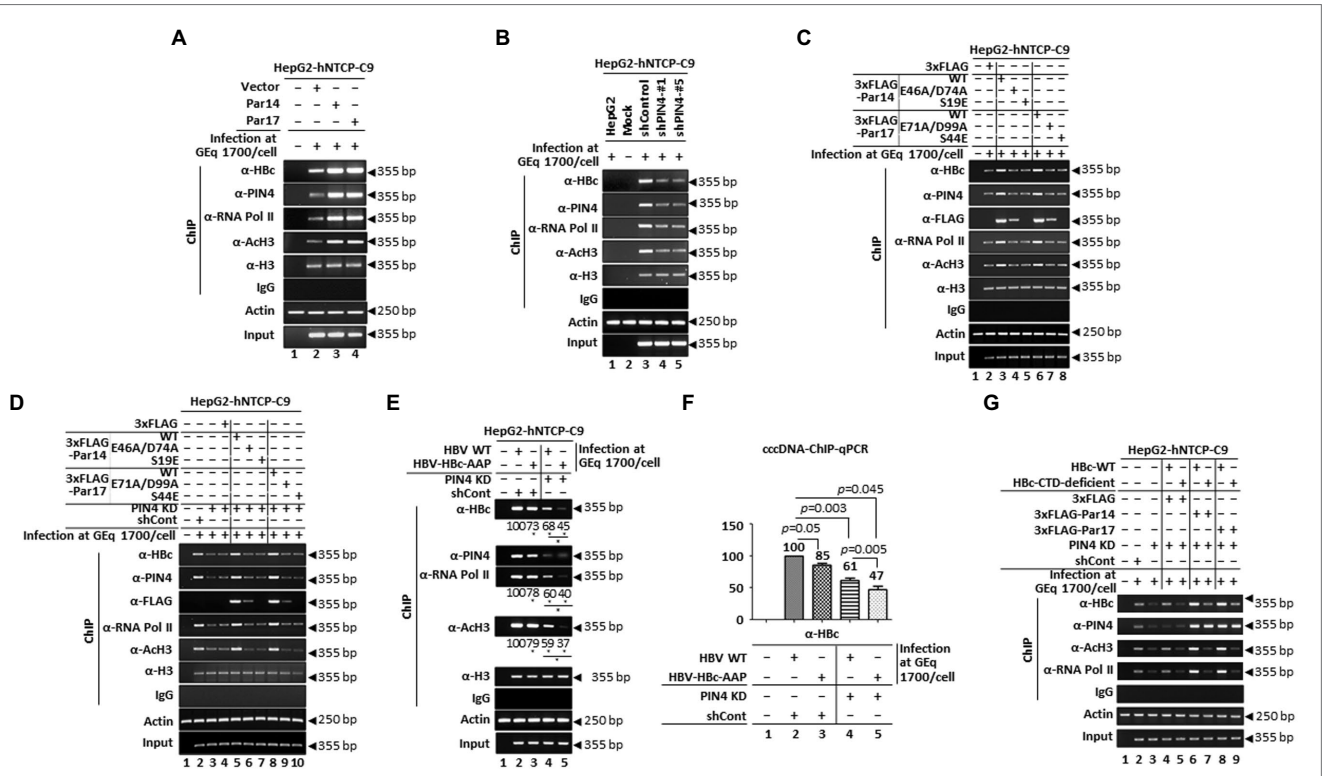


**FIGURE 9 |** The S19 and E46/D74 residues of Par14 and S44 and E71/D99 residues of Par17 promote recruitment of HBc into cccDNA *via* the HBc RP motif. **(A)** Overexpressed Par14 and Par17 increase recruitment of HBc into cccDNA. Vector- (lane 2), Par14- (lane 3), and Par17-transduced (lane 4) HepG2-hNTCP-C9 cells were infected with $1.7 \times 10^3$ GEq of HBV WT. Mock-infected HepG2-hNTCP-C9 cells were used a negative control (lane 1). **(B)** *PIN4* KD reduces binding of HBc to cccDNA. HepG2-hNTCP-C9-shControl (lane 3), HepG2-hNTCP-C9-shPIN4-#1 (lane 4), and HepG2-hNTCP-C9-shPIN4-#5 (lane 5) cells were infected with HBV as described above. HepG2 cells were infected (lane 1) and HepG2-hNTCP cells were mock-infected (lane 2) as negative controls. **(C,D)** Substrate- and DNA-binding residues of Par14 (E46/D74 and S19, respectively) and Par17 (E71/D99 and S44, respectively) are important for enhanced recruitment of HBc into cccDNA. HepG2-hNTCP-C9 cells were plated as described above and mock-transfected (lane 1) or transfected with 3 × FLAG (lane 2), 3 × FLAG-Par14 WT (lane 3), 3 × FLAG-Par14-E46A/D74A (lane 4), 3 × FLAG-Par14-S19E (lane 5), 3 × FLAG-Par17 WT (lane 6), 3 × FLAG-Par17-E71A/D99A (lane 7), or 3 × FLAG-Par17-S44E (lane 8) **(C)**. HepG2-hNTCP-C9 (lane 1), HepG2-hNTCP-C9-shControl (lane 2), and HepG2-hNTCP-C9-shPIN4-#1 (lanes 3–10) cells were seeded as described above. As additional controls, HepG2-hNTCP-C9-shPIN4-#1 cells were mock-transfected (lane 3) or transfected with 3 × FLAG (lane 4). HepG2-hNTCP-C9-shPIN4-#1 cells were transfected with 3 × FLAG-Par14 WT (lane 5), 3 × FLAG-Par14-E46A/D74A (lane 6), 3 × FLAG-Par14-S19E (lane 7), 3 × FLAG-Par17 WT (lane 8), 3 × FLAG-Par17-E71A/D99A (lane 9), or 3 × FLAG-Par17-S44E (lane 10) **(D)**. **(E,F)** The HBc RP motif is critical for recruitment of HBc into cccDNA. HepG2-hNTCP-C9 (lane 1), HepG2-hNTCP-C9-shControl (lanes 2 and 3), and HepG2-hNTCP-C9-shPIN4-#1 (lanes 4 and 5) cells were infected with HBV WT (lanes 2 and 4) or HBV-HBc-AAP mutant (lanes 3 and 5) virions at $1.7 \times 10^3$ GEq per cell as detailed in the "Materials and Methods" section. (G) The HBc CTD is important for recruitment of HBc into cccDNA. HepG2-hNTCP-C9 (lane 1), HepG2-hNTCP-C9-shControl (lane 2), and HepG2-hNTCP-C9 *PIN4*-KD (lane 3) cells were used as controls. HepG2-hNTCP-C9 *PIN4*-KD cells were co-transfected with 3 × FLAG plus HBc WT (lane 4), the HBc CTD-deficient construct (lane 5), 3 × FLAG-Par14 WT plus HBc WT (lane 6) or the HBc CTD-deficient construct (lane 7), or 3 × FLAG-Par17 WT plus HBc WT (lane 8) or the HBc CTD-deficient construct (lane 9). HepG2-hNTCP-C9-shControl (lane 2) and HepG2-hNTCP-C9 *PIN4*-KD (lanes 3–9) cells were infected with HBV as described above. At 9 days p.i., chromatin solutions were prepared as described previously [35] and subjected to immunoprecipitation with an anti-PIN4, anti-FLAG, anti-HBc, anti-RNA polymerase II (Abcam #ab817), anti-acetyl H3 (Merck Millipore #06–599), or anti-H3 antibody (positive control) or normal rabbit polyclonal IgG (negative control). Immunoprecipitated chromatin was analyzed by semi-quantitative PCR **(A–E,G)** or quantitative real-time PCR **(F)**. Relative levels of HBc, RNA polymerase II, acetyl H3, and HBV RNA were measured using ImageJ 1.46r. Representative data from three independent experiments are shown. Statistical significance in E and F was evaluated using Student's *t*-test. $^*p < 0.05$ (E) and exact *p*-values **(F)** relative to the corresponding controls are shown.

H3 onto cccDNA (**Figure 9A**, third and fourth panels, lanes 2 vs. 3 and 4; Saeed et al., 2019). Furthermore, Par14/Par17 overexpression enhanced recruitment of HBc onto cccDNA (**Figure 9A**, top panel, lanes 2 vs. 3 and 4). *PIN4* KD reduced recruitment onto cccDNA (**Figure 9B**, top, third, and fourth panels, lanes 3 vs. 4 and 5).

To assess whether the substrate- and DNA-binding residues of Par14/Par17 (Saeed et al., 2019) are involved in recruitment of HBc onto cccDNA, ChIP was subjected (**Figure 9C**). Recruitment of HBc onto cccDNA was reduced by Par14-E46A/D74A, Par14-S19E, Par17-E71A/D99A, and Par17-S44E compared with Par14 WT and Par17 WT (**Figure 9C**, top panel, lanes 3 vs. 4 and 5; lanes 6 vs. 7 and 8), indicating that the substrate-binding E46/D74 of Par14 and E71/D99 of Par17 and the DNA-binding S19 of Par14 and S44 of Par17 are important for HBc recruitment onto cccDNA. The same result was obtained when a similar experiment was conducted with *PIN4*-KD HepG2-hNTCP-C9 cells (**Figure 9D**, top panel, lanes 5 vs. 6 and 7; lanes 8 vs. 9 and 10), further strengthening our conclusion.

Is the Par14/Par17-interacting $^{133}$RP$^{134}$ motif of HBc important for its recruitment onto cccDNA? We performed ChIP. shControl and *PIN4*-KD HepG2-hNTCP-C9 cells were infected with virions from HBV WT- or HBV-HBc-AAP-transfected HepG2 cells (**Figures 9E,F**). Recruitment of HBc-AAP onto cccDNA was lower than that of HBc WT in control cells (**Figure 9E**, top panel, lane 2 vs. 3). Likewise, recruitment of HBc-AAP onto cccDNA was lower than that of HBc WT in *PIN4*-KD cells (**Figure 9E**, top panel, lane 4 vs. 5), indicating that the $^{133}$RP$^{134}$ motif of HBc is important for interactions of HBc, Par14/Par17, and cccDNA. To quantitate recruitment of HBc WT and HBc-AAP onto cccDNA in the presence of absence of Par14/Par17, quantitative real-time PCR was performed (**Figure 9F**). As expected, recruitment of HBc-AAP was lower than that of HBc WT in shControl and *PIN4*-KD cells (**Figure 9F**, lane 2 vs. 3; lane 4 vs. 5). In the absence of Par14/Par17, the reduced recruitment of HBc-AAP relative to HBc WT was more evident, with ratios of 100:85 vs. 61:47 (100:67; **Figure 9F**, lane 2 vs. 3; lane 4 vs. 5).

The HBc CTD contains highly basic residues (arginine-rich, protamine-like) that resemble histone tails and are critical for non-specific nucleic acid binding (Nassal, 1990; Yu and Summers, 1991; Hatton et al., 1992; Köck et al., 2004; Jung et al., 2012, 2014; Diab et al., 2018). Therefore, the CTD of HBc may bind to cccDNA and the RP motif of HBc may interact with Par14/Par17. To explore this possibility, we used a HBc CTD-deficient construct (Jung et al., 2012). Co-transfected *PIN4*-KD HepG2-hNTCP-C9 cells were then infected with HBV WT, as described previously (Yang et al., 2019). Here, HBc proteins were provided by transfection and infection (**Figure 9G**). Therefore, in the case of CTD-deficient HBc transfection, both CTD-deficient HBc and HBc WT proteins were present (Yang et al., 2019). Transfection of CTD-deficient HBc reduced recruitment of HBc onto cccDNA in the presence or absence of Par14/Par17 WT (**Figure 9G**, top panel, lane 4 vs. 5; lane 6 vs. 7; lane 8 vs. 9). Since CTD-deficient HBc lacks NLS, it cannot localize in the nucleus. However, when both HBc WT and CTD-deficient HBc is present, HBc WT recruitment onto cccDNA is reduced, indicating that CTD-deficient HBc might interfere HBc WT to localize in the nucleus with unknown mechanism, resulting the reduced recruitment of HBc WT onto cccDNA. As expected, Par14/Par17 overexpression upregulated recruitment of HBc WT and CTD-deficient HBc onto cccDNA (**Figure 9G** top

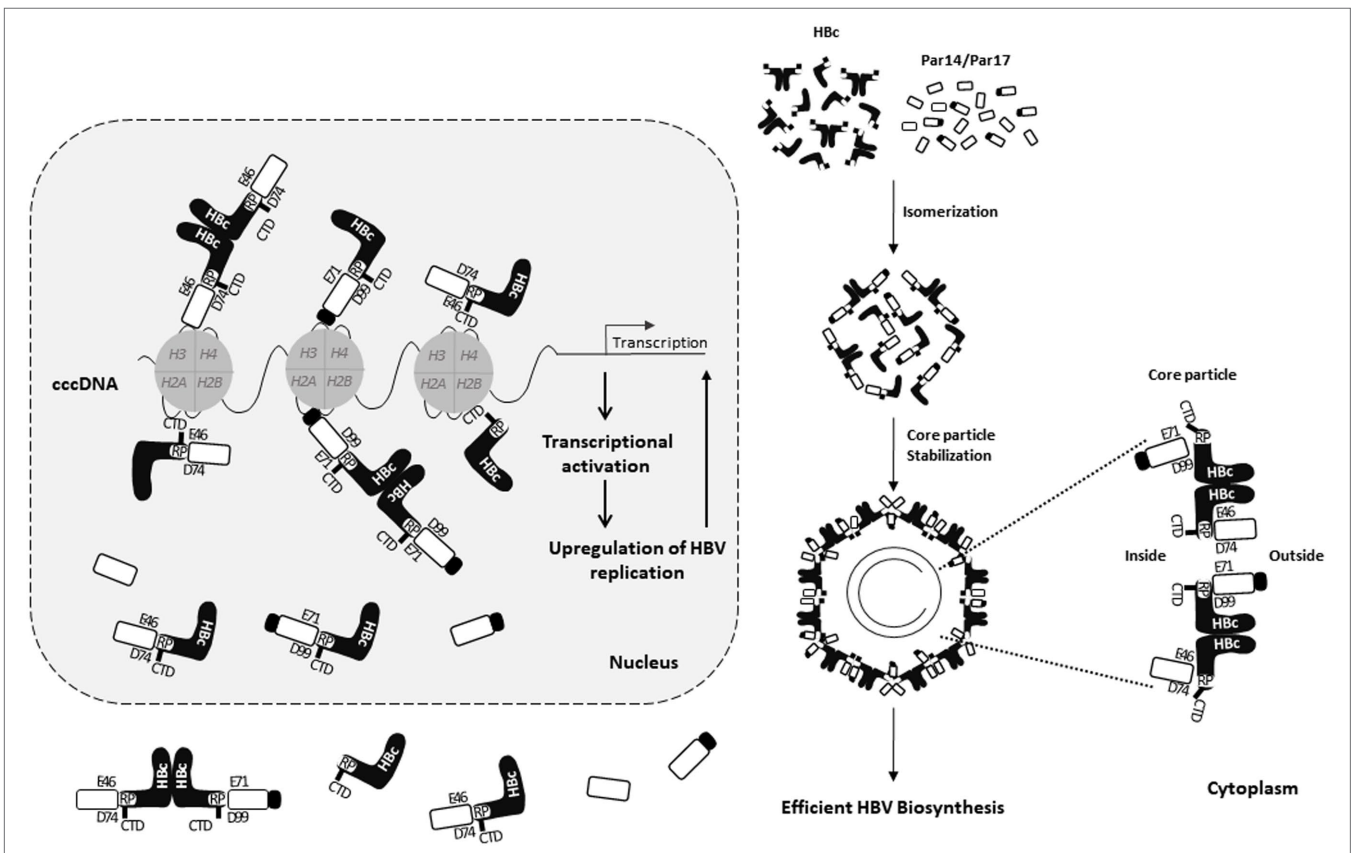


**FIGURE 10 |** Model of Par14/Par17–core particle interactions in the cytoplasm and interactions of Par14/Par17, HBc, and cccDNA in the nucleus. The HBV cccDNA minichromosome is associated with histone and non-histone cellular and viral proteins including HBc and HBx. In the nucleus, HBc binds to cccDNA and Par14/Par17 through its CTD and $^{133}$RP$^{134}$ motif, respectively. Par14 and Par17 in the nucleus also directly bind to cccDNA *via* S19 and S44, respectively, interact with HBc *via* the substrate-binding E46/D74 and E71/D99 residues, respectively, and promote recruitment of HBc into cccDNA. In the cytoplasm, Par14/Par17 bind to and stabilize HBc and enhance assembly and stability of the core particle by binding both outside and inside the core particle. Through these interactions in the nucleus and cytoplasm, HBV replication is upregulated.

panel, lane 4 vs. 6 and 8; lane 5 vs. 7 and 9), demonstrating that the CTD of HBc, in addition to its RP motif, is critical for recruitment of HBc onto cccDNA.

The E46/D74 and E71/D99 residues of Par14/Par17 bind to the $^{133}$RP$^{134}$ motif of HBc, the S19/44 residues of Par14/Par17 bind to cccDNA (Saeed et al., 2019), and the CTD of HBc binds to cccDNA (Chong et al., 2017). Therefore, HBc–Par14/Par17–cccDNA, HBc–cccDNA–Par14/Par17, or Par14/Par17–HBc–cccDNA interactions may occur in the nucleus (**Figure 10**).

Taken together, in addition to HBx–Par14/Par17–cccDNA interactions in the nucleus and HBx–Par14/Par17 interactions in the cytoplasm and mitochondria (Saeed et al., 2019), we demonstrate that interactions of HBc, Par14/Par17, and cccDNA in the nucleus and core particle–Par14/Par17 interactions in the cytoplasm can enhance HBV replication through increased transcriptional activity, increased core particle assembly and/or stability, and increased HBV DNA synthesis.

## DISCUSSION

Host PPIase parvulins affect HBV. Specifically, Par14/Par17 interact with two RP motifs of HBx to enhance HBx stability and promote HBV replication (Saeed et al., 2019), Pin1 interacts with phosphorylated SP motifs of HBx to facilitate HBx transactivation and hepatocarcinogenesis progression (Pang et al., 2007), and Pin1 binds to HBc *via* specific phosphorylated Thr$^{160}$-Pro and Ser$^{162}$-Pro motifs and stabilizes HBc in a phosphorylation-dependent manner for efficient HBV propagation (Nishi et al., 2020). We demonstrate here that other parvulin proteins, Par14/Par17, physically interact with HBc protein, as shown using core particle assembly-defective HBc-Y132A (**Figure 1**) and stabilize HBc through its $^{133}$RP$^{134}$ motif (**Figure 6** and **Supplementary S7 Figure**). We further show that Par14/Par17 physically interact with the core particle (**Figure 1**) and enhance its stability through the HBc RP motif (**Figure 6**).

Several host factors reportedly bind to HBc and affect the stabilities of HBc and/or the core particle. Pin1 stabilizes HBc but it is unknown whether it affects core particle stability (Nishi et al., 2020). Heat shock protein 90 (hsp90) binds to the HBc-149 dimer and increases core particle stability (Shim et al., 2011). NIRF, an E3 ubiquitin ligase, and hsp40/DnaJ proteins bind to HBc and decrease its stability *via* unknown binding sites (Sohn et al., 2006; Qian et al., 2012).

Likewise, the HBc CTD phosphorylation status affects core particle stability (Selzer and Zlotnick, 2015). Although many HBc CTD-binding proteins have been identified (Diab et al., 2018; Yang, 2018), not many HBc NTD-binding proteins are known. Although hsp90 and NIRF are speculated to be HBc NTP-binding proteins, the exact HBc-binding sites have not been identified (Shim et al., 2011; Qian et al., 2012). We present Par14/Par17 as HBc NTD-binding proteins that enhance HBV replication and have multiple roles (**Figures 6–10**; Saeed et al., 2019).

Structural studies of HBc revealed that the RP motif is located in an irregular proline-rich loop 6 ($^{128}$TPPAY*RP*PN$^{136}$) followed by helix α5 (aa 112–127; Wynne et al., 1999). Loop 6 is highly conserved among 10 genotypes of human and mammalian hepadnaviruses (**Figures 3A,B**). In this loop, Y132 mediates the HBc dimer–dimer interaction to facilitate core particle assembly, meaning the Y132A mutant is core particle assembly-defective (Wynne et al., 1999; Bourne et al., 2009). Similarly, the HBc-R133D and -R133E mutants were core particle assembly-defective (**Figure 4**) and dimer-positive (**Figure 5C**), indicating that R133 is also involved in HBc dimer–dimer interactions to facilitate core particle formation. Of note, the Y132, R133, and P134 residues are completely conserved (**Figures 3A,B**).

The results of cryo-scanning electron microscopy indicated that the HBc CTD shuttles between the interior and exterior of the core particle (Yu et al., 2013), partly due to differences in its charge balance (Selzer et al., 2015). Unlike hsp90, which is incorporated into the core particle (Shim et al., 2011), the Nedd4 ubiquitin ligase and γ2-adaptin, a ubiquitin-interacting adaptor, may interact with the core particle partly through the surface-exposed, late domain-like $^{129}$PPAY$^{132}$ motif (Rost et al., 2006). Here, we show that some fractions of Par14/Par17 bind outside the core particle, while other fractions of Par14/Par17 are incorporated into the core particle (**Figure 2A**). Par14/Par17 bind to the HBc RP motif in the core particle (**Figures 4, 5A,B**) and the HBc PPAY motif is at the dimer–dimer interface (Wynne et al., 1999). Therefore, we propose that shuttling of the HBc CTD between the interior and exterior of the core particle (Wang et al., 2012; Yu et al., 2013) starts from loop 6, including the $^{129}$PPAY$^{132}$ and $^{133}$RP$^{134}$ motifs, to the structurally disordered HBc CTD.

A previous study demonstrated that core particles by the HBc-R133A mutant migrate rapidly by NAGE (Wu et al., 2018). We further showed that core particles by the HBc-R133L, -R133H, -AAP, and AAA mutants also migrate rapidly (**Figures 4B,C**, second and third panels, lanes 2 vs. 4, 8, 9, 11, and 13) and fail to interact with Par14/Par17 (**Figures 4B,C**, top panel, lanes 2 vs. 4, 8, 9, 11, and 13). Interestingly, when R133 is changed to negatively charged D or E, core particle assembly is defective, as observed with the HBc-Y132A mutant (**Figures 4B,C**, top panel, lanes 2 vs. 4, 8, 9, 11, and 13). The E46/71 and D74/99 residues of Par14/Par17 are important for interactions with HBc and the core particle (**Figures 2B–D**); therefore, the R133D or R133E HBc mutant may repel Par14/Par17, rendering core particle assembly-defective. Taken together, we suggest that a positively charged residue at position 133 of HBc at the surface of the core particle changes the mobility of the core particle and ensures it is neither too stable nor unstable for replication (Jung et al., 2012; Wu et al., 2018) and that this is assisted through interactions with Par14/Par17.

Nuclear HBc plays prominent roles in modulating viral and host gene expression, splicing and nuclear export of viral transcripts, and cccDNA function.[7] HBc is a main component of HBV cccDNA (Bock et al., 2001; Guo et al., 2011; Lucifora and Protzer, 2016; Diab et al., 2018). HBc induces nucleosomal organization to positively regulate HBV transcription (Bock et al., 2001; Guo et al., 2011). However, HBc may not be absolutely required for cccDNA transcription (Zhang et al., 2014). Furthermore, repressive symmetric dimethylation of R3 of H4 (H4R3me2s) on cccDNA by PRMT5 occurs through its interaction with HBc (Zhang et al., 2017). Conversely, HBc positively regulates

HBV transcription through the interaction of its RP motif with Par14/Par17 (**Figures 8, 9** and **Supplementary Figures S12–S15**). Taken together, we postulate that HBc can function as both a negative and positive regulator of HBV transcription through its interactions with repressive modifiers, such as PRMT5, and activating modifiers, such as CREB-binding protein (Guo et al., 2011) and Par14/Par17 (**Figures 8–10**).

Consistent with the structural and regulatory roles of HBc in HBV replication (Zlotnick et al., 2015; Diab et al., 2018), our study further demonstrated that Par14/Par17 strengthen the structural roles of HBc and the core particle by enhancing their stabilities (**Figure 6**). The cccDNA–Par14/17–HBx complex promotes transcriptional activation (Saeed et al., 2019), and Par14/Par17 enhance recruitment of HBc into cccDNA and HBV transcription (**Figure 9** and **Supplementary Figures S12–S15**), strengthening the regulatory role of HBc. Taken together, we hypothesize that the chromatin remodelers Par14/Par17 induce unwinding of cccDNA *via* HBc and HBx proteins to activate transcription and ultimately augment HBV replication. This hypothesis should be investigated in the future. If this proves to be the case, targeting HBc, HBx, or Par14/Par17 might cure HBV infection by silencing cccDNA transcription.

Additionally, Iwamoto et al. (2017) demonstrated that microtubules are important for efficient HBV core particle formation and replication. Since Par14/Par17 can interact with tubulin and promote its polymerization (Thiele et al., 2011), whether Par14/Par17 facilitate HBV replication through an enhanced tubulin polymerization can be investigated in the future. Also, it should be investigated whether other HBV proteins, such as HBs or polymerase, might also interact with Par14/Par17 and affect HBV replication through their interaction.

### Statistical Analysis

Data are expressed as mean values ± standard deviations. Mean values were compared using Student's *t*-test. Values of $p < 0.05$ were considered statistically significant.

## DATA AVAILABILITY STATEMENT

The original contributions presented in the study are included in the article/**Supplementary Material**, further inquiries can be directed to the corresponding author.

## AUTHOR CONTRIBUTIONS

KK: study concept and design, study supervision, analysis and interpretation of data, obtained funding, drafting of the manuscript, and critical revision of the manuscript. US: acquisition of data, analysis and interpretation of data, and drafting of the manuscript. ZP: analysis and interpretation of data and statistical analysis. HK, JK, and FK: administrative, technical, or material support. Y-JC, SP, H-JS, HL, and JL: critical revision of the manuscript. All authors contributed to the article and approved the submitted version.

## FUNDING

This work was supported by the National Research Foundation Grants funded by the Korean Government (NRF-2019-R1A2C2005749).

## AUTHOR SUMMARY

The essential HBc protein plays structural and regulatory roles for HBV replication. We demonstrated that parvulin Par14/Par17 proteins can bind to both HBc and core particle, through a conserved RP motif on HBc. Through HBc– and/or core particle–Par14/Par17 interactions, HBc and core particle can be stabilized, and HBV replication can be upregulated. Also, Par14/Par17 were shown to promote HBc recruitment into cccDNA, like HBx. Our results indicate that in addition to the HBx–Par14/Par17–cccDNA interaction in the nucleus, the triple HBc, Par14/Par17, and cccDNA interaction in the nucleus, and the core particle–Par14/Par17 interaction in the cytoplasm are also important for HBV replication. These results suggest that inhibition or knockdown of Par14/Par17 may control HBV infection.

## SUPPLEMENTARY MATERIAL

The Supplementary Material for this article can be found online at: https://www.frontiersin.org/articless/10.3389/fmicb.2021.795047/full#supplementary-material

## REFERENCES

Belloni, L., Pollicino, T., de Nicola, F., Guerrieri, F., Raffa, G., and Fanciulli, M., et al. (2009). Nuclear HBx binds the HBV minichromosome and modifies the epigenetic regulation of cccDNA function. Available at: www.pnas.org/cgi/content/full/ (Accessed November 26, 2021).

Birnbaum, F., and Nassal, M. (1990). Hepatitis B virus nucleocapsid assembly: primary structure requirements in the core protein. *J. Virol.* 64, 3319–3330. doi: 10.1128/JVI.64.7.3319-3330.1990

Bock, C. T., Schwinn, S., Locarnini, S., Fyfe, J., Manns, M. P., and Trautwein, C. (2001). Structural organization of the hepatitis B virus minichromosome. *J. Mol. Biol.* 307, 183–196. doi: 10.1006/jmbi.2001.4481

Bourne, C. R., Katen, S. P., Fulz, M. R., Packianathan, C., and Zlotnick, A. (2009). A mutant hepatitis B virus core protein mimics inhibitors of icosahedral capsid self-assembly. *Biochemistry* 48, 1736–1742. doi: 10.1021/bi801814y

Cai, D., Nie, H., Yan, R., Guo, J.-T., Block, T. M., and Guo, H. (2013). A southern blot assay for detection of hepatitis B virus covalently closed circular DNA from cell cultures. *Methods Mol Biol.* 1030, 151–161. doi: 10.1007/978-1-62703-484-5_13

Chao, S.-H., Greenleaf, A. L., and Price, D. H. (2001). Juglone, an inhibitor of the peptidyl-prolyl isomerase pin1, also directly blocks transcription. *Nucleic Acids Res.* 29, 767–773. doi: 10.1093/nar/29.3.767

Chong, C. K., Cheng, C. Y. S., Tsoi, S. Y. J., Huang, F. Y., Liu, F., Seto, W. K., et al. (2017). Role of hepatitis B core protein in HBV transcription and recruitment of histone acetyltransferases to cccDNA minichromosome. *Antivir. Res.* 144, 1–7. doi: 10.1016/j.antiviral.2017.05.003

CLC Main workbench 21.0 software (2021). CLC Main workbench 8 software. Available at: https://www.qiagenbioinformatics.com/products/clc-main-workbench/ (Accessed October 1, 2021).

Cold Spring Harbor Laboratory (2015a). SDS–PAGE Sample Buffer (Nonreducing), Cold Spring Harb Protocol. Available at: http://cshprotocols.cshlp.org/content/2015/5/pdb.rec086991.full?rss=1 (Accessed October 1, 2021).

Cold Spring Harbor Laboratory (2015b). SDS–PAGE Sample Buffer (Reducing), Cold Spring Harb Protocol. Available at: http://cshprotocols.cshlp.org/content/2015/5/pdb.rec086942.full?text_only=true (Accessed October 1, 2021).

Cornberg, M., and Manns, M. P. (2018). Hepatitis: No cure for hepatitis B and D without targeting integrated viral DNA? *Nat. Rev. Gastroenterol. Hepatol.* 15, 195–196. doi: 10.1038/nrgastro.2017.185

Diab, A., Foca, A., Zoulim, F., Durantel, D., and Andrisani, O. (2018). The diverse functions of the hepatitis B core/capsid protein (HBc) in the viral life cycle: implications for the development of HBc-targeting antivirals. *Antivir. Res.* 149, 211–220. doi: 10.1016/j.antiviral.2017.11.015

Gallina, A., Bonelli, F., Zentilin, L., Rindi, G., Muttini, M., and Milanesi, G. (1989). A recombinant hepatitis B core antigen polypeptide with the protamine-like domain deleted self-assembles into capsid particles but fails to bind nucleic acids. *J. Virol.* 63, 4645–4652. doi: 10.1128/JVI.63.11.4645-4652.1989

Ganem, D. S. R. J. (2001). "The molecular biology of the hepatitis B viruses," in *Fields Virology. 4th Edn*. ed. Knipe (Philadelphia: Lippincott Williams & Wilkins).

Göthel, S. F., and Marahiel, M. A. (1999). Review peptidyl-prolyl cis-trans isomerases, a superfamily of Ubiquitous folding catalysts. *Cell Mol. Life Sci.* 55, 423–436. doi: 10.1007/s000180050299

Guo, Y. H., Li, Y. N., Zhao, J. R., Zhang, J., and Yan, Z. (2011). HBc binds to the CpG islands of HBV cccDNA and promotes an epigenetic permissive state. *Epigenetics* 6, 720–726. doi: 10.4161/epi.6.6.15815

Hatton, T., Zhou, S., and Standringl, D. N. (1992). RNA-and DNA-binding activities in hepatitis B virus capsid protein: a model for their roles in viral replication. *J. Virol.* 66, 5232–5241. doi: 10.1128/JVI.66.9.5232-5241.1992

Hennig, L., Christner, C., Kipping, M., Schelbert, B., Rücknagel, K. P., Grabley, S., et al. (1998). Selective inactivation of parvulin-like peptidyl-prolyl cis/trans isomerases by juglone. *Biochemistry* 37, 5953–5960. doi: 10.1021/bi973162p

Hu, J., and Seeger, C. (2015). Hepadnavirus genome replication and persistence. *Cold Spring Harb. Perspect. Med.* 5:a021386. doi: 10.1101/cshperspect.a021386

Iwamoto, M., Cai, D., Sugiyama, M., Suzuki, R., Aizaki, H., Ryo, A., et al. (2017). Functional association of cellular microtubules with viral capsid assembly supports efficient hepatitis B virus replication. *Sci. Rep.* 7:10620. doi: 10.1038/s41598-017-11015-4

Jung, J., Hwang, S. G., Chwae, Y.-J., Park, S., Shin, H.-J., and Kim, K. (2014). Phosphoacceptors threonine 162 and serines 170 and 178 within the carboxyl-terminal RRRS/T motif of the hepatitis B virus core protein make multiple contributions to hepatitis B virus replication. *J. Virol.* 88, 8754–8767. doi: 10.1128/jvi.01343-14

Jung, J., Kim, H.-Y., Kim, T., Shin, B.-H., Park, G.-S., Park, S., et al. (2012). C-terminal substitution of HBV core proteins with those from DHBV reveals that arginine-rich 167RRRSQSPRR175 domain is critical for HBV replication. *PLoS One* 7:e41087. doi: 10.1371/journal.pone.0041087

Kim, H. Y., Kim, H. Y., Jung, J., Park, S., Shin, H. J., and Kim, K. (2008). Incorporation of deoxyribonucleotides and ribonucleotides by a dNTP-binding cleft mutated reverse transcriptase in hepatitis B virus core particles. *Virology* 370, 205–212. doi: 10.1016/j.virol.2007.08.018

Kim, H. Y., Park, G. S., Kim, E. G., Kang, S. H., Shin, H. J., Park, S., et al. (2004). Oligomer synthesis by priming deficient polymerase in hepatitis B virus core particle. *Virology* 322, 22–30. doi: 10.1016/j.virol.2004.01.009

Ko, C., Chakraborty, A., Chou, W. M., Hasreiter, J., Wettengel, J. M., Stadler, D., et al. (2018). Hepatitis B virus genome recycling and de novo secondary infection events maintain stable cccDNA levels. *J. Hepatol.* 69, 1231–1241. doi: 10.1016/j.jhep.2018.08.012

Köck, J., Nassal, M., Deres, K., Blum, H. E., and von Weizsäcker, F. (2004). Hepatitis B virus nucleocapsids formed by carboxy-terminally mutated core proteins contain spliced viral genomes but lack full-size DNA. *J. Virol.* 78, 13812–13818. doi: 10.1128/jvi.78.24.13812-13818.2004

Liu, K., Luckenbaugh, L., Ning, X., Xi, J., and Hu, J. (2018). Multiple roles of core protein linker in hepatitis B virus replication. *PLoS Pathog.* 14:e1007085, 29782550. doi: 10.1371/journal.ppat.1007085

Lu, K. P., Finn, G., Lee, T. H., and Nicholson, L. K. (2007). Prolyl cis-trans isomerization as a molecular timer. *Nat. Chem. Biol.* 3, 619–629. doi: 10.1038/nchembio.2007.35

Lu, K. P., Hanes, S. D., and Hunter, T. (1996). A human peptidyl–prolyl isomerase essential for regulation of mitosis. *Nature* 380, 544–547. doi: 10.1038/380544a0

Lucifora, J., and Protzer, U. (2016). Attacking hepatitis B virus cccDNA-The holy grail to hepatitis B cure. *J. Hepatol.* 64, S41–S48. doi: 10.1016/j.jhep.2016.02.009

Matena, A., Rehic, E., Hönig, D., Kamba, B., and Bayer, P. (2018). Structure and function of the human parvulins Pin1 and Par14/17. *Biol. Chem.* 399, 101–125. doi: 10.1515/hsz-2017-0137

Mohd-Ismail, N. K., Lim, Z., Gunaratne, J., and Tan, Y. J. (2019). Mapping the interactions of HBV cccDNA with host factors. *Int. J. Mol. Sci.* 20:4276. doi: 10.3390/ijms20174276

Mueller, J. W., Kessler, D., Neumann, D., Stratmann, T., Papatheodorou, P., Hartmann-Fatu, C., et al. (2006). Characterization of novel elongated Parvulin isoforms that are ubiquitously expressed in human tissues and originate from alternative transcription initiation. *BMC Mol. Biol.* 7:9. doi: 10.1186/1471-2199-7-9

Nassal, M. (1990). Hepatitis B Virus nucleocapsid assembly: primary structure requirements in the core protein. *J. Virol.* 64, 3319–3330. doi: 10.1006/jmbi.2000.4481

Nassal, M. (1992). The arginine-rich domain of the hepatitis B virus core protein is required for pregenome encapsidation and productive viral positive-strand DNA synthesis but not for virus assembly. *J. Virol.* 66, 4107–4116. doi: 10.1128/JVI.66.7.4107-4116.1992

Ni, Y., Lempp, F. A., Mehrle, S., Nkongolo, S., Kaufman, C., Fälth, M., et al. (2014). Hepatitis B and D viruses exploit sodium taurocholate co-transporting polypeptide for species-specific entry into hepatocytes. *Gastroenterology* 146, 1070–1083. doi: 10.1053/j.gastro.2013.12.024

Nishi, M., Miyakawa, K., Matsunaga, S., Khatun, H., Yamaoka, Y., Watashi, K., et al. (2020). Prolyl isomerase Pin1 regulates the stability of hepatitis B virus core protein. *Front. Cell Dev. Biol.* 8:26. doi: 10.3389/fcell.2020.00026

Nkongolo, S., Ni, Y., Lempp, F. A., Kaufman, C., Lindner, T., Esser-Nobis, K., et al. (2014). Cyclosporin A inhibits hepatitis B and hepatitis D virus entry by cyclophilin-independent interference with the NTCP receptor. *J. Hepatol.* 60, 723–731. doi: 10.1016/j.jhep.2013.11.022

Pang, R., Lee, T. K. W., Poon, R. T. P., Fan, S. T., Wong, K. B., Kwong, Y. L., et al. (2007). Pin1 interacts with a specific serine-proline motif of hepatitis B virus X-protein to enhance hepatocarcinogenesis. *Gastroenterology* 132, 1088–1103. doi: 10.1053/j.gastro.2006.12.030

Piracha, Z. Z., Kwon, H., Saeed, U., Kim, J., Jung, J., Chwae, Y.-J., et al. (2018). Sirtuin 2 isoform 1 enhances hepatitis B virus RNA transcription and DNA synthesis through the AKT/GSK-3β/β-catenin signaling pathway. *J. Virol.* 92:e00955-18. doi: 10.1128/jvi.00955-18

Piracha, Z. Z., Saeed, U., Kim, J., Kwon, H., Chwae, Y.-J., Lee, H. W., et al. (2020). An alternatively spliced sirtuin 2 isoform 5 inhibits hepatitis B virus replication from cccDNA by repressing epigenetic modifications made by histone lysine methyltransferases. *J. Virol.* 94:e00926-20. doi: 10.1128/jvi.00926-20

Qian, G., Jin, F., Chang, L., Yang, Y., Peng, H., and Duan, C. (2012). NIRF, a novel ubiquitin ligase, interacts with hepatitis B virus core protein and promotes its degradation. *Biotechnol. Lett.* 34, 29–36. doi: 10.1007/s10529-011-0751-0

Revill, P. A., Chisari, F. V., Block, J. M., Dandri, M., Gehring, A. J., Guo, H., et al. (2019). A global scientific strategy to cure hepatitis B. *Lancet Gastroenterol. Hepatol.* 4, 545–558. doi: 10.1016/S2468-1253(19)30119-0

Rost, M., Mann, S., Lambert, C., Döring, T., Thomé, N., and Prange, R. (2006). γ2-adaptin, a novel ubiquitin-interacting adaptor, and Nedd4 ubiquitin ligase control hepatitis B virus maturation. *J. Biol. Chem.* 281, 29297–29308. doi: 10.1074/jbc.M603517200

Rulten, S., Thorpe, J., and Kay, J. (1999). Identification of eukaryotic Parvulin homologues: A new subfamily of Peptidylprolyl cis-trans Isomerases 1. Available at: http://www.idealibrary.com (Accessed November 26, 2021).

Saeed, U., Kim, J., Piracha, Z. Z., Kwon, H., Jung, J., Chwae, Y.-J., et al. (2019). Parvulin 14 and parvulin 17 bind to HBx and cccDNA and upregulate hepatitis B virus replication from cccDNA to virion in an HBx-dependent manner. *J. Virol.* 93:e01840-18. doi: 10.1128/jvi.01840-18

Saningong, A. D., and Bayer, P. (2015). Human DNA-binding peptidyl-prolyl cis/trans isomerase Par14 is cell cycle dependently expressed and associates with chromatin in vivo. *BMC Biochem.* 16:4. doi: 10.1186/s12858-015-0033-x

Seeger, C., and Mason, W. S. (2015). Molecular biology of hepatitis B virus infection. *Virology* 479–480, 672–686. doi: 10.1016/j.virol.2015.02.031

Selzer, L., Kant, R., Wang, J. C. Y., Bothner, B., and Zlotnick, A. (2015). Hepatitis B virus core protein phosphorylation sites affect capsid stability and transient exposure of the C-terminal domain. *J. Biol. Chem.* 290, 28584–28593. doi: 10.1074/jbc.M115.678441

Selzer, L., and Zlotnick, A. (2015). Assembly and release of hepatitis B virus. *Cold Spring Harb. Perspect. Med.* 5:a021394. doi: 10.1101/cshperspect.a021394

Shim, H. Y., Quan, X., Yi, Y. S., and Jung, G. (2011). Heat shock protein 90 facilitates formation of the HBV capsid via interacting with the HBV core protein dimers. *Virology* 410, 161–169. doi: 10.1016/j.virol.2010.11.005

Sohn, S. Y., Kim, S. B., Kim, J., and Ahn, B. Y. (2006). Negative regulation of hepatitis B virus replication by cellular Hsp40/DnaJ proteins through destabilization of viral core and X proteins. *J. Gen. Virol.* 87, 1883–1891. doi: 10.1099/vir.0.81684-0

Thiele, A., Krentzlin, K., Erdmann, F., Rauh, D., Hause, G., Zerweck, J., et al. (2011). Parvulin 17 promotes microtubule assembly by its peptidyl-prolyl cis/trans isomerase activity. *J. Mol. Biol.* 411, 896–909. doi: 10.1016/j.jmb.2011.06.040

Uchida, T., Takamiya, M., Takahashi, M., Miyashita, H., Ikeda, H., Terada, T., et al. (2003). Pin1 and Par14 peptidyl prolyl isomerase inhibitors block cell proliferation. *Chem. Biol.* 10, 15–24. doi: 10.1016/S

Venkatakrishnan, B., and Zlotnick, A. (2016). The structural biology of hepatitis B virus: form and function. *Annu. Rev. Virol.* 3, 429–451. doi: 10.1146/annurev-virology-110615-042238

Wang, J. C. Y., Dhason, M. S., and Zlotnick, A. (2012). Structural organization of pregenomic RNA and the carboxy-terminal domain of the capsid protein of hepatitis B virus. *PLoS Pathog.* 8:e1002919. doi: 10.1371/journal.ppat.1002919

Watashi, K., Liang, G., Iwamoto, M., Marusawa, H., Uchida, N., Daito, T., et al. (2013). Interleukin-1 and tumor necrosis factor-α trigger restriction of hepatitis B virus infection via a cytidine deaminase activation-induced cytidine deaminase (AID). *J. Biol. Chem.* 288, 31715–31727. doi: 10.1074/jbc.M113.501122

Watts, N. R., Conway, J. F., Cheng, N., Stahl, S. J., Belnap, D. M., Steven, A. C., et al. (2002). The morphogenic linker peptide of HBV capsid protein forms a mobile array on the interior surface. *EMBO J.* 21, 876–884. doi: 10.1093/emboj/21.5.876

World Health Organization Gobal Heptatitis report (2017). Global hepatitis report, 2017. Available at: http://www.who.int/hepatitis/publications/global-hepatitis-report2017/en/ (Accessed November 26, 2021).

Wu, S., Luo, Y., Viswanathan, U., Kulp, J., Cheng, J., Hu, Z., et al. (2018). CpAMs induce assembly of HBV capsids with altered electrophoresis mobility: implications for mechanism of inhibiting pgRNA packaging. *Antivir. Res.* 159, 1–12. doi: 10.1016/j.antiviral.2018.09.001

Wynne, S. A., Crowther, R. A., and Leslie, A. G. W. (1999). The crystal structure of the human hepatitis B virus capsid. *Mol. Cell.* 3, 771–780. doi: 10.1016/s1097-2765(01)80009-5

Xie, Q., Fan, F., Wei, W., Liu, Y., Xu, Z., Zhai, L., et al. (2017). Multi-omics analyses reveal metabolic alterations regulated by hepatitis B virus core protein in hepatocellular carcinoma cells. *Sci. Rep.* 7:41089. doi: 10.1038/srep41089

Yan, H., Zhong, G., Xu, G., He, W., Jing, Z., Gao, Z., et al. (2012). Sodium taurocholate cotransporting polypeptide is a functional receptor for human hepatitis B and D virus. *Elife* 1:e00049. doi: 10.7554/eLife.00049

Yang, F. (2018). Post-translational modification control of HBV biological processes. *Front. Microbiol.* 9:2661. doi: 10.3389/fmicb.2018.02661

Yang, G., Feng, J., Liu, Y., Zhao, M., Yuan, Y., Yuan, H., et al. (2019). HAT1 signaling confers to assembly and epigenetic regulation of HBV cccDNA minichromosome. *Theranostics* 9, 7345–7358. doi: 10.7150/thno.37173

Yoon, S., Jung, J., Kim, T., Park, S., Chwae, Y. J., Shin, H. J., et al. (2011). Adiponectin, a downstream target gene of peroxisome proliferator-activated receptor γ, controls hepatitis B virus replication. *Virology* 409, 290–298. doi: 10.1016/j.virol.2010.10.024

Yu, X., Jin, L., Jih, J., Shih, C., and Hong Zhou, Z. (2013). 3.5Å cryoEM structure of hepatitis B virus core assembled from full-length core protein. *PLoS One*:e69729, 8. doi: 10.1371/journal.pone.0069729

Yu, M., and Summers, J. (1991). A domain of the hepadnavirus capsid protein is specifically required for DNA maturation and virus assembly. *J. Virol.* 65, 2511–2517. doi: 10.1128/JVI.65.5.2511-2517.199

Zhang, W., Chen, J., Wu, M., Zhang, X., Zhang, M., Yue, L., et al. (2017). PRMT5 restricts hepatitis B virus replication through epigenetic repression of covalently closed circular DNA transcription and interference with pregenomic RNA encapsidation. *Hepatology* 66, 398–415. doi: 10.1002/hep.29133/suppinfo

Zhang, Y., Mao, R., Yan, R., Cai, D., Zhang, Y., Zhu, H., et al. (2014). Transcription of hepatitis B virus covalently closed circular DNA is regulated by CpG methylation during chronic infection. *PLoS One* 9:e110442. doi: 10.1371/journal.pone.0110442

Zlotnick, A., Cheng, N., Conway, J. F., Booy, F. P., Steven, A. C., and Stahl, S. J. (1996). et al, Dimorphism of hepatitis B virus capsids is strongly influenced by the c-terminus of the capsid protein. *Biochemistry* 35, 7412–7421. doi: 10.1021/bi9604800

Zlotnick, A., Venkatakrishnan, B., Tan, Z., Lewellyn, E., Turner, W., and Francis, S. (2015). Core protein: A pleiotropic keystone in the HBV lifecycle. *Antivir. Res.* 121, 82–93. doi: 10.1016/j.antiviral.2015.06.020

**Conflict of Interest:** The authors declare that the research was conducted in the absence of any commercial or financial relationships that could be construed as a potential conflict of interest.

**Publisher's Note:** All claims expressed in this article are solely those of the authors and do not necessarily represent those of their affiliated organizations, or those of the publisher, the editors and the reviewers. Any product that may be evaluated in this article, or claim that may be made by its manufacturer, is not guaranteed or endorsed by the publisher.

*Copyright © 2021 Saeed, Piracha, Kwon, Kim, Kalsoom, Chwae, Park, Shin, Lee, Lim and Kim. This is an open-access article distributed under the terms of the Creative Commons Attribution License (CC BY). The use, distribution or reproduction in other forums is permitted, provided the original author(s) and the copyright owner(s) are credited and that the original publication in this journal is cited, in accordance with accepted academic practice. No use, distribution or reproduction is permitted which does not comply with these terms.*

frontiers in Microbiology

ORIGINAL RESEARCH
published: 14 December 2021
doi: 10.3389/fmicb.2021.789991

# Significantly Low Levels of IgG Antibodies Against Oncogenic Merkel Cell Polyomavirus in Sera From Females Affected by Spontaneous Abortion

*Chiara Mazziotta[1,2], Giulia Pellielo[1], Mauro Tognon[1], Fernanda Martini[1,3]* and John Charles Rotondo[1,2]**

*[1] Department of Medical Sciences, University of Ferrara, Ferrara, Italy, [2] Center for Studies on Gender Medicine, Department of Medical Sciences, University of Ferrara, Ferrara, Italy, [3] Laboratory for Technologies of Advanced Therapies (LTTA), University of Ferrara, Ferrara, Italy*

OPEN ACCESS

**Edited by:**
*Chunfu Zheng,*
*University of Calgary, Canada*

**Reviewed by:**
*Yi-Quan Wu,*
*National Cancer Institute (NCI), United States*
*Yan Yan,*
*Wuxi No. 5 People's Hospital, China*

***Correspondence:**
*Fernanda Martini*
*mrf@unife.it*
*orcid.org/0000-0001-9137-0805*
*John Charles Rotondo*
*rtnjnc@unife.it*
*orcid.org/0000-0001-5179-1525*

**Specialty section:**
*This article was submitted to Virology, a section of the journal Frontiers in Microbiology*

**Received:** *05 October 2021*
**Accepted:** *27 October 2021*
**Published:** *14 December 2021*

**Citation:**
*Mazziotta C, Pellielo G, Tognon M, Martini F and Rotondo JC (2021) Significantly Low Levels of IgG Antibodies Against Oncogenic Merkel Cell Polyomavirus in Sera From Females Affected by Spontaneous Abortion. Front. Microbiol. 12:789991. doi: 10.3389/fmicb.2021.789991*

Merkel cell polyomavirus (MCPyV) is a small DNA tumor virus ubiquitous in humans. MCPyV establishes a clinically asymptomatic lifelong infection in healthy immunocompetent individuals. Viral infections are considered to be risk factors for spontaneous abortion (SA), which is the most common adverse complication of pregnancy. The role of MCPyV in SA remains undetermined. Herein, the impact of MCPyV infection in females affected by SA was investigated. Specifically, an indirect enzyme-linked immunosorbent assay (ELISA) method with two linear synthetic peptides/mimotopes mimicking MCPyV antigens was used to investigate immunoglobulin G (IgG) antibodies against MCPyV in sera from 94 females affected by SA [mean ± standard deviation (SD) age 35 ± (6) years] and from 96 healthy females undergoing voluntary pregnancy interruption [VI, mean (±SD) age 32 ± (7) years]. MCPyV seroprevalence and serological profiles were analyzed. The overall prevalence of serum IgG antibodies against MCPyV was 35.1% (33/94) and 37.5% (36/96) in SA and VI females, respectively ($p > 0.05$). Notably, serological profile analyses indicated lower optical densities (ODs) in females with SA compared to those undergoing VI ($p < 0.05$), thus indicating a reduced IgG antibody response in SA females. Circulating IgGs were identified in sera from SA and VI females. Our immunological findings indicate that a relatively reduced fraction of pregnant females carry serum anti-MCPyV IgG antibodies, while SA females presented a more pronounced decrease in IgG antibody response to MCPyV. Although yet to be determined, this immunological decrease might prompt an increase in MCPyV multiplication events in females experiencing abortive events. The role of MCPyV in SA, if present, remains to be determined.

**Keywords: spontaneous abortion, miscarriage, pregnancy, viral infection, Merkel cell polyomavirus, antibodies, IgG, immune system**

## INTRODUCTION

Merkel cell polyomavirus (MCPyV) is a small DNA tumor virus (Witkin et al., 2020). It is the main causative agent of Merkel cell carcinoma (MCC), which is a rare, but highly aggressive, non-melanoma skin cancer (Rotondo et al., 2017; Jin et al., 2019). MCPyV oncogenic activity is mediated by viral DNA integration into the host genome (Rotondo et al., 2017; Del Marmol and Lebbé, 2019; Pietropaolo et al., 2020), alongside the expression of two viral oncoproteins large T (LT) and small T (sT) antigens (Csoboz et al., 2020; Liu and You, 2020). Two additional MCPyV proteins are major capsid protein 1 (VP1) and minor capsid protein 2 (VP2), which present structural functions (Pietropaolo et al., 2020). VPs have previously been exploited as immunoantigens in studies focusing on the detection of immunoglobulin G (IgG) antibodies against MCPyV in humans (Touzé et al., 2010, 2011). Serological studies have indicated that MCPyV is ubiquitous in the healthy population, with varying rates reported as ranging from 60 to 80%, approximately (Carter et al., 2009; Kean et al., 2009; Pastrana et al., 2009; Faust et al., 2011; Tolstov et al., 2011; Touzé et al., 2011; Viscidi et al., 2011; Coursaget et al., 2013; Van Der Meijden et al., 2013; Šroller et al., 2014; Zhang et al., 2014; Vahabpour et al., 2016; Kamminga et al., 2018; Csoboz et al., 2020; Zhou et al., 2020; Mazziotta et al., 2021a,b). Initial exposure to MCPyV occurs early in life. Then, MCPyV establishes a lifelong, asymptomatic infection in healthy immunocompetent individuals (Hashida et al., 2016; Prezioso et al., 2019). However, in certain circumstances, such as during host immune system impairment, increased MCPyV replication levels/activity can occur, thereby leading to an increase in MCC occurrence (Rotondo et al., 2017; Tabachnick-Cherny et al., 2020; Decaprio, 2021).

Spontaneous abortion (SA) is the natural loss of pregnancy before the 20th week of gestation and represents the most common adverse complication in pregnancy. Approximately 10–20% of clinically recognized pregnancies end in a spontaneous loss of the embryo/fetus (Hertz-Picciotto and Samuels, 1988; American College of Obstetricians and Gynecologists Committee on Practice Bulletins—Gynecology, 2018).

Spontaneous abortion causes comprise genetic abnormalities in either partners, which may lead to abnormal chromosomal numbers or alterations (Eiben et al., 1990; Suzumori and Sugiura-Ogasawara, 2012; Dean et al., 2018). Additional SA causes include negative lifestyle factors, such as unhealthy diet/weight other than smoking, alcohol and drug abuse, and other factors, such as ethnicity, stress, and occupational/chemical exposures (De La Rochebrochard and Thonneau, 2002; Sopori, 2002; Lashen et al., 2004). Hormonal, anatomical, and autoimmune abnormalities, as well as male genetic/epigenetic factors, have also been identified (Toth et al., 2010; Rotondo et al., 2012, 2013, 2021a). Notably, although a variety of SA factors have been reported, other causes are yet to be determined (Miyaji et al., 2019; Fukuta et al., 2020). Indeed, nearly one-half of SA cases, defined as idiopathic, presents an undefined etiology (Jeve and Davies, 2014).

A growing number of studies have identified infectious agents as SA risk factors (Giakoumelou et al., 2016; Contini et al., 2018). Nearly 40% of SA cases are estimated to be linked to infectious agents, including viruses (Donders et al., 2000; Srinivas et al., 2006; Giakoumelou et al., 2016), while over 60% of females experience at least one infection during pregnancy (Collier et al., 2009). Viruses can therefore cause severe complications during pregnancy and are reported as associated with cases of stillbirth and preterm delivery, in addition to SA (Giakoumelou et al., 2016; Racicot and Mor, 2017).

Different human viruses, such as dengue, Zika, adeno- and adeno-associated viruses, human cytomegalovirus (HCMV), herpes simplex viruses 1 and 2 (HSV-1 and HSV-2), and the recently discovered severe acute respiratory syndrome coronavirus 2 (SARS-CoV-2), can potentially impact pregnancy outcome, ending, in the worst cases, in an SA event (Burton and Watson, 1997; Fisher et al., 2000; Giakoumelou et al., 2016; Azevedo et al., 2018; Carabali et al., 2018; de Freitas et al., 2018; Sayyadi-Dehno et al., 2019; Auriti et al., 2021; Rotondo et al., 2021b).

The limited amount of data available preclude robust conclusions on the clinical significance of polyomavirus (PyV) infections, including MCPyV, in SA from being made (Tagliapietra et al., 2019, 2020; Mazzoni et al., 2020). Footprints of viral DNAs from PyVs, including Simian virus 40 (SV40), JCPyV/BKPyV, and MCPyV, have been detected at low prevalence in umbilical cords, placenta, peripheral blood mononuclear cells (PBMCs), and/or chorionic villi from both pregnant and SA females (Sadeghi et al., 2010; Tagliapietra et al., 2019, 2020; Mazzoni et al., 2020). Immunological data have also indicated the presence of circulating IgGs against SV40, JCPyV, and BKPyV in the same study groups (Tagliapietra et al., 2019, 2020). A role in SA has been excluded for other PyVs, i.e., KIPyV and WUPyV (Sadeghi et al., 2010). Notably, until now, only one study has reported on the presence of circulating antibodies against MCPyV in pregnant females (Sadeghi et al., 2010), while MCPyV serology in females with SA is unknown.

The lack of immunological data in this field has raised the question of whether MCPyV infection might be linked to SA. To this purpose, we aimed to assess the MCPyV seroprevalence and serological profiles in two sets of sera belonging to females affected by SA, the case, and healthy females (HF) undergoing voluntary interruption of pregnancy (VI), as control.

## MATERIALS AND METHODS

### Human Sera

Human sera were obtained from females who had experienced SA ($n$ = 94), i.e., the case, and females undergoing VI ($n$ = 96), i.e., the control. SA and VI sera were from our archive (Tognon et al., 2020). Samples were collected within 12 h from the abortion. Samples were stored at −80°C until testing, as reported previously (Mazziotta et al., 2021a,b). The mean ages [± standard deviation (SD)] of SA and VI groups were 35 ± 6 and 32 ± 7 years ($p > 0.05$), respectively. SA and VI inclusion criteria were (i) patients aged 18–42 years; (ii) gestational age within the first 12 weeks; and (iii) for the VI group, females selected according to Italian Law 194, article 6, comma B. Exclusion criteria were (i) severe hormonal or uterine dysregulations; (ii)

immunosuppressive therapies known to cause SA events; (iii) genetic disorders; (iv) presence of infections, such as hepatitis B virus (HBV), human immunodeficiency virus (HIV), hepatitis C virus (HCV), and syphilis; (v) use of teratogenic drugs; and (vi) acquired/congenital immunodeficiency syndromes/diseases. Written informed consent was obtained from all subjects/patients according to the Declaration of Helsinki. The Ethical Committee of Ferrara, Italy, authorized the study (ID: 151078). In addition, immunological data from a set of sera belonging to a cohort of age-matched HF [$n$ = 95, mean age ± SD, 34 ± (9) years] ($p > 0.05$), from our previous study (Mazziotta et al., 2021b), were included herein for comparison.

## MCPyV Linear Synthetic Peptides

The indirect enzyme-linked immunosorbent assay (ELISA) employed in this study to detect IgGs to MCPyV in sera from SA and VI was recently developed and validated (Mazziotta et al., 2021a,b). The immunoassay uses two linear synthetic peptides/mimotopes, known as MCPyV VP1 S and VP2 F (or S and F peptides) for detecting circulating IgGs against MCPyV in healthy adult and elderly individuals, as described (Mazziotta et al., 2021a,b). The peptides were synthesized using standard procedures and purchased from UFPeptides s.r.l., Ferrara, Italy. Amino acid (a.a.) sequences of VP1 S (24 a.a. residues) and VP2 F (25 a.a. residues) peptides are as follows:

VP1 S: $NH_2$-NSPDLPTTSNWYTYTYDLQPKGSS-COOH
and
VP2 F: $NH_2$-SLSPTSRLQIQSNLVNLILNSRWVF-COOH.

## Indirect Enzyme-Linked Immunosorbent Assay

Indirect ELISA was performed as reported (Mazziotta et al., 2021a,b). S and F peptides, 5 μg each, were diluted in 100 μl of coating buffer 1X, pH 9.6 (Candor Bioscience, Wangen, Germany), which was used to coat each well of the immunological plates (Nunc-Immuno PolySorp, Thermo Fisher Scientific, Milan, Italy). The peptide-coated plates were incubated at 4°C for 16 h. Successively, immunological plates were rinsed three times with a washing buffer (Candor Bioscience, Wangen, Germany) to remove unbound peptides. For the blocking phase, 200 μl per well of blocking solution containing the casein and Tween detergent (Candor Bioscience, Wangen, Germany) was added to each well and incubated at 37°C for 90 min. Plates were washed three times with the washing buffer before serum samples were added. Each well was covered with 100 μl of serum samples diluted 1:20 in a low cross-buffer (Candor Bioscience, Wangen, Germany). Sera in each plate included (i) positive controls, that is, immune human sera derived from patients with MCPyV-positive MCC (Mazziotta et al., 2021b); (ii) negative controls, that is, three human MCPyV-negative sera (Mazziotta et al., 2021b); and (iii) sera from SA and VI under analysis. Immunological plates with sera were incubated at 37°C for 90 min. Each sample was analyzed in triplicate. Wells were washed three times, and then the secondary antibody was added to each sample. This solution consists of a goat anti-human IgG heavy (H)- and light (L)-chain-specific peroxidase conjugate (Calbiochem-Merck, Darmstadt, Germany) diluted 1:10,000 in a low cross-buffer. The solution was added to each well, whereas plates were incubated at room temperature (RT) for 90 min. After 90-min incubation, the plates were washed three times; then 100 μl of 2,2′-azino-bis-3-ethylbenzothiazoline-6-sulfonic acid (ABTS) solution (Sigma-Aldrich, Milan, Italy) was added to each well. Plates were incubated at RT for 45 min. ABTS reacted with the peroxidase enzyme to yield the color reaction. Finally, the plate was read with a spectrophotometer (Thermo Electron Corp., model Multiskan EX, Vantaa, Finland) at a wavelength (λ) of 405 nm. Color intensity in wells was determined by an optical density (OD) reading. The OD readings correspond to the amount of immune complexes formed by the specific antibodies binding to S and F synthetic peptides/mimotopes.

The cutoff for each S and F peptide was set in each indirect ELISA run, as the mean of the OD readings of negative control sera ($n$ = 3) plus three SDs of mean (mean + 3 SDs) (Classen et al., 1987; Saraswati et al., 2019; Mazziotta et al., 2021a,b), as described previously for other ELISA methods (Meyer, 2001; Lardeux et al., 2016).

Immune serum samples were considered MCPyV positive when reacting to both S and F synthetic peptides, in three replica ELISA experiments carried out by three independent operators, without data variability.

## Statistical Analysis

Merkel cell polyomavirus seroprevalence rates were statistically analyzed applying a two-sided chi-square test (Tognon et al., 2020; Oton-Gonzalez et al., 2021). Values were analyzed using the D'Agostino Pearson normality test, and parametric and non-parametric tests were applied according to normal and non-normal variables, respectively, as reported (Nakagawa and Schielzeth, 2010; Rotondo et al., 2020a). In detail, ODs were analyzed using a one-way analysis of variance (ANOVA) and Kruskal–Wallis multiple comparison tests, according to normal and non-normal variables, respectively [OD medians, 95% confidence interval (CI)]. The Spearman correlation coefficient $r$ was used to evaluate the OD concordance between S and F peptides. Statistical analyses were carried out using GraphPad Prism version 8.0 for Windows (GraphPad, La Jolla, CA, United States) (Rotondo et al., 2020b). A $p$-value $< 0.05$ was considered statistically significant (Mazzoni et al., 2020).

# RESULTS

## Indirect Enzyme-Linked Immunosorbent Assay Reliability Assessment

In the first phase of this investigation, the reliability of our immunoassay was assessed in sera from female patients with SA and those who had undergone VI, by determining the OD concordance between MCPyV VP1 S and VP2 F peptides. OD concordance between S and F peptides was evaluated using the Spearman correlation analysis in SA ($n$ = 94) and VI ($n$ = 96) sera. In addition, immunological data from a group of age-matched HF ($n$ = 95), which had previously been investigated in our

laboratory for MCPyV serology (Mazziotta et al., 2021b), were included herein for statistical comparisons. OD concordance between S and F peptides was therefore analyzed in SA, VI, and HF sera considered alone, as well as in combination ($n$ = 285). Results indicate a good degree of correlation between ODs for S and F peptides for the SA group, with a Spearman coefficient $r$ of 0.7727 ($p < 0.0001$) (**Figure 1A**), and for the VI group, with an $r$ of 0.6221 ($p < 0.0001$) (**Figure 1B**). A good correlation between S and F peptide ODs was also found in HF sera with an $r$ of 0.7686 ($p < 0.0001$) (**Figure 1C**). In addition, when evaluating the combined SA, VI, and HF sera, a good concordance between S and F was determined with an $r$ of 0.7854 ($p < 0.0001$) (**Figure 1D**). These data indicate that both peptides can be used simultaneously, therefore underlining that our assay is reliable in detecting anti-MCPyV IgGs in sera from SA and VI females.

## Detection of Serum IgG Antibodies Against MCPyV by Indirect Enzyme-Linked Immunosorbent Assay

Human sera, from SA ($n$ = 94) and VI ($n$ = 96) females, were analyzed by indirect ELISA for IgG Ab reactivity to MCPyV VP1 S and VP2 F peptides/mimotopes. The prevalence of anti-MCPyV IgGs was therefore determined in SA and VI groups. A statistically similar overall prevalence of 36.2% (34/94) and 43.6% (41/94) was obtained in SA sera, when tested with S and F peptides, respectively ($p > 0.05$) (**Table 1**). Comparable prevalence rates of 39.6% (38/96) and 47.9% (46/96) were obtained in VI sera reacting to S and F peptides, respectively ($p > 0.05$). With only a few exceptions, sera testing negative for S peptide did not react to F peptide and *vice versa*. In detail, 8.5% (8/94) of SA sera resulting negative for S peptide were positive for F peptide, while 1.1% (1/94) of sera tested F peptide negative, while being positive for S peptide. In VI, 10.4% (10/96) of sera tested F peptide positive were negative for S peptide, whereas 2.1% (2/96) of sera negative for F peptide were positive for S peptide.

In this study, sera were considered MCPyV positive when reacting with both mimotopes S and F, as previously reported (Mazziotta et al., 2021a,b).

The combined overall prevalence of IgGs against MCPyV, for both S and F peptides, was 35.1% (33/94) and 37.5% (36/96) in serum samples from SA and VI groups, respectively ($p > 0.05$).

## Serological Profiles of Serum IgG Antibodies Reacting to MCPyV

Serological profiles for IgG reactivity to MCPyV VP1 S and VP2 F peptides/mimotopes were analyzed, both for the single peptide and in combination. Immunological data were taken from sera belonging to SA ($n$ = 94) and VI ($n$ = 96) females. Results are reported as OD readings at λ 405 nm. The median [interquartile range (IQR)] ODs for S peptide and F peptide, alone and in combination, were then determined in SA and VI sera; then values were compared.

Serologic profile analysis indicated that the median (IQR) OD values for S peptide resulted as 0.09 (0.08–0.11) and 0.11 (0.09–0.12) in SA and VI groups, respectively (**Figure 2A**). The median (IQR) OD values for F peptide resulted as 0.11 (0.1–0.14) and 0.18 (0.13–0.23) in SA and VI groups, respectively (**Figure 2B**). Lastly, the median (IQR) OD values for combined S and F peptides resulted as 0.1 (0.09–0.13) in SA and 0.12 (0.1–0.18) in VI groups (**Figure 2C**). The difference in OD levels between SA and VI groups was statistically significant for both S and F peptides considered alone, as well as upon combining ODs of the two peptides ($p < 0.05$, for S peptide; $p < 0.0001$, for both F peptide alone and combined S and F peptides) (**Figure 2**).

## Serum IgG Reactivity to MCPyV in Females Experiencing Spontaneous Abortion and Healthy Females Who Had Undergone Voluntary Interruption vs. Healthy Non-pregnant Females

In a second phase, MCPyV seroprevalence and serologic profiles in SA ($n$ = 94) and VI ($n$ = 96) females were compared to those obtained in sera from a group of age-matched HF ($n$ = 95) females ($p > 0.05$), which had previously been investigated in our laboratory for MCPyV serology (Mazziotta et al., 2021b).

Merkel cell polyomavirus seroprevalence was found to be lower in both SA (35.1%, 33/94) and VI groups (37.5%, 36/96) than in the HF group (62.1%, 59/95) ($p < 0.001$). Serologic profile analysis indicated that S-peptide ODs were lower in both SA [$n$ = 94, median (IQR), 0.09, 0.08–0.11] and VI groups ($n$ = 96, 0.11, 0.09–0.12) than in HF ($n$ = 95, 0.17, 0.12–0.26, $p < 0.0001$) (**Figure 2A**). Similarly, F-peptide ODs were lower in both SA (0.11, 0.1–0.14) and VI (0.18, 0.13–0.23) compared to the HF group (0.3, 0.19–0.49, $p < 0.0001$) (**Figure 2B**). Furthermore, lower ODs for combined S- and F-peptides were detected in both SA (0.1, 0.09–0.13) and VI sera (0.12, 0.1–0.18) compared to HF (0.22, 0.15–0.34, $p < 0.0001$) (**Figure 2C**).

# DISCUSSION

The role of MCPyV in SA remains undetermined. Herein, MCPyV seroprevalence and serological profiles were investigated, for the first time, in sera from SA females using an indirect ELISA with two linear synthetic peptides/mimotopes, which mimic MCPyV VP antigens. The lack of immunological studies into the involvement of MCPyV in SA prompted us to apply our newly developed immunoassay (Mazziotta et al., 2021a,b). Sera were considered MCPyV positive when IgGs reacted to both S and F peptides (Mazziotta et al., 2021a,b).

Overall MCPyV-positive prevalence, resulted as 35.1% in SA, was comparable to the 37.5% determined in VI ($p > 0.05$). Our data indicate that both SA and VI female groups present circulating IgGs to MCPyV, while, at least in terms of seroprevalence, a relationship between MCPyV and SA might be unlikely.

The involvement of MCPyV infection in SA has been poorly investigated (Giakoumelou et al., 2016). Early findings indicate the presence of MCPyV DNA in uterine cervical cancer tissues (Imajoh et al., 2012), suggesting that, after infecting the uterus, this PyV could potentially participate as a SA risk factor.

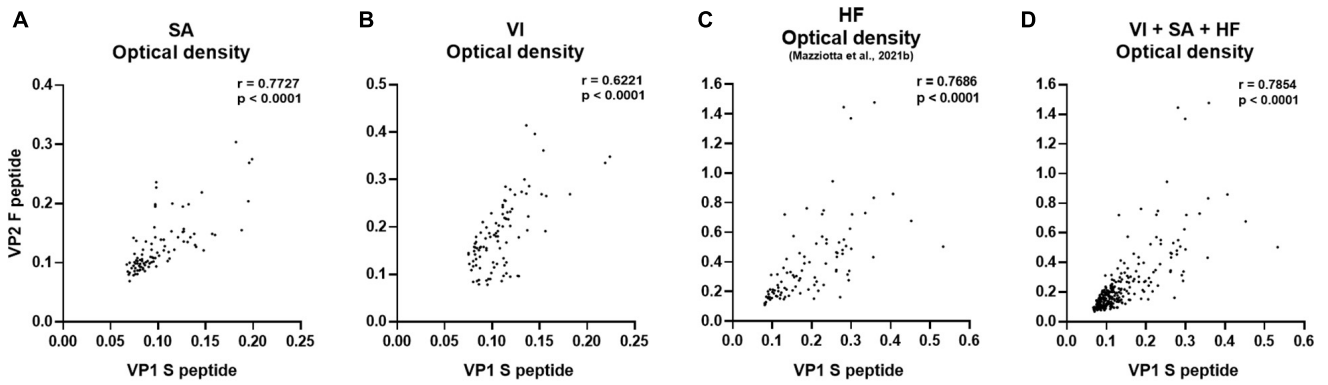


**FIGURE 1 |** Correlation of OD values obtained using MCPyV VP1 S and VP2 F mimotopes. The concordance in ODs between VP1 S and VP2 F peptides was evaluated in sera from females who had SA ($n$ = 94), the case; females undergoing VI ($n$ = 96), the control; age-matched HF ($n$ = 95); and the entire set of combined SA, VI, and HF sera ($n$ = 285), using Spearman correlation analysis. A good correlation between VP1 S and VP2 F peptide was found in SA, VI, and HF sera considered alone, as well as in combined SA, VI, and HF sera with an $r$ of 0.7727 and $p < 0.0001$ **(A)**, 0.6221 and $p < 0.0001$ **(B)**, 0.7686 and $p < 0.0001$ **(C)**, and 0.7854 and $p < 0.0001$ **(D)**, respectively.

**TABLE 1 |** Seroprevalence of IgG antibodies reacting with Merkel cell polyomavirus VP1 S and VP2 F peptides in sera from females who experienced spontaneous abortion (SA) and females undergoing voluntary interruption (VI).

| | | | Number of positive samples (%) | | |
|---|---|---|---|---|---|
| **Groups** | **Number of samples** | **Mean age (years) ± SD** | **VP1 S** | **VP2 F** | **VP1 S + VP2 F** |
| SA | 94 | 35 ± 6 | 34 (36.2) | 41 (43.6) | 33 (35.1) |
| VI | 96 | 32 ± 7 | 38 (39.6) | 46 (47.9) | 36 (37.5) |

*Serum samples were from SA (n = 94) and VI (n = 96) females.*
*Statistical analyses were performed using the two-sided chi-square test.*
*No statistical differences were detected between SA and VI groups (p > 0.05).*

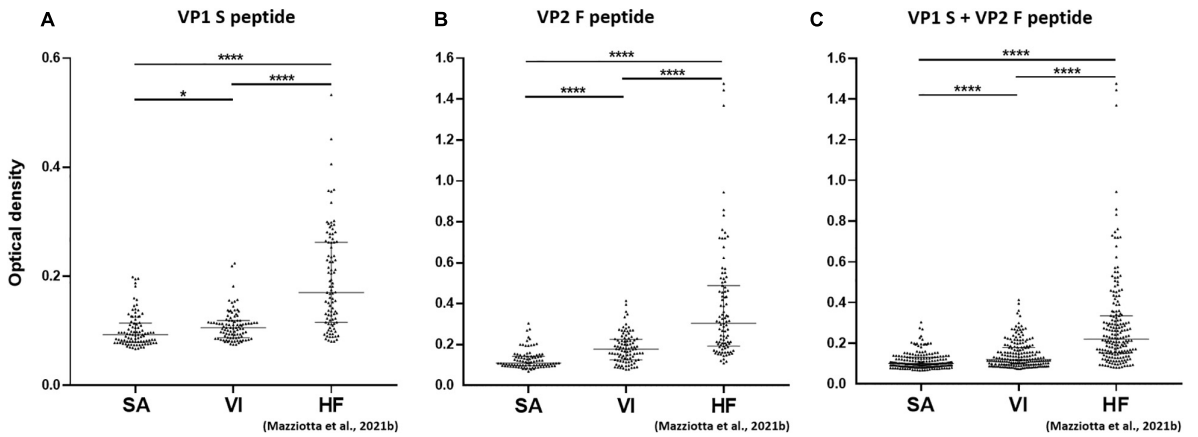


**FIGURE 2 |** Serological profiles of serum antibody reactivity to MCPyV VP1 S **(A)**, VP2 F **(B)** peptides, and combined S and F peptides **(C)** in females who had SA, females who had undergone VI, and age-matched HF. Immunologic data are from SA ($n$ = 94), VI ($n$ = 96), and HF ($n$ = 95) females, whereas data are reported as OD value readings at λ 405 nm for sera assayed in indirect ELISA. In the scatter dot plot, each dot represents the dispersion of ODs for each sample. The median is indicated by the line inside the scatter plot with the [interquartile range (IQR)] in SA and VI cohorts. **(A)** $^{*}p < 0.05$, $^{****}p < 0.0001$; **(B)** $^{****}p < 0.0001$; **(C)** $^{****}p < 0.0001$.

Nevertheless, few copies of MCPyV DNA and/or RNA molecules have been previously identified at low and similar prevalence in chorionic villi and PBMCs from SA and VI females (Tagliapietra et al., 2020), suggesting that MCPyV may not be involved in SA.

It is important to point out that SA females showed lower ODs compared to females who had undergone VI ($p < 0.05$), thus indicating a reduced anti-MCPyV IgG antibody response in females experiencing SA. In addition, both SA and VI

females exhibited lower rates and ODs compared to those determined in age-matched, non-pregnant HF (62.1%), which had been investigated in our previous study conducted on healthy individuals (Mazziotta et al., 2021b). These findings indicate not only that serum IgG antibody response to MCPyV may decline in pregnancy but also that this decline is *de facto* more pronounced in females experiencing SA.

Notably, to the best of our knowledge, this is the first study reporting on MCPyV serology in SA. Only one previous study has reported on MCPyV serology in pregnancy, describing a rate of nearly 46% in a cohort of pregnant females (Sadeghi et al., 2010), a proportion similar to that obtained herein in our study/control groups. Regarding the healthy population, previous works have reported that a considerable fraction of adults, both males and females, is exposed to an asymptomatic MCPyV infection, with seroprevalence rates ranging from 60 to 80%, according to the study under consideration (Carter et al., 2009; Kean et al., 2009; Pastrana et al., 2009; Faust et al., 2011; Tolstov et al., 2011; Touzé et al., 2011; Viscidi et al., 2011; Coursaget et al., 2013; Van Der Meijden et al., 2013; Šroller et al., 2014; Zhang et al., 2014; Vahabpour et al., 2016; Kamminga et al., 2018; Csoboz et al., 2020; Zhou et al., 2020; Mazziotta et al., 2021a,b). Our immunological findings, alongside those previously reported, cumulatively indicate that a relatively reduced fraction of pregnant females carries anti-MCPyV IgGs compared to the healthy population, while SA females have a lower IgG antibody response to MCPyV.

The similar rate of immunological decrease determined in SA and VI females compared to non-pregnant females might be accounted for by the well-known immune adaptation/modulation process occurring in pregnancy (Longman and Johnson, 2007). Pregnant females present a unique state of immunity, as they develop a tolerance for the semi-allogeneic embryo/fetus, compared to non-pregnant females (Giakoumelou et al., 2016). In other words, despite recognizing the paternal antigens expressed by the embryo/fetus, the maternal immune system undergoes an adaptation to hamper her/his rejection (Mor and Cardenas, 2010). This adaptation is mainly, but not only, due to a decrease in the production and/or function of (i) lymphocyte T and natural killer cells, involved in the adaptive immune response (Longman and Johnson, 2007); and (ii) B cells, deputies in the production of antibodies (Medina et al., 1993). A transient immune modulation during pregnancy can therefore affect how SA and VI females respond to viral agents, making them more susceptible to viral infections (Giakoumelou et al., 2016), probably including MCPyV infection. The diminished serum IgG antibody response to MCPyV in both SA and VI females compared to non-pregnant females might be a reflection of the transient modulation in the immune function being experienced during pregnancy. The lower IgG antibody response to MCPyV determined in SA females might be linked to their more increased susceptibility to MCPyV infection. However, the relationship between this possible immunologic dysregulation and SA is unknown.

Conditions of physiological immune impairment in the host can favor a minor response to MCPyV as a result of antiviral surveillance decline (Ma and Brewer, 2014). This phenomenon can lead to an increase in MCPyV replication levels/activity or reinfection, ultimately leading to MCC (Ma and Brewer, 2014). A higher MCC rate has been determined in patients with immunocompromising conditions such as oncologic patients (Yu and Dasanu, 2016; Zheng et al., 2019) as well as in patients/individuals being pharmacologically treated for organ transplantation and/or autoimmune diseases (Lanoy and Engels, 2010; Boldorini et al., 2014; Clarke et al., 2015; Rotondo et al., 2017; Pietropaolo et al., 2020). Notably, MCC cases have also been identified in pregnant females (Chao et al., 1990; Paterson et al., 2003; Kukko et al., 2008; Tyler, 2020), thus supporting the view that a dysregulation in transient immune modulation during pregnancy can, at least in certain circumstances, favor an increase in MCPyV activity. It should be recalled that, despite being oncogenic, MCPyV is ubiquitous in humans, while establishing a lifelong and asymptomatic infection in healthy immunocompetent individuals. The decreased IgG antibody response to MCPyV might account for greater tolerance to viral infections experienced during pregnancy, which in turn might potentially lead to an increase in MCPyV replication levels/activity in SA females, as reported for other viral agents (Giakoumelou et al., 2016). Indeed, previous findings indicate that maternal immune tolerance impairment may result in SA or preeclampsia (Wang and Li, 2020).

How a diminished antibody response to MCPyV in SA females might negatively impact embryo development remains to be determined. Following an increase in MCPyV multiplication, this PyV might reach the embryo/fetus from the mother *via* vertical transmission, through the mother's blood, as demonstrated for other viruses (Xu et al., 2015). As immune cells can allow viral crossing through placental barriers (Robbins and Bakardjiev, 2012; Cordeiro et al., 2015), a similar mechanism for MCPyV cannot be excluded. Notably, MCPyV DNA has been detected in white cells from pregnant females (Tagliapietra et al., 2020). An ascending transmission from the maternal reproductive system might be an alternative mechanism, as the uterine cervix may be prone to MCPyV infection (Imajoh et al., 2012). Likely, pregnancy may be affected following a maternal response to an MCPyV activity increase, even in the absence of a viral transmission, as found for other viruses (Mor and Cardenas, 2010; Racicot and Mor, 2017). Viral infections nearby placental barriers can trigger a mild inflammatory response represented by an increased cytokine production (Koga et al., 2009; Huang et al., 2014), promoting, in turn, an inflammatory response in the embryo/fetus, which can lead to pregnancy complications/abortion. A potential MCPyV activity increase may determine a mother's inflammatory response, ultimately affecting pregnancy. Excluding chorionic villi and PBMCs (Tagliapietra et al., 2020), an increase in MCPyV activity, if present, due to a reduced anti-MCPyV immunological response in SA females might occur in a tissue type, which is currently unknown. Notably, the reservoir cell type of MCPyV is still unclear (Liu et al., 2019). Evidently, due to the lack of molecular data, further studies should be performed.

It is important to underline that MCPyV activity in terms of DNA replication and gene expression was not investigated herein. Therefore, the hypothesis that MCPyV activity might

increase following a reduced antibody response to MCPyV, possibly making SA and VI females more susceptible to MCPyV infection, remains to be verified. Further studies evaluating the presence of viral DNA/RNA/proteins in key embryo development tissues including cord blood, amniotic fluids, cervical tissues, and fetal membranes should be conducted, as performed for other viruses (Giakoumelou et al., 2016). Since the basic immune conditions of SA, VI, and non-pregnant females might be different, determining the total IgG fraction, alongside IgGs to MCPyV, might help to better understand how pregnant females respond to MCPyV infection. Moreover, the prospective monitoring of the immunological status of pregnant females throughout the different gestation phases might be considered as an alternative investigative approach. These molecular and immunological experiments can be part of further investigations.

To avoid confounding variables, we excluded herein females who were positive for (i) congenital/acquired immunodeficiency syndromes or who were receiving immunosuppressive therapies; (ii) known causes of SA, i.e., genetic factors and anatomic/hormonal complications; and (iii) HIV, HBV, HCV, and syphilis infections. SA and VI females were similar in age ($p > 0.05$); samples were collected within 12 h from the abortion, while females were at a gestational age within the first 12 weeks.

In conclusion, our indirect ELISA proved to be reliable in identifying circulating IgGs reacting to MCPyV VP mimotopes in females experiencing SA and who had undergone VI. For the first time, IgG antibodies against oncogenic MCPyV were found in sera from SA females. Our results indicate that a reduced fraction of SA and VI females carries IgGs to MCPyV compared to healthy, non-pregnant females, while SA females presented a more pronounced decrease in IgG antibody response to MCPyV. Although yet to be determined, females experiencing abortive events might potentially present an increase in MCPyV multiplication events as a result of the immunological decline against MCPyV. Future investigations are needed to elucidate the relationship between MCPyV infection and SA.

## DATA AVAILABILITY STATEMENT

The raw data supporting the conclusions of this article will be made available by the authors, without undue reservation.

## ETHICS STATEMENT

The studies involving human participants were reviewed and approved by the Ethical Committee of Ferrara, Italy, authorized the study (ID: 151078). The patients/participants provided their written informed consent to participate in this study.

## AUTHOR CONTRIBUTIONS

JR: conceptualization. CM and JR: methodology. CM, JR, and GP: software. CM: formal analysis, resources, data curation, statistical analysis, and visualization. CM and GP: investigation. CM, MT, and JR: writing—original draft preparation. MT and FM: writing—review and editing. JR and MT: supervision. JR, MT, and FM: funding acquisition. All authors have read and agreed to the published version of the manuscript.

## FUNDING

This work was supported, in part, by grants MFAG 21956 (to JR), IG 21617 (to MT) from the Associazione Italiana per la Ricerca sul Cancro (AIRC), Milan, Italy, and University of Ferrara, FAR grants 2021 (to FM and MT).

## ACKNOWLEDGMENTS

We would like to thank Georgia Emma Gili for revising the English text of the manuscript.

## REFERENCES

American College of Obstetricians and Gynecologists Committee on Practice Bulletins—Gynecology (2018). ACOG Practice bulletin no. 200: early pregnancy loss. *Obstet. Gynecol.* 132, E197–E207. doi: 10.1097/AOG.0000000000002899

Auriti, C., De Rose, D., Santisi, A., Martini, L., Piersigilli, F., Bersani, I., et al. (2021). Pregnancy and viral infections: mechanisms of fetal damage, diagnosis and prevention of neonatal adverse outcomes from cytomegalovirus to SARS-CoV-2 and Zika virus. *Biochim. Biophys. Acta Mol. Basis Dis.* 1867:16 6198.

Azevedo, R. S. S., Araujo, M. T., Oliveira, C. S., Filho, A. J. M., Nunes, B. T. D., Henriques, D. F., et al. (2018). Zika virus epidemic in Brazil. II. Post-mortem analyses of neonates with microcephaly, stillbirths, and miscarriage. *J. Clin. Med.* 7:496. doi: 10.3390/jcm712 0496

Boldorini, R., Allegrini, S., Tognon, M., Miglio, U., Rossi, D., Pawlita, M., et al. (2014). Merkel cell carcinoma arising in inguinal lymph node in a patient with von Willebrand disease after multiple blood transfusions. *J. Clin. Virol.* 60, 73–75. doi: 10.1016/j.jcv.2014.0 2.007

Burton, G. J., and Watson, A. L. (1997). The structure of the human placenta: implications for initiating and defending against virus infections. *Rev. Med. Virol.* 7, 219–228.

Carabali, M., Austin, N., King, N. B., and Kaufman, J. S. (2018). The Zika epidemic and abortion in Latin America: a scoping review. *Glob. Heal. Res. Policy* 3:15. doi: 10.1186/s41256-018-0069-8

Carter, J. J., Paulson, K. G., Wipf, G. C., Miranda, D., Madeleine, M. M., Johnson, L. G., et al. (2009). Association of merkel cell polyomavirus-specific antibodies with merkel cell carcinoma. *J. Natl. Cancer Inst.* 101, 1510–1522. doi: 10.1093/jnci/djp332

Chao, T., Park, J., Rhee, H., and Greager, J. (1990). Merkel cell tumor of the back detected during pregnancy. *Plast. Reconstr. Surg.* 86, 347–351. doi: 10.1097/00006534-199008000-00028

Clarke, C. A., Robbins, H. A., Tatalovich, Z., Lynch, C. F., Pawlish, K. S., Finch, J. L., et al. (2015). Risk of Merkel cell carcinoma after solid organ transplantation. *J. Natl. Cancer Inst.* 107:dju382. doi: 10.1093/jnci/dj u382

Classen, D. C., Morningstar, J. M., and Shanley, J. D. (1987). Detection of antibody to murine cytomegalovirus by enzyme-linked immunosorbent and indirect immunofluorescence assays. *J. Clin. Microbiol.* 25, 600–604. doi: 10.1128/jcm.25.4.600-604.1987

Collier, S. A., Rasmussen, S. A., Feldkamp, M. L., and Honein, M. A. (2009). Prevalence of self-reported infection during pregnancy among control mothers in the National Birth Defects Prevention Study. *Birth Defects Res. Part A Clin. Mol. Teratol.* 85, 193–201. doi: 10.1002/BDRA.20540

Contini, C., Rotondo, J. C., Magagnoli, F., Maritati, M., Seraceni, S., Graziano, A., et al. (2018). Investigation on silent bacterial infections in specimens from pregnant women affected by spontaneous miscarriage. *J. Cell. Physiol.* 234, 100–107. doi: 10.1002/jcp.26952

Cordeiro, C. N., Tsimis, M., and Burd, I. (2015). Infections and brain development. *Obstet. Gynecol. Surv.* 70, 644–655. doi: 10.1097/OGX.0000000000000236

Coursaget, P., Samimi, M., Nicol, J. T. J., Gardair, C., and Touzé, A. (2013). Human Merkel cell polyomavirus: virological background and clinical implications. *APMIS* 121, 755–769. doi: 10.1111/apm.12122

Csoboz, B., Rasheed, K., Sveinbjørnsson, B., and Moens, U. (2020). Merkel cell polyomavirus and non-Merkel cell carcinomas: guilty or circumstantial evidence? *APMIS* 128, 104–120. doi: 10.1111/apm.13019

de Freitas, L. B., Pereira, C. C., Merçon-de-Vargas, P. R., and Spano, L. C. (2018). Human papillomavirus in foetal and maternal tissues from miscarriage cases. *J. Obstet. Gynaecol. (Lahore)* 38, 1083–1087. doi: 10.1080/01443615.2018.1454408

De La Rochebrochard, E., and Thonneau, P. (2002). Paternal age and maternal age are risk factors for miscarriage; results of a multicentre European study. *Hum. Reprod.* 17, 1649–1656. doi: 10.1093/humrep/17.6.1649

Dean, D. D., Agarwal, S., and Tripathi, P. (2018). Connecting links between genetic factors defining ovarian reserve and recurrent miscarriages. *J. Assist. Reprod. Genet.* 35, 2121–2128. doi: 10.1007/s10815-018-1305-3

Decaprio, J. A. (2021). Molecular Pathogenesis of Merkel Cell Carcinoma. *Annu. Rev. Pathol. Mech. Dis.* 16, 69–91. doi: 10.1146/annurev-pathmechdis-012419-032817

Del Marmol, V., and Lebbé, C. (2019). New perspectives in Merkel cell carcinoma. *Curr. Opin. Oncol.* 31, 72–83. doi: 10.1097/CCO.0000000000000508

Donders, G. G., Van Bulck, B., Caudron, J., Londers, L., Vereecken, A., and Spitz, B. (2000). Relationship of bacterial vaginosis and mycoplasmas to the risk of spontaneous abortion. *Am. J. Obstet. Gynecol.* 183, 431–437. doi: 10.1067/mob.2000.105738

Eiben, B., Bartels, I., Bahr-Porsch, S., Borgmann, S., Gatz, G., Gellert, G., et al. (1990). Cytogenetic analysis of 750 spontaneous abortions with the direct-preparation method of chorionic villi and its implications for studying genetic causes of pregnancy wastage. *Am. J. Hum. Genet.* 47, 656–663.

Faust, H., Pastrana, D. V., Buck, C. B., Dillner, J., and Ekström, J. (2011). Antibodies to Merkel cell polyomavirus correlate to presence of viral DNA in the skin. *J. Infect. Dis.* 203, 1096–1100. doi: 10.1093/infdis/jiq173

Fisher, S., Genbacev, O., Maidji, E., and Pereira, L. (2000). Human cytomegalovirus infection of placental cytotrophoblasts in vitro and in utero: implications for transmission and pathogenesis. *J. Virol.* 74, 6808–6820. doi: 10.1128/jvi.74.15.6808-6820.2000

Fukuta, K., Yoneda, S., Yoneda, N., Shiozaki, A., Nakashima, A., Minamisaka, T., et al. (2020). Risk factors for spontaneous miscarriage above 12 weeks or premature delivery in patients undergoing cervical polypectomy during pregnancy. *BMC Pregnancy Childbirth* 20:27. doi: 10.1186/s12884-019-2710-z

Giakoumelou, S., Wheelhouse, N., Cuschieri, K., Entrican, G., Howie, S. E. M., and Horne, A. W. (2016). The role of infection in miscarriage. *Hum. Reprod. Update* 22, 116–133. doi: 10.1093/humupd/dmv041

Hashida, Y., Kamioka, M., Tanaka, M., Hosokawa, S., Murakami, M., Nakajima, K., et al. (2016). Ecology of merkel cell polyomavirus in healthy skin among individuals in an asian cohort. *J. Infect. Dis.* 213, 1708–1716. doi: 10.1093/infdis/jiw040

Hertz-Picciotto, I., and Samuels, S. (1988). Incidence of early loss of pregnancy. *N. Engl. J. Med.* 319, 1483–1484. doi: 10.1056/NEJM198812013192214

Huang, Q. T., Chen, J. H., Zhong, M., Xu, Y. Y., Cai, C. X., Wei, S. S., et al. (2014). The risk of placental abruption and placenta previa in pregnant women with chronic hepatitis B viral infection: a systematic review and meta-analysis. *Placenta* 35, 539–545. doi: 10.1016/J.PLACENTA.2014.05.007

Imajoh, M., Hashida, Y., Nemoto, Y., Oguri, H., Maeda, N., Furihata, M., et al. (2012). Detection of Merkel cell polyomavirus in cervical squamous cell carcinomas and adenocarcinomas from Japanese patients. *Virol. J.* 91, 1–9. doi: 10.1186/1743-422X-9-154

Jeve, Y. B., and Davies, W. (2014). Evidence-based management of recurrent miscarriages. *J. Hum. Reprod. Sci.* 7, 159–169. doi: 10.4103/0974-1208.142475

Jin, H. T., Park, S. J., Choi, E. K., and Kim, Y. S. (2019). The frequency of Merkel cell polyomavirus in whole blood from immunocompetent and immunosuppressed patients with kidney disease and healthy donors. *Microb. Pathog.* 131, 75–80. doi: 10.1016/j.micpath.2019.03.020

Kamminga, S., Van Der Meijden, E., Feltkamp, M. C. W., and Zaaijer, H. L. (2018). Seroprevalence of fourteen human polyomaviruses determined in blood donors. *PLoS One* 13:e0206273. doi: 10.1371/journal.pone.0206273

Kean, J. M., Rao, S., Wang, M., and Garcea, R. L. (2009). Seroepidemiology of human polyomaviruses. *PLoS Pathog.* 5:e1000363. doi: 10.1371/journal.ppat.1000363

Koga, K., Cardenas, I., Aldo, P., Abrahams, V. M., Peng, B., Fill, S., et al. (2009). ORIGINAL ARTICLE: activation of TLR3 in the trophoblast is associated with preterm delivery. *Am. J. Reprod. Immunol.* 61, 196–212. doi: 10.1111/J.1600-0897.2008.00682.X

Kukko, H., Vuola, J., Suominen, S., and Koljonen, V. (2008). Merkel cell carcinoma in a young pregnant woman. *J. Plast. Reconstr. Aesthetic Surg.* 61, 1530–1533. doi: 10.1016/J.BJPS.2007.06.016

Lanoy, E., and Engels, E. A. (2010). Skin cancers associated with autoimmune conditions among elderly adults. *Br. J. Cancer* 103, 112–114. doi: 10.1038/sj.bjc.6605733

Lardeux, F., Torrico, G., and Aliaga, C. (2016). Calculation of the ELISA's cut-off based on the change-point analysis method for detection of *Trypanosoma cruzi* infection in Bolivian dogs in the absence of controls. *Mem. Inst. Oswaldo Cruz* 111, 501–504. doi: 10.1590/0074-02760160119

Lashen, H., Fear, K., and Sturdee, D. W. (2004). Obesity is associated with increased risk of first trimester and recurrent miscarriage: matched case-control study. *Hum. Reprod.* 19, 1644–1646. doi: 10.1093/humrep/deh277

Liu, W., Krump, N. A., Buck, C. B., and You, J. (2019). Merkel cell polyomavirus infection and detection. *J. Vis. Exp.* 7:e58950. doi: 10.3791/58950

Liu, W., and You, J. (2020). Molecular mechanisms of Merkel Cell polyomavirus transformation and replication. *Annu. Rev. Virol.* 7, 289–307. doi: 10.1146/annurev-virology-011720-121757

Longman, R. E., and Johnson, T. R. B. (2007). Viral respiratory disease in pregnancy. *Curr. Opin. Obstet. Gynecol.* 19, 120–125. doi: 10.1097/GCO.0B013E328028FDC7

Ma, J., and Brewer, J. D. (2014). Merkel cell carcinoma in immunosuppressed patients. *Cancers (Basel)* 6, 1328–1350. doi: 10.3390/CANCERS6031328

Mazziotta, C., Lanzillotti, C., Govoni, M., Pellielo, G., Mazoni, E., Tognon, M. G., et al. (2021a). Decreased IgG antibody response to viral protein mimotopes of oncogenic Merkel cell polyomavirus in sera from healthy elderly subjects. *Front. Immunol.* 12:738486.

Mazziotta, C., Lanzillotti, C., Torreggiani, E., Oton-Gonzalez, L., Iaquinta, M. R., Mazzoni, E., et al. (2021b). Serum antibodies against the oncogenic Merkel Cell Polyomavirus detected by an innovative immunological assay with mimotopes in healthy subjects. *Front. Immunol.* 12:676627. doi: 10.3389/fimmu.2021.676627

Mazzoni, E., Pellegrinelli, E., Mazziotta, C., Lanzillotti, C., Rotondo, J. C., Bononi, I., et al. (2020). Mother-to-child transmission of oncogenic polyomaviruses BKPyV, JCPyV and SV40. *J Infect* 163, 91–98. doi: 10.1016/j.jinf.2020.02.006

Medina, K. L., Smithson, G., and Kincade, P. W. (1993). Suppression of B lymphopoiesis during normal pregnancy. *J. Exp. Med.* 178, 1507–1515. doi: 10.1084/JEM.178.5.1507

Meyer, P. (2001). *Crowther J.R., The ELISA Guidebook, Methods in Molecular Biology*, Vol. 149. Totowa, NJ: Humana Press, 421. doi: 10.1016/s0923-2508(00)01178-5

Miyaji, M., Deguchi, M., Tanimura, K., Sasagawa, Y., Morizane, M., Ebina, Y., et al. (2019). Clinical factors associated with pregnancy outcome in women

with recurrent pregnancy loss. *Gynecol. Endocrinol.* 35, 913–918. doi: 10.1080/09513590.2019.1604657

Mor, G., and Cardenas, I. (2010). Review article: the immune system in pregnancy: a unique complexity. *Am. J. Reprod. Immunol.* 63, 425–433. doi: 10.1111/J.1600-0897.2010.00836.X

Nakagawa, S., and Schielzeth, H. (2010). Repeatability for Gaussian and non-Gaussian data: a practical guide for biologists. *Biol. Rev.* 85, 935–956. doi: 10.1111/j.1469-185X.2010.00141.x

Oton-Gonzalez, L., Rotondo, J. C., Cerritelli, L., Malagutti, N., Lanzillotti, C., Bononi, I., et al. (2021). Association between oncogenic human papillomavirus type 16 and Killian polyp. *Infect. Agent. Cancer* 16:3. doi: 10.1186/s13027-020-00342-3

Pastrana, D. V., Tolstov, Y. L., Becker, J. C., Moore, P. S., Chang, Y., and Buck, C. B. (2009). Quantitation of human seroresponsiveness to Merkel cell polyomavirus. *PLoS Pathog.* 5:e1000578. doi: 10.1371/journal.ppat.1000578

Paterson, C., Musselman, L., Chorneyko, K. S. R., and Rawlinson, J. (2003). Merkel cell (neuroendocrine) carcinoma of the anal canal: report of a case. *Dis. Colon Rectum* 46, 676–678. doi: 10.1007/S10350-004-6630-1

Pietropaolo, V., Prezioso, C., and Moens, U. (2020). merkel cell polyomavirus and merkel cell carcinoma. *Cancers (Basel)* 12:1774. doi: 10.3390/cancers12071774

Prezioso, C., Di Lella, F. M., Rodio, D. M., Bitossi, C., Trancassini, M., Mele, A., et al. (2019). Merkel cell polyomavirus dna detection in respiratory samples: study of a cohort of patients affected by cystic fibrosis. *Viruses* 11:571. doi: 10.3390/v11060571

Racicot, K., and Mor, G. (2017). Risks associated with viral infections during pregnancy. *J. Clin. Invest.* 127, 1591–1599. doi: 10.1172/JCI87490

Robbins, J. R., and Bakardjiev, A. I. (2012). Pathogens and the placental fortress. *Curr. Opin. Microbiol.* 15, 36–43. doi: 10.1016/J.MIB.2011.11.006

Rotondo, J. C., Bononi, I., Puozzo, A., Govoni, M., Foschi, V., Lanza, G., et al. (2017). Merkel cell carcinomas arising in autoimmune disease affected patients treated with biologic drugs including anti-TNF. *Clin. Cancer Res.* 23, 3929–3934. doi: 10.1158/1078-0432.CCR-16-2899

Rotondo, J. C., Bosi, S., Bazzan, E., Di Domenico, M., De Mattei, M., Selvatici, R., et al. (2012). Methylenetetrahydrofolate reductase gene promoter hypermethylation in semen samples of infertile couples correlates with recurrent spontaneous abortion. *Hum. Reprod.* 27, 3632–3638. doi: 10.1093/humrep/des319

Rotondo, J. C., Lanzillotti, C., Mazziotta, C., Tognon, M., and Martini, F. (2021a). Epigenetics of male infertility: the role of DNA methylation. *Front. Cell Dev. Biol.* 9:689624.

Rotondo, J. C., Martini, F., Maritati, M., Mazziotta, C., Di Mauro, G., Lanzillotti, C., et al. (2021b). SARS-CoV-2 infection: new molecular, phylogenetic, and pathogenetic insights. Efficacy of current vaccines and the potential risk of variants. *Viruses* 13:1687.

Rotondo, J. C., Oton-Gonzalez, L., Mazziotta, C., Lanzillotti, C., Iaquinta, M. R., Tognon, M., et al. (2020a). Simultaneous detection and viral DNA load quantification of different human papillomavirus types in clinical specimens by the high analytical droplet digital PCR method. *Front. Microbiol.* 11:591452. doi: 10.3389/fmicb.2020.591452

Rotondo, J. C., Oton-Gonzalez, L., Selvatici, R., Rizzo, P., Pavasini, R., Campo, G. C., et al. (2020b). SERPINA1 gene promoter is differentially methylated in peripheral blood mononuclear cells of pregnant women. *Front. Cell Dev. Biol.* 8:5505. doi: 10.3389/fcell.2020.550543

Rotondo, J. C., Selvatici, R., Di Domenico, M., Marci, R., Vesce, F., Tognon, M., et al. (2013). Methylation loss at H19 imprinted gene correlates with methylenetetrahydrofolate reductase gene promoter hypermethylation in semen samples from infertile males. *Epigenetics* 8, 990–997. doi: 10.4161/epi.25798

Sadeghi, M., Riipinen, A., Väisänen, E., Chen, T., Kantola, K., Surcel, H.-M., et al. (2010). Newly discovered KI, WU, and Merkel cell polyomaviruses: no evidence of mother-to-fetus transmission. *Virol. J.* 71, 1–5. doi: 10.1186/1743-422X-7-251

Saraswati, K., Phanichkrivalkosil, M., Day, N. P. J., and Blacksell, S. D. (2019). The validity of diagnostic cut-offs for commercial and in-house scrub typhus IgM and IgG ELISAs: a review of the evidence. *PLoS Negl. Trop. Dis.* 13:e0007158. doi: 10.1371/journal.pntd.0007158

Sayyadi-Dehno, Z., Seyed Khorrami, S. M., Ghavami, N., Ghotbi-Zadeh, F., Khushideh, M., Hosseini, M., et al. (2019). Molecular detection of adeno-associated virus DNA in cases of spontaneous and therapeutic abortion. *Fetal Pediatr. Pathol.* 38, 206–214. doi: 10.1080/15513815.2019.1576817

Sopori, M. (2002). Effects of cigarette smoke on the immune system. *Nat. Rev. Immunol.* 2, 372–377. doi: 10.1038/nri803

Srinivas, S. K., Ma, Y., Sammel, M. D., Chou, D., McGrath, C., Parry, S., et al. (2006). Placental inflammation and viral infection are implicated in second trimester pregnancy loss. *Am. J. Obstet. Gynecol.* 195, 797–802. doi: 10.1016/j.ajog.2006.05.049

Šroller, V., Hamšíková, E., Ludvíková, V., Vochozková, P., Kojzarová, M., Fraiberk, M., et al. (2014). Seroprevalence rates of BKV, JCV, and MCPyV polyomaviruses in the general czech republic population. *J. Med. Virol.* 86, 1560–1568. doi: 10.1002/jmv.23841

Suzumori, N., and Sugiura-Ogasawara, M. (2012). Genetic factors as a cause of miscarriage. *Curr. Med. Chem.* 17, 3431–3437. doi: 10.2174/092986710793176302

Tabachnick-Cherny, S., Pulliam, T., Church, C., Koelle, D. M., and Nghiem, P. (2020). Polyomavirus-driven Merkel cell carcinoma: prospects for therapeutic vaccine development. *Mol. Carcinog.* 59, 807–821. doi: 10.1002/mc.23190

Tagliapietra, A., Rotondo, J. C. C., Bononi, I., Mazzoni, E., Magagnoli, F., Maritati, M., et al. (2019). Footprints of BK and JC polyomaviruses in specimens from females affected by spontaneous abortion. *Hum. Reprod.* 34, 433–440. doi: 10.1093/humrep/dey375

Tagliapietra, A., Rotondo, J. C. J. C., Bononi, I., Mazzoni, E., Magagnoli, F., Gonzalez, L. O., et al. (2020). Droplet-digital PCR assay to detect Merkel cell polyomavirus sequences in chorionic villi from spontaneous abortion affected females. *J. Cell. Physiol.* 34, 1888–1894. doi: 10.1002/jcp.29213

Tognon, M., Tagliapietra, A., Magagnoli, F., Mazziotta, C., Oton-Gonzalez, L., Lanzillotti, C., et al. (2020). Investigation on spontaneous abortion and human papillomavirus infection. *Vaccines* 8:473. doi: 10.3390/vaccines8030473

Tolstov, Y. L., Knauer, A., Chen, J. G., Kensler, T. W., Kingsley, L. A., Moore, P. S., et al. (2011). Asymptomatic primary merkel cell polyomavirus infection among adults. *Emerg. Infect. Dis.* 17, 1371–1380. doi: 10.3201/eid1708.110079

Toth, B., Jeschke, U., Rogenhofer, N., Scholz, C., Würfel, W., Thaler, C. J., et al. (2010). Recurrent miscarriage: current concepts in diagnosis and treatment. *J. Reprod. Immunol.* 85, 25–32. doi: 10.1016/j.jri.2009.12.006

Touzé, A., Gaitan, J., Arnold, F., Cazal, R., Fleury, M. J., Combelas, N., et al. (2010). Generation of Merkel cell polyomavirus (MCV)-like particles and their application to detection of MCV antibodies. *J. Clin. Microbiol.* 48, 1767–1770. doi: 10.1128/JCM.01691-09

Touzé, A., Le Bidre, E., Laude, H., Fleury, M. J. J., Cazal, R., Arnold, F., et al. (2011). High levels of antibodies against merkel cell polyomavirus identify a subset of patients with merkel cell carcinoma with better clinical outcome. *J. Clin. Oncol.* 29, 1612–1619. doi: 10.1200/JCO.2010.31.1704

Tyler, K. H. (2020). *Cutaneous Disorders of Pregnancy*. Berlin: Springer.

Vahabpour, R., Aghasadeghi, M. R., Salehi-Vaziri, M., Mohajel, N., Keyvani, H., Nasimi, M., et al. (2016). Prevalence of Merkel cell polyomavirus in Tehran: an age-specific serological study. *Iran. Red Crescent Med. J.* 18, e26097. doi: 10.5812/ircmj.26097

Van Der Meijden, E., Bialasiewicz, S., Rockett, R. J., Tozer, S. J., Sloots, T. P., and Feltkamp, M. C. W. (2013). Different serologic behavior of MCPyV, TSPyV, HPyV6, HPyV7 and HPyV9 polyomaviruses found on the skin. *PLoS One* 8:e81078. doi: 10.1371/journal.pone.0081078

Viscidi, R. P., Rollison, D. E., Sondak, V. K., Silver, B., Messina, J. L., Giuliano, A. R., et al. (2011). Age-specific seroprevalence of merkel cell polyomavirus, BK virus, and JC virus. Clin. *Vaccine Immunol.* 18, 1737–1743. doi: 10.1128/CVI.05175-11

Wang, X., and Li, J. (2020). The mechanisms by which trophoblast-derived molecules induce maternal-fetal immune tolerance. *Cell Mol. Immunol.* 17, 1204–1207.

Witkin, A. E., Banerji, J., and Bullock, P. A. (2020). A model for the formation of the duplicated enhancers found in polyomavirus regulatory regions. *Virology* 543, 27–33. doi: 10.1016/j.virol.2020.01.013

Xu, Y. Y., Liu, H. H., Zhong, Y. W., Liu, C., Wang, Y., Jia, L. L., et al. (2015). Peripheral blood mononuclear cell traffic plays a crucial role in mother-to-infant transmission of hepatitis B virus. *Int. J. Biol. Sci.* 11, 266–273. doi: 10.7150/ijbs.10813

Yu, K. K., and Dasanu, C. A. (2016). Rapidly fatal dissemination of Merkel cell carcinoma in a patient treated with alemtuzumab for chronic lymphocytic leukemia. *Conn. Med.* 80, 353–358.

Zhang, C., Liu, F., He, Z., Deng, Q., Pan, Y., Liu, Y., et al. (2014). Seroprevalence of Merkel cell polyomavirus in the general rural population of Anyang. *China. PLoS One* 9:e106430. doi: 10.1371/journal.pone.0106430

Zheng, G., Chattopadhyay, S., Sud, A., Sundquist, K., Sundquist, J., Försti, A., et al. (2019). Second primary cancers in patients with acute lymphoblastic, chronic lymphocytic and hairy cell leukaemia. *Br. J. Haematol.* 185, 232–239. doi: 10.1111/bjh.15777

Zhou, X., Nakashima, K., Ito, M., Zhang, X., Sakai, S., Feng, C., et al. (2020). Prevalence and viral loads of polyomaviruses BKPyV, JCPyV, MCPyV, TSPyV and NJPyV and hepatitis viruses HBV, HCV and HEV in HIV-infected patients in China. *Sci. Rep.* 10:17066. doi: 10.1038/s41598-020-74244-0

**Conflict of Interest:** The authors declare that the research was conducted in the absence of any commercial or financial relationships that could be construed as a potential conflict of interest.

**Publisher's Note:** All claims expressed in this article are solely those of the authors and do not necessarily represent those of their affiliated organizations, or those of the publisher, the editors and the reviewers. Any product that may be evaluated in this article, or claim that may be made by its manufacturer, is not guaranteed or endorsed by the publisher.

*Copyright © 2021 Mazziotta, Pellielo, Tognon, Martini and Rotondo. This is an open-access article distributed under the terms of the Creative Commons Attribution License (CC BY). The use, distribution or reproduction in other forums is permitted, provided the original author(s) and the copyright owner(s) are credited and that the original publication in this journal is cited, in accordance with accepted academic practice. No use, distribution or reproduction is permitted which does not comply with these terms.*

frontiers in Microbiology

REVIEW
published: 24 December 2021
doi: 10.3389/fmicb.2021.808593

# The Role of Unfolded Protein Response in Coronavirus Infection and Its Implications for Drug Design

*Mei Xue and Li Feng**

*State Key Laboratory of Veterinary Biotechnology, Harbin Veterinary Research Institute, Chinese Academy of Agricultural Sciences (CAAS), Harbin, China*

Coronavirus is an important pathogen with a wide spectrum of infection and potential threats to humans and animals. Its replication occurs in the cytoplasm and is closely related to the endoplasmic reticulum (ER). Studies reported that coronavirus infection causes ER stress, and cells simultaneously initiate unfolded protein response (UPR) to alleviate the disturbance of ER homeostasis. Activation of the three branches of UPR (PERK, IRE1, and ATF6) modulates various signaling pathways, such as innate immune response, microRNA, autophagy, and apoptosis. Therefore, a comprehensive understanding of the relationship between coronavirus and ER stress is helpful to understand the replication and pathogenesis of coronavirus. This paper summarizes the current knowledge of the complex interplay between coronavirus and UPR branches, focuses on the effect of ER stress on coronavirus replication and coronavirus resistance to host innate immunity, and summarizes possible drug targets to regulate the impact of coronavirus infection.

**Keywords: coronavirus, endoplasmic reticulum stress, host innate immunity, drug targets, unfolded protein response (UPR)**

OPEN ACCESS

***Edited by:***
*Chunfu Zheng,*
*University of Calgary, Canada*

***Reviewed by:***
*Yiping Wang,*
*University of Florida, United States*
*Dan Li,*
*Lanzhou Veterinary Research Institute, Chinese Academy of Agricultural Sciences (CAAS), China*

***Correspondence:**
*Li Feng*
*fengli_h@163.com*

***Specialty section:***
*This article was submitted to Virology, a section of the journal Frontiers in Microbiology*

***Received:*** *03 November 2021*
***Accepted:*** *09 December 2021*
***Published:*** *24 December 2021*

***Citation:***
*Xue M and Feng L (2021) The Role of Unfolded Protein Response in Coronavirus Infection and Its Implications for Drug Design. Front. Microbiol. 12:808593. doi: 10.3389/fmicb.2021.808593*

## INTRODUCTION

Coronaviruses (order Nidovirales, family Coronaviridae, subfamily Coronavirinae) are a family of enveloped viruses with positive sense, non-segmented, single-stranded RNA genomes. According to the antigenicity relationship and subsequent sequence comparison of the whole virus genome, the *coronavirinae* is classified into four genera: the α-coronavirus, β-coronavirus, γ-coronavirus, and δ-coronavirus (Masters, 2006). Coronavirus infection has a wide spectrum, which causes lethal respiratory infections in humans, diarrhea in pigs and cattle, and bronchitis in poultry. Transmissible gastroenteritis virus (TGEV) and porcine epidemic diarrhea virus (PEDV), members of the α-coronavirus family (Masters, 2006), are the cause of economically important swine disease. PEDV and TGEV infect and destroy villous epithelial cells of the jejunum and ileum, resulting in lethal watery diarrhea and piglet dehydration (Van Nieuwstadt et al., 1989; Cruz et al., 2011). The two human α-coronavirus (HCoV-229E and HCoV-NL63) cause mild symptoms mainly restricted to the upper respiratory tract (Shaban et al., 2021). Human coronaviruses (SARS-CoV, SARS-CoV-2 and MERS-CoV) are a member of β-coronavirus. The emergence of SARS-CoV in 2003 and the SARS-CoV-2 still epidemic worldwide pose a great threat to human life (Ksiazek et al., 2003; Zarandi et al., 2021). γ-coronavirus mainly infects avian hosts. For example, avian infectious bronchitis virus (IBV) is an acute, highly contagious respiratory infectious disease in chickens.

Most strains can cause specific trachea lesions, but some can cause kidney and reproductive tract lesions. The infection of laying hens usually results in a decrease in egg production and egg quality. The disease is widely prevalent worldwide and is an important epidemic disease in the chicken industry (Cavanagh, 2007). Porcine deltacoronavirus (PDCoV) is an emerging porcine intestinal pathogenic coronavirus belonging to the δ-coronavirus family, which caused diarrhea and vomiting in piglets with an incidence rate and mortality rate as high as 50–100% (Zhang et al., 2019).

Coronaviruses are enveloped positive-sense RNA viruses that range in size from 26.4 to 31.7 kb (Hidalgo et al., 2021). The 5′-proximal two-thirds (~20–22 kb) of the genome consists of the two largest ORFs (ORF1a and ORF1b) that encode for the non-structural proteins (nsps). The 3′ one-third of the genome encodes the structural proteins-the highly glycosylated spike (S) protein, envelope (E), membrane (M), nucleocapsid (N), as well as several accessory proteins generally non-essential for replication in tissue culture but capable of inhibiting immune responses and enhancing pathogenesis (**Figure 1**). Infection begins when coronavirus S protein attaches to its complementary host receptor, allowing the virus to enter the host cells through endocytosis or direct fusion of the viral envelope with the cell membrane (Artika et al., 2020). After successfully enters the cells, coronavirus induces profound remodeling of the intracellular membrane network to generate double-membrane vesicles (DMVs). The viral genome RNA is translated to synthesize the viral proteins which are necessary for subsequent RNA replication and transcription. The structural proteins (S, M, and E) are synthesized, inserted, and folded in the ER and transported to the ER-Golgi apparatus intermediate compartment (ERGIC), which is the location of the coronavirus particle assembly, whereas N proteins are translated in the cytoplasm. Following assembly, the progeny virions accumulate in smooth-walled vesicles are transported to the cell surface, and ultimately fuse with the plasma membrane to release the mature virus particle (Artika et al., 2020).

Endoplasmic reticulum with normal function is essential for protein synthesis, folding, modification, and transport (Ron and Walter, 2007; Fung et al., 2014a; Hetz and Papa, 2017). Disturbances in the structure and function of the ER with the accumulation of unfolded/misfolded proteins lead to ER stress. The three major ER stress sensors [protein kinase R-like ER kinase (PERK), inositol-requiring enzyme 1 (IRE1), and activating transcription factor 6 (ATF6)] are activated by accumulated unfolded/misfolded proteins in the ER and initiated the unfolded protein response (UPR) (Credle et al., 2005; Ron and Walter, 2007; Hetz and Papa, 2017). The initiation marker of UPR is the expression of ER chaperone molecules, such as immunoglobulin heavy chain binding protein (BiP/GRP78) and glucose regulatory protein 94 (GRP94). UPR maintains ER homeostasis by turning off the translation of ER proteins and increasing their folding ability. However, UPR can induce apoptosis and cytokine production under sustained ER stress (Ron and Walter, 2007).

Coronavirus genome replication occurs in the cytoplasm, and the synthesis and translation of viral proteins are closely related to ER and its transducers. It is well documented that coronavirus replication causes ER stress and induces UPR in the infected cells. Coronaviruses, such as SARS-CoV-2, SARS-CoV, mouse hepatitis virus (MHV), IBV, TGEV, and PEDV, can all induce significant ER stress following infection (Versteeg et al., 2007; Krahling et al., 2009; DeDiego et al., 2011; Liao et al., 2013; Xue et al., 2018; Echavarria-Consuegra et al., 2021). GRP78 and GRP94 are overexpressed in SARS-CoV infected cells. Some SARS-CoV proteins have been shown to induce ER stress responses, such as spike protein, ORF3a, ORF6, ORF7a, ORF8ab, or ORF8b proteins (Chan et al., 2006; Ye et al., 2008; Minakshi et al., 2009; Sung et al., 2009; Shi et al., 2019). It is recognized that protein processing after synthesis is an important step in gene expression, and protein misfolding plays an important role in coronavirus infection. In the following chapters, we will summarize the latest knowledge on the signaling mechanism of coronavirus induced UPR and the regulation of UPR on coronavirus infection. The significance of the UPR in host innate immune response and possible drug targets will also be discussed.

## REGULATION OF CORONAVIRUS REPLICATION BY UNFOLDED PROTEIN RESPONSE

All three branches of the UPR were induced in MHV, SARS-CoV-2, PEDV, and TGEV infected cells (Versteeg et al., 2007; Xue et al., 2018; Chen et al., 2021; Echavarria-Consuegra et al., 2021). Pharmacological inhibition of the UPR greatly regulated coronavirus replication, revealing the importance of this pathway for successful coronavirus replication.

### The PERK Signaling

PERK belongs to the protein kinase family of the eukaryotic protein translation initiation complex. In the normal state, PERK binds to GRP78. Under conditions of ER stress, PERK dissociates from GRP78, phosphorylates itself, and forms a dimer. Activated PERK can specifically phosphorylate eukaryotic translation initiation factor 2α (eIF2α) at serine 51 (**Figure 2**). Studies based on transient transfection of SARS-CoV proteins have also implicated the involvement of the PERK branch of UPR (Chan et al., 2006; Krahling et al., 2009; DeDiego et al., 2011). For example, Chan et al. (2006) have shown that over-expression of SARS-CoV spike protein induces upregulation of the ER chaperones GRP78 and 94 through PERK activation. Later, the UPR activating domain of SARS-CoV S protein is mapped to the central region (amino acids 201–400) of the S1 subunit and seems to function independently of N-linked glycosylation (Siu et al., 2014). Interestingly, the accessory protein 3a of SARS-CoV, a small multipass transmembrane protein, also activates the ATF4 and Chop promoter activities and thus may potentially also activate the PERK branch of UPR (Minakshi et al., 2009). MHV infection leads to activation of PERK-eIF2α-ATF4 branch (**Figure 2**; Echavarria-Consuegra et al., 2021).

Virus replication is closely dependent on the host cellular protein synthetic machinery to produce viral proteins and particles. Several lines of evidence have indicated a link between

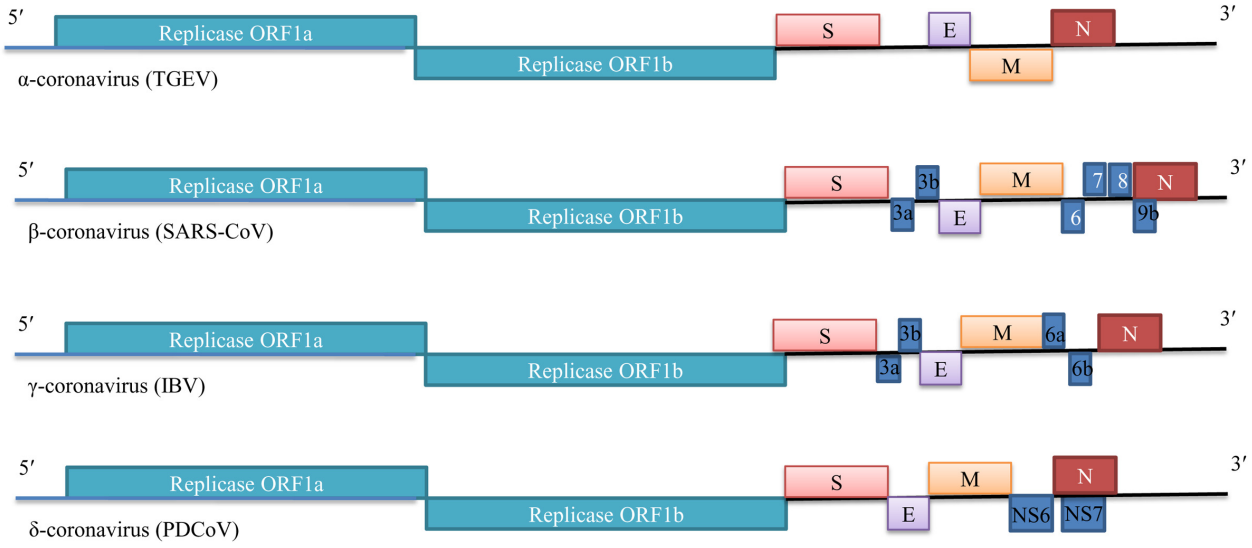


**FIGURE 1 |** Genome organization of selected members of genus Coronavirinae (TGEV, SARS-CoV, IBV and PDCoV).

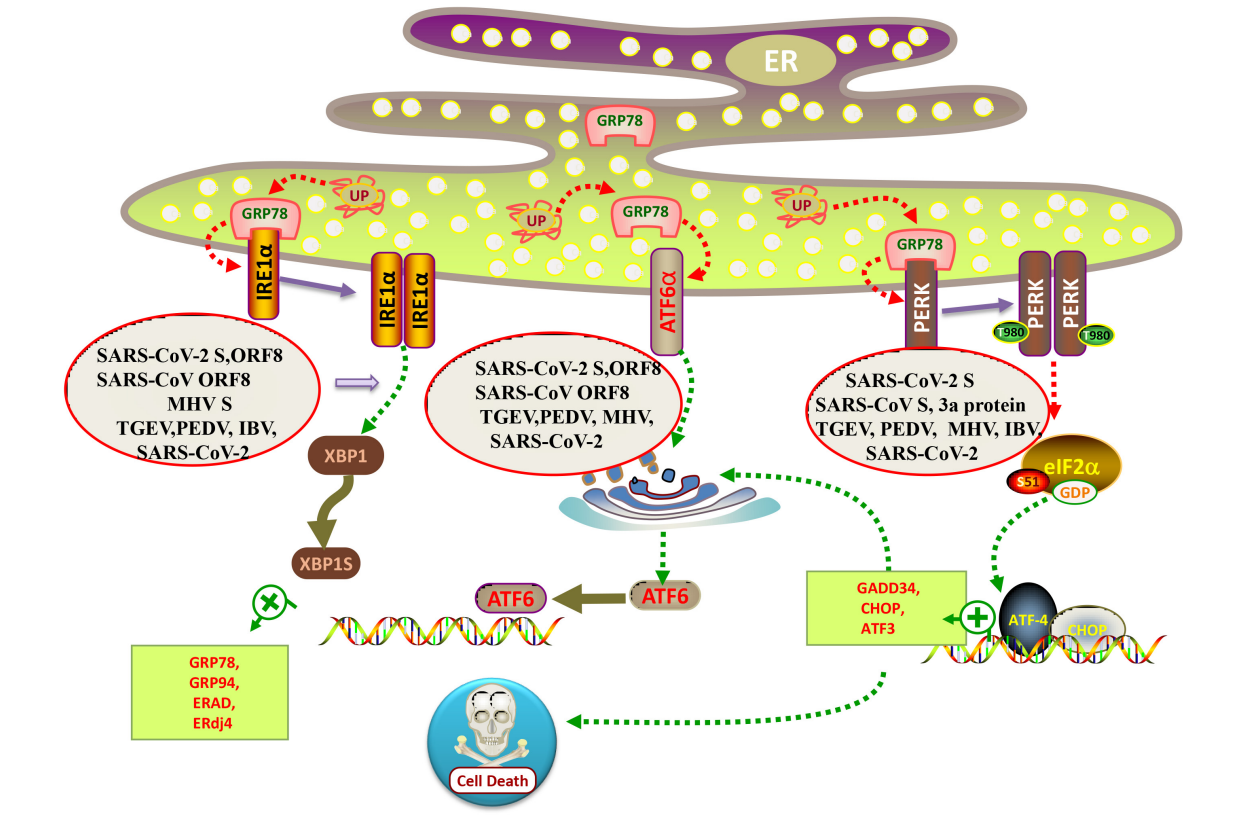


**FIGURE 2 |** Schematic diagram of coronavirus infection modulating the UPR arms. When misfolded proteins accumulate in the lumen of ER, chaperone binding immunoglobulin (BiP/GRP78) is separated from the lumen domains of the three ER sensors, allowing PERK and IRE1 to form a homodimer and activate the transport of ATF6 to the Golgi. All three branches of the UPR were induced in SARS-CoV-2, MHV, PEDV and TGEV infected cells. Individual over-expression of SARS-CoV and SARS-CoV-2 ORF8 protein is sufficient to induce the IRE1 and ATF6 pathway of UPR. While SARS-CoV-2 S protein activates all three branches of the UPR, SARS-CoV S protein only induces PERK pathway.

viral replication and the PERK pathway (Pavio et al., 2003; Datan et al., 2016; Landeras-Bueno et al., 2016; Zhou et al., 2016). Xue et al. (2018) demonstrated that infection with the α-coronavirus TGEV induced ER stress and triggered the three branches of UPR *in vitro* and *in vivo*. Treatment with thapsigargin (Tg) or tunicamycin (Tu) (the ER stress activator) significantly inhibits TGEV replication, indicating that ER stress negatively regulated TGEV replication. Further studies showed that although TGEV infection activated all three ATF6, IRE1, and PERK pathways, their effects on viral replication were different: PERK-eIF2α axis inhibits TGEV replication, IRE1 pathway contributes to virus replication, while ATF6 pathway does not affect TGEV replication. In addition, they demonstrated that phosphorylated eIF2α induced overall attenuation of protein translation, thereby down-regulating TGEV replication (Xue et al., 2018).

Intriguingly, using a recombinant TGEV virus lacking the accessory gene 7 (rTGEV-Δ7), Cruz et al. (2013) have demonstrated that the protein 7 of TGEV physically interacts with PP1 and promotes eIF2α dephosphorylation. Compared with the wild-type virus, cells infected with rTGEV-Δ7 have a much higher phosphorylated eIF2α, resulting in significant translation attenuation and drastic induction of GADD34 (a component of the PP1 complex responsible for the eIF2α dephosphorylation) (Cruz et al., 2013). In cells infected with PEDV, PERK is activated, as seen by an increase in autophosphorylation of PERK during virus infection. Notably, phosphorylation of PERK is dependent on the production of viral protein synthesis. The knockdown of PERK increased virus loads in the cells, consistent with the ER stress inhibitor, 4-phenylbutyrate (4-PBA) treatment (Wang et al., 2014).

In terms of γ-coronavirus, IBV infection activates the PERK-eIF2α-ATF4 and PKR-eIF2α-ATF4 pathways, resulting in the induction of ER stress-mediated proapoptotic pathways (Liao et al., 2013). Interestingly, IBV replication is not significantly affected by knockdown of PERK, indicating that similar to SARS-CoV, IBV is not sensitive to the antiviral activities of PERK *in vitro* (Liao et al., 2013). Thus, the effect of the PERK branch on virus replication is limited to the specific types of coronaviruses.

## The IRE1 Signaling

Mammalian IRE1 has two isoforms-IRE1α and IRE1β. IRE1α is a transmembrane protein with dual enzymatic activities, consisting of an ER luminal amino-terminal domain and a serine/threonine kinase domain plus a carboxyl-terminal ribonuclease (RNase) domain located on the cytosolic side of the protein. Under ER stress, IRE1 becomes an active kinase and autophosphorylates themselves. Splices of the 26-nucleotide intron lead to a frame-shift transcript, which encodes the spliced XBP1 protein (XBP1s) (Yoshida et al., 2001). XBP1s is a potent bZIP transcription factor that induces the expression of genes harboring the UPR element (UPRE) or the ER stress response element (ERSE) in the promoter sequences (Shuda et al., 2003). XBP1s regulate genes involved in protein entry into ER, folding, glycosylation, ER-associated degradation (ERAD), lipid biogenesis, and vesicular trafficking to counteract ER stress (Glimcher, 2010). The expression of at least two genes, the ER DNA J domain-containing protein 4 (ERdj4) and the protein kinase inhibitor of 58 kDa (p58IPK), are specifically induced by XBP1s, but not other UPR transcription factors (Lee et al., 2003).

The IRE1/XBP1 branch is involved in many viral infections. Herpes simplex virus 1 (HSV-1) can avoid cellular responses that are likely detrimental to viral replication by UL41 suppressing the IRE1/XBP1 pathway *via* its RNase activity (Zhang et al., 2017; Zhu and Zheng, 2020). Hepatitis C virus suppresses the IRE1/XBP1 pathway, and influenza A virus induces the IRE1/XBP1 pathway (Tardif et al., 2004; Hassan et al., 2012). For coronavirus, MHV S protein activates the IRE1α-XBP1 pathway (**Figure 2**; Versteeg et al., 2007). Neither infection with SARS-CoV nor overexpression of SARS-CoV S protein induces XBP1 mRNA splicing (Versteeg et al., 2007; DeDiego et al., 2011). Contrary to SARS-CoV, the expression of the SARS-CoV-2 S protein is sufficient to induce all three major signaling pathways of the UPR (Echavarria-Consuegra et al., 2021). IBV induced ER stress in infected cells and activated the IRE1α-XBP1 pathway at a late stage of infection. Both the kinase and RNase domains of IRE1 are necessary to protect infected cells from IBV induced apoptosis. IRE1 appears to convert it from a proapoptotic unspliced form to an antiapoptotic spliced form (Fung et al., 2014b). Previously, they demonstrated that the PERK branch of the UPR is activated at the early stage of IBV infection (Liao et al., 2013), leading to phosphorylation of eIF2α and upregulation of the Chop/GADD153 (C/EBP-homologous protein or growth arrest and DNA damage-inducible protein 153), which promotes IBV-induced apoptosis by suppressing the prosurvival extracellular signal-related kinase (ERK) (Liao et al., 2013). It is generally believed that when ER stress occurs, PERK is first activated, followed by ATF6 and IRE1 (Ron and Walter, 2007). It is interesting to consider the temporal control of UPR activation and its implication in coronavirus infection. From the host perspective, early activation of the PERK pathway and eIF2α phosphorylation induces translation attenuation, an effective antiviral defense mechanism. The induction of apoptosis through the eIF2α-ATF4-Chop pathway may also restrict virus replication. On the other hand, activation of IRE1 at the late stage of infection promotes the survival of infected cells, allowing more virions to be assembled and released before the infected cells succumb to apoptotic cell death.

In addition to the direct modulation of gene transcription, IRE1 cleaves and leads to the selective degradation of a small set of host microRNA (miRNA). SARS-CoV-2 and other human CoVs regulate host miRNAs to increase ER or ER membrane folding ability advantageously, block UPR related translation attenuation, inflammatory response, and apoptosis, and protect the virus from the influence of the immune system. For example, COVID-19-mediated reduction of host miR-34a-3p and miR-495-5p levels can increase the expression of XBP1s and BiP by increasing the folding ability of ER (Bartoszewski et al., 2020). The IRE1 pathway activated by TGEV infection can downregulate the host miR-30a-5p abundance, while miR-30a-5p targets the 3′UTR region of SOCS1 and SOCS3. The down-regulated expression of miR-30a-5p makes SOCS1 and SOCS3 negatively feedback regulate IFN antiviral signaling (Ma et al., 2018).

### The ATF6 Signaling

ATF6 resides in the ER membrane with a cytosolic amino-terminal domain and an ER luminal carboxyl-terminal domain. As a result of its activation, the amino-terminal domain of ATF6 is released by proteolysis. This portion of ATF6 translocates to the nucleus, where it cooperates with other proteins to form a complex that induces the expression of genes coding for chaperones or folding enzymes. A study of SARS-CoV has found one of the accessory proteins (8ab protein) directly binding to the ATF6 lumen domain, suggesting 8ab protein might facilitate protein folding and processing by modulating UPR (Sung et al., 2009). When SARS-CoV-2 ORF8 was transfected, IRE1α-XBP1 and ATF6 were the main pathways induced (Echavarria-Consuegra et al., 2021). In MHV infected cells, ATF6 was processed to its active form at 7 h after infection, but both full-length ATF6 and active ATF6 disappeared at the later stage of infection (Echavarria-Consuegra et al., 2021). In TGEV-infected cells, ATF6 was activated, but no significant difference in TGEV replication was found after ATF6 knockdown in ST and IPEC-J2 cells by siRNA compared with that of control siRNA. The results indicate that activation of the ATF6 branches is not responsible for suppressing TGEV replication by UPR (Xue et al., 2018).

## ENDOPLASMIC RETICULUM STRESS ON INNATE IMMUNE RESPONSE

In the innate immunity of the host, many cytokines are produced to fight the virus. Type I interferon (IFN-I) is the main antiviral molecule, but coronavirus has evolved a variety of strategies, including UPR, to combat IFN-I response during infection. MERS-CoV protein 4a is the first coronavirus protein identified as an antagonist of the dsRNA-dependent, PKR-mediated stress response and IFN-α/β pathways (Rabouw et al., 2016). SARS-CoV activates the PERK pathway of UPR, followed by eIF2α. The activation of the PERK pathway regulates innate immunity by inhibiting the IFN-I signaling. Mechanically, the 3a protein-induced serine phosphorylation and ubiquitination of the IFN alpha-receptor subunit 1 (IFNAR1) leading to lysosomal degradation of IFNAR1 (**Figure 3**; Minakshi et al., 2009). After TGEV infection, in addition to the classical signaling pathway (Ding et al., 2017), NF-kB can be activated by PERK-eIF2α to induce IFN-I production (Xue et al., 2018). As a member of the α-coronavirus family, PEDV inhibited IFN production, while TGEV induced high levels of IFN production. Surprisingly, the adequate IFN transcription could not suppress viral replication (Zhu et al., 2017). Ma et al. (2018) found a new strategy for TGEV to evade the IFN-I antiviral response by using the IRE1-miR-30a-5p/SOCS1/3 axis. The IRE1 axis reduced host miR-30a-5p abundance, resulting in increased negative feedback regulators of JAK-STAT signaling, SOCS1, and SOCS3. High expression of SOCS1 or 3 disrupted the antiviral effect of IFN-I (**Figure 3**; Ma et al., 2018). The data explain that TGEV evades the IFN-I antiviral response despite the intense induction of endogenous IFN-I.

The study of IBV found that the eIF2α phosphorylation leads to IκBα decrease, thereby activating NF-κB and promoting cytokine production. Activating the IRE1α-XBP1 signaling pathway is necessary for the production of IL-8 in IBV infected cells (Zhu et al., 2021). IRE1 kinase activity rather than RNase activity is involved in ER stress-mediated NF-κB activation. Therefore, UPR plays an important role in regulating IFN response and innate immunity of coronavirus-infected cells.

## THE UNFOLDED PROTEIN RESPONSE-DEPENDENT MOLECULAR MECHANISMS AS A THERAPEUTIC TARGET FOR CORONAVIRUS

Recent data suggest that the disturbance of UPR signal branches may play a role in developing and progressing various human diseases (Banerjee et al., 2020; Rozpedek-Kaminska et al., 2020). The ER stress inducer thapsigargin efficiently inhibits coronavirus (HCoV-229E, MERS-CoV, SARS-CoV-2) replication in different cell types, including primary differentiated human bronchial epithelial cells (Shaban et al., 2021). Thapsigargin exerts a profound antiviral effect on TGEV in two different cell types, including a non-transformed cell line originating from porcine jejunum epithelium (IPEC-J2) (Xue et al., 2018). This compound or its derivatives with better specificity, pharmacokinetics, and safety may be an interesting drug candidate suitable for alleviating the consequences of the potential CoV epidemic in the future. Sigma-1 receptor (Sig-1R) is a ligand-operated ER binding chaperone as an upstream regulator of ER stress and is, therefore, a candidate host protein for host-based re-utilization in patients with COVID-19 (Vela, 2020). Both andrographolide and melatonin provide useful adjuvant therapy for COVID-19 by impacting the UPR signaling pathways by inhibiting the ER stress transducers (Banerjee et al., 2020; Sureda et al., 2020). There is also evidence that 2-Deoxy-D-glucose (2-DG), an ER stress inducer, inhibits PEDV infection *via* altering viral protein translation during the early stage of virus infection and depressing the virus assembly (Wang et al., 2014). Coronavirus induces profound remodeling of primarily ER-derived membranes and triggers the formation of double-membrane vesicles (DMVs) for viral genome replication. Researchers determined the antiviral effect of a small complex inhibitor called K22 [(z)-N-(3-(4-(4-bromophenyl)-4-hydroxypiperidine-1-yl)-3-oxo-1-phenylpropyl-1-ene-2-yl) benzamide] in primary human epithelial cell cultures (Lundin et al., 2014). K22 exerts strong anti-coronavirus activity in the early stage of infection by preventing the formation of DMVs, leading to almost complete inhibition of RNA synthesis, including SARS-CoV and MERS-CoV (Lundin et al., 2014; Sureda et al., 2020). These data suggest that pharmacological regulation of the UPR signaling pathway may significantly inhibit coronavirus replication (**Table 1**). Therefore, targeting the ER stress-dependent UPR signaling branches may help to develop a new anti-coronavirus treatment strategy.

Small molecules targeting the PERK branch include GSK2606414, Salubrinal, GSK2656157, ISRIB, Guanabenz, Sepin1, Trazodone Hydrochloride, and Dibenzoylmethane,

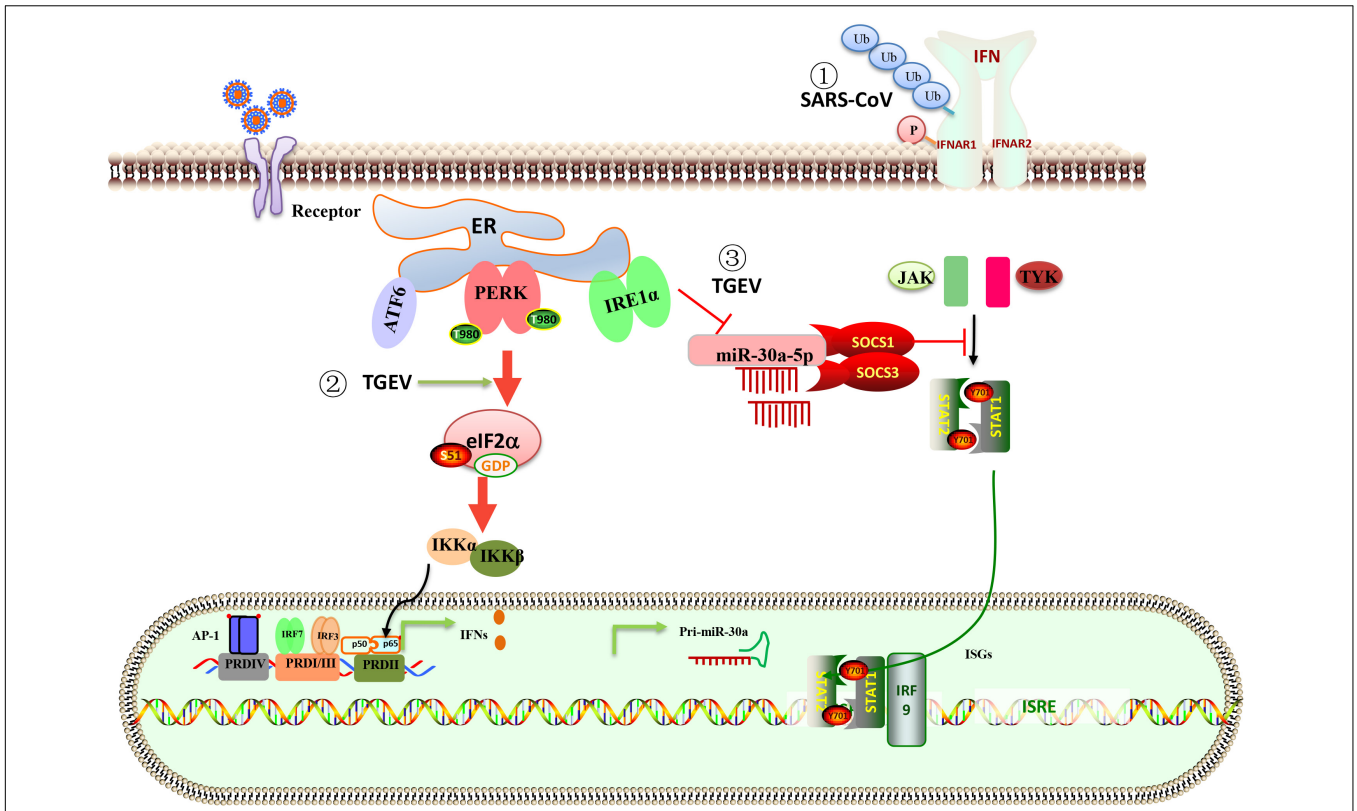


**FIGURE 3 |** Schematic representation of the interaction between ER stress, UPR, and innate immune system in response to coronavirus infection. (1) The PERK branch of UPR elicited by SARS-CoV 3a protein leads to ubiquitination, phosphorylation, and lysosomal degradation of IFNAR1 and inhibits IFN-I signaling. (2) TGEV infection activates the PERK-eIF2α pathway, the phosphorylation of eIF2α attenuates global protein synthesis, which decreases the levels of cytoplasm IκBα and leads to reduced inhibition of IκBα on NF-κB, promoting IFN-I production. (3) The IRE1 axis reduced host miR-30a-5p abundance, resulting in increased negative feedback regulators of JAK-STAT signaling, SOCS1 and SOCS3. High expression of SOCS1 or SOCS3 disrupted the antiviral effect of IFN-I. The data explain that TGEV evades the IFN-I antiviral response despite the intense induction of endogenous IFN-I.

**TABLE 1 |** A list of drugs that modulate ER stress and their anti-coronavirus activities.

| Compound | Biological activity | Antiviral activity | |
|---|---|---|---|
| | | Virus | References |
| Thapsigargin | ER stress inducer | HCoV-229E, MERS-CoV, SARS-CoV-2, TGEV | Xue et al., 2018; Shaban et al., 2021 |
| Sig-1R | Chaperone protein in ER | SARS-CoV-2 | Vela, 2020 |
| Andrographolide | A NF-κB inhibitor | SARS-CoV-2 | Banerjee et al., 2020; Sureda et al., 2020 |
| Melatonin | ATF6 inhibitor | SARS-CoV-2 | Banerjee et al., 2020; Sureda et al., 2020 |
| 2-DG | Inhibiting glycolysis via its actions on hexokinase | PEDV | Wang et al., 2014 |
| GSK2606414 | PERK inhibitor | SARS-CoV-2 | Sonkar et al., 2021 |
| Salubrinal | Selective inhibitor of eIF2α dephosphorylation | TGEV | Xue et al., 2018 |
| ISRIB | PERK inhibitor | MHV | Echavarria-Consuegra et al., 2021 |
| 4μ8C | IRE1α inhibitor | TGEV | Xue et al., 2018 |
| STF-083010 | Inhibits IRE1 endonuclease activity without affecting its kinase activity | SARS-CoV-2, MHV | Echavarria-Consuegra et al., 2021 |
| AEBSF | ATF6 inhibitor | SARS-CoV-2, MHV | Echavarria-Consuegra et al., 2021 |

LDN-0060609, Oxyresveratrol, β-Asarone, and Gastrodia Elata Derivatives (Rozpedek-Kaminska et al., 2020). GSK2606414 is the first-generation and highly selective PERK inhibitor characterized by 30 nm IC50 (the half-maximal inhibitory concentration) and good cell efficacy *in vitro* and *in vivo*. Its selectivity is > 385-fold over other eIF2α kinases. Recently, 12 inhibitors with high binding energies were used to treat COVID-19. GSK2606414 has shown a strong binding affinity

with SARS-CoV-2, but it was excluded from the study since its ability to be carcinogenic (Sonkar et al., 2021). GSK2606414 treatment of MHV-infected cells revealed a relief of translation inhibition (Echavarria-Consuegra et al., 2021). In another project, researchers have shown that the silencing of PERK by GSK2606414 considerably elevated TGEV replication in the cells. In addition, the increase in virus loads was correlated with the inhibition efficacy of p-PERK and p-eIF2α (Xue et al., 2018). Salubrinal selectively inhibited eIF2α dephosphorylation and evoked an increased level of p-eIF2α. Treatment of cells with salubrinal demonstrated the opposite effect to previously tested PERK inhibitors and caused a dose-dependent decrease in TGEV replication (Xue et al., 2018). When 2 μM ISRIB was used to treat MHV infected cells, it was found that the transcription of *Chop* decreased and the virus titers reduced by ∼sixfold (Echavarria-Consuegra et al., 2021). Thus, the latest data suggest that using small-molecule inhibitors of PERK-dependent UPR signaling pathways may help develop a novel and pioneering therapeutic strategy against coronavirus.

Small molecule inhibitors that selectively block IRE1α-XBP1 activation have been identified. Two major sites have been explored as targets for IRE1α inhibitors: the ATP binding site of the kinase domain and the catalytic core of the RNase domain. "Compound 3" and APY29 are both IRE1α kinase inhibitors which are reported to inhibit IRE1α-XBP1 by directly interfering with ATP binding in the IRE1α kinase domain (Wang et al., 2012). Small molecules targeting the RNase domain include 4μ8C, STF-083010, salicylaldehydes, toyocamycin, MKC-3946, and hydroxyl-aryl-aldehydes (HAA) (Cross et al., 2012; Jiang et al., 2015). Targeting the RNase activity of IRE1 could potentially be an ideal approach to modulate COVID-19 infection and pathogenesis *via* modulation of the secretome of macrophages. Inhibition of IRE1α RNase activity with small molecule 4μ8c suppressed TGEV replication (Ma et al., 2018). These data suggest that IRE1α-targeting might be a new strategy to cope with coronavirus infection.

AEBSF is a serine protease inhibitor, preventing ER stress-induced ATF6 cleavage, thereby inhibiting the transcriptional induction of ATF6 target genes (Chan et al., 2006). *Calreticulin* and *Grp94* transcription were significantly reduced in AEBSF treated MHV infected cells (Echavarria-Consuegra et al., 2021).

The combination of UPR inhibitors has a cumulative effect on virus release. Cells incubated with STF-083010 (targeting the IRE1α pathway) lead to ∼twofold reductions in MHV titers, while cells treated with STF-083010 and AEBSF (targeting the IRE1α and the ATF6 pathways) reduced virus titer ranged to ∼40- and ∼100-fold. Reductions in virus titer were observed in SARS-CoV-2 infected cells, and the reductions were generally much greater than those seen for MHV, with STF-083010/AEBSF combinations reducing SARS-CoV-2 titers to below the limit of detection (Echavarria-Consuegra et al., 2021).

## CONCLUSION

Coronavirus has posed a great threat to humans and animals. Despite decades of elegant investigations, the interactions between the host and coronaviruses during infection remain poorly understood. Recent studies have demonstrated that coronavirus infection induces ER stress in infected cells and activates the UPR. Notably, previous studies on coronavirus-induced UPR have been mainly focusing on individual branches of the UPR. It is important to note that the three branches of UPR are not functionally independent but rather operate as an integrated signaling network. The complex of GRP78 and three sensors, PERK, ATF6, and IRE1, regulated by viruses is probably evolved to either regulate the pathological process or optimize viral replication. UPR inhibitors may have dual therapeutic effects, which help reduce viral load and diminish the pathophysiology associated with coronavirus. Further investigation on the molecular interaction between viruses, ER stress, and innate immunity may yield important information to clarify coronavirus pathogenesis. The crosstalk between ER stress and antiviral activities suggests that novel therapeutic targets may have potential utility against coronavirus.

## AUTHOR CONTRIBUTIONS

MX conceived and drafted the manuscript. LF conceived and revised the manuscript. All authors read and approved the final manuscript for publication.

## FUNDING

This work was supported by grants from the National Natural Science Foundation of China (no. 31802198) and Natural Science Foundation of Heilongjiang Province (no. TD2020C002). The funding body had no role in the study's design, collection, analysis, and interpretation of data or the writing of this manuscript.

## ACKNOWLEDGMENTS

We are grateful to Pinghuang Liu (College of Veterinary Medicine, China Agricultural University) for providing useful inspiration.

## REFERENCES

Artika, I. M., Dewantari, A. K., and Wiyatno, A. (2020). Molecular biology of coronaviruses: current knowledge. *Heliyon* 6:e04743. doi: 10.1016/j.heliyon.2020.e04743

Banerjee, A., Czinn, S. J., Reiter, R. J., and Blanchard, T. G. (2020). Crosstalk between endoplasmic reticulum stress and anti-viral activities: a novel therapeutic target for COVID-19. *Life Sci.* 255:117842. doi: 10.1016/j.lfs.2020.117842

Bartoszewski, R., Dabrowski, M., Jakiela, B., Matalon, S., Harrod, K. S., Sanak, M., et al. (2020). SARS-CoV-2 may regulate cellular responses through depletion of specific host miRNAs. *Am. J. Physiol. Lung. Cell Mol. Physiol.* 319, L444–L455. doi: 10.1152/ajplung.00252.2020

Cavanagh, D. (2007). Coronavirus avian infectious bronchitis virus. *Vet. Res.* 38, 281–297.

Chan, C. P., Siu, K. L., Chin, K. T., Yuen, K. Y., Zheng, B., and Jin, D. Y. (2006). Modulation of the unfolded protein response by the severe acute respiratory syndrome coronavirus spike protein. *J. Virol.* 80, 9279–9287. doi: 10.1128/JVI.00659-06

Chen, Y. M., Gabler, N. K., and Burrough, E. R. (2021). Porcine epidemic diarrhea virus infection induces endoplasmic reticulum stress and unfolded protein response in jejunal epithelial cells of weaned pigs. *Vet. Pathol. [Online ahead of print]* 3009858211048622. doi: 10.1177/03009858211048622

Credle, J. J., Finer-Moore, J. S., Papa, F. R., Stroud, R. M., and Walter, P. (2005). On the mechanism of sensing unfolded protein in the endoplasmic reticulum. *Proc. Natl. Acad. Sci. U.S.A.* 102, 18773–18784. doi: 10.1073/pnas.0509487102

Cross, B. C., Bond, P. J., Sadowski, P. G., Jha, B. K., Zak, J., Goodman, J. M., et al. (2012). The molecular basis for selective inhibition of unconventional mRNA splicing by an IRE1-binding small molecule. *Proc. Natl. Acad. Sci. U.S.A.* 109, E869–E878. doi: 10.1073/pnas.1115623109

Cruz, J. L., Becares, M., Sola, I., Oliveros, J. C., Enjuanes, L., and Zuniga, S. (2013). Alphacoronavirus protein 7 modulates host innate immune response. *J. Virol.* 87, 9754–9767. doi: 10.1128/JVI.01032-13

Cruz, J. L., Sola, I., Becares, M., Alberca, B., Plana, J., Enjuanes, L., et al. (2011). Coronavirus gene 7 counteracts host defenses and modulates virus virulence. *PLoS Pathog.* 7:e1002090. doi: 10.1371/journal.ppat.1002090

Datan, E., Roy, S. G., Germain, G., Zali, N., Mclean, J. E., Golshan, G., et al. (2016). Dengue-induced autophagy, virus replication and protection from cell death require ER stress (PERK) pathway activation. *Cell Death Dis.* 7:e2127. doi: 10.1038/cddis.2015.409

DeDiego, M. L., Nieto-Torres, J. L., Jimenez-Guardeno, J. M., Regla-Nava, J. A., Alvarez, E., Oliveros, J. C., et al. (2011). Severe acute respiratory syndrome coronavirus envelope protein regulates cell stress response and apoptosis. *PLoS Pathog.* 7:e1002315. doi: 10.1371/journal.ppat.1002315

Ding, Z., An, K., Xie, L., Wu, W., Zhang, R., Wang, D., et al. (2017). Transmissible gastroenteritis virus infection induces NF-kappaB activation through RLR-mediated signaling. *Virology* 507, 170–178. doi: 10.1016/j.virol.2017.04.024

Echavarria-Consuegra, L., Cook, G. M., Busnadiego, I., Lefevre, C., Keep, S., Brown, K., et al. (2021). Manipulation of the unfolded protein response: a pharmacological strategy against coronavirus infection. *PLoS Pathog.* 17:e1009644. doi: 10.1371/journal.ppat.1009644

Fung, T. S., Huang, M., and Liu, D. X. (2014a). Coronavirus-induced ER stress response and its involvement in regulation of coronavirus-host interactions. *Virus Res.* 194, 110–123. doi: 10.1016/j.virusres.2014.09.016

Fung, T. S., Liao, Y., and Liu, D. X. (2014b). The endoplasmic reticulum stress sensor IRE1alpha protects cells from apoptosis induced by the coronavirus infectious bronchitis virus. *J. Virol.* 88, 12752–12764. doi: 10.1128/JVI.02138-14

Glimcher, L. H. (2010). XBP1: the last two decades. *Ann. Rheum Dis.* 69(Suppl. 1), i67–i71. doi: 10.1136/ard.2009.119388

Hassan, I. H., Zhang, M. S., Powers, L. S., Shao, J. Q., Baltrusaitis, J., Rutkowski, D. T., et al. (2012). Influenza A viral replication is blocked by inhibition of the inositol-requiring enzyme 1 (IRE1) stress pathway. *J. Biol. Chem.* 287, 4679–4689. doi: 10.1074/jbc.M111.284695

Hetz, C., and Papa, F. R. (2017). The unfolded protein response and cell fate control. *Mol. Cell.* 69, 169–181. doi: 10.1016/j.molcel.2017.06.017

Hidalgo, P., Valdes, M., and Gonzalez, R. A. (2021). Molecular biology of coronaviruses: an overview of virus-host interactions and pathogenesis. *Bol. Med. Hosp. Infant Mex* 78, 41–58. doi: 10.24875/BMHIM.20000249

Jiang, D., Niwa, M., and Koong, A. C. (2015). Targeting the IRE1alpha-XBP1 branch of the unfolded protein response in human diseases. *Semin. Cancer Biol.* 33, 48–56. doi: 10.1016/j.semcancer.2015.04.010

Krahling, V., Stein, D. A., Spiegel, M., Weber, F., and Muhlberger, E. (2009). Severe acute respiratory syndrome coronavirus triggers apoptosis via protein kinase R but is resistant to its antiviral activity. *J. Virol.* 83, 2298–2309. doi: 10.1128/JVI.01245-08

Ksiazek, T. G., Erdman, D., Goldsmith, C. S., Zaki, S. R., Peret, T., Emery, S., et al. (2003). A novel coronavirus associated with severe acute respiratory syndrome. *N. Engl. J. Med.* 348, 1953–1966.

Landeras-Bueno, S., Fernandez, Y., Falcon, A., Oliveros, J. C., and Ortin, J. (2016). Chemical genomics identifies the PERK-Mediated unfolded protein stress response as a cellular target for influenza virus inhibition. *MBio* 7:e00085-16. doi: 10.1128/mBio.00085-16

Lee, A. H., Iwakoshi, N. N., and Glimcher, L. H. (2003). XBP-1 regulates a subset of endoplasmic reticulum resident chaperone genes in the unfolded protein response. *Mol. Cell Biol.* 23, 7448–7459. doi: 10.1128/MCB.23.21.7448-7459.2003

Liao, Y., Fung, T. S., Huang, M., Fang, S. G., Zhong, Y., and Liu, D. X. (2013). Upregulation of CHOP/GADD153 during coronavirus infectious bronchitis virus infection modulates apoptosis by restricting activation of the extracellular signal-regulated kinase pathway. *J. Virol.* 87, 8124–8134. doi: 10.1128/JVI.00626-13

Lundin, A., Dijkman, R., Bergstrom, T., Kann, N., Adamiak, B., Hannoun, C., et al. (2014). Targeting membrane-bound viral RNA synthesis reveals potent inhibition of diverse coronaviruses including the middle East respiratory syndrome virus. *PLoS Pathog.* 10:e1004166. doi: 10.1371/journal.ppat.1004166

Ma, Y., Wang, C., Xue, M., Fu, F., Zhang, X., Li, L., et al. (2018). The coronavirus transmissible gastroenteritis virus evades the Type I interferon response through IRE1alpha-Mediated manipulation of the MicroRNA miR-30a-5p/SOCS1/3 axis. *J. Virol.* 92, e728–e718. doi: 10.1128/JVI.00728-18

Masters, P. S. (2006). The molecular biology of coronaviruses. *Adv. Virus Res.* 66, 193–292.

Minakshi, R., Padhan, K., Rani, M., Khan, N., Ahmad, F., and Jameel, S. (2009). The SARS Coronavirus 3a protein causes endoplasmic reticulum stress and induces ligand-independent downregulation of the type 1 interferon receptor. *PLoS One* 4:e8342. doi: 10.1371/journal.pone.0008342

Pavio, N., Romano, P. R., Graczyk, T. M., Feinstone, S. M., and Taylor, D. R. (2003). Protein synthesis and endoplasmic reticulum stress can be modulated by the hepatitis C virus envelope protein E2 through the eukaryotic initiation factor 2alpha kinase PERK. *J. Virol.* 77, 3578–3585. doi: 10.1128/jvi.77.6.3578-3585.2003

Rabouw, H. H., Langereis, M. A., Knaap, R. C., Dalebout, T. J., Canton, J., Sola, I., et al. (2016). Middle east respiratory coronavirus accessory protein 4a inhibits PKR-Mediated antiviral stress responses. *PLoS Pathog.* 12:e1005982. doi: 10.1371/journal.ppat.1005982

Ron, D., and Walter, P. (2007). Signal integration in the endoplasmic reticulum unfolded protein response. *Nat. Rev. Mol. Cell Biol.* 8, 519–529.

Rozpedek-Kaminska, W., Siwecka, N., Wawrzynkiewicz, A., Wojtczak, R., Pytel, D., Diehl, J. A., et al. (2020). The PERK-Dependent molecular mechanisms as a novel therapeutic target for neurodegenerative diseases. *Int. J. Mol. Sci.* 21:2108. doi: 10.3390/ijms21062108

Shaban, M. S., Muller, C., Mayr-Buro, C., Weiser, H., Meier-Soelch, J., Albert, B. V., et al. (2021). Multi-level inhibition of coronavirus replication by chemical ER stress. *Nat. Commun.* 12:5536. doi: 10.1038/s41467-021-25551-1

Shi, C. S., Nabar, N. R., Huang, N. N., and Kehrl, J. H. (2019). SARS-coronavirus open reading Frame-8b triggers intracellular stress pathways and activates NLRP3 inflammasomes. *Cell Death Discov.* 5:101. doi: 10.1038/s41420-019-0181-7

Shuda, M., Kondoh, N., Imazeki, N., Tanaka, K., Okada, T., Mori, K., et al. (2003). Activation of the ATF6, XBP1 and grp78 genes in human hepatocellular carcinoma: a possible involvement of the ER stress pathway in hepatocarcinogenesis. *J. Hepatol.* 38, 605–614. doi: 10.1016/s0168-8278(03)00029-1

Siu, K. L., Chan, C. P., Kok, K. H., Woo, P. C., and Jin, D. Y. (2014). Comparative analysis of the activation of unfolded protein response by spike proteins of severe acute respiratory syndrome coronavirus and human coronavirus HKU1. *Cell Biosci.* 4:3. doi: 10.1186/2045-3701-4-3

Sonkar, C., Doharey, P. K., Rathore, A. S., Singh, V., Kashyap, D., Sahoo, A. K., et al. (2021). Repurposing of gastric cancer drugs against COVID-19. *Comput. Biol. Med.* 137:104826. doi: 10.1016/j.compbiomed.2021.104826

Sung, S. C., Chao, C. Y., Jeng, K. S., Yang, J. Y., and Lai, M. M. (2009). The 8ab protein of SARS-CoV is a luminal ER membrane-associated protein and induces the activation of ATF6. *Virology* 387, 402–413. doi: 10.1016/j.virol.2009.02.021

Sureda, A., Alizadeh, J., Nabavi, S. F., Berindan-Neagoe, I., Cismaru, C. A., Jeandet, P., et al. (2020). Endoplasmic reticulum as a potential therapeutic target for covid-19 infection management? *Eur. J. Pharmacol.* 882:173288. doi: 10.1016/j.ejphar.2020.173288

Tardif, K. D., Mori, K., Kaufman, R. J., and Siddiqui, A. (2004). Hepatitis C virus suppresses the IRE1-XBP1 pathway of the unfolded protein response. *J. Biol. Chem.* 279, 17158–17164. doi: 10.1074/jbc.M312144200

Van Nieuwstadt, A. P., Zetstra, T., and Boonstra, J. (1989). Infection with porcine respiratory coronavirus does not fully protect pigs against intestinal transmissible gastroenteritis virus. *Vet. Rec.* 125, 58–60. doi: 10.1136/vr.125.3.58

Vela, J. M. (2020). Repurposing Sigma-1 receptor ligands for COVID-19 therapy? *Front. Pharmacol.* 11:582310. doi: 10.3389/fphar.2020.582310

Versteeg, G. A., Van De Nes, P. S., Bredenbeek, P. J., and Spaan, W. J. (2007). The coronavirus spike protein induces endoplasmic reticulum stress and upregulation of intracellular chemokine mRNA concentrations. *J. Virol.* 81, 10981–10990. doi: 10.1128/JVI.01033-07

Wang, L., Perera, B. G., Hari, S. B., Bhhatarai, B., Backes, B. J., Seeliger, M. A., et al. (2012). Divergent allosteric control of the IRE1alpha endoribonuclease using kinase inhibitors. *Nat. Chem. Biol.* 8, 982–989. doi: 10.1038/nchembio.1094

Wang, Y., Li, J. R., Sun, M. X., Ni, B., Huan, C., Huang, L., et al. (2014). Triggering unfolded protein response by 2-Deoxy-D-glucose inhibits porcine epidemic diarrhea virus propagation. *Antiviral Res.* 106, 33–41. doi: 10.1016/j.antiviral.2014.03.007

Xue, M., Fu, F., Ma, Y., Zhang, X., Li, L., Feng, L., et al. (2018). The PERK arm of the unfolded protein response negatively regulates transmissible gastroenteritis virus replication by suppressing protein translation and promoting Type I interferon production. *J. Virol.* 92, e431–e418. doi: 10.1128/JVI.00431-18

Ye, Z., Wong, C. K., Li, P., and Xie, Y. (2008). A SARS-CoV protein, ORF-6, induces caspase-3 mediated, ER stress and JNK-dependent apoptosis. *Biochim. Biophys. Acta* 1780, 1383–1387. doi: 10.1016/j.bbagen.2008.07.009

Yoshida, H., Matsui, T., Yamamoto, A., Okada, T., and Mori, K. (2001). XBP1 mRNA is induced by ATF6 and spliced by IRE1 in response to ER stress to produce a highly active transcription factor. *Cell* 107, 881–891. doi: 10.1016/s0092-8674(01)00611-0

Zarandi, P. K., Zinatizadeh, M. R., Zinatizadeh, M., Yousefi, M. H., and Rezaei, N. (2021). SARS-CoV-2: from the pathogenesis to potential anti-viral treatments. *Biomed. Pharmacother.* 137:111352. doi: 10.1016/j.biopha.2021.111352

Zhang, J., Chen, J., Shi, D., Shi, H., Zhang, X., Liu, J., et al. (2019). Porcine deltacoronavirus enters cells via two pathways: a protease-mediated one at the cell surface and another facilitated by cathepsins in the endosome. *J. Biol. Chem.* 294, 9830–9843. doi: 10.1074/jbc.RA119.007779

Zhang, P., Su, C., Jiang, Z., and Zheng, C. (2017). Herpes simplex virus 1 UL41 protein suppresses the IRE1/XBP1 signal pathway of the unfolded protein response via its RNase activity. *J. Virol.* 91, e2056–e2016. doi: 10.1128/JVI.02056-16

Zhou, Y., Qi, B., Gu, Y., Xu, F., Du, H., Li, X., et al. (2016). Porcine circovirus 2 deploys PERK pathway and GRP78 for its enhanced replication in PK-15 cells. *Viruses* 8:56. doi: 10.3390/v8020056

Zhu, H., and Zheng, C. (2020). The race between host antiviral innate immunity and the immune evasion strategies of herpes simplex virus 1. *Microbiol. Mol. Biol. Rev.* 84, e99–e20. doi: 10.1128/MMBR.00099-20

Zhu, L., Yang, X., Mou, C., and Yang, Q. (2017). Transmissible gastroenteritis virus does not suppress IFN-beta induction but is sensitive to IFN in IPEC-J2 cells. *Vet. Microbiol.* 199, 128–134. doi: 10.1016/j.vetmic.2016.12.031

Zhu, Q. C., Li, S., Yuan, L. X., Chen, R. A., Liu, D. X., and Fung, T. S. (2021). Induction of the proinflammatory chemokine Interleukin-8 is regulated by integrated stress response and AP-1 family proteins activated during coronavirus infection. *Int. J. Mol. Sci.* 22:5646. doi: 10.3390/ijms22115646

**Conflict of Interest:** The authors declare that the research was conducted in the absence of any commercial or financial relationships that could be construed as a potential conflict of interest.

**Publisher's Note:** All claims expressed in this article are solely those of the authors and do not necessarily represent those of their affiliated organizations, or those of the publisher, the editors and the reviewers. Any product that may be evaluated in this article, or claim that may be made by its manufacturer, is not guaranteed or endorsed by the publisher.

*Copyright © 2021 Xue and Feng. This is an open-access article distributed under the terms of the Creative Commons Attribution License (CC BY). The use, distribution or reproduction in other forums is permitted, provided the original author(s) and the copyright owner(s) are credited and that the original publication in this journal is cited, in accordance with accepted academic practice. No use, distribution or reproduction is permitted which does not comply with these terms.*

frontiers in Microbiology

REVIEW
published: 05 January 2022
doi: 10.3389/fmicb.2021.794431

# RNA Granules in Antiviral Innate Immunity: A Kaposi's Sarcoma-Associated Herpesvirus Journey

*Nishi R. Sharma[1]* and Zhi-Ming Zheng[2]**

[1] Department of Molecular Medicine, School of Interdisciplinary Studies, Jamia Hamdard University, New Delhi, India,
[2] Tumor Virus RNA Biology Section, HIV Dynamics and Replication Program, Center for Cancer Research, National Cancer Institute, National Institutes of Health, Frederick, MD, United States

OPEN ACCESS

**Edited by:**
*Douglas Paul Gladue, Plum Island Animal Disease Center, Agricultural Research Service, United States Department of Agriculture (USDA), United States*

**Reviewed by:**
*Junjie Zhang, Wuhan University, China*
*Genhong Cheng, University of California, Los Angeles, United States*

***Correspondence:**
*Nishi R. Sharma*
*nrsharma@jamiahamdard.ac.in*
*Zhi-Ming Zheng*
*zhengt@exchange.nih.gov*

**Specialty section:**
*This article was submitted to Virology, a section of the journal Frontiers in Microbiology*

**Received:** *13 October 2021*
**Accepted:** *02 December 2021*
**Published:** *05 January 2022*

**Citation:**
*Sharma NR and Zheng ZM (2022) RNA Granules in Antiviral Innate Immunity: A Kaposi's Sarcoma-Associated Herpesvirus Journey. Front. Microbiol. 12:794431. doi: 10.3389/fmicb.2021.794431*

RNA granules are cytoplasmic, non-membranous ribonucleoprotein compartments that form ubiquitously and are often referred to as foci for post-transcriptional gene regulation. Recent research on RNA processing bodies (PB) and stress granules (SG) has shown wide implications of these cytoplasmic RNA granules and their components in suppression of RNA translation as host intracellular innate immunity against infecting viruses. Many RNA viruses either counteract or co-opt these RNA granules; however, many fundamental questions about DNA viruses with respect to their interaction with these two RNA granules remain elusive. Kaposi's sarcoma-associated herpesvirus (KSHV), a tumor-causing DNA virus, exhibits two distinct phases of infection and encodes ∼90 viral gene products during the lytic phase of infection compared to only a few (∼5) during the latent phase. Thus, productive KSHV infection relies heavily on the host cell translational machinery, which often links to the formation of PB and SG. One major question is how KSHV counteracts the hostile environment of RNA granules for its productive infection. Recent studies demonstrated that KSHV copes with the translational suppression by cellular RNA granules, PB and SG, by expressing ORF57, a viral RNA-binding protein, during KSHV lytic infection. ORF57 interacts with Ago2 and GW182, two major components of PB, and prevents the scaffolding activity of GW182 at the initial stage of PB formation in the infected cells. ORF57 also interacts with protein kinase R (PKR) and PKR-activating protein (PACT) to block PKR dimerization and kinase activation, and thus inhibits eIF2α phosphorylation and SG formation. The homologous immediate-early regulatory protein ICP27 of herpes simplex virus type 1 (HSV-1), but not the EB2 protein of Epstein-Barr virus (EBV), shares this conserved inhibitory function with KSHV ORF57 on PB and SG. Through KSHV ORF57 studies, we have learned much about how a DNA virus in the infected cells is equipped to evade host antiviral immunity for its replication and productive infection. KSHV ORF57 would be an excellent viral target for development of anti-KSHV-specific therapy.

**Keywords: virus infections, innate immunity, KSHV, ORF57, stress granule (SG), processing bodies (PB), PKR, ago**

## INTRODUCTION

Representing the first line of defense for host cells against invading viral pathogens, the cellular innate immune system is equipped with germline-encoded pattern recognition receptors (PRRs) to recognize pathogen-derived and conserved pathogen-associated molecular patterns (PAMPs (Brennan and Bowie, 2010; Brubaker et al., 2015). This intricate framework, in response to recognition of antigens and non-self RNA/DNA, also facilitates mammalian cells to produce several inflammatory cytokines (IL-1β and IL-18, etc.) and type I interferons (IFNs) as a strategy of intrinsic defense against invading viral pathogens. Until now, six types of PRRs resulting in the transcription of type I IFNs in responses to the infections of RNA and DNA viruses have been identified, including toll-like receptors (TLRs), retinoic acid-inducible gene-I (RIG-I)-like receptors (RLRs), C-type lectin receptors (CLRs), absent in melanoma 2 (AIM2)-like receptors (ALRs), nucleotide-binding oligomerization domain (NOD)-like receptors (NLRs), and cytosolic DNA-sensing receptors such as cyclic GMP-AMP synthase (cGAS)-stimulator of interferon genes (STING; Thompson et al., 2011; Lee et al., 2016; Zevini et al., 2017; Wei and Lan, 2018; Hopfner and Hornung, 2020). At least 10 human TLRs (TLR1–TLR10), which are believed to function as dimers, are type I transmembrane proteins that are composed of an N-terminal leucine-rich repeat-containing ectodomain responsible for PAMP recognition, a transmembrane domain, and a cytoplasmic C-terminal TIR (Toll-interleukin-1 receptor homology) domain that activates downstream signal transduction (Bowie and O'Neill, 2000; Akira and Takeda, 2004). While some of these receptors (TLR1, TLR2, TLR4, TLR5, TLR6, and TLR10) reside on plasma membranes and recognize components of microbial cell walls and membranes such as lipoproteins and peptidoglycans, members of the TLR3 and TLR7 families are intracellular TLRs expressed in endosomes and lysosomes. In the battle with viral infections, TLR3 and TLR10 recognize double-stranded RNA (dsRNA; Lee et al., 2018; Wei and Lan, 2018), whereas TLR7, TLR8, and TLR9 make up the TLR7 family, with TLR7 and TLR8 detecting single-stranded RNA (ssRNA) and TLR9 recognizing unmethylated CpG DNA (Kawai and Akira, 2011).

The intracellular innate immune system has another dimension of antiviral defense in the form of RNA granules. In mammalian cells, formation of RNA granules allows flexibility for survival during adverse biological conditions. Two distinct non-membranous RNA granules, RNA processing bodies (P-bodies, PB) and stress granules (SG), are found in mammalian somatic cells (**Figure 1**), which regulate RNA metabolism and cellular homeostasis (Anderson and Kedersha, 2006, 2009). PB appear physiologically and comprise RNA and a unique composition of RNA-binding protein (RBP) markers including glycine/tryptophan-rich GW182, DDX6, and decapping/deadenylating enzymes (Eystathioy et al., 2003; **Figure 1**). PB are the cytoplasmic ribonucleoprotein (RNP) foci where small interfering RNA (siRNA)- or microRNA (miRNA)-guided mRNAs were once proposed the site for RNA processing and degradation (Cougot et al., 2004; Liu et al., 2005). The current observations suggest that mRNAs in PB are not degraded but remain translational after release from PB (Brengues et al., 2005; Aizer et al., 2014; Hubstenberger et al., 2017; Wilbertz et al., 2019). SG, on the other hand, appear in the cells only during stress and comprise stalled mRNAs and a unique composition of RBP markers TIA-1, G3BP1, and PABPC1 (**Figure 1**). SG initiate global translational arrest by storing mRNAs (Anderson and Kedersha, 2009) or exchange with either polysomes for translation or PB for RNA degradation (Anderson and Kedersha, 2009).

The formation of RNA granules is attributed to protein/RNA biomolecular condensates proposed to dynamically form by liquid-liquid phase separation, which reportedly depends on three factors: a dense network of redundant RNA-protein interactions; low-complexity sequences in proteins; and weak to intermediate interactions, including polyelectrolyte-polyelectrolyte interactions and between proteins-RNA interactions (Luo et al., 2018; Youn et al., 2019; Riggs et al., 2020). Recent reports suggest that SG and PB proteomes, in general, are biased toward the proteins with intrinsically disordered regions and have a high propensity to contain primary sequence features favoring phase separation (Protter and Parker, 2016; Protter et al., 2018). The latest success in the purification of PB using a fluorescence-activated particle sorting (FAPS)-based method from human epithelial cells helped to identify hundreds of proteins and thousands of accumulated and repressed mRNAs encoding regulatory processes (Hubstenberger et al., 2017).

A new user-friendly database[1] collating genes or proteins associated with SG or PB has been generated (Youn et al., 2019). A similar effort to study SG (Jain et al., 2016) revealed stable substructures, referred to as cores, within SG from sodium arsenite (ARS)-stressed U2OS cells by super-resolution microscopy, which could be purified using a series of differential centrifugations and then affinity purification. Proteomic analysis of these cores revealed a dense network of protein-protein interactions linking SG with human diseases. This study proposed a model of SG assembly and dynamics requiring ATP-dependent helicases and protein-remodeling complexes as conserved SG components. The study further suggested that SG contain a stable core structure surrounded by a dynamic shell with assembly, disassembly, and transitions between the core and shell modulated by numerous protein- and RNA-remodeling complexes. Using the same SG purification protocol, this group also described the SG transcriptome of yeast and mammalian cells (Khong et al., 2017) through RNA-Seq analysis of purified SG cores and single-molecule fluorescence *in situ* hybridization (smFISH) validation. This study revealed that only ∼10% of bulk mRNA molecules are accumulated in mammalian SG and only 185 genes have more than 50% of their mRNA molecules in SG. In general, almost every mRNA, and some non-coding RNAs (ncRNAs), could be targeted to SG, although the targeting efficiency varies from <1 to >95%.

Besides its role in cellular homeostasis, formation of RNA granules also represents a new paradigm of virus-host interaction. Mammalian RNA granules can elicit an antiviral response independent of type I IFNs and both PB and SG are important

[1] http://rnagranuledb.lunenfeld.ca/

**Major components in PB and SG in mammalian cells**

| PB specific | Shared | SG specific |
|---|---|---|
| 4E-T | eIF4E | TIA-1 |
| DCP1a, DCP2 | YB-1 | eIF3 |
| Hedls/GE-1 | Ago 1, 2 | eIF4A/B |
| Nesprin | HuR | eIF4G |
| CAF | Rap55/Lsm14 | DDX3 |
| CCR4-Not1 | XRN1 | Ataxin2 |
| GW182 | PMR1 | PABP |
| DDX6 | YB1 | G3BP1/2 |
| | FASTK | Staufen |
| | Roquin | FMRP/FXR1 |

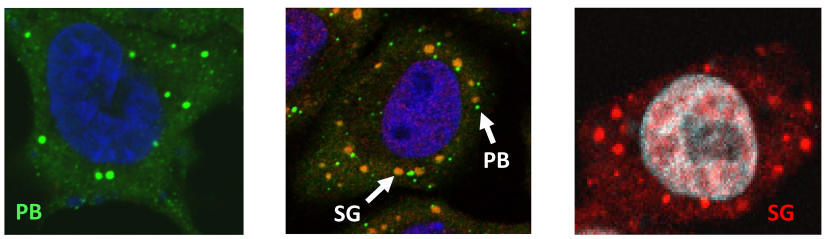


**FIGURE 1 |** Two major cellular RNA granules and their protein components. The table shows major specific or shared cellular protein components of PB and SG in mammalian cells. In the bottom panels, PB (green) and SG (red) are visible in HeLa cells after immunostaining with an anti-GW182 antibody under physiological conditions **(left)** or with an anti-TIA-1 antibody during stress induced by treatment with 0.5 mM $NaAS_2O_3$ (arsenite or ARS) for 30 min **(right)**. Middle panel showing the HeLa cells under ARS stress were double stained with an anti-GW182antibody for PB (green) and an anti-TIA-1 antibody for SG (yellow).

components of the host cell antiviral response (Zhang et al., 2019). For instance, suppression of PB and/or SG formation enhances human immunodeficiency virus type 1 (HIV-1) and Kaposi's sarcoma-associated herpesvirus (KSHV) production (Nathans et al., 2009; Sharma et al., 2019). A fascinating question remains, however, as to how viruses can inhibit PB and SG assembly. Moreover, virus infection imposes stress in host cells, causing a burden on the biosynthetic machineries of host cells including mRNA translation (McInerney et al., 2005) and thereby risking their own production by inducing SG. The overall understanding of whether SG are induced or suppressed by infected viruses continues to be an area of high interest. Notably, several RNA viruses show the ability to suppress the formation of SG by a viral factor (Emara and Brinton, 2007; White et al., 2007; Khaperskyy et al., 2012, 2014; Valiente-Echeverria et al., 2014). Recent reports provide profound evidence that DNA virus infections also regulate the formation of RNA granules in their host cells (Sharma et al., 2017, 2019; Zhang et al., 2019). In this brief review, we will use KSHV as an example to illustrate how a human DNA tumor virus regulates the formation of both PB and SG during KSHV lytic infection.

Kaposi's sarcoma-associated herpesvirus, or human herpesvirus 8 (HHV8), is a γ-2 herpesvirus (Chang et al., 1994). KSHV is the etiological agent of Kaposi's sarcoma, primary effusion lymphoma (PEL), and multicentric Castleman disease (MCD; Chang et al., 1994). Like other herpesviruses, KSHV has a large DNA genome of ∼165 kb that encodes nearly 90 open reading frames (ORFs) and several miRNAs and long non-coding RNAs (lncRNAs). Similar to other herpesviruses, KSHV, upon entering a susceptible host cell, causes lytic productive infection, but after lytic infection, establishes a latent infection within the host cell. While the latent infection features the highly restricted expression of only few viral genes (Zhong et al., 1996), the lytic program allows infectious virions to be shed and transmitted to new hosts. KSHV lytic expression commences the translation of all viral coding transcripts and thus imposes a stress on the host's translational machinery.

## KAPOSI'S SARCOMA-ASSOCIATED HERPESVIRUS REGULATION OF ANTIVIRAL PROCESSING BODIES FORMATION FOR LYTIC VIRUS INFECTION AND VIRION PRODUCTION

Kaposi's sarcoma-associated herpesvirus-infected B lymphocytes (BCBL-1, JSC-1, BC-3, and tonsil resting B cells) (Arvanitakis et al., 1996; Renne et al., 1996; Cannon et al., 2000; Hassman et al., 2011; Myoung and Ganem, 2011a) and epithelial cells (HEK293-derived Bac36 cells and the renal carcinoma cell line Caki-1-derived-iSLK.219, iSLK-Bac16 cells) (Majerciak et al., 2007; Myoung and Ganem, 2011b; Brulois et al., 2012; Sturzl et al., 2013) harbor an episomal KSHV genome at the latent stage but can be reactivated to lytic KSHV infection under hypoxia (Davis et al., 2001; Cai et al., 2006) or oxidative stress

conditions (Li et al., 2011; Ye et al., 2011) or in the presence of valproic acid (Shaw et al., 2000; Majerciak et al., 2007), butyrate (Renne et al., 1996; Miller et al., 1997), or 12-*O*-Tetradecanoyl-phorbol-13-acetate (TPA; Miller et al., 1997) by inducing the expression of two viral essential genes: a viral replication and transcription activator (RTA, or ORF50) and a viral mRNA regulator and stabilizer (MTA, mRNA transcript accumulation, or ORF57) (**Figure 2A**).

An early observation on PB suppression during KSHV lytic infection came from a study (Corcoran et al., 2012) showing that induction of KSHV lytic gene expression in iSLK cells led to elimination of cytoplasmic PB. This study demonstrated that ectopically expressed viral G-protein-coupled receptor (vGPCR) was capable of eliminating PB, but the role of vGPCR in preventing PB formation during KSHV lytic infection in the context of the KSHV genome was not defined. However, the study claimed that overexpressed ectopic vGPCR activates RhoA subfamily GTPases, the central regulator of actin reorganization, and activates the p38/MK2 pathway for the stabilization of ARE (AU-rich elements)-containing mRNAs and inhibits PB. In a separate study, PB dispersion in endothelial cells with latent KSHV infection was shown to be affected by ectopic expression of kaposin B protein *via* activation of a non-canonical Rho-GTPase signaling axis involving MK2, hsp27, p115RhoGEF, and RhoA, but in a ROCK1/2-independent manner (Corcoran et al., 2015). As the study was not conducted in the context of the KSHV genome with physiological expression of kaposin B, the role of kaposin B in regulating PB formation during KSHV latent infection was again inconclusive.

Using anti-GW182, anti-Dcp1A, and anti-DDX6 antibodies for immunofluorescence (IF) staining assays to investigate PB formation in KSHV-infected B lymphocytes or epithelial cells, we recently revealed that BCBL-1, HEK293-derived BAC36, and Caki-1-derived iSLK-BAC16 cells with KSHV latent infection are all capable of PB formation, but when reactivated with KSHV lytic infection, they displayed no PB or a dramatical reduction of PB formation (Sharma et al., 2019; Zhang et al., 2019; **Figure 2B**). Suppression of PB formation during KSHV lytic infection was found to be related to viral ORF57 expression, because the BAC36 cells containing an ORF57-null KSHV genome (BAC36-Δ57) lost

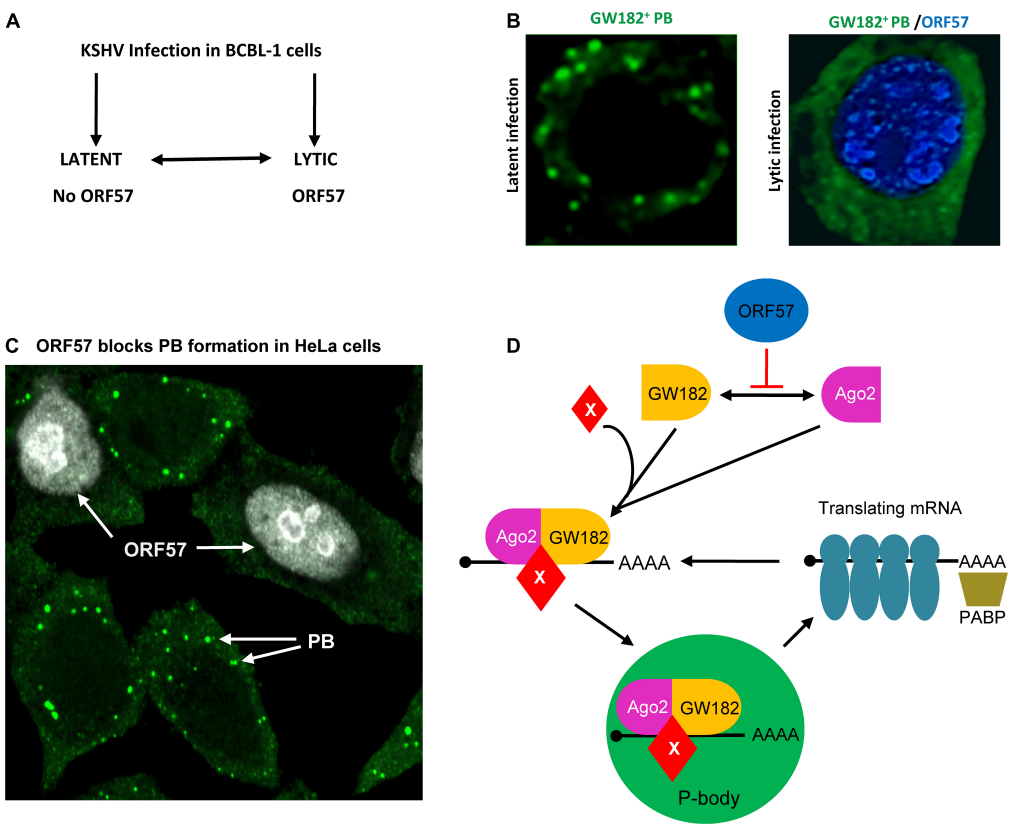


**FIGURE 2 |** Inhibition of PB assembly during Kaposi's sarcoma-associated herpesvirus (KSHV) lytic infection. **(A)** Flow diagram showing the exchangeable progression of lytic and latent phases of KSHV infection in BCBL-1 (B lymphocytes) cells. KSHV ORF57 is expressed only in viral lytic infection. **(B)** Left panel, a BCBL-1 cell carrying latent KSHV infection showing PB (green), after immunostaining with an anti-GW182antibody. Right panel, inhibition of PB assembly during KSHV lytic infection by expression of viral ORF57 (blue). **(C)** Inhibition of PB formation by ectopic ORF57 in HeLa cells. **(D)** Schematic model depicting the steps of KSHV ORF57 inhibition of PB formation during KSHV lytic infection by direct interaction with Ago2 and GW182. The mRNA translation can be stopped by RNA-induced silencing complex (RISC) including Ago2-GW182 complex with other factors shown as X. As a result, the translating mRNA can be stripped of ribosomes and the translational complex can be collapsed when binding to the Ago2-GW182-X complex. Panel **(D)** is modified from our previously published figure (Sharma et al., 2019).

this inhibition on PB formation (Sharma et al., 2019; Zhang et al., 2019). Further investigation by expression of ORF57 in HeLa cells in the absence of other KSHV proteins revealed that ORF57 expression is necessary to inhibit PB formation (**Figure 2C**), but its N-terminal ORF57 mutant lacking the protein-protein and protein-RNA interaction activities was not (Sharma et al., 2019; Zhang et al., 2019). Interestingly, HSV-1 ICP27 but not EBV EB2, two homologs of KSHV ORF57, also showed a strong inhibitory effect on PB formation in HeLa cells (Sharma et al., 2019; Zhang et al., 2019). The reason why EBV EB2 lacks such function in suppressing PB formation remains to be understood. Surprisingly, in this study (Sharma et al., 2019; Zhang et al., 2019), we found that miRNAs and the miRNA pathway do not contribute to PB formation as previously reported (Liu et al., 2005; Eulalio et al., 2007). PB formation is independent of mature miRNAs in Dicer-knockout cells or cells with efficient knockdown expression of Dicer or Ago2, a major component of RNA-induced silencing complex (RISC). We also found that knockdown of DCP1a expression had no effect on PB formation (Sharma et al., 2019; Zhang et al., 2019).

Mechanistically, KSHV ORF57 does not affect host cells expressing Ago2 and GW182, but suppresses PB formation by direct interaction with Ago2 and GW182 and affects the scaffolding activity of GW182 at the initial stage of PB formation (Sharma et al., 2019). By co-immunoprecipitation, we found that ORF57, but not its dysfunctional mutant, interacts with the N-terminal domain of Ago2 and separately with the motif 1 of the N-terminal GW-rich, Ago2-interacting domain of GW182 (**Figure 3**) in an RNA-independent manner (Sharma et al., 2019) and these interactions block the Ago2-GW182 interaction (Sharma et al., 2019) required for PB formation (Yao et al., 2011; **Figure 2D**). Importantly, knockdown of GW182 expression in KSHV-infected iSLK-Bac16 cells was found to block PB formation, subsequently promoting production of infectious KSHV virions by ∼100-fold in the cells with reactivated lytic infection (Sharma et al., 2019). Given that PB function is an important component of host innate immunity to prevent virus infection and replication and that viral ORF57 is essential for KSHV replication and virus production (Majerciak et al., 2007; BeltCappellino et al., 2019), the identified novel function of ORF57 in blocking PB formation in the KSHV-infected host cells has greatly advanced our understanding of how a DNA tumor virus could escape the hostile surveillance of host innate immunity to benefit its infection and replication.

## KAPOSI'S SARCOMA-ASSOCIATED HERPESVIRUS REGULATION OF MAMMALIAN ANTIVIRAL STRESS GRANULES

Mammalian cells undergo a distinct stage of "translational dormancy" during stress. Here, the translating pool of mRNAs forming polysomes dissembles and the resulting mRNA-translation initiation complexes along with many RBPs, including TIA-1, G3BP1, and PABP, aggregate to form SG (Kedersha et al., 2000; Kimball et al., 2003). During cellular stress, four different kinases (general control non-derepressible 2, GCN2; protein kinase R, PKR; PKR-like endoplasmic reticulum kinase, PERK; and heme regulated inhibitory, HRI) induce phosphorylation of eIF2α, a major trigger of cascaded reactions in SG formation, depending on the cause of stress (Donnelly et al., 2013; Panas et al., 2016). Both viral infection (Lloyd, 2013; Reineke and Lloyd, 2013) and ARS (Patel and Sen, 1998) activate

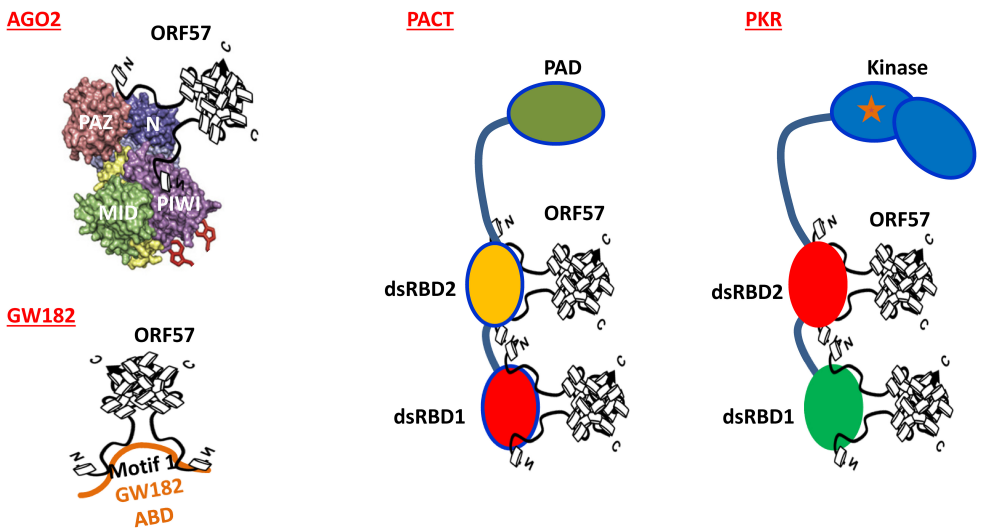


**FIGURE 3 |** Mechanisms of how KSHV ORF57 blocks the formation of both PB and SG in mammalian cell. Dimeric ORF57 interacts with the N domain of Ago2 and the motif 1 of GW182 Ago2-binding domain (ABD) to prevent Ago2-GW182 interaction, subsequently blocking PB formation in mammalian cells. Dimeric ORF57 also directly interacts with two dsRNA-binding domains (dsRBDs) of both PACT and PKR to block PKR dimerization and PKR kinase activation, thus preventing SG formation in the cells subjected to stress.

PKR phosphorylation, dimerization, and PKR kinase activity. ARS activates PKR kinase activity through binding with PKR-activating protein (PACT; Patel et al., 2000; Li et al., 2006). The typical SG assembly is mostly mediated by phosphorylated eIF2 (Kedersha et al., 1999), the alpha subunit of which, eIF2α, is phosphorylated by any of the four described kinases above. Thus, the formation of SG is initiated as a downstream event of elF2α phosphorylation. Normally, eIF2α is required to initiate mRNA translation by promoting the binding of $tRNA^{met}$ to the 40S ribosome in a GTP-dependent manner. Stress induces phosphorylation of eIF2α to attenuate eIF2α activity and thereby promotes prion-like TIA-1 aggregation/nucleation to form SG where mRNA translation is stalled (Donnelly et al., 2013). Among the four well-known eIF2α kinases, PKR (the key cellular sensor of dsRNAs) also serves to induce the innate immune response through virus infection-induced production of type I IFNs which bind to an IFN-stimulated response element (ISRE) in the PKR promoter and activate PKR transcription (Kuhen and Samuel, 1997). An early report claimed that KSHV blocks PKR phosphorylation by a short, artificial form (163 aa residues) of viral IFN regulatory factor 2 (vIRF-2) (36). Unfortunately, this report was misleading, because the actual vIRF-2 ORF splits into two separate exons, with exon 1 in K11.1 and exon 2 in K11 (Jenner et al., 2001; Cunningham et al., 2003), and encodes an authentic vIRF-2 bearing 680 aa residues. In other words, the annotated vIRF-2 ORF encoding 163 aa residues in an early report (36) was wrongly predicted from the KSHV genome (Russo et al., 1996; Neipel et al., 1997). We subsequently examined the functionality of the full-length authentic vIRF-2 bearing 680 aa residues in HeLa cells with or without ARS treatment and did not find its inhibitory effect on ARS-induced SG formation (Sharma et al., 2017).

Kaposi's sarcoma-associated herpesvirus regulation of SG formation was initially observed in our recent study (Sharma et al., 2017). By using SG-specific TIA-1 antibody staining (Gilks et al., 2004), we initially did not find any TIA-$1^+$ SG formation in BCBL-1 cells with latent or with lytic KSHV infection reactivated by butyrate (**Figure 4A**). However, after a 30-min treatment with 0.5 mM ARS, a common chemical inducer that causes oxidative stress (Kedersha et al., 1999), the BCBL-1 cells with KSHV latent infection appeared in many cytoplasmic TIA-$1^+$ SG, but did not do so when the cells were reactivated with virus lytic infection (**Figure 4B**). Data indicate that some KSHV lytic proteins may inhibit SG formation. To explore which viral lytic proteins might contribute to this negative regulation on SG formation, we compared HEK293-derived Bac36 cells containing a wild-type (wt) KSHV genome or an ORF57-null (Δ57) KSHV genome with latent or lytic KSHV infection for SG formation under ARS treatment. We found that both cells with a wt KSHV genome or Δ57 KSHV genome in latent infection were capable of forming SG under ARS treatment, but only the cells with a Δ57 genome in viral lytic infection did so, while the cells with a wt KSHV genome did not (Sharma et al., 2017). These data suggested that KSHV lytic protein ORF57 was most likely required for the observed suppression of SG formation.

Kaposi's sarcoma-associated herpesvirus ORF57 is an RBP with an intrinsically disordered, non-structural N-terminal domain and a structured α-helix-rich C-terminal domain (Majerciak et al., 2015; Majerciak and Zheng, 2015; Yuan et al., 2018). Early studies from our group and others demonstrated that ORF57 functions at the post-transcriptional level for viral gene expression by enhancement of RNA stability, splicing, and translation mostly through its N-terminal domain interaction with RNAs and various RBPs (Majerciak and Zheng, 2015; Vogt and Bohne, 2016). As described above, ORF57 also inhibits PB formation during KSHV lytic infection (Sharma et al., 2019). The independent ability of ORF57 to inhibit SG formation under ARS or poly I:C treatment was confirmed in HeLa and HEK293T cells with ectopic ORF57 in the absence of other KSHV lytic proteins (**Figure 4C**), but not an N-terminal dysfunctional ORF57 mutant (Sharma et al., 2017). Interestingly, by using HeLa cells with ectopic expression of other individual viral proteins, we discovered that KSHV ORF37 (vSOX) bearing intrinsic endoribonuclease activity also showed the activity to inhibit ARS-induced SG formation, but KSHV RTA, ORF45, ORF59, and LANA did not display such function (Sharma et al., 2017). Homologous protein HSV-1 ICP27, but surprisingly not EBV EB2, resembles KSHV ORF57 in the ability to block the PKR/eIF2α/SG pathway (Sharma et al., 2017).

Mechanistically, ORF57 functioning as a dimer (Majerciak et al., 2015; Yuan et al., 2018) was found to directly interact with PACT, PKR, PABPC1, and eIF4E independent of RNA (Massimelli et al., 2011, 2013; Sharma et al., 2017) but has no interaction with TIA-1, G3BP1, eIF4G, or eIF2α (Sharma et al., 2017). ORF57 interacts with PACT and PKR *via* its N-terminal domain interacting with the dsRNA-binding domain of PACT or PKR (**Figure 3**) and blocks PACT interaction with PKR, PKR activation, and kinase activity to phosphorylate eIF2α (Sharma et al., 2017; **Figure 4D**). This mechanistic function of ORF57 resembles the TAR RNA-binding protein (TRBP), which inhibits PKR activity *via* the interaction with PKR (Daher et al., 2009; Daniels and Gatignol, 2012), but differs from poliovirus 3C protease, which cleaves Ras-GAP SH3 domain–binding proteins (G3BP) (White et al., 2007), and Semliki Forest virus (SFV) nsP3 and HSV type 2 (HSV-2) ICP8, which suppress SG formation by their FGDF motifs interacting with G3BP (Panas et al., 2015). KSHV ORF57 does not have such an FGDF motif and does not interact with G3BP1. Moreover, ORF57 does not inhibit heat-induced phosphorylation of elF2α and SG formation, as it is independent of the PKR pathway (Sharma et al., 2017).

Most importantly, we demonstrated that KSHV ORF57 blocking PKR activation and SG formation is one of the ORF57 functions that promote KSHV gene expression and virus production, as seen in many other virus infections. The outcome of SG formation is to trigger the host cell antiviral response and inhibit virus production (Onomoto et al., 2014). By examining KSHV virion production in iSLK-BAC16 cells bearing a KSHV genome (Brulois et al., 2012) after treatment with a PKR-specific siRNA, we found that efficient knockdown of PKR expression from iSLK-BAC16 cells led to ∼78-fold increase of KSHV virion production over the cells with the normal level of PKR expression (Sharma et al., 2017). Consistently, a recent report also revealed that KSHV infection could result in downregulation of PKR (Gabaev et al., 2020).

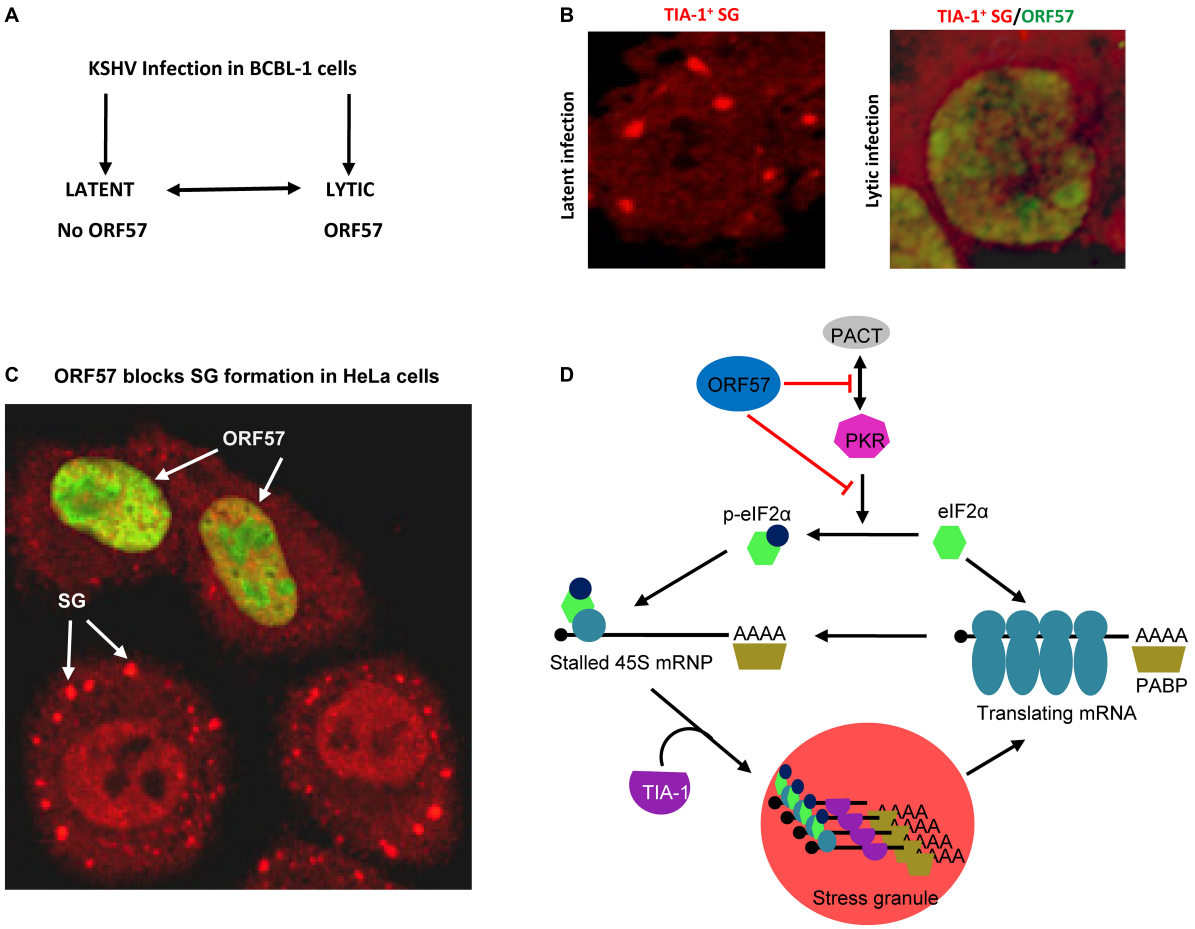


**FIGURE 4 |** Disruption of SG assembly during KSHV lytic infection. **(A)** Flow diagram showing the exchangeable progression of lytic and latent phases of KSHV infection in BCBL-1 (B lymphocytes) cells. **(B)** Left panel, a BCBL-1 cell carrying latent KSHV infection showing SG (red) by immunostaining with an anti-TIA-1 antibody after treatment with 0.5 mM arsenite for 30 mins. Right panel, inhibition of SG assembly during KSHV lytic infection by expression of viral ORF57 (green). **(C)** Ectopic ORF57 inhibiting SG formation in HeLa cells under ARS stress. **(D)** Schematic model depicting the ORF57 interactions with PACT and PKR to block PKR dimerization and activation and thus inhibit SG formation during KSHV lytic infection. Panel **(D)** is modified from our previously published figure (Sharma et al., 2019).

## FUTURE PERSPECTIVES

Finding that KSHV lytic infection prevents the formation of RNA granules by expressing viral ORF57 represents a new dimension in understanding how KSHV evades host innate immunity for efficient viral gene expression and eventually virus production. We have learned over the years that host humoral immunity and cell-mediated immunity are two types of specific immune responses to various infections by pathogens. To date, the host innate immune system has been recognized as an equally important mechanism of intrinsic defense against invading viruses in the infected cells. This innate immune system *via* pattern-recognition receptors, including TLRs, RLRs, ALRs, NLRs, CLRs, and intracellular DNA sensors such as cGAS and IFI16 (Kawasaki and Kawai, 2014; Lester and Li, 2014; Chan and Gack, 2016; Bermejo-Jambrina et al., 2018), detects viral components such as viral genomic DNA, ssRNA, dsRNA, RNA with 5′ triphosphate ends, and viral proteins and initiates intracellular antiviral responses. KSHV evades the host immune system in multiple ways by encoding various viral proteins (Lee et al., 2015, 2016). Some of them are homologous to cellular proteins and interfere with both innate and adaptive immune responses. Immune evasion of the IFN pathway and the TLR pathway by KSHV vIRFs and other host mimics is one of the important strategies for KSHV to escape from the host innate immune response (Lee et al., 2015). KSHV vIRF-1, -2, or -3 blocks TLR3-mediated activation of IFN-responsive promoter activity, and vIRF-1 decreases phosphorylation and nuclear translocation of IRF-3 in response to TLR3 activation (Jacobs et al., 2013). We found that ORF57 also blocks poly I:C-induced phosphorylation of TLR3 (Sharma et al., 2017).

Currently, host cell RNA granules have been recognized as functional components of intrinsic defense against invading viruses in the infected cells. However, almost all viruses have evolutionarily developed mechanisms to inhibit the formation of RNA granules for their replication and multiplication in the infected cells (Zhang et al., 2019). In this regard, KSHV ORF57 functioning as a dimer (Majerciak et al., 2015; Yuan et al., 2018)

has been demonstrated to interact with two major components, Ago2 and GW182 of PB and PACT and PKR of SG (**Figure 3**), to suppress the formation of PB and SG (Sharma et al., 2017, 2019; Zhang et al., 2019), respectively, leading to enhanced KSHV lytic infection and virus production by maintaining cellular translational machineries to function. Considering these unexpected findings, it would be important for us to address the following questions in future studies: (1) Can ORF57 function(s) that inhibit RNA granules be targeted for anti-KSHV therapeutics? (2) Can KSHV inhibition of PB through ORF57 be further explored to understand the mechanisms that regulate PB formation in mammalian cells? (3) Can identification of potential factors be associated with PKR activation during KSHV infection? (4) Can KSHV viral RNA species be determined to preferentially travel through these RNA granules? (5) Because the N-terminal half of KSHV ORF57 is intrinsically disordered like many other viral proteins (Majerciak and Zheng, 2015; Majerciak et al., 2015; Sharma et al., 2021), can the role of the intrinsic disordered region of KSHV ORF57 be ascertained in its inhibitory function toward RNA granules? (6) LSm14 (RAP55), a DDX6 interactor (Brandmann et al., 2018), is a common protein factor for assembly of both PB and SG and has the binding activity to viral RNA and DNA to mediate IRF3 activation and IFN-β induction in the early phase of virus infection (Li et al., 2012). Whether lytic KSHV infection affects LSm14 expression or its interaction with DDX6 remains to be investigated. (7) Since EBV EB2 is incapable of blocking assembly of both PB and SG, what is the distinct feature of EBV EB2 from its homologous proteins KSHV ORF57 and HSV-1 ICP27 in inhibition of PB and SG assembly? Taken together, KSHV regulation of RNA granule assembly represents an exciting area for further investigation.

## AUTHOR CONTRIBUTIONS

NS and ZMZ drafted the review and approved the final manuscript. Both authors contributed to the article and approved the submitted version.

## FUNDING

NS received support from the Ramalingaswami Re-entry Fellowship from the Department of Biotechnology (DBT), Ministry of Science and Technology, Government of India (BT/RLF/Re-entry/40/2018). ZMZ was supported by the Intramural Research Program of the National Institutes of Health, National Cancer Institute, Center for Cancer Research (ZIASC010357).

## ACKNOWLEDGMENTS

We thank Anne Arthur for proofreading of this manuscript.

## REFERENCES

Aizer, A., Kalo, A., Kafri, P., Shraga, A., Ben-Yishay, R., Jacob, A., et al. (2014). Quantifying mRNA targeting to P-bodies in living human cells reveals their dual role in mRNA decay and storage. *J. Cell Sci.* 127, 4443–4456. doi: 10.1242/jcs.152975

Akira, S., and Takeda, K. (2004). Toll-like receptor signaling. *Nat. Rev. Immunol.* 4, 499–511.

Anderson, P., and Kedersha, N. (2006). RNA granules. *J. Cell Biol.* 172, 803–808.

Anderson, P., and Kedersha, N. (2009). RNA granules: post-transcriptional and epigenetic modulators of gene expression. *Nat. Rev. Mol. Cell. Biol.* 10, 430–436. doi: 10.1038/nrm2694

Arvanitakis, L., Mesri, E. A., Nador, R. G., Said, J. W., Asch, A. S., Knowles, D. M., et al. (1996). Establishment and characterization of a primary effusion (body cavity-based) lymphoma cell line (BC-3) harboring Kaposi's sarcoma-associated herpesvirus (KSHV/HHV-8) in the absence of Epstein-Barr virus. *Blood* 88, 2648–2654.

BeltCappellino, A., Majerciak, V., Lobanov, A., Lack, J., Cam, M., and Zheng, Z. M. (2019). CRISPR/Cas9-mediated knockout and *in situ* inversion of the ORF57 gene from all copies of the kaposi's sarcoma-associated herpesvirus genome in BCBL-1 Cells. *J. Virol.* 93:e00628-19. doi: 10.1128/JVI.00628-19

Bermejo-Jambrina, M., Eder, J., Helgers, L. C., Hertoghs, N., Nijmeijer, B. M., Stunnenberg, M., et al. (2018). C-type lectin receptors in antiviral immunity and viral escape. *Front. Immunol.* 9:590. doi: 10.3389/fimmu.2018.00590

Bowie, A., and O'Neill, L. A. (2000). The interleukin-1 receptor/Toll-like receptor superfamily: signal generators for pro-inflammatory interleukins and microbial products. *J. Leukoc. Biol.* 67, 508–514. doi: 10.1002/jlb.67.4.508

Brandmann, T., Fakim, H., Padamsi, Z., Youn, J. Y., Gingras, A. C., Fabian, M. R., et al. (2018). Molecular architecture of LSM14 interactions involved in the assembly of mRNA silencing complexes. *EMBO. J.* 37:e97869. doi: 10.15252/embj.201797869

Brengues, M., Teixeira, D., and Parker, R. (2005). Movement of eukaryotic mRNAs between polysomes and cytoplasmic processing bodies. *Science* 310, 486–489. doi: 10.1126/science.1115791

Brennan, K., and Bowie, A. G. (2010). Activation of host pattern recognition receptors by viruses. *Curr. Opin. Microbiol.* 13, 503–507. doi: 10.1016/j.mib.2010.05.007

Brubaker, S. W., Bonham, K. S., Zanoni, I., and Kagan, J. C. (2015). Innate immune pattern recognition: a cell biological perspective. *Annu. Rev. Immunol.* 33, 257–290. doi: 10.1146/annurev-immunol-032414-112240

Brulois, K. F., Chang, H., Lee, A. S., Ensser, A., Wong, L. Y., Toth, Z., et al. (2012). Construction and manipulation of a new Kaposi's sarcoma-associated herpesvirus bacterial artificial chromosome clone. *J. Virol.* 86, 9708–9720. doi: 10.1128/JVI.01019-12

Cai, Q., Lan, K., Verma, S. C., Si, H., Lin, D., and Robertson, E. S. (2006). Kaposi's sarcoma-associated herpesvirus latent protein LANA interacts with HIF-1 alpha to upregulate RTA expression during hypoxia: latency control under low oxygen conditions. *J. Virol.* 80, 7965–7975. doi: 10.1128/JVI.00689-06

Cannon, J. S., Ciufo, D., Hawkins, A. L., Griffin, C. A., Borowitz, M. J., Hayward, G. S., et al. (2000). A new primary effusion lymphoma-derived cell line yields a highly infectious Kaposi's sarcoma herpesvirus-containing supernatant. *J. Virol.* 74, 10187–10193. doi: 10.1128/jvi.74.21.10187-10193.2000

Chan, Y. K., and Gack, M. U. (2016). Viral evasion of intracellular DNA and RNA sensing. *Nat. Rev. Microbiol.* 14, 360–373. doi: 10.1038/nrmicro.2016.45

Chang, Y., Cesarman, E., Pessin, M. S., Lee, F., Culpepper, J., Knowles, D. M., et al. (1994). Identification of herpesvirus-like DNA sequences in AIDS-associated Kaposi's sarcoma. *Science* 266, 1865–1869. doi: 10.1126/science.7997879

Corcoran, J. A., Johnston, B. P., and McCormick, C. (2015). Viral activation of MK2-hsp27-p115RhoGEF-RhoA signaling axis causes cytoskeletal rearrangements, p-body disruption and ARE-mRNA stabilization. *PLoS Pathog.* 11:e1004597. doi: 10.1371/journal.ppat.1004597

Corcoran, J. A., Khaperskyy, D. A., Johnston, B. P., King, C. A., Cyr, D. P., Olsthoorn, A. V., et al. (2012). Kaposi's sarcoma-associated herpesvirus

G-protein-coupled receptor prevents AU-rich-element-mediated mRNA decay. *J. Virol.* 86, 8859–8871. doi: 10.1128/JVI.00597-12

Cougot, N., Babajko, S., and Seraphin, B. (2004). Cytoplasmic foci are sites of mRNA decay in human cells. *J. Cell Biol.* 165, 31–40. doi: 10.1083/jcb.200309008

Cunningham, C., Barnard, S., Blackbourn, D. J., and Davison, A. J. (2003). Transcription mapping of human herpesvirus 8 genes encoding viral interferon regulatory factors. *J. Gen. Virol.* 84, 1471–1483. doi: 10.1099/vir.0.19015-0

Daher, A., Laraki, G., Singh, M., Melendez-Pena, C. E., Bannwarth, S., Peters, A. H., et al. (2009). TRBP control of PACT-induced phosphorylation of protein kinase R is reversed by stress. *Mol. Cell Biol.* 29, 254–265. doi: 10.1128/MCB.01030-08

Daniels, S. M., and Gatignol, A. (2012). The multiple functions of TRBP, at the hub of cell responses to viruses, stress, and cancer. *Microbiol. Mol. Biol. Rev.* 76, 652–666. doi: 10.1128/MMBR.00012-12

Davis, D. A., Rinderknecht, A. S., Zoeteweij, J. P., Aoki, Y., Read-Connole, E. L., Tosato, G., et al. (2001). Hypoxia induces lytic replication of Kaposi sarcoma-associated herpesvirus. *Blood* 97, 3244–3250. doi: 10.1182/blood.v97.10.3244

Donnelly, N., Gorman, A. M., Gupta, S., and Samali, A. (2013). The eIF2alpha kinases: their structures and functions. *Cell. Mol. Life. Sci.* 70, 3493–3511. doi: 10.1007/s00018-012-1252-6

Emara, M. M., and Brinton, M. A. (2007). Interaction of TIA-1/TIAR with West Nile and dengue virus products in infected cells interferes with stress granule formation and processing body assembly. *Proc. Natl. Acad. Sci. U.S.A.* 104, 9041–9046. doi: 10.1073/pnas.0703348104

Eulalio, A., Behm-Ansmant, I., Schweizer, D., and Izaurralde, E. (2007). P-body formation is a consequence, not the cause, of RNA-mediated gene silencing. *Mol. Cell. Biol.* 27, 3970–3981. doi: 10.1128/MCB.00128-07

Eystathioy, T., Jakymiw, A., Chan, E. K., Seraphin, B., Cougot, N., and Fritzler, M. J. (2003). The GW182protein colocalizes with mRNA degradation associated proteins hDcp1 and hLSm4 in cytoplasmic GW bodies. *RNA* 9, 1171–1173. doi: 10.1261/rna.5810203

Gabaev, I., Williamson, J. C., Crozier, T. W. M., Schulz, T. F., and Lehner, P. J. (2020). Quantitative Proteomics analysis of lytic KSHV infection in human endothelial cells reveals targets of viral immune modulation. *Cell Rep.* 33:108249. doi: 10.1016/j.celrep.2020.108249

Gilks, N., Kedersha, N., Ayodele, M., Shen, L., Stoecklin, G., Dember, L. M., et al. (2004). Stress granule assembly is mediated by prion-like aggregation of TIA-1. *Mol. Biol. Cell* 15, 5383–5398. doi: 10.1091/mbc.e04-08-0715

Hassman, L. M., Ellison, T. J., and Kedes, D. H. (2011). KSHV infects a subset of human tonsillar B cells, driving proliferation and plasmablast differentiation. *J. Clin. Invest.* 121, 752–768. doi: 10.1172/JCI44185

Hopfner, K. P., and Hornung, V. (2020). Molecular mechanisms and cellular functions of cGAS-STING signalling. *Nat. Rev. Mol. Cell. Biol.* 21, 501–521. doi: 10.1038/s41580-020-0244-x

Hubstenberger, A., Courel, M., Benard, M., Souquere, S., Ernoult-Lange, M., Chouaib, R., et al. (2017). P-body purification reveals the condensation of repressed mRNA regulons. *Mol. Cell* 68, 144–157.e5. doi: 10.1016/j.molcel.2017.09.003

Jacobs, S. R., Gregory, S. M., West, J. A., Wollish, A. C., Bennett, C. L., Blackbourn, D. J., et al. (2013). The viral interferon regulatory factors of Kaposi's sarcoma-associated herpesvirus differ in their inhibition of interferon activation mediated by toll-like receptor 3. *J. Virol.* 87, 798–806. doi: 10.1128/JVI.01851-12

Jain, S., Wheeler, J. R., Walters, R. W., Agrawal, A., Barsic, A., and Parker, R. (2016). ATPase-modulated stress granules contain a diverse proteome and substructure. *Cell* 164, 487–498. doi: 10.1016/j.cell.2015.12.038

Jenner, R. G., Alba, M. M., Boshoff, C., and Kellam, P. (2001). Kaposi's sarcoma-associated herpesvirus latent and lytic gene expression as revealed by DNA arrays. *J. Virol.* 75, 891–902. doi: 10.1128/JVI.75.2.891-902.2001

Kawai, T., and Akira, S. (2011). Toll-like receptors and their crosstalk with other innate receptors in infection and immunity. *Immunity* 34, 637–650. doi: 10.1016/j.immuni.2011.05.006

Kawasaki, T., and Kawai, T. (2014). Toll-like receptor signaling pathways. *Front. Immunol.* 5:461.

Kedersha, N. L., Gupta, M., Li, W., Miller, I., and Anderson, P. (1999). RNA-binding proteins TIA-1 and TIAR link the phosphorylation of eIF-2 alpha to the assembly of mammalian stress granules. *J.Cell Biol.* 147, 1431–1442. doi: 10.1083/jcb.147.7.1431

Kedersha, N., Cho, M. R., Li, W., Yacono, P. W., Chen, S., Gilks, N., et al. (2000). Dynamic shuttling of TIA-1 accompanies the recruitment of mRNA to mammalian stress granules. *J. Cell. Biol.* 151, 1257–1268. doi: 10.1083/jcb.151.6.1257

Khaperskyy, D. A., Emara, M. M., Johnston, B. P., Anderson, P., Hatchette, T. F., and McCormick, C. (2014). Influenza a virus host shutoff disables antiviral stress-induced translation arrest. *PLoS Pathog.* 10:e1004217. doi: 10.1371/journal.ppat.1004217

Khaperskyy, D. A., Hatchette, T. F., and McCormick, C. (2012). Influenza A virus inhibits cytoplasmic stress granule formation. *FASEB. J.* 26, 1629–1639. doi: 10.1096/fj.11-196915

Khong, A., Matheny, T., Jain, S., Mitchell, S. F., Wheeler, J. R., and Parker, R. (2017). The stress granule transcriptome reveals principles of mRNA accumulation in stress granules. *Mol. Cell* 68, 808–820e5. doi: 10.1016/j.molcel.2017.10.015

Kimball, S. R., Horetsky, R. L., Ron, D., Jefferson, L. S., and Harding, H. P. (2003). Mammalian stress granules represent sites of accumulation of stalled translation initiation complexes. *Am. J. Physiol. Cell. Physiol.* 284, C273–C284. doi: 10.1152/ajpcell.00314.2002

Kuhen, K. L., and Samuel, C. E. (1997). Isolation of the interferon-inducible RNA-dependent protein kinase Pkr promoter and identification of a novel DNA element within the 5′-flanking region of human and mouse Pkr genes. *Virology* 227, 119–130. doi: 10.1006/viro.1996.8306

Lee, H. R., Amatya, R., and Jung, J. U. (2015). Multi-step regulation of innate immune signaling by Kaposi's sarcoma-associated herpesvirus. *Virus Res.* 209, 39–44. doi: 10.1016/j.virusres.2015.03.004

Lee, H. R., Choi, U. Y., Hwang, S. W., Kim, S., and Jung, J. U. (2016). Viral inhibition of PRR-mediated innate immune response: learning from KSHV evasion strategies. *Mol. Cells* 39, 777–782. doi: 10.14348/molcells.2016.0232

Lee, S. M., Yip, T. F., Yan, S., Jin, D. Y., Wei, H. L., Guo, R. T., et al. (2018). Recognition of double-stranded RNA and regulation of interferon pathway by toll-like receptor 10. *Front. Immunol.* 9:516. doi: 10.3389/fimmu.2018.00516

Lester, S. N., and Li, K. (2014). Toll-like receptors in antiviral innate immunity. *J. Mol. Biol.* 426, 1246–1264.

Li, S., Peters, G. A., Ding, K., Zhang, X., Qin, J., and Sen, G. C. (2006). Molecular basis for PKR activation by PACT or dsRNA. *Proc. Natl. Acad. Sci. U.S.A.* 103, 10005–10010. doi: 10.1073/pnas.0602317103

Li, X., Feng, J., and Sun, R. (2011). Oxidative stress induces reactivation of Kaposi's sarcoma-associated herpesvirus and death of primary effusion lymphoma cells. *J. Virol.* 85, 715–724. doi: 10.1128/JVI.01742-10

Li, Y., Chen, R., Zhou, Q., Xu, Z., Li, C., Wang, S., et al. (2012). LSm14A is a processing body-associated sensor of viral nucleic acids that initiates cellular antiviral response in the early phase of viral infection. *Proc. Natl. Acad. Sci . U.S.A.* 109, 11770–11775. doi: 10.1073/pnas.1203405109

Liu, J., Valencia-Sanchez, M. A., Hannon, G. J., and Parker, R. (2005). MicroRNA-dependent localization of targeted mRNAs to mammalian P-bodies. *Nat. Cell. Biol.* 7, 719–723. doi: 10.1038/ncb1274

Lloyd, R. E. (2013). Regulation of stress granules and P-bodies during RNA virus infection. *Wiley Interdiscip. Rev. RNA* 4, 317–331. doi: 10.1002/wrna.1162

Luo, Y., Na, Z., and Slavoff, S. A. (2018). P-bodies: composition, properties, and functions. *Biochemistry* 57, 2424–2431. doi: 10.1021/acs.biochem.7b01162

Majerciak, V., and Zheng, Z. M. (2015). KSHV ORF57, a protein of many faces. *Viruses* 7, 604–633. doi: 10.3390/v7020604

Majerciak, V., Pripuzova, N., Chan, C., Temkin, N., Specht, S. I., and Zheng, Z. M. (2015). Stability of structured Kaposi's sarcoma-associated herpesvirus ORF57 protein is regulated by protein phosphorylation and homodimerization. *J. Virol.* 89, 3256–3274. doi: 10.1128/JVI.03721-14

Majerciak, V., Pripuzova, N., McCoy, J. P., Gao, S. J., and Zheng, Z. M. (2007). Targeted disruption of Kaposi's sarcoma-associated herpesvirus ORF57 in the viral genome is detrimental for the expression of ORF59, K8alpha, and K8.1 and the production of infectious virus. *J. Virol.* 81, 1062–1071. doi: 10.1128/JVI.01558-06

Massimelli, M. J., Kang, J. G., Majerciak, V., Le, S. Y., Liewehr, D. J., Steinberg, S. M., et al. (2011). Stability of a long noncoding viral RNA depends on a 9-nt core element at the RNA 5′ end to interact with viral ORF57 and cellular PABPC1. *Int. J. Biol. Sci.* 7, 1145–1160. doi: 10.7150/ijbs.7.1145

Massimelli, M. J., Majerciak, V., Kruhlak, M., and Zheng, Z. M. (2013). Interplay between polyadenylate-binding protein 1 and Kaposi's sarcoma-associated

herpesvirus ORF57 in accumulation of polyadenylated nuclear RNA, a viral long noncoding RNA. *J. Virol.* 87, 243–256. doi: 10.1128/JVI.01693-12

McInerney, G. M., Kedersha, N. L., Kaufman, R. J., Anderson, P., and Liljestrom, P. (2005). Importance of eIF2alpha phosphorylation and stress granule assembly in alphavirus translation regulation. *Mol. Biol. Cell* 16, 3753–3763. doi: 10.1091/mbc.e05-02-0124

Miller, G., Heston, L., Grogan, E., Gradoville, L., Rigsby, M., Sun, R., et al. (1997). Selective switch between latency and lytic replication of Kaposi's sarcoma herpesvirus and Epstein-Barr virus in dually infected body cavity lymphoma cells. *J. Virol.* 71, 314–324. doi: 10.1128/JVI.71.1.314-324.1997

Myoung, J., and Ganem, D. (2011a). Active lytic infection of human primary tonsillar B cells by KSHV and its noncytolytic control by activated CD4+ T cells. *J. Clin. Invest.* 121, 1130–1140. doi: 10.1172/JCI43755

Myoung, J., and Ganem, D. (2011b). Generation of a doxycycline-inducible KSHV producer cell line of endothelial origin: maintenance of tight latency with efficient reactivation upon induction. *J. Virol. Methods* 174, 12–21. doi: 10.1016/j.jviromet.2011.03.012

Nathans, R., Chu, C. Y., Serquina, A. K., Lu, C. C., Cao, H., and Rana, T. M. (2009). Cellular micro RNA and P bodies modulate host-HIV-1 interactions. *Mol. Cell* 34, 696–709. doi: 10.1016/j.molcel.2009.06.003

Neipel, F., Albrecht, J. C., and Fleckenstein, B. (1997). Cell-homologous genes in the Kaposi's sarcoma-associated rhadinovirus human herpesvirus 8: determinants of its pathogenicity? *J. Virol.* 71, 4187–4192.

Onomoto, K., Yoneyama, M., Fung, G., Kato, H., and Fujita, T. (2014). Antiviral innate immunity and stress granule responses. *Trends Immunol.* 35, 420–428. doi: 10.1016/j.it.2014.07.006

Panas, M. D., Ivanov, P., and Anderson, P. (2016). Mechanistic insights into mammalian stress granule dynamics. *J. Cell Biol.* 215, 313–323. doi: 10.1083/jcb.201609081

Panas, M. D., Schulte, T., Thaa, B., Sandalova, T., Kedersha, N., Achour, A., et al. (2015). Viral and cellular proteins containing FGDF motifs bind G3BP to block stress granule formation. *PLoS Pathog.* 11:e1004659. doi: 10.1371/journal.ppat.1004659

Patel, C. V., Handy, I., Goldsmith, T., and Patel, R. C. (2000). PACT, a stress-modulated cellular activator of interferon-induced double-stranded RNA-activated protein kinase, PKR. *J. Biol. Chem.* 275, 37993–37998. doi: 10.1074/jbc.M004762200

Patel, R. C., and Sen, G. C. (1998). PACT, a protein activator of the interferon-induced protein kinase, PKR. *EMBO J.* 17, 4379–4390.

Protter, D. S. W., and Parker, R. (2016). Principles and properties of stress granules. *Trends Cell Biol.* 34526, 668–679. doi: 10.1016/j.tcb.2016.05.004

Protter, D. S. W., Rao, B. S., Van Treeck, B., Lin, Y., Mizoue, L., Rosen, M. K., et al. (2018). Intrinsically disordered regions can contribute promiscuous interactions to RNP granule assembly. *Cell Rep.* 22, 1401–1412. doi: 10.1016/j.celrep.2018.01.036

Reineke, L. C., and Lloyd, R. E. (2013). Diversion of stress granules and P-bodies during viral infection. *Virology* 436, 255–267. doi: 10.1016/j.virol.2012.11.017

Renne, R., Zhong, W., Herndier, B., McGrath, M., Abbey, N., Kedes, D., et al. (1996). Lytic growth of Kaposi's sarcoma-associated herpesvirus (human herpesvirus 8) in culture. *Nat. Med.* 2, 342–346. doi: 10.1038/nm0396-342

Riggs, C. L., Kedersha, N., Ivanov, P., and Anderson, P. (2020). Mammalian stress granules and P bodies at a glance. *J. Cell Sci.* 133:jcs242487. doi: 10.1242/jcs.242487

Russo, J. J., Bohenzky, R. A., Chien, M. C., Chen, J., Yan, M., Maddalena, D., et al. (1996). Nucleotide sequence of the Kaposi sarcoma-associated herpesvirus (HHV8). *Proc. Natl. Acad. Sci. U.S.A.* 93, 14862–14867. doi: 10.1073/pnas.93.25.14862

Sharma, N. R., Gadhave, K., Kumar, P., Saif, M., Khan, M. M., Sarkar, D. P., et al. (2021). Analysis of the dark proteome of Chandipura virus reveals maximum propensity for intrinsic disorder in phosphoprotein. *Sci. Rep.* 11:13253. doi: 10.1038/s41598-021-92581-6

Sharma, N. R., Majerciak, V., Kruhlak, M. J., and Zheng, Z. M. (2017). KSHV inhibits stress granule formation by viral ORF57 blocking PKR activation. *PLoS Pathog.* 13:e1006677. doi: 10.1371/journal.ppat.1006677

Sharma, N. R., Majerciak, V., Kruhlak, M. J., Yu, L., Kang, J. G., Yang, A., et al. (2019). KSHV RNA-binding protein ORF57 inhibits P-body formation to promote viral multiplication by interaction with Ago2 and GW182. *Nucleic Acids Res.* 47, 9368–9385. doi: 10.1093/nar/gkz683

Shaw, R. N., Arbiser, J. L., and Offermann, M. K. (2000). Valproic acid induces human herpesvirus 8lytic gene expression in BCBL-1 cells. *AIDS* 14, 899–902. doi: 10.1097/00002030-200005050-00021

Sturzl, M., Gaus, D., Dirks, W. G., Ganem, D., and Jochmann, R. (2013). Kaposi's sarcoma-derived cell line SLK is not of endothelial origin, but is a contaminant from a known renal carcinoma cell line. *Int. J. Cancer* 132, 1954–1958. doi: 10.1002/ijc.27849

Thompson, M. R., Kaminski, J. J., Kurt-Jones, E. A., and Fitzgerald, K. A. (2011). Pattern recognition receptors and the innate immune response to viral infection. *Viruses* 3, 920–940. doi: 10.3390/v3060920

Valiente-Echeverria, F., Melnychuk, L., Vyboh, K., Ajamian, L., Gallouzi, I. E., Bernard, N., et al. (2014). eEF2 and Ras-GAP SH3 domain-binding protein (G3BP1) modulate stress granule assembly during HIV-1 infection. *Nat. Commun.* 5:4819. doi: 10.1038/ncomms5819

Vogt, C., and Bohne, J. (2016). The KSHV RNA regulator ORF57: target specificity and its role in the viral life cycle. *Wiley Interdiscip. Rev. RNA* 7, 173–185. doi: 10.1002/wrna.1323

Wei, X., and Lan, K. (2018). Activation and counteraction of antiviral innate immunity by KSHV: an update. *Sci. Bull.* 63, 1223–1234. doi: 10.1016/j.scib.2018.07.009

White, J. P., Cardenas, A. M., Marissen, W. E., and Lloyd, R. E. (2007). Inhibition of cytoplasmic mRNA stress granule formation by a viral proteinase. *Cell Host Microbe* 2, 295–305. doi: 10.1016/j.chom.2007.08.006

Wilbertz, J. H., Voigt, F., Horvathova, I., Roth, G., Zhan, Y., and Chao, J. A. (2019). Single-molecule imaging of mRNA localization and regulation during the integrated stress response. *Mol. Cell* 73, 946–958.e7. doi: 10.1016/j.molcel.2018.12.006

Yao, B., Li, S., Lian, S. L., Fritzler, M. J., and Chan, E. K. (2011). Mapping of Ago2-GW182 functional interactions. *Methods Mol. Biol.* 725, 45–62. doi: 10.1007/978-1-61779-046-1_4

Ye, F., Zhou, F., Bedolla, R. G., Jones, T., Lei, X., Kang, T., et al. (2011). Reactive oxygen species hydrogen peroxide mediates Kaposi's sarcoma-associated herpesvirus reactivation from latency. *PLoS Pathog.* 7:e1002054. doi: 10.1371/journal.ppat.1002054

Youn, J. Y., Dyakov, B. J. A., Zhang, J., Knight, J. D. R., Vernon, R. M., Forman-Kay, J. D., et al. (2019). Properties of stress granule and P-body proteomes. *Mol. Cell* 76, 286–294. doi: 10.1016/j.molcel.2019.09.014

Yuan, F., Gao, Z. Q., Majerciak, V., Bai, L., Hu, M. L., Lin, X. X., et al. (2018). The crystal structure of KSHV ORF57 reveals dimeric active sites important for protein stability and function. *PLoS Pathog.* 14:e1007232. doi: 10.1371/journal.ppat.1007232

Zevini, A., Olagnier, D., and Hiscott, J. (2017). Crosstalk between cytoplasmic RIG-I and STING sensing pathways. *Trends Immunol.* 38, 194–205. doi: 10.1016/j.it.2016.12.004

Zhang, Q., Sharma, N. R., Zheng, Z. M., and Chen, M. (2019). Viral regulation of RNA granules in infected cells. *Virol. Sin.* 34, 175–191. doi: 10.1007/s12250-019-00122-3

Zhong, W., Wang, H., Herndier, B., and Ganem, D. (1996). Restricted expression of Kaposi sarcoma-associated herpesvirus (human herpesvirus 8) genes in Kaposi sarcoma. *Proc. Natl. Acad. Sci. U.S.A.* 93, 6641–6646. doi: 10.1073/pnas.93.13.6641

**Conflict of Interest:** The authors declare that the research was conducted in the absence of any commercial or financial relationships that could be construed as a potential conflict of interest.

**Publisher's Note:** All claims expressed in this article are solely those of the authors and do not necessarily represent those of their affiliated organizations, or those of the publisher, the editors and the reviewers. Any product that may be evaluated in this article, or claim that may be made by its manufacturer, is not guaranteed or endorsed by the publisher.

*Copyright © 2022 Sharma and Zheng. This is an open-access article distributed under the terms of the Creative Commons Attribution License (CC BY). The use, distribution or reproduction in other forums is permitted, provided the original author(s) and the copyright owner(s) are credited and that the original publication in this journal is cited, in accordance with accepted academic practice. No use, distribution or reproduction is permitted which does not comply with these terms.*

frontiers in Microbiology

ORIGINAL RESEARCH
published: 10 January 2022
doi: 10.3389/fmicb.2021.799890

# Hsp90 Inhibitors Inhibit the Entry of Herpes Simplex Virus 1 Into Neuron Cells by Regulating Cofilin-Mediated F-Actin Reorganization

*Xiaowei Song[1], Yiliang Wang[1,2,3], Feng Li[1,2], Wenyan Cao[1,2,3], Qiongzhen Zeng[1,2,3], Shurong Qin[4], Zhaoyang Wang[1,2], Jiaoyan Jia[1,2], Ji Xiao[1], Xiao Hu[4], Kaisheng Liu[5], Yifei Wang[1]* and Zhe Ren[1]**

[1] Guangzhou Jinan Biomedicine Research and Development Center, Institute of Biomedicine, College of Life Science and Technology, Jinan University, Guangzhou, China, [2] Key Laboratory of Virology of Guangzhou, Jinan University, Guangzhou, China, [3] Key Laboratory of Bioengineering Medicine of Guangdong Province, Jinan University, Guangzhou, China, [4] College of Pharmacy, Jinan University, Guangzhou, China, [5] The Second Clinical Medical College, Shenzhen People's Hospital, Jinan University, Guangzhou, China

OPEN ACCESS

**Edited by:**
Chunfu Zheng,
University of Calgary, Canada

**Reviewed by:**
Yan Yan,
Wuxi No. 5 People's Hospital, China
Qinchang Zhu,
Shenzhen University, China

***Correspondence:**
Yifei Wang
twang-yf@163.com
Zhe Ren
rz62@163.com

**Specialty section:**
This article was submitted to Virology, a section of the journal Frontiers in Microbiology

**Received:** 22 October 2021
**Accepted:** 10 November 2021
**Published:** 10 January 2022

**Citation:**
Song X, Wang Y, Li F, Cao W, Zeng Q, Qin S, Wang Z, Jia J, Xiao J, Hu X, Liu K, Wang Y and Ren Z (2022) Hsp90 Inhibitors Inhibit the Entry of Herpes Simplex Virus 1 Into Neuron Cells by Regulating Cofilin-Mediated F-Actin Reorganization. Front. Microbiol. 12:799890. doi: 10.3389/fmicb.2021.799890

Herpes simplex virus 1 (HSV-1) is a common neurotropic virus, the herpes simplex encephalitis (HSE) caused by which is considered to be the most common sporadic but fatal encephalitis. Traditional antiviral drugs against HSV-1 are limited to nucleoside analogs targeting viral factors. Inhibition of heat shock protein 90 (Hsp90) has potent anti-HSV-1 activities *via* numerous mechanisms, but the effects of Hsp90 inhibitors on HSV-1 infection in neuronal cells, especially in the phase of virus entry, are still unknown. In this study, we aimed to investigate the effects of the Hsp90 inhibitors on HSV-1 infection of neuronal cells. Interestingly, we found that Hsp90 inhibitors promoted viral adsorption but inhibited subsequent penetration in neuronal cell lines and primary neurons, which jointly confers the antiviral activity of the Hsp90 inhibitors. Mechanically, Hsp90 inhibitors mainly impaired the interaction between Hsp90 and cofilin, resulting in reduced cofilin membrane distribution, which led to F-actin polymerization to promote viral attachment. However, excessive polymerization of F-actin inhibited subsequent viral penetration. Consequently, unidirectional F-actin polymerization limits the entry of HSV-1 virions into neuron cells. Our research extended the molecular mechanism of Hsp90 in HSV-1 infection in neuron cells and provided a theoretical basis for developing antiviral drugs targeting Hsp90.

**Keywords: herpes simplex virus 1, heat shock protein 90, virus entry, cofilin, F-actin**

## INTRODUCTION

Herpes simplex virus type 1 (HSV-1) is a neurotropic DNA virus belonging to the Herpesviridae family (Grinde, 2013). The infection of HSV-1 is extensive and causes disease diversity. In particular, HSV-1, as a neurotropic virus, spreads to the brain. After primary infection, HSV-1 can reach the central nervous system, resulting in substantial damage to neuronal cells (Wang et al., 2019; Marcocci et al., 2020). Herpes simplex encephalitis (HSE) induced by HSV-1 infection is the most common sporadic but fatal encephalitis. Although rare, HSE causes 70% mortality in

untreated patients (Whitley, 2006; Stahl et al., 2012; Piret and Boivin, 2020), and most survivors present severe neurological sequelae (Lafaille et al., 2019). Further research indicates that HSV-1 infection of neurons activates neurotoxic pathways typical of Alzheimer's disease (AD), and repeated HSV-1 reactivations in the brain of infected mice produce an AD-like phenotype. HSV-1 is gradually recognized as an important factor affecting AD development (Balin and Hudson, 2018; Eimer et al., 2018; Tzeng et al., 2018; Wang et al., 2020b).

The proliferation process of HSV-1 includes multiple stages (Ibáñez et al., 2018). Traditional antiviral drugs against HSV-1 are limited to nucleoside analogs targeting viral factors, and the treatment drugs are single; thus, novel therapeutic targets against HSV-1 infection-associated diseases are urgently needed (Wang et al., 2017). Virus propagation requires host proteins to participate; to find new antiviral targets from host proteins is an appropriate strategy for developing safe and effective anti-herpes simplex drugs (Wang et al., 2017). The heat shock protein 90 (Hsp90) as a molecular chaperone associates with various other proteins such as steroid receptors, protein kinases, and filamentous actin and activates or inhibits a range of client proteins (Buchner and Li, 2013; Schopf et al., 2017). Hsp90 is essential for many viruses to complete the multiplication cycle, including human immunodeficiency virus (HIV)-1, enterovirus 71 (EV71), HSV-1, and influenza virus (Wang et al., 2017). Recent studies have indicated that Hsp90 is a crucial host factor that is required by many viruses for multiple phases of their life cycle, such as virus entry and intracellular transport, viral gene expression, and viral protein maturation which requires Hsp90 regulation (Wang et al., 2017; Li et al., 2018). Hsp90 has attracted intensive attention in developing novel antiviral drugs because of their functions in the life cycle of multiple viruses. For example, Hsp90 inhibitors block HSV-1 nuclear egress and assembly in Vero cells (Ju et al., 2011; Xiang et al., 2012a; Li et al., 2018), and another research shows that Hsp90 is essential for the correct localization of HSV-1 DNA polymerase to the nucleus (Burch and Weller, 2005), and Hsp90 also promotes nuclear transport of HSV-1 capsid proteins by interacting with acetylated tubulin (Zhong et al., 2014). Furthermore, previous research showed that AT533 reduced the nuclear translocation of NF-κB and NLRP3 activation *via* inhibiting Hsp90 from attenuating HSV-1-induced inflammation (Li et al., 2019b). Hsp90 inhibitors have rarely reported their antiviral effects in neurons, and it is of great significance to study Hsp90 as a promising host target for antiviral infection in neurons.

Viral intracellular transportation mainly relies on the dynamic regulation of the cell's cytoskeleton, especially actin filaments, an important part of the cell cytoskeleton, which is closely related to early virus infection (Xiang et al., 2012b). Actin filaments are polymers formed by G-actin polymerization, mainly in the cortical area below the cell membrane (Sens and Plastino, 2015); F-actin dynamics is essential for early virus infection (Xiang et al., 2012b). Rho GTPase is a key regulator for regulating the actin dynamics, which is also closely related to viral infections (Favoreel et al., 2007; Van den Broeke et al., 2014). For example, the actin-depolymerizing factor (ADF)/cofilin regulates the microfilament framework (Favoreel et al., 2007; Ndozangue-Touriguine et al., 2008). Cofilin is essential for regulators of actin dynamics, is previously reported to sever actin filaments at low cofilin/actin ratios, and stabilizes filaments at high cofilin/actin ratios in mammalian neurons by binding to ADP–actin subunits in F-actin (Southwick, 2000; Bravo-Cordero et al., 2013; Wioland et al., 2017). When various intracellular and extracellular signal molecules stimulate cells, the microfilament can form filopodia, lamellipodia, and stress fibers (Taylor et al., 2011).

As an essential facet of virus–cell interactions, HSV interacts with the host cytoskeleton at various stages of the viral life cycle. The biphasic F-actin dynamics in HSV-1 neurons was demonstrated (Xiang et al., 2012b; Zheng et al., 2016). For example, F-actin dynamics plays a vital role in virus entry; we have shown that early infection of HSV-1 mobilizes F-actin reorganization to facilitate viral entry (Xiang et al., 2012b). F-Actin is polymerized to form pseudopods, which enrich the receptors required by the virus and facilitate further infection of the virus (Hu et al., 2016; Azab and Osterrieder, 2017), and previous studies have shown that the viral envelope glycoprotein gB binds to the receptor α3β1, activates Rho GTPases to cause the rearrangement of F-actin, and ultimately promotes virus entry into the cell (Naranatt et al., 2003). The entry of the virus into host cells, including adsorption and penetration, is the initial step of the infection process and is an ideal antiviral stage (Ibáñez et al., 2018). It is a good antiviral strategy to block the assembly of G-actin by regulating the polymerization and depolymerization of F-actin to inhibit virus entry (Zheng et al., 2016). Hsp90 is associated with filamentous actin (Kellermayer and Csermely, 1995; Taiyab and Rao, 2011), but the specific mechanism of Hsp90 regulating filamentous actin remains to be further explored. Herein, we further investigated the antiviral efficacy and mechanism of Hsp90 inhibitors in neuron cells and provided a theoretical basis for Hsp90 as a new anti-HSV-1 drug target point in HSE.

# MATERIALS AND METHODS

## Cell and Virus

A Vero cell line (ATCC, Manassas, VA, United States) was cultured as previously described (Li et al., 2019a), The neuroblastoma cell line SH-SY5Y (ATCC, United States) was purchased from the Cell Bank of the Chinese Academy of Sciences, and N2a cells, our laboratory stock, were cultured in Dulbecco's modified Eagle's medium (DMEM; Gibco, Grand Island, NY, United States) with 10% fetal bovine serum (FBS; Gibco). The reporter virus EGFP-HSV-1, which expresses eGFP fused with US11, was acquired from the Anti-Stress and Health Research Center, College of Pharmacy, Jinan University, Guangzhou, Guangdong, 510632, China. HSV-1 strain F was obtained from Hong Kong University and preserved in our laboratory elaborately. After repeated freezing and thawing three times, the viruses were propagated in Vero cells, centrifuged at 4°C, 1,000 rpm for 5 min to take the supernatant, and then stored at –80°C until used.

## Chemicals, Antibodies, and Reagents

17-N-Allylamino-17-demethoxygeldanamycin (17-AAG) was purchased from Selleck (S1141; Houston, TX, United States) and dissolved in dimethyl sulfoxide at a concentration of 10 mM. SNX-25a (AT533) was acquired according to previous reports [20] and dissolved in dimethyl sulfoxide at a concentration of 20 mM. In this study, SH-SY5Y cells were treated with 17-AAG (1.25 μM) or AT533 (1.00 μM), and N2a cells were treated with 17-AAG (0.63 μM) or AT533 (40.00 nM). Cytochalasin B was purchased from Sigma-Aldrich (14930-96-2, St. Louis, MO, United States). Antibodies, including anti-gB (ab6506) and anti-VP5 (ab6508), were purchased from Abcam (Cambridge, United Kingdom), as well as anti-cofilin (5175S), anti-p-cofilin (3313 S), anti-Hsp90 (ab13492), anti-Hsp90α (GTX109753), anti-Hsp90β (5087 S), anti-β-actin (GTX109639), and anti-GAPDH (5174 S). TRIzol reagent was bought from Tiangen (Beijing, China). All primer sequences are shown in **Supplementary Table 1**. siRNAs were purchased from GenePharma (Shanghai, China), and their sequences are shown in **Supplementary Table 2**.

## CCK8 Assay

The cytotoxicity of 17-AAG or AT533 on SH-SY5Y and N2a cells was evaluated by CCK8 assay. Both SH-SY5Y and N2a cells were seeded into 96-well plates to 90% confluence; then, various concentrations of the compound were added to the plate. After 24 h, each well was added with 10 μl of CCK8 solution and incubated at 37°C for another 2 h in the dark. The absorbance was then measured by an enzyme immunoassay reader at 450 nm.

## Quantitative Real-Time PCR

The total RNA of the different cell samples was extracted according to the manufacturer's specifications (TRIzol, DP424, Tiangen Biotech Co., Beijing, China) and was reverse transcribed using the Reverse Transcriptase Kit (RR036A-1, TaKaRa, Tokyo, Japan). Quantitative real-time PCR (qRT-PCR) was performed using a Bio-Rad CFX96 real-time PCR system with a total volume of 10 μl including 5 μl of SYBR Green Real-Time PCR Master Mix (RR820, TaKaRa, Japan), 4 μl of cDNA template, and 0.5 μl of each primer. Data were processed and analyzed by Bio-Rad CFX Manager software. The mRNA expression normalization was internally controlled by gene β-actin.

## Western Blotting

Cell samples were washed thrice with precooled PBS and lysed in SDS buffer (Beyotime, Shanghai, China) containing 1 mM PMSF (Beyotime). Lysates were heated at 100°C for 15 min and centrifuged at 12,000 × g for 15 min at 4°C. The protein concentrations were then measured with a bicinchoninic acid (BCA) protein assay kit (Beyotime), and the cell lysates were mixed with 5 × SDS-PAGE buffer (P0015, Beyotime, Shanghai, China) and boiled for 10 min. Subsequently, samples were subjected to 10–12% SDS-PAGE and transferred to a polyvinylidene fluoride (PVDF) membrane (Millipore, Bedford, MA, United States). The PVDF membranes were incubated with interesting primary antibodies overnight at 4°C after blocking with 5% skimmed milk for 1 h, then indicated with appropriate HRP-conjugated secondary antibodies (Invitrogen, Carlsbad, CA, United States) for 1 h at room temperature. Finally, target proteins were visualized by enhanced chemiluminescence.

## Detection of Herpes Simplex Virus 1 Binding and Internalization

The amount of virus binding to and internalized by cells was measured as described previously, just with minor modifications (Wang et al., 2020a). Cells were seeded 24 h prior to the experiment in 12-well plates at a 2 × 105/well density to determine the amount of virus binding. Cells were incubated for 1 h at 4°C, then infected with HSV-1 for another 1 h in the presence of 17-AAG or AT533. The unbound virus was removed with PBS after HSV-1 attachment. The total DNA of HSV-1 was extracted using the EasyPure® Viral DNA/RNA Kit (Trans, Beijing, China) to determine viral DNA copy numbers using qRT-PCR-based detection of the viral gene. To measure the amount of viral entry, cells were seeded 24 h prior to the experiment in 12-well plates at a $2 \times 10^5$/well density. Cells were incubated for 1 h at 4°C, then infected with HSV-1 for another 1 h, and then washed with PBS for three times before the cells were transferred to 37°C until the end of penetration; the HSV-1 internalized by cells was detected after extracellular viral particles and virions that bound to but did not enter the cells were removed by washing with PBS (pH 3.0). The cells were collected, and total DNA was extracted by EasyPure Viral DNA/RNA Kit, and targeted genes were analyzed by qRT-PCR. In addition, other experiments were performed on these cell samples according to the experimental objectives.

## Viral Plaque Assay

SH-SY5Y and Vero cells were seeded in 24-well plates at a density of 1.5 × 105/well, then the reduction of plaque formation was measured. Briefly, cells were incubated for 1 h at 4°C, then infected with HSV-1 for another 1 h. The virus inoculum was removed, and an overlay medium (maintenance medium containing 1% methylcellulose) was added to each well. After 72 h of incubation, cell monolayers were fixed with 4% paraformaldehyde and stained with 1% crystal violet. Finally, the plaque number was counted.

## Immunofluorescence Assay

Cells were seeded into confocal dishes to attain 70–80% confluence and treated based on various experimental requirements, and then samples were fixed with 4% paraformaldehyde for 20 min, permeabilized with 0.1% Triton X-100 for 5 min, and then blocked with 5% bovine serum albumin for 1 h. The samples were incubated overnight at 4°C with the anti-VP5 primary antibody then incubated with a fluorescently labeled secondary antibody for 1 h at room temperature, then actin filaments were stained by FITC-labeled phalloidin (red), and cell nuclei were stained with DAPI staining solution (C1006, Beyotime, Shanghai, China) for 10 min. Finally, a confocal laser scanning microscope was used to capture immunofluorescence images (LSM 510 meta; Zeiss).

## Immunoprecipitation Assay

Cells were lysed with 500 μl IP lysis buffer (P0013J, Beyotime, Shanghai, China) containing 1% PMSF, and the supernatant was collected by centrifugation at 14,000 g for 10 min at 4°C. Fifty microliters of supernatant was used as input, and the remaining supernatant was incubated with a primary antibody (Hsp90, cofilin) overnight at 4°C. Then, 40 μl of Protein A/G magnetic beads were incubated for 4 h on a vertical suspension at 4°C. The immunoprecipitation was collected and washed three times with ice PBS and resuspended in 30 μl of 1 × SDS-PAGE buffer. Finally, the sample was analyzed by Western blot.

## Flow Cytometry

Cells were infected with HSV-1 and treated with 17-AAG, AT533, or cytochalasin B, and the samples were processed accordingly according to the purpose of the experiment. Then, the cells were washed with PBS, fixed with 4% paraformaldehyde for 5 min, and permeabilized with 0.1% Triton X-100 for 5 min. Next, all samples were stained with 5% FITC phalloidin (40735ES75, YEASEN, China) for 40 min at 37°C. Finally, fluorescence was analyzed with a flow cytometer (Becton Dickinson, San Jose, CA, United States).

## Primary Cortical Neuron Extraction

The extraction of cortical neurons was measured as described previously (Meng et al., 2017). We extracted cortical neurons from C57BL/6J mice 1–2 days after birth. For example, 0.1 mg/ml L-polylysine (P8130-25, Solarbio, Beijing, China) was coated on a six-well plate overnight, washed with ultrapure water, and exposed to ultraviolet light in a biological safety cabinet and dried. C57BL/6J mice were sterilized with 75% alcohol, and the cerebral cortex was taken out and cut into pieces in a container of 2 ml D-Hanks solution, then 1 ml of 0.25% trypsin was added for digestion at 37°C, 5% $CO_2$ for 10 min. The tissue suspension was filtered with a primary cell strainer, and the cells were collected at 1,000 rpm, centrifuged for 5 min, and seeded in a six-well plate at $1.5 \times 10^6$ cells/well. Finally, the cells were cultured in a 37°C, 5% $CO_2$ incubator for 6 h, and then the adhesion of the cells was observed. After most of the cells have adhered, the medium was changed and a freshly prepared Neurobasal-A + B27 medium was added. The second day of replacing the Neurobasal-A + B27 medium was used as the first day of *in vitro* cell culture. On the third day, the Neurobasal-A + B27 medium was changed again. On the fifth day, neurons were separated and subjected to corresponding experiments.

## Statistical Analysis

Data were presented as mean ± SD of the results from at least two independent experiments. Significant differences between control and experimental groups were analyzed using Student's *t*-test. Differences were considered significant set at $^{*}p < 0.05$. $^{**}p < 0.01$; $^{***}p < 0.001$.

# RESULTS

## Hsp90 Inhibitors Inhibit Herpes Simplex Virus 1 Infection of Neuron Cells

Two different Hsp90 inhibitors, 17-AAG and AT533, were used to detect cytotoxicity and antiviral activity. Firstly, the cytotoxicity

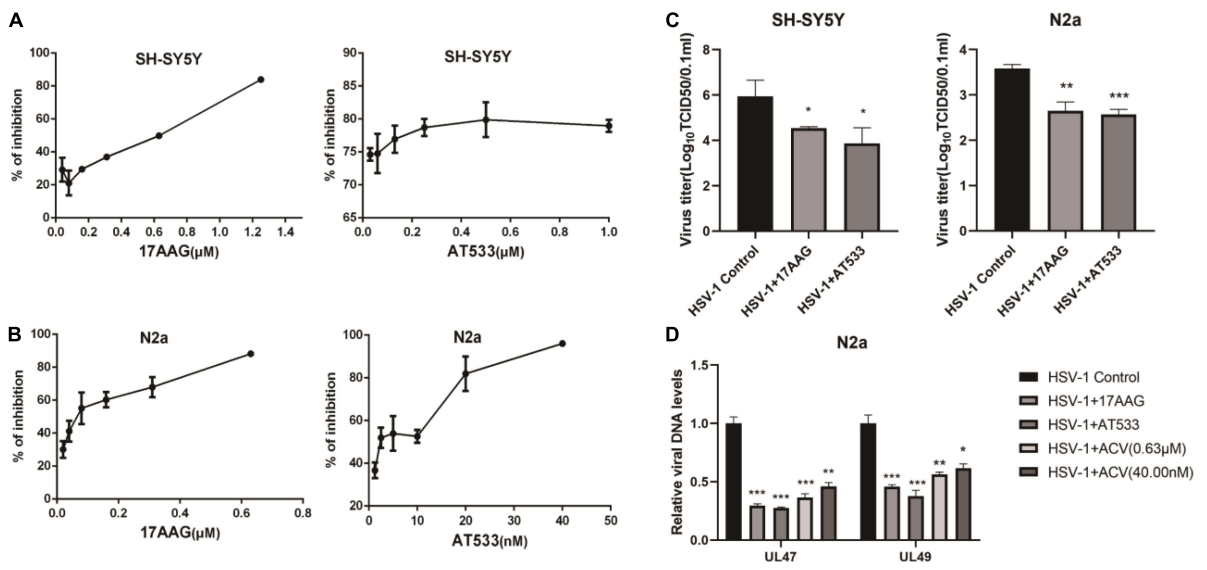


**FIGURE 1 |** The antiviral activity of Hsp90 inhibitors. **(A,B)** Hsp90 inhibitors exhibited an inhibitory effect on eGFP-HSV-1. SH-SY5Y and N2a cells were infected with eGFP-HSV-1 (MOI = 0.1) at different concentrations of 17-AAG or AT533 for 24 h. The fluorescence intensity was detected by a multifunctional enzyme marking instrument to calculate the virus inhibition rate. **(C)** SH-SY5Y and N2a cells were infected with HSV-1 (MOI = 0.1) in 17-AAG or AT533 for 24 h, and the cell suspensions were collected to measure the viral titer in Vero cells. **(D)** N2a cells were infected with HSV-1 (MOI = 0.1) in the presence of 17-AAG or AT533 for 24 h, and ACV was used as a positive control, then the total DNA of HSV-1 was extracted, and the levels of *UL47* and *UL49* were analyzed by qRT-PCR. Data are mean ± SD ($n = 3$). $^{*}p < 0.05$, $^{**}p < 0.01$, $^{***}p < 0.001$ versus the HSV-1 control group.

of Hsp90 inhibitors on SH-SY5Y and N2a cells was detected by CCK8 assay (**Supplementary Figures 1A,B**). In addition, we used eGFP-HSV-1 to infect SH-SY5Y and N2a cells for 24 h in the presence of Hsp90 inhibitors, respectively, and the antiviral activity of Hsp90 inhibitors was judged by the fluorescence intensity of eGFP (**Figures 1A,B**). Furthermore, we also assessed the effects of Hsp90 inhibitors on viral titers (**Figure 1C**), which indicated that 17-AAG and AT533 inhibited HSV-1 infection. HSV-1 DNA was also extracted by the Virus DNA/RNA Kit to detect the amount of HSV-1. The results show that 17-AAG and AT533 have better antiviral activity than ACV (Acyclovir) (**Figure 1D**).

## Hsp90 Inhibitors Promote Herpes Simplex Virus 1 Attachment

We consider that the adsorption of HSV-1 on the cell membrane surface is the first step in the virus proliferation process (Ibáñez et al., 2018). To explore the effect of Hsp90 inhibitors on the adsorption phase of HSV-1-infected neuron cells, two different Hsp90 inhibitors, 17-AAG and AT533, were treated as neuron cells. A simple diagram of HSV-1 attachment was shown (**Supplementary Figure 2A**). We firstly investigated the amount of HSV-1 bound to cells by quantifying the viral genome, a common method used for determining the amount of viral attachment during early infection (Wang et al., 2020a). Neuron cells are pretreated at 4°C for 1 h and then infected with HSV-1 1 h at 4°C, so that the virus can be infected simultaneously as much as possible, after the adsorption is completed. Hsp90 inhibitors were treated on the adsorption of HSV-1-infected SH-SY5Y and N2a cells, then HSV-1 DNA was extracted by the Virus DNA/RNA Kit for detection by qRT-PCR.

Interestingly, the results indicated that viral attachment was higher than control groups after Hsp90 inhibitors treatment (**Figures 2A,C**). Similarly, Hsp90 inhibitors pretreatment also promoted HSV-1 attachment (**Supplementary Figure 3**). The

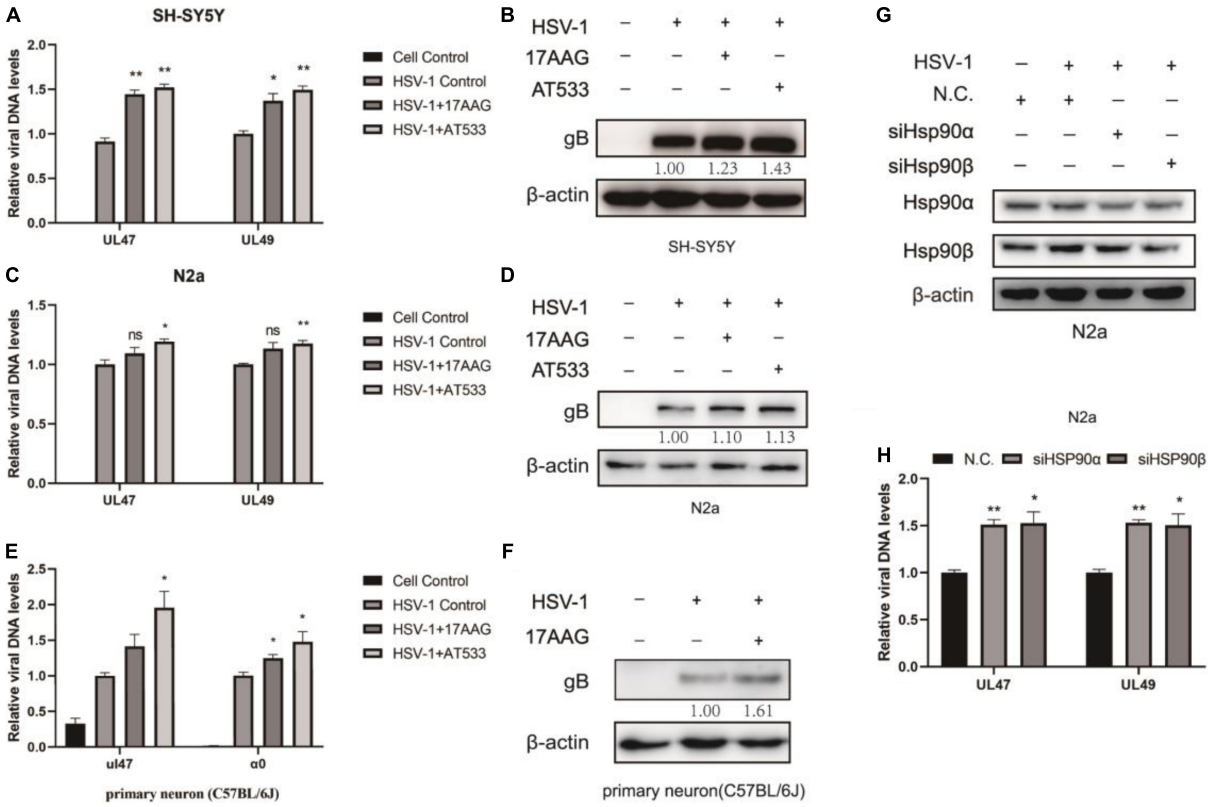


**FIGURE 2 |** Hsp90 inhibitors promote HSV-1 attachment. **(A)** Hsp90 inhibitors increased the amount of viral DNA. SH-SY5Y cells were incubated for 1 h at 4°C, then infected with HSV-1 (MOI = 20) for another 1 h in the presence of 17-AAG or AT533, and the unbound virus was removed after HSV-1 attachment. Total DNA of HSV-1 was extracted, and the expression level of *UL47* and *UL49* was subjected to qRT-PCR analysis. **(B)** Hsp90 inhibitors increased the amount of viral protein. SH-SY5Y cells were incubated for 1 h at 4°C, then infected with HSV-1 (MOI = 50) for another 1 h in the presence of 17-AAG or AT533, and the unbound virus was removed after HSV-1 attachment. The level of gB was detected by Western blot. **(C,D)** N2a cells were treated as **(A,B)** in the presence of Hsp90 inhibitors, and the total DNA and protein of HSV-1 were extracted for analysis. **(E)** Hsp90 inhibitors promoted the amount of viral DNA in primary cortical neurons. Primary cortical neurons were incubated for 1 h at 4°C, then infected with HSV-1 (MOI = 20) for another 1 h in the presence of 17-AAG or AT533, then viral DNA was extracted and then qRT-PCR was performed to measure viral DNA amounts. **(F)** 17-AAG promoted the amount of protein. Primary cortical neurons were incubated for 1 h at 4°C, then infected with HSV-1 (MOI = 50) for another 1 h in the presence of 17-AAG or AT533, the total proteins were extracted after HSV-1 attachment; protein levels were evaluated by Western blotting. **(G)** The efficiency of Hsp90α and Hsp90β knockdown was detected by Western blot for 48 h. **(H)** Hsp90α and Hsp90β knockdown also increased the level of HSV-1. Data are mean ± SD ($n = 3$). *$p < 0.05$, **$p < 0.01$ versus the HSV-1 control group.

level of gB, a viral protein carried by the virus particle itself, was increased than the virus control after the cells were treated with Hsp90 inhibitors (**Figures 2B,D**). Consistently, we also verified primary cortical neurons, and the cortical neurons of C57BL/6J mice were extracted as described previously (Meng et al., 2017). Cell morphology was shown (**Supplementary Figure 4A**), beyond the neuronal nuclear antigen (NeuN), a neuronal specific nuclear protein in vertebrates, as a neuronal nuclear antigen marker was detected, and the primary cortical neurons were separated with a purity of 95.76% (**Supplementary Figure 4B**). The DNA and protein levels were higher than the control group (**Figures 2E,F**). These results confirmed that Hsp90 inhibitors facilitated the adsorption of HSV-1 on neuron cells.

Hsp90α and Hsp90β are mainly involved in the virus proliferation cycle (Wang et al., 2017). Moreover, the knockdown efficiency was detected after Hsp90α and Hsp90β were knocked down by siRNA (**Figure 2G**). Samples were collected to extract viral DNA to determine the HSV-1 binding amount according to the "Detection of HSV-1 binding and internalization" method, and Hsp90α and Hsp90β knockdown promoted viral attachment (**Figure 2H**).

## Hsp90 Inhibitors Inhibit Herpes Simplex Virus 1 Penetration

Furthermore, Hsp90 is involved in multiple phases of the virus infection cycle (Wang et al., 2017). Thus, we further explored the effect of Hsp90 inhibitors on HSV-1 penetration, and a simple diagram of HSV-1 penetration was shown (**Supplementary Figure 2B**). The dynamic curve of HSV-1 penetration was tested (**Supplementary Figures 5A,B**). Firstly, neuronal cells were infected with HSV-1 for 1 h at 4°C; we found that

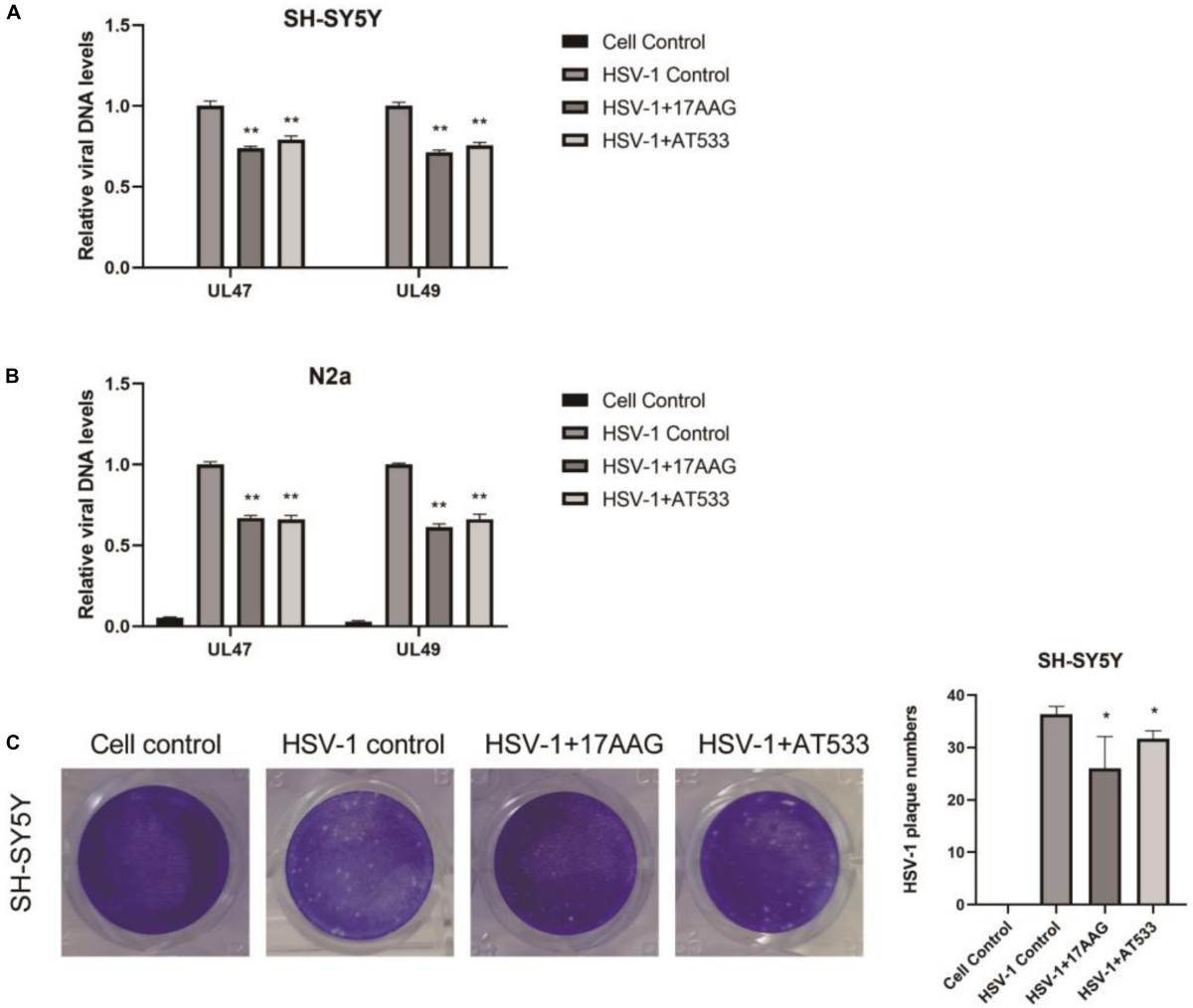


**FIGURE 3 |** Hsp90 inhibitors abrogate HSV-1 penetration. **(A,B)** 17-AAG and AT533 reduced the amount of viral DNA. SH-SY5Y and N2a cells were precooled for 1 h at 4°C, then infected with HSV-1 (MOI = 20) for another 1 h at 4°C. The unadsorbed viruses were removed, then SH-SY5Y cells were treated with 17-AAG or AT533 for 0.5 h at 37°C and washed with acidic PBS to remove the viruses on cell membranes. Total DNA of HSV-1 was extracted for analysis. **(C)** HSV-1 infection-mediated plaque formation units were significantly reduced. 17-AAG and AT533 processed the penetration stage, then HSV-1 plaque formation was measured after 72 h post-infection in SH-SY5Y cells. Data are mean ± SD ($n = 3$). *$p < 0.05$, **$p < 0.01$ versus the HSV-1 control group.

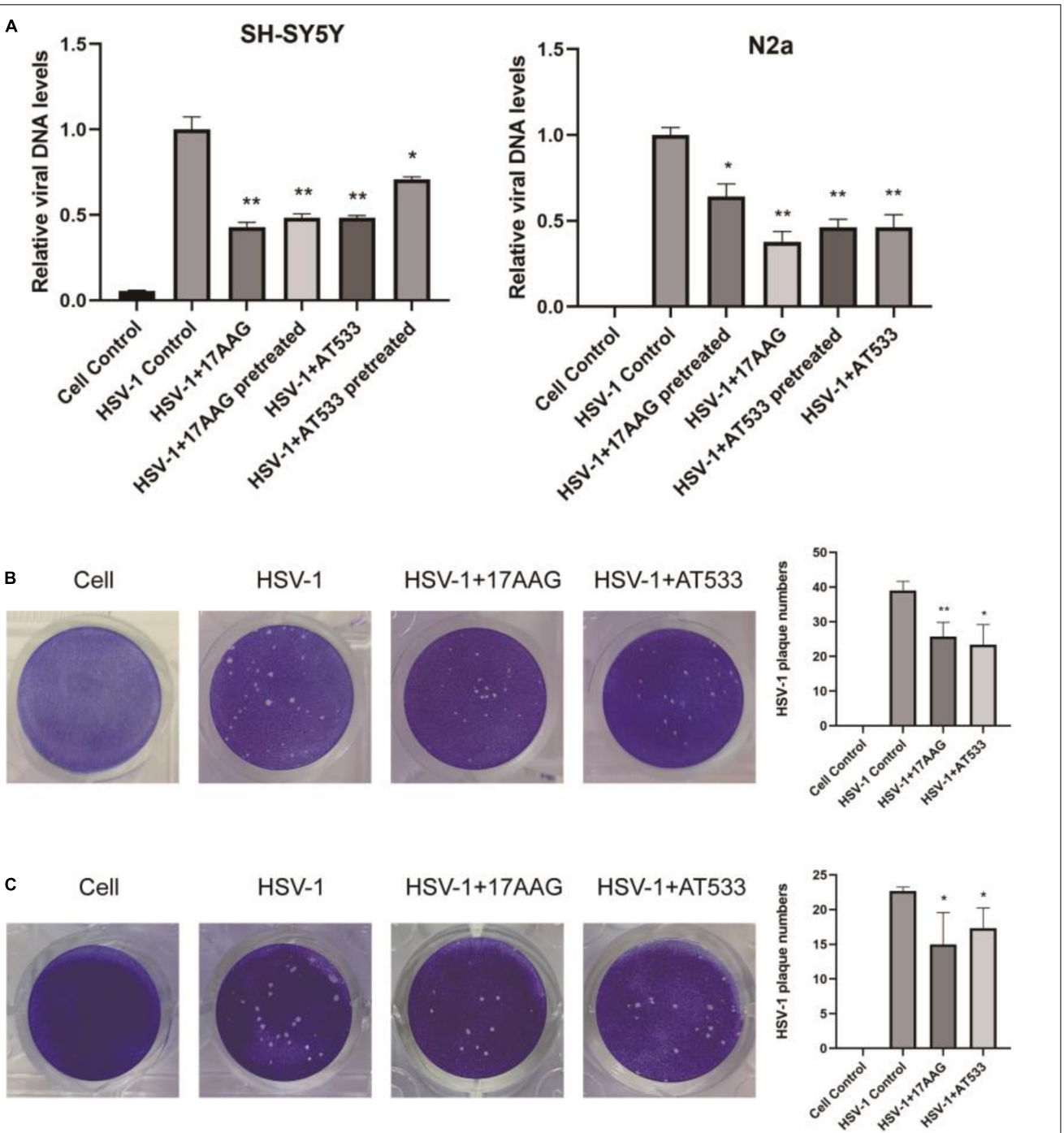


**FIGURE 4 |** Hsp90 inhibitors block viral entry. **(A)** SH-SY5Y and N2a cells were pretreated with 17-AAG or AT533 for 1 h at 4°C and washed with PBS to remove the inhibitors, then infected with HSV-1 (MOI = 20) for another 1 h at 4°C, then all groups were shifted to 37°C; at the same time, the treatment groups were treated with HSV-1 (MOI = 20) in the presence of Hsp90 inhibitors all the time. Finally, viral DNA was extracted, and then qRT-PCR was performed to measure viral *α0* DNA amounts. **(B)** Plaque-formation assay results showing that Hsp90 inhibitors limited HSV-1 entry; SH-SY5Y cells were incubated for 1 h at 4°C, then infected with HSV-1 (MOI = 20) for another 1 h at 4°C in the presence of Hsp90 inhibitors, and all groups were shifted to 37°C, then washed with acidic PBS; overlay medium was added to each well. After 72 h of incubation, cell monolayers were fixed with 4% paraformaldehyde and stained with 1% crystal violet. Finally, the number of plaques was counted. **(C)** N2a cells were infected with HSV-1 (MOI = 20) in the presence of Hsp90 inhibitors, then unbound virus was removed, and N2a cells were treated with the Hsp90 inhibitor again; all groups were shifted to 37°C for 30 min, then all samples were repeatedly frozen and thawed three times to collect the virus, and the plaque reduction experiment was performed on Vero cells to evaluate the level of a virus entering N2a cells. Data are mean ± SD ($n = 3$). $^{*}p < 0.05$, $^{**}p < 0.01$ versus the HSV-1 control group.

the intracellular virus reached a plateau after 30 min of virus infection at 37°C, indicating the end of viral penetration. To further confirm the effects of Hsp90 inhibitors on HSV-1 early infection, the internalized viral DNA was quantified using real-time PCR. As shown in **Figures 3A,B**, Hsp90 inhibitors inhibit the amount of intracellular virus DNA. Antiviral activity was evaluated by a plaque reduction assay (PRA); the amount of HSV-1 infection-mediated plaque formation units was also significantly reduced by Hsp90 inhibitors (**Figure 3C**). Therefore, the above experiment indicates that Hsp90 inhibitors inhibit virus penetration.

## Hsp90 Inhibitors Inhibit Herpes Simplex Virus 1 Entry

Considering that the process of virus entry into host cells includes adsorption and penetration stages, the comprehensive effect of Hsp90 inhibitors on HSV-1 entry into neuron cells is worthy of further investigation. HSV-1 DNA was extracted using the viral DNA/RNA kit and detected by qRT-PCR. As shown in **Figure 4A**, whether it was pretreated and treated with 17-AAG or AT533, the entry of HSV-1 was inhibited. In addition, plaque reduction experiments also show that Hsp90 inhibitors impaired HSV-1 from entering SH-SY5Y cells (**Figure 4B**). While it is not suitable for N2a cells to directly form plaque, after HSV-1 (MOI = 20) infected N2a cells, the virus was therefore collected to infect Vero cells for plaque reduction experiments; consistently, Hsp90 inhibitor treatment significantly reduced the number of viral plaque (**Figure 4C**). These results further demonstrated that Hsp90 inhibitors played an antiviral effect at HSV-1 entry.

## Hsp90 Inhibitors Induce F-Actin Assembly

Cell cytoskeleton, especially actin filaments, is an essential part of the cell structure, closely related to virus infection (Favoreel et al., 2007; Pollard and Cooper, 2009; Zheng et al., 2016; Miranda-Saksena et al., 2018). In the previous study, F-actin

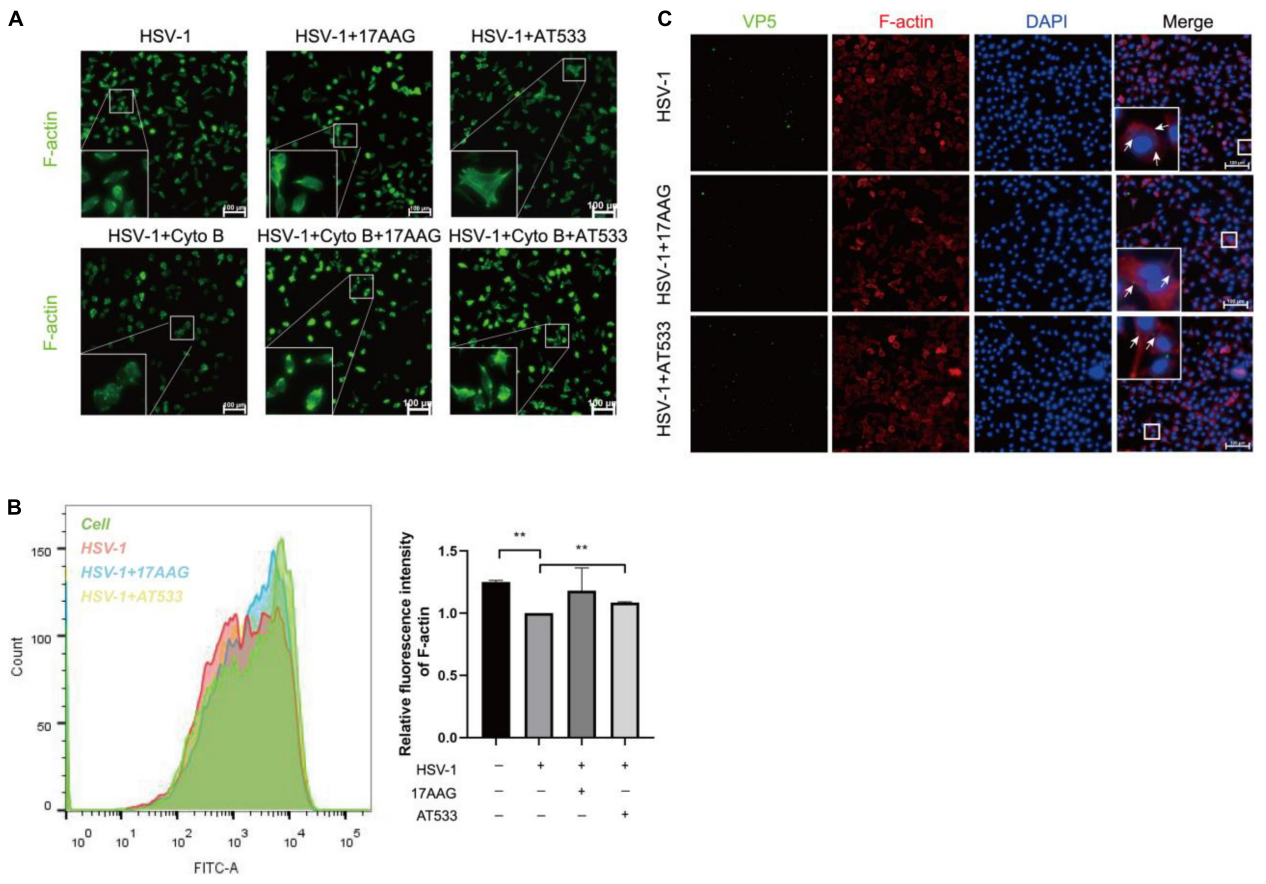


**FIGURE 5 |** Hsp90 inhibitors promote the aggregation of F-actin. **(A)** Hsp90 inhibitors induced F-actin assembly in HSV-1 entry. SH-SY5Y cells were precooled for 1 h at 4°C then treated with 17-AAG, AT533, or Cyto B (10 μM) for 1 h at 4°C and another 0.5 h at 37°C, then the cells were collected to be fixed, and F-actin was stained with FITC-phalloidin (F-actin, green) for analysis by immunofluorescence assay. **(B)** Hsp90 inhibitors induced F-actin assembly in HSV-1 penetration. SH-SY5Y cells were incubated for 1 h at 4°C, then infected with HSV-1 (MOI = 100) for another 1 h at 4°C, then cells were treated with 17-AAG or AT533 for 30 min at 37°C. Then, F-actin was stained with FITC-phalloidin for analysis by flow cytometry. Data are mean ± SD ($n = 2$). $^{**}p < 0.01$. **(C)** Hsp90 inhibitors impaired viral penetration by inducing F-actin assembly; SH-SY5Y cells were incubated for 1 h at 4°C, then infected with HSV-1 (MOI = 50) for another 1 h at 4°C, then cells were treated with 17-AAG or AT533 for 30 min at 37°C. The cells were then fixed and stained with anti-VP5 antibody (green), TRITC-phalloidin (F-actin, red), and DAPI (nucleus, blue), then analyzed by immunofluorescence assay. Scale bars, 100 μm. × 20.

dynamics plays a vital role in virus entry. We have shown that early infection of HSV-1 mobilizes F-actin reorganization to facilitate viral entry (Xiang et al., 2012b). Considering that HSV-1 modifies the actin filaments *via* cofilin to facilitate its infection of neurons, specifically, HSV-1 infection firstly enhances F-actin polymerization to promote virus binding, which is followed by continuous depolymerization of F-actin during the later stages to facilitate viral penetration (Xiang et al., 2012b; Zheng et al., 2014). It has been reported that disrupting the dynamics of F-actin is a good antiviral strategy. For example, amentoflavone, a polyphenol compound, disturbed cofilin-mediated F-actin assembly and significantly reduced HSV-1 infection (Li et al., 2019a). In addition, the disruption of F-actin dynamics by chemical inhibitors also significantly reduced the efficiency of early viral infection and intracellular HSV-1 replication (Pei et al., 2011; Xiang et al., 2012b; Spear et al., 2013; Yi et al., 2017). Thus, we firstly analyzed the possible effect of Hsp90 inhibitors on the F-actin of neuronal cells; cytochalasin B (Cyto B), an inhibitor of F-actin, was used to induce the depolymerization of existing actin filaments, and the results indicated that Hsp90 inhibitors promoted the polymerization of F-actin to prevent Cyto B-induced depolymerization with HSV-1 infection (**Figure 5A**). Next, F-actin was measured by flow cytometry as described previously (Li et al., 2019a). As shown in **Figure 5B**, Hsp90 inhibitors induced F-actin assembly in the presence of HSV-1 infection. Finally, the effect of Hsp90 inhibitors on F-actin with the stages of HSV-1 penetration was also analyzed (**Figure 5C**). These results indicated that Hsp90 inhibitors promoted F-actin polymerization to prevent HSV-1 from entering neuron cells.

## Hsp90 Inhibitors Lead to a Reduced Membrane Localization of Cofilin by Impairing Hsp90–Cofilin Interaction

Given Hsp90 is a molecular chaperone for folding, assembling, and stabilizing many client proteins, which is essential for these client proteins to perform their normal biological functions

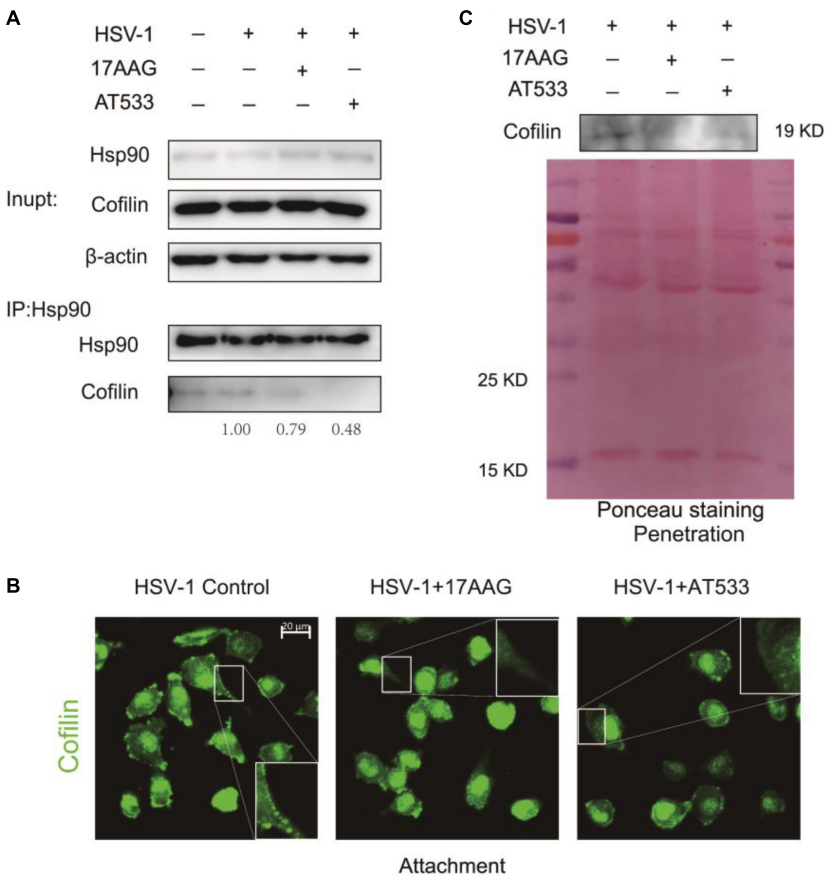


**FIGURE 6 |** Hsp90 inhibitors reduce cofilin cell membrane distribution. **(A)** The binding of Hsp90 to cofilin was reduced in the presence of Hsp90 inhibitors, and the whole-cell extracts were subjected to immunoprecipitation with Protein A/G magnetic beads, anti-Hsp90, and anti-cofilin for immunoprecipitation assay, and the samples were detected by Western blot assay. **(B)** Hsp90 inhibitors affected the intracellular localization of cofilin; SH-SY5Y cells were incubated for 1 h at 4°C, then infected with HSV-1 (MOI = 50) at 4°C for another 1 h in the presence of 17-AAG or AT533. The cells were then fixed and stained with anti-cofilin antibody (green). Scale bars, 20 μm, ×40. **(C)** Hsp90 inhibitors reduced the localization of cofilin protein levels on the cell membrane. SH-SY5Y cells were incubated for 1 h at 4°C and infected with HSV-1 (MOI = 50) at 4°C for another 1 h; the unbound virus was removed, then treated with 17-AAG or AT533 for 30 min at 37°C, and cells were washed with acidic PBS. The cell membrane proteins were extracted to detect the protein level of cofilin by Western blotting. Data are mean ± SD ($n$ = 3).

(Bravo-Cordero et al., 2013; Balin and Hudson, 2018), inhibition of Hsp90 function may result in the degradation or abnormal subcellular localization of client proteins (Prodromou, 2012). To clarify the reason why Hsp90 inhibitors facilitated F-actin polymerization, we analyzed the effect of Hsp90 inhibitors on the ADF/cofilin; the results of co-immunoprecipitation indicated that Hsp90 interacted with cofilin, and Hsp90 inhibitors led to a weakened interaction of cofilin (**Figure 6A**). However, Western blot assay showed that Hsp90 inhibitors did not affect the total amount of cofilin protein in the stage of HSV-1 attachment (**Supplementary Figures 6A,B**) or HSV-1 penetration **(Supplementary Figures 6C,D**).

We further examined the effect of Hsp90 inhibitors on the subcellular localization of cofilin during the HSV-1 infection. Immunofluorescence showed that the Hsp90 inhibitor affected the intracellular localization of cofilin, resulting in a significant decrease in the localization of cofilin at the cell edge (**Figure 6B**). Considering that actin filaments are mainly located on the area under the cell membrane, and cofilin is also located on the cell membrane and combines with F-actin to play a depolymerization effect (Nebl et al., 1996; Keezer et al., 2003), we extracted the cell membrane proteins to detect the level of cofilin, and the results confirmed that Hsp90 inhibitors cause a decrease in the level of cofilin on the cell membrane during the penetration stage of HSV-1 (**Figure 6C**), which may lead to the polymerization of F-actin, thereby inhibiting the entry of HSV-1 into neuron cells.

## DISCUSSION

HSE is the most common cause of sporadic fatal encephalitis worldwide (Whitley, 2006), and HSE shows the characteristics of high mortality and poor prognosis in all encephalitis, which is tightly associated with Herpes simplex virus 1 (HSV-1) infection of the neurons (Whitley et al., 1982; Whitley, 2006). Specifically, HSV-1 can spread from epithelial cells to neurons and cause pathological changes in the central nervous system (Wang et al., 2019). However, Hsp90 inhibitors have rarely reported their antiviral effects in neurons. This study demonstrated that Hsp90 inhibitors had antiviral activity against HSV-1 in nerve cell lines (**Figure 1**) and inhibited HSV-1 entry into neuronal cells (**Figure 4**). We consider that many viruses have evolved various methods of destroying the actin cytoskeleton to promote self-infection. For example, HIV and HSV-1 regulate the cofilin-mediated F-actin dynamic to facilitate virus entry (Yoder et al., 2008; Xiang et al., 2012b). The formation of pseudopods was beneficial to HSV-1 which adsorbs to the cell membrane, but the unidirectional polymerization of F-actin prevented HSV-1 penetration (Xiang et al., 2012b). We further examined the effect of Hsp90 inhibitors on ADF/cofilin. Specifically, both Western blotting assay and immunofluorescence experiments showed that Hsp90 inhibitors inhibited the molecular chaperone function of Hsp90 during HSV-1 infection, which reduced the subcellular localization of cofilin on the membrane to promote the assembly of actin structures (**Figure 6**). We hypothesize that the inhibition of HSV-1 penetration was a key rate-limiting step. Whether this phenomenon exists in non-neuronal cells remains to be further explored. It has been reported that geldanamycin, an Hsp90 inhibitor, has a significant inhibitory effect against HSV-1 in Vero cells (non-neural cells). Still, geldanamycin inhibits neither HSV-1 attachment nor penetration and mainly restrains HSV-1 replication *in vitro* (Li et al., 2004). However, in the enrichment of microfilament skeletons in synapses and dendritic spines in neuron cells, cofilin played an important role in the growth and development of nerves, including the formation of neurites, the directional growth of axons and dendrites, the formation of synapses, and the plasticity of neuronal cell dendritic spines (Sivadasan et al., 2016; Zheng et al., 2016; Tedeschi et al., 2019), which may be beneficial to Hsp90 inhibitors inhibiting the entry of HSV-1 into neuron cells by regulating cofilin-mediated F-actin reorganization.

In summary, this study demonstrated the effects of Hsp90 inhibitors 17-AAG and AT533 on HSV-1 infection of neuron cells. Specifically, we confirmed that Hsp90 inhibitors reduced membrane localization of cofilin by impairing Hsp90-cofilin interaction, which led to the unidirectional polymerization of F-actin. However, F-actin polymerization promoted viral attachment but inhibited subsequent viral penetration, which limited the entry of HSV-1 virions into neuron cells. Our research will provide a novel insight into the mechanism of Hsp90 inhibitors against HSV-1 and better extend the molecular mechanism of Hsp90 in HSV-1 infection in neuron cells.

## DATA AVAILABILITY STATEMENT

The original contributions presented in the study are included in the article/**Supplementary Material**, further inquiries can be directed to the corresponding author/s.

## ETHICS STATEMENT

The animal study was reviewed and approved by Medical Ethics Committee of Jinan University.

## AUTHOR CONTRIBUTIONS

XS, YLW, and FL conceived and designed the study. XS wrote the first draft of the manuscript. XS, WC, QZ, and JX developed and designed the methodology and specifically performed the experiments. SQ, ZW, JJ, and XH provided study materials. YLW commented or revised the manuscript. KL, ZR, and YFW were responsible for the management and coordination for the research activity planning and execution and acquisition of the financial support for the project leading to this publication. All authors have read and agreed to the published version of the manuscript.

## FUNDING

This work was supported by the Grants from the National Natural Science Foundation of China (Grant Nos. 81872908 and

82072274), the Science and Technology Program of Guangzhou, China (201604020178), the Youth Fund Project of China Natural Science Foundation (Grant No. 2020A1515110566), the Guangdong Natural Science Foundation (Grant No. 2019A1515010046), and the Science and Technology Foundation of Shenzhen (Grant No. JCYJ20200109144410181).

## SUPPLEMENTARY MATERIAL

The Supplementary Material for this article can be found online at: https://www.frontiersin.org/articles/10.3389/fmicb.2021.799890/full#supplementary-material

**Supplementary Figure 1 |** The cytotoxicity of Hsp90 inhibitors. **(A,B)** The cytotoxicity of Hsp90 inhibitors. SH-SY5Y and N2a cells were treated with different concentrations of 17AAG, AT533 for 24 h, and the cell survival was then calculated through CCK8 assay. Data are mean ± SD ($n$ = 3).

**Supplementary Figure 2 |** Simple diagram of HSV-1 attachment and penetration. **(A)** Cells were incubated for 1 h at 4°C, then infected with HSV-1 for another 1 h in the presence of 17AAG or AT533, and the unbound virus was removed after HSV-1 attachment **(B)** Cells were pre-cooled for 1 h at 4°C, then infected with HSV-1 for another 1h at 4°C. The unadsorbed viruses were removed, then the cells were treated with 17AAG or AT533 for indicated times at 37°C, and washed with acidic PBS to remove the viruses on cell membranes. All samples were collected to detect and analyze.

**Supplementary Figure 3 |** Hsp90 inhibitors pretreatment promoted HSV-1 attachment. SH-SY5Y cells were pretreated with 17AAG or AT533 for 1 h at 4°C, and washed with PBS to remove the inhibitors, then infected with HSV-1 (MOI = 20) in the absence of 17AAG and AT533 for another 1 h. Total DNA of HSV-1 was extracted for qRT-PCR analysis to detect the level of *UL47* gene. Data are mean ± SD ($n$ = 3). $^{**}P < 0.01$ versus HSV-1 control group.

**Supplementary Figure 4 |** The cell morphology of cortical neurons. **(A)** Primary cortical neurons were extracted from the cerebral cortex of C57BL/6J mice aged 1–2 days and cultured for 5 days *in vitro*, then the cell morphology was examined by an inverted microscope. Scale bars, 0.2 μm. **(B)** Primary cortical neurons of C57BL/6J mice were stained with anti-NeuN antibody (green) and DAPI (nucleus, blue), and the ratio of cortical neurons to total cells is shown (right). Scale bars, 50 μm. 20×. Data are mean ± SD ($n$ = 2).

**Supplementary Figure 5 |** The dynamic curve of HSV-1 penetration. SH-SY5Y and N2a cells were incubated for 1 h at 4°C, then infected with HSV-1 (MOI = 20) for another 1 h at 4°C in the presence of Hsp90 inhibitors, and all groups were shifted to 37°C, incubated for different times, then washed with acidic PBS. The total HSV-1 DNA was extracted for the qRT-PCR experiment to analyze the dynamic curve of HSV-1 penetration. Data are mean ± SD ($n$ = 3).

**Supplementary Figure 6 |** Hsp90 inhibitors do not affect the total amount of cofilin. **(A,B)** Hsp90 inhibitors did not alter cofilin protein levels at the stage of HSV-1 attachment. SH-SY5Y and N2a cells were incubated for 1 h at 4°C, then infected with HSV-1 (MOI = 50) for another 1 h in the presence of 17AAG or AT533. Then the unbound virus was removed, and the protein levels of cofilin were detected by Western blot. **(C,D)** Hsp90 inhibitors did not alter cofilin protein levels at the stage of HSV-1 penetration. SH-SY5Y and N2a cells were pre-cooled for 1 h at 4°C, then infected with HSV-1 (MOI = 50) for another 1h at 4°C. The unbound virus was removed, then cells were treated with 17AAG or AT533 for indicated times at 37°C, and washed with acidic PBS to remove the viruses on cell membranes, and the protein levels were detected by Western blot. Data are mean ± SD ($n$ = 3).

**Supplementary Table 1 |** List of Primers information for qRT-PCR in this research.

**Supplementary Table 2 |** The sequence of siRNAs used in this study.

## REFERENCES

Azab, W., and Osterrieder, K. (2017). "Initial contact: the first steps in herpesvirus entry," in *Cell Biology of Herpes Viruses*, ed. K. Osterrieder (Cham: Springer), 1–27. doi: 10.1007/978-3-319-53168-7_1

Balin, B. J., and Hudson, A. P. (2018). Herpes viruses and Alzheimer's disease: new evidence in the debate. *Lancet Neurol.* 17, 839–841. doi: 10.1016/S1474-4422(18)30316-8

Bravo-Cordero, J. J., Magalhaes, M. A., Eddy, R. J., Hodgson, L., and Condeelis, J. (2013). Functions of cofilin in cell locomotion and invasion. *Nat. Rev. Mol. Cell Biol.* 14, 405–415. doi: 10.1038/nrm3609

Buchner, J., and Li, J. (2013). Structure, function and regulation of the hsp90 machinery. *Biomed. J.* 36:106. doi: 10.4103/2319-4170.113230

Burch, A. D., and Weller, S. K. (2005). Herpes simplex virus type 1 DNA polymerase requires the mammalian chaperone hsp90 for proper localization to the nucleus. *J. Virol.* 79, 10740–10749. doi: 10.1128/JVI.79.16.10740-10749.2005

Eimer, W. A., Kumar, D. K. V., Shanmugam, N. K. N., Rodriguez, A. S., Mitchell, T., Washicosky, K. J., et al. (2018). Alzheimer's disease-associated β-amyloid is rapidly seeded by herpesviridae to protect against brain infection. *Neuron* 99, 56–63.e3. doi: 10.1016/j.neuron.2018.06.030

Favoreel, H. W., Enquist, L. W., and Feierbach, B. (2007). Actin and Rho GTPases in herpesvirus biology. *Trends Microbiol.* 15, 426–433. doi: 10.1016/j.tim.2007.08.003

Grinde, B. (2013). Herpesviruses: latency and reactivation–viral strategies and host response. *J. Oral Microbiol.* 5:22766. doi: 10.3402/jom.v5i0.22766

Hu, W., Zhu, L., Yang, X., Lin, J., and Yang, Q. (2016). The epidermal growth factor receptor regulates cofilin activity and promotes transmissible gastroenteritis virus entry into intestinal epithelial cells. *Oncotarget* 7:12206. doi: 10.18632/oncotarget.7723

Ibáñez, F. J., Farías, M. A., Gonzalez-Troncoso, M. P., Corrales, N., Duarte, L. F., Retamal-Díaz, A., et al. (2018). Experimental dissection of the lytic replication cycles of herpes simplex viruses *in vitro*. *Front. Microbiol.* 9:2406. doi: 10.3389/fmicb.2018.02406

Ju, H.-Q., Xiang, Y.-F., Xin, B.-J., Pei, Y., Lu, J.-X., Wang, Q.-L., et al. (2011). Synthesis and *in vitro* anti-HSV-1 activity of a novel Hsp90 inhibitor BJ-B11. *Bioorgan. Med. Chem. Lett.* 21, 1675–1677. doi: 10.1016/j.bmcl.2011.01.098

Keezer, S. M., Ivie, S. E., Krutzsch, H. C., Tandle, A., Libutti, S. K., and Roberts, D. D. (2003). Angiogenesis inhibitors target the endothelial cell cytoskeleton through altered regulation of heat shock protein 27 and cofilin. *Cancer Res.* 63, 6405–6412.

Kellermayer, M. S., and Csermely, P. (1995). ATP induces dissociation of the 90-kDa heat shock protein (hsp90) from F-actin: interference with the binding of heavy meromyosin. *Biochem. Biophys. Res. Commun.* 211, 166–174. doi: 10.1006/bbrc.1995.1792

Lafaille, F. G., Harschnitz, O., Lee, Y. S., Zhang, P., Hasek, M. L., Kerner, G., et al. (2019). Human SNORA31 variations impair cortical neuron-intrinsic immunity to HSV-1 and underlie herpes simplex encephalitis. *Nat. Med.* 25, 1873–1884. doi: 10.1038/s41591-019-0672-3

Li, F., Jin, F., Wang, Y., Zheng, D., Liu, J., Zhang, Z., et al. (2018). Hsp90 inhibitor AT-533 blocks HSV-1 nuclear egress and assembly. *J. Biochem.* 164, 397–406. doi: 10.1093/jb/mvy066

Li, F., Song, X., Su, G., Wang, Y., Wang, Z., Jia, J., et al. (2019a). Amentoflavone inhibits HSV-1 and ACV-resistant strain infection by suppressing viral early infection. *Viruses* 11:466. doi: 10.3390/v11050466

Li, F., Song, X., Su, G., Wang, Y., Wang, Z., Qing, S., et al. (2019b). AT-533, a Hsp90 inhibitor, attenuates HSV-1-induced inflammation. *Biochem. Pharmacol.* 166, 82–92. doi: 10.1016/j.bcp.2019.05.003

Li, Y.-H., Tao, P.-Z., Liu, Y.-Z., and Jiang, J.-D. (2004). Geldanamycin, a ligand of heat shock protein 90, inhibits the replication of herpes simplex virus type 1 *in vitro*. *Antimicrob. Agents Chemother.* 48, 867–872. doi: 10.1128/AAC.48.3.867-872.2004

Marcocci, M. E., Napoletani, G., Protto, V., Kolesova, O., Piacentini, R., Li Puma, D. D., et al. (2020). Herpes simplex virus-1 in the brain: the dark side of a sneaky infection. *Trends Microbiol.* 28, 808–820. doi: 10.1016/j.tim.2020.03.003

Meng, T., Cao, Q., Lei, P., Bush, A. I., Xiang, Q., Su, Z., et al. (2017). Tat-haFGF(14-154) upregulates ADAM10 to attenuate the Alzheimer phenotype of APP/PS1 mice through the PI3K-CREB-IRE1α/XBP1 pathway. *Mol. Ther. Nucleic Acids* 7, 439–452. doi: 10.1016/j.omtn.2017.05.004

Miranda-Saksena, M., Denes, C. E., Diefenbach, R. J., and Cunningham, A. L. (2018). Infection and transport of herpes simplex virus type 1 in neurons: role of the cytoskeleton. *Viruses* 10:92. doi: 10.3390/v10020092

Naranatt, P. P., Akula, S. M., Zien, C. A., Krishnan, H. H., and Chandran, B. (2003). Kaposi's sarcoma-associated herpesvirus induces the phosphatidylinositol 3-kinase-PKC-ζ-MEK-ERK signaling pathway in target cells early during infection: implications for infectivity. *J. Virol.* 77, 1524–1539. doi: 10.1128/JVI.77.2.1524-1539.2003

Ndozangue-Touriguine, O., Hamelin, J., and Bréard, J. (2008). Cytoskeleton and apoptosis. *Biochem. Pharmacol.* 76, 11–18. doi: 10.1016/j.bcp.2008.03.016

Nebl, G., Meuer, S. C., and Samstag, Y. (1996). Dephosphorylation of serine 3 regulates nuclear translocation of cofilin. *J. Biol. Chem.* 271, 26276–26280. doi: 10.1074/jbc.271.42.26276

Pei, Y., Xiang, Y.-F., Chen, J.-N., Lu, C.-H., Hao, J., Du, Q., et al. (2011). Pentagalloylglucose downregulates cofilin1 and inhibits HSV-1 infection. *Antiviral Res.* 89, 98–108. doi: 10.1016/j.antiviral.2010.11.012

Piret, J., and Boivin, G. (2020). Immunomodulatory strategies in herpes simplex virus Encephalitis. *Clin. Microbiol. Rev.* 33:e00105-19. doi: 10.1128/CMR.00105-19

Pollard, T. D., and Cooper, J. A. (2009). Actin, a central player in cell shape and movement. *Science* 326, 1208–1212. doi: 10.1126/science.1175862

Prodromou, C. (2012). The 'active life' of Hsp90 complexes. *Biochim. Biophys. Acta Mol. Cell Res.* 1823, 614–623. doi: 10.1016/j.bbamcr.2011.07.020

Schopf, F. H., Biebl, M. M., and Buchner, J. (2017). The HSP90 chaperone machinery. *Nat. Rev. Mol. Cell Biol.* 18, 345–360. doi: 10.1038/nrm.2017.20

Sens, P., and Plastino, J. (2015). Membrane tension and cytoskeleton organization in cell motility. *J. Phys. Condens. Matter* 27:273103. doi: 10.1088/0953-8984/27/27/273103

Sivadasan, R., Hornburg, D., Drepper, C., Frank, N., Jablonka, S., Hansel, A., et al. (2016). C9ORF72 interaction with cofilin modulates actin dynamics in motor neurons. *Nat. Neurosci.* 19, 1610–1618. doi: 10.1038/nn.4407

Southwick, F. S. (2000). Gelsolin and ADF/cofilin enhance the actin dynamics of motile cells. *Proc. Natl. Acad. Sci. U.S.A.* 97, 6936–6938. doi: 10.1073/pnas.97.13.6936

Spear, M., Guo, J., and Wu, Y. (2013). Novel anti-HIV therapeutics targeting chemokine receptors and actin regulatory pathways. *Immunol. Rev.* 256, 300–312. doi: 10.1111/imr.12106

Stahl, J. P., Mailles, A., and De Broucker, T. (2012). Herpes simplex encephalitis and management of acyclovir in encephalitis patients in France. *Epidemiol. Infect.* 140, 372–381. doi: 10.1017/s0950268811000483

Taiyab, A., and Rao, C. M. (2011). HSP90 modulates actin dynamics: inhibition of HSP90 leads to decreased cell motility and impairs invasion. *Biochim. Biophys. Acta Mol. Cell Res.* 1813, 213–221. doi: 10.1016/j.bbamcr.2010.09.012

Taylor, M. P., Koyuncu, O. O., and Enquist, L. W. (2011). Subversion of the actin cytoskeleton during viral infection. *Nat. Rev. Microbiol.* 9, 427–439. doi: 10.1038/nrmicro2574

Tedeschi, A., Dupraz, S., Curcio, M., Laskowski, C. J., Schaffran, B., Flynn, K. C., et al. (2019). ADF/cofilin-mediated actin turnover promotes axon regeneration in the adult CNS. *Neuron* 103, 1073–1085.e6. doi: 10.1016/j.neuron.2019.07.007

Tzeng, N.-S., Chung, C.-H., Lin, F.-H., Chiang, C.-P., Yeh, C.-B., Huang, S.-Y., et al. (2018). Anti-herpetic medications and reduced risk of dementia in patients with herpes simplex virus infections—a nationwide, population-based cohort study in Taiwan. *Neurotherapeutics* 15, 417–429. doi: 10.1007/s13311-018-0611-x

Van den Broeke, C., Jacob, T., and Favoreel, H. W. (2014). Rho'ing in and out of cells: viral interactions with Rho GTPase signaling. *Small GTPases* 5:e28318. doi: 10.4161/sgtp.28318

Wang, Y., Huang, L., Wang, Y., Luo, W., Li, F., Xiao, J., et al. (2020a). Single-cell RNA-sequencing analysis identifies host long noncoding RNA MAMDC2-AS1 as a co-factor for HSV-1 nuclear transport. *Int. J. Biol. Sci.* 16, 1586–1603. doi: 10.7150/ijbs.42556

Wang, Y., Song, X., Wang, Y., Huang, L., Luo, W., Li, F., et al. (2020b). Dysregulation of cofilin-1 activity-the missing link between herpes simplex virus type-1 infection and Alzheimer's disease. *Crit. Rev. Microbiol.* 46, 381–396. doi: 10.1080/1040841x.2020.1794789

Wang, Y., Jia, J., Wang, Y., Li, F., Song, X., Qin, S., et al. (2019). Roles of HSV-1 infection-induced microglial immune responses in CNS diseases: friends or foes? *Crit. Rev. Microbiol.* 45, 581–594. doi: 10.1080/1040841x.2019.1660615

Wang, Y., Jin, F., Wang, R., Li, F., Wu, Y., Kitazato, K., et al. (2017). HSP90: a promising broad-spectrum antiviral drug target. *Arch. Virol.* 162, 3269–3282. doi: 10.1007/s00705-017-3511-1

Whitley, R. J. (2006). Herpes simplex encephalitis: adolescents and adults. *Antiviral Res.* 71, 141–148. doi: 10.1016/j.antiviral.2006.04.002

Whitley, R. J., Soong, S.-J., Linneman, C., Liu, C., Pazin, G., and Alford, C. A. (1982). Herpes simplex encephalitis: clinical assessment. *JAMA* 247, 317–320. doi: 10.1001/jama.1982.03320280037026

Wioland, H., Guichard, B., Senju, Y., Myram, S., Lappalainen, P., Jégou, A., et al. (2017). ADF/cofilin accelerates actin dynamics by severing filaments and promoting their depolymerization at both ends. *Curr. Biol.* 27, 1956–1967.e7. doi: 10.1016/j.cub.2017.05.048

Xiang, Y.-F., Qian, C.-W., Xing, G.-W., Hao, J., Xia, M., and Wang, Y.-F. (2012a). Anti-herpes simplex virus efficacies of 2-aminobenzamide derivatives as novel HSP90 inhibitors. *Bioorgan. Med. Chem. Lett.* 22, 4703–4706. doi: 10.1016/j.bmcl.2012.05.079

Xiang, Y., Zheng, K., Ju, H., Wang, S., Pei, Y., Ding, W., et al. (2012b). Cofilin 1-mediated biphasic F-actin dynamics of neuronal cells affect herpes simplex virus 1 infection and replication. *J. Virol.* 86, 8440–8451. doi: 10.1128/JVI.00609-12

Yi, F., Guo, J., Dabbagh, D., Spear, M., He, S., Kehn-Hall, K., et al. (2017). Discovery of novel small-molecule inhibitors of LIM domain kinase for inhibiting HIV-1. *J. Virol.* 91:e02418-16. doi: 10.1128/JVI.02418-16

Yoder, A., Yu, D., Dong, L., Iyer, S. R., Xu, X., Kelly, J., et al. (2008). HIV envelope-CXCR4 signaling activates cofilin to overcome cortical actin restriction in resting CD4 T cells. *Cell* 134, 782–792. doi: 10.1016/j.cell.2008.06.036

Zheng, K., Kitazato, K., Wang, Y., and He, Z. (2016). Pathogenic microbes manipulate cofilin activity to subvert actin cytoskeleton. *Crit. Rev. Microbiol.* 42, 677–695.

Zheng, K., Xiang, Y., Wang, X., Wang, Q., Zhong, M., Wang, S., et al. (2014). Epidermal growth factor receptor-PI3K signaling controls cofilin activity to facilitate herpes simplex virus 1 entry into neuronal cells. *mBio* 5:e00958-13. doi: 10.1128/mBio.00958-13

Zhong, M., Zheng, K., Chen, M., Xiang, Y., Jin, F., Ma, K., et al. (2014). Heat-shock protein 90 promotes nuclear transport of herpes simplex virus 1 capsid protein by interacting with acetylated tubulin. *PLoS One* 9:e99425. doi: 10.1371/journal.pone.0099425

**Conflict of Interest:** The authors declare that the research was conducted in the absence of any commercial or financial relationships that could be construed as a potential conflict of interest.

**Publisher's Note:** All claims expressed in this article are solely those of the authors and do not necessarily represent those of their affiliated organizations, or those of the publisher, the editors and the reviewers. Any product that may be evaluated in this article, or claim that may be made by its manufacturer, is not guaranteed or endorsed by the publisher.

*Copyright © 2022 Song, Wang, Li, Cao, Zeng, Qin, Wang, Jia, Xiao, Hu, Liu, Wang and Ren. This is an open-access article distributed under the terms of the Creative Commons Attribution License (CC BY). The use, distribution or reproduction in other forums is permitted, provided the original author(s) and the copyright owner(s) are credited and that the original publication in this journal is cited, in accordance with accepted academic practice. No use, distribution or reproduction is permitted which does not comply with these terms.*

frontiers in Microbiology

ORIGINAL RESEARCH
published: 21 January 2022
doi: 10.3389/fmicb.2022.839845

# A Recombinant Porcine Reproductive and Respiratory Syndrome Virus Stably Expressing DsRed Protein Based on Bacterial Artificial Chromosome System

*Na Li[1], Yiyi Zhang[1], Lunguang Yao[1], Yunpeng Shi[2], Qin Zhao[3], Baicheng Huang[4]* and Yani Sun[3]**

[1] Key Laboratory of Ecological Security, Collaborative Innovation Centre of Water Security for Water Source Region of Mid-line of South-to-North Diversion Project of Henan Province, Henan Provincial Engineering and Technology Center of Health Products for Livestock and Poultry, School of Life Sciences and Agricultural Engineering, Nanyang Normal University, Nanyang, China, [2] Shijiazhuang Customs (Huanghua Port), Cangzhou, China, [3] College of Veterinary Medicine, Northwest A&F University, Yangling, China, [4] National Research Center for Veterinary Medicine, Luoyang, China

OPEN ACCESS

**Edited by:**
Chunfu Zheng,
University of Calgary, Canada

**Reviewed by:**
Bin Li,
Jiangsu Academy of Agricultural Sciences (JAAS), China
Gaopeng Hou,
Washington University School of Medicine in St. Louis, United States

***Correspondence:**
Baicheng Huang
hbch228@163.com
Yani Sun
sunyani@nwsuaf.edu.cn

**Specialty section:**
This article was submitted to Virology, a section of the journal Frontiers in Microbiology

**Received:** 20 December 2021
**Accepted:** 03 January 2022
**Published:** 21 January 2022

**Citation:**
Li N, Zhang Y, Yao L, Shi Y, Zhao Q, Huang B and Sun Y (2022) A Recombinant Porcine Reproductive and Respiratory Syndrome Virus Stably Expressing DsRed Protein Based on Bacterial Artificial Chromosome System. Front. Microbiol. 13:839845. doi: 10.3389/fmicb.2022.839845

Recombinant viruses possessing reporter proteins as tools are widely applied in investigating viral biology because of the convenience for observation. Previously, we generated a recombinant pathogenic porcine reproductive and respiratory syndrome virus (PRRSV) with enhanced green fluorescent protein (EGFP) reporter for monitoring virus spread and screening of neutralizing antibodies. PRRSV with different kinds of reporters can support more application scenarios. Here, we described a new genetically stable infectious clones of a highly pathogenic PRRSV (HP-PRRSV) harboring the DsRed (a red fluorescent protein isolated from the coral *Discosoma*) gene. In the recombinant infectious clone, the transcription regulatory sequence 2 (TRS2) of PRRSV was inserted between the open reading frame 7 (ORF7) and 3′UTR to drive the transcription of DsRed gene, which makes it a separate transcription unit in the viral genome. Using the bacterial artificial chromosome (BAC) system and cytomegalovirus (CMV) promoter, the recombinant HP-PRRSV with the DsRed insertion was successfully rescued and showed similar growth and replication patterns compared with the wild-type virus in the MARC-145 cells. In addition, the DsRed protein was stably expressed in the recombinant virus for at least 10 passages with consistent fluorescence intensity and density. Using the recombinant HP-PRRSV with DsRed protein, the virus tracking in MARC-145 was observed by live-cell imaging. Meanwhile, quantification of the DsRed fluorescence positive cells by flow cytometry provides an alternative to standard methods for testing the level of PRRSV infection. This recombinant PRRSV with DsRed fluorescence protein expression could be a useful tool for fundamental research on the viral biology and shows the new design for stable expression of foreign genes in PRRSV.

**Keywords: HP-PRRSV, DsRed, bacterial artificial chromosome, transcription regulatory sequence, reporter**

## INTRODUCTION

Porcine reproductive and respiratory syndrome (PRRS) is a widespread disease affecting domestic pigs, first reported in North America and Europe in the late 1980s (Wensvoort et al., 1991; Albina, 1997). The symptoms of PRRS include reproductive failure, pneumonia, and increased susceptibility to secondary bacterial infection. The causative agent of PRRS is the PRRS virus (PRRSV), which is in the *Arteriviridae* family of the order *Nidovirales*. PRRSV is an enveloped, single-stranded positive-sense RNA virus of approximately 15 kb in length that contains 9 open reading frames (ORFs) (Fang and Snijder, 2010). Two distinct viral genotypes of PRRSV are North American type and European type, only shared the genome identity by approximately 60%. In the early 2000s, the outbreak of highly pathogenic PRRS (HP-PRRS) inflicted serious economic losses, which characterized by high-grade fever with increased mortality in pigs of all ages (Tian et al., 2007). The modified attenuated and killed vaccines have been wildly used in the field (Charerntantanakul, 2012). However, there is no remarkably effective vaccine for controlling PRRSV infection in pigs.

In the past decade, reverse genetics technology was applied to many RNA viruses to generate recombinant mutant viruses for virology and biology studies (Racaniello and Baltimore, 1981; Bernstein et al., 1986; Gonzalez et al., 2002; Almazan et al., 2006; St-Jean et al., 2006; Park et al., 2012; Amarilla et al., 2021; Nouda et al., 2021). Many infectious clones of different PRRSV strains have been constructed, including North American and European type strains (Nielsen et al., 2003; Truong et al., 2004; Fang et al., 2006; Zhang et al., 2011; Sang et al., 2012; Wang et al., 2013). In various rescue systems, the bacterial artificial chromosomes (BAC) have the advantages of large antigen-capacity, high fidelity in replication, and the easier procedures of manipulation, which was applied both in DNA (Messerle et al., 1997; Borst et al., 1999; Suter et al., 1999; Kanda et al., 2004) and RNA virus (Almazan et al., 2000; Almazan et al., 2006; Wang et al., 2013). The reverse genetics technology with fluorescence protein insertion is a common strategy for recombinant virus labeling, which gives an intuitive convenience for virus observation by fluorescence microscopy or flow cytometer. The application of fluorescence proteins in virus labeling mainly focuses on the enhanced green fluorescent protein (EGFP). Previously, we generated a recombinant PRRSV with EGFP expression, and the transcription regulatory sequence for ORF6 (TRS6) was inserted between the ORF7 and 3′UTR to drive the transcription of the EGFP (Wang et al., 2013). The results showed that the recombinant PRRSV with EGFP was a useful tool for neutralizing antibodies screening. However, to study the real-time interaction of various proteins, it is necessary to achieve multi-fluorescence labeling for live-cell imaging (Wolff et al., 2006; Strickfaden et al., 2010; Behrens et al., 2017).

In this study, to produce a differentiated recombinant PRRSV for fluorescence capture, we developed an HP-PRRS virus (HP-PRRSV) infectious clone with a red fluorescence protein of DsRed (a red fluorescent protein isolated from the coral *Discosoma*) based on BAC system. The DsRed gene was inserted between the ORF7 gene and the 3′UTR region of the PRRSV genome and transcripted by TRS2 (the sequence length of TRS2 is shorter than that of TRS6). The expression levels and stability of the DsRed in the rescued recombinant PRRSV were investigated, in addition, the virus tracking in MARC-145 and the quantification of the DsRed fluorescence positive cells by flow cytometry were also studied.

## MATERIALS AND METHODS

### Plasmid and Cell Lines

The PRRSV infectious clone plasmid pBAC-SD16$^{FL}$-AM containing the whole viral genome derived from the HP-PRRSV strain (SD16 strain, GenBank: JX087437) was constructed based on the results on previous descriptions (Wang et al., 2013). MARC-145 cell line, derived from the embryonic African green monkey kidney cell line (MA-104), was cultured in the Dulbecco's modified Eagle's medium (DMEM) supplemented with 10% fetal bovine serum (FBS) (HyClone, South Logan, UT, United States) at 37°C in a 5% $CO_2$ incubator.

### Plasmid Construction With DsRed Gene Insertion

The plasmid with DsRed gene insertion was constructed as previously described (Wang et al., 2013). Briefly, the DsRed gene was amplified from pDsRed-Express-N1 Vector (Clontech, CA, United States) with primers 5′-GCGATCGC *TTGAACCAACTTTAGGCCTGAATTGAA*ATGGCCTCCTCCG AGGC-3′ (the *Asi*SI site is underlined and TRS2 sequence is in italics), and 5′-CAGCCCACGACGCGTCGCTACAGGAA CAGGTGGTG-3′ (the *Mlu*I site is underlined) by polymerase chain reaction (PCR). The amplified product was inserted into the pEasy$^{TM}$-blunt simple cloning vector to generate plasmids pEasy-TRS2-DsRed. After sequencing, the positive plasmids containing TRS2-DsRed genes and pBAC-SD16$^{FL}$-AM were digested with *Asi*SI and *Mlu*I, and then the digested products were ligated to generate plasmid pBAC-SD16$^{FL}$-TRS2-DsRed. The design of the recombinant PRRSV infection clone is shown in **Figure 1A**. The recombinant plasmid was identified by sequencing. Finally, the positive plasmid was extracted with the QIAfilter Plasmid Midi Kit (QIAGEN, Hilden, Germany) and transfected into MARC-145 cells.

### Transfection and Rescue of Recombinant Viruses

The recombinant PRRSV carrying DsRed was rescued according to the method in previous report (Wang et al., 2013). Briefly, MARC-145 cells in a 6-well plate (80% confluent) were transfected with the plasmids pBAC-SD16$^{FL}$-TRS2-DsRed using Attractene Transfection Reagent (QIAGEN, Hilden, Germany) following the manufacturers' instructions. After 2 days of incubation at 37°C and 5% $CO_2$, the cytopathic effect (CPE) in cells were checked daily, and the fluorescence was captured when the CPE was found. In addition, the culture supernatants from the transfected cells were used to infect MARC-145 cells to

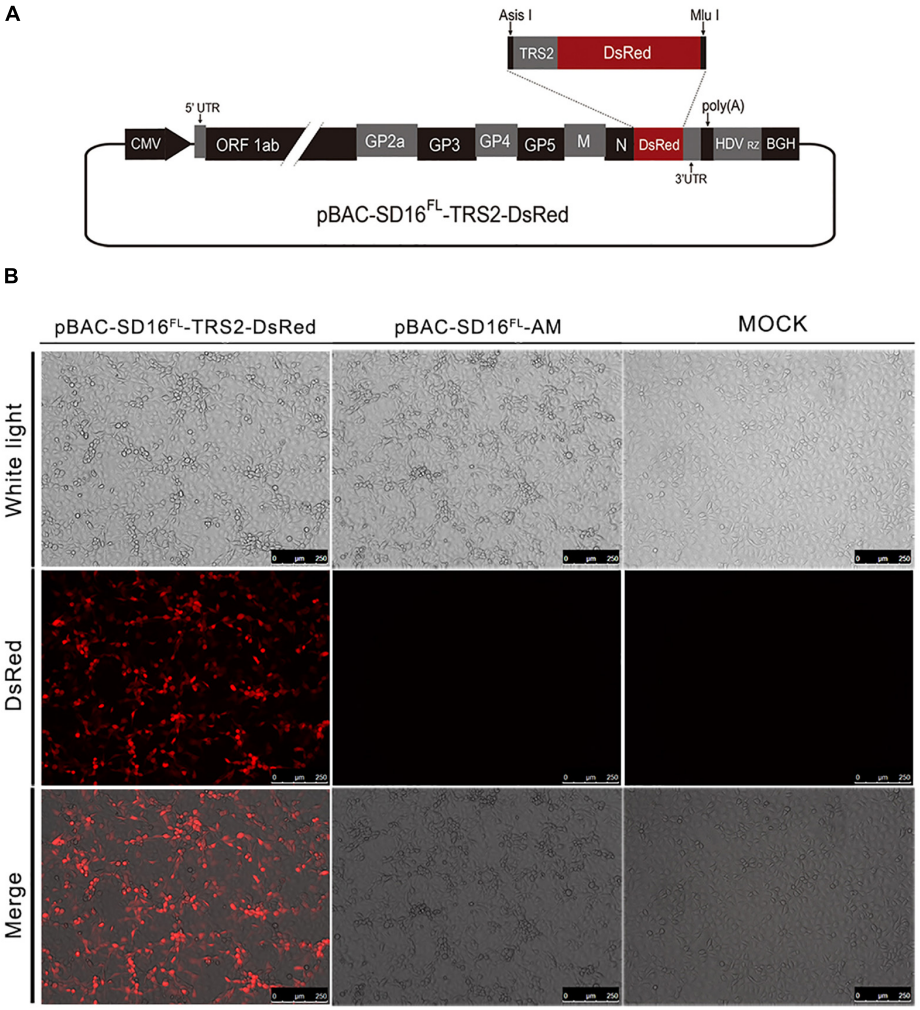


**FIGURE 1 |** Plasmid construction of pBAC-SD16$^{FL}$-TRS2-DsRed and DsRed expression in MARC-145 cells after transfection. **(A)** The DsRed gene was flanked by the transcription regulatory sequence 2 (TRS2) at the 5′end was inserted into plasmid pBAC-SD16$^{FL}$-AM to produce plasmid pBAC-SD16$^{FL}$-TRS2- DsRed using sites of *Asi*SI and *Mlu*I; **(B)** MARC-145 cells transfected with pBAC-SD16$^{FL}$-TRS2-DsRed or pBAC-SD16$^{FL}$-AM in a 6-well plate, after 48 h post-transfection, the fluorescence pictures in the live cells were captured by fluorescence microscopy.

propagate the rescued virus. The rescued viruses were confirmed by sequencing. The rescued virus was named rSD16/TRS2-DsRed.

## Immunofluorescence Assays

MARC-145 cells were cultured on glass coverslips in a 24-well plate and were infected with SD16 or rSD16/TRS2-DsRed (3rd passage) at a multiplicity of infection (MOI) of 0.01 for 48 h. Cells were fixed with 4% formaldehyde for 30 min at room temperature (RT) and permeabilized with 0.5% Triton X-100 in phosphate-buffered saline (PBS) for 10 min. Then, the cells were incubated with monoclonal antibody (mAb) against PRRSV nucleocapsid (N) protein (6D10) for 1 h at room temperature as previously described (Li et al., 2016). After that, the cells were still incubated with Alexa Fluor® 488 AffiniPure Goat Anti-Mouse IgG (Jackson, West Grove, PA, United States) for 1 h at RT. Finally, the cells were stained with 4-6-diamidino-2-phenylindole (DAPI) for 5 min at RT. Images were taken by Leica microscope. Mock-infected MARC-145 cells were used as controls.

## Western Blotting

MARC-145 cells were infected with SD16 or rSD16/TRS2-DsRed (3rd passage) at an MOI of 0.01. When 60% of the cells showed CPE, the infected cells were collected and lysed. The cellular proteins were separated by SDS-PAGE and transferred on a polyvinylidene difluoride (PVDF) membrane. The membrane was incubated with anti-α-Tubulin antibody (Sigma-Aldrich, MO, United States), mouse anti-DsRed mAb (Santa Cruz Biotechnology, United States) and 6D10 mAb overnight at 4°C. And then, it was incubated with peroxidase-conjugated goat anti-mouse IgG (Jackson, PA, United States) for 1 h at RT. Immuno-stained proteins were visualized using ECL Western Blotting Substrate (Pierce, CA, United States). Cellular proteins from mock-infected MARC-145 cells were used as controls.

## Imaging of Porcine Reproductive and Respiratory Syndrome Virus With DsRed Expression

MARC-145 cells were grown on a 35 mm cell culture dish to a density of 50–70% confluence and then infected with rSD16/TRS2-DsRed (MOI: 0.1) of different passages. After 1 h post-infection (hpi), the medium was removed and replaced with 2 mL of pre-warmed DMEM containing 3% FBS. The dish was placed at 37°C with 5% $CO_2$. The fluorescence of different passages of rSD16/TRS2-DsRed was captured by Leica microscope at 36 hpi. In live-cell imaging, MARC-145 cells were infected with rSD16/TRS2/DsRed at an MOI of 0.01 in a 35 mm cell culture dish. At 1 hpi, the medium was removed and replaced with 2 ml of pre-warmed DMEM containing 3% FBS. The dish was placed in the 37°C observation chamber containing 5% $CO_2$ (Leica CTR-Controller 3700, Wetzlar, Germany). DsRed signals and phase-contrast images were captured with the time interval of 1 min for 3 h by a live-cell station (Leica AF6000, Wetzlar, Germany). Subsequently, images were processed into a movie of 10 frames s-1 using QuickTime Pro.

## Determination of Growth Curves for Recombinant Porcine Reproductive and Respiratory Syndrome Virus

Recombinant virus rSD16/TRS2-DsRed was propagated in MARC-145 cells with an MOI of 1.0. The growth curves of rSD16/TRS2-DsRed and parental virus SD16 were compared. Briefly, 1 h after virus adsorption, MARC-145 cells were washed three times with PBS and incubated in DMEM with 3% FBS at 37°C, 5% $CO_2$. The supernatants were collected at various time points (12, 24, 36, 48, 60, and 72 hpi), and viral titers were calculated based on the $TCID_{50}$ data (Calculate by *Reed-Muench* method).

## Polymerase Chain Reaction Analysis of Viral RNA Isolation and Reverse Transcription

To determine the mRNA production of the DsRed gene in different passages, the viral RNA of rSD16/TRS2-DsRed (passages 1, 3, 5, 7, and 9) was extracted from supernatants of culture medium with the RNAiso Plus (Takara, Dalian, China) and then reverse-transcribed into cDNAs with M-MLV reverse transcriptase (Takara, Dalian, China). The target PCR fragments were amplified using the primer pairs of 5′-ATACTGTGCGCCTGATCCGC-3′ (located in the 3′ end of N protein) and 5′- TCGCCAATTAAACTTTACCCCCACA-3′ (located in the 5′ end of 3′UTR region).

# RESULTS

## Rescue of rSD16/Transcription Regulatory Sequence 2-DsRed

A vector pBAC-SD16$^{FL}$-AM with *Asi*SI and *Mlu*I sites between the ORF7 gene and the 3′UTR region of the viral genome was used to construct PRRSV infectious clone with DsRed. The DsRed gene was flanked by the unique *Asi*SI and *Mlu*I sites for its insertion into the plasmid pBAC-SD16$^{FL}$-AM, and its expression was driven by the transcription-regulating sequence of gene GP2a (TRS2) (**Figure 1A**). An apparent DsRed fluorescence was observed in the MARC-145 cells after transfection with pBAC-SD16$^{FL}$-TRS2-DsRed (**Figure 1B**), which means the successful expression of indictor protein.

## Replication Properties of Recombinant Viruses

The expression of DsRed and PRRSV N protein in MARC-145 cells infected with rSD16/TRS2-DsRed were identified by western blot using anti-DsRed and anti-PRRSV N protein mAbs as primary antibodies. As shown in **Figure 2A**, DsRed and PRRSV N protein were detected in rSD16/TRS2-DsRed infected cells, and DsRed was not detected in SD16-infected or normal MARC-145 cells. PRRSV N protein was also detected in virus-infected cells by immunofluorescence assays but not in the normal cells (**Figure 2C**). The replication ability of the recombinant virus with DsRed insertion was also compared by growth curves of SD16 and rSD16/TRS2-DsRed in MARC-145 cells. The supernatant of the culture medium of rSD16/TRS2-DsRed and the parental virus were collected at 12, 24, 36, 48, and 60 hpi, respectively. The viral titers were examined at the indicated time points. As shown in **Figure 2B**, the growth kinetics of recombinant PRRSV rSD16/TRS2-DsRed was not significantly different from the parental virus, and the titers peaked at 48 hpi for both viruses.

## Stability of DsRed Expression in Recombinant Viruses

The recombinant viruses were passaged in MARC-145 cells for at least 10 passages to investigate the stability of DsRed expression. As visualized by fluorescence microscopy, positive cells exhibited a sustained red fluorescence at different passages (**Figure 3A**). The viral titers of the recombinant virus in different passages were also detected by the $TCID_{50}$ method. As shown in **Figure 3B**, no significant changes of the viral titers were found in different passages. Furthermore, the presence of the DsRed gene in the viral genome was identified by RT-PCR. As shown in **Figure 3C**, all fragments were consistent with the expected length of about 750 bp. In addition, the PCR products were also sequenced, and the results showed no mutations in the DsRed gene (data not shown).

## Intercellular Spread of rSD16/Transcription Regulatory Sequence 2/DsRed

Live-cell imaging was performed in recombinant virus-infected MARC-145 cells to determine whether the rSD16/TRS2/DsRed could be used as a reporter virus. As shown in **Supplementary Movie 1**, the DsRed fluorescent in the recombinant virus-infected cells could be observed at approximately 24 hpi, and the fluorescence is distributed evenly in the cells. We also found that the DsRed fluorescence could be transported along intercellular connecting nanotube to neighboring cells. These results suggested that the recombinant PRRSV rSD16/TRS2/DsRed

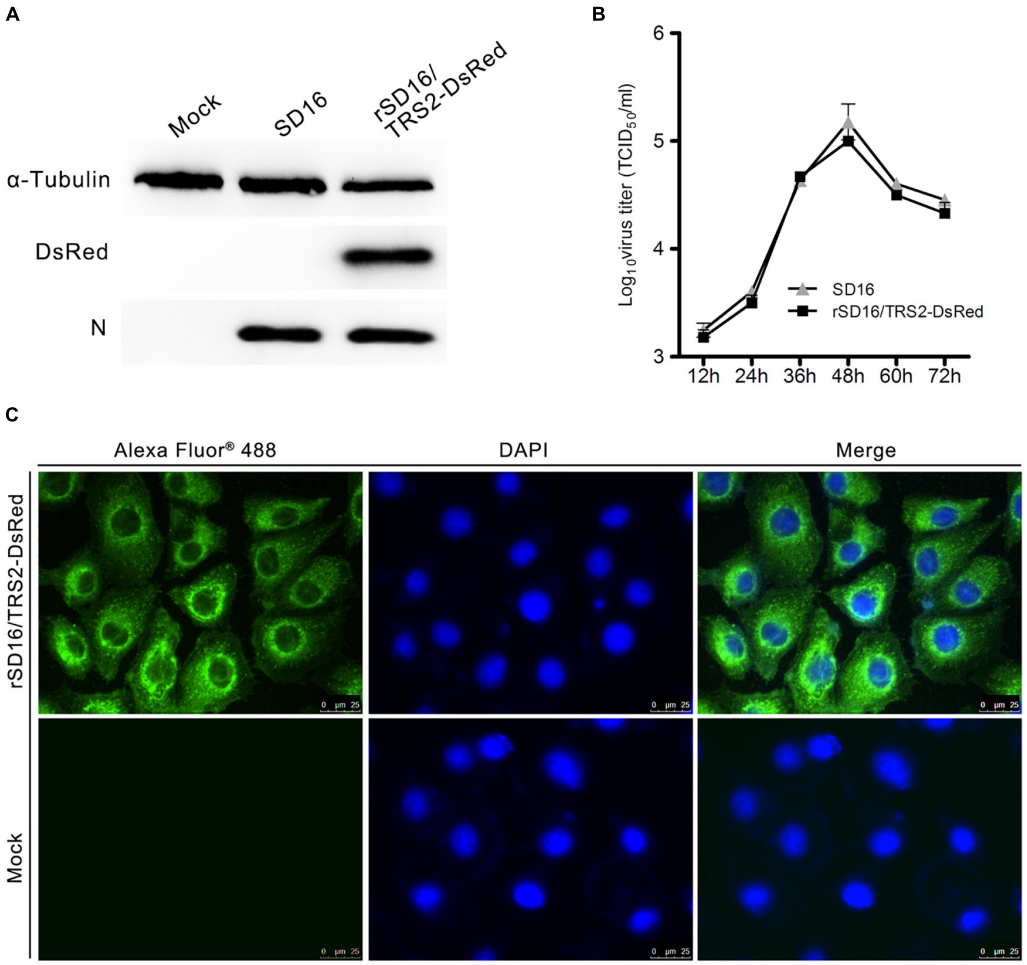


**FIGURE 2 |** DsRed protein expression and growth curve of rSD16/TRS2-DsRed. **(A)** After being infected with SD16 or rSD16/TRS2-DsRed (MOI of 0.1) for 36 h, the MARC-145 cells were lysed for the western blot analysis of PRRSV protein and DsRed expression, the MARC-145 cells infected with SD16 and normal MARC-145 cells were taken as the control; **(B)** MARC-145 cells were infected with SD16 or rSD16/TRS2-DsRed at the MOI of 1.0, and the progeny virus produced in the culture medium was measured at a series of times from 12 to 72 hpi by the method of $TCID_{50}$ detection, and all the data were expressed as the mean ± standard deviation (SD); **(C)** after infected with rSD16/TRS2-DsRed for 48 h, the MARC-145 cells were fixed for the immunofluorescence analysis using the monoclonal antibody of PRRSV N protein, the normal MARC-145 cells were the control.

can be used as a reporter virus to analyze the biological characterizations of PRRSV.

## DsRed as an Indicator of Recombinant Virus Infection

To validate the correlation between the DsRed and the viral infection, the DsRed fluorescence intensity from the infected virus was measured by flow cytometry. As shown in **Figure 4A**, a gradient manner of red fluorescence positive cells ratio in MARC-145 cells infected with rSD16/TRS2/DsRed in different hpi. The ratio of positive cells ranged from 5.49% at hpi of 24 (MOI: 0.1) to 35.72% at hpi of 48 (MOI: 1.0), indicating a high ratio of DsRed positive cells when the culture time was prolonged. Western blot analysis of PRRSV N protein and $TCID_{50}$ detection of culture supernatant were performed to verify whether the ratio of fluorescence positive cells is related to the virus infection. As shown in **Figures 4B,C**, the gradient manner is similar to the flow cytometry results of different hpi.

# DISCUSSION

One of the most important achievements in RNA virus research is the development of reverse genetics systems, which makes the possibility of the virus genetic manipulation (Ishibashi et al., 2017). Reverse genetics technology has been extensively utilized to explore various aspects of virus infection, including infection mechanisms, virulence, pathogenesis, immune responses, transmission characteristics, vaccine development, and antiviral screening tests (Hoenen et al., 2011). There are two strategies to construct a reverse genetics system for PRRSV depending on whether viral RNA or cDNA is used for transfection (Chaudhari and Vu, 2020). It has been demonstrated that the

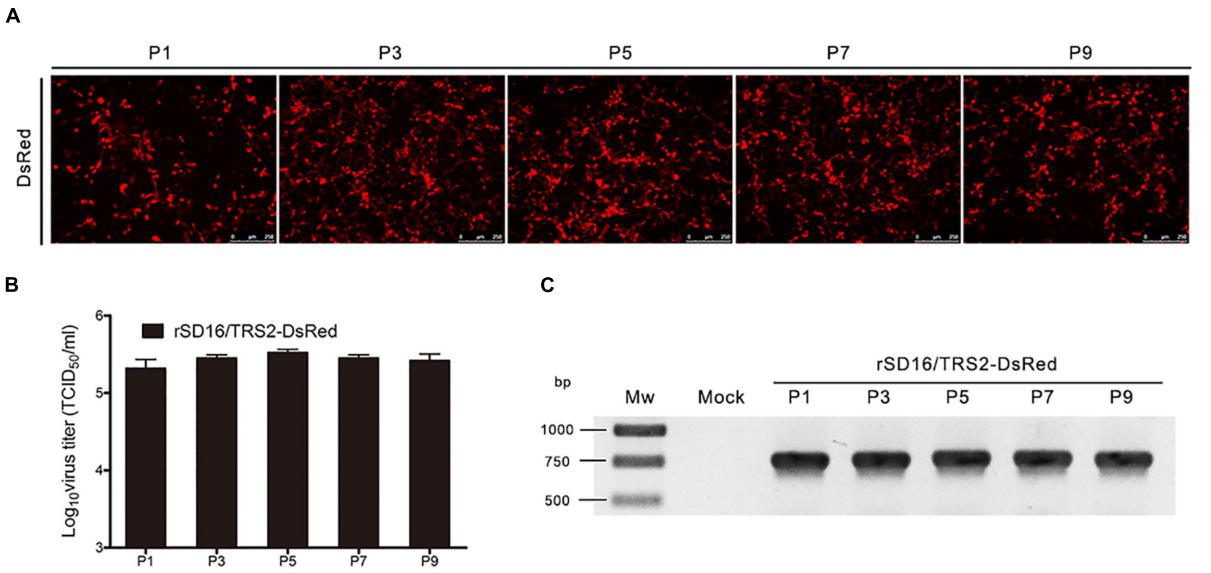


**FIGURE 3 |** Stable expression of DsRed in different passages of rSD16/TRS2-DsRed. **(A)** In different passages, fluorescence pictures of the recombinant virus were captured at 48 hpi by fluorescence microscopy; **(B)** titers of the recombinant virus were detected at different passages by $TCID_{50}$ method, all the tests were repeated three times; **(C)** mRNA production of DsRed gene at different passages of the recombinant virus were detected by reverse transcription PCR analysis.

DNA-based transfection system produces 10–100-fold higher viral titers than the RNA-based transfection system (Huang et al., 2009). The BAC system is based on the *Escherichia coli* (*E. coli*) F factor, in which replication is strictly controlled in *E. coli*. In BAC system, structural stability of inserted DNA in the host on the higher degree at the lower number of copies per cell (one or two per cell), beside the capability of maintaining large fragments (Shizuya et al., 1992), which applied in the rescue of many kinds of virus, comprising virus belongs to *Coronaviridae* (Almazan et al., 2000, 2006; Wang et al., 2013) and *Herpesviridae* (Messerle et al., 1997; Borst et al., 1999; Suter et al., 1999; Kanda et al., 2004; Li et al., 2011). Based on this system, we revealed that the ∼15.4 kb fragment of the PRRSV viral genome was inserted in the BAC plasmid for transfection more conveniently without steps like *in vitro* transcription.

Genetically recombinant viruses which express green and red fluorescent proteins are universally used as tools for studying replication and spread of diverse RNA viruses in living cells or animals (Kanai et al., 2019). Although PRRSV with EGFP has been generated (Wang et al., 2013), this is the first report of a recombinant HP-PRRSV expressing red fluorescence. DsRed, derived from the coral *Discosoma*, has an orange-red fluorescence and can form a stable tetramer, which is detectable by laser-based confocal microscopes and flow cytometers with an excitation at 568 nm (Hawley et al., 2001). It was possible to simultaneously measure the efficiency and fluorescence intensity of the transfected live cells. Compared with EGFP, DsRed has shown its tremendous advantages, including bright red fluorescence and high resistance against photo-bleaching (Garcia-Parajo et al., 2001). Recombinant viruses expressing DsRed proteins represent a better option to combine with genetically modified GFP-expressing cell lines or animals. Their reduced auto-fluorescence background captures the dynamics of viral infection and replication (Chiem et al., 2021). DsRed expression was used for the high-throughput hepatotoxicity test in drug screening and biomonitoring environmental toxicants in zebrafish (Zhang et al., 2014), the investigation of the host and tumor cell compartments (Jacobsen et al., 2013), and identification of MHC I-restricted epitope in mouse (Davey et al., 2013). In the cells, which were used in high-throughput scale detection of allergic sensitization (Wang et al., 2014), *in vivo* imaging of metastatic disease (Yu et al., 2012), genotoxicity, and oxidative stress assessment (Hendriks et al., 2011). As showed in this study, the DsRed fluorescence in the recombinant HP-PRRSV was observed in the MARC-145 cells with CPE (**Figure 1**).

Meanwhile, the growth kinetics of recombinant PRRSV rSD16/TRS2-DsRed showed no significant difference compared with that of the parental virus (**Figure 2**). The DsRed fluorescence intensity and the viral titers were stable at different passaged-recombinant PRRSV (**Figure 3**). Using the rSD16/TRS2/DsRed as a tool, the virus tracking in MARC-145 was observed by live-cell imaging (**Supplementary Movie 1**). Quantification of the DsRed fluorescence positive cells was carried out by using flow cytometry, which shows it is a quick and reliable way to detect the level of PRRSV infection (**Figure 4**).

In conclusion, a recombinant HP-PRRSV carrying the DsRed gene as a separate transcription unit based on the BAC system was successfully rescued. The recombinant viruses can be useful for studying PRRSV transcription and replication by visualization. In addition, the strategy using a TRS2-derived foreign gene expression provides a new method for expressing foreign genes in the PRRSV genome. In the studies of PRRSV visualization, to ensure the fluorescent proteins not interfering with the natural

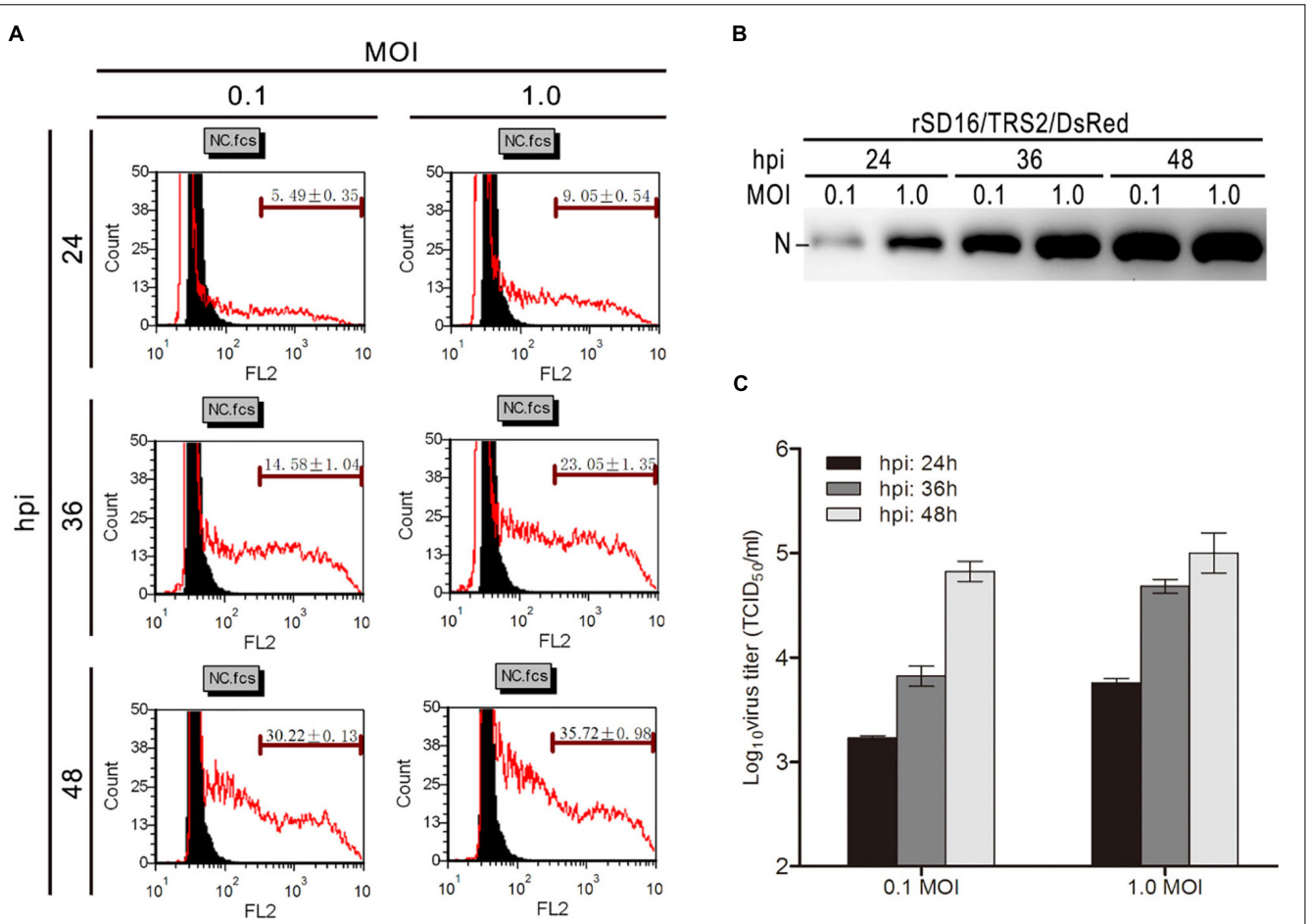


**FIGURE 4 |** DsRed as an indicator of recombinant PRRSV infection. **(A)** Different concentrations of DsRed in virus-infected cells detected by flow cytometry; **(B)** western blot analysis to detect PRRSV N proteins expression after infection with rSD16/TRS2/DsRed; **(C)** titers of culture supernatant were detected using the $TCID_{50}$ method, and all the tests were repeated three times.

infection state of the virus is still the challenge, which was just as reported in the study of PRV (Yang et al., 2020). In the future, CRISPR technology to achieve viral nucleic acid labeling can explain the biological characteristics of the virus that are closest to the real states.

## DATA AVAILABILITY STATEMENT

The original contributions presented in the study are included in the article/**Supplementary Material**, further inquiries can be directed to the corresponding authors.

## AUTHOR CONTRIBUTIONS

BH, YaS, and QZ conceived and designed the experiments. NL, BH, and YZ performed the experiments. NL, LY, and YuS analyzed the data of experiments and drafted the manuscript. All authors contributed to the article and approved the submitted version.

## FUNDING

This research was supported by the National Natural Science Foundation of China (Grant No. 31870917), the Program for Innovative Research Teams of Science and Technology in the University of Henan Province (Grant No. 20IRTSTHN024), and the Foundation of Nanyang Normal University (Grant No. 218264).

## SUPPLEMENTARY MATERIAL

The Supplementary Material for this article can be found online at: https://www.frontiersin.org/articles/10.3389/fmicb.2022.839845/full#supplementary-material

**Supplementary Movie 1 |** Live imaging of rSD16/TRS2/DsRed observed by live-cell microscopy. MARC-145 cells were infected with rSD16/TRS2/DsRed at an MOI of 0.01 in a 35 mm cell culture dish. DsRed fluorescence signals were acquired with the time interval of 1 min for 3 h using a live-cell station, as described in Materials and methods. Images were processed into a movie of six frames $s^{-1}$ by using QuickTime Pro. Scale bar, 50 μm.

## REFERENCES


Albina, E. (1997). Epidemiology of porcine reproductive and respiratory syndrome (PRRS): an overview. *Vet. Microbiol.* 55, 309–316. doi: 10.1016/s0378-1135(96)01322-3

Almazan, F., Dediego, M. L., Galan, C., Escors, D., Alvarez, E., Ortego, J., et al. (2006). Construction of a severe acute respiratory syndrome coronavirus infectious cDNA clone and a replicon to study coronavirus RNA synthesis. *J. Virol.* 80, 10900–10906. doi: 10.1128/JVI.00385-06

Almazan, F., Gonzalez, J. M., Penzes, Z., Izeta, A., Calvo, E., Plana-Duran, J., et al. (2000). Engineering the largest RNA virus genome as an infectious bacterial artificial chromosome. *Proc, Natl. Acad. Sci. U.S.A.* 97, 5516–5521. doi: 10.1073/pnas.97.10.5516

Amarilla, A. A., Sng, J. D. J., Parry, R., Deerain, J. M., Potter, J. R., Setoh, Y. X., et al. (2021). A versatile reverse genetics platform for SARS-CoV-2 and other positive-strand RNA viruses. *Nat. Commun.* 12:3431. doi: 10.1038/s41467-021-23779-5

Behrens, R. T., Aligeti, M., Pocock, G. M., Higgins, C. A., and Sherer, N. M. (2017). Nuclear export signal masking regulates HIV-1 rev trafficking and viral RNA nuclear export. *J. Virol.* 91:e02107-16. doi: 10.1128/JVI.02107-16

Bernstein, H. D., Sarnow, P., and Baltimore, D. (1986). Genetic complementation among poliovirus mutants derived from an infectious cDNA clone. *J. Virol.* 60, 1040–1049. doi: 10.1128/JVI.60.3.1040-1049.1986

Borst, E. M., Hahn, G., Koszinowski, U. H., and Messerle, M. (1999). Cloning of the human cytomegalovirus (HCMV) genome as an infectious bacterial artificial chromosome in *Escherichia coli*: a new approach for construction of HCMV mutants. *J. Virol.* 73, 8320–8329. doi: 10.1128/JVI.73.10.8320-8329.1999

Charerntantanakul, W. (2012). Porcine reproductive and respiratory syndrome virus vaccines: immunogenicity, efficacy and safety aspects. *World J, Virol.* 1, 23–30. doi: 10.5501/wjv.v1.i1.23

Chaudhari, J., and Vu, H. L. X. (2020). porcine reproductive and respiratory syndrome virus reverse genetics and the major applications. *Viruses* 12:1245. doi: 10.3390/v12111245

Chiem, K., Morales Vasquez, D., Park, J. G., Platt, R. N., Anderson, T., Walter, M. R., et al. (2021). Generation and characterization of recombinant SARS-CoV-2 expressing reporter genes. *J. Virol.* 95:e02209-20. doi: 10.1128/JVI.02209-20

Davey, G. M., Mueller, S. N., van Vliet, C., Gigowski, M., Zaid, A., Davies, B., et al. (2013). Identification of a MHC I-restricted epitope of DsRed in C57BL/6 mice. *Mol, Immunol.* 53, 450–452. doi: 10.1016/j.molimm.2012.10.003

Fang, Y., Rowland, R. R., Roof, M., Lunney, J. K., Christopher-Hennings, J., and Nelson, E. A. (2006). A full-length cDNA infectious clone of North American type 1 porcine reproductive and respiratory syndrome virus: expression of green fluorescent protein in the Nsp2 region. *J. Virol.* 80, 11447–11455. doi: 10.1128/JVI.01032-06

Fang, Y., and Snijder, E. J. (2010). The PRRSV replicase: exploring the multifunctionality of an intriguing set of nonstructural proteins. *Virus Res.* 154, 61–76. doi: 10.1016/j.virusres.2010.07.030

Garcia-Parajo, M. F., Koopman, M., van Dijk, E. M., Subramaniam, V., and van Hulst, N. F. (2001). The nature of fluorescence emission in the red fluorescent protein DsRed, revealed by single-molecule detection. *Proc. Nat. Acad. Sci. U.S.A.* 98, 14392–14397. doi: 10.1073/pnas.251525598

Gonzalez, J. M., Penzes, Z., Almazan, F., Calvo, E., and Enjuanes, L. (2002). Stabilization of a full-length infectious cDNA clone of transmissible gastroenteritis coronavirus by insertion of an intron. *J. Virol.* 76, 4655–4661. doi: 10.1128/jvi.76.9.4655-4661.2002

Hawley, T. S., Telford, W. G., Ramezani, A., and Hawley, R. G. (2001). Four-color flow cytometric detection of retrovirally expressed red, yellow, green, and cyan fluorescent proteins. *BioTechniques* 30, 1028–1034. doi: 10.2144/01305rr01

Hendriks, G., Atallah, M., Raamsman, M., Morolli, B., van der Putten, H., Jaadar, H., et al. (2011). Sensitive DsRed fluorescence-based reporter cell systems for genotoxicity and oxidative stress assessment. *Mutat. Res.* 709-710, 49–59. doi: 10.1016/j.mrfmmm.2011.02.013

Hoenen, T., Groseth, A., de Kok-Mercado, F., Kuhn, J. H., and Wahl-Jensen, V. (2011). Minigenomes, transcription and replication competent virus-like particles and beyond: reverse genetics systems for filoviruses and other negative stranded hemorrhagic fever viruses. *Antivir. Res.* 91, 195–208. doi: 10.1016/j.antiviral.2011.06.003

Huang, Y. W., Fang, Y., and Meng, X. J. (2009). Identification and characterization of a porcine monocytic cell line supporting porcine reproductive and respiratory syndrome virus (PRRSV) replication and progeny virion production by using an improved DNA-launched PRRSV reverse genetics system. *Virus Res.* 145, 1–8. doi: 10.1016/j.virusres.2009.05.013

Ishibashi, K., Matsumoto-Yokoyama, E., and Ishikawa, M. (2017). A tomato spotted wilt virus S RNA-based replicon system in yeast. *Sci. Rep.* 7:12647. doi: 10.1038/s41598-017-12687-8

Jacobsen, H. K., Sleire, L., Wang, J., Netland, I. A., Mutlu, E., Forde, H., et al. (2013). Establishment of a novel dsRed NOD/Scid mouse strain to investigate the host and tumor cell compartments. *Cancer Invest.* 31, 221–230. doi: 10.3109/07357907.2013.780075

Kanai, Y., Kawagishi, T., Nouda, R., Onishi, M., Pannacha, P., Nurdin, J. A., et al. (2019). Development of stable rotavirus reporter expression systems. *J. Virol.* 93:e01774-18. doi: 10.1128/JVI.01774-18

Kanda, T., Yajima, M., Ahsan, N., Tanaka, M., and Takada, K. (2004). Production of high-titer Epstein-Barr virus recombinants derived from Akata cells by using a bacterial artificial chromosome system. *J. Virol.* 78, 7004–7015. doi: 10.1128/JVI.78.13.7004-7015.2004

Li, Q., Wang, X., Wang, C., Yu, Y., Wang, G., Gao, J., et al. (2016). Intracellular expression of an anti-idiotypic antibody single-chain variable fragment reduces porcine reproductive and respiratory syndrome virus infection in MARC-145 cells. *Antivir. Ther.* 21, 161–170. doi: 10.3851/IMP2980

Li, Y., Wang, S., Zhu, H., and Zheng, C. (2011). Cloning of the herpes simplex virus type 1 genome as a novel luciferase-tagged infectious bacterial artificial chromosome. *Arch. Virol.* 156, 2267–2272. doi: 10.1007/s00705-011-1094-9

Messerle, M., Crnkovic, I., Hammerschmidt, W., Ziegler, H., and Koszinowski, U. H. (1997). Cloning and mutagenesis of a herpesvirus genome as an infectious bacterial artificial chromosome. *Proc. Natl. Acad, Sci, U.S.A.* 94, 14759–14763. doi: 10.1073/pnas.94.26.14759

Nielsen, H. S., Liu, G., Nielsen, J., Oleksiewicz, M. B., Botner, A., Storgaard, T., et al. (2003). Generation of an infectious clone of VR-2332, a highly virulent North American-type isolate of porcine reproductive and respiratory syndrome virus. *J. Virol.* 77, 3702–3711. doi: 10.1128/jvi.77.6.3702-3711.2003

Nouda, R., Minami, S., Kanai, Y., Kawagishi, T., Nurdin, J. A., Yamasaki, M., et al. (2021). Development of an entirely plasmid-based reverse genetics system for 12-segmented double-stranded RNA viruses. *Proc. Natl. Acad. Sci. U.S.A.* 118:e2105334118. doi: 10.1073/pnas.2105334118

Park, G. S., Lim, S. I., Hong, S. H., and Song, J. Y. (2012). Establishment and characterization of an infectious cDNA clone of a classical swine fever virus LOM strain. *J. Vet. Sci.* 13, 81–91. doi: 10.4142/jvs.2012.13.1.81

Racaniello, V. R., and Baltimore, D. (1981). Cloned poliovirus complementary DNA is infectious in mammalian cells. *Science* 214, 916–919. doi: 10.1126/science.6272391

Sang, Y., Shi, J., Sang, W., Rowland, R. R., and Blecha, F. (2012). Replication-competent recombinant porcine reproductive and respiratory syndrome (PRRS) viruses expressing indicator proteins and antiviral cytokines. *Viruses* 4, 102–116. doi: 10.3390/v4010102

Shizuya, H., Birren, B., Kim, U. J., Mancino, V., Slepak, T., Tachiiri, Y., et al. (1992). Cloning and stable maintenance of 300-kilobase-pair fragments of human DNA in *Escherichia coli* using an F-factor-based vector. *Proc. Natl. Acad. Sci. U.S.A.* 89, 8794–8797. doi: 10.1073/pnas.89.18.8794

St-Jean, J. R., Desforges, M., Almazan, F., Jacomy, H., Enjuanes, L., and Talbot, P. J. (2006). Recovery of a neurovirulent human coronavirus OC43 from an infectious cDNA clone. *J. Virol.* 80, 3670–3674. doi: 10.1128/JVI.80.7.3670-3674.2006

Strickfaden, H., Zunhammer, A., van Koningsbruggen, S., Kohler, D., and Cremer, T. (2010). 4D chromatin dynamics in cycling cells: theodor Boveri's hypotheses revisited. *Nucleus* 1, 284–297. doi: 10.4161/nucl.1.3.11969

Suter, M., Lew, A. M., Grob, P., Adema, G. J., Ackermann, M., Shortman, K., et al. (1999). BAC-VAC, a novel generation of (DNA) vaccines: a bacterial artificial chromosome (BAC) containing a replication-competent, packaging-defective virus genome induces protective immunity against herpes simplex virus 1. *Proc. Natl. Acad. Sci, U S.A.* 96, 12697–12702. doi: 10.1073/pnas.96.22.12697

Tian, K., Yu, X., Zhao, T., Feng, Y., Cao, Z., Wang, C., et al. (2007). Emergence of fatal PRRSV variants: unparalleled outbreaks of atypical PRRS in China and molecular dissection of the unique hallmark. *PLoS One* 2:e526. doi: 10.1371/journal.pone.0000526

Truong, H. M., Lu, Z., Kutish, G. F., Galeota, J., Osorio, F. A., and Pattnaik, A. K. (2004). A highly pathogenic porcine reproductive and respiratory syndrome virus generated from an infectious cDNA clone retains the in vivo virulence and transmissibility properties of the parental virus. *Virology* 325, 308–319. doi: 10.1016/j.virol.2004.04.046

Wang, C., Huang, B., Kong, N., Li, Q., Ma, Y., Li, Z., et al. (2013). A novel porcine reproductive and respiratory syndrome virus vector system that stably expresses enhanced green fluorescent protein as a separate transcription unit. *Vet. Res.* 44:104. doi: 10.1186/1297-9716-44-104

Wang, X., Cato, P., Lin, H. C., Li, T., Wan, D., Alcocer, M. J., et al. (2014). Optimisation and use of humanised RBL NF-AT-GFP and NF-AT-DsRed reporter cell lines suitable for high-throughput scale detection of allergic sensitisation in array format and identification of the ECM-integrin interaction as critical factor. *Mol. Biotechnol.* 56, 136–146. doi: 10.1007/s12033-013-9689-x

Wensvoort, G., Terpstra, C., Pol, J. M., ter Laak, E. A., Bloemraad, M., de Kluyver, E. P., et al. (1991). Mystery swine disease in The Netherlands: the isolation of Lelystad virus. *Vet. Q.* 13, 121–130. doi: 10.1080/01652176.1991.9694296

Wolff, H., Hadian, K., Ziegler, M., Weierich, C., Kramer-Hammerle, S., Kleinschmidt, A., et al. (2006). Analysis of the influence of subcellular localization of the HIV Rev protein on Rev-dependent gene expression by multi-fluorescence live-cell imaging. *Exp. Cell Res.* 312, 443–456. doi: 10.1016/j.yexcr.2005.11.020

Yang, Y. B., Tang, Y. D., Hu, Y., Yu, F., Xiong, J. Y., Sun, M. X., et al. (2020). Single virus tracking with quantum dots packaged into enveloped viruses using CRISPR. *Nano Lett.* 20, 1417–1427.

Yu, Z., Zhou, J., and Hoffman, R. M. (2012). Lentivirus-based DsRed-2-transfected pancreatic cancer cells for deep in vivo imaging of metastatic disease. *Methods Mol. Biol.* 872, 69–83.

Zhang, S., Zhou, Y., Jiang, Y., Li, G., Yan, L., Yu, H., et al. (2011). Generation of an infectious clone of HuN4-F112, an attenuated live vaccine strain of porcine reproductive and respiratory syndrome virus. *Virol. J.* 8:410. doi: 10.1186/1743-422X-8-410

Zhang, X., Li, C., and Gong, Z. (2014). Development of a convenient in vivo hepatotoxin assay using a transgenic zebrafish line with liver-specific DsRed expression. *PLoS One* 9:e91874. doi: 10.1371/journal.pone.0091874

**Conflict of Interest:** YuS was employed by Shijiazhuang Customs (Huanghua Port).

The remaining authors declare that the research was conducted in the absence of any commercial or financial relationships that could be construed as a potential conflict of interest.

**Publisher's Note:** All claims expressed in this article are solely those of the authors and do not necessarily represent those of their affiliated organizations, or those of the publisher, the editors and the reviewers. Any product that may be evaluated in this article, or claim that may be made by its manufacturer, is not guaranteed or endorsed by the publisher.

*Copyright © 2022 Li, Zhang, Yao, Shi, Zhao, Huang and Sun. This is an open-access article distributed under the terms of the Creative Commons Attribution License (CC BY). The use, distribution or reproduction in other forums is permitted, provided the original author(s) and the copyright owner(s) are credited and that the original publication in this journal is cited, in accordance with accepted academic practice. No use, distribution or reproduction is permitted which does not comply with these terms.*

frontiers in Microbiology

REVIEW
published: 03 February 2022
doi: 10.3389/fmicb.2022.845625

# The Emerging Role of RNA Modifications in the Regulation of Antiviral Innate Immunity

*Jie Tong[1,2*†], Wuchao Zhang[3†], Yuran Chen[1,2], Qiaoling Yuan[1,2], Ning-Ning Qin[1,2] and Guosheng Qu[1,2*]*

[1]College of Life Sciences, Hebei University, Baoding, China, [2]Institute of Life Sciences and Green Development, Hebei University, Baoding, China, [3]College of Veterinary Medicine, Hebei Agricultural University, Baoding, China

Posttranscriptional modifications have been implicated in regulation of nearly all biological aspects of cellular RNAs, from stability, translation, splicing, nuclear export to localization. Chemical modifications also have been revealed for virus derived RNAs several decades before, along with the potential of their regulatory roles in virus infection. Due to the dynamic changes of RNA modifications during virus infection, illustrating the mechanisms of RNA epigenetic regulations remains a challenge. Nevertheless, many studies have indicated that these RNA epigenetic marks may directly regulate virus infection through antiviral innate immune responses. The present review summarizes the impacts of important epigenetic marks on viral RNAs, including N6-methyladenosine ($m^6A$), 5-methylcytidine ($m^5C$), 2′-O-methylation (2′-O-Methyl), and a few uncanonical nucleotides (A-to-I editing, pseudouridine), on antiviral innate immunity and relevant signaling pathways, while highlighting the significance of antiviral innate immune responses during virus infection.

**Keywords: RNA modification, viral infection, RIG-I, IFN-I, antiviral innate immunity**

OPEN ACCESS

***Edited by:***
*Chunfu Zheng,*
*University of Calgary, Canada*

***Reviewed by:***
*Yue Ma,*
*Van Andel Institute, United States*
*Yan-Dong Tang,*
*Harbin Veterinary Research Institute (CAAS), China*

***Correspondence:**
*Jie Tong*
*tongjie2019@hbu.edu.cn*
*Guosheng Qu*
*guo_sheng_qu@126.com*

†*These authors have contributed equally to this work*

***Specialty section:***
*This article was submitted to Virology, a section of the journal Frontiers in Microbiology*

***Received:*** *30 December 2021*
***Accepted:*** *10 January 2022*
***Published:*** *03 February 2022*

***Citation:***
*Tong J, Zhang W, Chen Y, Yuan Q, Qin N-N and Qu G (2022) The Emerging Role of RNA Modifications in the Regulation of Antiviral Innate Immunity. Front. Microbiol. 13:845625. doi: 10.3389/fmicb.2022.845625*

## INTRODUCTION

Chemical modifications of RNA, also be designated as epitranscriptomic marks of RNA, are considered common features in most natural RNAs. To date, more than 140 posttranscriptional modifications have been discovered to function in the structural diversity and metabolism of RNAs (Zhao et al., 2017). While chemical modifications mainly appear in cellular RNAs such as messenger RNA (mRNA), ribosomal RNA (rRNA), and transfer RNA (tRNA) as well as other non-coding RNAs, numerous studies have indicated the pivotal roles of RNA epigenetic regulations in virus infection (McIntyre et al., 2018; Netzband and Pager, 2020). The most prevalent modifications in the virus genome include methylation of adenine and cytidine residues, such as N6-methyladenosine ($m^6A$), 5-methylcytidine ($m^5C$), or 7-methylguanosine ($m^7G$), 2′-O-methylation (2′-O-Methyl), as well as uncanonical nucleotides like A-to-I editing and pseudouridine (McIntyre et al., 2018). Although these chemical modifications are generally formed by cellular enzymes, virus-encoded methyltransferases have been implicated in several methylation modifications. Nearly all chemical modifications that are mediated by enzymes undergo dynamic and reversible changes during virus infection, which makes it difficult to define roles of epigenetic modifications in viral RNA metabolism or virus infection. Nevertheless, due to the rapid development of RNA biology, numbers of RNA modifications have been

found in genome of various viruses, which are supposed to influence virus infection to some extent (Courtney, 2021; Marchand and Motorin, 2021).

As the primary antiviral strategies, innate immune responses are invariably activated at the early stage of virus infection. Through recognizing the exogenous nucleic acids including virus-derived RNAs or DNAs by Toll-like receptors (TLRs; Creagh and O'Neill, 2006; Beutler, 2009; Lavelle et al., 2010), which belong to pattern-recognition receptors (PRRs), cytoplasmic receptors/adapters like myeloid differentiation factor-88 (MyD-88) or TIR-domain-containing adaptor protein inducing interferon-beta (TRIF) is recruited and in turn activates TNF receptor-associated factors (TRAFs; Creagh and O'Neill, 2006). Activation of TRAFs then gives rise to the activation of IFN response factor 3/7 (IRF3/7) and nuclear factor-κB (NF-κB) signaling pathways that induces type I interferons (IFNs) and proinflammatory cytokines expression (Bonizzi and Karin, 2004; Rius et al., 2008; Dev et al., 2011). Aside from the TLR pathway, another kind of PRRs named as retinoic acid-inducible gene I (RIG-I)-like receptor (RLR) family also has been identified as crucial cytosolic sensors of viral nucleic acids (Schustak et al., 2021). The mitochondrial antiviral-signaling protein (MAVS) is located in mitochondria or endoplasmic reticulum (ER) and considered as the receptor protein of RLR signaling pathway, by which IFN-β is effectively expressed at the early stage of virus infection (Hwang et al., 2013; Tong et al., 2021b). Both IFNs and proinflammatory cytokines have strong antiviral activities. A battery of studies have recently indicated the emerging roles of RNA modifications in regulating antiviral innate immune responses (Thompson et al., 2021). The present review will focus on the impacts of these epigenetic marks, especially on antiviral innate immunity and its relevant signaling pathways, while highlighting the significance of antiviral innate immune responses during virus infection.

# PREVALENT RNA MODIFICATIONS IN VIRUS

## N6-Methyladenosine

N6-Methyladenosine modification affects nearly all aspects of RNA biology, including stability, translation, splicing, nuclear export, and localization. Methylation modification, adding adenosine to N6 to form $m^6A$, is catalyzed by a large heterogeneous complex of proteins that are named as "writer," including METTL3, METTL14, or Wilms tumor 1-associated protein and KIAA1429 (Meyer and Jaffrey, 2017; Shi et al., 2019). In contrast, demethylases enzymes like fat mass and obesity-associated protein (FTO) or α-ketoglutarate-dependent dioxygenase AlkB homology 5 (ALKBH5) designated as "eraser" remove the methyl group (Jia et al., 2011; Zheng et al., 2013). The YTH domain family of proteins (YTHDC1, YTHDC2, YTHDF1, YTHDF3, and YTHDF3) and others named as "reader" recognize and bind to the $m^6A$ modification site to directly regulate the posttranscriptional functions of modified RNAs (Shi et al., 2019). $m^6A$ modifications are typically identified within the $DRA^mCH$ motif (D = G/A/U, R = A/G, and H = A/C/U); however, given the fact that only some of the DRACH motifs in eukaryote transcriptome are modified, there might exist some mechanisms for site-selective modification (Dominissini et al., 2012).

## 5-Methylcytidine

Another kind of RNA base methylation is the C5-methylation of RNA cytosine-$m^5C$. $m^5C$ widely exists in cytoplasmic and ribosomal RNA (rRNA), tRNA, mRNA, and some non-coding RNAs (Lewis et al., 2017; Bohnsack et al., 2019). In eukaryotes, $m^5C$ is catalyzed by enzymes of the NOL1/NOP2/SUN domain (NSUN) family and DNA methyltransferase family protein (DNMT2), a homolog of DNA methyltransferase (Reid et al., 1999). Recent studies showed $m^5C$ was present in numerous virus genomes and might have non-negligible effects on antiviral innate immunity (Winans and Beemon, 2019; Wnuk et al., 2020). For instance, a high level of $m^5C$ modifications in HIV-1 genomic RNA (gRNA) promoted the expression of viral genes by regulating splicing and the translation efficiency of viral mRNAs (Courtney et al., 2019). Silencing or inactivation of the major writer NSUN2 of $m^5C$ reduced the $m^5C$ abundance in HIV-1 transcripts and inhibited virus replication by disrupting the alternative splicing and the followed translation of HIV-1 mRNA (Kong et al., 2020).

## 2′-O-Methylation and 7-Methylguanosine

Cellular mRNA conventionally has a triphosphate at 5′ end (5′-ppp), which is converted to 5′-diphosphate (5′-pp) by RNA triphosphatase (Ramanathan et al., 2016). This conversion resulted in mRNA capping by guanylyltransferase and guanine-N7 methyltransferase (Shatkin, 1976). After adding a terminal guanosine base, the mRNA transcripts possess an $m^7G$ joined *via* a 5′, 5′-triphosphate bridge, designated as cap-0 (Shatkin, 1976). When a cellular 2′-O-methyltransferase, CMTR1, further modifies the mRNA, a methyl group is added at the 2′-O-hydroxyl position of the first nucleotide to form cap-1 RNA structure (Belanger et al., 2010). Meanwhile, a second 2′-O-methyl group can be added at the second nucleotide to form cap-2, catalyzed by another cellular methyltransferase CMTR2 (Werner et al., 2011; Smietanski et al., 2014). mRNA capping is considered one of the key factors in regulating RNA metabolism and function (Topisirovic et al., 2011), including stabilizing the mRNA and serving as a chemical marker to discriminate self from foreign RNA, the latter of which may interfere with the innate immune sensing of viral derived RNA (Hocine et al., 2010; Ramanathan et al., 2016). Some viruses, such as West Neil virus (WNV) or Dengue virus (DENV), encode 2′-O MTases that catalyze 2′-O-methyl adenosines inside the virus genome (Dong et al., 2012; Chang et al., 2016). Interestingly, this internal adonosine 2′-O-methyl activity requires the same K-D-K-E motif as that for 2′-O methylation of the 5′cap (Yap et al., 2010; Dong et al., 2012). Given that many viruses possess cap structures in their RNA components, this type of modification is supposed to play a pivotal role in antiviral innate immunity.

## Uncanonical Nucleotides

After the pseudouridine (ψ) was firstly identified in plant turnip yellow mosaic virus (TYMV) in 1998 (Becker et al., 1998),

the follow-up research continuously indicated the abundant ψ in RNA viruses, especially in positive-sense RNA viruses (McIntyre et al., 2018). Psedouridine occurs through isomerization of uridine-to-5-ribosyl uracil by pseudouridine synthases (PUS; Markham and Smith, 1951). Similar to ψ, the deamination of adenosine to inosine (A-to-I) that depends on the catalyzing of adenosine deaminase acting on RNA (ADAR) family is also considered RNA editing or uncanonical nucleotides (Chen et al., 2000; Bass, 2002; George et al., 2014; Chung et al., 2018; Eisenberg and Levanon, 2018). The difference is that inosine generally acts similarly to guanosine (G), whereas ψ remains the original capacity of uridine to some extent. Although U to ψ conversion does not change the Watson–Crick base-pairing with adenosine, in certain cases, ψ enables base pairing with any other nucleotides (Samuel, 2011; Pfaller et al., 2021). Both ψ and A-to-I editing may significantly convert RNA biology, including changing the coding preference of viral RNA dependent RNA polymerases, mediating alternative splice and even affecting RNA structures (Netzband and Pager, 2020; Pfaller et al., 2021).

## Mechanisms of Epigenetic Regulation in RNA Metabolism

Modified nucleotides may stabilize the functional RNA structures by reinforcing the hydrogen bond between Watson–Crick pairs, resulting in augmented thermal stability and reduced dynamics (Serra et al., 2004; Zhou et al., 2016; Frye et al., 2018). Under other circumstances, Watson–Crick base pairs consisting of modified nucleotides may induce an alternative folding representing significant alterations in the RNA secondary or tertiary structures, negatively affecting RNA stability (Durbin et al., 2016; Zhou et al., 2016; Roundtree et al., 2017; Wei and He, 2021). Moreover, the posttranscriptional introduction of modified nucleotides can affect RNA intermolecular interactions with other encountered molecules such as DNA partners, RNA binding proteins, or other RNAs (Zhao et al., 2017; Nachtergaele and He, 2018; Shi et al., 2019). Since all functions are regulated by structure to a certain degree, viral RNAs carrying modified nucleotides (or uncanonical nucleotides) commonly represent functional differences in virus life-cycle, thus mediating virus infection in host cells. Besides, some RNA viruses those complete their life-cycle in cytoplasm influence host cell genomic transcription inside the cell nucleus, for example, ZIKV infection affects some endogenous genes' trancription which occured inside the cell nucleus (Gokhale et al., 2020). In this case, epigenetic regulations may facilitate the virus to overcome the spatial barrier. To sum up, some of the demonstrated RNA modifications in virus genome as well as the correlative functions are listed in **Figure 1**. Notably, many viruses use epigenetic modifications as crucial tools to evade antiviral innate immune response.

# RNA MODIFICATIONS IN SENSING OF FOREIGN NUCLEIC ACIDS

Sensing the foreign molecules by the PRRs of the innate immune system serves as the initial step of the innate immune response (Akira et al., 2006; Takeuchi and Akira, 2010). Different PRRs must distinguish the non-self molecules from the self through chemical patterns. To date, several kinds of PRRs, including TLRs, RLRs, cyclic GMP-AMP synthase (cGAS; Schoggins et al., 2014; Aguirre et al., 2017; Ma et al., 2021; Yu et al., 2021), C-type lectin receptors (CLRs), nucleotide-binding oligomerization domain (NOD)-like receptors (NLRs), and AIM2-like receptors (ALRs), have been utilized by host cells in recognition of viral PAMPs (Akira et al., 2006; Crowl et al., 2017; Babamale and Chen, 2021; Chou et al., 2021; de Oliveira Mann and Hornung, 2021). As the most important component in virus particles, viral-derived RNAs/DNAs are released into the host cell cytoplasm at the early stage of infection. Thus, recognizing the distinction of epitranscriptomic modifications between cellular and pathogen nucleic acids is supposed to regulate antiviral innate immunity at the early stage of virus infection (**Figure 2**).

## Retinoic Acid-Inducible Gene I-Like Receptors

Retinoic acid-inducible gene I, melanoma differentiation-associated protein 5 (MDA5), and laboratory of genetics and physiology 2 (LGP2) are the three major homologous helicases of RLRs (Wu et al., 2013; Yu et al., 2018; Thoresen et al., 2021). RIG-I and MDA5 displayed similar component structures, including caspase activation domain in N-terminal, recruitment domains (CARDs) for communicating with downstream signals, a DExD/H-box helicase domain with RNA binding and ATP hydrolysis activity, and a C-terminal domain (CTD; Yoneyama et al., 2004; Jiang et al., 2011; Kowalinski et al., 2011; Yu et al., 2018). The pathogen-associated molecular patterns (PAMPs) motifs of RIG-I include exposed 5′triphosphate (5′ppp) or diphosphate of double-strand RNAs (dsRNA), panhandle structures of viral genomic RNA, and uridine-rich sequences, while MDA5 recognizes long dsRNA such as poly (I:C; Yoneyama et al., 2004; Hornung et al., 2006; Kato et al., 2006; Cui et al., 2008; Liu et al., 2018). RIG-I is expressed at a low level in non-infected cells, usually referred to as a resting state with RNA-binding and helicase domains covered by RDs (Kowalinski et al., 2011; Luo et al., 2011). Following recognition of PAMPs, RIG-I undergoes a conformational change that provides room for closer interaction with more PAMPs RNAs and begins to release the CARDs for MAVS interaction and signaling (Pichlmair et al., 2006; Peisley et al., 2013; Thoresen et al., 2021). When the complex consisting of RIG-I, MAVS, and other cytosolic proteins translocate from the cytoplasm to the associated mitochondrial membrane, RIG-I CARDs interact with the MAVS CARD to catalyze the filament formation of MAVS and then activates TBK1 and IKKε to initiate downstream signaling (Pichlmair et al., 2006; Peisley et al., 2013; Goubau et al., 2014).

### m$^6$A and RLRs

As one of the most common RNA modifications, m$^6$A has been widely involved in the innate immune sensing process and thus regulates viral pathogenesis. In some cases, viral RNA-loaded m$^6$A modification dampens the RIG-I mediated

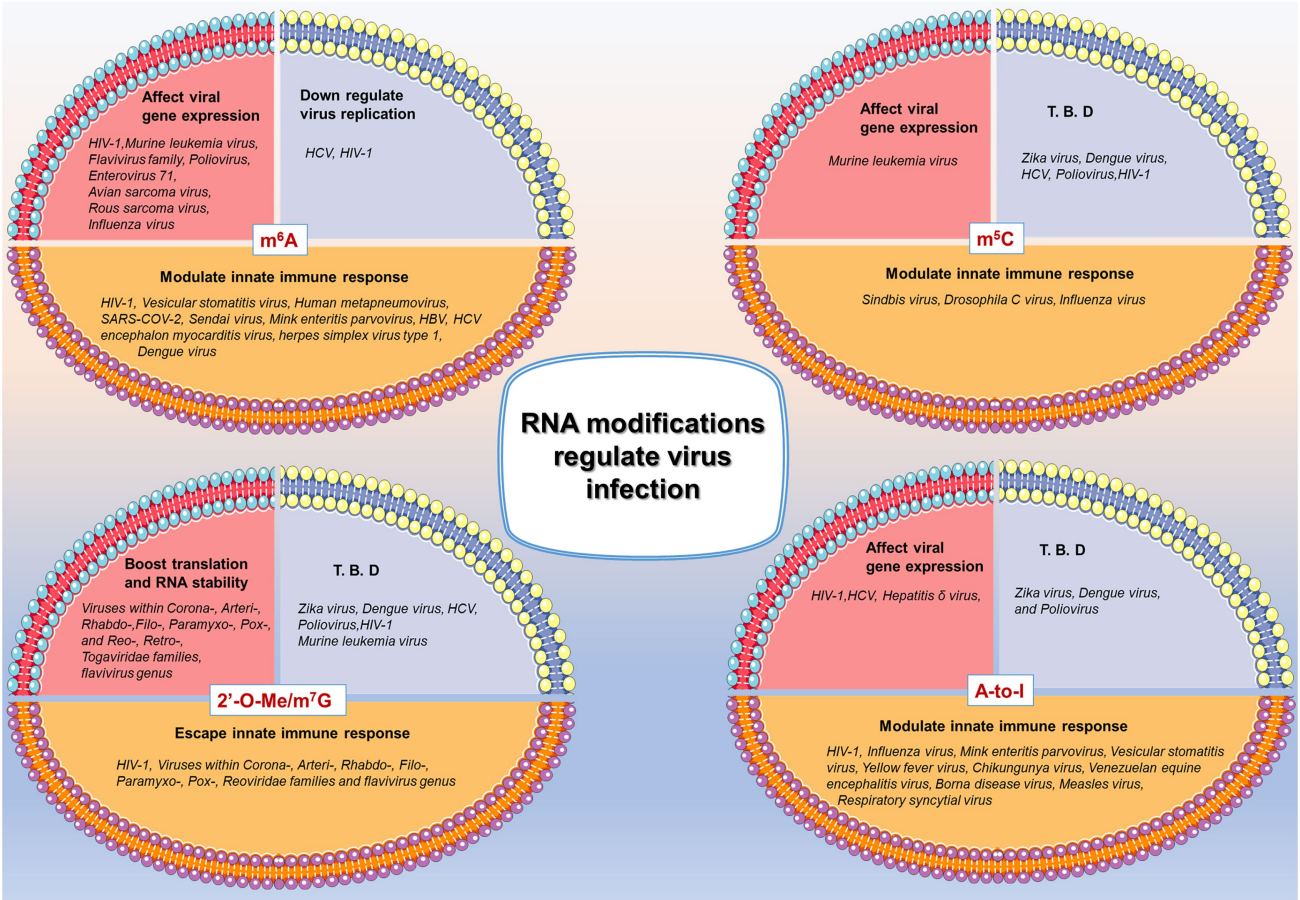


**FIGURE 1 |** Brief summary of RNA modifications in regulating virus infection. N6-methyladenosine ($m^6A$), 5-methylcytidine ($m^5C$), 2′-O-methylation (2′-O-Me)/7-methylguanosine ($m^7G$), and A-to-I editing (A-to-I) are listed as example of epigenetic regulations in virus infection. Three major effects are summarized in diverse virus infection, among which the modulation of innate immune response is the focus of the present review. T. B. D: To be determined. References are listed in the **Supplementary Table S1**.

RNA sensing and activation of the downstream transcription factors such as IRF3 and IRF7, which depresses the type I interferon (IFN-I) gene expression (Lu et al., 2020; Ge et al., 2021; Xue et al., 2021). One suggested mechanism is that $m^6A$ modification might harbor viral PAMPs motifs for RIG-I recognition and innate immune signaling. For example, $m^6A$ modifications in HIV RNAs undermined RIG-I sensing and type-I interferon induction in differentiated monocytic cells, while $m^6A$-deficient HIV-1 virions produced from FTO-overexpressing HEK293T cells induced high levels of IFN-I expression in a RIG-I-dependent manner (Chen et al., 2021). Consistently, in several families of negative-sense RNA viruses, such as Pneumoviridae (hMPV), Paramyxoviridae (SeV and MeV), and Rhabdoviridae (VSV), $m^6A$-deficient viral RNAs universally triggered RIG-I-dependent innate immune response much more efficiently compared to the $m^6A$-sufficient viral RNAs, suggesting a crucial role of $m^6A$ marker in RIG-I sensing process (Kim et al., 2020; Lu et al., 2020, 2021).

Further investigation demonstrated that these negative effects might be induced by $m^6A$ related enzymes, including YTHDFs and METTLs. Instead of encoding innate immune antagonist proteins, $m^6A$ modifications in viral RNAs enable the recruitment of the $m^6A$ enzymes, which subsequently sequestrates viral ds/ssRNA through their RNA binding ability to prevent RIG-I recognition. Specifically, $m^6A$ modification of hepatitis B and C viral RNAs suppressed the activation of RIG-I signaling, whereas single nucleotide mutation of $m^6A$ motif of viral RNAs (A8766C) enhanced RIG-I sensing activity (Kim et al., 2020). In this case, YTHDF2 was found to regulate HBV pgRNAs and HCV genomic RNAs to evade RIG-I recognition. Besides YTHDF itself, diverse RNA-binding proteins (RBPs) were identified to interact with YTHDF proteins. The interactions might also regulate RIG-I access to viral RNAs, which mediates the activation of RIG-I signaling pathways through indirect influences (Luo et al., 2012).

Moreover, reducing the $m^6A$ "writer" enzyme METTL3 not only downregulates the $m^6A$ levels in the 3′ end of SARS-COV-2 genome, but also improves the RIG-I binding to enhance the downstream innate immune signaling pathway and inflammatory gene expressions (Li et al., 2021). Similarly, as

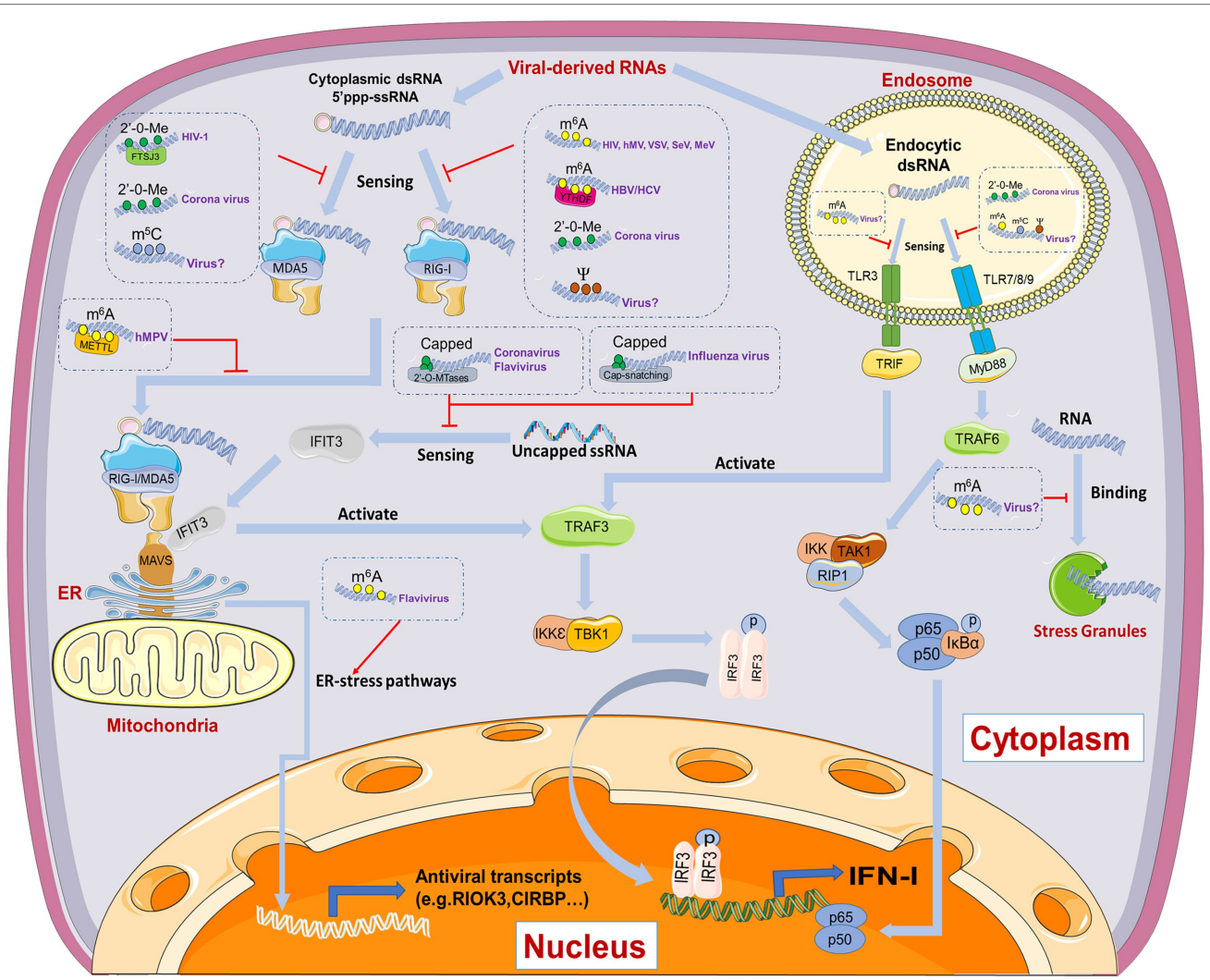


**FIGURE 2 |** Schematic diagram of mechanisms by which RNA modification regulating viral-derived RNA recognition and innate immune responses. $N^6$-methyladenosine ($m^6A$), 5-methylcytidine ($m^5C$), 2′-O-methylation (2′-O-Me), and pseudouridine (ψ) are demonstrated to inhibit melanoma differentiation-associated protein 5 (MDA5) or retinoic acid-inducible gene I (RIG-I) mediated sensing. METTL and YTHDF proteins are involved in these process. Inside the endosomes, 2′-O-Me are identified to block the TLR7-dependent type I interferon (IFN-I) response. Meanwhile, $m^6A$, $m^5C$, and ψ also prevent the Toll-like receptors (TLRs) activation inside the endosomes, although the relevance to virus infection still remains ambiguous. Moreover, $m^6A$ may regulate antiviral innate immunity through stress granules or endoplasmic reticulum (ER)-stress pathways, the latter of which has already been illustrated in Flavivirus infection.

for vesicular stomatitis virus (VSV) infection, METTL3 decreases viral dsRNA formation, thereby impeding virus-sensing efficacy by RIG-I and dampening antiviral immune signaling (Qiu et al., 2021). However, due to the lack of precise information about RIG-I PAMPs, the universal mechanisms of viral RNA $m^6A$ modification inhibiting RIG-I activation remains unclear. A potential clue has been elucidated in human metapneumovirus (hMPV) infection. Due to the indispensable role of conformational change in RIG-I activation, $m^6A$ modifications in virus genome might block the binding of viral RNAs to RIG-I, which disabled the conformational change of RIG-I, as well as the subsequent MAVS-TBK1 pathways. In this case, $m^6A$-deficient hMPV virion RNA induced much higher RIG-I expression (Lu et al., 2020).

## 2′-O-Methylation and RLRs

Besides $m^6A$ modifications, RNA 2′-O-methyl is a highly conserved process used by RNA viruses to evade sensing by cytosolic RNA sensor proteins (Daffis et al., 2010; Decroly et al., 2011; McFadden et al., 2017). Early studies indicated that the 2′-O-methyl commonly marks viral RNA as "self," which prevents RLRs and downstream signaling pathways (Hyde and Diamond, 2015; McFadden et al., 2017; Jaafar and Kieft, 2019). During HIV-1 infection, viral RNAs were methylated to carry internal 2′-O-methylations by the cellular methyltransferase FTSJ3 (Ringeard et al., 2019). When HIV-1 viruses were produced in FRSJ3 knock-out cells, the induction of IFNs was heavily enhanced in an MDA5-dependent manner (Zust et al., 2011; Ringeard et al., 2019). Similarly, 2′-O-methyls

on the coronavirus family viral RNAs also perturbed type I interferon production that is dependent on either the MDA5 or RIG-I sensing process (Zust et al., 2011; Devarkar et al., 2016).

Additionally, the virus facilitated the capping of viral RNAs at the 5′ terminal to disturb the innate immune sensing process (Bradrick, 2017; De Vlugt et al., 2018). Unlike cellular mRNA transcripts, some viruses, including flaviviruses and coronaviruses, encode enzymes with $m^7G$ and 2′-O-methyltransferase (2′-O-MTases) activity to cap their RNA, It has been showed that 2′-O-MTases-deficient virus are highly sensitive to IFN-I (Chen and Guo, 2016; Bradrick, 2017). Although, the precise factors that sense unmethylated RNAs as invading nucleic acid are still unclear, the interferon-induced protein with tetratricopeptide repeats (IFIT) family has been discovered to function in West neil virus, poxvirus, and coronavirus infection (Daffis et al., 2010). Interestingly, instead of encoding 2-O-MTases, the influenza virus applies a "cap-snatching" strategy to ensure the viral RNA 5′ end modifications that prevent the viral RNA from being sensed by IFIT proteins (De Vlugt et al., 2018).

### Other RNA Modifications and RLRs

Along with $m^6A$ modifications and 2′-O-methyl, other RNA chemical modifications also participate in RLRs sensing-dependent innate immune response (Ahmad et al., 2018). For example, RIG-I and MDA5 detection of dsRNA is blocked by adenosine deaminase acting on RNA (ADAR1), which catalyzes RNA A-to-I modification (Mannion et al., 2014; Yang et al., 2014; Ahmad et al., 2018; Tang et al., 2021). Although it is well-demonstrated how ADAR1-mediated A-to-I modifications impeded MDA5 activation in the mouse study (Liddicoat et al., 2015; de Reuver et al., 2021), MDA5-dependent sensing has rarely been found in A-to-I editing-induced innate immune response. In other cases of A-to-I editing in virus infection, suppression of innate immune IFN responses after virus infection is mainly mediated by cytoplasmic dsRNA sensors protein kinase R (PKR) and oligoadenylate synthetase (OAS; Yang et al., 2014; Radetskyy et al., 2018; Lamers et al., 2019). Rather than upstream dsRNA sensors, PKR, and OAS are identified as pivotal antiviral IFN stimulated genes (ISG). Thus, more details about ADAR1-mediated A-to-I modifications in antiviral innate immune response will be further discussed below.

Similar to A-to-I editing, pseudouridine modifications were shown to abolish RIG-I's filament formation and PAMPs RNA's binding (Peisley et al., 2013). Given the abundant pseudouridine modifications in RNA viruses, especially the positive-sense RNA viruses (McIntyre et al., 2018), this type of uncanonical nucleotides is suggested to regulate various aspects of the antiviral response.

## Toll-Like Receptors and Other PRRs

Another well-characterized PRRs, TLRs, are widely distributed invertebrates. TLRs are anchored in the cell membrane as type I transmembrane proteins (Akira et al., 2006). The ectodomain (N-terminal) of TLRs consists of several leucine-rich repeat (LRR), which connect to the C-terminal Toll/interleukin-1 receptor (TIR) domain by transmembrane (TM) domain (Akira et al., 2001; Kawasaki and Kawai, 2014). Studies have shown that most TLRs function as homology dimers (Kawai and Akira, 2011). Two TIR domains became close to forming a competent signaling state that recruits the adapter proteins (O'Neill et al., 2013). Nearly all the activated TLRs can trigger proinflammatory gene expression despite functioning in specific aspects of antiviral immunity (Kawai and Akira, 2011). To date, 10 TLRs have been identified in human cells. Four of them functioned as immune sensors by detecting pathogens-derived nucleotides (Kawasaki and Kawai, 2014). TLR3 recognizes long dsRNA and recruits TRIF as its dedicated adapter protein. Phosphorylated TRIF provides a signaling hub for IRF3 phosphorylation by TBK1, which then activates downstream signaling pathways of TRIF (Matsumoto et al., 2011; Oshiumi et al., 2011; Liu et al., 2015). TLR7 and TLR8 detect RNA debris as short RNA segments, while TLR9 enables sensing short DNA fragments that contain CG dinucleotide motifs (Chan et al., 2015; de Oliveira Mann and Hornung, 2021). TLR7, 8, and 9 can recruit the adapter protein MyD88 to form a complex known as the Myddosome. Myddsosome interact with IκB kinase and TGF-beta-activated kinase 1 (TAK1) complex to initiate NF-κB and MAPK signaling, respectively (Motshwene et al., 2009). Interestingly, the complex can also trigger IRF activation that depends on TASL that is only expressed in specific cells (Heinz et al., 2020). TASL is also capable of IRF phosphorylation, while in this case, IRF5 and IRF7, as well as IRF3, may be activated to drive antiviral gene expression (Wust et al., 2021).

Although several studies indicate the important roles of TLRs that usually sense long dsRNA inside endolysosome or outside the cells in antiviral innate immune response, they have rarely been found to be regulated by RNA modifications, partly because many RNA viruses expose their genomic dsRNA in the cytoplasm (Akira et al., 2001; Alexopoulou et al., 2001; Heil et al., 2004). Some studies have implied that the epigenetic marks of viral RNA interfere with the innate immune signaling pathway by preventing TLRs activation. For instance, the 2′-O-methyl marks on coronavirus RNAs avoid the recognition of TLR7 to evade the activation of the IFN signaling pathway, while this effect may also be achieved through MDA5 sensing signals (Zust et al., 2011). Coronaviruses replicating in MDA5 or TLR7 deficient mice are detected to the same extent as in IFNR-deficient mice. By employing *in vitro* modified RNA oligos, an early study showed that $m^6A$ limited the capacity of RNAs to activate TLR3, TLR7, and TLR8, while $m^5C$ and Ψ blocked the activation of TLR7 and TLR8 (Kariko et al., 2005). Recent studies applied CRISPER tools to map the function of $m^6A$ and demonstrated that $m^6A$ could suppress macrophage activation through TLR mediated signaling (Tong et al., 2021a). However, more evidence of virus RNA modifications regulating TLR mediated pathways in innate immune response remains to be discovered.

# RNA MODIFICATIONS IN REGULATING IFN SIGNALING PATHWAY

Interferon is a group of signal proteins synthesized and released by host cells in response to stress and infections. Interferon exists widely in human and other animal organisms with highly species specifictiy (Crow and Stetson, 2021). According to the

types of corresponding receptors, interferon can be divided into three types: IFN-I, type II interferon (IFN-II), and type III interferon (IFN-III; Hervas-Stubbs et al., 2011; Stanifer et al., 2019). After infected with viruses, cells release IFNs to restrict the virus infection and even degrade the virions. Although IFNs do not kill the virus directly, IFNs enable the transcription and production of several enzymes that interfere with the viral genome transcription or translation of viral protein components (Sadler and Williams, 2008).

Meanwhile, IFNs also improve the antiviral ability of the surrounding cells. Therefore, IFNs are commonly considered powerful tools and key components in the first line of innate immune defense against viruses infection.

Interferons function mainly through the interactions between IFN molecules and cell surface receptors. Upon specifical recognition and binding by IFNs, the IFN receptors undergo conformational changes, activating the JAK family proteins and promoting the recruitment and phosphorylation of signal transduction and transcriptional activation (STAT) proteins. The phosphorylated STAT is then dimerized and binds to IRF9 to form an ISGF3 complex, a transcriptional factor after transfer into the nucleus. The ISGF3 regulates the expression of numerous kinds of IFN stimulating genes ISGs, which exert strong antiviral effects (Darnell, 2012; Raftery and Stevenson, 2017). However, many viruses (e.g., SARA-COV-2 or influenza virus) encode structural and non-structural viral proteins that ablate the IFN signaling pathways through interaction with other cellular signaling pathways. This usually results in invalid STAT that fails to form phosphorylated ISGF3 complex, further abolishing the expression of antiviral ISGs (Mazewski et al., 2020; Yin et al., 2020; Jung and Lee, 2021). This process is concluded as an evasion of the innate immune response. Evading of the IFN-dependent innate immune response also relates to persistent infections. For example, direct binding of the Borna disease virus (BoDV) encoded P protein to TBK1 can antagonize the IRF3 activation, which prevents IFNβ induction (Unterstab et al., 2005). It is hypothesized that the ability of BoDV to prevent IRF3-dependent genes transcription might prevent the virus from activating the RLR signaling pathway and give rise to persistent BoDV infections in mammalian and avian hosts (Peng et al., 2007).

Whenever ISGs are successfully expressed, they will perform diverse antiviral effects. More than an important effector in IFN-dependent antiviral immune response, some ISGs can also be upregulated directly and independent of IFNs after virus infection. Although ISGs have different effects, on the whole, they all can resist or control infectious pathogens (Schneider et al., 2014; Fensterl et al., 2015). Previous studies showed that ISGs generally functioned by interacting with different co-factors, mediating antiviral effects by promoting viral RNA degradation, abrogating viral proteins translation, or combining both (Nguyen et al., 2001; Bick et al., 2003; Yang and Li, 2020). Moreover, secreted IFNs and induced ISGs may also activate NF-κB or other related innate immune signaling pathways to improve the release of proinflammatory cytokines and/or induce apoptosis that further restricts virus infection (Peteranderl and Herold, 2017).

## m$^6$A in IFN Producing and Effecting

The biological function of m$^6$A is mainly regulated by a methyltransferase (writer), demethylase (eraser), and m$^6$A binding protein (reader; Tong et al., 2018). Many studies have shown that RNA m$^6$A modification plays an important role in innate immune response, while the exact roles of m$^6$A in regulating antiviral IFN signaling displays in opposite aspect (Gokhale et al., 2016; Guo et al., 2020). In some cases, m$^6$A modifications in the virus genome promote the IFN and ISGs induction, whereas, under other circumstances, m$^6$A modification occurs to turn off the antiviral innate immune response. For example, the m$^6$A modifications at specific sites in the HBV transcript restricts the virus replication through IFN α-mediated response. Although HBV is a DNA virus, it replicates through transitional pre-genomic RNA (pgRNA). m$^6$A modification of A1907 in HBV pgRNA is the key regulator of IFN α-mediated pgRNA decay. Further investigation showed that ISG20 selectively degraded the m$^6$A HBV transcripts that are strictly regulated by m$^6$A reader YTHDF2 (Liu et al., 2017; Imam et al., 2020).

Contrary effects were found in encephalon myocarditis virus (EMCV), herpes simplex virus type 1 (HSV-1), and VSV infection. In these cases, YTHDF3 can inhibit the expression of ISGs by promoting the translation of transcriptional inhibitor FOXO3 (Zhang et al., 2019). RAW264.7 cells with YTHDF3 gene deletion have extensive antiviral activity against RNA and DNA virus, and this activity is mediated by the IFNAR1 signal (Zhang et al., 2019). Notably, m$^6$A modification, in this case, regulated the host cell transcripts to inhibit antiviral innate immune response instead of affecting viral RNAs. Indeed, this viral infection-induced host cell m$^6$A epitranscriptome diversity has commonly been found to regulate the antiviral innate immune response. During VSV infection, m$^6$A modifications in MAVS, TRAF3, and TRAF6 are demethylated by ALKBH5 through interacting with the RNA helicase DDX46, which leads these three transcripts to retention in nuclei. Abolished expression of these three transcripts prevents efficient IFN induction (Zheng et al., 2017). Similarly, human cytomegalovirus (hCMV) infection affects host m$^6$A modification machinery, including METTL14 and ALKBH5, reducing the IFNβ production. When knocking down the expression of METTL14, the production of IFNβ and subsequent signaling depending on the JAK/STAT pathway are enhanced, which decreases the production of infectious hCMV virion in infected cells (Rubio et al., 2018).

Interestingly, besides the direct influences of m$^6$A modification on HBV pgRNA, it also has been indicated that m$^6$A modification of tumor suppressor phosphatase and tensin homolog (PTEN) transcript is affected by HBV infection through invaliding PI3K/AKT pathway and inhibiting IRF-3 nuclear export (Kim et al., 2021). Other studies also indicated that DHX58, p65, and IKKγ, which bind to YTHDF2, are mediated by m$^6$A modification, potentially interfering with IFN induction during virus infection (Lichinchi et al., 2016). Besides, YTHDF1, METTL3, and METTL14 have also been found to increase the expression of ISGs like IFITM1 in an m$^6$A binding-dependent manner, which further indicated the m$^6$A methyltransferase complex might

promote the antiviral activity of type I IFN (McFadden et al., 2021).

Excluding the direct regulations of host transcripts by m$^6$A modification, interactions between RNA and RBPs may also be affected by m$^6$A modifications that subsequently affect antiviral IFN response (Bidet et al., 2014). For example, it has been found that during DENV-2 infection, three conserved RBPs, G3BP1, G3BP2, and CAPRIN1, are regulatory factors necessary for antiviral IFN response by promoting the efficient translation of PKR and IFITM2 mRNAs (Arguello et al., 2017; Edupuganti et al., 2017).

### Other RNA Modifications in IFN Producing and Effecting

As one of the most important signaling pathways in innate immune responses, IFN producing and effecting are likely regulated by diversity factors, probably due to numerous protein enzymes evolving in the IFN signaling pathway. For example, NSUN2, the methyltransferase of m$^5$C, has multiple effects on RNA biogenesis, including converting vault ncRNA to vtRNA (Bohnsack et al., 2019; Kong et al., 2020). The vtRNA has been shown to promote Influenza A virus (IAV) replication in A549 cells and mouse lungs through repressing PKR activation and the subsequent effects of interferon (Li et al., 2015; Wnuk et al., 2020). Similarly, DNMT2 has been reported to be required for efficient IFN responses in Drosophila C virus or Sindbis virus infected Drosophila (Durdevic et al., 2013; Bhattacharya et al., 2017).

Other studies also indicate an important role of ADARs, the enzymes mediating A-to-I editing, in modulating innate immune response during virus infection (Pfaller et al., 2021). ADAR1 has a proviral effect on Measles virus (MeV) and VSV infection that depends on PKR activation (Nie et al., 2007; Pfaller et al., 2015), while the suppression of innate immune response by ADAR2 is supposed to rely on STAT1 in the case of Chikungunya virus (CHIKV) and Venezuelan equine encephalitis virus (VEEV; Schoggins et al., 2011; Clavarino et al., 2012). In the case of other viruses, such as BoDV, IAV, and Yellow fever virus (YFV), the mechanisms of ADAR-regulated IFN response remain indistinct (Pfaller et al., 2021). Interestingly, during HIV-1 infection, ADAR1 and ADAR2 may have opposite effects on virus replication, through the forming of DNA:RNA heteroduplex or antiviral innate immune response, respectively (Clerzius et al., 2009; Doria et al., 2009; Pujantell et al., 2017).

## RNA MODIFICATIONS ALTERED SPECIFIC CELLULAR TRANSCRIPTS TO REGULATE ANTIVIRAL RESPONSES

Except for the viral RNA modifications, some RNA modification can also directly control the expression of cytokines or specific genes that important for antiviral responses. In Flavivirus infection, the m$^6$A abundance of host cell transcripts CIRBP and RIOK3 are altered through ER stress and RIG-I signaling respectively, which further regulate virus infection through antiviral immune response (Gokhale et al., 2016, 2020). m$^6$A modification also destroyed the binding of stress granules (SGs) proteins to their RNA partners (Arguello et al., 2017; Fu and Zhuang, 2020). These may explain the diverse function of G3BP1, G3BP2, and CAPRIN1 in virus infection. G3BP1 and CAPRIN1 functioned as proviral factors in vaccinia virus (VACV) and respiratory syncytial virus (RSV) infection, while in contrast, G3BP1 and G3BP2 performed antiviral activity against poliovirus (PV) and alphaviruses (Bidet et al., 2014; Eiermann et al., 2020).

5-Methylcytidine has also been described to affect the expresson of host cell genes, which include cell cycle regulator p21 and immunity-related protein IL-17A (Wnuk et al., 2020). There were also studies suggesting a potential role of m$^5$C in regulating other host genes, including those functioning in antiviral response.

## HOW EPIGENETIC MARKS REGULATE VIRUS INFECTION?

Compared to the heritable evolutions, epitranscriptomic marks on virus genomes that are controlled by various protein factors including endogenous modifying enzymes undergo more dynamic changes. This type of epigentic regulation has been identified to play important roles in virus-host arms race. On one hand, epigenetic modifications of the virus genome prevent the host from recognizing the viral-derived RNAs, thus invaliding the antiviral innate immune response. On the other hand, the host epitranscriptome profiles may vary with virus infection so as to induce expression of uncanonical antiviral genes that restircts virus replication. Notably, the changes to the host transcriptome likely occur in the late stage of virus infection. As a result, the epigenetic machinery tends to facilitate the virus infection at the early stage. However, the dynamic property of RNA modifications on both virus and host transcriptiomes has even complicated epigenetic regulation of the virus-host arms race. Nevertheless, it is worthwhile to harness epigenetic regulations to intervene virus infections and develop antiviral treatments on the future avenue of antiviral research.

## CONCLUSION

Despite the indistinct mechanisms, RNA modifications currently are identified to affect the infection of diverse kinds of viruses, in which the antiviral innate immunity is the most prevalent factor. In the near future, some RNA modifications, including m$^6$A and m$^5$C, may serve as crucial targets for the rational design of improved live attenuated vaccine candidates. Importantly, considering the complex effects of epigenetic modifications in host cell transcriptome, developing these types of antiviral drugs or vaccines still needs additional studies to confirm such assumptions.

## AUTHOR CONTRIBUTIONS

JT, WZ, and GQ: conceptualization and writing, review, and editing. JT and WZ: data curation and writing original draft. YC, QY, and N-NQ: visualization. All authors contributed to the article and approved the submitted version.

## FUNDING

This work was supported by Natural Science Foundation of Hebei Province, China (C2021201010), Hundreds Talents Program of Hebei Province, China (E2020050011), and Advanced Talents Incubation Program of the Hebei University (521000981413) to JT, the National Natural Science Foundation of China (31971227), the Science and Technology Project of Hebei Education Department (ZD2021010), and the Natural Science Foundation of Hebei Province, China (C2020201039).

## SUPPLEMENTARY MATERIAL

The Supplementary Material for this article can be found online at: https://www.frontiersin.org/articles/10.3389/fmicb.2022.845625/full#supplementary-material

## REFERENCES

Aguirre, S., Luthra, P., Sanchez-Aparicio, M. T., Maestre, A. M., Patel, J., Lamothe, F., et al. (2017). Dengue virus NS2B protein targets cGAS for degradation and prevents mitochondrial DNA sensing during infection. *Nat. Microbiol.* 2:17037. doi: 10.1038/nmicrobiol.2017.37

Ahmad, S., Mu, X., Yang, F., Greenwald, E., Park, J. W., Jacob, E., et al. (2018). Breaching self-tolerance to Alu duplex RNA underlies MDA5-mediated inflammation. *Cell* 172, 797.e13–810.e13. doi: 10.1016/j.cell.2017.12.016

Akira, S., Takeda, K., and Kaisho, T. (2001). Toll-like receptors: critical proteins linking innate and acquired immunity. *Nat. Immunol.* 2, 675–680. doi: 10.1038/90609

Akira, S., Uematsu, S., and Takeuchi, O. (2006). Pathogen recognition and innate immunity. *Cell* 124, 783–801. doi: 10.1016/j.cell.2006.02.015

Alexopoulou, L., Holt, A. C., Medzhitov, R., and Flavell, R. A. (2001). Recognition of double-stranded RNA and activation of NF-kappaB by toll-like receptor 3. *Nature* 413, 732–738. doi: 10.1038/35099560

Arguello, A. E., DeLiberto, A. N., and Kleiner, R. E. (2017). RNA chemical proteomics reveals the N(6)-methyladenosine (m(6)A)-regulated protein-RNA interactome. *J. Am. Chem. Soc.* 139, 17249–17252. doi: 10.1021/jacs.7b09213

Babamale, A. O., and Chen, S. T. (2021). Nod-like receptors: critical intracellular sensors for host protection and cell death in microbial and parasitic infections. *Int. J. Mol. Sci.* 22:11398. doi: 10.3390/ijms222111398

Bass, B. L. (2002). RNA editing by adenosine deaminases that act on RNA. *Annu. Rev. Biochem.* 71, 817–846. doi: 10.1146/annurev.biochem.71.110601.135501

Becker, H. F., Motorin, Y., Florentz, C., Giegé, R., and Grosjean, H. (1998). Pseudouridine and ribothymidine formation in the tRNA-like domain of turnip yellow mosaic virus RNA. *Nucleic Acids Res.* 26, 3991–3997. doi: 10.1093/nar/26.17.3991

Belanger, F., Stepinski, J., Darzynkiewicz, E., and Pelletier, J. (2010). Characterization of hMTr1, a human Cap1 2′-O-ribose methyltransferase. *J. Biol. Chem.* 285, 33037–33044. doi: 10.1074/jbc.M110.155283

Beutler, B. A. (2009). TLRs and innate immunity. *Blood* 113, 1399–1407. doi: 10.1182/blood-2008-07-019307

Bhattacharya, T., Newton, I. L. G., and Hardy, R. W. (2017). Wolbachia elevates host methyltransferase expression to block an RNA virus early during infection. *PLoS Pathog.* 13:e1006427. doi: 10.1371/journal.ppat.1006427

Bick, M. J., Carroll, J. W., Gao, G., Goff, S. P., Rice, C. M., and MacDonald, M. R. (2003). Expression of the zinc-finger antiviral protein inhibits alphavirus replication. *J. Virol.* 77, 11555–11562. doi: 10.1128/JVI.77.21.11555-11562.2003

Bidet, K., Dadlani, D., and Garcia-Blanco, M. A. (2014). G3BP1, G3BP2 and CAPRIN1 are required for translation of interferon stimulated mRNAs and are targeted by a dengue virus non-coding RNA. *PLoS Pathog.* 10:e1004242. doi: 10.1371/journal.ppat.1004242

Bohnsack, K. E., Hobartner, C., and Bohnsack, M. T. (2019). Eukaryotic 5-methylcytosine (m(5)C) RNA methyltransferases: mechanisms, cellular functions, and links to disease. *Genes* 10:102. doi: 10.3390/genes10020102

Bonizzi, G., and Karin, M. (2004). The two NF-kappaB activation pathways and their role in innate and adaptive immunity. *Trends Immunol.* 25, 280–288. doi: 10.1016/j.it.2004.03.008

Bradrick, S. S. (2017). Causes and consequences of flavivirus RNA methylation. *Front. Microbiol.* 8:2374. doi: 10.3389/fmicb.2017.02374

Chan, M. P., Onji, M., Fukui, R., Kawane, K., Shibata, T., Saitoh, S. I., et al. (2015). DNase II-dependent DNA digestion is required for DNA sensing by TLR9. *Nat. Commun.* 6:5853. doi: 10.1038/ncomms6853

Chang, D. C., Hoang, L. T., Mohamed Naim, A. N., Dong, H., Schreiber, M. J., Hibberd, M. L., et al. (2016). Evasion of early innate immune response by 2′-O-methylation of dengue genomic RNA. *Virology* 499, 259–266. doi: 10.1016/j.virol.2016.09.022

Chen, C. X., Cho, D. S., Wang, Q., Lai, F., Carter, K. C., and Nishikura, K. (2000). A third member of the RNA-specific adenosine deaminase gene family, ADAR3, contains both single- and double-stranded RNA binding domains. *RNA* 6, 755–767. doi: 10.1017/S1355838200000170

Chen, Y., and Guo, D. (2016). Molecular mechanisms of coronavirus RNA capping and methylation. *Virol. Sin.* 31, 3–11. doi: 10.1007/s12250-016-3726-4

Chen, S., Kumar, S., Espada, C. E., Tirumuru, N., Cahill, M. P., Hu, L., et al. (2021). N6-methyladenosine modification of HIV-1 RNA suppresses type-I interferon induction in differentiated monocytic cells and primary macrophages. *PLoS Pathog.* 17:e1009421. doi: 10.1371/journal.ppat.1009421

Chou, W. C., Rampanelli, E., Li, X., and Ting, J. P-Y. (2021). Impact of intracellular innate immune receptors on immunometabolism. *Cell. Mol. Immunol.* doi: 10.1038/s41423-021-00780-y [Epub ahead of print].

Chung, H., Calis, J. J. A., Wu, X., Sun, T., Yu, Y., Sarbanes, S. L., et al. (2018). Human ADAR1 prevents endogenous RNA from triggering translational shutdown. *Cell* 172, 811.e14–824.e14. doi: 10.1016/j.cell.2017.12.038

Clavarino, G., Claudio, N., Couderc, T., Dalet, A., Judith, D., Camosseto, V., et al. (2012). Induction of GADD34 is necessary for dsRNA-dependent interferon-beta production and participates in the control of chikungunya virus infection. *PLoS Pathog.* 8:e1002708. doi: 10.1371/journal.ppat.1002708

Clerzius, G., Gelinas, J. F., Daher, A., Bonnet, M., Meurs, E. F., and Gatignol, A. (2009). ADAR1 interacts with PKR during human immunodeficiency virus infection of lymphocytes and contributes to viral replication. *J. Virol.* 83, 10119–10128. doi: 10.1128/JVI.02457-08

Courtney, D. G. (2021). Post-transcriptional regulation of viral RNA through epitranscriptional modification. *Cells* 10:1129. doi: 10.3390/cells10051129

Courtney, D. G., Tsai, K., Bogerd, H. P., Kennedy, E. M., Law, B. A., Emery, A., et al. (2019). Epitranscriptomic addition of m(5)C to HIV-1 transcripts regulates viral gene expression. *Cell Host Microbe* 26, 217.e6–227.e6. doi: 10.1016/j.chom.2019.07.005

Creagh, E. M., and O'Neill, L. A. (2006). TLRs, NLRs and RLRs: a trinity of pathogen sensors that co-operate in innate immunity. *Trends Immunol.* 27, 352–357. doi: 10.1016/j.it.2006.06.003

Crow, Y. J., and Stetson, D. B. (2021). The type I interferonopathies: 10 years on. *Nat. Rev. Immunol.* 20, 1–13. doi: 10.1038/s41577-021-00633-9

Crowl, J. T., Gray, E. E., Pestal, K., Volkman, H. E., and Stetson, D. B. (2017). Intracellular nucleic acid detection in autoimmunity. *Annu. Rev. Immunol.* 35, 313–336. doi: 10.1146/annurev-immunol-051116-052331

Cui, S., Eisenacher, K., Kirchhofer, A., Brzózka, K., Lammens, A., Lammens, K., et al. (2008). The C-terminal regulatory domain is the RNA 5′-triphosphate sensor of RIG-I. *Mol. Cell* 29, 169–179. doi: 10.1016/j.molcel.2007.10.032

Daffis, S., Szretter, K. J., Schriewer, J., Li, J., Youn, S., Errett, J., et al. (2010). 2′-O methylation of the viral mRNA cap evades host restriction by IFIT family members. *Nature* 468, 452–456. doi: 10.1038/nature09489

Darnell, J. E. (2012). The JAK-STAT pathway at 20. *JAKSTAT* 1:2. doi: 10.4161/jkst.18726

de Oliveira Mann, C. C., and Hornung, V. (2021). Molecular mechanisms of nonself nucleic acid recognition by the innate immune system. *Eur. J. Immunol.* 51, 1897–1910. doi: 10.1002/eji.202049116

de Reuver, R., Dierick, E., Wiernicki, B., Staes, K., Seys, L., de Meester, E., et al. (2021). ADAR1 interaction with Z-RNA promotes editing of endogenous double-stranded RNA and prevents MDA5-dependent immune activation. *Cell Rep.* 36:109500. doi: 10.1016/j.celrep.2021.109500

De Vlugt, C., Sikora, D., and Pelchat, M. (2018). Insight into influenza: a virus cap-snatching. *Viruses* 10:641. doi: 10.3390/v10110641

Decroly, E., Ferron, F., Lescar, J., and Canard, B. (2011). Conventional and unconventional mechanisms for capping viral mRNA. *Nat. Rev. Microbiol.* 10, 51–65. doi: 10.1038/nrmicro2675

Dev, A., Iyer, S., Razani, B., and Cheng, G. (2011). NF-kappaB and innate immunity. *Curr. Top. Microbiol. Immunol.* 349, 115–143. doi: 10.1007/82_2010_102

Devarkar, S. C., Wang, C., Miller, M. T., Ramanathan, A., Jiang, F., Khan, A. G., et al. (2016). Structural basis for m7G recognition and 2′-O-methyl discrimination in capped RNAs by the innate immune receptor RIG-I. *Proc. Natl. Acad. Sci. U. S. A.* 113, 596–601. doi: 10.1073/pnas.1515152113

Dominissini, D., Moshitch-Moshkovitz, S., Schwartz, S., Salmon-Divon, M., Ungar, L., Osenberg, S., et al. (2012). Topology of the human and mouse m6A RNA methylomes revealed by m6A-seq. *Nature* 485, 201–206. doi: 10.1038/nature11112

Dong, H., Chang, D. C., Hua, M. H. C., Lim, S. P., Chionh, Y. H., Hia, F., et al. (2012). 2′-O methylation of internal adenosine by flavivirus NS5 methyltransferase. *PLoS Pathog.* 8:e1002642. doi: 10.1371/journal.ppat.1002642

Doria, M., Neri, F., Gallo, A., Farace, M. G., and Michienzi, A. (2009). Editing of HIV-1 RNA by the double-stranded RNA deaminase ADAR1 stimulates viral infection. *Nucleic Acids Res.* 37, 5848–5858. doi: 10.1093/nar/gkp604

Durbin, A. F., Wang, C., Gallo, A., Farace, M. G., and Michienzi, A. (2016). RNAs containing modified nucleotides fail to trigger RIG-I conformational changes for innate immune signaling. *mBio* 7, e00833–e00916. doi: 10.1128/mBio.00833-16

Durdevic, Z., Hanna, K., Gold, B., Pollex, T., Cherry, S., Lyko, F., et al. (2013). Efficient RNA virus control in *drosophila* requires the RNA methyltransferase Dnmt2. *EMBO Rep.* 14, 269–275. doi: 10.1038/embor.2013.3

Edupuganti, R. R., Geiger, S., Lindeboom, R. G. H., Shi, H., Hsu, P. J., Lu, Z., et al. (2017). N(6)-methyladenosine (m(6)A) recruits and repels proteins to regulate mRNA homeostasis. *Nat. Struct. Mol. Biol.* 24, 870–878. doi: 10.1038/nsmb.3462

Eiermann, N., Haneke, K., Sun, Z., Stoecklin, G., and Ruggieri, A. (2020). Dance with the devil: stress granules and signaling in antiviral responses. *Viruses* 12:984. doi: 10.3390/v12090984

Eisenberg, E., and Levanon, E. Y. (2018). A-to-I RNA editing—immune protector and transcriptome diversifier. *Nat. Rev. Genet.* 19, 473–490. doi: 10.1038/s41576-018-0006-1

Fensterl, V., Chattopadhyay, S., and Sen, G. C. (2015). No love lost between viruses and interferons. *Annu. Rev. Virol.* 2, 549–572. doi: 10.1146/annurev-virology-100114-055249

Frye, M., Harada, B. T., Behm, M., and He, C. (2018). RNA modifications modulate gene expression during development. *Science* 361, 1346–1349. doi: 10.1126/science.aau1646

Fu, Y., and Zhuang, X. (2020). $m^{(6)}A$-binding YTHDF proteins promote stress granule formation. *Nat. Chem. Biol.* 16, 955–963. doi: 10.1038/s41589-020-0524-y

Ge, Y., Ling, T., Wang, Y., Jia, X., Xie, X., Chen, R., et al. (2021). Degradation of WTAP blocks antiviral responses by reducing the $m^{(6)}A$ levels of IRF3 and IFNAR1 mRNA. *EMBO Rep.* 22:e52101. doi: 10.15252/embr.202052101

George, C. X., John, L., and Samuel, C. E. (2014). An RNA editor, adenosine deaminase acting on double-stranded RNA (ADAR1). *J. Interf. Cytokine Res.* 34, 437–446. doi: 10.1089/jir.2014.0001

Gokhale, N. S., McIntyre, A. B. R., Mattocks, M. D., Holley, C. L., Lazear, H. M., Mason, C. E., et al. (2020). Altered m(6)A modification of specific cellular transcripts affects flaviviridae infection. *Mol. Cell* 77, 542.e8–555.e8. doi: 10.1016/j.molcel.2019.11.007

Gokhale, N. S., McIntyre, A. B. R., McFadden, M. J., Roder, A. E., Kennedy, E. M., Gandara, J. A., et al. (2016). N6-methyladenosine in flaviviridae viral RNA genomes regulates infection. *Cell Host Microbe* 20, 654–665. doi: 10.1016/j.chom.2016.09.015

Goubau, D., Schlee, M., Deddouche, S., Pruijssers, A. J., Zillinger, T., Goldeck, M., et al. (2014). Antiviral immunity via RIG-I-mediated recognition of RNA bearing 5′-diphosphates. *Nature* 514, 372–375. doi: 10.1038/nature13590

Guo, G., Wang, H., Shi, X., Ye, L., Yan, K., Chen, Z., et al. (2020). Disease activity-associated alteration of mRNA $m^{(5)}C$ methylation in CD4(+) T cells of systemic lupus erythematosus. *Front. Cell Dev. Biol.* 8:430. doi: 10.3389/fcell.2020.00430

Heil, F., Hemmi, H., Hochrein, H., Ampenberger, F., Kirschning, C., Akira, S., et al. (2004). Species-specific recognition of single-stranded RNA via toll-like receptor 7 and 8. *Science* 303, 1526–1529. doi: 10.1126/science.1093620

Heinz, L. X., Lee, J., Kapoor, U., Kartnig, F., Sedlyarov, V., Papakostas, K., et al. (2020). TASL is the SLC15A4-associated adaptor for IRF5 activation by TLR7-9. *Nature* 581, 316–322. doi: 10.1038/s41586-020-2282-0

Hervas-Stubbs, S., Perez-Gracia, J. L., Rouzaut, A., Sanmamed, M. F., le Bon, A., and Melero, I. (2011). Direct effects of type I interferons on cells of the immune system. *Clin. Cancer Res.* 17, 2619–2627. doi: 10.1158/1078-0432.CCR-10-1114

Hocine, S., Singer, R. H., and Grünwald, D. (2010). RNA processing and export. *Cold Spring Harb. Perspect. Biol.* 2:a000752. doi: 10.1101/cshperspect.a000752

Hornung, V., Ellegast, J., Kim, S., Brzózka, K., Jung, A., Kato, H., et al. (2006). 5′-Triphosphate RNA is the ligand for RIG-I. *Science* 314, 994–997. doi: 10.1126/science.1132505

Hwang, S. Y., Hur, K. Y., Kim, J.-R., Cho, K.-H., Kim, S.-H., and Yoo, J.-Y. (2013). Biphasic RLR-IFN-beta response controls the balance between antiviral immunity and cell damage. *J. Immunol.* 190, 1192–1200. doi: 10.4049/jimmunol.1202326

Hyde, J. L., and Diamond, M. S. (2015). Innate immune restriction and antagonism of viral RNA lacking 2-O methylation. *Virology* 479–480, 66–74. doi: 10.1016/j.virol.2015.01.019

Imam, H., Kim, G. W., Mir, S. A., Khan, M., and Siddiqui, A. (2020). Interferon-stimulated gene 20 (ISG20) selectively degrades N6-methyladenosine modified hepatitis B virus transcripts. *PLoS Pathog.* 16:e1008338. doi: 10.1371/journal.ppat.1008338

Jaafar, Z. A., and Kieft, J. S. (2019). Viral RNA structure-based strategies to manipulate translation. *Nat. Rev. Microbiol.* 17, 110–123. doi: 10.1038/s41579-018-0117-x

Jia, G., Fu, Y., Zhao, X., Dai, Q., Zheng, G., Yang, Y., et al. (2011). $N^6$-methyladenosine in nuclear RNA is a major substrate of the obesity-associated FTO. *Nat. Chem. Biol.* 7, 885–887. doi: 10.1038/nchembio.687

Jiang, F., Ramanathan, A., Miller, M. T., Tang, G. Q., Gale, M., Patel, S. S., et al. (2011). Structural basis of RNA recognition and activation by innate immune receptor RIG-I. *Nature* 479, 423–427. doi: 10.1038/nature10537

Jung, H. E., and Lee, H. K. (2021). Current understanding of the innate control of toll-like receptors in response to SARS-CoV-2 infection. *Viruses* 13:2132. doi: 10.3390/v13112132

Kariko, K., Buckstein, M., Ni, H., and Weissman, D. (2005). Suppression of RNA recognition by toll-like receptors: the impact of nucleoside modification and the evolutionary origin of RNA. *Immunity* 23, 165–175. doi: 10.1016/j.immuni.2005.06.008

Kato, H., Takeuchi, O., Sato, S., Yoneyama, M., Yamamoto, M., Matsui, K., et al. (2006). Differential roles of MDA5 and RIG-I helicases in the recognition of RNA viruses. *Nature* 441, 101–105. doi: 10.1038/nature04734

Kawai, T., and Akira, S. (2011). Toll-like receptors and their crosstalk with other innate receptors in infection and immunity. *Immunity* 34, 637–650. doi: 10.1016/j.immuni.2011.05.006

Kawasaki, T., and Kawai, T. (2014). Toll-like receptor signaling pathways. *Front. Immunol.* 5:461. doi: 10.3389/fimmu.2014.00461

Kim, G. W., Imam, H., Khan, M., Mir, S. A., Kim, S. J., Yoon, S. K., et al. (2021). HBV-induced increased N6 methyladenosine modification of PTEN RNA affects innate immunity and contributes to HCC. *Hepatology* 73, 533–547. doi: 10.1002/hep.31313

Kim, G. W., Imam, H., Khan, M., and Siddiqui, A. (2020). $N^{(6)}$-Methyladenosine modification of hepatitis B and C viral RNAs attenuates host innate immunity via RIG-I signaling. *J. Biol. Chem.* 295, 13123–13133. doi: 10.1074/jbc.RA120.014260

Kong, W., Biswas, A., Zhou, D., Fiches, G., Fujinaga, K., Santoso, N., et al. (2020). Nucleolar protein NOP2/NSUN1 suppresses HIV-1 transcription and promotes viral latency by competing with tat for TAR binding and methylation. *PLoS Pathog.* 16:e1008430. doi: 10.1371/journal.ppat.1008430

Kowalinski, E., Lunardi, T., McCarthy, A. A., Louber, J., Brunel, J., Grigorov, B., et al. (2011). Structural basis for the activation of innate immune pattern-recognition receptor RIG-I by viral RNA. *Cell* 147, 423–435. doi: 10.1016/j.cell.2011.09.039

Lamers, M. M., van den Hoogen, B. G., and Haagmans, B. L. (2019). ADAR1: "editor-in-chief" of cytoplasmic innate immunity. *Front. Immunol.* 10:1763. doi: 10.3389/fimmu.2019.01763

Lavelle, E. C., Murphy, C., O'Neill, L. A. J., and Creagh, E. M. (2010). The role of TLRs, NLRs, and RLRs in mucosal innate immunity and homeostasis. *Mucosal Immunol.* 3, 17–28. doi: 10.1038/mi.2009.124

Lewis, C. J., Pan, T., and Kalsotra, A. (2017). RNA modifications and structures cooperate to guide RNA-protein interactions. *Nat. Rev. Mol. Cell Biol.* 18, 202–210. doi: 10.1038/nrm.2016.163

Li, F., Chen, Y., Zhang, Z., Ouyang, J., Wang, Y., Yan, R., et al. (2015). Robust expression of vault RNAs induced by influenza A virus plays a critical role in suppression of PKR-mediated innate immunity. *Nucleic Acids Res.* 43, 10321–10337. doi: 10.1093/nar/gkv1078

Li, N., Hui, H., Bray, B., Gonzalez, G. M., Zeller, M., Anderson, K. G., et al. (2021). METTL3 regulates viral m$^6$A RNA modification and host cell innate immune responses during SARS-CoV-2 infection. *Cell Rep.* 35:109091. doi: 10.1016/j.celrep.2021.109091

Lichinchi, G., Gao, S., Saletore, Y., Gonzalez, G. M., Bansal, V., Wang, Y., et al. (2016). Dynamics of the human and viral m(6)A RNA methylomes during HIV-1 infection of T cells. *Nat. Microbiol.* 1:16011. doi: 10.1038/nmicrobiol.2016.11

Liddicoat, B. J., Piskol, R., Chalk, A. M., Ramaswami, G., Higuchi, M., Hartner, J. C., et al. (2015). RNA editing by ADAR1 prevents MDA5 sensing of endogenous dsRNA as nonself. *Science* 349, 1115–1120. doi: 10.1126/science.aac7049

Liu, S., Cai, X., Cong, Q., Chen, X., Li, T., Du, F., et al. (2015). Phosphorylation of innate immune adaptor proteins MAVS, STING, and TRIF induces IRF3 activation. *Science* 347:aaa2630. doi: 10.1126/science.aaa2630

Liu, G., Lu, Y., Thulasi Raman, S. N., Xu, F., Wu, Q., Li, Z., et al. (2018). Nuclear-resident RIG-I senses viral replication inducing antiviral immunity. *Nat. Commun.* 9:3199. doi: 10.1038/s41467-018-05745-w

Liu, Y., Nie, H., Mao, R., Mitra, B., Cai, D., Yan, R., et al. (2017). Interferon-inducible ribonuclease ISG20 inhibits hepatitis B virus replication through directly binding to the epsilon stem-loop structure of viral RNA. *PLoS Pathog.* 13:e1006296. doi: 10.1371/journal.ppat.1006296

Lu, M., Xue, M., Wang, H.-T., Kairis, E. L., Ahmad, S., Wei, J., et al. (2021). Nonsegmented negative-sense RNA viruses utilize N$^{(6)}$-methyladenosine (m(6)A) as a common strategy to evade host innate immunity. *J. Virol.* 95, e01939–e02120. doi: 10.1128/JVI.01939-20

Lu, M., Zhang, Z., Xue, M., Zhao, B. S., Harder, O., Li, A., et al. (2020). N(6)-methyladenosine modification enables viral RNA to escape recognition by RNA sensor RIG-I. *Nat. Microbiol.* 5, 584–598. doi: 10.1038/s41564-019-0653-9

Luo, D., Ding, S. C., Vela, A., Kohlway, A., Lindenbach, B. D., and Pyle, A. M. (2011). Structural insights into RNA recognition by RIG-I. *Cell* 147, 409–422. doi: 10.1016/j.cell.2011.09.023

Luo, D., Kohlway, A., Vela, A., and Pyle, A. M. (2012). Visualizing the determinants of viral RNA recognition by innate immune sensor RIG-I. *Structure* 20, 1983–1988. doi: 10.1016/j.str.2012.08.029

Ma, Y., Wang, X., Luo, W., Xiao, J., Song, X., Wang, Y., et al. (2021). Roles of emerging RNA-binding activity of cGAS in innate antiviral response. *Front. Immunol.* 12:741599. doi: 10.3389/fimmu.2021.741599

Mannion, N. M., Greenwood, S. M., Young, R., Cox, S., Brindle, J., Read, D., et al. (2014). The RNA-editing enzyme ADAR1 controls innate immune responses to RNA. *Cell Rep.* 9, 1482–1494. doi: 10.1016/j.celrep.2014.10.041

Marchand, V., and Motorin, Y. (2021). Detection and functions of viral RNA modifications: perspectives in biology and medicine. *Virologie* 25, 5–20. doi: 10.1684/vir.2021.0884

Markham, R., and Smith, J. D. (1951). Structure of ribonucleic acid. *Nature* 168, 406–408. doi: 10.1038/168406a0

Matsumoto, M., Oshiumi, H., and Seya, T. (2011). Antiviral responses induced by the TLR3 pathway. *Rev. Med. Virol.* 21, 67–77. doi: 10.1002/rmv.680

Mazewski, C., Perez, R. E., Fish, E. N., and Platanias, L. C. (2020). Type I interferon (IFN)-regulated activation of canonical and non-canonical signaling pathways. *Front. Immunol.* 11:606456. doi: 10.3389/fimmu.2020.606456

McFadden, M. J., Gokhale, N. S., and Horner, S. M. (2017). Protect this house: cytosolic sensing of viruses. *Curr. Opin. Virol.* 22, 36–43. doi: 10.1016/j.coviro.2016.11.012

McFadden, M. J., McIntyre, A. B. R., Mourelatos, H., Abell, N. S., Gokhale, N. S., Ipas, H., et al. (2021). Post-transcriptional regulation of antiviral gene expression by N6-methyladenosine. *Cell Rep.* 34:108798. doi: 10.1016/j.celrep.2021.108798

McIntyre, W., Netzband, R., Bonenfant, G., Biegel, J. M., Miller, C., Fuchs, G., et al. (2018). Positive-sense RNA viruses reveal the complexity and dynamics of the cellular and viral epitranscriptomes during infection. *Nucleic Acids Res.* 46, 5776–5791. doi: 10.1093/nar/gky029

Meyer, K. D., and Jaffrey, S. R. (2017). Rethinking m$^6$A Readers, Writers, and Erasers. *Annu. Rev. Cell Dev. Biol.* 33, 319–342. doi: 10.1146/annurev-cellbio-100616-060758

Motshwene, P. G., Moncrieffe, M. C., Grossmann, J. G., Kao, C., Ayaluru, M., Sandercock, A. M., et al. (2009). An oligomeric signaling platform formed by the toll-like receptor signal transducers MyD88 and IRAK-4. *J. Biol. Chem.* 284, 25404–25411. doi: 10.1074/jbc.M109.022392

Nachtergaele, S., and He, C. (2018). Chemical modifications in the life of an mRNA transcript. *Annu. Rev. Genet.* 52, 349–372. doi: 10.1146/annurev-genet-120417-031522

Netzband, R., and Pager, C. T. (2020). Epitranscriptomic marks: emerging modulators of RNA virus gene expression. *Wiley Interdiscip. Rev. RNA* 11:e1576. doi: 10.1002/wrna.1576

Nguyen, L. H., Espert, L., Mechti, N., and Wilson, D. M. (2001). The human interferon- and estrogen-regulated ISG20/HEM45 gene product degrades single-stranded RNA and DNA in vitro. *Biochemistry* 40, 7174–7179. doi: 10.1021/bi010141t

Nie, Y., Hammond, G. L., and Yang, J. H. (2007). Double-stranded RNA deaminase ADAR1 increases host susceptibility to virus infection. *J. Virol.* 81, 917–923. doi: 10.1128/JVI.01527-06

O'Neill, L. A., Golenbock, D., and Bowie, A. G. (2013). The history of toll-like receptors—redefining innate immunity. *Nat. Rev. Immunol.* 13, 453–460. doi: 10.1038/nri3446

Oshiumi, H., Okamoto, M., Fujii, K., Kawanishi, T., Matsumoto, M., Koike, S., et al. (2011). The TLR3/TICAM-1 pathway is mandatory for innate immune responses to poliovirus infection. *J. Immunol.* 187, 5320–5327. doi: 10.4049/jimmunol.1101503

Peisley, A., Wu, B., Yao, H., Walz, T., and Hur, S. (2013). RIG-I forms signaling-competent filaments in an ATP-dependent, ubiquitin-independent manner. *Mol. Cell* 51, 573–583. doi: 10.1016/j.molcel.2013.07.024

Peng, G., Zhang, F., Zhang, Q., Wu, K., Zhu, F., and Wu, J. (2007). Borna disease virus P protein inhibits nitric oxide synthase gene expression in astrocytes. *Virology* 366, 446–452. doi: 10.1016/j.virol.2007.04.031

Peteranderl, C., and Herold, S. (2017). The impact of the interferon/TNF-related apoptosis-inducing ligand signaling axis on disease progression in respiratory viral infection and beyond. *Front. Immunol.* 8:313. doi: 10.3389/fimmu.2017.00313

Pfaller, C. K., George, C. X., and Samuel, C. E. (2021). Adenosine deaminases acting on RNA (ADARs) and viral infections. *Annu. Rev. Virol.* 8, 239–264. doi: 10.1146/annurev-virology-091919-065320

Pfaller, C. K., Mastorakos, G. M., Matchett, W. E., Ma, X., Samuel, C. E., and Cattaneo, R. (2015). Measles virus defective interfering RNAs are generated frequently and early in the absence of C protein and can be destabilized by adenosine deaminase acting on RNA-1-like hypermutations. *J. Virol.* 89, 7735–7747. doi: 10.1128/JVI.01017-15

Pichlmair, A., Schulz, O., Tan, C. P., Näslund, T. I., Liljeström, P., Weber, F., et al. (2006). RIG-I-mediated antiviral responses to single-stranded RNA bearing 5′-phosphates. *Science* 314, 997–1001. doi: 10.1126/science.1132998

Pujantell, M., Riveira-Munoz, E., Badia, R., Castellví, M., Garcia-Vidal, E., Sirera, G., et al. (2017). RNA editing by ADAR1 regulates innate and antiviral immune functions in primary macrophages. *Sci. Rep.* 7:13339. doi: 10.1038/s41598-017-13580-0

Qiu, W., Zhang, Q., Zhang, R., Lu, Y., Wang, X., Tian, H., et al. (2021). N$^{(6)}$-methyladenosine RNA modification suppresses antiviral innate sensing pathways via reshaping double-stranded RNA. *Nat. Commun.* 12:1582. doi: 10.1038/s41467-021-21904-y

Radetskyy, R., Daher, A., and Gatignol, A. (2018). ADAR1 and PKR, interferon stimulated genes with clashing effects on HIV-1 replication. *Cytokine Growth Factor Rev.* 40, 48–58. doi: 10.1016/j.cytogfr.2018.03.007

Raftery, N., and Stevenson, N. J. (2017). Advances in anti-viral immune defence: revealing the importance of the IFN JAK/STAT pathway. *Cell. Mol. Life Sci.* 74, 2525–2535. doi: 10.1007/s00018-017-2520-2

Ramanathan, A., Robb, G. B., and Chan, S.-H. (2016). mRNA capping: biological functions and applications. *Nucleic Acids Res.* 44, 7511–7526. doi: 10.1093/nar/gkw551

Reid, R., Greene, P. J., and Santi, D. V. (1999). Exposition of a family of RNA m(5)C methyltransferases from searching genomic and proteomic sequences. *Nucleic Acids Res.* 27, 3138–3145. doi: 10.1093/nar/27.15.3138

Ringeard, M., Marchand, V., Decroly, E., Motorin, Y., and Bennasser, Y. (2019). FTSJ3 is an RNA 2′-O-methyltransferase recruited by HIV to avoid innate immune sensing. *Nature* 565, 500–504. doi: 10.1038/s41586-018-0841-4

Rius, J., Guma, M., Schachtrup, C., Akassoglou, K., Zinkernagel, A. S., Nizet, V., et al. (2008). NF-kappaB links innate immunity to the hypoxic response through transcriptional regulation of HIF-1alpha. *Nature* 453, 807–811. doi: 10.1038/nature06905

Roundtree, I. A., Evans, M. E., Pan, T., and He, C. (2017). Dynamic RNA modifications in gene expression regulation. *Cell* 169, 1187–1200. doi: 10.1016/j.cell.2017.05.045

Rubio, R. M., Depledge, D. P., Bianco, C., Thompson, L., and Mohr, I. (2018). RNA $m^{(6)}A$ modification enzymes shape innate responses to DNA by regulating interferon beta. *Genes Dev.* 32, 1472–1484. doi: 10.1101/gad.319475.118

Sadler, A. J., and Williams, B. R. (2008). Interferon-inducible antiviral effectors. *Nat. Rev. Immunol.* 8, 559–568. doi: 10.1038/nri2314

Samuel, C. E. (2011). Adenosine deaminases acting on RNA (ADARs) are both antiviral and proviral. *Virology* 411, 180–193. doi: 10.1016/j.virol.2010.12.004

Schneider, W. M., Chevillotte, M. D., and Rice, C. M. (2014). Interferon-stimulated genes: a complex web of host defenses. *Annu. Rev. Immunol.* 32, 513–545. doi: 10.1146/annurev-immunol-032713-120231

Schoggins, J. W., MacDuff, D. A., Imanaka, N., Gainey, M. D., Shrestha, B., Eitson, J. L., et al. (2014). Pan-viral specificity of IFN-induced genes reveals new roles for cGAS in innate immunity. *Nature* 505, 691–695. doi: 10.1038/nature12862

Schoggins, J. W., Wilson, S. J., Panis, M., Murphy, M. Y., Jones, C. T., Bieniasz, P., et al. (2011). A diverse range of gene products are effectors of the type I interferon antiviral response. *Nature* 472, 481–485. doi: 10.1038/nature09907

Schustak, J., Twarog, M., Wu, X., Wu, H. Y., Huang, Q., and Bao, Y. (2021). Mechanism of nucleic acid sensing in retinal pigment epithelium (RPE): RIG-I mediates type I interferon response in human RPE. *J. Immunol. Res.* 2021:9975628. doi: 10.1155/2021/9975628

Serra, M. J., Smolter, P. E., and Westhof, E. (2004). Pronounced instability of tandem IU base pairs in RNA. *Nucleic Acids Res.* 32, 1824–1828. doi: 10.1093/nar/gkh501

Shatkin, A. J. (1976). Capping of eucaryotic mRNAs. *Cell* 9, 645–653. doi: 10.1016/0092-8674(76)90128-8

Shi, H., Wei, J., and He, C. (2019). Where, when, and how: context-dependent functions of RNA methylation writers, readers, and erasers. *Mol. Cell* 74, 640–650. doi: 10.1016/j.molcel.2019.04.025

Smietanski, M., Werner, M., Purta, E., Kaminska, K. H., Stepinski, J., Darzynkiewicz, E., et al. (2014). Structural analysis of human 2′-O-ribose methyltransferases involved in mRNA cap structure formation. *Nat. Commun.* 5:3004. doi: 10.1038/ncomms4004

Stanifer, M. L., Pervolaraki, K., and Boulant, S. (2019). Differential regulation of type I and type III interferon signaling. *Int. J. Mol. Sci.* 20:1445. doi: 10.3390/ijms20061445

Takeuchi, O., and Akira, S. (2010). Pattern recognition receptors and inflammation. *Cell* 140, 805–820. doi: 10.1016/j.cell.2010.01.022

Tang, Q., Rigby, R. E., Young, G. R., Hvidt, A. K., Davis, T., Tan, T. K., et al. (2021). Adenosine-to-inosine editing of endogenous Z-form RNA by the deaminase ADAR1 prevents spontaneous MAVS-dependent type I interferon responses. *Immunity* 54, 1961.e5–1975.e5. doi: 10.1016/j.immuni.2021.08.011

Thompson, M. G., Sacco, M. T., and Horner, S. M. (2021). How RNA modifications regulate the antiviral response. *Immunol. Rev.* 304, 169–180. doi: 10.1111/imr.13020

Thoresen, D., Wang, W., Galls, D., Guo, R., Xu, L., and Pyle, A. M. (2021). The molecular mechanism of RIG-I activation and signaling. *Immunol. Rev.* 304, 154–168. doi: 10.1111/imr.13022

Tong, J., Flavell, R. A., and Li, H.-B. (2018). RNA m(6)A modification and its function in diseases. *Front. Med.* 12, 481–489. doi: 10.1007/s11684-018-0654-8

Tong, J., Wang, X., Liu, Y., Ren, X., Wang, A., Chen, Z., et al. (2021a). Pooled CRISPR screening identifies m(6)A as a positive regulator of macrophage activation. *Sci. Adv.* 7:eabd4742. doi: 10.1126/sciadv.abd4742

Tong, J. F., Zhou, L., Li, S., Lu, L.-F., Li, Z.-C., Li, Z., et al. (2021b). Two duplicated Ptpn6 homeologs cooperatively and negatively regulate RLR-mediated IFN response in hexaploid gibel carp. *Front. Immunol.* 12:780667. doi: 10.3389/fimmu.2021.780667

Topisirovic, I., Svitkin, Y. V., Sonenberg, N., and Shatkin, A. J. (2011). Cap and cap-binding proteins in the control of gene expression. *Wiley Interdiscip. Rev. RNA* 2, 277–298. doi: 10.1002/wrna.52

Unterstab, G., Ludwig, S., Anton, A., Planz, O., Dauber, B., Krappmann, D., et al. (2005). Viral targeting of the interferon-{beta}-inducing Traf family member-associated NF-{kappa}B activator (TANK)-binding kinase-1. *Proc. Natl. Acad. Sci. U. S. A.* 102, 13640–13645. doi: 10.1073/pnas.0502883102

Wei, J., and He, C. (2021). Chromatin and transcriptional regulation by reversible RNA methylation. *Curr. Opin. Cell Biol.* 70, 109–115. doi: 10.1016/j.ceb.2020.11.005

Werner, M., Purta, E., Kaminska, K. H., Cymerman, I. A., Campbell, D. A., Mittra, B., et al. (2011). 2′-O-ribose methylation of cap2 in human: function and evolution in a horizontally mobile family. *Nucleic Acids Res.* 39, 4756–4768. doi: 10.1093/nar/gkr038

Winans, S., and Beemon, K. (2019). m(5)C goes viral. *Cell Host Microbe* 26, 154–155. doi: 10.1016/j.chom.2019.07.019

Wnuk, M., Slipek, P., Dziedzic, M., and Lewinska, A. (2020). The roles of host 5-methylcytosine RNA methyltransferases during viral infections. *Int. J. Mol. Sci.* 21:8176. doi: 10.3390/ijms21218176

Wu, B., Peisley, A., Richards, C., Yao, H., Zeng, X., Lin, C., et al. (2013). Structural basis for dsRNA recognition, filament formation, and antiviral signal activation by MDA5. *Cell* 152, 276–289. doi: 10.1016/j.cell.2012.11.048

Wust, S., Schad, P., Burkart, S., and Binder, M. (2021). Comparative analysis of six IRF family members in alveolar epithelial cell-intrinsic antiviral responses. *Cells* 10:2600. doi: 10.3390/cells10102600

Xue, M., Zhang, Y., Wang, H., Kairis, E. L., Lu, M., Ahmad, S., et al. (2021). Viral RNA N6-methyladenosine modification modulates both innate and adaptive immune responses of human respiratory syncytial virus. *PLoS Pathog.* 17:e1010142. doi: 10.1371/journal.ppat.1010142

Yang, S., Deng, P., Zhu, Z., Zhu, J., Wang, G., Zhang, L., et al. (2014). Adenosine deaminase acting on RNA 1 limits RIG-I RNA detection and suppresses IFN production responding to viral and endogenous RNAs. *J. Immunol.* 193, 3436–3445. doi: 10.4049/jimmunol.1401136

Yang, E., and Li, M. M. H. (2020). All about the RNA: interferon-stimulated genes that interfere with viral RNA processes. *Front. Immunol.* 11:605024. doi: 10.3389/fimmu.2020.605024

Yap, L. J., Luo, D., Chung, K. Y., Lim, S. P., Bodenreider, C., Noble, C., et al. (2010). Crystal structure of the dengue virus methyltransferase bound to a 5′-capped octameric RNA. *PLoS One* 5:e12836. doi: 10.1371/journal.pone.0012836

Yin, X., Langer, S., Herbert, K. M., Yoh, S., König, R., and Chanda, S. K. (2020). Sensor sensibility-HIV-1 and the innate immune response. *Cells* 9:254. doi: 10.3390/cells9010254

Yoneyama, M., Kikuchi, M., Natsukawa, T., Shinobu, N., Imaizumi, T., Miyagishi, M., et al. (2004). The RNA helicase RIG-I has an essential function in double-stranded RNA-induced innate antiviral responses. *Nat. Immunol.* 5, 730–737. doi: 10.1038/ni1087

Yu, P., Miao, Z., Li, Y., Bansal, R., Peppelenbosch, M. P., and Pan, Q. (2021). cGAS-STING effectively restricts murine norovirus infection but antagonizes the antiviral action of N-terminus of RIG-I in mouse macrophages. *Gut Microbes* 13:1959839. doi: 10.1080/19490976.2021.1959839

Yu, Q., Qu, K., and Modis, Y. (2018). Cryo-EM structures of MDA5-dsRNA filaments at different stages of ATP hydrolysis. *Mol. Cell* 72, 999.e6–1012.e6. doi: 10.1016/j.molcel.2018.10.012

Zhang, Y., Wang, X., Zhang, X., Wang, J., Ma, Y., Zhang, L., et al. (2019). RNA-binding protein YTHDF3 suppresses interferon-dependent antiviral responses by promoting FOXO3 translation. *Proc. Natl. Acad. Sci. U. S. A.* 116, 976–981. doi: 10.1073/pnas.1812536116

Zhao, B. S., Roundtree, I. A., and He, C. (2017). Post-transcriptional gene regulation by mRNA modifications. *Nat. Rev. Mol. Cell Biol.* 18, 31–42. doi: 10.1038/nrm.2016.132

Zheng, G., Dahl, J. A., Niu, Y., Fedorcsak, P., Huang, C. M., Li, C. J., et al. (2013). ALKBH5 is a mammalian RNA demethylase that impacts RNA metabolism and mouse fertility. *Mol. Cell* 49, 18–29. doi: 10.1016/j.molcel.2012.10.015

Zheng, Q., Hou, J., Zhou, Y., Li, Z., and Cao, X. (2017). The RNA helicase DDX46 inhibits innate immunity by entrapping m(6)A-demethylated antiviral transcripts in the nucleus. *Nat. Immunol.* 18, 1094–1103. doi: 10.1038/ni.3830

Zhou, K. I., Parisien, M., Dai, Q., Liu, N., Diatchenko, L., Sachleben, J. R., et al. (2016). $N^{(6)}$-methyladenosine modification in a long noncoding RNA hairpin predisposes its conformation to protein binding. *J. Mol. Biol.* 428, 822–833. doi: 10.1016/j.jmb.2015.08.021

Zust, R., Cervantes-Barragan, L., Habjan, M., Maier, R., Neuman, B. W., Ziebuhr, J., et al. (2011). Ribose 2′-O-methylation provides a molecular signature for the distinction of self and non-self mRNA dependent on the RNA sensor Mda5. *Nat. Immunol.* 12, 137–143. doi: 10.1038/ni.1979

**Conflict of Interest:** The authors declare that the research was conducted in the absence of any commercial or financial relationships that could be construed as a potential conflict of interest.

**Publisher's Note:** All claims expressed in this article are solely those of the authors and do not necessarily represent those of their affiliated organizations, or those of the publisher, the editors and the reviewers. Any product that may be evaluated in this article, or claim that may be made by its manufacturer, is not guaranteed or endorsed by the publisher.

*Copyright © 2022 Tong, Zhang, Chen, Yuan, Qin and Qu. This is an open-access article distributed under the terms of the Creative Commons Attribution License (CC BY). The use, distribution or reproduction in other forums is permitted, provided the original author(s) and the copyright owner(s) are credited and that the original publication in this journal is cited, in accordance with accepted academic practice. No use, distribution or reproduction is permitted which does not comply with these terms.*

frontiers in Microbiology

REVIEW
published: 03 February 2022
doi: 10.3389/fmicb.2021.780887

# Insights Into the Coinfections of Human Immunodeficiency Virus-Hepatitis B Virus, Human Immunodeficiency Virus-Hepatitis C Virus, and Hepatitis B Virus-Hepatitis C Virus: Prevalence, Risk Factors, Pathogenesis, Diagnosis, and Treatment

*Sagarika Shahriar[1,2†], Yusha Araf[1,3†], Rasel Ahmad[4], Pravakar Kattel[4], Ganga Sagar Sah[4], Tanjim Ishraq Rahaman[5], Rahila Zannat Sadiea[4], Shahnaj Sultana[4], Md. Sayeedul Islam[6], Chunfu Zheng[1,7]* and Md. Golzar Hossain[4]**

[1] Department of Immunology, School of Basic Medical Sciences, Fujian Medical University, Fuzhou, China, [2] Biotechnology Program, Department of Mathematics and Natural Sciences, BRAC University, Dhaka, Bangladesh, [3] Department of Genetic Engineering and Biotechnology, School of Life Sciences, Shahjalal University of Science and Technology, Sylhet, Bangladesh, [4] Department of Microbiology and Hygiene, Bangladesh Agricultural University, Mymensingh, Bangladesh, [5] Department of Biotechnology and Genetic Engineering, Faculty of Life Sciences, Bangabandhu Sheikh Mujibur Rahman Science and Technology University, Gopalganj, Bangladesh, [6] Department of Biological Sciences, Graduate School of Science, Osaka University, Osaka, Japan, [7] Department of Microbiology, Immunology and Infectious Diseases, University of Calgary, Calgary, AB, Canada

Human immunodeficiency virus, hepatitis B virus, and hepatitis C virus are three blood-borne viruses that can cause major global health issues by increasing severe morbidity. There is a high risk of coinfection with these viruses in individuals because of their same transmission routes through blood using shared needles, syringes, other injection equipment, sexual transmission, or even vertical transmission. Coinfection can cause various liver-related illnesses, non-hepatic organ dysfunction, followed by death compared to any of these single infections. The treatment of coinfected patients is complicated due to the side effects of antiviral medication, resulting in drug resistance, hepatotoxicity, and a lack of required responses. On the other hand, coinfected individuals must be treated with multiple drugs simultaneously, such as for HIV either along with HBV or HCV and HBV and HCV. Therefore, diagnosing, treating, and controlling dual infections with HIV, HBV, or HCV is complicated and needs further investigation. This review focuses on the current prevalence, risk factors, and pathogenesis of dual infections with HIV, HBV, and HCV. We also briefly overviewed the diagnosis and treatment of coinfections of these three blood-borne viruses.

**Keywords: coinfection, HIV, HBV, HCV, prevalence, risk factors, pathogenesis**

OPEN ACCESS

***Edited by:***
*Linqi Zhang,*
*Tsinghua University, China*

***Reviewed by:***
*Li Ye,*
*Guangxi Medical University, China*
*Jieli Hu,*
*Chongqing Medical University, China*

***Correspondence:**
*Md. Golzar Hossain*
*mghossain@bau.edu.bd*
*Chunfu Zheng*
*zheng.alan@hotmail.com*

*† These authors have contributed equally to this work*

***Specialty section:***
*This article was submitted to Virology, a section of the journal Frontiers in Microbiology*

***Received:*** *21 September 2021*
***Accepted:*** *21 December 2021*
***Published:*** *03 February 2022*

***Citation:***
*Shahriar S, Araf Y, Ahmad R, Kattel P, Sah GS, Rahaman TI, Sadiea RZ, Sultana S, Islam MS, Zheng C and Hossain MG (2022) Insights Into the Coinfections of Human Immunodeficiency Virus-Hepatitis B Virus, Human Immunodeficiency Virus-Hepatitis C Virus, and Hepatitis B Virus-Hepatitis C Virus: Prevalence, Risk Factors, Pathogenesis, Diagnosis, and Treatment. Front. Microbiol. 12:780887. doi: 10.3389/fmicb.2021.780887*

## INTRODUCTION

The coinfection of viruses can be a serious public health problem because most medicines are designed to control and manage a single infection. Acquired immunodeficiency syndrome (AIDS) caused by the human immunodeficiency virus (HIV) is one of the most important and prevalent disease conditions that has been spread among humans for the last two decades (Kim et al., 2000). More than 75 million people worldwide have been infected with HIV, and approximately 37 million individuals are currently living with this infection. Hepatitis B (HB) and hepatitis C (HC) viral infections are highly prevalent among HIV-infected individuals due to sharing the same transmission routes. Hepatitis caused by both hepatitis B virus (HBV) and hepatitis C virus (HCV) leads to severe liver disorder, and morbidity and mortality are now increasing due to coinfection with HIV (Easterbrook et al., 2012). Coinfection with HIV can modify the natural characteristics of HBV by genome replication status, higher rates of chronic infection, and liver disease progression (Ndifontiayong et al., 2021). The impact of HIV on HBV is critical, as HIV can provoke chronic HBV infection, which can lead to hepatocellular carcinoma (HCC) (Maponga et al., 2020). While in HIV-HCV coinfection, HIV increases the HCV viral load and accelerates liver disease progression (Rodrigo, 2020). HIV, HBV, and HCV are transmitted *via* blood, shared needles, syringes, and other injection equipment, sexually, or even from pregnant mothers to babies (Pfaender et al., 2016). The hepatotropic viruses, both HBV and HCV, attack the liver cell and cause inflammation. However, HIV can attack any targeted cell in the mucosal tissue and spread through the whole lymphoid system (Siebers and Finlay, 1996). As a result of shared transmission routes, HBV, HCV, and HIV can easily cause coinfection, more pervasive than an infection caused by either HBV or HCV.

On the other hand, patients dually infected with HCV and HBV carry a significantly higher risk of developing fulminant hepatic failure, liver cirrhosis, and HCC than those with HCV or HBV infection alone (Liu, 2014). A recent study showed that viral infections, such as HBV, HCV, and HIV, are the second most common cause of morbidity and mortality among patients with thalassemia (Bhuyan et al., 2021). Great attention should be paid to the stages of liver disease, virus predominance, and the presence of HIV infection and comorbidities to conduct a better treatment. Several other therapies are being assessed in these circumstances, along with highly active antiretroviral therapy (HAART) (Zhang et al., 2014). However, proper treatment for patients suffering from dual coinfection, either with HIV, HBV, or HCV, is yet to be discovered. The current review is focused on various aspects of HIV, HBV, or HCV coinfection, with a special emphasis on prevalence, risk factors, pathogenesis, diagnostic markers, and treatment.

## STRUCTURE AND REPLICATION OF HUMAN IMMUNODEFICIENCY VIRUS, HEPATITIS B VIRUS, AND HEPATITIS C VIRUS

### Human Immunodeficiency Virus

Human immunodeficiency virus infects humans with two types of lentiviruses of the Retroviridae family. The structure of HIV is roughly spherical with a diameter of about 120 nm and covered by an outer lipid envelope membrane (de Jongh et al., 1992). The viral genome consists of two identical single-stranded RNA molecules enclosed within the core of the virus particle along with three viral enzymes-reverse transcriptases (RT/RNAse), integrase, and protease (Bodsworth et al., 1991). The initial steps of infection are dependent on protein-protein interactions, where the surface protein GP120 of the virus binds to the CD4 receptors on host cells (Xiao et al., 2008). The attachment causes a conformational change by which channels are formed. Due to its high hydrophobicity, the virus particle is engulfed by the target cell's plasma membrane, and the reverse transcriptase enzyme transcribes the single-strand RNA genome into double-stranded DNA (dsDNA) (Ockenga et al., 1997). The dsDNA is then transported through the nucleopore complex into the nucleus and integrated within the host genome by the integrase enzyme, producing mRNA and translating it into structural and non-structural proteins (**Figure 1**). These proteins are then assembled to form viral progeny and finally released into the bloodstream (Yim and Lok, 2006; Miailhes et al., 2007).

### Hepatitis B Virus

Hepatitis B virus is a member of the Hepadnavirus family, infecting humans, whereas orthohepadnaviruses and avihepadnaviruses infect mammals and birds, respectively (Schaefer, 2007). The infectious virion is approximately 42 nm in diameter with an internal icosahedral symmetry core particle nucleocapsid. The viral genome is a double-stranded DNA around 3.2 kb in size (Ott et al., 2012). The positive strand is the incomplete inner one, and the negative strand is the completed outer one, and viral polymerase is linked to the 5′ end of the minus strand (Bosch et al., 1988; Hossain et al., 2020). The envelope is also the primary structure embedded with the surface antigens (HBsAg), which are the core components of detecting the presence of HBV infections by commercial immunoassays (Hossain and Ueda, 2017). In the first phase of infection, the virion attaches to host cells *via* sodium taurocholate co-transporting polypeptide (NTCP) that helps itself get uncoated by fusion (Yan et al., 2012; Li, 2015). Secondly, upon infection, the rcDNA of the virus is converted into plasmid-like covalently-closed circular DNA (cccDNA) inside the host cell nucleus (**Figure 2**). Finally, the cccDNA templates several genomic and subgenomic RNAs transcribed by cellular RNA polymerase II. The pregenomic RNA (pgRNA) is then selectively packaged into progeny capsids, and most

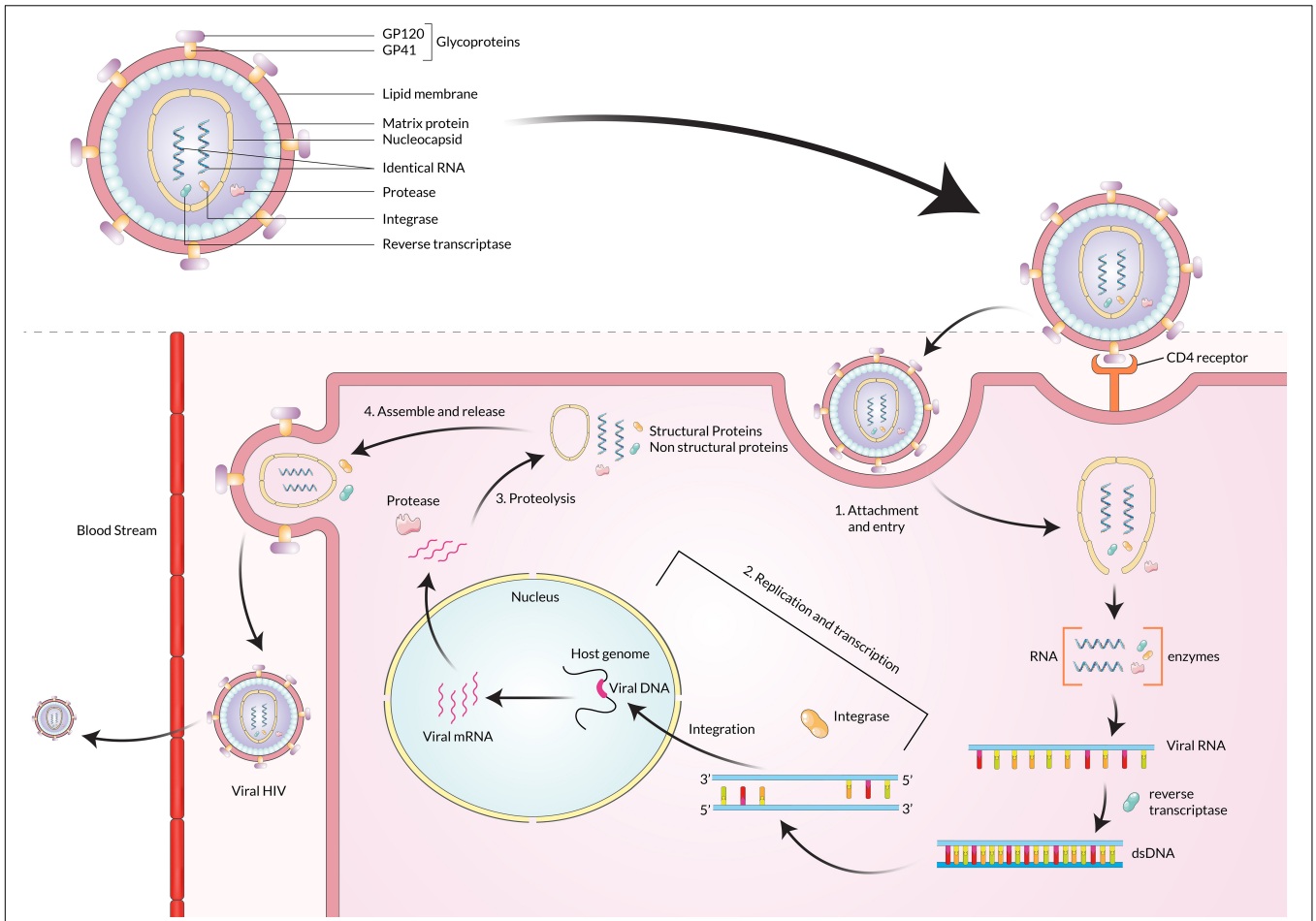


**FIGURE 1 |** After HIV GP120 binds with the receptors on the CD4 cell surface, the viral particle fuses with the membrane and enters the cell. The HIV genome ssRNA is reverse transcribed into the dsDNA using reverse transcriptase. The viral DNA is then integrated with the host cell DNA using integrase. The various structural and non-structural proteins are produced from the integrated DNA, and then viral particles are assembled and released from the cell.

of the pgRNA reversely transcribed into DNA within the capsids. Then the progeny viruses are released from the cells after being enveloped in the ER-Golgi/MVB (Lee et al., 2008; Hossain et al., 2020).

## Hepatitis C Virus

Hepatitis C virus is an enveloped virus that is a member of the genus Hepacivirus under the family Flaviviridae. The genome of the HCV is a positive-sense single-stranded RNA (ssRNA), around 9.6 kilobases in size (Kato, 2000). The ssRNA(+) is protected by a protein nucleocapsid and a lipid envelope membrane (Bukh et al., 1994). HCV infection into the host cells occurs by receptor-mediated endocytosis (Blanchard et al., 2006; Karangelis et al., 2010). The HCV particle binds with the hepatocyte surface molecules such as glycosaminoglycans, CD81, scavenger receptor class B type I (SR-BI), members of the claudin family (CLDN1, 6 and 9), and mannose-binding lectins DC-SIGN and L-SIGN (Barth et al., 2006; Helle and Dubuisson, 2008). Lipoproteins metabolism is also involved in the HCV attachment and replication steps (Grassi et al., 2016). The nucleocapsid is released in the cell cytoplasm from the virus-host cell molecule complex, and then the nucleocapsid is decapsidated to free the ssRNA(+) into the host cytoplasm. Due to its positive-sense properties, the viral RNA acts as mRNA and is directly translated by cap-dependent ribosomal machinery (El-Hage and Luo, 2003). A single polyprotein is translated from the mRNA, later processed to produce several structural and non-structural viral proteins. The six non-structural proteins are NS2, NS3, NS4A, NS4B, NS5A, and NS5B, which help in functions related to viral replication and are involved in host cell pathogenesis (Bartenschlager et al., 1994; Reed et al., 1995; Egger et al., 2002). The non-structural proteins help to make ssRNA(+) by using a ssRNA(−) template that is replicated by NS5B RNA-dependent RNA polymerase beforehand from one ssRNA(+) (Gosert et al., 2003). Finally, the assembled viral particle is incorporated with lipid droplets and released by one of the two predicted pathways such as very-low-density lipoproteins (VLDL) secretory pathway or endosomal sorting complex required for transport (ESCRT) pathway (**Figure 3**; Penin et al., 2004; Syed et al., 2010; Dubuisson and Cosset, 2014).

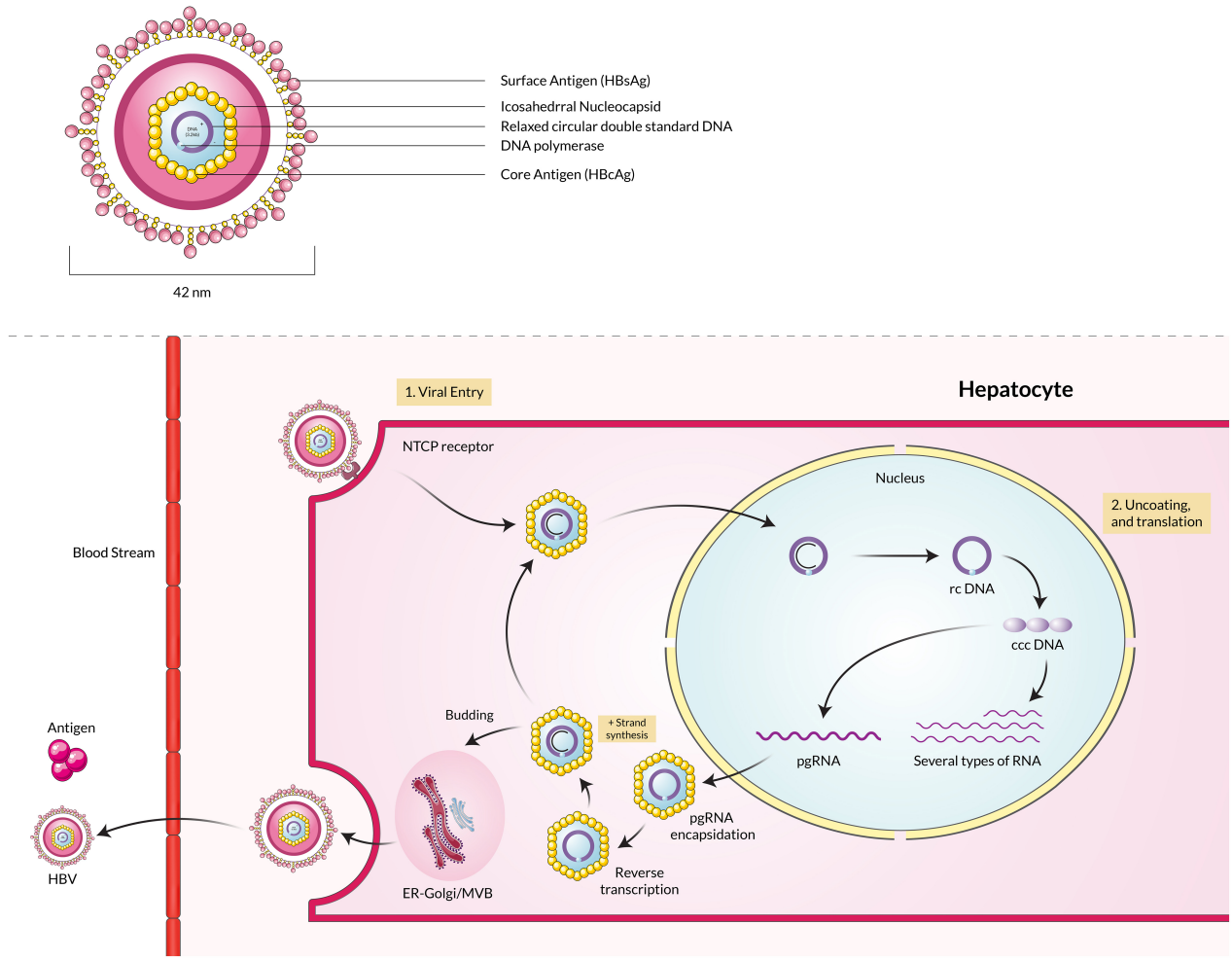


**FIGURE 2 |** Hepatitis B virus particle binds with the NTCP receptor, fuses with the membrane, and enters the host cell. The rcDNA is converted into cccDNA, transcribed into pgRNA, and finally packaged into the capsid. The capsid is enveloped by the ER-Golgi/MVB and released into the extracellular space.

# PREVALENCE OF COINFECTION

## Human Immunodeficiency Virus-Hepatitis B Virus

It is estimated that approximately 240 million people have chronic HBV infection (Sun et al., 2014). According to WHO, 37.5 million people were estimated to be living with HIV at the end of 2020. Because of shared routes of transmission, HBV coinfection among HIV-positive persons is common. In some regions, over two-thirds of HIV-infected persons have been reported with a history of HBV infection, which means 2–4 million people have HBV-HIV coinfection (Alter, 2006). However, the prevalence varies from region to region among HIV patients with chronic HBV infection (5–10%) due to local endemicity and acquisition mode. In western countries, the prevalence of HIV-HBV coinfection is estimated to be approximately 20% due to being acquired in adulthood, either by drug injection or through sexual transmission (Nyirenda et al., 2008). However, in Asia and sub-Saharan Africa, the endemicity is intermediate to high with 10–20% prevalence, acquired primarily in the perinatal period and early childhood (Lee et al., 2008; Nyirenda et al., 2008). In the United States, it is estimated that half of all patients with HIV infection have been exposed to HBV, which is 20 times higher than in the general US population. In the early 2000s, around 8% tested positive for hepatitis B surface antigen (HBsAg) or had detectable HBV DNA levels (Spradling et al., 2010). In a study conducted in Iran, the HIV-HBV prevalence in the general population and health care workers was very low. The highest prevalence was observed among injecting drug users at 1.88% and prisoners (0.13%) (**Table 1**; Bagheri Amiri et al., 2016).

## Human Immunodeficiency Virus-Hepatitis C Virus

Globally 37.5 million people live with HIV infection, and approximately 20–30% are infected with HCV (Hernandez and Sherman, 2011). As mentioned above, in the same

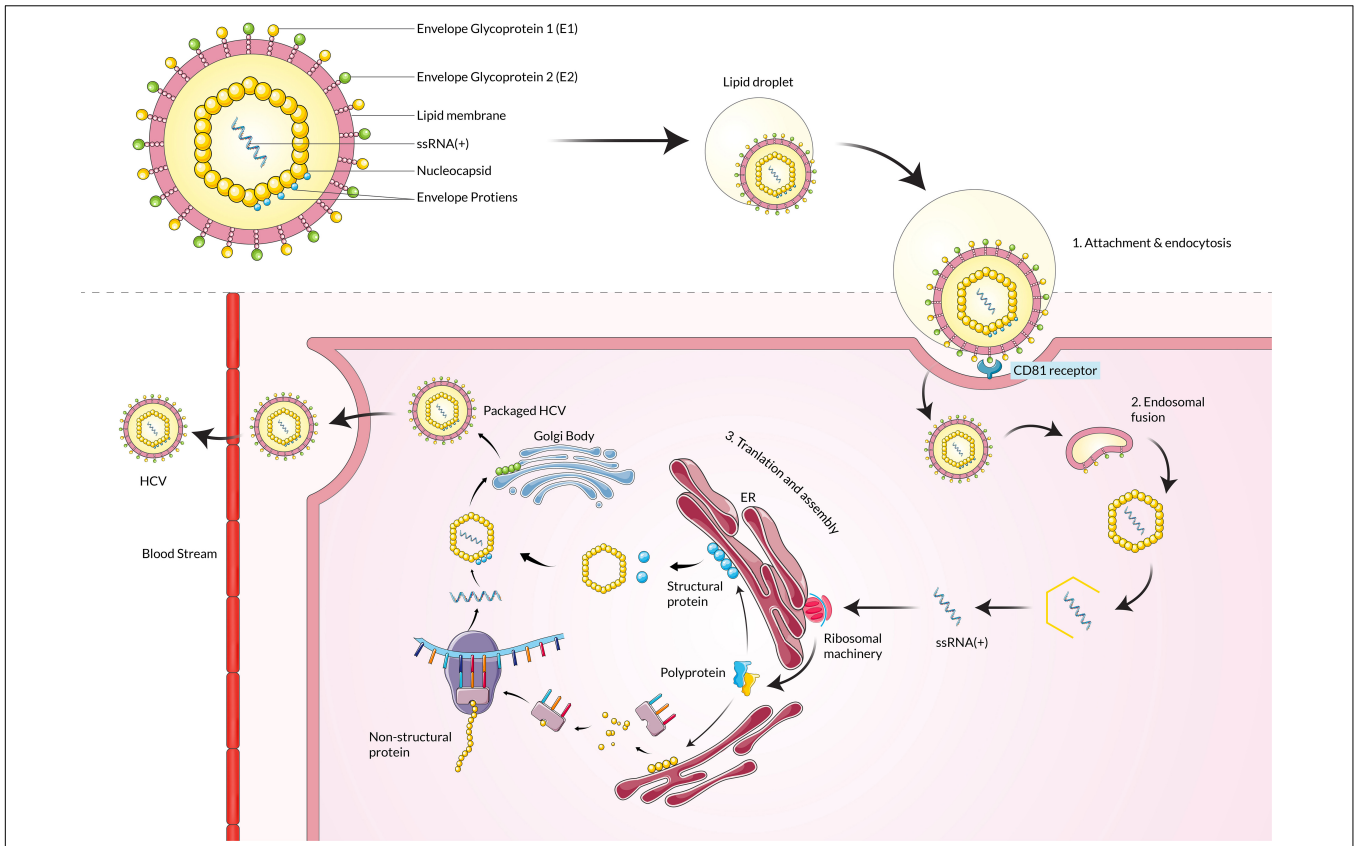


**FIGURE 3 |** Hepatitis C virus particle binds with the CD81 receptor, fuses with the membrane, and enters the host cell. Upon entering, the ssRNA(+) is translated by ribosomal machinery and produces both structural and non-structural proteins, which assemble and mature in the Golgi body and are then released into extracellular space.

**TABLE 1 |** Regional prevalence of HIV-HBV, HIV-HCV, and HBV-HCV coinfection.

| Coinfection | Region | Prevalence of risk factors among the cases | References |
|---|---|---|---|
| HIV-HBV | Globally | 2–4 million people have HBV-HIV coinfection | Alter, 2006 |
| | Western countries | 20% coinfection occurs due to drug injection and sexual intercourse | Nyirenda et al., 2008 |
| | Asia and Africa | 10–20% coinfection occurs during the perinatal period and early childhood | Lee et al., 2008; Nyirenda et al., 2008 |
| | United States | Half of the HIV infected patients are coinfected with HBV | Spradling et al., 2010 |
| | Iran | The prevalence of coinfection is higher in drug users (1.88%) and prisoners (0.13%) than general people | Bagheri Amiri et al., 2016 |
| HIV-HCV | Globally | 20–30% of 3.5 million HIV patients are infected with HCV | Hernandez and Sherman, 2011 |
| | | The prevalence of HIV-HCV coinfection among intravenous drug users is estimated to be around 90% | Sherman et al., 2002 |
| HBV-HCV | Globally | 10–15% of patients with chronic HBV infection are infected with HCV | Crespo et al., 1994; Ohkawa et al., 1994; Senturk et al., 2008 |
| | | 2–10% of anti-HCV-positive patients are HBsAg positive | |
| | India | The prevalence of HBV-HCV dual infection is 16% | Chakravarti et al., 2005 |
| | Egypt | The prevalence of coinfection is 0.7% | Mekky et al., 2013 |
| | United States | The prevalence of coinfection is 1.4% | Semnani et al., 2007 |

transmission route, the prevalence of HIV-HCV coinfection among intravenous drug users is estimated to be around 90% (Sherman et al., 2002). According to various reports, approximately 21% of adults with HIV tested positive with HCV infection (Yee et al., 2000). Besides percutaneous drug exposure, coinfection can also be seen in hemophiliacs who received

contaminated blood without routine serological screening (Di Martino et al., 2001). HCV is estimated to have a 10-fold higher risk of transmission than HIV through percutaneous routes; hence coinfected individuals are usually first infected by HCV (Kingsley et al., 1987). HCV is spread less efficiently by sexual transmission than HIV (Thomas et al., 1995; Gupta, 2013). The number of HIV-infected people chronically infected with HCV worldwide is approximately 2.3 million (**Table 1**; Garg et al., 2014).

### Hepatitis B Virus-Hepatitis C Virus

Due to the lack of large-scale population-based studies, the exact number of HBV-HCV coinfected patients is unknown; however, some regional studies have been done. One study reported that the prevalence of HBV-HCV dual infection is 16% in India (Chakravarti et al., 2005), while another reported the prevalence of coinfection is 0.7% in Egypt (Mekky et al., 2013). Data from different regions concluded that approximately 10–15% of patients with chronic HBV infection are also infected with HCV; on the other hand, about 2–10% of anti-HCV-positive patients are HBsAg positive (Crespo et al., 1994; Ohkawa et al., 1994; Senturk et al., 2008). Tyson et al. estimated that the prevalence of HBV-HCV coinfection was 1.4% in the US (**Table 1**; Semnani et al., 2007).

## RISK FACTORS OF COINFECTION

### Human Immunodeficiency Virus-Hepatitis B Virus

The risk factors for coinfection with HBV in HIV-positive individuals may vary in several aspects, including patient age, body mass index, sex, geographical location, current ART regime and duration, key population category, HIV viral load, marital status, and CD4+ T cell count. An epidemiological profile study of HBV-HIV coinfected people conducted in Nepal portrayed some risk factors, including being a spouse of a migrant laborer, a male or female sex worker, an intravenous drug user, or having an HCV-positive status (Bhattarai et al., 2018). Several studies reported that the prevalence of HIV-HBV coinfection among people who inject drugs (PWID) increases with age (Falade-Nwulia and Thio, 2011; Wing, 2017). Due to the chronic and sometimes asymptomatic nature of HIV and HBV infections, the individuals are likely at an even higher risk of chronic progression given the combined effects of age and related immune system dysfunction (Abdala et al., 2008). It is hypothesized that HIV-positive individuals are more likely to be infected with the hepatitis B virus (HBV) than HIV-negative individuals, possibly due to common risk factors. In addition, immunosuppression induced by HIV infection may cause reactivation or reinfection in those previously exposed to HBV (Thio et al., 2002). Other reports showed that coinfection prevalence was higher among men than women, especially in homosexual men, non-Hispanics than Hispanics, and among patients aged 35–44 than younger or older (Porras-Ramírez and Rico-Mendoza, 2020; **Figure 4**).

### Human Immunodeficiency Virus-Hepatitis C Virus

Human immunodeficiency virus-driven viral hepatitis exacerbates hepatic lesions and increases the transmission of HCV. Several risk factors associated with the HIV-HCV coinfection are shown in **Figure 4**. Some populations among HIV-positive patients worldwide have more frequent exposure to HCV infection due to engagement in high-risk behaviors, weak family and social support systems, and inadequate access to healthcare services (Health Policy Project, 2014). Coinfection risk factors also vary on epidemiological subjects such as age, marital status, sex, geographical location, HIV viral load, and CD4+ T cell count. In a Nepalese study, HIV-HCV coinfection was higher in individuals >40 years of age. It is more evident in homosexual men with multiple sexual contacts without a preservative (Götz et al., 2005). In a cohort, the incidence of HCV infection among HIV seropositive MSMs increased 10-fold (van de Laar et al., 2007). Moreover, HIV-positives with CD4+ T cell counts of >200 cells/μL were associated with a lower risk of coinfection with HCV. The study suggested that age and CD4+ T cell count may affect the risk for HIV-HCV coinfection (Bhattarai et al., 2018). Furthermore, the blood-borne transmission of the coinfection is 62–80% common among injection-drug users (Yehia et al., 2014). Several studies suggest that HIV and hepatitis transmission are associated with high-risk injection practices such as injection with a syringe previously used by another PWID (Ray Saraswati et al., 2015; Buchanan et al., 2017; Kilonzo et al., 2018). Individuals living with HIV-HCV coinfection are less likely to clear acute HCV infection and more likely to transmit the virus, particularly PWID who share used needles (Shapatava et al., 2006). In the case of mother-to-child, the risk of transmission to the fetus in coinfected women for HIV is between 5 and 25% times higher than in mothers infected by only HCV (Zanetti et al., 1999). Coinfected patients have higher HCV RNA loads and experience more rapid progression of HCV-related liver disease than those without HIV infection (Thomas et al., 2000). HIV infection was found in 13% of hemophiliacs coinfected with HIV and HCV, while HCV infection was detected in just 3% of 162 female sexual partners (Eyster et al., 1991). Other transmission routes, such as sexual intercourse or vertical transmission, have less risk of transmission than percutaneous exposures. The reported prevalence of sexual transmission of HCV-positive individuals is 2–8% and in newborn babies is 2–5%, but three times higher if the mother is HIV positive (Operskalski and Kovacs, 2011).

## PATHOGENESIS OF COINFECTION

### Human Immunodeficiency Virus-Hepatitis B Virus

The impact of HIV infection on HBV-induced hepatitis progression is significantly different from HBV infection on HIV disease progression. Around 10–15% developed chronic hepatitis B, which is less likely to be eliminated. HIV-HBV coinfection causes several symptoms, some of which can be

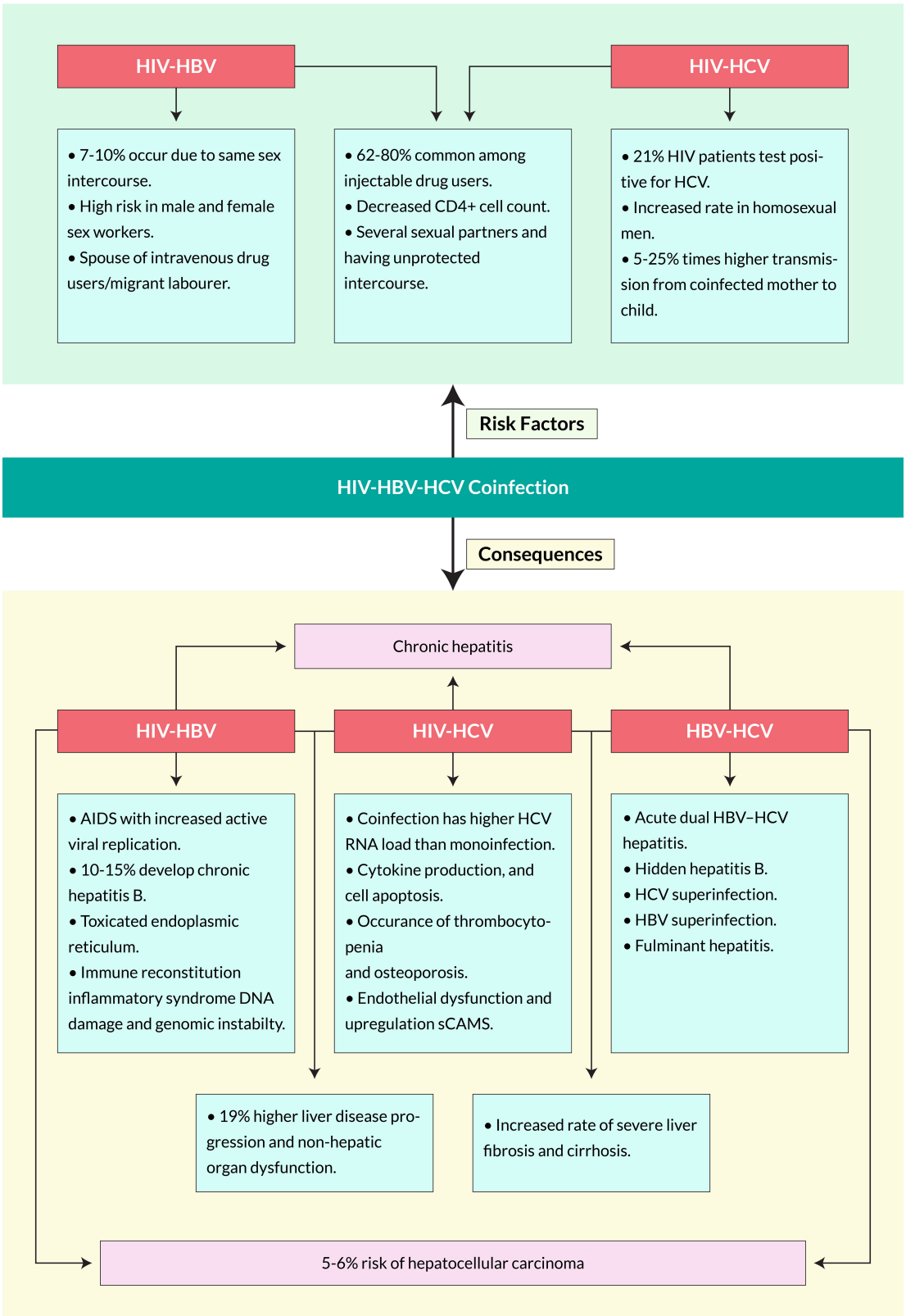


**FIGURE 4 |** Major risk factors and consequences of HIV, HBV, and HCV coinfection.

fatal. Mutations in the HBsAg coding sequence coinfected with HIV can accumulate HBsAg in hepatocytes and damage the host's endoplasmic reticulum and DNA damage (Pollicino et al., 2014). With HIV-HBV coinfection, immune reconstitution inflammatory syndrome (IRIS) is developed more profoundly (Shahani and Hamill, 2016). Acute HBV infection in 90–95% of adults can develop a broad and multispecific cellular immune response that can eliminate the virus by producing protective antibodies against HBsAg (Mahoney, 1999).

Moreover, chronic HBV-infected patients can develop anti-HBe associated with aging and aminotransferase (ALT) elevation (Liaw et al., 1988; Fattovich et al., 1991). In a 10-year study of 1536 Alaskan natives with chronic hepatitis B, 70 and 7% cleared HBeAg and HBsAg, respectively (McMahon et al., 2001). However, they might remain inactive carriers with HBsAg particles with either low or undetectable levels of HBV DNA (Fattovich et al., 1986; de Jongh et al., 1992). These inert carriers can significantly reduce the mortality rate twofold, although increased ALT can lead to fibrosis progression (Fattovich et al., 1990). However, when coinfection occurs with HIV, the mortality rate increases significantly in HBV patients elevating chronic liver diseases. Among 1000 people a year, 14.2% of them suffer from several chronic liver diseases when coinfected compared with 0.8% of people with HBV infection only (Thio et al., 2002). One study suggested that HIV-infected people had a greater clearance rate of HBsAg and HBeAg due to the degree of immunosuppression (Bodsworth et al., 1991). However, other studies showed that HIV infection reactivates HBV and accelerates the loss of anti-HBs, increases levels of HBV DNA, and significantly lowers the ALT levels (Biggar et al., 1987; Gilson et al., 1997). Although lower ALT levels indicate less hepatocyte destruction, anti-HBV therapy's effectiveness decreases in coinfected individuals. HIV coinfection has also been reported to create fibrosing cholestatic hepatitis, which leads to liver graft rejection in liver transplant recipients. An extremely high level of HBV antigen expression is observed in this specific liver disease due to a direct cytopathic effect (Davies et al., 1991; Xiao et al., 2008).

Although most studies show significant evidence of HBV infection acceleration due to HIV, the impact of HBV infection in HIV patients is still quite limited. A study found that among 80 gay men, 32 anti-HBc positive men progressed to get acquired immunodeficiency syndrome (AIDS) more rapidly (Eskild et al., 1992). Another study showed that HIV-HBV coinfected patients with AIDS had decreased survival than AIDS patients (Ockenga et al., 1997). The outcome of HBV infection varies according to the age and the current immune status of the host. For example, HBV infection persists in 50–90% of persons infected at birth or early childhood.

In contrast, fewer than 5% of HBV infections become chronic among HIV-uninfected adults (Yim and Lok, 2006). A multicenter-AIDS-cohort study suggested that coinfected patients had a mortality rate eight times higher than those singly infected. Moreover, the mortality related to hepatopathy due to hepatitis B has increased significantly since the highly active antiretroviral therapy (HAART), a treatment for HIV patients (Miailhes et al., 2007). Previous studies show that coinfection causes liver-related mortality 19 times that of a single infection (Thio et al., 2002). The mortality rate increased in individuals with lower CD4+ T-cell counts for the infection (Jaroszewicz et al., 2012; **Figure 4**).

## Human Immunodeficiency Virus-Hepatitis C Virus

Human immunodeficiency virus -Hepatitis C virus coinfected patients have higher HCV RNA loads and experience more rapid progression of HCV-related liver diseases than those without HIV infection (Hoofnagle and Di Bisceglie, 1991). Several studies suggested plenty of symptoms of the coinfection (**Figure 4**); however, these can vary over different factors, such as consumption of alcohol, age at acquisition of infection, race, sexual status, concomitant viral infection with HIV, time of illness, body mass index, and various genetic factors. HIV-HCV coinfected patients suffer from higher liver-related morbidity and mortality, non-hepatic organ dysfunction, and overall mortality than HCV single infected patients (Lo ReIII, Kallan et al., 2014). Moreover, coinfection causes an increased rate of severe liver fibrosis and cirrhosis (Fierer et al., 2013; Kirk et al., 2013). A meta-analysis of eight separate studies found that HIV-HCV coinfected patients had approximately two times higher risk of cirrhosis diagnosed on liver biopsy and around six times higher risk of decompensated liver disease than HCV-infected patients (Thein et al., 2008; Tuyama et al., 2010). Coinfection can cause immune dysfunction, cytokine production, and cell apoptosis, leading to severe immunodeficiency (Körner et al., 2009; Kovacs et al., 2010). It causes HIV-related mitochondrial translocation-induced immune activation and causes severe liver damage (Kim and Chung, 2009; Rotman and Liang, 2009). HIV- and HCV-associated chronic inflammation leads to endothelial dysfunction (Bedimo et al., 2010). Moreover, coinfection also causes thrombocytopenia and osteoporosis (Marks et al., 2009). It is estimated that 90% of HIV patients with acute HCV will gradually develop chronic HBV, which shows a higher prevalence in coinfected patients than singly-infected (Collin et al., 2009). Other reports suggest that coinfection also increases the rate of related diseases such as cryoglobulinemia, hemophilia, diabetes mellitus, and kidney-related infections (Sulkowski, 2001). It is confirmed that HIV infection substantially impacts mortality among HCV-infected individuals, mainly due to HIV-induced immunodeficiency (Singal and Anand, 2009).

## Hepatitis B Virus-Hepatitis C Virus

Hepatitis B virus-Hepatitis C virus coinfection is more frequently found in several high-risk populations, for example, persons who inject drugs, patients on hemodialysis and undergoing organ transplantation, HIV-positive, and β-thalassemia (Pallás et al., 1999; Aroldi et al., 2005; Reddy et al., 2005). Tyson et al. stated that the independent associations with HBV coinfection compared with HCV single infection were age ≤50 years, male sex, positive HIV status, history of hemophilia, sickle cell anemia, or thalassemia, history of blood transfusion, cocaine, and other drug uses. At the same time, there was decreased risk in patients of Hispanic ethnicity (Tyson et al., 2013). With hidden

hepatitis B, liver cirrhosis occurs in 33% of HCV coinfected patients and 19% of HCV carriers with undetectable HBV DNA (Fan et al., 2003). Superinfections cause the development of chronic hepatitis, for which the mortality rate is as high as 10% (Sterling and Sulkowski, 2004). Moreover, coinfection increases the rate of liver cirrhosis, chronic and fulminant hepatitis, and hepatocellular carcinoma (**Figure 4**).

## DIAGNOSIS OF COINFECTION

### Human Immunodeficiency Virus-Hepatitis B Virus

All patients infected with HIV must be tested for HBV and HCV and vice versa, as the transmission route is the same. The HIV-negative patients, only infected with any of the hepatitis viruses, are required to test for alanine aminotransferase (ALT), aspartate aminotransferase (AST), hemoglobin, white blood cell count, platelets, HBeAg, HBe antibody (anti-HBe), HBsAg antibody (anti-HBs), CD4 count, and HBV DNA quantification in the serum (Audsley et al., 2020). HBV DNA levels are a significant marker to detect coinfection (Lok and McMahon, 2009). Spontaneous sero-reversion can occur due to having a low CD4 count (<200/mm3) and is also a prime marker for HIV-HBV coinfection. Therefore, HBV serological tests should be repeated among HIV-infected patients with prior positivity for HBsAb for the reemergence of HBV infection (European Association for the Study of the Liver, 2012). Anti-HBc can also be found in HIV-positive patients due to having past HBV infection (Gandhi et al., 2005). The occurrence of a past infection is often termed "Occult HBV infection," which results in the presence of HBV DNA in the absence of HBsAg and has been reported in 2 to 10% of HIV-infected patients (Shire et al., 2007; Tsui et al., 2007). For HCC screening, coinfected patients with HBV-HIV should undergo serial liver ultrasound examinations and alpha-fetoprotein (AFP) serology every 6 months (European Association for the Study of the Liver, 2012). Severe conditions with HIV-HBV coinfection may require a liver biopsy. However, non-invasive measures, such as serum fibrosis markers and transient elastography, can help determine the degree of underlying fibrosis instead of biopsy (Moreno et al., 2009; Smith and Sterling, 2009). The markers suggest different parameters for detecting HIV-HBV coinfection depending on HBV infection types (**Table 2**).

### Human Immunodeficiency Virus-Hepatitis C Virus

Reverse transcriptase-nested polymerase chain reaction assays (RT-PCR) must be conducted for the screening of the persistent HCV 5′ untranslated region (5′ UTR) for the diagnosis of HCV RNA in HIV patients (Panigrahi et al., 1994). Liver fibrosis progression is more rapid in the context of HIV-HCV coinfection and is associated with lower CD4 cell counts (Martin et al., 1989; Puoti et al., 2001; Martinez-Sierra et al., 2003). Non-invasive measures of liver fibrosis can be a reliable diagnosis for HIV-HCV coinfection. The alanine aspartyl transferase (AST)-to-platelet ratio index (APRI) has been validated as a good predictor of significant liver fibrosis in both HCV single and coinfection when compared with liver biopsy (Wai et al., 2003; Lackner et al., 2005). One study suggested that, in coinfection, APRI score > 1.5 was 100% specific and 52% sensitive for predicting significant fibrosis (Al-Mohri et al., 2005). Forrester et al. reported that AST and alanine aminotransferase (ALT) levels were significantly higher ($P < 0.0001$), and platelet counts were lower ($P < 0.01$) in HIV-HCV coinfected individuals than in patients infected with only HIV (Forrester et al., 2012). Other markers such as alpha-2-macroglobulin, apolipoprotein A1, haptoglobin, γ-glutamyl transpeptidase (GGT), and bilirubin are also screened primarily focuses on HCV patients (**Table 2**; Imbert-Bismut et al., 2001; Morali et al., 2007).

### Hepatitis B Virus-Hepatitis C Virus

Laboratory evaluation for coinfection with all possible viral causes, including HBV and HCV, is performed in patients presenting with acute hepatitis resulting from any of the two viruses. In case of superinfection of HCV or HBV, silent or occult HBV, all the necessary parameters and confirmatory tests such as HBV DNA testing by polymerase chain reaction (PCR) should also be performed when clinically indicated. In acute infection with HBV and HCV, patients showed delayed HBsAg appearance and a shorter HBs antigenemia than those with acute HBV alone (Mimms et al., 1993). According to an Italian investigation that showed active HBV-HCV indicators in 30 patients with HCV infection, the chronicity rates were equivalent to individuals with a single infection with either of the viruses. Biphasic alanine aminotransferase elevation was also observed in the case of HBV-HCV coinfection (Yan and Lee, 2005). Several reports have documented that *de novo* HCV superinfection in the setting of chronic HBV infection can result in HBeAg seroconversion and clearance of HBsAg.

Moreover, fulminant hepatic failure was significantly higher among patients with underlying HBV infection than those singly infected (23 vs. 3%) (Wu et al., 1994). Hence, every marker should be adequately detected with a specific protocol. On the other hand, occult hepatitis B (OHB) is defined as the presence of HBV DNA in serum and the liver tissue without detectable HBsAg with or without anti-HBc or anti-HBs outside the pre-seroconversion window period (**Table 2**; Bréchot et al., 2001).

## PROSPECTIVE TREATMENTS

### Human Immunodeficiency Virus-Hepatitis B Virus Coinfection

The most common treatment for HIV-HBV coinfection is HBV-active ART, usually tenofovir together with either lamivudine or emtricitabine. This treatment significantly decreases the rate of HBeAg and HBsAg antigens in infected individuals (Boyd et al., 2016). Drugs such as interferon alfa, peginterferon alfa, adefovir, lamivudine, entecavir, tenofovir, emtricitabine are used to prevent the coinfection (**Table 3**). As HIV infection can accelerate the progression of HBV-related liver disease, treatment

**TABLE 2 |** Serological markers of HIV-HBV, HIV-HCV, and HBV-HCV coinfection.

| | HIV-HBV coinfection markers | HIV-HCV coinfection markers | HBV-HCV coinfection markers |
|---|---|---|---|
| Genomic level | ↑ HBV DNA | ↑ HCV RNA | ↑ HBV DNA |
| T-cell count | ↓ CD4 count (<200/mm3) | ↓ CD4 and CD8 ratio | - |
| Antigen/Antibody | ↑ HBsAb<br>↑ Anti-HBc | ↑Anti-HCV | Delayed HBsAg<br>↓ HBs antigenemia |
| Related infection | Occult infection:<br>↑HBV DNA<br>↓HBsAg | - | HCV superinfection and chronic HBV infection:<br>↑ HBeAg<br>↓ HBsAg |
| Enzyme markers | ↑ alpha-fetoprotein | ↑ AST:APRI<br>↑ APRI score (>1.5)<br>↓ AST *p*-value (<0.0001) | ↑ biphasic alanine aminotransferase |

of chronic hepatitis B is generally recommended for most HIV-infected patients with active HBV infection.

## Human Immunodeficiency Virus-Hepatitis C Virus Coinfection

Generally, HIV-HCV coinfection treatment focuses on eliminating a single infection first by decreasing the viral load alongside treating the secondary issues. A guideline is followed to treat HCV, but there is still a lack of information about HIV and HCV disease stage and viral load, HCV genotype, degree of hepatic fibrosis, and patient's readiness to tolerate and adhere to treatment (Soriano et al., 2007). The treatments are more likely to target the current standard pegylated interferon plus ribavirin (pegIFN + RBV) medication, predictors of the treatment response, adverse events of anti-HCV therapy, and HAART as both HIV-HCV therapeutic agents (**Table 4**). The most effective treatment to date for HCV infection is direct-acting antiviral (DAA) therapy. First-generation DAAs include the NS3/4A serine protease inhibitor telaprevir and the NS5B RNA polymerase inhibitor sofosbuvir (Messina et al., 2015). Clinical trials demonstrated that using these DAAs in combination with peginterferon and ribavirin gave sustained virologic response (SVR) to HCV genotype 1 infection, up to 75% for telaprevir and 90% for sofosbuvir (Walker et al., 2015). The second-generation DAA regimens paritaprevir/ritonavir/ombitasvir, dasabuvir (3D), and sofosbuvir/ledipasvir were approved by the United States Food and Drug Administration (FDA) for patients with HCV genotype 1, as these all-oral regimens showed improved efficacy, safety, and tolerability when compared to first-generation protease inhibitor regimens (Pawlotsky, 2014). However, many long-term studies have shown that patients with compensated cirrhosis who achieved SVR with interferon (IFN)-based therapy showed efficacy at first, but various side-effects and limited virological effectiveness was seen with long-term treatment. However, with DAAs, patients with compensated cirrhosis achieve SVR rates over 95% (Afdhal et al., 2014; Poordad et al., 2014; Krassenburg et al., 2021). Moreover, high rates of cure have also been observed in groups including patients with cirrhosis and HIV coinfection (Hawkins et al., 2016). Many open-labeled studies demonstrated that DAAs such as ledipasvir and sofosbuvir for 12 weeks provided high rates of SVR in the patients coinfected with HIV-1 and HCV genotype 1 or 4 (Naggie et al., 2015). Another study suggested that treatment with the all-oral, interferon-free 3D-plus-ribavirin regimen resulted in high SVR rates among patients co-infected with HCV genotype one and HIV-1 (Sulkowski et al., 2015).

**TABLE 3 |** Potential medications and their activity against HIV-HBV coinfected individuals.

| Drug | Direct activity against HIV and HBV | For chronic HBV in HIV-infected patients | References |
|---|---|---|---|
| Interferon Alfa | No | No | Johnson et al., 2007 |
| Peginterferon Alfa | Yes | No | Di Martino et al., 2002 |
| Lamivudine | Yes | No | Benhamou et al., 1999; Dore et al., 1999 |
| Emtricitabine | Yes | No | Lim et al., 2006; Saag, 2006 |
| Adefovir | No | No | Hadziyannis et al., 2003; Thio, 2006 |
| Tenofovir | Yes | Yes | Lada et al., 2004 |
| Entecavir | Yes | Yes | Tenney et al., 2004; Pessôa et al., 2008 |

## Hepatitis B Virus-Hepatitis C Virus Coinfection

Hepatitis B virus-Hepatitis C virus coinfection is more complex than a single infection with HBV or HCV alone. Hence, the general approach for treatment is first to identify the dominant virus, treat that virus as a single infection, and then monitor for reactivation of the other virus. Coinfection is typically treated with a nucleotide analog (such as lamivudine, entecavir, or tenofovir) along with PegIFN (Sulaiman, 1989). It is 35% effective in HBV and 50–60% effective in HCV when combined with ribavirin (Crockett and Keeffe, 2005). Moreover, direct-acting antiviral (DAA) is also used, which gives 90% efficacy for inhibiting HCV but no response for HBV (Calvaruso et al., 2018). It is recommended to vaccinate HBV patients because studies showed 60% efficacy to vaccinated cirrhotic patients (Roni et al., 2013). Liu et al. (2014) assessed that peg-IFN/RBV therapy is not only safe and effective but translates into significant clinical benefits such as reduction in liver-related complications and

**TABLE 4 |** Effects and side-effects of potential medications for HIV-HCV coinfected individuals.

| Drugs | Therapeutic effects | Side effects | References |
|---|---|---|---|
| HAART | Decreases HIV replication in liver<br>Decreases proinflammatory cytokines and necro-inflammatory activity | Increases Liver enzymes (LEE) and hepatotoxicity | Pascual-Pareja et al., 2009; Price et al., 2009 |
| Protease inhibitors | Decreases HCV replication | | Toma et al., 2009 |
| Efavirenz | Decreases hepatotoxicity | | Labarga et al., 2007 |
| NNRTI + pegIFN + RBV | Decreases synergistic HCV replication *in vitro* | Increases Mitochondrial toxicity | Labarga et al., 2007; Toma et al., 2009 |
| Simeprevir (SMV) + PR | Decreases hepatotoxicity | | Jacobson et al., 2014 |
| DAAs (Telaprevir/Sofosbuvir/Paritaprevir /Ritonavir/Ombitasvir) | Increase sustained virologic response upto 90% | | Naggie et al., 2015; Wyles et al., 2015 |

improved patient survival. However, in terms of viral dominance, it is not common to have codominance of both viruses. Hence, there is either HBV dominance, which means high HBV DNA levels and low HCV RNA levels, or HCV dominance, defined by the high HCV RNA levels and absent HBV DNA (Konstantinou and Deutsch, 2015). HBV dominance is likely to be more common in Asian patients, while HCV dominance is seen among North American coinfected and European patients (Nguyen et al., 2011). Therefore, it is suggested to diagnose the disease properly and determine the dominant side before treating a coinfected patient. An Italian study reported that 9 million IU of standard IFN 3 times weekly for 3 months could clear HCV in 31% of HCV-HBV coinfections (Villa et al., 2001). As previously mentioned, peg-IFN is one of the first-line choices for treating chronic HBV infection, and does not cause any side effects toward coinfected patients (Bihl et al., 2010). However, till present, no data have been published regarding the efficacy of direct-acting antivirals (DAAs) in combination with peg-IFN plus RBV or with IFN-free regimens in treating patients with chronic HBV-HCV coinfection.

## CONCLUSION AND FUTURE DIRECTIONS

Coinfection with HBV or HCV is common among HIV-infected individuals due to their similar modes of transmission. Any coinfection can reportedly lead to an increased risk of morbidity and mortality. Overall, the prevalence of hepatitis B and hepatitis C, with HIV coinfection, is 50.3%. Among these, HIV-HBV is 8.4%, HIV-HCV is 35.4%, and HBV-HCV is 5%. The characteristics of HIV-infected individuals can differ according to the coinfecting hepatitis viruses that can change their strains over time. Therefore, frequent screening and monitoring should be performed in both coinfected and singly infected patients due to the possibility of developing another secondary infection if measurable steps are not taken. In addition, one must get tested if their partner is positive for any infection or assume any symptoms.

Treatments for coinfected patients are complex due to the interaction of the two viruses and the potential for reactivation of one virus with antiviral therapy directed against only the other virus. Therefore, coinfected patients must undertake single infection treatment concurrently with dual antiviral therapy. Until today, highly active antiretroviral therapy (HAART) has been a breakthrough for treating patients with HIV, as the infection currently does not have any effective vaccination. HCV prevention is also based on direct-acting antiviral (DAA) treatments for short-term and curative measures.

Vaccination is given to prevent HBV with three consecutive doses for the long term. Early remedies for acute infection are also highly encouraged. However, several preventive strategies must be followed to prevent and control these blood and fluid-borne viral diseases. It is highly advisable to avoid percutaneous exposure incidents, such as needle injuries, sharp injuries, and splashes leading to exposure of the skin or mucosa to blood. Drug abuse and sharing the same needle or syringe are also high-risk behaviors toward these diseases. Safe sex and special care for pregnant women are recommended to prevent disease occurrence. Besides conventional therapy and treatments, CRISPR-Cas9-based antiviral strategies can also be implied to avoid hepatitis coinfection due to its relative versatility, specificity, and ease of use. Vaccines against HCV and HIV should be further studied and implemented at the earliest convenience. Polyvalent vaccines for these viral coinfections can also be an escalating preventive measure for the prospective times. Although current diagnostic technologies can detect viruses, they still rely on practical labor, expensive and limited resources. However, if nanotechnology (metal/inorganic nanoparticles, carbon nanotubes) combined with microfabrication can be used in diagnostic and therapeutic settings, the healthcare systems will undergo a revolutionary shift. These technologies with miniatured sensors can be used to easily detect viruses from an ultra-low volume of blood, serum, and plasma, allowing highly accurate diagnosis. However, further extensive studies should be conducted to diagnose and treat the coinfection of these blood-borne viral diseases.

## AUTHOR CONTRIBUTIONS

MGH designed and supervised the manuscript. SaS, YA, RA, PK, GS, TR, RS, and ShS searched and collected the literature.

SaS and YA wrote the preliminary draft manuscript. YA and TR designed the graphs. MSI and MGH reviewed the preliminary draft manuscript. CZ and MGH edited, revised, and finalized the manuscript. All authors read and approved the manuscript.

## ACKNOWLEDGMENTS

We are grateful to Luke Ueda-Sarson of Osaka University for his critical reading and English editing of the manuscript.

## REFERENCES

Abdala, N., Krasnoselskikh, T. V., Durante, A. J., Timofeeva, M. Y., Verevochkin, S. V., and Kozlov, A. P. (2008). Sexually transmitted infections, sexual risk behaviors and the risk of heterosexual spread of HIV among and beyond IDUs in St. Petersburg, Russia. *Eur. Addict. Res.* 14, 19–25. doi: 10.1159/000110407

Afdhal, N., Reddy, K. R., Nelson, D. R., Lawitz, E., Gordon, S. C., Schiff, E., et al. (2014). Ledipasvir and sofosbuvir for previously treated HCV genotype 1 infection. *N. Engl. J. Med.* 370, 1483–1493.

Al-Mohri, H., Cooper, C., Murphy, T., and Klein, M. B. (2005). Validation of a simple model for predicting liver fibrosis in HIV/hepatitis C virus-coinfected patients. *HIV Med.* 6, 375–378. doi: 10.1111/j.1468-1293.2005.00330.x

Alter, M. J. (2006). Epidemiology of viral hepatitis and HIV co-infection. *J. Hepatol.* 44, S6–S9. doi: 10.1016/j.jhep.2005.11.004

Aroldi, A., Lampertico, P., Montagnino, G., Passerini, P., Villa, M., Campise, M. R., et al. (2005). Natural history of hepatitis B and C in renal allograft recipients. *Transplantation* 79, 1132–1136. doi: 10.1097/01.tp.0000161250.83392.73

Audsley, J., Avihingsanon, A., Littlejohn, M., Bowden, S., Matthews, G. V., Fairley, C. K., et al. (2020). Long-term TDF-inclusive ART and progressive rates of HBsAg loss in HIV-HBV coinfection-lessons for functional HBV cure? *J. Acquir. Immune Defic. Syndr.* 84, 527–533. doi: 10.1097/QAI.0000000000002386

Bagheri Amiri, F., Mostafavi, E., and Mirzazadeh, A. (2016). HIV, HBV and HCV coinfection prevalence in Iran–a systematic review and meta-analysis. *PLoS One* 11:e0151946. doi: 10.1371/journal.pone.0151946

Bartenschlager, R., Ahlborn-Laake, L., Mous, J., and Jacobsen, H. (1994). Kinetic and structural analyses of hepatitis C virus polyprotein processing. *J. Virol.* 68, 5045–5055. doi: 10.1128/JVI.68.8.5045-5055.1994

Barth, H., Liang, T. J., and Baumert, T. F. (2006). Hepatitis C virus entry: molecular biology and clinical implications. *Hepatology* 44, 527–535. doi: 10.1002/hep.21321

Bedimo, R., Westfall, A. O., Mugavero, M., Drechsler, H., Khanna, N., and Saag, M. (2010). Hepatitis C virus coinfection and the risk of cardiovascular disease among HIV-infected patients. *HIV Med.* 11, 462–468. doi: 10.1111/j.1468-1293.2009.00815.x

Benhamou, Y., Bochet, M., Thibault, V., Di Martino, V., Caumes, E., Bricaire, F., et al. (1999). Long-term incidence of hepatitis B virus resistance to lamivudine in human immunodeficiency virus-infected patients. *Hepatology* 30, 1302–1306. doi: 10.1002/hep.510300525

Bhattarai, M., Baniya, J. B., Aryal, N., Shrestha, B., Rauniyar, R., Adhikari, A., et al. (2018). Epidemiological profile and risk factors for acquiring HBV and/or HCV in HIV-infected population groups in Nepal. *Biomed Res. Int.* 2018:9241679. doi: 10.1155/2018/9241679

Bhuyan, G. S., Noor, A. U. Z., Sultana, R., Noor, F. A., Sultana, N., Sarker, S. K., et al. (2021). Frequency of hepatitis B, C and HIV infections among transfusion-dependent beta thalassemia patients in Dhaka. *Infect. Dis. Rep.* 13, 89–95. doi: 10.3390/idr13010011

Biggar, R. J., Goedert, J. J., and Hoofnagle, J. (1987). Accelerated loss of antibody to hepatitis B surface antigen among immunodeficient homosexual men infected with HIV. *N. Engl. J. Med.* 316, 630–631. doi: 10.1056/NEJM198703053161015

Bihl, F., Alaei, M., and Negro, F. (2010). The new EASL guidelines for the management of chronic hepatitis B infection adapted for Swiss physicians. *Swiss Med. Wkly.* 140, 154–159.

Blanchard, E., Belouzard, S., Goueslain, L., Wakita, T., Dubuisson, J., Wychowski, C., et al. (2006). Hepatitis C virus entry depends on clathrin-mediated endocytosis. *J. Virol.* 80, 6964–6972. doi: 10.1128/JVI.00024-06

Bodsworth, N. J., Cooper, D. A., and Donovan, B. (1991). The influence of human immunodeficiency virus type 1 infection on the development of the hepatitis B virus carrier state. *J. Infect. Dis.* 163, 1138–1140. doi: 10.1093/infdis/163.5.1138

Bosch, V., Bartenschlager, R., Radziwill, G., and Schaller, H. (1988). The duck hepatitis B virus P-gene codes for protein strongly associated with the 5'-end of the viral DNA minus strand. *Virology* 166, 475–485. doi: 10.1016/0042-6822(88)90518-1

Boyd, A., Piroth, L., Maylin, S., Maynard-Muet, M., Lebossé, F., Bouix, C., et al. (2016). Intensification with pegylated interferon during treatment with tenofovir in HIV-hepatitis B virus co-infected patients. *J. Viral Hepat.* 23, 1017–1026. doi: 10.1111/jvh.12581

Bréchot, C., Thiers, V., Kremsdorf, D., Nalpas, B., Pol, S., and Paterlini-Bréchot, P. (2001). Persistent hepatitis B virus infection in subjects without hepatitis B surface antigen: clinically significant or purely "occult"? *Hepatology* 34, 194–203. doi: 10.1053/jhep.2001.25172

Buchanan, R., Khakoo, S. I., Coad, J., Grellier, L., and Parkes, J. (2017). Hepatitis C bio-behavioural surveys in people who inject drugs-a systematic review of sensitivity to the theoretical assumptions of respondent driven sampling. *Harm Reduct. J.* 14:44. doi: 10.1186/s12954-017-0172-z

Bukh, J., Purcell, R. H., and Miller, R. H. (1994). Sequence analysis of the core gene of 14 hepatitis C virus genotypes. *Proc. Natl. Acad. Sci. U.S.A.* 91, 8239–8243. doi: 10.1073/pnas.91.17.8239

Calvaruso, V., Ferraro, D., Licata, A., Bavetta, M. G., Petta, S., Bronte, F., et al. (2018). HBV reactivation in patients with HCV/HBV cirrhosis on treatment with direct-acting antivirals. *J. Viral Hepat.* 25, 72–79. doi: 10.1111/jvh.12754

Chakravarti, A., Verma, V., Jain, M., and Kar, P. (2005). Characteristics of dual infection of hepatitis B and C viruses among patients with chronic liver disease: a study from tertiary care hospital. *Trop. Gastroenterol.* 26, 183–187.

Collin, F., Duval, X., Le Moing, V., Piroth, L., Al Kaied, F., Massip, P., et al. (2009). Ten-year incidence and risk factors of bone fractures in a cohort of treated HIV1-infected adults. *AIDS* 23, 1021–1024. doi: 10.1097/QAD.0b013e3283292195

Crespo, J., Lozano, J. L., De La Cruz, F., Rodrigo, L., Rodríguez, M., San Miguel, G., et al. (1994). Prevalence and significance of hepatitis C viremia in chronic active hepatitis B. *Am. J. Gastroenterol.* 89, 1147–1151.

Crockett, S. D., and Keeffe, E. B. (2005). Natural history and treatment of hepatitis B virus and hepatitis C virus coinfection. *Ann. Clin. Microbiol. Antimicrob.* 4:13.

Davies, S. E., Portmann, B. C., O'grady, J. G., Aldis, P. M., Chaggar, K., Alexander, G. J., et al. (1991). Hepatic histological findings after transplantation for chronic hepatitis B virus infection, including a unique pattern of fibrosing cholestatic hepatitis. *Hepatology* 13, 150–157.

de Jongh, F. E., Janssen, H. L., De Man, R. A., Hop, W. C., Schalm, S. W., and Van Blankenstein, M. (1992). Survival and prognostic indicators in hepatitis B surface antigen-positive cirrhosis of the liver. *Gastroenterology* 103, 1630–1635. doi: 10.1016/0016-5085(92)91188-a

Di Martino, V., Rufat, P., Boyer, N., Renard, P., Degos, F., Martinot-Peignoux, M., et al. (2001). The influence of human immunodeficiency virus coinfection on chronic hepatitis C in injection drug users: a long-term retrospective cohort study. *Hepatology* 34, 1193–1199. doi: 10.1053/jhep.2001.29201

Di Martino, V., Thevenot, T., Colin, J. F., Boyer, N., Martinot, M., Degos, F., et al. (2002). Influence of HIV infection on the response to interferon therapy and the long-term outcome of chronic hepatitis B. *Gastroenterology* 123, 1812–1822. doi: 10.1053/gast.2002.37061

Dore, G. J., Cooper, D. A., Barrett, C., Goh, L. E., Thakrar, B., and Atkins, M. (1999). Dual efficacy of lamivudine treatment in human immunodeficiency virus/hepatitis B virus-coinfected persons in a randomized, controlled study (CAESAR). The CAESAR Coordinating Committee. *J. Infect. Dis.* 180, 607–613. doi: 10.1086/314942

Dubuisson, J., and Cosset, F. L. (2014). Virology and cell biology of the hepatitis C virus life cycle: an update. *J. Hepatol.* 61, S3–S13. doi: 10.1016/j.jhep.2014.06.031

Easterbrook, P., Sands, A., and Harmanci, H. (2012). Challenges and priorities in the management of HIV/HBV and HIV/HCV coinfection in resource-limited settings. *Semin. Liver Dis.* 32, 147–157. doi: 10.1055/s-0032-1316476

Egger, D., Wölk, B., Gosert, R., Bianchi, L., Blum, H. E., Moradpour, D., et al. (2002). Expression of hepatitis C virus proteins induces distinct membrane

alterations including a candidate viral replication complex. *J. Virol.* 76, 5974–5984. doi: 10.1128/jvi.76.12.5974-5984.2002

El-Hage, N., and Luo, G. (2003). Replication of hepatitis C virus RNA occurs in a membrane-bound replication complex containing nonstructural viral proteins and RNA. *J. Gen. Virol.* 84, 2761–2769. doi: 10.1099/vir.0.19305-0

Eskild, A., Magnus, P., Petersen, G., Sohlberg, C., Jensen, F., Kittelsen, P., et al. (1992). Hepatitis B antibodies in HIV-infected homosexual men are associated with more rapid progression to AIDS. *AIDS* 6, 571–574. doi: 10.1097/00002030-199206000-00008

European Association for the Study of the Liver (2012). EASL clinical practice guidelines: management of chronic hepatitis B virus infection. *J. Hepatol.* 57, 167–185.

Eyster, M. E., Alter, H. J., Aledort, L. M., Quan, S., Hatzakis, A., and Goedert, J. J. (1991). Heterosexual co-transmission of hepatitis C virus (HCV) and human immunodeficiency virus (HIV). *Ann. Intern. Med.* 115, 764–768. doi: 10.7326/0003-4819-115-10-764

Falade-Nwulia, O., and Thio, C. L. (2011). Liver disease, HIV and aging. *Sex. Health* 8, 512–520. doi: 10.1071/SH10163

Fan, C. L., Wei, L., Jiang, D., Chen, H. S., Gao, Y., Li, R. B., et al. (2003). Spontaneous viral clearance after 6-21 years of hepatitis B and C viruses coinfection in high HBV endemic area. *World J. Gastroenterol.* 9, 2012–2016. doi: 10.3748/wjg.v9.i9.2012

Fattovich, G., Brollo, L., Alberti, A., Realdi, G., Pontisso, P., Giustina, G., et al. (1990). Spontaneous reactivation of hepatitis B virus infection in patients with chronic type B hepatitis. *Liver* 10, 141–146. doi: 10.1111/j.1600-0676.1990.tb00449.x

Fattovich, G., Brollo, L., Giustina, G., Noventa, F., Pontisso, P., Alberti, A., et al. (1991). Natural history and prognostic factors for chronic hepatitis type B. *Gut* 32, 294–298. doi: 10.1136/gut.32.3.294

Fattovich, G., Rugge, M., Brollo, L., Pontisso, P., Noventa, F., Guido, M., et al. (1986). Clinical, virologic and histologic outcome following seroconversion from HBeAg to anti-HBe in chronic hepatitis type B. *Hepatology* 6, 167–172. doi: 10.1002/hep.1840060203

Fierer, D. S., Dieterich, D. T., Fiel, M. I., Branch, A. D., Marks, K. M., Fusco, D. N., et al. (2013). Rapid progression to decompensated cirrhosis, liver transplant, and death in HIV-infected men after primary hepatitis C virus infection. *Clin. Infect. Dis.* 56, 1038–1043. doi: 10.1093/cid/cis1206

Forrester, J. E., Rhee, M. S., Mcgovern, B. H., Sterling, R. K., Knox, T. A., and Terrin, N. (2012). The association of HIV viral load with indirect markers of liver injury. *J. Viral Hepat.* 19, e202–e211. doi: 10.1111/j.1365-2893.2011.01529.x

Gandhi, R. T., Wurcel, A., Lee, H., Mcgovern, B., Shopis, J., Geary, M., et al. (2005). Response to hepatitis B vaccine in HIV-1-positive subjects who test positive for isolated antibody to hepatitis B core antigen: implications for hepatitis B vaccine strategies. *J. Infect. Dis.* 191, 1435–1441. doi: 10.1086/429302

Garg, S., Brooks, J. T., Luo, Q., and Skarbinski, J. (2014). 1588: Prevalence of and factors associated with hepatitis C virus testing and infection among HIV-infected adults receiving medical care in the United States. *Open Forum Infect. Dis.* 1(Suppl. 1):S423.

Gilson, R. J., Hawkins, A. E., Beecham, M. R., Ross, E., Waite, J., Briggs, M., et al. (1997). Interactions between HIV and hepatitis B virus in homosexual men: effects on the natural history of infection. *AIDS* 11, 597–606. doi: 10.1097/00002030-199705000-00007

Gosert, R., Egger, D., Lohmann, V., Bartenschlager, R., Blum, H. E., Bienz, K., et al. (2003). Identification of the hepatitis C virus RNA replication complex in Huh-7 cells harboring subgenomic replicons. *J. Virol.* 77, 5487–5492. doi: 10.1128/jvi.77.9.5487-5492.2003

Götz, H. M., Van Doornum, G., Niesters, H. G., Den Hollander, J. G., Thio, H. B., and De Zwart, O. (2005). A cluster of acute hepatitis C virus infection among men who have sex with men–results from contact tracing and public health implications. *AIDS* 19, 969–974. doi: 10.1097/01.aids.0000171412.61360.f8

Grassi, G., Di Caprio, G., Fimia, G. M., Ippolito, G., Tripodi, M., and Alonzi, T. (2016). Hepatitis C virus relies on lipoproteins for its life cycle. *World J. Gastroenterol.* 22, 1953–1965. doi: 10.3748/wjg.v22.i6.1953

Gupta, P. (2013). Hepatitis C virus and HIV type 1 co-infection. *Infect. Dis. Rep.* 5:e7.

Hadziyannis, S. J., Tassopoulos, N. C., Heathcote, E. J., Chang, T. T., Kitis, G., Rizzetto, M., et al. (2003). Adefovir dipivoxil for the treatment of hepatitis B e antigen-negative chronic hepatitis B. *N. Engl. J. Med.* 348, 800–807. doi: 10.1056/NEJMoa021812

Hawkins, C., Grant, J., Ammerman, L. R., Palella, F., Mclaughlin, M., Green, R., et al. (2016). High rates of hepatitis C virus (HCV) cure using direct-acting antivirals in HIV/HCV-coinfected patients: a real-world perspective. *J. Antimicrob. Chemother.* 71, 2642–2645. doi: 10.1093/jac/dkw203

Health Policy Project (2014). *The Role of Policy, Advocacy, Governance, and Financing in Addressing the HIV Epidemic [Online]*. Available online at: https://www.healthpolicyproject.com/index.cfm?id=topics-KeyPopulations (accessed September 7, 2021).

Helle, F., and Dubuisson, J. (2008). Hepatitis C virus entry into host cells. *Cell. Mol. Life Sci.* 65, 100–112.

Hernandez, M. D., and Sherman, K. E. (2011). HIV/hepatitis C coinfection natural history and disease progression. *Curr. Opin. HIV AIDS* 6, 478–482. doi: 10.1097/COH.0b013e32834bd365

Hoofnagle, J. H., and Di Bisceglie, A. M. (1991). Serologic diagnosis of acute and chronic viral hepatitis. *Semin. Liver Dis.* 11, 73–83. doi: 10.1055/s-2008-1040426

Hossain, M. G., Akter, S., Ohsaki, E., and Ueda, K. (2020). Impact of the interaction of hepatitis B virus with mitochondria and associated proteins. *Viruses* 12:175. doi: 10.3390/v12020175

Hossain, M. G., and Ueda, K. (2017). Investigation of a novel hepatitis B virus surface antigen (HBsAg) escape mutant affecting immunogenicity. *PLoS One* 12:e0167871. doi: 10.1371/journal.pone.0167871

Imbert-Bismut, F., Ratziu, V., Pieroni, L., Charlotte, F., Benhamou, Y., and Poynard, T. (2001). Biochemical markers of liver fibrosis in patients with hepatitis C virus infection: a prospective study. *Lancet* 357, 1069–1075. doi: 10.1016/S0140-6736(00)04258-6

Jacobson, I. M., Dore, G. J., Foster, G. R., Fried, M. W., Radu, M., Rafalsky, V. V., et al. (2014). Simeprevir with pegylated interferon alfa 2a plus ribavirin in treatment-naive patients with chronic hepatitis C virus genotype 1 infection (QUEST-1): a phase 3, randomised, double-blind, placebo-controlled trial. *Lancet* 384, 403–413. doi: 10.1016/S0140-6736(14)60494-3

Jaroszewicz, J., Reiberger, T., Meyer-Olson, D., Mauss, S., Vogel, M., Ingiliz, P., et al. (2012). Hepatitis B surface antigen concentrations in patients with HIV/HBV co-infection. *PLoS One* 7:e43143. doi: 10.1371/journal.pone.0043143

Johnson, R. M., Ristig, M. B., Overton, E. T., Lisker-Melman, M., Cummings, O. W., and Aberg, J. A. (2007). Safety and tolerability of sequential pegylated IFN-alpha2a and tenofovir for hepatitis B infection in HIV(+) individuals. *HIV Clin. Trials* 8, 173–181. doi: 10.1310/hct0803-173

Karangelis, D. E., Kanakis, I., Asimakopoulou, A. P., Karousou, E., Passi, A., Theocharis, A. D., et al. (2010). Glycosaminoglycans as key molecules in atherosclerosis: the role of versican and hyaluronan. *Curr. Med. Chem.* 17, 4018–4026. doi: 10.2174/092986710793205354

Kato, N. (2000). Genome of human hepatitis C virus (HCV): gene organization, sequence diversity, and variation. *Microb. Comp. Genomics* 5, 129–151. doi: 10.1089/omi.1.2000.5.129

Kilonzo, S. B., Gunda, D. W., Mpondo, B. C. T., Bakshi, F. A., and Jaka, H. (2018). Hepatitis B virus infection in Tanzania: current status and challenges. *J. Trop. Med.* 2018:4239646. doi: 10.1155/2018/4239646

Kim, A. Y., and Chung, R. T. (2009). Coinfection with HIV-1 and HCV–a one-two punch. *Gastroenterology* 137, 795–814. doi: 10.1053/j.gastro.2009.06.040

Kim, A. Y., Chung, R. T., and Polsky, B. (2000). Human immunodeficiency virus and hepatitis B and C coinfection: pathogenic interactions, natural history, and therapy. *IDS Clin. Rev.* 12(Suppl. 1), 263–306.

Kingsley, L. A., Detels, R., Kaslow, R., Polk, B. F., Rinaldo, C. R. Jr., Chmiel, J., et al. (1987). Risk factors for seroconversion to human immunodeficiency virus among male homosexuals. Results from the Multicenter AIDS Cohort Study. *Lancet* 1, 345–349. doi: 10.1016/s0140-6736(87)91725-9

Kirk, G. D., Mehta, S. H., Astemborski, J., Galai, N., Washington, J., Higgins, Y., et al. (2013). HIV, age, and the severity of hepatitis C virus-related liver disease: a cohort study. *Ann. Intern. Med.* 158, 658–666. doi: 10.7326/0003-4819-158-9-201305070-00604

Konstantinou, D., and Deutsch, M. (2015). The spectrum of HBV/HCV coinfection: epidemiology, clinical characteristics, viralinteractions and management. *Ann. Gastroenterol.* 28, 221–228.

Körner, C., Krämer, B., Schulte, D., Coenen, M., Mauss, S., Fätkenheuer, G., et al. (2009). Effects of HCV co-infection on apoptosis of $CD4^+$ T-cells in HIV-positive patients. *Clin. Sci.* 116, 861–870.

Kovacs, A., Karim, R., Mack, W. J., Xu, J., Chen, Z., Operskalski, E., et al. (2010). Activation of CD8 T cells predicts progression of HIV infection in women coinfected with hepatitis C virus. *J. Infect. Dis.* 201, 823–834. doi: 10.1086/650997

Krassenburg, L. A. P., Maan, R., Ramji, A., Manns, M. P., Cornberg, M., Wedemeyer, H., et al. (2021). Clinical outcomes following DAA therapy in patients with HCV-related cirrhosis depend on disease severity. *J. Hepatol.* 74, 1053–1063. doi: 10.1016/j.jhep.2020.11.021

Labarga, P., Soriano, V., Vispo, M. E., Pinilla, J., Martin-Carbonero, L., Castellares, C., et al. (2007). Hepatotoxicity of antiretroviral drugs is reduced after successful treatment of chronic hepatitis C in HIV-infected patients. *J. Infect. Dis.* 196, 670–676. doi: 10.1086/520092

Lackner, C., Struber, G., Liegl, B., Leibl, S., Ofner, P., Bankuti, C., et al. (2005). Comparison and validation of simple noninvasive tests for prediction of fibrosis in chronic hepatitis C. *Hepatology* 41, 1376–1382. doi: 10.1002/hep.20717

Lada, O., Benhamou, Y., Cahour, A., Katlama, C., Poynard, T., and Thibault, V. (2004). In vitro susceptibility of lamivudine-resistant hepatitis B virus to adefovir and tenofovir. *Antivir. Ther.* 9, 353–363.

Lee, H. C., Ko, N. Y., Lee, N. Y., Chang, C. M., and Ko, W. C. (2008). Seroprevalence of viral hepatitis and sexually transmitted disease among adults with recently diagnosed HIV infection in Southern Taiwan, 2000-2005: upsurge in hepatitis C virus infections among injection drug users. *J. Formos. Med. Assoc.* 107, 404–411. doi: 10.1016/S0929-6646(08)60106-0

Li, W. (2015). The hepatitis B virus receptor. *Annu. Rev. Cell Dev. Biol.* 31, 125–147.

Liaw, Y. F., Tai, D. I., Chu, C. M., and Chen, T. J. (1988). The development of cirrhosis in patients with chronic type B hepatitis: a prospective study. *Hepatology* 8, 493–496.

Lim, S. G., Ng, T. M., Kung, N., Krastev, Z., Volfova, M., Husa, P., et al. (2006). A double-blind placebo-controlled study of emtricitabine in chronic hepatitis B. *Arch. Intern. Med.* 166, 49–56. doi: 10.1001/archinte.166.1.49

Liu, C. J. (2014). Treatment of patients with dual hepatitis C virus and hepatitis B virus infection: resolved and unresolved issues. *J. Gastroenterol. Hepatol.* 29, 26–30. doi: 10.1111/jgh.12421

Liu, C. J., Chu, Y. T., Shau, W. Y., Kuo, R. N., Chen, P. J., and Lai, M. S. (2014). Treatment of patients with dual hepatitis C and B by peginterferon α and ribavirin reduced risk of hepatocellular carcinoma and mortality. *Gut* 63, 506–514. doi: 10.1136/gutjnl-2012-304370

Lo Re, V. L. III, Kallan, M. J., Tate, J. P., Localio, A. R., Lim, J. K., Goetz, M. B., et al. (2014). Hepatic decompensation in antiretroviral-treated patients co-infected with HIV and hepatitis C virus compared with hepatitis C virus-monoinfected patients: a cohort study. *Ann. Intern. Med.* 160, 369–379. doi: 10.7326/M13-1829

Lok, A. S., and McMahon, B. J. (2009). Chronic hepatitis B: update 2009. *Hepatology* 50, 661–662.

Mahoney, F. J. (1999). Update on diagnosis, management, and prevention of hepatitis B virus infection. *Clin. Microbiol. Rev.* 12, 351–366. doi: 10.1128/CMR.12.2.351

Maponga, T. G., Glashoff, R. H., Vermeulen, H., Robertson, B., Burmeister, S., Bernon, M., et al. (2020). Hepatitis B virus-associated hepatocellular carcinoma in South Africa in the era of HIV. *BMC Gastroenterol.* 20:226. doi: 10.1186/s12876-020-01372-2

Marks, K. M., Clarke, R. M., Bussel, J. B., Talal, A. H., and Glesby, M. J. (2009). Risk factors for thrombocytopenia in HIV-infected persons in the era of potent antiretroviral therapy. *J. Acquir. Immune Defic. Syndr.* 52, 595–599. doi: 10.1097/QAI.0b013e3181b79aff

Martin, P., Di Bisceglie, A. M., Kassianides, C., Lisker-Melman, M., and Hoofnagle, J. H. (1989). Rapidly progressive non-A, non-B hepatitis in patients with human immunodeficiency virus infection. *Gastroenterology* 97, 1559–1561. doi: 10.1016/0016-5085(89)90405-8

Martinez-Sierra, C., Arizcorreta, A., Díaz, F., Roldán, R., Martín-Herrera, L., Pérez-Guzmán, E., et al. (2003). Progression of chronic hepatitis C to liver fibrosis and cirrhosis in patients coinfected with hepatitis C virus and human immunodeficiency virus. *Clin. Infect. Dis.* 36, 491–498. doi: 10.1086/367643

McMahon, B. J., Holck, P., Bulkow, L., and Snowball, M. (2001). Serologic and clinical outcomes of 1536 Alaska Natives chronically infected with hepatitis B virus. *Ann. Intern. Med.* 135, 759–768. doi: 10.7326/0003-4819-135-9-200111060-00006

Mekky, M. A., Nasr, A. M., Saleh, M. A., Wasif, N. K., Khalaf, M., Aboalam, H., et al. (2013). Virologic and histologic characterisation of dual hepatitis B and C co-infection in Egyptian patients. *Arab J. Gastroenterol.* 14, 143–147. doi: 10.1016/j.ajg.2013.11.003

Messina, J. P., Humphreys, I., Flaxman, A., Brown, A., Cooke, G. S., Pybus, O. G., et al. (2015). Global distribution and prevalence of hepatitis C virus genotypes. *Hepatology* 61, 77–87. doi: 10.1002/hep.27259

Miailhes, P., Trabaud, M. A., Pradat, P., Lebouché, B., Chevallier, M., Chevallier, P., et al. (2007). Impact of highly active antiretroviral therapy (HAART) on the natural history of hepatitis B virus (HBV) and HIV coinfection: relationship between prolonged efficacy of HAART and HBV surface and early antigen seroconversion. *Clin. Infect. Dis.* 45, 624–632. doi: 10.1086/520752

Mimms, L. T., Mosley, J. W., Hollinger, F. B., Aach, R. D., Stevens, C. E., Cunningham, M., et al. (1993). Effect of concurrent acute infection with hepatitis C virus on acute hepatitis B virus infection. *BMJ* 307, 1095–1097. doi: 10.1136/bmj.307.6912.1095

Morali, G., Maor, Y., Klar, R., Braun, M., Ben Ari, Z., Bujanover, Y., et al. (2007). Fibrotest-Actitest: the biochemical marker of liver fibrosis–the Israeli experience. *Isr. Med. Assoc. J.* 9, 588–591.

Moreno, S., García-Samaniego, J., Moreno, A., Ortega, E., Pineda, J. A., Del Romero, J., et al. (2009). Noninvasive diagnosis of liver fibrosis in patients with HIV infection and HCV/HBV co-infection. *J. Viral Hepat.* 16, 249–258. doi: 10.1111/j.1365-2893.2009.01088.x

Naggie, S., Cooper, C., Saag, M., Workowski, K., Ruane, P., Towner, W. J., et al. (2015). Ledipasvir and sofosbuvir for HCV in patients coinfected with HIV-1. *N. Engl. J. Med.* 373, 705–713.

Ndifontiayong, A. N., Ali, I. M., Sokoudjou, J. B., Ndimumeh, J. M., and Tume, C. B. (2021). The effect of HBV/HCV in response to HAART in HIV patients after 12 months in Kumba Health District in the South West Region of Cameroon. *Trop. Med. Infect. Dis.* 6:150. doi: 10.3390/tropicalmed6030150

Nguyen, L. H., Ko, S., Wong, S. S., Tran, P. S., Trinh, H. N., Garcia, R. T., et al. (2011). Ethnic differences in viral dominance patterns in patients with hepatitis B virus and hepatitis C virus dual infection. *Hepatology* 53, 1839–1845.

Nyirenda, M., Beadsworth, M. B., Stephany, P., Hart, C. A., Hart, I. J., Munthali, C., et al. (2008). Prevalence of infection with hepatitis B and C virus and coinfection with HIV in medical inpatients in Malawi. *J. Infect.* 57, 72–77. doi: 10.1016/j.jinf.2008.05.004

Ockenga, J., Tillmann, H. L., Trautwein, C., Stoll, M., Manns, M. P., and Schmidt, R. E. (1997). Hepatitis B and C in HIV-infected patients. Prevalence and prognostic value. *J. Hepatol.* 27, 18–24. doi: 10.1016/s0168-8278(97)80274-7

Ohkawa, K., Hayashi, N., Yuki, N., Hagiwara, H., Kato, M., Yamamoto, K., et al. (1994). Hepatitis C virus antibody and hepatitis C virus replication in chronic hepatitis B patients. *J. Hepatol.* 21, 509–514. doi: 10.1016/s0168-8278(94)80094-4

Operskalski, E. A., and Kovacs, A. (2011). HIV/HCV co-infection: pathogenesis, clinical complications, treatment, and new therapeutic technologies. *Curr. HIV/AIDS Rep.* 8, 12–22. doi: 10.1007/s11904-010-0071-3

Ott, J. J., Stevens, G. A., Groeger, J., and Wiersma, S. T. (2012). Global epidemiology of hepatitis B virus infection: new estimates of age-specific HBsAg seroprevalence and endemicity. *Vaccine* 30, 2212–2219. doi: 10.1016/j.vaccine.2011.12.116

Pallás, J. R., Fariñas-Alvarez, C., Prieto, D., and Delgado-Rodríguez, M. (1999). Coinfections by HIV, hepatitis B and hepatitis C in imprisoned injecting drug users. *Eur. J. Epidemiol.* 15, 699–704. doi: 10.1023/a:1007619614350

Panigrahi, A. K., Nanda, S. K., Dixit, R. K., Acharya, S. K., Zuckerman, A. J., and Panda, S. K. (1994). Diagnosis of hepatitis C virus-associated chronic liver disease in India: comparison of HCV antibody assay with a polymerase chain reaction for the 5' noncoding region. *J. Med. Virol.* 44, 176–179. doi: 10.1002/jmv.1890440211

Pascual-Pareja, J. F., Caminoa, A., Larrauri, C., González-García, J., Montes, M. L., Díez, J., et al. (2009). HAART is associated with lower hepatic necroinflammatory activity in HIV-hepatitis C virus-coinfected patients with CD4 cell count of more than 350 cells/microl at the time of liver biopsy. *AIDS* 23, 971–975. doi: 10.1097/qad.0b013e328329f994

Pawlotsky, J. M. (2014). New hepatitis C therapies: the toolbox, strategies, and challenges. *Gastroenterology* 146, 1176–1192. doi: 10.1053/j.gastro.2014.03.003

Penin, F., Brass, V., Appel, N., Ramboarina, S., Montserret, R., Ficheux, D., et al. (2004). Structure and function of the membrane anchor domain of hepatitis C

virus nonstructural protein 5A. *J. Biol. Chem.* 279, 40835–40843. doi: 10.1074/jbc.M404761200

Pessôa, M. G., Gazzard, B., Huang, A. K., Brandão-Mello, C. E., Cassetti, I., Mendes-Corrêa, M. C., et al. (2008). Efficacy and safety of entecavir for chronic HBV in HIV/HBV coinfected patients receiving lamivudine as part of antiretroviral therapy. *AIDS* 22, 1779–1787. doi: 10.1097/QAD.0b013e32830b3ab5

Pfaender, S., Von Hahn, T., Steinmann, J., Ciesek, S., and Steinmann, E. (2016). Prevention strategies for blood-borne viruses-in the era of vaccines, direct acting antivirals and antiretroviral therapy. *Rev. Med. Virol.* 26, 330–339. doi: 10.1002/rmv.1890

Pollicino, T., Cacciola, I., Saffioti, F., and Raimondo, G. (2014). Hepatitis B virus PreS/S gene variants: pathobiology and clinical implications. *J. Hepatol.* 61, 408–417. doi: 10.1016/j.jhep.2014.04.041

Poordad, F., Hezode, C., Trinh, R., Kowdley, K. V., Zeuzem, S., Agarwal, K., et al. (2014). ABT-450/r-ombitasvir and dasabuvir with ribavirin for hepatitis C with cirrhosis. *N. Engl. J. Med.* 370, 1973–1982.

Porras-Ramírez, A., and Rico-Mendoza, A. (2020). "Coinfection of hepatitis B and C in HIV patients: a review of the state of the art," in *Hepatitis B and C*, ed. L. Rodrigo (London: IntechOpen).

Price, P., Murdoch, D. M., Agarwal, U., Lewin, S. R., Elliott, J. H., and French, M. A. (2009). Immune restoration diseases reflect diverse immunopathological mechanisms. *Clin. Microbiol. Rev.* 22, 651–663. doi: 10.1128/CMR.00015-09

Puoti, M., Bonacini, M., Spinetti, A., Putzolu, V., Govindarajan, S., Zaltron, S., et al. (2001). Liver fibrosis progression is related to CD4 cell depletion in patients coinfected with hepatitis C virus and human immunodeficiency virus. *J. Infect. Dis.* 183, 134–137. doi: 10.1086/317644

Ray Saraswati, L., Sarna, A., Sebastian, M. P., Sharma, V., Madan, I., Thior, I., et al. (2015). HIV, hepatitis B and C among people who inject drugs: high prevalence of HIV and Hepatitis C RNA positive infections observed in Delhi, India. *BMC Public Health* 15:726. doi: 10.1186/s12889-015-2003-z

Reddy, G. A., Dakshinamurthy, K. V., Neelaprasad, P., Gangadhar, T., and Lakshmi, V. (2005). Prevalence of HBV and HCV dual infection in patients on haemodialysis. *Indian J. Med. Microbiol.* 23, 41–43. doi: 10.4103/0255-0857.13872

Reed, K. E., Grakoui, A., and Rice, C. M. (1995). Hepatitis C virus-encoded NS2-3 protease: cleavage-site mutagenesis and requirements for bimolecular cleavage. *J. Virol.* 69, 4127–4136. doi: 10.1128/JVI.69.7.4127-4136.1995

Rodrigo, L. (2020). *Hepatitis B and C*. London: IntechOpen.

Roni, D. A., Pathapati, R. M., Kumar, A. S., Nihal, L., Sridhar, K., and Tumkur Rajashekar, S. (2013). Safety and efficacy of hepatitis B vaccination in cirrhosis of liver. *Adv. Virol.* 2013:196704. doi: 10.1155/2013/196704

Rotman, Y., and Liang, T. J. (2009). Coinfection with hepatitis C virus and human immunodeficiency virus: virological, immunological, and clinical outcomes. *J. Virol.* 83, 7366–7374. doi: 10.1128/JVI.00191-09

Saag, M. S. (2006). Emtricitabine, a new antiretroviral agent with activity against HIV and hepatitis B virus. *Clin. Infect. Dis.* 42, 126–131. doi: 10.1086/498348

Schaefer, S. (2007). Hepatitis B virus taxonomy and hepatitis B virus genotypes. *World J. Gastroenterol.* 13, 14–21. doi: 10.3748/wjg.v13.i1.14

Semnani, S., Roshandel, G., Abdolahi, N., Besharat, S., Keshtkar, A. A., Joshaghani, H., et al. (2007). Hepatitis B/C virus co-infection in Iran: a seroepidemiological study. *Turk. J. Gastroenterol.* 18, 20–21.

Senturk, H., Tahan, V., Canbakan, B., Dane, F., Ulger, Y., Ozaras, R., et al. (2008). Clinicopathologic features of dual chronic hepatitis B and C infection: a comparison with single hepatitis B, C and delta infections. *Ann. Hepatol.* 7, 52–58.

Shahani, L., and Hamill, R. J. (2016). Therapeutics targeting inflammation in the immune reconstitution inflammatory syndrome. *Transl. Res.* 167, 88–103. doi: 10.1016/j.trsl.2015.07.010

Shapatava, E., Nelson, K. E., Tsertsvadze, T., and Del Rio, C. (2006). Risk behaviors and HIV, hepatitis B, and hepatitis C seroprevalence among injection drug users in Georgia. *Drug Alcohol Depend.* 82(Suppl. 1), S35–S38. doi: 10.1016/s0376-8716(06)80006-2

Sherman, K. E., Rouster, S. D., Chung, R. T., and Rajicic, N. (2002). Hepatitis C virus prevalence among patients infected with human immunodeficiency virus: a cross-sectional analysis of the US adult AIDS Clinical Trials Group. *Clin. Infect. Dis.* 34, 831–837. doi: 10.1086/339042

Shire, N. J., Rouster, S. D., Stanford, S. D., Blackard, J. T., Martin, C. M., Fichtenbaum, C. J., et al. (2007). The prevalence and significance of occult hepatitis B virus in a prospective cohort of HIV-infected patients. *J. Acquir. Immune Defic. Syndr.* 44, 309–314. doi: 10.1097/QAI.0b013e31802e29a9

Siebers, A., and Finlay, B. B. (1996). M cells and the pathogenesis of mucosal and systemic infections. *Trends Microbiol.* 4, 22–29. doi: 10.1016/0966-842x(96)81501-0

Singal, A. K., and Anand, B. S. (2009). Management of hepatitis C virus infection in HIV/HCV co-infected patients: clinical review. *World J. Gastroenterol.* 15, 3713–3724. doi: 10.3748/wjg.15.3713

Smith, J. O., and Sterling, R. K. (2009). Systematic review: non-invasive methods of fibrosis analysis in chronic hepatitis C. *Aliment. Pharmacol. Ther.* 30, 557–576. doi: 10.1111/j.1365-2036.2009.04062.x

Soriano, V., Puoti, M., Sulkowski, M., Cargnel, A., Benhamou, Y., Peters, M., et al. (2007). Care of patients coinfected with HIV and hepatitis C virus: 2007 updated recommendations from the HCV-HIV International Panel. *AIDS* 21:1073–1089. doi: 10.1097/QAD.0b013e3281084e4d

Spradling, P. R., Richardson, J. T., Buchacz, K., Moorman, A. C., and Brooks, J. T. (2010). Prevalence of chronic hepatitis B virus infection among patients in the HIV outpatient study, 1996-2007. *J. Viral Hepat.* 17, 879–886. doi: 10.1111/j.1365-2893.2009.01249.x

Sterling, R. K., and Sulkowski, M. S. (2004). Hepatitis C virus in the setting of HIV or hepatitis B virus coinfection. *Semin. Liver Dis.* 24(Suppl. 2), 61–68.

Sulaiman, H. A. (1989). The development of hepatocellular carcinoma from liver cirrhosis during a follow-up study. *Gastroenterol. Jpn.* 24, 567–572. doi: 10.1007/BF02773887

Sulkowski, M. S. (2001). Hepatitis C virus infection in HIV-infected patients. *Curr. Infect. Dis. Rep.* 3, 469–476.

Sulkowski, M. S., Eron, J. J., Wyles, D., Trinh, R., Lalezari, J., Wang, C., et al. (2015). Ombitasvir, paritaprevir co-dosed with ritonavir, dasabuvir, and ribavirin for hepatitis C in patients co-infected with HIV-1: a randomized trial. *JAMA* 313, 1223–1231. doi: 10.1001/jama.2015.1328

Sun, H. Y., Sheng, W. H., Tsai, M. S., Lee, K. Y., Chang, S. Y., and Hung, C. C. (2014). Hepatitis B virus coinfection in human immunodeficiency virus-infected patients: a review. *World J. Gastroenterol.* 20, 14598–14614. doi: 10.3748/wjg.v20.i40.14598

Syed, G. H., Amako, Y., and Siddiqui, A. (2010). Hepatitis C virus hijacks host lipid metabolism. *Trends Endocrinol. Metab.* 21, 33–40. doi: 10.1016/j.tem.2009.07.005

Tenney, D. J., Levine, S. M., Rose, R. E., Walsh, A. W., Weinheimer, S. P., Discotto, L., et al. (2004). Clinical emergence of entecavir-resistant hepatitis B virus requires additional substitutions in virus already resistant to lamivudine. *Antimicrob. Agents Chemother.* 48, 3498–3507. doi: 10.1128/AAC.48.9.3498-3507.2004

Thein, H. H., Yi, Q., Dore, G. J., and Krahn, M. D. (2008). Natural history of hepatitis C virus infection in HIV-infected individuals and the impact of HIV in the era of highly active antiretroviral therapy: a meta-analysis. *AIDS* 22, 1979–1991. doi: 10.1097/QAD.0b013e32830e6d51

Thio, C. L. (2006). Treatment of lamivudine-resistant hepatitis B in HIV-infected persons: is adefovir dipivoxil the answer? *J. Hepatol.* 44, 1–3. doi: 10.1016/j.jhep.2005.10.012

Thio, C. L., Seaberg, E. C., Skolasky, R. Jr., Phair, J., Visscher, B., Muñoz, A., et al. (2002). HIV-1, hepatitis B virus, and risk of liver-related mortality in the Multicenter Cohort Study (MACS). *Lancet* 360, 1921–1926. doi: 10.1016/s0140-6736(02)11913-1

Thomas, D. L., Astemborski, J., Rai, R. M., Anania, F. A., Schaeffer, M., Galai, N., et al. (2000). The natural history of hepatitis C virus infection: host, viral, and environmental factors. *JAMA* 284, 450–456. doi: 10.1001/jama.284.4.450

Thomas, D. L., Zenilman, J. M., Alter, H. J., Shih, J. W., Galai, N., Carella, A. V., et al. (1995). Sexual transmission of hepatitis C virus among patients attending sexually transmitted diseases clinics in Baltimore–an analysis of 309 sex partnerships. *J. Infect. Dis.* 171, 768–775. doi: 10.1093/infdis/171.4.768

Toma, S., Yamashiro, T., Arakaki, S., Shiroma, J., Maeshiro, T., Hibiya, K., et al. (2009). Inhibition of intracellular hepatitis C virus replication by nelfinavir and synergistic effect with interferon-alpha. *J. Viral Hepat.* 16, 506–512. doi: 10.1111/j.1365-2893.2009.01102.x

Tsui, J. I., French, A. L., Seaberg, E. C., Augenbraun, M., Nowicki, M., Peters, M., et al. (2007). Prevalence and long-term effects of occult hepatitis B virus

infection in HIV-infected women. *Clin. Infect. Dis.* 45, 736–740. doi: 10.1086/520989

Tuyama, A. C., Hong, F., Saiman, Y., Wang, C., Ozkok, D., Mosoian, A., et al. (2010). Human immunodeficiency virus (HIV)-1 infects human hepatic stellate cells and promotes collagen I and monocyte chemoattractant protein-1 expression: implications for the pathogenesis of HIV/hepatitis C virus-induced liver fibrosis. *Hepatology* 52, 612–622. doi: 10.1002/hep.23679

Tyson, G. L., Kramer, J. R., Duan, Z., Davila, J. A., Richardson, P. A., and El-Serag, H. B. (2013). Prevalence and predictors of hepatitis B virus coinfection in a United States cohort of hepatitis C virus-infected patients. *Hepatology* 58, 538–545. doi: 10.1002/hep.26400

van de Laar, T. J., Van Der Bij, A. K., Prins, M., Bruisten, S. M., Brinkman, K., Ruys, T. A., et al. (2007). Increase in HCV incidence among men who have sex with men in Amsterdam most likely caused by sexual transmission. *J. Infect. Dis.* 196, 230–238. doi: 10.1086/518796

Villa, E., Grottola, A., Buttafoco, P., Colantoni, A., Bagni, A., Ferretti, I., et al. (2001). High doses of alpha-interferon are required in chronic hepatitis due to coinfection with hepatitis B virus and hepatitis C virus: long term results of a prospective randomized trial. *Am. J. Gastroenterol.* 96, 2973–2977. doi: 10.1111/j.1572-0241.2001.04670.x

Wai, C. T., Greenson, J. K., Fontana, R. J., Kalbfleisch, J. D., Marrero, J. A., Conjeevaram, H. S., et al. (2003). A simple noninvasive index can predict both significant fibrosis and cirrhosis in patients with chronic hepatitis C. *Hepatology* 38, 518–526. doi: 10.1053/jhep.2003.50346

Walker, D. R., Pedrosa, M. C., Manthena, S. R., Patel, N., and Marx, S. E. (2015). Early view of the effectiveness of new direct-acting antiviral (DAA) regimens in patients with hepatitis C virus (HCV). *Adv. Ther.* 32, 1117–1127. doi: 10.1007/s12325-015-0258-5

Wing, E. J. (2017). The aging population with HIV infection. *Trans. Am. Clin. Climatol. Assoc.* 128, 131–144.

Wu, J. C., Chen, C. L., Hou, M. C., Chen, T. Z., Lee, S. D., and Lo, K. J. (1994). Multiple viral infection as the most common cause of fulminant and subfulminant viral hepatitis in an area endemic for hepatitis B: application and limitations of the polymerase chain reaction. *Hepatology* 19, 836–840.

Wyles, D. L., Ruane, P. J., Sulkowski, M. S., Dieterich, D., Luetkemeyer, A., Morgan, T. R., et al. (2015). Daclatasvir plus sofosbuvir for HCV in patients coinfected with HIV-1. *N. Engl. J. Med.* 373, 714–725. doi: 10.1056/NEJMoa1503153

Xiao, S. Y., Lu, L., and Wang, H. L. (2008). Fibrosing cholestatic hepatitis: clinicopathologic spectrum, diagnosis and pathogenesis. *Int. J. Clin. Exp. Pathol.* 1, 396–402.

Yan, B. M., and Lee, S. S. (2005). Acute coinfection with hepatitis B and hepatitis C viruses. *Can. J. Gastroenterol.* 19, 729–730. doi: 10.1155/2005/514813

Yan, H., Zhong, G., Xu, G., He, W., Jing, Z., Gao, Z., et al. (2012). Sodium taurocholate cotransporting polypeptide is a functional receptor for human hepatitis B and D virus. *eLife* 1:e00049.

Yee, T. T., Griffioen, A., Sabin, C. A., Dusheiko, G., and Lee, C. A. (2000). The natural history of HCV in a cohort of haemophilic patients infected between 1961 and 1985. *Gut* 47, 845–851. doi: 10.1136/gut.47.6.845

Yehia, B. R., Herati, R. S., Fleishman, J. A., Gallant, J. E., Agwu, A. L., Berry, S. A., et al. (2014). Hepatitis C virus testing in adults living with HIV: a need for improved screening efforts. *PLoS One* 9:e102766. doi: 10.1371/journal.pone.0102766

Yim, H. J., and Lok, A. S. (2006). Natural history of chronic hepatitis B virus infection: what we knew in 1981 and what we know in 2005. *Hepatology* 43, S173–S181. doi: 10.1002/hep.20956

Zanetti, A. R., Tanzi, E., and Newell, M. L. (1999). Mother-to-infant transmission of hepatitis C virus. *J. Hepatol.* 31(Suppl. 1), 96–100.

Zhang, F., Zhu, H., Wu, Y., Dou, Z., Zhang, Y., Kleinman, N., et al. (2014). HIV, hepatitis B virus, and hepatitis C virus co-infection in patients in the China National Free Antiretroviral Treatment Program, 2010-12: a retrospective observational cohort study. *Lancet Infect. Dis.* 14, 1065–1072. doi: 10.1016/S1473-3099(14)70946-6

**Conflict of Interest:** The authors declare that the research was conducted in the absence of any commercial or financial relationships that could be construed as a potential conflict of interest.

**Publisher's Note:** All claims expressed in this article are solely those of the authors and do not necessarily represent those of their affiliated organizations, or those of the publisher, the editors and the reviewers. Any product that may be evaluated in this article, or claim that may be made by its manufacturer, is not guaranteed or endorsed by the publisher.

*Copyright © 2022 Shahriar, Araf, Ahmad, Kattel, Sah, Rahaman, Sadiea, Sultana, Islam, Zheng and Hossain. This is an open-access article distributed under the terms of the Creative Commons Attribution License (CC BY). The use, distribution or reproduction in other forums is permitted, provided the original author(s) and the copyright owner(s) are credited and that the original publication in this journal is cited, in accordance with accepted academic practice. No use, distribution or reproduction is permitted which does not comply with these terms.*

frontiers in Microbiology

PERSPECTIVE
published: 10 February 2022
doi: 10.3389/fmicb.2022.840911

# The Hidden Enemy Within: Non-canonical Peptides in Virus-Induced Autoimmunity

*Manivel Lodha, Florian Erhard, Lars Dölken and Bhupesh K. Prusty**

*Institute for Virology and Immunobiology, Julius-Maximilians University of Würzburg, Würzburg, Germany*

Viruses play a key role in explaining the pathogenesis of various autoimmune disorders, whose underlying principle is defined by the activation of autoreactive T-cells. In many cases, T-cells escape self-tolerance due to the failure in encountering certain MHC-I self-peptide complexes at substantial levels, whose peptides remain invisible from the immune system. Over the years, contribution of unstable defective ribosomal products (DRiPs) in immunosurveillance has gained prominence. A class of unstable products emerge from non-canonical translation and processing of unannotated mammalian and viral ORFs and their peptides are cryptic in nature. Indeed, high throughput sequencing and proteomics have revealed that a substantial portion of our genomes comprise of non-canonical ORFs, whose generation is significantly modulated during disease. Many of these ORFs comprise short ORFs (sORFs) and upstream ORFs (uORFs) that resemble DRiPs and may hence be preferentially presented. Here, we discuss how such products, normally "hidden" from the immune system, become abundant in viral infections activating autoimmune T-cells, by discussing their emerging role in infection and disease. Finally, we provide a perspective on how these mechanisms can explain several autoimmune disorders in the wake of the COVID-19 pandemic.

**Keywords: viruses, cryptic peptides, autoimmunity, defective ribosomal products, non-canonical translation, COVID-19**

OPEN ACCESS

***Edited by:***
*Douglas Paul Gladue, Plum Island Animal Disease Center, Agricultural Research Service, United States Department of Agriculture (USDA), United States*

***Reviewed by:***
*Jorg Calis, University Medical Center Utrecht, Netherlands*

***Correspondence:**
*Bhupesh K. Prusty*
*bhupesh.prusty@uni-wuerzburg.de*

***Specialty section:***
*This article was submitted to Virology, a section of the journal Frontiers in Microbiology*

***Received:*** *21 December 2021*
***Accepted:*** *17 January 2022*
***Published:*** *10 February 2022*

***Citation:***
*Lodha M, Erhard F, Dölken L and Prusty BK (2022) The Hidden Enemy Within: Non-canonical Peptides in Virus-Induced Autoimmunity. Front. Microbiol. 13:840911. doi: 10.3389/fmicb.2022.840911*

## INTRODUCTION

One of the salient features of autoimmunity lies in the recognition of MHC class I associated self-peptides by T-cells that have escaped self-tolerance during their development and selection in the thymus. Self-peptides, not generated and presented at substantial levels for T-cells to undergo anergy and deletion, can cause T-cells to escape selection. Such cryptic peptides might be generated and presented under certain stimuli to activate self-specific T-cells, forming the fundamental basis of autoimmunity (Sercarz et al., 1993; Lanzavecchia, 1995). Over the years, many extrinsic factors including viral infections have served to explain autoimmunity through the generation of self-peptide mimics, bystander activation of T-cells and epitope spreading (Smatti et al., 2019). However, the exact nature and generation of such peptides remains loosely defined, hampering the development of broad range therapeutics and our understanding of these disorders.

Oligopeptides arising from the degradation of self and non-self-proteins enter the antigen presentation pathway, activating humoral and cell-mediated immune responses against infected and cancerous cells. While peptides derived from exogenous proteins,

acquired externally through the endo-lysosomal pathway are loaded on MHC-II molecules, peptides derived from endogenously synthesized proteins are presented on MHC-I (Vyas et al., 2008). Such peptides form the basis of $CD8^+$ T-cell immune responses that play an important role in various infections, tumors, and autoimmune disorders. However, efficient presentation of endogenous foreign peptides requires them to compete with both high and low-affinity self-peptides originating from the cellular proteome. This competition would be puzzling in viral infections, where slow synthesis and degradation of viral proteins cannot explain the rapid onset of the adaptive immune response (Yewdell et al., 1996).

In this context, the DRiPs (defective ribosomal products) hypothesis proposed by Yewdell and colleagues in 1996 describes a class of newly synthesized, highly unstable rapidly degraded polypeptides which forms the bulk of the antigenic repertoire in viral infections through their preferential presentation on MHC-I molecules (Yewdell et al., 1996; **Table 1**). Strong evidence in favor of DRiPs has explained immunosurveillance in infection and disease. A class of these products include peptides arising from non-canonical open reading frames (ORFs) (Yewdell et al., 2019)—translation initiation from alternative open reading frames (ARFs) (Bullock et al., 1997; Ronsin et al., 1999) at near-cognate start codons (e.g., CUG) (Schwab et al., 2004; Yang et al., 2016) or genomic regions previously deemed as untranslated (5′ or 3′ UTRs) (Laumont et al., 2016)—outside the annotated genome. High-throughput sequencing approaches combined with mass spectrometry have revealed that a substantial portion of our genome comprises of these non-canonical ORFs (Laumont et al., 2016; Erhard et al., 2018) and that their products are efficiently presented on MHC-I (Laumont et al., 2016; Erhard et al., 2018). Furthermore, the induction of cellular non-canonical translation is observed in cancers and viral infections (Laumont et al., 2016; Zanker et al., 2019; Chong et al., 2020). Given the immunological role of non-canonical gene products under infection and disease, we speculate that these peptides may play a role in autoimmunity, where they would be absent or weakly presented during T-cell selection, mediating their escape. Substantial synthesis, presentation, and processing of these peptides under infection, would then activate the circulating T-cells, triggering autoimmunity (**Figure 1**). To support our theory, we discuss the contribution of non-canonical translation products as MHC-I-associated peptides (MAPs), their significance in immunosurveillance and present evidence for their emerging role in autoimmunity in the context of viral infections, including COVID-19.

## GENERATION OF MHC-I ANTIGENIC PEPTIDES AND NON-CANONICAL TRANSLATION

Most canonical viral and cellular proteins are stable and exhibit normal turnover kinetics prior to their degradation *via* both proteasomal dependent and independent mechanisms (Yewdell et al., 2019). The resulting peptides are transported into the endoplasmic reticulum (ER) *via* TAP (transporter associated with antigen processing) where their N-termini are cleaved *via* ER aminopeptidases (ERAPs), generating oligopeptides to be loaded on MHC-I (Starck and Shastri, 2011). Peptide-deficient MHC-I molecules are rendered unstable and fail to reach the cell surface, but undergo recycling to and from the cell surface upon successfully loading MHC-I peptides (Ljunggren et al., 1990). During infection and cancer, foreign peptides must compete with these self-peptides to mark infected or cancerous cells for $CD8^+$ T-cell cytotoxicity. Besides, highly abundant herpesvirus proteins like EBNA (Dantuma et al., 2000) and LANA (Kwun et al., 2011) are extremely stable and less susceptible to immediate proteasomal degradation (van de Weijer et al., 2015). This makes it not only competitive, but also implausible for antigenic peptides to be presented in a timely manner (van de Weijer et al., 2015). A key feature of the antigen presentation pathway lies in selectively and preferentially presenting peptides on MHC molecules (Yewdell et al., 2019). This is achieved through rapidly degraded polypeptides derived from DRiPs and SLiPs (short-lived proteins) (Yewdell et al., 1996, 2019). The half-life of these proteins is in the order of minutes, ensuring rapid presentation of their peptides which is directly proportional to the translational rates of their source proteins. Many translational and post-translational mechanisms have explained the selectivity in presenting DRiPs (Yewdell et al., 2019). Accumulating evidence suggests that non-canonical translation is a prevalent phenomenon in mammalian cells, especially in infection and disease. These events include translation of loci outside the annotated genome, within 5′ and 3′ UTRs, at near-cognate start codons and include several alternative open reading frames (ARFs) and non-canonical ORFs resulting from premature stop-codon (PTC) read-through. Since these regions lie in previously unannotated or unknown regions, their peptide products are termed as cryptic peptides.

The concept of non-canonical translation emerged from the "pepton" hypothesis proposed by Boon and Van Pel (1989), where transfected genes devoid of distinct expression systems could produce polypeptides. Over the years, such translation events were observed for mammalian and viral genomes too. These non-canonical proteins gave rise to functional polypeptides as well as regulatory elements like upstream ORFs (uORFs) involved in translationally regulating their downstream ORFs (Vattem and Wek, 2004; Young and Wek, 2016). In fact, viruses could modulate non-canonical translation as seen in Vaccinia and Semliki Forest virus (SFV) (Townsend et al., 1988; Berglund et al., 2007), where insertion of genes into the respective viral vectors, led to the synthesis of novel polypeptides providing a rich source of DRiPs. Influenza DRiPs studies performed by Yewdell and colleagues laid the foundation to describe the role of non-canonical translation in antigen presentation. By cloning a Kb restricted model epitope, SIINFEKL, into IAV Neuraminidase (NA), they were able to distinguish non-canonical NA derived DRiPs products from the full-length NA protein. The translation of NA DRiP occurred independently of full-length NA mRNA initiating at CUG (Dolan et al., 2010) by specifically preventing nuclear export of NA mRNA, drastically reducing NA protein synthesis, without hampering levels of the NA DRiP product. Indeed, non-canonical translation is governed by several factors,

**TABLE 1 |** Glossary of terminologies representing the nature of peptides in this study.

| | |
|---|---|
| Canonical ORFs | ORFs encoding functional gene products/proteins exhibiting high stability and normal turnover kinetics in line with the conventional antigen processing and presentation pathway (Yewdell et al., 2019). |
| Non-canonical ORFs | ORFs ncoding highly unstable gene products, exhibiting distinct biological properties (Yewdell et al., 2019) including ORFs initiating at non-AUG start codons (Starck and Shastri, 2011) and may include unannotated ORFs comprising sORFs, uORFs, and ARFs (Erhard et al., 2018). |
| ARF (Alternative open reading frame) | ARFs comprise ORFs initiating within a gene body where such an ORF does not constitute the dominant canonical ORF representing the locus. Such initiation can be attributed to alternative transcription and translation start sites (Whisnant et al., 2020). |
| Annotated ORFs | ORFs currently annotated for a given organism. |
| Unannotated ORFs | ORFs identified from high-throughput sequencing experiments but currently not annotated. |
| uORF (upstream ORF) | Upstream ORFs are located upstream of a canonical ORF, which may function in regulating their downstream ORFs (Vattem and Wek, 2004) or provide a source of antigenic peptides (Starck and Shastri, 2016). |
| sORF (short ORF) | Short ORFs <100 aa in length, whose products would include unstable polypeptides which may perform biological functions or provide a source of antigenic peptides (Erhard et al., 2018). |
| Cryptic peptides | The term cryptic peptides include "hidden" or "invisible" peptides originating from genomic loci not previously annotated/studied (Erhard et al., 2020). Such peptides can be translated by both non-canonical and previously unannotated ORFs. In the context of autoimmunity, these peptides are "hidden" or "invisible" as described by Lanzavecchia (1995), due to their absence or low levels of expression which can hamper their antigen presentation, thereby explaining T-cells escaping self-tolerance against these peptides. |
| DRiPs (Defective ribosomal products) | The term DRiPs (Defective ribosomal products) coined by Yewdell et al. (1996), was used to describe a source of nascent polypeptides, highly unstable in nature exhibiting half-lives in the order of minutes and capable of producing MHC-I antigenic peptides. Such peptides are preferentially degraded due to their instability and biogenesis—including alterations in translation, ribosomal modifications and post-translational mechanisms including their rapid degradation and channeling (Yewdell et al., 2019). |

including differential usage of ribosomal proteins, which strictly control the global translation and MHC-I presentation of non-AUG and ARF derived polypeptides (Wei et al., 2019). These studies highlight key features of non-canonical proteins by shedding light on the differences in their processing pathways to provide a wealth of antigenic peptides.

## IMMUNOLOGICAL SIGNIFICANCE OF NON-CANONICAL TRANSLATION AND DEFECTIVE RIBOSOMAL PRODUCTS

The contribution of cryptic peptides in antigen presentation emerged from pioneering studies by Shastri and colleagues. They demonstrated an antigenic peptide whose source protein initiated at a non-canonical codon, CUG, translating a leucine instead of a methionine, and could activate specific alloreactive T cell clones (Schwab et al., 2004). Decoding CUG was a result of translational control mediated by eIF2A phosphorylation under cellular stress and was not affected by compounds affecting initiation at AUG (Schwab et al., 2004). Phosphorylation of eIF2A is a hallmark of cellular stress, often seen in viral infections and plays a role in the translational regulation of upstream ORFs (uORFs) (Vattem and Wek, 2004; Young and Wek, 2016). These uORFs also form a source of cryptic peptides as observed in the 5′ UTR cryptic product of the VEGF gene in renal cell carcinoma (Weinzierl et al., 2008). It was later shown that translation initiation at CUG could be enhanced *via* inflammatory stimuli and viral infections by modulating the ribosomal machinery (Prasad et al., 2016). More recently, the contribution of interferon in rapidly synthesizing and presenting DRiPs was observed in the context of MHC associated peptides (Komov et al., 2021).

Viruses have adopted several means of translational control. Non-canonical translation has been reported for Plautia stali intestinal virus through internal ribosome entry site (IRES) dependent translation of the capsid protein, initiating at a non-canonical CAA codon (Sasaki and Nakashima, 2000). Non-canonical translation also forms a source of antigenic epitopes as observed in the case of Influenza (IAV) DRiPs synthesis (Dolan et al., 2010; Yang et al., 2016), portraying their immunological role in viral infections. Generation of these anti-viral cryptic epitopes through non-canonical translation has been well documented and reviewed in retroviruses (Starck and Shastri, 2011) where ribosomal frameshifting and ARFs have contributed to non-conventional epitopes derived from gag, pol and env genes in murine AIDS, HIV and Simian Immunodeficiency Virus (SIV) (Mayrand et al., 1998; Cardinaud et al., 2004; Ho and Green, 2006). Protective $CD8^+$ T-cell responses were elicited in these cases, especially in SIV infection of rhesus macaques, where a substantial portion of T-cell responses were attributed to cryptic peptides arising from ARFs (Maness et al., 2010). The fact that ARF derived epitopes appeared to be more immunologically dominant than classical epitopes upon assaying PBMCs against both ARF and non-ARF epitopes (Maness et al., 2010) warrant the use of such peptides in therapy to trigger cytotoxic $CD8^+$ T cells. In case of HIV, acquired mutations in ARF derived epitopes prevented their presentation, stressing on the importance of these epitopes in immunosurveillance and how viruses could evolve to antagonize immune responses (Maness et al., 2007; Berger et al., 2010). Significant improvements in understanding the plethora of gene products encoded by genomes came from studies employing ribosome profiling, a technique applied to study translation events by sequencing ribosome protected RNA (Ingolia et al., 2012). Ribosome

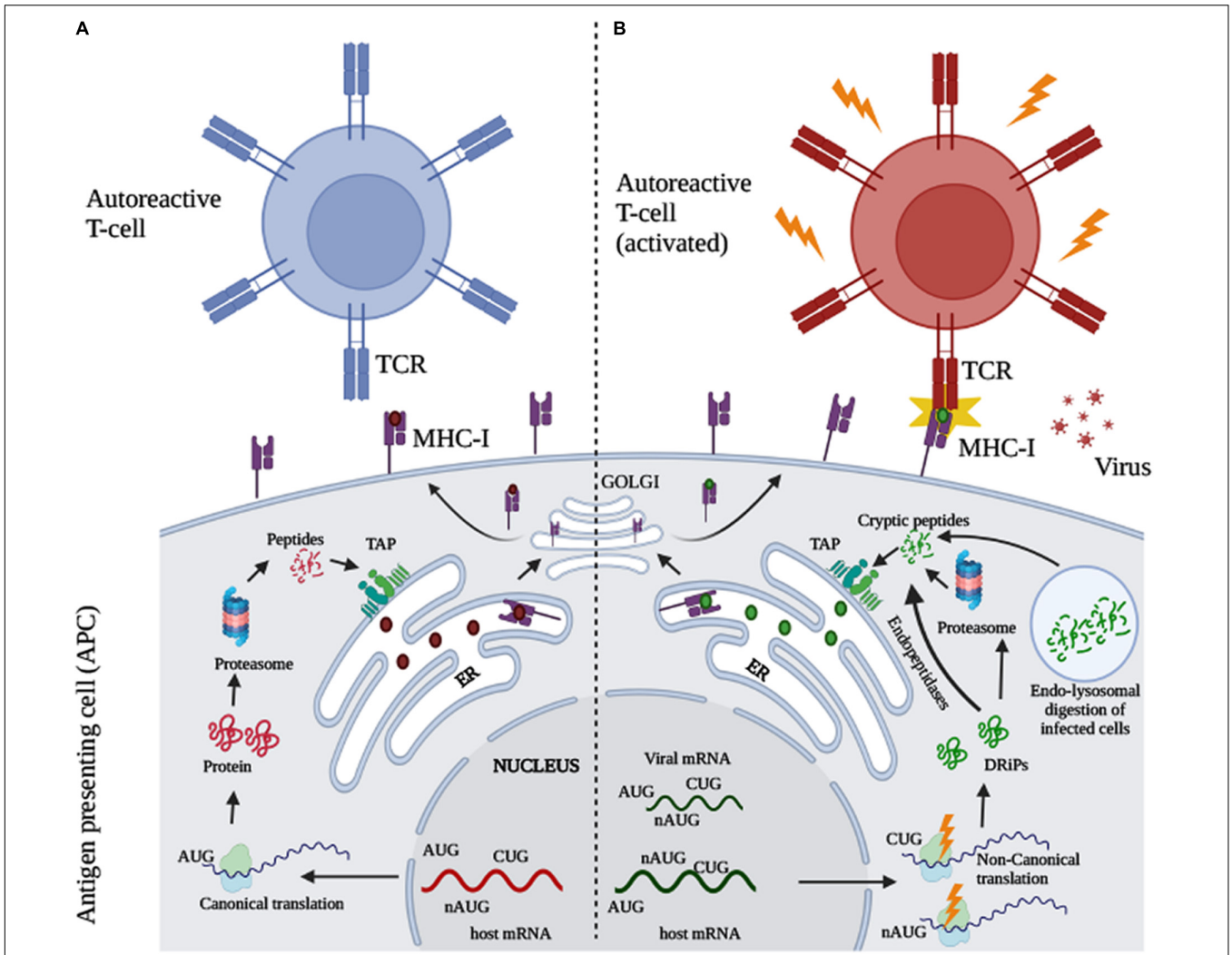


**FIGURE 1 |** Role of non-canonical translation in virus-induced autoimmunity. **(A)** Proteins synthesized from canonical open reading frames (ORFs) are degraded *via* the proteasomal degradation pathway. The peptides produced thereof localize to the endoplasmic reticulum (ER) *via* TAP and are loaded on MHC-I molecules. The presented complexes however, fail to activate autoreactive T-cells as T cells against a majority of self-peptides are eliminated during the selection process in the thymus. **(B)** During viral infection, stress responses alter the translational machinery to synthesize novel proteins/polypeptides from both viral and cellular non-canonical ORFs, initiating at non-canonical AUG (nAUG) or other codons (e.g., CUG). These novel proteins are highly unstable and are preferentially degraded *via* several mechanisms including both proteasomal independent and dependent mechanisms, cytoplasmic endopeptidases and peptides formed through endo-lysosomal digestion of infected cells. The novel cryptic peptides, previously invisible to the immune system can now activate specific T-cell clones triggering an autoimmune-like response (Created using biorender.com).

profiling revealed hundreds of novel open reading frames in several viruses and cancers, severely undermining our knowledge of the coding capacity of mammalian and viral genomes (Stern-Ginossar et al., 2012; Arias et al., 2014; Chong et al., 2020; Whisnant et al., 2020; Ruiz Cuevas et al., 2021). These novel ORFs comprised of many short open reading frames (sORFs), which formed the major component of the non-canonical "ORFeome." Such sORFs resemble DRiPs products in that the encoded microproteins commonly initiate at near-cognate start codons, appear to be highly unstable and disordered in structure (Ruiz Cuevas et al., 2021). The instability of sORFs makes it challenging to detect them through conventional proteomic methods including shot gun mass spectrometry (MS) (Erhard et al., 2018). However, sORF-derived peptides (SEPs), like DRiPs, would efficiently enter the antigen presentation pathway. Indeed, such peptides were better recovered by MHC-I peptidomics due to the ability of MHC-I molecules to form stable complexes with antigenic peptides and like DRiPs, the extent of their presentation correlated with their translational rates (Erhard et al., 2018). MHC-I-peptidomics revealed that approximately 10% of the MHC-I-immunopeptidome comprised of cryptic peptides originating from non-canonical ORFs (Erhard et al., 2018; Ruiz Cuevas et al., 2021). Immunopeptidomic studies (Erhard et al., 2020) and proteogenomic approaches utilizing MS coupled with high-throughput sequencing improved the identification of novel

neo-antigens in tumors supporting the role of non-canonical peptides in immunity which were efficiently presented on MHC-I molecules (Laumont et al., 2016; Chong et al., 2020; Ouspenskaia et al., 2021).

## NON-CANONICAL TRANSLATION AND DEFECTIVE RIBOSOMAL PRODUCTS IN AUTOIMMUNITY

T-cell lymphocytes expressing either $CD4^+$ or $CD8^+$ TCRs are capable of recognizing antigen associated MHC class II and I molecules respectively (Kumar et al., 2018). During their development in the thymus, T-cells undergo positive and negative selection, where T-cells recognizing self-antigen MHC complexes with low to moderate affinity undergo proliferation, whereas strong interactions with high affinity self-antigen MHC complexes leads to cell death, preventing autoimmunity, while some of the cells differentiate into regulatory T-cells (Takaba and Takayanagi, 2017). The self-tolerant T-cells selected recognize abnormal or foreign peptides during infection and disease. However, some T-cells escape tolerance and are activated when exposed to self-peptides which may not have been expressed during their development at optimal levels. These "invisible" peptides are therefore cryptic in nature and may not be sufficiently expressed during T-cell selection (Sercarz et al., 1993; Lanzavecchia, 1995). In certain cases, cryptic epitopes would have lower affinity for MHC molecules and may not be presented due to competition with the high affinity epitopes. However, inflammatory stimuli and co-stimulatory signals might alter their expression and processing, thereby activating self-reactive T-cells.

Evidence for T-cells reactive toward self-cryptic epitopes has been extensively reviewed for a variety of autoimmune disorders (Warnock and Goodacre, 1997). Studies conducted for rhesus polypeptides involved in autoimmune hemolytic anemia (AIHA) analyzed T-cell responses toward the full-length autoantigen and synthetic peptides derived from the same (Barker and Elson, 1994). The study described *in vitro* experiments with intact protein which failed to elicit self-specific T-cell responses as opposed to peptide constructs, indicating that the latter comprised of a pool of cryptic peptides for which T-cells had escaped self-tolerance *in vivo*, and that these peptides were not synthesized *in vivo*, explaining their cryptic nature. The fact that full-length proteins could not trigger such responses implied that their processing pathways did not efficiently present cryptic epitopes to activate the T-cells. A similar finding was reported for proteolytic protein (PLP) involved in multiple sclerosis (MS) (Markovic-Plese et al., 1995) and thyroid peroxidase (TPO) involved in Grave's disease (Quaratino et al., 1996) where the antigenic peptides significantly differed for both endogenously and exogenously processed TPO proteins. These features of cryptic autoantigens bear close resemblance to DRiPs and non-canonical translation products. Cartilage autoantigens in Rheumatoid arthritis (RA) (Buttle et al., 1995) rapidly degrading to give rise to antigenic peptides draws similarities to the unstable nature of DRiPs, explaining their preferential presentation during disease. Epitope processing is also regulated by changes in the activity of cytosolic endopeptidases that play an important role in exposing cryptic epitopes within the myelin basic protein (MBD) (Anderton et al., 2002). Whether these peptides originate from non-canonical translation events remains an open question since most of the studies exploited synthetic peptide constructs, making it difficult to comment on the nature and generation of their source proteins, compounded by the lack of studies in this direction.

Recent studies provide a clearer picture to explain the involvement of non-canonical translation in autoimmune disorders. $CD8^+$ T-cell isolated from Reiter's syndrome patients led to the identification of an autoreactive T cells specific toward an epitope encoded by human Interleukin-10 (IL-10) (Saulquin et al., 2002). T-cells were activated upon transfecting the nucleotide sequence encoding the epitope but failed to generate immune responses when utilizing synthetic peptides. It was later found by mutational analysis, that this epitope was formed because of non-canonical frameshifting, resulting in a peptide encoded by both ORF1 and ORF2. Given the immunosuppressive role of IL-10, the deletion of IL-10 producing cells could have a profound impact on the pathology of Reiter's syndrome. The potential for non-canonical self-peptides to be immunologically relevant has also been observed in therapeutics. Defective proteins synthesized due to a premature stop codon (PTC) form the basis of diseases like cystic fibrosis and Duchenne muscular dystrophy (Goodenough et al., 2014). The use of aminoglycosides has the potential to cause read-through leading to the synthesis of full-length proteins to overcome this. However, stop codon read-through opens possibilities of non-canonical translation events downstream, which has been observed in gentamicin treated cells leading to the development of immunologically relevant self-peptides.

A breakthrough in understanding the contribution of non-canonical translation products or DRiPs to autoimmunity comes from recent studies in Type I diabetes (T1D) (Kracht et al., 2017). In their elegant study, Kracht and colleagues report a novel DRiP encoded by Insulin mRNA (INS-DRiP) in the non-canonical +2 open reading frame initiating at an AUG start codon. The cryptic epitope encoded by INS-DRiPs efficiently entered the antigen presentation pathway and was surprisingly loaded on both HLA I and II molecules. Such a response would generate both $CD8^+$ T-cell cytotoxic responses and autoantibodies through $CD4^+$ helper T-cells.

## CAN VIRUSES INDUCE AUTOIMMUNITY THROUGH NON-CANONICAL PEPTIDES AND DEFECTIVE RIBOSOMAL PRODUCTS?—A THEORY

Viruses have shown to contribute to the pathophysiology of several autoimmune disorders through a broad range of mechanisms (Smatti et al., 2019). They can encode for cross-reactive structural or molecular "mimics" of several autoantigens

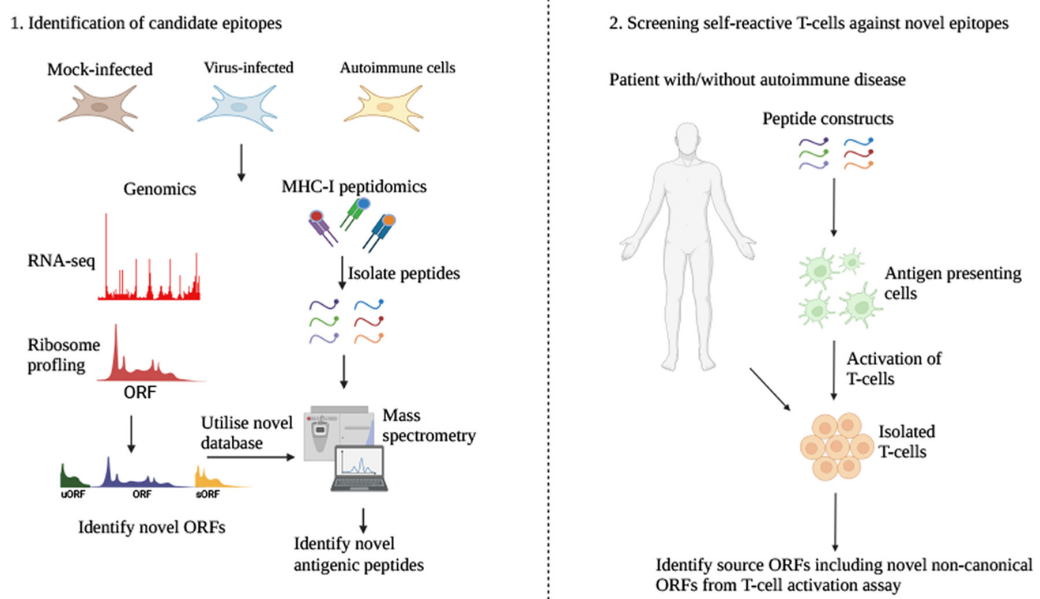


**FIGURE 2 |** Assessing the role of non-canonical viral ORFs in virus-induced autoimmunity. To support our presented hypothesis, a proteogenomic approach should be adopted to identify novel ORFs combining RNA-seq and ribosome profiling methods for the displayed conditions (1). The novel database would then be utilized to identify novel antigenic epitopes presented by MHC-I complexes through solubilization of peptides stably bound to MHC-I, which would significantly improve the determination of highly unstable non-canonical ORFs of lengths <100 aa, which would otherwise be challenging to detect using conventional proteomics. The identified peptides should then be utilized for uptake by antigen presenting cells *in vitro* to assess self-reactivity of T-cells isolated from patients with and without autoimmune diseases and with a history of chronic viral infection for the virus under study (2). This methodology would help determine both the proportion and immunological repertoire of non-canonical peptides playing a role in virus-induced autoimmunity. By deciphering their expression under various conditions and cell lines (1), one could determine both the non-canonical nature and expression of ORFs and if indeed their absence or weak expression could explain an escape in immunological self-tolerance for the specific peptide and its source protein. sORF, short ORF; uORF, upstream ORF; APCs, antigen presenting cells (Created using biorender.com).

that can activate self-specific T-cells and autoantibodies—a concept defined as molecular mimicry. On the other hand, certain viruses induce autoimmunity through bystander activation of T-cells and antigen presenting cells (APCs) as well as epitope spreading. These mechanisms rely on the exposure of self-peptides to autoreactive T-cells through destruction of host cells stimulated by APCs and a pro-inflammatory microenvironment. Several viruses including IAV, Coxsackie viruses and herpesviruses including HCMV, EBV, HSV-1, and HHV-6A mediate self-reactivity through these processes (Smatti et al., 2019). While the mechanisms modulate the clinical symptoms of autoimmune disorders, they do not provide adequate information about how self-reactive cells were generated at the first place nor provide information about the synthesis and processing of autoantigenic peptides. Thymic T-cells must have escaped tolerance due to poor availability of certain peptides which remain "hidden" or are cryptic and viral infections may contribute in generating such peptides through non-canonical synthesis or processing of their source proteins (Sercarz et al., 1993; Lanzavecchia, 1995).

Indeed, evidence to define the role of cryptic peptides in virus-induced autoimmunity emerged from studies in HIV infections where the viral membrane protein, gp120 was able to modulate the processing of endogenous $CD4^+$ to generate self-peptides (Salemi et al., 1995). Expression of gp120 led to an increase in $CD4^+$ endocytic processing, generating novel epitopes which in turn generated anti-CD4 autoantibodies. Synthesis and presentation of less immunodominant and normally absent epitopes was also observed in the case of Theiler's virus mediated MS (Miller et al., 1997). Differences in the processing and magnitude of antigen presentation between non-canonical and canonical peptides must play a crucial role. In the case of HSV-1-induced HSK, peptides originating from the viral protein, UL6 appeared to be cross-reactive when exposed to corneal T-cell clones in murine models (Zhao et al., 1998; Smatti et al., 2019). However, HSK studies in patients did not result in the isolation of T cells cross-reactive with UL6 indicating other mechanisms at play, which may involve self-antigens expressed at sufficiently high levels to trigger autoimmune T-cells (Verjans et al., 2000). Similarly, for EBV, anti-Ro antibodies found in SLE patients were cross-reactive with the EBV EBNA-1 protein (Poole et al., 2006). Synthetic peptides derived from Ro generated a broad range of antibodies against several epitopes including autoantibodies in mice, while immunization with intact Ro protein only produced antibodies against the immunizing peptide indicating differences in peptide processing during viral infections. While epitope spreading and mimicry explain the development of autoimmunity in

viral infections, mechanistic differences in the generation of autoantigens must be addressed.

The most profound example for virus induced autoimmunity in the context of non-canonical translation comes from studies in IAV infection, where generation of viral DRiPs resulting from non-canonical translation through an ARF also results in the generation of a cellular ARF DRiP product (Zanker et al., 2019). The study described for the first time that viruses can induce cellular DRiPs, which has implications in understanding virus-induced autoimmunity. The authors conclude by stating that viruses might trigger autoimmunity by simply generating DRiPs. This might explain the preferential presentation of autoantigens under infection which generally remain hidden from developing T-cells. Perhaps a large amount of DRiPs derived peptides originate from non-canonical ORFs and remain invisible to the immune system under normal conditions that do not permit expression of such ORFs. Ribosome profiling conducted in human Beta cells in both normal and type 1 diabetes (T1D) conditions (Thomaidou et al., 2021) have revealed a novel set of non-canonical polypeptides which might unveil neo-antigens in T1D. Future studies to understand the role of novel ORFs in autoimmunity might explain several non-canonical autoantigens. Indeed, viruses encode many non-canonical ORFs that may play a role in better understanding virus-induced autoimmunity (Stern-Ginossar et al., 2012; Arias et al., 2014; Whisnant et al., 2020).

## A PERSPECTIVE ON SARS-CoV2 INDUCED AUTOIMMUNITY—CAN CRYPTIC PEPTIDES PLAY A ROLE?

Recent evidence has indicated that severe acute respiratory syndrome coronavirus 2 (SARS-CoV2) affects the outcome of autoimmune disorders. The virus responsible for the COVID-19 pandemic has been associated with the development of pediatric inflammatory multisystemic syndrome (PIMS) or Kawasaki-like disease in children as well as Guillain-Barre syndrome (GBS) and Miller Fisher syndrome (MFS) (Dotan et al., 2021). Clinical studies establishing an association between SLE and SARS-CoV2 disease firmly establish a link between the two (Gracia-Ramos and Saavedra-Salinas, 2021; Sjöwall et al., 2021; Zamani et al., 2021). As observed in other viruses, the mechanisms triggering autoimmunity must be similar for SARS-CoV2. *In silico* studies have predicted 23 peptides shared by the virus and the human proteome present in the canonical ORFs of SARS-CoV2 (Karami Fath et al., 2021), of which three were experimentally confirmed to bind to HLA. However, the significance of these peptides to function as cross-reactive mimics is yet to be confirmed.

SARS-CoV2 utilizes ACE-2 receptors for virus entry (Jackson et al., 2021). ACE-2 is highly expressed in patients with COVID-19. A theory proposing the role of soluble ACE-2 in autoimmunity posits that ACE-2 molecules circulating in plasma would be endocytosed by APCs to produce novel antigens that can trigger autoantibodies (McMillan et al., 2021). The synthesis of such novel peptides can occur due to alternative processing of soluble ACE-2 in the endo-lysosomal compartment or the engulfment of non-canonical ACE-2 polypeptides. At the translational level, peptides might be generated from cellular proteins by non-canonical translation. Certainly, autoantibodies against cellular proteins including anti-Ro have been observed in patients affected by COVID-19 (Fujii et al., 2020). Differences in the variety of non-canonical epitopes arising from Ro protein and transfected Ro nucleotide sequence is a clear example of non-canonical translational regulation (Poole et al., 2006). The induction of several cytokines like IL-6 and a strong pro-inflammatory response is a classical feature of COVID-19 which may promote cryptic translation due to stress-mediated alteration of the translational machinery (Chen et al., 2020). While the contribution of non-canonical translation in SARS-CoV2 induced autoimmunity remains speculative, ribosome profiling has revealed cryptic products encoded by SARS-CoV2 (Finkel et al., 2021), expanding our view of the viruses' coding capacity. Since epitopes are predicted using a proteomic database to screen for antigenic peptides, non-canonical proteins, particularly unstable and difficult to detect *via* proteomics, are neglected without knowledge of their ORF sequence. ORF prediction through ribosome profiling coupled with MHC-I peptidomics will hence improve epitope detection and validation for various diseases (Erhard et al., 2018) to better understand the role of non-canonical gene products in autoimmunity (**Figure 2**). Indeed, some of the cryptic products encoded by SARS-CoV2 were confirmed through proteomics (Schmidt et al., 2021).

## DISCUSSION

We provide a perspective on how non-canonical translation and generation of cryptic epitopes can improve our understanding of autoimmune disorders in the context of viral infections. The theory discussed would help explain how T cells escape self-tolerance and how cryptic antigens might trigger them. Non-canonical expression of cryptic peptides due to infection and cellular stress will explain why they remain hidden from T cells under normal conditions. Although direct evidence for the contribution of non-canonical translation remains elusive, ribosome profiling data coupled with mass spectrometry has highlighted the breadth of cryptic gene products in mammalian and viral genomes, laying the foundation for their functional characterization in the context of immunosurveillance. Autoantigen-ome studies in A549 lung cells (Wang et al., 2021) have revealed abnormal levels of around 291 altered autoantigens in SARS-CoV2 infection, out of which only 191 autoantigens are known to promote self-reactivity. These autoantigens could explain post infection sequelae persistent after acute COVD-19 disease in several patients, termed as "Long COVID"- whose symptoms and abnormalities share close resemblance to myalgic encephalomyelitis/chronic fatigue syndrome (ME/CFS) which is often associated with viral infections (Mackay, 2021). The fact that

more than a third of the autoantigens remain unidentified in the context of autoimmunity, raise the possibility of cryptic peptides playing a role in "Long COVID" disease. Perhaps modulation of the cellular proteome by SARS-CoV2 infection would govern the atlas of putative self-peptides involved in autoimmunity.

## DATA AVAILABILITY STATEMENT

The original contributions presented in the study are included in the article, further inquiries can be directed to the corresponding author.

## AUTHOR CONTRIBUTIONS

ML and BKP conceived the idea. ML, FE, LD, and BKP wrote the manuscript. All authors contributed to the article and approved the submitted version.

## FUNDING

BKP was funded by the ME Research United Kingdom and the Amar Foundation, United States. ML, FE, and LD were funded by the DFG Research unit FOR 2830.

## REFERENCES

Anderton, S. M., Viner, N. J., Matharu, P., Lowrey, P. A., and Wraith, D. C. (2002). Influence of a dominant cryptic epitope on autoimmune T cell tolerance. *Nat. Immunol.* 3, 175–181. doi: 10.1038/ni756

Arias, C., Weisburd, B., Stern-Ginossar, N., Mercier, A., Madrid, A. S., Bellare, P., et al. (2014). KSHV 2.0: a comprehensive annotation of the Kaposi's sarcoma-associated *herpesvirus* genome using next-generation sequencing reveals novel genomic and functional features. *PLoS Pathog.* 10:e1003847. doi: 10.1371/journal.ppat.1003847

Barker, R. N., and Elson, C. J. (1994). Multiple self epitopes on the rhesus polypeptides stimulate immunologically ignorant human T cells in vitro. *Eur. J. Immunol.* 24, 1578–1582. doi: 10.1002/eji.1830240719

Berger, C. T., Carlson, J. M., Brumme, C. J., Hartman, K. L., Brumme, Z. L., Henry, L. M., et al. (2010). Viral adaptation to immune selection pressure by HLA class I-restricted CTL responses targeting epitopes in HIV frameshift sequences. *J. Exp. Med.* 207, 61–75. doi: 10.1084/jem.20091808

Berglund, P., Finzi, D., Bennink, J. R., and Yewdell, J. W. (2007). Viral alteration of cellular translational machinery increases defective ribosomal products. *J. Virol.* 81, 7220–7229. doi: 10.1128/JVI.00137-07

Boon, T., and Van Pel, A. (1989). T cell-recognized antigenic peptides derived from the cellular genome are not protein degradation products but can be generated directly by transcription and translation of short subgenic regions. A hypothesis. *Immunogenetics* 29, 75–79. doi: 10.1007/BF00395854

Bullock, T. N., Patterson, A. E., Franlin, L. L., Notidis, E., and Eisenlohr, L. C. (1997). Initiation codon scanthrough versus termination codon readthrough demonstrates strong potential for major histocompatibility complex class I-restricted cryptic epitope expression. *J. Exp. Med.* 186, 1051–1058. doi: 10.1084/jem.186.7.1051

Buttle, D. J., Bramwell, H., and Hollander, A. P. (1995). Proteolytic mechanisms of cartilage breakdown: a target for arthritis therapy? *Clin. Mol. Pathol.* 48, M167–M177. doi: 10.1136/mp.48.4.m167

Cardinaud, S., Moris, A., Février, M., Rohrlich, P. S., Weiss, L., Langlade-Demoyen, P., et al. (2004). Identification of cryptic MHC I-restricted epitopes encoded by HIV-1 alternative reading frames. *J. Exp. Med.* 199, 1053–1063. doi: 10.1084/jem.20031869

Chen, L. Y. C., Hoiland, R. L., Stukas, S., Wellington, C. L., and Sekhon, M. S. (2020). Confronting the controversy: interleukin-6 and the COVID-19 cytokine storm syndrome. *Eur. Respir. J.* 56:2003006. doi: 10.1183/13993003.03006-2020

Chong, C., Müller, M., Pak, H., Harnett, D., Huber, F., Grun, D., et al. (2020). Integrated proteogenomic deep sequencing and analytics accurately identify non-canonical peptides in tumor immunopeptidomes. *Nat. Commun.* 11:1293. doi: 10.1038/s41467-020-14968-9

Dantuma, N. P., Heessen, S., Lindsten, K., Jellne, M., and Masucci, M. G. (2000). Inhibition of proteasomal degradation by the gly-Ala repeat of Epstein-Barr virus is influenced by the length of the repeat and the strength of the degradation signal. *Proc. Natl. Acad. Sci. U.S.A.* 97, 8381–8385. doi: 10.1073/pnas.140217397

Dolan, B. P., Knowlton, J. J., David, A., Bennink, J. R., and Yewdell, J. W. (2010). RNA polymerase II inhibitors dissociate antigenic peptide generation from normal viral protein synthesis: a role for nuclear translation in defective ribosomal product synthesis? *J. Immunol.* 185, 6728–6733. doi: 10.4049/jimmunol.1002543

Dotan, A., Muller, S., Kanduc, D., David, P., Halpert, G., and Shoenfeld, Y. (2021). The SARS-CoV-2 as an instrumental trigger of autoimmunity. *Autoimmun. Rev.* 20:102792. doi: 10.1016/j.autrev.2021.102792

Erhard, F., Dölken, L., Schilling, B., and Schlosser, A. (2020). Identification of the cryptic HLA-I immunopeptidome. *Cancer Immunol. Res.* 8, 1018–1026. doi: 10.1158/2326-6066.CIR-19-0886

Erhard, F., Halenius, A., Zimmermann, C., L'Hernault, A., Kowalewski, D. J., Weekes, M. P., et al. (2018). Improved Ribo-seq enables identification of cryptic translation events. *Nat. Methods* 15, 363–366. doi: 10.1038/nmeth.4631

Finkel, Y., Mizrahi, O., Nachshon, A., Weingarten-Gabbay, S., Morgenstern, D., Yahalom-Ronen, Y., et al. (2021). The coding capacity of SARS-CoV-2. *Nature* 589, 125–130. doi: 10.1038/s41586-020-2739-1

Fujii, H., Tsuji, T., Yuba, T., Tanaka, S., Suga, Y., Matsuyama, A., et al. (2020). High levels of anti-SSA/Ro antibodies in COVID-19 patients with severe respiratory failure: a case-based review : high levels of anti-SSA/Ro antibodies in COVID-19. *Clin. Rheumatol.* 39, 3171–3175. doi: 10.1007/s10067-020-05359-y

Goodenough, E., Robinson, T. M., Zook, M. B., Flanigan, K. M., Atkins, J. F., Howard, M. T., et al. (2014). "Cryptic MHC class I-binding peptides are revealed by aminoglycoside-induced stop codon read-through into the 3′. UTR. *Proc. Natl. Acad. Sci. U.S.A.* 111, 5670–5675. doi: 10.1073/pnas.1402670111

Gracia-Ramos, A. E., and Saavedra-Salinas, M. (2021). Can the SARS-CoV-2 infection trigger systemic lupus erythematosus? A case-based review. *Rheumatol. Int.* 41, 799–809. doi: 10.1007/s00296-021-04794-7

Ho, O., and Green, W. R. (2006). Cytolytic CD8+ T cells directed against a cryptic epitope derived from a retroviral alternative reading frame confer disease protection. *J. Immunol.* 176, 2470–2475. doi: 10.4049/jimmunol.176.4.2470

Ingolia, N. T., Brar, G. A., Rouskin, S., McGeachy, A. M., and Weissman, J. S. (2012). The ribosome profiling strategy for monitoring translation in vivo by deep sequencing of ribosome-protected mRNA fragments. *Nat. Protoc.* 7, 1534–1550. doi: 10.1038/nprot.2012.086

Jackson, C. B., Farzan, M., Chen, B., and Choe, H. (2021). Mechanisms of SARS-CoV-2 entry into cells. *Nat. Rev. Mol. Cell Biol.* 23, 3–20.

Karami Fath, M., Jahangiri, A., Ganji, M., Sefid, F., Payandeh, Z., Hashemi, Z. S., et al. (2021). SARS-CoV-2 proteome harbors peptides which are able to trigger autoimmunity responses: implications for infection, vaccination, and population coverage. *Front. Immunol.* 12:705772. doi: 10.3389/fimmu.2021.705772

Komov, L., Melamed Kadosh, D., Barnea, E., and Admon, A. (2021). The Effect of Interferons on Presentation of Defective Ribosomal Products as HLA Peptides. *Mol. Cell Proteomics* 20:100105. doi: 10.1016/j.mcpro.2021.100105

Kracht, M. J., van Lummel, M., Nikolic, T., Joosten, A. M., Laban, S., van der Slik, A. R., et al. (2017). Autoimmunity against a defective ribosomal insulin gene product in type 1 diabetes. *Nat. Med.* 23, 501–507. doi: 10.1038/nm.4289

Kumar, B. V., Connors, T. J., and Farber, D. L. (2018). Human T cell development, localization, and function throughout life. *Immunity* 48, 202–213. doi: 10.1016/j.immuni.2018.01.007

Kwun, H. J., da Silva, S. R., Qin, H., Ferris, R. L., Tan, R., Chang, Y., et al. (2011). The central repeat domain 1 of Kaposi's sarcoma-associated herpesvirus (KSHV) latency associated-nuclear antigen 1 (LANA1) prevents cis MHC class I peptide presentation. *Virology* 412, 357–365. doi: 10.1016/j.virol.2011.01.026

Lanzavecchia, A. (1995). How can cryptic epitopes trigger autoimmunity? *J. Exp. Med.* 181, 1945–1948. doi: 10.1084/jem.181.6.1945

Laumont, C. M., Daouda, T., Laverdure, J. P., Bonneil, E., Caron-Lizotte, O., Hardy, M. P., et al. (2016). Global proteogenomic analysis of human MHC class I-associated peptides derived from non-canonical reading frames. *Nat. Commun.* 7:10238. doi: 10.1038/ncomms10238

Ljunggren, H. G., Stam, N. J., Ohlén, C., Neefjes, J. J., Höglund, P., Heemels, M. T., et al. (1990). Empty MHC class I molecules come out in the cold. *Nature* 346, 476–480. doi: 10.1038/346476a0

Mackay, A. (2021). A paradigm for post-covid-19 fatigue syndrome analogous to ME/CFS. *Front. Neurol.* 12:701419. doi: 10.3389/fneur.2021.701419

Maness, N. J., Valentine, L. E., May, G. E., Reed, J., Piaskowski, S. M., Soma, T., et al. (2007). AIDS virus specific CD8+ T lymphocytes against an immunodominant cryptic epitope select for viral escape. *J. Exp. Med.* 204, 2505–2512. doi: 10.1084/jem.20071261

Maness, N. J., Walsh, A. D., Piaskowski, S. M., Furlott, J., Kolar, H. L., Bean, A. T., et al. (2010). CD8+ T cell recognition of cryptic epitopes is a ubiquitous feature of AIDS virus infection. *J. Virol.* 84, 11569–11574. doi: 10.1128/JVI.01419-10

Markovic-Plese, S., Fukaura, H., Zhang, J., Al-Sabbagh, A., Southwood, S., Sette, A., et al. (1995). T cell recognition of immunodominant and cryptic proteolipid protein epitopes in humans. *J. Immunol.* 155, 982–992.

Mayrand, S. M., Schwarz, D. A., and Green, W. R. (1998). An alternative translational reading frame encodes an immunodominant retroviral CTL determinant expressed by an immunodeficiency-causing retrovirus. *J. Immunol.* 160, 39–50.

McMillan, P., Dexhiemer, T., Neubig, R. R., and Uhal, B. D. (2021). COVID-19-A theory of autoimmunity against ACE-2 explained. *Front. Immunol.* 12:582166. doi: 10.3389/fimmu.2021.582166

Miller, S. D., Vanderlugt, C. L., Begolka, W. S., Pao, W., Yauch, R. L., Neville, K. L., et al. (1997). Persistent infection with Theiler's virus leads to CNS autoimmunity via epitope spreading. *Nat. Med.* 3, 1133–1136. doi: 10.1038/nm1097-1133

Ouspenskaia, T., Law, T., Clauser, K. R., Klaeger, S., Sarkizova, S., Aguet, F., et al. (2021). Unannotated proteins expand the MHC-I-restricted immunopeptidome in cancer. *Nat. Biotechnol.* doi: 10.1038/s41587-021-01021-3 [Epub ahead of print].

Poole, B. D., Scofield, R. H., Harley, J. B., and James, J. A. (2006). Epstein-Barr virus and molecular mimicry in systemic lupus erythematosus. *Autoimmunity* 39, 63–70. doi: 10.1080/08916930500484849

Prasad, S., Starck, S. R., and Shastri, N. (2016). Presentation of cryptic peptides by MHC class I is enhanced by inflammatory stimuli. *J. Immunol.* 197, 2981–2991. doi: 10.4049/jimmunol.1502045

Quaratino, S., Feldmann, M., Dayan, C. M., Acuto, O., and Londei, M. (1996). Human self-reactive T cell clones expressing identical T cell receptor beta chains differ in their ability to recognize a cryptic self-epitope. *J. Exp. Med.* 183, 349–358. doi: 10.1084/jem.183.2.349

Ronsin, C., Chung-Scott, V., Poullion, I., Aknouche, N., Gaudin, C., and Triebel, F. (1999). A non-AUG-defined alternative open reading frame of the intestinal carboxyl esterase mRNA generates an epitope recognized by renal cell carcinoma-reactive tumor-infiltrating lymphocytes in situ. *J. Immunol.* 163, 483–490.

Ruiz Cuevas, M. V., Hardy, M. P., Holly, J., Bonneil, E., Durette, C., Courcelles, M., et al. (2021). Most non-canonical proteins uniquely populate the proteome or immunopeptidome. *Cell Rep.* 34:108815. doi: 10.1016/j.celrep.2021.108815

Salemi, S., Caporossi, A. P., Boffa, L., Longobardi, M. G., and Barnaba, V. (1995). HIVgp120 activates autoreactive CD4-specific T cell responses by unveiling of hidden CD4 peptides during processing. *J. Exp. Med.* 181, 2253–2257. doi: 10.1084/jem.181.6.2253

Sasaki, J., and Nakashima, N. (2000). Methionine-independent initiation of translation in the capsid protein of an insect RNA virus. *Proc. Natl. Acad. Sci. U.S.A.* 97, 1512–1515. doi: 10.1073/pnas.010426997

Saulquin, X., Scotet, E., Trautmann, L., Peyrat, M. A., Halary, F., Bonneville, M., et al. (2002). +1 Frameshifting as a novel mechanism to generate a cryptic cytotoxic T lymphocyte epitope derived from human interleukin 10. *J. Exp. Med.* 195, 353–358. doi: 10.1084/jem.20011399

Schmidt, N., Lareau, C. A., Keshishian, H., Ganskih, S., Schneider, C., Hennig, T., et al. (2021). The SARS-CoV-2 RNA-protein interactome in infected human cells. *Nat. Microbiol.* 6, 339–353. doi: 10.1038/s41564-020-00846-z

Schwab, S. R., Shugart, J. A., Horng, T., Malarkannan, S., and Shastri, N. (2004). Unanticipated antigens: translation initiation at CUG with leucine. *PLoS Biol.* 2:e366. doi: 10.1371/journal.pbio.0020366

Sercarz, E. E., Lehmann, P. V., Ametani, A., Benichou, G., Miller, A., and Moudgil, K. (1993). Dominance and crypticity of T cell antigenic determinants. *Annu. Rev. Immunol.* 11, 729–766. doi: 10.1146/annurev.iy.11.040193.003501

Sjöwall, J., Azharuddin, M., Frodlund, M., Zhang, Y., Sandner, L., Dahle, C., et al. (2021). SARS-CoV-2 antibody isotypes in systemic lupus erythematosus patients prior to vaccination: associations with disease activity, antinuclear antibodies, and immunomodulatory drugs during the first year of the pandemic. *Front. Immunol.* 12:724047. doi: 10.3389/fimmu.2021.724047

Smatti, M. K., Cyprian, F. S., Nasrallah, G. K., Al Thani, A. A., Almishal, R. O., and Yassine, H. M. (2019). Viruses and autoimmunity: a review on the potential interaction and molecular mechanisms. *Viruses* 11:762. doi: 10.3390/v11080762

Starck, S. R., and Shastri, N. (2011). Non-conventional sources of peptides presented by MHC class I. *Cell. Mol. Life Sci.* 68, 1471–1479. doi: 10.1007/s00018-011-0655-0

Starck, S. R., and Shastri, N. (2016). Nowhere to hide: unconventional translation yields cryptic peptides for immune surveillance. *Immunol. Rev.* 272, 8–16. doi: 10.1111/imr.12434

Stern-Ginossar, N., Weisburd, B., Michalski, A., Le, V. T., Hein, M. Y., Huang, S. X., et al. (2012). Decoding human cytomegalovirus. *Science* 338, 1088–1093.

Takaba, H., and Takayanagi, H. (2017). The mechanisms of T cell selection in the thymus. *Trends Immunol.* 38, 805–816.

Thomaidou, S., Slieker, R. C., van der, A. R., Slik, J. Boom, Mulder, F., Munoz-Garcia, A., et al. (2021). Long RNA sequencing and ribosome profiling of inflamed β-cells reveal an extensive translatome landscape. *Diabetes* 70, 2299–2312. doi: 10.2337/db20-1122

Townsend, A., Bastin, J., Gould, K., Brownlee, G., Andrew, M., Coupar, B., et al. (1988). Defective presentation to class I-restricted cytotoxic T lymphocytes in vaccinia-infected cells is overcome by enhanced degradation of antigen. *J. Exp. Med.* 168, 1211–1224.

van de Weijer, M. L., Luteijn, R. D., and Wiertz, E. J. (2015). Viral immune evasion: lessons in MHC class I antigen presentation. *Semin. Immunol.* 27, 125–137. doi: 10.1016/j.smim.2015.03.010

Vattem, K. M., and Wek, R. C. (2004). Reinitiation involving upstream ORFs regulates ATF4 mRNA translation in mammalian cells. *Proc. Natl. Acad. Sci. U.S.A.* 101, 11269–11274. doi: 10.1073/pnas.0400541101

Verjans, G. M., Remeijer, L., Mooy, C. M., and Osterhaus, A. D. (2000). Herpes simplex virus-specific T cells infiltrate the cornea of patients with herpetic stromal keratitis: no evidence for autoreactive T cells. *Invest. Ophthalmol. Vis. Sci.* 41, 2607–2612.

Vyas, J. M., Van der Veen, A. G., and Ploegh, H. L. (2008). The known unknowns of antigen processing and presentation. *Nat. Rev. Immunol.* 8, 607–618. doi: 10.1038/nri2368

Wang, J. Y., Zhang, W., Roehrl, M. W., Roehrl, V. B., and Roehrl, M. H. (2021). An autoantigen profile of human A549 lung cells reveals viral and host etiologic molecular attributes of autoimmunity in COVID-19. *J. Autoimmun.* 120:102644. doi: 10.1016/j.jaut.2021.102644

Warnock, M. G., and Goodacre, J. A. (1997). Cryptic T-cell epitopes and their role in the pathogenesis of autoimmune diseases. *Br. J. Rheumatol.* 36, 1144–1150.

Wei, J., Kishton, R. J., Angel, M., Conn, C. S., Dalla-Venezia, N., Marcel, V., et al. (2019). Ribosomal proteins regulate MHC class i peptide generation for immunosurveillance. *Mol. Cell* 73, 1162.e–1173.e. doi: 10.1016/j.molcel.2018.12.020

Weinzierl, A. O., Maurer, D., Altenberend, F., Schneiderhan-Marra, N., Klingel, K., Schoor, O., et al. (2008). A cryptic vascular endothelial growth factor T-cell epitope: identification and characterization by mass spectrometry and T-cell assays. *Cancer Res.* 68, 2447–2454. doi: 10.1158/0008-5472.CAN-07-2540

Whisnant, A. W., Jürges, C. S., Hennig, T., Wyler, E., Prusty, B., Rutkowski, A. J., et al. (2020). Integrative functional genomics decodes herpes simplex virus 1. *Nat. Commun.* 11:2038. doi: 10.1038/s41467-020-15992-5

Yang, N., Gibbs, J. S., Hickman, H. D., Reynoso, G. V., Ghosh, A. K., Bennink, J. R., et al. (2016). Defining viral defective ribosomal products: standard

and alternative translation initiation events generate a common peptide from influenza a virus M2 and M1 mRNAs. *J. Immunol.* 196, 3608–3617. doi: 10.4049/jimmunol.1502303

Yewdell, J. W., Antón, L. C., and Bennink, J. R. (1996). Defective ribosomal products (DRiPs): a major source of antigenic peptides for MHC class I molecules? *J. Immunol.* 157, 1823–1826.

Yewdell, J. W., Dersh, D., and Fåhraeus, R. (2019). Peptide channeling: the key to MHC class I immunosurveillance? *Trends Cell Biol.* 29, 929–939. doi: 10.1016/j.tcb.2019.09.004

Young, S. K., and Wek, R. C. (2016). Upstream open reading frames differentially regulate gene-specific translation in the integrated stress response. *J. Biol. Chem.* 291, 16927–16935. doi: 10.1074/jbc.R116.733899

Zamani, B., Moeini Taba, S. M., and Shayestehpour, M. (2021). Systemic lupus erythematosus manifestation following COVID-19: a case report. *J. Med. Case Rep.* 15:29. doi: 10.1186/s13256-020-02582-8

Zanker, D. J., Oveissi, S., Tscharke, D. C., Duan, M., Wan, S., Zhang, X., et al. (2019). Influenza a virus infection induces viral and cellular defective ribosomal products encoded by alternative reading frames. *J. Immunol.* 202, 3370–3380. doi: 10.4049/jimmunol.1900070

Zhao, Z. S., Granucci, F., Yeh, L., Schaffer, P. A., and Cantor, H. (1998). Molecular mimicry by herpes simplex virus-type 1: autoimmune disease after viral infection. *Science* 279, 1344–1347. doi: 10.1126/science.279.5355.1344

**Conflict of Interest:** The authors declare that the research was conducted in the absence of any commercial or financial relationships that could be construed as a potential conflict of interest.

**Publisher's Note:** All claims expressed in this article are solely those of the authors and do not necessarily represent those of their affiliated organizations, or those of the publisher, the editors and the reviewers. Any product that may be evaluated in this article, or claim that may be made by its manufacturer, is not guaranteed or endorsed by the publisher.

*Copyright © 2022 Lodha, Erhard, Dölken and Prusty. This is an open-access article distributed under the terms of the Creative Commons Attribution License (CC BY). The use, distribution or reproduction in other forums is permitted, provided the original author(s) and the copyright owner(s) are credited and that the original publication in this journal is cited, in accordance with accepted academic practice. No use, distribution or reproduction is permitted which does not comply with these terms.*

frontiers in Microbiology

OPINION
published: 16 February 2022
doi: 10.3389/fmicb.2022.843587

# What Should Be Learned From Repurposed Antivirals Against SARS-CoV-2?

*Miguel Angel Martinez**

*IrsiCaixa, Hospital Universitari Germans Trias i Pujol, Universitat Autònoma de Barcelona, Badalona, Spain*

**Keywords: antiviral, repurposed drugs, virus therapy, SARS-CoV-2, emerging viruses**

Since severe acute respiratory syndrome coronavirus 2 (SARS-CoV-2) was first identified in 2019, more than 270 million infections have been reported, and the death toll from the associated coronavirus disease 2019 (COVID-19) has reached 5.5 million. The magnitude of this pandemic has encouraged the repurposing of numerous drugs, with the aim of rapidly curbing the morbidity, mortality, and spread of this new disease. However, this approach has had limited success. Only vaccine development and the repurposing of dexamethasone have impacted COVID-19 severity. Drug repurposing is, perhaps, an effective strategy for identifying antivirals, but there are no shortcuts for drug development. The identification of effective drugs, regardless of previous approval, requires time and funding to confirm and understand the drug target, the drug's toxicity, and its proper use. The lessons learned with COVID-19 should provide a roadmap for approaching drug discovery, when confronting SARS-CoV-2 and other current and future viral threats.

From the beginning of the SARS-CoV-2 pandemic in China, it was clear that severe COVID-19 was an inflammatory acute respiratory distress syndrome (ARDS). Indeed, early in the pandemic, COVID-19 progression from mild to moderate to severe was associated with immune dysfunction, hyper-inflammatory response, and sepsis (Zhou et al., 2020). Later studies showed that some patients infected with SARS-CoV-2 developed severe pneumonia and ARDS (Grant et al., 2021). Consequently, both antiviral and immunomodulatory drugs were contemplated and administered early in the pandemic (Martinez, 2020; Cross et al., 2021). Early studies (Tay et al., 2020) searched for parallelisms between SARS-CoV-2-related pneumonia and pneumonias connected to other human coronavirus diseases, such as severe acute respiratory syndrome (SARS-CoV) and Middle East respiratory syndrome (MERS-CoV). However, the pathobiology of SARS-CoV-2-related pneumonia seems to be distinct from pneumonia caused by other respiratory viral and bacterial pathogens; the SARS-CoV-2-related pneumonia displays unusual clinical features and has a longer clinical course than severe pneumonia (Gattinoni et al., 2020; Grant et al., 2021). An accurate clinical characterization of SARS-CoV-2 infections, based on known clinical syndromes, is critical for the identification of effective therapies (Cross et al., 2021).

Understandably, early in the SARS-CoV-2 pandemic, several repurposed drugs were quickly translated to the clinic. However, over the 2 last years, the results have been rather poor (Edwards, 2020; Edwards and Hartung, 2021; Martinez, 2021). The repurposed drugs for combating COVID-19 were selected either without a hypothetical basis or with mechanistic hypothetical approaches. Unfortunately, when those candidates were tested in clinical studies, none proved effective against SARS-CoV-2. Given that the repurposed drugs were optimized for a different target, dosage, or tissue, their pharmacology was probably not appropriate for the new indication (Edwards, 2020; Dahlin et al., 2021). In addition, the cellular assays designed for repurposing antivirals, including phenotypic and high-throughput screening assays, are frequently subject to interfering or undesirable bioactive mechanisms (Dahlin et al., 2021). Remarkably, most of the repurposed drugs tested during this pandemic were administered off-label and outside of properly designed observational or clinical trials. However, unsuccessful approaches might reduce the public trust

OPEN ACCESS

***Edited by:***
*Chunfu Zheng,*
*University of Calgary, Canada*

***Reviewed by:***
*Steven De Jonghe,*
*KU Leuven, Belgium*

***Correspondence:**
*Miguel Angel Martinez*
*mmartinez@irsicaixa.es*

***Specialty section:***
*This article was submitted to Virology, a section of the journal Frontiers in Microbiology*

***Received:*** *26 December 2021*
***Accepted:*** *26 January 2022*
***Published:*** *16 February 2022*

***Citation:***
*Martinez MA (2022) What Should Be Learned From Repurposed Antivirals Against SARS-CoV-2? Front. Microbiol. 13:843587. doi: 10.3389/fmicb.2022.843587*

in evidence-based medicine (Cross et al., 2021). Therefore, clinical trials and methodologies for identifying effective drugs should be designed based on methodologies with the highest likelihood of success.

Antiviral drugs target key processes in the virus life cycle. These processes include virus cell entry, genome replication, translation, protein processing, and virus particle generation. More than two-thirds of all antivirals approved for human use target viral enzymes, such as viral RNA/DNA polymerases and viral proteases (De Clercq and Li, 2016; Tompa et al., 2021). Importantly, in the last 30 years, no antiviral drug has been approved in the absence of a specific viral target. Thus, perhaps the main drawback of the repurposed antiviral drugs that have been tested unsuccessfully against SARS-CoV-2 has been the absence of an evident mechanism of action (**Table 1**).

Hits from antiviral screening based on biochemical or cell-culture assays must be treated with skepticism. Chloroquine and hydroxychloroquine represent a clear example of misinterpreted cell culture results. The efficacy of chloroquine and hydroxychloroquine against SARS-CoV-2 in tissue cultures was determined with African green monkey kidney-derived Vero cells. However, when Vero cells were engineered to express TMPRSS2, a cellular protease that activates SARS-CoV-2 for entry into lung cells, the genetic manipulation rendered SARS-CoV-2–infected Vero cells insensitive to chloroquine (Hoffmann et al., 2020). Accordingly, chloroquine could not block SARS-CoV-2 infections in TMPRSS2-expressing human lung Calu-3 cells; thus, chloroquine targets a viral activation pathway that is not present in human lung cells. Therefore, the drug is unlikely to protect against the spread of SARS-CoV-2. Another example of a misinterpretation of cell culture results was recently reported (Tummino et al., 2021) in a study that demonstrated that phospholipidosis was a shared mechanism underlying the antiviral activity of many repurposed drugs for SARS-CoV-2 (Tummino et al., 2021). Conversely, drugs that were active against the same targets, but did not induce phospholipidosis, were not effective against viruses. Those results strongly suggested that a failure to induce phospholipidosis could explain why most drugs that were selected for repurposing to date lacked clinical efficacy against SARS-CoV-2. In future pandemics, the target specificity of candidate antivirals should be examined before initiating treatment to exclude non-specific mechanisms during drug development. Target specificity should be accompanied by safety profiles and a determination of the pharmacokinetics/pharmacodynamics of selected drugs. Viruses manipulate many cellular processes during their life-cycles; thus, when a tested drug modifies a cellular pathway, it frequently leads to a false-positive hit.

Even when a drug mechanism of action is known, the preclinical data must be interpreted with caution. At the beginning of the SARS-CoV-2 pandemic, remdesivir, developed by Gilead, was the most promising antiviral drug for combating SARS-CoV-2. Initial interest in the drug was based on its potency in cell culture models of SARS-CoV-2, including primary human airway epithelial cells (Pruijssers et al., 2020). Moreover, remdesivir displayed specificity against the RNA-dependent RNA polymerase (RdRp) of other coronaviruses (Agostini et al., 2018), such as SARS-CoV and MERS-CoV. Moreover, it showed prophylactic and therapeutic efficacy in a rhesus macaque model of a MERS-CoV infection (de Wit et al., 2020). However, the clinical efficacy of remdesivir for COVID-19 remains controversial. Several trials have found no significant differences between remdesivir-treated and control groups in the time-to-clinical-improvement or mortality (Yan and Muller, 2021). Previous work with remdesivir also showed impressive preclinical and animal-model results against Ebola virus (Warren et al., 2016); however, those results were not confirmed in clinical studies (Mulangu et al., 2019).

In severe cases, SARS-CoV-2 induces an overexpression of inflammatory cytokines. Accordingly, immunomodulatory therapies, such as Anakinra (anti-interleukin 1b) and Tocilizumab (anti-interleukin 6), were repurposed for COVID-19. However, monotherapies with these compounds were unsuccessful. Remarkably, broad-spectrum immune-modulators, such as dexamethasone or baricitinib (anti-Janus kinase) have shown better efficacy in severe COVID-19 cases (Tomazini et al., 2020; Abani et al., 2021; Kalil et al., 2021). The pathogenesis of COVID-19 is different from those of other respiratory diseases. Consequently, repurposing immunomodulatory therapies might be more difficult than initially thought. Additionally, immunomodulatory therapies that might be useful for severe COVID-19 might be harmful in mild or moderate COVID-19, where the immune system can work effectively to control viral replication and disease (Cross et al., 2021).

Historically, repurposing drugs has only been successful in a few cases (Edwards, 2020). Examples are aspirin, for treating coronary artery disease; erythromycin, for treating impaired gastric motility; sildenafil for treating erectile dysfunction; thalidomide for treating multiple myeloma; and imatinib for treating gastrointestinal stromal tumors (Corsello et al., 2017). Most of those achievements were serendipitous. Nevertheless, those chance discoveries have promoted systematic searches for other drugs that might be repurposed. These explorations have mainly relied on high-throughput screening technologies and computational modeling with large datasets (Edwards, 2020). Currently, several libraries of approved drugs are available for rapid screening to identify candidates for repurposing against the targeted disease. Unfortunately, systematic, hypothesis-free, large-scale screening of these drug libraries has yet to yield effective treatments for most targeted diseases.

Effective vaccines against SARS-CoV-2 have been developed with extraordinary speediness. Vaccines have prevented COVID-19 development, but they have not generated sterilizing immunity in a significant percentage of individuals; thus, viral transmission remains possible after a vaccination (Krammer, 2020; Cromer et al., 2021). The continuous emergence of SARS-CoV-2 variants, such as the Delta or Omicron variant, has challenged the efficacy of current vaccines. The Omicron outbreak in southern Africa might be due to its capacity to infect people that have been vaccinated or have recovered from COVID-19 caused by Delta and other variants. At this stage, there is a need for an antiviral that effectively combats

**TABLE 1 |** Most relevant repurposed antiviral drugs against SARS-CoV-2.

| Antiviral drug | Approved target disease | Drug target | COVID-19 clinical trial reference |
|---|---|---|---|
| Favipiravir | Influenza virus | Virus RdRp | Doi et al., 2020 |
| Hydroxychloroquine | Malaria | Hemozoin biocrystallization | Axfors et al., 2021; WHO Solidarity Trial Consortium, 2021 |
| Ivermectin | Antiparasitic | Glutamate-gated chloride channels | Baker and Reardon, 2021; Popp et al., 2021 |
| Interferon beta-1a | Multiple sclerosis | Reduce inflammation | WHO Solidarity Trial Consortium, 2021 |
| Lopinavir | HIV-1 | Virus protease | Cao et al., 2020; WHO Solidarity Trial Consortium, 2021 |
| Remdesivir | SARS-CoV-2 | Virus RdRp | Wang et al., 2020; WHO Solidarity Trial Consortium, 2021 |

**TABLE 2 |** Approved direct acting antiviral drugs against SARS-CoV-2.

| Antiviral drug | Drug target | Delivery | References |
|---|---|---|---|
| Molnupiravir (MK-4482/EIDD-2801) | Virus RdRp | Oral | Jayk Bernal et al., 2021 |
| Nirmatrelvir (PF-07321332) | Virus main protease | Oral | Owen et al., 2021 |
| Remdesivir (GS-5734) | Virus RdRp | Intravenous | Wang et al., 2020; WHO Solidarity Trial Consortium, 2021 |

SARS-CoV-2 to prevent more severe disease, hospitalizations, and deaths.

A combination of vaccines and antiviral drugs should be a powerful tool for controlling the morbidity, mortality, and spread of SARS-CoV-2. Antivirals should target SARS-CoV-2 infections early to prevent rapid viral replication. In addition to the approved antiviral, remdesivir, which is delivered intravenously, two additional oral drugs, molnupiravir and nirmatrelvir (paxlovid), have completed human phase 3 clinical trials and have been approved (**Table 2**). Molnupiravir, a cytidine ribonucleoside analog first developed to inhibit influenza virus replication, was shown to inhibit the SARS-CoV-2 RdRp (Painter et al., 2021). Molnupiravir can pair ambiguously, as cytidine or uridine, with viral RNA. This pairing introduces an elevated mutation load that generates non-infectious virus particles. Molnupiravir, promoted by Merck for SARS-CoV-2 clinics, has the potential to be a broad-based inhibitor; it acts against a number of RNA viruses, including seasonal influenza virus, MERS-CoV, and encephalitic alphaviruses, such as Venezuelan, Eastern, and Western equine encephalitis viruses. Phase 3 clinical trial data from Merck have shown that a 5-day course of molnupiravir reduced hospitalization or mortality by ∼50%, compared to placebo, in patients with mild or moderate COVID-19. Nevertheless, the efficacy of molnupiravir was reduced from 50 to 30% in the published peer-reviewed data of the former phase 3 trial (Jayk Bernal et al., 2021). Nirmatrelvir inhibits the main SARS-CoV-2 protease (Owen et al., 2021). Protease inhibitors have been shown to be powerful antivirals, as demonstrated with human immunodeficiency virus type 1 (HIV-1) and hepatitis C virus (HCV). In a phase 3 clinical trial, nirmatrelvir was combined with ritonavir, an HIV-1 protease inhibitor that prevents enzymes in the liver from breaking down the antiviral. This combination showed 89% efficacy in preventing COVID-19 hospitalization and death. Still, the data for nirmatrelvir, generated by Pfizer, have not yet been peer-reviewed. These two promising antivirals will probably be effective against SARS-CoV-2 variants of concern, because these variants are characterized by mutations in the viral spike protein and other regions that are targeted by the immune system and/or by vaccines. Nevertheless, it should not be overlooked that monotherapy with any of these antivirals may induce viral drug resistance. This has been a familiar problem with other virus infections, like HIV-1 and HCV, which require treatments with a combination of antiviral drugs.

The emergence of new human viruses, such as HIV-1, HCV, Ebola virus, and Zika virus, has taught us that every new emerging virus has a distinct life style and a pathogenic course that was unknown in preceding viral infections. Moreover, SARS-CoV-2 is likely to become a permanent, endemic virus, like the previous, recently emerged human viruses. Repurposing drugs has been an appealing strategy for the rapid translation of drugs to the clinic. However, despite the enthusiasm for this strategy, it has not produced any effective treatments for COVID-19, or any other viral disease, including those caused by recent emergent viruses, such as Zika virus and Ebola virus. Drug development requires time, funding, and collaboration among clinical investigators, virologists, immunologists, and pharmacologists. It is important to know and understand the drug's target, toxicity, and pharmacodynamics, in addition to the key viral kinetic time-points and specific (or broad) immune phenomena. This approach may take more time, but it could be useful for fighting SARS-CoV-2 and for developing drugs to combat newly emerging viruses and future pandemics.

## AUTHOR CONTRIBUTIONS

The author confirms being the sole contributor of this work and has approved it for publication.

## FUNDING

This work was supported by the Spanish Ministry of Science and Innovation (PID2019-103955RB-100).

## REFERENCES


Abani, O., Abbas, A., Abbas, F., Abbas, M., Abbasi, S., Abbass, H., et al. (2021). Tocilizumab in patients admitted to hospital with COVID-19 (RECOVERY): a randomised, controlled, open-label, platform trial. *Lancet* 397, 1637–1645. doi: 10.1016/S0140-6736(21)00676-0

Agostini, M. L., Andres, E. L., Sims, A. C., Graham, R. L., Sheahan, T. P., Lu, X., et al. (2018). Coronavirus susceptibility to the antiviral remdesivir (GS-5734) is mediated by the viral polymerase and the proofreading exoribonuclease. *MBio* 9, e00221–e00218. doi: 10.1128/mBio.00221-18

Axfors, C., Schmitt, A. M., Janiaud, P., van't Hooft, J., Abd-Elsalam, S., Abdo, E. F., et al. (2021). Mortality outcomes with hydroxychloroquine and chloroquine in COVID-19 from an international collaborative meta-analysis of randomized trials. *Nat. Commun.* 12, 1–13. doi: 10.1038/s41467-021-22446-z

Baker, N., and Reardon, S. (2021). Coronapod: ivermectin, what the science says. *Nature* doi: 10.1038/d41586-021-02178-2. [Epub ahead of print].

Cao, B., Wang, Y., Wen, D., Liu, W., Wang, J., Fan, G., et al. (2020). A trial of lopinavir-ritonavir in adults hospitalized with severe COVID-19. *N. Engl. J. Med.* 382, 1787–1799. doi: 10.1056/NEJMoa2001282

Corsello, S. M., Bittker, J. A., Liu, Z., Gould, J., McCarren, P., Hirschman, J. E., et al. (2017). The Drug Repurposing Hub: a next-generation drug library and information resource. *Nat. Med.* 23, 405–408. doi: 10.1038/nm.4306

Cromer, D., Juno, J. A., Khoury, D., Reynaldi, A., Wheatley, A. K., Kent, S. J., et al. (2021). Prospects for durable immune control of SARS-CoV-2 and prevention of reinfection. *Nat. Rev. Immunol.* 21, 395–404. doi: 10.1038/s41577-021-00550-x

Cross, G., Ho, J. S. Y., Zacharias, W., Jeyasekharan, A. D., and Marazzi, I. (2021). Emergency drug use in a pandemic: harsh lessons from COVID-19. *Cell* 184, 5497–5500. doi: 10.1016/j.cell.2021.09.025

Dahlin, J. L., Auld, D. S., Rothenaigner, I., Haney, S., Sexton, J. Z., Nissink, J. W. M., et al. (2021). Nuisance compounds in cellular assays. *Cell Chem. Biol.* 28, 356–370. doi: 10.1016/j.chembiol.2021.01.021

De Clercq, E., and Li, G. (2016). Approved antiviral drugs over the past 50 years. *Clin. Microbiol. Rev.* 29, 695–747. doi: 10.1128/CMR.00102-15

de Wit, E., Feldmann, F., Cronin, J., Jordan, R., Okumura, A., Thomas, T., et al. (2020). Prophylactic and therapeutic remdesivir (GS-5734) treatment in the rhesus macaque model of MERS-CoV infection. *Proc. Natl. Acad. Sci. U. S. A.* 117, 6771–6776. doi: 10.1073/pnas.1922083117

Doi, Y., Hibino, M., Hase, R., Yamamoto, M., Kasamatsu, Y., Hirose, M., et al. (2020). A prospective, randomized, open-label trial of early versus late favipiravir therapy in hospitalized patients with COVID-19. *Antimicrob. Agents Chemother.* 64, e01897–e01820. doi: 10.1128/AAC.01897-20

Edwards, A. (2020). What are the odds of finding a COVID-19 drug from a lab repurposing screen? *J. Chem. Inf. Model.* 60, 5727–5729. doi: 10.1021/acs.jcim.0c00861

Edwards, A., and Hartung, I. V. (2021). No shortcuts to SARS-CoV-2 antivirals. *Science* 373, 488–489. doi: 10.1126/science.abj9488

Gattinoni, L., Coppola, S., Cressoni, M., Busana, M., Rossi, S., and Chiumello, D. (2020). COVID-19 does not lead to a "typical" acute respiratory distress syndrome. *Am. J. Respir. Crit. Care Med.* 201, 1299–1300. doi: 10.1164/rccm.202003-0817LE

Grant, R. A., Morales-Nebreda, L., Markov, N. S., Swaminathan, S., Querrey, M., Guzman, E. R., et al. (2021). Circuits between infected macrophages and T cells in SARS-CoV-2 pneumonia. *Nature* 590, 635–641. doi: 10.1038/s41586-020-03148-w

Hoffmann, M., Mösbauer, K., Hofmann-Winkler, H., Kaul, A., Kleine-Weber, H., Krüger, N., et al. (2020). Chloroquine does not inhibit infection of human lung cells with SARS-CoV-2. *Nature* 585, 588–590. doi: 10.1038/s41586-020-2575-3

Jayk Bernal, A., Gomes da Silva, M. M., Musungaie, D. B., Kovalchuk, E., Gonzalez, A., Delos Reyes, V., et al. (2021). Molnupiravir for oral treatment of COVID-19 in nonhospitalized patients. *N. Engl. J. Med* doi: 10.1056/NEJMoa2116044. [Epub ahead of print].

Kalil, A. C., Patterson, T. F., Mehta, A. K., Tomashek, K. M., Wolfe, C. R., Ghazaryan, V., et al. (2021). Baricitinib plus remdesivir for hospitalized adults with COVID-19. *N. Engl. J. Med.* 384, 795–807. doi: 10.1056/NEJMoa2031994

Krammer, F. (2020). SARS-CoV-2 vaccines in development. *Nature* 586, 516–527. doi: 10.1038/s41586-020-2798-3

Martinez, M. A. (2020). Compounds with therapeutic potential against novel respiratory 2019 coronavirus. *Antimicrob. Agents Chemother.* 64, e00399–e00320. doi: 10.1128/AAC.00399-20

Martinez, M. A. (2021). Lack of effectiveness of repurposed drugs for COVID-19 treatment. *Front. Immunol.* 12, 635371. doi: 10.3389/fimmu.2021.635371

Mulangu, S., Dodd, L. E., Davey, R. T., Tshiani Mbaya, O., Proschan, M., Mukadi, D., et al. (2019). A randomized, controlled trial of ebola virus disease therapeutics. *N. Engl. J. Med.* 381, 2293–2303. doi: 10.1056/NEJMoa1910993

Owen, D. R., Allerton, C. M. N., Anderson, A. S., Aschenbrenner, L., Avery, M., Berritt, S., et al. (2021). An oral SARS-CoV-2 M pro inhibitor clinical candidate for the treatment of COVID-19. *Science* 374, 1586–1593. doi: 10.1126/science.abl4784

Painter, W. P., Holman, W., Bush, J. A., Almazedi, F., Malik, H., Eraut, N. C. J. E., et al. (2021). Human safety, tolerability, and pharmacokinetics of molnupiravir, a novel broad-spectrum oral antiviral agent with activity against SARS-CoV-2. *Antimicrob. Agents Chemother.* 65, e022428–e022420. doi: 10.1128/AAC.02428-20

Popp, M., Stegemann, M., Metzendorf, M. I., Gould, S., Kranke, P., Meybohm, P., et al. (2021). Ivermectin for preventing and treating COVID-19. *Cochrane database Syst. Rev.* 7, CD015017. doi: 10.1002/14651858.CD015017

Pruijssers, A. J., George, A. S., Schäfer, A., Leist, S. R., Gralinksi, L. E., Dinnon, K. H., et al. (2020). Remdesivir inhibits SARS-CoV-2 in human lung cells and chimeric SARS-CoV expressing the SARS-CoV-2 RNA polymerase in mice. *Cell Rep.* 32, 107940. doi: 10.1016/j.celrep.2020.107940

Tay, M. Z., Poh, C. M., Rénia, L., MacAry, P. A., and Ng, L. F. P. (2020). The trinity of COVID-19: immunity, inflammation and intervention. *Nat. Rev. Immunol.* 20, 363–374. doi: 10.1038/s41577-020-0311-8

Tomazini, B. M., Maia, I. S., Cavalcanti, A. B., Berwanger, O., Rosa, R. G., Veiga, V. C., et al. (2020). Effect of dexamethasone on days alive and ventilator-free in patients with moderate or severe acute respiratory distress syndrome and COVID-19: the CoDEX randomized clinical trial. *JAMA* 324, 1307–1316. doi: 10.1001/jama.2020.17021

Tompa, D. R., Immanuel, A., Srikanth, S., and Kadhirvel, S. (2021). Trends and strategies to combat viral infections: a review on FDA approved antiviral drugs. *Int. J. Biol. Macromol.* 172, 524–541. doi: 10.1016/j.ijbiomac.2021.01.076

Tummino, T. A., Rezelj, V. V., Fischer, B., Fischer, A., O'Meara, M. J., Monel, B., et al. (2021). Drug-induced phospholipidosis confounds drug repurposing for SARS-CoV-2. *Science* 373, 541–547. doi: 10.1126/science.abi4708

Wang, Y., Zhang, D., Du, G., Du, R., Zhao, J., Jin, Y., et al. (2020). Remdesivir in adults with severe COVID-19: a randomised, double-blind, placebo-controlled, multicentre trial. *Lancet* 395, 1569–1578. doi: 10.1016/S0140-6736(20)31022-9

Warren, T. K., Jordan, R., Lo, M. K., Ray, A. S., Mackman, R. L., Soloveva, V., et al. (2016). Therapeutic efficacy of the small molecule GS-5734 against Ebola virus in rhesus monkeys. *Nature* 531, 381–385. doi: 10.1038/nature17180

WHO Solidarity Trial Consortium (2021). Repurposed antiviral drugs for COVID-19 - interim WHO solidarity trial results. *N. Engl. J. Med.* 384, 497–511. doi: 10.1056/NEJMoa2023184

Yan, V. C., and Muller, F. L. (2021). Why remdesivir failed: Preclinical assumptions overestimate the clinical efficacy of remdesivir for COVID-19 and Ebola. *Antimicrob. Agents Chemother.* 65, e01117–e01121. doi: 10.1128/AAC.01117-21

Zhou, F., Yu, T., Du, R., Fan, G., Liu, Y., Liu, Z., et al. (2020). Clinical course and risk factors for mortality of adult inpatients with COVID-19 in Wuhan, China: a retrospective cohort study. *Lancet* 395, 1054–1062. doi: 10.1016/S0140-6736(20)30566-3

**Conflict of Interest:** The author declares that the research was conducted in the absence of any commercial or financial relationships that could be construed as a potential conflict of interest.

**Publisher's Note:** All claims expressed in this article are solely those of the authors and do not necessarily represent those of their affiliated organizations, or those of the publisher, the editors and the reviewers. Any product that may be evaluated in this article, or claim that may be made by its manufacturer, is not guaranteed or endorsed by the publisher.

*Copyright © 2022 Martinez. This is an open-access article distributed under the terms of the Creative Commons Attribution License (CC BY). The use, distribution or reproduction in other forums is permitted, provided the original author(s) and the copyright owner(s) are credited and that the original publication in this journal is cited, in accordance with accepted academic practice. No use, distribution or reproduction is permitted which does not comply with these terms.*

frontiers in Microbiology

REVIEW
published: 24 February 2022
doi: 10.3389/fmicb.2022.839624

# The Role of Deubiquitinases in Virus Replication and Host Innate Immune Response

*Qinglin Zhang[1], Qizhen Jia[1], Wenying Gao[2]* and Wenyan Zhang[2]**

*[1] College of Life Sciences of Jilin University, Changchun, China, [2] Center for Pathogen Biology and Infectious Diseases, Institute of Virology and AIDS Research, Key Laboratory of Organ Regeneration and Transplantation of the Ministry of Education, The First Hospital of Jilin University, Changchun, China*

As a critical post-translational modification, ubiquitination is known to affect almost all the cellular processes including immunity, signaling pathways, cell death, cancer development, and viral infection by controlling protein stability. Deubiquitinases (DUBs) cleave ubiquitin from proteins and reverse the process of ubiquitination. Thus, DUBs play an important role in the deubiquitination process and serve as therapeutic targets for various diseases. DUBs are found in eukaryotes, bacteria, and viruses and influence various biological processes. Here, we summarize recent findings on the function of DUBs in modulating viral infection, the mechanism by which viral DUBs regulate host innate immune response, and highlight those DUBs that have recently been discovered as antiviral therapeutic targets.

**Keywords: DUBs, ubiquitin, PTM, viral infection, antiviral innate immunity**

OPEN ACCESS

***Edited by:***
*Chunfu Zheng,*
*University of Calgary, Canada*

***Reviewed by:***
*Fei Guo,*
*MOH Key Laboratory of Systems Biology of Pathogens, Institute of Pathogen Biology, Chinese Academy of Medical Sciences and Peking Union Medical College, China*
*Yong-Hui Zheng,*
*Michigan State University, United States*

****Correspondence:***
*Wenying Gao*
*gaowenying@jlu.edu.cn*
*Wenyan Zhang*
*zhangwenyan@jlu.edu.cn*

***Specialty section:***
*This article was submitted to Virology, a section of the journal Frontiers in Microbiology*

***Received:*** *20 December 2021*
***Accepted:*** *12 January 2022*
***Published:*** *24 February 2022*

***Citation:***
*Zhang Q, Jia Q, Gao W and Zhang W (2022) The Role of Deubiquitinases in Virus Replication and Host Innate Immune Response. Front. Microbiol. 13:839624. doi: 10.3389/fmicb.2022.839624*

## INTRODUCTION

Post-translational modifications (PTMs) play an important role in altering proteins without changing the nucleotide sequence of the organism's DNA or RNA, thus enhancing their response and adaptation to complex environmental variations. PTMS includes methylation, acetylation, phosphorylation, hydroxylation, and ubiquitination (Deribe et al., 2010). Among them, ubiquitination and deubiquitination significantly regulate various cellular processes in eukaryotes, such as signals transduction, protein trafficking, cell motility, transcription, apoptosis, cancer development (Yang et al., 2013; Seo et al., 2018; Tang et al., 2018; Mennerich et al., 2019; Jin et al., 2020; Li et al., 2021). Moreover, the ubiquitination and deubiquitination also exert diverse functions in archaea, bacteria, and viruses (Fuchs et al., 2018; Hermanns and Hofmann, 2019; Wu et al., 2020). The process of ubiquitination involves the conjugation of ubiquitin (Ub) or Ub-like modifiers (Ubl) [for example, the small ubiquitin-like modifier (SUMO), the ubiquitin-like protein (NEDD8), and IFN-induced 15-kd protein (ISG15)] to substrate proteins by three types of enzymes, including E1 ubiquitin-activating enzyme, E2 ubiquitin-conjugating enzyme, an E3 ubiquitin-protein ligase, and the sequential cascades of E1-E2-E3 enzymes have been well studied (Deribe et al., 2010; Zheng and Shabek, 2017; Hu et al., 2020). The important molecule ubiquitin contains seven lysine residues (K6, K11, K27, K29, K33, K48, and K63) and an N-terminus methionine (M1) serving as ubiquitination sites, which result in various polyubiquitin chain linkage types. "Ubiquitin code" is comprised by the architecture of polyubiquitin chain linkage-type, the number of modified sites, the length of the added ubiquitin molecules, and dictates the fate of the substrates (Komander and Rape, 2012). For example, the K48-linked polyubiquitin chain often leads to proteasome degradation of the protein substrate, whereas K63-linked polyubiquitin mainly involves non-degradative roles such as innate immunity or intracellular trafficking of modified proteins (Oshiumi et al., 2013; Song et al., 2016;

Okamoto et al., 2017). The conjugation of ubiquitin is reversible since deubiquitinases (DUBs) can cleave peptide or isopeptide bonds between ubiquitin and substrate protein or conjoined ubiquitin molecules. "Ubiquitin code" also dictates a wide variety of distinct DUBs activities and preferences, which has been well-reviewed (Clague et al., 2019).

The study of molecular pathways of deubiquitination was initiated in the 1990s and then further investigated and elucidated (Tobias and Varshavsky, 1991; Baker et al., 1992; Papa and Hochstrasser, 1993; Wilkinson, 1997). DUBs are key effectors of the removal of ubiquitin, which reverses the fate of the modified proteins as well as the following molecular and cellular functions of the proteins (Clague et al., 2013; Kategaya et al., 2017; Clague et al., 2019). DUBs have nearly 100 family members, which are classified into seven families, ubiquitin-specific proteases (USPs), ovarian tumor proteases (OTUs), ubiquitin carboxyl-terminal hydrolases (UCHs), Ataxin-3 like proteins (Josephins), MIU-containing new DUB family (MIUDY), zinc-finger ubiquitin protease 1 (ZUB/ZUFSP), and Jab/MPN domain-associated metalloisopeptidases (JAMMs) (Hermanns and Hofmann, 2019). Each possesses unique cleavage specificity owing to its structural characteristics (Mevissen and Komander, 2017).

The protein levels of individual DUB and their intracellular localization are important for DUBs function in the cellular process. The estimated copy number of DUBs ranges from the low hundreds (limit of detection) to hundreds of thousands per cell. A systemic subcellular localization screen by GFP (Green fluorescent protein)-tagged DUBs in HeLa cells, combined with individual studies, showed that DUBs distribute in a variety of defined structures, such as the nucleolus (USP36 and USP39), plasma membrane (USP6 and JOSD1), microtubule [USP21 and CYLD (cylindromatosis)], Golgi (USP33V3 and USP32) (reviewed in Clague et al., 2019). DUBs are associated with almost all biological functions and diseases. For example, USP14, CYLD, and UCHL1 regulate cardiac hypertrophy by the different mechanism (Wang et al., 2015; Liu et al., 2016; Bi et al., 2020; Qi et al., 2020). Some DUBs regulate tumorigenesis and migration by their intrinsic oncogenic or tumor suppressor activities (UCHL1 and CYLD), or by controlling key epigenetic changes that affect cancer development (USP22), or by affecting the protein levels and/or activities of various cancer-related proteins (USP7 and USP28) (Sacco et al., 2010; Nicholson and Suresh Kumar, 2011; Wang and Dent, 2014; Harrigan et al., 2018; Xiao et al., 2019). In addition, DUBs have also been reported to function in interferon (IFN) antiviral signaling, dependent or independent of their deubiquitinase activity (Wang L. et al., 2013; Zhong et al., 2013; Fan et al., 2014; Pauli et al., 2014; Zhang et al., 2015; Gu et al., 2017; Qian et al., 2018; Liu et al., 2020).

Virus infection induces a host immune response, and leads to multiple serious diseases, including fever, chronic hepatitis, acquired immunodeficiency syndrome (AIDS), and cervical cancer (Tanuma et al., 2016; De Nola et al., 2019; Gallardo et al., 2019; Thomas, 2019). Furthermore, COVID-19 caused by SARS coronavirus 2 (SARS-CoV-2) has resulted in over 12,340,000 cases and 2,710,000 deaths worldwide until the end of March 2021 (Yamamoto et al., 2020). Therefore, investigations have focused on the molecular mechanisms that regulate or mediate virus replication (García et al., 2017; Kumar et al., 2018; Luo et al., 2018; Zhu et al., 2020). DUBs are known to participate in virus-related cellular activities (Zhang et al., 2011; Saxena and Kumar, 2014). Isaacson and Ploegh (2009) had summarized the effect of Ub, Ubl, and deubiquitination in viral infection, and then Gu and Shi (2016) reviewed the mechanism used by viruses to bypass or employ DUBs to evade the host immune defense. As an interesting therapeutic target, the clinical development of selective DUB inhibitors has been well-reviewed (Harrigan et al., 2018). Here, we mainly summarize the recent studies on the role of DUBs in viral replication, including host-encoded- and virus-encoded DUBs, and the influence of DUBs on the innate immunity of the host. Our review aims to provide a brief insight into the above fields and highlight the potential therapeutic targets of virus infection.

## HOST-ENCODED DEUBIQUITINASES

### Host-Encoded Deubiquitinases Regulate Viral Replication by Affecting Innate Immune Response

The innate immune response begins with pathogen recognition. Pathogen-associated molecular patterns (PAMPs) are structural characteristics that broadly exist in various pathogens and are recognized by germline-encoded pattern-recognition receptors (PRRs). Activated PRRs initiate cellular signaling pathways which defend against the invading microbes (Akira et al., 2006). PRRs include Toll-like receptors (TLRs), RIG-I-like receptors (RLRs), NOD-like receptors (NLRs), and C-type lectin receptors (CLRs). Both TLRs and RLRs are responsible for sensing viral infection. Upon recognition, TLRs recruit adaptor proteins, including MyD88 (Myeloid differentiation primary response protein 88), TIRAP (Toll/interleukin 1 receptor domain-containing adaptor protein), TRIF (toll/interleukin 1 receptor-domain-containing adapter-inducing interferon-β), and TRAM (a transverse rectus abdominis), and lead to activation of the TRAF3-TBK1-IRF3 axis to induce type I IFN (IFN-I), or the TRAF6-TAK1-IKK axis to activate nuclear factor κ-light-chain-enhancer of activated B cells (NF-κB) and stimulate inflammatory cytokines (Kawai and Akira, 2011; Lim and Staudt, 2013; Ivashkiv and Donlin, 2014). As a typical member of the RLRs family, Retinoic acid-inducible gene I (RIG-I) interacts with a mitochondrial activator of virus signaling (MAVS), the essential signaling adaptor protein of RIG-I, and causes the activation of TBK1 (TANK-binding kinase 1) and IKKε (IκB kinase ε) (Kell and Gale, 2015; Chow et al., 2018). As the TLR and RIG-I signaling have crosslinks and have been well characterized, we summarize recent studies on regulating host-encoded DUBs in viral replication *via* TLR, RIG-I, or STING signaling (**Figure 1**). In most cases, host DUBs exert their deubiquitinating activity to reverse the ubiquitination and degradation of key molecular regulators of TLR or RIG-I signaling, including TRAF3 (TNF-receptor-associated factor 3), TBK1, MAVS (Mitochondria antiviral signaling protein), and other molecules, resulting in their stabilization, thereby altering the strength of the innate immune response to restrict the

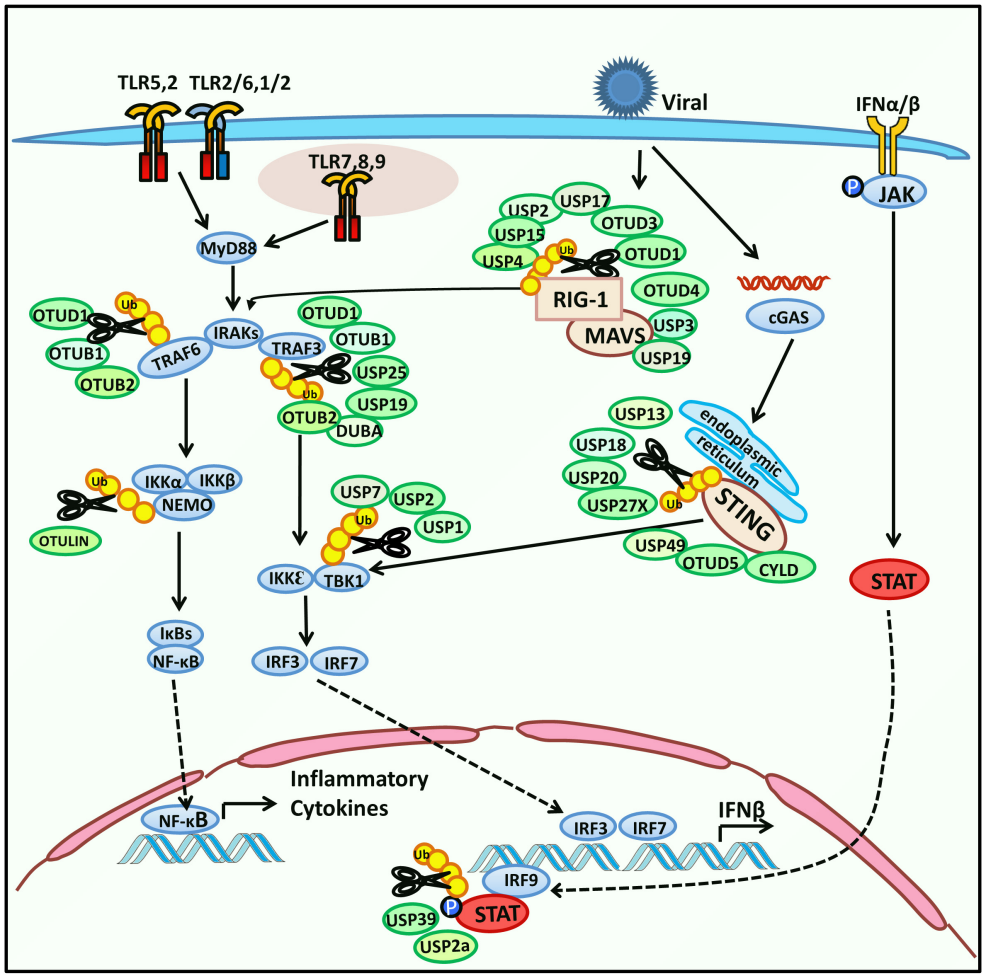


**FIGURE 1 |** Regulation of host-encoded DUBs in innate immune response. Toll-like receptors (TLRs) are a type of pattern-recognition receptors (PRRs) that recognize pathogen-associated molecular patterns (PAMPs) and subsequently change their conformation to initiate downstream signaling. TLRs are located on the cell membrane, phagosome membrane, endosome, and endoplasmic reticulum (TLRs on endosomes and endoplasmic reticulum are not shown). TLRs can activate the expression of NF-κB or IRF3 and subsequently induce the expression of inflammatory cytokines or IFN-β in the nucleus. Activated TLRs recruit adaptor proteins, including TIRAP, MyD88, TRAM, and TRIF. First, the adaptors interact with IRAKs and TRAF6 and then activate NF-κB through the TAK1-IKK-IκB axis. Second, the adaptors mediate the expression of IRF3 *via* TRIF-TRAF3-TBK1 signaling. In addition, another PRR, RIG-I, which belongs to the RIG-I-like receptors (RLRs) family, is responsible for sensing RNA of pathogens. It interacts with MAVS, which further induces both NF-κB and IRF3. Stimulator of interferon genes (STING), located on the endoplasmic reticulum senses cytoplasmic DNA and regulates IFN signaling by activating TBK1 and IRF3. IFN-β induces the phosphorylation of JAK and expression of interferon-stimulated genes (ISGs) by activating the downstream JAK-STAT pathway. Host-encoded DUBs interact with the above signaling molecules to modulate the innate immune response. Their deubiquitinating function and substrates are shown in the schematic.

proliferation of the virus. Located on the endoplasmic reticulum, STING (the stimulator of IFN genes) is responsible for sensing cytoplasmic DNA and exerts its function by activating TBK1 and IRF3 (IFN regulatory factor 3) thus stimulating IFN-I production (Tanaka and Chen, 2012).

Studies on host DUBs' function in innate immune response could be dated to the beginning of the 21st century. The tumor suppressor CYLD was originally reported to be a deubiquitinase that negatively regulates NF-κB *via* its deubiquitinase activity in 2003 (Kovalenko et al., 2003; Trompouki et al., 2003). The subsequent studies showed that CYLD is a negative regulator targeting RIG-I by the removal of K63-linked RIG-I polyubiquitin chains, resulting in the inactivation of IKKε/TBK1, and eventually inhibiting IFN promoter (Friedman et al., 2008; Zhang et al., 2008). In 2018, CYLD was reported to positively regulate STING-mediated antiviral signaling by the cleavage of K48-linked ubiquitination of STING and the blockage of its degradation, thus sustaining the level of STING and triggering the antiviral response (Zhang et al., 2018b). Zinc finger protein A20 (A20) is an OTU domain DUB and also has E3 ubiquitin ligase activity. It has been reported that A20 functions as a potent inhibitor of NF-κB signaling through the cooperative activity of its two ubiquitin-editing domains or antagonizing the interactions between TRAF6, TRAF2, and cIAP1 with the E2 ligases Ubc13 and UbcH5c, which are required for TRAF6 ubiquitination and NF-κB activation (Wertz et al., 2004;

Shembade et al., 2010). A20 has been reported to be a negative regulator of antiviral signaling by binding to TRIF and inhibition of TRIF-mediated activation of ISRE and IFN-β as well as Sendai virus (SeV) triggered NF-κB promoter, and blocks RIG-I-induced activation of NF-κ B-, IRF3- and IRF7-dependent promoters (Wang et al., 2004; Lin et al., 2006). So far, there are few studies of host-encoded DUBs other than USP and OTU family which regulate innate immune responses, so here we are focusing on these two DUB family members.

## Ubiquitin-Specific Proteases

Among the seven families of DUB families, the USP family is the largest DUB family, with more than 60 USPs identified (Yuan T. et al., 2018). Many USPs participate in the regulation of viral replication and are widely involved in RIG-I-induced antiviral immunity, such as USP17, USP3, USP4. In 2010, USP17 was identified in virus-induced IFN signaling, whose role in viral immunology is explored much earlier. Knockdown of USP17 increases the ubiquitination level of RIG-I and another RLR, MDA5, and reduces the production of SeV-induced IRF3 and IFN-β (Chen et al., 2010). It has been demonstrated that RIG-I K63-linked ubiquitination mediated by the E3 ubiquitin ligase tripartite motif protein 25 (TRIM25) is required for its activation and the stimulation of IFN signaling (Gack et al., 2007). In 2013, USP3 was reported to inhibit the type-I IFN pathway by binding to the K63-linked polyubiquitin chains of RIG-I and cleaving them, resulting in the negative regulation of RIG-I ubiquitination. Knockdown of USP3 promotes the phosphorylation of IRF3 and enhances the resistance of cells to viral infection (Cui et al., 2014). As a positive regulator of RIG-I-induced IFN signaling, USP4 interacts and removes K48-linked polyubiquitin chains of RIG-I and prevents RIG-I from degradation. Overexpression of USP4 suppresses VSV replication, while the knockdown of USP4 has the opposite effect (Wang L. et al., 2013). There are two contradictory reports about the regulation mechanism of USP15 on antiviral signaling (Pauli et al., 2014; Zhang et al., 2015). The first research reveals that USP15 deubiquitinates K48-linked ubiquitination of TRIM25 and prevents the degradation of TRIM25, which indicates that USP15 indirectly enhances TRIM25- and RIG-I-dependent production of IFN-I and the antiviral activity (Pauli et al., 2014). However, the other research claims that USP15 serves as a negative regulator of RIG-I signaling by deconjugating K63-linked polyubiquitin chains from RIG-I, resulting in the suppression of RIG-I-mediated antiviral responses. Interestingly, this research also points out that a part of this inhibition effect is independent of the DUB activity of USP15 (Zhang et al., 2015). Enterovirus 71 (EV71) infection induces the expression of host DUB USP19, and USP19 removes K63-linked ubiquitination of TRAF3, thereby inhibiting the antiviral IFN signaling. Knockdown of USP19 promotes cellular antiviral immunity and represses the replication of EV-71 (Gu et al., 2017). USP21 is the same negative regulator of the IFN signaling as USP19 by targeting and deubiquitinating K63-linked ubiquitination of RIG-I, though the specific site of deubiquitination has not been clarified (Fan et al., 2014). USP25 has been identified as a regulator of TLR signaling by removing the cIAP2 (cellular inhibitor of apoptosis 2)-mediated K48-linked ubiquitination of TRAF3, resulting in the blockage of TRAF3 degradation. The deficiency of USP25 enhances the extent of ubiquitination of TRAF3 and accelerates its degradation after TLR4 activation, which potentiates TLR4-induced activation of MAPK and NF-κB signaling, but suppresses the activation of IRF3 (IFN regulatory factor 3). Therefore, USP25 enables a balance between proinflammatory cytokines and type I IFNs by maintaining cellular TRAF3 level (Zhong et al., 2013).

USP1 forms a complex with USP1-associated factor 1 (UAF1), which reduces K48-linked ubiquitination of TBK1 and stabilizes it, resulting in the downstream activation of IRF3 and promotion of IFN-β secretion. The USP1-UAF1 inhibitor ML323 suppresses the expression of IFN-β and enhances virus replication *in vitro* and *in vivo*. This finding indicates a positive-regulatory effect of USP1 on IFN signaling (Yu et al., 2017). Another study reported that in contrast to USP1 and USP39, USP7 acts as a negative regulator of IFN signaling. Overexpression of USP7 enhances the stabilization of the E3 ligase TRIM27, thus promoting the ubiquitination and degradation of TBK1 and vesicular stomatitis virus (VSV) replication, whereas knockdown and knockout of endogenous USP7 inhibit TBK1 ubiquitination and degradation and increase IFN-β expression (Cai et al., 2018). Like USP7, USP5 is a restrictive factor for red-spotted grouper nervous necrosis virus (RGNNV)-induced IFN response in sea perch. Overexpression of USP5 leads to inhibition of other RLR signaling pathway-related genes, including MAVS, TRAF3, and TBK1, and strongly represses the IFN-I promoter's activation in zebra fish increases RGNNV replication *in vitro*. However, the mechanism by which USP5 influences RLR signaling genes needs to be elucidated further (Jia et al., 2020). Knockdown of USP39, another positive regulator of the IFN pathway, notably promotes viral replication. Interestingly, USP39 does not influence IFN-I production but affects IFN downstream JAK/STAT signaling. USP39 downregulates STAT K6-linked ubiquitination, thus stabilizing STAT (Peng et al., 2020). USP2a also targets STAT and functions as a regulator of antiviral signaling. STAT is mainly located in the nucleus, and USP2a could translocate into the nucleus and reduce the K48-linked ubiquitination and degradation of pY701-STAT1 (STAT activation depends on phosphorylation at tyrosine 701). Therefore, USP2a maintains the level of pY701-STAT induced by IFN and promotes antiviral immunity (Ren et al., 2016). USP2b targets TBK1 and negatively regulates IFN-β signaling by the cleavage of K63-linked polyubiquitin chains of TBK1, thus inhibiting the kinase activity of TBK1. Overexpression of USP2b promotes the replication of vesicular stomatitis virus (VSV), whereas the knockdown of USP2b represses VSV replication (Zhang et al., 2014).

As a negative regulator of cellular antiviral responses that targets STING, USP13 deconjugates K27- and K63-linked polyubiquitin chains of STING and then prevents the recruitment of TBK1 to STING. The knockdown of USP13 activates IRF3 and NF-κB and enhances antiviral immunity. Consistently, the deficiency of USP13 inhibits Herpes simplex virus (HSV-1) infection (Sun et al., 2017). USP49 has a similar function as USP13 (Ye et al., 2019). USP18 recruits USP20 and deconjugates

K48-linked ubiquitination of STING, thereby protecting STING from proteasomal degradation and promoting the production of type-I IFN. The knockdown of USP20 or USP18 promotes STING ubiquitination and degradation and impairs IRF3 and NF-κB pathways, thereby reducing the resistance of mice to HSV-1 infection (Zhang et al., 2016). USP27X also targets, and the mechanism involves cyclic GMP-AMP synthase (cGAS), a cytosolic DNA sensor catalyzing the formation of a second messenger cGAMP. cGAMP binds to STING and promotes the IFN-I signaling. USP27X interacts with cGAS and removes its K48-linked ubiquitination, thereby leading to the stabilization of cGAS and the enhancement of IFN production (Guo et al., 2019).

## Ovarian Tumor Proteases

Deubiquitinases in the OTU superfamily were originally identified from different organisms and affect antiviral immunity as well as virus proliferation (Kayagaki et al., 2007; Li et al., 2010). Deubiquitinating enzyme A (DUBA) was identified in 2007 to act as a negative regulator of IFN signaling, which removes K63-linked ubiquitination of TRAF3, resulting in the dissociation of TRAF3 from TBK1 (Kayagaki et al., 2007). OTUB1 and OTUB2 negatively regulate type-I IFN signaling by deubiquitinating TRAF3 and TRAF6 after viral infection (Li et al., 2010). OTUD1 could also inhibit IFN response. OTUD1 could be induced by an RNA virus and could upregulate the level of protein Smurf1. Smurf1 could ubiquitinate and degrade each component of the MAVS/TRAF3/TRAF6 signalosome (Zhang et al., 2018a). OTUD3 is an acetylation-dependent DUB. Its DUB activity relies on K129 acetylation, and it could remove the K63-linked ubiquitination of MAVS, hence repressing antiviral response. OTUD3 acetylation would be removed upon virus infection, and the DUB activity would be blocked. Therefore, OTUD3 is controlled to timely response to virus infection (Zhang et al., 2020). OTUD5 exerts DUB activity by cleaving STING K48, enhancing STING stability, and thus promoting type-I IFN signaling (Guo et al., 2020). Similarly, OTUD4 deubiquitinates and stabilizes MAVS and promotes antiviral signaling. Knockdown of OTUD4 inhibits the activation of NF-κB and IRF3, resulting in the suppression of their downstream genes, thus enabling the VSV replication (Liuyu et al., 2019). OTULIN is an ovarian tumor domain deubiquitinase that possesses linear linkage specificity. PRRSV infection enhances the expression of OTULIN, and overexpression of OTULIN increases PRRSV propagation. OTULIN is recruited by PRRSV Nsp11 and removes linear ubiquitination targeting NEMO, a subunit of the IKK complex, resulting in the reduction of IFN-I production (Su et al., 2018).

## Host-Encoded Deubiquitinases Modulate Virus Replication *via* Viral Proteins

In addition to modulating innate immune signaling pathways, host DUBs also regulate viral replication *via* the interaction with virus-encoded proteins. Due to the selective pressure of evolution, viruses have evolved to recruit host proteins to assist their propagation, and host deubiquitinases are widely involved (**Table 1**). USP7 is the first identified DUB that interacts with ICP0 of HSV-1, mediating the stability of ICP0 or modulating TLR-mediated innate response (Everett et al., 1997; Boutell et al., 2005; Daubeuf et al., 2009). USP7 has been demonstrated to participate in the replication of multiple viruses, including Epstein-Barr virus (EBV), Merkel cell polyomavirus (MCPyV), and Human immunodeficiency virus type 1 (HIV-1) (Holowaty and Frappier, 2004). USP7 directly binds to the large T (LT)-antigen of MCPyV, an early viral gene product that plays a significant role in viral replication, which promotes the binding affinity of LT to the viral origin of replication and decreases viral DNA replication. This process is not related to the deubiquitinase activity of USP7 (Czech-Sioli et al., 2020). USP7 also serves as an enhancer of viral replication. Inhibition of USP7 decreases the replication of human adenoviral species C (HAdV-C5), most adenoviral species A as well as clinical isolates, and HIV (Ali et al., 2017; Kosulin et al., 2018). HIV Tat is produced in the early phase of HIV infection and is mainly responsible for transacting transcription and promoting viral production. USP7 stabilizes Tat by deubiquitylating and blocking it from proteasomal degradation, resulting in the promotion of virus propagation (Ali et al., 2017). In EBV infected cells, the EBNA1 protein binds to specific recognition sites *oriP* in the latent origin of replication required for the viral genome's replication and maintenance. USP7 greatly stimulates EBNA1-DNA interactions and enhances the ability of EBNA1 to activate transcription by modifying histone in a deubiquitinase-dependent manner (Sarkari et al., 2009). Similarly, in Kaposi's sarcoma herpesvirus (KSHV), USP7 interacts with the viral latency-associated nuclear antigen 1 (LANA), which is involved in latent viral replication and maintenance of the viral genome, thus enhancing the latent viral DNA replication of KSHV (Holowaty et al., 2003; Jager et al., 2012). vIRF1 of KSHV was identified as a novel interaction partner of USP7, which deregulates USP7 to inhibit p53-mediated antiviral responses (Chavoshi et al., 2016).

In high-risk human papillomavirus (HPV)-induced cancer, USP46 recruited by oncoprotein E6 leads to deubiquitination and stabilization of Cdt2/DTL, a component of the E3 ligase $CRL4^{Cdt2}$, and represses the level of epigenetic regulator Set8, which promotes cell proliferation. Thus, depletion of USP46 inhibits HPV-transformation-induced tumor growth through the E6-USP46-Cdt2-Set8 pathway (Kiran et al., 2018). HPV E1 helicase, which possesses DNA unwinding activity and enhances viral DNA replication, could form a complex with UAF1 and any one of USP1, USP12 and USP46. Besides USP1, the catalytic activity-negative USP12 and USP46 also decrease viral replication, and E1-UAF1 binding is essential for the effect (Lehoux et al., 2014). Therefore, USP1, USP12, and USP46 promote viral replication *via* interacting with the E1-UAF1 complex.

Similarly, inhibition of USP14 causes the repression of replication of several flaviviruses, indicating the crucial role of USP14 in viral propagation (Nag and Finley, 2012; Perry et al., 2012). WP1130, a small molecule inhibitor, can inhibit Murine norovirus 1 (MNV-1) replication, and chemical proteomics showed that USP14 is the target of WP1130. The downregulation of USP14 by pharmacologic inhibition or siRNA-mediated knockdown reduces the expression of the MNV-1 non-structural

**TABLE 1 |** Host-encoded DUBs and the targeted viruses, proteins, or genes.

| Host-encoded DUBs | Targeted viruses or genes, proteins | The mechanism | References |
|---|---|---|---|
| USP1/USP12/USP46 | Human papillomavirus (HPV) E1 helicase | Unwinding DNA and enhancing viral DNA replication | Lehoux et al., 2014 |
| USP14 | Murine norovirus 1 (MNV-1) VPg gene | Non-structural gene | Perry et al., 2012 |
| USP 7 | HIV-1 Tat | Promoting viral production | Ali et al., 2017 |
| | Herpes simplex virus type 1 (HSV-1) ICP0 (Vmw110) | Non-specific activator of gene expression | Everett et al., 1997 |
| | Epstein-Barr virus (EBV) EBNA1 | Initiating EBV latent genome replication | Sarkari et al., 2009 |
| | Kaposi's sarcoma herpesvirus (KSHV) LANA<br>vIRF1 | Working in latent viral replication<br>Inhibit p53-mediated antiviral responses | Chavoshi et al., 2016 |
| | Merkel cell polyomavirus (MCPyV) | Working in viral replication | Czech-Sioli et al., 2020 |
| | red-spotted grouper nervous necrosis virus (RGNNV) | Strongly represses the activation of the IFN-I promoter | Jia et al., 2020 |
| | TRIM27 | Enhances the stabilization of the E3 ligase TRIM27 | Cai et al., 2018 |
| USP15 | HIV Nef | Necessary for AIDS pathogenicity | Pyeon et al., 2016 |
| | HIV Gag | HIV structural protein | |
| USP11 | Influenza A virus RNA | A component of viral RNA replication complex | Liao et al., 2010 |
| OTULIN | PRRSV Nsp11 | OTULIN is recruited by PRRSV Nsp11 and removes linear ubiquitination targeting NEMO | Su et al., 2018 |
| USP19, DUBA | TRAF3 | Removes K63-linked ubiquitination of TRAF3 | Kayagaki et al., 2007; Gu et al., 2017 |
| USP25 | TRAF3 | The enhancement of TRAF3 degradation | Zhong et al., 2013 |
| CYLD; USP18 and USP20 | STING | The cleavage of K48-linked ubiquitination of STING | Zhang et al., 2016; Zhang et al., 2018b |
| USP13/49 | STING | Deconjugates K27- and K63-linked polyubiquitin chains of STING | Sun et al., 2017; Ye et al., 2019 |
| USP17 | RIG-I | Increases the ubiquitination level of RIG-I | Chen et al., 2010 |
| USP3/21/19 | RIG-I | Removes K63-linked polyubiquitin chains of RIG-I | Cui et al., 2014; Fan et al., 2014 |
| USP4 | RIG-I | Interacts and removes K48-linked polyubiquitin chains of RIG-I | Wang L. et al., 2013 |
| USP15 | TRIM25/RIG-I | Enhanced the TRIM25- and RIG-I-Dependent production of IFN-I and suppressed RNA virus replication | Pauli et al., 2014; Zhang et al., 2015 |
| USP1 | TBK1 | Reduces K48-linked ubiquitination of TBK1 and stabilizes it | Yu et al., 2017 |
| USP2a | STAT | Reduce the K48-linked ubiquitination and degradation of pY701-STAT1 | Ren et al., 2016 |
| USP39 | STAT | Downregulates STAT K6-linked ubiquitination, thus stabilizing STAT | Peng et al., 2020 |
| USP2b | TBK1 | Inhibits the kinase activity of TBK1 | Zhang et al., 2014 |
| USP27X | cGAS-STING | Removes cGAS K48-linked ubiquitination | Guo et al., 2019 |
| DUBA | TRAF3 | Removes K63-linked ubiquitination of TRAF3 | Kayagaki et al., 2007 |
| OTUB1, OTUB2 | TRAF3 and TRAF6 | Deubiquitinating TRAF3 and TRAF6 | Li et al., 2010 |
| OTUD1 | Smurf1 | Upregulate the level of protein Smurf1 | Zhang et al., 2018a |
| OTUD3, OTUD4 | MAVS | Deubiquitinates and stabilizes MAVS | Liuyu et al., 2019; Zhang et al., 2020 |
| OTUD5 | STING | Cleaving STING K48, enhancing STING stability | Guo et al., 2020 |

gene VPg, suggesting the essential role of USP14 in effective MNV-1 inhibition (Perry et al., 2012).

Host DUBs also block the activity of crucial proteins during viral replication, thus exhibiting a negative regulatory function. Liao et al. reported that downregulation of USP11 results in higher level of influenza A virus (IAV) RNA, indicating that USP11 inhibits IAV replication. Moreover, the inhibitory effect of USP11 on viral genome replication requires its deubiquitinase activity. USP11 interacts with and deubiquitinates the nucleoprotein (NP) protein, a component of the viral RNA replication complex (Liao et al., 2010). In contrast to the positive role of USP7 in HIV-1 replication, USP15 represses the replication of HIV-1 by inducing the degradation of HIV-1 Nef and Gag proteins (Pyeon et al., 2016).

## VIRUS-ENCODED DEUBIQUITINASES

Deubiquitinases are widely presented in various viruses and significantly influence viral activity. During viral infection, a set of DUBs encoded by viruses mainly target various signaling molecules of innate immune pathways to suppress antiviral immunity, thus ensuring viral replication (Kumari and Kumar, 2018). In addition, some virus-encoded DUBs regulate viral replication through other mechanisms or mechanisms remaining unknown. Most viral DUB activity is mediated by papain-like proteases (PLPs) (Zheng et al., 2008; Frieman et al., 2009; Wang G. et al., 2011; Sun et al., 2012; van Kasteren et al., 2013; Xing et al., 2013; Chen et al., 2014; Yang et al., 2014; Yuan et al., 2015; Li et al., 2016). The adenovirus protease adenain was initially demonstrated to possess a deubiquitinating function in *in vitro* experiments (Balakirev et al., 2002). Then viral PLPs encoded by coronavirus family member such as SARS-CoV was reported to remove ubiquitin from substrate proteins (Barretto et al., 2005; Lindner et al., 2005; Bekes et al., 2016; Shin et al., 2020). UL36 encoded by HSV-1 and Marek's disease virus (MDV), UL48 of HCMV are ubiquitin-specific cysteine proteases and have deubiquitinating activity (Kattenhorn et al., 2005; Wang et al., 2006; Jarosinski et al., 2007). DUB activity is strictly conserved in several other herpesviruses such as EBV, which encodes BPLF1 exhibiting deubiquitinating activity (Whitehurst et al., 2009). DUBs encoded by other viral genes are relatively few. For example, the DUB of nairoviruses resides in the polymerase protein but is not essential for RNA replication (van Kasteren et al., 2012). Previous studies have systematically summarized the role of viral DUBs in innate immunity (Gu and Shi, 2016;

**TABLE 2 |** Virus-encoded DUBs and the targeted proteins or genes.

| Virus-encoded DUBs | Targeted protein(s) or gene(s) | Mechanism | References |
|---|---|---|---|
| Adenovirus protease Adenain | N/A | Deubiquitinates a number of cellular proteins | Balakirev et al., 2002 |
| SARS PLP | ISG15 | Cleave replicase substrates; cleave K48-linked polyUb chains of ISG15 | Barretto et al., 2005; Lindner et al., 2005; Bekes et al., 2016; Shin et al., 2020 |
| | TRAF3, TRAF6 | Inhibits the production of IFNs and pro-inflammatory cytokines | Li et al., 2016 |
| HcoV-NL63 PLP2 | N/A | Antagonizes the induction of IFN-I independent of protease and DUB activity | Clementz et al., 2010; Yuan et al., 2015 |
| HSV-1 UL36 | Proliferating cell nuclear antigen (PCNA) | Blocks the polymerase-η-mediated DNA damage-response translation synthesis (TLS) pathway | Kattenhorn et al., 2005 |
| | TRAF3, ISRE promoter | Inhibits IFN-I production or counteracts the IFN-I-mediated signaling pathway | Wang S. et al., 2013; Yuan H. et al., 2018 |
| | IκBα | The inactivation of the NF-κB pathway and the inhibition of IFN-β production | Ye et al., 2017 |
| MDV UL36 | N/A | Contributes to malignant outgrowths | Jarosinski et al., 2007 |
| HCMV UL48 | N/A | Facilitates production of infectious virus | Wang et al., 2006; Kim et al., 2009 |
| | TRAF6, TRAF3, IRAK1, IRF7, STING | Promotes oncogenesis by inhibiting innate immunity of the host | Kumari et al., 2017 |
| | RIP1 | Inhibits TNFα-induced NF-κB activation | Kwon et al., 2017 |
| EBV BPLF1 | EBV ribonucleotide reductase (RR) | Interacts with, deubiquitinates, and influences the activity of the EBV RR | Whitehurst et al., 2009 |
| | IκBα, TRAF6, NEMO | Suppresses TLR-mediated activation of NF-κB | Saito et al., 2013; van Gent et al., 2014 |
| | PCNA | Attenuates polymerase η recruitment to DNA damage sites | Whitehurst et al., 2012 |
| CCHFV OTU | NP | Associating with viral genomic RNA to form RNP complexes, initiate replication or transcription | Scholte et al., 2019 |
| KSHV ORF64 | RIG-I | Inhibition of RIG-I-mediated signaling | Inn et al., 2011 |
| Arteri- and nairovirus DUBs | RIG-I | Control innate immune signaling | van Kasteren et al., 2012 |
| TYMV PRO domain | 66K RdRp | Ensures the replication of viral RNA | Fieulaine et al., 2020 |
| HEV PCP | RIG-I, TBK1 | Reduces IFN production | Nan et al., 2014 |
| FMDV Ppro | RIG-1, TBK1, TRAF3, TRAF6 | Blocks the IFN-β promoter | Wang D. et al., 2011 |
| PEDV PLP2 | IRF3 | Negatively regulates type I interferon pathway | Xing et al., 2013 |
| TGEV PL1 | RIG-I, STING | Antagonizes production of IFN- β | Hu et al., 2017 |
| PRRSV nsp2 | IκBα | Antagonizes the type I interferon induction by interfering with the NF-kappaB signaling pathway | Sun et al., 2010 |
| MHV-A59 PLP2 | IRF3<br>TBK1 | Blocks IRF3-, TBK1- and CARDIF-mediated IFN-β reporter activity | Zheng et al., 2008; Wang G. et al., 2011 |

*N/A represents not applicable.*

Zheng and Gao, 2020), here, we focus on the recent studies on how viral DUBs modulate the innate immune response and detail the signaling pathways that involve viral DUBs (**Table 2**).

## Effect of Virus-Encoded Deubiquitinases on Retinoic Acid-Inducible Gene-I and Toll-Like Receptor Signaling

Viral DUB could influence the TLR pathway to antagonize innate immunity, and PLP2 encoded by Human coronavirus NL63 (HCoV-NL63) is a typical DUB targeting TLR signaling. HCoV-NL63 PLP2 was identified to possess DUB activity, and it could cleave both K48- and K63-linked polyubiquitin chains, thereby antagonizing IFN, although the inhibition effect is independent of its DUB activity (Clementz et al., 2010). In 2015, another study suggested one potential mechanism of HCoV-NL63 PLP2 antagonism to IFN signaling, but it is associated with PLP2 DUB activity. PLP2 is claimed to induce p53 degradation *via* deubiquitination and stabilization of the oncoprotein MDM2, an E3 ligase degrading p53. p53 could activate the transcription of IRF7. Hence, PLP2 blocks IFN-β signaling through the MDM2-p53-IRF7 pathway and facilitates viral replication (Yuan et al., 2015).

Multiple viral DUBs mainly target RIG-I signaling to regulate IFN response. The DUB activity of Crimean-Congo Hemorrhagic Fever virus (CCHFV) OTU is essential for inhibiting RIG-I-mediated IFN-β response and inactivated OTU DUB suppresses viral replication. OTU represses the RIG-I-mediated IFN-β response by removing ubiquitin (Ub) from RIG-I CARDs. Moreover, OTU DUB also inhibits the IFN-β response by blocking the activation of both IRF3 and NF-κB, indicating that CCHFV OTU DUB ensures the sufficient replication of the virus *via* multiple cellular signaling pathways (Scholte et al., 2017). KSHV ORF64 DUB, both arteri- and nairovirus DUBs decrease the ubiquitination of RIG-I, thus inactivating RIG-I-mediated IFN signaling (Inn et al., 2011; van Kasteren et al., 2012). DUBs can also repress MAVS-mediated IFN-β induction (van Kasteren et al., 2012). The interaction between herpesvirus BPLF1 and the 14-3-3-TRIM25 complex is essential for the induction of TRIM25 aggregates. TRIM25 ubiquitinates RIG-I, thus promoting RIG-I-triggered IFN signaling (Gupta et al., 2019).

Some viral DUBs can act on various RIG-I and TLR pathways adaptors. SARS-CoV infection inhibits IFN production as well as the upregulation of IFN-stimulated genes. SARS-CoV PLP interacts with IRF3 to block its phosphorylation and translocation into the nucleus and interrupts IRF3-mediated IFN signaling of either RIG-I or TLR pathway (Devaraj et al., 2007). However, a later study reported that SARS-CoV PLP does not directly interact with IRF3 and inhibit IRF3 phosphorylation *in vitro* but suppresses IRF3 signaling. PLP blocks both IRF3 and NF-κB signaling by deubiquitinating IKBα, while DUB activity of PLP is necessary for pathway antagonism but not sufficient by itself (Frieman et al., 2009). In addition, SARS coronavirus PLP also suppresses the TLR7 signaling pathway by removing K63-linked polyubiquitin of TRAF3 and TRAF6, thereby inhibiting the production of IFNs and pro-inflammatory cytokines (Li et al., 2016). Seneca Valley Virus (SVV) 3C protease represses the ubiquitination of RIG-I, TBK1, and TRAF3, thus inhibiting the expression of IFN-β and promoting virus replication (Xue et al., 2018). The PCP domain of hepatitis E virus (HEV) deubiquitinates RIG-I and TBK-1, thereby reducing IFN production (Nan et al., 2014). The leader proteinase ($L^{pro}$) of the foot-and-mouth disease virus (FMDV) has DUB activity and strongly reduces ubiquitination of several key molecular regulators in the IFN-I response pathway, including RIG-1, TBK1, TRAF3, and TRAF6. Loss of DUB activity abolishes the ability of $L^{pro}$ to block the IFN-β promoter (Wang D. et al., 2011).

## Effect of Virus-Encoded Deubiquitinases on STING Signaling

Some virus-encoded DUBs act on STING and influence downstream signaling. HSV-1 VP1-2 blocks IFN-I production by directly interacting with and deubiquitinating STING. In contrast, the VP1-2 mutant that lacks DUB activity enhances IFN expression due to increased STING ubiquitination as well as STING, TBK1, and IRF3 phosphorylation (Bodda et al., 2020). In addition, ORF64 DUB of MHV68 is essential for antagonizing the STING-dependent pathway which is induced by viral genomic DNA (Sun et al., 2015).

Human cytomegalovirus (HCMV) pUL48 blocks PRR-mediated IFN-I signaling through deubiquitinating a variety of key molecules, including STING, TRAF3, TRAF6, IRAK1, and IRF7 (Kumari et al., 2017). Upon ectopic expression, both CoV-NL63 PLP2 and SARS-CoV membrane-anchored PLpro domain (PLpro-TM) inhibit the formation of STING dimer and block the assembly of STING-MAVS-TBK1/IKKε complexes, thus inhibiting the activation of IRF3 and disrupting the signaling of IFN induction (Sun et al., 2012). It has also been demonstrated that SARS-Cov PLpro-TM represses the ubiquitination of RIG-I, STING, TRAF3, TBK1, and IRF3, thus inhibiting the assembly of the STING-TRAF3-TBK1 complex and the activation of IFN expression (Chen et al., 2014).

Some DUBs directly interact with RIG-I or STING and deubiquitinate them, resulting in suppression of STING- and RIG-I-mediated IFN-β signaling, such as porcine epidemic diarrhea virus (PEDV) PLP2 and transmissible gastroenteritis virus (TGEV) PL1 (Xing et al., 2013; Hu et al., 2017).

## Effect of Virus-Encoded Deubiquitinases on NF-κB Signaling

Some viral DUBs target NF-κB signaling to manipulate immune responses (Sun et al., 2010; Kwon et al., 2017; Ye et al., 2017). HSV-1 UL36 and porcine reproductive and respiratory syndrome virus (PRRSV) nsp2 both deubiquitinate K48-linked IκBα and prevent its degradation, resulting in the inactivation of the NF-κB pathway and the inhibition of IFN-β production (Sun et al., 2010; Ye et al., 2017). UL48 and UL45 encoded by HCMV that contain DUB activity, target receptor-interacting protein kinase 1 to inhibit NF-κB signaling (Kwon et al., 2017). EBV BPLF1 deubiquitinates IκBα, TRAF6 and NEMO, thus suppressing the activation of the NF-κB pathway at multiple steps. BPLF1 also inhibits NF-κB upstream TLR signaling, and reduces the production of IL-8 (van Gent et al., 2014).

EBV BPLF1 deubiquitinates TRAF6, which is further associated with latent membrane protein 1 (LMP1) and inhibits NF-κB signaling, thereby increasing EBV DNA replication (Saito et al., 2013). SARS-CoV PLP antagonizes IFN and NF-κB signaling pathway by interfering with the activation of the important signaling proteins, IRF3 and IκBα in the respective pathways (Frieman et al., 2009).

## Effect of Virus-Encoded Deubiquitinases on Crosslinking Signaling Molecules

Besides the DUBs listed above, some viral DUBs act on the common downstream molecules of the TLR/RIG-I/STING signaling pathways. MHV-A59 PLP2 deubiquitinases IRF3 and inhibits its nuclear translocation *via* its DUB activity, thereby blocking IRF3-, TBK1-, and CARDIF-mediated IFN-β reporter activity (Zheng et al., 2008). Further studies also show that MHV-A59 PLP2 deubiquitinates TBK1 and inhibits its kinase activity, thereby preventing IRF3 from phosphorylation and inactivating IFN-β signaling (Wang G. et al., 2011). HSV-1 UL36USP deubiquitinates TRAF3 and prevents recruitment of TBK1, and inactivates the IFN-β promoter (Wang S. et al., 2013). It also binds to the IFNAR2 subunit, thus preventing JAK1-IFNAR2 interaction. Therefore, UL36USP antagonizes IFN-mediated JAKs and STAT activation (Yuan H. et al., 2018). MERS-Cov PLpro inhibits IRF3 phosphorylation and nuclear translocation, thus antagonizing the IFN-β pathway (Yang et al., 2014).

## Other Mechanisms of Virus-Encoded Deubiquitinases in the Regulation of Viral Replication

In several RNA viruses, virus-encoded DUBs affect and mediate viral replication. CCHFV OTU is required for viral replication, and occupancy of the synthetic ubiquitin variant (UbV-CC4) on CCHFV OTU directly interrupts viral RNA synthesis, thus blocking viral replication without targeting IFN signaling. CCHFV replication requires NP protein to associate with viral genomic RNA to form ribonucleoprotein (RNP) complexes and then interact with the L protein to initiate replication or transcription. In the presence of UbV-CC4, fewer NPs interact with the L protein, which indicates that UbV-CC4 inhibits CCHFV replication by interfering with the formation of replication complexes (Scholte et al., 2019). Turnip yellow mosaic virus (TYMV) PRO/DUB enzyme mediates the RNA-dependent RNA polymerase (RdRp) level, thereby regulating viral replication. The PRO domain cleaves TYMV-encoded 206 K polyprotein and produces 66 K RdRp. RdRp undergoes ubiquitination and degradation, whereas the DUB activity inhibits the degradation of the 66K RdRp and ensures the replication of viral RNA (Fieulaine et al., 2020). Among DNA viruses, HSV UL36USP and EBV BPLF1 enhance the sensitivity of cells to DNA-damaging agents to facilitate virus proliferation through its DUB activity (Whitehurst et al., 2012; Dong et al., 2017). In brief, UL36USP or BPLF1 deubiquitinates proliferating cell nuclear antigen (PCNA) and inhibits the subsequent formation of polymerase-η (pol-η) foci, thereby blocking the pol-η-mediated DNA damage-response translation synthesis (TLS) pathway (Dong et al., 2017).

Some DUB-mediated mechanisms have not yet been elucidated. PRRSV PLP2 possesses DUB activity and is essential for viral replication. However, the DUB activity is independent of the TNF-α pathway (Zhou et al., 2019). CCHFV L protein exhibits DUB activity but does not affect virus proliferation and innate immune responses (Tchesnokov et al., 2020). The reduction of FMDV DUB activity results in virus attenuation, but it is independent of interference with the expression of IFN (Medina et al., 2020). Murine cytomegalovirus (MCMV) encodes M48 DUB and MCK2 (MCMV-encoded chemokine 2), a viral C-C chemokine that enhances the host immune response. Blocking M48 DUB activity reduces MCMV replication, at least in the natural host, and promotes MCK2-induced immune response (Hilterbrand et al., 2017).

# DEUBIQUITINASES SERVE AS TARGETS FOR THERAPY

Being intrinsically attractive targets for drug development, the progress in the development of DUBs inhibitors or pharmacological modulation of DUB activities, in particular, the disease ranging from oncology to neurodegeneration, have been well-reviewed (Harrigan et al., 2018). As DUBs are crucial for virus replication, and participate in multiple signaling pathways during immune response, they present ideal targets for diagnosing and treating viral infections.

Perry et al. (2012) demonstrated that WP1130, a small molecule inhibitor of a subset of cellular DUBs, displays antiviral activity against murine and human norovirus, suggesting the importance of DUBs in modulating virus replication. Compound 9, a novel small molecule inhibitor derived from WP1130, markedly reduces the replication of murine norovirus, and amplifies the Norwalk virus genome (Charbonneau et al., 2014). A set of WP1130 derivatives retain the broad-spectrum antiviral function, acting on a variety of RNA viruses, including Sindbis virus and LaCrosse virus (Gonzalez-Hernandez et al., 2014). In addition, the 2-cyano-3-acrylamide compound C6 also facilitates the suppression of intracellular replication of murine norovirus by repressing DUB activity (Passalacqua et al., 2016). Overexpression of gga-miR-30d reduces the proliferation of infectious bronchitis virus (IBV), and USP47 is a target of gga-miR-30d in cells (Li et al., 2020). The DUBs inhibitors P22077 and PR-619 targeting USP7 and USP47 impair Gag processing, thereby blocking HIV-1 replication (Setz et al., 2017).

Efforts have also been focused on developing inhibitors against virus DUBs, and some have shown promise to be efficient antiviral drugs. The inhibitors targeting EBV DUB BPLF1, or thiopurine analog 6-mercaptopurine (6MP) and 6-thioguanine (6TG) targeting SARS-CoV PLpro all have been proved to be effective and promising new therapeutic strategies (Chen et al., 2009; Atkins et al., 2020). Thiopurine analog 6MP and 6TG that have long been used in cancer chemotherapy were found not only to be specific inhibitors for the SARS-CoV PLpro but also

to be potential inhibitors of USP14 by computer docking analysis (Chen et al., 2009). GRL0617 binds to SARS-CoV PLP, abolishes its deubiquitinase activity, and thus inhibits viral replication (Ratia et al., 2008). HCMV UL48 and HSV UL36 execute DUB activity in K63 and K48 ubiquitin linkages. HCMV UL48 C24 mutant with mutations in the active site residues that completely abolish DUB activity results in a notable decrease in HCMV viral protein expression and virus proliferation (Kim et al., 2009). Furthermore, naphthalene inhibitor targeting SARS-CoV-2 PLP suppresses the activity of PLP and viral replication by interfering with its deubiquitinating activity (Ratia et al., 2006; Freitas et al., 2020).

## CONCLUSION AND PERSPECTIVE

Deubiquitinases are crucial regulators of viral replication and exert their function in multiple steps of signaling pathways to modulate host innate immune response. Among them, host-encoded DUBs play an indispensable role in PTMs, as they reverse the process of ubiquitination and allow for the fine-tuning of Ub modification. As key regulators of viral replication, host DUBs have two major functional mechanisms. First, they widely participate in innate immune pathways, deubiquitinate and stabilize critical signaling molecules, thus enhancing the strength of the antiviral immune response. Second, host DUBs interact with viral proteins that are important for replication and affect viral replication positively or negatively. In addition, viruses encode DUBs or protein domains that possess DUB activity.

In most cases, the biological function of viral DUBs is to antagonize the host immune system and ensure its proliferation. Like host DUBs, viral DUBs may also be involved in many steps of innate immune signaling to suppress their function. Moreover, viral DUBs regulate viral replication through a variety of mechanisms. Based on these biological roles, both host and viral DUBs represent potential targets for treating diseases.

For DUB-targeted therapy, more effort is needed to further elucidate the cellular pathways involving DUBs and identify DUB substrates. As only a few viral DUBs have been characterized thus far, we need to explore other viral DUBs that remain largely unknown. Moreover, chemical techniques may be employed to identify novel inhibitors of DUBs, and small-molecule antiviral drugs.

## AUTHOR CONTRIBUTIONS

QZ, WG, and QJ wrote this manuscript. WZ revised this manuscript. All authors contributed to the article and approved the submitted version.

## FUNDING

This work was supported in part by funding from the National key R&D Program of China (2021YFC2301900 and 2301904); the National Natural Science Foundation of China (81930062 and 81672004 to WZ and 31900457 to WG); the Science and Technology Department of Jilin Province (20190101003JH, 20190201272JC, and 20200201331JC); and the Key Laboratory of Molecular Virology, Jilin Province (20102209).

## REFERENCES

Akira, S., Uematsu, S., and Takeuchi, O. (2006). Pathogen recognition and innate immunity. *Cell* 124, 783–801. doi: 10.1016/j.cell.2006.02.015

Ali, A., Raja, R., Farooqui, S. R., Ahmad, S., and Banerjea, A. C. (2017). USP7 deubiquitinase controls HIV-1 production by stabilizing Tat protein. *Biochem. J.* 474, 1653–1668. doi: 10.1042/BCJ20160304

Atkins, S. L., Motaib, S., Wiser, L. C., Hopcraft, S. E., Hardy, P. B., Shackelford, J., et al. (2020). Small molecule screening identifies inhibitors of the Epstein-Barr virus deubiquitinating enzyme, BPLF1. *Antiviral Res.* 173:104649. doi: 10.1016/j.antiviral.2019.104649

Baker, R. T., Tobias, J. W., and Varshavsky, A. (1992). Ubiquitin-specific proteases of Saccharomyces cerevisiae. Cloning of UBP2 and UBP3, and functional analysis of the UBP gene family. *J. Biol. Chem.* 267, 23364–23375.

Balakirev, M. Y., Jaquinod, M., Haas, A. L., and Chroboczek, J. (2002). Deubiquitinating function of adenovirus proteinase. *J. Virol.* 76, 6323–6331. doi: 10.1128/jvi.76.12.6323-6331.2002

Barretto, N., Jukneliene, D., Ratia, K., Chen, Z., Mesecar, A. D., and Baker, S. C. (2005). The papain-like protease of severe acute respiratory syndrome coronavirus has deubiquitinating activity. *J. Virol.* 79, 15189–15198. doi: 10.1128/JVI.79.24.15189-15198.2005

Bekes, M., van der Heden, van Noort, G. J., Ekkebus, R., Ovaa, H., Huang, T. T., et al. (2016). Recognition of Lys48-Linked Di-ubiquitin and Deubiquitinating Activities of the SARS Coronavirus Papain-like Protease. *Mol. Cell* 62, 572–585. doi: 10.1016/j.molcel.2016.04.016

Bi, H. L., Zhang, X. L., Zhang, Y. L., Xie, X., Xia, Y. L., Du, J., et al. (2020). The deubiquitinase UCHL1 regulates cardiac hypertrophy by stabilizing epidermal growth factor receptor. *Sci. Adv.* 6:eaax4826. doi: 10.1126/sciadv.aax4826

Bodda, C., Reinert, L. S., Fruhwurth, S., Richardo, T., Sun, C., Zhang, B. C., et al. (2020). HSV1 VP1-2 deubiquitinates STING to block type I interferon expression and promote brain infection. *J. Exp. Med.* 217:20191422. doi: 10.1084/jem.20191422

Boutell, C., Canning, M., Orr, A., and Everett, R. D. (2005). Reciprocal activities between herpes simplex virus type 1 regulatory protein ICP0, a ubiquitin E3 ligase, and ubiquitin-specific protease USP7. *J. Virol.* 79, 12342–12354. doi: 10.1128/JVI.79.19.12342-12354.2005

Cai, J., Chen, H. Y., Peng, S. J., Meng, J. L., Wang, Y., Zhou, Y., et al. (2018). USP7-TRIM27 axis negatively modulates antiviral type I IFN signaling. *FASEB J.* 32, 5238–5249. doi: 10.1096/fj.201700473RR

Charbonneau, M. E., Gonzalez-Hernandez, M. J., Showalter, H. D., Donato, N. J., Wobus, C. E., and O'Riordan, M. X. (2014). Small molecule deubiquitinase inhibitors promote macrophage anti-infective capacity. *PLoS One* 9:e104096. doi: 10.1371/journal.pone.0104096

Chavoshi, S., Egorova, O., Lacdao, I. K., Farhadi, S., Sheng, Y., and Saridakis, V. (2016). Identification of Kaposi Sarcoma Herpesvirus (KSHV) vIRF1 Protein as a Novel Interaction Partner of Human Deubiquitinase USP7. *J. Biol. Chem.* 291, 6281–6291. doi: 10.1074/jbc.M115.710632

Chen, R., Zhang, L., Zhong, B., Tan, B., Liu, Y., and Shu, H. B. (2010). The ubiquitin-specific protease 17 is involved in virus-triggered type I IFN signaling. *Cell Res.* 20, 802–811. doi: 10.1038/cr.2010.41

Chen, X., Chou, C. Y., and Chang, G. G. (2009). Thiopurine analogue inhibitors of severe acute respiratory syndrome-coronavirus papain-like protease, a deubiquitinating and deISGylating enzyme. *Antivir. Chem. Chemother.* 19, 151–156. doi: 10.1177/095632020901900402

Chen, X., Yang, X., Zheng, Y., Yang, Y., Xing, Y., and Chen, Z. (2014). SARS coronavirus papain-like protease inhibits the type I interferon signaling

pathway through interaction with the STING-TRAF3-TBK1 complex. *Protein Cell* 5, 369–381. doi: 10.1007/s13238-014-0026-3

Chow, K. T., Gale, M. Jr., and Loo, Y. M. (2018). RIG-I and Other RNA Sensors in Antiviral Immunity. *Annu. Rev. Immunol.* 36, 667–694. doi: 10.1146/annurev-immunol-042617-053309

Clague, M. J., Barsukov, I., Coulson, J. M., Liu, H., Rigden, D. J., and Urbé, S. (2013). Deubiquitylases From Genes to Organism. *Physiol. Rev.* 93, 1289–1315. doi: 10.1152/physrev.00002.2013

Clague, M. J., Urbe, S., and Komander, D. (2019). Breaking the chains: deubiquitylating enzyme specificity begets function. *Nat. Rev. Mol. Cell Biol.* 20, 338–352. doi: 10.1038/s41580-019-0099-1

Clementz, M. A., Chen, Z., Banach, B. S., Wang, Y., Sun, L., Ratia, K., et al. (2010). Deubiquitinating and interferon antagonism activities of coronavirus papain-like proteases. *J. Virol.* 84, 4619–4629. doi: 10.1128/JVI.02406-09

Cui, J., Song, Y., Li, Y., Zhu, Q., Tan, P., Qin, Y., et al. (2014). USP3 inhibits type I interferon signaling by deubiquitinating RIG-I-like receptors. *Cell Res.* 24, 400–416. doi: 10.1038/cr.2013.170

Czech-Sioli, M., Siebels, S., Radau, S., Zahedi, R. P., Schmidt, C., Dobner, T., et al. (2020). The Ubiquitin-Specific Protease Usp7, a Novel Merkel Cell Polyomavirus Large T-Antigen Interaction Partner, Modulates Viral DNA Replication. *J. Virol.* 94:19. doi: 10.1128/JVI.01638-19

Daubeuf, S., Singh, D., Tan, Y., Liu, H., Federoff, H. J., Bowers, W. J., et al. (2009). HSV ICP0 recruits USP7 to modulate TLR-mediated innate response. *Blood* 113, 3264–3275. doi: 10.1182/blood-2008-07-168203

De Nola, R., Menga, A., Castegna, A., Loizzi, V., Ranieri, G., Cicinelli, E., et al. (2019). The Crowded Crosstalk between Cancer Cells and Stromal Microenvironment in Gynecological Malignancies: Biological Pathways and Therapeutic Implication. *Int. J. Mol. Sci.* 20:ijms20102401. doi: 10.3390/ijms20102401

Deribe, Y. L., Pawson, T., and Dikic, I. (2010). Post-translational modifications in signal integration. *Nat. Struct. Mol. Biol.* 17, 666–672. doi: 10.1038/nsmb.1842

Devaraj, S. G., Wang, N., Chen, Z., Chen, Z., Tseng, M., Barretto, N., et al. (2007). Regulation of IRF-3-dependent innate immunity by the papain-like protease domain of the severe acute respiratory syndrome coronavirus. *J. Biol. Chem.* 282, 32208–32221. doi: 10.1074/jbc.M704870200

Dong, X., Guan, J., Zheng, C., and Zheng, X. (2017). The herpes simplex virus 1 UL36USP deubiquitinase suppresses DNA repair in host cells *via* deubiquitination of proliferating cell nuclear antigen. *J. Biol. Chem.* 292, 8472–8483. doi: 10.1074/jbc.M117.778076

Everett, R. D., Meredith, M., Orr, A., Cross, A., Kathoria, M., and Parkinson, J. (1997). A novel ubiquitin-specific protease is dynamically associated with the PML nuclear domain and binds to a herpesvirus regulatory protein. *EMBO J.* 16, 1519–1530. doi: 10.1093/emboj/16.7.1519

Fan, Y., Mao, R., Yu, Y., Liu, S., Shi, Z., Cheng, J., et al. (2014). USP21 negatively regulates antiviral response by acting as a RIG-I deubiquitinase. *J. Exp. Med.* 211, 313–328. doi: 10.1084/jem.20122844

Fieulaine, S., Witte, M. D., Theile, C. S., Ayach, M., Ploegh, H. L., Jupin, I., et al. (2020). Turnip yellow mosaic virus protease binds ubiquitin suboptimally to fine-tune its deubiquitinase activity. *J. Biol. Chem*295, 13769–13783. doi: 10.1074/jbc.RA120.014628

Freitas, B. T., Durie, I. A., Murray, J., Longo, J. E., Miller, H. C., Crich, D., et al. (2020). Characterization and Noncovalent Inhibition of the Deubiquitinase and deISGylase Activity of SARS-CoV-2 Papain-Like Protease. *ACS Infect. Dis.* 6, 2099–2109. doi: 10.1021/acsinfecdis.0c00168

Friedman, C. S., O'Donnell, M. A., Legarda-Addison, D., Ng, A., Cardenas, W. B., Yount, J. S., et al. (2008). The tumour suppressor CYLD is a negative regulator of RIG-I-mediated antiviral response. *EMBO Rep.* 9, 930–936. doi: 10.1038/embor.2008.136

Frieman, M., Ratia, K., Johnston, R. E., Mesecar, A. D., and Baric, R. S. (2009). Severe acute respiratory syndrome coronavirus papain-like protease ubiquitin-like domain and catalytic domain regulate antagonism of IRF3 and NF-kappaB signaling. *J. Virol.* 83, 6689–6705. doi: 10.1128/JVI.02220-08

Fuchs, A. C. D., Maldoner, L., Wojtynek, M., Hartmann, M. D., and Martin, J. (2018). Rpn11-mediated ubiquitin processing in an ancestral archaeal ubiquitination system. *Nat. Commun.* 9:2696. doi: 10.1038/s41467-018-05198-1

Gack, M. U., Shin, Y. C., Joo, C. H., Urano, T., Liang, C., Sun, L., et al. (2007). TRIM25 RING-finger E3 ubiquitin ligase is essential for RIG-I-mediated antiviral activity. *Nature* 446, 916–920. doi: 10.1038/nature05732

Gallardo, C., Soler, A., Rodze, I., Nieto, R., Cano-Gómez, C., Fernandez-Pinero, J., et al. (2019). Attenuated and non-haemadsorbing (non-HAD) genotype II African swine fever virus (ASFV) isolated in Europe, Latvia 2017. *Transboundary Emerg. Dis.* 66, 1399–1404. doi: 10.1111/tbed.13132

García, L. L., Padilla, L., and Castaño, J. C. (2017). Inhibitors compounds of the flavivirus replication process. *Virol. J.* 14:95. doi: 10.1186/s12985-017-0761-1

Gonzalez-Hernandez, M. J., Pal, A., Gyan, K. E., Charbonneau, M. E., Showalter, H. D., Donato, N. J., et al. (2014). Chemical derivatives of a small molecule deubiquitinase inhibitor have antiviral activity against several RNA viruses. *PLoS One* 9:e94491. doi: 10.1371/journal.pone.0094491

Gu, Z., and Shi, W. (2016). Manipulation of viral infection by deubiquitinating enzymes: new players in host-virus interactions. *Future Microbiol.* 11, 1435–1446. doi: 10.2217/fmb-2016-0091

Gu, Z., Shi, W., Zhang, L., Hu, Z., and Xu, C. (2017). USP19 suppresses cellular type I interferon signaling by targeting TRAF3 for deubiquitination. *Future Microbiol.* 12, 767–779. doi: 10.2217/fmb-2017-0006

Guo, Y., Jiang, F., Kong, L., Li, B., Yang, Y., Zhang, L., et al. (2019). Cutting Edge: USP27X Deubiquitinates and Stabilizes the DNA Sensor cGAS to Regulate Cytosolic DNA-Mediated Signaling. *J. Immunol.* 203, 2049–2054. doi: 10.4049/jimmunol.1900514

Guo, Y., Jiang, F., Kong, L., Wu, H., Zhang, H., Chen, X., et al. (2020). OTUD5 promotes innate antiviral and antitumor immunity through deubiquitinating and stabilizing STING. *Cell Mol. Immunol.* 2020:5. doi: 10.1038/s41423-020-00531-5

Gupta, S., Yla-Anttila, P., Sandalova, T., Sun, R., Achour, A., and Masucci, M. G. (2019). 14-3-3 scaffold proteins mediate the inactivation of trim25 and inhibition of the type I interferon response by herpesvirus deconjugases. *PLoS Pathog.* 15:e1008146. doi: 10.1371/journal.ppat.1008146

Harrigan, J. A., Jacq, X., Martin, N. M., and Jackson, S. P. (2018). Deubiquitylating enzymes and drug discovery: emerging opportunities. *Nat. Rev. Drug Discov.* 17, 57–78. doi: 10.1038/nrd.2017.152

Hermanns, T., and Hofmann, K. (2019). Bacterial DUBs: deubiquitination beyond the seven classes. *Biochem. Soc. Transact.* 47, 1857–1866. doi: 10.1042/BST20190526

Hilterbrand, A. T., Boutz, D. R., Marcotte, E. M., and Upton, J. W. (2017). Murine Cytomegalovirus Deubiquitinase Regulates Viral Chemokine Levels To Control Inflammation and Pathogenesis. *mBio* 8:16. doi: 10.1128/mBio.01864-16

Holowaty, M. N., and Frappier, L. (2004). HAUSP/USP7 as an Epstein-Barr virus target. *Biochem. Soc. Trans.* 32(Pt 5), 731–732. doi: 10.1042/BST0320731

Holowaty, M. N., Zeghouf, M., Wu, H., Tellam, J., Athanasopoulos, V., Greenblatt, J., et al. (2003). Protein profiling with Epstein-Barr nuclear antigen-1 reveals an interaction with the herpesvirus-associated ubiquitin-specific protease HAUSP/USP7. *J. Biol. Chem.* 278, 29987–29994. doi: 10.1074/jbc.M303977200

Hu, X., Tian, J., Kang, H., Guo, D., Liu, J., Liu, D., et al. (2017). Transmissible Gastroenteritis Virus Papain-Like Protease 1 Antagonizes Production of Interferon-beta through Its Deubiquitinase Activity. *Biomed. Res. Int.* 2017:7089091. doi: 10.1155/2017/7089091

Hu, Y., Bai, X., Zhang, C., Chakrabarti, S., Tang, B., Xiong, H., et al. (2020). Ubiquitination-activating enzymes UBE1 and UBA6 regulate ubiquitination and expression of cardiac sodium channel Nav1.5. *Biochem. J.* 477, 1683–1700. doi: 10.1042/BCJ20200138

Inn, K. S., Lee, S. H., Rathbun, J. Y., Wong, L. Y., Toth, Z., Machida, K., et al. (2011). Inhibition of RIG-I-mediated signaling by Kaposi's sarcoma-associated herpesvirus-encoded deubiquitinase ORF64. *J. Virol.* 85, 10899–10904. doi: 10.1128/JVI.00690-11

Isaacson, M. K., and Ploegh, H. L. (2009). Ubiquitination, ubiquitin-like modifiers, and deubiquitination in viral infection. *Cell Host Microbe* 5, 559–570. doi: 10.1016/j.chom.2009.05.012

Ivashkiv, L. B., and Donlin, L. T. (2014). Regulation of type I interferon responses. *Nat. Rev. Immunol.* 14, 36–49. doi: 10.1038/nri3581

Jager, W., Santag, S., Weidner-Glunde, M., Gellermann, E., Kati, S., Pietrek, M., et al. (2012). The ubiquitin-specific protease USP7 modulates the replication of Kaposi's sarcoma-associated herpesvirus latent episomal DNA. *J. Virol.* 86, 6745–6757. doi: 10.1128/JVI.06840-11

Jarosinski, K., Kattenhorn, L., Kaufer, B., Ploegh, H., and Osterrieder, N. (2007). A herpesvirus ubiquitin-specific protease is critical for efficient T cell lymphoma formation. *Proc. Natl. Acad. Sci. U S A.* 104, 20025–20030. doi: 10.1073/pnas.0706295104

Jia, P., Zhang, W., Xiang, Y., Lu, X., Liu, W., Jia, K., et al. (2020). Ubiquitin-specific protease 5 was involved in the interferon response to RGNNV in sea perch

(Lateolabrax japonicus). *Fish Shellfish Immunol.* 103, 239–247. doi: 10.1016/j.fsi.2020.04.065

Jin, Y., Zhao, X., Zhang, Q., Zhang, Y., Fu, X., Hu, X., et al. (2020). Cancer-associated mutation abolishes the impact of TRIM21 on the invasion of breast cancer cells. *Int. J. Biol. Macromol.* 142, 782–789. doi: 10.1016/j.ijbiomac.2019.10.019

Kategaya, L., Di Lello, P., Rougé, L., Pastor, R., Clark, K. R., Drummond, J., et al. (2017). USP7 small-molecule inhibitors interfere with ubiquitin binding. *Nature* 550, 534–538. doi: 10.1038/nature24006

Kattenhorn, L. M., Korbel, G. A., Kessler, B. M., Spooner, E., and Ploegh, H. L. (2005). A deubiquitinating enzyme encoded by HSV-1 belongs to a family of cysteine proteases that is conserved across the family Herpesviridae. *Mol. Cell* 19, 547–557. doi: 10.1016/j.molcel.2005.07.003

Kawai, T., and Akira, S. (2011). Toll-like receptors and their crosstalk with other innate receptors in infection and immunity. *Immunity* 34, 637–650. doi: 10.1016/j.immuni.2011.05.006

Kayagaki, N., Phung, Q., Chan, S., Chaudhari, R., Quan, C., O'Rourke, K. M., et al. (2007). DUBA: a deubiquitinase that regulates type I interferon production. *Science* 318, 1628–1632. doi: 10.1126/science.1145918

Kell, A. M., and Gale, M. Jr. (2015). RIG-I in RNA virus recognition. *Virology* 47, 110–121. doi: 10.1016/j.virol.2015.02.017

Kim, E. T., Oh, S. E., Lee, Y. O., Gibson, W., and Ahn, J. H. (2009). Cleavage specificity of the UL48 deubiquitinating protease activity of human cytomegalovirus and the growth of an active-site mutant virus in cultured cells. *J. Virol.* 83, 12046–12056. doi: 10.1128/JVI.00411-09

Kiran, S., Dar, A., Singh, S. K., Lee, K. Y., and Dutta, A. (2018). The Deubiquitinase USP46 Is Essential for Proliferation and Tumor Growth of HPV-Transformed Cancers. *Mol. Cell* 72, 823.e–835.e. doi: 10.1016/j.molcel.2018.09.019

Komander, D., and Rape, M. (2012). The ubiquitin code. *Annu. Rev. Biochem.* 81, 203–229. doi: 10.1146/annurev-biochem-060310-170328

Kosulin, K., Lam, E., Heim, A., Dobner, T., and Rodriguez, E. (2018). Broad-spectrum antiviral activity of the deubiquitinase inhibitor HBX against human adenoviruses. *Antivir. Ther.* 23, 475–483. doi: 10.3851/IMP3230

Kovalenko, A., Chable-Bessia, C., Cantarella, G., Israel, A., Wallach, D., and Courtois, G. (2003). The tumour suppressor CYLD negatively regulates NF-kappaB signalling by deubiquitination. *Nature* 424, 801–805. doi: 10.1038/nature01802

Kumar, R., Khandelwal, N., Thachamvally, R., Tripathi, B. N., Barua, S., Kashyap, S. K., et al. (2018). Role of MAPK/MNK1 signaling in virus replication. *Virus Res.* 253, 48–61. doi: 10.1016/j.virusres.2018.05.028

Kumari, P., and Kumar, H. (2018). Viral deubiquitinases: role in evasion of anti-viral innate immunity. *Crit. Rev. Microbiol.* 44, 304–317. doi: 10.1080/1040841X.2017.1368999

Kumari, P., Saha, I., Narayanan, A., Narayanan, S., Takaoka, A., Kumar, N. S., et al. (2017). Essential role of HCMV deubiquitinase in promoting oncogenesis by targeting anti-viral innate immune signaling pathways. *Cell Death Dis.* 8:e3078. doi: 10.1038/cddis.2017.461

Kwon, K. M., Oh, S. E., Kim, Y. E., Han, T. H., and Ahn, J. H. (2017). Cooperative inhibition of RIP1-mediated NF-kappaB signaling by cytomegalovirus-encoded deubiquitinase and inactive homolog of cellular ribonucleotide reductase large subunit. *PLoS Pathog.* 13:e1006423. doi: 10.1371/journal.ppat.1006423

Lehoux, M., Gagnon, D., and Archambault, J. (2014). E1-mediated recruitment of a UAF1-USP deubiquitinase complex facilitates human papillomavirus DNA replication. *J. Virol.* 88, 8545–8555. doi: 10.1128/JVI.00379-14

Li, H., Li, J., Zhai, Y., Zhang, L., Cui, P., Feng, L., et al. (2020). Gga-miR-30d regulates infectious bronchitis virus infection by targeting USP47 in HD11 cells. *Microb. Pathog.* 141:103998. doi: 10.1016/j.micpath.2020.103998

Li, R., Ahmad, I., Li, S., Johnson, S., Liangliang, S., and Zheng, Y.-H. (2021). Cul3-KLHL20 E3 ubiquitin ligase plays a key role in the arms race between HIV-1 and host restriction. *Res. Square* 2021:v1. doi: 10.21203/rs.3.rs-912958/v1

Li, S. W., Wang, C. Y., Jou, Y. J., Huang, S. H., Hsiao, L. H., Wan, L., et al. (2016). SARS Coronavirus Papain-Like Protease Inhibits the TLR7 Signaling Pathway through Removing Lys63-Linked Polyubiquitination of TRAF3 and TRAF6. *Int. J. Mol. Sci.* 17:ijms17050678. doi: 10.3390/ijms17050678

Li, S., Zheng, H., Mao, A. P., Zhong, B., Li, Y., Liu, Y., et al. (2010). Regulation of virus-triggered signaling by OTUB1- and OTUB2-mediated deubiquitination of TRAF3 and TRAF6. *J. Biol. Chem.* 285, 4291–4297. doi: 10.1074/jbc.M109.074971

Liao, T. L., Wu, C. Y., Su, W. C., Jeng, K. S., and Lai, M. M. (2010). Ubiquitination and deubiquitination of NP protein regulates influenza A virus RNA replication. *EMBO J.* 29, 3879–3890. doi: 10.1038/emboj.2010.250

Lim, K. H., and Staudt, L. M. (2013). Toll-like receptor signaling. *Cold Spring Harb. Perspect. Biol.* 5:a011247. doi: 10.1101/cshperspect.a011247

Lin, R., Yang, L., Nakhaei, P., Sun, Q., Sharif-Askari, E., Julkunen, I., et al. (2006). Negative regulation of the retinoic acid-inducible gene I-induced antiviral state by the ubiquitin-editing protein A20. *J. Biol. Chem.* 281, 2095–2103. doi: 10.1074/jbc.M510326200

Lindner, H. A., Fotouhi-Ardakani, N., Lytvyn, V., Lachance, P., Sulea, T., and Menard, R. (2005). The papain-like protease from the severe acute respiratory syndrome coronavirus is a deubiquitinating enzyme. *J. Virol.* 79, 15199–15208. doi: 10.1128/JVI.79.24.15199-15208.2005

Liu, J., Jin, L., Chen, X., Yuan, Y., Zuo, Y., Miao, Y., et al. (2020). USP12 translocation maintains interferon antiviral efficacy by inhibiting CBP acetyltransferase activity. *PLoS Pathog.* 16:e1008215. doi: 10.1371/journal.ppat.1008215

Liu, N., Chai, R., Liu, B., Zhang, Z., Zhang, S., Zhang, J., et al. (2016). Ubiquitin-specific protease 14 regulates cardiac hypertrophy progression by increasing GSK-3β phosphorylation. *Biochem. Biophys. Res. Commun.* 478, 1236–1241. doi: 10.1016/j.bbrc.2016.08.100

Liuyu, T., Yu, K., Ye, L., Zhang, Z., Zhang, M., Ren, Y., et al. (2019). Induction of OTUD4 by viral infection promotes antiviral responses through deubiquitinating and stabilizing MAVS. *Cell Res.* 29, 67–79. doi: 10.1038/s41422-018-0107-6

Luo, Q., Zhang, L., Wei, F., Fang, Q., Bao, F., Mi, S., et al. (2018). mTORC1 Negatively Regulates the Replication of Classical Swine Fever Virus Through Autophagy and IRES-Dependent Translation. *iScience* 3, 87–101. doi: 10.1016/j.isci.2018.04.010

Medina, G. N., Azzinaro, P., Ramirez-Medina, E., Gutkoska, J., Fang, Y., Diaz-San Segundo, F., et al. (2020). Impairment of the DeISGylation Activity of Foot-and-Mouth Disease Virus Lpro Causes Attenuation *In Vitro* and *In Vivo*. *J. Virol.* 94:20. doi: 10.1128/JVI.00341-20

Mennerich, D., Kubaichuk, K., and Kietzmann, T. (2019). DUBs, Hypoxia, and Cancer. *Trends Cancer* 5, 632–653. doi: 10.1016/j.trecan.2019.08.005

Mevissen, T. E. T., and Komander, D. (2017). Mechanisms of Deubiquitinase Specificity and Regulation. *Annu. Rev. Biochem.* 86, 159–192. doi: 10.1146/annurev-biochem-061516-044916

Nag, D. K., and Finley, D. (2012). A small-molecule inhibitor of deubiquitinating enzyme USP14 inhibits Dengue virus replication. *Virus Res.* 165, 103–106. doi: 10.1016/j.virusres.2012.01.009

Nan, Y., Yu, Y., Ma, Z., Khattar, S. K., Fredericksen, B., and Zhang, Y. J. (2014). Hepatitis E virus inhibits type I interferon induction by ORF1 products. *J. Virol.* 88, 11924–11932. doi: 10.1128/JVI.01935-14

Nicholson, B., and Suresh Kumar, K. G. (2011). The multifaceted roles of USP7: new therapeutic opportunities. *Cell Biochem. Biophys.* 60, 61–68. doi: 10.1007/s12013-011-9185-5

Okamoto, M., Kouwaki, T., Fukushima, Y., and Oshiumi, H. (2017). Regulation of RIG-I Activation by K63-Linked Polyubiquitination. *Front. Immunol.* 8:1942. doi: 10.3389/fimmu.2017.01942

Oshiumi, H., Miyashita, M., Matsumoto, M., and Seya, T. (2013). A distinct role of Riplet-mediated K63-Linked polyubiquitination of the RIG-I repressor domain in human antiviral innate immune responses. *PLoS Pathog.* 9:e1003533. doi: 10.1371/journal.ppat.1003533

Papa, F. R., and Hochstrasser, M. (1993). The yeast DOA4 gene encodes a deubiquitinating enzyme related to a product of the human tre-2 oncogene. *Nature* 366, 313–319. doi: 10.1038/366313a0

Passalacqua, K. D., Charbonneau, M. E., Donato, N. J., Showalter, H. D., Sun, D., Wen, B., et al. (2016). Anti-infective Activity of 2-Cyano-3-Acrylamide Inhibitors with Improved Drug-Like Properties against Two Intracellular Pathogens. *Antimicrob. Agents Chemother.* 60, 4183–4196. doi: 10.1128/AAC.03021-15

Pauli, E. K., Chan, Y. K., Davis, M. E., Gableske, S., Wang, M. K., Feister, K. F., et al. (2014). The ubiquitin-specific protease USP15 promotes RIG-I-mediated antiviral signaling by deubiquitylating TRIM25. *Sci. Signal* 7:ra3. doi: 10.1126/scisignal.2004577

Peng, Y., Guo, J., Sun, T., Fu, Y., Zheng, H., Dong, C., et al. (2020). USP39 Serves as a Deubiquitinase to Stabilize STAT1 and Sustains Type I IFN-Induced Antiviral Immunity. *J. Immunol.* 205, 3167–3178. doi: 10.4049/jimmunol.1901384

Perry, J. W., Ahmed, M., Chang, K. O., Donato, N. J., Showalter, H. D., and Wobus, C. E. (2012). Antiviral activity of a small molecule deubiquitinase inhibitor occurs *via* induction of the unfolded protein response. *PLoS Pathog.* 8:e1002783. doi: 10.1371/journal.ppat.1002783

Pyeon, D., Timani, K. A., Gulraiz, F., He, J. J., and Park, I. W. (2016). Function of ubiquitin (Ub) specific protease 15 (USP15) in HIV-1 replication and viral protein degradation. *Virus Res.* 223, 161–169. doi: 10.1016/j.virusres.2016.07.009

Qi, L., Zang, H., Wu, W., Nagarkatti, P., Nagarkatti, M., Liu, Q., et al. (2020). CYLD exaggerates pressure overload-induced cardiomyopathy *via* suppressing autolysosome efflux in cardiomyocytes. *J. Mol. Cell Cardiol.* 145, 59–73. doi: 10.1016/j.yjmcc.2020.06.004

Qian, L., Zuo, Y., Deng, W., Miao, Y., Liu, J., Yuan, Y., et al. (2018). MCPIP1 is a positive regulator of type I interferons antiviral activity. *Biochem. Biophys. Res. Commun.* 498, 891–897. doi: 10.1016/j.bbrc.2018.03.076

Ratia, K., Pegan, S., Takayama, J., Sleeman, K., Coughlin, M., Baliji, S., et al. (2008). A noncovalent class of papain-like protease/deubiquitinase inhibitors blocks SARS virus replication. *Proc. Natl. Acad. Sci. U S A.* 105, 16119–16124. doi: 10.1073/pnas.0805240105

Ratia, K., Saikatendu, K. S., Santarsiero, B. D., Barretto, N., Baker, S. C., Stevens, R. C., et al. (2006). Severe acute respiratory syndrome coronavirus papain-like protease: structure of a viral deubiquitinating enzyme. *Proc. Natl. Acad. Sci. U S A.* 103, 5717–5722. doi: 10.1073/pnas.0510851103

Ren, Y., Zhao, P., Liu, J., Yuan, Y., Cheng, Q., Zuo, Y., et al. (2016). Deubiquitinase USP2a Sustains Interferons Antiviral Activity by Restricting Ubiquitination of Activated STAT1 in the Nucleus. *PLoS Pathog.* 12:e1005764. doi: 10.1371/journal.ppat.1005764

Sacco, J. J., Coulson, J. M., Clague, M. J., and Urbe, S. (2010). Emerging roles of deubiquitinases in cancer-associated pathways. *IUBMB Life* 62, 140–157. doi: 10.1002/iub.300

Saito, S., Murata, T., Kanda, T., Isomura, H., Narita, Y., Sugimoto, A., et al. (2013). Epstein-Barr virus deubiquitinase downregulates TRAF6-mediated NF-kappaB signaling during productive replication. *J. Virol.* 87, 4060–4070. doi: 10.1128/JVI.02020-12

Sarkari, F., Sanchez-Alcaraz, T., Wang, S., Holowaty, M. N., Sheng, Y., and Frappier, L. (2009). EBNA1-mediated recruitment of a histone H2B deubiquitylating complex to the Epstein-Barr virus latent origin of DNA replication. *PLoS Pathog.* 5:e1000624. doi: 10.1371/journal.ppat.1000624

Saxena, N., and Kumar, V. (2014). The HBx oncoprotein of hepatitis B virus deregulates the cell cycle by promoting the intracellular accumulation and re-compartmentalization of the cellular deubiquitinase USP37. *PLoS One* 9:e111256. doi: 10.1371/journal.pone.0111256

Scholte, F. E. M., Hua, B. L., Spengler, J. R., Dzimianski, J. V., Coleman-McCray, J. D., Welch, S. R., et al. (2019). Stable Occupancy of the Crimean-Congo Hemorrhagic Fever Virus-Encoded Deubiquitinase Blocks Viral Infection. *mBio* 10:19. doi: 10.1128/mBio.01065-19

Scholte, F. E. M., Zivcec, M., Dzimianski, J. V., Deaton, M. K., Spengler, J. R., Welch, S. R., et al. (2017). Crimean-Congo Hemorrhagic Fever Virus Suppresses Innate Immune Responses *via* a Ubiquitin and ISG15 Specific Protease. *Cell Rep.* 20, 2396–2407. doi: 10.1016/j.celrep.2017.08.040

Seo, J. H., Agarwal, E., Bryant, K. G., Caino, M. C., Kim, E. T., Kossenkov, A. V., et al. (2018). Syntaphilin Ubiquitination Regulates Mitochondrial Dynamics and Tumor Cell Movements. *Cancer Res.* 78:4215. doi: 10.1158/0008-5472.CAN-18-0595

Setz, C., Friedrich, M., Rauch, P., Fraedrich, K., Matthaei, A., Traxdorf, M., et al. (2017). Inhibitors of Deubiquitinating Enzymes Block HIV-1 Replication and Augment the Presentation of Gag-Derived MHC-I Epitopes. *Viruses* 9:v9080222. doi: 10.3390/v9080222

Shembade, N., Ma, A., and Harhaj, E. W. (2010). Inhibition of NF-kappaB signaling by A20 through disruption of ubiquitin enzyme complexes. *Science* 327, 1135–1139. doi: 10.1126/science.1182364

Shin, D., Mukherjee, R., Grewe, D., Bojkova, D., Baek, K., Bhattacharya, A., et al. (2020). Papain-like protease regulates SARS-CoV-2 viral spread and innate immunity. *Nature* 587, 657–662. doi: 10.1038/s41586-020-2601-5

Song, G., Liu, B., Li, Z., Wu, H., Wang, P., Zhao, K., et al. (2016). E3 ubiquitin ligase RNF128 promotes innate antiviral immunity through K63-linked ubiquitination of TBK1. *Nat. Immunol.* 17, 1342–1351. doi: 10.1038/ni.3588

Su, Y., Shi, P., Zhang, L., Lu, D., Zhao, C., Li, R., et al. (2018). The Superimposed Deubiquitination Effect of OTULIN and Porcine Reproductive and Respiratory Syndrome Virus (PRRSV) Nsp11 Promotes Multiplication of PRRSV. *J. Virol.* 92:18. doi: 10.1128/JVI.00175-18

Sun, C., Schattgen, S. A., Pisitkun, P., Jorgensen, J. P., Hilterbrand, A. T., Wang, L. J., et al. (2015). Evasion of innate cytosolic DNA sensing by a gammaherpesvirus facilitates establishment of latent infection. *J. Immunol.* 194, 1819–1831. doi: 10.4049/jimmunol.1402495

Sun, H., Zhang, Q., Jing, Y. Y., Zhang, M., Wang, H. Y., Cai, Z., et al. (2017). USP13 negatively regulates antiviral responses by deubiquitinating STING. *Nat. Commun.* 8:15534. doi: 10.1038/ncomms15534

Sun, L., Xing, Y., Chen, X., Zheng, Y., Yang, Y., Nichols, D. B., et al. (2012). Coronavirus papain-like proteases negatively regulate antiviral innate immune response through disruption of STING-mediated signaling. *PLoS One* 7:e30802. doi: 10.1371/journal.pone.0030802

Sun, Z., Chen, Z., Lawson, S. R., and Fang, Y. (2010). The cysteine protease domain of porcine reproductive and respiratory syndrome virus nonstructural protein 2 possesses deubiquitinating and interferon antagonism functions. *J. Virol.* 84, 7832–7846. doi: 10.1128/JVI.00217-10

Tanaka, Y., and Chen, Z. J. (2012). STING specifies IRF3 phosphorylation by TBK1 in the cytosolic DNA signaling pathway. *Sci. Signal* 5:ra20. doi: 10.1126/scisignal.2002521

Tang, Y., Joo, D., Liu, G., Tu, H., You, J., Jin, J., et al. (2018). Linear ubiquitination of cFLIP induced by LUBAC contributes to TNFα-induced apoptosis. *J. Biol. Chem.* 293, 20062–20072. doi: 10.1074/jbc.RA118.005449

Tanuma, J., Lee, K. H., Haneuse, S., Matsumoto, S., Nguyen, D. T., Nguyen, D. T., et al. (2016). Incidence of AIDS-Defining Opportunistic Infections and Mortality during Antiretroviral Therapy in a Cohort of Adult HIV-Infected Individuals in Hanoi, 2007-2014. *PLoS One* 11:e0150781. doi: 10.1371/journal.pone.0150781

Tchesnokov, E. P., Bailey-Elkin, B. A., Mark, B. L., and Gotte, M. (2020). Independent inhibition of the polymerase and deubiquitinase activities of the Crimean-Congo Hemorrhagic Fever Virus full-length L-protein. *PLoS Negl. Trop. Dis.* 14:e0008283. doi: 10.1371/journal.pntd.0008283

Thomas, D. L. (2019). Global Elimination of Chronic Hepatitis. *New Engl. J. Med.* 380, 2041–2050. doi: 10.1056/NEJMra1810477

Tobias, J. W., and Varshavsky, A. (1991). Cloning and functional analysis of the ubiquitin-specific protease gene UBP1 of Saccharomyces cerevisiae. *J. Biol. Chem.* 266, 12021–12028. doi: 10.1016/s0021-9258(18)99059-9

Trompouki, E., Hatzivassiliou, E., Tsichritzis, T., Farmer, H., Ashworth, A., and Mosialos, G. (2003). CYLD is a deubiquitinating enzyme that negatively regulates NF-kappaB activation by TNFR family members. *Nature* 424, 793–796. doi: 10.1038/nature01803

van Gent, M., Braem, S. G., de Jong, A., Delagic, N., Peeters, J. G., Boer, I. G., et al. (2014). Epstein-Barr virus large tegument protein BPLF1 contributes to innate immune evasion through interference with toll-like receptor signaling. *PLoS Pathog.* 10:e1003960. doi: 10.1371/journal.ppat.1003960

van Kasteren, P. B., Bailey-Elkin, B. A., James, T. W., Ninaber, D. K., Beugeling, C., Khajehpour, M., et al. (2013). Deubiquitinase function of arterivirus papain-like protease 2 suppresses the innate immune response in infected host cells. *Proc. Natl. Acad. Sci. U S A.* 110, E838–E847. doi: 10.1073/pnas.1218464110

van Kasteren, P. B., Beugeling, C., Ninaber, D. K., Frias-Staheli, N., van Boheemen, S., Garcia-Sastre, A., et al. (2012). Arterivirus and nairovirus ovarian tumor domain-containing Deubiquitinases target activated RIG-I to control innate immune signaling. *J. Virol.* 86, 773–785. doi: 10.1128/JVI.06277-11

Wang, D., Fang, L., Li, P., Sun, L., Fan, J., Zhang, Q., et al. (2011). The leader proteinase of foot-and-mouth disease virus negatively regulates the type I interferon pathway by acting as a viral deubiquitinase. *J. Virol.* 85, 3758–3766. doi: 10.1128/JVI.02589-10

Wang, G., Chen, G., Zheng, D., Cheng, G., and Tang, H. (2011). PLP2 of mouse hepatitis virus A59 (MHV-A59) targets TBK1 to negatively regulate cellular type I interferon signaling pathway. *PLoS One* 6:e17192. doi: 10.1371/journal.pone.0017192

Wang, H., Lai, Y., Mathis, B. J., Wang, W., Li, S., Qu, C., et al. (2015). Deubiquitinating enzyme CYLD mediates pressure overload-induced cardiac maladaptive remodeling and dysfunction *via* downregulating Nrf2. *J. Mol. Cell Cardiol.* 84, 143–153. doi: 10.1016/j.yjmcc.2015.04.012

Wang, J., Loveland, A. N., Kattenhorn, L. M., Ploegh, H. L., and Gibson, W. (2006). High-molecular-weight protein (pUL48) of human cytomegalovirus is a competent deubiquitinating protease: mutant viruses altered in its active-site cysteine or histidine are viable. *J. Virol.* 80, 6003–6012. doi: 10.1128/JVI.00401-06

Wang, L., and Dent, S. Y. (2014). Functions of SAGA in development and disease. *Epigenomics* 6, 329–339. doi: 10.2217/epi.14.22

Wang, L., Zhao, W., Zhang, M., Wang, P., Zhao, K., Zhao, X., et al. (2013). USP4 positively regulates RIG-I-mediated antiviral response through deubiquitination and stabilization of RIG-I. *J. Virol.* 87, 4507–4515. doi: 10.1128/JVI.00031-13

Wang, S., Wang, K., Li, J., and Zheng, C. (2013). Herpes simplex virus 1 ubiquitin-specific protease UL36 inhibits beta interferon production by deubiquitinating TRAF3. *J. Virol.* 87, 11851–11860. doi: 10.1128/JVI.01211-13

Wang, Y. Y., Li, L., Han, K. J., Zhai, Z., and Shu, H. B. (2004). A20 is a potent inhibitor of TLR3- and Sendai virus-induced activation of NF-kappaB and ISRE and IFN-beta promoter. *FEBS Lett.* 576, 86–90. doi: 10.1016/j.febslet.2004.08.071

Wertz, I. E., O'Rourke, K. M., Zhou, H., Eby, M., Aravind, L., Seshagiri, S., et al. (2004). De-ubiquitination and ubiquitin ligase domains of A20 downregulate NF-kappaB signalling. *Nature* 430, 694–699. doi: 10.1038/nature02794

Whitehurst, C. B., Ning, S., Bentz, G. L., Dufour, F., Gershburg, E., Shackelford, J., et al. (2009). The Epstein-Barr virus (EBV) deubiquitinating enzyme BPLF1 reduces EBV ribonucleotide reductase activity. *J. Virol.* 83, 4345–4353. doi: 10.1128/JVI.02195-08

Whitehurst, C. B., Vaziri, C., Shackelford, J., and Pagano, J. S. (2012). Epstein-Barr virus BPLF1 deubiquitinates PCNA and attenuates polymerase eta recruitment to DNA damage sites. *J. Virol.* 86, 8097–8106. doi: 10.1128/JVI.00588-12

Wilkinson, K. D. (1997). Regulation of ubiquitin-dependent processes by deubiquitinating enzymes. *FASEB J.* 11, 1245–1256. doi: 10.1096/fasebj.11.14.9409543

Wu, C., Shi, B., Yang, D., Zhang, K., Li, J., Wang, J., et al. (2020). Porcine Reproductive and Respiratory Syndrome Virus Promotes SLA-DR-Mediated Antigen Presentation of Nonstructural Proteins To Evoke a Nonneutralizing Antibody Response <em>*In Vivo*</em>. *J. Virol.* 94, e1423–e1420. doi: 10.1128/JVI.01423-20

Xiao, Z., Chang, L., Kim, J., Zhang, P., Hang, Q., Yap, S., et al. (2019). USP37 is a SNAI1 deubiquitinase. *Am. J. Cancer Res.* 9, 2749–2759.

Xing, Y., Chen, J., Tu, J., Zhang, B., Chen, X., Shi, H., et al. (2013). The papain-like protease of porcine epidemic diarrhea virus negatively regulates type I interferon pathway by acting as a viral deubiquitinase. *J. Gen. Virol.* 94(Pt 7), 1554–1567. doi: 10.1099/vir.0.051169-0

Xue, Q., Liu, H., Zhu, Z., Yang, F., Xue, Q., Cai, X., et al. (2018). Seneca Valley Virus 3C protease negatively regulates the type I interferon pathway by acting as a viral deubiquitinase. *Antiviral Res.* 160, 183–189. doi: 10.1016/j.antiviral.2018.10.028

Yamamoto, V., Bolanos, J. F., Fiallos, J., Strand, S. E., Morris, K., Shahrokhinia, S., et al. (2020). COVID-19: Review of a 21st Century Pandemic from Etiology to Neuro-psychiatric Implications. *J. Alzheimer's Dis.* 77, 459–504. doi: 10.3233/JAD-200831

Yang, W.-L., Jin, G., Li, C.-F., Jeong, Y. S., Moten, A., Xu, D., et al. (2013). Cycles of Ubiquitination and Deubiquitination Critically Regulate Growth Factor–Mediated Activation of Akt Signaling. *Sci. Signal.* 6:ra3. doi: 10.1126/scisignal.2003197

Yang, X., Chen, X., Bian, G., Tu, J., Xing, Y., Wang, Y., et al. (2014). Proteolytic processing, deubiquitinase and interferon antagonist activities of Middle East respiratory syndrome coronavirus papain-like protease. *J. Gen. Virol.* 95(Pt 3), 614–626. doi: 10.1099/vir.0.059014-0

Ye, L., Zhang, Q., Liuyu, T., Xu, Z., Zhang, M. X., Luo, M. H., et al. (2019). USP49 negatively regulates cellular antiviral responses *via* deconjugating K63-linked ubiquitination of MITA. *PLoS Pathog.* 15:e1007680. doi: 10.1371/journal.ppat.1007680

Ye, R., Su, C., Xu, H., and Zheng, C. (2017). Herpes Simplex Virus 1 Ubiquitin-Specific Protease UL36 Abrogates NF-kappaB Activation in DNA Sensing Signal Pathway. *J. Virol.* 91:16. doi: 10.1128/JVI.02417-16

Yu, Z., Song, H., Jia, M., Zhang, J., Wang, W., Li, Q., et al. (2017). USP1-UAF1 deubiquitinase complex stabilizes TBK1 and enhances antiviral responses. *J. Exp. Med.* 214, 3553–3563. doi: 10.1084/jem.20170180

Yuan, H., You, J., You, H., and Zheng, C. (2018). Herpes Simplex Virus 1 UL36USP Antagonizes Type I Interferon-Mediated Antiviral Innate Immunity. *J. Virol.* 92:18. doi: 10.1128/JVI.01161-18

Yuan, L., Chen, Z., Song, S., Wang, S., Tian, C., Xing, G., et al. (2015). p53 degradation by a coronavirus papain-like protease suppresses type I interferon signaling. *J. Biol. Chem.* 290, 3172–3182. doi: 10.1074/jbc.M114.619890

Yuan, T., Yan, F., Ying, M., Cao, J., He, Q., Zhu, H., et al. (2018). Inhibition of Ubiquitin-Specific Proteases as a Novel Anticancer Therapeutic Strategy. *Front. Pharmacol.* 9:1080. doi: 10.3389/fphar.2018.01080

Zhang, H., Wang, D., Zhong, H., Luo, R., Shang, M., Liu, D., et al. (2015). Ubiquitin-specific Protease 15 Negatively Regulates Virus-induced Type I Interferon Signaling *via* Catalytically-dependent and -independent Mechanisms. *Sci. Rep.* 5:11220. doi: 10.1038/srep11220

Zhang, L., Wei, N., Cui, Y., Hong, Z., Liu, X., Wang, Q., et al. (2018b). The deubiquitinase CYLD is a specific checkpoint of the STING antiviral signaling pathway. *PLoS Pathog.* 14:e1007435. doi: 10.1371/journal.ppat.1007435

Zhang, L., Liu, J., Qian, L., Feng, Q., Wang, X., Yuan, Y., et al. (2018a). Induction of OTUD1 by RNA viruses potently inhibits innate immune responses by promoting degradation of the MAVS/TRAF3/TRAF6 signalosome. *PLoS Pathog.* 14:e1007067. doi: 10.1371/journal.ppat.1007067

Zhang, L., Zhao, X., Zhang, M., Zhao, W., and Gao, C. (2014). Ubiquitin-specific protease 2b negatively regulates IFN-beta production and antiviral activity by targeting TANK-binding kinase 1. *J. Immunol.* 193, 2230–2237. doi: 10.4049/jimmunol.1302634

Zhang, M., Lee, A. J., Wu, X., and Sun, S. C. (2011). Regulation of antiviral innate immunity by deubiquitinase CYLD. *Cell Mol. Immunol.* 8, 502–504. doi: 10.1038/cmi.2011.42

Zhang, M., Wu, X., Lee, A. J., Jin, W., Chang, M., Wright, A., et al. (2008). Regulation of IkappaB kinase-related kinases and antiviral responses by tumor suppressor CYLD. *J. Biol. Chem.* 283, 18621–18626. doi: 10.1074/jbc.M801451200

Zhang, M., Zhang, M. X., Zhang, Q., Zhu, G. F., Yuan, L., Zhang, D. E., et al. (2016). USP18 recruits USP20 to promote innate antiviral response through deubiquitinating STING/MITA. *Cell Res.* 26, 1302–1319. doi: 10.1038/cr.2016.125

Zhang, Z., Fang, X., Wu, X., Ling, L., Chu, F., Li, J., et al. (2020). Acetylation-Dependent Deubiquitinase OTUD3 Controls MAVS Activation in Innate Antiviral Immunity. *Mol. Cell* 79:e307. doi: 10.1016/j.molcel.2020.06.020

Zheng, D., Chen, G., Guo, B., Cheng, G., and Tang, H. (2008). PLP2, a potent deubiquitinase from murine hepatitis virus, strongly inhibits cellular type I interferon production. *Cell Res.* 18, 1105–1113. doi: 10.1038/cr.2008.294

Zheng, N., and Shabek, N. (2017). Ubiquitin Ligases: Structure, Function, and Regulation. *Annu. Rev. Biochem.* 86, 129–157. doi: 10.1146/annurev-biochem-060815-014922

Zheng, Y., and Gao, C. (2020). Fine-tuning of antiviral innate immunity by ubiquitination. *Adv. Immunol.* 145, 95–128. doi: 10.1016/bs.ai.2019.11.004

Zhong, B., Liu, X., Wang, X., Liu, X., Li, H., Darnay, B. G., et al. (2013). Ubiquitin-specific protease 25 regulates TLR4-dependent innate immune responses through deubiquitination of the adaptor protein TRAF3. *Sci. Signal.* 6:ra35. doi: 10.1126/scisignal.2003708

Zhou, S., Ge, X., Kong, C., Liu, T., Liu, A., Gao, P., et al. (2019). Characterizing the PRRSV nsp2 Deubiquitinase Reveals Dispensability of Cis-Activity for Replication and a Link of nsp2 to Inflammation Induction. *Viruses* 11:v11100896. doi: 10.3390/v11100896

Zhu, Z., Li, W., Zhang, X., Wang, C., Gao, L., Yang, F., et al. (2020). Foot-and-Mouth Disease Virus Capsid Protein VP1 Interacts with Host Ribosomal Protein SA To Maintain Activation of the MAPK Signal Pathway and Promote Virus Replication. *J. Virol.* 94, e1350–e1319. doi: 10.1128/JVI.01350-19

**Conflict of Interest:** The authors declare that the research was conducted in the absence of any commercial or financial relationships that could be construed as a potential conflict of interest.

**Publisher's Note:** All claims expressed in this article are solely those of the authors and do not necessarily represent those of their affiliated organizations, or those of the publisher, the editors and the reviewers. Any product that may be evaluated in this article, or claim that may be made by its manufacturer, is not guaranteed or endorsed by the publisher.

*Copyright © 2022 Zhang, Jia, Gao and Zhang. This is an open-access article distributed under the terms of the Creative Commons Attribution License (CC BY). The use, distribution or reproduction in other forums is permitted, provided the original author(s) and the copyright owner(s) are credited and that the original publication in this journal is cited, in accordance with accepted academic practice. No use, distribution or reproduction is permitted which does not comply with these terms.*

frontiers in Microbiology

ORIGINAL RESEARCH
published: 28 February 2022
doi: 10.3389/fmicb.2022.862352

# Isolation and Genetic Characterization of Parvoviruses From Dogs, Cats, Minks, and Raccoon Dogs in the Eastern Region of Shandong Province, China

*Jiakai Zhao[1,2], Hao Zhang[1,2], Lu Zhang[1,2], Qiang Zhang[1,2], Ning Zhou[1,2], Taofeng Du[1,2], Qin Zhao[1,2], En-Min Zhou[1,2], Yongkun Du[3]* and Yani Sun[1,2]**

[1]Department of Preventive Veterinary Medicine, College of Veterinary Medicine, Northwest Agriculture and Forestry University, Yangling, China, [2]Scientific Observing and Experimental Station of Veterinary Pharmacology and Diagnostic Technology, Ministry of Agriculture, Yangling, China, [3]College of Veterinary Medicine, Henan Agricultural University, Zhengzhou, China

OPEN ACCESS

**Edited by:**
Chunfu Zheng,
University of Calgary, Canada

**Reviewed by:**
Gaopeng Hou,
Washington University School of Medicine in St. Louis, United States
Biyun Xue,
The University of Iowa, United States

***Correspondence:**
Yongkun Du
mututushen@163.com
Yani Sun
sunyani@nwsuaf.edu.cn

**Specialty section:**
This article was submitted to Virology, a section of the journal Frontiers in Microbiology

**Received:** 25 January 2022
**Accepted:** 03 February 2022
**Published:** 28 February 2022

**Citation:**
Zhao J, Zhang H, Zhang L, Zhang Q, Zhou N, Du T, Zhao Q, Zhou E-M, Du Y and Sun Y (2022) Isolation and Genetic Characterization of Parvoviruses From Dogs, Cats, Minks, and Raccoon Dogs in the Eastern Region of Shandong Province, China. Front. Microbiol. 13:862352. doi: 10.3389/fmicb.2022.862352

The eastern region of Shandong province, China, is an intensive economic mink and raccoon dog breeding area. To investigate the molecular variations of parvovirus in cats, dogs, minks, and raccoon dogs from this region, feline panleukopenia virus (FPV), canine parvovirus 2 (CPV-2), mink enteritis virus (MEV), and raccoon dog parvovirus (RDPV) were separately isolated and characterized from the respective animals with gastroenteritis. PCR amplification showed that there were 15/18 (83.3%), 9/13 (69.2%), 8/11 (72.7%), and 3/7 (42.9%) samples from the diseased animals separately positive for FPV, CPV-2, MEV, and RDPV. Of these, a total of six FPV, six MEV, four CPV-2, and three RDPV strains were successfully isolated using F81 cells. Next, the near-complete genomes of 19 parvovirus isolates were amplified and analyzed. The viral particle 2 (VP2) sequence alignment showed that they shared 97.2–100% nucleotide similarity. Phylogenetic analysis showed that the five FPV isolates were in the same branch, and an FPV isolate was closely related with MEV and RDPV isolates obtained in this study. These suggested that cross-species infection occurred in the Shandong region between the FPV, MEV, and RDPV. For the four CPV-2 isolates, three were antigenic variant strains CPV-2a, and the other was antigenic variant strain CPV-2c. Additionally, the mutations that had emerged in the VP2 amino acids of CPV-2 also occurred in the VP2 from the FPV, MEV, and RDPV isolates. This study suggested that the continuous evolution of the parvovirus may be accelerated in areas with a high density of economic animal trading/breeding, and controlling parvovirus infection in these animals remains a challenge.

**Keywords: canine parvovirus 2, feline panleukopenia virus, genetic characterization, mink enteritis virus, raccoon dog parvovirus, phylogenetic analysis**

## INTRODUCTION

*Parvoviridae* is divided into the three subfamilies: *Parvovirinae*, *Densovirinae,* and *Hamaparparvovirinae*, and these are distinguished primarily by their respective ability to infect vertebrate and arthropod hosts.[1] Feline panleukopenia virus (FPV), canine parvovirus 2 (CPV-2), mink enteritis virus (MEV), and raccoon dog parvovirus (RDPV) belong to the species *Carnivore protoparvovirus 1* (genus *Protoparvovirus*, family *Parvovirinae*; Cotmore et al., 2019). They are all autonomous, linear, single-stranded, and negative-sense DNA viruses with a genome of approximately 5 kb (Johnson et al., 1974; Ohshima and Mochizuki, 2009). The four viruses are very closely related, showing more than 98% genome similarity (Battilani et al., 2011; Cotmore et al., 2014, 2019). The complete viral genome contains two large open reading frames encoding for two structural (VP1 and VP2) and two non-structural (NS1 and NS2) proteins (Reed et al., 1988). The VP2 protein contains the primary antigenic epitopes of viral particles and plays an important role in viral pathogenicity and hosts ranges (Truyen, 2006).

Feline panleukopenia, a disease of cats caused by FPV, was initially reported in the 1920s and can infect many species within the *Carnivora* order, including cats, dogs, minks, raccoon dogs, and foxes (Steinel et al., 2000). As a highly contagious sickness occurring in cats, FPV infection causes severe leukopenia and gastroenteritis (Steinel et al., 2001; Muz et al., 2012). In 1952, MEV, the causative pathogen of viral enteritis in minks, was characterized (Wills, 1952; Yuan et al., 2014). In the 1970s, it was documented that MEV was serologically and biochemically related to FPV and a variant strain of FPV (Parrish, 1990). As a variant of feline parvovirus, CPV-2 was first recognized in the mid-1970s and was shown to cause severe fatal epizootics of gastroenteritis in dogs (Appel et al., 1979; Truyen, 1999; Hoelzer and Parrish, 2010). Three variants of CPV-2, CPV-2a, CPV-2b, and CPV-2c have been identified worldwide (Li et al., 2019). It also had a broad host range and naturally infected cats (*Felis catus*), raccoons (*Procyon lotor*), and raccoon dogs (*Nyctereutes procyonoides*; Allison et al., 2012). RDPV was first isolated from raccoon dogs in China in 2018 and is known as a variant of CPV-2 (Jia-Yu et al., 2018). Once the raccoon dog is infected with parvovirus, it experiences severe enteritis, including vomiting, hemorrhagic diarrhea, depression, loss of appetite, and dehydration (Jia-Yu et al., 2018). The infections caused by these four viruses seriously affect the health of pets and the development of particular economic animal industries in China (Barker et al., 1983; Steinel et al., 2001). In addition, it was documented that the CPV-2 can infect species among dogs, cats, minks, and raccoon dogs, and FPV can infect species among cats and minks, particularly in areas where special economic animals are intensively raised, which presents a considerable challenge for the prevention and control of the four diseases (Truyen et al., 1995; Lu et al., 2020).

The eastern region of Shandong province in China is an intensive area of economic mink and raccoon dog breeding. Between 2018 and 2019, the incidence of gastroenteritis in dogs, cats, minks, and raccoon dogs in this area increased, resulting in major economic consequences. In the present study, the fecal samples from the diseased cats and dogs and intestinal samples from the minks and raccoon dogs from this area were collected and used to isolate parvovirus. Next, the genetic characterizations of these isolated parvoviruses were analyzed.

[1]http://www.ictv.global/report/parvoviridae

**TABLE 1** | Primers used in this study.

| Primers | Sequences (5′–3′) | Size (bp) |
|---|---|---|
| VP2-S1 | GGATTTCTACGGGTACTTTC | 571 |
| VP2-S2 | GGTGTGCCACTAGTTCCAGTAT | |
| P1 | GTCTGGCAACCAGTATACTGAGG | 2,400 |
| P2 | GATGTTGATGGATGATCTGG | |
| P3 | TCTCGCCAGCAGATCAACGCTT | 2,026 |
| P4 | CATAAAAACATAGTAAGTATG | |

## MATERIALS AND METHODS

### Ethics Statement

Based on the Guide for the Care and Use of Laboratory Animals of the Northwest Agriculture and Forestry University (NWAFU) recommendations, the clinical samples were collected for processing. The protocols were approved by the IACUC of NWAFU (approval no. 20180014/02).

### Cells and Samples

F81 cells were purchased from American Type Culture Collection, cultured in RPMI 1640 (Biological Industries) supplemented with 10% fetal bovine serum (FBS; Gibco; Thermo Fisher Scientific, Inc.), in a humidified incubator at 37°C with 5% $CO_2$.

Between 2018 and 2019, 18 fecal samples from cats and 13 samples from dogs were collected from the Veterinary Hospital in the eastern region of Shandong province, China. The cats and dogs exhibited diarrhea, emesis, and dehydration, which approximately accounts for 11.5% of the hospital cases. In addition, the 11 minks from which intestinal samples were obtained and the seven raccoon dogs also exhibited diarrhea and were collected from seven farms with the amount of livestock being 1860 minks and 395 raccoon dogs also located in the Shandong province; the Veterinary Hospital is located near these farms. All samples were first emulsified in 1 ml 0.1 M phosphate-buffered saline (pH 7.4) and centrifuged at 3,500 *g* for 10 min at 4°C. Next, the supernatants were collected and used for DNA extraction and virus isolation.

### Detection of Viral DNA From the Samples

First, universal primer pairs were designed for detecting the viral DNA of FPV, CPV-2, MEV, and RDPV. Based on the highly conserved VP2 gene of the four viral genomes, a primer pair (VP2-S1 and VP2-S2) was designed and synthesized (**Table 1**). The expected size of amplification with the primers was approximately 571 base pairs (bp). Second, the total viral DNA was extracted

from 200 µl of the supernatants mentioned above from the samples after processing using the EasyPure Viral DNA/RNA kit (TransGen Biotech, CO., Ltd.) to the manufacturer's instructions. Briefly, the unique lysate was used to cleave the virus and release DNA, which was adsorbed by a silica gel-membrane centrifuge column (TransGen Biotech, CO., Ltd.) and centrifuged with 10,000 *g* for 2 min at 4°C to purify viral DNA effectively. The target DNA fragments were amplified by PCR using the primer pairs VP2-S1 and VP2-S2. The PCR reaction consisted of 1 U TransTaq® HiFi DNA Polymerase (TransGen Biotech, Co., Ltd.), 5 µl TransTaq® HiFi Buffer 10 X (TransGen Biotech, Co., Ltd.), 10 mM each dNTP (4 µl, TransGen Biotech, Co., Ltd.), 100 ng viral DNA, and 10 µM of each primer (1 µl). The amplification conditions were as follows: Initial denaturation at 94°C for 5 min; followed by 34 cycles of denaturation at 94°C for 30 s, annealing at 55°C for 35 s and extension at 72°C for 35 s; and with a final extension of 72°C for 5 min. The PCR products were analyzed by electrophoresis using a 1% agarose gel and sequenced by TINGKE Biological Technology Company. The obtained sequences were analyzed for genetic identification by performing BLAST searches.[2]

## Viral Isolation

To isolate the virus, the supernatants from the clinical samples positive on PCR detection were filtered through a 0.22-µm Millipore filter (Millipore Sigma) and subsequently inoculated into F81 cells of $2 \times 10^7$ cells in a final volume of 100 µl. The inoculated cells were maintained with 3% FBS at 37°C in a humidified 5% $CO_2$ incubator and monitored daily for the cytopathic effects (CPEs), including floating, rounding, or disintegration. When a CPE was observed in 80% of the inoculated cells, the cells were collected and freeze-thawed three times. After centrifugation with 8,000 *g* for 10 min at 4°C, the virus's supernatants were collected and stored −80°C. If no CPE was observed in the inoculated cells, the supernatants were further inoculated until a CPE was observed. All supernatants were added to F81 cells for five passages. Next, an indirect immunofluorescence assay (IFA) was performed on the F81 cells inoculated with the five-passaged supernatants for confirming viral isolation. In addition, the five-passaged supernatants were also assessed for viral DNA by PCR as described above.

## Immunofluorescence Assay

To confirm that the virus had been successfully isolated and had infected the cells, IFA was performed. Briefly, after the F81 cells in the six-well plates were inoculated and cultured with the supernatants containing the virus for 2 days, they were fixed for 30 min at 4°C with pre-cooled 70% ethanol. Then, the cells were incubated in 1% BSA for 1 h at 37°C to block non-specific protein–protein interactions. Subsequently, the cells were incubated with mouse anti-CPV-2 monoclonal antibodies cross-reacting with FPV, MEV, and RDPV (Qianxun Biological Company, catalog. no: Ab-015) using the dilution of 1:50 overnight at 4°C. The secondary antibody used was a FITC-goat anti-mouse IgG antibody (Jackson ImmunoResearch Laboratories, Inc., catalog. no: 115–035\ u2013003) with a dilution of 1:200 and incubated for 1 h at 37°C. Finally, a fluorescent strain (4′,6-diamidino-2-phenylindole, DAPI) for 5 min at room temperature was used to stain the cell nucleus. The cells were observed under a fluorescence microscope with a 10× objective (Leica AF6000, Germany).

## Amplification of the Near-Complete Genome of the Four Viruses

To amplify the near-complete genome of FPV, CPV-2, MEV, and RDPV isolated in the present study, the two primer pairs (P1, P2, P3, and P4) were designed based on the reference sequences in GenBank (accession no. MH106700). The sequences of the primers are shown in **Table 1**. The expected product size was 2,400 bp with the primers P1 and P2 and 2,026 bp with the primers P3 and P4. PCR was performed as described above for detecting the viral DNA from the five-passaged supernatants, with the only difference being the viral template DNA. The conditions for PCR amplification were also the same as that described above, except that the 35 s of extension time was extended to 1 min. The positive PCR products were purified using an *EasyPure*® PCR Purification kit (TransGen Biotech, Co., Ltd.) and then cloned into a pMD-19-T vector (Takara Bio, Inc.) based on the manufacturer's protocol. The plasmids were transformed into competent *Escherichia coli* DH5α cells. For sequencing, the positive clones were sent to Sangon Biotech, Co., Ltd. The near-complete genomic sequences were edited and assembled using the EditSeq program 7.1.0 of the Lasergene software package (DNASTAR, Madison, WI, United States). All the sequences were determined from at least three independent PCR products.

## Sequences and Phylogenetic Analysis

Based on the near-complete genome, the phylogenetic tree was constructed using the sequences obtained in the present study and partially referenced sequences from GenBank using the neighbor-joining method in MEGA 6.0 software. The GenBank accession nos. of the FPV, CPV-2, MEV, and RDPV sequences are shown in **Table 2**. The robustness of the tree was assessed by bootstrap analyses using 1,000 re-samplings of the data.

In addition, the complete VP2 gene sequences were also obtained by editing from the near-complete genome. Next, the amino acid sequences of the VP2 protein were determined by the translation of the VP2 gene using the EditSeq program. The obtained amino acid sequences of the VP2 protein from the present study and GenBank were aligned using the MegAlign program 7.1.0 of the Lasergene software package (DNASTAR, Madison, WI). Furthermore, the phylogenetic tree based on the VP2 amino acid sequences was constructed using MEGA 6.0 software with 1,000 bootstrap replications (Tamura et al., 2007). The accessions nos. of the sequences downloaded from the GenBank are shown in **Figure 1**.

# RESULTS

## Genetic Identification of FPV, CPV-2, MEV, and RDPV From the Clinical Samples

A total of 18 clinical fecal samples from the cats were tested for the target gene of FPV by PCR, and the results showed that the

[2]http://www.ncbi.nlm.nih.gov/BLAST

**TABLE 2** | Nucleotide and amino acid homology of the isolates.

| Isolates | | Identity (%) | | | | | | | | | | | | | | | | | | |
|---|---|---|---|---|---|---|---|---|---|---|---|---|---|---|---|---|---|---|---|---|
| | Accession number | 1 | 2 | 3 | 4 | 5 | 6 | 7 | 8 | 9 | 10 | 11 | 12 | 13 | 14 | 15 | 16 | 17 | 18 | 19 |
| CPV-SD/2019/1 | OK384305 | | 100 | 99.8 | 99.3 | 99.3 | 98.3 | 98.3 | 98.3 | 98.3 | 98.3 | 98.5 | 99.0 | 99.1 | 99.1 | 99.1 | 99.1 | 99.1 | 99.0 | 99.0 |
| CPV-SD/2019/2 | OK384306 | 100 | | 99.8 | 99.3 | 99.3 | 98.3 | 98.3 | 98.3 | 98.3 | 98.3 | 98.5 | 99.0 | 99.1 | 99.1 | 99.1 | 99.1 | 99.1 | 99.0 | 99.0 |
| CPV-SD/2019/3 | OK384307 | 100 | 100 | | 99.0 | 99.1 | 98.1 | 98.1 | 98.1 | 98.1 | 98.1 | 98.3 | 98.9 | 99.0 | 99.0 | 99.0 | 99.0 | 98.9 | 98.9 | 98.9 |
| CPV-SD/2019/4 | OK384308 | 99.3 | 99.3 | 99.3 | | 98.7 | 98.0 | 98.0 | 98.0 | 98.0 | 98.0 | 97.9 | 98.5 | 98.6 | 98.6 | 98.6 | 98.6 | 98.7 | 98.5 | 98.5 |
| FPV-SD/2019/1 | OK384309 | 99.1 | 99.1 | 99.1 | 98.8 | | 98.0 | 98.0 | 98.0 | 98.0 | 98.0 | 99.1 | 99.7 | 99.8 | 99.8 | 99.8 | 99.8 | 98.8 | 99.6 | 99.6 |
| FPV-SD/2019/2 | OK384310 | 97.4 | 97.4 | 97.4 | 97.1 | 97.6 | | 100 | 100 | 100 | 100 | 97.2 | 97.7 | 97.9 | 97.8 | 97.9 | 97.9 | 98.6 | 97.7 | 97.7 |
| FPV-SD/2019/3 | OK384311 | 97.4 | 97.4 | 97.4 | 97.1 | 97.6 | 100 | | 100 | 100 | 100 | 97.2 | 97.7 | 97.9 | 97.8 | 97.9 | 97.9 | 98.6 | 97.7 | 97.7 |
| FPV-SD/2019/4 | OK384312 | 97.4 | 97.4 | 97.4 | 97.1 | 97.6 | 100 | 100 | | 100 | 100 | 97.2 | 97.7 | 97.9 | 97.8 | 97.9 | 97.9 | 98.6 | 97.7 | 97.7 |
| FPV-SD/2019/5 | OK384313 | 97.4 | 97.4 | 97.4 | 97.1 | 97.6 | 100 | 100 | 100 | | 100 | 97.2 | 97.7 | 97.9 | 97.8 | 97.9 | 97.9 | 98.6 | 97.7 | 97.7 |
| FPV-SD/2019/6 | OK384314 | 97.4 | 97.4 | 97.4 | 97.1 | 97.6 | 100 | 100 | 100 | 100 | | 97.2 | 97.7 | 97.9 | 97.8 | 97.9 | 97.9 | 98.6 | 97.7 | 97.7 |
| MEV-SD/2019/1 | OK384315 | 97.4 | 97.4 | 97.4 | 97.1 | 98.3 | 95.9 | 95.9 | 95.9 | 95.9 | 95.9 | | 99.1 | 99.3 | 99.3 | 99.3 | 99.3 | 98.0 | 99.1 | 99.1 |
| MEV-SD/2019/2 | OK384316 | 98.8 | 98.8 | 98.8 | 98.5 | 99.7 | 97.3 | 97.3 | 97.3 | 97.3 | 97.3 | 98.3 | | 99.8 | 99.9 | 99.8 | 99.8 | 98.5 | 99.7 | 99.7 |
| MEV-SD/2019/3 | OK384317 | 99.0 | 99.0 | 99.0 | 98.6 | 99.8 | 97.4 | 97.4 | 97.4 | 97.4 | 97.4 | 98.5 | 99.8 | | 99.9 | 100 | 100 | 98.7 | 99.8 | 99.8 |
| MEV-SD/2019/4 | OK384318 | 99.0 | 99.0 | 99.0 | 98.6 | 99.8 | 97.4 | 97.4 | 97.4 | 97.4 | 97.4 | 98.5 | 99.8 | 100 | | 99.9 | 99.9 | 98.6 | 99.8 | 99.8 |
| MEV-SD/2019/5 | OK384319 | 99.0 | 99.0 | 99.0 | 98.6 | 99.8 | 97.4 | 97.4 | 97.4 | 97.4 | 97.4 | 98.5 | 99.8 | 100 | 100 | | 100 | 98.7 | 99.8 | 99.8 |
| MEV-SD/2019/6 | OK384320 | 99.0 | 99.0 | 99.0 | 98.6 | 99.8 | 97.4 | 97.4 | 97.4 | 97.4 | 97.4 | 98.5 | 99.8 | 100 | 100 | 100 | | 98.7 | 99.8 | 99.8 |
| RDPV-SD/2019/1 | OK384321 | 98.5 | 98.5 | 98.5 | 98.1 | 98.5 | 97.9 | 97.9 | 97.9 | 97.9 | 97.9 | 96.8 | 98.1 | 98.3 | 98.3 | 98.3 | 98.3 | | 98.6 | 98.6 |
| RDPV-SD/2019/2 | OK384322 | 99.0 | 99.0 | 99.0 | 98.6 | 99.8 | 97.4 | 97.4 | 97.4 | 97.4 | 97.4 | 98.5 | 99.8 | 100 | 100 | 100 | 100 | 98.3 | | 100 |
| RDPV-SD/2019/3 | OK384323 | 99.0 | 99.0 | 99.0 | 98.6 | 99.8 | 97.4 | 97.4 | 97.4 | 97.4 | 97.4 | 98.5 | 99.8 | 100 | 100 | 100 | 100 | 98.3 | 100 | |

*VP2 nucleotide sequence homology is shown in the gray background and VP2 amino acid homology is shown in white background.*

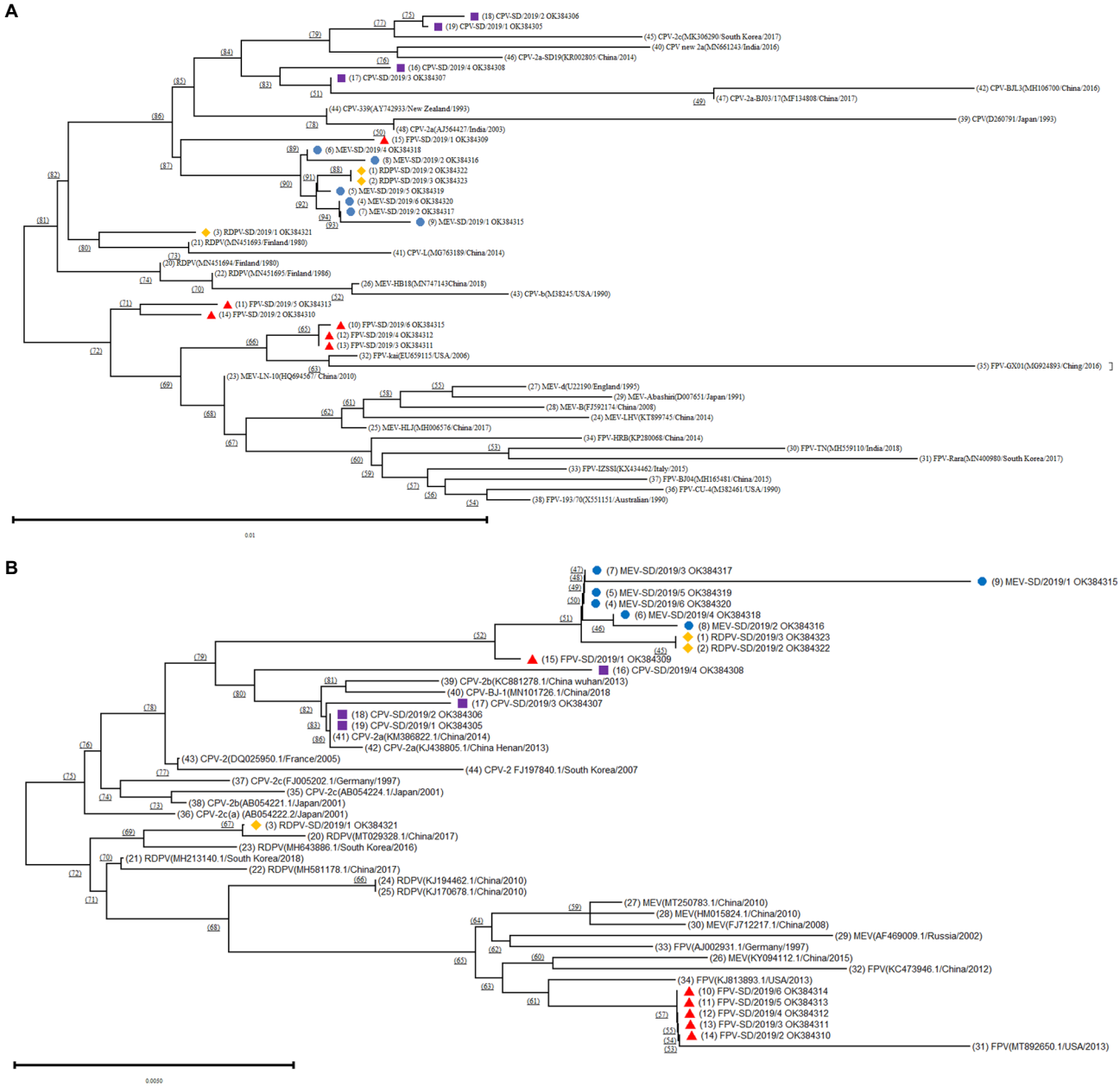


**FIGURE 1 |** Phylogenetic tree analysis based on the different FPV, canine parvovirus-2 (CPV-2), MEV, and RDPV isolates in the present study and reference isolates from GenBank. **(A)** Construction of the phylogenetic tree based on the near-complete genomes of the different isolates. **(B)** Construction of the phylogenetic tree based on the sequence of the VP2 gene of the different isolates. ■ Represents the CPVs isolated in this study; ▲ represents the FPVs isolated in this study; ● represents the MEVs isolated in this study; and ◆ represents the RDPVs isolated in this study.

expected size (571 bp) bands were successfully amplified in 15 of 18 samples. For the canine samples, it was shown that nine out of 13 samples were positive. In the mink samples, eight out of 11 were positive, and three out of seven were positive in the raccoon dog samples. Next, the 35 positive PCR products were sequenced, and BLAST analysis was performed. The blast results showed that the 15 sequences of the isolates from cats, nine from dogs, eight from minks, and three from raccoon dogs showed high similarity with the VP2 genes of FPV, CPV-2, MEV, and RDPV separately (data not shown).

## Isolation and Identification of FPV, CPV-2, MEV, and RDPV From the Samples

The positive FPV, CPV-2, MEV, and RDPV samples identified by PCR were inoculated into the F81 cells. At 2 days

post-inoculation, the cells inoculated with cat, dog, mink, and raccoon dog viral isolates showed the obvious CPEs, including floating, rounding, disintegration, and increased granularity. The IFA results showed that fluorescence was observed in these inoculated cells, indicating that the viruses in the samples successfully proliferated in the F81 cells (**Figure 2**). In addition, after five passages in the cells, the supernatants containing the viral stock were still positive for the viral DNA based on PCR amplification. The amplified sequences shared 100% similarity with the respective sequences obtained from the inoculated samples (data not shown). These results indicated that the six FPV, four CPV-2, six MEV, and three RDPV strains were successfully isolated from the clinical feces.

## Amplification and Analysis of the Near-Complete Genomes of FPV, CPV-2, MEV, and RDPV Isolates

The near-complete genomes of six FPV, four CPV-2, six MEV, and three RDPV isolates were amplified using the viral stock from the five-passaged supernatant in the cell as the templates. The sequences of the near-complete genomes were assembled

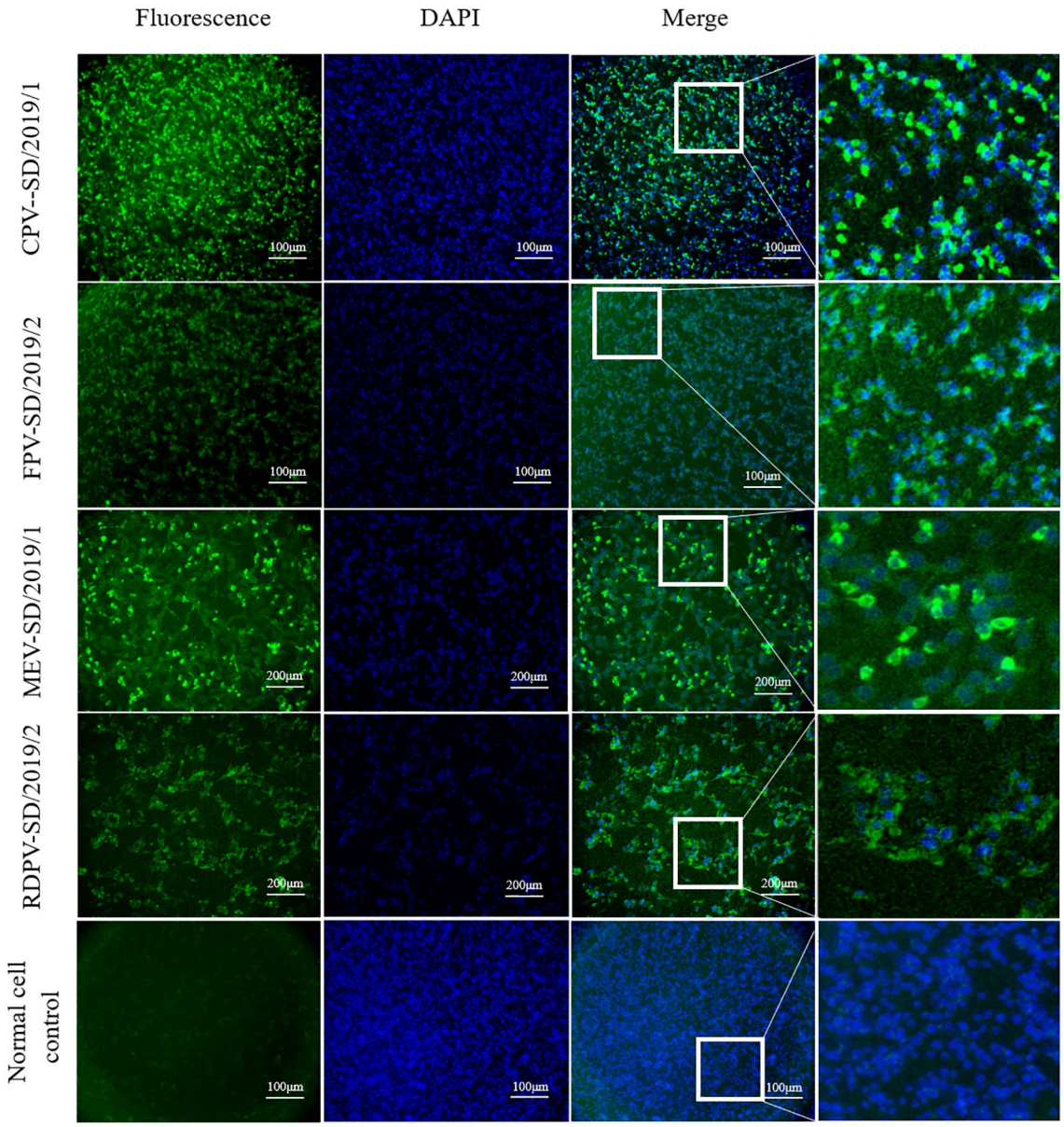


**FIGURE 2 |** Detection of feline panleukopenia virus (FPV), canine parvovirus (CPV), mink enteritis virus (MEV), and raccoon dog parvovirus (RDPV) in the infected F81 cells by indirect immunofluorescence assay with monoclonal antibodies against the viral particle 2 (VP2) protein of parvovirus.

by two overlapping fragment sequences based on at least three independent viral DNA sequences obtained. The near-complete genomes of these isolates were 4,194 nt in length and contained the complete VP1, VP2, and part of the NS1 and NS2 genes. Then, six near-complete genomes of FPV were obtained and termed FPV-SD/2019/1–6. The four CPV-2 sequences were termed CPV-2-SD/2019/1–4. The six MEV genomes were termed MEV-SD/2019/1–6, and the three RDPV genomes were termed RDPV-SD/2019/1–3. All the viral sequences were submitted to GenBank, and the accessions nos. Are presented in **Table 2**. BLAST analysis showed the nucleotide homologies of the near-complete sequences among the 19 isolates were 98.4–100%, while 97.6–99.9% with the reference strains from the GenBank (**Table 3**). Out of which, four MEV isolates share low identity (97.6%) with an FPV isolate from South Korea in 2017, CPV-2-SD/2019/3 shares high homology (99.9%) with CPV-2 strain from China in 2018 (**Table 3**).

## Alignment of the Amino Acid Sequences of VP2 Proteins From the FPV, CPV-2, MEV, and RDPV Isolates

The PCR products of all the VP2 genes from the isolates were cloned into the pMD19-T vector and sequenced. A comparative analysis of the VP2 nucleotide sequences from these strains was performed with the reference strains from the GenBank. BLAST analysis showed that the nucleotide identity of VP2 gene sequences among the 19 isolates was 97.2–100%, and the amino acid identity was 97.4–100% (**Table 2**). The nucleotide and amino acid homology among the four CPV-2 strains were separately 99.0–100% and 99.3–100% (**Table 2**). Among the six isolated FPV strains, amino acid and nucleotide similarity were 97.6–100% and 98.0–100%, respectively (**Table 2**). For the six MEV strains, amino acid and nucleotide similarities were separately 99.1–100% and 99.8–100% (**Table 2**). For the three RDPVs, amino acid and nucleotide similarities were separately 98.6–100% and 98.3–100% (**Table 2**).

The 13 key amino acid sites in the VP2 protein determining the viral antigenicity and host range were also analyzed and classified (Buonavoglia et al., 2001; Govindasamy et al., 2003). For CPV-2, based on the key amino acid mutation at residue 426 (Asp426Glu) in the VP2 protein (Buonavoglia et al., 2001), the results showed that CPV-2-SD/2019/1, CPV-2-SD/2019/2, and CPV-2-SD/2019/3 strains were the same as the antigenic subtype CPV-2a, and the CPV-2-SD/2019/4 strain was the same as CPV-2c (**Table 4**). Interestingly, one FPV strain (FPV-SD/2019/1) possessed only one amino acid mutation (Gly300Ser) compared with the reference CPV-2a strain (**Table 4**). The other five strains, FPV-SD/2019/2, FPV-SD/2019/3, FPV-SD/2019/4, FPV-SD/2019/5, and FPV-SD/2019/6, had an amino acid mutation (Leu562Val) when compared with the reference strain (**Table 4**). The six MEV and two RDPV strains (RDPV-SD/2019/2 and RDPV-SD/2019/3) possessed the same key amino acids but possessed one amino acid mutation (Ala300Ser) compared with the reference CPV-2 strain. The key amino acids of RDPV-SD/2019/1 were the same as the reference CPV-2 strain (**Table 4**).

## Phylogenetic Analysis of Different FPV, CPV-2, MEV, and RDPV Isolates

The phylogenetic tree based on the near-complete genomes showed that the CPV-2 isolates in the present study and reference strains from GenBank were present on the same branch (**Figure 1A**). Interestingly, the one FPV (FPV-SD/2019/1), all six MEV and two RDPV (RDPV-SD/2019/2 and RDPV-SD/2019/3) isolated from the present study were located in the same branch and had a close relationship with CPV-2 isolates (**Figure 1A**). The results indicated that these isolates might be different variants of the same virus, suggesting that the parvoviruses in circulation in cats, minks, and raccoon dogs were initially derived from the same viral strain. However, the other five FPV isolates (FPV-SD/2019/2–6) and MEV and FPV strains from GenBank were located on the same big branch (**Figure 1A**). The FPV-SD/2019/3, FPV-SD/2019/4, and FPV-SD/2019/6 isolates showed further FPV-SD/2019/2 and FPV-SD/2019/5 sequences relationships with the reference sequences of MEV and FPV strains (**Figure 1A**). Another RDPV isolate (RDPV-SD/2019/1) exhibited a close relationship with the reference sequence of the RDPV strain from GenBank (**Figure 1A**).

The phylogenetic tree based on the VP2 amino acid sequences was similar to that of the near-complete genomes (**Figure 1B**). It also showed that the FPV-SD/2019/1, RDPV-SD/2019/2, RDPV-SD/2019/3, all six MEV, and four CPV-2 isolates were located on the same big branch (**Figure 1B**). However, the other five FPV isolates in the study were all on the same branch in the phylogenetic tree constructed based on the VP2 sequences, which was different from the tree based on the genome (**Figure 1**).

# DISCUSSION

FPV and CPV-2 belong to the genus *Protoparvovirus* in the subfamily *Parvovirinae* and cause serious diseases in cats, dogs, minks, and raccoon dogs (Steinel et al., 2001). These contagious viral diseases are characterized by severe leukopenia, nervous system disorders, and acute hemorrhagic gastroenteritis (Truyen, 2006). Sequence alignments and phylogenetic trees drawn in the present study showed that the four viruses exhibit a high degree of identity and may come from the same ancestral virus. Additionally, it was hypothesized that FPV might be the ancestral virus from which CPV-2, MEV, and RDPV originated for the respective hosts. However, it has been documented that FPV can directly infect minks, and raccoon dogs can be directly infected by CPV-2, indicating that these viruses can cause cross-species infections without adaptive variation. Thus, the four viruses seriously harm the health of pets and the development of the commercial animal breeding industry. In the eastern region of Shandong, the breeding density of minks and raccoon dogs is high, and pet dogs and cats are also raised in these farms. Thus, the epidemiology of the two viruses' infection in the region was investigated, and FPV and CPV-2 were isolated and characterized from the cats, dogs, minks, and raccoon dogs, in the present study. A total of 19 variants of parvovirus, including

**TABLE 3 |** Genome nucleotide homology of the isolates and the reference viruses.

| Isolates | Identity (%) | | | | | | | | | | | | | | | | | | | | | | | | | | | | | | |
|---|---|---|---|---|---|---|---|---|---|---|---|---|---|---|---|---|---|---|---|---|---|---|---|---|---|---|---|---|---|---|---|
| | 1 | 2 | 3 | 4 | 5 | 6 | 7 | 8 | 9 | 10 | 11 | 12 | 13 | 14 | 15 | 16 | 17 | 18 | 19 | 20 | 21 | 22 | 23 | 24 | 25 | 26 | 27 | 28 | 29 | 30 | 31 | 32 |
| **CPV-SD/2019/1** | 99.9 | 99.5 | 99.2 | 99.0 | 98.8 | 98.7 | 98.6 | 98.7 | 98.6 | 99.0 | 98.9 | 99.0 | 99.0 | 99.0 | 99.0 | 99.1 | 99.0 | 99.0 | 99.5 | 99.5 | 99.3 | 99.4 | 98.5 | 98.7 | 98.0 | 97.9 | 98.6 | 98.7 | 98.3 | 98.7 | 99.3 |
| **CPV-SD/2019/2** | | 99.4 | 99.1 | 99.0 | 98.7 | 98.6 | 98.5 | 98.6 | 98.5 | 98.9 | 98.9 | 98.9 | 99.0 | 99.0 | 98.9 | 99.0 | 98.9 | 98.9 | 99.4 | 99.4 | 99.2 | 99.3 | 98.5 | 98.6 | 97.9 | 97.8 | 98.5 | 98.6 | 98.1 | 98.6 | 99.2 |
| **CPV-SD/2019/3** | | | 99.7 | 99.1 | 99.2 | 98.8 | 98.7 | 99.0 | 98.7 | 99.4 | 99.3 | 99.4 | 99.4 | 99.4 | 99.4 | 99.4 | 99.3 | 99.3 | 99.9 | 99.5 | 99.4 | 99.0 | 98.6 | 98.8 | 98.2 | 97.9 | 98.7 | 98.8 | 98.3 | 98.8 | 99.4 |
| **CPV-SD/2019/4** | | | | 99.9 | 99.1 | 98.6 | 98.6 | 98.9 | 98.6 | 99.1 | 99.1 | 99.1 | 99.2 | 99.2 | 99.2 | 99.1 | 99.2 | 99.1 | 99.1 | 99.7 | 99.3 | 99.3 | 99.3 | 98.5 | 98.6 | 98.0 | 97.8 | 98.5 | 98.6 | 98.0 | 98.7 | 99.3 |
| **FPV-SD/2019/1** | | | | | 98.7 | 99.2 | 99.2 | 98.5 | 99.2 | 99.2 | 99.2 | 99.2 | 99.3 | 99.2 | 99.2 | 99.2 | 99.0 | 99.2 | 99.2 | 99.1 | 99.3 | 99.2 | 98.5 | 98.7 | 98.6 | 98.0 | 97.9 | 98.6 | 98.7 | 98.0 | 98.8 | 99.2 |
| **FPV-SD/2019/2** | | | | | | 99.5 | 99.5 | 99.7 | 99.4 | 98.9 | 98.8 | 98.9 | 98.9 | 98.9 | 98.9 | 98.9 | 99.2 | 98.8 | 98.8 | 99.2 | 99.2 | 99.3 | 98.4 | 99.0 | 99.3 | 98.6 | 98.5 | 99.0 | 99.1 | 99.0 | 99.2 | 99.3 |
| **FPV-SD/2019/3** | | | | | | | 100.0 | 99.3 | 100.0 | 98.5 | 98.4 | 98.5 | 98.5 | 98.5 | 98.5 | 98.5 | 98.9 | 98.4 | 98.4 | 98.7 | 99.1 | 99.2 | 98.3 | 99.2 | 99.2 | 98.6 | 98.5 | 99.1 | 99.2 | 98.8 | 99.3 | 99.2 |
| **FPV-SD/2019/4** | | | | | | | | 99.3 | 100.0 | 98.4 | 98.4 | 98.4 | 98.5 | 98.5 | 98.4 | 98.9 | 98.4 | 98.4 | 98.7 | 99.1 | 99.2 | 98.2 | 99.2 | 99.3 | 98.6 | 98.5 | 99.1 | 99.2 | 98.9 | 99.3 | 99.2 |
| **FPV-SD/2019/5** | | | | | | | | | 99.3 | 99.2 | 99.0 | 99.2 | 99.1 | 99.1 | 99.2 | 99.0 | 99.0 | 99.0 | 99.0 | 99.0 | 99.0 | 99.1 | 98.3 | 98.8 | 99.1 | 98.5 | 98.3 | 98.9 | 99.1 | 98.8 | 99.0 | 99.2 |
| **FPV-SD/2019/6** | | | | | | | | | | 98.4 | 98.4 | 98.4 | 98.5 | 98.5 | 98.4 | 98.9 | 98.4 | 98.4 | 98.7 | 99.1 | 99.2 | 98.2 | 99.1 | 99.2 | 98.6 | 98.5 | 99.1 | 99.2 | 98.8 | 99.3 | 99.2 |
| **MEV-SD/2019/1** | | | | | | | | | | | 99.8 | 100.0 | 99.9 | 100.0 | 100.0 | 99.0 | 99.9 | 99.9 | 99.3 | 99.2 | 99.1 | 98.5 | 98.3 | 98.5 | 97.9 | 97.6 | 98.4 | 98.5 | 97.9 | 98.5 | 99.1 |
| **MEV-SD/2019/2** | | | | | | | | | | | | 99.8 | 99.9 | 99.8 | 99.8 | 99.0 | 99.8 | 99.8 | 99.3 | 99.1 | 99.0 | 98.4 | 98.3 | 98.4 | 97.8 | 97.6 | 98.3 | 98.5 | 97.8 | 98.4 | 99.0 |
| **MEV-SD/2019/3** | | | | | | | | | | | | | 99.9 | 100.0 | 99.0 | 99.0 | 99.9 | 99.9 | 99.3 | 99.2 | 99.1 | 98.5 | 98.3 | 98.5 | 97.9 | 97.6 | 98.4 | 98.5 | 97.9 | 98.5 | 99.1 |
| **MEV-SD/2019/4** | | | | | | | | | | | | | | 100.0 | 99.9 | 99.1 | 99.9 | 99.9 | 99.4 | 99.3 | 99.1 | 98.5 | 98.4 | 98.5 | 97.9 | 97.7 | 98.4 | 98.6 | 97.9 | 98.5 | 99.1 |
| **MEV-SD/2019/5** | | | | | | | | | | | | | | | 100.0 | 99.1 | 99.9 | 99.9 | 99.4 | 99.3 | 99.1 | 98.5 | 98.4 | 98.5 | 97.9 | 97.7 | 98.4 | 98.6 | 97.9 | 98.5 | 99.1 |
| **MEV-SD/2019/6** | | | | | | | | | | | | | | | | 99.0 | 99.9 | 99.9 | 99.3 | 99.2 | 99.1 | 98.5 | 98.3 | 98.5 | 97.9 | 97.6 | 98.4 | 98.5 | 97.9 | 98.5 | 99.1 |
| **RDPV-SD/2019/1** | | | | | | | | | | | | | | | | | 99.0 | 99.0 | 99.3 | 99.4 | 99.5 | 98.7 | 98.9 | 98.9 | 98.3 | 98.1 | 98.8 | 98.9 | 98.6 | 99.0 | 99.6 |
| **RDPV-SD/2019/2** | | | | | | | | | | | | | | | | | | 100.0 | 99.3 | 99.2 | 99.0 | 98.5 | 98.3 | 98.4 | 97.8 | 97.6 | 98.3 | 98.5 | 97.9 | 98.5 | 99.1 |
| **RDPV-SD/2019/3** | | | | | | | | | | | | | | | | | | | 99.3 | 99.2 | 99.0 | 98.5 | 98.3 | 98.4 | 97.8 | 97.6 | 98.3 | 98.5 | 97.9 | 98.5 | 99.1 |
| **CPV (China, 2018)** | | | | | | | | | | | | | | | | | | | | 94.1 | 91.8 | 98.9 | 91.9 | 95.3 | 94.4 | 94.1 | 98.7 | 94.3 | 98.2 | 90.6 | 99.4 |
| **CPV-L (China, 2018)** | | | | | | | | | | | | | | | | | | | | | 97.8 | 99.0 | 97.2 | 98.7 | 98.1 | 97.9 | 99.0 | 98.0 | 98.7 | 97.3 | 99.7 |
| **CPV (USA, 2018)** | | | | | | | | | | | | | | | | | | | | | | 98.9 | 93.2 | 98.1 | 96.4 | 96.2 | 99.1 | 97.2 | 98.8 | 94.0 | 99.9 |
| **CPV-2c (South Korea, 2018)** | | | | | | | | | | | | | | | | | | | | | | | 98.1 | 98.2 | 97.6 | 97.4 | 99.2 | 98.2 | 97.8 | 98.3 | 98.9 |
| **FPV (China, 2019)** | | | | | | | | | | | | | | | | | | | | | | | | 99.1 | 98.5 | 98.4 | 99.2 | 99.2 | 99.3 | 97.8 | 99.1 |
| **FPV-L (China, 2018)** | | | | | | | | | | | | | | | | | | | | | | | | | 98.7 | 98.7 | 99.2 | 99.2 | 99.0 | 99.1 | 99.2 |
| **FPV (India, 2018)** | | | | | | | | | | | | | | | | | | | | | | | | | | 98.5 | 98.6 | 98.7 | 98.0 | 97.1 | 98.6 |
| **FPV (South Korea, 2017)** | | | | | | | | | | | | | | | | | | | | | | | | | | | 98.4 | 98.4 | 97.7 | 96.9 | 98.4 |
| **MEV (China, 2018)** | | | | | | | | | | | | | | | | | | | | | | | | | | | | 99.5 | 99.2 | 99.4 | 99.1 |
| **MEV (China, 2019)** | | | | | | | | | | | | | | | | | | | | | | | | | | | | | 99.2 | 99.3 | 99.2 |
| **MEV (England, 1996)** | | | | | | | | | | | | | | | | | | | | | | | | | | | | | | 99.5 | 98.8 |
| **MEV (Japan, 2007)** | | | | | | | | | | | | | | | | | | | | | | | | | | | | | | | 99.3 |
| **RDPV (Finland, 1980)** | | | | | | | | | | | | | | | | | | | | | | | | | | | | | | | |

**TABLE 4** | Amino acid sequence variations in the VP2 proteins.

| Strains | Accession number | Amino acid residues | | | | | | | | | | | | | Genotype |
|---|---|---|---|---|---|---|---|---|---|---|---|---|---|---|---|
| | | 80 | 87 | 93 | 101 | 103 | 297 | 300 | 305 | 323 | 426 | 562 | 564 | 568 | |
| **CPV-b** | **PVCPVC** | **R** | **M** | **N** | **I** | **A** | **S** | **A** | **D** | **N** | **N** | **V** | **S** | **G** | **CPV-2** |
| **CPV-2a** | **TQ686671** | **R** | **L** | **N** | **T** | **A** | **A** | **G** | **Y** | **N** | **N** | **V** | **S** | **G** | **CPV-2a** |
| **LCPV-V204** | **AB054221** | **R** | **L** | **N** | **T** | **A** | **A** | **G** | **Y** | **N** | **D** | **V** | **S** | **G** | **CPV-2b** |
| **HRB-A6** | **KT156832** | **R** | **L** | **N** | **T** | **A** | **A** | **D** | **Y** | **N** | **E** | **V** | **S** | **G** | **CPV-2c** |
| CPV-SD/2019/1 | OK384305 | R | L | N | T | A | A | G | Y | N | N | V | S | G | CPV-2a |
| CPV-SD/2019/2 | OK384306 | R | L | N | T | A | A | G | Y | N | N | V | S | G | CPV-2a |
| CPV-SD/2019/3 | OK384307 | R | L | N | T | A | A | G | Y | N | N | V | S | G | CPV-2a |
| CPV-SD/2019/4 | OK384308 | R | L | N | T | A | A | G | Y | N | E | V | S | G | CPV-2c |
| **PLI-IV** | **D88287** | **K** | **M** | **K** | **T** | **V** | **S** | **A** | **D** | **D** | **N** | **L** | **N** | **A** | **FPV** |
| FPV-SD/2019/1 | OK384309 | R | L | N | T | A | A | S | Y | N | N | V | S | G | CPV-2 |
| FPV-SD/2019/2 | OK384310 | K | M | K | T | V | S | A | D | D | N | V | N | A | FPV |
| FPV-SD/2019/3 | OK384311 | K | M | K | T | V | S | A | D | D | N | V | N | A | FPV |
| FPV-SD/2019/4 | OK384312 | K | M | K | T | V | S | A | D | D | N | V | N | A | FPV |
| FPV-SD/2019/5 | OK384313 | K | M | K | T | V | S | A | D | D | N | V | N | A | FPV |
| FPV-SD/2019/6 | OK384314 | K | M | K | T | V | S | A | D | D | N | V | N | A | FPV |
| **MEV-SD1** | **KY094112** | **K** | **M** | **K** | **T** | **V** | **S** | **A** | **D** | **D** | **N** | **V** | **N** | **A** | **MEV** |
| MEV-SD/2019/1 | OK384315 | R | L | N | T | A | A | S | Y | N | N | V | S | G | CPV-2 |
| MEV-SD/2019/2 | OK384316 | R | L | N | T | A | A | S | Y | N | N | V | S | G | CPV-2 |
| MEV-SD/2019/3 | OK384317 | R | L | N | T | A | A | S | Y | N | N | V | S | G | CPV-2 |
| MEV-SD/2019/4 | OK384318 | R | L | N | T | A | A | S | Y | N | N | V | S | G | CPV-2 |
| MEV-SD/2019/5 | OK384319 | R | L | N | T | A | A | S | Y | N | N | V | S | G | CPV-2 |
| MEV-SD/2019/6 | OK384320 | R | L | N | T | A | A | S | Y | N | N | V | S | G | CPV-2 |
| **RDPV-DP1** | **MF996332** | **R** | **M** | **N** | **I** | **A** | **A** | **A** | **D** | **N** | **N** | **L** | **S** | **G** | **RDPV** |
| RDPV-SD/2019/1 | OK384321 | R | M | N | I | A | A | A | D | N | N | L | S | G | CPV-2 |
| RDPV-SD/2019/2 | OK384322 | R | L | N | T | A | A | S | Y | N | N | V | S | G | CPV-2 |
| RDPV-SD/2019/3 | OK384323 | R | L | N | T | A | A | S | Y | N | N | V | S | G | CPV-2 |

*The font in bold is the reference strains, and the normal font is the strains isolated in this study.*

six FPV, four CPV-2, six MEV, and three RDPV variants, were isolated and characterized from the four species with enteritis disease in this region. Interestingly, the phylogenetic trees showed one FPV in the middle branches between MEV and RDPV branches, suggesting that there may be a cross-species infection in this region, which also highlights the potential challenge in controlling parvovirus disease in the region.

Feline panleukopenia virus and CPV-2 are two closely related viruses and are widely hypothesized to be variants of FPV infecting a new host (Parrish, 1990). Previous studies have reported that new variants of CPV-2 have acquired the ability to infect felines, allowing them to infect both dogs and cats (Decaro et al., 2010; Clegg et al., 2012). Four mutations in VP2 protein at residues 87, 300, and 305 have been shown to alter the host range in parvoviruses (Stucker et al., 2012). In the present study, we found only one amino acid (Gly300Ser) in the VP2 sequence of FPV-SD/2019/1 isolate that was inconsistent with reference CPV-2a strain and CPV-2a isolates, and other amino acids are consistent, providing novel evidence for the continued emergence of CPV-2 in the feline population in China. We also found only one amino acid (Gly300Ser) in the VP2 sequence of MEV-SD/2019/1–6 isolates inconsistent with CPV-2a isolates, and other amino acids are consistent suggest that CPV-2 cross-infected minks. RDPV was originally derived from CPV-2, suggesting that CPV-2 cross-infected a raccoon dog and mutated during adaptation (Allison et al., 2012). Typically, the genes of RDPV isolates were very similar to that of the original CPV-2, but there were four mutations in the VP2 gene. However, only one amino acid (Gly300Ser) in the VP2 gene of RDPV-SD/2019/1 and RDPV-SD/2019/2 was inconsistent with CPV-2a, and this mutation was consistent with the FPV-SD/2019/1 isolated in the present study. These findings suggested that the cross-species infection of CPV-2a and FPV is more complex than previously suggested, especially given that the isolates were obtained from the mixed breeding region for pets and special economic animals.

To prevent parvovirus infection, these farms of special economic animals in this region were immunized with commercial attenuated vaccines for dogs. However, the outbreak of viral enteritis still occurred on the farms of minks and raccoon dogs, indicating that the commercial dog parvovirus vaccine may not provide complete protection against MEV and RDPV infection in the minks and raccoon dogs. By comparing VP2 amino acids of all isolates in the study, we found that, although the identity between MEV and RDPV and CPV-2 was high, there were still some mutations of key amino acids. These mutations may change the viral antigenicity and cause immunization failure. Thus, molecular epidemiological investigations are necessary to identify the genetic mutation sites of the new viral strains, which is of great significance for revising the immunization plan.

## CONCLUSION

Collectively, 19 parvovirus variants were successfully isolated from dogs, cats, minks, and raccoon dogs with viral enteritis in the eastern region of Shandong, China. Genetic analysis of these isolates showed that cross-species infections among FPV and CPV-2 occurred in this region's cats, dogs, minks, and raccoon dogs. Thus, in the areas with a high density of mixed farming in China, the continuous evolution of the parvovirus in different species will likely be accelerated, increasing the difficulty in controlling these animals' viral spread, thus requiring continuous epidemiological surveillance.

## DATA AVAILABILITY STATEMENT

The datasets presented in this study can be found in online repositories. The names of the repository/repositories and accession number(s) can be found in the article/supplementary material.

## AUTHOR CONTRIBUTIONS

YS and YD jointly conceived the study. JZ did the experiments and wrote the manuscript. HZ, LZ, and NZ performed the sample collection. QZ and TD contributed to data analyses. QZ, E-MZ, YS, and YD revised the paper. All authors contributed to the article and approved the final manuscript.

## FUNDING

The study is mainly funded by grants from the National Natural Science Foundation of China (no. 31402233) to QZ and Tang Scholar of Cyrus Tang Foundation to QZ.

## REFERENCES

Allison, A. B., Harbison, C. E., Pagan, I., Stucker, K. M., Kaelber, J. T., Brown, J. D., et al. (2012). Role of multiple hosts in the cross-species transmission and emergence of a pandemic parvovirus. *J. Virol.* 86, 865–872. doi: 10.1128/JVI.06187-11

Appel, M. J., Scott, F. W., and Carmichael, L. E. (1979). Isolation and immunisation studies of a canine parco-like virus from dogs with haemorrhagic enteritis. *Vet. Rec.* 105, 156–159. doi: 10.1136/vr.105.8.156

Barker, I. K., Povey, R. C., and Voigt, D. R. (1983). Response of mink, skunk, red fox and raccoon to inoculation with mink virus enteritis, feline panleukopenia and canine parvovirus and prevalence of antibody to parvovirus in wild carnivores in Ontario. *Can. J. Comp. Med.* 47, 188–197.

Battilani, M., Balboni, A., Ustulin, M., Giunti, M., Scagliarini, A., and Prosperi, S. (2011). Genetic complexity and multiple infections with more parvovirus species in naturally infected cats. *Vet. Res.* 42:43. doi: 10.1186/1297-9716-42-43

Buonavoglia, C., Martella, V., Pratelli, A., Tempesta, M., Cavalli, A., Buonavoglia, D., et al. (2001). Evidence for evolution of canine parvovirus type 2 in Italy. *J. Gen. Virol.* 82, 3021–3025. doi: 10.1099/0022-1317-82-12-3021

Clegg, S. R., Coyne, K. P., Dawson, S., Spibey, N., Gaskell, R. M., and Radford, A. D. (2012). Canine parvovirus in asymptomatic feline carriers. *Vet. Microbiol.* 157, 78–85. doi: 10.1016/j.vetmic.2011.12.024

Cotmore, S. F., Agbandje-McKenna, M., Canuti, M., Chiorini, J. A., Eis-Hubinger, A. M., Hughes, J., et al. (2019). ICTV virus taxonomy profile: Parvoviridae. *J. Gen. Virol.* 100, 367–368. doi: 10.1099/jgv.0.001212

Cotmore, S. F., Agbandje-McKenna, M., Chiorini, J. A., Mukha, D. V., Pintel, D. J., Qiu, J., et al. (2014). The family Parvoviridae. *Arch. Virol.* 159, 1239–1247. doi: 10.1007/s00705-013-1914-1

Decaro, N., Buonavoglia, D., Desario, C., Amorisco, F., Colaianni, M. L., Parisi, A., et al. (2010). Characterisation of canine parvovirus strains isolated from cats with feline panleukopenia. *Res. Vet. Sci.* 89, 275–278. doi: 10.1016/j.rvsc.2010.03.001

Govindasamy, L., Hueffer, K., Parrish, C. R., and Agbandje-McKenna, M. (2003). Structures of host range-controlling regions of the capsids of canine and feline parvoviruses and mutants. *J. Virol.* 77, 12211–12221. doi: 10.1128/JVI.77.22.12211-12221.2003

Hoelzer, K., and Parrish, C. R. (2010). The emergence of parvoviruses of carnivores. *Vet. Res.* 41:39. doi: 10.1051/vetres/2010011

Jia-Yu, Y., Qian, Z., Fei-Fei, D., Chuan-Jie, T., Hui, P., Yuan-Yuan, S., et al. (2018). Emergence of novel canine parvovirus type 2 and its pathogenesis in raccoon dogs. *Vet. Microbiol.* 216, 7–12. doi: 10.1016/j.vetmic.2018.01.016

Johnson, R. H., Siegl, G., and Gautschi, M. (1974). Characteristics of feline panleucopaenia virus strains enabling definitive classification as parvoviruses. *Arch. Gesamte Virusforsch.* 46, 315–324. doi: 10.1007/BF01240073

Li, C., Tang, J., Chen, Z., Niu, G., and Liu, G. (2019). A divergent canine parvovirus type 2c (CPV-2c) isolate circulating in China. *Infect. Genet. Evol.* 73, 242–247. doi: 10.1016/j.meegid.2019.05.004

Lu, R., Yu, Y., Zhu, X., Shi, Q., Wang, Y., Wang, J., et al. (2020). Molecular characteristics of the capsid protein VP2 gene of canine parvovirus type 2 amplified from raccoon dogs in Hebei province, *China. Arch. Virol.* 165, 2453–2459. doi: 10.1007/s00705-020-04714-3

Muz, D., Oğuzoğlu, T. C., Timurkan, M. O., and Akın, H. (2012). Characterization of the partial VP2 gene region of canine parvoviruses in domestic cats from Turkey. *Virus Genes* 44, 301–308. doi: 10.1007/s11262-011-0703-8

Ohshima, T., and Mochizuki, M. (2009). Evidence for recombination between feline panleukopenia virus and canine parvovirus type 2. *J. Vet. Med. Sci.* 71, 403–408. doi: 10.1292/jvms.71.403

Parrish, C. R. (1990). Emergence, natural history, and variation of canine, mink, and feline parvoviruses. *Adv. Virus Res.* 38, 403–450. doi: 10.1016/s0065-3527(08)60867-2

Reed, A. P., Jones, E. V., and Miller, T. J. (1988). Nucleotide sequence and genome organization of canine parvovirus. *J. Virol.* 62, 266–276. doi: 10.1128/jvi.62.1.266-276.1988

Steinel, A., Munson, L., van Vuuren, M., and Truyen, U. (2000). Genetic characterization of feline parvovirus sequences from various carnivores. *J. Gen. Virol.* 81, 345–350. doi: 10.1099/0022-1317-81-2-345

Steinel, A., Parrish, C. R., Bloom, M. E., and Truyen, U. (2001). Parvovirus infections in wild carnivores. *J. Wildl. Dis.* 37, 594–607. doi: 10.7589/0090-3558-37.3.594

Stucker, K. M., Pagan, I., Cifuente, J. O., Kaelber, J. T., Lillie, T. D., Hafenstein, S., et al. (2012). The role of evolutionary intermediates in the host adaptation of canine parvovirus. *J. Virol.* 86, 1514–1521. doi: 10.1128/JVI.06222-11

Tamura, K., Dudley, J., Nei, M., and Kumar, S. (2007). MEGA4: molecular evolutionary genetics analysis (MEGA) software version 4.0. *Mol. Biol. Evol.* 24, 1596–1599. doi: 10.1093/molbev/msm092

Truyen, U. (1999). Emergence and recent evolution of canine parvovirus. *Vet. Microbiol.* 69, 47–50. doi: 10.1016/S0378-1135(99)00086-3

Truyen, U. (2006). Evolution of canine parvovirus--a need for new vaccines? *Vet. Microbiol.* 117:9–13. doi:10.1016/j.vetmic.2006.04.003

Truyen, U., Gruenberg, A., Chang, S. F., Obermaier, B., Veijalainen, P., and Parrish, C. R. (1995). Evolution of the feline-subgroup parvoviruses and the control of canine host range in vivo. *J. Virol.* 69, 4702–4710. doi: 10.1128/jvi.69.8.4702-4710.1995

Wills, C. G. (1952). Notes on infectious enteritis of mink and its relationship to feline enteritis. *Can. J. Comp. Med. Vet. Sci.* 16, 419–420

Yuan, D., Wang, J., Li, Z., Mao, Y., Sun, J. Z., Xi, J., et al. (2014). Establishment of a rescue system for an autonomous parvovirus mink enteritis virus. *Virus Res.* 183, 1–5. doi: 10.1016/j.virusres.2014.01.012

**Conflict of Interest:** The authors declare that the research was conducted in the absence of any commercial or financial relationships that could be construed as a potential conflict of interest.

**Publisher's Note:** All claims expressed in this article are solely those of the authors and do not necessarily represent those of their affiliated organizations, or those of the publisher, the editors and the reviewers. Any product that may be evaluated in this article, or claim that may be made by its manufacturer, is not guaranteed or endorsed by the publisher.

*Copyright © 2022 Zhao, Zhang, Zhang, Zhang, Zhou, Du, Zhao, Zhou, Du and Sun. This is an open-access article distributed under the terms of the Creative Commons Attribution License (CC BY). The use, distribution or reproduction in other forums is permitted, provided the original author(s) and the copyright owner(s) are credited and that the original publication in this journal is cited, in accordance with accepted academic practice. No use, distribution or reproduction is permitted which does not comply with these terms.*

frontiers in Microbiology

ORIGINAL RESEARCH
published: 02 March 2022
doi: 10.3389/fmicb.2022.846079

# The Construction and Immunogenicity Analyses of Recombinant Pseudorabies Virus With NADC30-Like Porcine Reproductive and Respiratory Syndrome Virus-Like Particles Co-expression

*Jun Zhao[1*†], Ling Zhu[1,2†], Lei Xu[1], Fengqing Li[1], Huidan Deng[1], Yao Huang[1], Sirui Gu[1], Xianggang Sun[1], Yuancheng Zhou[3] and Zhiwen Xu[1,2*]*

[1] College of Veterinary Medicine, Sichuan Agricultural University, Chengdu, China, [2] Key Laboratory of Animal Disease and Human Health of Sichuan Province, Chengdu, China, [3] Animal Breeding and Genetics Key Laboratory of Sichuan Province, Sichuan Animal Science Academy, Chengdu, China

Porcine reproductive and respiratory syndrome (PRRS) and pseudorabies (PR) are highly infectious swine diseases and cause significant financial loss in China. The respiratory system and reproductive system are the main target systems. Previous studies showed that the existing PR virus (PRV) and PRRS virus (PRRSV) commercial vaccines could not provide complete protection against PRV variant strains and NADC30-like PRRSV strains in China. In this study, the PRV variant strain XJ and NADC30-like PRRSV strain CHSCDJY-2019 are used as the parent for constructing a recombinant pseudorabies virus (rPRV)-NC56 with gE/gI/TK gene deletion and co-expressing NADC30-like PRRSV GP5 and M protein. The rPRV-NC56 proliferated stably in BHK-21 cells, and it could stably express GP5 and M protein. Due to the introduction of the self-cleaving 2A peptide, GP5 and M protein were able to express independently and form virus-like particles (VLPs) of PRRSV in rPRV-NC56-infected BHK-21 cells. The rPRV-NC56 is safe for use in mice; it can colonize and express the target protein in mouse lungs for a long time. Vaccination with rPRV-NC56 induces PRV and NADC30-like PRRSV specific humoral and cellular immune responses in mice, and protects 100% of mice from virulent PRV XJ strain. Furthermore, the virus-neutralizing antibody (VNA) elicited by rPRV-NC56 showed significantly lower titer against SCNJ-2016 (HP-PRRSV) than that against CHSCDJY-2019 (NADC30-like PRRSV). Thus, rPRV-NC56 appears to be a promising candidate vaccine against NADC30-like PRRSV and PRV for the control and eradication of the variant PRV and NADC30-like PRRSV.

**Keywords: PRV variant, NADC30-like PRRSV, VLPs, viral-vectored vaccine, immunogenicity analyses**

OPEN ACCESS

***Edited by:***
*Chunfu Zheng,*
*University of Calgary, Canada*

***Reviewed by:***
*Xiangang Zou,*
*Chongqing CAMAB Biotech Ltd., China*
*Zhiqiang Huang,*
*Karolinska Institutet (KI), Sweden*

****Correspondence:***
*Jun Zhao*
*zhaojunjoy@126.com*
*Zhiwen Xu*
*abtcxzw@126.com*

*† These authors have contributed equally to this work*

***Specialty section:***
*This article was submitted to Virology, a section of the journal Frontiers in Microbiology*

***Received:*** *30 December 2021*
***Accepted:*** *24 January 2022*
***Published:*** *02 March 2022*

***Citation:***
*Zhao J, Zhu L, Xu L, Li F, Deng H, Huang Y, Gu S, Sun X, Zhou Y and Xu Z (2022) The Construction and Immunogenicity Analyses of Recombinant Pseudorabies Virus With NADC30-Like Porcine Reproductive and Respiratory Syndrome Virus-Like Particles Co-expression. Front. Microbiol. 13:846079. doi: 10.3389/fmicb.2022.846079*

## INTRODUCTION

Porcine reproductive and respiratory syndrome (PRRS) appeared in Europe and the United States in the 1990s and became a problem that plagued the global pig industry ever since. PRRS virus (PRRSV) is a single-stranded positive-strand RNA virus with capsule, belonging to the arteritis virus family and arteritis virus genus, with a diameter of 50–65 nm. The pig is the natural host of PRRSV. The lungs are the main target organ *in vivo*, and porcine alveolar macrophages (PAMs) are the main target cells of PRRSV infection *in vitro*. Heparin sulfate, vimentin, CD151, CD169, and CD163 are the main receptors of PRRSV infection (Nan et al., 2017). Because of the great differences in genes and proteins between the PRRSV-1 and PRRSV-2, they are divided into two species (Kuhn et al., 2016). According to the classification system, the PRRSV-1 was divided into three subtypes (subtypes 1–3), and the PRRSV-2 was classified into nine lineages with several sublineages in each lineage (Shi et al., 2010a,b). The main prevalent PRRSV-2 strains in China are types 1, 3, 5, 8, and 9 (Chen et al., 2019; Han et al., 2020). Lineage 1 PRRSV contains representative strains, such as NADC30, JL580, NADC34, and RFLP 1-4-4. Lineage 3 PRRSV is mainly prevalent in South China and has low pathogenicity, including representative strains such as QYYZ and GM2. Lineage 5 mainly contains the classical PRRSV strain represented by VR-2332. Lineage 8 contains highly virulent strains represented by TJ, JXA1, TA-12, and classical PRRSV strains represented by CH-1a. Lineage 9 was discovered in Xinjiang in 2011. Since the emergence of PRRSV strains in China, the most popular strains are lineage 8, including classic strain (CH-1a) and HP-PRRSV in 2006 (Deng et al., 2012). The NADC30-like strain in lineage 1 appeared in the United States in 2008 and in China in 2013. Since then, the detection rate of clinical samples in nine provinces such as North China, East China, South China, and Central China has gradually increased (Guo et al., 2018, 2019; Jiang et al., 2020). The results of challenge protection experiment using NADC30-like PRRSV strains showed that the most widely used commercial vaccines in China cannot effectively protect pigs from the attack of NADC30-like PRRSV strain. Pigs infected with NADC30-like PRRSV strain after vaccination still have obvious clinical symptoms, high viremia, and virus load in various tissues (Bai et al., 2016; Zhou et al., 2017; Wei et al., 2019; Chen et al., 2021). At present, there is no commercial PRRSV vaccine developed with NADC30-like PRRSV strain. Therefore, the development of a PRRSV vaccine against NADC30-like PRRSV is particularly important to combat the continuously increasing epidemic of NADC30-like PRRS outbreaks.

Virus-neutralizing antibodies, the key weapon of the body to resist virus infection, is the main evaluation index of many effective vaccines to prevent virus infection (Robinson et al., 2015). The PRRSV virion surface contains at least seven envelope proteins, GP2a, GP2b, GP3, GP4, GP5, M, and N protein, respectively. GP5 and M protein are the major envelope proteins, and they are disulfide-linked heterodimers. The minor glycoprotein GP2a, GP3, and GP4 form noncovalent heterotrimers (Trible et al., 2015). Multiple previous studies have identified multiple neutralization epitopes distributed on major structural protein (GP5 and M) and minor glycoprotein (GP2a, GP3, and GP4) (Vanhee et al., 2011). In the last years, a lot of effort has been put into VLPs for vaccine development to control human or animal disease (Kang et al., 2021; Lampinen et al., 2021; Marin et al., 2021; Wang et al., 2021). Previous studies showed that GP5 and M protein interaction, GP2, GP3, GP4, and E protein interaction, GP5, GP4, GP3, GP2a, and M protein interaction, and GP5, M, and N protein interaction of PRRSV could form VLPs (Uribe-Campero et al., 2015; Binjawadagi et al., 2016; García Durán et al., 2016).

Pseudorabies virus (PRV) belongs to the family Herpesviridae, subfamily Alphaherpesvirinae (Müller et al., 2011; Tang Y. D. et al., 2016) and can infect pigs, cattle, sheep, and many other livestock and wild animals, causing fever, severe itching, and encephalomyelitis in infected animals. Pigs are the main reservoir host and infection source of PRV, and are threatened by pseudorabies (PR) at all ages (Müller et al., 2011; Zhang et al., 2015). PRV infection mainly causes disorder of the nervous system and respiratory system in piglets and the abortion of pregnant sows (Weigel et al., 2003; Wang et al., 2015; Lamote et al., 2016; Sun et al., 2016). In the 1970s, The Bartha-K61 vaccine was imported into China from Hungary and effectively controlled the prevalence of PR (Tong et al., 2015). However, variant PRV emerges in many Bartha-K61 vaccinated farms in the Northern provinces of China since 2011 (An et al., 2013; Gu et al., 2018).

Pseudorabies virus is a double-stranded DNA virus of approximately 150 kb in length, which contains almost 70 open reading frames (ORFs) that encode 70–100 viral proteins including structural, nonstructural, and virulence-associated protein (Klupp et al., 2004). The large genome of the PRV contains many nonessential genes with many insertion sites that can integrate and express heterologous genes, including the TK, gE, gI, and gG genes. The absence of these nonessential genes results in a diminished virulence phenotype of the virus while having no significant effect on the immune response (Klupp et al., 2004; Olsen et al., 2006). At present, PRV has developed into a powerful vector system for expressing exogenous protein, which can carry and express the main immunogenic genes and protein of other viruses, such as PCV2 Cap, PCV3 Cap, PPV VP2, ASFV CD2v, HP-PRRSV GP5, and M proteins (Freuling et al., 2017; Feng et al., 2020; Zheng et al., 2020; Yao et al., 2021). These bivalent or trivalent recombinant vaccines developed with a PRV live virus vector can stimulate the body to produce a specific immune response to the target virus without affecting the autogenous immune effect of PRV. In this study, based on the functional characteristics of PRRSV GP5 and M proteins, we construct a recombinant PRV strain, named recombinant pseudorabies virus (rPRV)-NC56. It expresses the NADC30-like PRRSV GP5 and M proteins stably, and the two proteins assemble into VLPs intracellularly. The safety and ability to elicit humoral and cellular immune responses of rPRV-NC56 were evaluated in mice to provide evidence for the

future vaccine development against both NADC30-like PRRSV and variant PRV.

## MATERIALS AND METHODS

### Viruses, Cells, and Plasmids

PRV-XJ (Genbank accession No. MW893682.1) strain was obtained from specimens of pseudorabies-infected pigs at Sichuan Province in 2015 by our lab, and it has been proven to be a potential PR vaccine with good immunogenicity (Yin et al., 2017). PRV XJ-ΔgE/gI/TK-EGFP was built and stored in our lab. All viruses were propagated in BHK-21 cells in Dulbecco's modified Eagle's medium (DMEM) (12100046, Gibco) supplemented with 10% fetal bovine serum (10099133C, Gibco). Baby hamster Syrian kidney cells (BHK-21) and HEK293T cells were purchased and cultured in DMEM medium containing 10% fetal bovine serum in our lab. The single-guide RNA (sgRNA) lentiCRISPR V2 plasmid of gE gene (GGGCAGGAACGTCCAGATCC), TK gene (CTCGACGGCGCCTACGGCAC, GCCGCGTAC GGCGACCACATC), and pEGFP-gI/28K plasmid containing gI and 28K homologous arms of PRV were constructed by our lab.

The NADC30-like PRRSV ORF5 and ORF6 genes were amplified from the CHSCDJY-2019 strain genome (Genbank accession No. MT075480.1) (Zhao et al., 2021). The nucleotide sequences of self-cleaving T2A and P2A peptides were added to the donor template by PCR amplification, and the donor template (T2A-ORF6-P2A-ORF5) was obtained by fusion PCR amplification. The recombinant transfer plasmid (pEGFP-2A-NC-OFR5-6) was constructed by Seamless Cloning Kit (D7010FT, Beyotime) with the donor template and the pEGFP-gI/28K (digestion with EcoR I and Bcl I; 1611 and 1045A, Takara), and named as pEGFP-2A-NADC30-like-ORF6-ORF5 (pEGFP-2A-NC-OFR5-6) (**Supplementary Figure 1**). All the sequences of the primers are listed in **Supplementary Table 1**.

### Generation of Recombinant Virus and PCR Identification

The PRV-XJ genomic DNA was extracted according to the Omega DNA extraction kit instructions. PRV-XJ genomic DNA (3 μg), pEGFP-2A-NC-OFR5-6 plasmid (5 μg), and sgRNA-gE plasmid (5 μg), with a molar ratio of 20:1, were cotransfected into the well-developed HEK293T cells using Lipofectamine 3000 Transfection Reagent (L3000015, Thermo). After transfection, the cells were cultured under 37°C until cytopathic effect (CPE) occurred. Virus supernatant was taken to inoculate BHK-21 cells, green fluorescence plaques were picked out, and three rounds of plaque purification were performed. The purified viruses were named rPRV-ΔgE/gI-NC-ORF5-6. The rPRV-ΔgE/gI-NC-ORF5-6 viral DNA was extracted. The rPRV-ΔgE/gI-NC-ORF5-6 (3 μg) and two sgRNA of TK genes (5 μg each), with a molar ratio of 20:1, were cotransfected into the well-developed HEK293T cells using Lipofectamine 3000 transfection Reagent. Pure recombinant PRV were plaque purified, named as rPRV-NC56.

The viral DNA of the purified virus rPRV-NC56 and PRV-XJ was extracted by the Genomic DNA Purification Kit (K182001, Thermo). The TK, gE, and gB genes and insert nucleic acid sequence (ORF6-P2A-ORF5) were detected by PCR. The detection primers are shown in **Supplementary Table 1**. The PCR products were agarose gel electrophoresis, the target bands were recovered and purified, and sequencing was done by Sangon Biotech (Shanghai) Co., Ltd.

### Immunofluorescence Assay for GP5 and M Protein Expression Detection

The purified recombinant virus rPRV-NC56 was inoculated in a 12-well plate filled with monolayer BHK-21 cells with 0.05 MOI. Furthermore, an equal amount of parental involvement strain PRV XJ was set up as a negative control. The BHK-21 cells were fixed with paraformaldehyde, permeabilized with 0.2% X-Triton (9002-93-1, Sangon Biotech), followed by incubation with rabbit anti-GP5 polyclonal (bs-4504R, Bioss) or rabbit anti-M polyclonal antibody (bs-4507R, Bioss) for 1 h at 37°C, respectively. After three washes with PBS (20012050, Gibco), the cells were stained with corallite 594-conjugated goat anti-rabbit IgG (SA00013-4, Proteintech) and DAPI (C0060, Solarbio) (0.5 μg/ml) for 30 min at 37°C, and cells were washed with PBS three times. The GP5 and M proteins were observed under an inverted fluorescence microscope.

### Western Blotting Analysis for GP5, M, gE, and gB Protein Expression Detection

The rPRV-NC56 and PRV XJ were, respectively, inoculated in a six-well plate for the fifth generation with 0.1 MOI. After 36 h, the BHK-21 cells were lysed with RIPA lysis solution (P0013B, Beyotime), and the supernatant was collected by centrifugation at 12,000 r/min for 5 min. Then the supernatant was boiled with 5× SDS-PAGE loading buffer for 20 min and centrifuged at 15,000 r/min for 15 min. After 12% SDS-PAGE electrophoresis (1610185, Bio-Rad Laboratories), the gel was electrotransferred to a nitrocellulose membrane (1620117, Bio-Rad Laboratories). Membranes were blocked with 5% skim milk in PBS for 1 h at 37°C. After three washings with PBST (PBS containing 1% Tween 20), the nitrocellulose membranes were, respectively, incubated overnight at 4°C with a primary antibody. The primary antibodies used in this study were rabbit anti-PRRSV GP5 polyclonal antibody (bs-4504R, Bioss), rabbit anti-RRRSV M polyclonal antibody (bs-4507R, Bioss), mouse anti-PRV gE monoclonal antibody (82289, TianTech), anti-PRV gB (The gB polyclonal antibodies were obtained from rabbits immunized with gB protein in our lab), and rabbit anti-β-actin monoclonal antibody (66009-1-Ig, Proteintech). After three washings with PBST, nitrocellulose membranes were incubated with horseradish peroxidase-conjugated goat anti-mouse or goat anti-rabbit secondary antibody (D110087 and D110058, Sangon Biotech) for 1 h at room temperature, respectively, then washed with PBST, and developed using SuperSignal™ West Pico PLUS chemiluminescent substrate (34580, Thermo) according to the manufacturer's instructions.

## Virus One-Step Growth Curve and Plaque Assays

The virus growth kinetics of rPRV-NC56, rPRV XJ-ΔgE/gI/TK-EGFP, and PRV-XJ was compared. The 0.1 MOI virus was inoculated when the growth density reached 80% of BHK-21 cells in T25 cell culture flask. The cell supernatants were collected at different time points (0, 4, 8, 12, 24, 36, 48, 64 hpi) after inoculation; the $TCID_{50}$ of the viruses was measured. Three replicated tests were taken for each sample, and the values were averaged to draw a one-step growth curve.

The 100 $TCID_{50}$ of rPRV-NC56, rPRV XJ-ΔgE/gI/TK-EGFP, and parental virus PRV-XJ were placed into six-well plates full of BHK-21 cells, respectively. After incubating at 37°C for 1 h, the cells were covered with DMEM containing 1% low-melting point agarose. The infected BHK-21 cells were maintained at 37°C and 5% $CO_2$ for 96 h, and were stained with formaldehyde–crystal violet staining solution containing 1% crystal violet and 4% formaldehyde. The morphology and size of virus plaques were analyzed using Image Pro Plus (v 7.0).

## Transmission Electron Microscopic Observation of Porcine Reproductive and Respiratory Syndrome Virus-Like Particles

A 1/1,000 dose of the rPRV-NC56, rPRV XJ-ΔgE/gI/TK-EGFP, PRV-XJ, and CHSCDJY-2019 was, respectively, inserted into a T75 cell culture flask full of monolayer Marc-145 cells, and the cells were collected in a centrifuge tube when they were more than 80% diseased. Cells were centrifuged at 1,500 r/min for 10 min, and the supernatant was discarded. Glutaraldehyde fixative (0.5%) was slowly added along the tube wall and was left for 10 min at 4°C. Then it was centrifuged at 15,000 r/min for 15 min, the supernatant was discarded, and 3% glutaraldehyde fixative was slowly added to fix it. The cell culture clumps after fixation were sent to Chengdu Lilai Biological Co., Ltd. The formation of rPRV-NC56, rPRV XJ-ΔgE/gI/TK-EGFP, PRV-XJ, and CHSCDJY-2019 strains and the formation of PRRSV VLPs were observed under an electron microscope. To assess the formation and release of VLPs, infections with rPRV-NC56 and CHSCDJY-2019 were performed in Marc-145 cells. The VLPs were condensed from the supernatant by 100-KDa MWCO centrifugal concentrator (UFC9100, Millipore), and the unassembled GP5 and M proteins were removed. All the fractions obtained were analyzed by SDS-PAGE and Western blot.

## Safety, Immunogenicity, and Challenge in Mice

Ninety healthy BALB/c mice (25 g) were randomly divided into nine groups (10 mice/each). Groups A–C, D–F, G–H, and I were inoculated with different concentrations of rPRV-NC56 ($10^{6.0}$, $10^{7.0}$, and $10^{8.0}$ $TCID_{50}$), rPRV XJ-ΔgE/gI/TK-EGFP ($10^{6.0}$, $10^{7.0}$, and $10^{8.0}$ $TCID_{50}$), PRV-XJ ($10^{2.0}$ and $10^{3.0}$ $TCID_{50}$), and DMEM with intramuscularly (i.m.) (200 μl/dose), and were continuously observed for 14 days. Blood was collected from the tail vein of 10 mice in each group at 1 and 3 days for IL-6 and TNF-α (KMC0061 and BMS607-3, Thermo) detection, respectively.

Sixty BALB/c mice were divided into two groups: 30 mice in one group were immunized with rPRV-NC56 [i.m. at 200 μl/dose ($10^6$ $TCID_{50}$)], and 30 mice in the other groups were injected with equal volume of PBS. The immunized mice were killed at 1-day postvaccination (dpv), 3 dpv, 5 dpv, 7 dpv, and 21 dpv, and the lung tissues were collected for PRRSV GP5 protein immunohistochemistry (IHC) detection and PRV gB gene real-time quantitative polymerase chain reaction (qPCR) detection. The PRV gB segment was cloned into the PMD-18T vector (6011, TAKARA) to construct the PMD18T-gB recombinant plasmid and generate a standard curve. gB forward, 5′-CGGCAAGTGCGTCTCC-3′ and reverse, 5′-TGTAGGTGTCGTTGGTGGTG-3′. The IHC detection was sent to Chengdu Lilai Biological Co., Ltd., and 8–12 fields under ×400 magnification were selected for each sample to count the positive cells using image Pro Plus (V 7.0).

Seventy-two BALB/c mice were randomly divided into three groups of 24 each, and the three groups were inoculated with rPRV-NC56 and rPRV XJ-ΔgE/gI/TK-EGFP and DMEM, respectively. The viruses were intramuscularly injected into mice at a dose of 200 μl ($10^6$ $TCID_{50}$), and the other one group was injected with 200 μl of DMEM as control. Three groups were booster immunized with the same dose 2 weeks postvaccination (wpv). Blood was collected from the tail vein of 10 mice in each group at 1–6 weeks after the first immunization. Levels of PRV gB, NADC30-like PRRSV GP5, and M-specific antibodies in the serum were measured by enzyme-linked immunosorbent assay (ELISA). The splenocytes from 10 mice at 4 wpv were isolated and, respectively, stimulated *in vitro* with $10^6$ $TCID_{50}$ of UV-inactivated CHSCDJY-2019 (NADC30-like PRRSV) and SCNJ-2016 (HP-PRRSV) strains as the antigen. Meanwhile, the specific CD8 T lymphocytes were detected by cell proliferation assay. The secretion of IL-2, IL-4, and IFN-γ (BMS601, BMS613, and BMS606-2, Thermo) in the blood of mice on weeks 2, 4, and 6 were measured by cytokine assay kits.

The mice in each group were challenged at week 8 after primary vaccination via footpad injection of 10× $LD_{50}$ of the PRV XJ ($LD_{50}$ = $10^{2.74}$ $TCID_{50}$/ml). The serum of each group of mice was collected at 3 days postchallenge (dpc) to detect IL-6 and TNF-α (KMC0061 and BMS607-3, Thermo). All mice were monitored for 14 days after the challenge and humanely euthanized. The main organs and tissues of each group of mice were sent to Chengdu Lilai Biological Co., Ltd. for hematoxylin–eosin (HE) staining and histopathological observation after fixing with 4% paraformaldehyde.

## Enzyme-Linked Immunosorbent Assay for Antibodies and Cytokine

The serum of each group of mice was collected and subjected to anti-gB antibody by commercial ELISA kit (IDEXX,

United States). Mouse IL-2, IL-4, IFN-γ, TNF-α, and IL-6 ELISA kits were purchased from Thermo Fisher Scientific (MA, United States). All operations were carried out according to the instructions of commercial ELISA kit. NADC30-like PRRSV anti-GP5 and anti-M antibody were detected by NADC30-like GP5 and M antibody ELISA assays constructed in our lab (Zhang, 2021).

## Neutralizing Antibody Assay

BHK-21 or Marc-145 cells were cultured in 96-well plates. The serum was inactivated at 56°C for 30 min, and serial double dilutions (1:2n) were mixed with an equal volume of the PRV-XJ or PRRSV CHSCDJY-2019 and SCNJ-2016 containing 200 $TCID_{50}$; the mixture was incubated at 37°C for 1 h. The mixture was incubated with BHK-21 or Marc-145 cells in a 96-well plate at 37°C for 5–7 days. The CPE in each pore was observed and counted under inverted microscope. Neutralizing antibody titers were calculated as the average of three measurements according to the Reed–Muench method (Hong et al., 2007; Robinson et al., 2015).

## Flow Cytometry

In order to detect the number of $CD3^+/CD4^+/CD8^+$ cells in the spleen of mice, the spleen cells of mice were isolated at 2 wpv after primary immunization. The dispersed spleen cells were adjusted to $10^7$/ml and mixed with the PE-Cy anti-mouse CD8α (70-AM008A04-100, MULTI), FITC anti-mouse CD4 (70-AM00401-100, MULTI), and APC Hamster Anti-Mouse CD3ε (70-AM003E07-100, MULTI) for 30 min at 37°C. Subsequently, the cells were washed three times with PBS and analyzed by flow cytometry.

## Statistical Analysis

All data are expressed as the means ± standard errors (SEs). The data analysis between different groups was analyzed by two-tailed Student's *t*-test and/or one-way analysis of variance (ANOVA) of the GraphPad Prism 8.0 software. A value of $p \leq 0.05$ was considered statistically significant ($^*p < 0.05$, $^{**}p < 0.01$, and $^{***}p < 0.001$).

# RESULTS

## Generation and Characterization of the Recombinant Pseudorabies Virus-NC56

The target gene (CMV-EGFP-T2A-ORF6-P2A-ORF5-SV40) was inserted in the location of gE and gI gene deletion of PRV XJ strain by CRISPR/Cas9-mediated homologous recombination, and the TK gene was deleted by CRISPR/Cas9 (**Figure 1A**). The inserted target fragment is driven by CMV endogenous promoter, and the independent expression of EGFP, M, and GP5 proteins is realized by ribosomal jump translation of 2A cleavage peptide. The first generation of CRISPR/Cas9-mediated recombinant viruses (rPRV-ΔgE/gI-NC-ORF5-6) were harvested after infection with a 0.1 MOI of PRV XJ, which showed the highest efficiency for gene recombination. rPRV-ΔgE/gI-NC-ORF5-6 proliferated continuously in BHK-21 cells for five generations. PCR detection results of the five generations of rPRV-ΔgE/gI-NC-ORF5-6 cultures showed that gE and gI genes were negative, and gB, TK, and partial inserted target genes (ORF6-P2A-ORF5) were positive (**Figure 1C**). The TK gene of rPRV-ΔgE/gI-NC-ORF5-6 was deleted by CRISPR/Cas9, and the recombinant virus rPRV-ΔgE/gI/TK-NC-ORF5-6 (rPRV-NC56) was obtained (**Figure 1B**). The results of PCR detection of TK gene of F1–F5 generations of rPRV-NC56 and PRV-XJ showed that there were 661- and 1,579-bp charged swimming bands, respectively (**Figure 1D**).

The NADC30-like PRRSV GP5, M protein expression in BHK-21 cells that were infected with rPRV-NC56 were confirmed by indirect immunofluorescence assay (IFA) and Western blot. The expression of PRV gE and gB proteins of the recombinant virus was verified by Western blot. The PRV XJ strain was used as the control. For assessment of the NADC30-like PRRSV GP5 and M protein and PRV gE, gB protein expression, BHK-21 cells infected with rPRV-NC56 or PRV XJ were lysed by RIPA lysis solution, and the cell lysates were analyzed by Western blot. The expression of β-actin was detected in all groups with Western blot. The band specifically recognized by the rabbit anti-GP5 and anti-M antibody appeared in the BHK-21 cells infected with rPRV-NC56 but not in those infected with PRV XJ strain (**Figure 2A**). The band specifically recognized by the rabbit anti-gB antibody appeared in the BHK-21 cells infected with rPRV-NC56 and PRV XJ strain. The band specifically recognized by the rabbit anti-gE antibody showed in the BHK-21 cells infected with PRV XJ strain but not in those infected with rPRV-NC56 (**Figure 2B**). The expression of GP5 and M proteins in rPRV-NC56- and PRV XJ-infected BHK-21 cells was identified by IFA. The identification results showed that rPRV-NC56-infected BHK-21 cells were positive and PRV XJ-infected BHK-21 cells were negative (**Figure 2C**).

## Biological Characteristics of Recombinant Pseudorabies Virus-NC56

We analyzed the one-step growth curves and plaque experiments of rPRV-NC56, rPRV XJ-ΔgE/gI/TK-EGFP, and PRV XJ strains to determine whether the insertion and expression of foreign fragments affect the biological characteristics of the virus. One-step growth curve showed that within 18 h after rPRV-NC56 infected BHK-21 cells, the virus titer in the supernatant was lower than that of the parent strain PRV-XJ and rPRV XJ-ΔgE/gI/TK-EGFP, and from 24 h after infection, the titer of rPRV-NC56 was similar to those of PRV-XJ and rPRV XJ-ΔgE/gI/TK-EGFP in BHK-21 cells (**Figure 3A**). The empty spot areas of rPRV-NC56 and rPRV XJ-ΔgE/gI/TK-EGFP were not significantly different, but they have a plaque size of about 60% of the parental PRV XJ strain (**Figure 3B**). In addition, the gene deletion and the stability of the foreign gene carrying the recombinant virus (F1–F21) were verified by PCR. The recombinant viruses were identified by PCR for deletion of gE, gI, and TK genes. There were no electrophoretic

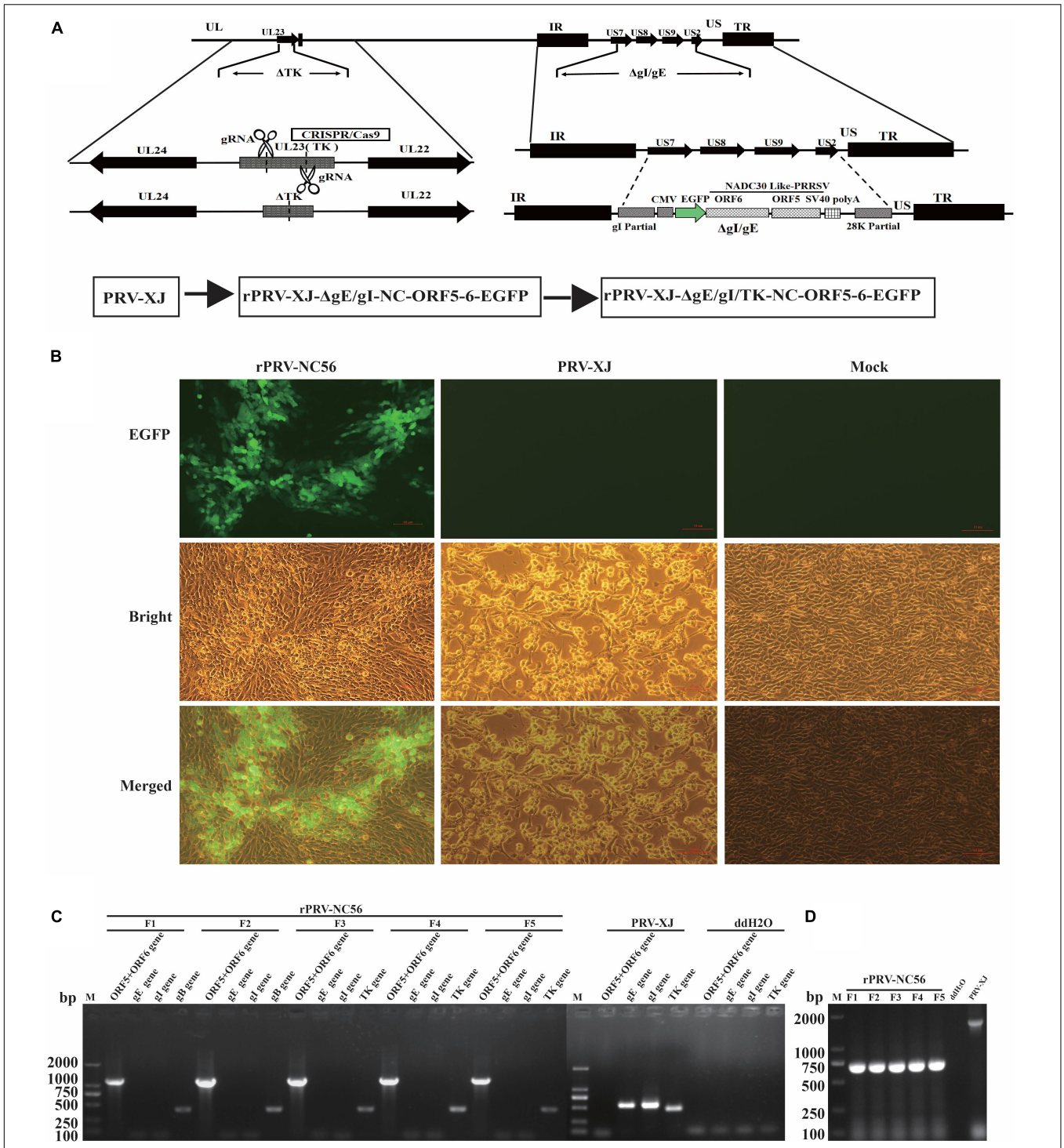


**FIGURE 1 |** Construction of recombinant pseudorabies virus (rPRV)-NC56. **(A)** Schematic diagram of recombinant pseudorabies virus (PRV) construction strategy. **(B)** Baby hamster Syrian kidney (BHK-21) cells infected with rPRV-NC56 and PRV XJ were observed under fluorescence microscope. **(C)** PCR identification results of the gE, gI, gB, TK, and partial inserted target genes (ORF5-6) of rPRV-ΔgE/gI-NC-ORF5-6 cultures. **(D)** PCR identification of the CRISPR/Cas9 deletion of the TK gene.

bands for gE, gI genes, and the TK gene and inserted foreign gene (ORF6-P2A-ORF5), respectively, showed an electrophoretic band of about 661 and 1,191 bp, which was consistent with the expected results, indicating that gE, gI, and TK genes were effectively absent, and the inserted foreign gene was stably carried (**Figure 3C**).

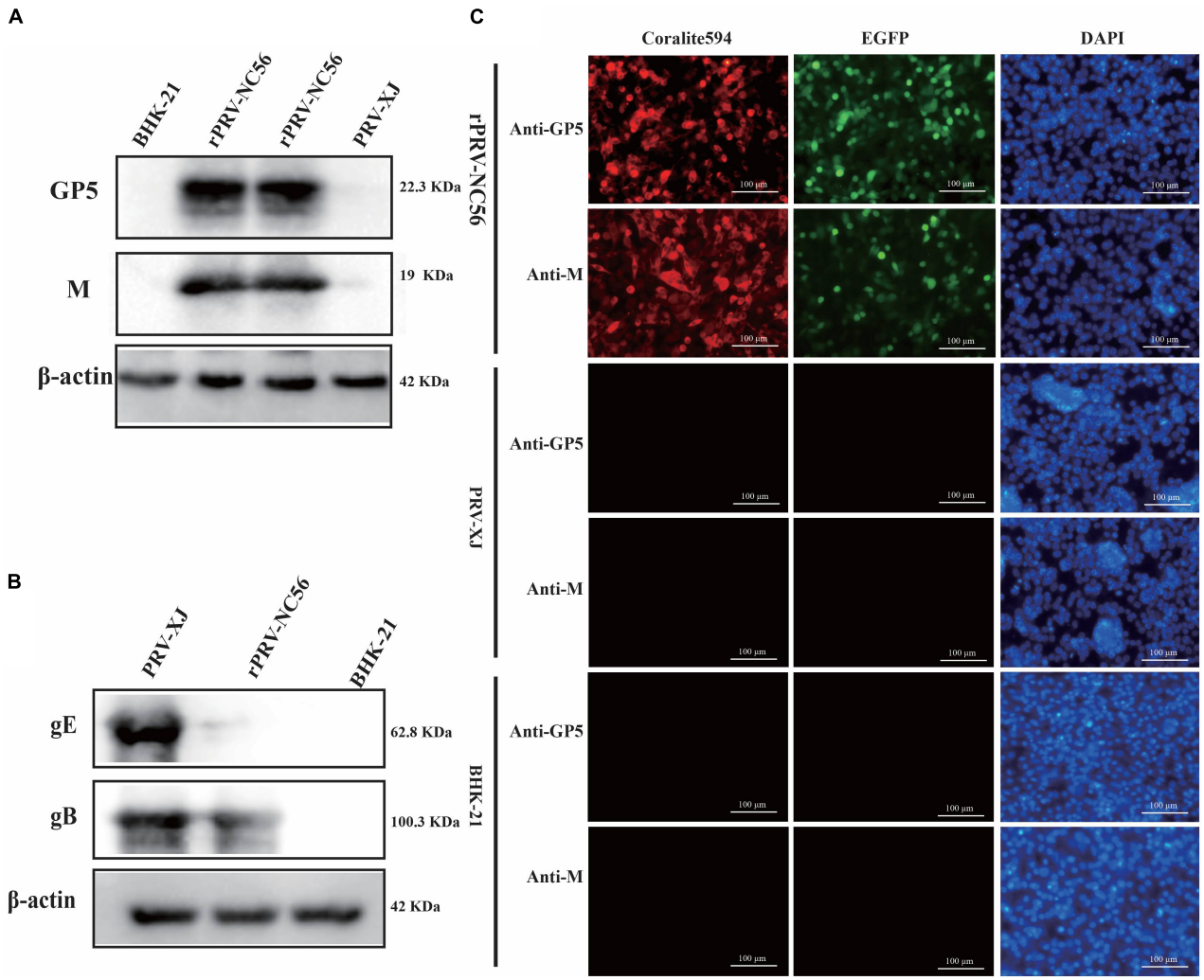


**FIGURE 2 |** Western blot and immunofluorescence assay (IFA) identification of recombinant pseudorabies virus rPRV-NC56. **(A)** Western blotting analysis of NADC30-like porcine reproductive and respiratory syndrome virus (PRRSV) GP5 and M proteins in BHK-21 cells infected with rPRV-NC56. **(B)** Western blotting analysis of PRV gE and gB protein in BHK-21 cells infected with rPRV-NC56. **(C)** Detection of the GP5 and M protein expression through an IFA. Green, EGFP; red, GP5 protein-positive cells; blue, DAPI-stained BHK-21 cell nucleus. DAPI, 4′,6-diamidino-2-phenylindole.

## Observation of Recombinant Pseudorabies Virus-NC56 Virus Particles and Porcine Reproductive and Respiratory Syndrome Virus-Like Particles by Transmission Electron Microscopic

The difference of virus particle structure between rPRV-NC56, rPRV XJ-ΔgE/gI/TK-EGFP, and PRV XJ strains, and the formation of VLPs by NADC30-like PRRSV GP5 and M proteins expressed by the rPRV-NC56 virus was investigated by an electron microscope. As in **Figure 4A**, the mature envelope PRV virus particles with the size of about 120–130 nm were found in the cytoplasm in Marc-145 cells infected with rPRV-NC56, rPRV XJ-ΔgE/gI/TK-EGFP, and PRV XJ. A similar morphology of viral particles was found to exist in all three groups and show the typical structure of PRV. Mature PRRSV virus particles with a size of about 40–60 nm can be found in the vesicles of Marc-145 cells infected by PRRSV CHSCDJY-2019. Interestingly, mature PRV virus particles of about 120–130 nm and nucleic acid-free 40- to 60-nm PRRSV VLPs can concurrently be found in the vesicles of BHK-21 cells infected with rPRV-NC56 (**Figure 4A**). The specific bands of GP5 and M proteins were detected in the rPRV-NC56 infection group and the CHSCDJY-2019 infection group in the supernatant of Marc-145 cells infected with rPRV-NC56 and CHSCDJY-2019 (**Figure 4B**).

## Safety of Recombinant Pseudorabies Virus-NC56 in Mice

We used mice to evaluate the safety of the recombinant virus, and the results are shown in **Figure 5**.

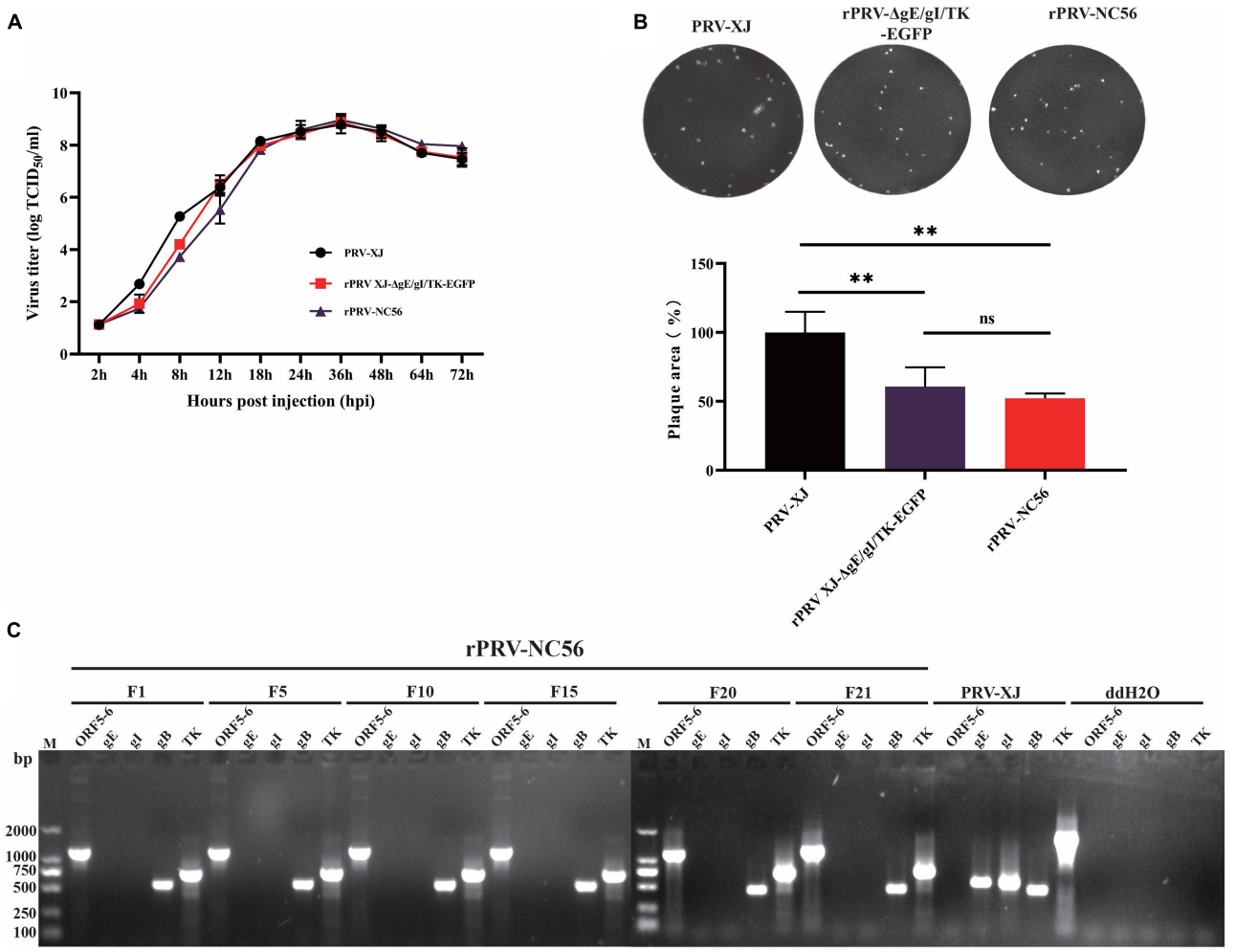


**FIGURE 3 |** Biological characterization of recombinant pseudorabies virus rPRV-NC56. **(A)** One-step growth curves of PRV XJ, rPRV XJ-ΔgE/gI/TK-EGFP, and rPRV-NC56 in BHK-21 cells. **(B)** Comparison of plaque size of BHK-21 cells infected with PRV XJ, rPRV XJ-ΔgE/gI/TK-EGFP, and rPRV-NC56. **(C)** PCR identification of gE, gI, gB, TK, and a partially inserted target gene (ORF5-6) in cell cultures from generations 1, 5, 10, 15, 20, and 21 of rPRV-NC56. $^{**}p < 0.01$.

After injection with different doses of rPRV-NC56, rPRV XJ-ΔgE/gI/TK-EGFP, and DMEM culture medium, the mice showed no clinical symptoms and death during the observation period (14 days). The mice injected with $10^3$ $TCID_{50}$/ml of PRV XJ showed itching and bite symptoms, and all of them died within 7 days. The $10^2$ $TCID_{50}$/ml of PRV XJ-infected mouse group died (50%) within 8 days (**Figure 5A**). PRV XJ infection led to a significant increase in the IL-6 and TNF-α expression in serum at 3 dpi, whereas the IL-6 and TNF-α expression in rPRV-NC56 and rPRV XJ-ΔgE/gI/TK-EGFP infected groups had no significant differences (**Figures 5B,C**). Meanwhile we analyzed the pathological changes in the brain tissues of mice in each group. The results of pathological analysis showed that PRV XJ infection led to a disordered arrangement of cell layers in the cerebral cortex and degeneration and necrosis of neuronal cells, but the rPRV-NC56 and rPRV XJ-ΔgE/gI/TK-EGFP infection groups had no pathological changes (**Figure 5D**). The results showed that rPRV-NC56 virus is safe for mice.

## The Recombinant Pseudorabies Virus-NC56 Can Colonize and Express the Target Protein in the Lung of Mice for a Long Time

To investigate the proliferation and the expression of target gene in the lungs of rPRV-NC56-immunized mice, we identified the colonization and target protein expression in the lungs of mice immunized with rPRV-NC56 at different times by qPCR and IHC, respectively. The results of IHC detection are shown in **Figures 6A,B**. A few GP5 IHC-positive cells could be found in the lung at 1 dpv after rPRV-NC56 i.m. immunization; the number of positive cells gradually increased at 3 dpv, the most at 5 dpv, and the positive cells could still be found in the lung until 21 dpv. The viral genome DNA in the lung was detected by qPCR. The calibration equation is Y = −3.295X + 33.868, E = 97.6%, $R^2$ = 1.000, Slope = −33.382, y-int = 33.868. In the results shown in **Figure 6C**, gB gene could be detected in the lung at 1 dpv after

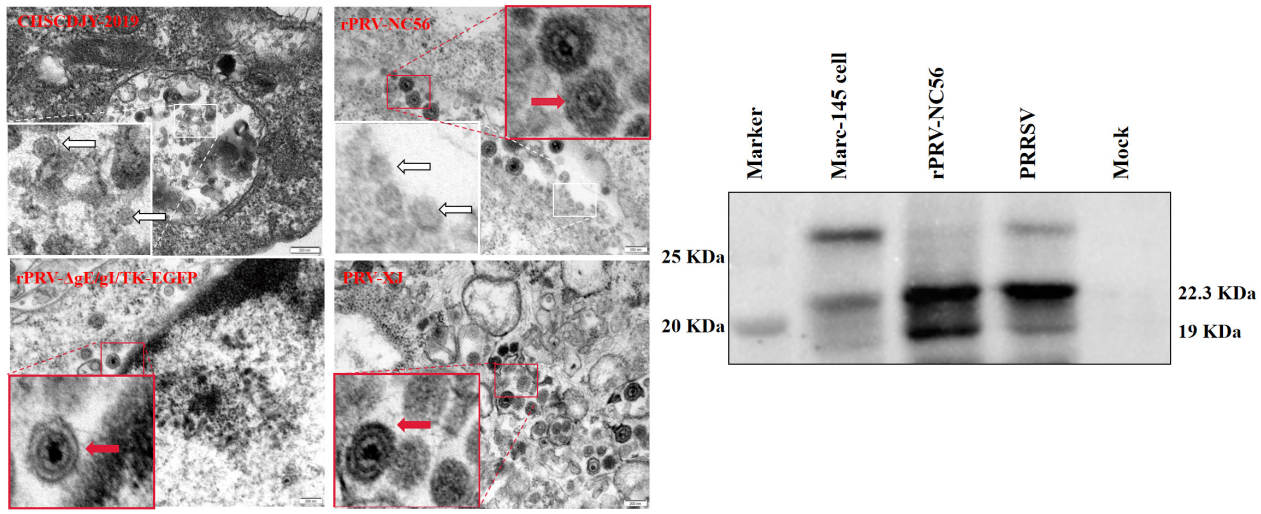


**FIGURE 4 |** Transmission electron microscopy analysis of PRRSV, PRV XJ, rPRV XJ-ΔgE/gI/TK-EGFP, and rPRV-NC56 in Marc-145 cells. **(A)** PRRSV CHSCDJY-2019 PRV XJ, rPRV XJ-ΔgE/gI/TK-EGFP, and rPRV-NC56 in Marc-145 cells. The red arrow indicates PRV virus particles, and the white arrow indicates PRRSV virus particles and virus-like particles. **(B)** PRRSV GP5 and M proteins in ultrafiltration cell culture supernatant of Marc-145 cells infected with rPRV-NC56 were identified by Western blotting. Virus-like particles (VLPs) assembled by GP5 and M proteins will be intercepted by ultrafiltration column (100 kDa).

rPRV-NC56 immunization, which lasted until the 21st day, and the copies of gB gene was the highest at 5 dpv.

## NADC30-Like Porcine Reproductive and Respiratory Syndrome Virus-Specific Antibodies and Pseudorabies Virus-Specific gB Antibodies Can Be Induced by Recombinant Pseudorabies Virus-NC56 in Mice

To evaluate the specific antibody response to rPRV-NC56, indirect ELISA assays and specific virus-neutralizing antibody (VNA) test were used to detect antigen-specific antibodies and neutralizing antibody, and the results are shown in **Figure 7**. The results showed that low antibodies were detected in all vaccinated groups after 2 wpv for the primary vaccination, and the antibodies to gB and GP5, and M turned positive after 1 wpv for the booster vaccination. The virus-specific antibody levels (OD450 values) were gradually increased over time after vaccination. The GP5- and M-specific antibodies were not detected in the control and rPRV XJ-ΔgE/gI/TK-EGFP-immunized mouse group (**Figures 7A,B**). All mouse groups vaccinated with rPRV-NC56 and rPRV XJ-ΔgE/gI/TK-EGFP contained similar levels of gB antibodies in the postimmunization serum (**Figure 7C**). The rPRV-NC56 and rPRV XJ-ΔgE/gI/TK-EGFP vaccinated group exhibited similar neutralization titers against PRV XJ ($p = 0.14$), and the VNA titers of the control group was lower than 1:2 (**Figure 7D**). The rPRV-NC56 vaccinated group exhibited higher levels of VNA titers against PRRSV CHSCDJY-2019 than SCNJ-2016 (**Figures 7E,F**). This result indicates that rPRV-NC56 induces humoral immunity specific for PRRSV GP5 and M protein and does not affect viral production PRV gB antibodies.

## The Innate Immune Cytokines Were Induced by Recombinant Pseudorabies Virus-NC56 in Mice

Potent induction of adaptive immunity depends on efficient activation of the innate immune system. Cytokines, such as IFN-γ, IL-2, IL-4, and IL-6, can enhance adaptive immune response and play an important role in regulating innate and adaptive immunity (Striz et al., 2014). IL-2, IL-4, and IFN-γ were measured by ELISA in the peripheral blood of each mouse group. The rPRV-NC56- and rPRV XJ-ΔgE/gI/TK-EGFP-immunized mice compared with the control group showed significant upregulation of IL-2, IL-4, and IFN-γ (**Figure 8**). IL-2 in the peripheral blood of rPRV-NC56- and rPRV XJ-ΔgE/gI/TK-EGFP-immunized mice at 2, 4, and 6 wpv was continuously increased after primary vaccination, and IL-4 and IFN-γ in the peripheral blood of rPRV-NC56- and rPRV XJ-ΔgE/gI/TK-EGFP-immunized mice were the highest (**Figures 8A–C**). The majority of T cells produce IL-2, IL-4, and IFN-γ during robust T-cell responses.

## The Specific T-Cell Immune Responses Were Induced by Recombinant Pseudorabies Virus-NC56 in Mice

We detected the activation of lymphocytes in spleen and the proliferation of splenocytes stimulated by target antigen to investigate the cellular responses induced by rPRV-NC56 immunization of mice. The splenocytes of rPRV-NC56-immunized mice increased significantly after being stimulated

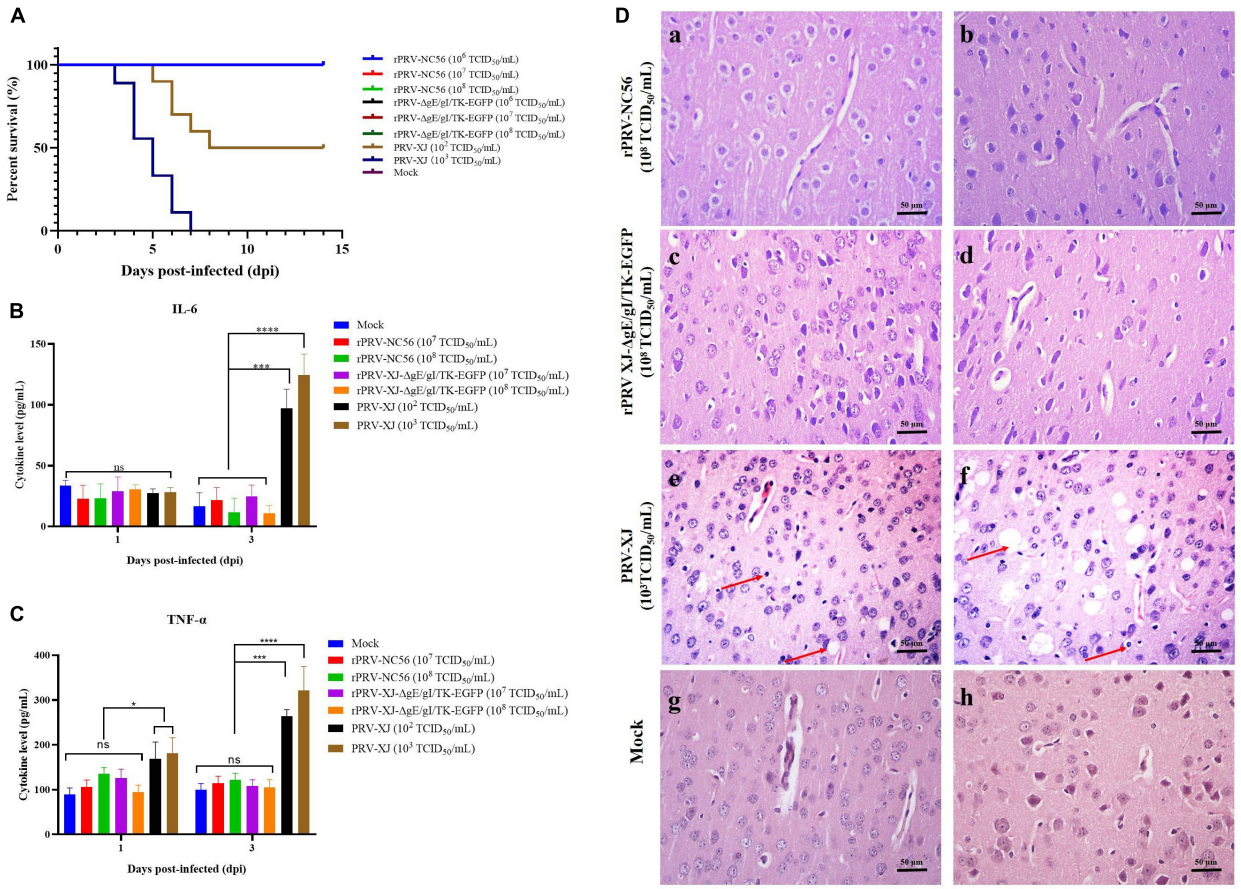


**FIGURE 5 |** The safety assessment of rPRV-NC56. **(A)** Survival rate of mice infected with different titers of PRV XJ, rPRV XJ-ΔgE/gI/TK-EGFP, and rPRV-NC56. **(B)** Plasma IL-6 was detected by enzyme-linked immunosorbent assay (ELISA). **(C)** Plasma TNF-α was detected by ELISA. **(D)** Pathological observation of HE staining in brain tissue of mice infected with PRV XJ, rPRV XJ-ΔgE/gI/TK-EGFP, and rPRV-NC56 (×400). a, c, and e were granulocyte layers in the cerebral cortex, and b, d, and f were the pyramidal cell layers in the cerebral cortex. *$p < 0.05$; **$p < 0.01$; ***$p < 0.005$; and ****$p < 0.001$. Neuronal necrosis and vacuolar degeneration are indicated by red arrows.

by inactivated PRRSV CHSCDJY-2019 and SCNJ-2016 as stimulants, but CHSCDJY-2019 could cause a stronger proliferative response than SCNJ-2016 (**Figure 8D**). The percentage of $CD3^+$, $CD4^+$, and $CD8^+$ T-cell subpopulations in splenic were detected by flow cytometry at 4 wpv. The $CD3^+$, $CD4^+$ and $CD8^+$ T-cell ratios were different between the three groups (**Figure 9**). The $CD3^+$, $CD8^+$, and $CD4^+$ T-cell ratios of rPRV-NC56- and rPRV XJ-ΔgE/gI/TK-EGFP-immunized mouse group had no significant difference, but they were significantly higher than those in the control group ($p < 0.05$ and $p < 0.01$).

## The Recombinant Pseudorabies Virus-NC56 Strains Can Protect Mice 100% From Challenge by the Virulent Strain

To further investigate the protective immunity of rPRV-NC56, after 4 weeks of booster vaccination, the immunized mice were challenged with $1 \times 10^{3.74}$ $TCID_{50}$ of PRV XJ by intramuscular injection. All mice were observed for 14 dpc. During the observation period, no clinical symptoms related to pseudorabies were observed in mice immunized with RPRV-NC56 and rPRV XJ-ΔgE/gI/TK-EGFP, and no mice died (**Figure 10A**). The mice in the control group began to die at 3 dpc, and all mice died at 5 dpc. At 3 dpc, the blood of all challenged mice was collected from the tail vein to detect the inflammatory cytokines IL-6 and TNF-α. There was a highly significant upregulation of IL-6 and TNF-α in the control group compared with the rPRV-NC56, rPRV XJ-ΔgE/gI/TK-EGFP immune group, while there was no significance in the rPRV-NC56 and rPRV XJ-ΔgE/gI/TK-EGFP immune group (**Figure 10B**).

Histopathological examination of mice brain, heart, liver, spleen, lungs, and kidneys were performed at 5 dpc. The rPRV-NC56- and rPRV XJ-ΔgE/gI/TK-EGFP-vaccinated group did not display significant histopathological changes in the tissues. However, in the control group, there were neuronal cell degeneration, necrosis, and vacuolization in the cortical region of the brain, hemorrhage in the heart and liver, vacuolar degeneration and necrosis of the liver cells, unclear demarcation of white pulp and red pulp and thickening of the trabecular

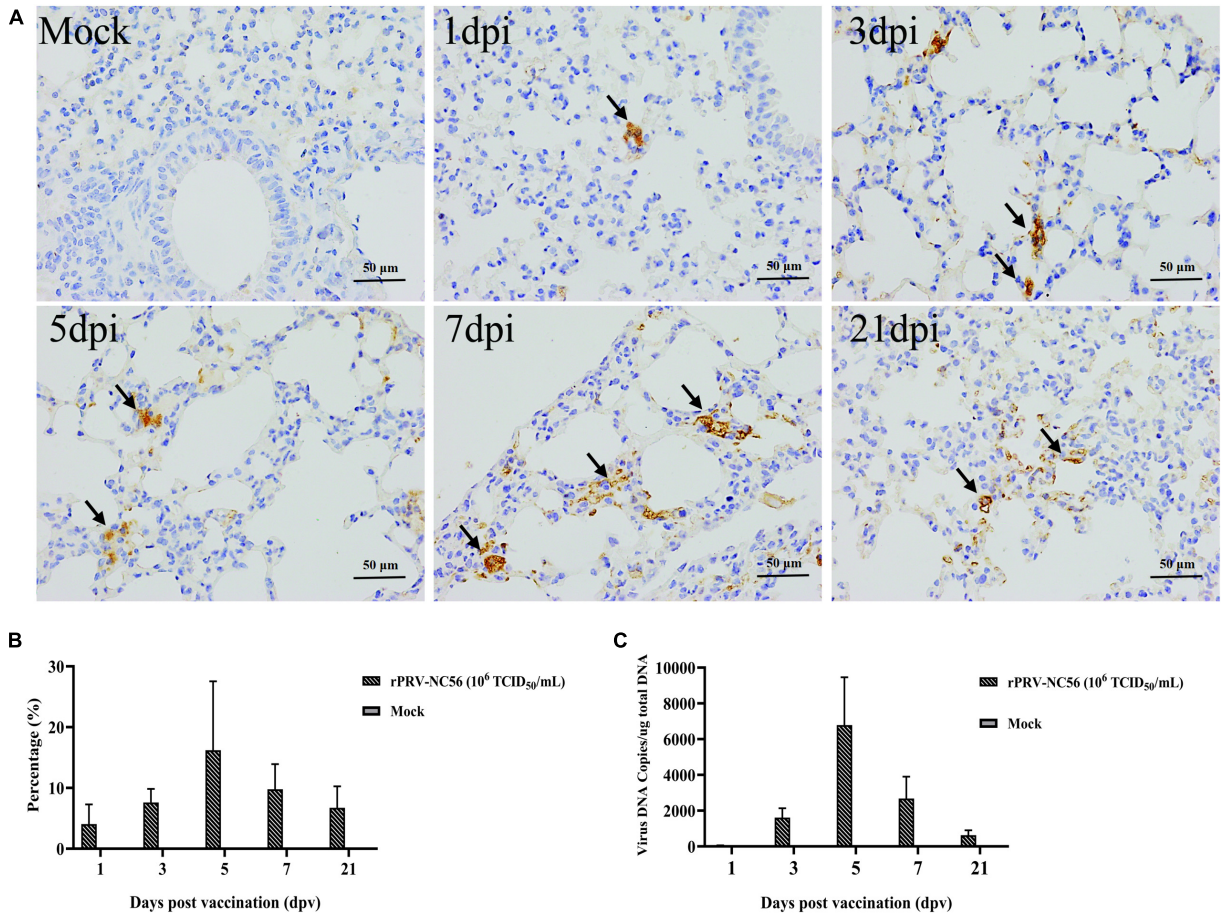


**FIGURE 6 |** The colonization properties of rPRV-NC56 in mouse lungs. **(A)** IHC identification of GP5 protein expression in the mouse lungs of rPRV-NC56-infected mice at 1, 3, 5, 7, and 21 dpv. The brown precipitate indicated by the black arrow indicates the cells expressing GP5 protein (×400). **(B)** Percentage of positive cells expressing GP5 protein identified by IHC. **(C)** qPCR identification of gB gene in the lungs of rPRV-NC56-immunized mice.

meshwork in the spleen, thickening of the alveolar wall, degeneration and necrosis of some alveolar epithelial cells and inflammatory cell infiltration in the lung interstitium in the lung, glomerular edema, and cell necrosis in the kidneys (**Figure 10C**).

## DISCUSSION

Porcine reproductive and respiratory syndrome remains a major challenge in the pig industry and causes significant economic loss annually. Vaccine immunity remains an important means to control the PRRSV outbreak and epidemic. The continuous evolution of PRRSV, resulting in simultaneous outbreaks and epidemics of multisubtype strains, has made PRRS prevention and control more complicated. The NADC30-like PRRSV strain is the main epidemic strain with the second detection rate compared with the HP-PRRSV strain in China (Sun et al., 2020). Whether the currently available commercial PRRSV vaccine based on classical PRRSV and HP-PRRSV strains can prevent or worsen the diseases infected by the new subtype PRRSV strains requires to be further confirmed. Several studies have reported the evaluation of the protective effect of commercial PRRSV vaccine on NADC30-like PRRSV strain. Ingelvac PRRS MLV (United States) and modified live virus (MLV) vaccine derived from classical PRRSV (VR2332) or HP-PRRSV (TJ and JXA1) have been reported to provide optimistic cross protection for some NADC30-like PRRSV strains isolated in China (Zhang et al., 2018; Wei et al., 2019; Chai et al., 2020). However, some studies have shown that the above commercial vaccines can only provide limited protection against some NADC30 PRRSV strains (FJWQ16, HNhx, and CHsx1401) (Bai et al., 2016; Zhou et al., 2017; Wei et al., 2019; Chen et al., 2021). PRRSV CHSCDJY-2019 was isolated from the serum of piglets with severe respiratory clinical symptoms and viremia. It was the result of the recombination of NADC30 strain with TJ-like PRRSV and HP-PRRSV (Zhao et al., 2021). GP5 is the major glycoprotein of PRRSV and carries the major neutralizing epitope (Popescu et al., 2017). M is the most conserved membrane protein in PRRSV, which can cause strong cellular immune response (Bautista et al., 1999; Murtaugh et al., 2010). The formation of disulfide-linked complexes between GP5 and M through disulfide bonds is the key mechanism

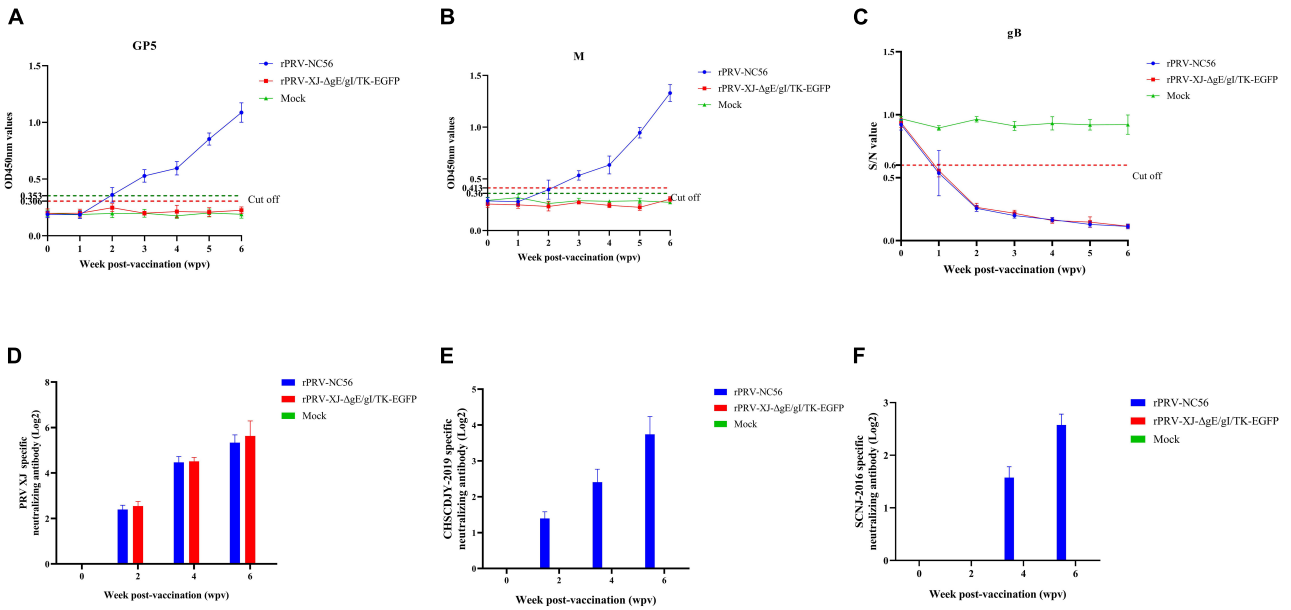


**FIGURE 7 |** Immune responses after immunization with rPRV-NC56. **(A)** The GP5-specific antibodies were calculated by ELISA. **(B)** The M-specific antibodies were calculated by ELISA. **(C)** The gB-specific antibodies were calculated by ELISA. **(D)** Detection results of anti-PRV XJ-neutralizing antibody titer in the serum of immunized mice. **(E)** Detection results of anti-PRRSV CHSCDJY-2019-neutralizing antibody titer in the serum of immunized mice. **(F)** Detection results of anti-PRRSV SCNJ-2016-neutralizing antibody titer in the serum of immunized mice.

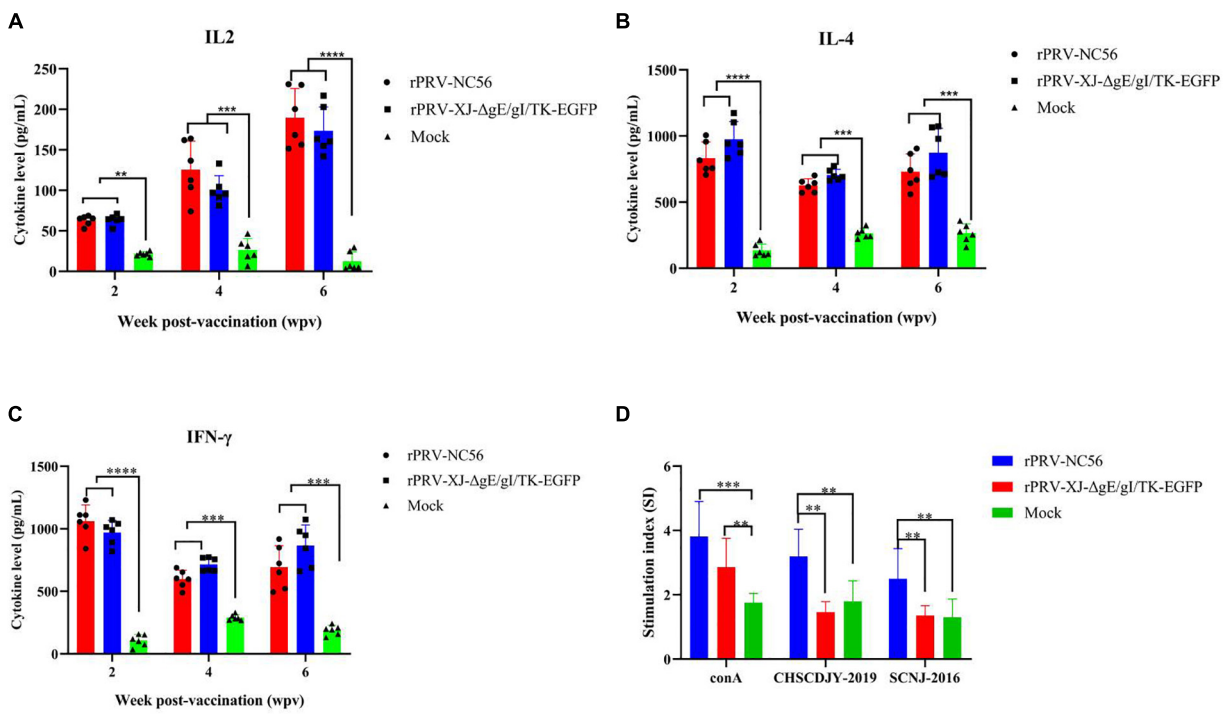


**FIGURE 8 |** The T cellular response analyses of blood sample from rPRV XJ-ΔgE/gI/TK-EGFP, rPRV-NC56, and nonvaccinated groups. **(A)** Plasma IL-2 was detected by ELISA. **(B)** Plasma IL-4 was detected by ELISA. **(C)** Plasma IFN-γ was detected by ELISA. **(D)** Splenic lymphocytes were assayed for T-cell-specific proliferative responses using the MTT kit. *$p < 0.05$; **$p < 0.01$; ***$p < 0.005$; and ****$p < 0.001$.

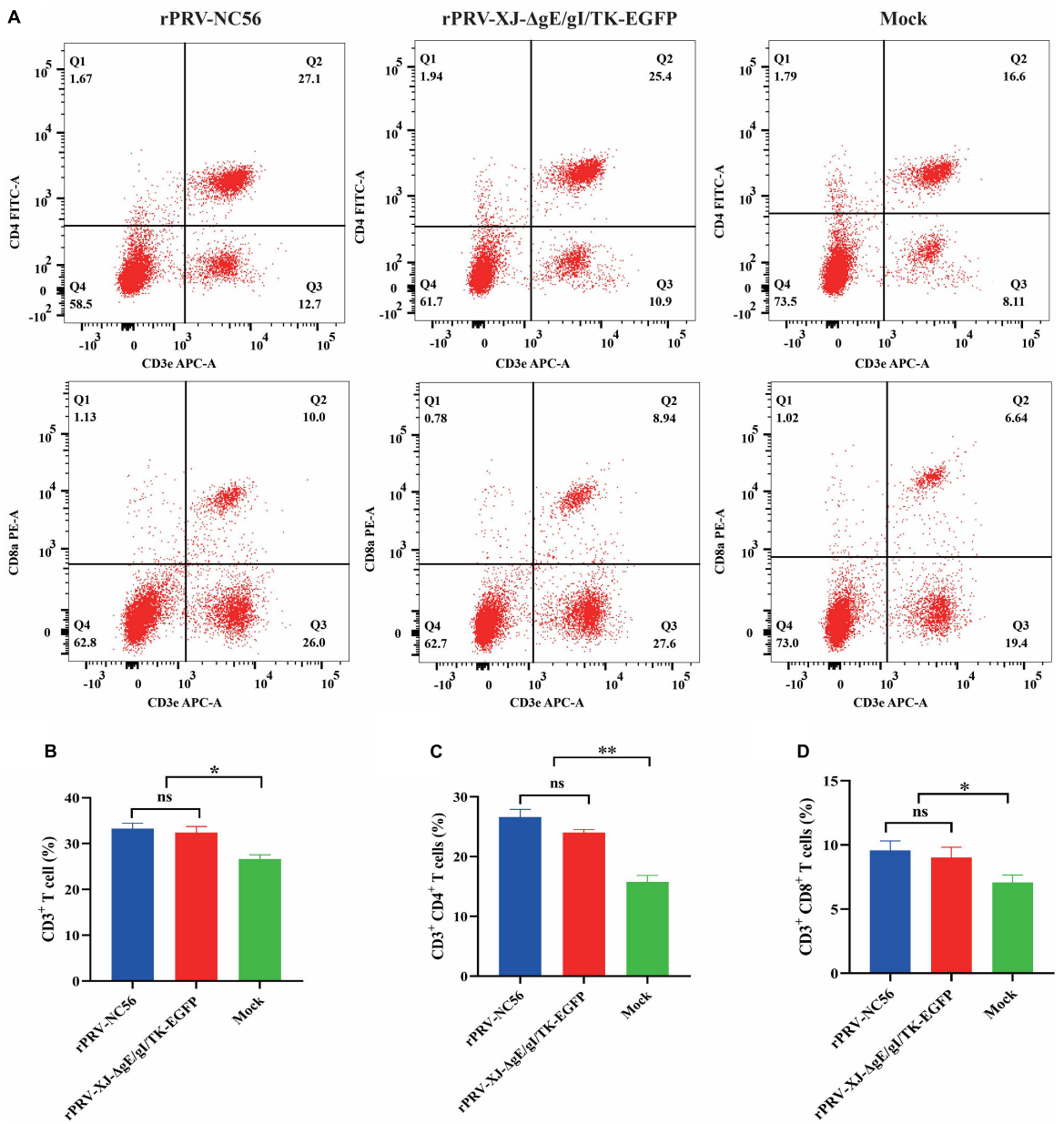


**FIGURE 9 |** Flow cytometric analysis of $CD3^+/CD4^+/CD8^+$ cells in the spleen of rPRV XJ-ΔgE/gI/TK-EGFP, rPRV-NC56, and nonvaccinated groups. **(A)** Flow cytometry analysis of $CD3^+$, $CD3^+$ $CD4^+$, and $CD3^+$ $CD8^+$ T-cell populations at 2 weeks postvaccination (wpv) after immunization ($n$ = 6/each group). The data show the percentage of $CD3^+$ **(B)**, $CD3^+$ $CD4^+$ **(C)**, and $CD3^+$ $CD8^+$ **(D)** T cells in the total splenocytes. By GraphPad Prism 5.0, unpaired $t$-test, $^*p < 0.05$; $^{**}p < 0.01$; $^{***}p < 0.005$; and $^{****}p < 0.001$.

for the production of VLPs (Mardassi et al., 1996). Fusion expression of GP5 and M proteins or multigene co-expression can cause more neutralizing antibodies against GP5 than GP5 protein alone (Jiang et al., 2006, 2007; Zheng et al., 2007).

The expression of foreign genes by gene deletion-attenuated PRV live virus vector is a very mature antigen presentation system. In previous studies, we have confirmed that piglets immunized with JXA1-R vaccine will still have elevated body temperature, respiratory symptoms, severe viremia, and lung pathological changes after being infected with CHSCDJY-2019 (data not published). In the present study, we constructed a recombinant pseudorabies virus (rPRV-NC56) co-expressing GP5 and M proteins of NADC30-like PRRSV. The gE, gI, and TK genes of the recombinant virus were knocked out at the same time as foreign gene insertion. In order to enable GP5 and M proteins to express independently without affecting each other's later modification, self-cleavage T2A and P2A

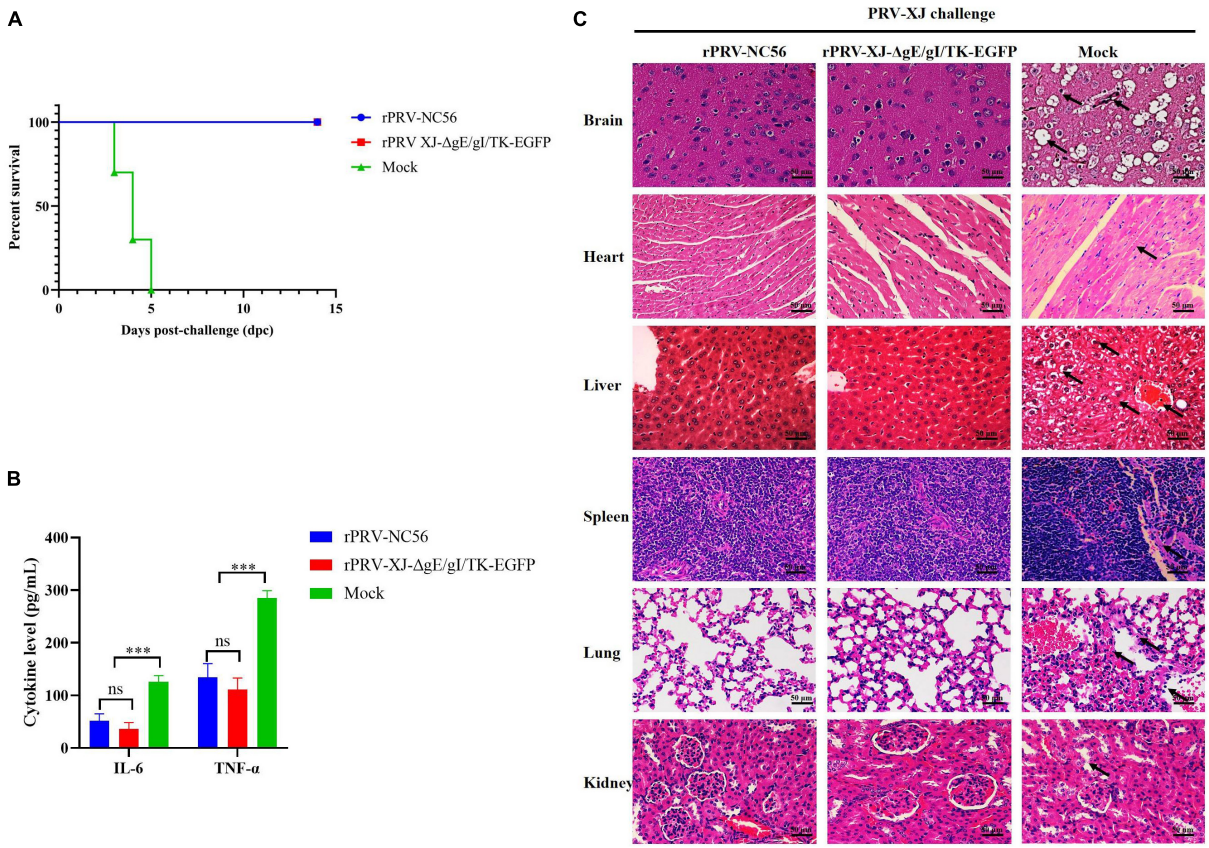


**FIGURE 10 |** Recombinant pseudorabies virus-NC56 has a 100% protective capacity against challenge by virulent PRV XJ. **(A)** The survival rate of rPRV XJ-ΔgE/gI/TK-EGFP, rPRV-NC56, and nonvaccinated mice groups challenged with PRV XJ strain. **(B)** The results of inflammatory cytokines (IL-6 and TNF-α) in the serum of mice in each group at 3 dpc by ELISA. **(C)** Histopathological examination of mice brain, heart, liver, spleen, lungs, and kidneys at 5 days postchallenge (dpc) (×400). *$p < 0.05$; **$p < 0.01$; ***$p < 0.005$; and ****$p < 0.001$. Pathological lesions in all tissues were described in the results.

peptides were introduced (Tang X. et al., 2016). The rPRV-NC56 carries the foreign gene to proliferate within BHK-21 cells for 21 generations. This strain is a potential marker vaccine for PRRSV DIVA and a targeted vaccine against NADC30-like PRRSV strain. In addition, PRV gE, gI, and TK gene-deficient live attenuated vaccine can colonize the host for a long time and cause a strong immune response (Hu et al., 2015; Wang et al., 2020). Therefore, we anticipate that the foreign gene would be persistently expressed, together with PRV replication, to constantly stimulate immune responses in the host. In addition, several studies have confirmed that PRRSV GP5 and M proteins can assemble into VLPs, and independently expressed GP5 and M proteins are capable of self-assembling intracellular assembly into VLPs (Binjawadagi et al., 2016; García Durán et al., 2016; Xu et al., 2021). PRRSV VLPs can induce a stronger immune response than commercial vaccines (Nam et al., 2013). In this study, we found that the virus particles of pseudorabies virus and VLPs of PRRSV in BHK-21 cells were infected with rPRV-NC56. The morphology and size of PRRSV VLPs (approximately 40–60 nm) expressed by rPRV-NC56 were largely similar to PRRSV virions and PRRSV VLPs composed of GP5 and M proteins expressed by baculovirus (Nam et al., 2013; Binjawadagi et al., 2016; Xu et al., 2021). We detected the Viral gene copies and the number of infection-positive cells in the lung tissue of rPRV-NC56-immunized mice by qRT-PCR and IHC. The rPRV-NC56 can colonize and express foreign protein in lung tissue for a long time in mice. From 3 to 21 dpv after immunization, the gB gene of rPRV-NC56 can be detected in the lungs, and IHC can detect the sustained expression of GP5 protein in the lungs.

Mouse is the natural host of PRV and the research model for PRV vaccine development and neural transmission. We evaluated the safety and immunogenicity of rPRV-NC56 in mice. The inflammatory cytokines IL-6 and TNF-α in the serum of high-dose rPRV-NC56-immunized mice did not change significantly, while they were significantly upregulated in the serum of PRV XJ-infected mice. No pathological changes were found in the brain of mice immunized with high-dose rPRV-NC56, compared with PRV XJ-infected mice. This is consistent with previous studies, indicating that the NADC30-like PRRSV/PRV bivalent vaccine is safe and will not cause clinical symptoms and histopathological changes in mice (Zhao et al., 2020). After the second immunization, specific antibodies and neutralizing antibodies against PRV and PRRSV in mice inoculated with rPRV-NC56 increased continuously. The neutralizing antibody

titer of NADC30-like PRRSV in the serum of rPRV-NC56-immunized mice was higher than that of HP-PRRSV. PRRSV infection has been reported to decrease in $CD4^+$ T cells and increase in $CD8^+$ T cells in piglets (Tingstedt and Nielsen, 2004; Dwivedi et al., 2012). In this study, rPRV-NC56 could effectively activate the specific T-cell immune system, and $CD3^+$ and $CD3^+$ $CD8^+$ T cells increased significantly after inoculation with attenuated strain compared with other groups. However, there was no significant difference in the $CD4^+$ T cell level in the experimental and control groups. This may also have been an association between the PRRSV GP5 and M proteins expressed by rPRV-NC56.

The stimulation of T-cell-mediated IFN-γ response upon immunization is a major focus for assessing the improvement of vaccine efficacy. There is a positive correlation between the frequency of virus-specific IFN-γ-secreting cells and the clinical outcome upon PRRSV infection after immunization with the PRRSV vaccine (Martelli et al., 2009). Meanwhile, IFN-γ plays a key role in innate and adaptive immunity induced by herpes simplex virus and PRV (Paludan et al., 2002; Yao et al., 2007).

We investigated the proliferative response of rPRV-NC56-immunized mice spleen cells stimulated by NADC30-like PRRSV and inactivated HP-PRRSV. The stimulation index and IFN-γ concentrations in the cell culture medium of the inactivated NADC30-like PRRSV stimulation group were significantly higher than that of the inactivated HP-PRRSV stimulation group, indicating that there was a significant difference in cell response between the two subtypes of PRRSVs. The concentrations of IL-2, IL-4, and IFN-γ in the sera of rPRV-NC56- and rPRV XJ-ΔgE/gI/TK-EGFP-immunized mice were similar, but significantly upregulated compared with the nonimmunized group. IL-2 is produced by T cells, which are capable of promoting killer cell differentiation and effector, B-cell proliferative differentiation, and macrophage activation. IL-4 is produced by Th2 subsets of cells, promoting proliferation and differentiation of B cells and enhance the humoral immune response.

## CONCLUSION

In conclusion, we constructed a recombinant pseudorabies virus (rPRV-NC56) co-expressing NADC30-like PRRSV GP5 and M proteins. The GP5 and M proteins were autonomously loaded into VLPs in cells. The rPRV-NC56 colonizes the lung tissue of mice for prolonged periods and continuously expresses NADC30-like PRRSV GP5 and M proteins. The rPRV-NC56, similar to rPRV XJ-ΔgE/gI/TK-EGFP, could effectively activate protective immunity and produce specific antibodies. The rPRV-NC56 could activate high levels of neutralizing antibodies against PRV and NADC30-like PRRSV. Vaccination and challenge experiments showed that rPRV-NC56 elicited complete protection of mice against PRV. The rPRV-NC56 vaccine could serve as a DIVA vaccine in the further control and eradication of PRRSV. The evaluation of the safety and immunogenicity of rPRV-NC56 based on the PRV natural host mouse model can provide a reference for rPRV-NC56 in conducting vaccine evaluation studies on animals.

## DATA AVAILABILITY STATEMENT

The original contributions presented in the study are included in the article/**Supplementary Material**, further inquiries can be directed to the corresponding author.

## ETHICS STATEMENT

The animal study was reviewed and approved by the Sichuan Provincial Laboratory Animal Management Committee [License No: SYXK (chuan) 2019-187].

## AUTHOR CONTRIBUTIONS

ZX and LZ conceived the project. JZ designed the experiments and wrote the manuscript. JZ, FL, LX, and YZ performed most of the experiments. XS, HD, SG, and YH contributed the materials and participated in the discussion. ZX supervised the work and edited the final version of the manuscript, which was read and approved by all authors.

## FUNDING

This work was supported by the Key Research and Development Project of Sichuan Science and Technology Plan: Research and Integration Demonstration of Key Technologies for Improving Quality and Efficiency of Sichuan Pig Industry Cain (2020YFN0147), Program Sichuan Veterinary Medicine and Drug Innovation Group of China Agricultural Research System (CARS-SVDIP). The funders had no role in the design of the collection, analysis, and interpretation of data.

## SUPPLEMENTARY MATERIAL

The Supplementary Material for this article can be found online at: https://www.frontiersin.org/articles/10.3389/fmicb.2022.846079/full#supplementary-material

## REFERENCES

An, T.-Q., Peng, J.-M., Tian, Z.-J., Zhao, H.-Y., Li, N., Liu, Y.-M., et al. (2013). Pseudorabies virus variant in bartha-K61-vaccinated pigs, China, 2012. *Emerg. Infect. Dis.* 19, 1749–1755. doi: 10.3201/eid1911.130177

Bai, X., Wang, Y., Xu, X., Sun, Z., Xiao, Y., Ji, G., et al. (2016). Commercial vaccines provide limited protection to NADC30-like PRRSV infection. *Vaccine* 34, 5540–5545. doi: 10.1016/j.vaccine.2016.09.048

Bautista, E. M., Suárez, P., and Molitor, T. W. (1999). T cell responses to the structural polypeptides of porcine reproductive and respiratory

syndrome virus. *Arch. Virol.* 144, 117–134. doi: 10.1007/s007050050489

Binjawadagi, B., Lakshmanappa, Y. S., Longchao, Z., Dhakal, S., Hiremath, J., Ouyang, K., et al. (2016). Development of a porcine reproductive and respiratory syndrome virus-like-particle-based vaccine and evaluation of its immunogenicity in pigs. *Arch. Virol.* 161, 1579–1589. doi: 10.1007/s00705-016-2812-0

Chai, W., Liu, Z., Sun, Z., Su, L., Zhang, C., and Huang, L. (2020). Efficacy of two porcine reproductive and respiratory syndrome (PRRS) modified-live virus (MLV) vaccines against heterologous NADC30-like PRRS virus challenge. *Vet. Microbiol.* 248:108805. doi: 10.1016/j.vetmic.2020.108805

Chen, N., Ye, M., Huang, Y., Li, S., Xiao, Y., Li, X., et al. (2019). Identification of two porcine reproductive and respiratory syndrome virus variants sharing high genomic homology but with distinct virulence. *Viruses* 11:875. doi: 10.3390/v11090875

Chen, X.-X., Zhou, X., Guo, T., Qiao, S., Guo, Z., Li, R., et al. (2021). Efficacy of a live attenuated highly pathogenic PRRSV vaccine against a NADC30-like strain challenge: implications for ADE of PRRSV. *BMC Vet .Res.* 17:260. doi: 10.1186/s12917-021-02957-z

Deng, Y., Pan, Y., Wang, D., Zhou, Q., Bi, Y., Chen, F., et al. (2012). Complete genome sequence of porcine reproductive and respiratory syndrome virus strain QY2010 reveals a novel subgroup emerging in China. *J. Virol.* 86, 7719–7720. doi: 10.1128/JVI.00977-12

Dwivedi, V., Manickam, C., Binjawadagi, B., Linhares, D., Murtaugh, M. P., and Renukaradhya, G. J. (2012). Evaluation of immune responses to porcine reproductive and respiratory syndrome virus in pigs during early stage of infection under farm conditions. *Virol. J.* 9:45. doi: 10.1186/1743-422X-9-45

Feng, Z., Chen, J., Liang, W., Chen, W., Li, Z., Chen, Q., et al. (2020). The recombinant pseudorabies virus expressing African swine fever virus CD2v protein is safe and effective in mice. *Virol. J.* 17:180. doi: 10.1186/s12985-020-01450-7

Freuling, C. M., Müller, T. F., and Mettenleiter, T. C. (2017). Vaccines against pseudorabies virus (PrV). *Vet. Microbiol.* 206, 3–9. doi: 10.1016/j.vetmic.2016.11.019

García Durán, M., Costa, S., Sarraseca, J., de La Roja, N., García, J., García, I., et al. (2016). Generation of porcine reproductive and respiratory syndrome (PRRS) virus-like-particles (VLPs) with different protein composition. *J. Virol. Methods* 236, 77–86. doi: 10.1016/j.jviromet.2016.03.021

Gu, J., Hu, D., Peng, T., Wang, Y., Ma, Z., Liu, Z., et al. (2018). Epidemiological investigation of pseudorabies in Shandong Province from 2013 to 2016. *Transbound. Emerg. Dis.* 65, 890–898. doi: 10.1111/tbed.12827

Guo, Z., Chen, X.-X., Li, R., Qiao, S., and Zhang, G. (2018). The prevalent status and genetic diversity of porcine reproductive and respiratory syndrome virus in China: a molecular epidemiological perspective. *Virol. J.* 15:2. doi: 10.1186/s12985-017-0910-6

Guo, Z., Chen, X.-X., Li, X., Qiao, S., Deng, R., and Zhang, G. (2019). Prevalence and genetic characteristics of porcine reproductive and respiratory syndrome virus in central China during 2016-2017: NADC30-like PRRSVs are predominant. *Microb. Pathog.* 135:103657. doi: 10.1016/j.micpath.2019.103657

Han, G., Lei, K., Xu, H., and He, F. (2020). Genetic characterization of a novel recombinant PRRSV2 from lineage 8, 1 and 3 in China with significant variation in replication efficiency and cytopathic effects. *Transbound. Emerg. Dis.* 67, 1574–1584. doi: 10.1111/tbed.13491

Hong, Q., Qian, P., Li, X.-M., Yu, X.-L., and Chen, H.-C. (2007). A recombinant pseudorabies virus co-expressing capsid proteins precursor P1-2A of FMDV and VP2 protein of porcine parvovirus: a trivalent vaccine candidate. *Biotechnol. Lett.* 29, 1677–1683. doi: 10.1007/s10529-007-9459-6

Hu, R.-M., Zhou, Q., Song, W.-B., Sun, E.-C., Zhang, M.-M., He, Q.-G., et al. (2015). Novel pseudorabies virus variant with defects in TK, gE and gI protects growing pigs against lethal challenge. *Vaccine* 33, 5733–5740. doi: 10.1016/j.vaccine.2015.09.066

Jiang, W., Jiang, P., Li, Y., Tang, J., Wang, X., and Ma, S. (2006). Recombinant adenovirus expressing GP5 and M fusion proteins of porcine reproductive and respiratory syndrome virus induce both humoral and cell-mediated immune responses in mice. *Vet. Immunol. Immunopathol.* 113, 169–180. doi: 10.1016/j.vetimm.2006.05.001

Jiang, Y., Fang, L., Xiao, S., Zhang, H., Pan, Y., Luo, R., et al. (2007). Immunogenicity and protective efficacy of recombinant pseudorabies virus expressing the two major membrane-associated proteins of porcine reproductive and respiratory syndrome virus. *Vaccine* 25, 547–560. doi: 10.1016/j.vaccine.2006.07.032

Jiang, Y., Li, G., Yu, L., Li, L., Zhang, Y., Zhou, Y., et al. (2020). Genetic diversity of porcine reproductive and respiratory syndrome virus (PRRSV) from 1996 to 2017 in China. *Front. Microbiol.* 11:618. doi: 10.3389/fmicb.2020.00618

Kang, S.-J., Bae, S.-M., Lee, H.-J., Jeong, Y.-J., Lee, M.-A., You, S.-H., et al. (2021). Porcine circovirus (PCV) genotype 2d-based virus-like particles (VLPs) induced broad cross-neutralizing antibodies against diverse genotypes and provided protection in dual-challenge infection of a PCV2d virus and a type 1 porcine reproductive and respiratory syndrome virus (PRRSV). *Pathogens* 10:1145. doi: 10.3390/pathogens10091145

Klupp, B. G., Hengartner, C. J., Mettenleiter, T. C., and Enquist, L. W. (2004). Complete, annotated sequence of the pseudorabies virus genome. *J. Virol.* 78, 424–440. doi: 10.1128/jvi.78.1.424-440.2004

Kuhn, J. H., Lauck, M., Bailey, A. L., Shchetinin, A. M., Vishnevskaya, T. V., Bào, Y., et al. (2016). Reorganization and expansion of the nidoviral family Arteriviridae. *Arch. Virol.* 161, 755–768. doi: 10.1007/s00705-015-2672-z

Lamote, J. A. S., Glorieux, S., Nauwynck, H. J., and Favoreel, H. W. (2016). The US3 protein of pseudorabies virus drives viral passage across the basement membrane in porcine respiratory mucosa explants. *J. Virol.* 90, 10945–10950. doi: 10.1128/JVI.01577-16

Lampinen, V., Heinimäki, S., Laitinen, O. H., Pesu, M., Hankaniemi, M. M., Blazevic, V., et al. (2021). Modular vaccine platform based on the norovirus-like particle. *J. Nanobiotechnol.* 19:25. doi: 10.1186/s12951-021-00772-0

Mardassi, H., Massie, B., and Dea, S. (1996). Intracellular synthesis, processing, and transport of proteins encoded by ORFs 5 to 7 of porcine reproductive and respiratory syndrome virus. *Virology* 221, 98–112. doi: 10.1006/viro.1996.0356

Marin, A., Chowdhury, A., Valencia, S. M., Zacharia, A., Kirnbauer, R., Roden, R. B. S., et al. (2021). Next generation polyphosphazene immunoadjuvant: synthesis, self-assembly and in vivo potency with human papillomavirus VLPs-based vaccine. *Nanomedicine* 33:102359. doi: 10.1016/j.nano.2021.102359

Martelli, P., Gozio, S., Ferrari, L., Rosina, S., de Angelis, E., Quintavalla, C., et al. (2009). Efficacy of a modified live porcine reproductive and respiratory syndrome virus (PRRSV) vaccine in pigs naturally exposed to a heterologous European (Italian cluster) field strain: clinical protection and cell-mediated immunity. *Vaccine* 27, 3788–3799. doi: 10.1016/j.vaccine.2009.03.028

Müller, T., Hahn, E. C., Tottewitz, F., Kramer, M., Klupp, B. G., Mettenleiter, T. C., et al. (2011). Pseudorabies virus in wild swine: a global perspective. *Arch. Virol.* 156, 1691–1705. doi: 10.1007/s00705-011-1080-2

Murtaugh, M. P., Stadejek, T., Abrahante, J. E., Lam, T. T. Y., and Leung, F. C.-C. (2010). The ever-expanding diversity of porcine reproductive and respiratory syndrome virus. *Virus Res.* 154, 18–30. doi: 10.1016/j.virusres.2010.08.015

Nam, H.-M., Chae, K.-S., Song, Y.-J., Lee, N.-H., Lee, J.-B., Park, S.-Y., et al. (2013). Immune responses in mice vaccinated with virus-like particles composed of the GP5 and M proteins of porcine reproductive and respiratory syndrome virus. *Arch. Virol.* 158, 1275–1285. doi: 10.1007/s00705-013-1612-z

Nan, Y., Wu, C., Gu, G., Sun, W., Zhang, Y.-J., and Zhou, E.-M. (2017). Improved vaccine against PRRSV: current progress and future perspective. *Front. Microbiol.* 8:1635. doi: 10.3389/fmicb.2017.01635

Olsen, L. M., Ch'ng, T. H., Card, J. P., and Enquist, L. W. (2006). Role of pseudorabies virus Us3 protein kinase during neuronal infection. *J. Virol.* 80, 6387–6398. doi: 10.1128/JVI.00352-06

Paludan, S. R., Melchjorsen, J., Malmgaard, L., and Mogensen, S. C. (2002). Expression of genes for cytokines and cytokine-related functions in leukocytes infected with Herpes simplex virus: comparison between resistant and susceptible mouse strains. *Eur. Cytokine Netw.* 13, 306–316.

Popescu, L. N., Trible, B. R., Chen, N., and Rowland, R. R. R. (2017). GP5 of porcine reproductive and respiratory syndrome virus (PRRSV) as a target for homologous and broadly neutralizing antibodies. *Vet. Microbiol.* 209, 90–96. doi: 10.1016/j.vetmic.2017.04.016

Robinson, S. R., Li, J., Nelson, E. A., and Murtaugh, M. P. (2015). Broadly neutralizing antibodies against the rapidly evolving porcine reproductive and respiratory syndrome virus. *Virus Res.* 203, 56–65. doi: 10.1016/j.virusres.2015.03.016

Shi, M., Lam, T. T.-Y., Hon, C.-C., Hui, R. K.-H., Faaberg, K. S., Wennblom, T., et al. (2010a). Molecular epidemiology of PRRSV: a phylogenetic perspective. *Virus Res.* 154, 7–17. doi: 10.1016/j.virusres.2010.08.014

Shi, M., Lam, T. T.-Y., Hon, C.-C., Murtaugh, M. P., Davies, P. R., Hui, R. K.-H., et al. (2010b). Phylogeny-based evolutionary, demographical, and geographical dissection of North American type 2 porcine reproductive and respiratory syndrome viruses. *J. Virol.* 84, 8700–8711. doi: 10.1128/JVI.02551-09

Striz, I., Brabcova, E., Kolesar, L., and Sekerkova, A. (2014). Cytokine networking of innate immunity cells: a potential target of therapy. *Clin. Sci. (Lond.)* 126, 593–612. doi: 10.1042/CS20130497

Sun, Y., Luo, Y., Wang, C.-H., Yuan, J., Li, N., Song, K., et al. (2016). Control of swine pseudorabies in China: opportunities and limitations. *Vet. Microbiol.* 183, 119–124. doi: 10.1016/j.vetmic.2015.12.008

Sun, Y.-K., Chen, Y.-J., Cai, Y., Li, Q., Xie, J.-X., Liang, G., et al. (2020). Insights into the evolutionary history and epidemiological characteristics of the emerging lineage 1 porcine reproductive and respiratory syndrome viruses in China. *Transbound. Emerg. Dis.* 67, 2630–2641. doi: 10.1111/tbed.13613

Tang, X., Liu, X., Tao, G., Qin, M., Yin, G., Suo, J., et al. (2016a). "Self-cleaving" 2A peptide from porcine teschovirus-1 mediates cleavage of dual fluorescent proteins in transgenic *Eimeria tenella*. *Vet. Res.* 47:68. doi: 10.1186/s13567-016-0351-z

Tang, Y.-D., Liu, J.-T., Wang, T.-Y., An, T.-Q., Sun, M.-X., Wang, S.-J., et al. (2016b). Live attenuated pseudorabies virus developed using the CRISPR/Cas9 system. *Virus Res.* 225, 33–39. doi: 10.1016/j.virusres.2016.09.004

Tingstedt, J.-E., and Nielsen, J. (2004). Cellular immune responses in the lungs of pigs infected in utero with PRRSV: an immunohistochemical study. *Viral Immunol.* 17, 558–564. doi: 10.1089/vim.2004.17.558

Tong, W., Liu, F., Zheng, H., Liang, C., Zhou, Y.-J., Jiang, Y.-F., et al. (2015). Emergence of a Pseudorabies virus variant with increased virulence to piglets. *Vet. Microbiol.* 181, 236–240. doi: 10.1016/j.vetmic.2015.09.021

Trible, B. R., Popescu, L. N., Monday, N., Calvert, J. G., and Rowland, R. R. R. (2015). A single amino acid deletion in the matrix protein of porcine reproductive and respiratory syndrome virus confers resistance to a polyclonal swine antibody with broadly neutralizing activity. *J. Virol.* 89, 6515–6520. doi: 10.1128/JVI.03287-14

Uribe-Campero, L., Monroy-García, A., Durán-Meza, A. L., Villagrana-Escareño, M. V., Ruíz-García, J., Hernández, J., et al. (2015). Plant-based porcine reproductive and respiratory syndrome virus VLPs induce an immune response in mice. *Res. Vet. Sci.* 102, 59–66. doi: 10.1016/j.rvsc.2015.07.012

Vanhee, M., van Breedam, W., Costers, S., Geldhof, M., Noppe, Y., and Nauwynck, H. (2011). Characterization of antigenic regions in the porcine reproductive and respiratory syndrome virus by the use of peptide-specific serum antibodies. *Vaccine* 29, 4794–4804. doi: 10.1016/j.vaccine.2011.04.071

Wang, T., Xiao, Y., Yang, Q., Wang, Y., Sun, Z., Zhang, C., et al. (2015). Construction of a gE-deleted pseudorabies virus and its efficacy to the new-emerging variant PRV challenge in the form of killed vaccine. *Biomed. Res. Int.* 2015:684945. doi: 10.1155/2015/684945

Wang, Y., Wu, H., Wang, B., Qi, H., Jin, Z., Qiu, H.-J., et al. (2020). A nanoluc luciferase reporter pseudorabies virus for live imaging and quantification of viral infection. *Front. Vet. Sci.* 7:566446. doi: 10.3389/fvets.2020.566446

Wang, Z., Liu, M., Zhao, H., Wang, P., Ma, W., Zhang, Y., et al. (2021). Induction of robust and specific humoral and cellular immune responses by bovine viral diarrhea virus virus-like particles (BVDV-VLPs) Engineered with baculovirus expression vector system. *Vaccines (Basel)* 9:350. doi: 10.3390/vaccines9040350

Wei, C., Dai, A., Fan, J., Li, Y., Chen, A., Zhou, X., et al. (2019). Efficacy of Type 2 PRRSV vaccine against challenge with the Chinese lineage 1 (NADC30-like) PRRSVs in pigs. *Sci. Rep.* 9:10781. doi: 10.1038/s41598-019-47239-9

Weigel, R. M., Hahn, E. C., and Scherba, G. (2003). Survival and immunization of raccoons after exposure to pseudorabies (Aujeszky's disease) virus gene-deleted vaccines. *Vet. Microbiol.* 92, 19–24. doi: 10.1016/s0378-1135(02)00350-4

Xu, W., Du, S., Li, T., Wu, S., Jin, N., Ren, L., et al. (2021). Generation and evaluation of recombinant baculovirus coexpressing Gp5 and M proteins of porcine reproductive and respiratory syndrome virus Type 1. *Viral Immunol.* 34, 697–707. doi: 10.1089/vim.2021.0018

Yao, L., Cheng, Y., Wu, H., Ghonaim, A. H., Fan, S., Li, W., et al. (2021). The construction and immunogenicity analyses of a recombinant pseudorabies virus with porcine circovirus type 3 capsid protein co-expression. *Vet. Microbiol.* 264, 109283. doi: 10.1016/j.vetmic.2021.109283

Yao, Q., Qian, P., Cao, Y., He, Y., Si, Y., Xu, Z., et al. (2007). Synergistic inhibition of pseudorabies virus replication by porcine alpha/beta interferon and gamma interferon in vitro. *Eur. Cytokine Netw.* 18, 71–77. doi: 10.1684/ecn.2007.0088

Yin, Y., Xu, Z., Liu, X., Li, P., Yang, F., Zhao, J., et al. (2017). A live gI/gE-deleted pseudorabies virus (PRV) protects weaned piglets against lethal variant PRV challenge. *Virus Genes* 53, 565–572. doi: 10.1007/s11262-017-1454-y

Zhang, C., Guo, L., Jia, X., Wang, T., Wang, J., Sun, Z., et al. (2015). Construction of a triple gene-deleted Chinese Pseudorabies virus variant and its efficacy study as a vaccine candidate on suckling piglets. *Vaccine* 33, 2432–2437. doi: 10.1016/j.vaccine.2015.03.094

Zhang, H., Xia, M., Wang, W., Ju, D., Cao, L., Wu, B., et al. (2018). An attenuated highly pathogenic chinese PRRS viral vaccine confers cross protection to pigs against challenge with the emerging PRRSV NADC30-like strain. *Virol. Sin.* 33, 153–161. doi: 10.1007/s12250-018-0027-0

Zhang, R. (2021). *Establishment And Preliminary Application Of An Indirect ELISA Method For NADC30-Like PRRSV GP5 Protein and M Protein.* Ph.D. thesis. Chengdu: Sichuan Agricultural University.

Zhao, J., Zhu, L., Huang, J., Yang, Z., Xu, L., Gu, S., et al. (2021). Genetic characterization of a novel recombined porcine reproductive and respiratory syndrome virus 2 among Nadc30-like, Jxa1-like and TJ-like strains. *Vet. Med. Sci.* 7, 697–704. doi: 10.1002/vms3.402

Zhao, Y., Wang, L.-Q., Zheng, H.-H., Yang, Y.-R., Liu, F., Zheng, L.-L., et al. (2020). Construction and immunogenicity of a gE/gI/TK-deleted PRV based on porcine pseudorabies virus variant. *Mol. Cell Probes* 53:101605. doi: 10.1016/j.mcp.2020.101605

Zheng, H.-H., Wang, L.-Q., Fu, P.-F., Zheng, L.-L., Chen, H.-Y., and Liu, F. (2020). Characterization of a recombinant pseudorabies virus expressing porcine parvovirus VP2 protein and porcine IL-6. *Virol. J.* 17:19. doi: 10.1186/s12985-020-1292-8

Zheng, Q., Chen, D., Li, P., Bi, Z., Cao, R., Zhou, B., et al. (2007). Co-expressing GP5 and M proteins under different promoters in recombinant modified vaccinia virus ankara (rMVA)-based vaccine vector enhanced the humoral and cellular immune responses of porcine reproductive and respiratory syndrome virus (PRRSV). *Virus Genes* 35, 585–595. doi: 10.1007/s11262-007-0161-5

Zhou, L., Yang, B., Xu, L., Jin, H., Ge, X., Guo, X., et al. (2017). Efficacy evaluation of three modified-live virus vaccines against a strain of porcine reproductive and respiratory syndrome virus NADC30-like. *Vet. Microbiol.* 207, 108–116. doi: 10.1016/j.vetmic.2017.05.031

**Conflict of Interest:** The authors declare that the research was conducted in the absence of any commercial or financial relationships that could be construed as a potential conflict of interest.

**Publisher's Note:** All claims expressed in this article are solely those of the authors and do not necessarily represent those of their affiliated organizations, or those of the publisher, the editors and the reviewers. Any product that may be evaluated in this article, or claim that may be made by its manufacturer, is not guaranteed or endorsed by the publisher.

*Copyright © 2022 Zhao, Zhu, Xu, Li, Deng, Huang, Gu, Sun, Zhou and Xu. This is an open-access article distributed under the terms of the Creative Commons Attribution License (CC BY). The use, distribution or reproduction in other forums is permitted, provided the original author(s) and the copyright owner(s) are credited and that the original publication in this journal is cited, in accordance with accepted academic practice. No use, distribution or reproduction is permitted which does not comply with these terms.*

frontiers in Microbiology

ORIGINAL RESEARCH
published: 04 March 2022
doi: 10.3389/fmicb.2022.862580

# MiR-103a-3p Promotes Zika Virus Replication by Targeting OTU Deubiquitinase 4 to Activate p38 Mitogen-Activated Protein Kinase Signaling Pathway

*Haiyan Ye[1], Lan Kang[1], Xipeng Yan[2], Shilin Li[1], Yike Huang[1], Rongrong Mu[1], Xiaoqiong Duan[1]* and Limin Chen[1,2]**

[1]*Institute of Blood Transfusion, Chinese Academy of Medical Sciences and Peking Union Medical College, Chengdu, China,* [2]*The Joint Laboratory on Transfusion-Transmitted Diseases (TTDs) Between Institute of Blood Transfusion, Chinese Academy of Medical Sciences and Nanning Blood Center, Nanning Blood Center, Nanning, China*

OPEN ACCESS

**Edited by:**
*Chunfu Zheng,*
*University of Calgary, Canada*

**Reviewed by:**
*Haizhen Zhu,*
*Hunan University, China*
*Qiang Liu,*
*University of Saskatchewan, Canada*

***Correspondence:**
*Xiaoqiong Duan*
*xiaoqiongduan@yahoo.com*
*Limin Chen*
*limin_chen_99@yahoo.com*

**Specialty section:**
*This article was submitted to Virology, a section of the journal Frontiers in Microbiology*

**Received:** *26 January 2022*
**Accepted:** *18 February 2022*
**Published:** *04 March 2022*

**Citation:**
*Ye H, Kang L, Yan X, Li S, Huang Y, Mu R, Duan X and Chen L (2022) MiR-103a-3p Promotes Zika Virus Replication by Targeting OTU Deubiquitinase 4 to Activate p38 Mitogen-Activated Protein Kinase Signaling Pathway. Front. Microbiol. 13:862580. doi: 10.3389/fmicb.2022.862580*

**Background:** MicroRNAs (miRNAs) play critical roles in regulating virus infection and replication. However, the mechanism by which miRNA regulates Zika virus (ZIKV) replication remains elusive. We aim to explore how the differentially expressed miR-103a-3p regulates ZIKV replication and to clarify the underlying molecular mechanism.

**Methods:** Small RNA sequencing (RNA-Seq) was performed to identify differentially expressed miRNAs in A549 cells with or without ZIKV infection and some of the dysregulated miRNAs were validated by quantitative real time PCR (qRT-PCR). The effect of miR-103a-3p on ZIKV replication was examined by transfecting miR-103a-3p mimic or negative control (NC) into A549 cells with or without p38 mitogen-activated protein kinase (MAPK) inhibitor SB203580 and expression levels of ZIKV NS5 mRNA and NS1 protein were detected by qRT-PCR and Western blot, respectively. The potential target genes for miR-103a-3p were predicted by four algorithms and further validated by mutation analysis through luciferase reporter assay. The predicated target gene OTU deubiquitinase (DUB) 4 (OTUD4) was over-expressed by plasmid transfection or silenced by siRNA transfection into cells prior to ZIKV infection. Activation status of p38 MAPK signaling pathway was revealed by looking at the phosphorylation levels of p38 (p-p38) and HSP27 (p-HSP27) by Western blot.

**Results:** Thirty-five differentially expressed miRNAs in ZIKV-infected A549 cells were identified by RNA-Seq analysis. Five upregulated and five downregulated miRNAs were further validated by qRT-PCR. One of the validated upregulated miRNAs, miR-103a-3p significantly stimulated ZIKV replication both at mRNA (NS5) and protein (NS1) levels. We found p38 MAPK signaling was activated following ZIKV infection, as demonstrated by the increased expression of the phosphorylation of p38 MAPK and HSP27. Blocking p38 MAPK signaling pathway using SB203580 inhibited ZIKV replication and attenuated the stimulating effect of miR-103a-3p on ZIKV replication. We further identified OTUD4 as a direct target gene of miR-103a-3p.

MiR-103a-3p over-expression or OTUD4 silencing activated p38 MAPK signaling and enhanced ZIKV replication. In contrast, OTUD4 over-expression inhibited p38 MAPK activation and decreased ZIKV replication. In addition, OTUD4 over-expression attenuated the stimulating effect of miR-103a-3p on ZIKV replication and activation of p38 MAPK signaling.

**Conclusion:** Zika virus infection induced the expression of miR-103a-3p, which subsequently activated p38 MAPK signaling pathway by targeting OTUD4 to facilitate ZIKV replication.

**Keywords: MiR-103a-3p, Zika virus, flavivirus, OTUD4, p38 MAPK signaling pathway**

## INTRODUCTION

As an arthropod-borne single-stranded positive RNA virus belonging to the *Flavivirus* genus in the *Flaviviridae* family (Lanciotti et al., 2008), Zika virus (ZIKV) was first identified from a rhesus monkey in Uganda in 1947 (Dick et al., 1952). There have been at least three outbreaks of ZIKV infection in the past two decades and the most recent ZIKV outbreak occurred in Brazil in 2015. Since then, ZIKV has spread to over 94 countries, which poses a serious global public health threat (Filgueiras et al., 2021). Although approximately 80% of individuals infected with ZIKV are asymptomatic (Patterson et al., 2016), it is noteworthy that accumulating evidence suggests that ZIKV infection is associated with neurologic disorders, such as microcephaly in infants and Guillain-Barré syndrome (GBS) in adults (Filgueiras et al., 2021). Up till now, no vaccine or specific anti-viral drugs are licensed for prevention or treatment of ZIKV infection (Mwaliko et al., 2021). One of the main reasons lies in the fact that the pathogenesis of ZIKV infection and how this virus evades host immune response have not been fully elucidated.

P38 mitogen-activated protein kinases (MAPKs) are a class of serine/threonine protein kinases that play critical roles in various cellular process, including virus infection (Chander et al., 2021). Upon stimulation, p38 MAPK is phosphorylated by upstream kinases mitogen-activated protein kinase kinase 3 (MKK3) or mitogen-activated protein kinase kinase 6 (MKK6) and subsequently causes cascade phosphorylation of substrates, including MAPK activated protein kinase 2 (MAPKAPK2) and heat shock protein 27 (HSP27; Kostenko and Moens, 2009; Cuadrado and Nebreda, 2010). It has been reported that p38 MAPK can be activated by several viruses, including hepatitis C virus (HCV), herpes simplex virus type 1 (HSV-1), severe fever with thrombocytopenia syndrome virus (SFTSV; Cheng et al., 2020) enterovirus 71 (EV71; Peng et al., 2014), severe acute respiratory syndrome coronavirus 2 (SARS-CoV-2; Grimes and Grimes, 2020; Ma et al., 2020), and ZIKV (Zhu et al., 2017; Muthuraj et al., 2021). Interestingly, data from previous studies indicated that some viruses, such as hepatitis B virus (HBV), HSV-1, respiratory syncytial virus (RSV), and influenza A virus (IAV), can utilize the p38 MAPK to benefit their replication (Chander et al., 2021), which makes p38 MAPK inhibitor as a promising therapeutic approach for virus infection.

OTU deubiquitinase 4 (OTUD4) is a member of OTD deubiquitinase (DUB) family, which participates in various physiological and pathological processes, such as embryonic development of zebrafish, repair of DNA alkylation damage, and innate immune response (Tse et al., 2009; Zhao et al., 2015, 2018; Liuyu et al., 2019). Zhao et al. (2018) revealed that OTUD4 negatively modulated TLR-mediated NF-κB activation and silencing of OTUD4 increased the phosphorylation of p38 MAPK upon the stimulation of IL-1β. Nevertheless, the role of OTUD4 and p38 MAPK signal pathway in ZIKV replication has not been elucidated.

MicroRNAs (miRNAs) are a class of small endogenous non-coding RNAs with a length of approximately 22 nucleotides. MiRNAs can post-transcriptionally inhibit the expression of their target genes through degrading mRNAs or inhibiting their translation following the base complementary pairing between miRNAs seed sequence and specific mRNAs sequence of target genes, primarily in the 3′-untranslated regions (3′UTRs; Bartel, 2004). Many miRNAs have been reported to engage in ZIKV infection (Estevez-Herrera et al., 2021). For example, miR-142-5p was found to be downregulated by ZIKV infection, while miR-142-5p overexpression suppressed ZIKV replication (Seong et al., 2020). Zhang et al. (2019a) demonstrated that ZIKV infection increased miR-9 expression and decreased its target gene GDNF, which were associated with microcephaly in mice. Shukla et al. (2021) demonstrated that miR-146a induced by ZIKV-NS1 protein suppressed cellular antiviral response in human microglial cells. MiRNAs have also been involved in the regulation of p38 MAPK signaling pathway. MiR-744, miR-124a, and miR-24 could effectively inhibit the phosphorylation of p38 MAPK in influenza A virus infected cells (McCaskill et al., 2017). In this study, we found that ZIKV infection induced miR-103a-3p expression which stimulates ZIKV replication and activation of p38 MAPK signaling pathway, while blocking p38 MAPK signaling suppressed ZIKV replication. Mechanistically, we identified OTUD4 as a direct target gene for miR-103a-3p. Increased miR-103a-3p expression leads to downregulation OTUD4 to stimulate ZIKV replication through the activation of p38 MAPK signaling pathway. Therefore, miR-103a-3p may be one of the host genes exploited by ZIKV to benefit its replication in host cells. Targeting miR-103a-3p or p38 MAPK signaling may be a viable approach for the better control of ZIKV infection.

## MATERIALS AND METHODS

### Cell Culture and Zika Virus

A549 and 293T cells were obtained from West China Hospital, Sichuan University. The cells were grown in Dulbecco's modified

Eagle's medium (DMEM; Hyclone, United States) supplemented with 10% fetal bovine serum (FBS; Biological Industries, Israel) and 1% mycoplasma prevention reagent (Transgen, China) at 37°C with 5% $CO_2$ in a humidified incubator. ZIKV (GZ01 strain) was generously provided by Dr. Chengfeng Qin (Beijing Institute of Microbiology and Epidemiology, China). ZIKV was propagated and tittered in A549 cells as previously described (Wang et al., 2020). ZIKV stock was stored in aliquots at −80°C freezer for further use.

## Small RNA Sequencing and Data Analysis

A549 cells with or without ZIKV infection by multiplicity of infection (MOI) of 0.5 were harvested at 48 h post-infection for analysis of intracellular miRNAs. The preparation of libraries and the procedure of sequencing were performed by Novogene Co., Ltd (Beijing, China). Briefly, 3 μg total RNA per sample was processed for the small RNA library. Sequencing libraries were generated using NEBNext® Multiplex Small RNA Library Prep Set for Illumina® (NEB, United States) followed by products purification on 8% polyacrylamide gel to isolate the 140–160 bp DNA fragments. Library quality was assessed on a DNA High Sensitivity Chip using the Agilent Bioanalyzer 2100 system (Agilent Technologies, United States). Next, small RNA sequencing (RNA-Seq) was performed on an Illumina Hiseq 4,000 platform and 50 bp single-end reads were generated.

The small RNA-Seq data analysis was performed by Novogene Co., Ltd (Beijing, China). Raw data was assessed by internal quality control and filtered by several criteria to obtain clean reads. Reads were then aligned to the human reference genome using Bowtie (Langmead et al., 2009). The DESeq R package (1.8.3) was used to identify differentially expressed miRNAs following ZIKV infection. The *p*-values were adjusted using the Benjamini & Hochberg method to control the false-discovery rate. An adjusted $p < 0.05$ was deemed differentially expressed miRNAs. The complete raw small RNA sequencing data have been deposited in NCBI's Gene Expression Omnibus (GEO) with the accession number of GSE146423.[1]

## ZIKV Infection and Treatment of Cells With P38 MAPK Inhibitor

A549 cells were infected with ZIKV by MOI of 0.5 for 4 h at 37°C. After 4 h virus incubation, the medium was aspirated. Cells were washed three times with phosphate-buffered saline (PBS; Hyclone, United States) and then replenished with fresh medium. p38 MAPK inhibitor SB203580 (APExBIO, United States) was dissolved in dimethyl sulfoxide (DMSO) to prepare a 10 mM stock solution and stored at −20°C freezer for further use. SB203580 stock was diluted to indicated concentration in cell culture medium and the cells were pretreated 1 h before ZIKV infection.

## Transfection of Cells With MiR-103a-3p Mimic, siRNA, Plasmid DNA

MiR-103a-3p mimic and negative control (NC) were purchased from RiBoBio (RiBoBio Inc., China) and transfected into A549 or 293T cells at a final concentration of 10 nM using RNAiMAX reagent (Invitrogen, United States) according to the manufacturer's instructions. Small interfering RNA targeted OTUD4 (GGAAC UAGACACGUUGGAATT) and a NC siRNA (UUCUCCGAA CGUGUCACGUTT) were chemically synthesized by Sangon Biotech (Sangon Biotech, China). Transfection of siRNA at a final concentration of 20 nM was performed using the RNAiMAX regent according to the manufacturer's recommended procedures. Recombinant plasmid expressing OTUD4 was constructed by cloning the amplified human full-length OTUD4 cDNA into the expression vector P3×FLAG-CMV-7.1 (Fenghbio, China). The correct insertion of the OTUD4 gene was verified by DNA-sequencing. The recombinant OTUD4 plasmid and the corresponding empty vector were transiently transfected into A549 cells at a final concentration of 1 μg/ml using the Lipofectamine 3000 reagent (Invitrogen, United States) following the manufacturer's instructions.

## RNA Isolation, Reverse Transcription, and qRT-PCR

Total cellular RNA was extracted using Trizol reagent (Invitrogen, United States). The first-strand cDNA was synthesized from 1 μg of total RNA by reverse transcription using ReverTra Ace®qPCR RT Master Mix (Toyobo, Japan) according to the manufacturer's protocol. To validate the differentially expressed miRNAs induced by ZIKV infection, we use miRNAs specific primers (**Table 1**). The qRT-PCR analysis was carried out using SYBR Green Real-time Master Mix (Novoprotein, China) on a CFX96 Real-Time System (Bio-Rad, United States). The mRNA level of each gene was calculated by using $2^{-\triangle\triangle Ct}$ method, normalized to GAPDH or U6. The sequences of primers used in this study are listed in **Table 1**.

## Western Blotting and Antibodies

Total protein of cells was extracted by radioimmune precipitation assay (RIPA) lysis buffer containing PMSF protease inhibitor (Biosharp, China) and phosphatase inhibitor cocktail (Transgen, China). The lysates were centrifugated at 15,000*g* for 20 min at 4°C and the supernatant was collected. Protein concentrations were quantified by BCA Protein Assay Kit (Beyotime, China). A total of 30 μg protein was boiled at 98°C for 5 min and loaded into SDS-PAGE gels. Then the separated protein bands were transferred to a PVDF membrane (Millipore, United States). The membrane was blocked with 5% bovine serum albumin (BSA) (Solarbio, China) at room temperature for 2 h, and then incubated with specific primary antibody at 4°C overnight. The primary antibodies used were as follows: anti-GADPH (Proteintech, China), anti-β-actin (Proteintech, China), anti-FLAG (Sigma, United States), anti-p-p38 MAPK phosphorylated Thr180/Tyr182 (Cell Signaling Technology, United States), anti-p38 MAPK (Cell Signaling Technology, United States), anti-p-HSP27 phosphorylated Ser82 (Cell Signaling Technology, United States), anti-HSP27 (Proteintech, China), anti-ZIKV NS1 (GeneTex, United States), and anti-OTUD4 (Proteintech, China). After washing with Tris-buffered saline with 0.1% Tween-20 (TBST), the membrane was incubated with horseradish peroxidase (HRP)-conjugated goat anti-mouse IgG or anti-rabbit IgG secondary antibodies (Proteintech, China) at room temperature for 1 h. Finally, the membrane was washed

[1]https://www.ncbi.nlm.nih.gov/geo/query/acc.cgi?acc=GSE146423

**TABLE 1** | qRT-PCR primer sequences.

| Gene name | | Primer sequences (5′-3′) |
|---|---|---|
| miR-103a-3p | RT | GTCGTATCCAGTGCAGGGTCCGAG GTATTCGCACTGGATACGACTCATAG |
| | Forward | TTAGCAGCATTGTACAGGG |
| miR-4454 | RT | GTCGTATCCAGTGCAGGGTCCGAG GTATTCGCACTGGATACGACTGGTGC |
| | Forward | TTAGGATCCGAGTCACGG |
| miR-203a-3p | RT | GTCGTATCCAGTGCAGGGTCCGAG GTATTCGCACTGGATACGACCTAGTG |
| | Forward | GTGAAATGTTTAGGACCACT |
| miR-203b-5p | RT | GTCGTATCCAGTGCAGGGTCCGAG GTATTCGCACTGGATACGACTGTGAA |
| | Forward | CAGGTAGTGGTCCTAAACATT |
| miR-210-3p | RT | GTCGTATCCAGTGCAGGGTCCGAG GTATTCGCACTGGATACGACTCAGCC |
| | Forward | TGTGCGTGTGACAGCG |
| miR-495-3p | RT | GTCGTATCCAGTGCAGGGTCCGAG GTATTCGCACTGGATACGACAAGAAG |
| | Forward | CGAAACAAACATGGTGCA |
| miR-543 | RT | GTCGTATCCAGTGCAGGGTCCGAG GTATTCGCACTGGATACGACAAGAAG |
| | Forward | GAAACATTCGCGGTGC |
| miR-654-5p | RT | GTCGTATCCAGTGCAGGGTCCGAG GTATTCGCACTGGATACGACGCACAT |
| | Forward | TGGTGGGCCGCAGAA |
| miR-493-5p | RT | GTCGTATCCAGTGCAGGGTCCGAG GTATTCGCACTGGATACGACAATGAA |
| | Forward | TGGTTGTACATGGTAGGCTT |
| miR-376c-3p | RT | GTCGTATCCAGTGCAGGGTCCGAG GTATTCGCACTGGATACGACACGTGG |
| | Forward | TCGGAACATAGAGGAAATTC |
| miRNA | Reverse | GCAGGGTCCGAGGTATTC |
| OTUD4 | Forward | CTAACTCCTGCGGTGCCTTCTT |
| | Reverse | GCTGAATCAGGTCCAGTGGTCA |
| GZ01-NS5 | Forward | CCTTGGATTCTTGAACGAGGA |
| | Reverse | AGAGCTTCATTCTCCAGATCAA |
| U6 | Forward | CTCGCTTCGGCAGCACA |
| | Reverse | AACGCTTCACGAATTTGCGT |
| GAPDH | Forward | GCCTCCTGCACCACCAACTG |
| | Reverse | ACGCCTGCTTCACCACCTTC |

and incubated with chemiluminescent HRP substrate (Milipore, United States) to detect the immunoreactive bands using a ChemiDoc imaging system (Bio-Rad, United States). Densitometry was performed with ImageJ software.

## Bioinformatic Analysis of miR-103a-3p Target Genes

The putative miR-103a-3p targets were predicted by four different algorithms, including PicTar,[2] TargetScan,[3] miRanda,[4] and miRMap.[5] Venn's diagram was drawn by Venny2.1.[6]

[2]http://www.pictar.org/
[3]http://www.targetscan.org/
[4]http://microrna.sanger.ac.uk/
[5]https://mirmap.ezlab.org/
[6]https://bioinfogp.cnb.csic.es/tools/venny/index.html

## Luciferase Reporter Assay

The putative binding sites between OTUD4 3′UTR and miR-103a-3p seed sequence were predicted by Targetscan. Wild-type or mutant OTUD4 3′UTR sequences that containing the binding sites of miR-103a-3p seed sequence were constructed into the 3′UTR of the Renilla luciferase gene in the dual-luciferase reporter vector pmiR-RB-Report™ (Ribobio, China). The reporter plasmid also included a firefly luciferase gene, which was used as a reference for normalization. The reporter plasmids were co-transfected with miR-103a-3p mimic or negative control into 293T cells using Lipofectamine 3000 transfection reagent (Invitrogen, United States). At 48 h post-transfection, the cells were lysed for Firefly and Renilla luciferase measurement by dual-luciferase reporter assay (Promega, United States) according to the manufacture's protocol. The luciferase activities were measured on EnSpire Multimode Plate Reader (PerkinElmer, United States). The Renilla luciferase/Firefly luciferase activity ratio was calculated to determine the binding between miR-103a-3p and cloned 3′UTR of OTUD4.

## Cell Viability Assay

A549 cells were seeded in 96-well plates and treated with SB203580 or transfected with miR-103a-3p mimic, OTUD4 plasmid, OTUD4 siRNA and corresponding negative controls. After 48 h post treatment or transfection, cell viability was detected by Cell Counting Kit 8 (CCK8; Biosharp, China) according to the manufacture's instruction. In brief, 10 μl CCK8 solution was added to each well and incubated for 2 h at 37°C. Sample absorbance was determined at 450 nm on EnSpire Multimode Plate Reader (PerkinElmer, United States). The cell viability was calculated by using $(OD_{experiment} - OD_{blank})/(OD_{control} - OD_{blank}) \times 100\%$.

## Statistical Analysis

Statistical analyses and calculations were performed with GraphPad Prism 8 software. All the data presented are representative of at least three independent experiments, unless stated otherwise. Data are expressed as mean ± SD. A two-tailed Student's *t*-tests were performed to determine the difference, and value of $p < 0.05$ was considered statistically significant.

# RESULTS

## Differentially Expressed miRNAs in ZIKV-Infected A549 Cells

Our previous study demonstrated that ZIKV could efficiently infect A549 cells (Liao et al., 2020). To investigate the miRNA expression profiles following ZIKV infection, we performed small RNA-seq in A549 cells with or without ZIKV infection. Around 35 dysregulated miRNAs were identified in A549 cells following ZIKV infection compared to uninfected cells ($p < 0.05$; **Figure 1A**). Five upregulated and five downregulated miRNAs were selected for further validation by qRT-PCR. As shown in **Figures 1B,C**, the qRT-PCR results for these miRNAs were consistent with the RNA-seq results. Among these dysregulated miRNAs, miR-103a-3p was highly induced by ZIKV infection and our result is supported by most recent study that miR-103a-3p was upregulated in extracellular vesicles (EVs) during ZIKV infection (Tabari et al.,

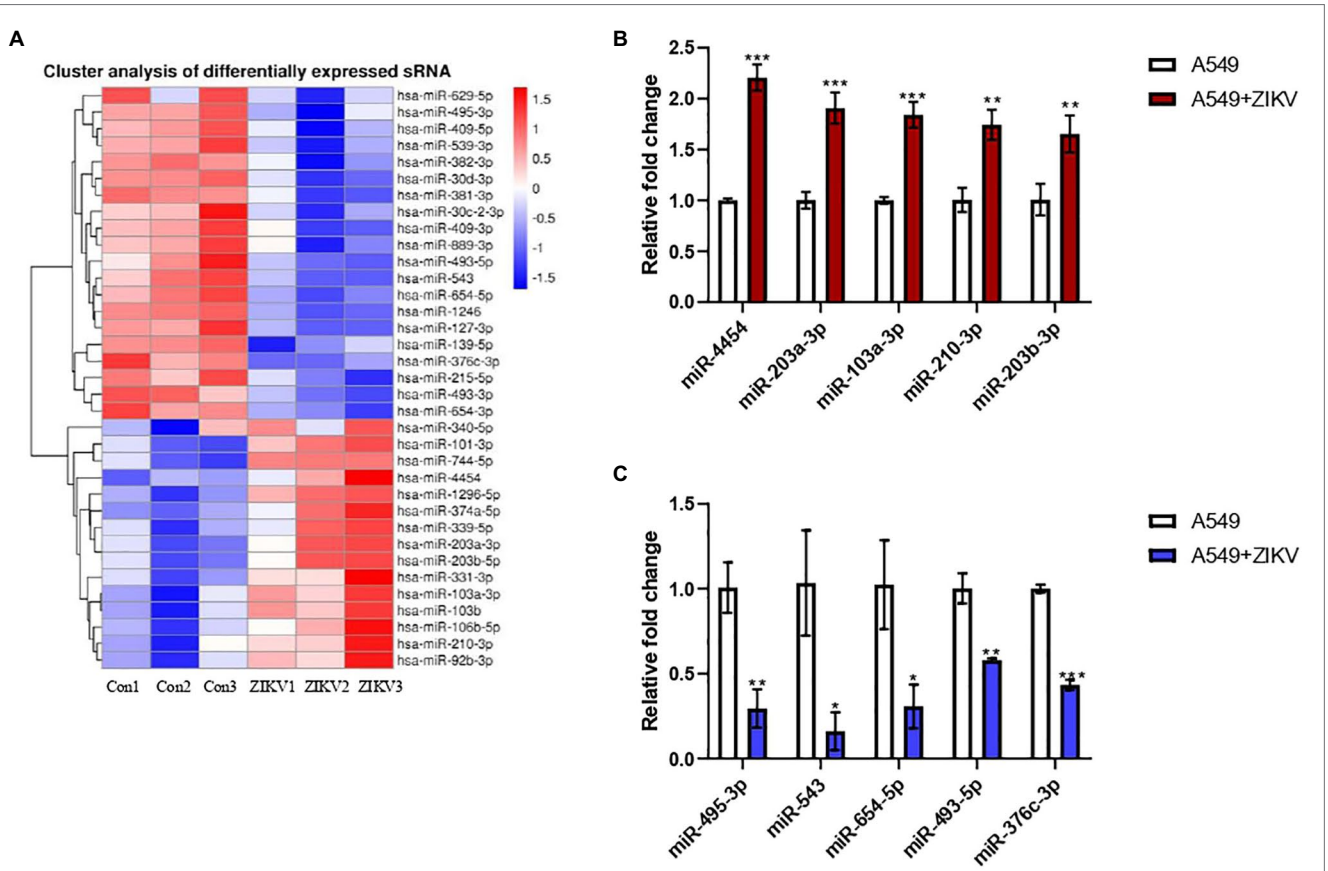


**FIGURE 1 |** Differentially expressed host MicroRNAs (miRNAs) between A549 and Zika virus (ZIKV) infected A549 cells. A549 cells were infected with ZIKV infection by multiplicity of infection (MOI) of 0.5 and the infected cells were harvested at 48 h post-infection for miRNA profiling by RNA sequencing (RNA-seq) and the data were compared with those obtained from un-infected A549 cells. **(A)** Heat map analysis of the miRNAs expression. Red indicates upregulation and blue indicates downregulation. **(B)** Five upregulated candidate miRNAs were selected to verify by qRT-PCR. **(C)** Five downregulated candidate miRNAs were selected to verify by qRT-PCR. Data are normalized to U6 and presented as mean ± SD. Error bars indicate SD ($n \geq 3$). *$p < 0.05$, **$p < 0.01$, and ***$p < 0.001$.

2020). Up till now, no studies on the effect of miR-103a-3p on viral replication have been reported; therefore, we choose it for further investigation using ZIKV as a model virus.

## MiR-103a-3p Stimulates ZIKV Replication

In order to determine the effect of miR-103a-3p on ZIKV replication, we transfected miR-103a-3p mimic or the corresponding negative control into A549 cell. As shown in **Figure 2A**, miR-103a-3p was successfully over-expressed in A549 cells with or without ZIKV infection following transfection. MiR-103a-3p over-expression significantly promoted ZIKV RNA replication and ZIKV NS1 protein expression (**Figures 2B,C**). In addition, we confirmed that either miR-103a-3p mimic or negative control transfection had no effect on cell viability (**Figure 2D**). Taken together, these results indicate that ZIKV infection induced miR-103a-3p expression to promote its replication both at mRNA and protein levels.

## MiR-103a-3p Stimulates ZIKV Replication Through Activation of the p38 MAPK Signaling Pathway

Many viruses have been reported to utilize p38 MAPK in order to facilitate their replication (Chander et al., 2021). We next move forward to investigate whether p38 MAPK signaling pathway is involved in miR-103a-3p regulation of ZIKV infection. Firstly, we confirmed that p38 MAPK signaling pathway was activated upon ZIKV infection in A549 cells. As shown in **Supplementary Figures S1A,B**, increased phosphorylation of p38 MAPK was observed in ZIKV-infected A549 cells both in time-dependent and MOI-dependent manners. Blocking p38 MAPK pathway using SB203580 inhibited ZIKV RNA replication and ZIKV NS1 protein expression in a dose-dependent manner (**Figures 3A,B**). SB203580 treatment alone did not affect miR-103a-3p expression in A549 cells, but slightly inhibited the expression of miR-103a-3p induced by ZIKV infection (**Supplementary Figure S2**). Consistent with the previous study (Kumar et al., 1999), SB203580 inhibited the phosphorylation of HSP27 (down-stream of p38 MAPK pathway) but increased p38 MAPK phosphorylation slightly (**Figure 3B**). Next, we found miR-103a-3p over-expression activated p38 MAPK signaling pathway. The phosphorylation levels of p38 MAPK and HSP27 were significantly increased following miR-103a-3p upregulation in A549 cells with or without ZIKV infection (**Figure 3C**). SB203580 treatment attenuated the stimulating effect of miR-103a-3p on ZIKV RNA replication and ZIKV NS1 expression, as well as the

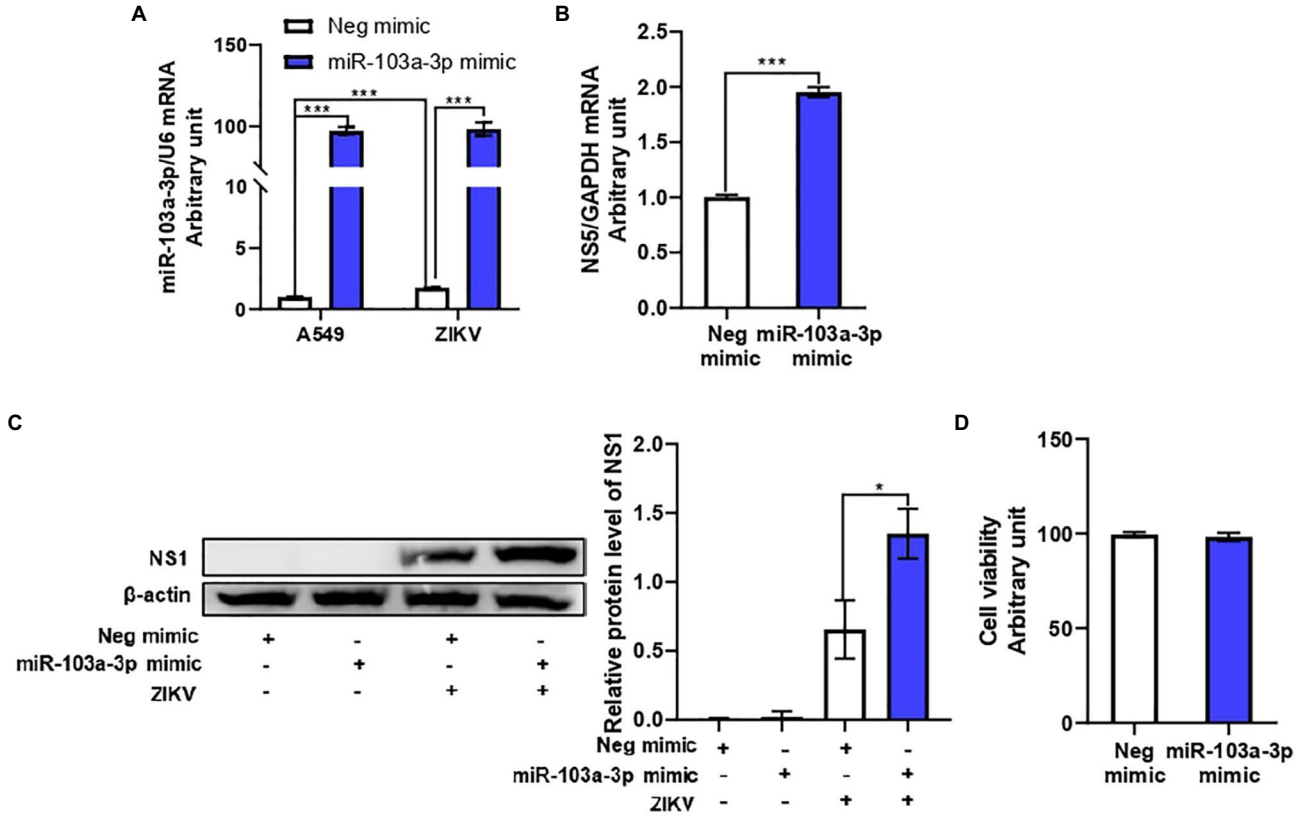


**FIGURE 2 |** miR-103a-3p stimulates ZIKV replication in A549 cells. A549 cells were transfected with miR-103a-3p mimic or corresponding negative control at a final concentration of 10 nM and infected with ZIKV at a MOI of 0.5. Total RNA and protein of cells were harvested at 48 h post infection for qRT-PCR and Western blot analysis, respectively. **(A)** Level of miR-103a-3p over-expression. **(B)** MiR-103a-3p over-expression promotes ZIKV NS5 RNA expression. **(C)** MiR-103a-3p over-expression enhances ZIKV NS1 protein level. **(D)** miR-103a-3p mimic or negative control transfection does not affect cell viability. Data are presented as mean ± SD. Error bars indicate SD ($n \geq 3$). *$p < 0.05$ and ***$p < 0.001$.

induction of p-HSP27 (**Figures 3D,E**). Besides, we did not observe significant effect of SB203580 treatment on cell viability (**Figure 3F**). Collectively, these results suggest that miR-103a-3p stimulates ZIKV replication through activation p38 MAPK signaling pathway.

## OTUD4 Is a Target of miR-103a-3p

After, we clarified miR-103a-3p stimulated ZIKV replication through activation of the p38 MAPK signaling pathway, we next moved on to investigate the target gene of miR-103a-3p. We employed four different prediction algorithms to predict the possible target genes of miR-103a-3p and 177 genes overlapped in all the four algorithms were obtained (**Supplementary Figure S3**). Among these genes, OTUD4 was closely relevant to host antiviral response and p38 MAPK signaling pathway according to previously studies (Zhao et al., 2018; Liuyu et al., 2019). Interestingly, one possible binding site for miR-103a-3p at the 3′UTR region of OTUD4 was identified (**Figure 4A**). By qRT-PCR and Western blot, we found OTUD4 expression was significantly downregulated by over-expression of miR-103a-3p compared to negative control (**Figure 4B**). To further confirm whether OTUD4 is a direct target gene of miR-103a-3p, we performed mutation analysis by dual-luciferase assays. As expected, miR-103a-3p significantly repressed Renilla/Firefly luciferase activity when co-transfected with the wild-type OTUD4 3′UTR plasmid but not of the 3′UTR mutant plasmid (**Figure 4C**). Taken together, these results support that OTUD4 is a target gene of miR-103a-3p.

## OTUD4 Inhibits ZIKV Replication Through Suppression of p38 MAPK Signaling Pathway

Next, we sought to explore the regulatory effect of OTUD4 on ZIKV replication. OTUD4 was over-expressed by transfection with Flag-OTUD4 plasmid. Transfection of OTUD4 plasmid led to a remarkable upregulation of OTUD4 mRNA and protein expression in A549 cells with or without ZIKV infection (**Figures 5A,C**). OTUD4 over-expression significantly inhibited ZIKV RNA replication and ZIKV NS1 protein level compared with empty vector group (**Figures 5B,C**). Additionally, we further validated the anti-ZIKV effect of OTUD4 by downregulation through siRNA transfection. OTUD4 siRNA could efficiently suppress its mRNA and protein expression in A549 cells in the presence or absence of ZIKV infection (**Figures 5D,F**). As expected, silencing of OTUD4 significantly promoted ZIKV RNA replication and ZIKV NS1 protein level compared with

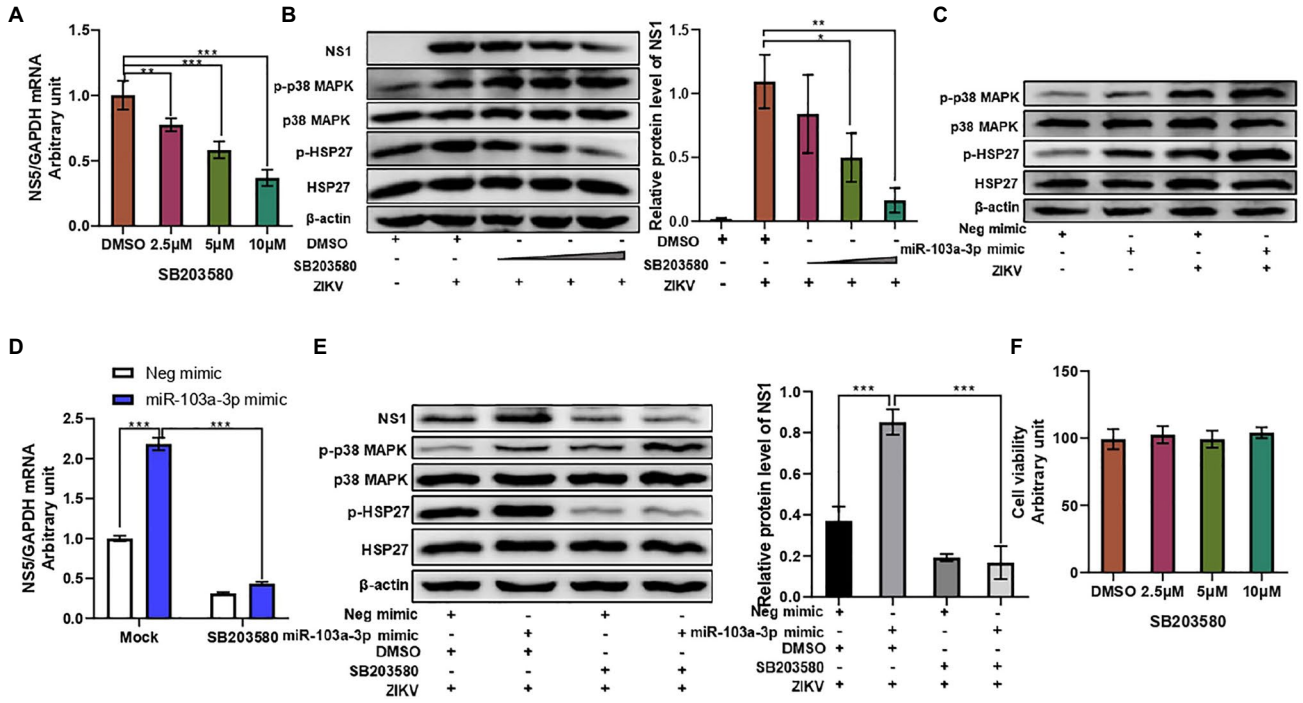


**FIGURE 3 |** miR-103a-3p stimulates ZIKV replication through activation of p38 MAPK signaling pathway. A549 cells were pretreated with SB203580 at indicated dose for 1 h or transfected with miR-103a-3p mimic or corresponding negative control and infected with ZIKV (MOI = 0.5) for 48 h. Total RNA and protein of cells were harvested at 48 h post infection for qRT-PCR or Western blot analysis. **(A)** SB203580 inhibits ZIKV RNA replication in a dose-dependent manner. **(B)** SB203580 inhibits ZIKV NS1 expression and p-HSP17 but increases p-p38 MAPK protein levels in a dose-dependent manner. **(C)** Over-expression of miR-103a-3p increases p-p38 MAPK and p-HSP27 protein levels. **(D)** SB203580 treatment attenuates the stimulating effect of miR-103a-3p on ZIKV RNA replication. **(E)** SB203580 abrogates the stimulating effect of miR-103a-3p on ZIKV NS1 and p-HSP27, but not of p-p38 MAPK protein levels. **(F)** The selected dose of SB203580 does not affect cell viability. Data are presented as mean ± SD. Error bars indicate SD ($n \geq 3$). $^{*}p < 0.05$, $^{**}p < 0.01$, and $^{***}p < 0.001$.

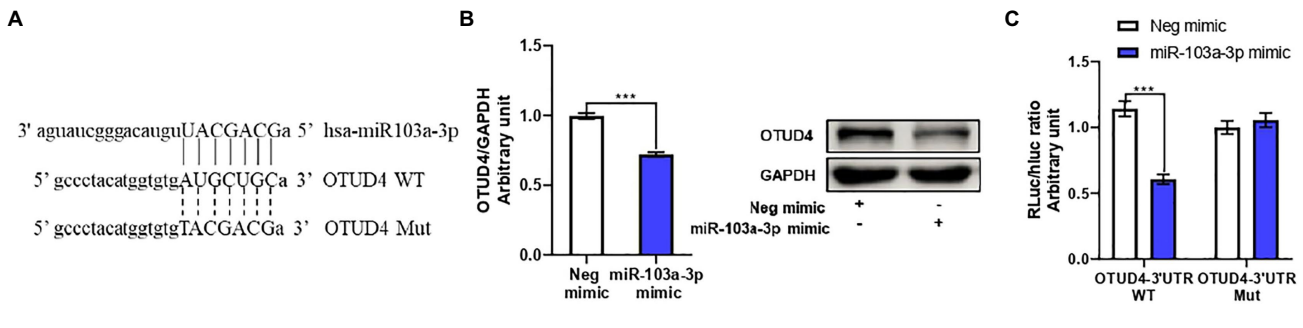


**FIGURE 4 |** OTU deubiquitinase 4 (OTUD4) is a target gene of miR-103a-3p. A549 cells were transfected with miR-103a-3p or co-transfected with miR-103a-3p and luciferase reporter plasmid. Total RNA, protein, and lysates of cells were harvested at 48 h post transfection for qRT-PCR, Western blot, and Luciferase reporter assays. **(A)** The putative binding sites in wide-type (WT) and corresponding mutant (MUT) sites of miR-103a-3p seed sequence on the 3′-untranslated region (3′UTR) of OTUD4. **(B)** miR-103a-3p decreases both mRNA and protein levels of OTUD4. **(C)** The luciferase activity is decreased in the group co-transfected of miR-103a-3p mimic and OTUD4-3′UTR-WT plasmid, but not of OTUD4-3′UTR-Mut plasmid. Data are presented as mean ± SD. Error bars indicate SD ($n \geq 3$). $^{***}p < 0.001$.

negative control group (**Figures 5E,F**). Furthermore, to determine whether OTUD4 could counteract the pro-viral effect of miR-103a-3p on ZIKV replication, we co-transfected miR-103a-3p and OTUD4 plasmid into A549 cells in the presence of ZIKV infection. As expected, OTUD4 over-expression abrogated the stimulating effect of miR-103a-3p on ZIKV replication (**Figures 5G,H**). We further assessed the effect of OTUD4 on p38 MAPK pathway in ZIKV-infected A549 cells. We found OTUD4 over-expression inhibited the phosphorylation of both p38 MAPK and HSP27 (**Figure 5C**), while OTUD4 knock down upregulated the phosphorylation of p38 MAPK and HSP27 (**Figure 5F**). Moreover, OTUD4 attenuated the activation effect of miR-103a-3p on the p38 MAPK signaling pathway as shown by the decreased phosphorylation levels of both p-p38 MAPK and p-HSP27 in the presence of OTUD4 over-expression (**Figure 5H**). Besides, OTUD4 knock-down or over-expression

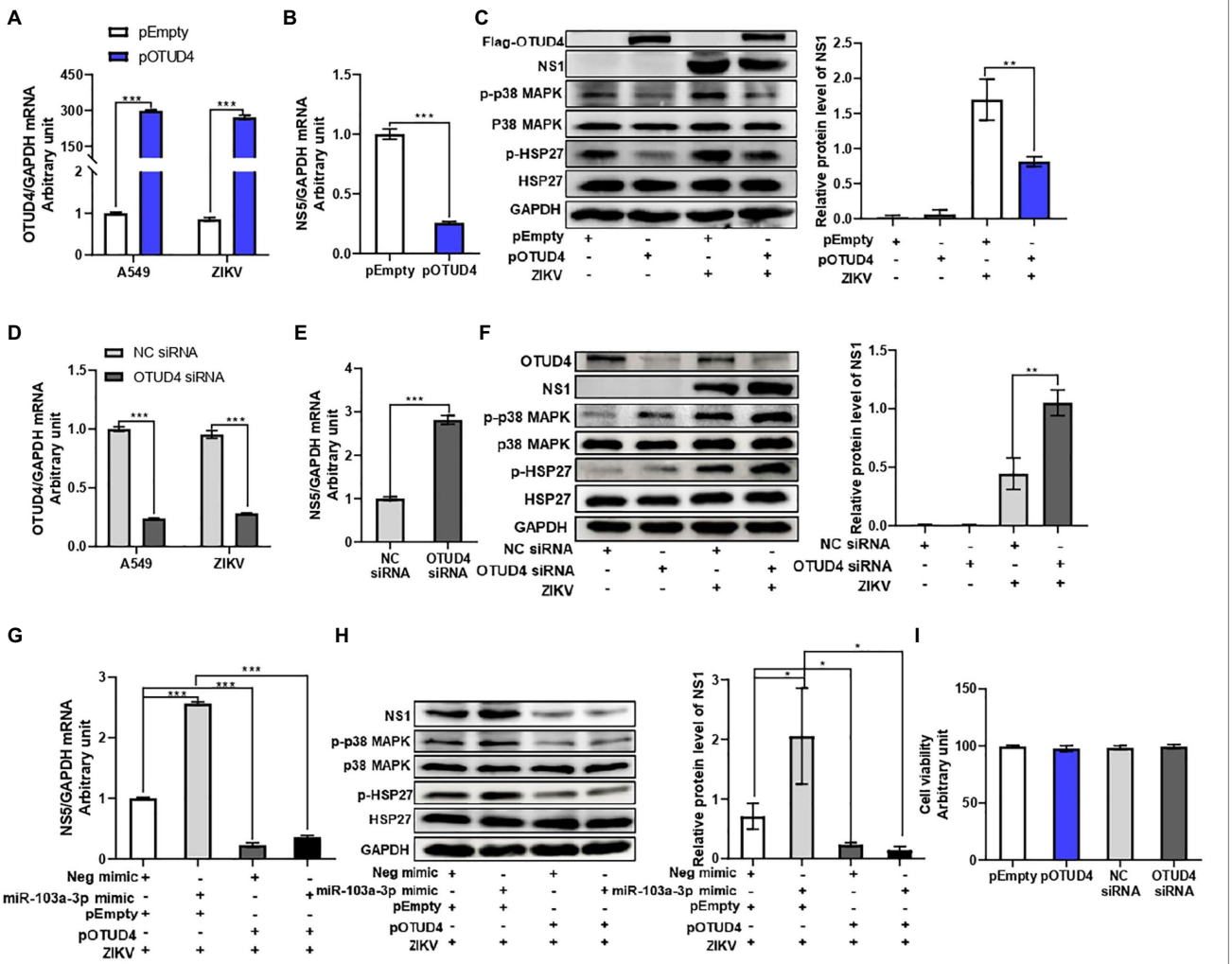


**FIGURE 5 |** OTU deubiquitinase 4 regulates ZIKV replication through activating p38 MAPK signaling pathway. pOTUD4, OTUD4 siRNA and corresponding control were transfected into A549 cells and then cells were infected ZIKV (MOI = 0.5). Total RNA and protein of cells were harvested at 48 h post infection for qRT-PCR and Western blot analysis, respectively. **(A)** The mRNA expression level of OTUD4 is significantly increased following pOTUD4 transfection compared to pEmpty. **(B)** OTUD4 over-expression inhibits ZIKV NS5 mRNA expression compared to pEmpty. **(C)** Over-expression of OTUD4 decreases ZIKV NS1, p-p38 MAPK, and p-HSP27 protein levels compared to pEmpty. **(D)** The mRNA expression level of OTUD4 is inhibited by OTUD4 siRNA transfection compared to NC siRNA. **(E)** OTUD4 knock-down significantly promotes ZIKV RNA expression compared to NC siRNA. **(F)** Silencing of OTUD4 increases ZIKV NS1, p-p38 MAPK, and p-HSP27 protein levels compared to NC siRNA. **(G)** Over-expression of OTUD4 abrogates the stimulating effect of miR-103a-3p on ZIKV RNA replication. **(H)** OTUD4 over-expression reduces the promoting effect of miR-103a-3p on ZIKV NS1, p-p38 MAPK, and p-HSP27 protein levels. **(I)** pOTUD4 and OTUD4 siRNA transfection into A549 cells did not affect cell viability. Data are presented as mean ± SD. Error bars indicate SD ($n \geq 3$). $^{*}p < 0.05$, $^{**}p < 0.01$ and $^{***}p < 0.001$.

did not affect cell viability (**Figure 5I**). Taken together, these findings indicate that OTUD4 not only inhibits ZIKV replication through suppression of p38 MAPK signaling pathway but also attenuates the stimulating effect of miR-103a-3p on ZIKV replication.

## DISCUSSION

In the past few years, accumulating evidence has suggested that miRNAs regulate a variety of biological processes including host immune responses, apoptosis, and viral infections (Fani et al., 2018). Although miRNAs play important roles in the pathogenesis of *flavivirus* infections, only a few studies attempt to analyze how ZIKV infection alters host miRNA expression (Kozak et al., 2017; Dang et al., 2019; Seong et al., 2020; Tabari et al., 2020). Interestingly, we found different research groups showed significantly different results of the miRNAs expression profiles induced by ZIKV infection, which may be due to different ZIKV lineages, sample harvested time and cell lines used in different studies. ZIKV was reported to infect lung in animal models. One study showed that in

a primate model, ZIKV was subcutaneously injected into pregnant rhesus macaques, and vRNA could be detected in the lungs of fetus (Nguyen et al., 2017). Another study demonstrated that primary cells from lung tissues of tree shrew permissive to ZIKV infection (Zhang et al., 2019b). In addition, human lung epithelial A549 cells have been shown to be permissive to infection by most flaviviruses including ZIKV (Frumence et al., 2016; Liao et al., 2020) and are a suitable model for studying host-virus interactions. In this study, we first performed a small RNA sequencing to identify dysregulated miRNAs profiles during the course of ZIKV (GZ01 strain) infection in A549 cells. As shown in **Figure 1**, although slightly differences within the three samples for each group were observed in cluster analysis, 35 miRNAs were statistically differentially regulated in ZIKV-infected A549 cells ($p < 0.05$). We further confirmed the expression levels of 10 miRNAs obtained by RNA-Seq using qRT-PCR, which were consistent with RNA-Seq results.

MiR-103a-3p is one of the upregulated miRNAs induced by ZIKV infection. A recent study also reported that miR-103a-3p was upregulated in EVs during ZIKV infection (Tabari et al., 2020). MiR-103a-3p has multiple functions involved in the regulation of inflammation, immune response, and development of a variety of cancers (Geng et al., 2014; Hu et al., 2018; Lu et al., 2019; Li et al., 2020, 2021). However, to date, the effect of miR-103a-3p on the regulation of pathogen infection has not been reported. Therefore, we focus on miR-103a-3p to explore the role of miR-103a-3p in ZIKV replication and its underlying mechanisms. We upregulated the expression level of miR-103a-3p by transfection to study its role in ZIKV replication. We found that over-expression of miR-103a-3p stimulated ZIKV replication both at NS5 mRNA and NS1 protein levels (**Figure 2**) without affecting the cell viability. These results indicated that miR-103a-3p may be one of the host genes ZIKV exploited to benefit its own replication.

P38 MAPK signaling pathway has been reported to be involved in the pathogenesis of many viruses (Sreekanth et al., 2016; Grimes and Grimes, 2020). It has been well documented that several viruses facilitate their replication by activating p38 MAPK signaling pathway (Chander et al., 2021). For example, SARS-CoV-2 may directly activate p38 MAPK signaling to induce overwhelming inflammation, as well as simultaneously utilizes p38 MAPK signaling pathway to facilitate its replication (Grimes and Grimes, 2020). Similarly, activated p38α has been shown to interact with HCV core protein to promote oligomerization of the HCV core protein, and subsequently facilitates HCV replication, while disruption of the p38α-core interaction by SB203580 inhibits HCV assembly. In addition, similar results were also observed in SFTSV and HSV-1 infections (Cheng et al., 2020). However, whether ZIKV infection activates p38 MAPK signaling is controversially. One earlier study reported that ZIKV infection activated p38 MAPK signaling pathway in Müller cells (Zhu et al., 2017). Another study also showed that ZIKV activated p38 MAPK in JAR, JEG-3, and HTR-8 cells (Muthuraj et al., 2021). However, one study failed to show any effect of ZIKV infection on p38 MAPK activity (Cheng et al., 2020). These earlier studies used different virus strains, cell lines, and sample harvesting time, which may contribute to different findings. In this current study, we confirmed that ZIKV infection induced p38 MAPK activation in both time-dependent and MOI-dependent manners (**Supplementary Figure S1**), while blockage of p38 MAPK activity by inhibitor SB203580 repressed ZIKV replication (**Figure 3B**). In addition, pretreatment of SB203580 alone did not affect miR-103a-3p in A549 cells, but slightly inhibited the ZIKV induced miR-103a-3p expression (**Supplementary Figure S2**), which indicated that ZIKV induced miR-103a-3p is associate with the ZIKV infection and independent of p38 MAPK pathway. Quite interestingly, we observed a slight increase in phosphorylation of p38 MAPK in the presence of SB203580 in A549 cells. Kumar et al. (1999) also observed similar phenomenon and speculated that it may be due to inaccessibility of phosphatase responsible for p38 MAPK dephosphorylation in the presence of SB203580. Alternatively, the p38 MAPK enzyme may be stabilized in a state that is more accessible to MKK6 due to SB203580 binding. Therefore, the binding of SB203580 in the ATP binding pocket of p38 MAPK interferes with its catalytic activity but does not inhibit p38 MAPK phosphorylation by upstream kinases. HSP27 is one of effector molecule downstream of the p38 MAPK signaling pathway and can be activated by virus infection (Mathew et al., 2009). It has been reported that adenovirus infection activates p38 MAPK, and HSP27, which is required for virus nuclear targeting (Suomalainen et al., 2001). HSP27 or p-HSP27 depletion can reduce HSV-1 production significantly (Mathew et al., 2009). These studies implied that HSP27 plays an important role in regulating virus infection.

Our data indicated that either ZIKV infection or miR-103a-3p alone could effectively activated p38 MAPK signaling pathway as shown by the increased level of p-p38 MAPK and p-HSP27 (**Figure 3C**). After we confirmed that miR-103a-3p could stimulate ZIKV replication and p38 MAPK signaling pathway was activated following ZIKV infection, we moved on to clarify whether the stimulating effect of miR-103a-3p on ZIKV replication is mediated by p38 MAPK signaling pathway. To this end, an inhibitor of p38 MAPK signaling pathway (SB203580) was used. We found the stimulating effect of miR-103a-3p on ZIKV replication was attenuated if the activation of p38 MAPK signaling pathway was inhibited by SB203580 (**Figures 3D,E**), which indicates that p38 MAPK signaling pathway is involved in the regulation of ZIKV replication by miR-103a-3p.

MicroRNAs normally function through downregulation of their target genes. In order to further understand the molecular mechanism by which miR-103a-3p stimulates ZIKV replication, we used four different prediction algorithms to predict the possible target genes of miR-103a-3p. As shown in **Supplementary Figure S3**, 177 overlapping genes predicted by all four algorithms were obtained. Among these genes, OTUD4 was previously reported to be associated with host antiviral response and p38 MAPK pathway (Zhao et al., 2018; Liuyu et al., 2019). As a k48-specific DUB, OTUD4 could stabilize MAVS by preventing its degradation to facilitate

antiviral response (Liuyu et al., 2019). Furthermore, OTUD4 was identified as a phospho-activated k63 DUB, which targeted toll-like receptor (TLR)-associated factor MyD88 and negatively regulated TLR-mediated activation of NF-κB; Moreover, silencing of OTUD4 has been shown to enhance the phosphorylation of p38 MAPK in cells upon IL-1β stimulation (Zhao et al., 2018), which may indicate OTUD4 is a negative regulator of p38 MAPK signaling pathway. In our current study, we first identified a potential binding site for miR-103a-3p at the 3′UTR region of OTUD4 (**Figure 4A**). Using mutation analysis, we were able to confirm that OTUD4 is indeed one of the target genes of miR-103a-3p (**Figure 4C**). We further assessed the effect of OTUD4 on ZIKV replication and activation of p38 MAPK signaling pathway. As shown in **Figure 5**, over-expression of OTUD4 inhibited, while silencing of OTUD4 promoted ZIKV replication both at NS5 mRNA and NS1 protein levels. We also observed decreased phosphorylation of p38 MAPK and HSP27 in OTUD4 over-expressed cells, while increased in OTUD4 silenced cells in the presence or absence of ZIKV infection. Most importantly, OTUD4 attenuated the simulating effect of miR-103a-3p on ZIKV replication together with inhibition of p38 MAPK signaling pathway (**Figures 5G,H**).

In summary, data from our current study indicated that ZIKV infection induced miR-103a-3p upregulation, which in turn was exploited by ZIKV to promote its own replication through targeting OTUD4 to activate p38 MAPK signaling pathway (**Figure 6**). Our research revealed a novel miRNA-mediated activation of the p38 MAPK signaling pathway to promote ZIKV replication, implying that miR-103a-3p is one of the host genes exploited by ZIKV to benefit its replication and targeting this gene or the p38 MAPK signaling pathway may be a potential novel strategy to treat ZIKV infection.

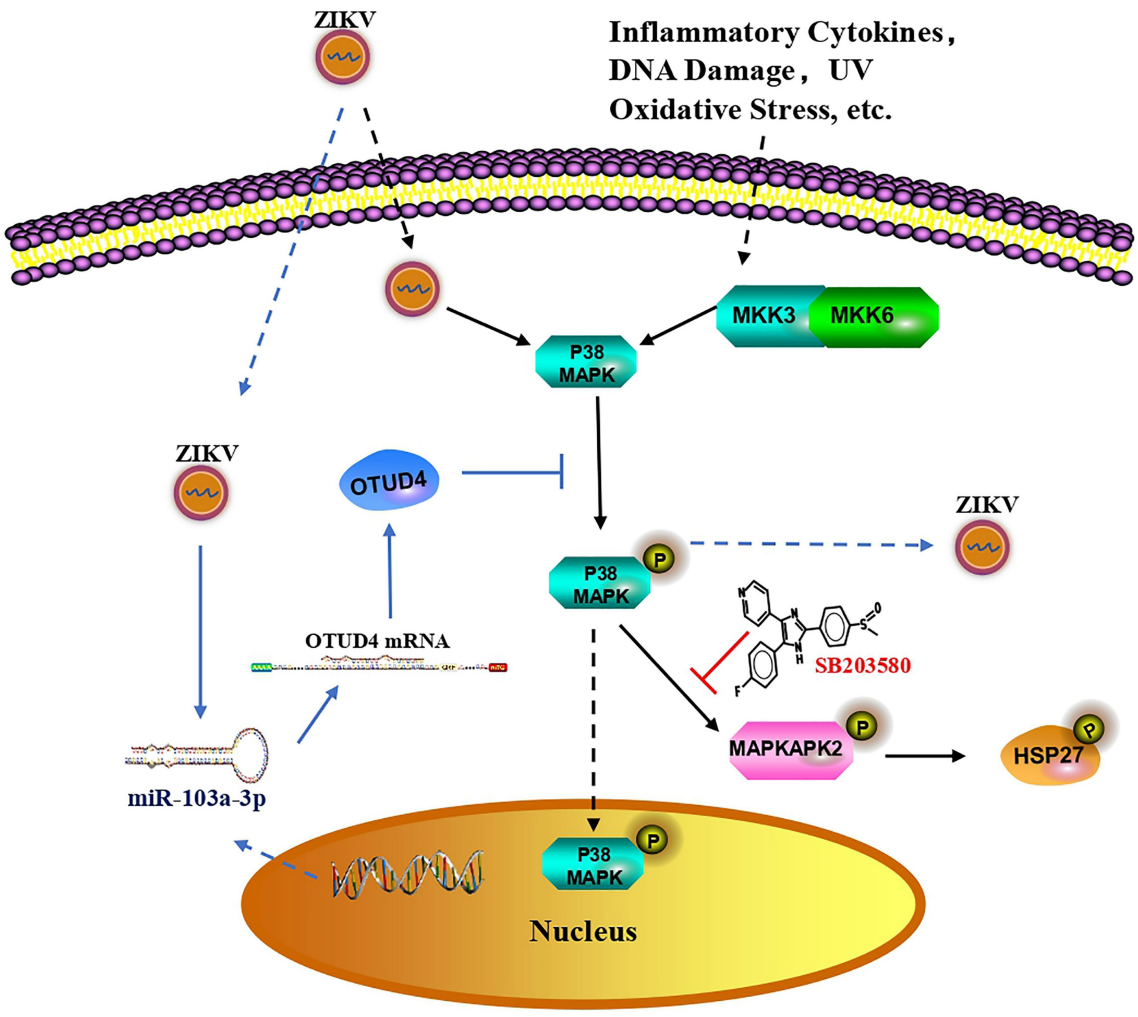


**FIGURE 6 |** Proposed model for miR-103a-3p regulates ZIKV replication. In response to ZIKV infection, p38 MAPK is activated as shown by increased phosphorylated of HSP27 which facilitates ZIKV replication. Suppressed activity of p38 MAPK by SB203580 inhibits ZIKV replication. ZIKV infection also induces miR-103a-3p expression, which targets OTUD4 to regulate p38 MAPK signaling pathway to stimulate ZIKV replication. MiR-103a-3p is one of the host genes exploited by ZIKV to benefit its replication and targeting this gene or the p38 MAPK signaling pathway may be a potential novel strategy to treat ZIKV infection.

## CONCLUSION

We conclude that miR-103a-3p plays an important role in regulating ZIKV replication. MiR-103a-3p stimulates ZIKV replication by targeting OTUD4 to activate the p38 MAPK signaling pathway and targeting miR-103a-3p or p38 MAPK signaling may provide a viable approach for the treatment of ZIKV infection.

## DATA AVAILABILITY STATEMENT

The datasets presented in this study can be found in online repositories. The names of the repository/repositories and accession number(s) can be found in the article/ **Supplementary Material**.

## AUTHOR CONTRIBUTIONS

HY, XD, and LC conceived and designed the project. HY, LK, XY, YH, and RM performed the experiments. HY, XD, and SL analyzed and interpreted the data. HY drafted the initial manuscript. SL, XD, and LC reviewed and critically revised the initial draft. All authors contributed to the article and approved the submitted version.

## FUNDING

This work is supported by Natural Science Foundation of China (NSFC 82102383) and the central government directed special funds for local science and technology development project (No 2021ZYD0085) to XD; by National Key Research and Development Program of China (2018YFE0107500), and the Science and Technology Partnership Program, Ministry of Science and Technology of China (KY201904011) to LC.

## ACKNOWLEDGMENTS

The authors are grateful to Chengfeng Qin for providing Zika virus.

## SUPPLEMENTARY MATERIAL

The Supplementary Material for this article can be found online at: https://www.frontiersin.org/articles/10.3389/fmicb.2022.862580/full#supplementary-material

**Supplementary Figure S1 |** Zika virus (ZIKV) infection activates p38 mitogen-activated protein kinase (MAPK) signaling pathway in A549 cells. ZIKV infected A549 cells at indicated multiplicity of infection (MOI) and harvested cells at indicated time post infection. **(A)** ZIKV infection increases p-p38 MAPK protein level in a time-dependent manner. **(B)** ZIKV infection enhances p-p38 MAPK protein level in a MOI-dependent manner at 48 h post infection.

**Supplementary Figure S2 |** Zika virus -induced miR-103a-3p expression is slightly inhibited by SB203580 pretreatment. A549 cells were pretreated with SB203580 for 1 h and infected with ZIKV at a MOI of 0.5. Cells were harvested at 48 h post infection. SB20350 inhibited ZIKV-induced miR-103a-3p expression. Data are presented as mean ± SD. Error bars indicate SD ($n \geq 3$). $^{**}p < 0.01$ and $^{***}p < 0.001$.

**Supplementary Figure S3 |** Bioinformatics analysis of miR-103a-3p target gene. Four different prediction algorithms were used to predict the putative miR-103a-3p targets. Around 177 targets genes are overlapped in four prediction datasets.

## REFERENCES

Bartel, D. P. (2004). MicroRNAs: genomics, biogenesis, mechanism, and function. *Cell* 116, 281–297. doi: 10.1016/s0092-8674(04)00045-5

Chander, Y., Kumar, R., Khandelwal, N., Singh, N., Shringi, B. N., Barua, S., et al. (2021). Role of p38 mitogen-activated protein kinase signalling in virus replication and potential for developing broad spectrum antiviral drugs. *Rev. Med. Virol.* 31, 1–16. doi: 10.1002/rmv.2217

Cheng, Y., Sun, F., Wang, L., Gao, M., Xie, Y., Sun, Y., et al. (2020). Virus-induced p38 MAPK activation facilitates viral infection. *Theranostics* 10, 12223–12240. doi: 10.7150/thno.50992

Cuadrado, A., and Nebreda, A. R. (2010). Mechanisms and functions of p38 MAPK signalling. *Biochem. J.* 429, 403–417. doi: 10.1042/BJ20100323

Dang, J. W., Tiwari, S. K., Qin, Y., and Rana, T. M. (2019). Genome-wide integrative analysis of zika-virus-infected neuronal stem cells reveals roles for microRNAs in cell cycle and Stemness. *Cell Rep.* 27, 3618.e5–3628.e5. doi: 10.1016/j.celrep.2019.05.059

Dick, G. W., Kitchen, S. F., and Haddow, A. J. (1952). Zika virus. I. Isolations and serological specificity. *Trans. R. Soc. Trop. Med. Hyg.* 46, 509–520. doi: 10.1016/0035-9203(52)90042-4

Estevez-Herrera, J., Perez-Yanes, S., Cabrera-Rodriguez, R., Marquez-Arce, D., Trujillo-Gonzalez, R., Machado, J. D., et al. (2021). Zika virus pathogenesis: a battle for immune evasion. *Vaccine* 9:294. doi: 10.3390/vaccines9030294

Fani, M., Zandi, M., Rezayi, M., Khodadad, N., Langari, H., and Amiri, I. (2018). The role of microRNAs in the viral infections. *Curr. Pharm. Des.* 24, 4659–4667. doi: 10.2174/1381612825666190110161034

Filgueiras, I. S., Torrentes de Carvalho, A., Cunha, D. P., Mathias da Fonseca, D. L., El Khawanky, N., Freire, P. P., et al. (2021). The clinical spectrum and immunopathological mechanisms underlying ZIKV-induced neurological manifestations. *PLoS Negl. Trop. Dis.* 15:e0009575. doi: 10.1371/journal.pntd.0009575

Frumence, E., Roche, M., Krejbich-Trotot, P., El-Kalamouni, C., Nativel, B., Rondeau, P., et al. (2016). The south pacific epidemic strain of zika virus replicates efficiently in human epithelial A549 cells leading to IFN-beta production and apoptosis induction. *Virology* 493, 217–226. doi: 10.1016/j.virol.2016.03.006

Geng, L., Sun, B., Gao, B., Wang, Z., Quan, C., Wei, F., et al. (2014). MicroRNA-103 promotes colorectal cancer by targeting tumor suppressor DICER and PTEN. *Int. J. Mol. Sci.* 15, 8458–8472. doi: 10.3390/ijms15058458

Grimes, J. M., and Grimes, K. V. (2020). p38 MAPK inhibition: a promising therapeutic approach for COVID-19. *J. Mol. Cell. Cardiol.* 144, 63–65. doi: 10.1016/j.yjmcc.2020.05.007

Hu, X., Miao, J., Zhang, M., Wang, X., Wang, Z., Han, J., et al. (2018). miRNA-103a-3p promotes human gastric cancer cell proliferation by targeting and suppressing ATF7 in vitro. *Mol. Cell* 41, 390–400. doi: 10.14348/molcells.2018.2078

Kostenko, S., and Moens, U. (2009). Heat shock protein 27 phosphorylation: kinases, phosphatases, functions and pathology. *Cell. Mol. Life Sci.* 66, 3289–3307. doi: 10.1007/s00018-009-0086-3

Kozak, R. A., Majer, A., Biondi, M. J., Medina, S. J., Goneau, L. W., Sajesh, B. V., et al. (2017). MicroRNA and mRNA dysregulation in astrocytes infected with zika virus. *Viruses* 9:297. doi: 10.3390/v9100297

Kumar, S., Jiang, M. S., Adams, J. L., and Lee, J. C. (1999). Pyridinylimidazole compound SB 203580 inhibits the activity but not the activation of p38

mitogen-activated protein kinase. *Biochem. Biophys. Res. Commun.* 263, 825–831. doi: 10.1006/bbrc.1999.1454

Lanciotti, R. S., Kosoy, O. L., Laven, J. J., Velez, J. O., Lambert, A. J., Johnson, A. J., et al. (2008). Genetic and serologic properties of zika virus associated with an epidemic, yap state, Micronesia, 2007. *Emerg. Infect. Dis.* 14, 1232–1239. doi: 10.3201/eid1408.080287

Langmead, B., Trapnell, C., Pop, M., and Salzberg, S. L. (2009). Ultrafast and memory-efficient alignment of short DNA sequences to the human genome. *Genome Biol.* 10:R25. doi: 10.1186/gb-2009-10-3-r25

Li, H., Huhe, M., and Lou, J. (2021). MicroRNA-103a-3p promotes cell proliferation and invasion in non-small-cell lung cancer cells through Akt pathway by targeting PTEN. *Biomed. Res. Int.* 2021, 7590976–7591110. doi: 10.1155/2021/7590976

Li, R., Liang, P., Yuan, J., and He, F. (2020). Exosomal miR-103a-3p ameliorates lipopolysaccharide-induced immune response in BEAS-2B cells via NF-kappaB pathway by targeting transducin beta-like 1X related protein 1. *Clin. Exp. Pharmacol. Physiol.* 47, 620–627. doi: 10.1111/1440-1681.13241

Liao, X., Xie, H., Li, S., Ye, H., Li, S., Ren, K., et al. (2020). 2′, 5'-Oligoadenylate synthetase 2 (OAS2) inhibits zika virus replication through activation of type iota IFN signaling pathway. *Viruses* 12:418. doi: 10.3390/v12040418

Liuyu, T., Yu, K., Ye, L., Zhang, Z., Zhang, M., Ren, Y., et al. (2019). Induction of OTUD4 by viral infection promotes antiviral responses through deubiquitinating and stabilizing MAVS. *Cell Res.* 29, 67–79. doi: 10.1038/s41422-018-0107-6

Lu, Q., Ma, Z., Ding, Y., Bedarida, T., Chen, L., Xie, Z., et al. (2019). Circulating miR-103a-3p contributes to angiotensin II-induced renal inflammation and fibrosis via a SNRK/NF-kappaB/p65 regulatory axis. *Nat. Commun.* 10:2145. doi: 10.1038/s41467-019-10116-0

Ma, Q., Pan, W., Li, R., Liu, B., Li, C., Xie, Y., et al. (2020). Liu Shen capsule shows antiviral and anti-inflammatory abilities against novel coronavirus SARS-CoV-2 via suppression of NF-kappaB signaling pathway. *Pharmacol. Res.* 158:104850. doi: 10.1016/j.phrs.2020.104850

Mathew, S. S., Della Selva, M. P., and Burch, A. D. (2009). Modification and reorganization of the cytoprotective cellular chaperone Hsp27 during herpes simplex virus type 1 infection. *J. Virol.* 83, 9304–9312. doi: 10.1128/JVI.01826-08

McCaskill, J. L., Ressel, S., Alber, A., Redford, J., Power, U. F., Schwarze, J., et al. (2017). Broad-spectrum inhibition of respiratory virus infection by microRNA mimics targeting p38 MAPK signaling. *Mol. Ther. Nucleic Acids* 7, 256–266. doi: 10.1016/j.omtn.2017.03.008

Muthuraj, P. G., Sahoo, P. K., Kraus, M., Bruett, T., Annamalai, A. S., Pattnaik, A., et al. (2021). Zika virus infection induces endoplasmic reticulum stress and apoptosis in placental trophoblasts. *Cell Death Dis.* 7:24. doi: 10.1038/s41420-020-00379-8

Mwaliko, C., Nyaruaba, R., Zhao, L., Atoni, E., Karungu, S., Mwau, M., et al. (2021). Zika virus pathogenesis and current therapeutic advances. *Pathog. Glob. Health.* 115, 21–39. doi: 10.1080/20477724.2020.1845005

Nguyen, S. M., Antony, K. M., Dudley, D. M., Kohn, S., Simmons, H. A., Wolfe, B., et al. (2017). Highly efficient maternal-fetal zika virus transmission in pregnant rhesus macaques. *PLoS Pathog.* 13:e1006378. doi: 10.1371/journal.ppat.1006378

Patterson, J., Sammon, M., and Garg, M. (2016). Dengue, zika and chikungunya: emerging arboviruses in the new world. *West. J. Emerg. Med.* 17, 671–679. doi: 10.5811/westjem.2016.9.30904

Peng, H., Shi, M., Zhang, L., Li, Y., Sun, J., Zhang, L., et al. (2014). Activation of JNK1/2 and p38 MAPK signaling pathways promotes enterovirus 71 infection in immature dendritic cells. *BMC Microbiol.* 14:147. doi: 10.1186/1471-2180-14-147

Seong, R. K., Lee, J. K., Cho, G. J., Kumar, M., and Shin, O. S. (2020). mRNA and miRNA profiling of Zika virus-infected human umbilical cord mesenchymal stem cells identifies miR-142-5p as an antiviral factor. *Emerg. Microbes Infect.* 9, 2061–2075. doi: 10.1080/22221751.2020.1821581

Shukla, A., Rastogi, M., and Singh, S. K. (2021). Zika virus NS1 suppresses the innate immune responses via miR-146a in human microglial cells. *Int. J. Biol. Macromol.* 193, 2290–2296. doi: 10.1016/j.ijbiomac.2021.11.061

Sreekanth, G. P., Chuncharunee, A., Sirimontaporn, A., Panaampon, J., Noisakran, S., Yenchitsomanus, P. T., et al. (2016). SB203580 modulates p38 MAPK signaling and dengue virus-induced liver injury by reducing MAPKAPK2, HSP27, and ATF2 phosphorylation. *PLoS One* 11:e0149486. doi: 10.1371/journal.pone.0149486

Suomalainen, M., Nakano, M. Y., Boucke, K., Keller, S., and Greber, U. F. (2001). Adenovirus-activated PKA and p38/MAPK pathways boost microtubule-mediated nuclear targeting of virus. *EMBO J.* 20, 1310–1319. doi: 10.1093/emboj/20.6.1310

Tabari, D., Scholl, C., Steffens, M., Weickhardt, S., Elgner, F., Bender, D., et al. (2020). Impact of zika virus infection on human neural stem cell microRNA signatures. *Viruses* 12:1219. doi: 10.3390/v12111219

Tse, W. K., Eisenhaber, B., Ho, S. H., Ng, Q., Eisenhaber, F., and Jiang, Y. J. (2009). Genome-wide loss-of-function analysis of deubiquitylating enzymes for zebrafish development. *BMC Genomics* 10:637. doi: 10.1186/1471-2164-10-637

Wang, Y., Ren, K., Li, S., Yang, C., and Chen, L. (2020). Interferon stimulated gene 15 promotes zika virus replication through regulating Jak/STAT and ISGylation pathways. *Virus Res.* 287:198087. doi: 10.1016/j.virusres.2020.198087

Zhang, H., Chang, Y., Zhang, L., Kim, S. N., Otaegi, G., Zhang, Z., et al. (2019a). Upregulation of MicroRNA miR-9 is associated with microcephaly and zika virus infection in mice. *Mol. Neurobiol.* 56, 4072–4085. doi: 10.1007/s12035-018-1358-4

Zhang, L., Shen, Z. L., Feng, Y., Li, D. Q., Zhang, N. N., Deng, Y. Q., et al. (2019b). Infectivity of zika virus on primary cells support tree shrew as animal model. *Emerg. Microbes Infect.* 8, 232–241. doi: 10.1080/22221751.2018.1559707

Zhao, Y., Majid, M. C., Soll, J. M., Brickner, J. R., Dango, S., and Mosammaparast, N. (2015). Noncanonical regulation of alkylation damage resistance by the OTUD4 deubiquitinase. *EMBO J.* 34, 1687–1703. doi: 10.15252/embj.201490497

Zhao, Y., Mudge, M. C., Soll, J. M., Rodrigues, R. B., Byrum, A. K., Schwarzkopf, E. A., et al. (2018). OTUD4 is a phospho-activated K63 deubiquitinase that regulates MyD88-dependent signaling. *Mol. Cell* 69, 505.e5–516.e5. doi: 10.1016/j.molcel.2018.01.009

Zhu, S., Luo, H., Liu, H., Ha, Y., Mays, E. R., Lawrence, R. E., et al. (2017). p38MAPK plays a critical role in induction of a pro-inflammatory phenotype of retinal muller cells following zika virus infection. *Antivir. Res.* 145, 70–81. doi: 10.1016/j.antiviral.2017.07.012

**Conflict of Interest:** The authors declare that the research was conducted in the absence of any commercial or financial relationships that could be construed as a potential conflict of interest.

**Publisher's Note:** All claims expressed in this article are solely those of the authors and do not necessarily represent those of their affiliated organizations, or those of the publisher, the editors and the reviewers. Any product that may be evaluated in this article, or claim that may be made by its manufacturer, is not guaranteed or endorsed by the publisher.

*Copyright © 2022 Ye, Kang, Yan, Li, Huang, Mu, Duan and Chen. This is an open-access article distributed under the terms of the Creative Commons Attribution License (CC BY). The use, distribution or reproduction in other forums is permitted, provided the original author(s) and the copyright owner(s) are credited and that the original publication in this journal is cited, in accordance with accepted academic practice. No use, distribution or reproduction is permitted which does not comply with these terms.*

frontiers in Microbiology

REVIEW
published: 04 March 2022
doi: 10.3389/fmicb.2022.865592

# Innate Immune Evasion by Human Respiratory Syncytial Virus

*Yan Ouyang[1†], Hongqun Liao[1,2†], Yan Hu[3†], Kaiyuan Luo[1], Shaowen Hu[4] and Huifang Zhu[1,2,4,5*]*

[1]Neonatal/Pediatric Intensive Care Unit, Children's Medical Center, First Affiliated Hospital of Gannan Medical University, Ganzhou, China, [2]Ganzhou Key Laboratory of Immunotherapeutic Drugs Developing for Childhood Leukemia, Ganzhou, China, [3]Department of Gynecology, The Third Affiliated Hospital of Kunming Medical University, Kunming, China, [4]Basic Medical College of Gannan Medical University, Ganzhou, China, [5]Institute of Children's Medical, First Affiliated Hospital of Gannan Medical University, Ganzhou, China

Respiratory syncytial virus (RSV) is the leading cause of severe respiratory infection in young children. Nearly all individuals become infected in their early childhood, and reinfections with RSV are common throughout life. Primary infection with RSV is usually involved in the symptom of bronchiolitis and pneumonia in the lower respiratory tract, which accounts for over 3 million hospitalizations and approximately 66,000 deaths annually worldwide. Despite the widespread prevalence and high morbidity and lethality rates of diseases caused by RSV infection, there is currently no licensed RSV vaccine. During RSV infection, innate immunity plays the first line of defense to suppress RSV infection and replication. However, RSV has evolved multiple mechanisms to evade the host's innate immune responses to gain a window of opportunity for efficient viral replication. This review discusses the comprehensive interaction between RSV infection and the host antiviral innate immunity and updates recent findings on how RSV modulates the host innate immune response for survival, which may provide novel insights to find potent drug targets and vaccines against RSV.

**Keywords: respiratory syncytial virus, innate immune response, PRRs, RLRs, TLRs, NLRs**

OPEN ACCESS

***Edited by:***
*Chunfu Zheng,*
*University of Calgary, Canada*

***Reviewed by:***
*Chenhe Su,*
*Wistar Institute, United States*
*Mei Xue,*
*Harbin Veterinary Research Institute (CAAS), China*

***Correspondence:**
*Huifang Zhu*
*zhuhuifang1985@163.com*

*[†]These authors have contributed equally to this work*

***Specialty section:***
*This article was submitted to Virology, a section of the journal Frontiers in Microbiology*

***Received:*** *30 January 2022*
***Accepted:*** *17 February 2022*
***Published:*** *04 March 2022*

***Citation:***
*Ouyang Y, Liao H, Hu Y, Luo K, Hu S and Zhu H (2022) Innate Immune Evasion by Human Respiratory Syncytial Virus. Front. Microbiol. 13:865592. doi: 10.3389/fmicb.2022.865592*

## INTRODUCTION

Respiratory syncytial virus (RSV) is an enveloped virus belonging to the *Pneumovirus* genus in the *Paramyxoviridae* family. It contains a single-stranded, negative-sense RNA genome, which is 15.2 kb in size and comprises 10 genes that encode 11 viral proteins (**Figure 1**). These include two major surface proteins, the glycoprotein (G) and the gusion protein (F), and an envelope protein, the small hydrophobic (SH) protein. In addition, the matrix (M) proteins, the M2 gene-encoded two distinct matrix proteins M2-1 and M2-2, the nucleoprotein (N), the phosphoprotein (P), and the RNA polymerase large nucleoprotein (L), are located in the nucleocapsid. Two other non-structural (NS) proteins, NS1 and NS2, are characterized by their immunomodulatory functions. The airway epithelium is the primary target of RSV infection by binding viral G protein to cell-surface glycosaminoglycans. After attaching to epithelial cells, the viral surface F protein will mediate host cell membrane fusion to facilitate RSV entry.

Meanwhile, airway epithelial cells are also the first site for the activation of host innate immune responses against RSV infection through a wide variety of pattern recognition receptors

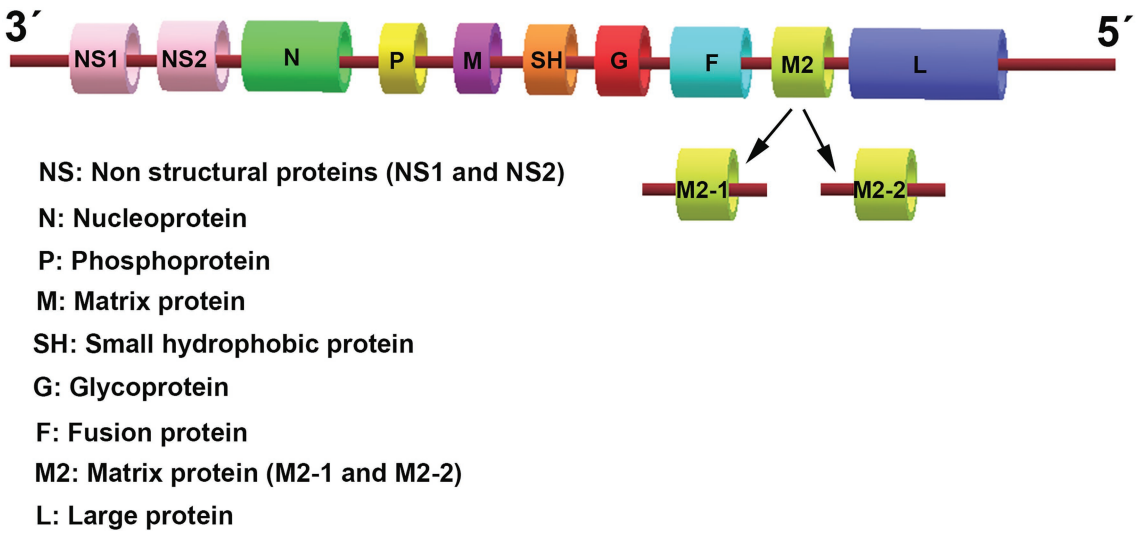


**FIGURE 1 |** The genomic organization of respiratory syncytial virus (RSV). The RSV genome is approximately 15.2 kb in size and encodes 10 genes that transcribe 11 proteins. The genome sequence from 3′ to 5′ successively encodes the non-structural (NS) proteins 1 and 2 (NS1/2), the nucleocapsid (N), the phosphoprotein (P), the matrix (M) protein, the small hydrophobic (SH) protein, the attachment (G) protein, the fusion (F) glycoproteins, the M2 gene-encoded two distinct matrix proteins M2-1 and M2-2, and the large polymerase (L) protein.

(PRRs), including the toll-like receptors (TLRs) and the cytoplasmic retinoic acid-inducible gene (RIG)-I like receptors (RLRs). On the one hand, recognition of pathogen-associated molecular patterns (PAMPs) results in activation of antiviral type I interferon (IFN-I) response, which restricts virus replication and transmission; on the other hand, RSV has evolved several mechanisms to evade the host immune response and promote virus replication through interactions between RSV proteins and immune components. In this review, we discuss the interactions between RSV proteins and host factors that modulate the immune response and the implications of these interactions for the course of an RSV infection (**Figure 2**).

## INNATE IMMUNE RESPONSE AGAINST RSV INFECTION

RSV infection is the leading cause of bronchiolitis and pneumonia in children. Although the symptoms in most patients would spontaneously relieve within a week, approximately 1 to 3% of infants with RSV infection require hospitalization for supportive care, which is responsible for approximately 50% of all types of pneumonia in infancy. It is proposed that reinfections with RSV are common throughout an individual's lifespan, and the early exposure to RSV infection in life can lead to an increased susceptibility to suffering from recurrent allergic wheezing and asthma. The first infection usually evokes inadequate immunological memory, and reinfection may exacerbate inflammatory response in the respiratory tract promoting airway damage during virus clearance. In that case, on the one hand, RSV infection in the respiratory tract induces innate immune responses by the host to facilitate the efficient clearance of the virus; on the other hand, the exacerbated host immune response during RSV infection may also partly be responsible for lung pathology, characterized by immune cell infiltration to the lungs. Therefore, the host immune response also contributes to respiratory diseases following RSV infection, except for the immune protection role.

The host's innate immunity is powerful in the first-line defense of viral infection. Multiple elements of the innate immune system, including diverse innate cell types, various PRRs, and a large array of cytokines and chemokines, contribute to the control of RSV infection. Generally, innate cellular immunity against virus infection is primarily mediated by IFN-I, which then exerts the pleiotropic effects by inducing a variety of IFN-stimulated genes (ISGs). Unique viral proteins/genomes and replication products from RSV are natural PAMPs to evoke host innate immune response through PRRs. To date, three major classes of PRRs: TLRs, RLRs, and NOD-like receptors (NLRs) are demonstrated to be involved in the detection of RSV, leading to the induction of cytokines, chemokines, and IFN-I, which subsequently facilitate the clearance of the virus.

### RSV Infection Triggers TLRs Pathway

TLRs are type I transmembrane receptor proteins composed of an extracellular domain containing multiple leucine-rich repeats, a transmembrane region, and a cytoplasmic tail containing the conserved TIR domain. The TLR family members typically recognize evolutionarily conserved structures of many pathogens, such as bacterial lipopolysaccharide, bacterial and viral nucleic acids, peptidoglycans, lipoproteins. Ten different TLRs (TLR1-10) have been identified in humans. They are largely divided into two subgroups depending on their cellular localization and respective ligands. One group is composed of TLR1 ~ 6, which are expressed on cell surfaces and recognize microbial membrane components such as lipoproteins and

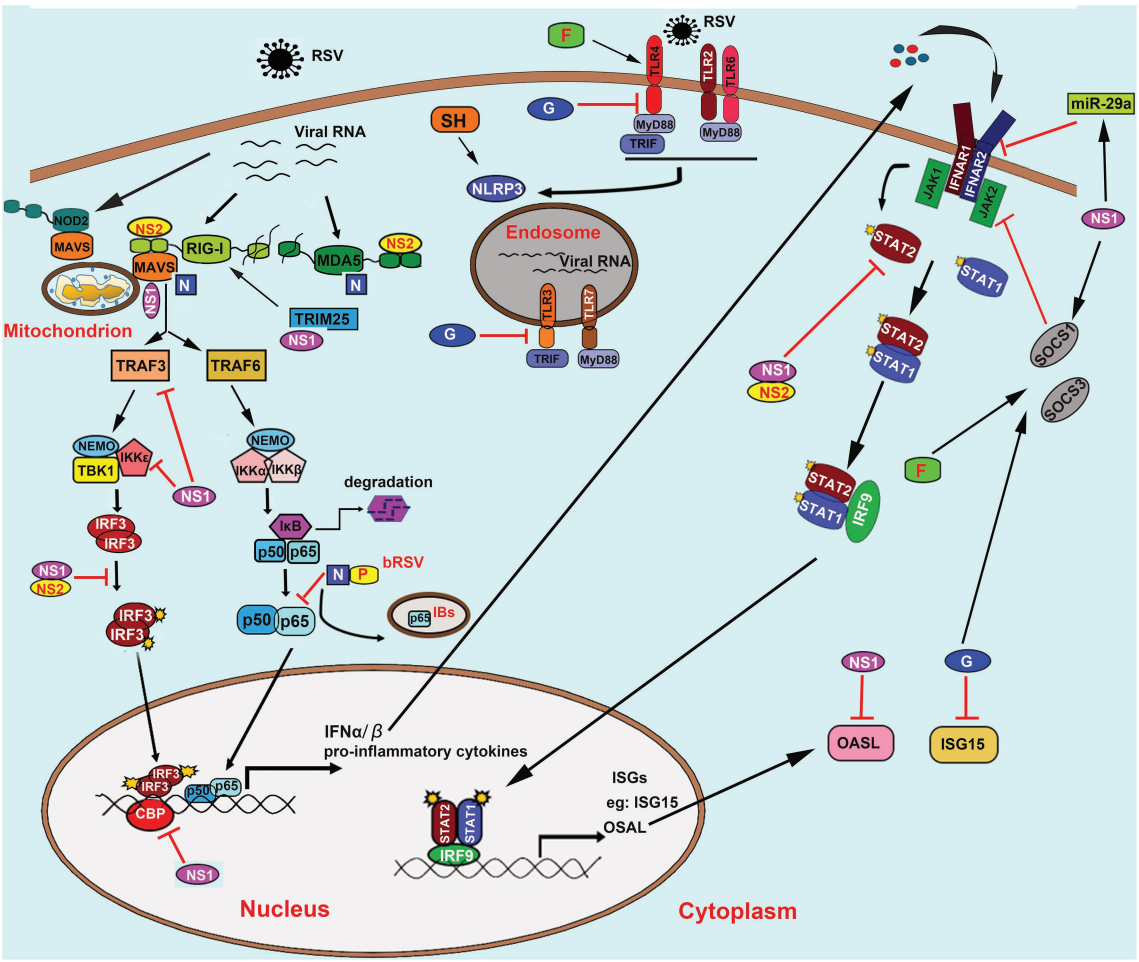


**FIGURE 2 |** Innate recognition of RSV and its immune evasion mechanisms. RSV is recognized by TLRs including TLR2/6, TLR4, TLR3, and TLR7; RLRs including RIG-I and MDA5; NLRs including NOD2 and NLRP3. NS1/2 mainly mediates the innate immune evasion mechanisms caused by RSV converged in interfering with the RLRs signaling pathway by direct binding to RIG-I, MDA5, adaptor proteins MAVS, and TRIM25. Besides, NS1/2 also induces the decrease of TRAF3, IKKε, and blocks the phosphorylation of IRF3 and its association to transcriptional coactivator CBP. Moreover, NS1/2 also prevents the JAK/STAT signaling by promoting the degradation of STAT2 and OASL and inhibits the IFNAR synthesis *via* inducing the expression of miR-29a. Besides, NS1 can also induce the expression of SOCS1 in a RIG-I and TLR3-independent pathway, which further inhibits the phosphorylation of STAT2. The N protein binds to MDA5 and MAVS to inhibit their activation. The bovine RSV (bRSV) N protein can also cooperate with P protein to promote the formation of IBs-like structures to capture the p65 subunit of NF-κB, which further prevents its translocation to the nucleus. On the one hand, the soluble G protein blocks the TLR3/4-mediated IFN-β production. On the other hand, it also impedes the ISG15 expression. The G protein and F protein induce both SOCS1 and SOCS3, which subsequently interferes with the JAK–STAT pathway to block the IFN-I response. Abbreviation: RSV, respiratory syncytial virus; TLRs, toll-like receptors; RIG-I, retinoic acid-inducible gene I; MDA5, melanoma differentiation associated gene 5; NOD2, nucleotide-binding oligomerization domain 2; NLRP3, the NOD, leucine-rich repeat (LRR)-containing protein 3; NS1/2, non-structural (NS) protein 1 or 2; MAVS, mitochondrial antiviral-signaling protein; TRIM25, tripartite motif-containing protein 25; TRAF3/6, tumor necrosis factor (TNF) receptor-associated factor (TRAF) adapter protein 3 or 6; NF-κB, nuclear factor kappa-B; IκB, inhibitor of NF-κB; IKKε, inhibitor of IκB kinase ε; IRF3, interferon regulatory factor 3; JAK, Janus kinase; STAT, signal transducer and activation of transcription; OASL, 2′-5′-Oligoadenylate synthetases-like protein; IFNAR, IFN-α receptors; SOCS1/3, suppressor of cytokine signaling protein 1 or 3; N; nucleoprotein; P, phosphoprotein; G, glycoprotein; IBs, inclusion bodies; IFN-α/β, interferon α or β; ISG15, IFN-stimulated gene 15; CBP, cAMP (cyclic adenosine monophosphate) response element-binding protein (CREB)-binding protein.

proteins; the other group is composed of TLR3, TLR7, TLR8, and TLR9, which are expressed in endosomes and recognize microbial nucleic acids.

TLRs are constitutively expressed on epithelial cells lining the skin and the respiratory, endothelial cells, and immune cells. The activation of TLRs signaling pathways leads to antiviral cytokines that support viral clearance. Several TLRs have been reported to be involved in RSV recognition. For example, TLR2, TLR3, and TLR4 on epithelial cells have been implicated in inducing cytokines and chemokines upon RSV infection (Rudd et al., 2005; Murawski et al., 2009). Leukocytes expressed TLR2, TLR3, TLR4, TLR6, and TLR7 can interact with RSV and promote immune responses following infection. Alveolar macrophages are the primary source of IFN-I in RSV-infected mice during the early periods of infection (Goritzka et al., 2015), but the IFN-I production by macrophages and dendritic cells (DCs) from wild-type (WT) and TLR1, -2, -4, -6, and-7 knock-out (KO) mice is very similar following RSV infection, indicating that TLRs

are essential for IFN-I production in this. While in another study, mice plasmacytoid dendritic cells (pDCs) were reported to induce IFN-I production through TLR7-MyD88 signaling pathway, but not the RLR-MAVS (mitochondrial antiviral-signaling protein) pathway *in vivo* (Kim et al., 2019). TLR2, which is expressed on immune cells and tissues, generally forms heterodimers with TLR1 or TLR6 to activate innate immunity. Genetic analysis of TLR-KO BALB/c mice demonstrated that TLR2/6 signaling, but not TLR2/1 signaling, is involved in early cytokine and chemokine production in response to RSV, while the induction of IFN-I was independent on TLR2 signaling (Murawski et al., 2009). TLR3 can detect double-stranded RNA (dsRNA) during viral infection. It is reported that TLR3 also contributes to cytokine production in human lung cells infected with RSV, independent of the IFN-I signaling (Rudd et al., 2005). On airway epithelial cells, the TLR4/CD14 complex is the main extracellular receptor recognizing RSV through interacting with viral F protein to activate the nuclear factor kappa-B (NF-κB)-mediated cytokine response, including the secretion of IL-6, IL-8, and IL-10 (Kurt-Jones et al., 2000; Haynes et al., 2001; Haeberle et al., 2002). Similarly, in murine peritoneal macrophages, F protein was also reported to induce IL-6 secretion dependent on the TLR4/CD4 signaling (Haeberle et al., 2002). In addition, RSV infection also upregulates TLR4 expression on airway epithelial cells in mice and peripheral blood monocytes and upper airways from infants with RSV bronchiolitis (Gagro et al., 2004). However, some other studies did not find a role for purified F protein in stimulating TLR4-dependent activation of NF-κB (Marr and Turvey, 2012). Therefore, the role of TLR4 in response to RSV infection is currently debated.

## RSV Infection Triggers the RLRs Pathway

The RLRs family comprises RIG-I and MDA5, widely expressed in most cell types, such as fibroblasts, epithelial cells, macrophages, and DCs. They are cytosolic RNA helicases/ATPases that possess two N-terminal caspase activation and recruitment (CARD) domains, a central DExD/H-box helicase domain and a C-terminal RNA-binding domain (CTD; Rehwinkel and Gack, 2020). They can recognize cytosolic pathogenic-derived ssRNA and short dsRNA to activate the downstream signaling pathway by the interaction between the CARD domain and the adaptor protein MAVS, which subsequently leads to the recruitment of members of the TNF (tumor necrosis factor) receptor-associated factor (TRAF) adapter proteins, mainly including TRAF3 and TRAF6 to promote the activation of interferon regulatory factor 3 or 7 (IRF3/7) and NF-κB, respectively (Seth et al., 2005). These activated transcription factors then translocate from the cytoplasm into the nucleus, ultimately inducing the production of IFN-I and the inflammatory genes. RIG-I senses 5′-triphosphate blunted ends in the presence of short ss/dsRNA (Cui et al., 2008; Jiang et al., 2011), while MDA5 predominantly recognizes long dsRNA without sequence specificity (Wu et al., 2013).

Sasai and colleagues first reported the involvement of RLRs in RSV infection in 2006 (Sasai et al., 2006). Their study demonstrated that RIG-I is essential for IFN-β induction in HeLa cells, dependent on RSV replication. RIG-I's critical role in recognizing RSV was also shown in airway epithelial cells (Liu et al., 2007). It was demonstrated that the expression of RIG-I and MDA5 were upregulated, but only RIG-I could specifically bind to RSV RNA (RSV A2 strain) in human bronchiolar carcinoma cell line A549, which was confirmed by immunoprecipitation assay. Besides, the knockdown of RIG-I by siRNA approach could significantly block the activation of NF-κB and IRF3 and the production of IFN-β (Liu et al., 2007). Moreover, data from another literature also indicated that both IFN-α/β and IFN-λ (IFN-III) were induced by RSV infection in A549 cells in RIG-I-dependent pathway (Okabayashi et al., 2011). In RSV-infected hTERT-NECs, which is one type of immortalized human nasal epithelial cells (NECs) through transfection with the human telomerase reverse transcriptase gene, suppression of RIG-I expression but not MDA5 by short interfering RNA (siRNA) technology significantly reduced IFN-λ1 production, indicating that RIG-I but not MDA5 contributed to the main role in inducing the expression of IFN-III. However, studies from another group showed that both RIG-I and MDA5 could co-localize with RSV genomic RNA (RSV A2 strain) in the small inclusion bodies (IBs) in A549 cells by immunofluorescence assay (Lifland et al., 2012). A clinical study observed a significant positive correlation between RSV viral load and RIG-1 mRNA levels in these RSV-infected infants with bronchiolitis (Scagnolari et al., 2009). Also, in human primary PBMCs isolated from healthy volunteers, the expression of RIG-I was upregulated following RSV infection (Vissers et al., 2012). These studies demonstrate that RIG-I seems to been particularly important for host to defense against RSV infection. Similar results were also obtained in an *in vivo* infectious model (Demoor et al., 2012). The MAVS (the adaptor protein for RIG-I and MDA5) deficient mice produced reduced amount of IFN-I infection, as well as other pro-inflammatory cytokines, including interleukin-6 (IL-6), tumor necrosis factor-α (TNF-α), monocyte chemoattractant protein-1 (MCP-1), and IL-1β in response to RSV (Demoor et al., 2012).

## RSV Infection Triggers the NLRs Pathway

The NLR family of PRRs is intracellular cytoplasmic sensors that play a crucial role in the innate immune response against invading pathogens. There are 22 identified NLRs in humans and at least 33 NLRs in mice. Structurally, they share a central NOD (nucleotide-binding and oligomerization domain) domain, N-terminal effector domain, and C-terminal leucine-rich repeats (LRRs). Based on the different functions of the N-terminal effector domain, NLRs can be divided into four subfamilies: the acidic transactivation domain (NLRA), the baculoviral inhibitory repeat-like domain (NLRB), the caspase activation and recruitment domain (NLRC), and the pyrin domain (NLRP). They are widely involved in various intracellular activities, including inflammasome assembly, signaling transduction, transcription activation, and autophagy.

NOD2, a member of the NLRC subfamily, was recently demonstrated to be involved in recognizing ssRNA virus by activating the IFN-I-mediated innate antiviral responses. It is reported that RSV infection could rapidly increase NOD2 expression (within 2h) after RSV and plays a critical role in the induction of IFN-β in 293 cells and PBMCs in a MAVS-dependent manner (Sabbah et al., 2009; Vissers et al., 2012). Mechanically, NOD2 could translocate to the mitochondria and interact with MAVS to activate IRF3 and NF-κB, resulting in the induction of IFN-I

(Sabbah et al., 2009). Similar results were obtained from the mice model *in vivo*. It has been shown that, compared with the WT mice, the susceptibility of RSV and lung disease were significantly enhanced in NOD2-deficient mice. Moreover, the activation of IRF3 and production of IFN-I were also reduced in NOD2-deficient mice (Sabbah et al., 2009). These data indicate that NOD2 functions as an important PRR for RSV recognition and plays a critical role in the host's innate immune defense against RSV infection.

NLRP3 [the nucleotide-binding oligomerization domain (NOD), leucine-rich repeat (LRR)-containing protein 3], another member of the NLR family, plays a crucial role in the innate immune response and inflammation by recruiting proCASP1 to the inflammasome, which ultimately leads to the proteolytic activation of the pro-inflammatory cytokines interleukin-1β (IL-1β) and interleukin-18. Recent evidence indicates that NLRP3 is also reported to be activated following RSV infection in mouse bone marrow-derived macrophages. The TLR2/Myd88 signaling pathway was demonstrated to be essential for the activation of NF-κB and subsequent expression of pro-IL-1β and NLRP3 caused by RSV infection (Segovia et al., 2012). Moreover, evidence from another research demonstrates that RSV appears to stimulate the inflammasome activation through both the TLR4 signaling and SH protein on its own. Upon the infection of RSV (strain A2) in primary human lung epithelial cells, the knocking down of TLR4, but not TLR3, TLR7, TLR8, or RIG-I results in a reduced expression of pro-IL-1β and IL-1β. In this process, TLR4 may act as a sensor for RSV recognition to trigger inflammasome activation during virus invasion.

Further study demonstrated that the RSV mutants lacking the viroporin SH could not trigger inflammasome activation. It was observed that during RSV infection, the SH protein accumulated in lipid rafts of the Golgi apparatus, which further enhances membrane permeability and promotes the entry of small molecules into cells; meanwhile, interestingly, NLRP3 was also shown to accumulate in the Golgi apparatus. It was inferred that the functions of SH viroporin may facilitate the trafficking of NLRP3 from the cytoplasm to the Golgi, which is essential for the inflammasome activation (Triantafilou et al., 2013).

However, the NLRP3-mediated excessive inflammation seemed to be responsible for lung tissue damage (Shen et al., 2018). Therefore, NLRP3 was suggested as a potential therapeutic target to protect lung disease from RSV infection.

## EVASION OF INNATE IMMUNE RESPONSE BY RSV

The interaction between host innate immunity and RSV is a long-term tug of war. On the one hand, the RSV infection evokes the production of IFN-I and numerous downstream ISGs to limit viral replication; on the other hand, RSV has evolved specialized strategies to modulate and suppress the IFN-I response to gain a window of opportunity for efficient virus replication and setting-up of the infection. Human epithelial cells, including A549, Hep-2, and HEK293 infected with either RSV A2 strain or clinical isolates, failed to produce IFN-α, suggesting that RSV could block the ongoing IFN-I signaling. However, understanding the innate immune evasion mechanisms employed by RSV is helpful for the design of target therapy. This review will focus on the implicated strategies for RSV to antagonize the host antiviral immune response.

### RSV Impedes the RLRs Signaling Pathway

Numerous groups have highlighted the role of NS proteins in suppressing innate immune signaling. It was indicated that the infection of recombinant human RSV with single or double deletions of NS genes (ΔNS1, ΔNS2, and ΔNS1/2) in A549 cells produce higher levels of IFN-I compared to WT virus (Spann et al., 2004). Moreover, in human macrophage and epithelial cells, the infection of RSV virus with both NS1 and NS2 genes deficient evokes higher IFN-I production than that of single deletions, suggesting that RSV exhibited a cooperative interaction between NS1 and NS2 to block the IFN-I singling pathway (Spann et al., 2004). Similar results were also observed in bovine RSV NS1 and NS2 proteins, which show cooperation in antagonizing IFN-I-mediated antiviral activity (Schlender et al., 2000). NS proteins exhibit multiple mechanisms to target different signals involved in the PRR signaling pathway to evade the IFN-I-mediated antiviral immune responses.

The importance of RIG-I in RSV recognition has been discussed above. However, NS1 and NS2 could interfere with the RIG-I-mediated antiviral signaling in various ways. In 293T cells, the direct interaction between NS2 and the CARD domains on RIG-I is confirmed by a coimmunoprecipitation (Co-IP) assay. This interaction prevents the signal transduction from RIG-I to downstream adaptor protein MAVS, which subsequently suppresses further induction of IFN-I and ISGs (Ling et al., 2009). Recently, a combined biochemical and structural analysis of NS2 protein confirmed again that NS2 could bind the CARD domain of both RIG-I and MDA5. It was revealed that the N terminus of NS2 is essential for binding an inactive form of RIG-I and MDA5, which subsequently prevented the transduction of downstream signaling and IFN-I production (Pei et al., 2021). During RSV infection in A549 cells, NS1 was visualized to be co-localized with MAVS in the mitochondria, and the direct interaction was further determined by Co-IP experiments (Boyapalle et al., 2012). Similarly, the interaction between NS1 and MAVS prevents signal transduction from RIG-I to MAVS without significantly affecting either RIG-I or MAVS expression. The tripartite motif-containing protein 25 (TRIM25) is an important E3-ubiquitin ligase responsible for delivering the K63-linked polyubiquitin chain to the CARDs domain in RIG-I to induce its oligomerization and activation. Evidence shows that the ectopic expression of NS1 could interact with TRIM25 and then interfere with the RIG-I ubiquitination to block the IFN-I signaling pathway (Ban et al., 2018). TRAF3 is essential for activating IRF3 and IRF7, which serves as the integration point of signals from both the RIG-I- and TLR-mediated IFN-I pathways. It is reported that the ectopic expression of either NS1 or NS2 reduces the protein level of TRAF3 in A549 cells, while only infection with NS1-deficient RSV, but not NS2-deficient virus increases the levels of TRAF3

compared to WT virus infection. Besides, the ectopic expression of NS1 but not NS2 decreases the levels of IKKε (inhibitor of IκB kinase ε), which is a Ser/Thr kinase of the IKK downstream of TRAF3. The further structure–activity studies demonstrated that the C-terminal 20 residues of NS1 were required to decrease IKKε (Swedan et al., 2009). These results suggest that NS1 can block the IFN-I signaling by reducing the presence of adaptors downstream RLRs. Moreover, NS1 and NS2 can also cooperatively block translocation of IRF3 to the nucleus, as shown by the increased nuclear presence in either NS1-deficient or NS2-deficient RSV-infected cells, which occurs by preventing the upstream phosphorylation of IRF3, or binding and sequestering IRF3 to prevent downstream association (Spann et al., 2005). Evidence from another study reveals a novel mechanism utilized by NS1 to impede the IFN-I signaling pathway. It is reported that NS1 does not affect RSV-induced phosphorylation and nuclear translocation of IRF3 but prevents its association to transcriptional coactivator CBP [cAMP response element-binding protein (CREB)-binding protein] and subsequently reduced binding of IRF3 to the IFN-β promoter in A549 cells (Ren et al., 2011).

RSV strains deficient in NS1 and NS2 expression show incomplete suppression of IFN-I production in human macrophage and epithelial cells, indicating that some other immunomodulatory proteins may help to the evasion of the early antiviral response. The N protein is essential for RSV assembly and replication as part of the nucleocapsid that functions as a template for replication and transcription by the viral polymerase complex. It is reported that the RSV N protein could co-localize with MDA5 in viral inclusion bodies (IBs) and antagonize the IFN-I response by interacting with MAVS (Lifland et al., 2012). Moreover, a recent study suggested that bovine RSV (bRSV) infection could also promote the formation of IBs-like structures induced by both viral N and P proteins. Interestingly, these organelles (IBs-like structures) can capture the p65 subunit of NF-κB, which further prevents its translocation to the nucleus (Jobe et al., 2020). It is a novel mechanism for viral antagonism of the IFN-I signaling pathway.

## RSV Subverts the TLRs Signaling Pathway

The glycoprotein protein (G) of RSV is responsible for the attachment of the virus particle to the target cell. It is expressed as membrane-anchored (mG) and secreted (sG) forms, containing a central fractalkine-like CX3C motif. It was demonstrated that the G protein was implicated in altering cytokine and chemokine expression in pulmonary leukocytes (Tripp, 2004). In the mouse infection model, the RSV F protein was reported to be an effector to trigger the production of IFN-β *via* interaction with TLR4 (Kurt-Jones et al., 2000; Haynes et al., 2001); while in monocyte-derived dendritic cells (mDCs), the soluble G protein was demonstrated to inhibit TLR3/4-mediated IFN-β production (Shingai et al., 2008). But the mechanism was not revealed in this study. The suppressor of cytokine signaling (SOCS) proteins family, especially SOCS1 and SOCS3 have elicited interest as negative regulators of IFN-I and pro-inflammatory cytokine signaling (Yoshimura et al., 2007). In macrophages and dendritic cells, both SOCS1 and SOCS3 were demonstrated to play an important regulatory role modulating TLR signaling (Takagi et al., 2004). Data from an RSV mutant virus lacking the G gene showed that the G protein has an important role in modulating SOCS1 and SOCS3, which subsequently downregulated the expression of IFN-I through the TLR signaling pathway (Oshansky et al., 2009).

## RSV Interferes With the JAK/STAT Signaling Pathway and Downstream ISGs

The antiviral activities of IFN-I are initiated by the engagement of IFNα/β to their cognate receptors IFNAR1/2 (IFNα receptors 1 and 2), which subsequently activate the downstream signaling cascades, namely JAK (Janus kinase)/STAT (signal transducer, and activation of transcription), resulting in the induction of various IFN-stimulated genes (ISGs). At present, more than 300 ISG proteins are identified to participate in the host's antiviral immune responses. Multiple reports suggest that the NS proteins, singly or together, also affect the JAK/STAT signaling to block the production of ISGs, among which the STAT2 is shown to be the major target to be degraded caused by the NS proteins. An earlier study suggested RSV infection with a high inoculum at a multiplicity of infection (MOI) of 10 or ectopic expression of NS1 and NS2 in human epithelial cells A549 significantly decreased the protein level of STAT2 and fully inhibited IFN-β responsiveness (Lo et al., 2005). In contrast, a study from another group demonstrated that NS2 alone is sufficient and necessary for RSV to promote STAT2 degradation. During RSV infection in human tracheobronchial epithelial (hTBE) cells, the expression of NS2 under conditions could markedly decrease the protein levels of STAT2. Nonetheless, RSV infection with NS2 deletion did not affect STAT2 expression (Ramaswamy et al., 2006).

Moreover, when hTBE cells were pretreated with non-specific proteasome inhibitor MG-132, NS2 could not alter the expression of STAT2, indicating that NS2 mediated the degradation of STAT2 through a proteasome-dependent manner (Ramaswamy et al., 2006). But the complicated mechanism utilized by NS2 was still unclear in this research. Later, studies from the same group revealed that the C-terminal 10 residues were required for NS2 to decrease STAT2 (Swedan et al., 2009). Besides, the C-terminal DLNP tetrapeptide was also reported to be critical for NS2 to mediate the degradation of STAT2 *via* direct binding to the host microtubule-associated protein 1B (MAP1B) in the mitochondria. It was inferred that the bound of NS2 and MAP1B complex could serve as docking for mitochondrial receptors or recruit other host proteins to promote the destruction of STAT2 (Swedan et al., 2011). In addition to negatively regulating the TLRs signaling pathway to suppress IFN-I production, the SOCS proteins could also block the activation of the JAK/STAT signaling pathway *via* a negative feedback regulatory mechanism, of which SOCS1 and SOCS3 appear to be the most effective regulators (O'Shea et al., 2002; Akhtar and Benveniste, 2011). Mechanically, SOCS binds to JAK and inhibits the activity of its catalytic kinase reaction to block the JAK/STAT signal transduction pathway to inhibit STAT phosphorylation. It has been demonstrated that the NS1 protein

can form a functional E3 ligase like SOCS, in which a putative elongin C and cullin 2 binding consensus sequences were identified by bioinformatic analysis (Elliott et al., 2007). The *in vitro* protein pulldown experiments also suggested that NS1 could act as a scaffold on which a multisubunit E3 ligase complex can be formed, which was essential for NS1/2-induced STAT2 degradation *via* a ubiquitin-dependent proteasomal mechanism (Elliott et al., 2007). Afterward, the NS1 was shown to induce the expression of SOCS1 in a RIG-I and TLR3-independent pathway, which further inhibit the phosphorylation of STAT2. It is a novel mechanism for NS1 to subvert the JAK/STAT pathway through an indirect way (Xu et al., 2014).

In addition, NS1 protein was also proved to inhibit the IFNAR synthesis through a viral replication-dependent manner. MicroRNAs (miRNAs) are small non-protein-coding RNA molecules of approximately 20 ~ 22 nucleotides encoded in the genome that bind to mRNA, leading to mRNA degradation or translational suppression. Viral infection, especially with RNA viruses, can usually cause the change of some cellular microRNA expression, potentially to the benefit of the virus. Data from the dual-luciferase reporter assay system demonstrated that during RSV replication in A549 cells, NS1 could upregulate the expression of miR-29a, which in turn targeted the mRNA of the *IFNAR* gene for degradation, resulting in the downregulation of protein translation of IFNAR. It is a novel mechanism for NS1 to subvert the JAK/STAT pathway through inducing the expression of miRNA as a negative regulator of IFNAR synthesis (Zhang et al., 2016).

The 2′-5′-oligoadenylate synthetases (OAS) are a family of ISGs characterized by their ability to synthesize 2′-5′-oligoadenylate and further induce RNA degradation. They consist of four OAS isoforms: OAS1, OAS2, OAS3, and OASL (2′-5′-oligoadenylate synthetases-like protein; Zhu et al., 2015). It was reported that OASL could inhibit viral replication during RSV infection. However, the NS1 protein seemed to possess the capacity to promote the degradation of OASL through a proteasome-dependent manner (Dhar et al., 2015). Moreover, the G protein also impedes the ISG15 expression in mouse lung epithelial (MLE)-15 cells, a type II pneumocyte cell line representing the distal bronchiolar and alveolar epithelium. ISG15 is an important ISG protein released from cells to mediate extracellular cytokine-like activities and exhibits a close link to IFN-I-mediated antiviral signal transduction. It has been shown that in MLE-15 cells, the infection of RSV with G gene deletion (RSVΔG) could stimulate significantly higher levels of ISG15 compared to that of the WT virus, indicating that the G protein plays a critical role in modifying the expression of ISG15 (Moore et al., 2008). Besides, the G protein could also mimic CX3C chemokine fractalkine (also named CX3CL1) due to the similar structure (Tripp et al., 2001). The bound of G protein to the CX3C receptor remarkably impairs the innate immune response to RSV infection. While the deletion of the CX3CL1 motif in G protein results in increased levels of IFN-I/III, indicating that the interruption of CX3C-CX3CR1 interaction by G protein greatly benefits RSV to evade IFN-I/III-mediated innate immune response (Chirkova et al., 2013).

## CONCLUDING REMARKS

It is more than 60 years since human RSV was first discovered in 1957 (Chanock et al., 1957), and RSV has become one of the most important pathogens causing respiratory disease worldwide, especially in young children. Globally, RSV causes approximately 60,000 deaths of hospitalized children younger than 5 years old each year (Shi et al., 2017). There is still no approved means for the effective prevention and treatment of RSV infection. Researchers have devoted themselves to studying the interaction between RSV and the host innate immune system in the past decades. The innate immune response plays an important role in defense against RSV infection. The elucidation of the recognition mechanism and viral innate immune evasion strategies caused by RSV contributes to designing novel drugs targeting potential regulatory molecules in the host innate immune pathway. Although the viral genome size is quite small and only encodes 11 viral proteins, RSV has evolved effective strategies to manipulate the host's innate immune responses. In particular, the non-structural proteins NS1 and NS2 were suggested to degrade or sequester multiple signaling proteins that affect both IFN induction and IFN effector functions. The involved evasion mechanisms employed by NS1/2 are diverse, among which the proteasome-mediated direct degradation of target signals is most widely studied. In addition, NS proteins also indirectly affect the IFN-I response, such as inducing the expression of SOCSs and miRNAs to regulate the signaling pathway negatively in STATs and IFNARs levels, respectively. Intriguingly, the evasion strategies utilized by RSV are mainly concentrated on interfering with the pivotal signal molecules implicated in the RLRs pathway, such as receptors RIG-I and MDA5, adaptor protein MAVS, and transcription factors IRF3 and NF-κB.

However, the current knowledge regarding the NLRs, especially whether and how RSV blocks the NLRP3-mediated innate immune pathway, is still unknown. The present studies that characterize the role of NLRP3-mediated inflammasome are supposed to contribute mainly to RSV immunopathology and lung inflammation (Malinczak et al., 2021). NLRP3 inflammasome is suggested as a potential therapeutic target to attenuate severe RSV disease and limit childhood asthma development. In addition, the NF-κB induced pro-inflammatory cytokines expression is also considered to promote RSV-associated acute bronchiolitis (Zhang et al., 2021). A new understanding of the critical role of NLRP3 and NF-κB in triggering the antiviral innate immune response and aggravating the severity of the respiratory diseases during RSV infection is challenged. Therefore, additional studies on the interaction between RSV and host defense immune signaling are encouraged. These studies may provide novel antiviral therapeutic strategies to target viral components or cellular immune signals.

## AUTHOR CONTRIBUTIONS

HZ, YO, and HL contributed ideas for the review and wrote the manuscript. KL and SH constructed the figures. HZ and YH edited and revised the manuscript. All authors contributed to the article and approved the submitted version.

## FUNDING

This work was supported by the Natural Science Foundation of Jiangxi Province (20202BAB216002), the Key Research Project of Gannan Medical University (ZD201906), the National Natural Science Foundation of China (82003043), and the training plan for academic and technical leaders of major disciplines in Jiangxi Province (20212BCJL23049).

## REFERENCES

Akhtar, L. N., and Benveniste, E. N. (2011). Viral exploitation of host SOCS protein functions. *J. Virol.* 85, 1912–1921. doi: 10.1128/JVI.01857-10

Ban, J., Lee, N. R., Lee, N. J., Lee, J. K., Quan, F. S., and Inn, K. S. (2018). Human respiratory syncytial virus NS 1 targets TRIM25 to suppress RIG-I Ubiquitination and subsequent RIG-I-mediated antiviral signaling. *Viruses* 10:716. doi: 10.3390/v10120716

Boyapalle, S., Wong, T., Garay, J., Teng, M., San Juan-Vergara, H., Mohapatra, S., et al. (2012). Respiratory syncytial virus NS1 protein colocalizes with mitochondrial antiviral signaling protein MAVS following infection. *PLoS One* 7:e29386. doi: 10.1371/journal.pone.0029386

Chanock, R., Roizman, B., and Myers, R. (1957). Recovery from infants with respiratory illness of a virus related to chimpanzee coryza agent (CCA). I. Isolation, properties and characterization. *Am. J. Hyg.* 66, 281–290. doi: 10.1093/oxfordjournals.aje.a119901

Chirkova, T., Boyoglu-Barnum, S., Gaston, K. A., Malik, F. M., Trau, S. P., Oomens, A. G., et al. (2013). Respiratory syncytial virus G protein CX3C motif impairs human airway epithelial and immune cell responses. *J. Virol.* 87, 13466–13479. doi: 10.1128/JVI.01741-13

Cui, S., Eisenacher, K., Kirchhofer, A., Brzozka, K., Lammens, A., Lammens, K., et al. (2008). The C-terminal regulatory domain is the RNA 5′-triphosphate sensor of RIG-I. *Mol. Cell* 29, 169–179. doi: 10.1016/j.molcel.2007.10.032

Demoor, T., Petersen, B. C., Morris, S., Mukherjee, S., Ptaschinski, C., De Almeida Nagata, D. E., et al. (2012). IPS-1 signaling has a nonredundant role in mediating antiviral responses and the clearance of respiratory syncytial virus. *J. Immunol.* 189, 5942–5953. doi: 10.4049/jimmunol.1201763

Dhar, J., Cuevas, R. A., Goswami, R., Zhu, J., Sarkar, S. N., and Barik, S. (2015). 2′-5′-Oligoadenylate synthetase-like protein inhibits respiratory syncytial virus replication and is targeted by the viral nonstructural protein 1. *J. Virol.* 89, 10115–10119. doi: 10.1128/JVI.01076-15

Elliott, J., Lynch, O. T., Suessmuth, Y., Qian, P., Boyd, C. R., Burrows, J. F., et al. (2007). Respiratory syncytial virus NS1 protein degrades STAT2 by using the Elongin-Cullin E3 ligase. *J. Virol.* 81, 3428–3436. doi: 10.1128/JVI.02303-06

Gagro, A., Tominac, M., Krsulovic-Hresic, V., Bace, A., Matic, M., Drazenovic, V., et al. (2004). Increased toll-like receptor 4 expression in infants with respiratory syncytial virus bronchiolitis. *Clin. Exp. Immunol.* 135, 267–272. doi: 10.1111/j.1365-2249.2004.02364.x

Goritzka, M., Makris, S., Kausar, F., Durant, L. R., Pereira, C., Kumagai, Y., et al. (2015). Alveolar macrophage-derived type I interferons orchestrate innate immunity to RSV through recruitment of antiviral monocytes. *J. Exp. Med.* 212, 699–714. doi: 10.1084/jem.20140825

Haeberle, H. A., Takizawa, R., Casola, A., Brasier, A. R., Dieterich, H. J., Van Rooijen, N., et al. (2002). Respiratory syncytial virus-induced activation of nuclear factor-kappaB in the lung involves alveolar macrophages and toll-like receptor 4-dependent pathways. *J. Infect. Dis.* 186, 1199–1206. doi: 10.1086/344644

Haynes, L. M., Moore, D. D., Kurt-Jones, E. A., Finberg, R. W., Anderson, L. J., and Tripp, R. A. (2001). Involvement of toll-like receptor 4 in innate immunity to respiratory syncytial virus. *J. Virol.* 75, 10730–10737. doi: 10.1128/JVI.75.22.10730-10737.2001

Jiang, F., Ramanathan, A., Miller, M. T., Tang, G. Q., Gale, M. Jr., Patel, S. S., et al. (2011). Structural basis of RNA recognition and activation by innate immune receptor RIG-I. *Nature* 479, 423–427. doi: 10.1038/nature10537

Jobe, F., Simpson, J., Hawes, P., Guzman, E., and Bailey, D. (2020). Respiratory syncytial virus sequesters NF-kappaB subunit p65 to cytoplasmic inclusion bodies to inhibit innate immune signaling. *J. Virol.* 94, e01380–e01320. doi: 10.1128/JVI.01380-20

Kim, T. H., Oh, D. S., Jung, H. E., Chang, J., and Lee, H. K. (2019). Plasmacytoid dendritic cells contribute to the production of IFN-beta via TLR7-MyD88-dependent pathway and CTL priming during respiratory syncytial virus infection. *Viruses* 11:730. doi: 10.3390/v11080730

Kurt-Jones, E. A., Popova, L., Kwinn, L., Haynes, L. M., Jones, L. P., Tripp, R. A., et al. (2000). Pattern recognition receptors TLR4 and CD14 mediate response to respiratory syncytial virus. *Nat. Immunol.* 1, 398–401. doi: 10.1038/80833

Lifland, A. W., Jung, J., Alonas, E., Zurla, C., Crowe, J. E. Jr., and Santangelo, P. J. (2012). Human respiratory syncytial virus nucleoprotein and inclusion bodies antagonize the innate immune response mediated by MDA5 and MAVS. *J. Virol.* 86, 8245–8258. doi: 10.1128/JVI.00215-12

Ling, Z., Tran, K. C., and Teng, M. N. (2009). Human respiratory syncytial virus nonstructural protein NS2 antagonizes the activation of beta interferon transcription by interacting with RIG-I. *J. Virol.* 83, 3734–3742. doi: 10.1128/JVI.02434-08

Liu, P., Jamaluddin, M., Li, K., Garofalo, R. P., Casola, A., and Brasier, A. R. (2007). Retinoic acid-inducible gene I mediates early antiviral response and toll-like receptor 3 expression in respiratory syncytial virus-infected airway epithelial cells. *J. Virol.* 81, 1401–1411. doi: 10.1128/JVI.01740-06

Lo, M. S., Brazas, R. M., and Holtzman, M. J. (2005). Respiratory syncytial virus nonstructural proteins NS1 and NS2 mediate inhibition of Stat2 expression and alpha/beta interferon responsiveness. *J. Virol.* 79, 9315–9319. doi: 10.1128/JVI.79.14.9315-9319.2005

Malinczak, C. A., Schuler, C. F., Duran, A. J., Rasky, A. J., Mire, M. M., Nunez, G., et al. (2021). NLRP3-Inflammasome inhibition during respiratory virus infection abrogates lung immunopathology and long-term airway disease development. *Viruses* 13:692. doi: 10.3390/v13040692

Marr, N., and Turvey, S. E. (2012). Role of human TLR4 in respiratory syncytial virus-induced NF-kappaB activation, viral entry and replication. *Innate Immun.* 18, 856–865. doi: 10.1177/1753425912444479

Moore, E. C., Barber, J., and Tripp, R. A. (2008). Respiratory syncytial virus (RSV) attachment and nonstructural proteins modify the type I interferon response associated with suppressor of cytokine signaling (SOCS) proteins and IFN-stimulated gene-15 (ISG15). *Virol. J.* 5:116. doi: 10.1186/1743-422X-5-116

Murawski, M. R., Bowen, G. N., Cerny, A. M., Anderson, L. J., Haynes, L. M., Tripp, R. A., et al. (2009). Respiratory syncytial virus activates innate immunity through toll-like receptor 2. *J. Virol.* 83, 1492–1500. doi: 10.1128/JVI.00671-08

Okabayashi, T., Kojima, T., Masaki, T., Yokota, S., Imaizumi, T., Tsutsumi, H., et al. (2011). Type-III interferon, not type-I, is the predominant interferon induced by respiratory viruses in nasal epithelial cells. *Virus Res.* 160, 360–366. doi: 10.1016/j.virusres.2011.07.011

Oshansky, C. M., Krunkosky, T. M., Barber, J., Jones, L. P., and Tripp, R. A. (2009). Respiratory syncytial virus proteins modulate suppressors of cytokine signaling 1 and 3 and the type I interferon response to infection by a toll-like receptor pathway. *Viral Immunol.* 22, 147–161. doi: 10.1089/vim.2008.0098

O'Shea, J. J., Gadina, M., and Schreiber, R. D. (2002). Cytokine signaling in 2002: new surprises in the Jak/Stat pathway. *Cell* 109, S121–S131. doi: 10.1016/s0092-8674(02)00701-8

Pei, J., Wagner, N. D., Zou, A. J., Chatterjee, S., Borek, D., Cole, A. R., et al. (2021). Structural basis for IFN antagonism by human respiratory syncytial virus nonstructural protein 2. *Proc. Natl. Acad. Sci. U. S. A.* 118:e2020587118. doi: 10.1073/pnas.2020587118

Ramaswamy, M., Shi, L., Varga, S. M., Barik, S., Behlke, M. A., and Look, D. C. (2006). Respiratory syncytial virus nonstructural protein 2 specifically inhibits type I interferon signal transduction. *Virology* 344, 328–339. doi: 10.1016/j.virol.2005.09.009

Rehwinkel, J., and Gack, M. U. (2020). RIG-I-like receptors: their regulation and roles in RNA sensing. *Nat. Rev. Immunol.* 20, 537–551. doi: 10.1038/s41577-020-0288-3

Ren, J., Liu, T., Pang, L., Li, K., Garofalo, R. P., Casola, A., et al. (2011). A novel mechanism for the inhibition of interferon regulatory factor-3-dependent gene expression by human respiratory syncytial virus NS1 protein. *J. Gen. Virol.* 92, 2153–2159. doi: 10.1099/vir.0.032987-0

Rudd, B. D., Burstein, E., Duckett, C. S., Li, X., and Lukacs, N. W. (2005). Differential role for TLR3 in respiratory syncytial virus-induced chemokine expression. *J. Virol.* 79, 3350–3357. doi: 10.1128/JVI.79.6.3350-3357.2005

Sabbah, A., Chang, T. H., Harnack, R., Frohlich, V., Tominaga, K., Dube, P. H., et al. (2009). Activation of innate immune antiviral responses by Nod2. *Nat. Immunol.* 10, 1073–1080. doi: 10.1038/ni.1782

Sasai, M., Shingai, M., Funami, K., Yoneyama, M., Fujita, T., Matsumoto, M., et al. (2006). NAK-associated protein 1 participates in both the TLR3 and the cytoplasmic pathways in type I IFN induction. *J. Immunol.* 177, 8676–8683. doi: 10.4049/jimmunol.177.12.8676

Scagnolari, C., Midulla, F., Pierangeli, A., Moretti, C., Bonci, E., Berardi, R., et al. (2009). Gene expression of nucleic acid-sensing pattern recognition receptors in children hospitalized for respiratory syncytial virus-associated acute bronchiolitis. *Clin. Vaccine Immunol.* 16, 816–823. doi: 10.1128/CVI.00445-08

Schlender, J., Bossert, B., Buchholz, U., and Conzelmann, K. K. (2000). Bovine respiratory syncytial virus nonstructural proteins NS1 and NS2 cooperatively antagonize alpha/beta interferon-induced antiviral response. *J. Virol.* 74, 8234–8242. doi: 10.1128/jvi.74.18.8234-8242.2000

Segovia, J., Sabbah, A., Mgbemena, V., Tsai, S. Y., Chang, T. H., Berton, M. T., et al. (2012). TLR2/MyD88/NF-kappaB pathway, reactive oxygen species, potassium efflux activates NLRP3/ASC inflammasome during respiratory syncytial virus infection. *PLoS One* 7:e29695. doi: 10.1371/journal.pone.0029695

Seth, R. B., Sun, L., Ea, C. K., and Chen, Z. J. (2005). Identification and characterization of MAVS, a mitochondrial antiviral signaling protein that activates NF-kappaB and IRF 3. *Cell* 122, 669–682. doi: 10.1016/j.cell.2005.08.012

Shen, C., Zhang, Z., Xie, T., Xu, J., Yan, J., Kang, A., et al. (2018). Jinxin oral liquid inhibits human respiratory syncytial virus-induced excessive inflammation associated with blockade of the NLRP3/ASC/Caspase-1 pathway. *Biomed. Pharmacother.* 103, 1376–1383. doi: 10.1016/j.biopha.2018.04.174

Shi, T., McAllister, D. A., O'Brien, K. L., Simoes, E. A. F., Madhi, S. A., Gessner, B. D., et al. (2017). Global, regional, and national disease burden estimates of acute lower respiratory infections due to respiratory syncytial virus in young children in 2015: a systematic review and modelling study. *Lancet* 390, 946–958. doi: 10.1016/S0140-6736(17)30938-8

Shingai, M., Azuma, M., Ebihara, T., Sasai, M., Funami, K., Ayata, M., et al. (2008). Soluble G protein of respiratory syncytial virus inhibits toll-like receptor 3/4-mediated IFN-beta induction. *Int. Immunol.* 20, 1169–1180. doi: 10.1093/intimm/dxn074

Spann, K. M., Tran, K. C., Chi, B., Rabin, R. L., and Collins, P. L. (2004). Suppression of the induction of alpha, beta, and lambda interferons by the NS1 and NS2 proteins of human respiratory syncytial virus in human epithelial cells and macrophages [corrected]. *J. Virol.* 78, 4363–4369. doi: 10.1128/jvi.78.8.4363-4369.2004

Spann, K. M., Tran, K. C., and Collins, P. L. (2005). Effects of nonstructural proteins NS1 and NS2 of human respiratory syncytial virus on interferon regulatory factor 3, NF-kappaB, and proinflammatory cytokines. *J. Virol.* 79, 5353–5362. doi: 10.1128/JVI.79.9.5353-5362.2005

Swedan, S., Andrews, J., Majumdar, T., Musiyenko, A., and Barik, S. (2011). Multiple functional domains and complexes of the two nonstructural proteins of human respiratory syncytial virus contribute to interferon suppression and cellular location. *J. Virol.* 85, 10090–10100. doi: 10.1128/JVI.00413-11

Swedan, S., Musiyenko, A., and Barik, S. (2009). Respiratory syncytial virus nonstructural proteins decrease levels of multiple members of the cellular interferon pathways. *J. Virol.* 83, 9682–9693. doi: 10.1128/JVI.00715-09

Takagi, H., Sanada, T., Minoda, Y., and Yoshimura, A. (2004). Regulation of cytokine and toll-like receptor signaling by SOCS family genes. *Nihon Rinsho* 62, 2189–2196. doi: 10.1016/j.gene.2012.12.009

Triantafilou, K., Kar, S., Vakakis, E., Kotecha, S., and Triantafilou, M. (2013). Human respiratory syncytial virus viroporin SH: a viral recognition pathway used by the host to signal inflammasome activation. *Thorax* 68, 66–75. doi: 10.1136/thoraxjnl-2012-202182

Tripp, R. A. (2004). Pathogenesis of respiratory syncytial virus infection. *Viral Immunol.* 17, 165–181. doi: 10.1089/0882824041310513

Tripp, R. A., Jones, L. P., Haynes, L. M., Zheng, H., Murphy, P. M., and Anderson, L. J. (2001). CX3C chemokine mimicry by respiratory syncytial virus G glycoprotein. *Nat. Immunol.* 2, 732–738. doi: 10.1038/90675

Vissers, M., Remijn, T., Oosting, M., de Jong, D. J., Diavatopoulos, D. A., Hermans, P. W., et al. (2012). Respiratory syncytial virus infection augments NOD2 signaling in an IFN-beta-dependent manner in human primary cells. *Eur. J. Immunol.* 42, 2727–2735. doi: 10.1002/eji.201242396

Wu, B., Peisley, A., Richards, C., Yao, H., Zeng, X., Lin, C., et al. (2013). Structural basis for dsRNA recognition, filament formation, and antiviral signal activation by MDA5. *Cell* 152, 276–289. doi: 10.1016/j.cell.2012.11.048

Xu, X., Zheng, J., Zheng, K., Hou, Y., Zhao, F., and Zhao, D. (2014). Respiratory syncytial virus NS1 protein degrades STAT2 by inducing SOCS1 expression. *Intervirology* 57, 65–73. doi: 10.1159/000357327

Yoshimura, A., Naka, T., and Kubo, M. (2007). SOCS proteins, cytokine signalling and immune regulation. *Nat. Rev. Immunol.* 7, 454–465. doi: 10.1038/nri2093

Zhang, L., Wan, Y., Ma, L., Xu, K., and Cheng, B. (2021). Inhibition of NF-kappaB/IL-33/ST2 axis ameliorates acute bronchiolitis induced by respiratory syncytial virus. *J. Immunol. Res.* 2021:6625551. doi: 10.1155/2021/6625551

Zhang, Y., Yang, L., Wang, H., Zhang, G., and Sun, X. (2016). Respiratory syncytial virus non-structural protein 1 facilitates virus replication through miR-29a-mediated inhibition of interferon-alpha receptor. *Biochem. Biophys. Res. Commun.* 478, 1436–1441. doi: 10.1016/j.bbrc.2016.08.142

Zhu, J., Ghosh, A., and Sarkar, S. N. (2015). OASL-a new player in controlling antiviral innate immunity. *Curr. Opin. Virol.* 12, 15–19. doi: 10.1016/j.coviro.2015.01.010

**Conflict of Interest:** The authors declare that the research was conducted in the absence of any commercial or financial relationships that could be construed as a potential conflict of interest.

**Publisher's Note:** All claims expressed in this article are solely those of the authors and do not necessarily represent those of their affiliated organizations, or those of the publisher, the editors and the reviewers. Any product that may be evaluated in this article, or claim that may be made by its manufacturer, is not guaranteed or endorsed by the publisher.

*Copyright © 2022 Ouyang, Liao, Hu, Luo, Hu and Zhu. This is an open-access article distributed under the terms of the Creative Commons Attribution License (CC BY). The use, distribution or reproduction in other forums is permitted, provided the original author(s) and the copyright owner(s) are credited and that the original publication in this journal is cited, in accordance with accepted academic practice. No use, distribution or reproduction is permitted which does not comply with these terms.*

frontiers in Microbiology

ORIGINAL RESEARCH
published: 04 March 2022
doi: 10.3389/fmicb.2022.865644

# Heat Shock Protein A6 Is Especially Involved in Enterovirus 71 Infection

*Jiaoyan Jia[1,2†], Ge Liu[1†], Jianfeng Zhong[2], Ran Yan[2], Xun Song[2], Kai Zheng[2], Zhe Ren[3], Zhendan He[1*] and Qinchang Zhu[1,2*]*

[1]College of Pharmacy, Shenzhen Technology University, Shenzhen, China, [2]School of Pharmaceutical Sciences, Shenzhen University, Shenzhen, China, [3]Institute of Biomedicine, College of Life Science and Technology, Jinan University, Guangzhou, China

Hand foot and mouth disease (HFMD) caused by Enterovirus 71 (EV71) infection is still a major infectious disease threatening children's life and health in the absence of effective antiviral drugs due to its high prevalence and neurovirulence. A study of EV71-specific host response might shed some light on the reason behind its unique epidemiologic features and help to find means to conquer EV71 infection. We reported that host heat shock protein A6 (HSPA6) was induced by EV71 infection and involved infection in both Rhabdomyosarcoma (RD) cells and neurogliocytes. Most importantly, we found that EV71 did not induce the expression of other heat shock proteins HSPA1, HSPA8, and HSPB1 under the same conditions, and other HFMD-associated viruses including CVA16, CVA6, CVA10, and CVB1-3 did not induce the upregulation of HSPA6. In addition, EV71 infection enhanced the cytoplasmic aggregation of HSPA6 and its colocalization with viral capsid protein VP1. These findings suggest that HSPA6 is a potential EV71-specific host factor worthy of further study.

**Keywords: HFMD, EV71, heat shock proteins, HSPA6, host factor, specificity**

OPEN ACCESS

***Edited by:***
*Chunfu Zheng,*
*University of Calgary, Canada*

***Reviewed by:***
*Xinlei Li,*
*Nationwide Children's Hospital, United States*
*Guanyi Zhang,*
*Louisiana State University, United States*

***Correspondence:**
*Zhendan He*
*hezhendan@sztu.edu.cn*
*Qinchang Zhu*
*zhuqinchang@sztu.edu.cn*

[†]*These authors have contributed equally to this work*

***Specialty section:***
*This article was submitted to Virology, a section of the journal Frontiers in Microbiology*

***Received:*** *30 January 2022*
***Accepted:*** *17 February 2022*
***Published:*** *04 March 2022*

***Citation:***
*Jia J, Liu G, Zhong J, Yan R, Song X, Zheng K, Ren Z, He Z and Zhu Q (2022) Heat Shock Protein A6 Is Especially Involved in Enterovirus 71 Infection. Front. Microbiol. 13:865644. doi: 10.3389/fmicb.2022.865644*

## INTRODUCTION

Enterovirus 71 (EV71) from the Picornaviridae family is one of the common causative pathogens for hand foot and mouth disease (HFMD), which is usually a self-limiting, mild childhood disease with typical clinical manifestations of fever, mouth sores, skin rash on hands, mouth, and/or feet (Wong et al., 2010). Nevertheless, it can cause neurological complications such as myocarditis, aseptic meningitis, encephalitis, neurogenic pulmonary edema, and even death in severe cases. HFMD has emerged as a major concern among pediatric infectious diseases during the past 20 years, particularly in the Asia-Pacific (Koh et al., 2016). Countries such as Taiwan, Singapore, Malaysia, Vietnam, and China have encountered outbreaks of HFMD epidemics and millions of infections since the late 1990s. Around 13 million HFMD cases were reported in China from 2008 to 2015, including 123,261 severe cases and more than 3,322 deaths (Yang et al., 2017).

There are more than 20 enteroviruses that can cause HFMD (Klein and Chong, 2015), but EV71 is the most clinically significant serotype, being associated with severe disease outcomes more frequently than other common causes such as coxsackievirus A16 (CVA16) and A6 (CVA6). It was reported that around 60% of clinical HFMD and more than 70% of severe HFMD were caused by EV71 infection (Huang et al., 2015; Wang et al., 2015). It is estimated

that around 0.2–1% of children with EV71 infection develop neurological complications (Lee and Chang, 2010; Aw-Yong et al., 2019). The reason why EV71 is more prevalent and more likely to cause severe disease when compared with other enteroviruses is currently largely unknown.

Recombination and mutation were reported to occur extensively throughout the genome of EV71 and to be possible key factors affecting the virulence of EV71 (Mandary and Poh, 2018). New EV71 variant arose from the recombination of part of the EV71 genome with 5'-NTR of poliovirus may have acquired virulence determinants to give rise to clinical complications (Brown and Pallansch, 1995). Although several mutations such as E145G/Q and D164E in VP1, LysP930 in 2A, GP272, UP488, and AP700/UP700 in the 5'-NTR are highly conserved in the neuro-virulent strains across different genotypes of EV71 (Li et al., 2011), there is still no solid evidence to confirm their roles in virulence. Excessive secretion of cytokines including IL-1β, IL-6, IL-10, IL-17A, monocyte chemotactic protein 1 (MCP-1), and IFN-γ were reported to be linked to EV71 severity (Aw-Yong et al., 2019). The single nucleotide polymorphisms (SNPs) of type I IFN receptor 1 (IFNAR1) were found to be associated with the susceptibility and severity to EV71 infection (Zou et al., 2015). EV71-specific host responses may be related to the prevalence of virulence of EV71, but they have rarely been studied.

Heat shock protein A6 (HSPA6, also known as Hsp70B') is a member of the highly conserved heat shock protein 70 kDa (Hsp70) family, which generally plays a wide range of roles in cellular functions in health and disease (Evans et al., 2010; Rosenzweig et al., 2019). Besides HSPA6, more than 13 Hsp70 isoforms have been identified in the human Hsp70 family, classified as inducible or constitutive and organ or tissue specificity (Radons, 2016; Ambrose and Chapman, 2021). Although there is a high sequence homology between the members, a considerable difference in function has been observed in the Hsp70 family (Daugaard et al., 2007; Hageman et al., 2011; Radons, 2016). For instance, HSPA1A (Hsp70-1) is one of the major cytoplasmic stress-inducible Hsp70s that has a preferential contribution to DNA repair and tumor immune response (Multhoff et al., 1995; Duan et al., 2014). HSPA8 (Hsc70) is constitutively expressed in both cytoplasm and nucleus and is associated with cellular housekeeping functions, while HSPA9 (Hsp70-9) is expressed in mitochondria and is not induced by heat stress and is correlated with muscle activity and mitochondrial respiration (Radons, 2016). Although sharing high sequence identity (81–85%) and partly overlapping cellular stress-response functions with HSPA1A, HSPA6 has unique induction characteristics, different substrates, and thus potential distinct functions (Daugaard et al., 2007; Hageman et al., 2011; Deane and Brown, 2017). HSPA6 is a strictly stress-inducible Hsp70 in higher mammals such as primates, swine, and goats but not rodents (Parsian et al., 2000; Ramirez et al., 2015), and has varied expression patterns between cell types (Noonan et al., 2007; Banerjee et al., 2014; Kuballa et al., 2015), suggesting it is newly evolved Hsp70. HSPA6 has been reported to protect human neuronal cells from cellular stress (Deane and Brown, 2018) and might be associated with earlier recurrence of human hepatocellular carcinoma (Yang et al., 2015). Compared to other widely studied Hsp70s like HSPA1A, very little is known about the functions of HSPA6.

Hsp70 family has been positively involved in viral infection, but most studies focus on general Hsp70 without paying much attention to particular isoforms (Kim and Oglesbee, 2012; Yang et al., 2020). Hsp70 functions at distinct steps of the viral cycle in a virus or isoform-specific manner (Phillips et al., 1991; Lahaye et al., 2012; Manzoor et al., 2014; Taguwa et al., 2015). For instance, HSPA1 and HSPA8 but not HSPA2, HSPA6, and HSPA14 were found to be recruited to zika virus-induced compartments and required for virus replication (Taguwa et al., 2019). HSPA1A, HSPA1B, and HSPA8 are required for dengue virus infection at steps of entry, replication, and virion production, while HSPA5 and HSPA9 are not (Taguwa et al., 2015). On the other side, HSPA5 was found to contribute to the entry and replication of the Japanese encephalitis virus (JEV), a member of the Flaviviridae family-like dengue virus (Nain et al., 2017). In addition, Hsp70s have been reported to participate in the infection of several enteroviruses. HSPA1A was reported to promote coxsackievirus B3 (CVB3) translation initiation and elongation through the Akt-mTORC1 pathway (Wang et al., 2017). Hsp70 (actually HSPA9) was reported to facilitate EV71 infection *in vitro* as a supplementary receptor (Xu et al., 2019). HSPA8 (Hsc70) was found to assist EV71 replication through upregulating the activity of viral the internal ribosome entry site (IRES; Dong et al., 2018). Another study also reported that HSPA8 and HSPA9 regulated all phases of the EV71 life cycle (Su et al., 2020). However, so far, there is no study addressing the specificity of Hsp70 in the infection of HFMD-associated viruses.

We reported that HSPA6 was induced by EV71 infection and involved infection in both RD cells and neurogliocytes. For the first time, we also show that EV71 did not induce the expression of HSPA1, HSPA8, and HSPB1 under the same conditions, and several other common HFMD-associated viruses did not induce the upregulation of HSPA6. In addition, EV71 infection enhanced the cytoplasmic aggregation of HSPA6 and its colocalization with viral capsid protein VP1. These findings suggest that HSPA6 is a potential EV71-specific host factor worthy of further study.

# MATERIALS AND METHODS

## Cell and Viruses

Vero cells (African green monkey kidney cells, ATCC, CCL-81), RD cells (human muscle rhabdomyosarcoma; ATCC, CCL-136), and U251 cells (human brain glioma cells, BNCC,341988) were cultivated in Dulbecco's modified Eagle's medium (DMEM; Gibco) supplemented with 10% fetal bovine serum, 100 U/ml penicillin and 100 μg/ml streptomycin at 37°C with 5% $CO_2$. EV71 C4/BrCr strains and Coxsackievirus A16 (CVA16) were kindly provided by Dr. Tao Peng, Guangzhou Medical University, China. Coxsackievirus B1, B2, B3, A6, and A10 (CVB1, CVB2, CVB3, CVA6, and CVA10) were obtained from ATCC. The viruses were propagated, titred in RD or Vero cells, and used at the

indicated multiplicity of infection (MOI). EV71 C4 is a clinically isolated strain (Xu et al., 2017), mainly used EV71 in this study.

## Transcriptome Analysis and RT-PCR

RD cells were infected with the EV71 virus at a multiplicity of infection (MOI) of 0.2 for 8 h, and then the cells were collected and subjected to RNA extraction and transcriptomic sequencing analyses as described previously (Huang et al., 2020). The transcriptomes were sequenced on Illumina HiSeq2500 by Gene Denovo Biotechnology Co. (Guangzhou, China). Gene differential expression analysis was performed using DESeq2 software on EV71 infected (V) vs. uninfected groups (Ctrl). The genes/transcripts with the parameter of false discovery rate (FDR) below 0.05 and absolute fold change ≥2 were considered differentially expressed genes/transcripts.

For RT-PCR, RD or U251 cells were treated and/or infected as indicated, followed by RNA extraction. RD cells were infected with EV71 at an MOI of 0.2 for 8 h or 24 h, while U251 cells were infected with EV71 at an MOI of 1 for 24 h or 48 h. An active compound pendulectin (PDL, 10 μM) was used as antiviral control. According to the manufacturer's protocol, total RNA was extracted using TaKaRa MiniBEST Universal RNA Extraction Kit (TaKaRa, Shiga, Japan). RNA samples were subjected to cDNA synthesis with PrimeScript RT Reagent Kit (TaKaRa, Shiga, Japan). PCR amplified and detection was performed with TB Green Premix Ex Taq II (TaKaRa, Shiga, Japan) in the QTOWER3G real-time PCR system (Jena, Germany). The relative gene expression was determined by using the $2^{-\Delta\Delta CT}$ comparative method. GAPDH was used as the normalizing gene. Quantitative RT-PCR primer sequences were as follows: HSPA6 forward (5'-AGTACAAGGCTGAGGATGAGGC-3') and reverse (5'-AAGGACTTCCCGACACTTGTCTT-3'); HSPA1A forward (5'-GACGCGAAGCGGCTGATT-3') and reverse (5'-TCGGGGTAGAATGCCTTGG-3'); HSPB1 forward (5'-TACATCTCCCGGTGCTTCACG-3') and reverse (5'-ATCTCGTTGGACTGCGTGGC-3'); HSPA8 forward (5'-ACTCCAAGCTATGTCGCCTTT-3') and reverse (5'-TGGCATCAAAAACTGTGTTGGT-3'). EV71 positive-strand forward (5'-GCAGCCCAAAAGAACTTCAC-3') and reverse (5'-ATTTCAGCAGCTTGGAGTGC-3'); EV71 negative-strand forward (5'-TGCGTGGTGATGGTGGAGTT-3') and reverse (5'-GCCACAGCAGGCAAACAGAG-3'); EV-A71 VP1 forward (5'-CACACAGGTGAGCAGTCATCG-3') and reverse (5'-GTCTCAATCATGCTCTCGTCACT-3'); CVA6 VP1 forward (5'-TAAGCACGTGAGAGCTTGGG-3') and reverse (5'-CCGCCTTCATAATCCGTGGT-3'); CVA16 VP1 forward (5'-AGCCGTGCTGGTCTTGTTAG-3') and reverse (5'-TGGGGGACTAGCTCTCCATT-3'); CVB2 VP1 forward (5'-ACCGTGGACGATTACAACTGG-3') and reverse (5'-ATGCCTAAACTCGGACCAACC-3'). GAPDH forward (5'-GATTCCACCCATGGCAAATTCCA-3') and reverse (5'-TGGTGATGGGATTTCCATTGATGA-3').

## Western Blot Analysis

Cells were treated as indicated and Western blotted as previously described (Liu et al., 2015). Briefly, the cells were lysed and assessed using 4–20% sodium dodecyl sulfate–polyacrylamide gel electrophoresis (SurePAGE, Bis-Tris gels, Genscript, Nanjing, China). Proteins were transferred to polyvinylidene difluoride membranes (Millipore, Bedford, MA, United States) and probed with primary antibodies against HSPA6 (sc-374589, Santa Cruz Biotechnology), HSPA1A (PA534772, Invitrogen), HSPA8 (PA5-27337, Invitrogen), HSPB1 (PA1017, Invitrogen), EV71 VP1 (GTX132339, GeneTex), CVA6 VP1 (GTX132346, GeneTex), GAPDH (ab9485, Abcam) or α-Tubulin (ab179484, Abcam). Protein bands were visualized with Pierce™ ECL Western blotting substrate (Thermo Scientific, Rockford, IL, United States). Protein levels were determined by scanning the bands' intensities and analyzed using Quantity One software (Bio-Rad, Hercules, CA, United States).

## RNA Interference (RNAi)-Directed Knockdown

RD cells in 12-well plate were cultured to 60–80% confluence and then transfected with siRNAs targeting HSPA6 gene or SCARB2 (Scavenger Receptor Class B Member 2) gene or negative control siRNA targeting no known genes (si-NC) using Lipofectamine™ RNAiMAX Transfection Reagent (Life Technologies, Carlsbad, United States) according to the manufacturer's protocol. siRNAs were chemically synthesized by Guangzhou Ruibo Biotech Co., Ltd., China. Cells were infected with the virus 24 h after transfection. After 48 h of infection, the gene and protein expression levels were evaluated with RT-PCR and Western blotting, respectively. After 72 h of infection, the culture supernatants were collected, and the daughter virus production was analyzed with plaque reduction assay. At the same time, the cytopathic effect (CPE) caused by EV71 infection was measured by Alamar blue reagent as described previously (Zhu et al., 2011).

## Confocal Microscopy Analysis

RD cells grown on a glass-bottomed dish were infected with EV71 C4 strain (MOI = 0.2) for 8 h or 24 h and then were fixed with 4% paraformaldehyde and permeabilized with 0.1% Triton X-100. Then the cells were blocked with 5% BSA and then incubated with the indicated primary antibodies in 1% BSA at 4°C overnight. After three washes with PBS, the cells were incubated with a secondary antibody in 1% BSA for 1 h at room temperature in the dark and washed three times with PBS. The samples were then exposed to VP1 (GTX132339) / Alexa Fluor 488 or HSPA6 (sc-374,589) /Alexa Fluor 594 (Beyotime Biotechnology, Jiangsu, China) and observed under a Nikon A1 confocal microscope. The nuclei of the cells were stained with 4,6-diamidino-2-phenylindole (DAPI, Molecular Probes). Images and Z-stacks were acquired with NIS-Elements imaging software. Orthogonal views were generated in Imaris Software.

## Plaque Reduction Assay

RD cells were first transfected with siRNA against HSPA6 or SCARB2 or negative control siRNA (si-NC) for 24 h as described above. Then, the cells were infected with the EV71 C4 strain.

After 48 h of infection, the culture supernatant was collected and subjected to plaque reduction assay as described previously (Zhu et al., 2011). The cells were finally stained with 1% crystal violet. The titer of the virus in the culture supernatant was calculated according to the number of forming plaques.

## Statistics Analysis

All the data presented herein are mean ± standard derivation values. Statistical comparisons were analyzed with a two-tailed Student's t-test or one-way ANOVA followed by Dunnett's post-hoc test using GraphPad Prism version 8.0.2 for Windows (GraphPad Software, California, United States). **Indicates $p < 0.01$ and * indicates $p < 0.05$. $p$ values <0.05 were considered statistically significant.

# RESULTS

## EV71 Infection Specially Upregulates HSPA6 Gene Expression

Comparative transcriptome analysis was firstly performed and found that the expression of HSPA6 mRNA was upregulated in EV71 infected RD cells (**Figure 1A**), which could be inhibited by the treatment of penduletin (PDL), an active compound against EV71 we previously reported (data not showed; Zhu et al., 2011). RD cells were infected with EV71 at an MOI of 0.2 for 8 h or 24 h again and then subjected to RT-PCR. The expression of HSPA6 and other three heat shock proteins, including HSPA1A, HSPA8, and HSPB1 and viral genes, were measured. Results showed that EV71 infection significantly upregulated HSPA6 expression in RD cells but had no significant effect on the other three heat shock proteins (**Figures 1B,D**). The upregulation of HSPA6 in infected cells was completely inhibited by simultaneous treatment of PDL, which was in accord with the expression of viral VP1 gene and positive viral strand (**Figures 1B,C**). In addition, human brain glioma cells (U251) were normally infected with 1MOI of EV71 (**Supplementary Figure S1**), and the expression of HSPA6 mRNA in the cells was also found to be upregulated (**Figure 1D**). These results suggested that EV71 infection specially upregulates the mRNA expression of HSPA6 but not the other three heat shock proteins.

## EV71 Infection Specially Upregulates HSPA6 Protein Expression

To evaluate the inducible effect of EV71 infection on HSPA6 expression at the protein level, RD cells were infected with EV71 for 8 or 24 h and then subjected to Western blotting analysis for HSPA6, HSPA1A, HSPA8, HSPB1, and viral capsid protein VP1. PDL here was used as antiviral control. Results showed that the inducible effect of EV71 infection on HSPA6 and other three heat shock proteins was not significant when detection was performed at 8 h post-infection (hpi; **Figure 2**). When detection was conducted at 24 hpi, EV71 infection was

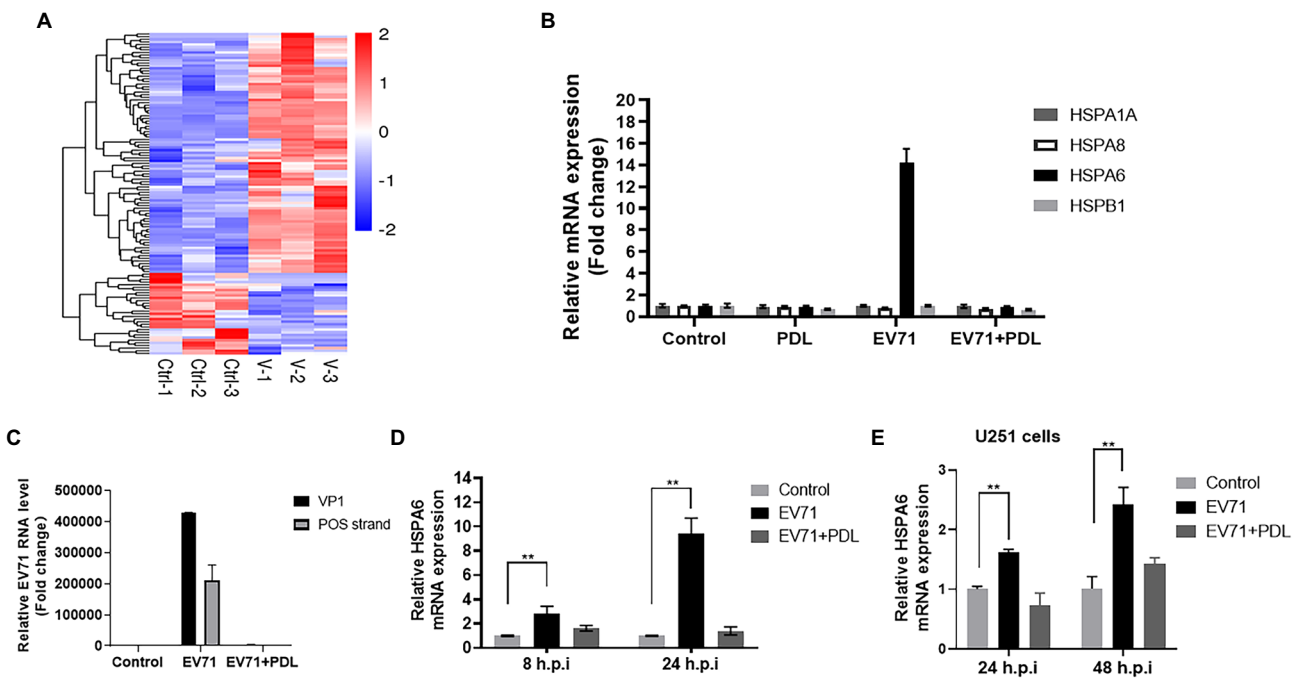


**FIGURE 1 |** EV71 infection specially upregulates HSPA6 gene expression. **(A)** Heat map of RNA-Seq transcriptome analysis for genes changed in RD cells infected with EV71 for 8 h. **(B)** RT-PCR measurement of HSPA6 and HSPA1, HSPA8, and HSPB1 expression in RD cells infected with EV71 for 8 h. **(C)** RT-PCR measurement of EV71 VP1 gene and positive (POS) strand in RD cells infected with EV71 for 8 h. **(D)** RT-PCR measurement of HSPA6 expression in RD cells infected with EV71 for 8 h and 24 h. **(E)** RT-PCR measurement of HSPA6 expression in U251 cells infected with EV71 for 24 h and 48 h. Control presented cell control, and PDL presented treating the cells with 10 μM of pendulectin at the same time of EV71 infection (**$p < 0.01$).

found to upregulate the expression of HSPA6 significantly, but it did not affect the expression of the other three heat shock proteins (**Figures 2A,B**). The upregulation of HSPA6 protein caused by EV71 infection was inhibited by the treatment of PDL that possessed strong antiviral activity against EV71. These results are consistent with the observations from the above RT-PCR analysis, which confirms that EV71 infection especially upregulates the expression of HSPA6 at both mRNA and protein levels.

## HSPA6 Knockdown Inhibits EV71 Replication and Protein Expression

To explore the role of HSPA6 in the infection of EV71, RNAi-directed knockdown of HSPA6 was performed in EV71 infected RD cells, and the viral replication and protein synthesis in the cells were measured. Results showed that siRNA targeting HSPA6 caused a dose-dependent decrease in HSPA6 mRNA level and EV71 VP1 mRNA level and the amount of both viral positive and negative strands (**Figure 3A**). A similar dose-dependent reduction was also observed in the synthesis of viral protein VP1 (**Figure 3B**). SCARB2 is an important receptor for EV71 infection. Here siRNA targeting the SCARB2 gene was used as a positive control for RNAi. These results showed that silencing of HSPA6 led to inhibition of EV71 replication and viral protein synthesis, which suggests that HSPA6 plays a role in EV71 infection.

## HSPA6 Knockdown Inhibits EV71 CPE Formation and Daughter Virus Production

To further study the role of HSPA6 in EV71 infection, the effect of silencing HSPA6 on CPE formation and daughter virus production was investigated. PDL and siRNA targeting SCARB2 were used as positive controls. Results showed that siRNA targeting HSPA6 significantly protected the cells from CPE caused by EV71 infection in a dose-dependent manner (**Figure 4A**). When the daughter virus production was considered, siRNA targeting HSPA6 significantly reduced the production of the EV71 daughter virus in the culture supernatant (**Figure 4B**). These results suggest that HSPA 6 plays an important role in EV71 infection.

## EV71 Infection Enhances the Cytoplasmic Aggregation of HSPA6

To provide a clue for understanding how HSPA6 involve in EV71 infection, the distribution of HSPA6 in EV71 infected cells was investigated with confocal microscopy. RD cells were infected with EV71 for 8 and 24 h, and an immunofluorescence staining was performed with specific antibodies. Results showed that EV71 infection enhanced the cytoplasmic aggregation of HSPA 6 at 24 hpi (**Figure 5**). Moreover, the aggregated HSPA6 was found to colocalize with viral VP1 protein (**Figure 5B**). We also observed that HSPA6 cellular levels were significantly elevated at 24 h post-EV71 infection than uninfected cells

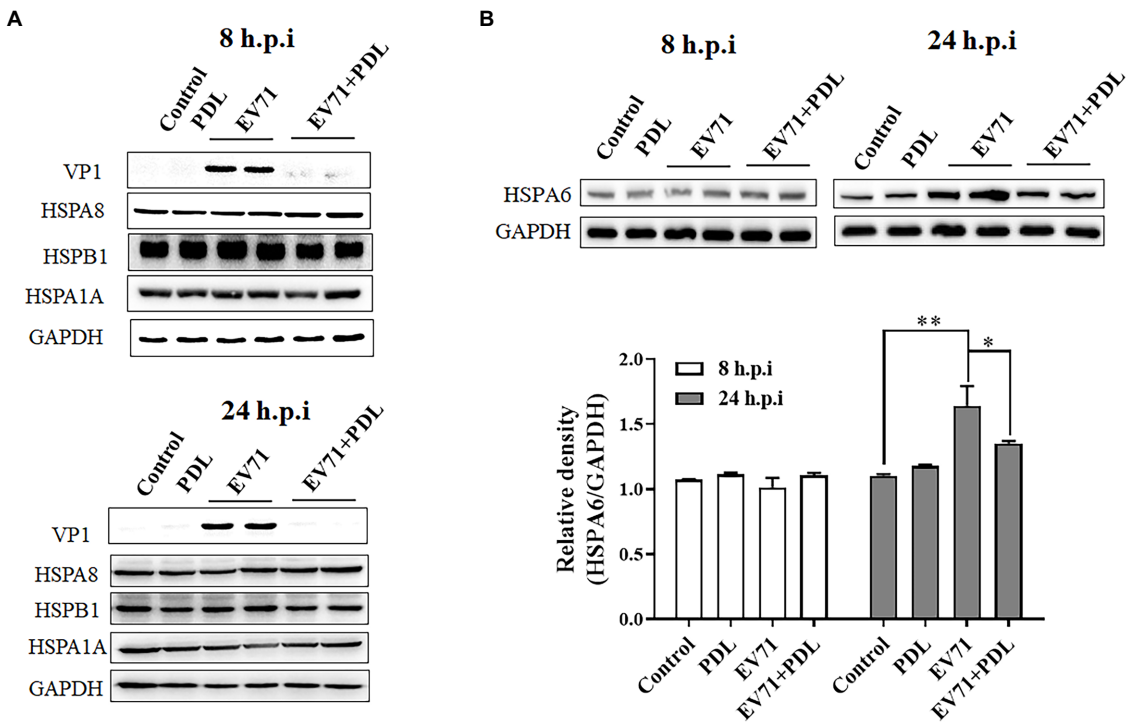


**FIGURE 2 |** EV71 infection specially upregulates HSPA6 protein expression. **(A)** Western blotting analysis of HSPA1A, HSPA8, HSPB1, and viral VP1 expression in RD cells infected with EV71 for 8 or 24 h. **(B)** Western blotting analysis of HSPA6 expression in RD cells infected with EV71 for 8 or 24 h. The relative expression of HSPA6 was quantitatively analyzed based on the bands' intensities from the Western blotting analysis. PDL (10 μM) here was used as anti-EV71 control ($^{*}p < 0.05$, $^{**}p < 0.01$).

(**Figure 5B**). This observation was consistent with the results from RT-PCR and Western blotting performed above.

## HSPA6 Is Involved in the Infection of EV71 but Not Other HFMD-Associated Viruses

To investigate the inducible effect of other HFMD-associated viruses on HSPA6 expression, RD or Vero cells were infected with different HFMD-associated viruses including EV71 C4 strain, EV71 BrCr strain, CVA6, CVA10, CVA16, and CVB1-3 at MOI of 0.2 for 8 h, and then subjected to RT-PCR analysis for HSPA6 mRNA level. Results showed that only EV71, including strain C4 and BrCr, upregulated the expression of HSPA6, while other viruses showed no obvious effect on HSPA6 expression (**Figure 6A**). Western blotting was also performed to analyze the expression of HSPA6 protein in RD cells infected with 0.2 MOI of EV71 or CVA6 at 36 hpi. Results showed that the expression of HSPA6 protein was upregulated in RD cells infected with EV71 but not in the cells infected with CVA6. To further investigate the connection between HSPA6 and these non-EV71 HFMD-associated viruses, the cells were transfected with 100 nM of si-HSPA6 or si-NC for 24 h and then infected with the viruses for 72 h, followed by the cell survival detection with Alamar blue reagent. Results showed

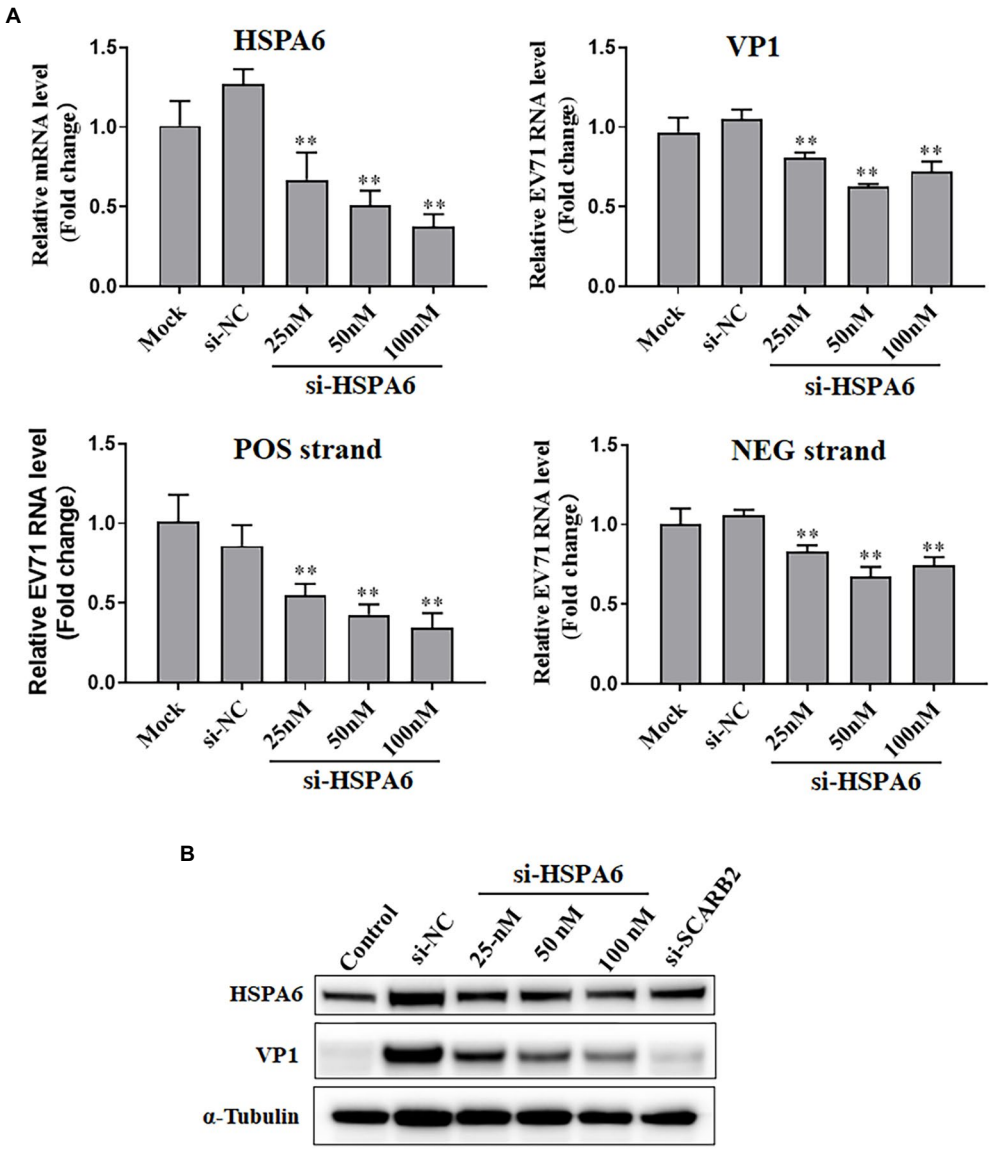


**FIGURE 3 |** HSPA6 knockdown inhibits EV71 replication and protein expression. **(A)** RT-PCR measurement of HSPA6 as well as viral VP1, positive (POS) strand, and negative (NEG) strand expression in RD cells transfected with siRNAs targeting HSPA6 (si-HSPA6) and infected with EV71. **(B)** Western blotting analysis of protein level of HSPA6 protein and viral VP1 in RD cells transfected with siRNAs and infected with EV71. Mock is the infected but untreated control, si-NC is the negative control siRNA targeting no known genes. Control in B is the cell control without viral infection and siRNA transfection. si-SCARB2 is siRNA targeting the receptor of EV71, using it as the positive control (vs. si-NC, $^{**}p < 0.01$).

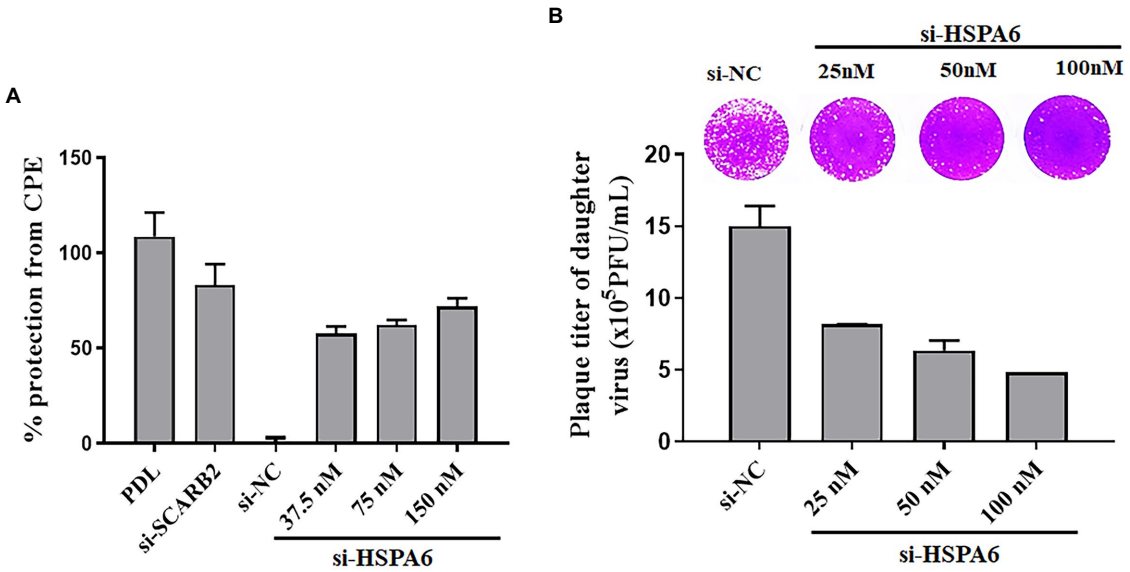


**FIGURE 4 |** HSPA6 knockdown inhibits EV71 CPE formation and daughter virus production. **(A)** siRNA targeting HSPA6 protected RD cells from EV71-induced CPE. **(B)** siRNA targeting HSPA6 inhibited the production of the EV71 daughter virus. RD cells were transfected with siRNAs for 24 h and then infected with 0.2 MOI EV71 for 72 h, followed by cytopathic analysis. At the same time, the culture supernatant was subjected to plaque reduction assay.

that silencing of HSPA6 did not affect the infection of CVA6, CVA10, CVA16, and CVB1-3 (**Figure 6B**), which was different from the observation for EV71 infection. These results suggest that HSPA6 is especially involved in the infection of EV71 but not other HFMD-associated viruses.

## DISCUSSION

HFMD caused by EV71 infection is still a major infectious disease threatening children's life and health in the absence of effective antiviral drugs due to its high prevalence and severe rate. The study of EV71 infection-related host factors, especially EV71 specific host factors, will help to answer the reasons for the special virulence of EV71 and help find effective ways of antiviral treatment.

PDL is a flavonoid compound with significant anti EV71 activity that we found earlier (Zhu et al., 2011). In the process of tracing the action target of PDL, based on differential transcriptome analysis, we found that EV71 infection can significantly upregulate the expression of HSPA6, including in its most sensitive cell line RD cells and human nervous system-derived U251 cells (**Figure 1**). Through further research, we found that EV71 only upregulated HSPA6, but not HSPA1, HSPA8, and HSPB1. HSPA1, a major stress-inducible Hsp70 protein member, has been reported to be involved in the infection of Zika virus, Dengue virus, and CVB3 virus (Taguwa et al., 2015, 2019; Wang et al., 2017). HSPA8 is a constitutively expressed Hsp70, the most important Hsp70 protein in Zika virus infection (Taguwa et al., 2019). Moreover, through the knockdown experiment, some studies found that HSPA8 regulates the IRES of EV71 and is required at all stages of the EV71 life cycle (Dong et al., 2018; Su et al., 2020), but here we do not see that EV71 infection can conversely upregulate the expression of HSPA8 (**Figures 1, 2**). Previously reported that HSPB1 can be upregulated by EV71 infection at a higher MOI and play a supportive role in EV71 replication (Dan et al., 2019). However, we found no significant change in the expression of HSPB1 under a relatively low MOI infection of EV71 (**Figures 1, 2**). During our study, another group also independently found and first reported the induction effect of EV71 on HSPA6 protein, which is consistent with our findings (Su et al., 2021). They infected RD cells with EV71 C strain and found that HSPA6 is induced to support EV71 replication cycle in an IRES-dependent manner. But the specificity of the induction of HSPA6 was not considered and human nervous system-derived cells were not used in their study. In addition, we further investigate the distribution of HSPA6 in EV71 infected cells and tested the specificity of induction of HSPA6 using other HFMD-associated viruses.

As an important stress response protein of the body, heat shock protein often plays different roles in different viral infections, assists the virus infection, or helps the body resist the virus infection. To further clarify the significance of upregulating HSPA6 in EV71 infection, we downregulated the expression of the HSPA6 gene in cells by RNAi and observed its effect on EV71 virus infection. We found that downregulation of HSPA6 could inhibit the replication of EV71 virus, the synthesis of viral protein, the production of daughter virus, and its cytopathic effect (**Figures 3, 4**), indicating that HSPA6 is important for the life cycle of EV71 infection. Nevertheless, the mechanism behind it is unclear. A study suggested that HSPA6 may play a role in EV71 infection by promoting the IRES activity of EV71 (Su et al., 2021). Through confocal microscopy analysis, we found that EV71 infection can not only induce HSPA6

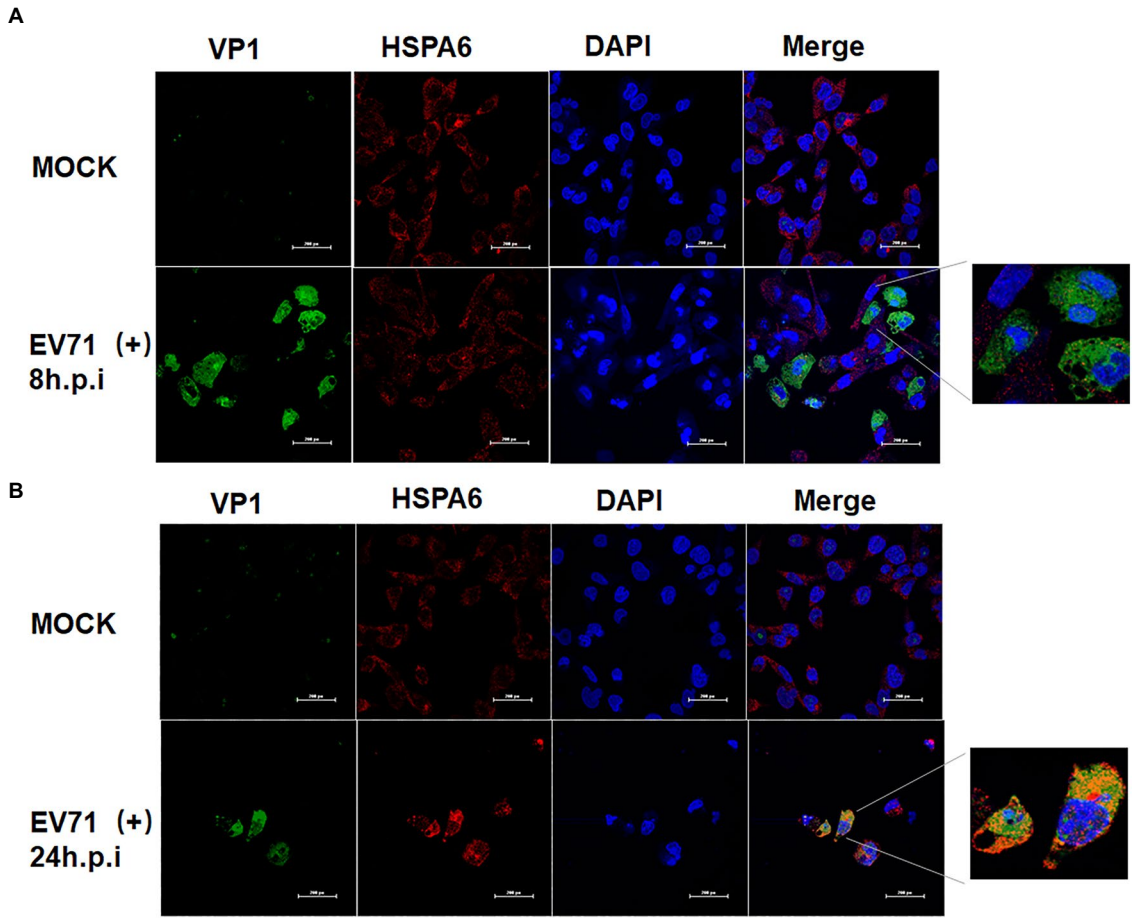


**FIGURE 5 |** EV71 infection enhances the cytoplasmic aggregation of HSPA6. **(A)** Confocal microscopy analysis of RD cells infected with EV71 at 8 hpi. **(B)** Confocal microscopy analysis of RD cells infected with EV71 at 24 hpi. Cells were stained with VP1/ Alexa Fluor 488, HSPA6/Alexa Fluor 594, and nuclei/DAPI.

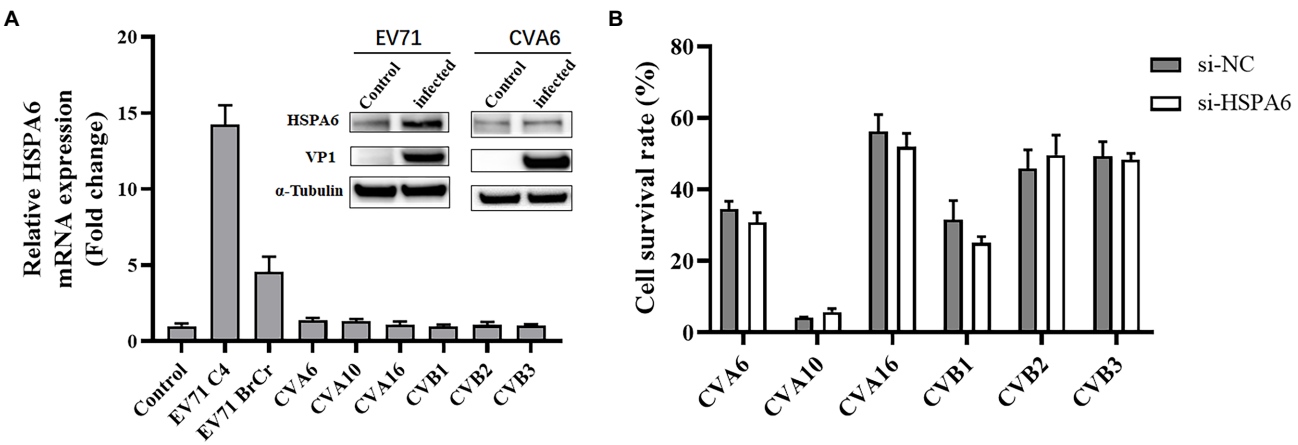


**FIGURE 6 |** HSPA6 is involved in the infection of EV71 but not other HFMD-associated viruses. **(A)** RT-PCR and Western blotting analysis of HSPA6 expression in RD cells infected with various HFMD viruses. RD cells were infected with 0.2 MOI of EV71 C4 strain, EV71 BrCr strain, CVA6, and CVA10, while Vero cells were infected with 1MOI of CVA16 and CVB1-3. After 8 h infection, the cells were subjected to RT-PCR analysis. Western blotting was also performed to analyze the expression of HSPA6 protein in RD cells infected with 0.2 MOI of EV71 or CVA6 at 36 hpi. **(B)** Survival analysis of RD cells transfected with siRNA targeting HSPA6 and infected with various viruses. RD cells or Vero cells were transfected with 100 nM of si-HSPA6 or si-NC for 24 h and then infected with the viruses for 72 h, followed by the cell survival detection with Alamar blue reagent.

expression but also enhance the aggregation of HSPA6 in the cytoplasm and colocalization with viral protein VP1 (**Figure 5**), suggesting that HSPA6 may be involved in virus assembly.

In addition to EV7, various enteroviruses can cause HFMD in infants, including the most common CVA16, CVA6, and CVA10. To determine whether the induction and dependence of EV71 on HSPA6 are specific in HFMD-associated enteroviruses, we studied the HSPA6 induction effects of six enteroviruses besides two EV71 strains. We found that all of these viruses except EV71 did not significantly upregulate HSPA6 mRNA in RD cells at 8 hpi (**Figure 6A**). This result is consistent with the detection of HSPA6 at the protein level. At the same time, the expression of HSPA6 was downregulated by RNAi, and there was no significant effect on the cytopathic effect of these viruses except EV71 (**Figure 6B**). These results suggest that the induction and dependence of EV71 on HSPA6 are specific in these HFMD-associated enteroviruses.

Interestingly, we found that EV71 infection can upregulate the expression of HSPA6 in human neurogliocytes (**Figure 1E**) but not in neuronal SH-SY5Y cells (data not shown). According to the Human Protein Atlas online database,[1] HSPA6 is brain-enriched. EV-71 is the most popular and most deadly virus than the other HFDM associated viruses. But the reason why EV71 is more prevalent and more likely to cause severe neurological complications is currently largely unknown. Our findings suggest HSPA6 is a EV71-specific host factor, which hold the potential to be a drug target or biomarkers for EV71 infection. Whether the phenomenon of EV71 specific induction and dependence on HSPA6 is related to the unique neurovirulence of EV71 still needs more in-depth research.

## CONCLUSION

This study has shown that HSPA6, a member of the host Hsp70 family, was induced by EV71 infection and was involved in EV71 virus replication, protein synthesis, daughter virus production, and cytopathic effect. At the same time, this study, for the first time, found that EV71 has relative specificity in the induction and dependence of HSPA6. Under the same conditions, EV71 did not induce the expression of HSPA1, HSPA8, and HSPB1 genes, and several other common HFMD-associated viruses did not induce the upregulation of HSPA6. This study suggests that HSPA6 is a potential EV71-specific host factor worthy of further study.

[1]www.proteinatlas.org

## DATA AVAILABILITY STATEMENT

The datasets presented in this study can be found in online repositories. The names of the repository/repositories and accession number(s) can be found at: SRA NCBI, accession number PRJNA803808.

## AUTHOR CONTRIBUTIONS

JJ planned the experiments and carried out the experiment. GL analyzed the data and wrote the manuscript. JZ and RY carried out the experiment. XS, KZ, and ZR analyzed the data and reviewed the manuscript. ZH supervised the project. QZ conceived the original idea, wrote the manuscript, and acquired financial support. All authors contributed to the article and approved the submitted version.

## FUNDING

This project was funded by the Science and Technology Program of Guangdong Province (2018A030313252), the Shenzhen Science and Technology Project (JCYJ20170818095732006, JCYJ20190808122605563), and the Shenzhen Peacock Plan and the Fundamental Research Funds for Shenzhen Technology University.

## ACKNOWLEDGMENTS

We thank Professor Tao Peng of Guangzhou Medical University for providing EV71 and CVA16.

## SUPPLEMENTARY MATERIAL

The Supplementary Material for this article can be found online at: https://www.frontiersin.org/articles/10.3389/fmicb.2022.865644/full#supplementary-material

## REFERENCES

Ambrose, A. J., and Chapman, E. (2021). Function, therapeutic potential, and inhibition of Hsp70 chaperones. *J. Med. Chem.* 64, 7060–7082. doi: 10.1021/acs.jmedchem.0c02091

Aw-Yong, K. L., NikNadia, N., Tan, C. W., Sam, I. C., and Chan, Y. F. (2019). Immune responses against enterovirus A71 infection: Implications for vaccine success. *Rev. Med. Virol.* 29:e2073. doi: 10.1002/rmv.2073

Banerjee, D., Upadhyay, R. C., Chaudhary, U. B., Kumar, R., Singh, S., Ashutosh, et al. (2014). Seasonal variation in expression pattern of genes under HSP70 family in heat- and cold-adapted goats (Capra hircus). *Cell Stress Chaperones* 19, 401–408. doi: 10.1007/s12192-013-0469-0

Brown, B. A., and Pallansch, M. A. (1995). Complete nucleotide sequence of enterovirus 71 is distinct from poliovirus. *Virus Res.* 39, 195–205. doi: 10.1016/0168-1702(95)00087-9

Dan, X., Wan, Q., Yi, L., Lu, J., Jiao, Y., Li, H., et al. (2019). Hsp27 responds to and facilitates Enterovirus A71 replication by enhancing viral internal ribosome entry site-mediated translation. *J. Virol.* 93:18. doi: 10.1128/JVI.02322-18

Daugaard, M., Rohde, M., and Jaattela, M. (2007). The heat shock protein 70 family: highly homologous proteins with overlapping and distinct functions. *FEBS Lett.* 581, 3702–3710. doi: 10.1016/j.febslet.2007.05.039

Deane, C. A. S., and Brown, I. R. (2017). Differential targeting of Hsp70 heat shock proteins HSPA6 and HSPA1A with components of a protein

disaggregation/refolding machine in differentiated human neuronal cells following thermal stress. *Front. Neurosci.* 11:227. doi: 10.3389/fnins.2017.00227

Deane, C. A. S., and Brown, I. R. (2018). Knockdown of heat shock proteins HSPA6 (Hsp70B') and HSPA1A (Hsp70-1) sensitizes differentiated human neuronal cells to cellular stress. *Neurochem. Res.* 43, 340–350. doi: 10.1007/s11064-017-2429-z

Dong, Q., Men, R., Dan, X., Chen, Y., Li, H., Chen, G., et al. (2018). Hsc70 regulates the IRES activity and serves as an antiviral target of enterovirus A71 infection. *Antivir. Res.* 150, 39–46. doi: 10.1016/j.antiviral.2017.11.020

Duan, Y., Huang, S., Yang, J., Niu, P., Gong, Z., Liu, X., et al. (2014). HspA1A facilitates DNA repair in human bronchial epithelial cells exposed to Benzo[a] pyrene and interacts with casein kinase 2. *Cell Stress Chaperones* 19, 271–279. doi: 10.1007/s12192-013-0454-7

Evans, C. G., Chang, L., and Gestwicki, J. E. (2010). Heat shock protein 70 (hsp70) as an emerging drug target. *J. Med. Chem.* 53, 4585–4602. doi: 10.1021/jm100054f

Hageman, J., van Waarde, M. A. W. H., Zylicz, A., Walerych, D., and Kampinga, H. H. (2011). The diverse members of the mammalian HSP70 machine show distinct chaperone-like activities. *Biochem. J.* 435, 127–142. doi: 10.1042/BJ20101247

Huang, Z., Ma, A., Yang, S., Liu, X., Zhao, T., Zhang, J., et al. (2020). Transcriptome analysis and weighted gene co-expression network reveals potential genes responses to heat stress in turbot Scophthalmus maximus. *Comp. Biochem. Physiol. Part D Genomics Proteomics* 33:100632. doi: 10.1016/j.cbd.2019.100632

Huang, X., Wei, H., Wu, S., du, Y., Liu, L., Su, J., et al. (2015). Epidemiological and etiological characteristics of hand, foot, and mouth disease in Henan, China, 2008-2013. *Sci. Rep.* 5:8904. doi: 10.1038/srep08904

Kim, M. Y., and Oglesbee, M. (2012). Virus-heat shock protein interaction and a novel axis for innate antiviral immunity. *Cell* 1, 646–666. doi: 10.3390/cells1030646

Klein, M., and Chong, P. (2015). Is a multivalent hand, foot, and mouth disease vaccine feasible? *Hum. Vaccin. Immunother.* 11, 2688–2704. doi: 10.1080/21645515.2015.1049780

Koh, W. M., Bogich, T., Siegel, K., Jin, J., Chong, E. Y., Tan, C. Y., et al. (2016). The epidemiology of hand, foot and mouth disease in Asia: a systematic review and analysis. *Pediatr. Infect. Dis. J.* 35, e285–e300. doi: 10.1097/INF.0000000000001242

Kuballa, P., Baumann, A. L., Mayer, K., Bär, U., Burtscher, H., and Brinkmann, U. (2015). Induction of heat shock protein HSPA6 (HSP70B') upon HSP90 inhibition in cancer cell lines. *FEBS Lett.* 589, 1450–1458. doi: 10.1016/j.febslet.2015.04.053

Lahaye, X., Vidy, A., Fouquet, B., and Blondel, D. (2012). Hsp70 protein positively regulates rabies virus infection. *J. Virol.* 86, 4743–4751. doi: 10.1128/JVI.06501-11

Lee, M. S., and Chang, L. Y. (2010). Development of enterovirus 71 vaccines. *Expert Rev. Vaccines* 9, 149–156. doi: 10.1586/erv.09.152

Li, R., Zou, Q., Chen, L., Zhang, H., and Wang, Y. (2011). Molecular analysis of virulent determinants of enterovirus 71. *PLoS One* 6:e26237. doi: 10.1371/journal.pone.0026237

Liu, G., Asanoma, K., Takao, T., Tsukimori, K., Uchi, H., Furue, M., et al. (2015). Aryl hydrocarbon receptor SNP -130 C/T associates with dioxins susceptibility through regulating its receptor activity and downstream effectors including interleukin 24. *Toxicol. Lett.* 232, 384–392. doi: 10.1016/j.toxlet.2014.11.025

Mandary, M. B., and Poh, C. L. (2018). Changes in the EV-A71 genome through recombination and spontaneous mutations: Impact on Virulence. *Viruses* 10:320. doi: 10.3390/v10060320

Manzoor, R., Kuroda, K., Yoshida, R., Tsuda, Y., Fujikura, D., Miyamoto, H., et al. (2014). Heat shock protein 70 modulates influenza A virus polymerase activity. *J. Biol. Chem.* 289, 7599–7614. doi: 10.1074/jbc.M113.507798

Multhoff, G., Botzler, C., Wiesnet, M., Müller, E., Meier, T., Wilmanns, W., et al. (1995). A stress-inducible 72-kDa heat-shock protein (HSP72) is expressed on the surface of human tumor cells, but not on normal cells. *Int. J. Cancer* 61, 272–279. doi: 10.1002/ijc.2910610222

Nain, M., Mukherjee, S., Karmakar, S. P., Paton, A. W., Paton, J. C., Abdin, M. Z., et al. (2017). GRP78 is an important host factor for Japanese encephalitis virus entry and replication in mammalian cells. *J. Virol.* 91:16. doi: 10.1128/JVI.02274-16

Noonan, E. J., Place, R. F., Rasoulpour, R. J., Giardina, C., and Hightower, L. E. (2007). Cell number-dependent regulation of Hsp70B' expression: evidence of an extracellular regulator. *J. Cell. Physiol.* 210, 201–211. doi: 10.1002/jcp.20875

Parsian, A. J., Sheren, J. E., Tao, T. Y., Goswami, P. C., Malyapa, R., van Rheeden, R., et al. (2000). The human Hsp70B gene at the HSPA7 locus of chromosome 1 is transcribed but non-functional. *Biochim. Biophys. Acta* 1494, 201–205. doi: 10.1016/S0167-4781(00)00203-7

Phillips, B., Abravaya, K., and Morimoto, R. I. (1991). Analysis of the specificity and mechanism of transcriptional activation of the human hsp70 gene during infection by DNA viruses. *J. Virol.* 65, 5680–5692. doi: 10.1128/jvi.65.11.5680-5692.1991

Radons, J. (2016). The human HSP70 family of chaperones: where do we stand? *Cell Stress Chaperones* 21, 379–404. doi: 10.1007/s12192-016-0676-6

Ramirez, V. P., Stamatis, M., Shmukler, A., and Aneskievich, B. J. (2015). Basal and stress-inducible expression of HSPA6 in human keratinocytes is regulated by negative and positive promoter regions. *Cell Stress Chaperones* 20, 95–107. doi: 10.1007/s12192-014-0529-0

Rosenzweig, R., Nillegoda, N. B., Mayer, M. P., and Bukau, B. (2019). The Hsp70 chaperone network. *Nat. Rev. Mol. Cell Biol.* 20, 665–680. doi: 10.1038/s41580-019-0133-3

Su, Y. S., Hsieh, P. Y., Li, J. S., Pao, Y. H., Chen, C. J., and Hwang, L. H. (2020). The heat shock protein 70 family of chaperones regulates All phases of the Enterovirus A71 life cycle. *Front. Microbiol.* 11:1656. doi: 10.3389/fmicb.2020.01656

Su, Y. S., Hwang, L. H., and Chen, C. J. (2021). Heat shock protein A6, a novel HSP70, is induced During Enterovirus A71 infection to facilitate internal ribosomal entry site-mediated translation. *Front. Microbiol.* 12:664955. doi: 10.3389/fmicb.2021.664955

Taguwa, S., Maringer, K., Li, X., Bernal-Rubio, D., Rauch, J. N., Gestwicki, J. E., et al. (2015). Defining Hsp70 subnetworks in dengue virus replication reveals key vulnerability in Flavivirus infection. *Cell* 163, 1108–1123. doi: 10.1016/j.cell.2015.10.046

Taguwa, S., Yeh, M. T., Rainbolt, T. K., Nayak, A., Shao, H., Gestwicki, J. E., et al. (2019). Zika virus dependence on host Hsp70 provides a protective strategy against infection and disease. *Cell Rep.* 26, 906.e3–920.e3. doi: 10.1016/j.celrep.2018.12.095

Wang, F., Qiu, Y., Zhang, H. M., Hanson, P., Ye, X., Zhao, G., et al. (2017). Heat shock protein 70 promotes coxsackievirus B3 translation initiation and elongation via Akt-mTORC1 pathway depending on activation of p70S6K and Cdc2. *Cell. Microbiol.* 19, e12725. doi: 10.1111/cmi.12725

Wang, Y., Zou, G., Xia, A., Wang, X., Cai, J., Gao, Q., et al. (2015). Enterovirus 71 infection in children with hand, foot, and mouth disease in Shanghai, China: epidemiology, clinical feature and diagnosis. *Virol. J.* 12:83. doi: 10.1186/s12985-015-0308-2

Wong, S. S., et al. (2010). Human enterovirus 71 and hand, foot and mouth disease. *Epidemiol. Infect.* 138, 1071–1089. doi: 10.1017/S0950268809991555

Xu, T., Lin, Z., Wang, C., Li, Y., Xia, Y., Zhao, M., et al. (2019). Heat shock protein 70 as a supplementary receptor facilitates enterovirus 71 infections *in vitro*. *Microb. Pathog.* 128, 106–111. doi: 10.1016/j.micpath.2018.12.032

Xu, Y., Ma, S., Zhu, L., Huang, Z., Chen, L., Xu, Y., et al. (2017). Clinically isolated enterovirus A71 subgenogroup C4 strain with lethal pathogenicity in 14-day-old mice and the application as an EV-A71 mouse infection model. *Antivir. Res.* 137, 67–75. doi: 10.1016/j.antiviral.2016.11.008

Yang, B., Liu, F., Liao, Q., Wu, P., Chang, Z., Huang, J., et al. (2017). Epidemiology of hand, foot and mouth disease in China, 2008 to 2015 prior to the introduction of EV-A71 vaccine. *Euro Surveill.* 22:16-00824. doi: 10.2807/1560-7917.ES.2017.22.50.16-00824

Yang, J., Xu, Y., Yan, Y., Li, W., Zhao, L., Dai, Q., et al. (2020). Small molecule inhibitor of ATPase activity of HSP70 as a broad-Spectrum inhibitor against Flavivirus infections. *ACS Infect. Dis.* 6, 832–843. doi: 10.1021/acsinfecdis.9b00376

Yang, Z., Zhuang, L., Szatmary, P., Wen, L., Sun, H., Lu, Y., et al. (2015). Upregulation of heat shock proteins (HSPA12A, HSP90B1, HSPA4, HSPA5 and HSPA6) in tumour tissues is associated with poor outcomes from HBV-related early-stage hepatocellular carcinoma. *Int. J. Med. Sci.* 12, 256–263. doi: 10.7150/ijms.10735

Zhu, Q. C., Wang, Y., Liu, Y. P., Zhang, R. Q., Li, X., Su, W. H., et al. (2011). Inhibition of enterovirus 71 replication by chrysosplenetin and penduletin. *Eur. J. Pharm. Sci.* 44, 392–398. doi: 10.1016/j.ejps.2011.08.030

Zou, R., Zhang, G., Li, S., Wang, W., Yuan, J., Li, J., et al. (2015). A functional polymorphism in IFNAR1 gene is associated with susceptibility and severity of HFMD with EV71 infection. *Sci. Rep.* 5:18541. doi: 10.1038/srep18541

**Conflict of Interest:** The authors declare that the research was conducted in the absence of any commercial or financial relationships that could be construed as a potential conflict of interest.

**Publisher's Note:** All claims expressed in this article are solely those of the authors and do not necessarily represent those of their affiliated organizations, or those of the publisher, the editors and the reviewers. Any product that may be evaluated in this article, or claim that may be made by its manufacturer, is not guaranteed or endorsed by the publisher.

*Copyright © 2022 Jia, Liu, Zhong, Yan, Song, Zheng, Ren, He and Zhu. This is an open-access article distributed under the terms of the Creative Commons Attribution License (CC BY). The use, distribution or reproduction in other forums is permitted, provided the original author(s) and the copyright owner(s) are credited and that the original publication in this journal is cited, in accordance with accepted academic practice. No use, distribution or reproduction is permitted which does not comply with these terms.*

frontiers in Microbiology

MINI REVIEW
published: 08 March 2022
doi: 10.3389/fmicb.2022.852431

# Multifunctional pMGF505-7R Is a Key Virulence-Related Factor of African Swine Fever Virus

*Li Huang[1,2], Jiangnan Li[1,2], Jun Zheng[1,2], Dan Li[3] and Changjiang Weng[1,2]**

[1] Division of Fundamental Immunology, National African Swine Fever Para-Reference Laboratory, State Key Laboratory of Veterinary Biotechnology, Harbin Veterinary Research Institute, Chinese Academy of Agricultural Sciences, Harbin, China, [2] Heilongjiang Provincial Key Laboratory of Veterinary Immunology, Harbin, China, [3] State Key Laboratory of Veterinary Etiological Biology, Lanzhou Veterinary Research Institute, Chinese Academy of Agricultural Sciences, Lanzhou, China

African swine fever virus (ASFV) is the etiological agent of African swine fever (ASF), and it is an enveloped, icosahedral, double-stranded DNA virus with a genome length ranging from 170 to 193 kb. The ASFV genome contains at least five multigene families (MGFs): MGF100, MGF110, MGF300, MGF360, and MGF505 at the right and left terminal variable regions. The members of the same MGF family are most similar and have conserved sequence motifs, whereas the genetic diversity of different MGF families varies widely. MGF genes play a crucial role in determining ASFV host range, virulence and reducing early cell death post-infection. pMGF505-7R is a multifunctional protein. Recent research advances of pMGF505-7R provide a few new clues to understand the functions of pMGF505-7R either in antagonizing the induction of type I IFN production and IFN downstream signaling or in suppressing inflammatory responses by inhibition of NF-κB signaling and NLRP3 inflammasome, which may be related to ASFV infection-induced pathogenesis.

**Keywords: ASFV, pMGF505-7R, multifunction, virulence, innate immune, inflammatory response**

OPEN ACCESS

***Edited by:***
*Chunfu Zheng,*
*University of Calgary, Canada*

***Reviewed by:***
*Hongjun Chen,*
*Shanghai Veterinary Research Institute (CAAS), China*
*Jianzhong Zhu,*
*Yangzhou University, China*

****Correspondence:***
*Changjiang Weng*
*wengchji@163.com*

***Specialty section:***
*This article was submitted to Virology, a section of the journal Frontiers in Microbiology*

***Received:*** *11 January 2022*
***Accepted:*** *31 January 2022*
***Published:*** *08 March 2022*

***Citation:***
*Huang L, Li J, Zheng J, Li D and Weng C (2022) Multifunctional pMGF505-7R Is a Key Virulence-Related Factor of African Swine Fever Virus. Front. Microbiol. 13:852431. doi: 10.3389/fmicb.2022.852431*

## CLASSIFICATION AND CHARACTERIZATION OF AFRICAN SWINE FEVER VIRUS MULTIGENE FAMILIES

African swine fever virus (ASFV) is the etiological agent of African swine fever (ASF), and it is an enveloped, icosahedral, double-stranded DNA virus with a genome length ranging from 170 to 193 kb. The ASFV genome contains at least five multigene families (MGFs): MGF100, MGF110, MGF300, MGF360, and MGF505 at the right and left terminal variable regions. The members of the same MGF family are most similar and have conserved sequence motifs, whereas the genetic diversity of different MGF families varies widely. Zsak et al. (2001a,b) demonstrated that MGF360 and MGF505 genes are expressed early after infection, which play a crucial role in determining host range and reducing early cell death post-infection. Compared with a highly pathogenic isolate Benin 97/1, Chapman et al. (2008) showed that the non-pathogenic isolate OURT88/3 lacks eight MGF genes (MGF360-9L, 10L, 11L, 12L, 13L, 14L, MGF505-1R, 2R), suggesting MGF360/MGF505 may play a role in virulence. Interestingly, IFN priming of primary PAMs limited replication of the attenuated OURT88/3 but not virulent isolates indicating that MGF360 and MGF505 genes also enable ASFV to overcome the IFN-induced antiviral state

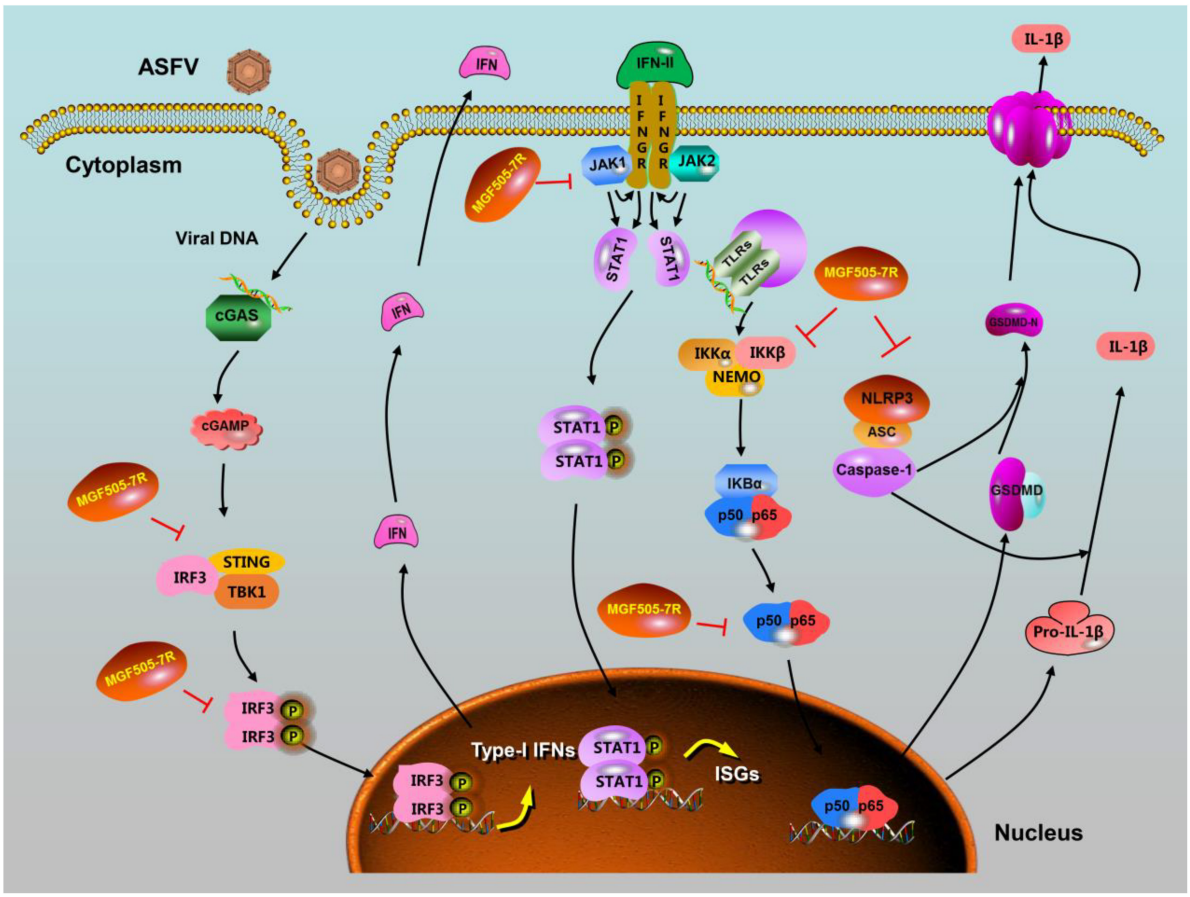


**FIGURE 1 |** ASFV pMGF505-7R is a multifunctional protein involved in viral pathogenesis.

(Golding et al., 2016). Consistently, a study revealed that the enhanced type I interferon (IFN-I) responses were observed in the PAMs infected with a recombinant virus Pr4Δ35 derived from the highly virulent strain Pr4 with deletion of MGF360 and MGF530 (Afonso et al., 2004). Subsequently, many recombinant viruses with deletion of MGF360 and MGF530 from three different genotypes also reduced virulence in pigs (O'Donnell et al., 2015). Until now, the functions of the members of these MGF families have not been well characterized.

## AFRICAN SWINE FEVER VIRUS pMGF505-7R SUPPRESSES IFN-I PRODUCTION

Accumulating evidence suggests that several ASFV-encoded MGF proteins can suppress the IFN-I induction. For example, pMGF360-15R/pA276R was found to inhibit the induction of IFN-I via both TLR3 and the cytosolic sensing pathways by inhibiting IRF3 through a mechanism independent of IRF7 and NF-κB (Correia et al., 2013). pMGF505-7R/pA528R was found to inhibit the induction of IFN-I through the inhibition of IRF3 and NF-κB (Correia et al., 2013). Recently, ASFV pMGF505-7R was found to exert a negative regulatory effect on the cGAS-STING signaling pathway at the STING level (Li et al., 2021a). An ASFV-ΔMGF505-7R recombinant virus derived from ASFV CN/GS/2018 strain induced more IFN-β production than wild-type ASFV infection in PAMs. Mechanistically, pMGF505-7R promoted the expression of the autophagy-related protein ULK1 to degrade STING (Li et al., 2021a). Li et al. (2021c) also noticed that pMGF505-7R interacted with and inhibited the nuclear translocation of IRF3, resulting in blocking IFN-I production. Of note, the replication ability of ASFV-ΔMGF505-7R was reduced compared with wild-type ASFV *in vivo*, and the ASFV-ΔMGF505-7R virus was fully attenuated in pigs. Altogether, these results showed that MGF505-7R may be a new key virulence-related factor.

## AFRICAN SWINE FEVER VIRUS pMGF505-7R MODULATES THE IFN SIGNALING PATHWAY

Treatment of ASFV-infected cells with IFN-I did not reduce the replication of virulent ASFV isolates. Consistently, ASFV lacking the gene of MGF360 and MGF505 families is partially sensitive to IFN-I compared to its parent virus (Golding et al., 2016). These results suggest that the ASFV developed strategies to inhibit IFN-I induced host antiviral state. On the other

hand, it is well known that the binding of secreted IFN-II (γ) to their respective receptors (IFNGR1/IFNGR2) in the viral-infected cells or neighboring cells initiates the Janus kinase (JAK)-signal transducer and activator of transcription (STAT) pathway. The process leads to the phosphorylation of STAT1 by JAK1 and JAK2, resulting in formation of a STAT1 dimer which then translocates to the nucleus to activate transcription of IFN-regulated genes including IFN stimulated genes (ISGs). These ISGs have a variety of antiviral activities, including the production of chemokines and other proteins involved in activating the innate and adaptive responses to restrict virus replication (Mazewski et al., 2020).

It has been reported that ASFV infection suppresses JAK-STAT signaling to evade the immune response. For example, pMGF505-7R was reported to inhibit both the type I and type II IFN signaling pathways, limiting the effect of IFN-I and IFN-II on the JAK-STAT signaling pathway and the expression of ISGs (Correia et al., 2013). Recently, Li et al. (2021b) reported that pMGF505-7R from ASFV CN/GS/2018 strain interacts with JAK1/JAK2 and mediates their degradation by up-regulating the E3 ubiquitin ligase RNF125 expression and inhibiting the expression of Hes5. Consistently, ASFV-ΔMGF505-7R derived from ASFV CN/GS/2018 strain induced higher levels of IRF1 expression and displayed compromised replication both in PAMs and pigs compared with wild-type ASFV (Li et al., 2021b). MGF505-7R deficiency attenuated the virulence of the ASFV and pathogenesis of ASF in pigs, suggesting that the MGF-505-7R gene plays a critical role in the virulence of the ASFV and pathogenesis of ASF by antagonizing IFN-I production and IFN (I and II) downstream JAK-STAT signaling.

## AFRICAN SWINE FEVER VIRUS pMGF505-7R INHIBITS THE ACTIVATION OF THE NF-κB SIGNALING PATHWAY AND NLRP3 INFLAMMASOME

Inflammatory factors are key components of host antiviral responses released from the pathogens-infected macrophages. Recently, ASFV pMGF505-7R was found to regulate ASFV pathogenicity by inhibiting IL-1β and IFN-I production (Li et al., 2021c). ASFV HLJ/18 isolate infection induced low levels of IL-1β in PAMs, even in the presence of strong inducers such as LPS and poly(dA:dT). Additionally, ASFV HLJ/18 strain infection-induced IL-1β production is depended on TLRs/NF-κB signaling pathway and NLRP3 inflammasome. Subsequently, several members of the MGF360 and MGF505 families were found to significantly inhibit IL-1β maturation and secretion. Among them, pMGF505-7R had the strongest inhibitory effect. Mechanistically, pMGF505-7R not only interacted with IKKα in the IKK complex to inhibit NF-κB activation and but also bound to NLRP3 to inhibit inflammasome formation, resulting in decreased IL-1β production. Consistent with these results, A528R can suppress the NF-κB p65 phosphorylation and nuclear translocation, and the antiviral and antibacterial activity (Liu et al., 2021), while an ASFV-ΔMGF505-7R recombinant virus derived from ASFV HLJ/18 induced higher levels of IL-1β in PAMs compared with its parental ASFV HLJ/18 strain. Importantly, the virulence of ASFV-ΔMGF505-7R is reduced in piglets, which may occur due to induction of higher IL-1β and IFN-I production *in vivo*.

Although both the two groups confirmed that the virulence of the two ASFV-ΔMGF505-7R recombinant viruses, derived from ASFV HLJ/18 strain and ASFV CN/GS/2018 strain, respectively, were attenuated compared with wild-type ASFV (Li et al., 2021a,b,c). Zheng's group found that the ASFV-ΔMGF505-7R virus derived from the ASFV CN/GS/2018 strain, was fully attenuated in pigs (Li et al., 2021a) while Weng's group showed that nearly 40% of piglets inoculated with the ASFV-ΔMGF505-7R virus derived from ASFV HLJ/18 strain still died, suggesting that this recombinant ASFV-ΔMGF505-7R retains some of its virulence. The differences of experimental results between the two groups may be caused by the usage of different ASFV isolates with different genetic backgrounds or by using different does of virus to challenge the pigs, and the specific reasons still need to be further investigated in the future.

## CONCLUSION

Taken together, pMGF505-7R is a multifunctional protein. Recent research advances of pMGF505-7R provide a few new clues to understand the functions of pMGF505-7R either in antagonizing the induction of IFN-I and IFN downstream signaling or in suppressing inflammatory responses by inhibition of NF-κB signaling and NLRP3 inflammasome (**Figure 1**), which may be related to ASFV infection-induced pathogenesis. pMGF505-7R, as a multifunctional protein, may have other functions not found, and needs to be further explored. The current progress in understanding of pMGF505-7R might help design antiviral agents or live-attenuated vaccines to control ASF.

## AUTHOR CONTRIBUTIONS

CW and LH wrote the manuscript. LH and JZ drew the diagram. JL and DL modified the manuscript. All authors contributed to the article and approved the submitted version.

## FUNDING

This study was supported by the National Natural Science Foundation of China (31941002).

## REFERENCES

Afonso, C. L., Piccone, M. E., Zaffuto, K. M., Neilan, J., Kutish, G. F., Lu, Z., et al. (2004). African swine fever virus multigene family 360 and 530 genes affect host interferon response. *J. Virol.* 78, 1858–1864. doi: 10.1128/jvi.78.4.1858-1864.2004

Chapman, D. A. G., Tcherepanov, V., Upton, C., and Dixon, L. K. (2008). Comparison of the genome sequences of non-pathogenic and pathogenic

African swine fever virus isolates. *J. Gen. Virol.* 89(Pt 2), 397–408. doi: 10.1099/vir.0.83343-0

Correia, S., Ventura, S., and Parkhouse, R. M. (2013). Identification and utility of innate immune system evasion mechanisms of ASFV. *Virus Res.* 173, 87–100. doi: 10.1016/j.virusres.2012.10.013

Golding, J. P., Goatley, L., Goodbourn, S., Dixon, L. K., Taylor, G., and Netherton, C. L. (2016). Sensitivity of African swine fever virus to type I interferon is linked to genes within multigene families 360 and 505. *Virology* 493, 154–161. doi: 10.1016/j.virol.2016.03.019

Li, D., Yang, W., Li, L., Li, P., Ma, Z., Zhang, J., et al. (2021a). African Swine Fever Virus MGF-505-7R Negatively Regulates cGAS-STING-Mediated Signaling Pathway. *J. Immunol.* 206, 1844–1857. doi: 10.4049/jimmunol.2001110

Li, J., Song, J., Kang, L., Huang, L., Zhou, S., Hu, L., et al. (2021c). pMGF505-7R determines pathogenicity of African swine fever virus infection by inhibiting IL-1beta and type I IFN production. *PLoS Pathog.* 17:e1009733. doi: 10.1371/journal.ppat.1009733

Li, D., Zhang, J. H., Yang, W., Li, P., Ru, Y., Kang, W., et al. (2021b). African swine fever virus protein MGF-505-7R promotes virulence and pathogenesis by inhibiting JAK1- and JAK2-mediated signaling. *J. Biol. Chem.* 297:101190. doi: 10.1016/j.jbc.2021.101190

Liu, X., Ao, D., Jiang, S., Xia, N., Xu, Y., Shao, Q., et al. (2021). African Swine Fever Virus A528R Inhibits TLR8 Mediated NF-kappaB Activity by Targeting p65 Activation and Nuclear Translocation. *Viruses* 13:2046. doi: 10.3390/v13102046

Mazewski, C., Perez, R. E., Fish, E. N., and Platanias, L. C. (2020). Type I interferon (IFN)-regulated activation of canonical and non-canonical signaling pathways. *Front. Immunol.* 11:606456. doi: 10.3389/fimmu.2020.606456

O'Donnell, V., Holinka, L. G., Gladue, D. P., Sanford, B., Krug, P. W., Lu, X., et al. (2015). African swine fever virus Georgia isolate harboring deletions of MGF360 and MGF505 genes is attenuated in swine and confers protection against challenge with virulent parental virus. *J. Virol.* 89, 6048–6056. doi: 10.1128/JVI.00554-15

Zsak, L., Lu, Z., Burrage, T. G., Neilan, J. G., Kutish, G. F., Moore, D. M., et al. (2001a). African swine fever virus multigene family 360 and 530 genes are novel macrophage host range determinants. *J. Virol.* 75, 3066–3076. doi: 10.1128/JVI.75.7.3066-3076.2001

Zsak, L., Sur, J. H., Burrage, T. G., Neilan, J. G., and Rock, D. L. (2001b). African Swine Fever Virus (Asfv) Multigene Families 360 and 530 Genes Promote Infected Macrophage Survival. *ScientificWorldJournal* 1:97. doi: 10.1100/tsw.2001.202

**Conflict of Interest:** The authors declare that the research was conducted in the absence of any commercial or financial relationships that could be construed as a potential conflict of interest.

**Publisher's Note:** All claims expressed in this article are solely those of the authors and do not necessarily represent those of their affiliated organizations, or those of the publisher, the editors and the reviewers. Any product that may be evaluated in this article, or claim that may be made by its manufacturer, is not guaranteed or endorsed by the publisher.

*Copyright © 2022 Huang, Li, Zheng, Li and Weng. This is an open-access article distributed under the terms of the Creative Commons Attribution License (CC BY). The use, distribution or reproduction in other forums is permitted, provided the original author(s) and the copyright owner(s) are credited and that the original publication in this journal is cited, in accordance with accepted academic practice. No use, distribution or reproduction is permitted which does not comply with these terms.*

frontiers in Microbiology

ORIGINAL RESEARCH
published: 10 March 2022
doi: 10.3389/fmicb.2022.865124

# Reactivation of Occult Hepatitis B Virus Infection During Long-Term Entecavir Antiviral Therapy

*Chunyan Yuan†, Jing Peng†, Renxiang Xia†, Jian He, Tianji Qiu and Yunqing Yao**

*Department of Infectious Diseases, The First Affiliated Hospital of Chongqing Medical University, Chongqing, China*

Up to now, it has not been clear whether occult hepatitis B virus (HBV) infection (OBI) can be treated with antiviral therapy whether OBI can develop drug resistance gene mutation or not. We report a middle-aged female patient with OBI who showed HBV reactivation (HBVr) during more than 3 years of intermittent entecavir (ETV) antiviral therapy: seropositive HBV surface antigen (HBsAg), increased e antigen (HBeAg), and repeatedly elevated serum HBV DNA. Genotype analysis showed that the patient was infected with HBV type B. Genetic sequencing of HBV showed the mutants of S143T, D144G, and G145R in the S gene region, and the mutant of site 1896 in the pre-Core region coexisted with the wild type (G1896A/G). No mutation was found in other HBV gene segments. Drug resistance gene analysis found RtL229W mutant, resistant to lamivudine but sensitive to ETV and other nucleoside analogs. This case of OBI provides us with the following clinical experiences: Firstly, it is necessary to detect HBV genotype, mutation, and drug-resistant genes at the initial diagnosis, which can be helpful for reasonable treatment. Secondly, identifying the risk factors and mechanisms associated with HBVr could help quantify the risk of HBVr and manage the clinical consequences. Thirdly, the OBI patients with hepatitis B e antigen-positive, HBV DNA $> 1 \times 10^3$ IU/ml should be recommended regular and continuous antiviral therapy as soon as possible to prevent the occurrence of hepatocirrhosis and hepatocellular carcinoma (HCC).

**Keywords: occult hepatitis B virus infection, antiviral therapy, S gene mutation, pre-C gene mutation, drug-resistant, entecavir, reactivation**

OPEN ACCESS

***Edited by:***
*Chunfu Zheng,*
*University of Calgary, Canada*

***Reviewed by:***
*Limin Chen,*
*Chinese Academy of Medical Sciences and Peking Union Medical College, China*
*Yan Yan,*
*Wuxi No.5 People's Hospital, China*

****Correspondence:***
*Yunqing Yao*
*yaoyunqing@hospital.cqmu.edu.cn*

*†These authors have contributed equally to this work*

***Specialty section:***
*This article was submitted to Virology, a section of the journal Frontiers in Microbiology*

***Received:*** *29 January 2022*
***Accepted:*** *14 February 2022*
***Published:*** *10 March 2022*

***Citation:***
*Yuan C, Peng J, Xia R, He J, Qiu T and Yao Y (2022) Reactivation of Occult Hepatitis B Virus Infection During Long-Term Entecavir Antiviral Therapy. Front. Microbiol. 13:865124. doi: 10.3389/fmicb.2022.865124*

## INTRODUCTION

Occult hepatitis B virus (HBV) infection (OBI) is defined as surface antigen (HBsAg) seronegative, core antibody (HBcAb) seropositive, and HBV DNA positive in serum or liver (de Almeida and de Paula, 2021). OBI may result in HBV reactivation (HBVr), acute exacerbations, cirrhosis, and hepatocellular carcinoma (HCC; Mak et al., 2020). For OBI patients or HBV exposure (HBsAg-negative but HBcAb-positive; Pattullo, 2015), according to the recent American Association for the Study of Liver Diseases (AASLD) recommendation guideline, HBVr could be defined as (1) HBV DNA is detectable; or (2) reverse HBsAg seroconversion occurs (reappearance of HBsAg; Terrault et al., 2018; Onorato et al., 2021).

The occurrence of HBVr largely depends on the primary disease requiring chemotherapy or immunosuppressive therapy, host immunity, underlying disease, and the immunosuppressive agents used. The main risk factors associated with HBVr could be divided into three categories: (1) host factors (such as male sex, older age, presence of liver cirrhosis, and type of underlying diseases); (2) virological factors (the extent of HBV replication is most important); and (3) type of immunosuppressive regimen. The HBVr rate ranges from 8.9 to 41.5% in occult HBV infection patients receiving rituximab-containing chemotherapy in different studies using the definitions of HBsAg seroreversion or detectable HBV DNA (Shih and Chen, 2021).

Here, we report a unique case of OBI who developed HBV reactivation during the long term of antiviral therapy but without chemotherapy or immunosuppressive therapy.

## MEDICAL CONDITION AT INITIAL DIAGNOSIS

In April 2018, a 55-year-old woman was diagnosed with occult HBV infection during the medical examination. She had no symptoms and signs of liver disease. She denied the history of any liver disease, hepatitis virus infection, anti-HBV treatment, tumor, chemotherapy, biological therapy or immunosuppressive therapy, blood transfusion, diabetes, and tuberculosis. She denied drinking or smoking. She submitted that her mother and a brother had died of liver cancer but had no clear family history of chronic hepatitis B. Her husband and children had no HBV infection.

The laboratory examination results showed that blood routine tests, urine routine tests, liver function, kidney function, and alpha-fetal protein (AFP) were normal.

Hepatitis B virus serological testing showed that HBsAg was negative (less than 0.05 IU/ml), surface antibody (HBsAb) was positive (53.69 mIU/ml, more than ULT 10 mIU/ml), e antigen (HBeAg) was positive (45.42 S/Co, more than 1.0 S/Co), e antibody (HBeAb) was negative (0, less than 1.0 S/Co), and HBcAb was positive (9.37 S/Co, more than 1.0 S/Co. Details shown in **Table 1**).

Serological tests showed that hepatitis A, C, D, and E virus markers were negative.

Real-Time PCR-Fluorescence Quantitation showed that the serum load of HBV DNA was $2.32 \times 10^3$ IU/ml. HBV Genotype analysis showed that type B.

Abdominal ultrasound revealed mild fatty liver but no fibrosis, cirrhosis, or HCC. Liver Stiffness Measurement (LSM) was 5.5 kPA (range of normal value was 4.0–7.0 kPA).

## THE FIRST STAGE OF ANTIVIRAL THERAPY AND FOLLOW-UP

After the initial diagnosis of OBI, the patient was recommended oral entecavir (ETV) therapy (single dose 50 mg daily) and long-term outpatient follow-up.

In May 2018, 4 weeks after initiation of ETV treatment, follow-up tests showed that a load of serum HBV DNA dropped below 100 IU/ml (Minimum detection value line). There were no significant changes in other serum markers of HBV except HBsAb was about 10 mIU/ml more than before (63.50 mIU/ml. Details shown in **Table 1**). There were no significant drug-related adverse events.

In November 2018, 30 weeks after ETV treatment, follow-up tests showed that serum HBV DNA was still less than 100 IU/ml, HBeAg was much less than that of initial diagnosis (26.93 S/Co. Details shown in **Table 1**). Interestingly, HBsAb also decreased significantly from last time (38.50 mIU/ml. Details are shown in **Table 1**).

The patient had no symptoms and signs of liver disease.

The laboratory examination results showed that blood routine tests, urine routine tests, liver function, kidney function, and AFP were normal.

Abdominal ultrasound revealed no fatty liver, fibrosis, cirrhosis, or HCC. The result of LSM was normal.

There were no significant drug-related adverse events.

The patient was advised to continue ETV antiviral therapy.

## THE FIRST REACTIVATION OF HBV AND DRUG RESISTANCE GENETIC TESTING

On a subsequent follow-up visit (July 2019), test results showed that the serum load of HBV rebounded to $2.79 \times 10^3$ IU/ml (Details shown in **Table 1**). Interestingly, serum levels of HBsAb, HBeAg, and HBcAb were higher than those in November 2018 (Details shown in **Table 1**). Meanwhile, serum HBsAg was still negative, and there was no other abnormal detection. The patient had no symptoms and signs of liver disease.

Further examination of the patient's medical history revealed that the patient had spontaneously stopped taking ETV for 6 months.

In addition, drug resistance gene examination of HBV showed that RtL229W mutant, resistant to lamivudine but sensitive to ETV and other nucleoside analogs (Details shown in **Table 2**).

**TABLE 1** | The serological and molecular characterization results during intermittent antiviral therapy from April 2018 to August 2021.

| Date | HBsAg (IU/ml) | HBsAb (mIU/ml) | HBeAg (S/Co) | HBeAb (S/Co) | HBcAb (S/Co) | HBV DNA (IU/ml) |
|---|---|---|---|---|---|---|
| April 2018 | 0 | 53.69 | 45.42 | 0 | 9.37 | $2.32 \times 10^3$ |
| May 2018 | 0 | 63.50 | 44.60 | 0 | 9.41 | <100 |
| November 2018 | 0 | 38.50 | 26.93 | 0 | 7.66 | <100 |
| July 2019 | 0 | 66.76 | 36.76 | 0 | 9.62 | $2.79 \times 10^3$ |
| October 2019 | 0 | 36.51 | 29.79 | 0 | 8.73 | <100 |
| September 2020 | 0.10 | 22.08 | 27.71 | 0 | 7.74 | <100 |
| August 2021 | 0.45 | 0 | 66.50 | 0 | 8.09 | $5.93 \times 10^3$ |

Subsequently, this patient was recommended to take ETV antiviral therapy again.

## THE SECOND STAGE OF ANTIVIRAL THERAPY AND FOLLOW-UP

In October 2019, 3 months of ETV oral treatment, follow-up test results showed that the patient's serum load of HBV decreased to less than 100 IU/ml, serum level of HBsAb, HBeAg, and HBcAb also decreased to than those in July 2019 (Details shown in **Table 1**). Meanwhile, serum HBsAg was still negative, and there was no other abnormal detection. The patient had no symptoms and signs of liver disease. There were no significant drug-related adverse events.

The patient was encouraged to continue ETV antiviral therapy.

## THE SECOND REACTIVATION OF HBV

In September 2020, 14 months of uninterrupted ETV oral treatment, follow-up test results showed that the patient's serum HBsAg became positive (0.10 IU/ml, more than ULT 0.05 IU/ml. Details shown in **Table 1**), while the serum HBV DNA was undetectable, serum level of HBsAb, HBeAg, and HBcAb further decreased to less than those in October 2019 (all were positive. Details shown in **Table 1**).

There was no other abnormal detection, no symptoms, and no signs of liver disease. There were no significant drug-related adverse events.

The patient was encouraged to continue ETV antiviral therapy.

## THE THIRD REACTIVATION OF HBV AND GENETIC VARIATION DETECTION

Unfortunately, in August 2021, the patient spontaneously stopped ETV oral therapy for 6 months before seeing a physician. Follow-up test results showed that the patient's serum HBsAg increased to 0.45 IU/ml, much higher than that of September 2020 (positive, ULT 0.05 IU/ml), the serum load of HBV DNA also increased to $5.93 \times 10^3$ IU/ml from negative, serum levels of HBeAg and HBcAb were higher than those in September 2020, while serum HBsAb was negative (Details shown in **Table 1**).

The patient denied any symptoms and signs of liver disease and other diseases. There was no other abnormal laboratory detection. There were no significant drug-related adverse events.

Abdominal ultrasound revealed no fatty liver, fibrosis, cirrhosis, or HCC. The result of LSM was normal.

Mutation analysis of this patient's HBV showed there were three mutants (S143T, D144G, and G145R) in the S gene region, and the mutant of site 1896 in the pre-Core region coexisted with the wild type (G1896A/G), but no mutation in the pre-S1, pre-S2, and BCP gene regions (Details shown in **Table 3**).

In summary, due to the S gene mutation and drug resistance gene, the patient had become a chronic HBV infection from OBI.

**TABLE 2** | The results of drug resistance gene examination of hepatitis B virus (HBV; July 2019).

| Drug | Genetic locus | | | Potential phenotype | Comprehensive phenotype |
|---|---|---|---|---|---|
| lamivudine (LAM) | major: rtM204I | rtM204V | rtM204S | S | U |
| | minor: rtL80I | rtL80V | rtV173L | S | |
| | rtL180M | rtA181T | rtA181V | | |
| | undetermined: rtV207I | rtV207L | rtV207M | | |
| | rtS213T | rtL229F | rtL229G | U | |
| | rtL229M | rtL229V | rtL229W | | |
| tibivudine (LdT) | major: rtM204I | rtM204V | rtM204S | S | S |
| | minor: rtV173L | rtL180M | | S | |
| emtricitabine (FTC) | major: rtM204I | rtM204V | rtM204S | S | S |
| | minor: rtV173L | rtL180M | | S | |
| adefovir (ADV) | major: rtA181S | rtA181T | rtA181V | S | S |
| | rtN236T | rtN236V | | | |
| | undetermined: rtV84M | rtS85A | rtS85T | S | |
| | rtV214A | rtQ215H | rtQ215P | | |
| | rtQ215S | rtI233V | rtP237H | | |
| | rtN/H238D | rtN/H238S | rtN/H238T | | |
| tenofovir (TDF) | major: rtA194T | rtA194M | | S | S |
| | minor: rtN236T | rtN236V | | S | |
| entecavir (ETV) | major: rtT184A | rtT184C | rtT184F | S | S |
| | rtT184G | rtT184I | rtT184L | | |
| | rtT184M | rtT184S | rtS202C | | |
| | rtS202G | rtS202I | rtM250I | | |
| | rtM250L | rtM250V | | | |
| | minor: rtI169T | rtV173L | rtL180M | S | |
| | rtM204I | rtM204V | rtM204S | | |

**TABLE 3** | The results of mutation analysis of HBV (August 2021).

| Gene site | | Wild type/mutant |
|---|---|---|
| pre-C | 1862 | Wild type (G1862) |
| | 1896 | mutant coexists with the wild type (G1896A/G) |
| | 1899 | Wild type (G1899) |
| BCP | 1762 | Wild type (A1762) |
| | 1764 | Wild type (G1764) |
| pre-S1 Deletion mutation | No deletion mutations were detected | |
| pre-S2 Promoter mutation | Wild type promoter (ATG) | |
| pre-S2 Deletion mutation | No deletion mutations were detected | |
| S | 118 | Wild type (T118) |
| | 120 | Wild type (P120) |
| | 126 | Wild type (T/I126) |
| | 127 | Wild type (P127) |
| | 129 | Wild type (Q129) |
| | 131 | Wild type (T131) |
| | 133 | Wild type (M133) |
| | 143 | mutant type (S143T) |
| | 144 | mutant type (D144G) |
| | 145 | mutant type (G145R) |

## DISCUSSION

The case presented here represents a one-of-a-kind serological profile of HBV infection. Negative HBeAg is a common finding in OBI patients. OBI with positive HBeAg has been described but uncommon (Zhou et al., 2009; Han et al., 2015; Raimondo et al., 2019). Because HBeAg is associated with a high level of HBV replication, we can speculate that an escape mutant appeared at the time of diagnosis while the wild-type virus was still present in the patient. Patients are infected with "S-escape" mutations, which result in modified HBsAg that can evade standard assays. Unfortunately, we could not complete the gene sequencing from 2018 to 2020. The S gene sequencing in August 2021 revealed that mutations were detected at three amino acid sites (S143T, D144G, and G145R), while HBsAg was positive, which could be due to wild-type accounting for a large proportion at the time. A high level of HBV DNA is linked to e-antigen status and virus mutation. Although HBeAg is not part of the virus particle and is not required for infectivity or viral replication, its presence in the bloodstream correlates with high levels of viral replication in hepatic tissue. Furthermore, OBI infected with "S-escape" mutations has a higher viral load. As a result, the patient with negative HBsAg but positive HBeAg may represent a distinct type of OBI that warrants further investigation.

The case demonstrates the efficacy of antiviral therapy, as no study has previously reported on the antiviral response in patients with OBI. The patient requires antiviral therapy for the following reasons. In individuals with chronic hepatitis B, the level of HBV DNA is a well-described risk factor for progressive liver disease and a marker of viral replication and antiviral treatment efficacy. Furthermore, the patient's family had a history of liver cancer. After antiviral therapy, the HBV load was undetectable, and the titer of e antigen gradually decreased, indicating that antiviral therapy was feasible for this patient. The patient had no hepatitis symptoms or signs during treatment, and his alanine aminotransferase level was normal. Further research is needed to determine whether these indicators, such as serum HBV DNA, e-antigen status, and virus mutation, can be used as an antiviral therapeutic indicator in OBI.

After HBV infection, the virus genome remains in host hepatocytes and can reactivate. Common triggers include inappropriate antiviral drug withdrawal and the use of immunosuppressive therapies. The reactivation of HBV in this patient could be attributed to the untimely discontinuation of antiviral medications. In this case, drug withdrawal occurred twice. The first occurred in July 2019, resulting in a resurgence of the virus. The second withdrawal resulted in chronic hepatitis B with HBeAg positivity from OBI. As a result, improper medication withdrawal may result in disease progression. We also speculated whether long-term untreated OBI with positive HBeAg would more likely to result in the occurrence of adverse consequences such as liver cirrhosis and HCC, which has been reported in OBI with HBeAg negativity (Perisetti et al., 2021; Huang et al., 2022).

Whether HBV reactivation was caused by latent virus replication or a new HBV subtype infection is unknown. Given the coexistence of wild (G1896) and mutant (A1896) types of pre-C in the patient in August 2021, it is reasonable to assume that HBsAg was caused by the reactivation of the latent virus, which was now dominated by wild-type virus. Previous studies using nucleotide analog (NA) therapy demonstrated that the wild-type virus could replace pre-Core/BCP mutants during antiviral therapy (Cho et al., 2000; Lau et al., 2020). During the follow-up period, the patient may evolve from the coexistence of wild and mutant sequences to the sole wild-type virus. Assume, however, that the patient continues to discontinue antiviral therapy with increased mutant strains. In that case, subsequent follow-up visits may reveal negative HBeAg, which may not improve the disease. Furthermore, because the S gene's open reading frame partially overlaps with that of the reverse transcriptase (RT) gene, mutations in the S gene cause antiviral resistance mutations to appear in the RT domain. The variation of S gene not only Strongly Affect HBsAg Detection (Kuhns et al., 2021; Wang et al., 2021), but also leads to HBV drug resistance and immune escape (Delfino et al., 2021). Drug resistance must be considered when a patient experiences a poor curative effect during a follow-up visit.

Finally, in our case, antiviral therapy effectively inhibited viral replication in OBI with positive HBeAg and detectable serum HBV DNA. Nonetheless, abrupt drug discontinuation can hasten the progression of the disease. It is still debatable whether OBI requires antiviral therapy. Long-term observation of large cohorts is needed to elucidate the potential impact of antiviral treatment on OBI. We recommend NA antiviral therapy for OBI patients with positive HBeAg and high serum HBV DNA, especially for patients with a family history of chronic hepatitis B and/or HCC. Meanwhile, detection of HBV gene variation and drug resistance genes should be strengthened both before and during treatment to optimize

antiviral therapy and efficacy. Strengthening patient compliance education is helpful to guarantee the curative effect of antiviral therapy.

## DATA AVAILABILITY STATEMENT

The original contributions presented in the study are included in the article/supplementary material, further inquiries can be directed to the corresponding author.

## ETHICS STATEMENT

Ethical review and approval was not required for the study on human participants in accordance with the local legislation and institutional requirements. Written informed consent for participation was not required for this study in accordance with the national legislation and the institutional requirements.

## AUTHOR CONTRIBUTIONS

All authors listed have made a substantial, direct, and intellectual contribution to the work and approved it for publication.

## FUNDING

This work was supported by a grant from the Medical Science and Technology Fund of Chongqing Municipal Public Health Bureau (Grant No. 2015ZDXM008).

## REFERENCES

Cho, S. W., Hahm, K. B., and Kim, J. H. (2000). Reversion from precore/core promoter mutants to wild-type hepatitis B virus during the course of lamivudine therapy. *Hepatology* 32, 1163–1169. doi: 10.1053/jhep.2000.19618

de Almeida, N.A.A., and de Paula, V.S. (2021). Occult hepatitis B virus (HBV) infection and challenges for hepatitis elimination: a literature review. *J. Appl. Microbiol.* doi: 10.1111/jam.15351 [Epub ahead of print]

Delfino, C. M., Giorgio, M., García, G., Puch, S. S., Outon, E., and Mathet, V. L. (2021). Drug-resistant and immune-escape hepatitis B virus mutants, occult hepatitis B infection and coinfections in public hospital patients from Argentina. *Virus Genes* 57, 327–337. doi: 10.1007/s11262-021-01850-z

Han, Z., Liu, Y., Pan, J., Bi, Y., Liu, J., and Zhou, Y. H. (2015). Occult hepatitis B virus infection with positive hepatitis B e antigen. *Clin. Chim. Acta* 438, 266–268. doi: 10.1016/j.cca.2014.09.007

Huang, Y., Li, W., Hu, H.-T., Ruan, S.-M., Xian, M.-F., Xie, X.-Y., et al. (2022). Contrast-enhanced US diagnostic algorithm of hepatocellular carcinoma in patients with occult hepatitis B. *Abdom. Radiol.* 47, 608–617. doi: 10.1007/s00261-021-03343-x

Kuhns, M. C., Holzmayer, V., Anderson, M., McNamara, A. L., Sauleda, S., Mbanya, D., et al. (2021). Molecular and serological characterization of hepatitis B virus (HBV)-positive samples with very low or undetectable levels of HBV surface antigen. *Viruses* 13:2053. doi: 10.3390/v13102053

Lau, K. C. K., Joshi, S. S., Mahoney, D. J., Mason, A. L., van Marle, G., Osiowy, C., et al. (2020). Differences in HBV replication, APOBEC3 family expression, and inflammatory cytokine levels between wild-type HBV and pre-core (G1896A) or basal core promoter (A1762T/G1764A) mutants. *Front. Microbiol.* 11:1653. doi: 10.3389/fmicb.2020.01653

Mak, L.-Y., Wong, D. K.-H., Pollicino, T., Raimondo, G., Blaine Hollinger, F., and Yuen, M.-F. (2020). Occult hepatitis B infection and hepatocellular carcinoma: epidemiology, virology, hepatocarcinogenesis and clinical significance. *J. Hepatol.* 73, 952–964. doi: 10.1016/j.jhep.2020.05.042

Onorato, L., Pisaturo, M., Camaioni, C., Grimaldi, P., Codella, A. V., Calò, F., et al. (2021). Risk and prevention of hepatitis B virus reactivation during immunosuppression for non-oncological diseases. *J. Clin. Med.* 10:5201. doi: 10.3390/jcm10215201

Pattullo, V. (2015). Hepatitis B reactivation in the setting of chemotherapy and immunosuppression—prevention is better than cure. *World J. Hepatol.* 7, 954–967. doi: 10.4254/wjh.v7.i7.954

Perisetti, A., Goyal, H., Yendala, R., Thandassery, R. B., and Giorgakis, E. (2021). Non-cirrhotic hepatocellular carcinoma in chronic viral hepatitis: current insights and advancements. *World J. Gastroenterol.* 27, 3466–3482. doi: 10.3748/wjg.v27.i24.3466

Raimondo, G., Locarnini, S., Pollicino, T., Levrero, M., Zoulim, F., Lok, A. S., et al. (2019). Update of the statements on biology and clinical impact of occult hepatitis B virus infection. *J. Hepatol.* 71, 397–408. doi: 10.1016/j.jhep.2019.03.034

Shih, C.-A., and Chen, W. C. (2021). Prevention of hepatitis B reactivation in patients requiring chemotherapy and immunosuppressive therapy. *World J. Clin. Cases* 9, 5769–5781. doi: 10.12998/wjcc.v9.i21.5769

Terrault, N. A., Lok, A. S. F., McMahon, B. J., Chang, K. M., Hwang, J. P., Jonas, M. M., et al. (2018). Update on prevention, diagnosis, and treatment of chronic hepatitis B: AASLD hepatitis B guidance. *Hepatology* 67, 1560–1599. doi: 10.1002/hep.29800

Wang, H., Liao, F., Xie, J., Gao, W., Wang, M., Huang, J., et al. (2021). E2 site mutations in S protein strongly affect hepatitis B surface antigen detection in the occult hepatitis B virus. *Front. Microbiol.* 12:664833. doi: 10.3389/fmicb.2021.664833

Zhou, Y. H., Zhou, J., Li, L., Bi, Y., Liu, Y., Pan, J., et al. (2009). A novel hepatitis B virus mutant coexisting with wild type virus in a carrier with negative HBsAg yet positive HBeAg and anti-HBs. *J. Clin. Virol.* 46, 363–366. doi: 10.1016/j.jcv.2009.09.012

**Conflict of Interest:** The authors declare that the research was conducted in the absence of any commercial or financial relationships that could be construed as a potential conflict of interest.

**Publisher's Note:** All claims expressed in this article are solely those of the authors and do not necessarily represent those of their affiliated organizations, or those of the publisher, the editors and the reviewers. Any product that may be evaluated in this article, or claim that may be made by its manufacturer, is not guaranteed or endorsed by the publisher.

*Copyright © 2022 Yuan, Peng, Xia, He, Qiu and Yao. This is an open-access article distributed under the terms of the Creative Commons Attribution License (CC BY). The use, distribution or reproduction in other forums is permitted, provided the original author(s) and the copyright owner(s) are credited and that the original publication in this journal is cited, in accordance with accepted academic practice. No use, distribution or reproduction is permitted which does not comply with these terms.*

frontiers in Microbiology

ORIGINAL RESEARCH
published: 10 March 2022
doi: 10.3389/fmicb.2022.836831

# Human Immunodeficiency Virus-1 Latency Reversal *via* the Induction of Early Growth Response Protein 1 to Bypass Protein Kinase C Agonist-Associated Immune Activation

*Lilly M. Wong[1], Dajiang Li[1], Yuyang Tang[1], Gema Méndez-Lagares[2], George R. Thompson III[2], Dennis J. Hartigan-O'Connor[2], Satya Dandekar[2] and Guochun Jiang[1,3]**

[1] UNC HIV Cure Center, Institute of Global Health and Infectious Diseases, The University of North Carolina at Chapel Hill, Chapel Hill, NC, United States, [2] Department of Medical Microbiology and Immunology, University of California, Davis, Davis, CA, United States, [3] Department of Biochemistry and Biophysics, The University of North Carolina at Chapel Hill, Chapel Hill, NC, United States

OPEN ACCESS

**Edited by:**
*Chunfu Zheng,*
*University of Calgary, Canada*

**Reviewed by:**
*Huanzhang Zhu,*
*Fudan University, China*
*Jinbiao Liu,*
*Jinan University, China*

***Correspondence:**
*Guochun Jiang*
*Guochun_Jiang@med.unc.edu*

**Specialty section:**
*This article was submitted to Virology, a section of the journal Frontiers in Microbiology*

**Received:** *16 December 2021*
**Accepted:** *28 January 2022*
**Published:** *10 March 2022*

**Citation:**
*Wong LM, Li D, Tang Y, Méndez-Lagares G, Thompson GR III, Hartigan-O'Connor DJ, Dandekar S and Jiang G (2022) Human Immunodeficiency Virus-1 Latency Reversal via the Induction of Early Growth Response Protein 1 to Bypass Protein Kinase C Agonist-Associated Immune Activation. Front. Microbiol. 13:836831. doi: 10.3389/fmicb.2022.836831*

Human Immunodeficiency Virus-1 (HIV) remains a global health challenge due to the latent HIV reservoirs in people living with HIV (PLWH). Dormant yet replication competent HIV harbored in the resting CD4+ T cells cannot be purged by antiretroviral therapy (ART) alone. One approach of HIV cure is the "Kick and Kill" strategy where latency reversal agents (LRAs) have been implemented to disrupt latent HIV, expecting to eradicate HIV reservoirs by viral cytopathic effect or immune-mediated clearance. Protein Kinase C agonists (PKCa), a family of LRAs, have demonstrated the ability to disrupt latent HIV to an extent. However, the toxicity of PKCa remains a concern *in vivo*. Early growth response protein 1 (EGR1) is a downstream target of PKCa during latency reversal. Here, we show that PKCa induces EGR1 which directly drives Tat-dependent HIV transcription. Resveratrol, a natural phytoalexin found in grapes and various plants, induces *Egr1* expression and disrupts latent HIV in several HIV latency models *in vitro* and in CD4+ T cells isolated from ART-suppressed PLWH *ex vivo*. In the primary CD4+ T cells, resveratrol does not induce immune activation at the dosage that it reverses latency, indicating that targeting EGR1 may be able to reverse latency and bypass PKCa-induced immune activation.

**Keywords: HIV latency, protein kinase C, EGR1, kick and kill, HIV cure, immune response, HIV reservoir**

## INTRODUCTION

Integration of human immunodeficiency virus-1 (HIV) provirus in the human genome allows HIV to persist in resting CD4+ T cells in people living with HIV (PLWH), known as latent HIV reservoirs. Prolonged use of antiretroviral therapy (ART) mitigates progression of HIV infection; however, it is not a cure as it fails to eradicate latent HIV infected immune cells. Models indicate

that long-term ART would need to be sustained for a minimum of 60 years due to the inability to purge the reservoirs (Finzi et al., 1999; Crooks et al., 2015; Siliciano and Siliciano, 2015). Thus, the consequence of discontinuing ART leads to rapid viral rebound, usually within weeks. Therefore, current ART has no impact on the quiescent viral reservoirs due to the extremely low levels of HIV expressed in the immune cells. An approach to directly target latent HIV reservoirs is urgently needed.

A widely explored approach for HIV cure is "kick and kill," where small molecule agents, also known as latency reversal agents (LRAs), are used to stimulate HIV expression ("kick") for successive viral cytopathic effects or immune clearance ("kill") (Archin et al., 2012; Deeks, 2012). Epigenetic reprogramming at the HIV long terminal repeat (LTR) with histone deacetylase inhibitors (HDACi) and NF-κB activation with protein kinase C agonists (PKCa) constitute two of the major classes of LRAs (Abner and Jordan, 2019). Some HDACi such as Vorinostat, Romidepsin, and Panobinostat have advanced into clinical trials or in a clinic setting (Archin et al., 2012; Tsai et al., 2016; Kroon et al., 2020; Rosas-Umbert et al., 2020). Archin et al. (2012) presented a proof-of-concept study for the use of Vorinostat in HIV-infected individuals where increased HIV RNA expression was found in eight participants after a single dose of Vorinostat, providing the first evidence of LRA *in vivo*. However, no reservoir reduction was observed (Archin et al., 2012; Tsai et al., 2016). A study by Kroon et al. (2020) indicated that the time for viral rebound to occur and the overall size of the latent HIV reservoir may not be impacted by Vorinostat administration in ART-suppressed HIV-positive individuals. Previous studies involving PKCa portray robust latency reversal compared with HDACi *in vitro* (Jiang et al., 2014; Stoszko et al., 2019) and, to a lesser extent, *ex vivo* (Jiang et al., 2014, 2015; Pandelo Jose et al., 2014; Darcis et al., 2015; Cary et al., 2016; Spivak and Planelles, 2018; Yang et al., 2019). PKCa and their derivatives have been tested in several pre-clinic models (Gutierrez et al., 2016; Marsden et al., 2017, 2020; Jiang et al., 2019; Okoye et al., 2022), indicating their potential for latency reversal *in vivo*. Some PKCa such as FDA-approved ingenol compounds (PEP005, trademark name: PICATO for topical use) showed potency in the reactivation of latent HIV after topical application to the skin of PLWH on ART (Jiang et al., 2019). However, an initial double-blind Phase 1 trial of bryostatin-1 failed to reactivate latent HIV in ART-suppressed PLWH (Gutierrez et al., 2016). While the low dosages administered were safe in conclusion, further studies are needed to evaluate whether a higher dosage would be effective and safe (Gutierrez et al., 2016). These initial studies indicate that although PKCa are candidates for latency reversal, the use of this group of small molecular agents remains a concern as many of the LRAs act upon host cells and may cause toxicity of immune cells *in vivo* at the dosages that reverse latency (Pardons et al., 2019). PKCa are strong transcriptional activators of PKC/NF-κB, and in turn can cause a cascade of signaling events as an undesired immune response (i.e., T-cell activation and inflammation) (Jiang et al., 2014). Therefore, evaluating the basic mechanism of action by PKCa is necessary to potentiate the use of PKCa *in vivo*. Studies are underway to pursue new derivatives of PKCa, such as ingenol compounds GSK445A and SUW133, to efficiently disrupt latent HIV for eradication with minimal side effects and immune activation *in vivo* (Kim et al., 2022; Okoye et al., 2022), which support the concept that appropriate PKCa can be achieved by synthesizing new PKCa family compounds for the cure of HIV (Wender et al., 2008; Beans et al., 2013; Marsden et al., 2017, 2018, 2020; Jiang et al., 2019; Okoye et al., 2022). Recently, it was discovered that the family compounds of PKCa trigger a conserved downstream signaling of EGR pathway to induce HIV transcription from latency, which was significantly dampened when EGR proteins were knocked down (Vemula et al., 2017). This indicates that EGR protein is the effector of PKCa, in which EGR signaling is an essential molecular mechanism of latency reversal elicited by the family of PKCa. This may represent an alternative approach to disrupt latent HIV. Nevertheless, it is unknown whether EGR proteins directly regulate HIV transcription and whether a direct induction of EGR disrupts latent HIV without the induction of the subsequent immune activation. In this study, we aimed to address these important questions for the role of EGR1 in HIV cure.

## RESULTS

### Early Growth Response Protein 1 Is Highly Correlated With Human Immunodeficiency Virus-1 Transcription or Latency Reversal Induced by Families of Protein Kinase C Agonists

We first investigated whether EGR1 was associated with HIV transcription. J-Lat A1, Jurkat cell model of HIV latency, was treated with several PKCa (phorbol 12-myristate 13-acetate (PMA), prostratin, bryostatin-1 and PEP005) at optimized concentrations (Darcis et al., 2015; Jiang et al., 2015) to determine if there was any enhancement of EGR1 expression in HIV reactivated cells (**Figure 1**). Consistent with previous observations (Pandelo Jose et al., 2014; Darcis et al., 2015; Jiang et al., 2015; Vemula et al., 2017), we found that the commonly used PKCa induced robust HIV expression (up to 1,000-fold) in the J-Lat model of HIV latency whereas at the same time, we observed thousands-fold change in *EGR1* expression (**Figures 1A,B**). Furthermore, we examined the expression of Target of EGR1 (TOE1), which has been characterized as a direct downstream target of EGR1 and functions as an inhibitor of HIV replication (Sperandio et al., 2015). Surprisingly, *TOE1* expression did not change across the PKCa-treated cells, indicating that TOE1 may not be directly related with EGR1 even though EGR1 was highly induced by PKCa in the Jurkat cells (**Figure 1C**). To confirm whether EGR1 protein expression was indeed induced by PKCa, whole protein lysates were collected from J-Lat A1 cells that were treated with PEP005, prostratin or bryostatin-1 where PEP005 and prostratin had induced the highest EGR1 expression while bryostatin-1 had minimal impact on EGR1 expression (**Figure 1D**). Furthermore, we conducted a linear regression analysis of EGR1 expression compared to HIV reactivation where the observed $R_2$ value is 0.637 with $p = 0.0175$, suggesting that EGR1 is highly correlated to the

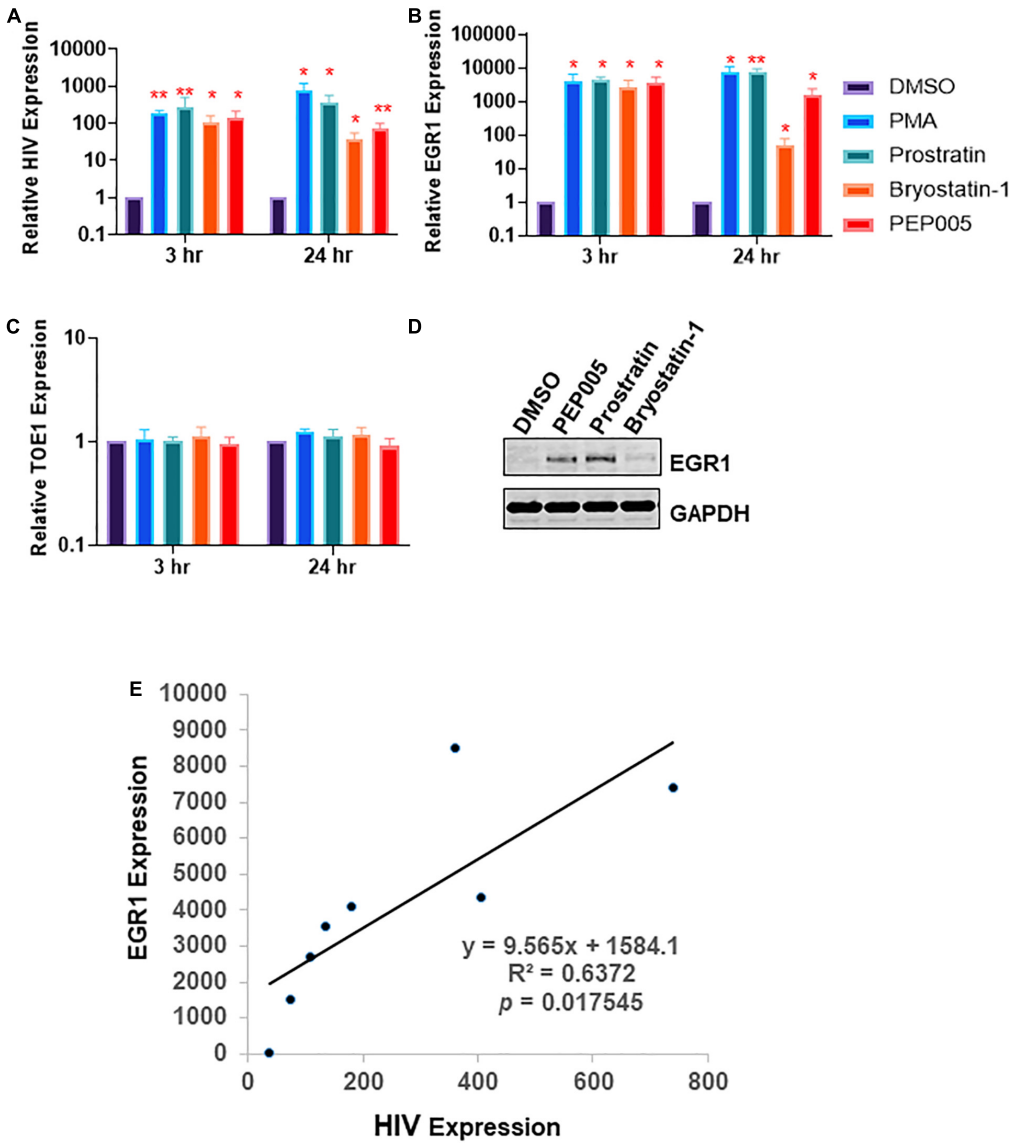


**FIGURE 1 |** Protein Kinase C agonist (PKCa) response gene, *early growth response protein 1* (*EGR1*), is associated with human immunodeficiency virus-1 (HIV) transcription or latency reversal. **(A–C)** J-Lat A1 cells were treated with 50 ng/mL phorbol 12-myristate 13-acetate (PMA), 2 μM prostratin, 10 nM bryostatin-1 or 12 nM PEP005. Cells were harvested 3 and 24 h post-treatment. The expression of HIV, *EGR1* or *TOE* was analyzed by RT-qPCR ($n = 3$). $^{*}p < 0.05$; $^{**}p < 0.01$, compared with control treatment and analyzed by two-tailed *T*-test. Data are represented as mean ± SEM. **(D)** J-Lat A1 cells were treated with 5 μM prostratin, 20 nM bryostatin-1 or 24 nM PEP005. Cells were harvested 4 h post-treatment with PKCa and subjected to Western blot to measure EGR1 protein expression. **(E)** *EGR1* expression and HIV reactivation were plotted to determine linear regression.

triggered HIV reactivation (**Figure 1E**). EGR1 may serve as the common downstream factor to induce HIV latency reversal prompted by the family of PKCa as discovered previously (Vemula et al., 2017).

If EGR1 is involved in latency reversal, it should be associated with HIV transcription. We tested this hypothesis in a previously reported primary CD4+ T cell model of HIV latency (Bradley et al., 2018). In brief, CD4+ T cells were isolated from HIV-negative donors and were subsequently infected with GFP-tagged NL4.3Δ6 HIV. A few days post-infection, the GFP+ positive cells were sorted by flow cytometry where the GFP+ cells were continued to culture. Then, a second flow cytometry was performed to selectively isolate GFP-negative cells. These GFP-negative HIV genome containing cells represent the latently infected CD4 + T cells where HIV expression can be reactivated by α-CD3/CD28 beads. After the beads were removed, GFP expression waned, indicating the reestablishment of the latent state (**Figure 2A**). In the process of HIV transcription, EGR1 expression was at its highest at 2 days post-stimulation with α-CD3/CD28 beads where the highest levels of HIV transcription was also observed. Then, it quickly diminished as HIV returned to its latent state (**Figure 2B**). These data are consistent to

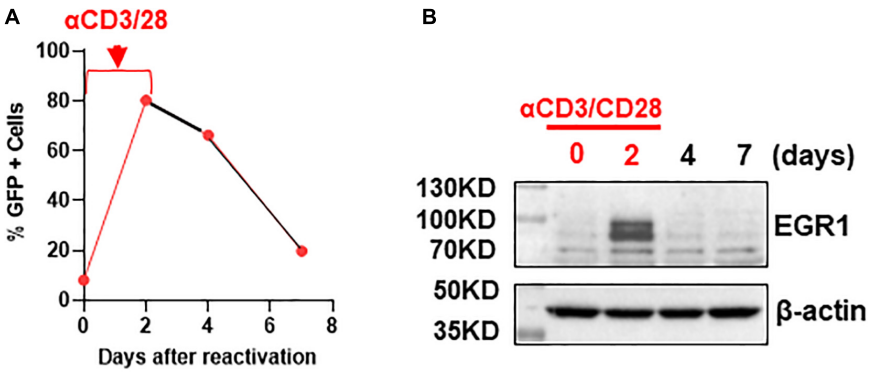


**FIGURE 2 |** Early growth response protein 1 protein is induced after T cell activation *via* αCD3/CD28 stimulation but waned when HIV re-entered the latent state. **(A)** Transcription of HIV in the primary CD4+ T cell model of HIV latency. The percentage of GFP positive cells was analyzed by flow cytometry at 0, 2, 4, and 7 days ($n = 3$). **(B)** EGR1 protein expression was analyzed in the primary T cell model of HIV latency during the activation of HIV and when HIV returned to latency where β-actin served as a loading control.

previous reports and suggest that EGR1 may be involved in HIV transcription.

## Early Growth Response Protein 1 Directly Induces Tat-Dependent Human Immunodeficiency Virus-1 Transcription

To see whether EGR plays a direct role in PKCa-induced HIV latency reversal or HIV transcription, we knocked down EGR1 by its specific siRNA in TZM-bl reporter cells. Relative *EGR1* expression compared to the control EGR1 siRNA decreased 2.5-fold (**Figure 3A**). HIV expression was evaluated in the presence of PEP005, a PKCa to reactivate latent HIV and induce EGR1 (**Figures 1**, **2**), where *EGR1* expression decreased 2.5-fold (**Figure 3B**). We wanted to determine whether Tat-driven transcription is directly regulated by EGR1 expression. *EGR1* was knocked down in the TZM-bl cells where cells were transfected with plasmid encoding HIV Tat afterward. Transfection of HIV Tat highly induced HIV transcription, which was significantly inhibited when *EGR1* was knocked down (**Figure 3C**). In the same model, TZM-bl cells were transfected with plasmids encoding EGR1, Tat, or Tat plus EGR1 (**Figure 3D**). Notably, there was 8.6 fold increase of Tat-induced HIV transcription in the presence of EGR1 plasmids compared with cells transfected with Tat plasmids alone (**Figure 3D**). Taken together, our data suggest that EGR1 may directly participate in the transcriptional machinery. This may partially explain the role of EGR1 as a conserved downstream effector of PKCa during latency reversal.

## Resveratrol Induces *Early Growth Response Protein 1* Where Early Growth Response Protein 1 Is Recruited to Human Immunodeficiency Virus-1 Long Terminal Repeat to Reactivate Human Immunodeficiency Virus-1 From Latency

Our studies above point to an interesting concept: the induction of EGR1 may be able to drive HIV transcription from latency, which could bypass the undesired side effects PKCa may elicit (French et al., 2020). Resveratrol has been described as an inducer of EGR1, which is involved in HIV transcription (Krishnan and Zeichner, 2004). However, its underlying mechanism is unclear. To evaluate the potential of resveratrol as an EGR1 agonist (EGRa), we first tested its activity in several models of HIV latency. We tested several concentrations of resveratrol and observed *EGR1* induction in a dose-dependent manner in J-Lat A1 cells (**Figure 4A**). Importantly, this also induced EGR1 enrichment at the HIV LTR (**Figure 4B**). GFP expression, a measure of HIV transcription at the protein level, increased in a dose-dependent manner (**Figures 4C,F**). In both J-Lat A1 and 2D10 cell models of HIV latency, no toxicity or minimal impact of cell proliferation was observed even at the highest tested concentration (60 μM) (**Figures 4D,E,G,H**). These data suggest that EGR1, after induction by resveratrol, may serve as a HIV transcription factor after its recruitment to HIV promoter to induce HIV transcription and/or latency reversal.

## Resveratrol Serves as a Stimulator to Enhance Human Immunodeficiency Virus-1 Transcription Induced by Other Latency Reversal Agents

Current LRAs alone may not be potent enough to disrupt latent HIV and/or present the viral antigen for the subsequent killing of HIV+ immune cells (Margolis et al., 2016; Hosmane et al., 2017; Dashti et al., 2020). To this end, we then decided to test whether resveratrol enhances HIV reactivation when combined with other known LRAs such as AZD5582, SAHA, OTX-015 and PEP005. We focused on these LRAs because: (1) it has been shown that PKCa has the best synergy with bromodomain inhibitors to disrupt latent HIV (Darcis et al., 2015; Jiang et al., 2015); (2) OTX-015, a bromodomain inhibitor, is able to disrupt latent HIV, and is under clinical trials for the cure of cancer (Lu et al., 2016; Yin et al., 2020); (2) SAHA and crotonate (NaCr) are epigenetic inducers

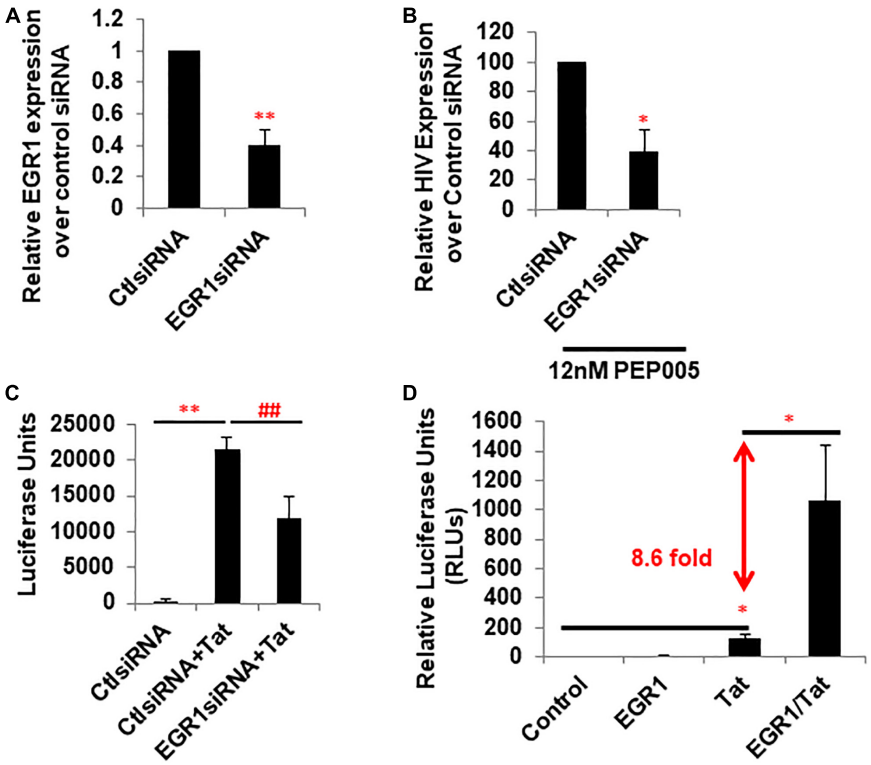


**FIGURE 3 |** Expression of EGR1 is associated with Tat-dependent HIV transcription. **(A)** TZM-bl cells were transfected with control or EGR1 siRNA. Cells were harvested 48 h post-knockdown and subjected to RT-qPCR ($n = 3$). $^{**}p < 0.01$, compared with control siRNA and analyzed by two-tailed *T*-test. Data are represented as mean ± SEM. **(B)** TZM-bl cells were transfected with control or EGR1 siRNA. Then, these cells were treated with 12 nM PEP005 48 h post-knockdown. Cells were harvested 24 h post-LRA treatment and subjected to RT-qPCR ($n = 3$). $^{*}p < 0.05$, compared with control siRNA and analyzed by two-tailed *T*-test. Data are represented as mean ± SEM. **(C)** TZM-bl cells were transfected by control or EGR1 siRNA in panel **(B)**, which were then transfected with empty vector or pcDNA-flag-Tat. Cells were harvested after 48 h and subjected to luciferase assay. $^{**}p < 0.01$, compared with control siRNA and analyzed by two-tailed *T*-test. $^{\#\#}p < 0.01$, compared with control siRNA with Tat and analyzed by two-tailed *T*-test. Data are represented as mean ± SEM. **(D)** TZM-bl cells were transfected with empty vector, pcDNA3-EGR1, pcDNA-Flag-Tat, or in combination. Cells were harvested 24 h post-transfection and subjected to luciferase assay. $^{*}p < 0.05$, compared with control siRNA and analyzed by two-tailed *T*-test.

(Archin et al., 2012; Jiang et al., 2018). SAHA and other HDACi have been tested in a clinic and/or pre-clinic setting; (3) Unlike PKCa-driven canonical NF-κB (cNF-κB) signaling, AZD5582 is a new generation of LRA that drives non-canonical NF-κB (ncNF-κB) signaling activation which displayed potential as a LRA in animal models (Nixon et al., 2020). We aimed to see whether a robust enhancement of latency reversal can be achieved. In order to achieve optimal latency reversal without triggering cellular toxicity, 40 μM of resveratrol was used during the combination treatment (**Figure 4**). Overall, we observed the enhancement of HIV transcription in most of those combinations compared with single LRA, except for PEP005 in combination with resveratrol in J-Lat A1 and NaCr in 2D10 cells (**Figures 5A,D**). No toxicity was observed in either J-Lat A1 or 2D10 cells (**Figures 5C,E**). When analyzed with Bliss independence assay, among all the other combinations, only the combination of AZD5582 with resveratrol showed a synergy in both J-Lat A1 and 2D10 cell models of HIV latency (**Figures 5D,F**). These data further support an idea that combination treatment may be better to induce HIV from latency where the combination of resveratrol with the activation of ncNF-κB by AZD5582 displays the optimal latency reversal.

## Resveratrol Induces Human Immunodeficiency Virus-1 Transcription in the Primary CD4+ T Cells Isolated From Antiretroviral Therapy-Suppressed People Living With Human Immunodeficiency Virus-1

Often times, LRAs can disrupt latent HIV *in vitro* but fails to recapitulate in patient cells *ex vivo* and/or *in vivo*, reflecting the extreme difficulty to eradicate HIV reservoirs in patients (Grau-Exposito et al., 2019). To evaluate the potential of resveratrol as an EGRa, we continued to test its activity in the primary CD4+ T cells isolated from PLWH receiving ART (**Table 1**). We aimed to test both its activity alone and in combination with AZD5582 since only the combination of resveratrol with AZD5582 showed synergy in both of the HIV latency models *in vitro,* compared with other combinations (**Figure 5**). We found that resveratrol

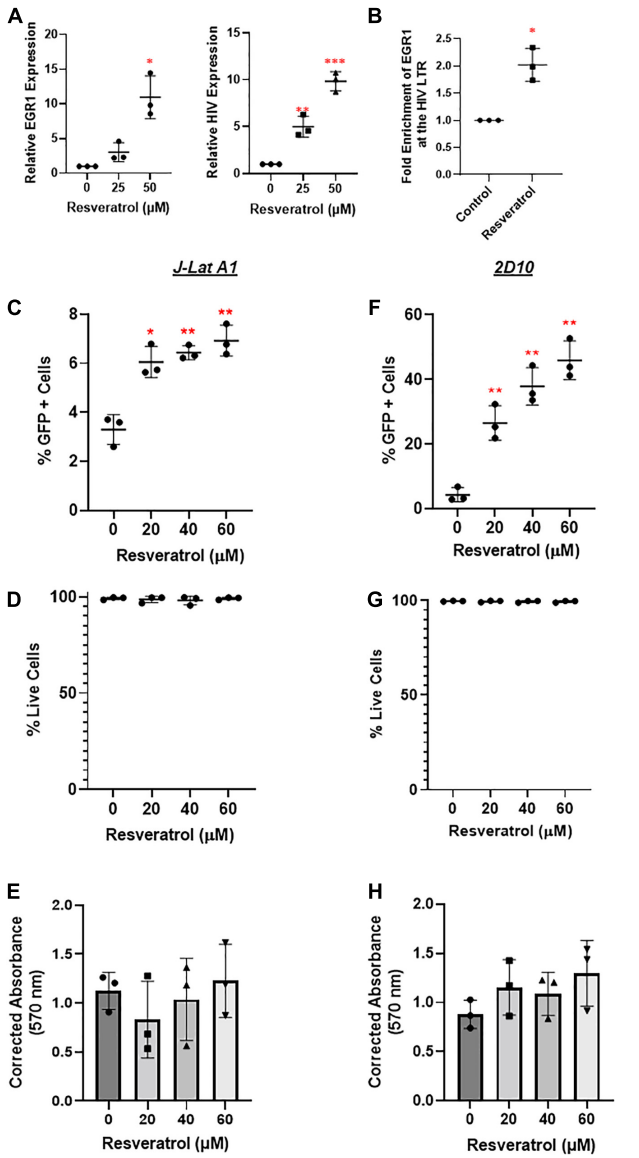


**FIGURE 4 |** Resveratrol induces *EGR1* expression and reactivates latent HIV *in vitro*. **(A)** J-Lat A1 cells were treated with resveratrol at 25 and 50 μM. Cells were harvested for RT-qPCR analysis ($n = 3$) 24 h post-treatment. $^{*}p < 0.05$; $^{**}p < 0.01$, $^{***}p < 0.001$ compared with control treatment and analyzed by two-tailed *T*-test. **(B)** J-Lat A1 cells were treated with resveratrol at 40 μM for 24 h. Cells were harvested and cross-linked with 1% formaldehyde to prepare chromatin. ChIP assay was performed with control IgG and anti-EGR antibodies. The enrichment of EGR1 at the HIV promoter was measured by SYBR green PCR with the specific primers targeting HIV long terminal repeat (LTR) region. $^{*}p < 0.05$; compared with control treatment and analyzed by two-tailed *T*-test. J-Lat A1 **(C–E)** and 2D10 **(F–H)** cells were treated with resveratrol (20, 40, and 60 μM). The percentage of GFP-positive cells and cell viability were analyzed by flow cytometry 24 h post-treatment while the cell proliferation was measured by 3-(4,5-dimethylthiazol-2-yl) -2,5-diphenyltetrazolium bromide (MTT) assay. $^{*}p < 0.05$; $^{**}p < 0.01$, compared with control treatment and analyzed by two-tailed *T*-test ($n = 3$).

alone was able to induce HIV transcription from latency in 4 of 6 samples while AZD5582 alone also disrupted latent HIV in 4 of 6 samples. Although PMA/ionomycin is among one of the more potent LRAs, it failed to induce HIV transcription in 2 of 6 samples. Different from latency models *in vitro*, combination treatment only enhanced latency reversal in 2 of 6 samples of primary CD4 + T cells isolated from PLWH. These data suggest that EGRa may be able to induce HIV transcription from latency in some, but not all, of the patient immune cells. Different from *in vitro* cell line model of latency, less samples achieved enhanced latency reversal. These observations further strengthen the idea that the latent HIV is extremely hard to disrupt and CD4 + T cells from PLWH may establish latency differently (**Figure 6**).

## Resveratrol Does Not Induce Immune Activation in the Primary CD4+ T Cells Isolated From Human Immunodeficiency Virus-1 Negative Donors

Resveratrol may be able to disrupt latent HIV *in vitro* and *ex vivo* (**Figures 3**, **6**). We next decided to examine its impact in immune activation. We evaluated this in the CD3+, CD4+ and CD8+ subsets of T cells in the PBMCs from HIV negative donors (**Figure 7**). We found that resveratrol did not change the percentage of the CD3+, CD4+, or CD8+ T cells, nor did it trigger CD69 and HLA-DR expression across these cells. PD-1 expression was unchanged in these resveratrol-treated cells compared to control-treated cells. These data suggest that resveratrol may not significantly induce immune activation.

# DISCUSSION

Current strategies of HIV cure are faced with the challenge of latent HIV reservoirs, which are extremely difficult to disrupt. "Kick and kill" flushes out the hidden HIV from the latently infected CD4+ T cells for immune clearance (Deeks, 2012). Among the currently available and highly active LRAs are PKCa (Wender et al., 2008; DeChristopher et al., 2012; Jiang et al., 2015; Cary et al., 2016; Lu et al., 2016; Wang et al., 2017). However, there remains concerns of toxicity when using PKCa due to the potential for cytokine storms induced by cNF-κB activation, indicating a need to further study the mechanisms of action involved in PKCa. Due to these concerns, alternative approaches are being pursued, including IAP inhibitors to activate ncNF-κB signaling (Nixon et al., 2020; Wong and Jiang, 2021; Li et al., 2022), synthesis of a new generation of PKCa through analog development (Wender et al., 2006; Jiang et al., 2014; Marsden et al., 2018; Okoye et al., 2022), or exploiting Chinese traditional medicine such as Kansui (Jiang et al., 2014; Cary et al., 2016; Wang et al., 2017). Here, we evaluated an alternative approach to circumvent cNF-κB activation by PKCa by directly activating its downstream effector protein, EGR1, and assessed its related side effects of immune activation.

Previous studies have shown that EGR family proteins serve as the common downstream effectors of PKCa during its action to disrupt latent HIV (Vemula et al., 2017). EGR knockdown prevented robust latency reversal when treated with PKCa (Vemula et al., 2017). Therefore, it may be useful to find a compound that can induce EGR family protein

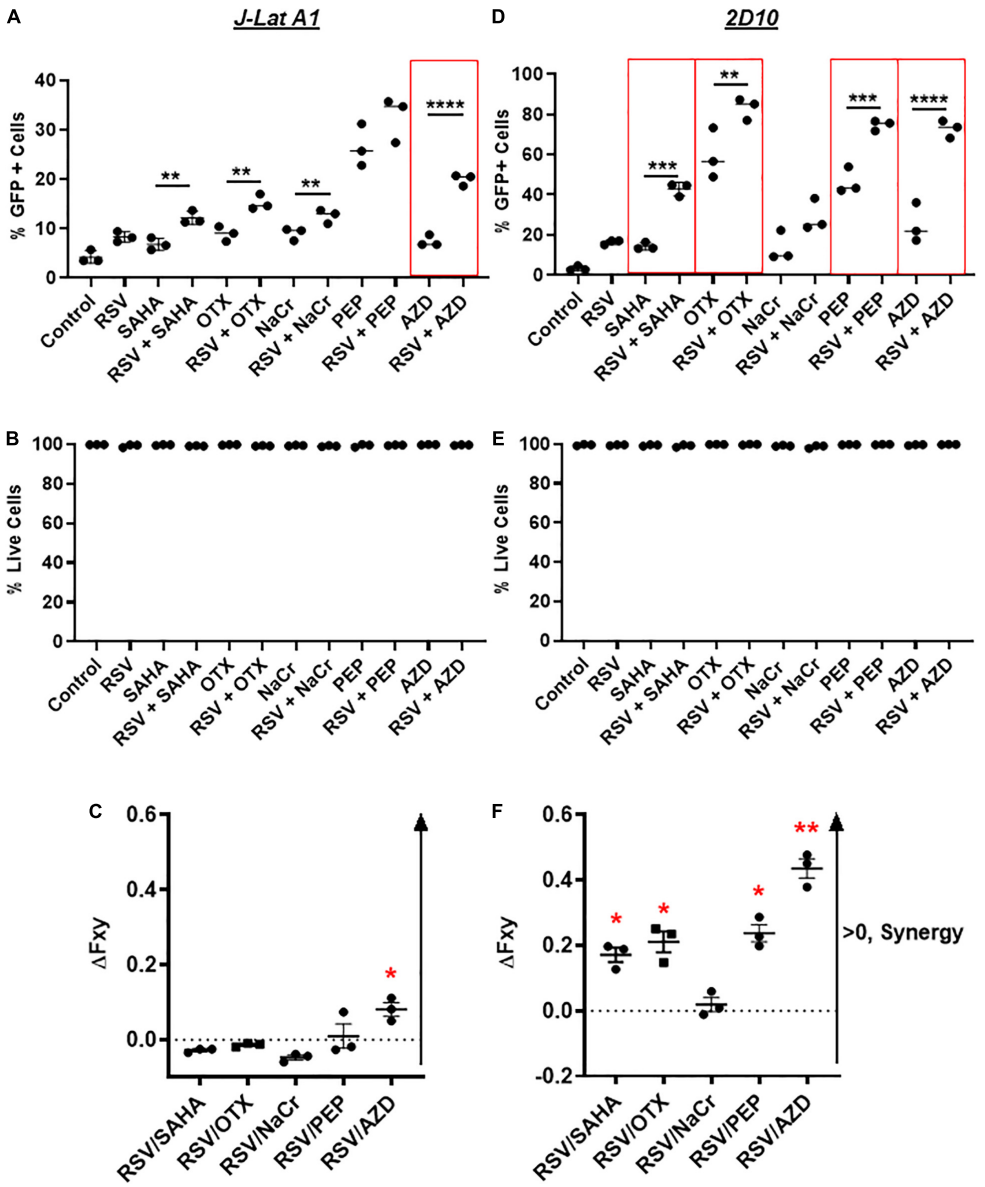


**FIGURE 5 |** Resveratrol enhances latency reversal in combination with AZD5582 and other established LRAs *in vitro*. J-Lat A1 cells **(A,B)** and 2D10 cells **(D,E)** were treated with 40 μM resveratrol (RSV), 500 nM suberoylanilide hydroxamic acid (SAHA), 10 nM OTX-015 (OTX), 40 mM crotonate (NaCr), 12 nM PEP005, 10 nM AZD5582 or in combination with 40 μM resveratrol. The percentage of GFP-positive cells and cell viability were analyzed by flow cytometry 24 h post-treatment ($n = 3$). $^{**}p < 0.01$; $^{***}p < 0.001$; $^{****}p < 0.0001$, compared with single LRA treatment and analyzed by One-way ANOVA. Bliss independence analysis was performed to evaluate the synergistic effect of resveratrol with other LRAs in comparison with the single LRA in J-Lat A1 **(C)** and 2D10 **(F)** cells. $^{*}p < 0.05$; $^{**}p < 0.01$, compared between faxyP and faxyO by two-tailed *t*-test analysis.

**TABLE 1 |** Patient information in this study.

| Patient ID | Age | Sex | Viral load (copies/ml) | CD4 count (cells/μl) | Duration of ART (years) | ART regimen |
|---|---|---|---|---|---|---|
| 1 | 33 | M | Undetectable | 854 | 1 | Triumeq |
| 2 | 60 | M | Undetectable | 742 | 19 | Triumeq |
| 3 | 33 | M | Undetectable | 681 | 21 | Odefsey |
| 4 | 39 | M | 30 | 826 | 20 | Triumeq |
| 5 | 68 | M | Undetectable | 376 | 31 | Triumeq |
| 6 | 56 | M | 47 | 412 | 25 | Ritonavir/ Darunavir/ Raltegravir |

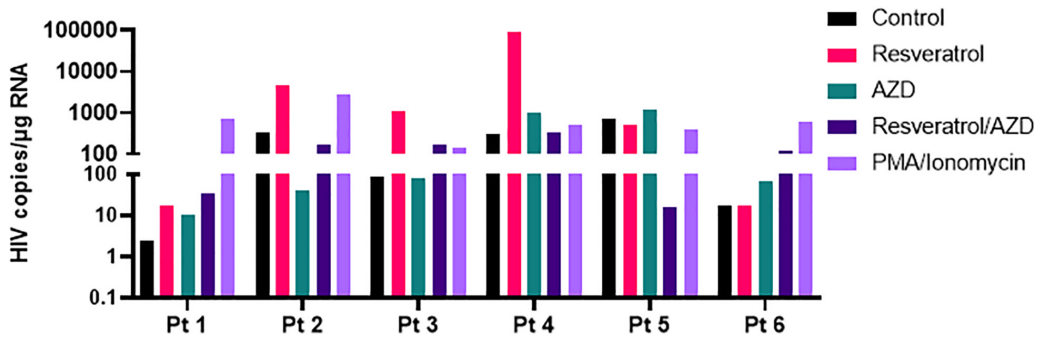


**FIGURE 6 |** Resveratrol reactivates latent HIV in the primary CD4+ T cells isolated from ART-suppressed PLWH. Total CD4+ T cells from ART-suppressed PLWH were treated with 40 μM resveratrol, 100 nM AZD5582 (AZD), 200 ng/mL PMA/2 μM ionomycin or in combination with RSV and AZD. Cells were harvested 24 h post-treatment, and copies of cell-associated HIV RNA were analyzed by ddPCR after normalization to the reference gene TBP.

to force HIV transcription from latency. Our data showed the strong correlation between *EGR1* expression and HIV reactivation in several cell models of HIV latency where active transcription was responsive to the peak EGR1 expression. When *EGR1* is knocked down, PEP005-induced HIV transcription or latency reversal was reduced. This is consistent to previous observations (Vemula et al., 2017). Importantly, our data indicate a direct role of EGR1 in HIV transcription since EGR1 was recruited to HIV LTR during latency reversal by EGRa. It can directly drive Tat-dependent HIV transcription. It is possible that EGR1 serves as a transcription factor to directly or indirectly interact with HIV LTR for its action. However, the underlying molecular mechanism is unclear, which warrants further investigation in future.

Resveratrol, a natural phytoalexin commonly found in red wine, has been used as a preventative measure for cardiovascular disease (Zeng et al., 2017; Cheng et al., 2020). Due to its naturally occurring state, others are investigating whether it could be repurposed for other disease treatments (Zeng et al., 2017). Interestingly, resveratrol has been implicated in the disruption of HIV latency; however, the mechanism is unclear, nor can it disrupt latent HIV in the patient-derived CD4+ T cells (Sampey et al., 2020). Our data showed that resveratrol induces *EGR1* expression and can reactivate latent HIV in several cellular models of HIV latency. This was observed in the majority of, but not all, the samples of the CD4 + T cells isolated from PLWH on ART. It has been shown that resveratrol induces histone acetylation to drive HIV transcription (Zeng et al., 2017). However, we failed to detect the activity of acetylation at H3K9 at the dosage of latency reversal in the Jurkat model of HIV latency (**Supplementary Figure 1**). It is worth pointing out that resveratrol may have some the other signaling targets, in addition to EGR1 (Tsai et al., 2017).

Together, our data support an idea that it is possible to develop an alternative approach to directly activate EGR1, the common downstream effector of PKCa, by EGRa to disrupt latent HIV, avoiding PKC/cNF-κB-induced immune activation. While EGR1 serves as an alternative therapeutic target to reverse HIV latency, studies are needed to develop a potent and specific inducer of EGR1 to reverse HIV latency in patient immune cells.

# MATERIALS AND METHODS

## Cell Culture

J-Lat A1 and 2D10 cell models of HIV latency were maintained in RPMI 1640 medium with 10% fetal bovine serum (Avantor, Allentown, PA, United States), 1% penicillin-streptomycin (Gibco, Waltham, MA, United States), and 1% L-glutamine (Gibco) in 37°C incubator with 5% $CO_2$. TZM-bl cells were maintained in DMEM medium with 10% fetal clone II serum (FCS II, Cytiva, Marlborough, MA, United States), 1% penicillin-streptomycin (Gibco), 1% HEPES (Gibco), and 1% L-glutamine (Gibco). TZM-bl is a HIV transcription/replication reporter cell line derived from HeLa where it constitutively expresses CD4, CXCR4, and CCR5. The HIV-Tat responsive TZM-bl cell line includes firefly luciferase reporter gene where the enzymatic output can be used to enlighten our understanding of HIV. These cell lines were provided by the National Institutes of Health (NIH) AIDS Reagent Program. The following reagents were used to test the reactivation of latent HIV: dimethyl sulfoxide (Sigma-Aldrich, St. Louis, MO, United States), phorbol 12-myristate 13-acetate (PMA) (Sigma-Aldrich), prostratin (Sigma-Aldrich), bryostatin-1 (Tocris Bioscience, Bristol, United Kingdom), PEP005 (Tocris Bioscience), resveratrol (RSV) (Celbiochem, San Diego, CA, United States) suberoylanilide hydroxamic acid (SAHA) (Santa Cruz, CA, United States), OTX-015 (Xcess Bioscience Inc., San Diego, CA, United States), crotonate (Sigma) and AZD5582 (ChemieTek, Indianapolis, IN, United States).

## Human Immunodeficiency Virus-1 Gene Expression Measurement by Real-Time Quantitative PCR

Cellular RNA was extracted by RNeasy mini kit (Qiagen). Extracted RNA was digested by DNase 1 (Invitrogen, Waltham, MA, United States) where first-strand cDNA was synthesized with SuperScript™ III Reverse Transcriptase (Invitrogen), dNTPs (Qiagen, Germantown, MA, United States), 0.1 M DTT (Invitrogen), Ribolock RNase Inhibitor (Thermo Scientific, Waltham, MA, United States) and Random Primers (Invitrogen) where it was carried out in Veriti™ 96-Well Thermal Cycler

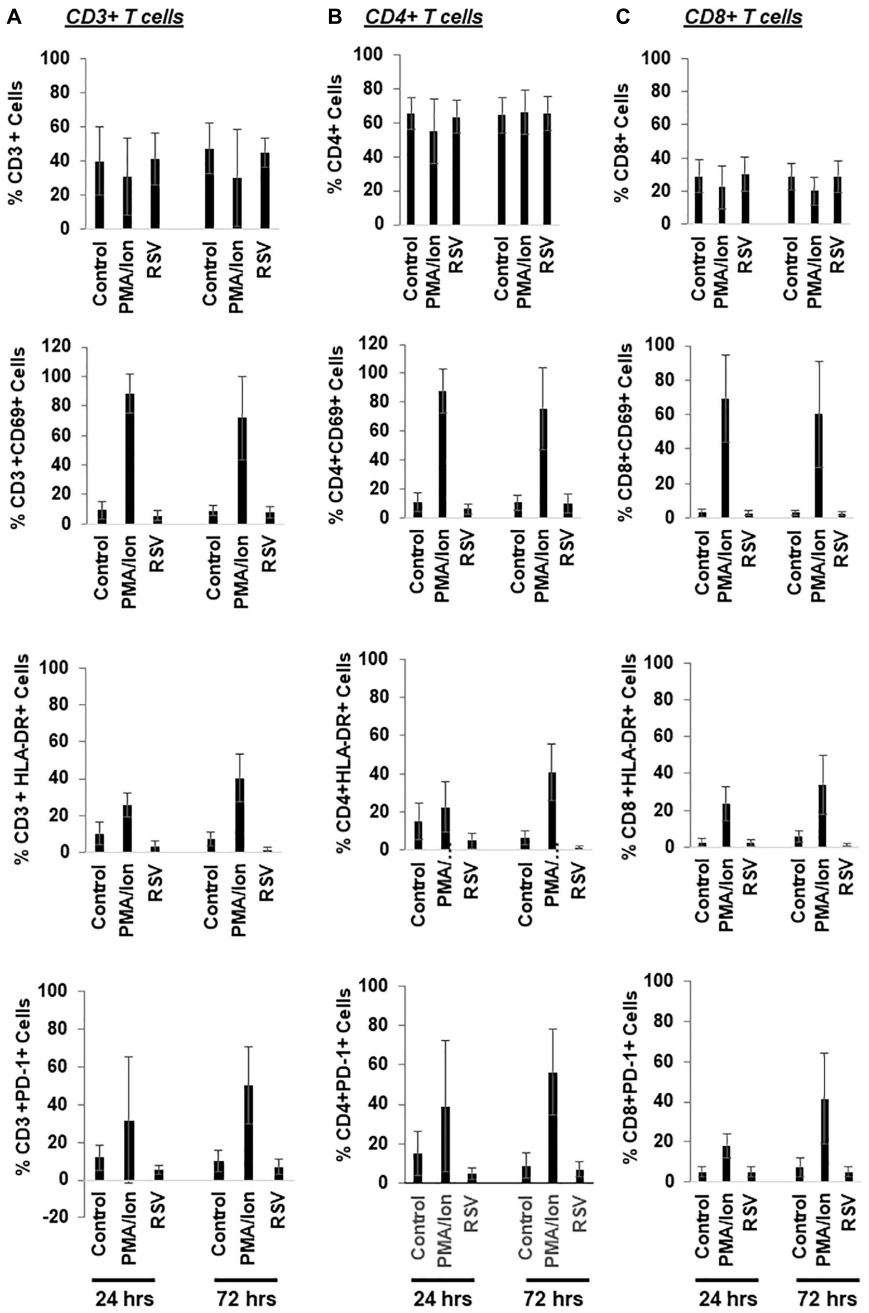


**FIGURE 7 |** Resveratrol bypasses immune activation in the primary CD4+ T cells isolated from HIV negative donors. **(A–C)** PBMCs from healthy donors were treated with DMSO, 40 μM resveratrol (RSV) or 200 ng/mL PMA plus 2 μM ionomycin for 24 or 72 h. Cells were then collected for flow cytometry analysis. Percentage of immune activation/suppression markers in T cell subsets (CD3+, CD4+, CD8+, and PD-1+) was analyzed by flowjo ($n$ = 5).

(Applied Biosystems, Waltham, MA, United States). HIV reactivation was quantified by Taqman quantitative RT-PCR (RT-qPCR) on the QuantStudio 5 system (Applied Biosystems) with HIV pre-gag primers/probe set as previously described (Jiang et al., 2015). Housekeeping genes, glyceraldehyde-3-phosphate dehydrogenase (GAPDH) and TATA-box binding protein (TBP) primers/probe sets were used for endogenous controls (Applied Biosystems).

## Evaluation of Human Immunodeficiency Virus-1 Reactivation by Flow Cytometry

Cells were cultured in 12-well plates at $1 \times 10^6$ cells/well. Cells were treated with LRAs. Twenty four hours post-treatment, cells were measured for endogenous GFP expression and cell viability by flow cytometry. Cells were stained with LIVE/DEAD Fixable Far Red stain (Invitrogen) to quantify cell viability by flow

cytometry. Flow cytometry results were analyzed by FlowJo™ v10.8 Software (BD Life Sciences, Franklin Lakes, NJ, United States).

## 3-(4,5-Dimethylthiazol-2-yl)-2,5-Diphenyltetrazolium Bromide Assay to Determine Cellular Viability/Proliferation After Latency Reversal

Cells were cultured in 96-well plates at $5 \times 10^4$ cells/well in 100 μl culture medium and treated with LRAs. To assess proliferation of the cells, CellTiter 96 Non-Radioactive Cell Proliferation Assay (Promega, Madison, MI, United States) was used. Twenty-four hours post-treatment, 15 μl of the Dye Solution was added to each well. The plate was incubated at 37°C for another 4 h. After incubation with the Dye Solution, 100 μl of the Solubilization Solution/Stop Mix was added to each well. One hour after addition of the Solubilization Solution/Stop Mix, the absorbance was measured at 570 nm wavelength with Synergy H1 (BioTek, Winooski, VY, United States). Absorbance values of samples were subtracted from the average reference absorbance values to determine the corrected absorbance value at 570 nm for each sample.

## Western Blot

Cells were lysed in RIPA buffer (Sigma-Aldrich) supplemented with 1X Protease/Phosphatase Inhibitor Cocktail (Cell Signaling, Danvers, MA, United States) and separated on 4–20% gradient SDS/PAGE (Novex). Proteins were transferred on nitrocellulose membranes and incubated with primary antibodies overnight at 4°C. The primary antibodies used for Western blotting were rabbit anti-EGR1 (#4153S; Cell Signaling), rabbit anti-GAPDH (#5174S; Cell Signaling) and rabbit anti-β-actin (#4970S; Cell Signaling). The secondary antibody used was HRP linked anti-rabbit IgG (#7074P2; Cell Signaling). Chemiluminescence (ECL) was used to detect protein abundance.

## Primary CD4+ T Cell Model of Human Immunodeficiency Virus-1 Latency

The primary CD4 + T cell model of latency was used as described (Bradley et al., 2018). Cells were reactivated with αCD3/CD28 beads for 2 days which were then harvested for protein in RIPA buffer (Sigma-Aldrich) supplemented with protease/phosphatase inhibitors cocktail (Cell Signaling). Protein expression of EGR1, GAPDH, or β-actin was evaluated. Cells were also harvested for the evaluation of GFP expression by flow cytometry at 0, 2, 4, and 7 days.

## Gene Knockdown by Small Interfering RNA and Transfections

Gene knockdown was achieved by Human EGR1 siRNA (E-006526-00-0005, Dharmacon) or scrambled control siRNAs (D-001910-10-20, Dharmacon) in TZM-bl cells. Cells were incubated with the siRNAs for 48 h where cells were then re-suspended in DMEM medium with 10% fetal bovine serum (VWR), 1% penicillin/streptomycin (Gibco), 1% L-glutamine (Gibco), and 1% HEPES (Gibco) for 24 h. Cells were harvested where RNA was extracted to check relative Egr1 expression in TZM-bl cells. To observe whether LRAs impact HIV expression in the case of Egr1 knockdown, cells were treated with 12 nM PEP005. RNA was extracted from the treated cells to check relative HIV expression. The expression plasmid, pcDNA-Flag-Tat, was transfected into TZM-bl cells after Egr1 knockdown. Cells were harvested for luciferase to determine impact. To determine whether Egr1 synergized with Tat, cells were transfected with pCDNA3.1, pcDNA3-Egr1, pcDNA-Flag-Tat, or in combination. Cells were harvested for luciferase activity.

## Luciferase Assays

Luciferase quantification was completed according to manufacturer's instructions for the Luciferase Assay System (Promega).

## Chromatin Immunoprecipitation

In total, $5 \times 10^6$ J-Lat A1 cells were treated with RSV. Twenty four hours post-treatment, protein-DNA bound in the cells were fixed in 1% formaldehyde for 10 min where the crosslinking was then quenched with 0.125 M glycine for 5 min. Cells were washed 3 times in cold PBS where cell pellets were stored in −80°C. Frozen, cross-linked pellets were re-suspended in ice-cold cell lysis buffer (Lysis Buffer 1) [50 mM HEPES–NaOH (pH 7.5); 140 mM NaCl; 1 mM EDTA; 10% glycerol; 0.5% NP-40; 0.25% Triton X100; protease/phosphatase inhibitor cocktail] for 10 min. After centrifugation (2,700 × *g*; 5 min; 4°C), the nuclear pellet was re-suspended in ice-cold nuclei swelling buffer (Lysis Buffer 2) [10 mM Tris–HCl (pH 8.0); 200 mM NaCl; 1 mM EDTA; 0.5 mM EGTA] for 5 min. After centrifugation (2,700 × *g*; 5 min; 4°C), the nuclear pellets were gently re-suspended in Lysis Buffer 3 [10 mM Tris–HCl (pH 8.0)]. After centrifugation (2,700 × *g*; 5 min; 4°C), the nuclei were re-suspended in 150 μl sonication buffer [0.1% SDS; 1 mM EDTA; 10 mM Tris–HCl (pH 8.0); protease/phosphatase inhibitor cocktail]. The nuclear lysates were sonicated with Bioruptor Pico (Diagenode) to obtain 300–1,000 bp chromatin. Nuclei fragments were collected and diluted in ChIP dilution buffer [2 mM EDTA; 5 mM Tris–HCl (pH 8.0); 1% NP-40; 150 mM NaCl; protease/phosphatase inhibitor cocktail). Approximately 100 μg of DNA was incubated overnight at 4°C with rabbit isotype control IgG (Cell Signaling) and rabbit anti-EGR1 (#4153S; Cell Signaling). Immune complexes were incubated with Dynabeads Protein G under rotation for 2 h at 4°C. Following washes with low salt wash buffer, high salt wash buffer, IP wash buffer and TE wash buffer, immunoprecipitation was eluted in 100 μl elution buffer (1% SDS, 0.1 M $NaHCO_3$). Immunoprecipitation was incubated with RNase A, proteinase K, then 5 M NaCl for reverse-crosslinking step overnight. DNA was recovered by ChIP Clean and Concentrator (Zymo, Irvine, CA, United States). Immunoprecipitated DNA was quantitated by SYBR green qPCR targeting HIV LTR region of HIV genome.

## Primary CD4$^+$ T Cell Isolation, Treatment, and Digital Droplet PCR Assays

Primary CD4+ T cells were isolated with EasySep Human CD4+ T cell enrichment kit (Stemcell Technologies; Vancouver, BC, Canada). Primary CD4+ T cells were plated at $1 \times 10^6$ cells/well and treated with DMSO, resveratrol (40 μM), AZD (100 nM), resveratrol and AZD and PMA (200 ng/ml)/ionomycin (2 μM). Twenty four hours post-treatment, cells were harvested for RNA extraction by RNeasy mini kit (Qiagen). RNA copy was measured by digital droplet PCR with pre-gag primer/probe sequences (Yukl et al., 2018). All participants were provided informed consent, and the study was approved by the UC Davis Institutional Review Board. The patient information has been included in **Table 1**.

## Bliss Independent Analysis

Synergy of resveratrol with other LRA in latency reversal was determined by the Bliss independence analysis (Laird et al., 2015; Jiang et al., 2018). % of GFP+ cells was normalized with that in PMA-treated cells. For drugs x and y, the predicted fraction in the cells with combination treatment (faxyP) is calculated as the equation faxyP = (fax + fay) − (fax) (fay). The observed combination value (FaxyO) is when the cells were treated by both drug x and drug y together. Then, Δfaxy, i.e., faxyO–faxyP, was defined as synergy if Δ faxy > 0, additive effect if Δ faxy = 0, or antagonism if Δ faxy < 0. Statistical significance was determined using a two-tailed *t*-test between faxyO and faxyP, where $^*p < 0.05$ was considered significant.

## Statistical Analysis

Statistical analysis was performed with Prism GraphPad 9.1. Means and standard errors were calculated for all data points from at least three independent experiments. Statistical significance was determined with One-way ANOVA or two-tailed student's *t*-test, where *p* value <0.05 was considered significant.

# DATA AVAILABILITY STATEMENT

The raw data supporting the conclusions of this article will be made available by the authors, without undue reservation.

# AUTHOR CONTRIBUTIONS

GJ conceived the study. LW, DL, and YT performed the experiments in latency models *in vitro and ex vivo*. GM-L and DH-O'C analyzed the phenotypes of primary T cell subsets. GT coordinated the patient blood samples. SD supported the initial study. LW and GJ assembled the data and wrote the manuscript. All authors contributed to the article, read, and revised initial draft and approved the manuscript.

# FUNDING

GJ was supported by Qura Therapeutics (2019-01), University of North Carolina at Chapel Hill Center for AIDS Research (P30AI50410), and NIAID/CARE (1UM1AI126619).

# ACKNOWLEDGMENTS

We thank Edward Browne for his primary CD4+ T cell model of latency. We extend our appreciation to the participants who donated samples for this study. Don Nguyen was involved in the initial work of this study at UC Davis.

# SUPPLEMENTARY MATERIAL

The Supplementary Material for this article can be found online at: https://www.frontiersin.org/articles/10.3389/fmicb.2022.836831/full#supplementary-material

**Supplementary Figure 1 |** Resveratrol does not mediate histone acetylation in cell model of HIV latency. 2D10 cells were treated with varying concentrations of resveratrol (20, 40, 60, and 80 μM) where the treatment of 500 nM suberoylanilide hydroxamic acid (SAHA) served as histone acetylation control. Total histone proteins were extracted and histone acetylation at the 9th lysine residue of histone H3 protein (H3K9Ac) was visualized by Western blot with the total histone H3 proteins (Total H3) as the loading control.

# REFERENCES

Abner, E., and Jordan, A. (2019). HIV "shock and kill" therapy: in need of revision. *Antivir. Res.* 166, 19–34. doi: 10.1016/j.antiviral.2019.03.008

Archin, N. M., Liberty, A. L., Kashuba, A. D., Choudhary, S. K., Kuruc, J. D., Crooks, A. M., et al. (2012). Administration of vorinostat disrupts HIV-1 latency in patients on antiretroviral therapy. *Nature* 487, 482–485.

Beans, E. J., Fournogerakis, D., Gauntlett, C., Heumann, L. V., Kramer, R., Marsden, M. D., et al. (2013). Highly potent, synthetically accessible prostratin analogs induce latent HIV expression in vitro and ex vivo. *Proc. Natl. Acad. Sci. U.S.A.* 110, 11698–11703. doi: 10.1073/pnas.1302634110

Bradley, T., Ferrari, G., Haynes, B. F., Margolis, D. M., and Browne, E. P. (2018). Single-Cell Analysis of Quiescent HIV Infection Reveals Host Transcriptional Profiles that Regulate Proviral Latency. *Cell Rep.* 25, 107-117. doi: 10.1016/j.celrep.2018.09.020

Cary, D. C., Fujinaga, K., and Peterlin, B. M. (2016). Euphorbia Kansui Reactivates Latent HIV. *PLoS One* 11:e0168027. doi: 10.1371/journal.pone.0168027

Cheng, C. K., Luo, J. Y., Lau, C. W., Chen, Z. Y., Tian, X. Y., and Huang, Y. (2020). Pharmacological basis and new insights of resveratrol action in the cardiovascular system. *Br. J. Pharmacol.* 177, 1258–1277.

Crooks, A. M., Bateson, R., Cope, A. B., Dahl, N. P., Griggs, M. K., Kuruc, J. D., et al. (2015). Precise Quantitation of the Latent HIV-1 Reservoir: implications for Eradication Strategies. *J. Infect Dis.* 212, 1361–1365. doi: 10.1093/infdis/jiv218

Darcis, G., Kula, A., Bouchat, S., Fujinaga, K., Corazza, F., Ait-Ammar, A., et al. (2015). An In-Depth Comparison of Latency-Reversing Agent Combinations in Various In Vitro and Ex Vivo HIV-1 Latency Models Identified Bryostatin-1+JQ1 and Ingenol-B+JQ1 to Potently Reactivate Viral

Gene Expression. *PLoS Pathog.* 11:e1005063. doi: 10.1371/journal.ppat.1005063

Dashti, A., Waller, C., Mavigner, M., Schoof, N., Bar, K. J., Shaw, G. M., et al. (2020). SMAC mimetic plus triple combination bispecific HIVxCD3 DART(R) molecules in SHIV.C.CH505-infected, ART-suppressed rhesus macaques. *J. Virol.* 94, e793–e720. doi: 10.1128/JVI.00793-20

DeChristopher, B. A., Loy, B. A., Marsden, M. D., Schrier, A. J., Zack, J. A., and Wender, P. A. (2012). Designed, synthetically accessible bryostatin analogues potently induce activation of latent HIV reservoirs in vitro. *Nat. Chem.* 4, 705–710. doi: 10.1038/nchem.1395

Deeks, S. G. (2012). HIV: shock and kill. *Nature* 487, 439–440. doi: 10.1038/487439a

Finzi, D., Blankson, J., Siliciano, J. D., Margolick, J. B., Chadwick, K., Pierson, T., et al. (1999). Latent infection of CD4+ T cells provides a mechanism for lifelong persistence of HIV-1, even in patients on effective combination therapy. *Nat. Med.* 5, 512–517. doi: 10.1038/8394

French, A. J., Natesampillai, S., Krogman, A., Correia, C., Peterson, K. L., Alto, A., et al. (2020). Reactivating latent HIV with PKC agonists induces resistance to apoptosis and is associated with phosphorylation and activation of BCL2. *PLoS Pathog.* 16:e1008906. doi: 10.1371/journal.ppat.1008906

Grau-Exposito, J., Luque-Ballesteros, L., Navarro, J., Curran, A., Burgos, J., Ribera, E., et al. (2019). Latency reversal agents affect differently the latent reservoir present in distinct CD4+ T subpopulations. *PLoS Pathog.* 15:e1007991. doi: 10.1371/journal.ppat.1007991

Gutierrez, C., Serrano-Villar, S., Madrid-Elena, N., Perez-Elias, M. J., Martin, M. E., Barbas, C., et al. (2016). Bryostatin-1 for latent virus reactivation in HIV-infected patients on antiretroviral therapy. *AIDS* 30, 1385–1392. doi: 10.1097/QAD.0000000000001064

Hosmane, N. N., Kwon, K. J., Bruner, K. M., Capoferri, A. A., Beg, S., Rosenbloom, D. I., et al. (2017). Proliferation of latently infected CD4(+) T cells carrying replication-competent HIV-1: potential role in latent reservoir dynamics. *J. Exp. Med.* 214, 959–972. doi: 10.1084/jem.20170193

Jiang, G., Maverakis, E., Cheng, M. Y., Elsheikh, M. M., Deleage, C., Mendez-Lagares, G., et al. (2019). Disruption of latent HIV in vivo during the clearance of actinic keratosis by ingenol mebutate. *JCI Insight* 4:e126027. doi: 10.1172/jci.insight.126027

Jiang, G., Mendes, E. A., Kaiser, P., Sankaran-Walters, S., Tang, Y., Weber, M. G., et al. (2014). Reactivation of HIV latency by a newly modified Ingenol derivative via protein kinase Cdelta-NF-kappaB signaling. *AIDS* 28, 1555–1566. doi: 10.1097/QAD.0000000000000289

Jiang, G., Mendes, E. A., Kaiser, P., Wong, D. P., Tang, Y., Cai, I., et al. (2015). Synergistic Reactivation of Latent HIV Expression by Ingenol-3-Angelate, PEP005, Targeted NF-kB Signaling in Combination with JQ1 Induced p-TEFb Activation. *PLoS Pathog* 11:e1005066. doi: 10.1371/journal.ppat.1005066

Jiang, G. C., Nguyen, D., Archin, N. M., Yukl, S. A., Mendez-Lagares, G., Tang, Y. Y., et al. (2018). HIV latency is reversed by ACSS2-driven histone crotonylation. *J. Clin. Invest.* 128, 1190–1198. doi: 10.1172/JCI98071

Kim, J. T., Zhang, T. H., Carmona, C., Lee, B., Seet, C. S., Kostelny, M., et al. (2022). Latency reversal plus natural killer cells diminish HIV reservoir in vivo. *Nat. Commun.* 13:121. doi: 10.1038/s41467-021-27647-0

Krishnan, V., and Zeichner, S. L. (2004). Host cell gene expression during human immunodeficiency virus type 1 latency and reactivation and effects of targeting genes that are differentially expressed in viral latency. *J. Virol.* 78, 9458–9473. doi: 10.1128/JVI.78.17.9458-9473.2004

Kroon, E., Ananworanich, J., Pagliuzza, A., Rhodes, A., Phanuphak, N., Trautmann, L., et al. (2020). A randomized trial of vorinostat with treatment interruption after initiating antiretroviral therapy during acute HIV-1 infection. *J. Virus Erad.* 6:100004. doi: 10.1016/j.jve.2020.100004

Laird, G. M., Bullen, C. K., Rosenbloom, D. I., Martin, A. R., Hill, A. L., Durand, C. M., et al. (2015). Ex vivo analysis identifies effective HIV-1 latency-reversing drug combinations. *J. Clin. Invest.* 125, 1901–1912. doi: 10.1172/JCI80142

Li, D., Dewey, M. G., Wang, L., Falcinelli, S. D., Wong, L. M., Tang, Y., et al. (2022). Crotonylation sensitizes IAPi-induced disruption of latent HIV by enhancing p100 cleavage into p52. *iScience* 25:103649. doi: 10.1016/j.isci.2021.103649

Lu, P., Qu, X., Shen, Y., Jiang, Z., Wang, P., Zeng, H., et al. (2016). The BET inhibitor OTX015 reactivates latent HIV-1 through P-TEFb. *Sci. Rep.* 6:24100.

Margolis, D. M., Garcia, J. V., Hazuda, D. J., and Haynes, B. F. (2016). Latency reversal and viral clearance to cure HIV-1. *Science* 353:aaf6517. doi: 10.1126/science.aaf6517

Marsden, M. D., Loy, B. A., Wu, X., Ramirez, C. M., Schrier, A. J., Murray, D., et al. (2017). In vivo activation of latent HIV with a synthetic bryostatin analog effects both latent cell "kick" and "kill" in strategy for virus eradication. *PLoS Pathog.* 13:e1006575. doi: 10.1371/journal.ppat.1006575

Marsden, M. D., Wu, X., Navab, S. M., Loy, B. A., Schrier, A. J., DeChristopher, B. A., et al. (2018). Characterization of designed, synthetically accessible bryostatin analog HIV latency reversing agents. *Virology* 520, 83–93. doi: 10.1016/j.virol.2018.05.006

Marsden, M. D., Zhang, T. H., Du, Y., Dimapasoc, M., Soliman, M. S. A., Wu, X., et al. (2020). Tracking HIV Rebound following Latency Reversal Using Barcoded HIV. *Cell Rep. Med.* 1:100162.

Nixon, C. C., Mavigner, M., Sampey, G. C., Brooks, A. D., Spagnuolo, R. A., Irlbeck, D. M., et al. (2020). Systemic HIV and SIV latency reversal via non-canonical NF-kappaB signalling in vivo. *Nature* 578, 160–165.

Okoye, A. A., Fromentin, R., Takata, H., Brehm, J. H., Fukazawa, Y., Randall, B., et al. (2022). The ingenol-based protein kinase C agonist GSK445A is a potent inducer of HIV and SIV RNA transcription. *PLoS pathog.* 18:e1010245. doi: 10.1371/journal.ppat.1010245

Pandelo Jose, D., Bartholomeeusen, K., da Cunha, R. D., Abreu, C. M., Glinski, J., da Costa, T. B., et al. (2014). Reactivation of latent HIV-1 by new semi-synthetic ingenol esters. *Virology* 46, 328–339. doi: 10.1016/j.virol.2014.05.033

Pardons, M., Fromentin, R., Pagliuzza, A., Routy, J. P., and Chomont, N. (2019). Latency-Reversing Agents Induce Differential Responses in Distinct Memory CD4 T Cell Subsets in Individuals on Antiretroviral Therapy. *Cell Rep.* 29, 2783–2795. doi: 10.1016/j.celrep.2019.10.101

Rosas-Umbert, M., Ruiz-Riol, M., Fernandez, M. A., Marszalek, M., Coll, P., Manzardo, C., et al. (2020). In vivo Effects of Romidepsin on T-Cell Activation, Apoptosis and Function in the BCN02 HIV-1 Kick&Kill Clinical Trial. *Front. Immunol.* 11:418. doi: 10.3389/fimmu.2020.00418

Sampey, G. C., Iordanskiy, S., Pleet, M. L., DeMarino, C., Romerio, F., Mahieux, R., et al. (2020). Identification of Modulators of HIV-1 Proviral Transcription from a Library of FDA-Approved Pharmaceuticals. *Viruses* 12:1067. doi: 10.3390/v12101067

Siliciano, J. M., and Siliciano, R. F. (2015). The Remarkable Stability of the Latent Reservoir for HIV-1 in Resting Memory CD4+ T Cells. *J. Infect. Dis.* 212, 1345–1347. doi: 10.1093/infdis/jiv219

Sperandio, S., Barat, C., Cabrita, M. A., Gargaun, A., Berezovski, M. V., Tremblay, M. J., et al. (2015). TOE1 is an inhibitor of HIV-1 replication with cell-penetrating capability. *Proc. Natl. Acad. Sci.* 112, E3392–E3401. doi: 10.1073/pnas.1500857112

Spivak, A. M., and Planelles, V. (2018). Novel Latency Reversal Agents for HIV-1 Cure. *Annu. Rev. Med.* 69, 421–436. doi: 10.1146/annurev-med-052716-031710

Stoszko, M., Ne, E., Abner, E., and Mahmoudi, T. (2019). A broad drug arsenal to attack a strenuous latent HIV reservoir. *Curr. Opin. Virol.* 38, 37–53. doi: 10.1016/j.coviro.2019.06.001

Tsai, H. Y., Ho, C. T., and Chen, Y. K. (2017). Biological actions and molecular effects of resveratrol, pterostilbene, and 3'-hydroxypterostilbene. *J. Food Drug Anal.* 25, 134–147. doi: 10.1016/j.jfda.2016.07.004

Tsai, P., Wu, G., Baker, C. E., Thayer, W. O., Spagnuolo, R. A., Sanchez, R., et al. (2016). In vivo analysis of the effect of panobinostat on cell-associated HIV RNA and DNA levels and latent HIV infection. *Retrovirology* 13:36. doi: 10.1186/s12977-016-0268-7

Vemula, S. V., Maxwell, J. W., Nefedov, A., Wan, B. L., Steve, J., Newhard, W., et al. (2017). Identification of proximal biomarkers of PKC agonism and evaluation of their role in HIV reactivation. *Antivir. Res.* 139, 161–170. doi: 10.1016/j.antiviral.2016.11.014

Wang, P., Lu, P., Qu, X., Shen, Y., Zeng, H., Zhu, X., et al. (2017). Reactivation of HIV-1 from Latency by an Ingenol Derivative from Euphorbia Kansui. *Sci. Rep.* 7:9451.

Wender, P. A., Dechristopher, B. A., and Schrier, A. J. (2008). Efficient synthetic access to a new family of highly potent bryostatin analogues via a Prins-driven macrocyclization strategy. *J. Am. Chem. Soc.* 130, 6658–6659. doi: 10.1021/ja8015632

Wender, P. A., Horan, J. C., and Verma, V. A. (2006). Total synthesis and initial biological evaluation of new B-ring-modified bryostatin analogs. *Org. Lett.* 8, 5299–5302. doi: 10.1021/ol0620904

Wong, L. M., and Jiang, G. (2021). NF-kappaB sub-pathways and HIV cure: a revisit. *EBioMedicine* 63:103159. doi: 10.1016/j.ebiom.2020.103159

Yang, H., Li, X., Yang, X., Lu, P., Wang, Y., Jiang, Z., et al. (2019). Dual effects of the novel ingenol derivatives on the acute and latent HIV-1 infections. *Antivir. Res.* 169:104555.

Yin, M., Guo, Y., Hu, R., Cai, W. L., Li, Y., Pei, S., et al. (2020). Potent BRD4 inhibitor suppresses cancer cell-macrophage interaction. *Nat. Commun.* 11:1833.

Yukl, S. A., Kaiser, P., Kim, P., Telwatte, S., Joshi, S. K., Vu, M., et al. (2018). HIV latency in isolated patient CD4(+) T cells may be due to blocks in HIV transcriptional elongation, completion, and splicing. *Sci. Transl. Med.* 10:eaa9927. doi: 10.1126/scitranslmed.aap9927

Zeng, X., Pan, X., Xu, X., Lin, J., Que, F., Tian, Y., et al. (2017). Resveratrol Reactivates Latent HIV through Increasing Histone Acetylation and Activating Heat Shock Factor 1. *J. Agric. Food Chem.* 65, 4384–4394. doi: 10.1021/acs.jafc.7b00418

**Conflict of Interest:** The authors declare that the research was conducted in the absence of any commercial or financial relationships that could be construed as a potential conflict of interest.

**Publisher's Note:** All claims expressed in this article are solely those of the authors and do not necessarily represent those of their affiliated organizations, or those of the publisher, the editors and the reviewers. Any product that may be evaluated in this article, or claim that may be made by its manufacturer, is not guaranteed or endorsed by the publisher.

*Copyright © 2022 Wong, Li, Tang, Méndez-Lagares, Thompson, Hartigan-O'Connor, Dandekar and Jiang. This is an open-access article distributed under the terms of the Creative Commons Attribution License (CC BY). The use, distribution or reproduction in other forums is permitted, provided the original author(s) and the copyright owner(s) are credited and that the original publication in this journal is cited, in accordance with accepted academic practice. No use, distribution or reproduction is permitted which does not comply with these terms.*

frontiers in Microbiology

ORIGINAL RESEARCH
published: 11 March 2022
doi: 10.3389/fmicb.2022.861734

# Vitamin D3 Suppresses Human Cytomegalovirus-Induced Vascular Endothelial Apoptosis *via* Rectification of Paradoxical m6A Modification of Mitochondrial Calcium Uniporter mRNA, Which Is Regulated by METTL3 and YTHDF3

*Wenbo Zhu*[1], *Hongbo Zhang*[1,2*†] *and Shao Wang*[3*†]

[1]*Clinical Medical Research Center, First Affiliated Hospital, University of South China, Hengyang, China,* [2]*Department of Microbiology and Immunology, LSU Health Sciences Center, Shreveport, LA, United States,* [3]*Institute of Animal Husbandry and Veterinary Medicine, Fujian Academy of Agriculture Science, Fuzhou, China*

OPEN ACCESS

**Edited by:**
*Chunfu Zheng,*
*University of Calgary, Canada*

**Reviewed by:**
*Tuo Yang,*
*University of Pittsburgh, United States*
*Yufeng Song,*
*University of Virginia, United States*

***Correspondence:**
*Hongbo Zhang*
*hongboflood@163.com*
*Shao Wang*
*365415005@qq.com*

*†These authors have contributed equally to this work and shared the corresponding authorship*

**Specialty section:**
*This article was submitted to Virology, a section of the journal Frontiers in Microbiology*

**Received:** *25 January 2022*
**Accepted:** *17 February 2022*
**Published:** *11 March 2022*

**Citation:**
*Zhu W, Zhang H and Wang S (2022) Vitamin D3 Suppresses Human Cytomegalovirus-Induced Vascular Endothelial Apoptosis via Rectification of Paradoxical m6A Modification of Mitochondrial Calcium Uniporter mRNA, Which Is Regulated by METTL3 and YTHDF3. Front. Microbiol. 13:861734. doi: 10.3389/fmicb.2022.861734*

Human cytomegalovirus (HCMV) infection can induce apoptosis of vascular endothelial cells, which may be the most important element of development and progression of reported atherosclerosis caused by HCMV. As there are no specific drugs to clear HCMV infection, exploration of relevant drugs and mechanisms that can intervene in HCMV-induced atherosclerosis is urgently needed. The present study confirmed that vitamin D3 protected vascular endothelial cells from HCMV-induced apoptosis by inhibiting endoplasmic reticulum (ER) and mitochondrial apoptosis pathway. Mechanistically, HCMV infection could induce aberrantly elevated m6A modification, especially the increases of methyltransferases-"writers" (METTL3) and m$^6$A binding proteins-"readers" (YTHDF3). METTL3 methylates mitochondrial calcium uniporter (MCU), the main contributor to HCMV-induced apoptosis of vascular endothelial cells, at three m6A residues in the 3′-UTR, which promotes the association of the YTHDF3 with methylated MCU mRNA and subsequently increases the translation and expression of MCU. Further analysis shows that ALKBH5 is the demethylases-"eraser" of MCU mRNA, which can negatively regulate the m6A modification process of MCU. Conversely, vitamin D3 downregulated the METTL3 by inhibiting the activation of AMPK, thereby inhibiting the m6A modification of MCU and cell apoptosis. Our findings extend the understanding of m6A driven machinery in virus-induced vascular endothelium damage and highlight the significance of vitamin D3 in the intervention of HCMV-induced atherosclerosis.

**Keywords: HCMV, vascular endothelial cells, apoptosis, MCU, m6A modification**

## INTRODUCTION

Human cytomegalovirus (HCMV) is a member of the *Herpesviridae* family and infects a broad range of cell types in human beings. In the normal human population, it can establish a latent infection with a mostly asymptomatic clinical outcome. However, reactivation from latent state under some circumstances or infection of an immunocompromised population can lead to severe clinical symptoms and even lethal outcomes (Khoshnevis and Tyring, 2002; Crough and Khanna, 2009; Manandhar et al., 2019). Apoptosis is a programmed cell death process that can be regulated by a variety of signals. On the one hand, HCMV viruses have developed a set of apoptosis-inhibiting mechanisms in order to establish a long-term persistent infection (Zhu et al., 1995; Goldmacher, 2005; Andoniou and Degli-Esposti, 2006; Brune, 2011). On the other hand, HCMV can also induce apoptosis in many cell types, mediating HCMV-induced pathological processes and viral transmission (Moon et al., 2003; Lee et al., 2013; Nakamura et al., 2013; Shao et al., 2016). It is unclear when HCMV induces apoptosis and when it causes apoptosis inhibition, probably in the context of different cellular environments and virus strains. Notably, HCMV infection can induce apoptosis of vascular endothelial cells (Shen et al., 2004; Utama et al., 2006), which may be closely related to the reported atherosclerosis caused by HCMV.

Vitamin D is a multifunctional lipid soluble hormone that is essential in a variety of physiological and pathological processes. Vitamin D3 and its metabolites regulate the transcription of target genes and exert biological effects through the vitamin D receptor (VDR). Accumulating evidence has shown that vitamin D3 deficiency is strongly associated with the development of atherosclerosis (Mozos and Marginean, 2015; Bennett and Lavie, 2017; Chen et al., 2018). Multiple mechanisms involved in occurrence and development of atherosclerosis are regulated by the VDR signaling, including improving endothelial function (Kim et al., 2020), inhibiting the formation of foam cells (Oh et al., 2009; Szeto et al., 2012), and suppressing the proliferation of vascular smooth muscle cells (Chen et al., 2010). Mostly, vitamin D3 can protect endothelial cells from apoptosis induced by radiation, immune damage, and oxidative stress (Dehghani et al., 2013; Polidoro et al., 2013; Marampon et al., 2016). However, whether vitamin D3 can protect vascular endothelial cells from HCMV-induced apoptosis is not yet known. As there are no specific drugs to clear HCMV infection, exploring related mechanisms can help us find interventions for HCMV-induced atherosclerosis.

$N^6$-methyladenosine ($m^6A$), the most prevalent post-transcriptional modification (PTMs) in mammalian mRNAs, is involved in a variety of physiological and pathological processes (Song et al., 2019). The $m^6A$ modification can be dynamically regulated by methyltransferases-"writers" (METTL3, METTL14, and WTAP), demethylases-"erasers" (ALKBH5 and FTO), and $m^6A$ binding proteins-"readers" (YTHDF1-3 and YTHDC1). This epigenetic regulatory mechanism has been reported to modulate alternative splicing, RNA stability, translation efficiency, and nuclear export (Wang et al., 2014, 2015; Zhao et al., 2014; Xiao et al., 2016). However, the status of m6A modification and the underlying regulatory mechanisms in HCMV-induced pathology are not fully understood. Mitochondrial calcium uniporter (MCU) located on the mitochondrial inner membrane is an important channel protein mediating mitochondrial calcium uptake. A lot of evidence has shown that MCU can promote apoptosis through the mitochondrial pathway and endoplasmic reticulum stress (Guan et al., 2019; Li et al., 2020). The previous study indicated that PTMs such as AMP-activated protein kinase-dependent phosphorylation regulated the mitochondrial calcium uptake and activity of MCU (Zhao et al., 2019). However, it is still unknown whether $m^6A$ modification at the nucleotide level can control the activity and expression of MCU and which enzyme mediates this modification. Understanding these issues will provide the opportunity to develop new therapeutic strategies to control the occurrence of apoptosis.

In the present study, utilizing an HCMV VHL/E-infected human aortic endothelial cell apoptosis model, we found for the first time that vitamin D3 protects vascular endothelial cells from HCMV-induced apoptosis by reducing the elevated translation of MCU induced by HCMV through METTL3- and YTHDF3-dependent mechanisms *via* VDR/AMPK/METTL3 pathway.

**Abbreviations:** HCMV, Human cytomegalovirus; VDR, Vitamin D receptor; m6A, $N^6$-methyladenosine; MCU, Mitochondrial calcium uniporter; PTMs, Post-translational modifications; HAECs, Primary human aortic endothelial cells; RPE-1, Retinal pigment epithelial cells; Bcl-2, B-cell lymphoma-2; Bax, Bcl2-Associated X; GRP78, Glucose-regulated protein 78; CHOP, C/EBP homologous protein; AMPK, Adenosine 5′-monophosphate (AMP)-activated protein kinase; PGC-1α, Peroxisome proliferator-activated receptor-γcoactivator-1α; TFAM, Transcription factor A, mitochondrial; NRF-1, Nuclear respiratory factor 1; ATP5G1, ATP synthase, H+ transporting, mitochondrial F0 complex, subunit C1(subunit 9); Cox5a, Cytochrome *c* oxidase subunit 5A; MFN1, Mitofusin 1; MFN2, Mitofusin 2; Drp 1, Dynamin related protein 1; FIS 1, Fission, mitochondrial 1; MTFP1, Mitochondrial fission process 1; METTL3, Methyltransferase 3, N6-adenosine-methyltransferase complex catalytic subunit; METTL14, Methyltransferase 14, N6-adenosine-methyltransferase subunit; WTAP, WT1 associated protein; ALKBH5, AlkB homolog 5, RNA demethylase; FTO, Fat mass and obesity-associated protein; YTHDC1, YTH domain containing 1; YTHDF1, YTH N6-methyladenosine RNA-binding protein 1; YTHDF2, YTH N6-methyladenosine RNA-binding protein 2; YTHDF3, YTH N6-methyladenosine RNA-binding protein 3.

## MATERIALS AND METHODS

### Cell Lines and Virus Infection

Primary human aortic endothelial cells (HAECs) were obtained from PromoCell (Heidelberg, Germany) and cultured or passaged in the endothelial cell growth medium MV2 (PromoCell, C-22022, Germany) supplemented with 10% fetal bovine serum and 1% penicillin–streptomycin at 37°C in a humidified atmosphere of 5% $CO_2$. Cell detachment was performed with 0.05% trypsin in ethylene diamine tetra acetic acid (EDTA; Thermo Fisher, 25300120, United States). All cells used were between passages 3 and 8.

The human cytomegalovirus (HCMV) VHL/E strain was used in this study. The virus was propagated in Retinal Pigment epithelial cells (RPE-1). The RPE-1 cells were harvested after

HCMV infection and underwent a freeze /thaw process to release the virus. Infection of HAECs was conducted at a multiplicity of infection (MOI) of 5 as determined by titration on RPE-1 cells. Then, the HAECs were incubated at 37°C for 2 h to absorb the virus, washed three times with phosphate buffer solution (PBS), and added with fresh complete medium. Cell fractions or supernatants were harvested at various postinfectious times.

## Chemical Reagents and Antibodies

Chemical reagents used in this study and indicated working concentrations were as follows: 1α,25(OH)2-vitamin D3 (100nM, 10 nM, and 1 nM; Sigma, United States, D1530), AICAR (1 mM; Sigma, United States, A9978), Spermine (10 μM; Sigma, United States, S3256), and Ru360 (5 μM; Sigma, United States, 557440). The following antibodies were used as: anti-p53 (Cell Signaling, #9282, United States), anti-Bax (Cell Signaling, #5023, United States), anti-Bcl-2 (Cell Signaling, #2870, United States), anti-cytochrome *c* (Cell Signaling, #4272, United States), anti-CHOP (Abcam, ab11419, United States), anti-GRP78 (Abcam, ab21685, United States), anti-beta actin (Proteintech, 66009-1-Ig, United States), anti-m6A antibody (Invitrogen, MA5-33030, United States), anti-METTL3 (Abcam, ab195352, United States), anti-METTL14 (Abcam, ab220030, United States), anti-YTHDC1 (Abcam, ab259990, United States), anti-YTHDF1 (Abcam, ab220162, United States), anti-YTHDF2 (Abcam, ab220163, United States), anti-YTHDF3 (Abcam, ab255267, United States), anti-ALKBH5 (Abcam, ab195377, United States), anti-FTO (Abcam, ab126605, United States), anti-phospho-AMPK alpha2 (Abcam, ab109402, United States), anti-AMPK alpha 2 (Abcam, ab214425, United States), anti-VDR (Proteintech, 67192-1-Ig, United States), anti-MCU (Abcam, ab219827, United States), and anti-Cytomegalovirus glycoprotein B antibody (Abcam, ab6499, United States).

## Cell Transfection, Plasmids, and siRNA Knockdown

MCU-3′UTR with either wild type or mutant (m6A site was replaced by T) were inserted into downstream of pGL3 Luciferase Reporter Vectors (Promega, E1751, United States) to construct pGL3-MCU-WT plasmid or pGL3-MCU-mut plasmid. The full-length and truncated forms of the human gene [YTHDF1 (GenBank accession no. NP_060268.2), YTHDF2 (GenBank accession no. NP_001166599.1), YTHDF3 (GenBank accession no. NP_001264742.1), △YTH, and YTH], each with a hemagglutinin (HA) tag sequence (YPYDVPDYA), were amplified by PCR and cloned into HindIII and BamHI sites of pcDNA3.1(+) (Invitrogen, V87020, United States) to produce pHA-YTHDF1, pHA-YTHDF2, pHA-YTHDF3, pHA-△YTH, and pHA-YTH. Human METTL3 (GenBank accession no. NP_062826.2) or human ALKBH5 (GenBank accession no. NP_060228.3) or human FTO (GenBank accession no. NP_001073901.1) cDNA was generated by PCR and cloned into pFlag-CMV2 expression plasmid (Sigma, E7033, United States) to produce pFlag-METTL3, pFlag-ALKBH5, or pFlag-FTO.

All RNA duplexes were obtained from GenePharma Company (Shanghai, China). The corresponding sequences are listed as follows:

| Gene | siRNAs sequences |
|---|---|
| METTL3 | siMETTL3-1: 5'-CUGCAAGUAUGUUCACUAUGA-3' |
| | siMETTL3-2: 5'-AGGAGCCAGCCAAGAAAUCAA-3' |
| METTL14 | siMETTL14: 5'-UUUAACACGGCACCAAUGC-3' |
| ALKBH5 | siALKBH5-1: 5'-ACAAGUACUUCUUCGGCGA-3' |
| | siALKBH5-2: 5'-GCGCCGUCAUCAACGACUA-3' |
| FTO | siFTO: 5'-AAAUAGCCGCUGCUUGUGAGA-3' |
| YTHDF1 | siYTHDF1: 5'-UUCAUGAACAACUAGACGCGG-3' |
| YTHDF2 | siYTHDF2: 5'-GCCCAAUAAUGCAUAUACU-3' |
| YTHDF3 | siYTHDF3-1: 5'-UUCGCCUGUUUCCUCUGCU-3' |
| | siYTHDF3-2: 5'-UAUCAUUGCCAAAUCCAGC-3' |
| MCU | siMCU: 5'-GCCAGAGACAGACAAUACU-3' |
| VDR | siVDR: 5'-AGUUCAUUCUGACAGAUGA-3' |
| Negative control | 5'-UUCUCCGAACGUGUCACGU-3' |

Cell transfection was performed by using Lipofectamine 2000 (Invitrogen; Thermo Fisher Scientific, 11668019, United States) for plasmids and Lipofectamine RNAiMAX (Invitrogen, Thermo Fisher Scientific, 13778030, United States) for siRNA according to the manufacturer's protocols.

## Luciferase Reporter Assay

Primary human aortic endothelial cells were plated at a density of $2 \times 10^5$ per well in a 12-well plate. HAECs in each were transiently transfected with 750 ng pGL3 Luciferase Reporter Vectors (Promega, E1751, United States) fused with or without the wild-type or mutated MCU-3′-UTR and 100 ng Renilla luciferase reporter vectors plus METTL3 siRNAs or YTHDF1-3 siRNAs using Lipofectamine 3000 (Thermo Fisher Scientific, L3000015, United States). At 12 h post-transfection, cells were infected with the indicated dose of HCMV. Cells were harvested 24 h after infection, and a dual-luciferase reporter assay kit (Promega, E1910, United States) was applied to assess the luciferase activities according to the manufacturer's instructions. Renilla luciferase activity was used to standardize transfection efficiency. Each experiment was subjected to at least three times replication.

## Western Blot Assay

Indicated cells were lysed using high intensive radio immunoprecipitation assay (RIPA) buffer (Beyotime, China, P0013B). The cell suspension was centrifuged at $14{,}000 \times g$ for 10 min at 4°C. The protein supernatant was collected and concentration was determined by a BCA Assay Kit (CWBIO, China, CW0014S). The equal amounts of protein were separated by sodium dodecyl sulfate-polyacrylamide gel electrophoresis (SDS-PAGE) at 100 V for 1.5 h and electrotransfer into polyvinylidene difluoride membranes (PVDF; Millipore, ISEQ00010, United States) at 200 mA for 2 h. Then, the membranes were blocked with 5% non-fat milk for 1 h at room temperature and incubated with the indicated primary antibodies overnight at 4°C. Next day, after being washed three times with TBST [20 mM Tris–HCl, 500 mM NaCl, and 0.1%

Tween 20 (pH 7.5)], membranes were incubated with HRP-conjugated secondary antibodies at indicated concentration for 2 h at room temperature. The signals were detected using Super-enhanced chemiluminescence detection reagents (Applygen Technologies, P1030, China). The intensity of the protein bands was quantified using NIH ImageJ software.

To detect phosphorylated MCU, phosphorylation-tag gels (Jingke, China, 195-17991) containing $Zn^{2+}$ ions were used for SDS-PAGE, which can specifically capture phosphorylated proteins in gel. After Western blotting with anti-MCU antibodies, phosphorylated proteins were showed as slower migration bands compared to corresponding unphosphorylated proteins.

## Caspase-3/9 Activity Assay

Caspase-3 and caspase-9 activities were measured using 30 μg protein obtained from extracted cells and Caspase-3/9 Activity Assay Kit (Beyotime Institute of Biotechnology; China; catalog no. C1115 and C1158) following the manufacturer's instructions. Cells were incubated with Ac-DEVD-pNA (caspase-3 substrate) and Ac-LEHD-pNA (caspase-9 substrate) at 37°C for 2 h. Optical densities were determined at 405 nm using a colorimetric microplate reader. The relative caspase activity was recorded as the ratio to that of the control group.

## RNA Isolation and Real-Time PCR

Total RNA from cells was extracted by Trizol reagent (Invitrogen, 15596018, United States) following the manufacturer's instructions. Purity of RNA was determined by measuring A260nm/A280nm absorption ratio with ultraviolet spectrophotometer. The cDNA synthesis was generated with Maxima H Minus First Strand cDNA Synthesis Kit with DNase I (Thermo Scientific, #K1682, United States) for reverse transcription according to the manufacturer's instructions. qRT-PCR was performed using TB GreenTM Premix Ex TaqTM II (Takara, Cat. #RR820A, Japan) on an ABI-7500 Real-time PCR System (Applied Biosystems, United States). GAPDH gene expression was used as internal control for the normalization. A two-step PCR program was performed for gene amplification. The PCR conditions were set to pre-denaturation at 95°C for 30s, followed by 40 cycles at 95°C for 10s and 60°C for 34 s. The $2^{-\triangle\triangle Ct}$ method was used to determine the relative gene expression. All primers used in this study are as follows:

| Genes | Primers | Sequences |
|---|---|---|
| GAPDH | Forward | AGCCTCAAGATCATCAGCAATGCC |
| GAPDH | Reverse | TGTGGTCATGAGTCCTTCCACGAT |
| PGC-1α | Forward | CAGAGAGTATGAGAAGCGAGAG |
| PGC-1α | Reverse | AGCATCACAGGTATAACGGTAG |
| TFAM | Forward | TTCCAAGAAGCTAAGGGTGATT |
| TFAM | Reverse | AGAAGATCCTTTCGTCCAACTT |
| NRF-1 | Forward | GCTACTTACACCGAGCATAGTA |
| NRF-1 | Reverse | CTCAAATACATGAGGCCGTTTC |
| ATP5G1 | Forward | GACACAGCAGCCAAGTTTATTG |
| ATP5G1 | Reverse | CCAAGAATGGCATAGGAGAAGA |
| Cox5a | Forward | GGGTAACATACTTCAACAAGCC |
| Cox5a | Reverse | AGTTGGTCTAAGTTCCTGGATG |
| MFN1 | Forward | ACAAGGTGAATGAGCGGCTTTCC |
| MFN1 | Reverse | TCTTTCCATGTGCTGTCTGCGTAC |
| MFN2 | Forward | GTGCTTCTCCCTCAACTATGAC |
| MFN2 | Reverse | ATCCGAGAGAGAAATGGAACTC |
| Drp1 | Forward | GAGATGGTGTTCAAGAACCAAC |
| Drp1 | Reverse | CAATAACCTCACAATCTCGCTG |
| FIS1 | Forward | AGTACGCCTGGTGCCTGGTG |
| FIS1 | Reverse | GCTGTTCCTCCTTGCTCCCTTTG |
| MTFP1 | Forward | CCATTGACAAAGGCAAGAAGG |
| MTFP1 | Reverse | CTAGAGCCTGCCATACAAAGG |
| METTL3 | Forward | CTTCAGCAGTTCCTGAATTAGC |
| METTL3 | Reverse | ATGTTAAGGCCAGATCAGAGAG |
| METTL14 | Forward | ACCAAAATCGCCTCCTCCCAAATC |
| METTL14 | Reverse | AGCCACCTCTTTCTCCTCGGAAG |
| WTAP | Forward | CTGACAAACGGACCAAGTAATG |
| WTAP | Reverse | AAAGTCATCTTCGGTTGTGTTG |
| FTO | Forward | GTTCACAACCTCGGTTTAGTTC |
| FTO | Reverse | CATCATCATTGTCCACATCGTC |
| ALKBH5 | Forward | GCAAGGTGAAGAGCGGCATCC |
| ALKBH5 | Reverse | GTCCACCGTGTGCTCGTTGTAC |
| YTHDC1 | Forward | ATCATCTTCCGTTCGTGCTGTCC |
| YTHDC1 | Reverse | ATACACCCTTCGCTTTGGCAAGAG |
| YTHDF1 | Forward | ATGACAATGACTTTGAGCCCTA |
| YTHDF1 | Reverse | AGGGAGTAAGGAAATCCAATGG |
| YTHDF2 | Forward | ACTTCTCAGCATGGGGAAATAA |
| YTHDF2 | Reverse | TATTCATGCCAGGAGCCTTATT |
| YTHDF3 | Forward | GCTCCACCAACCCAACCAGTTC |
| YTHDF3 | Reverse | CTGAGGTCCTTGTTGCTGCTGTG |
| MCU | Forward | ATTTGGGAGCTGTTTATTGCAG |
| MCU | Reverse | GCCTCACAGATATCACAGGTAA |

## Cell Apoptosis Analysis

Apoptosis of primary HAECs was detected by flow cytometry according to the manufacturer's instructions of the FITC Annexin-V apoptosis detection kit (BD pharmingen, United States, cat. No 556547). After various treatments, cells were washed with PBS and digested with 0.25% trypsin without EDTA. Next, cells were centrifuged at 500 *g* for 5 min, washed twice with cold PBS, and resuspended in 100 μl binding buffer. Thereafter, 5 μl of PI and 5 μl of Annexin V-FITC were added and incubated for 15 min in the dark. Finally, 400 μl of binding buffer was added and shaken on an oscillator for a bit. Apoptosis was analyzed using a BD FACSAria™ II cell sorter (BD Biosciences, San Jose, California, United States) at 488 nm.

## RNA m6A Dot Blots

A dot blot assay used to measure the level of mRNA m6A methylation was performed as follows. Total RNA was isolated. The isolated RNA was denatured at 95°C for 3 min, followed by immediate chilling on ice. The denatured RNA (100 ng) was spotted on a Nitrocellulose membrane (GE Healthcare, RPN203B, United States). Then, the membranes were ultraviolet (UV) crosslinked with a StratageneStratalinker 2,400 UV Crosslinker and were blocked in blocking buffer (5% non-fat milk in PBST) for 1 h. N6-Methyladenosine (m6A) recombinant rabbit monoclonal antibody (Invitrogen, MA5-33030, United States) was incubated with the membrane overnight at 4°C with a dilution of 1:1,000. After washing three times with 1 × PBST, a corresponding horseradish peroxidase conjugated secondary antibody (Cell Signaling Technology, 7074S, United States) was diluted 1:5,000 and incubated with the membranes for 1 h at room temperature.

After extensive washing, the membrane was visualized by Super-enhanced chemiluminescence detection reagents (Applygen Technologies, P1030, China). To determine whether each dot possess an equal amount of RNA, the RNAs with same amount were spotted on the membrane and stained with 0.02% methylene blue in 0.3 M sodium acetate (pH 5.2) as a control.

## M6a MeRIP-qRT-PCR

MeRIP assays were performed with Magna MeRIP m6A Kit (Millipore, 17-10499, United States) to detect the m6A modification on specific genes according to the manufacturer's instructions. In brief, 300 μg total RNAs were chemically fragmented into about 300 nucleotides fragments by incubation at 94°C for 3 min in fragmentation buffer (10 mmol/L Tris-HCl, 10 mmol/L $ZnCl_2$, and pH 7.0). Then, the RNA samples were immunoprecipitation with anti-m6A antibody (Invitrogen, MA5-33030, United States) or anti-rabbit IgG (Sigma-Aldrich, R2655, United States). The mixed solution was further incubated with pre-washed dynabeads Protein A/G for 2 h at 4°C. The methylated RNAs were eluted with N6-methyladenosine 5′-monophosphate sodium salt (6.7 mM) at 4°C for 1 h and precipitated with 5 mg of glycogen, one-tenth volumes of 3 M sodium acetate in a 2.5 volume of 100% ethanol at −80°C overnight. Further enrichment of m6A was quantified by qRT-PCR and normalized to the input ($\%\text{Input} = 1/10 \times 2^{Ct\ [IP]-Ct\ [input]}$).

## RNA Immunoprecipitation

RNA immunoprecipitation assay was carried out by using Magna RIP RNA-binding Protein immunoprecipitation kit (Millipore Sigma, 17-700, United States) according to the manufacturer's instructions. Indicated cells were transfected with the same amount of HA-tagged plasmids (HA-YTHDF1, HA-YTHDF2, HA-YTHDF3, HA-△YTH, and HA-YTH) or HA plasmids as a control. All cells were subjected to the same treatment. Cell extracts were prepared with RIP buffer (100 mM KCl, 5 mM $MgCl_2$, 1 mM DTT, 10 mM HEPES, and 0.5% NP-40, pH 7.0) and protease inhibitor (Beyotime, China, P1005) and then incubated with 5 μg of normal antibodies against mouse IgG (Millipore Sigma, 12-371, United States), YTHDF1-3, or HA (Abcam, ab18181, United States) overnight at 4°C. RNA enriched by HA RIP of cells expressing untagged protein was served as negative control. Associated RNA-protein complexes were brought down by protein A/G beads. RT-PCR analysis was performed to determine RNA transcripts associated with indicated protein, and the data were normalized to input.

## Statistical Analyses

Results were presented as mean ± standard deviation (SD) and statistical analyses were performed with GraphPad Prism 6 software. Statistical significance was calculated by two-tailed Student's *t*-test. All experiments were repeated at least three times and a $p$ value less than 0.05 was considered to statistically significant.

# RESULTS

## Vitamin D3 Protected HAECs From HCMV-Induced Apoptosis by Inhibiting ER and Mitochondrial Apoptosis Pathway

To elucidate the protective effect of vitamin D3 on vascular endothelial cells, we constructed a HAECs apoptosis model by infection with HCMV VHL/E strain and detected apoptosis of HAECs by FCM with Annexin V-FITC/PI. As shown in **Figure 1A**, HCMV infection could obviously increase the ratio of apoptotic cells (60.7%) compared to control (11.94%). When HAECs were co-treated with 100 nM vitamin D3 for 4 days, the ratio of apoptosis induced by HCMV infection was evident decreased (28.6%).

As HCMV proteins can traffic into mitochondria through mitochondria-associated membranes (Williamson and Colberg-Poley, 2009), quantitative PCR assays were performed to evaluate mitochondrial function-related genes. The results showed that the expression of genes regulating mitochondrial fusion (MFN1 and MFN2) was decreased after HCMV infection, while the expression of genes regulating mitochondrial division (Drp1 and FIS1) was upregulated. In contrast, vitamin D3-treated cells exhibited significantly enhanced mitochondrial homeostasis and improved disturbance in mitochondrial division and fusion (**Figure 1B**). In addition, the genes relate to mitochondrial biogenesis (PGC-1α, TFAM, and NRF1) and oxidative phosphorylation (ATP5G1 and Cox5a) were also decreased after HCMV infection. Vitamin D3 treatment enhanced overall mitochondrial biosynthesis and function of electron transport chain (**Figure 1C**).

To detect the effect of the mitochondrial apoptotic pathway or ER apoptotic pathway in vitamin D3-mediated protection on HAECs apoptosis induced by HCMV, expression of mitochondrial apoptotic pathway-related protein (Bcl-2, Bax, and cytochrome *c*) and ER apoptotic pathway-related protein (GRP78 and CHOP) were detected by Western blot. As shown in **Figure 1D**, compared to control group, the Bcl-2 protein expression was obviously decreased, and the expression of p53, Bax, Cytochrome *c*, GRP78, and CHOP was obviously increased in HCMV-infected cells. After addition of 100 nM vitamin D3, Bcl-2 expression was obviously increased, while the expression of mitochondrial apoptosis-related protein (Bax and Cytochrome *c*) or ER apoptosis-related protein (GRP78 and CHOP) was obviously decreased.

The caspase-3 and caspase-9 activities were detected by a fluorescent analysis kit. As shown in **Figure 1E**, after adding vitamin D3, the caspase-3 and caspase-9 activities were obviously suppressed in HCMV-induced HAECs, indicating apoptosis of HAECs was suppressed by vitamin D3.

To further explore whether the protective effect of vitamin D3 on vascular endothelial cells was related to its effect on HCMV replication, single-cycle viral replication kinetic in HAECs of HCMV single-treatment and vitamin D3 co-treatment groups was plotted. The results showed that the viral replication kinetics were similar in the two groups, and the HCMV replicate indistinguishably in HAECs between HCMV infection alone or with vitamin D3 co-treatment (**Figure 1F**).

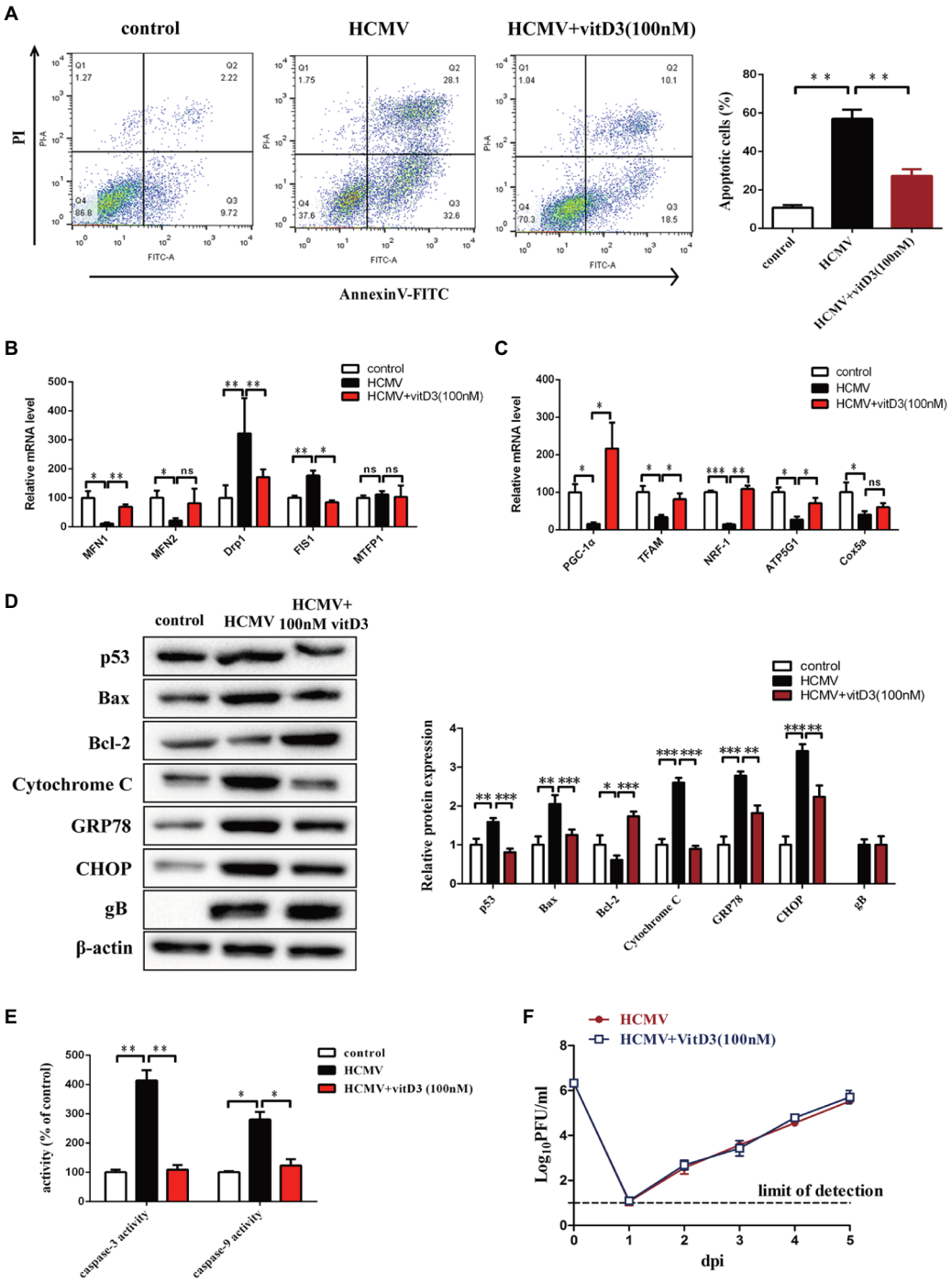


**FIGURE 1 |** The role of vitD3 on human cytomegalovirus (HCMV)-induced apoptosis of human aortic endothelial cells (HAECs). HAECs were mock-infected (control) or infected with VHL/E strain of HCMV [multiplicity of infection (MOI) = 5] for 4 days. In the vitD3-treated group, HAECs were continuously added with 100 nM vitD3 from the second to the fourth day of HCMV infection. After 4 days, HAECs were harvested for the following experiments. **(A)** Detection of cellular apoptosis in different groups by flow cytometric assay with Annexin-V/PI double staining and quantitative analysis. Left, representative images of flow cytometry; right, statistical charts. Apoptotic cells are calculated as the percentage of Annexin-V single-positive plus Annexin-V/PI double-positive cells. **(B,C)** qPCR analysis of mitochondrial gene expression in the corresponding groups. **(D)** Representative Western blot immunolabeling of proteins representing apoptosis, using β-actin as the loading control. Left, representative graphs of three independent experiments; right, statistical charts with densitometric analysis. gB, a HCMV gene used to quantify HCMV infection. **(E)** The caspase-3 and caspase-9 activities were measured by Caspase-3/9 fluorescent Assay kits. **(F)** Single-cycle viral replication kinetic curves from HAECs infected at an MOI of 5 were plotted by determining the titer in plaque forming unit (PFU) from supernatants collected at the indicated times postinfected. All data are from experiments performed in triplicate and presented as the mean ± standard deviation (SD). Student's *t*-test, $*p < 0.05$, $**p < 0.01$, and $***p < 0.001$. ns: no significant difference.

## Vitamin D3 Negatively Regulates the Elevated m6A Modification Levels Induced by HCMV Infection and Inhibits HCMV-Induced Apoptosis by Suppressing METTL3 Expression in HAECs

Previous study demonstrated that HCMV infection could induce aberrantly elevated m6A modification (Rubio et al., 2018). To determine whether m6A modification was involved in the vitamin D3-mediated protection on HAECs apoptosis induced by HCMV, the levels of m6A modification were measured using m6A mRNA dot blot. Consistent with the results in previous study, the levels of m6A modification were significantly increased in HAECs following HCMV infection. However, the increase in the levels of HCMV-induced m6A modification was inhibited by the addition of vitamin D3 (**Figure 2A**).

Given that the m$^6$A modification is dynamically regulated by methyltransferases-"writers" (METTL3, METTL14, and WTAP), demethylases-"erasers" (ALKBH5 and FTO), and m$^6$A binding proteins-"readers" (YTHDF1-3 and YTHDC1), we examined the expression of the key m6A modification-related genes at the mRNA level and protein level by quantitative PCR and Western blot. It was observed that the mRNA levels of METTL3, METTL14, YTHDF1, YTHDF2, and YTHDF3 were significantly increased in HAECs following HCMV infection. However, when the cells were co-treated with vitamin D3, the HCMV-induced elevated mRNA levels of METTL3 and METTL14 were inhibited, but the HCMV-induced elevated mRNA levels of YTHDF1, YTHDF2, and YTHDF3 were not inhibited (**Figure 2B**). Similar results were observed in protein expression by Western blot (**Figure 2C**). These results indicate that vitamin D3 negatively regulates HCMV-induced elevated m6A modification by inhibiting the expression of methyltransferases (METTL3 and METTL14).

Since vitamin D3 both inhibits m6A modification and protects arterial endothelial cells from HCMV-induced apoptosis, we hypothesized that the abnormal m6A modification may be involved in HCMV-induced apoptosis. We then assessed the effects of METTL3, METTL14, and YTHDF1-3 silencing on the HCMV-induced apoptosis in HAECs by flow cytometry with Annexin V-FITC/PI double staining. As seen in **Figure 2D**, the proportion of apoptotic cells during HCMV infection was significantly reduced after METTL3 or YTHDF3 knockdown. In contrast, the amount of HCMV-induced apoptosis was unaffected in the presence of METTL14, YTHDF1, or YTHDF2 silencing (**Figure 2D; Supplementary Figures 1A,B**). These data suggest that vitamin D3 protects arterial endothelial cells from HCMV-induced apoptosis in part by inhibiting METTL3 expression.

## Vitamin D3 Inhibits HCMV-Induced Apoptosis and Inhibits HCMV-Induce Increase in m6A Methylation *via* the VDR/AMPK Pathway

As we all know, vitamin D receptor signaling plays a key role in mediating the effect of vitamin D3. Vitamin D3 and its metabolites regulate the transcription of target genes and exert biological effects through the VDR. Furthermore, AMPK phosphorylation is regulated by Vitamin D3 *via* VDR and plays a protective role in a variety of pathological processes (Choi et al., 2013; Chang and Kim, 2019). Thus, to better understand how vitamin D3 inhibits HCMV-induced apoptosis and inhibits HCMV-induced increase in m6A modification, these two upstream pathway molecules were analyzed. First, we examined whether AMPK phosphorylation and VDR expression were altered under HCMV infection with or without vitamin D3 treatment. As shown in **Figure 3A**, AMPKα2 phosphorylation was obviously increased in the HCMV-infected group compared to the control group, yet significantly decreased after vitamin D3 co-treatment. In contrast, total AMPK protein levels and VDR expression did not change under HCMV infection with or without vitamin D3 treatment. These findings indicate that vitamin D3 treatment attenuated the increase in AMPK phosphorylation.

To directly address the role of AMPK or VDR on the effect of vitamin D3, we treated HAECs with AMPK activator (AICAR) or siVDR. The knockdown efficiency of VDR was shown in **Figure 3B**. In addition, activation of AMPK by AICAR upregulated the p-AMPKα2 level (**Figure 3C**). We then assessed the role of VDR and AMPK in vitamin D3-mediated inhibition of m6A modification by m6A mRNA dot blot and Western blot assays. Consistent with the previous results, the m6A mRNA dot blot assays showed that vitamin D3 treatment attenuated the increase in HCMV-induced m6A modification. However, when VDR was absent or the activator of AMPK (AICAR) was added, the level of HCMV-induced m6A modification was again increased (**Figure 3D**). Western blot assays showed the similar results, vitamin D3 treatment attenuated the HCMV-induced increase in the expression of m6A modification-related proteins (METTL3 or METTL14). However, when VDR was deleted or AMPK activator (AICAR) was added, the effect of vitamin D3 was diminished and METTL3 or METTL14 expression was elevated again. In contrast, YTHDF1-3 expression was increased under HCMV infection but was not affected by vitamin D3, VDR, and AMPK activity (**Figures 3E,F**).

To determine the role of VDR and AMPK in vitamin D3-mediated inhibition of apoptosis induced by HCMV infection, flow cytometry with Annexin V-FITC/PI double staining was performed. As shown in **Figure 3G**, vitamin D3 treatment protected the HAECs from HCMV-induced apoptosis, and AICAR co-treatment or VDR deletion rose the percentage of apoptosis again. Taken together, these data suggest that vitamin D3 inhibits HCMV-induced apoptosis and HCMV-induce increase in m6A methylation *via* the VDR/AMPK pathway.

## Vitamin D3 Reduces the HCMV-Induced Increase in MCU Expression *via* the VDR/AMPK Pathway and MCU Contributes To HCMV-Induced Apoptosis in HAECs

Given the known role of the mitochondrial protein MCU in regulating apoptosis by modulating mitochondrial function and ER stress (Guan et al., 2019; Li et al., 2020), we hypothesized that MCU may contribute to HCMV-induced apoptosis. To

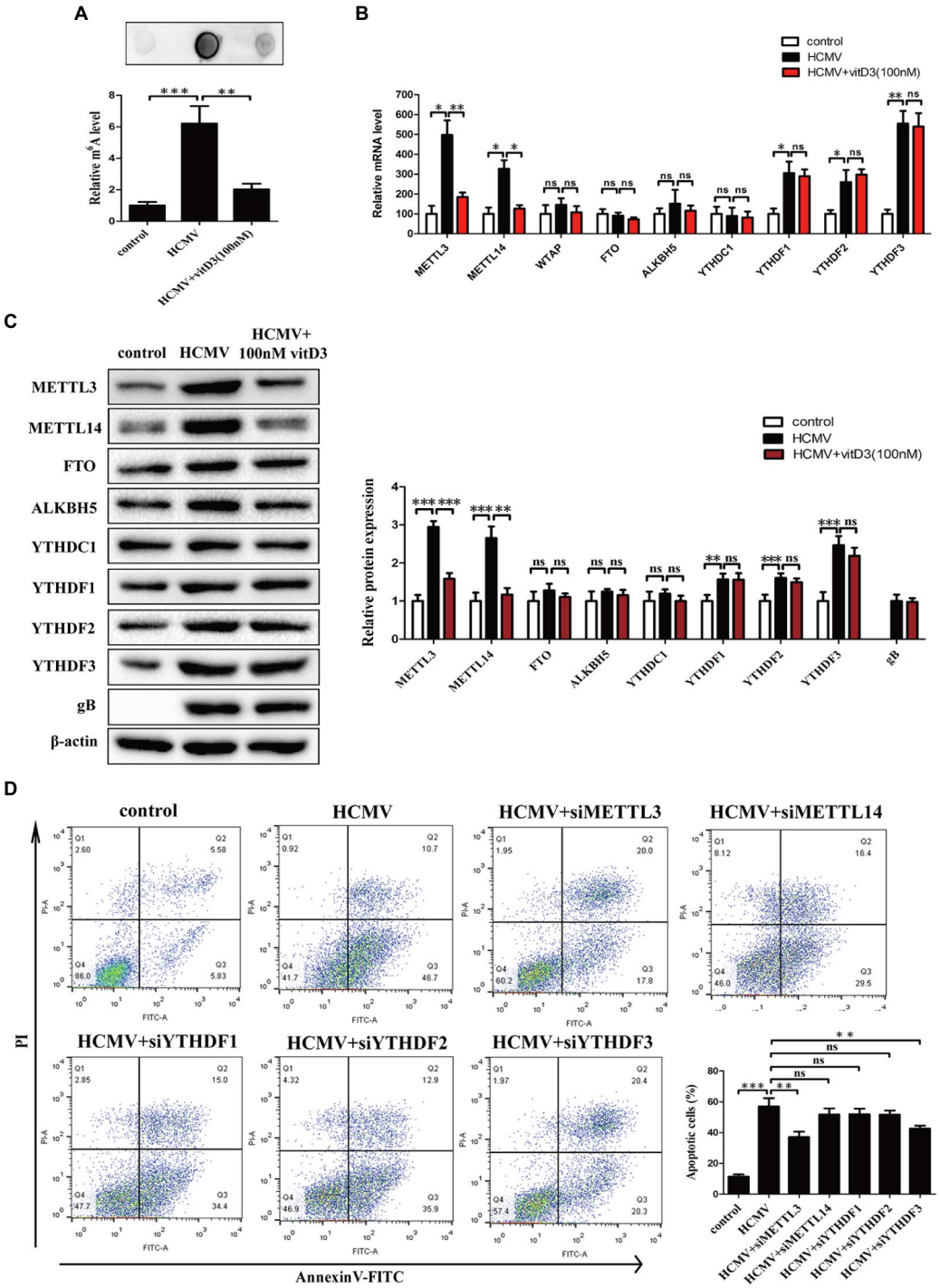


**FIGURE 2 |** Vitamin D3 negatively regulates the elevated m6A methylation levels induced by HCMV infection and inhibits HCMV-induced apoptosis by suppressing METTL3 expression in HAECs. HAECs were uninfected (control) or infected with VHL/E strain of HCMV [multiplicity of infection (MOI) = 5] for 4 days. In the vitD3-treated group, HAECs were continuously added with 100 nM vitD3 from the second to the fourth day of HCMV infection. After 4 days, HAECs were harvested for the following experiments. **(A)** RNA dot blot analysis of total m6A levels in the corresponding groups. Top, representative images of RNA dot blot; bottom, statistical charts for quantification of RNA dots. **(B)** qPCR analysis of mRNA levels of m6A modification-associated genes. **(C)** Western blot analysis of protein levels of m6A modification-associated genes. Left, representative graphs of three independent experiments; right, statistical charts with densitometric analysis. gB, a HCMV gene used to quantify HCMV infection. **(D)** Apoptosis was detected by Annexin-V/PI-labeled flow cytometric assay in different treatment groups and quantitative analysis. HAECs were transfected with siRNA of the indicated genes for 12 h and then exposed to HCMV. Left, representative images of flow cytometry; right, statistical charts. Apoptotic cells are calculated as the percentage of Annexin-V single-positive plus Annexin-V/PI double-positive cells. All data are expressed as the mean±SD of triplicate experiments. Columns, mean; error bars, SD. Student's *t*-test, $*p < 0.05$, $**p < 0.01$, and $***p < 0.001$. ns: no significant difference.

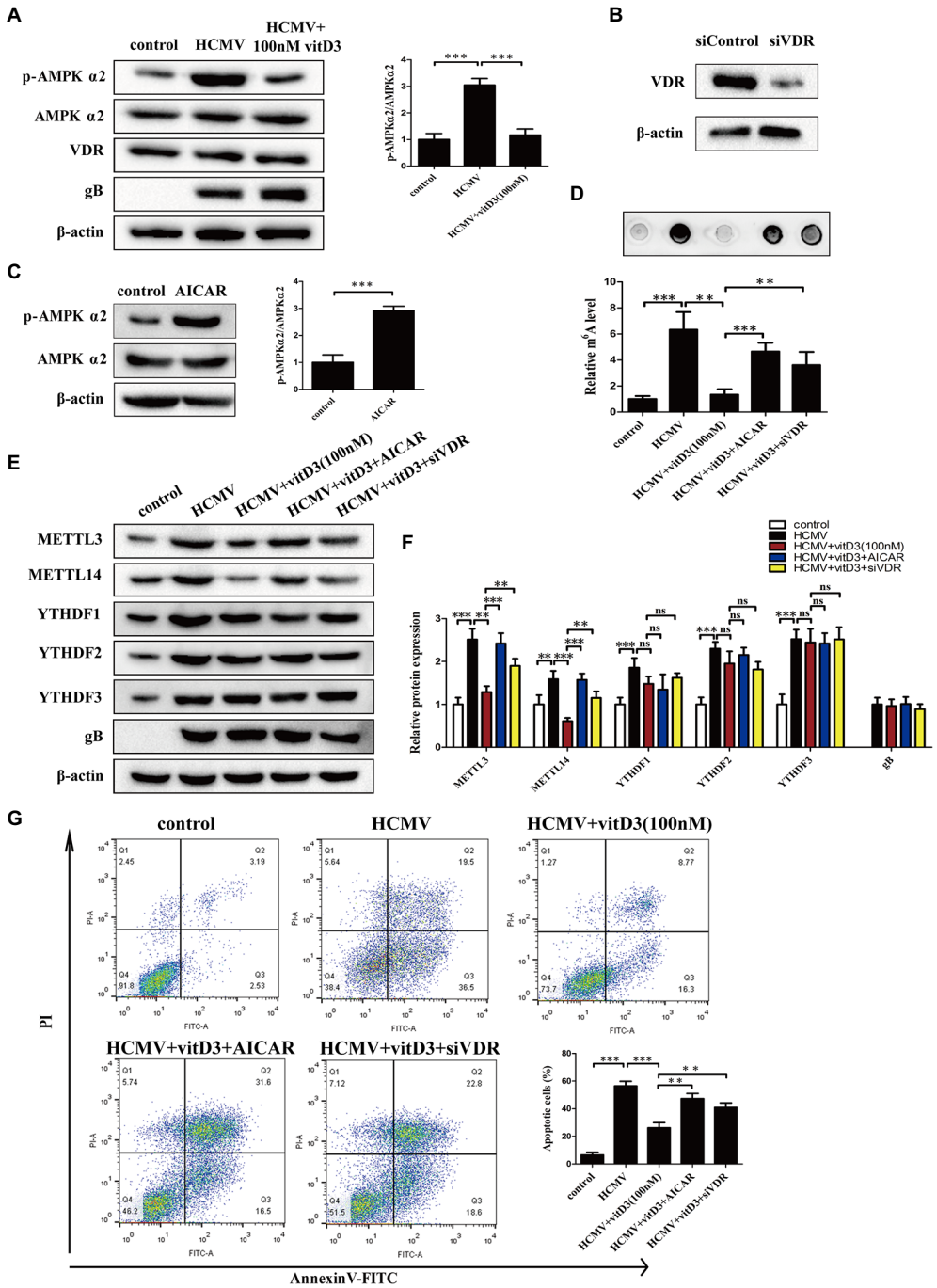


**FIGURE 3 |** Vitamin D3 inhibits HCMV-induced apoptosis and increased m6A methylation through the VDR/AMPK pathway. **(A)** The expression levels of p-AMPKα2, total AMPKα2, and VDR were detected by Western blotting in HAECs. Left, representative image of three independent experiments; right, statistical histogram representing the ratio of p-AMPKα2 to total AMPKα2. gB, a HCMV gene used to quantify HCMV infection. **(B)** Western blot analysis for knockdown efficiency of VDR in HAECs with siRNA (siVDR). **(C)** Western blot analysis to verify the effect of AMPK activator (AICAR) to increase p-AMPK levels. Left, representative image of triplicate experiments; right, statistical histogram representing the ratio of p-AMPKα2 to total AMPKα2. **(D)** RNA dot blot analysis verifies that vitD3 inhibits the HCMV-induced increase in total m6A levels through the VDR/AMPK pathway. HAECs were exposed to HCMV and simultaneously treated with vitD3 (100 nM) and AICAR (1 mM) for 4 days, or HAECs were transfected with siVDR for 12 h and then exposed to HCMV and vitD3. Top, representative images of RNA dot blot; bottom, statistical charts for quantification of RNA dots. **(E)** Representative Western blotting graphs verify that VitD3-induced alterations in m6A modification-associated proteins are *via* the VDR/AMPK pathway. **(F)** Histogram representing a densitometric analysis performed to quantify the relative intensity of the indicated bands detected by Western blotting. **(G)** Apoptosis rate detected by Annexin-V/PI-labeled flow cytometric assay in different treatment groups shows that vitD3 inhibits HCMV-induced apoptosis through VDR/AMPK pathway. Left, representative images of flow cytometry; right, statistical charts. All data are presented as the mean ± SD of triplicate experiments. Student's *t*-test, $^{**}p < 0.01$ and $^{***}p < 0.001$. ns: no significant difference.

test this hypothesis, we first examined the expression levels of MCU under different treatment conditions. It was observed that both total MCU protein and phosphorylated MCU protein were significantly increased after HCMV infection, and this increase was reversed after the addition of vitamin D3 and restored after exposure to AICAR or siVDR (**Figures 4A–C**). This finding indicated that vitamin D3 could reduce the HCMV-induced increase in total and phosphorylated MCU expression *via* the VDR/AMPK pathway.

To further determine whether MCU contributes to HCMV-induced apoptosis in HAECs, cellular apoptosis was measured using flow cytometry with Annexin V-FITC/PT double staining. We introduced Ru360 as MCU inhibitor or spermine as MCU activator, which has no effect on apoptosis of HAECs in normal state. HCMV infection induced a high percentage of apoptosis, which could be significantly reduced by MCU inhibition (Ru360 or siMCU) and further increased with spermine (**Figure 4D; Supplementary Figure 1C**). Additionally, apoptosis was estimated by apoptosis-related proteins including p53, Bax, Bcl-2, cytochrome *c*, GRP78, and CHOP by Western blot. In coincidence with flow cytometry results, HCMV infection induced the increment of p53, Bax, cytochrome *c*, GRP78, and CHOP, and the decrement of Bcl-2, and Ru360 or siMCU dampened these apoptotic changes while spermine enhanced apoptosis (**Figures 4E,F**).

The caspase-3 and caspase-9 activities were detected by a fluorescent analysis kit. As shown in **Supplementary Figure 1D**, the caspase-3 and caspase-9 activities were obviously increased under HCMV infection. This change could be reversed by MCU inhibition (Ru360 or siMCU) or be accelerated by MCU activator (spermine). These data confirm that MCU was upregulated during HCMV infection and contributed to HCMV-induced apoptosis.

## METTL3 Upregulates MCU Protein Expression (but Not mRNA) by Catalyzing Its m6A Methylation in Mock-Infected or HCMV-Infected HAECs

Since HCMV infection induced both elevated levels of m6A modification and MCU expression, and both m6A modification and MCU contribute to HCMV-induced apoptosis, we wondered whether the altered MCU expression was the consequence of HCMV-mediated m6A methylation modification. First, we investigated whether METTL3 or METTL14 (two m6A methyltransferases upregulated by HCMV infection) regulate MCU expression. It was observed that siRNA-mediated knockdown of METTL3 in HAECs significantly reduced MCU protein levels, while having no effect on p-MCU expression (**Figure 5A**). Conversely, we observed a dose-dependent increase in MCU protein levels in HAECs in response to METTL3 overexpression (**Figure 5B**). However, there was no change in MCU mRNA levels in HAECs either by knockdown of METTL3 or overexpression of METTL3 (**Figure 5C**). In contrast, METTL14 had no regulatory effect on MCU expression, as MCU protein expression was unchanged by either knocking down METLL14 or overexpressing METTL14 (**Supplementary Figures 1E,F**). In addition, knockdown of METTL3 in HCMV-infected HAECs similarly reduced the increase in protein expression of MCU induced by HCMV infection (mRNA expression was not affected; **Figures 5D,E**).

To further test the hypothesis that altered MCU expression was the consequence of METTL3-mediated m6A methylation modification, total cellular RNA was immunoprecipitated with an antibody recognizing m6A, and qRT-PCR was performed on the immunoprecipitated RNA to amplify the MCU 3′-UTR. We found that HCMV exposure led to an increase in MCU mRNA m6A methylation levels in HAECs. However, silencing METTL3 but not METTL14 resulted in decreased MCU m6A methylation levels under HCMV infection conditions, suggesting that MCU mRNA may be subject to METTL3-dependent m6A methylation (**Figure 5F**).

To further demonstrate that MCU mRNA is a direct target of METTL3-dependent m6A methylation, we searched for sequences within the MCU 3′-UTR. Sequence analysis of the MCU 3′-UTR revealed three matches to the 5′-RRACU-3′ (methylated adenosine residue is underlined) m6A consensus sequence (**Figure 5G**). In addition, a luciferase reporter plasmid that contained the entire MCU 3′-UTR was transiently transfected into HAECs, followed by exposure to HCMV infection and measurement of luciferase activity (**Figure 5H**). It was observed that HCMV infection significantly increased luciferase activity, whereas this effect was rescued by METTL3 knockdown in HAECs. Next, the adenine residues of the m6A consensus sequence in the MCU 3′-UTR were mutated (5′-GGACU-3′ to 5′-GGTCU-3′ of mRNA; **Supplementary Figure 1G**), and the WT and mutant reporters were compared by luciferase assay. Mutations of the adenosine residues in three identified m6A-consistent sequences lead to a decrease in luciferase activity in HAECs, suggesting that the mutation prevented m6A methylation and consequently reduced the translation efficiency of the luciferase-MCU-3′-UTR fusion mRNA (**Figure 5I**). Taken together, these results presented in **Figure 5** indicate that HCMV infection-induced METTL3 expression increases MCU mRNA methylation and translation efficiency.

## YTHDF3 Binds to MCU mRNA and Promotes MCU Protein Translation Through a METTL3-Mediated m6A-Dependent Manner

It was observed that the levels of $m^6A$ binding proteins-"readers" (YTHDF1-3) were elevated in response to HCMV infection in our previous results. Importantly, YTHDF1-3 reportedly regulates mRNA or protein expression and have been shown to bind to m6A-modified RNA (Fu et al., 2014; Wang et al., 2015; Zhang et al., 2019, 2020). To further explain the correlation between m6A methylation and MCU abundance, we investigated whether YTHDF1-3 was involved in the METTL3-mediated increase in translation of MCU mRNA. We first tested whether YTHDF1-3 interacted with MCU mRNA. RIP-qRT-PCR experiments showed that YTHDF1-3 all interacted with MCU mRNA. HCMV infection not only upregulated YTHDF3 expression but also promoted

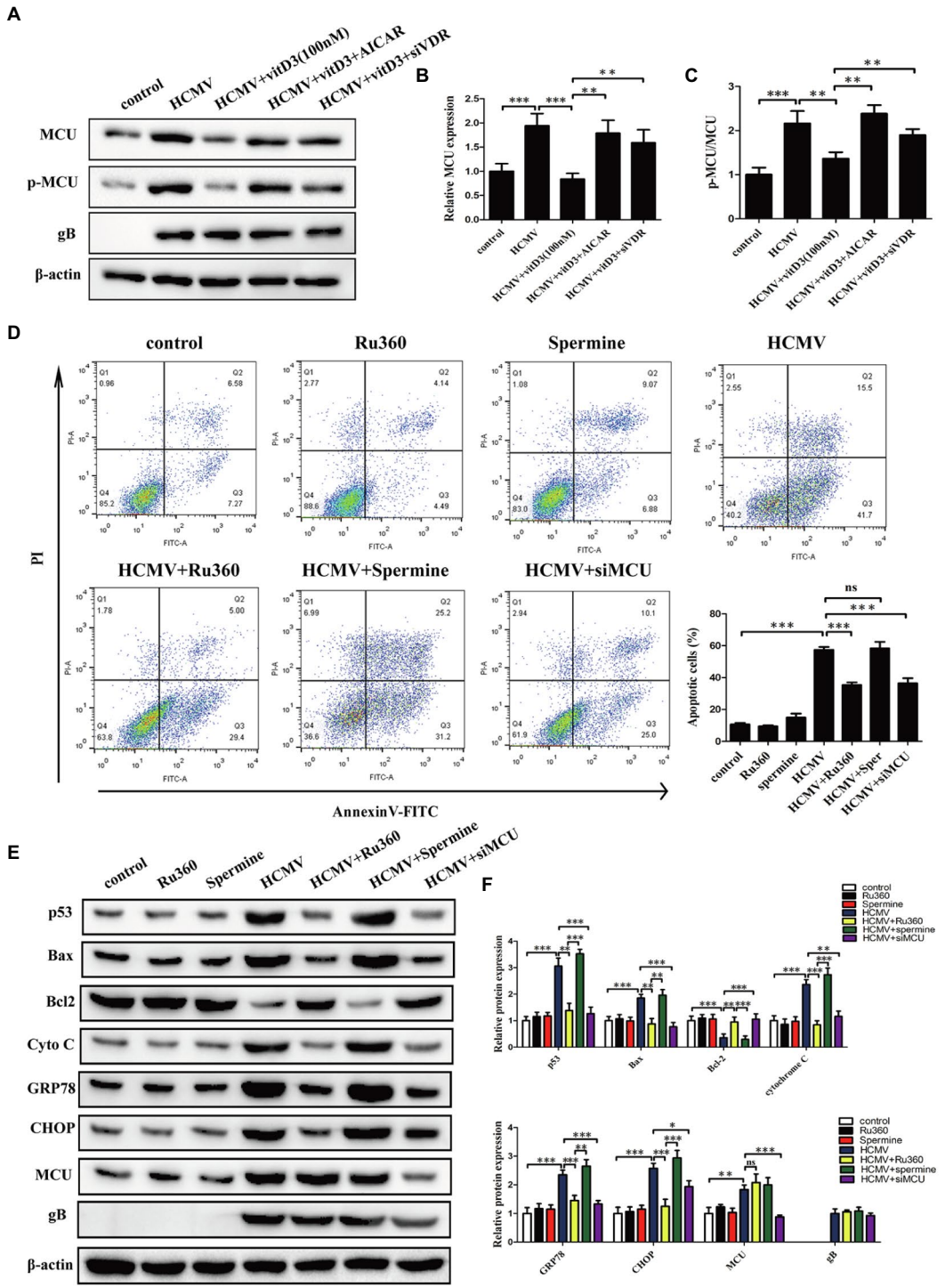


**FIGURE 4 |** Vitamin D3 reduces MCU expression *via* the VDR/AMPK pathway and MCU contributes to HCMV-induced apoptosis. **(A)** Representative Western blotting graphs verify that vitD3 reduces HCMV-induced increase in MCU (phosphorylated and total MCU) expression *via* the VDR/AMPK pathway. **(B)** Statistical histogram representing a densitometric analysis performed to quantify the relative intensity of the total MCU expressive bands detected by Western blotting in **(A)**. **(C)** Statistical histogram representing a densitometric analysis performed to quantify the ratio of p-MCU to total MCU in **(A)**. **(D)** Representative Annexin-V/PI double-labeled flow cytometric assay shows that MCU inhibition attenuates the apoptosis induced by HCMV. Left, representative images of flow cytometry; right, statistical charts. **(E)** Representative Western blotting graphs verify that MCU inhibition attenuates the expression of apoptosis-associated proteins. HAECs were exposed to HCMV or not with or without Ru360 (5 μM) or spermine (10 μM). gB, a HCMV gene used to quantify HCMV infection. **(F)** Statistical histogram representing a densitometric analysis performed to quantify the relative intensity of the indicated bands detected by Western blotting in **(E)**. All data are expressed as the mean ± SD of triplicate experiments. Student's *t*-test, $*p < 0.05$, $**p < 0.01$, and $***p < 0.001$. ns: no significant difference.

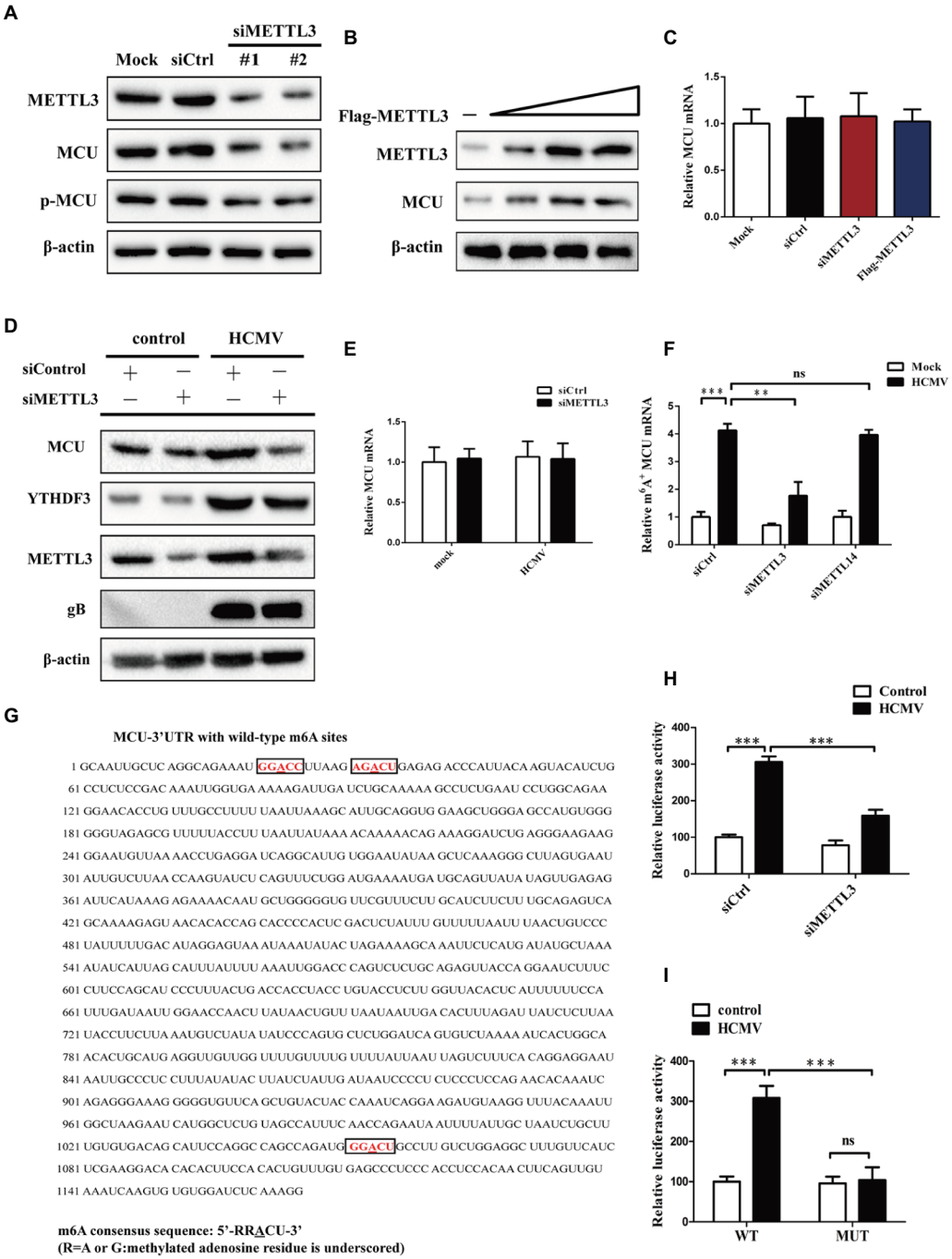


**FIGURE 5 |** METTL3 upregulates MCU protein expression (but not mRNA) by catalyzing its m6A methylation in mock-infected or HCMV-infected HAECs. **(A)** Western blot analysis of MCU protein levels after knockdown of METTL3 in mock-infected HAECs. **(B)** Western blot analysis of MCU protein levels after overexpression of METTL3 in mock-infected HAECs. HAECs were transfected with a different dose of METTL3 expression plasmids and then subjected to immunoblot. **(C)** qRT-PCR analysis to quantify the relative MCU mRNA level after knockdown or overexpression of METTL3 in mock-infected HAECs. **(D)** Western blot analysis of MCU protein level after METTL3 knockdown in HCMV-infected HAECs. **(E)** qRT-PCR analysis to quantify the relative MCU mRNA level after knockdown of METTL3 in HCMV-infected HAECs. **(F)** m6A immunoprecipitation and qRT-PCR were performed to determine the change of MCU mRNA with m6A methylation. HAECs with or without knockdown of METTL3 or METTL14 were exposed to HCMV. **(G)** Sequence analysis of the MCU 3′-UTR revealed three matches to the 5′-RRACU-3′ (underlined are methylated adenosine residue) m6A consensus sequence. **(H)** Luciferase assays were performed by transfecting HAECs with a reporter plasmid containing luciferase coding sequences followed by the MCU 3′-UTR or empty vector only containing luciferase. The ratio indicating the luciferase activity in cells transfected with MCU 3′-UTR relative to empty vector was determined. **(I)** Luciferase assays were performed in HAECs transfected with WT or mutant (MUT) luciferase-MCU 3′-UTR reporters. The ratio of luciferase activity in cells transfected with MCU-3′UTR relative to empty vector was determined. All data are expressed as the mean ± SD of triplicate experiments. Student's *t*-test, $^{**}p < 0.01$ and $^{***}p < 0.001$. ns: no significant difference.

its binding to MCU mRNA, and this interaction was significantly decreased after METTL3 knockdown (**Figure 6A**). In contrast, silencing METTL3 did not affect the association of YTHDF1 or YTHDF2 with MCU mRNA (**Figures 6B,C**). Moreover, to identify the MCU RNA-binding domain of YTHDF3, we stably expressed YTHDF3 deletion mutants in HAECs followed by exposure to HCMV infection. We found that only full-length YTHDF3 could bind to MCU

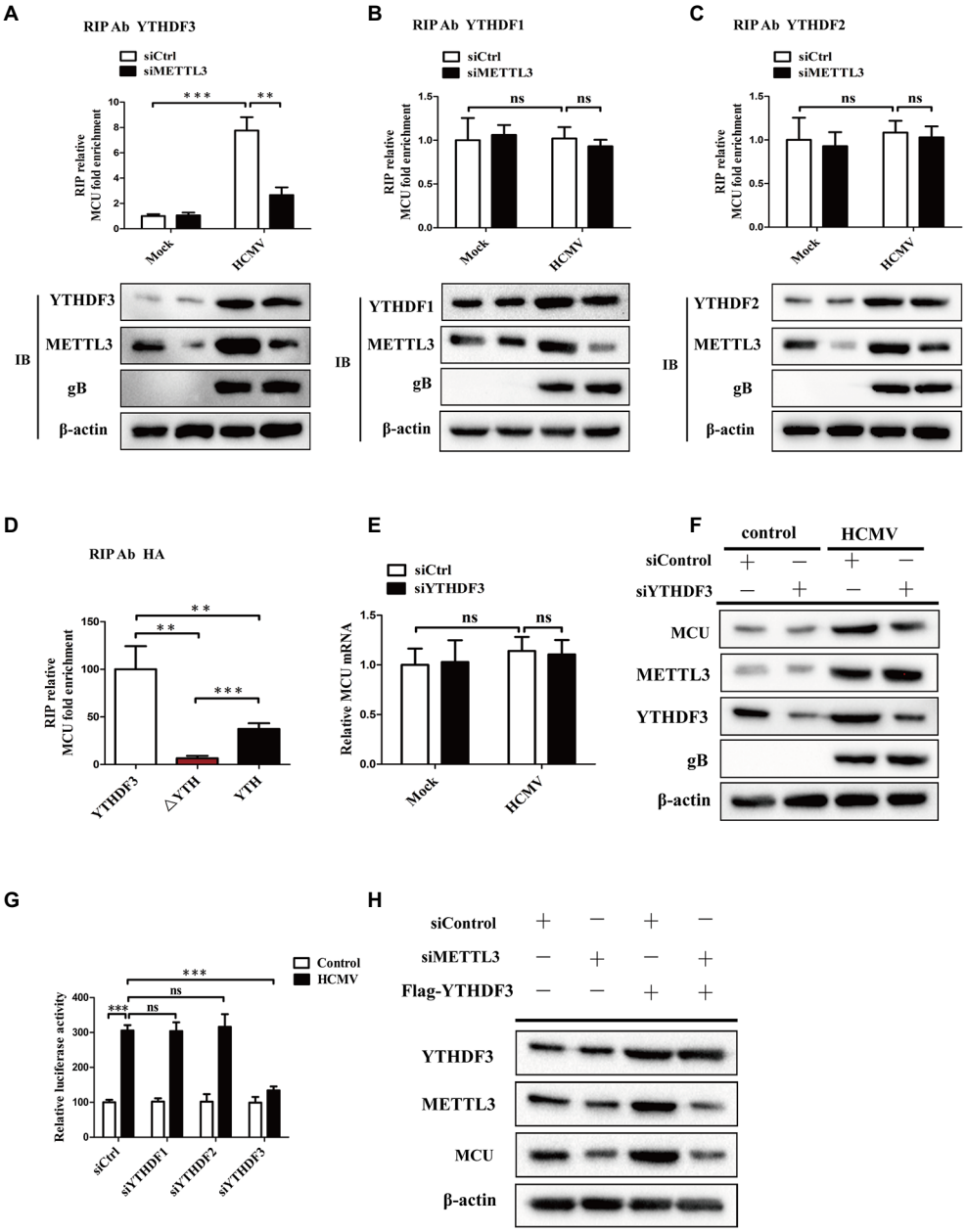


**FIGURE 6 |** YTHDF3 promotes translation of MCU protein by binding to the MCU mRNA dependently of METTL3-mediated m6A modification. **(A–C)**, RIP analysis of the interaction of YTHDF3 **(A)** or YTHDF1 **(B)** or YTHDF2 **(C)** with MCU mRNA using total cell lysates of HAECs with or without METTL3 knockdown under mock-infected or HCMV-infected condition. Enrichment of MCU mRNA with an antibody against YTHDF3 or YTHDF1 or YTHDF2 was measured by qRT-PCR and normalized to input. Western blotting was performed as indicated. **(D)** MCU RNA enrichment by HA RIP qPCR. Cells were transfected with HA-YTHDF3, HA-△YTH, or HA-YTH, then exposed to HCMV infection. Magnetic beads coated with 5ug of antibody against HA were incubated with indicated cell lysates. **(E)** qRT-PCR analysis of MCU mRNA in HAECs with or without YTHDF3 knockdown under mock-infected or HCMV-infected condition. **(F)** Western blotting of MCU protein expression in HAECs with or without YTHDF3 knockdown under mock-infected or HCMV-infected condition. **(G)** Luciferase assays analysis of changes in translation efficiency of luciferase-MCU 3′-UTR mRNA by knockdown of YTHDF1-3. **(H)** Western blotting analysis to identify whether the impact of YTHDF3 on MCU protein expression was dependent on METTL3. Cells were transfected with Flag-YTHDF3 with or without METTL3 knockdown. All data are expressed as the mean ± SD of triplicate experiments. *p* values were calculated with student's *t*-test, $^{**}p < 0.01$ and $^{***}p < 0.001$. ns: no significant difference.

mRNA. Deletion of the YTH domain (△YTH) of YTHDF3 abrogated the binding to MCU mRNA. MCU mRNA was enriched by the YTH domain by about 5-fold more than the △YTH mutant, but YTH alone did not regain the full ability of binding target RNAs (**Figure 6D**).

We then investigated whether YTHDF3 could regulate MCU expression by regulating the translation of MCU mRNA. As shown in **Figures 6E,F**, YTHDF3 knockdown attenuated the MCU protein expression induced by HCMV infection but did not affect the MCU mRNA levels. The luciferase assays also showed decreased MCU 3′-UTR luciferase activity in HAECs after YTHDF3 knockdown, but not in YTHDF1 or YTHDF2 (**Figure 6G**). In addition, elevated MCU protein expression was observed in YTHDF3 overexpressed HAECs and this increase was significantly reduced by METTL3 knockdown (**Figure 6H**). These data suggest that YTHDF3 plays a vital role in the regulation of MCU expression by promoting MCU protein translation *via* a METTL3-mediated m6A-dependent manner.

## ALKBH5 Not FTO Reverses HCMV-Mediated m6A Modification of MCU mRNA in HAECs

In mammalian cells, m6A methylation modification is a dynamic and reversible process. ALKBH5 and FTO, as two mammalian RNA demethylases, can reverse m6A methylation in cells (Meyer and Jaffrey, 2017). Although our previous results showed that the expression of ALKBH5 and FTO did not change after HCMV infection, we still wondered whether ALKBH5 or FTO was involved in the HCMV-mediated m6A methylation of MCU mRNA. We first measured the change in total mRNA and protein levels of MCU upon ALKBH5 knockdown in HCMV uninfected HAECs. The results showed that knockdown of ALKBH5 significantly increased protein abundance of MCU, but not mRNA (**Figures 7A,B**). In contrast, FTO knockdown did not change the expression of MCU mRNA and protein, suggesting that MCU may not be a direct target of FTO in HAECs (**Figures 7C,D**). Next, we tested the change in total mRNA and protein levels of MCU upon ALKBH5 overexpression in HCMV-infected HAECs. It was also observed that ALKBH5 overexpression strongly reduced the increased levels of MCU protein induced by HCMV infection but did not affect the total MCU mRNA (**Figures 7E,F**). These data suggest that MCU mRNA may be a substrate for ALKBH5 demethylase and this demethylase may not affect the stability but affect the translation efficiency of MCU mRNA.

To further investigate this idea, we performed methylated RNA immunoprecipitation (MeRIP) with m6A antibody of HCMV-infected HAECs in combination with qRT-PCR to determine the levels of MCU m6A methylation following ALKBH5 overexpression. Our results confirmed that m6A methylation on MCU mRNA was strongly increased in response to HCMV infection, whereas ALKBH5 overexpression significantly reduced the increased m6A levels of MCU mRNA induced by HCMV and this reduction was not observed by FTO overexpression (**Figure 7G**). These data indicate that ALKBH5 mainly affects MCU expression through its demethylation activity. As ALKBH5 can regulate MCU protein levels without effect on MCU mRNA, we wondered whether YTHDF3 was involved in the regulation of MCU protein by ALKBH5. Our experiments showed that the increased levels of MCU protein induced by ALKBH5 knockdown were significantly reduced by simultaneously silencing the YTHDF3 (**Figure 7H**), suggesting that the regulation of MCU protein by ALKBH5 is dependent on the effect of YTHDF3 on MCU mRNA translation process.

Next, the effects of ALKBH5 on apoptosis in HCMV-infected HAECs were examined. As shown in **Figure 7I**, the overexpression of ALKBH5 inhibited the apoptosis of HCMV-infected HAECs.

Based on the above results, as shown in **Figure 8**, it was concluded that HCMV induces apoptosis of vascular endothelial cells by promoting increased translation of MCU *via* METTL3- and YTHDF3-dependent m6A methylation mechanisms. In contrast, vitamin D3 downregulates the METTL3 by inhibiting the activation of AMPK, thereby inhibiting the m6A modification of MCU and cell apoptosis.

# DISCUSSION

Growing evidence indicates that HCMV infection may be the initiating factor of atherosclerosis and that it plays important roles in the occurrence and development of atherosclerosis (Hsich et al., 2001; Jia et al., 2017; Zhu and Liu, 2020). In the process of HCMV-induced atherosclerosis, the dysfunction and even apoptosis of vascular endothelial cells are the distinctive features (Shen et al., 2004; Utama et al., 2006). Since there is no specific drug to clear HCMV infection, there is an urgent need to find effective drugs to treat HCMV infection-related vascular endothelial cell damage. In the present study, we found that vitamin D3 could protect vascular endothelial cells from HCMV-induced apoptosis. Further exploring the mechanisms involved, we found that HCMV infection leads to an overall increase in the level of m6A modification in vascular endothelial cells. Moreover, it was found that HCMV infection could promote vascular endothelial cell apoptosis by increasing MCU protein expression in an m6A-mediated pattern. Further identification revealed that METTL3 is the methylation enzyme of MCU mRNA and YTHDF3 is the "reader" of MCU m6A locus. YTHDF3 can bind to the 3′UTR of MCU that undergoes m6A modification and promote the translation efficiency of MCU protein. Vitamin D3, on the other hand, can inhibit AMPK activation through VDR and reduce METTL3 expression (a downstream target of AMPK), thereby reducing MCU protein expression and ameliorating HCMV-induced apoptosis in vascular endothelia cells.

Vitamin D3 receptor (VDR), a member of the nuclear receptor family of transcription factors, is widely expressed on vascular tissues, such as vascular endothelial cells and vascular smooth muscle cells (Latic and Erben, 2020). This suggests that vitamin D3 plays an important role in the regulation

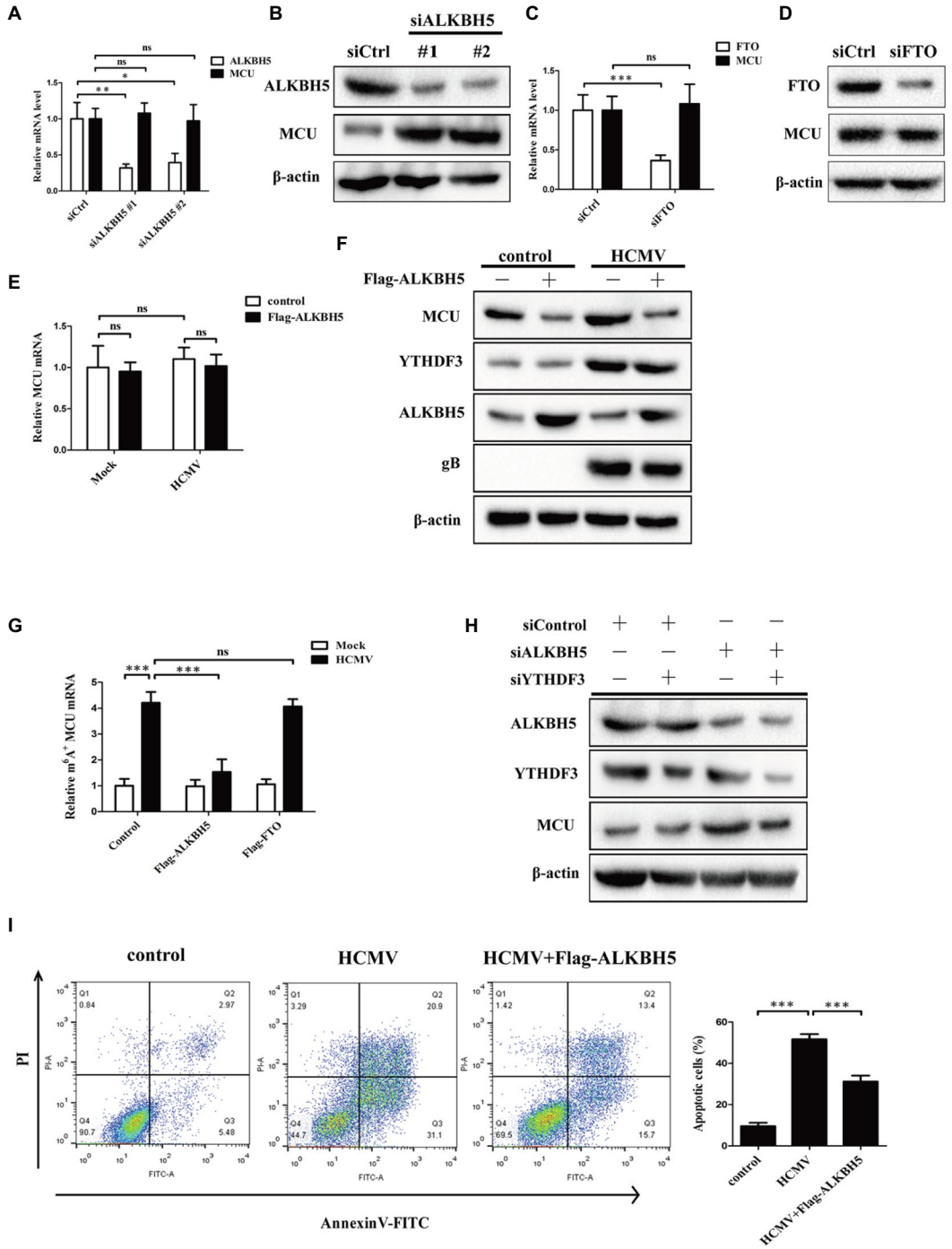


**FIGURE 7 |** ALKBH5, but not FTO, reverses HCMV-mediated m6A modification of MCU mRNA in HAECs. **(A)** qRT-PCR analysis of MCU mRNA expression in HAECs with or without ALKBH5 knockdown. Samples were normalized to GAPDH mRNA. **(B)** Representative Western blotting of MCU in HAECs with or without ALKBH5 knockdown. **(C)** qRT-PCR analysis of MCU mRNA expression in HAECs with or without FTO knockdown. Samples were normalized to GAPDH mRNA. **(D)** Representative Western blotting of MCU protein expression in HAECs with or without FTO knockdown. **(E)** qRT-PCR analysis of MCU mRNA expression in HAECs with or without ALKBH5 overexpression under mock-infected or HCMV-infected condition. **(F)** Representative Western blotting of MCU protein expression in HAECs with or without ALKBH5 overexpression under mock-infected or HCMV-infected condition. **(G)** m6A immunoprecipitation and qRT-PCR were performed to identify changes in MCU mRNA that underwent m6A methylation modification in HAECs with or without overexpression of ALKBH5 or FTO under mock-infected or HCMV-infected condition. **(H)** Western blotting analysis was performed to determine whether the effect of ALKBH5 on MCU protein expression was dependent on the promotion of MCU translation by YTHDF3. **(I)** Annexin-V/PI double-labeled flow cytometric assay shows that ALKBH5 overexpression attenuates the apoptosis induced by HCMV. Left, representative images of flow cytometry; right, statistical charts. All data are expressed as the mean ± SD of triplicate experiments. Values of $p$ were calculated with student's $t$-test, $*p<0.05$, $**p<0.01$, and $***p<0.001$. ns: no significant difference.

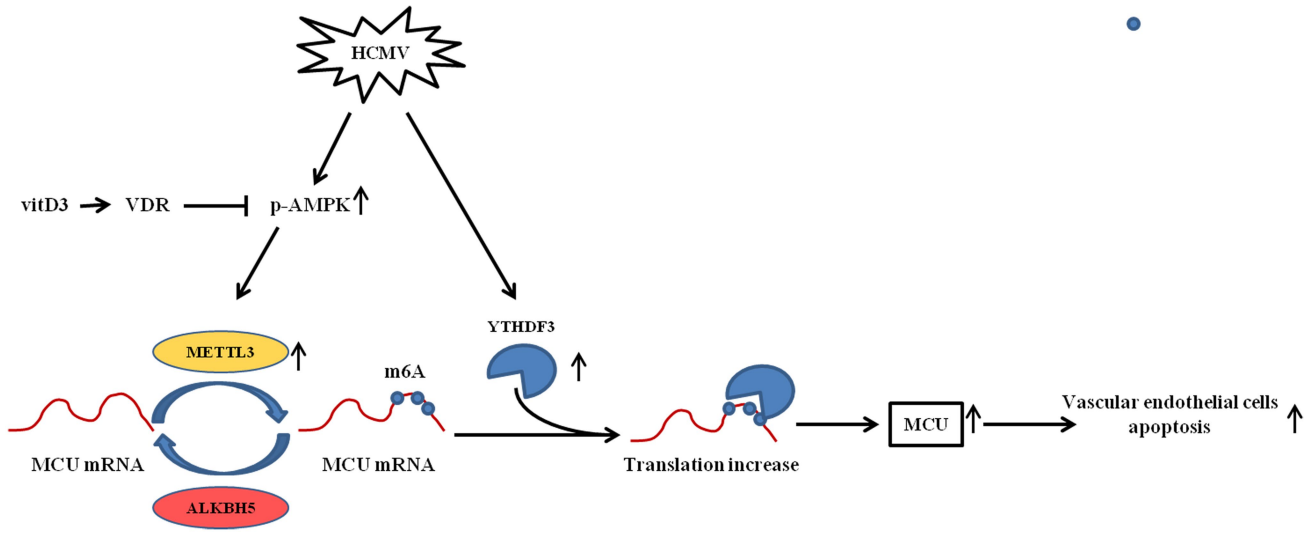


**FIGURE 8 |** The mechanism diagram of vitamin D3 inhibiting HCMV-induced apoptosis in HAECs. HCMV infection upregulates the expression of METTL3 and YTHDF3. METTL3 methylates MCU at three m6A residues in the 3′-UTR, thereby promoting the binding of RNA-binding protein YTHDF3 to MCU-methylated mRNA and promoting the translation of MCU mRNA. Increased MCU protein expression is responsible for HCMV-induced apoptosis. Vitamin D3 inhibits METTL3 expression *via* the VDR/AMPK pathway, thereby suppressing the MCU m6A modification and MCU-induced apoptosis.

of physiological function of blood vessels. A growing body of evidence suggests that vitamin D3 protects endothelial cells function from radiation, immune damage, and oxidative stress-induced injury (Dehghani et al., 2013; Polidoro et al., 2013; Marampon et al., 2016). In line with the above study, this study also found that vitamin D3 produced a protective effect on vascular endothelial cells against damage caused by HCMV infection. In addition, this anti-apoptotic ability was not due to inhibition of HCMV viral replication. Although it has been reported in the literature that vitamin D3 induces HCMV lytic replication marked by upregulation of HCMV gene expression and production of infectious virus (Wu and Miller, 2015), our experiments did not find the vitamin D3 could affect HCMV replication in vascular endothelial cells. Signaling analysis showed that vitamin D3 could downregulate the elevated level of p-AMPK induced by HCMV infection. Treatment with AICAR (an AMPK activator) or knockdown of the VDR attenuated the anti-apoptotic ability of vitamin D3 in HCMV-infected vascular endothelial cells, suggesting that vitamin D3 exerts its endothelial protective function through the VDR/AMPK axis.

As the most prevalent and abundant RNA modification in eukaryotes, N6-methyladenosine (m6A) modification has also attracted increasing attention in the regulation of cell fate (e.g., apoptosis; Shen et al., 2021; Yuan et al., 2021). Previous study showed that the overall abundance of cellular m6A writers METTL3/14, erasers ALKBH5 and FTO, and reader proteins increased in response to HCMV infection in normal human dermal fibroblasts (NHDFs; Rubio et al., 2018). Our experiments saw consistent results in vascular endothelial cells, with a slight difference that we did not see an increase in the demethylases ALKBH5 and FTO after HCMV infection. To understand the role of m6A modification in HCMV-induced apoptosis in endothelial cells, we knocked down the m6A writers METTL3/14 and the reader protein. We found that knockdown of METTL3 and YTHDF3 alleviated HCMV-induced apoptosis, suggesting that METTL3 and YTHDF3 mediated HCMV-triggered apoptosis in endothelial cells. In addition, vitamin D3 treatment downregulated the elevated expression of METTL3/14 induced by HCMV. However, this downregulation was reversed when AICAR was co-added, indicating that METTL3/14 is a downstream target of the AMPK pathway.

Aberrant expression or phosphorylation modification status of MCU causes disorder of the mitochondrial $Ca^{2+}$ transients, leading to cell death (Guan et al., 2019; Zhao et al., 2019; Li et al., 2020). In our present study, elevated amounts of total and phosphorylated proteins of MCU triggered by HCMV infection were also observed. Intervention with Ru360, an inhibitor of MCU function, or knock down the expression of MCU did attenuate HCMV-induced apoptosis. Further exploration indicated that treatment with vitamin D3 could downregulate the elevated level of MCU induced by HCMV *via* VDR/AMPK axis. Since inhibition of AMPK activation by vitamin D3 can reduce both METTL3/14 and MCU expression, we speculate that m6A modification may be involved in the regulation of MCU expression. Our study demonstrated that the methyltransferase METTL3, but not METTL14, mediated the methylation modification of MCU. Despite the identification of the biological significance of METTL3-mediated m6A modification, the mechanism of how m6A regulates MCU expression remains elusive. RNA metabolism regulation of m6A-modified mRNAs by so-called m6A readers is a fascinating field that has just started to be unveiled recently.

The m6A readers, such as the YTH domain-containing proteins (YTHDF1, 2, and 3), selectively bind to m6A-modified RNAs and play a distinctive function. YTHDF2 has been implicated in RNA transport, instability, and degradation (Fu et al., 2014). While YTHDF1 and YTHDF3 can promote translation of m6A-modified mRNA through an interaction with the ribosomal proteins of 40S/60S subunits (Wang et al., 2015; Li et al., 2017). Since all three readers were increased in HCMV-infected endothelial cells, we identified that YTHDF3, but not YTHDF1 or YTHDF2, could bind to the 3′UTR of MCU mRNA that underwent m6A modification and promote translation to facilitate MCU protein expression without affecting mRNA expression. As m6A modification is a dynamic process, I further identified ALKBH5 as a demethylase in the process of MCU m6A modification, and knockdown of ALKBH5 resulted in elevated methylation levels and elevated expression of MCU. Hence, in our current study, we propose a novel model in which METTL3 methylates MCU at three m6A residues in the 3′UTR, thereby promoting the association of RNA-binding protein YTHDF3 with MCU mRNA and promoting the translation of MCU protein. Supporting our findings, one study reported that m6A modification could alter RNA conformation to influence interaction with RNA-binding protein (Liu et al., 2017).

In conclusion, we established a model of HCMV-induced apoptosis in vascular endothelial cells and confirmed that HCMV promoted increased translation of MCU through METTL3 and YTHDF3-dependent manner, thereby promoting apoptosis. Conversely, vitamin D3 can downregulate the METTL3 by inhibiting the activation of AMPK, thereby inhibiting the m6A modification of MCU and cell apoptosis. Our findings extended the understanding of m6A driven machinery in virus-induced vascular endothelium damage and highlighted the significance of vitamin D3 in the intervention of HCMV-induced atherosclerosis.

## DATA AVAILABILITY STATEMENT

The original contributions presented in the study are included in the article/**Supplementary Material**, further inquiries can be directed to the corresponding authors.

## AUTHOR CONTRIBUTIONS

WZ and HZ designed and performed experiments, analyzed the data, and wrote the manuscript. HZ and SW guided the research and critically revised the manuscript. All authors have read and approved the final manuscript.

## FUNDING

This work was supported by the grants from the Natural Science Foundation of Hunan province (no. 2020JJ8031) and the cooperation project of FAAS (DWHZ2021-02).

## SUPPLEMENTARY MATERIAL

The Supplementary Material for this article can be found online at: https://www.frontiersin.org/articles/10.3389/fmicb.2022.861734/full#supplementary-material

**Supplementary Figure 1 | (A–C)** Western blot analysis for knockdown efficiency of YTHDF1 **(A)**, YTHDF2 **(B)**, and MCU **(C)** in HAECs with siRNA. **(D)** Effect of MCU activity on caspase-3 and caspase-9 activities using Caspase-3/9 fluorescent assay kits. **(E)** Knockdown of METTL14 in HAECs does not affect MCU protein expression. **(F)** Overexpression of METTL14 in HAECs does not affect MCU protein expression. **(G)** Sequence display of MCU 3′-UTR with mutated m6A sites. All data are expressed as the mean ± SD of triplicate experiments. Values of $p$ were calculated with student's $t$-test, $^{**}p < 0.01$ and $^{***}p < 0.001$. ns: no significant difference.

## REFERENCES

Andoniou, C. E., and Degli-Esposti, M. A. (2006). Insights into the mechanisms of CMV-mediated interference with cellular apoptosis. *Immunol. Cell Biol.* 84, 99–106. doi: 10.1111/j.1440-1711.2005.01412.x

Bennett, A. L., and Lavie, C. J. (2017). Vitamin D metabolism and the implications for atherosclerosis. *Adv. Exp. Med. Biol.* 996, 185–192. doi: 10.1007/978-3-319-56017-5_15

Brune, W. (2011). Inhibition of programmed cell death by cytomegaloviruses. *Virus Res.* 157, 144–150. doi: 10.1016/j.virusres.2010.10.012

Chang, E., and Kim, Y. (2019). Vitamin D ameliorates fat accumulation with AMPK/SIRT1 activity in C2C12 skeletal muscle cells. *Nutrients* 11, 2806–2822. doi: 10.3390/nu11112806

Chen, S., Law, C. S., Grigsby, C. L., Olsen, K., and Gardner, D. G. (2010). A role for the cell cycle phosphatase Cdc25a in vitamin D-dependent inhibition of adult rat vascular smooth muscle cell proliferation. *J. Steroid Biochem. Mol. Biol.* 122, 326–332. doi: 10.1016/j.jsbmb.2010.08.007

Chen, F. H., Liu, T., Xu, L., Zhang, L., and Zhou, X. B. (2018). Association of serum vitamin D level and carotid atherosclerosis: a systematic review and meta-analysis. *J. Ultrasound Med.* 37, 1293–1303. doi: 10.1002/jum.14494

Choi, M., Park, H., Cho, S., and Lee, M. (2013). Vitamin D3 supplementation modulates inflammatory responses from the muscle damage induced by high-intensity exercise in SD rats. *Cytokine* 63, 27–35. doi: 10.1016/j.cyto.2013.03.018

Crough, T., and Khanna, R. (2009). Immunobiology of human cytomegalovirus: from bench to bedside. *Clin. Microbiol. Rev.* 22, 76–98. doi: 10.1128/CMR.00034-08

Dehghani, L., Meamar, R., Etemadifar, M., Sheshde, Z. D., Shaygannejad, V., Sharifkhah, M., et al. (2013). Can vitamin D suppress endothelial cells apoptosis in multiple sclerosis patients? *Int. J. Prev. Med.* 4, S211–S215.

Fu, Y., Dominissini, D., Rechavi, G., and He, C. (2014). Gene expression regulation mediated through reversible m(6)A RNA methylation. *Nat. Rev. Genet.* 15, 293–306. doi: 10.1038/nrg3724

Goldmacher, V. S. (2005). Cell death suppression by cytomegaloviruses. *Apoptosis* 10, 251–265. doi: 10.1007/s10495-005-0800-z

Guan, L., Che, Z., Meng, X., Yu, Y., Li, M., Yu, Z., et al. (2019). MCU up-regulation contributes to myocardial ischemia-reperfusion injury through calpain/OPA-1-mediated mitochondrial fusion/mitophagy inhibition. *J. Cell. Mol. Med.* 23, 7830–7843. doi: 10.1111/jcmm.14662

Hsich, E., Zhou, Y. F., Paigen, B., Johnson, T. M., Burnett, M. S., and Epstein, S. E. (2001). Cytomegalovirus infection increases development of atherosclerosis in Apolipoprotein-E knockout mice. *Atherosclerosis* 156, 23–28. doi: 10.1016/S0021-9150(00)00608-0

Jia, Y. J., Liu, J., Han, F. F., Wan, Z. R., Gong, L. L., Liu, H., et al. (2017). Cytomegalovirus infection and atherosclerosis risk: a meta-analysis. *J. Med. Virol.* 89, 2196–2206. doi: 10.1002/jmv.24858

Khoshnevis, M., and Tyring, S. K. (2002). Cytomegalovirus infections. *Dermatol. Clin.* 20, 291–299. doi: 10.1016/S0733-8635(01)00007-9

Kim, D. H., Meza, C. A., Clarke, H., Kim, J. S., and Hickner, R. C. (2020). Vitamin D and endothelial function. *Nutrients* 12, 575–591. doi: 10.3390/nu12020575

Latic, N., and Erben, R. G. (2020). Vitamin D and cardiovascular disease, with emphasis on hypertension, atherosclerosis, and heart failure. *Int. J. Mol. Sci.* 21, 6483–6497. doi: 10.3390/ijms21186483

Lee, G. C., Lee, J. H., Kim, B. Y., and Lee, C. H. (2013). Mitochondria-targeted apoptosis in human cytomegalovirus-infected cells. *J. Microbiol. Biotechnol.* 23, 1627–1635. doi: 10.4014/jmb.1306.06023

Li, A., Chen, Y. S., Ping, X. L., Yang, X., Xiao, W., Yang, Y., et al. (2017). Cytoplasmic m(6)A reader YTHDF3 promotes mRNA translation. *Cell Res.* 27, 444–447. doi: 10.1038/cr.2017.10

Li, Y., Wang, C., Lian, Y., Zhang, H., Meng, X., Yu, M., et al. (2020). Role of the mitochondrial calcium uniporter in Mg(2+)-free-induced epileptic hippocampal neuronal apoptosis. *Int. J. Neurosci.* 130, 1024–1032. doi: 10.1080/00207454.2020.1715978

Liu, N., Zhou, K. I., Parisien, M., Dai, Q., Diatchenko, L., and Pan, T. (2017). N6-methyladenosine alters RNA structure to regulate binding of a low-complexity protein. *Nucleic Acids Res.* 45, 6051–6063. doi: 10.1093/nar/gkx141

Manandhar, T., Ho, G. T., Pump, W. C., Blasczyk, R., and Bade-Doeding, C. (2019). Battle between host immune cellular responses and HCMV immune evasion. *Int. J. Mol. Sci.* 20, 3626–3651. doi: 10.3390/ijms20153626

Marampon, F., Gravina, G. L., Festuccia, C., Popov, V. M., Colapietro, A., Sanita, P., et al. (2016). Vitamin D protects endothelial cells from irradiation-induced senescence and apoptosis by modulating MAPK/SirT1 axis. *J. Endocrinol. Investig.* 39, 411–422. doi: 10.1007/s40618-015-0381-9

Meyer, K. D., and Jaffrey, S. R. (2017). Rethinking m(6)A readers, writers, and erasers. *Annu. Rev. Cell Dev. Biol.* 33, 319–342. doi: 10.1146/annurev-cellbio-100616-060758

Moon, M. S., Lee, G. C., Kim, J. H., Yi, H. A., Bae, Y. S., and Lee, C. H. (2003). Human cytomegalovirus induces apoptosis in promonocyte THP-1 cells but not in promyeloid HL-60 cells. *Virus Res.* 94, 67–77. doi: 10.1016/S0168-1702(03)00134-5

Mozos, I., and Marginean, O. (2015). Links between vitamin D deficiency and cardiovascular diseases. *Biomed. Res. Int.* 2015:109275. doi: 10.1155/2015/109275

Nakamura, H., Liao, H., Minami, K., Toyoda, M., Akutsu, H., Miyagawa, Y., et al. (2013). Human cytomegalovirus induces apoptosis in neural stem/progenitor cells derived from induced pluripotent stem cells by generating mitochondrial dysfunction and endoplasmic reticulum stress. *Herpesviridae* 4:2. doi: 10.1186/2042-4280-4-2

Oh, J., Weng, S., Felton, S. K., Bhandare, S., Riek, A., Butler, B., et al. (2009). 1,25(OH)2 vitamin D inhibits foam cell formation and suppresses macrophage cholesterol uptake in patients with type 2 diabetes mellitus. *Circulation* 120, 687–698. doi: 10.1161/CIRCULATIONAHA.109.856070

Polidoro, L., Properzi, G., Marampon, F., Gravina, G. L., Festuccia, C., Di Cesare, E., et al. (2013). Vitamin D protects human endothelial cells from H(2)O(2) oxidant injury through the Mek/Erk-Sirt1 axis activation. *J. Cardiovasc. Transl. Res.* 6, 221–231. doi: 10.1007/s12265-012-9436-x

Rubio, R. M., Depledge, D. P., Bianco, C., Thompson, L., and Mohr, I. (2018). RNA m(6) A modification enzymes shape innate responses to DNA by regulating interferon beta. *Genes Dev.* 32, 1472–1484. doi: 10.1101/gad.319475.118

Shao, Y., Qi, Y., Huang, Y., Liu, Z., Ma, Y., Guo, X., et al. (2016). Human cytomegalovirus-encoded miR-US4-1 promotes cell apoptosis and benefits discharge of infectious virus particles by targeting QARS. *J. Biosci.* 41, 183–192. doi: 10.1007/s12038-016-9605-1

Shen, W., Li, H., Su, H., Chen, K., and Yan, J. (2021). FTO overexpression inhibits apoptosis of hypoxia/reoxygenation-treated myocardial cells by regulating m6A modification of Mhrt. *Mol. Cell. Biochem.* 476, 2171–2179. doi: 10.1007/s11010-021-04069-6

Shen, Y. H., Utama, B., Wang, J., Raveendran, M., Senthil, D., Waldman, W. J., et al. (2004). Human cytomegalovirus causes endothelial injury through the ataxia telangiectasia mutant and p53 DNA damage signaling pathways. *Circ. Res.* 94, 1310–1317. doi: 10.1161/01.RES.0000129180.13992.43

Song, H., Feng, X., Zhang, H., Luo, Y., Huang, J., Lin, M., et al. (2019). METTL3 and ALKBH5 oppositely regulate m(6)A modification of TFEB mRNA, which dictates the fate of hypoxia/reoxygenation-treated cardiomyocytes. *Autophagy* 15, 1419–1437. doi: 10.1080/15548627.2019.1586246

Szeto, F. L., Reardon, C. A., Yoon, D., Wang, Y., Wong, K. E., Chen, Y., et al. (2012). Vitamin D receptor signaling inhibits atherosclerosis in mice. *Mol. Endocrinol.* 26, 1091–1101. doi: 10.1210/me.2011-1329

Utama, B., Shen, Y. H., Mitchell, B. M., Makagiansar, I. T., Gan, Y., Muthuswamy, R., et al. (2006). Mechanisms for human cytomegalovirus-induced cytoplasmic p53 sequestration in endothelial cells. *J. Cell Sci.* 119, 2457–2467. doi: 10.1242/jcs.02974

Wang, X., Lu, Z., Gomez, A., Hon, G. C., Yue, Y., Han, D., et al. (2014). N6-methyladenosine-dependent regulation of messenger RNA stability. *Nature* 505, 117–120. doi: 10.1038/nature12730

Wang, X., Zhao, B. S., Roundtree, I. A., Lu, Z., Han, D., Ma, H., et al. (2015). N(6)-methyladenosine modulates messenger RNA translation efficiency. *Cell* 161, 1388–1399. doi: 10.1016/j.cell.2015.05.014

Williamson, C. D., and Colberg-Poley, A. M. (2009). Access of viral proteins to mitochondria via mitochondria-associated membranes. *Rev. Med. Virol.* 19, 147–164. doi: 10.1002/rmv.611

Wu, S. E., and Miller, W. E. (2015). The human cytomegalovirus lytic cycle is induced by 1,25-dihydroxyvitamin D3 in peripheral blood monocytes and in the THP-1 monocytic cell line. *Virology* 483, 83–95. doi: 10.1016/j.virol.2015.04.004

Xiao, W., Adhikari, S., Dahal, U., Chen, Y. S., Hao, Y. J., Sun, B. F., et al. (2016). Nuclear m(6)A reader YTHDC1 regulates mRNA splicing. *Mol. Cell* 61, 507–519. doi: 10.1016/j.molcel.2016.01.012

Yuan, Q., Zhu, H., Liu, H., Wang, M., Chu, H., and Zhang, Z. (2021). METTL3 regulates PM2.5-induced cell injury by targeting OSGIN1 in human airway epithelial cells. *J. Hazard. Mater.* 415:125573. doi: 10.1016/j.jhazmat.2021.125573

Zhang, S., Deng, W., Liu, Q., Wang, P., Yang, W., and Ni, W. (2020). Altered m(6) A modification is involved in up-regulated expression of FOXO3 in luteinized granulosa cells of non-obese polycystic ovary syndrome patients. *J. Cell. Mol. Med.* 24, 11874–11882. doi: 10.1111/jcmm.15807

Zhang, Y., Wang, X., Zhang, X., Wang, J., Ma, Y., Zhang, L., et al. (2019). RNA-binding protein YTHDF3 suppresses interferon-dependent antiviral responses by promoting FOXO3 translation. *Proc. Natl. Acad. Sci. U. S. A.* 116, 976–981. doi: 10.1073/pnas.1812536116

Zhao, H., Li, T., Wang, K., Zhao, F., Chen, J., Xu, G., et al. (2019). AMPK-mediated activation of MCU stimulates mitochondrial Ca(2+) entry to promote mitotic progression. *Nat. Cell Biol.* 21, 476–486. doi: 10.1038/s41556-019-0296-3

Zhao, X., Yang, Y., Sun, B. F., Shi, Y., Yang, X., Xiao, W., et al. (2014). FTO-dependent demethylation of N6-methyladenosine regulates mRNA splicing and is required for adipogenesis. *Cell Res.* 24, 1403–1419. doi: 10.1038/cr.2014.151

Zhu, W., and Liu, S. (2020). The role of human cytomegalovirus in atherosclerosis: a systematic review. *Acta Biochim. Biophys. Sin.* 52, 339–353. doi: 10.1093/abbs/gmaa005

Zhu, H., Shen, Y., and Shenk, T. (1995). Human cytomegalovirus IE1 and IE2 proteins block apoptosis. *J. Virol.* 69, 7960–7970. doi: 10.1128/jvi.69.12.7960-7970.1995

**Conflict of Interest:** The authors declare that the research was conducted in the absence of any commercial or financial relationships that could be construed as a potential conflict of interest.

**Publisher's Note:** All claims expressed in this article are solely those of the authors and do not necessarily represent those of their affiliated organizations, or those of the publisher, the editors and the reviewers. Any product that may be evaluated in this article, or claim that may be made by its manufacturer, is not guaranteed or endorsed by the publisher.

*Copyright © 2022 Zhu, Zhang and Wang. This is an open-access article distributed under the terms of the Creative Commons Attribution License (CC BY). The use, distribution or reproduction in other forums is permitted, provided the original author(s) and the copyright owner(s) are credited and that the original publication in this journal is cited, in accordance with accepted academic practice. No use, distribution or reproduction is permitted which does not comply with these terms.*

frontiers in Microbiology

ORIGINAL RESEARCH
published: 14 March 2022
doi: 10.3389/fmicb.2022.865336

# Long-Term Expansion of Porcine Intestinal Organoids Serves as an *in vitro* Model for Swine Enteric Coronavirus Infection

*Min Zhang[1,2†], Lilei Lv[2†], Hongming Cai[2,3], Yanhua Li[4], Fei Gao[2,5], Lingxue Yu[2,5], Yifeng Jiang[2,5], Wu Tong[2,5], Liwei Li[2,5], Guoxin Li[2,5], Guangzhi Tong[1,2,5*] and Changlong Liu[2,5*]*

[1] College of Veterinary Medicine, Northeast Agricultural University, Harbin, China, [2] Shanghai Veterinary Research Institute, Chinese Academy of Agricultural Sciences, Shanghai, China, [3] Key Laboratory of Fujian-Taiwan Animal Pathogen Biology, College of Animal Sciences, Fujian Agriculture and Forestry University, Fuzhou, China, [4] College of Veterinary Medicine, Yangzhou University, Yangzhou, China, [5] Jiangsu Co-innovation Center for the Prevention and Control of Important Animal Infectious Disease and Zoonosis, Yangzhou University, Yangzhou, China

OPEN ACCESS

**Edited by:**
Chunfu Zheng,
University of Calgary, Canada

**Reviewed by:**
Shao-Lun Zhai,
Institute of Animal Health, Guangdong Academy of Agricultural Sciences (GDAAS), China
Xiangdong Li,
Yangzhou University, China
Huachun Cui,
University of Alabama at Birmingham, United States

***Correspondence:**
Guangzhi Tong
gztong@shvri.ac.cn
Changlong Liu
liuchanglong@shvri.ac.cn

[†] These authors have contributed equally to this work

**Specialty section:**
This article was submitted to Virology, a section of the journal Frontiers in Microbiology

**Received:** 29 January 2022
**Accepted:** 21 February 2022
**Published:** 14 March 2022

**Citation:**
Zhang M, Lv L, Cai H, Li Y, Gao F, Yu L, Jiang Y, Tong W, Li L, Li G, Tong G and Liu C (2022) Long-Term Expansion of Porcine Intestinal Organoids Serves as an in vitro Model for Swine Enteric Coronavirus Infection. Front. Microbiol. 13:865336. doi: 10.3389/fmicb.2022.865336

A reliable and reproducible model *in vitro* for swine enteric coronaviruses infection would be intestinal models that support virus replication and can be long-term cultured and manipulated experimentally. Here, we designed a robust long-term culture system for porcine intestinal organoids from the intestinal crypt or single LGR5$^{+}$ stem cell by combining previously defined insights into the growth requirements of the intestinal epithelium of humans. We showed that long-term cultured swine intestinal organoids were expanded *in vitro* for more than 6 months and maintained the potential to differentiate into different types of cells. These organoids were successfully infected with porcine enteric coronavirus, including porcine epidemic diarrhea virus (PEDV) and transmissible gastroenteritis virus (TGEV), and were capable of supporting virus replication and progeny release. RNA-seq analysis showed robust induction of transcripts associated with antiviral signaling in response to enteric coronavirus infection, including hundreds of interferon-stimulated genes and cytokines. Moreover, gene set enrichment analysis indicated that PEDV infection could suppress the immune response in organoids. This 3D intestinal organoid model offers a long-term, renewable resource for investigating porcine intestinal infections with various pathogens.

**Keywords: long-term 3D culture, porcine intestinal organoids, swine enteric coronaviruses, interferon-stimulated genes, immune suppression**

## INTRODUCTION

Porcine epidemic diarrhea virus (PEDV), transmissible gastroenteritis virus (TGEV), and porcine delta coronavirus (PDCoV) are major pathogenic swine enteric viruses, which belong to the family Coronaviridae. PEDV, TGEV, and PDCoV are highly contagious and are a major cause of illness and death in piglets (Jung and Saif, 2015; Jung et al., 2016). These viruses can cause endemics or large-scale epidemics in major pig-producing countries, which lead to severe economic losses in the swine industry. So far, no effective treatments are available for any of these swine

enteric coronaviruses (CoVs) that have resisted eradication efforts in different countries (Vlasova et al., 2020).

Swine enteric CoVs share tropism for swine intestinal epithelial cells *in vivo* (Sungsuwan et al., 2020). Infection of any of these enteric coronaviruses can damage the jejunum and ileum of neonatal piglets up to 3 weeks of age (Vlasova et al., 2020). However, most *in vitro* studies of swine enteric CoVs have been performed in non-targeting cell lines. Vero cells from African green monkey kidneys have been used for PEDV propagation since it was described by Hofmann and Wyler (1988). Other immortalized cell lines permissive for PEDV include MARC-145, LLC-PK1, Huh7, and so forth (Liu et al., 2015; Zhang et al., 2016, 2017). PK-15 cells derived from porcine kidney and swine testicle-derived ST cells are used for TGEV isolation and propagation *in vitro* (Wang et al., 2019). The conclusions obtained from those non-targeting cells may not represent the true response to virus infection in targeting cells. Therefore, several swine intestine epithelial cell lines were developed like IPEC-J2 and IPI-21, which derived from pig jejunum and ileum, respectively. However, the viral infectivity in IPEC-J2 and IPI-21 cells are controversial, and it is increasingly evident that these cell models are not sufficient to fully understand swine enteric CoVs diseases (Zhao et al., 2014; Wang et al., 2019). Thus, the development of a reliable and reproducible model *in vitro* for swine enteric Covs infection is urgently needed for investigations of CoVs.

Unlike the immortalized cell lines models, organoids are self-organizing 3D structures grown from adult stem cells and recapitulate key aspects of the organ from which those cells derive (Clevers, 2016). The establishment of mouse intestinal organoids in 2009 advanced our understanding of the intestinal epithelium and led to numerous opportunities to study virus pathogenesis and host-pathogen interactions in this particular model (Sato et al., 2009; Artegiani and Clevers, 2018). Long-term cultures in which organoids can differentiate and recapitulate normal crypt-villus architecture have been established from the mouse and human intestines (Sato et al., 2011). Organoids derived from the porcine intestine have been produced using different culture systems (Powell and Behnke, 2017; Derricott et al., 2019; Li et al., 2019; Li Y. et al., 2020; Vermeire et al., 2021). However, these approaches may not allow long-term expansion of swine intestinal epithelium from adult pig individuals *in vitro*.

Long-term expansion of organoids culture requires suitable matrices creating a 3D condition as well as the appropriate medium providing necessary niche factors, which recapitulates the *in vivo* stem cell niche and able to sustain stem cell the capacity for self-renewal and the potential to differentiation (Clevers, 2016; Artegiani and Clevers, 2018). The media supplemented with wnt3a, R-spondin1, noggin, and the epidermal growth factor is sufficient to support the long-term expansion of mouse intestinal organoids, whereas the addition of nicotinamide, along with an inhibitor of ALK and an inhibitor of p38, was required for long-term culture of human small intestine organoids (Sato et al., 2011).

In this study, we designed a long-term culture to robust expand the porcine intestinal organoids by combining previously defined insights into the growth requirements of the intestinal epithelium. Studies of these cultures indicated that those swine intestinal organoids could self-renew for 6 months. These intestinal organoids were susceptible to infection by porcine enteric coronavirus PEDV and TGEV. We conclude that long-term expansion organoids represent versatile models for the *in vitro* study of swine enteric coronaviruses infection.

# MATERIALS AND METHODS

## Animal and Viruses

All experimental procedures and animal care protocols were approved by the Care and Use of Laboratory Animals of Shanghai Veterinary Research Institute (SHVRI), Chinese Academy of Agricultural Sciences, China. The PEDV-SD strain (GenBank accession No.MZ596343) and TGEV H16 (GenBank accession no.FJ755618) stocks were prepared and titrated on the Vero E6 cells and LLC-PK1 cells by TCID50, respectively.

## Cell Culture and Conditioned Media

L-WRN cells (CRL-3276) were obtained from American Type Culture Collection, and cultured in high glucose DMEM (Hyclone) supplemented with penicillin (100 U/mL), streptomycin (100 μg/mL) (Sigma-Aldrich), Geneticin (500 μg/ml) (Invitrogen), Hygromycin (500 μg/ml) (Invitrogen; Cat#: 10687010), and 10% fetal bovine serum (Gibco). Mycoplasma infection screening was performed with the LookOut Mycoplasma PCR Detection Kit (Sigma-Aldrich) as recommended by the manufacturer using cultured cell supernatant. The L-WRN conditioned media was made as previously described using the L-WRN cell line (Miyoshi and Stappenbeck, 2013).

## Porcine Intestinal Tissue Processing, Crypt Isolation, and Organoids Culture

Porcine intestinal crypts from the duodenum, jejunum, or ileum were prepared from specific-pathogen-free 10 days old piglets using previously described protocols with minor modification (Fujii et al., 2015). Briefly, the intestinal sections were cut and opened longitudinally. The mucosal layer and villi were removed by scraping with a microscope slide, and 2-4 cm of intestinal sections were cut into 5-mm segments. The dissected pieces were washed 5-10 times with PBS until the supernatant was free of debris, and then the washed pieces were incubated in cold PBS supplemented with 2.5 mM EDTA for 40 min at 4°C with gently rotating. Then pieces were pelleted and pipetted up and down in 10 ml of cold PBS vigorously to release crypts. The supernatant containing crypts was centrifuged at 400 *g* for 3 min. The crypts were washed twice with cold PBS and resuspended in Matrigel (Corning) with about 100–150 crypts per 50 μl of Matrigel. Dispense 50 μl of the crypt-Matrigel suspension into the center of each well of a 37°C pre-warmed 24-well plate. The Matrigel was polymerized for 15 min at 37°C, porcine intestinal organoids (PIO) medium plus 10 μM of ROCK inhibitor was added, and crypts were incubated at 37°C, 5% $CO_2$. The composition of PIO medium is: Advanced DMEM/F12,

100 μg/ml primocin, 2 mM GlutaMax, 10 mM HEPES, 1 × N2, 1 × B27, 1 mM N-Acetyl-Cysteine, 10 mM Nicotinamide, 50% L-WRN conditioned medium, 50 ng/ml human EGF, 500 nM A83-01 and 3 μM SB202190 (**Supplementary Table 1**).

## Organoids Passage, Cryopreservation, and Resuscitation

The intestinal organoids culture medium was refreshed every 3 days until organoids were approximately ten times the original size. Matrigel was broken up with medium using a 1-ml pipet tip and transferred from the well to a 15-ml tube to passage the organoids. The organoids were centrifuged at 400 *g* for 3 min, and the medium and most of Matrigel were removed. The organoids were incubated with 1 ml of TrypLE Express (Invitrogen) at 37°C for 5 min. Basal medium (Advanced DMEM/F12, 100 U/ml penicillin, 100 μg/ml streptomycin, 2 mM GlutaMax, 10 mM HEPES) was added, and cells were spun down at 400 g for 3 min. The pellet was resuspended in Matrigel and plated in droplets of 50 μl each well of 24-well plate. After allowing the Matrigel to solidify, PIO medium supplemented with 10 μM ROCK inhibitor was added to the plates, and organoids were cultured at 37°C 5% $CO_2$.

On day 4 or 5 of culture, the medium was removed from wells, and 1 ml of Recovery Cell Culture Freezing Medium (Invitrogen) was added. Organoids-containing Matrigel was scraped and transferred into 2-ml cryovials. Place tubes in a freezing container and incubate the tubes at −80°C for at least 1 day. Then transfer the frozen cryovials to a liquid nitrogen storage tank.

To recover the frozen organoids, cryovials containing organoids were removed from liquid nitrogen and thawed quickly in a 37°C water bath. The organoids were transferred into a 15-ml centrifuge tube, and 10 ml of basal medium were added. The organoids were pelleted down at 4°C at 400 g for 3 min. Then, the organoids were resuspended with Matrigel and plated in droplets of 50 μl each well of 24-well plate. After allowing the Matrigel to solidify, PIO medium supplemented with 10 μM ROCK inhibitor was added to the plates, and organoids were cultured at 37°C, 5% $CO_2$.

## Organoids Differentiation

For swine intestinal organoid differentiation, organoids were plated in Matrigel with PIO media. At 2–3 days after plating in Matrigel, organoids were cultured with PIO medium with DMSO or PIO medium 5% L-WRN conditioned medium containing 5 mM DAPT for 2 days. After treatment, organoids were harvested, and the total RNAs were purified using Trizol.

## Organoids Proliferation Assay and 5-Ethynyl-2′-Deoxyuridine Imaging

Single-cell suspensions from swine intestinal organoids were generated by TrypLE and counted. About 3,000 cells per replicate were plated in Matrigel and incubated in the PIO medium described above. At the indicated time points, 700 uM resazurin (Sigma) in PBS was added 10% by volume to each treatment well. Cells were incubated for 5 h in 37°C, 5% $CO_2$ incubator, and then fluorescence was measured on BioTek Epoch Microplate Spectrophotometer (BioTek).

The proliferation of organoids was also evaluated by Click-iT Plus EdU Imaging Kit (Invitrogen). In brief, organoid cells were incubated with EdU for 6 h fixed in 4% paraformaldehyde in DPBS and incubated for 15 min at room temperature. After washing 3 times with DPBS, the organoids were permeabilized and blocked with blocking buffer (0.1% Triton-X 100 and 3% BSA in DPBS) for 20 min at room temperature. Click-iT Plus reaction cocktail was added and incubated with cells for 30 min. The cells were counterstained with Hoechst for 10 min. Images were taken by Olympus IX81 fluorescence microscope.

## Histology and Imaging

Organoids were collected and fixed in 4% paraformaldehyde (PFA). Pellet fixed organoids at 400 g for 5 min, and wash with 1 ml PBS. Aspirate supernatant as much as possible, then mix 20 μl of organoids at 1:1 with molten 2% low melt agarose to tube. Immediately pipette onto parafilm to form a small dome, allow to cool. Then the small dome was put in a mold and filled with low melt agarose to form a block, followed by dehydration, paraffin embedding, sectioning, and standard H&E staining. Images were acquired on a Leica Eclipse E600 microscope.

## Quantitative Reverse Transcription Polymerase Chain Reaction

Total RNA was purified from organoids using TRIzol (Thermo Fisher Scientific, Shanghai, China). The reverse transcription reaction was carried out with 1 μg of total RNA using a PrimeScript first-strand cDNA synthesis kit (Takara, Beijing, China). Quantitative real-time PCR was performed using SYBR Premix Ex Taq (Takara, Beijing, China) and a LightCycler 96 instrument (Roche, Shanghai, China). The relative quantities of the genes were calculated using GAPDH as a reference, using the formula: $2^{-[Ct(Gene)-Ct(GAPDH)]}$. The primer sequences for each gene are provided in **Supplementary Table 2**.

## Transmissible Gastroenteritis Virus Infection and Porcine Epidemic Diarrhea Virus

Organoids were harvested in a cold basal medium washed once to remove Matrigel and digested using TrypLE express. After digestion, organoids were washed once in a Basal medium. TGEV and PEDV infections were performed at a multiplicity of infection (MOI) of 0.1 in Basal medium (Trypsin was added to Basal medium at a concentration of 5 μg/ml for PEDV infection). After 2 h of virus adsorption at 37°C 5% $CO_2$, cultures were washed twice with excess Basal medium to remove unbound virus. Organoids were re-embedded into 50 μl of Matrigel in 24-well tissue culture plates and cultured in 500 μl of PIO medium. Each well contained about 100,000 cells. Samples were taken at indicated time points by harvesting the medium in the well (supernatant) and the cells by resuspending the matrigel droplet containing organoids into 500 μl Basal medium.

## Immunofluorescent Staining of Organoids

Remove the culture medium from the wells, add 1 ml of ice-cold cell recovery solution (Corning) to each well and collect all organoids to a 15-ml tube. Fill up to 10 ml with ice-cold 1% (wt/vol) PBS-BSA and spin down at 300 g for 5 min at 4°C. Remove the supernatant. Gently resuspend the pellet of organoids in 1 ml of 4% PFA and incubate at 4°C for 45 min. Wash the pellet of organoids twice with 10 ml cold PBST and spin down at 300 g for 5 min at 4°C. For blocking the organoids, resuspend the pellet in 1 ml cold blocking buffer (0.1% triton-X100, 1% BSA in PBS). Incubate at 4°C for 15 min and wash the organoids' pellet twice with 10 ml ice-cold 1% BSA/PBS and spin down at 300 g for 5 min at 4°C. Resuspend the pellet of organoids in mouse monoclonal antibody against TGEV N (1:800 Shanghai Youlong Biotech) or rabbit monoclonal antibody against PEDV N (1:500, Shanghai Ango Biotech) and incubate at 4°C overnight. Wash the pellet of organoids twice with 10 ml ice-cold PBS and spin down at 300 g for 5 min at 4°C. Resuspend the pellet of organoids in 1 ml of goat anti-mouse IgG (H + L) Cross-Adsorbed Secondary Antibody, Alexa Fluor 488 (1:1000, Invitrogen) or goat anti-rabbit IgG (H + L) Cross-Adsorbed Secondary Antibody, Alexa Fluor 488 (1:1000, Invitrogen) and incubate at 37°C for 1 h. Wash the pellet of organoids twice with 10 ml ice-cold PBS and spin down at 300 g for 5 min at 4°C. Resuspend the pellet of organoids in 1 ml 0.1% DAPI in PBS incubate at room temperature 15 min. Wash the pellet of organoids twice with 10 ml ice-cold PBS and spin down at 300 g for 5 min at 4°C. Add 50 μl of fructose-glycerol clearing solution (mix 33 ml of glycerol, 7 ml of dH2O, and 29.7 g of fructose) using a 200-μl tip with the end cut off and resuspend organoids gently. Cut off the end of a 200-μl tip and use it to transfer 20 μl of the organoids in the middle of the slide and place a coverslip on top. Gently apply pressure to both sides of the coverslip to firmly attach. Images were taken by Nikon Model Eclipse fluorescence microscope.

## RT-qPCR Assay for Viral Genome Copy Number

For viral genome copy number detection, total RNA was extracted from cultured organoids with RNeasy Mini Kit (QIAGEN), and RNA in the supernatant was extracted with QIAamp Viral RNA Mini Kit. RNA was then reverse transcribed into cDNA by reverse transcriptase mix (Takara). Total RNAs were extracted and then was synthesized into cDNA by reverse transcriptase (Thermo Fisher Scientific). Quantitative real-time PCR experiments were performed in triplicate to detect the sequence that codes nucleocapsid of PEDV or TGEV. Absolute quantitative RNA levels were calculated using standard curves derived from a virus stock.Primers used in this experiment: TGEV-qPCR-F: 5′-CTTCAACCCCATAACCCTCCAG-3′; TGEV-qPCR-R: 5′-GCCCTTCACCATGCGATAGC-3′; PEDV-qPCR-F: 5′-GAAGGCGCAAAGACTGAACC-3′; PEDV-qPCR-R:5′-TTGCCATTGCCACGACTCCT-3′.

## RNA-Seq and Analysis

Total RNA was extracted from porcine intestinal organoids using the miRNeasy Minikit (Qiagen). RNA quality was assessed by an Agilent bioanalyzer, and 1 μg was used for library preparation using the TruSeq Stranded mRNA Library Preparation kit (Illumina) per the manufacturer's instructions. Sequencing was performed on an Illumina Novaseq 6000. RNA-seq FASTQ data were processed and mapped to the sus scrofa reference genome (sus scrofa11) using TopHat. Uniquely mapped reads were assembled into genes guided by Ensembl sus scrofa annotation file[1]. Differentially expressed genes between infections were evaluated using DESeq2 (Love et al., 2014) at a significance cutoff of FDR (False Discovery Rate) $P < 0.01$ unless otherwise stated. Pearson's coefficient was calculated using the cor function with default parameters in R[2]. The hierarchical clustering analysis of samples and gene expression patterns in different samples was carried out using the ComplexHeatmap function (Gu et al., 2016). Heat maps based on z-score of FPKM values were also generated using ComplexHeatmap. Gene set enrichment analysis (GSEA) (Subramanian et al., 2005) was performed with GSEA 4.1.0 software[3]. Briefly, All log2FoldChange of annotated genes from DESeq2 output were ranked and the analysis was performed using the standard weighted enrichment statistic against gene sets derived from the GO (Gene Ontology) Biological Process ontology in the Molecular Signatures Database[4]. All RNA-seq data sets have been deposited in the Gene Expression Omnibus database with the accession number GSE182240.

## Statistical Analysis

All data were analyzed with R (see text footnote 2)and GraphPad Prism 9 (GraphPad, San Diego, CA, United States) and provided as mean ± SD unless otherwise indicated. Statistical analyses were performed using an unpaired Student's *t*-test. The significance level (*P* value) was set at $< 0.05$ (*), $< 0.01$ (**), and $< 0.001$ (***).

## Data Availability Statement

All RNA-seq data sets have been deposited in the Gene Expression Omnibus database with the accession number GSE182240. All other data is available from the author upon reasonable request.

# RESULTS

## Generation and Long-Term Expansion of Epithelial Organoids From Porcine Duodenum, Jejunum, and Ileum

A reliable and reproducible model *in vitro* for swine enteric coronavirus infection would be intestinal models that support virus replication and can be cultured long-term. Organoids

[1]http://asia.ensembl.org/Sus_scrofa/Info/Annotation

[2]https://www.r-project.org/

[3]https://www.gsea-msigdb.org/gsea/index.jsp

[4]https://www.gsea-msigdb.org/gsea/msigdb/collections.jsp#C5

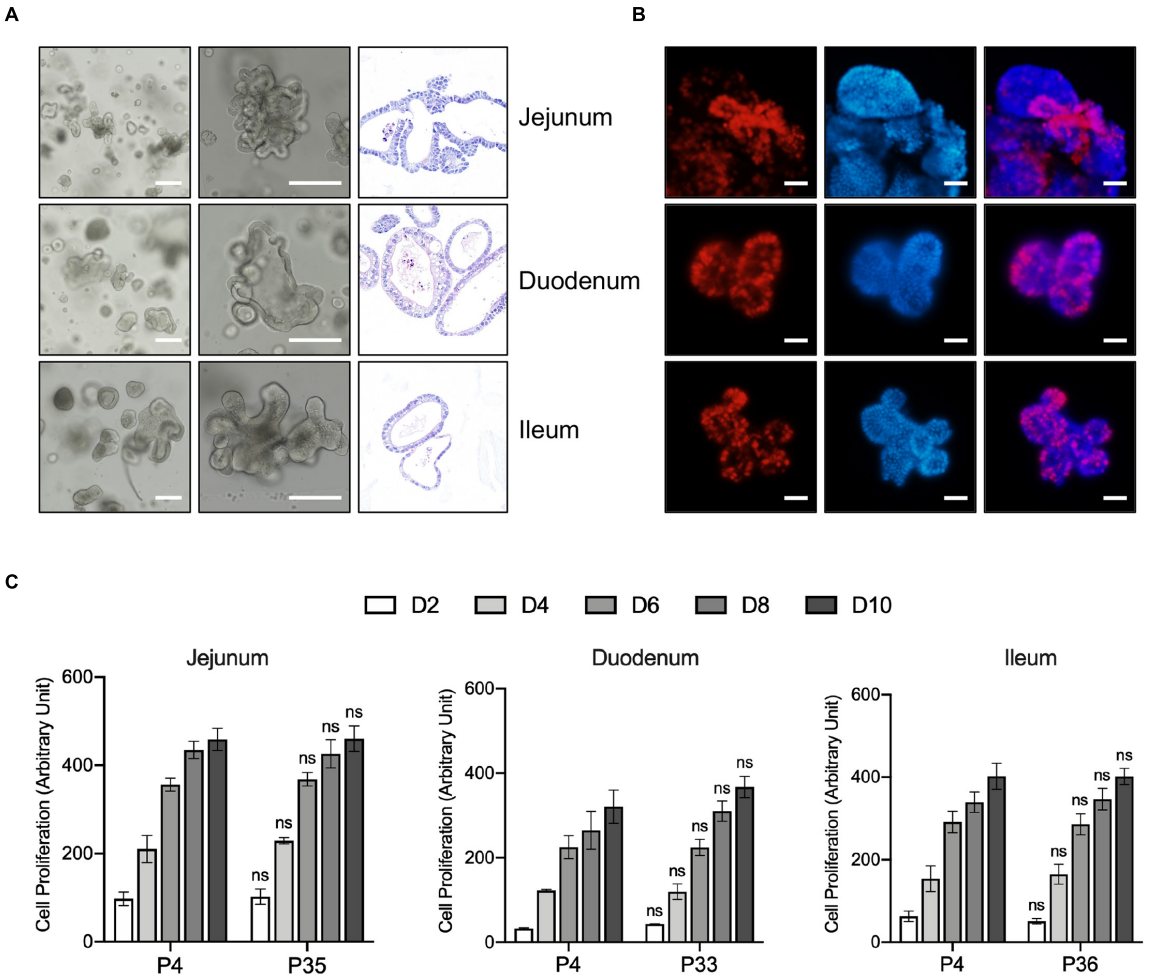


**FIGURE 1 |** Generation, Characterization, and long-term expansion of porcine intestinal organoids. **(A)** Left and middle panel: representative images show the morphology of intestinal organoids from early passage of the porcine duodenum, jejunum, and ileum. Right panel: Representative H&E staining images of the porcine intestinal organoid showing the structure of organoids. Scale bar = 500 μm. **(B)** Organoids were cultured for 4 days and incubated with the thymidine analog EdU (red) for 6 h. Images were analyzed by fluorescence microscopy, and nuclei were counterstained with Hoechst (blue). Scale bar = 200 μm. **(C)** The proliferation capacity of porcine duodenum, jejunum, and ileum organoids at early and late passage numbers was measured by resazurin at the indicated time points. Statistics analysis was performed between early and late passage at the indicated time points. Error bars represent standard deviations of technical triplicates ($n$ = 3). ns, not significant.

derived from the porcine intestine have been produced, whereas long-term expansion of swine intestinal organoids has not been well established (Derricott et al., 2019; Li et al., 2019; Li Y. et al., 2020). To explore the long-term culture for porcine small intestinal organoids, we apply the culture medium of human intestinal organoids with minor modifications to the culture of porcine intestinal organoids.

The crypts of duodenum, jejunum, and ileum from 10-day old pig were isolated and embedded in basement membrane extract (Matrigel) and covered with porcine intestinal organoids (PIO) medium, which is modified from human intestinal organoids culture system. The organoids with a crypt-villus architecture formed in several days (**Figure 1A**) resembled that seen in human organoid cultures, which is already well established in our laboratory (Liu et al., 2018). Also, the structure and composition of organoids were confirmed by hematoxylin and eosin (H&E) stain (**Figure 1A**).

The proliferating cells, including LGR5 + cells and transit-amplifying cells within the organoid crypt domains, were confirmed by 5-ethynyl-2′-deoxyuridine (EdU) staining. The result showed that proliferating cells were present throughout the organoids under this culture condition (**Figure 1B**). Porcine intestinal organoids grow very robustly and rapidly and need to be passaged every 5–6 days under this culture condition. Porcine intestinal organoids were passaged by enzyme digestion at 1:4 to 1:6 ratios for at least 35 passages, which equates to approximately 6 months in culture, proliferating at comparable rates regardless of passage number (**Figure 1C**). Altogether, our culture conditions allow long-term expansion of porcine intestinal organoids.

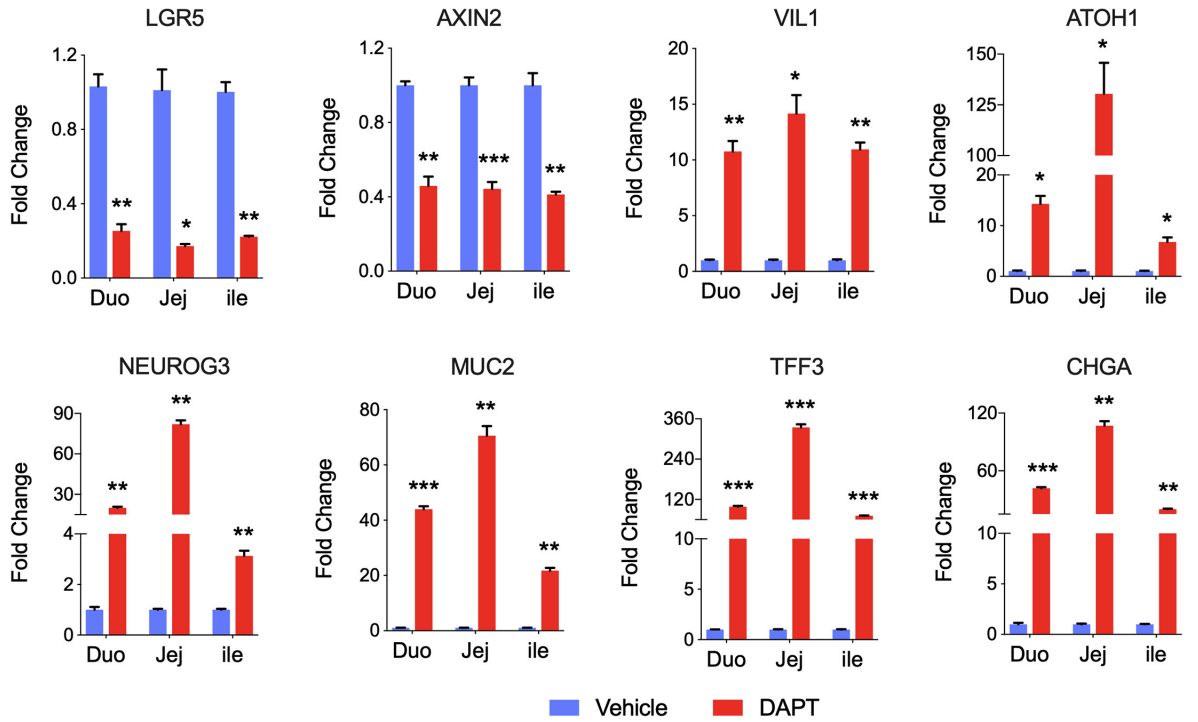


**FIGURE 2 |** Differentiation of long-term cultured porcine intestinal organoids. qPCR gene expression analysis for LGR5, AXIN2, VIL1, ATOH1, NEUROG3, MUC2, TFF3, and CHGA. RNA was collected from the late passage of duodenum, jejunum, and ileal organoids that had been passaged for at least 30 passages, allowed to recover overnight in PIO medium, and then cultured with PIO medium with DMSO or 5% L-WRN conditioned medium with the addition of 5 mM DAPT for an additional 2 days. Data are presented as fold change relative to organoids in PIO medium. Statistics analysis were performed between DMSO and DAPT treated group (*$P < 0.05$, **$P < 0.01$, ***$P < 0.001$, $n = 3$, technical repeat).

## Long-Term Cultured Porcine Intestinal Organoids Retain a Differentiation Program

Above we showed that porcine intestinal organoids could proliferation for several months suggesting those long-term cultured organoids are capable of self-renewal. We then sought to determine the potential of differentiation of these long-term organoids. Wnt signaling is essential for maintaining crypt proliferation and intestinal stem cell function *in vivo* (Van De Wetering et al., 2002; Pinto et al., 2003). And the reduced Wnt signaling activity induces differentiation in mouse and human intestinal epithelial organoids. Therefore, we examined mRNA expression of differentiated cell markers in duodenum, jejunum, and ileum organoids grown in PIO medium with DAPT. DAPT is an inhibitor of the γ-secretase complex, which plays a crucial role in activating the Notch signaling. Therefore, DAPT indirectly inhibits the Notch pathway. Inhibition of the Notch pathway promotes the differentiation of mouse and human organoids (Ootani et al., 2009; Jung et al., 2011; Patel et al., 2013) and rapidly reduces the proportion of proliferating cells in rectal and ileal lines (VanDussen et al., 2015).

As expected, intestinal stem cell marker LGR5 expression was greatly decreased, and expression of differentiated cell markers was generally increased in intestinal organoids cultured with DAPT compared with vehicle DMSO control. We also examined other stem cell marker Axin2, and the mRNA level was dramatically decreased after differentiation (**Figure 2**). The expression level of villin (VIL1) for enterocytes increased, demonstrating that organoid cells could differentiate into enterocytes, which are major targets of PEDV and TGEV *in vivo* (Cui et al., 2020). The addition of DAPT in the differentiation medium was important for inducing the expression of secretory cell markers (VanDussen et al., 2015), including transcription factors atonal homolog 1 (ATOH1) and neurogenin 3 (NEUROG3), which were significantly upregulated in DAPT treatment culture (**Figure 2**). The mRNA levels of goblet cell markers mucin 2 (MUC2) and trefoil factor 3 (TFF3) as well as endocrine cell marker chromogranin A (CHGA) increased significantly compared to undifferentiated intestinal organoids (**Figure 2**). These data indicated that long-term cultured porcine intestinal organoids maintained differentiation potential.

## Long-Term Cultured Intestinal Organoids Are Susceptible to Infection by Porcine Enteric Coronaviruses

To investigate whether long-term cultured porcine organoids could be infected by swine enteric virus, two well-characterized swine enteric coronaviruses, PEDV and TGEV, were used to infect jejunum organoids. PEDV primarily infects the small intestine and can replicate in the duodenum, jejunum, and ileum

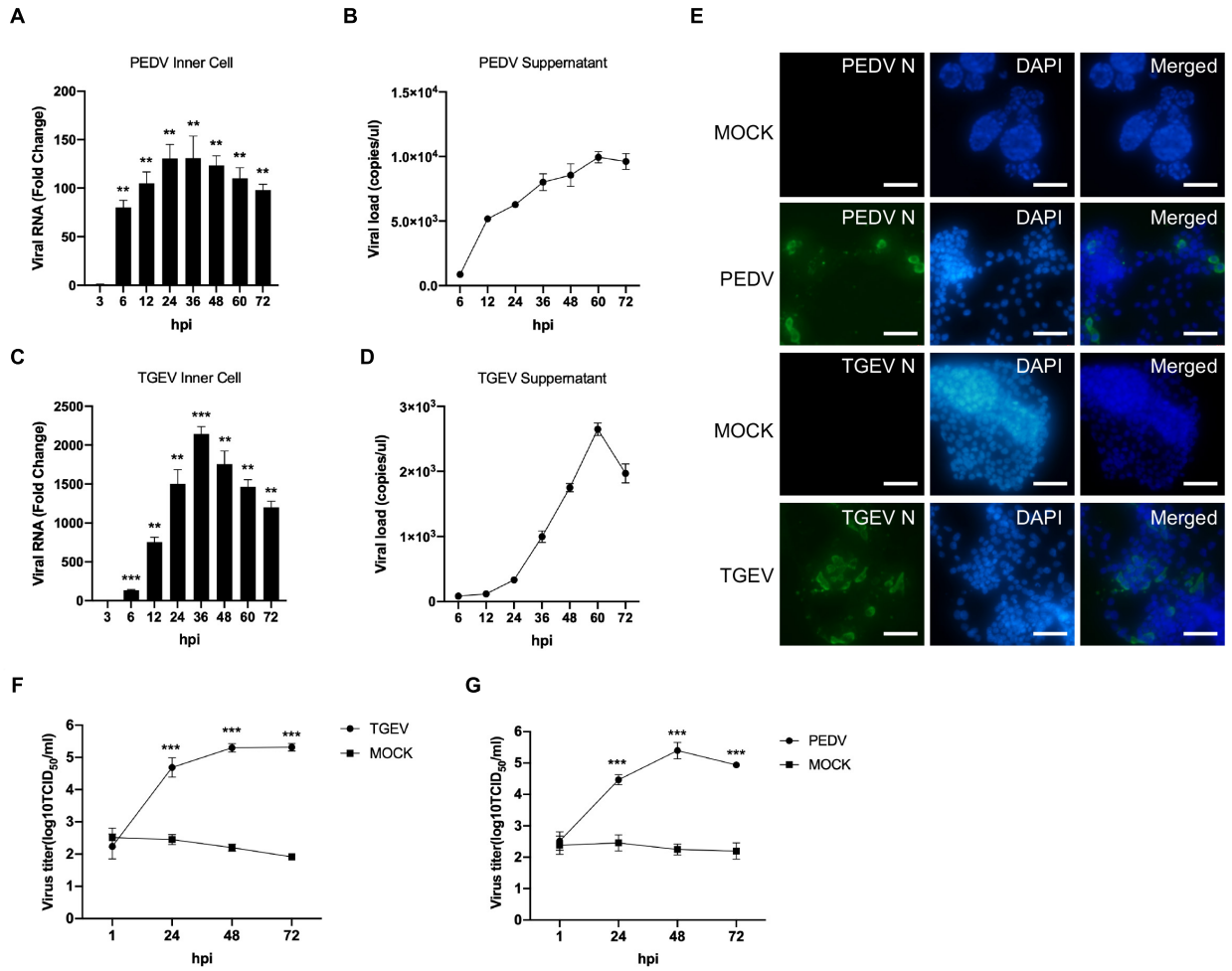


**FIGURE 3 |** PEDV and TGEV replicate in porcine intestinal organoids. **(A–D)** PEDV or TGEV genomic levels in supernatants and inner cells of infected jejunum organoids at indicated time points after infection were quantified using an RT-PCR assay. Error bars represent standard deviations of technical triplicates. hpi, hours post-infection; $^{**}P < 0.01$, $^{***}P < 0.001$, $n = 3$ per group. **(E)** TGEV-infected, PEDV-infected, or MOCK-infected jejunum organoids were collected at 48 hpi, fixed, permeabilized, and stained with TGEV N protein (green) or PEDV N protein antibody (green). DAPI was used for nuclear staining. Images were taken using a microscope. Scale bar = 200 μm. **(F,G)** The infectious PEDV or TGEV in the supernatant of organoids was titrated by $TCID_{50}$ assay on Vero or LLC-PK1 cell line. $^{***}P < 0.001$, $n = 3$ per group.

region of the small intestine *in vivo* (Li et al., 2019; Zhang et al., 2020). Previous studies showed that the load of PEDV in the jejunum was significantly higher than that in other tissues (Li et al., 2018). So we choose long-term cultured porcine jejunum organoids for further investigation. Accessing the apical surface is challenging because the apical surface of the organoids is enclosed within organoids. To make the apical surface of organoids accessible to virus challenges. First, organoids were broken up into chunks with TrypLE and then were incubated with 0.1 MOI of PEDV. Infected organoids and culture supernatant were then collected at different time points post-infection for viral replication detection by RT-qPCR. The results showed that the numbers of PEDV genomes inner cells of organoids were substantially increased after PEDV infection (**Figure 3A**), indicating that PEDV can infect long-term culture porcine intestinal organoids. In addition, viral load in culture supernatant remained increasing with the culture duration and peaked at 60 hpi (**Figure 3B**). PEDV infection in jejunum organoids 24 h post-infection was further confirmed by an anti-PEDV nucleocapsid immunofluorescence assay (IFA) (**Figure 3E**). In a parallel TGEV infection experiment, we inoculated porcine jejunum organoids with the TGEV at 0.1 MOI. A kinetic of viral genome replication in organoids (**Figure 3C**) and viral copies in the supernatant can be observed (**Figure 3D**), and the TGEV infection in organoids also was confirmed by IFA at 24 hpi with an anti-TGEV nucleocapsid antibody (**Figure 3E**). Furthermore, the infectious PEDV or TGEV in the supernatant of organoids culture was titrated by $TCID_{50}$ assay. The results showed that infectious viral titers of the PEDV and TGEV remained increasing with the culture duration (**Figures 3F,G**). Collectively, these data show that long-term cultured swine intestinal organoids are permissive to swine enteric CoVs

A

| Samples | Replicates | Total Reads | Uniquely Aligned Reads | Uniquely Aligned Rate |
|---|---|---|---|---|
| MOCK Infected | Replicate 1 | 40,298,362 | 37,364,925 | 92.7% |
| | Replicate 2 | 47,504,504 | 43,955,581 | 92.5% |
| PEDV Infected | Replicate 1 | 41,202,422 | 38,368,476 | 93.1% |
| | Replicate 2 | 48,512,614 | 44,983,710 | 92.7% |
| TGEV Infected | Replicate 1 | 45,013,176 | 40,328,200 | 89.6% |
| | Replicate 2 | 40,314,062 | 36,003,469 | 89.3% |

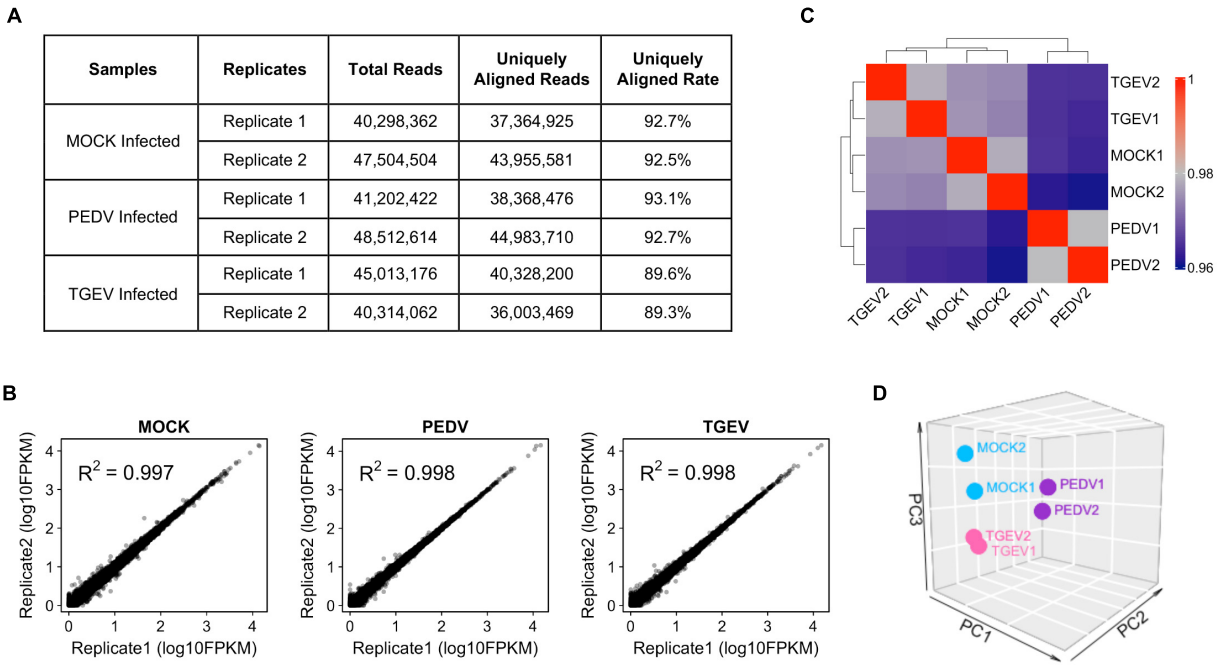


**FIGURE 4 |** Overview of RNA-seq results from MOCK, PEDV, or TGEV infected porcine jejunum organoids. **(A)** Summary of total and uniquely aligned reads for each sample of coronavirus infected porcine jejunum organoids. **(B)** Scatterplot evaluation of the reproducibility of two different biological repeats. **(C)** Correlation heat map of MOC, PEDV, or TGEV infected organoids based on all genes expression. The colors represent pairwise Pearson correlations derived from the expression values of all genes. The hierarchical clustering is based on minus correlation distance. **(D)** PCA analysis was performed on the FPKM expression matrix of all samples.

infection and are capable of supporting virus replication and progeny release.

## Transcriptome Analysis of Swine Enteric Coronaviruses Infection of Porcine Intestinal Organoids

The cells transcript landscape with enterovirus infections of the swine gastrointestinal tract remains unknown. With the goal of better understanding how porcine intestinal organoids respond to swine enteric CoVs infection, we performed RNA sequencing (RNA-seq) experiments using porcine intestinal organoids infected with 0.1 MOI of PEDV or TGEV and evaluated the transcript landscape of long-term cultured porcine jejunum organoids at 48 h after viral challenges. We obtained more than 36 million uniquely mapped reads for each sample (**Figure 4A**), with two biological replicates of each sample being highly reproducible (**Figure 4B**). **Figure 4C** shows the correlation heatmap of the different virus-infected organoid samples. Organoids infected with the same virus clustered tightly together. Consistent with the sample correlation analysis, we observed that RNA-seq samples from PEDV-, TGEV-, or MOCK-infected organoids could be distinguished when visualized by principal component analysis (PCA) (**Figure 4D**).

Next, we examined changes in gene expression induced upon TGEV or PEDV infection compared to MOCK infection. The volcano plot of the result showed that there were 749 significantly differentially expressed genes (**Supplementary Table 3**), which included 485 upregulated and 264 downregulated genes in response to TGEV infection compared to that in uninfected organoids (**Figure 5A**). In contrast, there were 5104 significantly differentially expressed genes (**Supplementary Table 4**), which included 2597 upregulated and 2507 downregulated genes in response to PEDV infection compared to MOCK-infected organoids (**Figure 5B**). Among the highly upregulated genes in TGEV infection, most of them were interferon-stimulated genes (ISGs), including OAS2, MX1, IFI6, ISG12(A), MX2, IFITM3, USP18, OASL, IFIT2, BST2, and IFIT5 (**Figure 5C**). In PEDV infection, ISGs including OAS2, MX1, IFI6, IFIT2, IFI44, ISG12(A), and MX2 ranked in the top 25 of upregulated genes (**Figure 5D**). Other upregulated genes in both PEDV and TGEV infection, such as HERC5, HERC6, and CXCL8 (IL8), are inflammatory cytokines related to the inflammatory response, ZBP1 is Z-DNA binding protein inducing type-I interferon production, and DDX60 functions as an antiviral factor and promotes RIG-I-like receptor-mediated signaling (**Figure 5E**). These results showed that enteric CoVs infection could substantially change the transcript landscape of porcine intestinal organoids.

Swine enteric coronaviruses infection induce transcripts associated antiviral signaling in long-term culture organoids.

We further examined the difference in gene expression between TGEV and PEDV infected organoids. Unsupervised hierarchical cluster analysis of all differentially expressed genes in TGEV and PEDV infected organoids showed that there were four groups: (1) those that are downregulated in PEDV infection

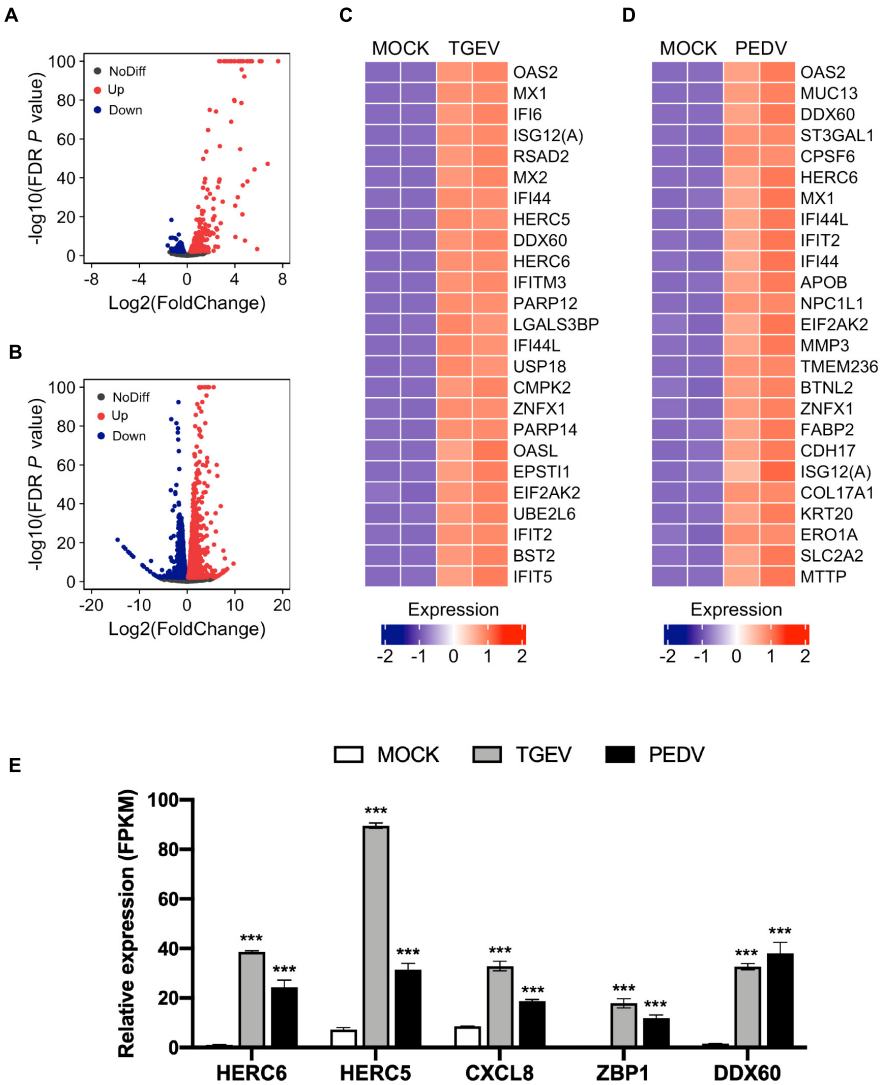


**FIGURE 5 |** Global differential gene expression analysis of TGEV and PEDV infected organoids. **(A)** Volcano plots comparing differential gene expression levels between MOCK infected and TGEV infected organoids and **(B)** between MOCK infected and PEDV infected organoids. Red dots: up-regulated genes (FDR $P < 0.01$); Blue dots: down-regulated genes (FDR $P < 0.01$); Black dots: no difference genes. **(C)** Heatmap depicting the 25 most significantly enriched genes (FDR $P < 0.01$) upon TGEV infection in swine intestinal organoids. **(D)** Heatmap shows the top 25 enriched genes (FDR $P < 0.01$) from PEDV infected organoids. The colored bar represents the z-score of FPKM values. **(E)** RNA-seq based gene expression values (FPKM) for HERC6, HERC5, CXCL8, ZBP1, DDX60 in PEDV-, TGEV- and MOCK-infected organoids. Asterisks indicate statistically significant differences (***$P < 0.001$) for expression in MOCK-infected organoids relative to expression values in PEDV-infected or TGEV-infected organoids. Statistics analysis were performed between MOCK and PEDV- or TGEV-infected organoids.

(group 1); (2) those that are repressed in both TGEV and PEDV infection (group 2); (3) those that are activated in both TGEV and PEDV infection (group 3); (4) those that are highly upregulated in PEDV infection (group 4). These data suggest that PEDV and TGEV induce different transcriptomes in porcine intestinal organoids (**Figure 6A**).

We then performed gene sets enrichment analysis (GSEA) to evaluate the global change of porcine intestinal organoids in response to CoVs infection. Infection with TGEV elicited a broad signature associated with antiviral signaling, including cytokines and ISGs attributed to type I and III IFN responses (**Figure 6B** and **Supplementary Table 5**). PEDV also induced transcripts associated with antiviral signaling but to a much lower level than TGEV infection (**Figure 6C** and **Supplementary Table 6**), suggesting that PEDV counteracts the host's innate immune response. PEDV develops a set of elaborate mechanisms to evade or inhibit the host antiviral innate immune response during virus evolution. These results are consistent with the innate immune suppression in PEDV infection (Li S. et al., 2020). We confirmed this by analyzing the ISGs that can be induced by human enteroviruses as well as the coronavirus infection in human intestinal organoids (Drummond et al., 2017; Lamers et al., 2020) and found that most of these ISGs were upregulated upon TGEV infection, but to fewer ISGs upregulated and much lower level

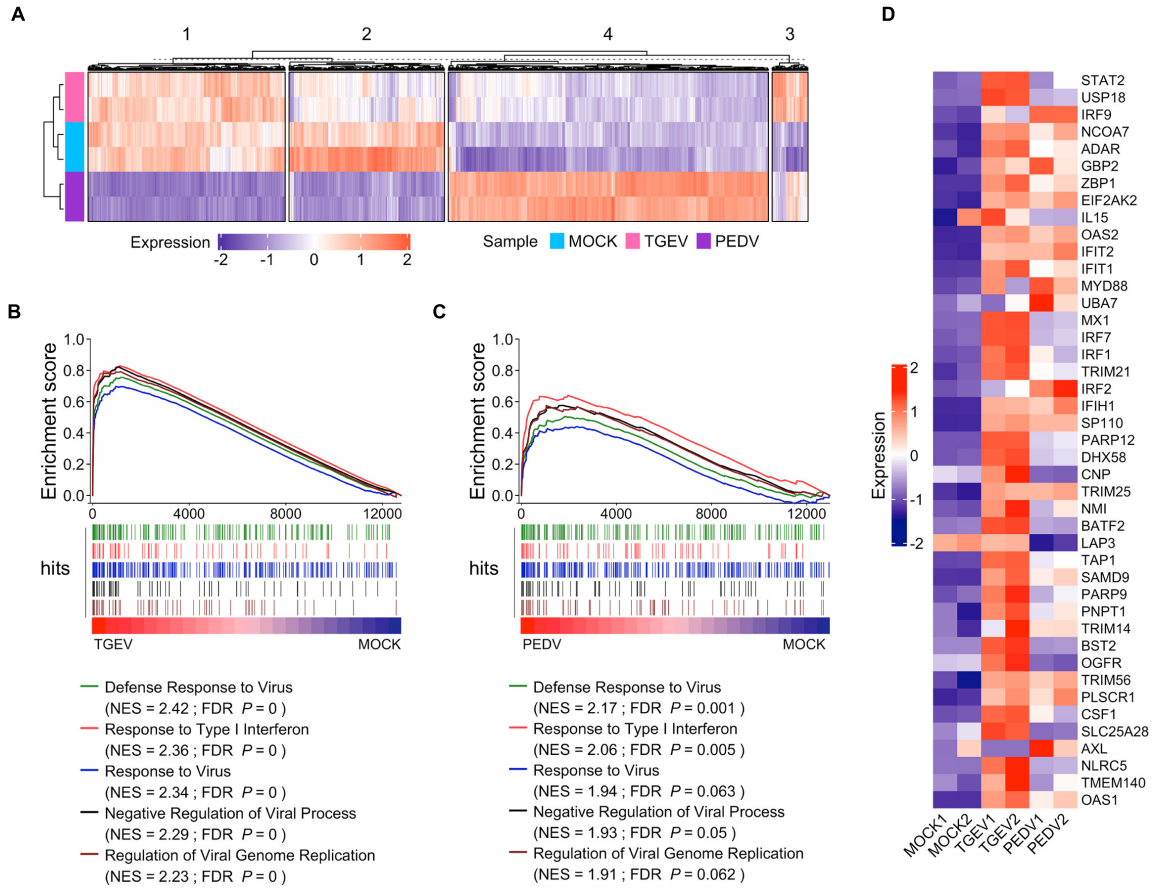


**FIGURE 6 |** Enteric coronavirus infection induces transcripts associated with antiviral signaling in long-term culture organoids. **(A)** The unsupervised hierarchical cluster of all differentially expressed genes in PEDV and TGEV infection was divided into four groups. The colored bar represents the Z-score of the FPKM value of each gene. **(B)** GSEA plots showing top five gene signatures from GO biological process in transcriptomes of TGEV- vs. MOCK-infected organoids. **(C)** GSEA plots showing the corresponding signatures in PEDV- vs. MOCK-infected organoids, NES: normalized enrichment score; FDR *P*: False discovery rate adjusted *P* values. **(D)** Heatmaps depicting ISGs reported in Drummond et al. (2017) upon TGEV infection or PEDV infection in porcine intestinal organoids. The colored bar represents the z-score of FPKM of each gene.

in PEDV infection (**Figure 6D**). Altogether, these results showed that enteric coronavirus infection-induced transcripts associated with antiviral signaling in long-term cultured organoids suggest that long-term expansion organoids represent versatile models for the *in vitro* study of innate immune response to swine enteric CoVs infection.

## Porcine Epidemic Diarrhea Virus Infection Induces a Transcriptional Immunosuppression Program

In addition to inducing lower levels of ISGs and cytokines in PEDV infected organoids, our GSEA showed, interestingly, that "negative regulation of lymphocyte activation" (**Figure 7A**), "negative regulation of leukocyte proliferation" (**Figure 7B**), and "negative regulation of T cell proliferation" (**Figure 7C**) were identified as the top regulated processes (**Supplementary Table 6**). Activation-induced proliferation and clonal expansion of antigen-specific lymphocytes are a hallmark of pathogens' adaptive immune response. Therefore, we examined genes expression levels in these three gene sets found that PEDV infection organoids present a unique expression pattern (**Figure 7D**), in which many genes involved in these three gene sets were dramatically upregulated, including phospholipase A2 inhibitory protein (ANXA1), RING finger and CCCH-type zinc finger domain-containing protein 1 (RC3H1), pulmonary surfactant-associated protein D (SFTPD) (**Figure 7E**). These results imply that the PEDV infection may induce a subset of cytokines, which affect lymphocyte activation and T cell proliferation, which in turn may damage the adaptive immune response during PEDV infection.

## DISCUSSION

Intestinal organoids represent a significant advantage over traditional cell line models and provide a unique opportunity to explore host-pathogen interactions in an *ex vivo* system that

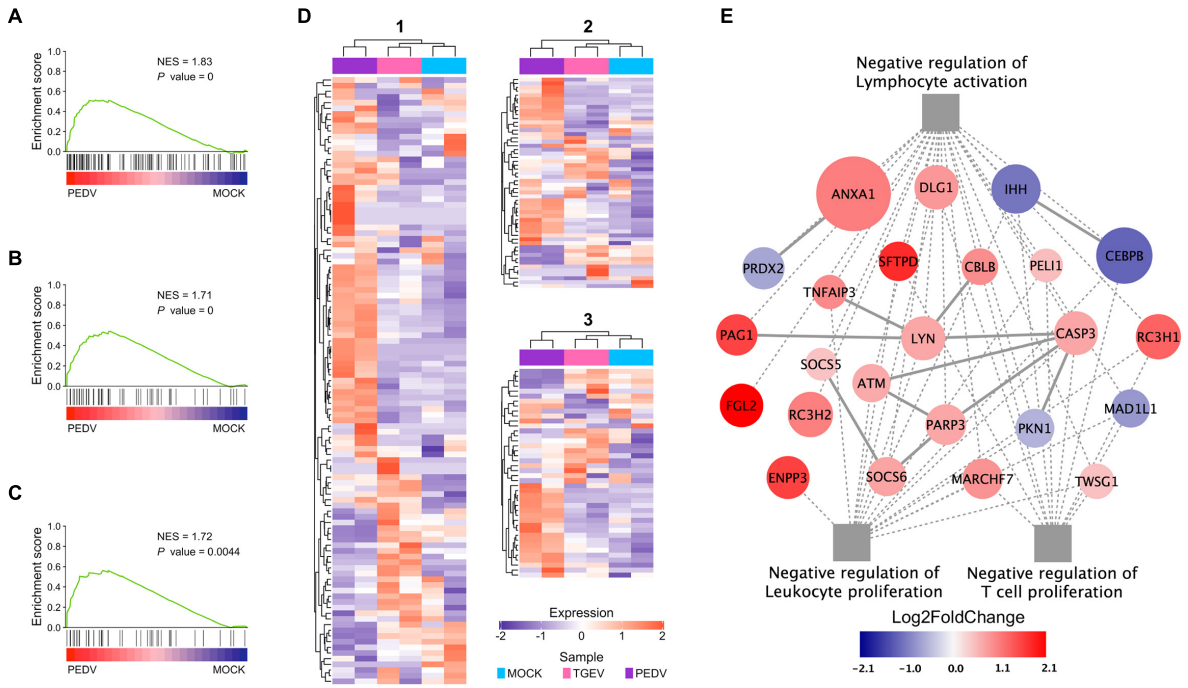


**FIGURE 7 |** Functional analysis of PEDV on adaptive immune suppression. **(A–C)** GSEA plots show gene signatures of negative regulation of lymphocyte activation, leukocyte proliferation, and negative regulation of T cell proliferation. NES: normalized enrichment score; *P* value: FDR adjusted. **(D)** Heatmaps depicting gene expression levels of three gene signatures, 1: Negative regulation of lymphocyte activation; 2: Negative regulation of leukocyte proliferation 3: Negative regulation of T cell proliferation. The colored bar represents the z-score of FPKM of each gene. **(E)** The interaction diagram of the negative regulation of lymphocyte activation, leukocyte proliferation, and T cell proliferation. Network nodes and edges represent proteins and protein-protein associations. Gray solid lines represent protein-protein interaction from STRING Database. The gray dot lines represent the GO biological processes. The red to dark blue color bar represents the fold change of gene expression level from increasing to decreasing. The significance of the gene expression represented by –log10(*P*-value) was shown by relative diameters of a circle with the largest diameter as most significant.

recapitulates the complicated cellularity of the gastrointestinal tract. Swine intestinal organoids have been established with different culture systems. One previous study shows that WRN conditioned media is sufficient for *in vitro* propagation of porcine intestinal organoids (Powell and Behnke, 2017). However, WRN conditioned media only didn't support the long-term expansion of swine intestinal organoids in our study (data not shown). Although others have generated swine intestinal organoids with commercial mouse intestinal organoids growth medium (Li et al., 2019; Li Y. et al., 2020), a study shows that porcine intestinal organoids cultured with IntestiCult$^{TM}$ organoid growth medium for mouse intestinal organoids seem as such less useful to study the interaction of enterotoxins or pathogens with the intestinal epithelium (Vermeire et al., 2021). In addition, the mouse organoid growth medium may not allow long-term expansion of swine intestinal organoids. Here, we describe a versatile approach by modifying previously defined insights in the growth requirements of the intestinal epithelium of humans (Sato et al., 2011; Liu et al., 2018) to establish swine intestinal epithelial organoids. Major differences to other swine intestinal organoid models are their long-term piglet expansion. Studies of these cultures indicate that those swine intestinal organoids can self-renew in culture for 6 months at least. The differentiation experiment of these long-term cultured organoids also indicated that the organoids under this culture condition maintained differentiation potential.

A challenge in using organoids to study virus-host interactions is that the apical surface is enclosed within the organoids, and therefore it is difficult to access the virus, which hampers the application of intestinal organoids in virus-host interaction studies. Several techniques, including microinjection, 3D to 2D culture, and apical-out organoid culture, were developed (Co et al., 2019; Li Y. et al., 2020). However, the procedures of these methods were relatively complicated. This study used TrypLE to break intestinal organoids into large pieces and incubated them with swine enteric coronaviruses. The virus infection experiment indicated that this technique was efficient for the virus to access the apical surface of organoids. This approach for organoid infection was also reported to be used for CoVID-19 infection of human intestinal organoids (Lamers et al., 2020).

Subsequently, two swine enteric coronaviruses, PEDV and TGEV, were employed to verify the infectivity of long-term cultured porcine intestinal organoids. We exposed long-term cultured porcine jejunum organoids to TGEV and PEDV at an MOI of 0.1. Samples were harvested at multiple time points after infection and processed for the viral load analyses. Culture supernatants contained lower infectious virus levels than inside organoids, implying that the Matrigel may impede virus release.

The limited virus in supernatant would be overcome by using a bioreactor and organoids-on-a-chip (Meran et al., 2020; Nikolaev et al., 2020), in which organoids were cultured without basement membrane extract.

Previous studies have not investigated the transcriptome change of porcine intestinal organoids upon enteric viral infection (Li et al., 2019; Li Y. et al., 2020). Here, we evaluated the transcriptional landscape of organoids upon swine enteric virus infection by RNA sequencing. Cells typically respond to virus infection by mounting an innate antiviral response to limit the spread of the infection and aid in inducing an adaptive immune response that will eventually clear the virus. The current study detected the robust induction of transcripts associated with antiviral signaling in response to swine enteric coronavirus infection of intestinal organoids, including many ISGs, cytokines, and chemokines (**Supplementary Tables 3**, **4**). Upon infection, the small intestinal epithelium secretes pro-inflammatory mediators, such as IL8 (CXCL8) (Vermeire et al., 2021). Our data show similar swine enteric CoVs infection responses in the long-term cultured organoids. The RNA-seq result showed an upregulated IL8 expression when exposed to CoVs. IL8 functions as a chemotactic factor that attracts neutrophils, basophils, and T-cells during the inflammatory process. PEDV has evolved strategies to suppress and/or evade these immune responses, which can dramatically influence the course of the infection, including pathogenesis and persistence in the host (Li S. et al., 2020). In agreement with the previous results, we showed that PEDV could compromise the innate immune response in long-term cultured organoids. Moreover, our GSEA results implied that PEDV might damage the adaptive immune response during PEDV infection through negative lymphocyte activation and/or proliferation regulation.

In summary, we designed a robust long-term culture system to expand the porcine intestinal organoids. These intestinal organoids were susceptible to infection by porcine enteric coronavirus PEDV and TGEV. Our findings provide important insights into events associated with PEDV and TGEV infection and demonstrate that swine intestinal organoids can be used as an *in vitro* model to define the complicated cross-talk between enteric coronavirus and the intestinal epithelium. This 3D intestinal organoid model offers a long-term, renewable resource for investigating porcine intestinal infections with various pathogens.

## DATA AVAILABILITY STATEMENT

The datasets presented in this study can be found in online repositories. The names of the repository/repositories and accession number(s) can be found in the article/ **Supplementary Material**.

## ETHICS STATEMENT

The animal study was reviewed and approved by the Ethical Committee of the Shanghai Veterinary Research Institute, Chinese Academy of Agricultural Sciences.

## AUTHOR CONTRIBUTIONS

CL and GT: conceptualization, supervision, and funding acquisition. MZ, LLv, HC, WT, and CL: methodology. CL, MZ, and LY: software. YJ, HC, and LY: validation. CL, MZ, and LLv: formal analysis and data curation. MZ, LLv, and HC: investigation. FG, GL, WT, YL, and LLi: resources. CL: writing—original draft preparation. CL, GT, LY, and FG: writing—review and editing. YJ and CL: visualization. CL and FG: project administration. All authors have read and agreed to the published version of the manuscript.

## FUNDING

This work was sponsored by the Shanghai Pujiang Program (No. 21PJ1416300), Natural Science Foundation of Shanghai (No. 21ZR1477200), Central Public-interest Scientific Institution Basal Research Fund (No. 2019JB09), and Agricultural Science and Technology Innovation Program (No. CAAS-ASTIP-2016-SHVRI-2004-1).

## SUPPLEMENTARY MATERIAL

The Supplementary Material for this article can be found online at: https://www.frontiersin.org/articles/10.3389/fmicb.2022.865336/full#supplementary-material

## REFERENCES

Artegiani, B., and Clevers, H. (2018). Use and application of 3D-organoid technology. *Hum. Mol. Genet.* 27, R99–R107. doi: 10.1093/hmg/ddy187

Clevers, H. (2016). Modeling development and disease with organoids. *Cell* 165, 1586–1597. doi: 10.1016/j.cell.2016.05.082

Co, J. Y., Margalef-Catala, M., Li, X., Mah, A. T., Kuo, C. J., Monack, D. M., et al. (2019). Controlling epithelial polarity: a human enteroid model for host-pathogen interactions. *Cell Rep.* 26, 2509.e2504–2520.e2504. doi: 10.1016/j.celrep.2019.01.108

Cui, T., Theuns, S., Xie, J., Van Den Broeck, W., and Nauwynck, H. J. (2020). Role of porcine aminopeptidase N and sialic Acids in porcine coronavirus infections in primary porcine enterocytes. *Viruses* 12:402. doi: 10.3390/v12040402

Derricott, H., Luu, L., Fong, W. Y., Hartley, C. S., Johnston, L. J., Armstrong, S. D., et al. (2019). Developing a 3D intestinal epithelium model for livestock species. *Cell Tissue Res.* 375, 409–424. doi: 10.1007/s00441-018-2924-9

Drummond, C. G., Bolock, A. M., Ma, C., Luke, C. J., Good, M., and Coyne, C. B. (2017). Enteroviruses infect human enteroids and induce antiviral signaling in a cell lineage-specific manner. *Proc. Natl. Acad. Sci. U.S.A.* 114, 1672–1677. doi: 10.1073/pnas.1617363114

Fujii, M., Matano, M., Nanki, K., and Sato, T. (2015). Efficient genetic engineering of human intestinal organoids using electroporation. *Nat. Protoc.* 10, 1474–1485.

Gu, Z., Eils, R., and Schlesner, M. (2016). Complex heatmaps reveal patterns and correlations in multidimensional genomic data. *Bioinformatics* 32, 2847–2849. doi: 10.1093/bioinformatics/btw313

Hofmann, M., and Wyler, R. (1988). Propagation of the virus of porcine epidemic diarrhea in cell culture. *J. Clin. Microbiol.* 26, 2235–2239. doi: 10.1128/jcm.26.11.2235-2239.1988

Jung, K., Hu, H., and Saif, L. J. (2016). Porcine deltacoronavirus infection: etiology, cell culture for virus isolation and propagation, molecular epidemiology and pathogenesis. *Virus Res.* 226, 50–59. doi: 10.1016/j.virusres.2016.04.009

Jung, K., and Saif, L. J. (2015). Porcine epidemic diarrhea virus infection: etiology, epidemiology, pathogenesis and immunoprophylaxis. *Vet. J.* 204, 134–143. doi: 10.1016/j.tvjl.2015.02.017

Jung, P., Sato, T., Merlos-Suarez, A., Barriga, F. M., Iglesias, M., Rossell, D., et al. (2011). Isolation and in vitro expansion of human colonic stem cells. *Nat. Med.* 17, 1225–1227. doi: 10.1038/nm.2470

Lamers, M. M., Beumer, J., Van Der Vaart, J., Knoops, K., Puschhof, J., Breugem, T. I., et al. (2020). SARS-CoV-2 productively infects human gut enterocytes. *Science* 369, 50–54. doi: 10.1126/science.abc1669

Li, L., Fu, F., Guo, S., Wang, H., He, X., Xue, M., et al. (2019). Porcine intestinal enteroids: a new model for studying enteric coronavirus porcine epidemic diarrhea virus infection and the host innate response. *J. Virol.* 93, e1682–e1618. doi: 10.1128/JVI.01682-18

Li, S., Yang, J., Zhu, Z., and Zheng, H. (2020). Porcine epidemic diarrhea virus and the host innate immune response. *Pathogens* 9:367. doi: 10.3390/pathogens9050367

Li, Y., Yang, N., Chen, J., Huang, X., Zhang, N., Yang, S., et al. (2020). Next-generation porcine intestinal organoids: an apical-out organoid model for swine enteric virus infection and immune response investigations. *J. Virol.* 94, e1006–e1020. doi: 10.1128/JVI.01006-20

Li, Y., Wu, Q., Huang, L., Yuan, C., Wang, J., and Yang, Q. (2018). An alternative pathway of enteric PEDV dissemination from nasal cavity to intestinal mucosa in swine. *Nat. Commun.* 9:3811. doi: 10.1038/s41467-018-06056-w

Liu, C., Banister, C. E., Weige, C. C., Altomare, D., Richardson, J. H., Contreras, C. M., et al. (2018). PRDM1 silences stem cell-related genes and inhibits proliferation of human colon tumor organoids. *Proc. Natl. Acad. Sci. U.S.A.* 115, E5066–E5075. doi: 10.1073/pnas.1802902115

Liu, C., Tang, J., Ma, Y., Liang, X., Yang, Y., Peng, G., et al. (2015). Receptor usage and cell entry of porcine epidemic diarrhea coronavirus. *J. Virol.* 89, 6121–6125. doi: 10.1128/JVI.00430-15

Love, M. I., Huber, W., and Anders, S. (2014). Moderated estimation of fold change and dispersion for RNA-seq data with DESeq2. *Genome Biol.* 15:550. doi: 10.1186/s13059-014-0550-8

Meran, L., Massie, I., Campinoti, S., Weston, A. E., Gaifulina, R., Tullie, L., et al. (2020). Engineering transplantable jejunal mucosal grafts using patient-derived organoids from children with intestinal failure. *Nat. Med.* 26, 1593–1601. doi: 10.1038/s41591-020-1024-z

Miyoshi, H., and Stappenbeck, T. S. (2013). In vitro expansion and genetic modification of gastrointestinal stem cells in spheroid culture. *Nat. Protoc.* 8, 2471–2482. doi: 10.1038/nprot.2013.153

Nikolaev, M., Mitrofanova, O., Broguiere, N., Geraldo, S., Dutta, D., Tabata, Y., et al. (2020). Homeostatic mini-intestines through scaffold-guided organoid morphogenesis. *Nature* 585, 574–578. doi: 10.1038/s41586-020-2724-8

Ootani, A., Li, X., Sangiorgi, E., Ho, Q. T., Ueno, H., Toda, S., et al. (2009). Sustained in vitro intestinal epithelial culture within a Wnt-dependent stem cell niche. *Nat. Med.* 15, 701–706. doi: 10.1038/nm.1951

Patel, K. K., Miyoshi, H., Beatty, W. L., Head, R. D., Malvin, N. P., Cadwell, K., et al. (2013). Autophagy proteins control goblet cell function by potentiating reactive oxygen species production. *EMBO J.* 32, 3130–3144. doi: 10.1038/emboj.2013.233

Pinto, D., Gregorieff, A., Begthel, H., and Clevers, H. (2003). Canonical Wnt signals are essential for homeostasis of the intestinal epithelium. *Genes Dev.* 17, 1709–1713. doi: 10.1101/gad.267103

Powell, R. H., and Behnke, M. S. (2017). WRN conditioned media is sufficient for in vitro propagation of intestinal organoids from large farm and small companion animals. *Biol. Open* 6, 698–705. doi: 10.1242/bio.021717

Sato, T., Stange, D. E., Ferrante, M., Vries, R. G., Van Es, J. H., Van Den Brink, S., et al. (2011). Long-term expansion of epithelial organoids from human colon, adenoma, adenocarcinoma, and Barrett's epithelium. *Gastroenterology* 141, 1762–1772.

Sato, T., Vries, R. G., Snippert, H. J., Van De Wetering, M., Barker, N., Stange, D. E., et al. (2009). Single Lgr5 stem cells build crypt-villus structures in vitro without a mesenchymal niche. *Nature* 459, 262–265. doi: 10.1038/nature07935

Subramanian, A., Tamayo, P., Mootha, V. K., Mukherjee, S., Ebert, B. L., Gillette, M. A., et al. (2005). Gene set enrichment analysis: a knowledge-based approach for interpreting genome-wide expression profiles. *Proc. Natl. Acad. Sci. U.S.A.* 102, 15545–15550. doi: 10.1073/pnas.0506580102

Sungsuwan, S., Jongkaewwattana, A., and Jaru-Ampornpan, P. (2020). Nucleocapsid proteins from other swine enteric coronaviruses differentially modulate PEDV replication. *Virology* 540, 45–56. doi: 10.1016/j.virol.2019.11.007

Van De Wetering, M., Sancho, E., Verweij, C., De Lau, W., Oving, I., Hurlstone, A., et al. (2002). The beta-catenin/TCF-4 complex imposes a crypt progenitor phenotype on colorectal cancer cells. *Cell* 111, 241–250. doi: 10.1016/s0092-8674(02)01014-0

VanDussen, K. L., Marinshaw, J. M., Shaikh, N., Miyoshi, H., Moon, C., Tarr, P. I., et al. (2015). Development of an enhanced human gastrointestinal epithelial culture system to facilitate patient-based assays. *Gut* 64, 911–920. doi: 10.1136/gutjnl-2013-306651

Vermeire, B., Gonzalez, L. M., Jansens, R. J. J., Cox, E., and Devriendt, B. (2021). Porcine small intestinal organoids as a model to explore ETEC-host interactions in the gut. *Vet. Res.* 52:94.

Vlasova, A. N., Wang, Q., Jung, K., Langel, S. N., Malik, Y. S., and Saif, L. J. (2020). "Porcine coronaviruses," in *Emerging and Transboundary Animal Viruses*, eds Y. Malik, R. Singh, and M. Yadav (Singapore: Springer), 79–110.

Wang, X., Fang, L., Liu, S., Ke, W., Wang, D., Peng, G., et al. (2019). Susceptibility of porcine IPI-2I intestinal epithelial cells to infection with swine enteric coronaviruses. *Vet Microbiol* 233, 21–27. doi: 10.1016/j.vetmic.2019.04.014

Zhang, Q., Ma, J., and Yoo, D. (2017). Inhibition of NF-kappaB activity by the porcine epidemic diarrhea virus nonstructural protein 1 for innate immune evasion. *Virology* 510, 111–126. doi: 10.1016/j.virol.2017.07.009

Zhang, Q., Shi, K., and Yoo, D. (2016). Suppression of type I interferon production by porcine epidemic diarrhea virus and degradation of CREB-binding protein by nsp1. *Virology* 489, 252–268. doi: 10.1016/j.virol.2015.12.010

Zhang, S., Cao, Y., and Yang, Q. (2020). Transferrin receptor 1 levels at the cell surface influence the susceptibility of newborn piglets to PEDV infection. *PLoS Pathog* 16:e1008682. doi: 10.1371/journal.ppat.1008682

Zhao, S., Gao, J., Zhu, L., and Yang, Q. (2014). Transmissible gastroenteritis virus and porcine epidemic diarrhoea virus infection induces dramatic changes in the tight junctions and microfilaments of polarized IPEC-J2 cells. *Virus Res.* 192, 34–45. doi: 10.1016/j.virusres.2014.08.014

**Conflict of Interest:** The authors declare that the research was conducted in the absence of any commercial or financial relationships that could be construed as a potential conflict of interest.

The reviewer XL declared a shared affiliation with the authors YL, FG, LY, YJ, WT, LLi, GL, GT, and CL to the handling editor at the time of the review.

**Publisher's Note:** All claims expressed in this article are solely those of the authors and do not necessarily represent those of their affiliated organizations, or those of the publisher, the editors and the reviewers. Any product that may be evaluated in this article, or claim that may be made by its manufacturer, is not guaranteed or endorsed by the publisher.

*Copyright © 2022 Zhang, Lv, Cai, Li, Gao, Yu, Jiang, Tong, Li, Li, Tong and Liu. This is an open-access article distributed under the terms of the Creative Commons Attribution License (CC BY). The use, distribution or reproduction in other forums is permitted, provided the original author(s) and the copyright owner(s) are credited and that the original publication in this journal is cited, in accordance with accepted academic practice. No use, distribution or reproduction is permitted which does not comply with these terms.*

frontiers in Microbiology

ORIGINAL RESEARCH
published: 18 March 2022
doi: 10.3389/fmicb.2022.860851

# Genetic Characteristics of Porcine Hemagglutinating Encephalomyelitis Coronavirus: Identification of Naturally Occurring Mutations Between 1970 and 2015

*Amina Nawal Bahoussi[1†], Yan-Yan Guo[1†], Rui-Zhu Shi[1], Pei-Hua Wang[1], Ya-Qian Li[1], Chang-Xin Wu[1,2,3] and Li Xing[1,2,3]**

[1]Institute of Biomedical Sciences, Shanxi University, Taiyuan, China, [2]Shanxi Provincial Key Laboratory of Medical Molecular Cell Biology, Shanxi University, Taiyuan, China, [3]Shanxi Provincial Key Laboratory for Prevention and Treatment of Major Infectious Diseases, Taiyuan, China

OPEN ACCESS

**Edited by:**
Chunfu Zheng,
University of Calgary,
Canada

**Reviewed by:**
Daxin Peng,
Yangzhou University,
China
Hongjie Fan,
Nanjing Agricultural University,
China

***Correspondence:**
Li Xing
xingli107@gmail.com

†These authors have contributed equally to this work

**Specialty section:**
This article was submitted to Virology, a section of the journal Frontiers in Microbiology

**Received:** 23 January 2022
**Accepted:** 21 February 2022
**Published:** 18 March 2022

**Citation:**
Bahoussi AN, Guo Y-Y, Shi R-Z, Wang P-H, Li Y-Q, Wu C-X and Xing L (2022) Genetic Characteristics of Porcine Hemagglutinating Encephalomyelitis Coronavirus: Identification of Naturally Occurring Mutations Between 1970 and 2015. Front. Microbiol. 13:860851. doi: 10.3389/fmicb.2022.860851

Porcine hemagglutinating encephalomyelitis virus (PHEV) is a *Betacoronavirus* characterized by neurological symptoms and a worldwide prevalence. Although PHEV is one of the earliest discovered porcine coronaviruses, it remains poorly studied. The full-length genome of the earliest PHEV strain collected in 1970 in the United States (PHEV/67 N/US/1970) was determined in October 2020. Using this virus as a prototype, we comparatively analyzed all available PHEV full-length sequences during 1970–2015. In phylogenetic trees based on PHEV full-length or spike glycoprotein open reading frame genomic sequences, PHEV/67 N/US/1970 was sorted into a clade different from that of viruses isolated in the United States in 2015. Intriguingly, United States and Belgium viruses isolated in 2015 and 2005, respectively, revealed multiple deletion mutation patterns compared to the strain PHEV/67 N/US/1970, leading to a truncated or a non-functional NS2A coding region. In addition, the genomic similarity analysis showed a hypervariability of the spike glycoprotein coding region, which can affect at least eight potential linear B cell epitopes located in the spike glycoprotein. This report indicates that PHEVs in the United States underwent a significant genetic drift, which might influence PHEV surveillance in other countries.

**Keywords: porcine hemagglutinating encephalomyelitis virus, coronavirus, spike glycoprotein, receptor-binding domain, genomic mutation, B cell epitope**

## INTRODUCTION

Coronaviruses (CoVs) rank among the largest groups of enveloped positive-sense, single-stranded RNA viruses, which fall under the *Coronavirinae* subfamily, *Coronaviridae* family, in *Nidovirales* order (Payne, 2017). In humans and vertebrates, the clinical picture of CoVs is dominated by the infection of three major systems, including the respiratory, digestive, and central nervous systems (CNS; Chen et al., 2020). CoVs are classified into four genera: *Alpha-CoV, Beta-CoV,*

*Gamma-CoV*, and *Deltacoronavirus* (de Groot et al., 2012). Human CoVs are generally attributed to a zoonotic origin before leaping into an intermediate host or directly to humans (Guan et al., 2003). The severe acute respiratory syndrome coronavirus 1 (SARS-CoV-1) in 2002/2003 (Ksiazek et al., 2003), the Middle East respiratory syndrome coronavirus (MERS-CoV) in 2012 and the novel severe acute respiratory syndrome coronavirus 2 (SARS-CoV-2) first identified in December 2019 in Wuhan, China (Zhou et al., 2020), confirmed that CoVs are likely originated in animals. The emergence of these three zoonotic severe *Betacoronavirus* outbreaks in less than two decades indicates the adaptation potentials of CoVs, their genetic plasticity, and the expansion of host range, which prompts us to explore the evolutionary characters of another mammal *Betacoronavirus*: the porcine hemagglutinating encephalomyelitis virus (PHEV).

Pigs are a natural host of six viruses from the *Coronaviridae* family (Wang et al., 2019), four of which were identified as *Alpha-CoVs*, including transmissible gastroenteritis virus (TGEV; Doyle and Hutchings, 1946), porcine epidemic diarrhea virus (PEDV; Wood, 1977), porcine respiratory coronavirus (PRCV; Pensaert et al., 1986), and the newly discovered swine acute diarrhea syndrome coronavirus (SADS-CoV; Gong et al., 2017; Pan et al., 2017; Zhou et al., 2018); one *Beta-CoV* PHEV (Greig et al., 1962); and the porcine *Deltacoronavirus* (PDCoV; Woo et al., 2012).

Porcine hemagglutinating encephalomyelitis virus is one of the earliest identified and isolated porcine CoVs and the only known neurotropic virus in pigs (Mora-Diaz et al., 2019). PHEV infection was first reported in the Ontario province of Canada in 1957 (Roe and Alexander, 1958) and the viral pathogen was first isolated from the brains of encephalitis piglets in 1962 (Greig et al., 1962). Since then, PHEV infection has been reported in countries of America, Europe, and Asia, including the United States (Cutlip and Mengeling, 1972), Argentina (Quiroga et al., 2008), Great Britain (Cartwright et al., 1969), Belgium (Sasseville et al., 2001), Japan (Hirano and Ono, 1998), South Korea (Rho et al., 2011), and China (Gao et al., 2011; Dong et al., 2014).

In neonatal pigs, PHEV infection causes vomiting and wasting disease (VWD) or encephalomyelitis (Mengeling et al., 1972; Andries and Pensaert, 1981) with approximately 100% mortality rate and a high prevalence in the United States (Mora-Diaz et al., 2020). The primary replication of PHEV starts in the upper respiratory tract and tonsils, with non-specific clinical signs, including sneezing, coughing, and transient fever of 1–2 days (Andries and Pensaert, 1980; Hirahara et al., 1987). During the incubation, PHEV can penetrate the CNS (Andries and Pensaert, 1980) and invade predominantly neurons with a massive activation of the surrounding microglia and an obvious inflammation of CNS (J. Zhang et al., 2021). During the early stage of PHEV infection, microglial activation leads to a monumental proinflammatory cytokine release (IL-1β, IL-6, TNF-α, and IFN-γ) to limit the viral replication (Zhang et al., 2021). However, an excessive microglial activation at a late stage, with a blood–brain barrier (BBB) destruction and a monocytes/macrophages infiltration of CNS, aggravates PHEV infection (Zhang et al., 2021). Furthermore, PHEV causes lysosomal disorders by decreasing the expression of progranulin protein (Lan et al., 2020), a significant accumulation of autophagosomes (APs) in nerve cells (Li et al., 2021) and other neurological dysfunctions (Mora-Diaz et al., 2021a). Although pigs of any age can be infected, the clinical manifestation depends on the age at PHEV-infection time (Hirano, 2004). In older pigs, PHEV is highly seroprevalent and usually subclinical (Dong et al., 2014; Mora-Diaz et al., 2020). However, a recent report showed the persistent virus shedding in feces and oral fluid with an active humoral immune response (IgM, IgG) in subclinical grower pigs suggesting an active viral replication attenuated by the immune response (Mora-Diaz et al., 2021b).

Porcine hemagglutinating encephalomyelitis virus belongs to *Betacoronavirus* genus, *Embecovirus* subgenus (Zhi et al., 2005; Llanes et al., 2020). The RNA genome of PHEV is about ~30 kb in length and shows a short untranslated region (UTR) at both ends (Fehr and Perlman, 2015). The genome is flanked with a 5′MET cap and a 3′ polyA tail (Fehr and Perlman, 2015) and contains at least 11 predicted open reading frames (ORFs; Vijgen et al., 2006; Shi et al., 2018). The first two-thirds of the viral genome is occupied by replicase ORF which encodes replicase polyprotein, a precursor for multiple nonstructural proteins (Nsps; Sola et al., 2015). The one-third 3′ region of the viral genome encodes five major structural proteins (hemagglutinin-esterase protein, HE; spike glycoprotein, S; envelope protein, E; membrane protein, M; and nucleocapsid protein, N) and three non-structural proteins (NS2A, NS4.9, and NS12.7; Weiss and Navas-Martin, 2005; Vijgen et al., 2006; Wang et al., 2019). Among them, N protein is the most abundant structural protein that binds to viral genome RNA. M and E are membrane proteins (Wang et al., 2019). Whereas, HE protein which is not present in other *Beta-CoVs,* is characterized by hemagglutinating (HA), acetyl-esterase (AE) or receptor-destroying and binding activities (Cornelissen et al., 1997).

The S glycoprotein of coronaviruses is a viral envelope protein with a binding specificity regulated by a receptor-binding domain (RBD; Bosch et al., 2003; Dong et al., 2015). S glycoprotein facilitates the attachment of the virion and its penetration into the host cells by recognizing and interacting with a proper cellular receptor (Schultze et al., 1992). During the entry of viral particles, S glycoprotein is cleaved into two subunits, named S1 and S2 subunits (Walls et al., 2016). S glycoprotein of PHEV is composed of about 1,349 amino acids (aa; Dong et al., 2015) and contains several conserved domains as determined in NCBI conserved domain database (CDD; Marchler-Bauer et al., 2017). The S1 subunit contains N-terminal domain (NTD, aa 16–298) and S1 receptor-binding domain (S1-RBD, aa 311–608), whereas the S2 subunit contains an S2 domain (aa 784–1,276), a transmembrane structure (TM, aa 1,294–1,316), and a cytosolic tail at the C-terminus. The S1-RBD of PHEV has been shown to bind specifically to neural cell adhesion molecules (NCAM), also named CD56 (Dong et al., 2015), which is involved in neuronal infection and injuries (Gao et al., 2010). The S2 subunit controls the membrane fusion between virion and cell during viral entry into the host cells (Bosch et al., 2003; Walls et al., 2016).

In China, PHEV was first reported in a pig farm in Beijing in 1985, then in Jilin, Liaoning, Shandong, and other provinces (Gao et al., 2011; Chen et al., 2012; Dong et al., 2014). In 2007, two pig farms in Changchun City and Siping City, Jilin Province of China, had outbreaks of PHEV, with mortality rates of 47.6 and 100%, respectively (Gao et al., 2011; Shi et al., 2018). In 2015, the influenza-like respiratory disease occurred in display pigs in Michigan, United States, and PHEV was finally identified in the specimens of clinically sick pigs (Lorbach et al., 2017). Currently, there is no commercially available vaccine against PHEV. The small interfering RNA (siRNA) technique has been suggested to have the potential to partially block the replication of PHEV by targeting the spike glycoprotein and replicase polyprotein genes (Lan et al., 2012) or cell host-specific proteins (Hu et al., 2020). Therefore, surveillance of this virus is the key to preventing the occurrence of an outbreak. In October 2020, the complete genome sequence of the virus PHEV/67 N/US/1970 collected in the United States in 1970 was determined. It represents the earliest full-length genome sequence information so far. In this study, we used this virus as a prototype to compare and analyze the full-length sequences of all other viral isolates and discussed the genome structure, genome similarity, and B cell epitopes to explore the evolutionary relationship and heredity of PHEV diversity, providing critical information for formulating disease control strategies suitable for PHEV.

# MATERIALS AND METHODS

## Phylogenetic Tree Construction and Genomic Similarity Analysis

Fourteen full-length genome sequences of PHEVs isolated since 1970 were retrieved from NCBI GenBank. The viruses in this report were identified by their GenBank ID, name, country, and year of collection in a format as [GenBank ID: virus name (country-year of collection)]. The sequence of the virus PHEV/67 N/US/1970 (GenBank ID: MW165134.1) collected in 1970 was included in this analysis as a prototype reference. The phylogenetic trees were constructed using the neighbor-joining method embedded in the MEGA-X software (Kumar et al., 2004, 2018) based on PHEV full-length genomic sequence or the full-length sequence of individual ORFs. 1,000 repeated bootstrap analysis was applied to determine the percentage reliability value of each internal node of the phylogenetic tree. SimPlot ver.3.5.1 (Lole et al., 1999) was used to generate a similarity map of full-length PHEV genome.

## Prediction of Linear B Cell Epitopes in S Glycoprotein of PHEV

To analyze the potential linear B cell epitopes in PHEV S glycoprotein, we used the BepiPred-2.0 server, running under IEDB (the immune epitope database, https://www.iedb.org/; Jespersen et al., 2017). The epitope and non-epitope amino acids were determined from the crystal structure using a Random Forest algorithm (Jespersen et al., 2017). Residues with scores higher than the threshold (set to 0.5) were predicted to be part of an epitope.

## Three-Dimensional Modeling of PHEV S Glycoprotein Domains

I-TASER (Iterative Threading ASSEmbly Refinement) is a hierarchical method for protein structure modeling and structure-based functional annotation (Roy et al., 2010; Yang et al., 2015). I-TASER first identified structural templates from the RCSB protein data bank (PDB) by multiple threading approach LOMETS, then the construction of the full-length atomic models by iterative template-based fragment assembly simulations. I-TASER was performed to visualize the tertiary structure of three regions of PHEV S glycoprotein, including the NTD-containing region (aa 16–310), S1-RBD-containing region (aa 311–783), and S2 domain (aa 784–1,276).

# RESULTS

## Phylogenetic Analysis Reveals Two Separate Evolutionary Clades of PHEVs

To determine the genomic characters, variation, and relationship between PHEV strains, we performed a phylogenetic analysis of the entire genomes or individual ORF sequences of PHEV isolates available since 1970 in the NCBI GenBank database using MEGA-X software (Kumar et al., 2004, 2018). We built phylogenetic trees based on 14 variants, isolated from the United States (11), China (2), and Belgium (1). The genomic sequence of PHEV/67 N/US/1970 virus (GenBank ID: MW165134.1) collected in the United States in 1970 was available in the NCBI GenBank database in October 2020, providing the earliest genetic information of PHEV. Therefore, this strain was included as a reference to explore the genetic diversity and evolution of PHEV over time. As indicated in **Figure 1A**, the phylogenetic tree of PHEV complete genome exhibits two main clades, where PHEV/67 N/US/1970 strain clustered together in one clade with strains isolated from Belgium in 2005 (PHEV/VW572, GenBank ID: DQ011855.1) and China in 2008 (PHEV/JL/2008, GenBank ID: KY994645.1) and 2014 (PHEV/CC14, GenBank ID: MF083115.1). The remaining strains isolated from the United States in 2015 (a total of 10) clustered together into another independent clade, which can be further divided into three lineage groups. To further understand the evolution of PHEV, we proceeded to individual ORF sequence-based phylogenetic analysis. In the phylogenetic tree of S glycoprotein ORF (**Figure 1B**), PHEV strains were sorted into two different evolutionary clades, similar to that of full-length viral genome (**Figure 1A**). In replicase polyprotein ORF-based phylogenetic tree, PHEV/67 N/US/1970 is still genetically closer to the strains isolated in China and Belgium (**Figure 1G**). However, in the phylogenetic trees based on ORFs of HE protein (**Figure 1C**), membrane protein (**Figure 1D**), envelop protein (**Figure 1E**), and nucleocapsid protein (**Figure 1F**), PHEV strains fell in different lineage groups other than groups indicated in the full-length genome phylogenetic tree (**Figure 1A**).

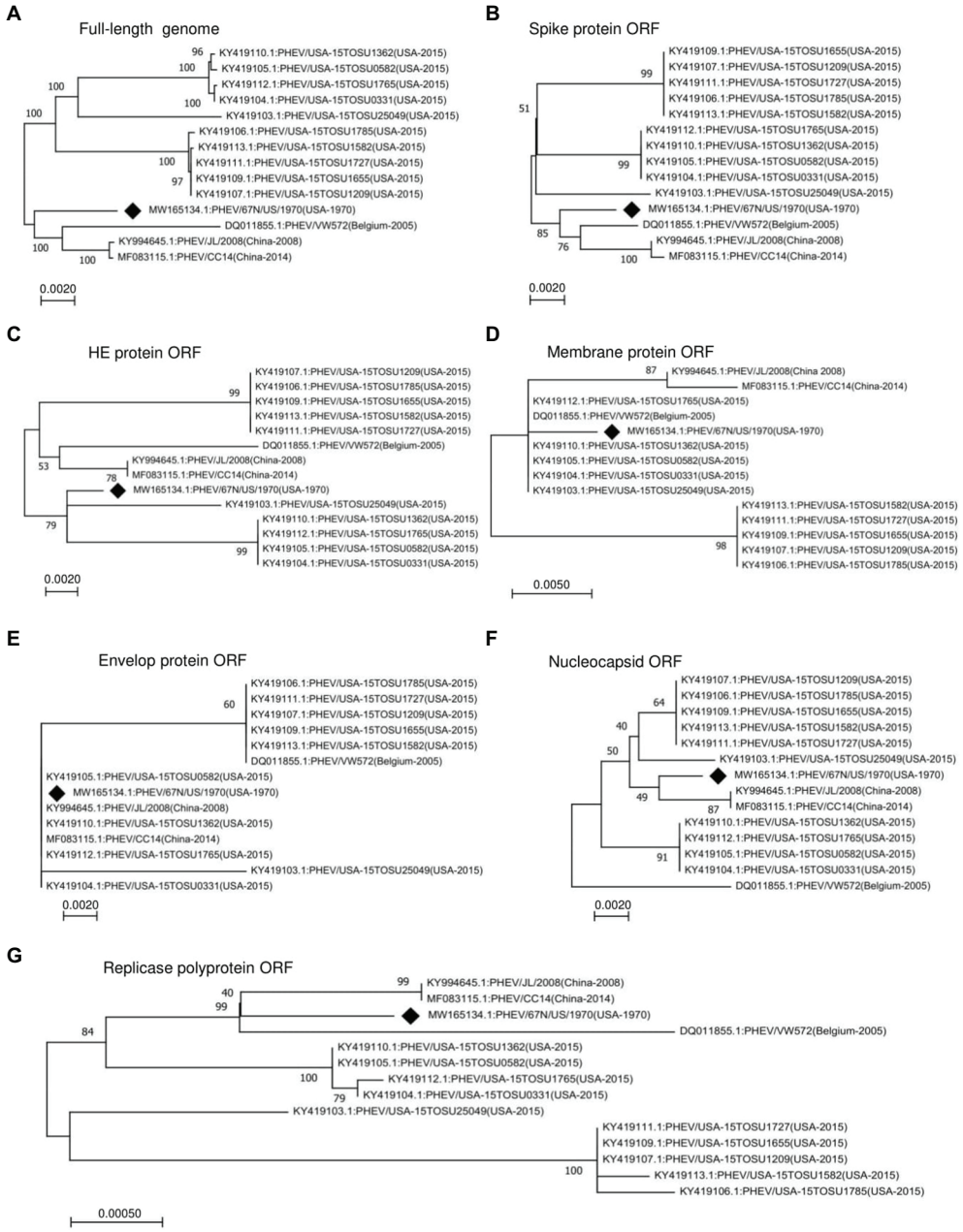


**FIGURE 1 |** Phylogenetic analysis of 14 PHEV strains isolated between 1970 and 2015. Phylogenetic trees were constructed using the neighbor-joining algorithm in the MEGA-X software and based on **(A)** Full-length genome, or individual ORFs including **(B)** spike glycoprotein ORF, **(C)** HE glycoprotein ORF, **(D)** membrane protein ORF, **(E)** envelope protein ORF, **(F)** nucleocapsid protein ORF, and **(G)** replicase polyprotein ORF. The numbers on each branch are the bootstrap values (%) in 1000 replicates. The scale bar indicates the amino acid substitution at each position. The strain PHEV/67 N/US/1970 isolated in the United States in 1970 was labeled with a black diamond.

## Two Highly Variable Regions of PHEV Genome: NS2A ORF and S Glycoprotein ORF

To further analyze the genetic characteristics and connectivity between PHEV strains, we conducted a genomic similarity analysis using SimPlot ver.3.5.1 software (Lole et al., 1999). Six viruses were included as representatives for each lineage group according to the whole genomic sequence-based phylogenetic tree (**Figure 1A**) and PHEV/USA-15TOSU1209 (GenBank ID: KY419107.1) was used as the query strain. As shown in **Figure 2**, the complete genome of PHEV/USA-15TOSU1209 (GenBank ID: KY419107.1) showed a great genomic similarity (>96%) with the included strains except for the region containing S glycoprotein and NS2A accessory protein ORFs that have the lowest genomic similarity, indicating their hypervariability. Sequence alignment revealed multiple deletion patterns in NS2A ORF region (**Figure 3**) of PHEVs isolated in the United States

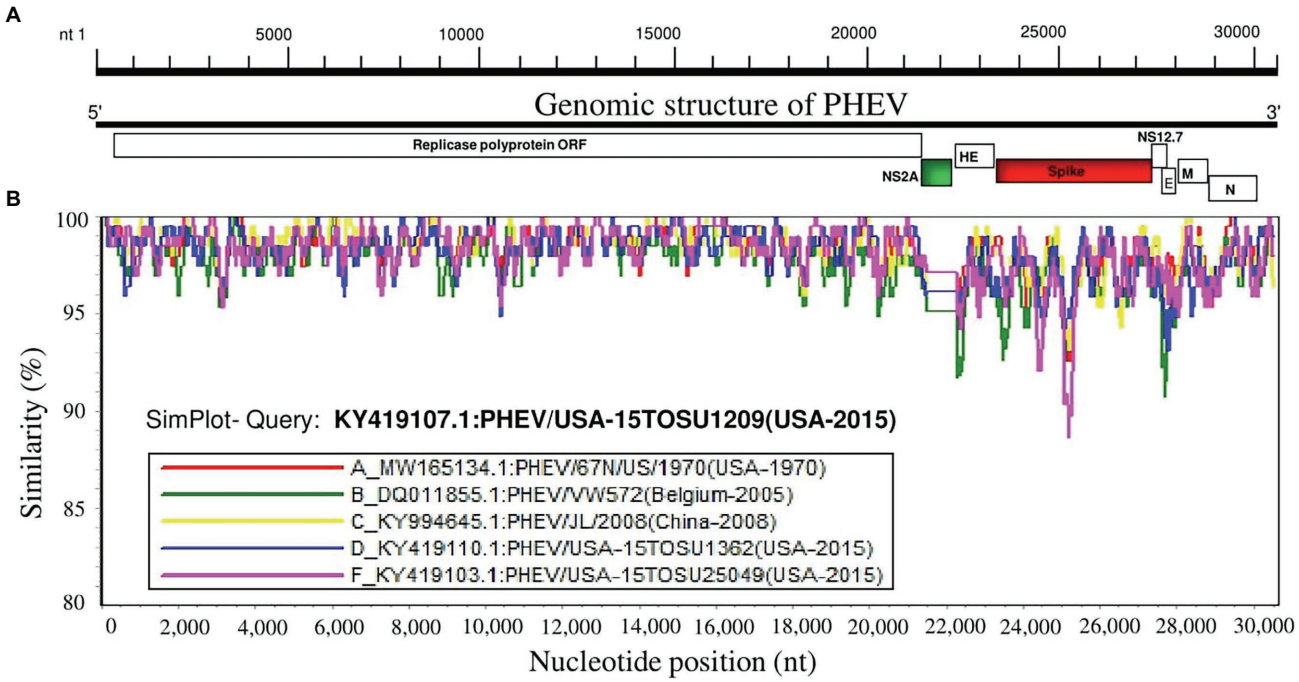


**FIGURE 2 |** Similarity map of the full-length genome sequence of representative PHEV isolates. **(A)** Schematic diagram of the complete PHEV genomic structure. From the 5′end to the 3′ end are Replicase polyprotein ORF, accessory protein NS2A ORF, HE protein ORF, spike glycoprotein ORF, accessory protein NS12.7 ORF, envelope protein ORF (E), membrane protein ORF (M) and nucleocapsid protein ORF (N). **(B)** SimPlot similarity analysis results using SimPlot ver.3.5.1 (Lole et al., 1999). Virus PHEV/USA-15TOSU1209 (GenBank ID: KY419107.1) was used as the query sequence to compare with five other representative strains from the United States, China, and Belgium.

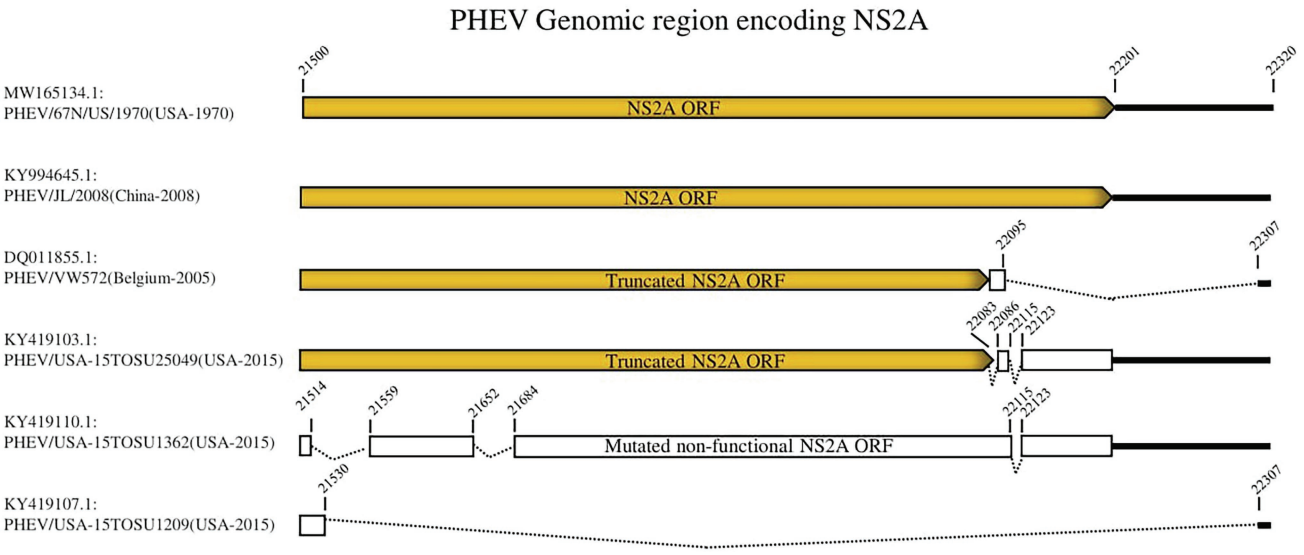


**FIGURE 3 |** Deletion patterns in NS2A ORF region. The yellow box indicates the expression of full-length or truncated NS2A. The white box indicates the region of non-functional expression. Deleted regions are indicated with dashed lines. The numbers indicate the nucleotide positions relative to the genome of PHEV/67 N/US/1970 strain (GenBank ID: MW165134.1).

in 2015 and Belgium in 2005. Compared with PHEV/67 N/US/1970 (**Figure 3**), viruses isolated from China in 2008 (PHEV/JL/2008) and 2014 (PHEV/CC14, Data not shown) have no deletion mutations in the NS2A ORF region. In contrast, NS2A of viruses PHEV/VW572 from Belgium in 2005 and PHEV/USA-15TOSU25049 from the United States in 2015 has small

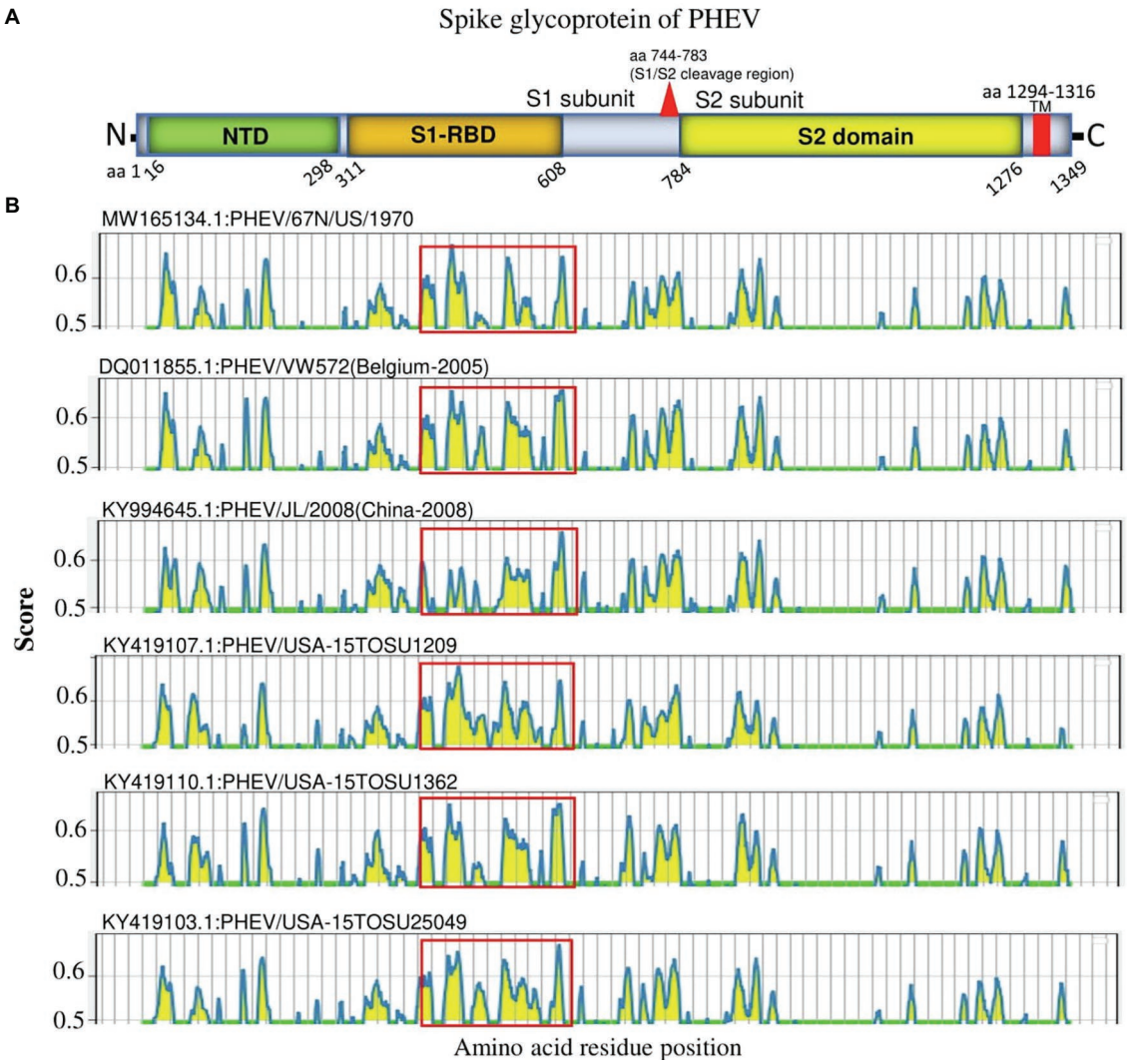


**FIGURE 4 |** Linear B cell epitope map of the full-length S glycoprotein of PHEV. **(A)** Diagram of the main features of PHEV S glycoprotein, including NTD (aa 16–298), S1-RBD (aa 311–608), S2 domain (aa 784–1,276), and transmembrane domain (TM; aa 1,294–1,316). Numbers refer to the amino acid positions corresponding to PHEV/67 N/US/1970 S glycoprotein. **(B)** Mapping of linear B cell epitopes using the BepiPred-2.0 server. The *Y*-axes represents the residue score, and the X-axes represents the amino acid position, which is also relative to the diagram on the top **(A)**. The predicted epitopes are indicated in yellow.

deletions of 39 and 38 amino acids at the C-terminus, respectively. The representative viruses isolated in the United States in 2015 (PHEV/USA-15TOSU1362 and PHEV/USA-15TOSU1209) exhibited multiple deletions all through the NS2A ORF region, resulting in a non-functional expression of NS2A (**Figure 3**).

## Linear B Cell Epitopes in S Glycoprotein of PHEV

S glycoprotein of coronaviruses is the major viral antigen that induces the generation of neutralizing antibodies during host infection, making it a major target protein for vaccine development (Du et al., 2009). Since S glycoprotein ORF of PHEV is found relatively highly variable (**Figure 2**), we assessed the effects of detected genomic variations on the antigenicity of S glycoprotein. For this aim, the linear B-cell epitopes on S glycoprotein of six representative viruses analyzed in genomic similarity analysis (**Figure 2**) were predicted using BepiPred-2.0 epitope prediction server (Jespersen et al., 2017). As indicated in **Figure 4**, a significant difference in the distribution of potential B cell epitopes was seen in S1-RBD (aa 311–608), whereas there were minor differences for the remaining part of S glycoprotein. Viruses PHEV/USA-15TOSU25049 (GenBank ID: KY419103.1) and PHEV/67 N/US/1970 (GenBank ID: MW165134.1) isolated in the same country (United States), were sorted into separate evolutionary clades in either full-length genome-based (**Figure 1A**) or S glycoprotein ORF-based phylogenetic tree (**Figure 1B**). However, compared with other viral strains, both viruses were genetically closer to each other in the S glycoprotein ORF-based phylogenetic tree (**Figure 1B**). Thus, the three-dimensional structures of NTD, S1-RBD, and S2 domains of these two viruses were modeled using I-TASER (Roy et al., 2010; Yang et al., 2015) to visualize the minimal amino acid

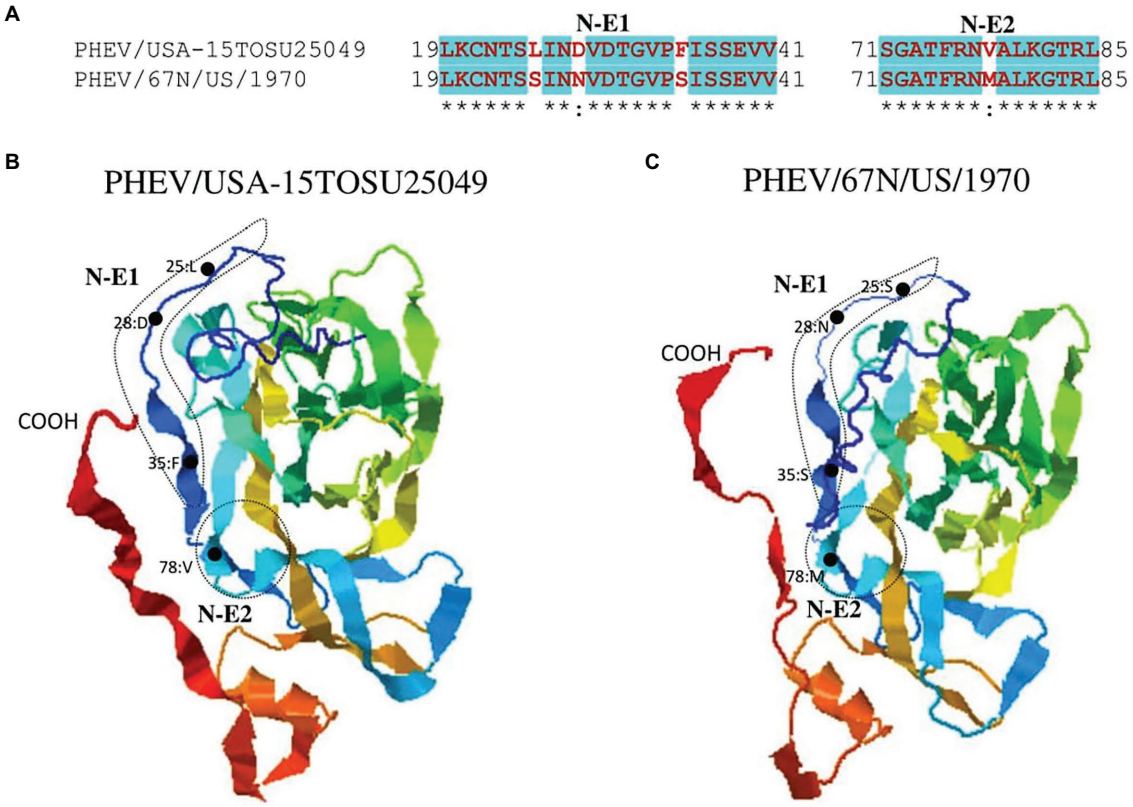


**FIGURE 5 |** Comparison of linear B cell epitopes affected by amino acid variations in the NTD of S glycoprotein between PHEV/USA-15TOSU25049 and PHEV/67 N/US/1970. **(A)** Amino acids of the predicted linear B cell epitope are indicated with bold red letters, while numbers refer to their positions relative to the corresponding full-length S glycoprotein. Three-dimensional view of epitopes of PHEV/USA-15TOSU25049 **(B)** and PHEV/67 N/US/1970 **(C)**. The tertiary structure was modeled using I-TASER. The predicted epitopes are circled, and amino acid variations are marked with black dots.

variations seen in two main evolutionary clades in the potential linear B cell epitopes. For NTD or S2 domains of viruses PHEV/USA-15TOSU25049 and PHEV/67 N/US/1970, only two linear B cell epitopes were affected by amino acid variations (**Figures 5** and **6**, respectively), whereas four predicted epitopes were affected in S1-RBD (**Figure 7**). The mutations T571I and R574S eliminated the epitope S1-E4 in PHEV/67 N/US/1970. No amino acid insertions or deletions were seen in the potential linear B cell epitopes. In summary, the S1-RBD may be one of the main factors driving the antigenic drift of S glycoprotein of PHEV.

## DISCUSSION

Although PHEV was one of the earliest identified and isolated swine CoVs, it remains after decades poorly documented and less studied with limited availability of genome sequences. In this report, we conducted a phylogenetic analysis based on the complete genome of the earliest isolated PHEV strain in the United States in 1970, available in October 2020, with 13 other isolates from different countries, including 10 from the United States, two from China, and one from Belgium. The phylogenetic tree showed two main clades, where the earliest United States strain (PHEV/67 N/US/1970) clustered together with the two strains from China and one from Belgium, whereas the other 10 United States variants (isolated in 2015) clustered together in another independent clade (**Figures 1A,B**), demonstrating the existence of two different circulating PHEV groups in the United States. Furthermore, NS2A and S glycoprotein ORFs were highly variable in PHEV genome, altering the expression of a normal NS2A and the composition of linear B cell epitopes in the S glycoprotein, particularly S1-RBD.

Compared with other *Beta-CoVs* from a supposed common ancestor such as human coronavirus OC43 and bovine coronavirus (Vijgen et al., 2006), NS2A of PHEV is shorter with a missing of ~84 amino acids at the C-terminus (Vijgen et al., 2006; Lau et al., 2012). NS2A belongs to the 2H phosphoesterase superfamily (Mazumder et al., 2002; Snijder et al., 2003), but its function in coronavirus replication is still unknown. In previous reports, mutation deletions in NS2A of PHEVs have been linked to severe respiratory manifestations in pigs (Lorbach et al., 2017; Wang et al., 2019), suggesting that the detected NS2A deletions might be involved in the pathogenicity of PHEV-mediated respiratory syndrome.

Besides NS2A, the S glycoprotein of coronaviruses is a direct target of cellular and humoral immune responses and a vaccine design focus since it represents the main viral surface antigen (Buchholz et al., 2004; Zhi et al., 2005; Tortorici et al., 2019; Dai and Gao, 2021). S glycoprotein mutations help escape the immune response and promote animal-human transmission through

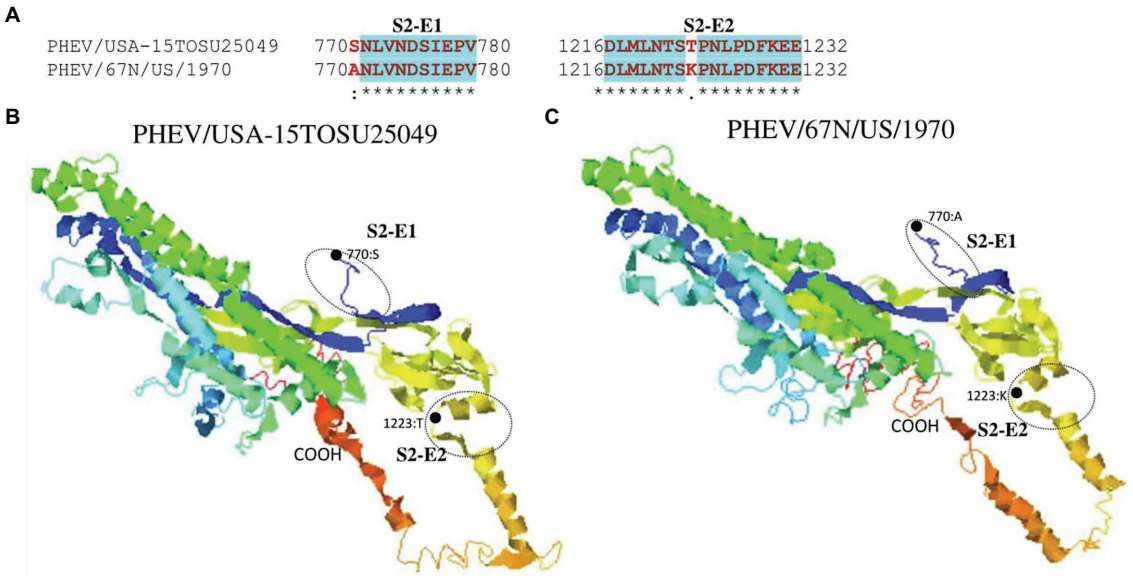


**FIGURE 6 |** Comparison of linear B cell epitopes affected by amino acid variations in the S2 domain between PHEV/USA-15TOSU25049 and PHEV/67 N/US/1970. **(A)** Amino acids of the predicted linear B cell epitope are indicated with bold red letters, while numbers refer to their positions relative to the full-length S glycoprotein. Three-dimensional view of epitopes in the S2 domain of PHEV/USA-15TOSU25049 **(B)** and PHEV/67 N/US/1970 **(C)**. The predicted epitopes are circled, and the amino acid variations are marked with black dots.

adaptation potentials (Zhang et al., 2006). The hypervariability of S glycoprotein is the main cause of changes in tissue tropism (Gallagher and Buchmeier, 2001; Hulswit et al., 2016). The deletion of about 216 or 227 amino acid residues in the N-terminus of S glycoprotein of TGEV has causally changed the enteric tissue tropism to a respiratory tissue tropism (named PRCV; Laude et al., 1993; Vaughn et al., 1995), which may be linked to the distribution of receptors over tissues or their different usage by different CoV strains (Whitworth et al., 2019). PDEV with the large deletion in the N terminus of S glycoprotein (about 194–216 amino acid residues) has shown a partial attenuation, although the tissue tropism was not altered (Hou et al., 2017). During PHEV infection, a crucial interaction between S glycoprotein and NCAM was identified (Gao et al., 2010), with a fragment (aa 291–548) in S1 subunit as a minimum number of amino acids essential to binding NCAM (Dong et al., 2015). Contrary to NS2A ORF region of PHEV, which showed significant deletions (**Figure 3**), S glycoprotein ORF did not undergo any deletion pattern.

Porcine hemagglutinating encephalomyelitis virus is the unique porcine neurotropic CoV with the potential to invade the central nervous system. Neurologic symptoms in PHEV-infected piglets with respiratory or digestive signs indicate the involvement of neurobiological pathways, which might be related to multiple cellular receptors in tissues of three major above mentioned systems. In the latest report, cell-surface glycans, including sialic acid (SA) and heparan sulfate (HS) were found to act as critical cellular factors involved in the attachment of PHEV (Hu et al., 2022). Altogether, this indicates the complexity of the underlying mechanisms of PHEV S glycoprotein interaction with cellular receptors.

S glycoprotein is a great inducer of neutralizing antibodies and encompasses multiple epitopes, making it an important target and informative source for CoVs vaccine design (Du et al., 2009), including the licensed vaccines against SARS-CoV-1 (Du et al., 2009) and the SARS-CoV-2 vaccines used to fight against the ongoing COVID-19 pandemic (Samrat et al., 2020; Dai and Gao, 2021). Like multiple coronaviruses, the hypervariability and the high dissimilarity of PHEV S glycoprotein ORF detected in this study impacted the potential B cell epitopes. The mutations affected at least eight potential linear B cell epitopes on S glycoprotein, half of which were located in the S1-RBD. This information is of great value for the vaccine design and the surveillance of genetic diversity of PHEV.

## DATA AVAILABILITY STATEMENT

Publicly available datasets were analyzed in this study. This data can be found here: Porcine hemagglutinating encephalomyelitis virus strain PHEV/67 N/US/1970, complete genome GenBank: MW165134.1.

## AUTHOR CONTRIBUTIONS

AB, YG, and LX: conceptualization. AB, YG, PW, YL, and RS: data analysis. AB, YG, and LX: visualization and writing. CW and LX: administration. AB, YG, and LX: manuscript revision. All authors contributed to the article and approved the submitted version.

## ACKNOWLEDGMENTS

The authors thank all the persons who contributed to the collection and production of PHEV genomic sequences in GenBank.

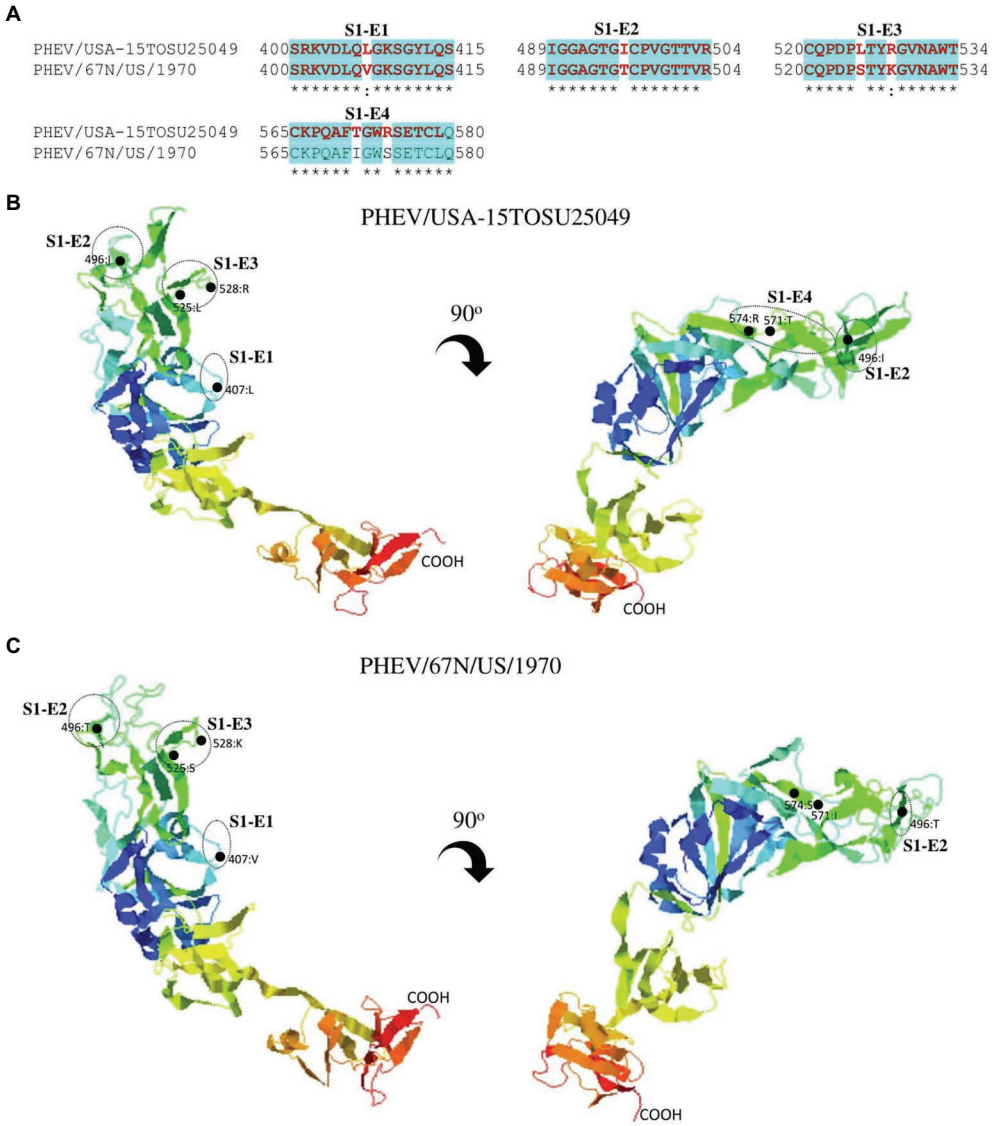


**FIGURE 7 |** Comparison of linear B cell epitopes affected by amino acid variations in the S1-RBD between PHEV/USA-15TOSU25049 and PHEV/67 N/US/1970. **(A)** Amino acids of the predicted linear B cell epitope are indicated with bold red letters, while numbers refer to their positions relative to the corresponding full-length S glycoprotein. Three-dimensional view of epitopes in the S1-RBD of PHEV/USA-15TOSU25049 **(B)** or PHEV/67 N/US/1970 **(C)**. The predicted epitopes are circled, and amino acid variations are marked with black dots.

## REFERENCES


Andries, K., and Pensaert, M. B. (1980). Immunofluorescence studies on the pathogenesis of hemagglutinating encephalomyelitis virus infection in pigs after oronasal inoculation. *Am. J. Vet. Res.* 41, 1372–1378.

Andries, K., and Pensaert, M. (1981). Vomiting and wasting disease, a coronavirus infection of pigs. *Adv. Exp. Med. Biol.* 142, 399–408. doi: 10.1007/978-1-4757-0456-3_33

Bosch, B. J., van der Zee, R., de Haan, C. A., and Rottier, P. J. (2003). The coronavirus spike protein is a class I virus fusion protein: structural and functional characterization of the fusion core complex. *J. Virol.* 77, 8801–8811. doi: 10.1128/JVI.77.16.8801-8811.2003

Buchholz, U. J., Bukreyev, A., Yang, L., Lamirande, E. W., Murphy, B. R., Subbarao, K., et al. (2004). Contributions of the structural proteins of severe acute respiratory syndrome coronavirus to protective immunity. *Proc. Natl. Acad. Sci. U. S. A.* 101, 9804–9809. doi: 10.1073/pnas.0403492101

Cartwright, S. F., Lucas, M., Cavill, J. P., Gush, A. F., and Blandford, T. B. (1969). Vomiting and wasting disease of piglets. *Vet. Rec.* 84, 175–176. doi: 10.1136/vr.84.7.175

Chen, Y., Liu, Q., and Guo, D. (2020). Emerging coronaviruses: genome structure, replication, and pathogenesis. *J. Med. Virol.* 92, 418–423. doi: 10.1002/jmv.25681

Chen, K., Zhao, K., Song, D., He, W., Gao, W., Zhao, C., et al. (2012). Development and evaluation of an immunochromatographic strip for rapid detection of porcine hemagglutinating encephalomyelitis virus. *Virol. J.* 9:172. doi: 10.1186/1743-422X-9-172

Cornelissen, L. A., Wierda, C. M., van der Meer, F. J., Herrewegh, A. A., Horzinek, M. C., Egberink, H. F., et al. (1997). Hemagglutinin-esterase, a novel structural protein of torovirus. *J. Virol.* 71, 5277–5286. doi: 10.1128/jvi.71.7.5277-5286.1997

Cutlip, R. C., and Mengeling, W. L. (1972). Lesions induced by hemagglutinating encephalomyelitis virus strain 67N in pigs. *Am. J. Vet. Res.* 33, 2003–2009

Dai, L., and Gao, G. F. (2021). Viral targets for vaccines against COVID-19. *Nat. Rev. Immunol.* 21, 73–82. doi: 10.1038/s41577-020-00480-0

de Groot, R., Baker, S., Baric, R., Enjuanes, L., Gorbalenya, A., Holmes, K., et al. (2012). "Virus taxonomy" in *Ninth Report of the International Committee on Taxonomy of Viruses: Family Coronaviridae*. eds. A. King, M. Adams, E. Cartens and E. Lefkowitz (San Diego, CA: Elsevier Academic Press), 806–828.

Dong, B., Gao, W., Lu, H., Zhao, K., Ding, N., Liu, W., et al. (2015). A small region of porcine hemagglutinating encephalomyelitis virus spike protein interacts with the neural cell adhesion molecule. *Intervirology* 58, 130–137. doi: 10.1159/000381060

Dong, B., Lu, H., Zhao, K., Liu, W., Gao, W., Lan, Y., et al. (2014). Identification and genetic characterization of porcine hemagglutinating encephalomyelitis virus from domestic piglets in China. *Arch. Virol.* 159, 2329–2337. doi: 10.1007/s00705-014-2070-y

Doyle, L. P., and Hutchings, L. M. (1946). A transmissible gastroenteritis in pigs. *J. Am. Vet. Med. Assoc.* 108, 257–259

Du, L., He, Y., Zhou, Y., Liu, S., Zheng, B.-J., and Jiang, S. (2009). The spike protein of SARS-CoV — a target for vaccine and therapeutic development. *Nat. Rev. Microbiol.* 7, 226–236. doi: 10.1038/nrmicro2090

Fehr, A. R., and Perlman, S. (2015). Coronaviruses: an overview of their replication and pathogenesis. *Methods Mol. Biol.* 1282, 1–23. doi: 10.1007/978-1-4939-2438-7_1

Gallagher, T. M., and Buchmeier, M. J. (2001). Coronavirus spike proteins in viral entry and pathogenesis. *Virology* 279, 371–374. doi: 10.1006/viro.2000.0757

Gao, W., He, W., Zhao, K., Lu, H., Ren, W., Du, C., et al. (2010). Identification of NCAM that interacts with the PHE-CoV spike protein. *Virol. J.* 7, 254. doi: 10.1186/1743-422X-7-254

Gao, W., Zhao, K., Zhao, C., Du, C., Ren, W., Song, D., et al. (2011). Vomiting and wasting disease associated with hemagglutinating encephalomyelitis viruses infection in piglets in Jilin. *China. Virol J* 8, 130. doi: 10.1186/1743-422x-8-130

Gong, L., Li, J., Zhou, Q., Xu, Z., Chen, L., Zhang, Y., et al. (2017). A new bat-HKU2-like coronavirus in swine, China, 2017. *Emerg. Infect. Dis.* 23, 1607–1609. doi: 10.3201/eid2309.170915

Greig, A. S., Mitchell, D., Corner, A. H., Bannister, G. L., Meads, E. B., and Julian, R. J. (1962). A hemagglutinating virus producing encephalomyelitis in baby pigs. *Can. J. Comp. Med. Vet. Sci.* 26, 49–56

Guan, Y., Zheng, B. J., He, Y. Q., Liu, X. L., Zhuang, Z. X., Cheung, C. L., et al. (2003). Isolation and characterization of viruses related to the SARS coronavirus from animals in southern China. *Science* 302, 276–278.

Hirahara, T., Yasuhara, H., Kodama, K., Nakai, M., and Sasaki, N. (1987). Isolation of hemagglutinating encephalomyelitis virus from respiratory tract of pigs in Japan. *Nihon Juigaku Zasshi* 49, 85–93. doi: 10.1292/jvms1939.49.85

Hirano, N. (2004). Neurotropism of swine Haemagglutinating encephalomyelitis virus (coronavirus) in mice depending upon host age and route of infection. *J. Comp. Pathol.* 130, 58–65. doi: 10.1016/S0021-9975(03)00083-5

Hirano, N., and Ono, K. (1998). A serological survey of human coronavirus in pigs of the Tohoku District of Japan. *Adv. Exp. Med. Biol.* 440, 491–494. doi: 10.1007/978-1-4615-5331-1_63

Hou, Y., Lin, C. M., Yokoyama, M., Yount, B. L., Marthaler, D., Douglas, A. L., et al. (2017). Deletion of a 197-amino-acid region in the N-terminal domain of spike protein attenuates porcine epidemic diarrhea virus in piglets. *J. Virol.* 91. doi: 10.1128/JVI.00227-17

Hu, S., Li, Z., Lan, Y., Guan, J., Zhao, K., Chu, D., et al. (2020). MiR-10a-5p-mediated Syndecan 1 suppression restricts porcine Hemagglutinating encephalomyelitis virus replication. *Front. Microbiol.* 11, 105. doi: 10.3389/fmicb.2020.00105

Hu, S., Zhao, K., Lan, Y., Shi, J., Guan, J., Lu, H., et al. (2022). Cell-surface glycans act as attachment factors for porcine hemagglutinating encephalomyelitis virus. *Vet. Microbiol.* 265:109315. doi: 10.1016/j.vetmic.2021.109315

Hulswit, R. J., de Haan, C. A., and Bosch, B. J. (2016). Coronavirus spike protein and tropism changes. *Adv. Virus Res.* 96, 29–57. doi: 10.1016/bs.aivir.2016.08.004

Jespersen, M. C., Peters, B., Nielsen, M., and Marcatili, P. (2017). BepiPred-2.0: improving sequence-based B-cell epitope prediction using conformational epitopes. *Nucleic Acids Res.* 45, W24–W29. doi: 10.1093/nar/gkx346

Ksiazek, T. G., Erdman, D., Goldsmith, C. S., Zaki, S. R., Peret, T., Emery, S., et al. (2003). A novel coronavirus associated with severe acute respiratory syndrome. *N. Engl. J. Med.* 348, 1953–1966. doi: 10.1056/NEJMoa030781

Kumar, S., Stecher, G., Li, M., Knyaz, C., and Tamura, K. (2018). MEGA X: molecular evolutionary genetics analysis across computing platforms. *Mol. Biol. Evol.* 35, 1547–1549. doi: 10.1093/molbev/msy096

Kumar, S., Tamura, K., and Nei, M. (2004). MEGA3: integrated software for molecular evolutionary genetics analysis and sequence alignment. *Brief. Bioinform.* 5, 150–163. doi: 10.1093/bib/5.2.150

Lan, Y., Li, Z., Wang, Z., Wang, X., Wang, G., Zhang, J., et al. (2020). An experimental model of neurodegenerative disease based on porcine Hemagglutinating encephalomyelitis virus-related Lysosomal abnormalities. *Mol. Neurobiol.* 57, 5299–5306. doi: 10.1007/s12035-020-02105-y

Lan, Y., Lu, H., Zhao, K., He, W., Chen, K., Wang, G., et al. (2012). In vitro inhibition of porcine hemagglutinating encephalomyelitis virus replication with siRNAs targeting the spike glycoprotein and replicase polyprotein genes. *Intervirology* 55, 53–61. doi: 10.1159/000323523

Lau, S. K., Woo, P. C., Yip, C. C., Fan, R. Y., Huang, Y., Wang, M., et al. (2012). Isolation and characterization of a novel Betacoronavirus subgroup A coronavirus, rabbit coronavirus HKU14, from domestic rabbits. *J. Virol.* 86, 5481–5496. doi: 10.1128/JVI.06927-11

Laude, H., Van Reeth, K., and Pensaert, M. (1993). Porcine respiratory coronavirus: molecular features and virus-host interactions. *Vet. Res.* 24, 125–150

Li, Z., Gao, F., Lan, Y., Guan, J., Zhang, J., Lu, H., et al. (2021). Porcine Hemagglutinating encephalomyelitis virus triggers neural autophagy independently of ULK1. *J. Virol.* 95:e0085121. doi: 10.1128/JVI.00851-21

Llanes, A., Restrepo, C. M., Caballero, Z., Rajeev, S., Kennedy, M. A., and Lleonart, R. (2020). Betacoronavirus genomes: how genomic information has been used to Deal with past outbreaks and the COVID-19 pandemic. *Int. J. Mol. Sci.* 21:24546. doi: 10.3390/ijms21124546

Lole, K. S., Bollinger, R. C., Paranjape, R. S., Gadkari, D., Kulkarni, S. S., Novak, N. G., et al. (1999). Full-length human immunodeficiency virus type 1 genomes from subtype C-infected seroconverters in India, with evidence of intersubtype recombination. *J. Virol.* 73, 152–160. doi: 10.1128/JVI.73.1.152-160.1999

Lorbach, J. N., Wang, L., Nolting, J. M., Benjamin, M. G., Killian, M. L., Zhang, Y., et al. (2017). Porcine Hemagglutinating encephalomyelitis virus and respiratory disease in exhibition swine, Michigan, USA, 2015. *Emerg. Infect. Dis.* 23, 1168–1171. doi: 10.3201/eid2307.170019

Marchler-Bauer, A., Bo, Y., Han, L., He, J., Lanczycki, C. J., Lu, S., et al. (2017). CDD/SPARCLE: functional classification of proteins via subfamily domain architectures. *Nucleic Acids Res.* 45, D200–D203. doi: 10.1093/nar/gkw1129

Mazumder, R., Iyer, L. M., Vasudevan, S., and Aravind, L. (2002). Detection of novel members, structure-function analysis and evolutionary classification of the 2H phosphoesterase superfamily. *Nucleic Acids Res.* 30, 5229–5243. doi: 10.1093/nar/gkf645

Mengeling, W. L., Boothe, A. D., and Ritchie, A. E. (1972). Characteristics of a coronavirus (strain 67N) of pigs. *Am. J. Vet. Res.* 33, 297–308

Mora-Diaz, J. C., Magtoto, R., Houston, E., Baum, D., Carrillo-Avila, J. A., Temeeyasen, G., et al. (2020). Detecting and monitoring porcine Hemagglutinating encephalomyelitis virus: an underresearched betacoronavirus. *mSphere* 5:199. doi: 10.1128/mSphere.00199-20

Mora-Diaz, J. C., Pineyro, P. E., Houston, E., Zimmerman, J., and Gimenez-Lirola, L. G. (2019). Porcine Hemagglutinating encephalomyelitis virus: a review. *Front Vet Sci* 6, 53. doi: 10.3389/fvets.2019.00053

Mora-Diaz, J. C., Pineyro, P. E., Rauh, R., Nelson, W., Sankoh, Z., Gregg, E., et al. (2021a). Porcine Hemagglutinating encephalomyelitis virus infection In vivo and ex vivo. *J. Virol.* 95. doi: 10.1128/JVI.02335-20

Mora-Diaz, J. C., Temeeyasen, G., Magtoto, R., Rauh, R., Nelson, W., Carrillo-Avila, J. A., et al. (2021b). Infection and immune response to porcine hemagglutinating encephalomyelitis virus in grower pigs. *Vet. Microbiol.* 253:108958. doi: 10.1016/j.vetmic.2020.108958

Pan, Y., Tian, X., Qin, P., Wang, B., Zhao, P., Yang, Y. L., et al. (2017). Discovery of a novel swine enteric alphacoronavirus (SeACoV) in southern China. *Vet. Microbiol.* 211, 15–21. doi: 10.1016/j.vetmic.2017.09.020

Payne, S. (2017). "Chapter 17 – family coronaviridae" in *Viruses*. ed. S. Payne (Cambridge, MA: Academic Press), 149–158.

Pensaert, M., Callebaut, P., and Vergote, J. (1986). Isolation of a porcine respiratory, non-enteric coronavirus related to transmissible gastroenteritis. *Vet. Q.* 8, 257–261. doi: 10.1080/01652176.1986.9694050

Quiroga, M. A., Cappuccio, J., Piñeyro, P., Basso, W., Moré, G., Kienast, M., et al. (2008). Hemagglutinating encephalomyelitis coronavirus infection in pigs. *Argentina. Emerg Infect Dis* 14, 484–486. doi: 10.3201/eid1403.070825

Rho, S., Moon, H. J., Park, S. J., Kim, H. K., Keum, H. O., Han, J. Y., et al. (2011). Detection and genetic analysis of porcine hemagglutinating encephalomyelitis virus in South Korea. *Virus Genes* 42, 90–96. doi: 10.1007/s11262-010-0551-y

Roe, C. K., and Alexander, T. J. (1958). A disease of nursing pigs previously unreported in Ontario. *Can. J. Comp. Med. Vet. Sci.* 22, 305–307

Roy, A., Kucukural, A., and Zhang, Y. (2010). I-TASSER: a unified platform for automated protein structure and function prediction. *Nat. Protoc.* 5, 725–738. doi: 10.1038/nprot.2010.5

Samrat, S. K., Tharappel, A. M., Li, Z., and Li, H. (2020). Prospect of SARS-CoV-2 spike protein: potential role in vaccine and therapeutic development. *Virus Res.* 288:198141. doi: 10.1016/j.virusres.2020.198141

Sasseville, M. J., Gélinas, A., Sawyer, N., Boutin, M., and Dea, S. J. S. U. (2001). Biological and molecular characteristics of an HEV isolate associated with recent acute outbreaks of encephalomyelitis in Quebec pig farms. *Adv. Exp. Med. Biol.* 494, 57–62. doi: 10.1007/978-1-4615-1325-4_8

Schultze, B., Cavanagh, D., and Herrler, G. (1992). Neuraminidase treatment of avian infectious bronchitis coronavirus reveals a hemagglutinating activity that is dependent on sialic acid-containing receptors on erythrocytes. *Virology* 189, 792–794. doi: 10.1016/0042-6822(92)90608-R

Shi, J., Zhao, K., Lu, H., Li, Z., Lv, X., Lan, Y., et al. (2018). Genomic characterization and pathogenicity of a porcine hemagglutinating encephalomyelitis virus strain isolated in China. *Virus Genes* 54, 672–683. doi: 10.1007/s11262-018-1591-y

Snijder, E. J., Bredenbeek, P. J., Dobbe, J. C., Thiel, V., Ziebuhr, J., Poon, L. L., et al. (2003). Unique and conserved features of genome and proteome of SARS-coronavirus, an early split-off from the coronavirus group 2 lineage. *J. Mol. Biol.* 331, 991–1004. doi: 10.1016/S0022-2836(03)00865-9

Sola, I., Almazán, F., Zúñiga, S., and Enjuanes, L. (2015). Continuous and discontinuous RNA synthesis in coronaviruses. *Annu Rev Virol* 2, 265–288. doi: 10.1146/annurev-virology-100114-055218

Tortorici, M. A., Walls, A. C., Lang, Y., Wang, C., Li, Z., Koerhuis, D., et al. (2019). Structural basis for human coronavirus attachment to sialic acid receptors. *Nat. Struct. Mol. Biol.* 26, 481–489. doi: 10.1038/s41594-019-0233-y

Vaughn, E. M., Halbur, P. G., and Paul, P. S. (1995). Sequence comparison of porcine respiratory coronavirus isolates reveals heterogeneity in the S, 3, and 3-1 genes. *J. Virol.* 69, 3176–3184. doi: 10.1128/jvi.69.5.3176-3184.1995

Vijgen, L., Keyaerts, E., Lemey, P., Maes, P., Van Reeth, K., Nauwynck, H., et al. (2006). Evolutionary history of the closely related group 2 coronaviruses: porcine hemagglutinating encephalomyelitis virus, bovine coronavirus, and human coronavirus OC43. *J. Virol.* 80, 7270–7274. doi: 10.1128/JVI.02675-05

Walls, A. C., Tortorici, M. A., Bosch, B.-J., Frenz, B., Rottier, P. J. M., DiMaio, F., et al. (2016). Cryo-electron microscopy structure of a coronavirus spike glycoprotein trimer. *Nature* 531, 114–117. doi: 10.1038/nature16988

Wang, L., Eggett, T. E., Lanka, S., Fredrickson, R. L., Li, G., Zhang, Y., et al. (2019). Development of a triplex real-time RT-PCR assay for detection and differentiation of three US genotypes of porcine hemagglutinating encephalomyelitis virus. *J. Virol. Methods* 269, 13–17. doi: 10.1016/j.jviromet.2019.04.008

Wang, Q., Vlasova, A. N., Kenney, S. P., and Saif, L. J. (2019). Emerging and re-emerging coronaviruses in pigs. *Curr. Opin. Virol.* 34, 39–49. doi: 10.1016/j.coviro.2018.12.001

Weiss, S. R., and Navas-Martin, S. (2005). Coronavirus pathogenesis and the emerging pathogen severe acute respiratory syndrome coronavirus. *Microbiol. Mol. Biol. Rev.* 69, 635–664. doi: 10.1128/MMBR.69.4.635-664.2005

Whitworth, K. M., Rowland, R. R. R., Petrovan, V., Sheahan, M., Cino-Ozuna, A. G., Fang, Y., et al. (2019). Resistance to coronavirus infection in amino peptidase N-deficient pigs. *Transgenic Res.* 28, 21–32. doi: 10.1007/s11248-018-0100-3

Woo, P. C., Lau, S. K., Lam, C. S., Lau, C. C., Tsang, A. K., Lau, J. H., et al. (2012). Discovery of seven novel mammalian and avian coronaviruses in the genus deltacoronavirus supports bat coronaviruses as the gene source of alphacoronavirus and betacoronavirus and avian coronaviruses as the gene source of gammacoronavirus and deltacoronavirus. *J. Virol.* 86, 3995–4008. doi: 10.1128/jvi.06540-11

Wood, E. N. (1977). An apparently new syndrome of porcine epidemic diarrhoea. *Vet. Rec.* 100, 243–244. doi: 10.1136/vr.100.12.243

Yang, J., Yan, R., Roy, A., Xu, D., Poisson, J., and Zhang, Y. (2015). The I-TASSER suite: protein structure and function prediction. *Nat. Methods* 12, 7–8. doi: 10.1038/nmeth.3213

Zhang, J., Li, Z., Lu, H., Shi, J., Gao, R., Ma, Y., et al. (2021). Evidence of microglial immune response following coronavirus PHEV infection of CNS. *Front. Immunol.* 12:804625. doi: 10.3389/fimmu.2021.804625

Zhang, C. Y., Wei, J. F., and He, S. H. (2006). Adaptive evolution of the spike gene of SARS coronavirus: changes in positively selected sites in different epidemic groups. *BMC Microbiol.* 6:88. doi: 10.1186/1471-2180-6-88

Zhi, Y., Kobinger, G. P., Jordan, H., Suchma, K., Weiss, S. R., Shen, H., et al. (2005). Identification of murine CD8 T cell epitopes in codon-optimized SARS-associated coronavirus spike protein. *Virology* 335, 34–45. doi: 10.1016/j.virol.2005.01.050

Zhou, P., Fan, H., Lan, T., Yang, X. L., Shi, W. F., Zhang, W., et al. (2018). Fatal swine acute diarrhoea syndrome caused by an HKU2-related coronavirus of bat origin. *Nature* 556, 255–258. doi: 10.1038/s41586-018-0010-9

Zhou, P., Yang, X.-L., Wang, X.-G., Hu, B., Zhang, L., Zhang, W., et al. (2020). A pneumonia outbreak associated with a new coronavirus of probable bat origin. *Nature* 579, 270–273. doi: 10.1038/s41586-020-2012-7

**Conflict of Interest:** The authors declare no conflict of interest concerning the research, authorship, or publication of the article.

**Publisher's Note:** All claims expressed in this article are solely those of the authors and do not necessarily represent those of their affiliated organizations, or those of the publisher, the editors and the reviewers. Any product that may be evaluated in this article, or claim that may be made by its manufacturer, is not guaranteed or endorsed by the publisher.

*Copyright © 2022 Bahoussi, Guo, Shi, Wang, Li, Wu and Xing. This is an open-access article distributed under the terms of the Creative Commons Attribution License (CC BY). The use, distribution or reproduction in other forums is permitted, provided the original author(s) and the copyright owner(s) are credited and that the original publication in this journal is cited, in accordance with accepted academic practice. No use, distribution or reproduction is permitted which does not comply with these terms.*

frontiers in Microbiology

REVIEW
published: 24 March 2022
doi: 10.3389/fmicb.2022.866271

# Genome-Wide Approaches to Unravel the Host Factors Involved in Chikungunya Virus Replication

*Atsushi Tanaka[1]* and Youichi Suzuki[2]**

[1] Division of Research Animal Laboratory and Translational Medicine, Research and Development Center, Osaka Medical and Pharmaceutical University, Takatsuki, Japan, [2] Department of Microbiology and Infection Control, Faculty of Medicine, Osaka Medical and Pharmaceutical University, Takatsuki, Japan

Chikungunya virus (CHIKV), the causative agent of Chikungunya fever (CHIKVF) that is often characterized by fever, headache, rash, and arthralgia, is transmitted to humans by *Aedes* mosquito bites. Although the mortality rate associated with CHIKV infection is not very high, CHIKVF has been confirmed in more than 40 countries, not only in tropical but also in temperate areas. Therefore, CHIKV is a growing major threat to the public health of the world. However, a specific drug is not available for CHIKV infection. As demonstrated by many studies, the processes completing the replication of CHIKV are assisted by many host factors, whereas it has become clear that the host cell possesses some factors limiting the virus replication. This evidence will provide us with an important clue for the development of pharmacological treatment against CHIKVF. In this review, we briefly summarize cellular molecules participating in the CHIKV infection, particularly focusing on introducing recent genome-wide screen studies that enabled illuminating the virus-host interactions.

**Keywords: Chikungunya virus, host factors, genome-wide screen, replication, antivirals**

OPEN ACCESS

***Edited by:***
*Chunfu Zheng,*
*University of Calgary, Canada*

***Reviewed by:***
*Melinda Ann Brindley,*
*University of Georgia, United States*
*Xiaochuan Liu,*
*University of California, Riverside, United States*

****Correspondence:***
*Atsushi Tanaka*
*atsushi.tanaka@ompu.ac.jp*
*Youichi Suzuki*
*californiacircle@gmail.com*

***Specialty section:***
*This article was submitted to Virology, a section of the journal Frontiers in Microbiology*

***Received:*** *31 January 2022*
***Accepted:*** *26 February 2022*
***Published:*** *24 March 2022*

***Citation:***
*Tanaka A and Suzuki Y (2022) Genome-Wide Approaches to Unravel the Host Factors Involved in Chikungunya Virus Replication. Front. Microbiol. 13:866271. doi: 10.3389/fmicb.2022.866271*

## INTRODUCTION

Chikungunya virus (CHIKV) is an enveloped RNA virus that causes Chikungunya fever (CHIKF) in humans. CHIKV is classified into the *Alphavirus* genus in the *Togaviridae* family, which is composed of more than 30 recognized viruses (Ahola et al., 2021). Most alphaviruses are transmitted by mosquitoes, and therefore they are also often referred to as arboviruses (arthropod-borne viruses) (Ahola et al., 2021). A CHIKV particle is approximately 70 nm in size and contains a single-stranded, positive-sense RNA genome (approximately 12 kb in length) within an icosahedral capsid structure. Four non-structural (nsP1, nsP2, nsP3, and nsP4) and five structural (C, E3, E2, 6k, and E1) proteins are encoded in the 5′-terminal two-thirds and 3′-terminal one-third portion of the viral genome, respectively (Campion et al., 2015).

Chikungunya virus strains are categorized into Asian, East/Central South African (ECSA), and West African (WA) lineages based on the E1 gene sequence (Weaver and Forrester, 2015). Although CHIKF had been regarded as an endemic disease that caused sporadic epidemics in Africa and Asia, the massive outbreak that started in 2004 in coastal Kenya increased awareness of CHIKV infection and led to its recognition as a re-emerging global disease (Weaver and Forrester, 2015). It is noteworthy that the ECSA lineage having an alanine to valine substitution at position 226 of the E1 protein was shown to play a key role in the spread of CHIKV during the outbreak (Volk et al., 2010). Supporting this, *in vitro* studies revealed that the A226V substitution in E1 enhanced the replication fitness of CHIKV in the *Aedes albopictus* mosquito, which thrives in both

tropical and temperate regions (Tsetsarkin et al., 2007; Vazeille et al., 2007; Weaver and Forrester, 2015). However, it has also been demonstrated that E1-A226V was not a sole determinant for the molecular adaptation of the CHIKV ECSA lineage to the *Ae. albopictus* cell (Wikan et al., 2012; Suzuki et al., 2021).

Clinical symptoms of CHIKVF generally include a sudden onset of fever, myalgia, and arthralgia after an incubation period of 2–6 days (Couderc and Lecuit, 2015). However, it has been reported that around 15% of infected people show no symptoms (Lemant et al., 2008). Arthralgia occurs symmetrically in the extremities, especially in the wrists, ankles, and toes, frequently accompanied by skin rash, headache, myalgia, lymphadenopathy, and nausea (Couderc and Lecuit, 2015). In the acute phase, the viral RNA per milliliter of blood reaches up to $10^9$ copies, and the high level of viremia was shown to be often correlated with the severity of the medical condition (Parola et al., 2006; Staikowsky et al., 2009). Although these symptoms are mostly resolved within 10 days, in some patients, polyarthritis develops, and joint pain persists for months to years (Couderc and Lecuit, 2015). The chronic disease is not likely to be a persistent infection of CHIKV; the mechanism that leads to the chronicity of these joint symptoms remains unclear (Schwartz and Albert, 2010). Mortality associated with CHIKV infection is not high (Josseran et al., 2006), whereas the risk of severe disease increases in young children, elderly people, and individuals undergoing the treatment for hypertension, diabetes, or heart disease, in which encephalitis, cardiovascular disorder, renal failure, hepatitis, and myocarditis may occur (Schwartz and Albert, 2010).

Although CHIKVF is generally considered a non-fatal self-limiting disease, CHIKV infection, particularly that associated with prolonged arthralgia, has a negative impact on the health-related quality of life of patients (Soumahoro et al., 2009; Staikowsky et al., 2009; Kumar et al., 2021). Therefore, the development of safe and effective antiviral drugs is required for the treatment of CHIKV infection (Burt et al., 2017). To date, many small molecule inhibitors against CHIKV have been developed, and their anti-CHIKV activities have been validated in *in vitro* experiments. However, since the cellular proteins targeted by the inhibitors (such as kinases and chaperone molecules) are often involved in critical biological activities of the host, the application of candidate inhibitors to the treatment of CHIKV-infected individuals remains an obstacle (Haese et al., 2022). In this respect, a comprehensive understanding of the molecular interactions between the virus and host cell should provide helpful insights into the more promising druggable target(s) for the development of anti-CHIKV agents. In this review, we focus on several cellular factors promoting or restricting CHIKV infection identified by genome-wide screen approaches.

## SURVEY OF CELLULAR PROTEINS INVOLVED IN THE ATTACHMENT OF CHIKUNGUNYA VIRUS

When a mosquito infected with a mosquito-borne virus such as CHIKV bites a target host, the virus is injected into the small blood vessels and capillaries of the animal along with the mosquito saliva, which acts as an anti-vasoconstrictor and an anticoagulant (Ribeiro and Francischetti, 2002). Hence, blood cells are considered the primary target cells for CHIKV infection (Her et al., 2010). However, many other types of cells have been reported to be susceptible to CHIKV (Wikan et al., 2012; Roberts et al., 2017).

The replication of CHIKV in humans begins with the attachment of virus particles to the surface of the target cell. The CHIKV virion is enveloped by the lipid bilayer membrane, which contains 80 viral envelope spikes trimerized with the heterodimer of E1-E2 glycoproteins (Simizu et al., 1984; Jose et al., 2009; Voss et al., 2010; Yap et al., 2017). E1 is a class II pH-triggered membrane fusion protein that is positioned at the base of the spike, and the top of E1 is covered by a protector protein, E2, which is located on the distal end of the spike (Li et al., 2010; Modis, 2013). Thus far, several cell surface proteins have been implicated as attachment receptors for CHIKV (Schnierle, 2019). A recent CRISPR-Cas9-based genome-wide screen revealed that the cell adhesion molecule Mxra8 (also known as DICAM, ASP, or Limitrin) is a receptor molecule mediating the entry of multiple alphaviruses, notably CHIKV (Zhang et al., 2018). Mxra8 is reported to be involved in cell-cell adhesion through a heterophilic interaction with αVβ3 integrin and associated with osteoclast differentiation and angiogenesis (Jung et al., 2012; Han et al., 2013). Cryo-electron microscopy (cryo-EM) and mutagenesis studies revealed that Mxra8 binds by wedging into a cleft created by two adjacent CHIKV E2-E1 heterodimers in one trimeric spike and engaging a neighboring spike; they also showed that Mxra8 binds to a surface-exposed region across the A and B domains of CHIKV E2, with speculated residues W64, D71, T116, and I121 in the A domain and I190, Y199, and I217 in the B domain (as shown in **Figure 1**), which emerged as essential for optimal Mxra8-Fc binding. Of interest is that CD147, identified as a novel cellular protein involved in CHIKV entry, was found to have a structural topology similar to that of Mxra8 in its two immunoglobulin-like domains (Caluwé et al., 2021). More importantly, human monoclonal antibodies competing for the interaction of CHIKV E2 glycoprotein and Mxra8 were shown to be protective against CHIKV infection in mice (Zhang et al., 2019; Powell et al., 2020), holding promise as a therapeutic antibody drug for the treatment of CHIKF. However, it is unclear whether Mxra8 is a necessary and sufficient receptor for CHIKV infection since some CHIKV-susceptible cell lines do not express Mxra8, and CHIKV is still able to infect the Mxra8 knockout mice.

It is well known that cell surface glycosaminoglycans (GAGs) bind to various bioactive proteins such as cell growth factors, cytokines, chemokines, enzymes, and protease inhibitors to regulate their activities (Sarrazin et al., 2011). In addition, they are also reported as the primary attachment factors, co-receptors, or the molecule that concentrates virion on the cell surface before entry for various virus infections (Rostand and Esko, 1997; Shukla et al., 1999; Aquino and Park, 2016). GAGs are unbranched, high-molecular-weight polysaccharides that contain repeating disaccharide units of N-acetylglucosamine (GlcNAc) and D-glucuronic acid (GlcA) in the heparan sulfate (HS) backbone and disaccharide units of GalNAc and GlcA in the

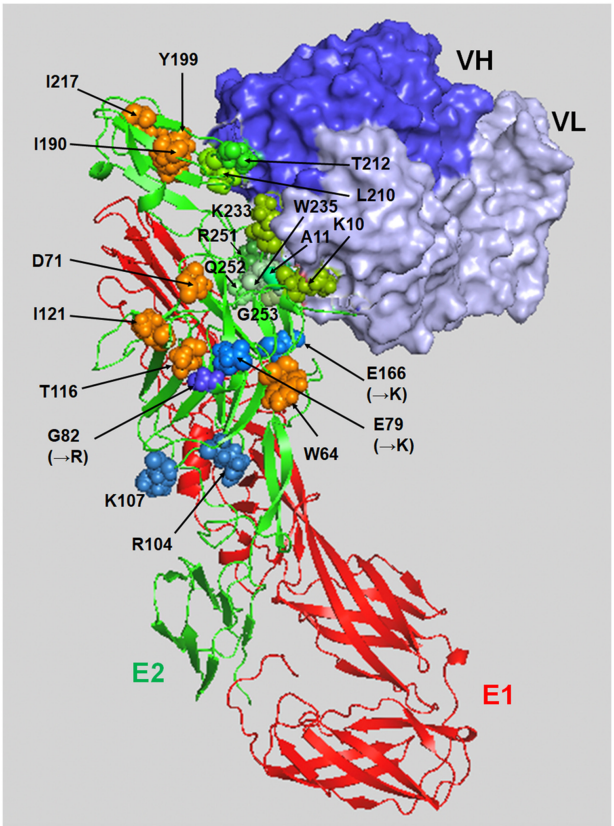


**FIGURE 1 |** A binding model of the E2-E1 heterodimer and NAb CHE19 on the CHIKV Thai#16856 spike. The binding of CHE19 Fab fragment (surface drawings, blue: the heavy chain, light blue: light chain) on the E2-E1 heterodimer (ribbon drawings reconstructed using PDB ID 3N42, red: the E1 glycoprotein, green: the E2 glycoprotein) is shown. The residues shown as green spheres (K10, A11, L210, T212, K233, W235, R251, Q252, and G253) are in contact within 4 Å of the heavy atoms of the NAb CHE19 paratope. The optimal binding sites of Mxra8-Fc are shown as orange spheres (W64, D71, T116, I121, I190, Y199, and I217). The residues shown as blue spheres are as follows; R104 and K107 in the predicted E2 amino acids for HS binding, and the residues substituted to the positively charged ones in 181/25 vaccine strain [G82(→R)] and mutant [E79(→K) and E166(→K)] in mutant CHIKV. Those positively charged residues are responsible for HS binding. This image was visualized using PyMOL software.

chondroitin sulfate (CS) backbone. GAGs attach to specific sites on the core proteins, generating proteoglycans (Häcker et al., 2005). Several studies using a live attenuated vaccine strain (181/25) and mutant CHIKV revealed that the viral determinant responsible for GAG dependency was in the E2 protein (Levitt et al., 1986; Silva et al., 2013; Gardner et al., 2014; Weber et al., 2017). Point mutations within the E2 protein (e.g., E79K, G82R, or E166K, shown in **Figure 1**) have been found in attenuated vaccine strains and in mutant viruses that exhibited enhanced GAG dependency but reduced *in vivo* pathogenicity (Gardner et al., 2014). In the attenuated CHIKV strain 181/25, the substitution of a residue at 82 (arginine to glycine) in the E2 glycoprotein showed a higher titer in the spleen and serum of mice at early times after inoculation (Ashbrook et al., 2014). Our previous genome-wide approach using knockout HAP1 cell libraries generated by a piggyBac-transposon-based exon-trapping vector found that the authentic clinical isolate CHIKV also utilizes the cell surface GAGs for entry to the target cell (Tanaka et al., 2017). We showed that a clinical CHIKV isolate (Thai#16856 strain) and prototype CHIKV (Ross strain), which contained the 79E, 82G, and 166E in E2, had a higher affinity to HS and that the N-sulfated HS was the minimum structure required for efficient CHIKV binding and infection on HAP1 cells (Tanaka et al., 2017). In addition, although the CS, another GAG, has been reported to be associated with viral infection, including CHIKV, CS may participate at later steps of CHIKV replication after virion binding (Banfield et al., 1995; Kato et al., 2010; Kim et al., 2011; Jinno-Oue et al., 2013; Silva et al., 2013; Zhang et al., 2013; Tanaka et al., 2017). Interestingly, previous studies have shown that pentosan polysulfate, an HS-like molecule, was capable of reducing the viral titer of alphaviruses including CHIKV *in vitro* and *in vivo*, indicating the potential therapeutic use of the GAG mimetic for the treatment of CHIKV infection in humans (Herrero et al., 2015; Supramaniam et al., 2018).

## ENTRY AND MEMBRANE FUSION PROCESS

Endocytosis is one of the major machineries for the entry of many viruses into target cells (Smith and Helenius, 2004). In the case of CHIKV infection, clathrin-dependent endocytosis is considered to be the main pathway for virion uptake into cells (Bernard et al., 2010; Kielian et al., 2010), although micropinocytosis is also reported as a route of CHIKV entry (Lee et al., 2019; Izumida et al., 2020). After internalization of the virion, membrane fusion between CHIKV and the cell occurs within the endosomal compartment, which is triggered by the low pH environment of the endosomes. This acidic pH then induces the dissociation of E1 from the E1/E2 glycoprotein dimer of CHIKV, followed by the penetration of E1 into the cell membrane (Kielian et al., 2010). Although the details of the structural change of E2 remain unclear, the R104 and K107 of E2 were shown to induce conformational change, and these residues were expected to configure the HS-binding pocket (**Figure 1**). Additionally, these two positive-charge residues forming the HS-binding sequence motif (XBXXBX, where B is a basic residue) were conserved in all CHIKV strains (Sahoo and Chowdary, 2019). Recently, we revealed that the E2 proteins of cell-bound CHIKV were easily lost during viral internalization, which was also observed in the cells that inhibited the endosome acidification *via* bafilomycin A1 treatment, suggesting that part of the conformational changes in E2 occurs before endosome acidification (Tumkosit et al., 2019). In addition, a CHIKV-neutralizing monoclonal antibody (NAb), CHE19, recognizes the E2 protein (**Figure 1**), which inhibits viral membrane fusion by stabilizing the E2-E1 heterodimer instead of E3, blocking the elimination of E2 (Tumkosit et al., 2020). CHIKV E2 may promptly suffer degradation by some type of existing protease cell membrane, as reported in other enveloped viruses (Lu et al., 1996; Abe et al., 2013; Bertram et al., 2013;

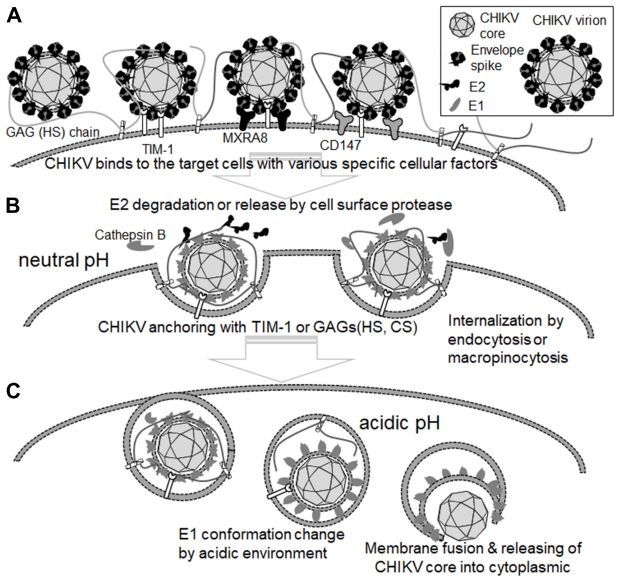


**FIGURE 2 |** Role of cellular proteins in the attachment and entry steps of CHIKV. **(A)** CHIKV virion binds to the target cells with cell surface molecules, including HS-proteoglycan, Mxra8, and CD147. **(B)** E2 is degraded and eliminated from CHIKV virion by cell surface protease such as cathepsin B at the neutral pH. CHIKV virions bearing no E2 are anchored by TIM-1, HS-/CS-proteoglycan, and internalized by endocytosis or micropinocytosis. **(C)** The conformation of the E1 protein is changed at the acidic pH. Then, the membrane of CHIKV virions and the target cell membrane are fused by the E1 protein, resulting in the release of the CHIKV core into the cytoplasm of the target cell.

Park et al., 2016). Indeed, it was recently shown that cathepsin B protease facilitated CHIKV envelope-mediated infection *via* endocytosis or macropinocytosis (Izumida et al., 2020). Thus, the binding position of neutralizing antibody CHE19 may be a target site for the protease that digests the E2 of the CHIKV virion after binding. Given that cell surface proteases dissociate the E2 of the virion bound to the target cell during the CHIKV entry, it is plausible that GAGs or the T-cell immunoglobulin and mucin domain 1 (TIM-1) (Kirui et al., 2021) may be used as an anchoring factor for tethering the E2-lacking virion on the cell surface in the endosome (**Figure 2**).

A genome-wide screen study employing small interfering RNA (siRNA) identified fuzzy homolog (FUZ) and TSPAN9 as cellular proteins that promoted the entry process of CHIKV (Ooi et al., 2013). Depletions of FUZ and TSPAN9 showed a significant reduction of CHIKV in human cells, and the FUZ depletion was likely to hamper the internalization step of another alphavirus, Semliki Forest virus (SFV) (Ooi et al., 2013). In contrast, the silencing of TSPAN9 inhibited the intracellular membrane fusion of alphavirus in endosomes, and it was characteristic of the viruses that fused in early endosomes, such as CHIKV (Ooi et al., 2013; Duijl-Richter et al., 2015; Stiles and Kielian, 2016). Additionally, the siRNA screen study by Ooi et al. revealed that Archain 1 (ARCN1), a subunit of the COPI coatomer complex, promoted the binding of alphaviruses SFV and Sindbis virus (SINV), therefore providing new insight into the involvement of cellular factors in the early events of alphavirus infection including CHIKV infection (Ooi et al., 2013).

## APPLICATION OF A GENOME-WIDE SCREEN TO INVESTIGATE THE CELLULAR FACTORS ESSENTIAL TO INTRACELLULAR CHIKUNGUNYA VIRUS REPLICATION

After entry into the target, an open reading frame (ORF) encoding nsP1–4 is first translated from the viral RNA released into the cytoplasm, which yields precursors of the non-structural protein. It has been well demonstrated that the majority of CHIKV isolates possess an opal stop codon (UGA) between the nsP3 and nsP4 genes that produces an nsP123 precursor; on the other hand, a full-length nsP1234 polyprotein is generated by the readthrough of the opal stop codon (Li and Rice, 1993; Jones et al., 2017). The nsP4 that is initially cleaved from the nsP1234 precursor functions as an RNA-dependent RNA polymerase (RdRp), together with nsP123, for the synthesis of negative-sense RNA, which, in turn, serves as a template for the amplification of full-length (49S) positive-sense RNA (Schwartz and Albert, 2010; Ahola et al., 2021). In contrast to the non-structural protein expression, structural protein is translated from the subgenomic (26S) RNA that is transcribed under the internal promoter sequence between two ORFs of non-structural and structural proteins (Ahola et al., 2021). The capsid (C) protein, which is cleaved from a structural protein precursor by its autoprotease activity, associates with 49S genomic RNA to form a nucleocapsid core (Schwartz and Albert, 2010; Ahola et al., 2021). Concurrently, the rest of the structural proteins containing E glycoproteins are processed and matured through the translocation from the endoplasmic reticulum (ER) to Golgi compartments and assembled with a nucleocapsid below the plasma membrane. Eventually, the mature virion egresses from the infected cell *via* budding (Schwartz and Albert, 2010).

nsP3 is an accessory protein necessary for the nsP4's RNA polymerase activity and has been shown to possess ADP-ribosylhydrolase activity in its N-terminal domain, whereas the C-terminal domain is hypervariable (Eckei et al., 2017; McPherson et al., 2017). In a recent study, CRISPR-Cas9-based genetic screening found four-and-a-half LIM domain protein 1 (FHL1) as a host factor essential for CHIKV replication (Meertens et al., 2019). FHL1, a member of the FHL family of proteins that are characterized by the existence of LIM domains, is predominantly expressed in skeletal muscle and is thought to be involved in muscle development and maintenance (Shathasivam et al., 2010). In CHIKV-infected cells, FHL1 interacted with the hypervariable domain of nsP3 and appeared to play a critical role in viral RNA synthesis (Meertens et al., 2019). It was also demonstrated that FHL1-deficient mice were less susceptible to CHIKV infection, and more importantly, virus replication was greatly impaired in fibroblasts and myoblasts derived from Emery-Dreifuss muscular dystrophy (EDMD) patients, in which the FHL1 gene was

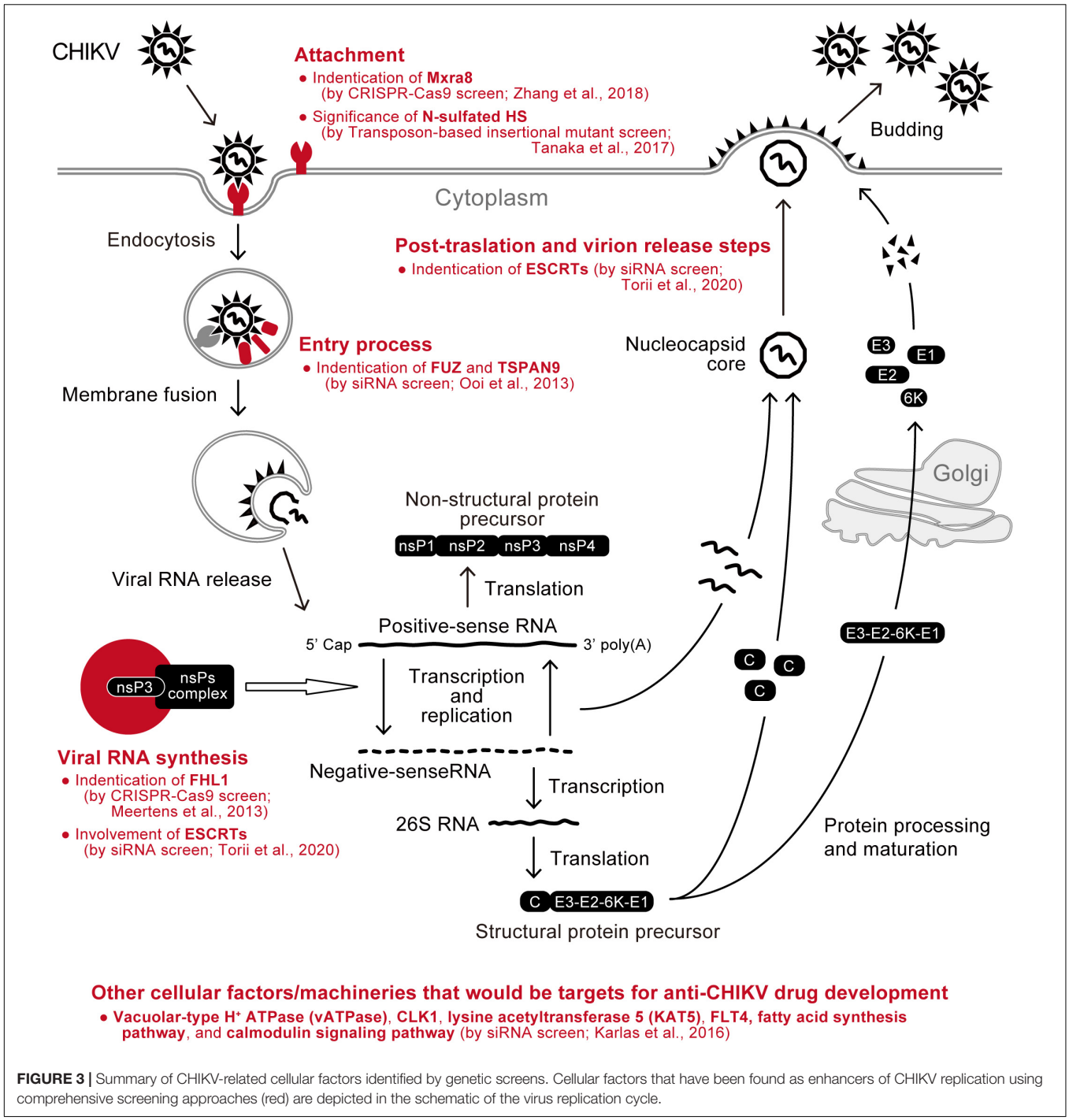


**FIGURE 3 |** Summary of CHIKV-related cellular factors identified by genetic screens. Cellular factors that have been found as enhancers of CHIKV replication using comprehensive screening approaches (red) are depicted in the schematic of the virus replication cycle.

mutated (Gueneau et al., 2009; Shathasivam et al., 2010). This genome-wide screening study demonstrates that FHL1 is a major determinant for the susceptibility of humans to CHIKV. In addition, since the expression of FHL1 is mainly found in skeletal muscle cells, the molecular interaction between nsP3 and FHL1 would influence the progression of arthritis in CHIKV-infected patients. Therefore, this host-virus interaction could be a promising target for the development of antivirals against CHIKV disease (Meertens et al., 2019).

A study using a set of siRNA libraries targeting cellular factors involved in membrane trafficking revealed critical roles of endosomal sorting complexes required for transport (ESCRT) proteins in the intracellular replication of CHIKV (Torii et al., 2020). ESCRT, originally discovered in yeast cells, are a network of the cytoplasmic protein complex, which has been demonstrated to regulate cellular membrane fission events, including the multivesicular body (MVB) formation and cytokinesis (Henne et al., 2011; Morita, 2012). One impact of the

ESCRT system in virology is that many enveloped viruses, such as human immunodeficiency virus type 1 (HIV-1), exploit the ESCRT proteins for their replication (Meng and Lever, 2021). As for CHIKV replication, siRNA-mediated depletion of 13 ESCRT genes markedly reduced the level of virus replication in HEK293T cells. Interestingly, some of the ESCRT factors were found to be required for CHIKV RNA synthesis and the post-translation step, which was presumably at the extracellular release step of the virion, as reported in HIV-1 (Torii et al., 2020). Hence, this siRNA screen study sheds light on the important role of the ESCRT pathway in the biology of CHIKV.

The genome-wide loss-of-function screen approach has also been employed to seek a druggable cellular target suitable for inhibiting CHIKV replication. Karlas et al. performed transfection of a large set of siRNA libraries using HEK-293 cells, followed by infection with green fluorescent protein (GFP)-expressing CHIKV, and identified 156 enhancing and 41 inhibitory genes for virus replication (Karlas et al., 2016). Then, by querying the enhancer hits against the databases of drugs whose target molecules have been experimentally proven, 52 chemical compounds were selected as antiviral candidates against CHIKV, and 20 of them indeed inhibited CHIKV *in vitro*. Furthermore, three drugs targeting the fatty acid synthesis pathway, calmodulin signaling pathway, or fms-related tyrosine kinase 4, all of which were identified as cellular enhancers for CHIKV infection using an siRNA library screen, significantly reduced virus replication in C57BL/6 mice (Karlas et al., 2016). Therefore, this is a proof-of-concept study demonstrating that the genome-wide screen is beneficial for a comprehensive survey of potential antiviral agents against CHIKV (**Figure 3**).

## FUNCTIONAL cDNA EXPRESSION CLONING TO FIND CELLULAR INHIBITORY FACTORS AGAINST CHIKUNGUNYA VIRUS

Generally, the loss-of-function genetic screen using the siRNA and CRISPR-Cas9 system provides insights into the dependencies of the virus on host factors and machinery, whereas the gain-of-function screen, which ectopically expresses a certain set of functional genes, is able to identify cellular factors that limit virus replication. Particularly, it has been demonstrated that the gain-of-function screen using a cDNA library is a powerful approach in a comprehensive study of host antiviral mechanisms such as interferon (IFN)-stimulated genes (Schoggins et al., 2011; Kane et al., 2016; Schoggins, 2019). Recently, we applied an expression-cloning screen using the cDNA library, which was generated from type I IFN-treated human cells, to CHIKV infection (Sakaguchi et al., 2020). The African green monkey–derived Vero cell is highly permissive of CHIKV and exhibits a massive cytopathic effect with the infection (Schwartz and Albert, 2010). However, when Vero cells were transduced with a pool of HIV vectors carrying the IFN-related cDNA library and subsequently subjected to a challenge infection with CHIKV, many cells that survived the viral infection were obtained. Then a long-read sequencing analysis using the MinION sequencer (Clarke et al., 2009) showed that cDNAs encoding three different mitochondrial proteins (TOM7, S100A16, and ECI1 lacking the N-terminal 59 amino acids) were introduced to the CHIKV-resistant cells. The inhibitory activities of these cellular factors were confirmed by an over-expression experiment using human Huh7 cells (Sakaguchi et al., 2020). One plausible molecular mechanism by which these cellular factors limit the CHIKV replication would be that the expression of TOM7 and S100A16 reinforced the function of mitochondria, resulting in the up-modulation of cellular innate immune response (Kim et al., 2018). Meanwhile, the expression of the N-terminally deleted ECl1 may function as a dominant-negative mutant for the lipid metabolism, which is usually catalyzed by wild-type ECI1 in the mitochondria and shown to be required for the replication of RNA viruses (Takahashi et al., 2007; Rasmussen et al., 2011). Although endogenous expressions of these mitochondria-related proteins were not changed in human cells upon IFN treatment (Sakaguchi et al., 2020), this study illustrates the usefulness of the gain-of-function cDNA library screening approach in the search for cellular inhibitors against CHIKV.

## CONCLUDING REMARKS

As seen in many human pathogenic viruses, CHIKV hijacks the host machinery to create a favorable environment for virus replication (Wong and Chu, 2018). On the other hand, the host cells harbor countermeasure mechanisms that restrict CHIKV replication (Schwartz and Albert, 2010; Schneider et al., 2014). Understanding these virus-host relationships, which are key factors influencing disease pathogenesis and progression, should reveal the Achilles' heel of CHIKV and be a basis for the future development of an anti-CHIKV drug. In particular, antiviral agents targeting the molecular interactions between CHIKV and cellular factors hold the promise of avoiding the emergence of resistant viruses (Wong and Chu, 2018). From this viewpoint, recent advances in genome-wide screening technologies could provide a complete molecular picture of the cellular environments where CHIKV replicates in the near future (Ramage and Cherry, 2014). In this review, we summarized the CHIKV-related host factors that have been identified by several genome-wide screen studies (**Figure 3**). Notwithstanding, it will be important to determine precisely whether the host factors identified are necessary for CHIKV infection and pathogenesis.

## AUTHOR CONTRIBUTIONS

AT and YS contributed to the conceptualization, writing, review, and editing of this manuscript. Both authors have read and agreed to the submission of the manuscript.

## FUNDING

This work was supported by AMED under Grant Number JP21fk0108123.

## REFERENCES


Abe, M., Tahara, M., Sakai, K., Yamaguchi, H., Kanou, K., Shirato, K., et al. (2013). TMPRSS2 is an activating protease for respiratory parainfluenza viruses. *J. Virol.* 87, 11930–11935. doi: 10.1128/jvi.01490-13

Ahola, T., McInerney, G., and Merits, A. (2021). Alphavirus RNA replication in vertebrate cells. *Adv. Virus Res.* 111, 111–156. doi: 10.1016/bs.aivir.2021.07.003

Aquino, R. S., and Park, P. W. (2016). Glycosaminoglycans and infection. *Front. Biosci.* 21, 1260–77. doi: 10.2741/4455

Ashbrook, A. W., Burrack, K. S., Silva, L. A., Montgomery, S. A., Heise, M. T., Morrison, T. E., et al. (2014). Residue 82 of the Chikungunya virus E2 attachment protein modulates viral dissemination and arthritis in mice. *J. Virol.* 88, 12180–12192. doi: 10.1128/jvi.01672-14

Banfield, B. W., Leduc, Y., Esford, L., Visalli, R. J., Brandt, C. R., and Tufaro, F. (1995). Evidence for an interaction of herpes simplex virus with chondroitin sulfate proteoglycans during infection. *Virology* 208, 531–539. doi: 10.1006/viro.1995.1184

Bernard, E., Solignat, M., Gay, B., Chazal, N., Higgs, S., Devaux, C., et al. (2010). Endocytosis of Chikungunya virus into mammalian cells: role of clathrin and early endosomal compartments. *PLoS One* 5:e11479. doi: 10.1371/journal.pone.0011479

Bertram, S., Dijkman, R., Habjan, M., Heurich, A., Gierer, S., Glowacka, I., et al. (2013). TMPRSS2 activates the human coronavirus 229E for cathepsin-independent host cell entry and is expressed in viral target cells in the respiratory epithelium. *J. Virol.* 87, 6150–6160. doi: 10.1128/jvi.03372-12

Burt, F. J., Chen, W., Miner, J. J., Lenschow, D. J., Merits, A., Schnettler, E., et al. (2017). Chikungunya virus: an update on the biology and pathogenesis of this emerging pathogen. *Lancet Infect. Dis.* 17, e107–e117. doi: 10.1016/s1473-3099(16)30385-1

Caluwé, L. D., Coppens, S., Vereecken, K., Daled, S., Dhaenens, M., Ostade, X. V., et al. (2021). The CD147 protein complex is involved in entry of Chikungunya virus and related alphaviruses in human cells. *Front. Microbiol.* 12:615165. doi: 10.3389/fmicb.2021.615165

Campion, E. W., Weaver, S. C., and Lecuit, M. (2015). Chikungunya virus and the global spread of a mosquito-borne disease. *N. Engl. J. Med.* 372, 1231–1239. doi: 10.1056/nejmra1406035

Clarke, J., Wu, H.-C., Jayasinghe, L., Patel, A., Reid, S., and Bayley, H. (2009). Continuous base identification for single-molecule nanopore DNA sequencing. *Nat. Nanotechnol.* 4, 265–270. doi: 10.1038/nnano.2009.12

Couderc, T., and Lecuit, M. (2015). Chikungunya virus pathogenesis: from bedside to bench. *Antiviral Res.* 121, 120–131. doi: 10.1016/j.antiviral.2015.07.002

Duijl-Richter, M. K. S., van, Hoornweg, T. E., Rodenhuis-Zybert, I. A., and Smit, J. M. (2015). Early events in Chikungunya virus infection - From virus cell binding to membrane fusion. *Viruses* 7, 3647–3674. doi: 10.3390/v7072792

Eckei, L., Krieg, S., Bütepage, M., Lehmann, A., Gross, A., Lippok, B., et al. (2017). The conserved macrodomains of the non-structural proteins of Chikungunya virus and other pathogenic positive strand RNA viruses function as mono-ADP-ribosylhydrolases. *Sci. Rep.* 7:41746. doi: 10.1038/srep41746

Gardner, C. L., Hritz, J., Sun, C., Vanlandingham, D. L., Song, T. Y., Ghedin, E., et al. (2014). Deliberate attenuation of Chikungunya virus by adaptation to heparan sulfate-dependent infectivity: a model for rational arboviral vaccine design. *PLoS Negl. Trop. Dis.* 8:e2719. doi: 10.1371/journal.pntd.0002719

Gueneau, L., Bertrand, A. T., Jais, J.-P., Salih, M. A., Stojkovic, T., Wehnert, M., et al. (2009). Mutations of the FHL1 gene cause Emery-Dreifuss muscular dystrophy. *Am. J. Hum. Genet.* 85, 338–353. doi: 10.1016/j.ajhg.2009.07.015

Häcker, U., Nybakken, K., and Perrimon, N. (2005). Heparan sulphate proteoglycans: the sweet side of development. *Nat. Rev. Mol. Cell Bio.* 6, 530–541. doi: 10.1038/nrm1681

Haese, N., Powers, J., and Streblow, D. N. (2022). Small molecule inhibitors targeting Chikungunya virus. *Curr. Top. Microbiol. Immunol.* 435, 107–139. doi: 10.1007/82_2020_195

Han, S.-W., Jung, Y.-K., Lee, E.-J., Park, H.-R., Kim, G.-W., Jeong, J.-H., et al. (2013). DICAM inhibits angiogenesis *via* suppression of AKT and p38 MAP kinase signalling. *Cardiovasc. Res.* 98, 73–82. doi: 10.1093/cvr/cvt019

Henne, W. M., Buchkovich, N. J., and Emr, S. D. (2011). The ESCRT pathway. *Dev. Cell* 21, 77–91. doi: 10.1016/j.devcel.2011.05.015

Her, Z., Malleret, B., Chan, M., Ong, E. K. S., Wong, S.-C., Kwek, D. J. C., et al. (2010). Active Infection of human blood monocytes by Chikungunya virus triggers an innate immune response. *J. Immunol.* 184, 5903–5913. doi: 10.4049/jimmunol.0904181

Herrero, L. J., Foo, S.-S., Sheng, K.-C., Chen, W., Forwood, M. R., Bucala, R., et al. (2015). Pentosan polysulfate: a novel glycosaminoglycan-like molecule for effective treatment of alphavirus-induced cartilage destruction and inflammatory disease. *J. Virol.* 89, 8063–8076. doi: 10.1128/jvi.00224-15

Izumida, M., Hayashi, H., Tanaka, A., and Kubo, Y. (2020). Cathepsin B protease facilitates Chikungunya virus envelope protein-mediated infection *via* endocytosis or macropinocytosis. *Viruses* 12:722. doi: 10.3390/v12070722

Jinno-Oue, A., Tanaka, A., Shimizu, N., Mori, T., Sugiura, N., Kimata, K., et al. (2013). Inhibitory effect of chondroitin sulfate type E on the binding step of human T-cell leukemia virus type 1. *AIDS Res. Hum Retroviruses* 29, 621–629. doi: 10.1089/aid.2012.0156

Jones, J. E., Long, K. M., Whitmore, A. C., Sanders, W., Thurlow, L. R., Brown, J. A., et al. (2017). Disruption of the opal stop codon attenuates Chikungunya virus-induced arthritis and pathology. *Mbio* 8, e1456–17. doi: 10.1128/mbio.01456-17

Jose, J., Snyder, J. E., and Kuhn, R. J. (2009). A structural and functional perspective of alphavirus replication and assembly. *Future Microbiol.* 4, 837–856. doi: 10.2217/fmb.09.59

Josseran, L., Paquet, C., Zehgnoun, A., Caillere, N., Tertre, A. L., Solet, J.-L., et al. (2006). Chikungunya disease outbreak, Reunion Island. *Emerg. Infect. Dis.* 12, 1994–1995. doi: 10.3201/eid1212.060710

Jung, Y., Han, S., Kim, G., Jeong, J., Kim, H., and Choi, J. (2012). DICAM inhibits osteoclast differentiation through attenuation of the integrin αVβ3 pathway. *J. Bone Miner. Res.* 27, 2024–2034. doi: 10.1002/jbmr.1632

Kane, M., Zang, T. M., Rihn, S. J., Zhang, F., Kueck, T., Alim, M., et al. (2016). Identification of interferon-stimulated genes with antiretroviral activity. *Cell Host Microbe.* 20, 392–405. doi: 10.1016/j.chom.2016.08.005

Karlas, A., Berre, S., Couderc, T., Varjak, M., Braun, P., Meyer, M., et al. (2016). A human genome-wide loss-of-function screen identifies effective Chikungunya antiviral drugs. *Nat. Commun.* 7:11320. doi: 10.1038/ncomms11320

Kato, D., Era, S., Watanabe, I., Arihara, M., Sugiura, N., Kimata, K., et al. (2010). Antiviral activity of chondroitin sulphate E targeting dengue virus envelope protein. *Antiviral Res.* 88, 236–243. doi: 10.1016/j.antiviral.2010.09.002

Kielian, M., Chanel-Vos, C., and Liao, M. (2010). Alphavirus entry and membrane fusion. *Viruses* 2, 796–825. doi: 10.3390/v2040796

Kim, E., Okumura, M., Sawa, H., Miyazaki, T., Fujikura, D., Yamada, S., et al. (2011). Paradoxical effects of chondroitin sulfate-E on Japanese encephalitis viral infection. *Biochem. Biophys. Res. Commun.* 409, 717–722. doi: 10.1016/j.bbrc.2011.05.072

Kim, S.-J., Ahn, D.-G., Syed, G. H., and Siddiqui, A. (2018). The essential role of mitochondrial dynamics in antiviral immunity. *Mitochondrion* 41, 21–27. doi: 10.1016/j.mito.2017.11.007

Kirui, J., Abidine, Y., Lenman, A., Islam, K., Gwon, Y.-D., Lasswitz, L., et al. (2021). The phosphatidylserine receptor TIM-1 enhances authentic Chikungunya virus cell entry. *Cells* 10:1828. doi: 10.3390/cells10071828

Kumar, R., Ahmed, S., Parray, H. A., and Das, S. (2021). Chikungunya and arthritis: an overview. *Travel. Med. Infect. Dis.* 44:102168. doi: 10.1016/j.tmaid.2021.102168

Lee, C. H., Regina, Hussain, K. M., and Chu, J. J. H. (2019). Macropinocytosis dependent entry of Chikungunya virus into human muscle cells. *PLoS Negl. Trop. Dis.* 13:e0007610. doi: 10.1371/journal.pntd.0007610

Lemant, J., Boisson, V., Winer, A., Thibault, L., André, H., Tixier, F., et al. (2008). Serious acute Chikungunya virus infection requiring intensive care during the Reunion Island outbreak in 2005-2006. *Crit. Care. Med.* 36, 2536–2541. doi: 10.1097/ccm.0b013e318183f2d2

Levitt, N. H., Ramsburg, H. H., Hasty, S. E., Repik, P. M., Cole, F. E., and Lupton, H. W. (1986). Development of an attenuated strain of Chikungunya virus for use in vaccine production. *Vaccine* 4, 157–162. doi: 10.1016/0264-410x(86)90003-4

Li, G., and Rice, C. M. (1993). The signal for translational readthrough of a UGA codon in Sindbis virus RNA involves a single cytidine residue immediately downstream of the termination codon. *J. Virol.* 67, 5062–5067. doi: 10.1128/jvi.67.8.5062-5067.1993

Li, L., Jose, J., Xiang, Y., Kuhn, R. J., and Rossmann, M. G. (2010). Structural changes of envelope proteins during alphavirus fusion. *Nature* 468, 705–708. doi: 10.1038/nature09546

Lu, X., Block, T. M., and Gerlich, W. H. (1996). Protease-induced infectivity of hepatitis B virus for a human hepatoblastoma cell line. *J. Virol.* 70, 2277–2285. doi: 10.1128/jvi.70.4.2277-2285.1996

McPherson, R. L., Abraham, R., Sreekumar, E., Ong, S.-E., Cheng, S.-J., Baxter, V. K., et al. (2017). ADP-ribosylhydrolase activity of Chikungunya virus macrodomain is critical for virus replication and virulence. *Proc. Natl. Acad. Sci. U. S. A.* 114, 1666–1671. doi: 10.1073/pnas.1621485114

Meertens, L., Hafirassou, M. L., Couderc, T., Bonnet-Madin, L., Kril, V., Kümmerer, B. M., et al. (2019). FHL1 is a major host factor for Chikungunya virus infection. *Nature* 574, 259–263. doi: 10.1038/s41586-019-1578-4

Meng, B., and Lever, A. M. L. (2021). The interplay between ESCRT and viral factors in the enveloped virus life cycle. *Viruses* 13:324. doi: 10.3390/v13020324

Modis, Y. (2013). Class II fusion proteins. *Adv. Exp. Med. Biol.* 790, 150–166. doi: 10.1007/978-1-4614-7651-1_8

Morita, E. (2012). Differential requirements of mammalian ESCRTs in multivesicular body formation, virus budding and cell division. *FEBS J.* 279, 1399–1406. doi: 10.1111/j.1742-4658.2012.08534.x

Ooi, Y. S., Stiles, K. M., Liu, C. Y., Taylor, G. M., and Kielian, M. (2013). Genome-wide RNAi screen identifies novel host proteins required for alphavirus entry. *PLoS Pathog.* 9:e1003835. doi: 10.1371/journal.ppat.1003835

Park, J.-E., Li, K., Barlan, A., Fehr, A. R., Perlman, S., McCray, P. B., et al. (2016). Proteolytic processing of Middle East respiratory syndrome coronavirus spikes expands virus tropism. *Proc. Natl. Acad. Sci. U. S. A.* 113, 12262–12267. doi: 10.1073/pnas.1608147113

Parola, P., Lamballerie, X., de, Jourdan, J., Rovery, C., Vaillant, V., Minodier, P., et al. (2006). Novel Chikungunya virus variant in travelers returning from Indian Ocean Islands. *Emerg. Infect. Dis.* 12, 1493–1499. doi: 10.3201/eid1210.060610

Powell, L. A., Miller, A., Fox, J. M., Kose, N., Klose, T., Kim, A. S., et al. (2020). Human mAbs broadly protect against arthritogenic alphaviruses by recognizing conserved elements of the Mxra8 receptor-binding site. *Cell Host Microbe.* 28, 699–711.e7. doi: 10.1016/j.chom.2020.07.008

Ramage, H., and Cherry, S. (2014). Virus-host interactions: from unbiased genetic screens to function. *Annu. Rev. Virol.* 2, 1–28. doi: 10.1146/annurev-virology-100114-055238

Rasmussen, A. L., Diamond, D. L., McDermott, J. E., Gao, X., Metz, T. O., Matzke, M. M., et al. (2011). Systems virology identifies a mitochondrial fatty acid oxidation enzyme, dodecenoyl coenzyme A delta isomerase, required for hepatitis C virus replication and likely pathogenesis. *J. Virol.* 85, 11646–11654. doi: 10.1128/jvi.05605-11

Ribeiro, J. M. C., and Francischetti, I. M. B. (2002). Role of arthropod saliva in blood feeding: sialome and post-sialome perspectives. *Annu. Rev. Entomol.* 48, 73–88. doi: 10.1146/annurev.ento.48.060402.102812

Roberts, G. C., Zothner, C., Remenyi, R., Merits, A., Stonehouse, N. J., and Harris, M. (2017). Evaluation of a range of mammalian and mosquito cell lines for use in Chikungunya virus research. *Sci. Rep.* 7:14641. doi: 10.1038/s41598-017-15269-w

Rostand, K. S., and Esko, J. D. (1997). Microbial adherence to and invasion through proteoglycans. *Infect. Immun.* 65, 1–8. doi: 10.1128/iai.65.1.1-8.1997

Sahoo, B., and Chowdary, T. K. (2019). Conformational changes in Chikungunya virus E2 protein upon heparan sulfate receptor binding explain mechanism of E2-E1 dissociation during viral entry. *Biosci. Rep.* 39:BSR20191077. doi: 10.1042/bsr20191077

Sakaguchi, S., Suzuki, Y., Emi, A., Wu, H., and Nakano, T. (2020). Identification of cellular inhibitors against Chikungunya virus replication by a cDNA expression cloning combined with MinION sequencing. *Biochem. Biophys. Res. Commun.* 530, 617–623. doi: 10.1016/j.bbrc.2020.07.036

Sarrazin, S., Lamanna, W. C., and Esko, J. D. (2011). Heparan sulfate proteoglycans. *Cold Spring Harb. Perspect. Biol.* 3:a004952. doi: 10.1101/cshperspect.a004952

Schneider, W. M., Chevillotte, M. D., and Rice, C. M. (2014). Interferon-stimulated genes: a complex web of host defenses. *Annu. Rev. Immunol.* 32, 513–545. doi: 10.1146/annurev-immunol-032713-120231

Schnierle, B. S. (2019). Cellular attachment and entry factors for Chikungunya virus. *Viruses* 11:1078. doi: 10.3390/v11111078

Schoggins, J. W. (2019). Interferon-stimulated genes: what do they all do? *Ann. Rev. Virol.* 6, 1–18. doi: 10.1146/annurev-virology-092818-015756

Schoggins, J. W., Wilson, S. J., Panis, M., Murphy, M. Y., Jones, C. T., Bieniasz, P., et al. (2011). A diverse range of gene products are effectors of the type I interferon antiviral response. *Nature* 472, 481–485. doi: 10.1038/nature09907

Schwartz, O., and Albert, M. L. (2010). Biology and pathogenesis of Chikungunya virus. *Nat. Rev. Microbiol.* 8, 491–500. doi: 10.1038/nrmicro2368

Shathasivam, T., Kislinger, T., and Gramolini, A. O. (2010). Genes, proteins and complexes: the multifaceted nature of FHL family proteins in diverse tissues. *J. Cell. Mol. Med.* 14, 2702–2720. doi: 10.1111/j.1582-4934.2010.01176.x

Shukla, D., Liu, J., Blaiklock, P., Shworak, N. W., Bai, X., Esko, J. D., et al. (1999). A novel role for 3-O-sulfated heparan sulfate in herpes simplex virus 1 entry. *Cell* 99, 13–22. doi: 10.1016/s0092-8674(00)80058-6

Silva, L. A., Khomandiak, S., Ashbrook, A. W., Weller, R., Heise, M. T., Morrison, T. E., et al. (2013). A single-amino-acid polymorphism in Chikungunya virus E2 glycoprotein influences glycosaminoglycan utilization. *J. Virol.* 88, 2385–2397. doi: 10.1128/jvi.03116-13

Simizu, B., Yamamoto, K., Hashimoto, K., and Ogata, T. (1984). Structural proteins of Chikungunya virus. *J. Virol.* 51, 254–258. doi: 10.1128/jvi.51.1.254-258.1984

Smith, A. E., and Helenius, A. (2004). How viruses enter animal cells. *Science* 304, 237–242. doi: 10.1126/science.1094823

Soumahoro, M.-K., Gérardin, P., Boëlle, P.-Y., Perrau, J., Fianu, A., Pouchot, J., et al. (2009). Impact of Chikungunya virus infection on health status and quality of life: a retrospective cohort study. *PLoS One* 4:e7800. doi: 10.1371/journal.pone.0007800

Staikowsky, F., Talarmin, F., Grivard, P., Souab, A., Schuffenecker, I., Roux, K. L., et al. (2009). Prospective study of Chikungunya virus acute infection in the Island of La Réunion during the 2005–2006 outbreak. *PLoS One* 4:e7603. doi: 10.1371/journal.pone.0007603

Stiles, K. M., and Kielian, M. (2016). Role of TSPAN9 in alphavirus entry and early endosomes. *J. Virol.* 90, 4289–4297. doi: 10.1128/jvi.00018-16

Supramaniam, A., Liu, X., Ferro, V., and Herrero, L. J. (2018). Prophylactic antiheparanase activity by PG545 is antiviral *in vitro* and protects against Ross River virus disease in mice. *Antimicrob. Agents Chemother.* 62, e01959–17. doi: 10.1128/aac.01959-17

Suzuki, Y., Tanaka, A., Maeda, Y., Emi, A., Fujioka, Y., Sakaguchi, S., et al. (2021). Construction and characterization of an infectious clone generated from Chikungunya virus SL11131 strain. *Virology* 552, 52–62. doi: 10.1016/j.virol.2020.09.006

Takahashi, M., Watari, E., Shinya, E., Shimizu, T., and Takahashi, H. (2007). Suppression of virus replication *via* down-modulation of mitochondrial short chain enoyl-CoA hydratase in human glioblastoma cells. *Antiviral Res.* 75, 152–158. doi: 10.1016/j.antiviral.2007.02.002

Tanaka, A., Tumkosit, U., Nakamura, S., Motooka, D., Kishishita, N., Priengprom, T., et al. (2017). Genome-wide screening uncovers the significance of N-sulfation of heparan sulfate as a host cell factor for Chikungunya virus infection. *J. Virol.* 91, e0432–17. doi: 10.1128/jvi.00432-17

Torii, S., Orba, Y., Sasaki, M., Tabata, K., Wada, Y., Carr, M., et al. (2020). Host ESCRT factors are recruited during Chikungunya virus infection and are required for the intracellular viral replication cycle. *J. Biol. Chem.* 295, 7941–7957. doi: 10.1074/jbc.ra119.012303

Tsetsarkin, K. A., Vanlandingham, D. L., McGee, C. E., and Higgs, S. (2007). A single mutation in Chikungunya virus affects vector specificity and epidemic potential. *PLoS Pathog.* 3:e201. doi: 10.1371/journal.ppat.0030201

Tumkosit, U., Maeda, Y., Kishishita, N., Siripanyaphinyo, U., Omori, H., Chetanachan, P., et al. (2019). The use of green fluorescent protein-tagged virus-like particles as a tracer in the early phase of Chikungunya infection. *Virus Res.* 272:197732. doi: 10.1016/j.virusres.2019.197732

Tumkosit, U., Siripanyaphinyo, U., Takeda, N., Tsuji, M., Maeda, Y., Ruchusatsawat, K., et al. (2020). Anti-Chikungunya virus monoclonal antibody that inhibits viral fusion and release. *J. Virol.* 94, e00252–20. doi: 10.1128/jvi.00252-20

Vazeille, M., Moutailler, S., Coudrier, D., Rousseaux, C., Khun, H., Huerre, M., et al. (2007). Two Chikungunya isolates from the outbreak of La Reunion (Indian Ocean) exhibit different patterns of infection in the mosquito, Aedes albopictus. *PLoS One* 2:e1168. doi: 10.1371/journal.pone.0001168

Volk, S. M., Chen, R., Tsetsarkin, K. A., Adams, A. P., Garcia, T. I., Sall, A. A., et al. (2010). Genome-scale phylogenetic analyses of Chikungunya virus reveal independent emergences of recent epidemics and various evolutionary rates. *J. Virol.* 84, 6497–6504. doi: 10.1128/jvi.01603-09

Voss, J. E., Vaney, M.-C., Duquerroy, S., Vonrhein, C., Girard-Blanc, C., Crublet, E., et al. (2010). Glycoprotein organization of Chikungunya virus particles revealed by X-ray crystallography. *Nature* 468, 709–712. doi: 10.1038/nature09555

Weaver, S. C., and Forrester, N. L. (2015). Chikungunya: evolutionary history and recent epidemic spread. *Antiviral Res.* 120, 32–39. doi: 10.1016/j.antiviral.2015.04.016

Weber, C., Berberich, E., von Rhein, C., Henß, L., Hildt, E., and Schnierle, B. S. (2017). Identification of functional determinants in the Chikungunya virus E2 protein. *PLoS Negl. Trop. Dis.* 11:e0005318. doi: 10.1371/journal.pntd.0005318

Wikan, N., Sakoonwatanyoo, P., Ubol, S., Yoksan, S., and Smith, D. R. (2012). Chikungunya virus infection of cell lines: analysis of the East, Central and South African lineage. *PLoS One* 7:e31102. doi: 10.1371/journal.pone.0031102

Wong, K. Z., and Chu, J. J. H. (2018). The interplay of viral and host factors in Chikungunya virus infection: targets for antiviral strategies. *Viruses* 10:294. doi: 10.3390/v10060294

Yap, M. L., Klose, T., Urakami, A., Hasan, S. S., Akahata, W., and Rossmann, M. G. (2017). Structural studies of Chikungunya virus maturation. *Proc. Natl. Acad. Sci. U. S. A.* 114, 13703–13707. doi: 10.1073/pnas.1713166114

Zhang, R., Earnest, J. T., Kim, A. S., Winkler, E. S., Desai, P., Adams, L. J., et al. (2019). Expression of the Mxra8 receptor promotes alphavirus infection and pathogenesis in mice and Drosophila. *Cell Rep.* 28, 2647–2658.e5. doi: 10.1016/j.celrep.2019.07.105

Zhang, R., Kim, A. S., Fox, J. M., Nair, S., Basore, K., Klimstra, W. B., et al. (2018). Mxra8 is a receptor for multiple arthritogenic alphaviruses. *Nature* 557, 570–574. doi: 10.1038/s41586-018-0121-3

Zhang, X., Zheng, Z., Shu, B., Liu, X., Zhang, Z., Liu, Y., et al. (2013). Human astrocytic cells support persistent coxsackievirus B3 infection. *J. Virol.* 87, 12407–12421. doi: 10.1128/jvi.02090-13

**Conflict of Interest:** The authors declare that the research was conducted in the absence of any commercial or financial relationships that could be construed as a potential conflict of interest.

**Publisher's Note:** All claims expressed in this article are solely those of the authors and do not necessarily represent those of their affiliated organizations, or those of the publisher, the editors and the reviewers. Any product that may be evaluated in this article, or claim that may be made by its manufacturer, is not guaranteed or endorsed by the publisher.

*Copyright © 2022 Tanaka and Suzuki. This is an open-access article distributed under the terms of the Creative Commons Attribution License (CC BY). The use, distribution or reproduction in other forums is permitted, provided the original author(s) and the copyright owner(s) are credited and that the original publication in this journal is cited, in accordance with accepted academic practice. No use, distribution or reproduction is permitted which does not comply with these terms.*

frontiers in Microbiology

ORIGINAL RESEARCH
published: 25 March 2022
doi: 10.3389/fmicb.2022.862907

# The Immunity Protection of Central Nervous System Induced by Pseudorabies Virus DelgI/gE/TK in Mice

*Lei Xu[1†], Jian-feng Wei[1†], Jun Zhao[1], Si-yao Xu[1], Feng-qin Lee[1], Min-cai Nie[1], Zhi-wen Xu[1], Yuan-cheng Zhou[2,3] and Ling Zhu[1]**

[1] Key Laboratory of Animal Diseases and Human Health of Sichuan Province, College of Veterinary Medicine, Sichuan Agricultural University, Chengdu, China, [2] Livestock and Poultry Biological Products Key Laboratory of Sichuan Province, Sichuan Animal Science Academy, Chengdu, China, [3] Animal Breeding and Genetics Key Laboratory of Sichuan Province, Sichuan Animal Science Academy, Chengdu, China

Based on a variant strain, we constructed a gE/gI/TK-deleted pseudorabies virus (PRV). A total of 18 female mice were randomized to a vaccination group to receive PRV XJ delgE/gI/TK, a vehicle group to receive Dulbecco's modified Eagle's medium, and a mock group to confirm the protection of PRV delgE/gI/TK on the central nervous system in mice. Subsequently, the vaccination and vehicle groups were infected with PRV XJ. The mice in the vehicle group showed more severe neurological symptoms and higher viral loads than those in the vaccination group. The exudation of Evans blue and the expression of tight junction protein showed no difference in all groups. HE staining showed vacuolar neuronal degeneration in the vehicle group brain, but no tissue lesions were observed in the vaccination group. TNF-α, IL-6, and synuclein were upregulated in the brain of mice in the vehicle group, while those were inhibited among mice in the vaccination group. IFN-β, IFN-γ, ISG15, Mx1, and OAS1 showed no difference in the brain between the vaccination and vehicle groups. In addition, TNF-α and IL-6 were inhibited, and antiviral factors were increased in the intestine of the mice in the vaccination group compared to those in the vehicle group. Our study showed that PRV XJ delgE/gI/TK inhibited neurological damage and the inflammation of the intestine and brain induced by PRV and activated the innate immunity of the intestine.

**Keywords: pseudorabies virus, neurological damage, intestinal immunity, blood–brain barrier, inflammation**

OPEN ACCESS

***Edited by:***
*Chunfu Zheng,*
*University of Calgary, Canada*

***Reviewed by:***
*Wenyu Lin,*
*Massachusetts General Hospital and Harvard Medical School, United States*
*Changxu Song,*
*South China Agricultural University, China*

***Correspondence:**
*Ling Zhu*
*abtczl72@126.com*

*† These authors have contributed equally to this work*

***Specialty section:***
*This article was submitted to Virology, a section of the journal Frontiers in Microbiology*

***Received:*** *26 January 2022*
***Accepted:*** *14 February 2022*
***Published:*** *25 March 2022*

***Citation:***
*Xu L, Wei J-f, Zhao J, Xu S-y, Lee F-q, Nie M-c, Xu Z-w, Zhou Y-c and Zhu L (2022) The Immunity Protection of Central Nervous System Induced by Pseudorabies Virus DelgI/gE/TK in Mice. Front. Microbiol. 13:862907. doi: 10.3389/fmicb.2022.862907*

## INTRODUCTION

Pseudorabies virus (PRV), also known as Aujeszky's disease virus, is a member of *Herpesviridae*, subfamily *Alphaherpesvirinae*, and genus *Varicellovirus* (Pomeranz et al., 2005). This disease was controlled and eradicated from the swine population in most parts of China before 2011 using Bartha-K61 strain inoculation of PRV-infected swine herds. Nevertheless, since October 2011, pseudorabies outbreaks among the Bartha-K61-immunized swine population have spread quickly in China, which caused significant economic losses to the swine industry. The virus genome analysis showed that the re-emerging PRV belongs to a variant strain of genotype-2, and the Bartha-K61 vaccine cannot provide complete protection against the challenge with the emerging PRV variants. Compared with the PRV classical strain, the PRV variants showed stronger virulence, infectious ability, faster transmission speed, more serious clinical symptoms, and higher mortality

rates. In a study by Yang et al. (2016) porcine infected with the variant PRV exhibited more serious respiratory symptoms and neurological signs, more severe damage to organs, and more extensive virus distribution and viral loads in different organs compared to classical PRV. Various animals are susceptible to PRV, including cats, rabbits, dogs, cattle, sheep, and goats, but only porcine are the natural host and reservoir (Zhang et al., 2015; He et al., 2019; Laval and Enquist, 2020). PRV infection causes high mortality in young piglets, growth retardation in growing pigs, and reproductive failure in sow. The major clinical symptoms include fever, itchiness, respiratory symptoms, ataxia, and tetany (An et al., 2013; Wu et al., 2013; Luo et al., 2014). PRV has been thought to cause diseases only in animals. However, recent evidence has shown that PRV might cause encephalitis in humans, which has severe clinical manifestations, including fever, sweating, weakness, status epilepticus, and even death, and the prognosis of patients is extremely poor (Wang et al., 2019a; Yang et al., 2019; Ou et al., 2020), which poses a serious threat to public health and safety. In late 2015, a PRV strain which caused a large number of deaths of piglets was isolated and named PRV XJ. Our study constructed a gE/gI/TK-deleted PRV based on the PRV XJ strain and evaluated the central nervous system protection of PRV XJ delgE/gI/TK and the intestinal immunity induced by PRV XJ delgE/gI/TK.

## MATERIALS AND METHODS

### Virus and Cells

The PRV XJ strain (GenBank accession no. MW893682), a variant strain, was isolated and identified by our laboratory. PRV XJ del gI/gE, in which the gI and gE genes are deleted, was constructed by our laboratory. All the viruses were propagated in BHK-21 cells cultured in Dulbecco's modified Eagle's medium (DMEM) supplemented with 10% (v/v) fetal bovine serum.

### Generation of PRV XJ DelgE/gI/TK

Briefly, single guide RNAs (sgRNA) targeting the TK gene were designed with the CRISPR design tool[1] (**Table 1**) and cloned into the lenticrispr-V2 vector, which was designated TK-sgRNA. The TK-sgRNA was verified by sequencing. BHK-21 cells were co-transfected with 1.5 μg of PUC57-TK-RED and 1.5 μg of CRISPR/Cas9 plasmid lentivrispr-V2 carrying the two sgRNAs targeting the TK gene. The BHK-21 cells were inoculated with PRV XJ del gI/gE when the red fluorescence proteins were expressed. When a distinct cytopathic effect was observed, the cultures were collected and subjected to six rounds of plaque purification. The gE/gI/TK-deleted virus was verified by PCR using gB, gE, and TK primers, respectively (**Table 1**). Finally, the purified gE/gI/TK-deleted virus was designated XJ del gE/gI/TK.

### One-Step Growth Kinetics

One-step growth kinetics was conducted to compare the growth kinetics of PRV XJ delgE/gI/TK with the parental virus PRV XJ. The BHK-21 cells were infected with the virus at a multiplicity of infection of 1. The cells were harvested at successive intervals after infection and stored at −80°C. A virus one-step growth curve was drawn based on 50% tissue culture infectious dose ($TCID_{50}$).

[1]https://zlab.bio/guide-design-resources

**TABLE 1 |** Primers for recombinant virus construction and detection.

| Primer name | Sequence | Size/position |
|---|---|---|
| gE-F | ATCTGGACGTTCCTGCCC | 534 bp |
| gE-R | GTAGATGCAGGGCTCGTACA | |
| gB-F | CGGCAAGTGCGTCTCCAAG | 255 bp |
| gB-R | AGGGCGAAGGAGTCGTAGGG | |
| TK-F | CATCCTCCGGATCTACCTCGACGGC | 742 bp |
| TK-R | CACACCCCCATCTCCGACGTGAAGG | |
| sgRNA1 | CTCGACGGCGCCTACGGCAC | 22–41 |
| | GTGCCGTAGGCGCCGTCGAG | |
| sgRNA1 | GCCGCGTACGGCGACCACATC | 902–921 |
| | GATGTGGTCGCCGTACGCGG | |
| gE-sF | CTTCCACTCGCAGCTCTTCT | 165 bp |
| gE-sR | TAGATGCAGGGCTCGTACAC | |

**TABLE 2 |** Primers for qRT-PCR.

| Primer | Sequence |
|---|---|
| gE-F | CTTCCACTCGCAGCTCTTCT |
| gE-R | TAGATGCAGGGCTCGTACAC |
| β-actin-F | CATCCGTAAAGACCTCTATGCCAAC |
| β-actin-R | ATGGAGCCACCGATCCACA |
| Occludin-F | CCTCCAATGGCAAAGTGAAT |
| Occludin-R | CTCCCCACCTGTCGTGTAGT |
| TNF-α-F | ATCCGCGACGTGGAACTG |
| TNF-α-R | ACCGCCTGGAGTTCTGGAA |
| IFN-γ-F | TCAAGTGGCATAGATGTGGAAGAA |
| IFN-γ-R | TGGCTCTGCAGGATTTTCATG |
| IL-6-F | TTGCCTTCTTGGGACTGATG |
| IL-6-R | ATTGCCATTGCACAACTCTT |
| IFN-β-F | GACGTGGGAGATGTCCTCAAC |
| IFN-β-R | GGTACCTTTGCACCCTCCAGTA |
| ISG15-F | CTCCTTAATTCCAGGGGACCT |
| ISG15-R | CGTCATGGAGTTAGTCACGG |
| Mx1-F | ACCAGGGTGGCTGTAGG |
| Mx1-R | CAGGTTGGGCATCACAT |
| OAS1-F | CATCCAGGAAATTCGGAGACAG |
| OAS1-R | GGCAGGACATCAAACTCCACCTC |

### Animals and Experiment Design

Eighteen female Kunming mice were divided randomly into three groups (vaccination group, vehicle group, and mock group) with six mice in each group. All mice had free access to food and water and were kept at room temperature (23 ± 1.5°C). The mice in the vaccination group were intramuscularly injected with $10^6$ $TCID_{50}$ PRV XJ delgI/gE/TK. Furthermore, booster vaccinations were performed at week 2. The mice in the vehicle and mock groups were intramuscularly injected with DMEM. Moreover, the mice in the vaccination and vehicle groups were challenged with $10^4$ $TCID_{50}$ PRV XJ strain *via* intramuscular injection at

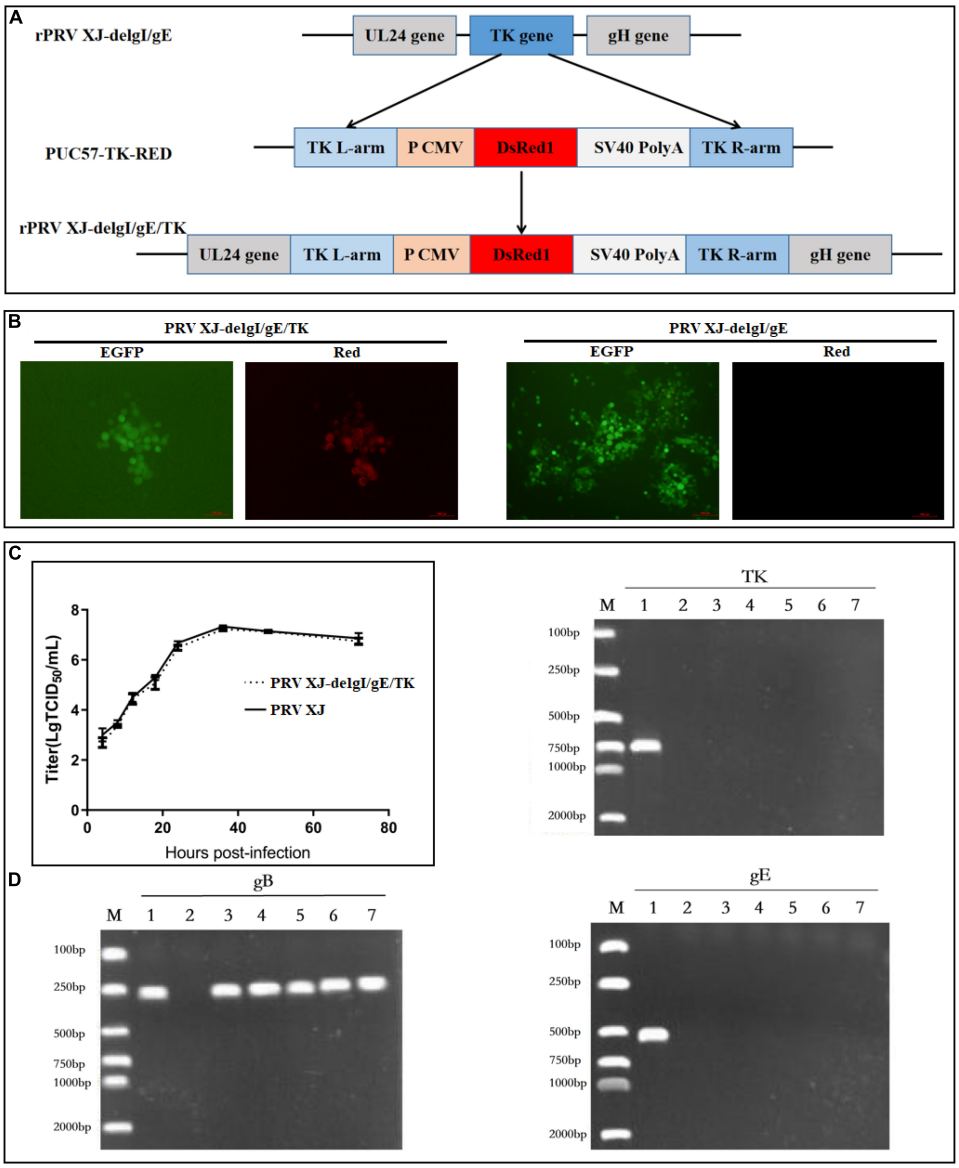


**FIGURE 1 |** Construction and identification of PRV XJ delgE/gI/TK. **(A)** Schematic diagram of the construction for PRV XJ delgE/gI/TK. **(B)** Identification of rescued pseudorabies virus (PRV) from the distinct cytopathic effect cells with green and red fluorescence under the fluorescence microscope. **(C)** One-step growth curves. The BHK-21 cells were infected with PRV XJ or PRV XJ delgE/gI/TK at multiplicity of infection = 1. At designated time points, the cells were harvested, and the viral titers were measured. **(D)** gE/gI/TK deletion was verified in PRV XJ delgE/gI/TK genome by PCR. M, DL 2000 Marker; 1, PRV XJ; 2, $H_2O$; 3–7, F6–F10.

week 2 after the booster vaccinations. Furthermore, the mice in the mock group were injected with DMEM. All mice were weighed and recorded after the challenge. Determination of the mean time to death and clinical evaluation were performed as described earlier (Sehl et al., 2020). All animal experiments were conducted in accordance with the guidelines of the local animal welfare bodies and the Sichuan Agricultural University Ethics Committee (SYXK2019-187).

## Evans Blue Extravasation

The permeability of the blood–brain barrier was determined using Evans blue dye; 2% Evans blue (2 ml/kg) was injected into the tail vein of the mice before they were sacrificed. The brain was dissected, weighed, homogenized with 50% trichloroacetic acid, and centrifuged (12,000 *g*, 15 min). The Evans blue contents of the supernatant were measured, based on absorbance at 620 nm, with a spectrophotometer and were calculated according to a standard curve.

## Quantitative Real-Time PCR Assay

The fresh intestine and brain of mice were dissected to analyze the expression of inflammation factors and antiviral factors in the intestine and brain. According to the manufacturer's protocols, total RNA was extracted from the mice's brain and

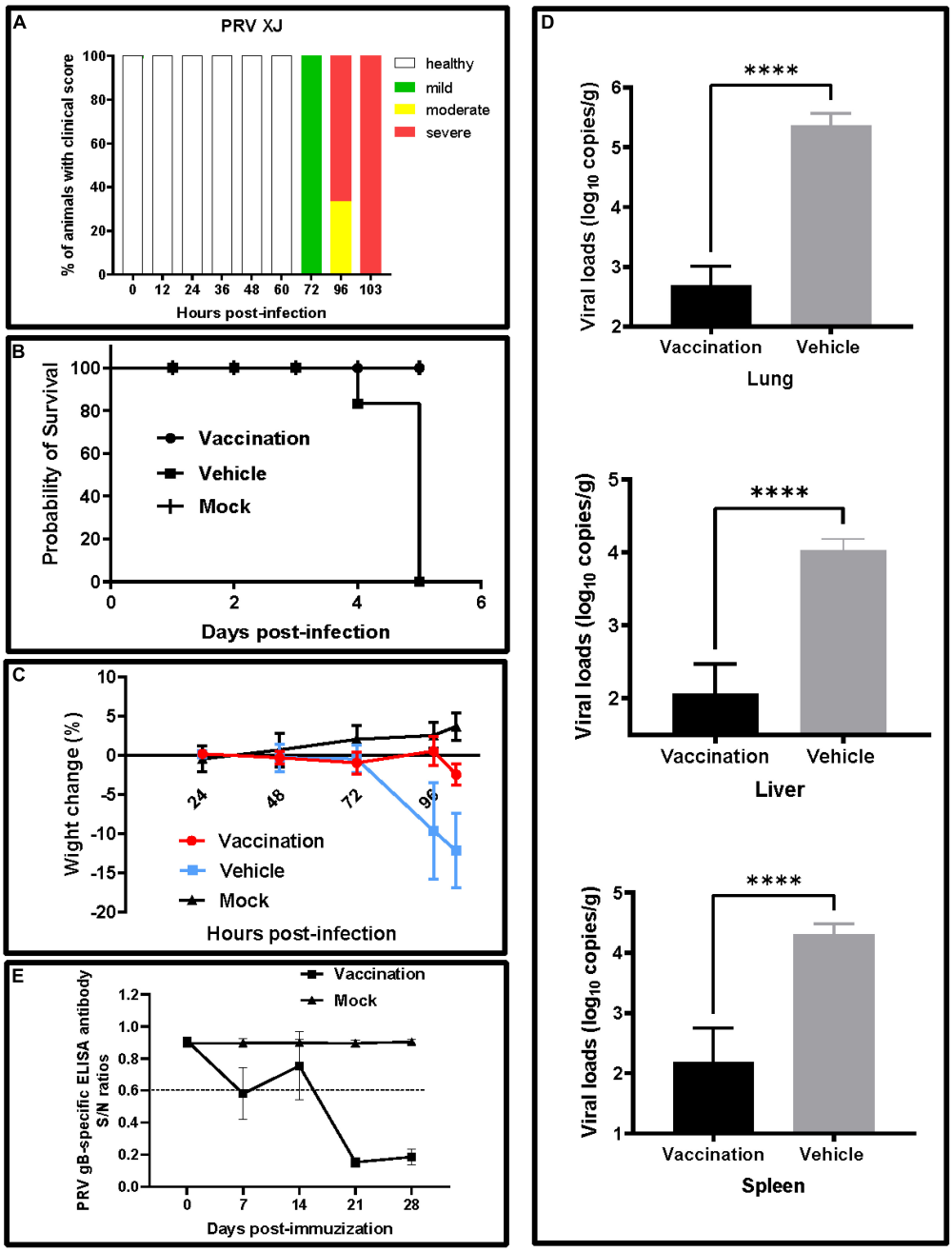


**FIGURE 2 |** Clinical signs and viral loads of experimental mice. **(A)** Clinical score. The frequency of sick animals infected with pseudorabies virus (PRV) XJ. Based on a scoring system (**Supplementary Table 1**), the animals were categorized into either healthy (white) and mildly (green), moderately (yellow), or severely affected (red). **(B)** Survival curves for mice after a virulent challenge with PRV XJ. The survival percentages were presented as a Kaplan–Meier plot ($n$ = 6 per group). **(C)** Weight change of mice in each group after immunization and challenge. **(D)** The viral DNA loads in the lung, liver, and spleen were determined by qRT-PCR. The viral DNA copy numbers were measured with specific primers for the gE gene. **(E)** Development of PRV gB-specific antibody. ****$p < 0.0001$.

intestine using RNAiso Plus. RNA concentration and purity were measured by ScanDrop using the A260 value and the ratio of A260/280, respectively. Reverse transcription reactions were performed using PrimeScript RT Kit. Quantitative RT-PCR was carried out on Roche Lightcycler96 instrument using TB Green Premix Ex Taq according to the manufacturer's instructions. The forward and reverse primer sequences for each gene are provided in **Table 2**. Gene expression was quantified using the $2^{-\Delta\Delta CT}$ method.

Total DNA was extracted from different tissues of the mice using a universal genomic DNA kit. The viral loads in tissue samples from the challenged animals were determined with the

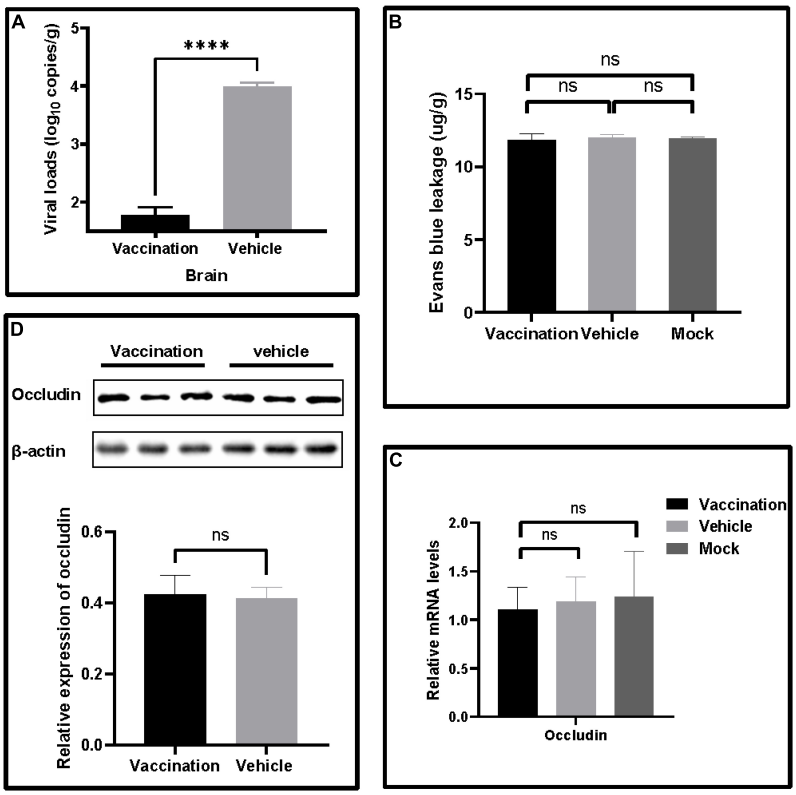


**FIGURE 3 |** The effects on blood–brain barrier leakage after pseudorabies virus XJ challenge. **(A)** The viral DNA loads in the brain were determined by qRT-PCR. **(B)** Quantitative analysis of Evans blue dye extravasation. **(C)** The fold changes normalized with β-actin as an internal control of occludin mRNA levels in the brain after the challenge. **(D)** Western blot analysis and relative quantification of the band density of occludin. Data represent mean ± SD. ****$p < 0.0001$.

qRT-PCR assay for the PRV gE gene using gE-specific primer (**Table 1**). The gene copy number for each sample was expressed as log10 copies per gram of tissue sample.

## Histopathology and Immunohistochemistry

The tissues were dissected, collected, and fixed in 4% paraformaldehyde for at least 72 h. The fixed tissues were embedded in paraffin wax and cut into 4-μm sections. The tissue sections were subjected to histopathological analysis by staining with hematoxylin and eosin.

Immunostaining was performed according to the streptavidin–biotin–peroxidase complex (SABC) immunoprecipitation kit. In brief, the sections were deparaffinized and rehydrated using xylene and graded concentrations of alcohol. Endogenous peroxidase activity was inhibited with 3% hydrogen peroxide for 15 min at room temperature. Then, the antigen epitope was subsequently unmasked using a citrate buffer *via* incubation with 100°C water bath for 15 min. Non-specific antigens were blocked with 5% bovine serum albumin (BSA). The sections were incubated with Syn1 (A17362, Abclonal, 1:200) overnight at 4°C in a moist chamber and rinsed three times with PBS. Then, the sections were incubated with a biotinylated secondary antibody for 30 min, followed by incubation with the SABC for 30 min. The sections were visualized using 3,3-diaminobenzidine and subsequently counterstained with hematoxylin for better visualization. The tissue sections were viewed with an Eclipse 50i microscope equipped with a camera. Images were captured using NIS-Elements 2.30 software.

## Western Blotting

Brain proteins were harvested and homogenized in lysis buffer containing protease inhibitor phenylmethanesulfony fluoride. The protein concentration was determined with the BCA Protein Assay Kit. Briefly, equal amounts of total protein were resolved by sodium dodecyl sulfate–polyacrylamide gel electrophoresis and then transferred onto a polyvinylidene fluoride membrane. The membrane blots were saturated with 5% BSA in phosphate-buffered saline with Tween 20 (PBST) for 2 h at room temperature and then incubated overnight at 4°C with primary antibodies against Syn1 (A17362, Abclonal, 1:1,000), β-actin (AC026, Abclonal, 1:50,000), and occludin (A2601, Abclonal, 1:1,000). After incubation, the membrane was washed three times with PBST and incubated with HRP Goat Anti-Rabbit IgG (H + L) (AS014, Abclonal, 1:10,000). The signals were visualized with SuperSignal$^{TM}$ West Pico Plus Chemiluminescent Substrate. The gray intensity of proteins was measured using ImageJ software.

## Enzyme-Linked Immunosorbent Assay

Blood samples were collected at 0, 7, 14, 21, and 28 days post-vaccination (dpv). The serum was separated by centrifugation after coagulation, and PRV-specific gB antibodies in serum were detected using ELISA kits (IDEXX, Bern, Switzerland) according to the manufacturer's directions. The optical density at 650 nm was measured by a microplate reader (Bio-Rad, Hercules, CA, United States).

## Statistical Analysis

Statistical analysis was undertaken by one-way analysis of variance with GraphPad 7.04 software. All results were expressed as mean ± standard deviation from at least three replicates and were representative of three independent experiments. The value of $P < 0.05$ was considered statistically significant.

# RESULTS

## Construction and Characterization of PRV XJ Del gE/gI/TK

The gE/gI/TK-deleted candidate strain was constructed with homologous recombination and CRISPR/Cas9 system, as shown in **Figure 1A**. Following the co-transfection of PUC57-TK-RED and the CRISPR/Cas9-TK-sgRNA plasmid, the BHK-21 cells were inoculated with PRV XJ del gE/gI. Then, the gE/gI/TK-deleted PRV plaques were isolated by plaque purification (**Figure 1B**). The gE-, TK-, and gB-specific primers were used to identify the gene deletion strain. The specific PCR products of gE and TK were not observed in PRV XJ delgE/gI/TK, whereas the gB gene could be detected (**Figure 1C**), which indicated that the PRV XJ delgE/gI/TK virus was constructed successfully. The reconstituted PRV XJ delgE/gI/TK growth features were analogous to that of the parental PRV XJ in BHK-21 cells (**Figure 1D**).

## PRV XJ DelgE/gI/TK Protects Mice Against Variant PRV XJ Strain

At 3 days post-infection with the PRV XJ strain, all mice of the vehicle group showed clinical symptoms, including curved back, ruffled fur, pruritus, auto-mutilation, and dyspnea, and died at 5 days post-infection (**Figures 2A,B**). All mice in the vaccination and mock groups survived throughout the experiments, and no clinical signs were observed. Before the challenge, there were no significant differences in the weight gain of mice in each group. After the challenge, the mice in the vehicle group lost weight, but the mice in the vaccination group inoculated with PRV XJ delgE/gI/TK had weight changes similar to those in the mock group (**Figure 2C**). The viral loads were monitored in different tissues using qRT-PCR. The viral genome could be detected in the lung, spleen, and liver from the vaccination and vehicle groups. All tissue viral loads of the vaccination group were lower than those of the vehicle group (**Figure 2D**). The gB-specific antibodies of the vaccinated group were detected at 7 dpv. Then, the gB antibody levels decreased at 14 dpv. Finally, the gB antibodies levels increased again when booster vaccinations were performed and kept steadily increasing until 28 dpv. On the contrary, the gB-specific antibodies failed to be detected in the mock group (**Figure 2E**).

## PRV XJ Strain Infections Had No Effects on Blood–Brain Barriers in Mice

The viral loads of the brain were determined to confirm the protection of PRV XJ delgE/gI/TK on the central nervous system. The brain viral loads of the vaccination group were significantly lower than those of the vehicle group (**Figure 3A**). Furthermore, all mice were injected with Evans blue dye by tail vein injection to examine whether the PRV XJ delgE/gI/TK protected the blood–brain barrier permeability of mice. Evans blue was not detected in these mice (**Figure 3B**). Similarly, the tight junction protein occludin mRNA and the occludin protein levels were detected. The occludin mRNA levels of all mice brains showed no difference (**Figure 3C**). The occludin expression was no different in all groups (**Figure 3D**). These results altogether suggested that PRV XJ strain infections did not affect the mice's blood–brain barrier permeability.

## PRV XJ DelgE/gI/TK Protects the Central Nervous System From Neurological Damage Induced by PRV XJ

To investigate the protection of PRV XJ delgE/gI/TK on the central nervous system in mice, we measured and compared the neurological damage in the brain of a different group. The histopathological examination showed vacuolar neuronal degeneration, neuron phagocytosis, and nuclear cleavage in the vehicle group, and no histopathological changes were observed in the vaccination group (**Figure 4A**). The expression of SYN1 protein in the brain was evaluated by immunohistochemistry. The brain of the vehicle group exhibited more SYN1 expression than the vaccination group (**Figure 4B**). Furthermore, Western blotting confirmed those results (**Figure 4C**). Those results suggested that PRV XJ delgE/gI/TK protected the central nervous system from neurological damage induced by PRV XJ. In addition, the pro-inflammatory and antiviral factor mRNA levels in the brain and intestine were determined. In the brain, the TNF-α and IL-6 mRNA levels of the vaccination group were significantly decreased compared with the vehicle group and showed no difference between the vaccination and mock groups, and the mRNA levels of IFN-β, IFN-γ, ISG15, Mx1, and OAS1 showed no difference between the vaccination group and the vehicle group but were significantly increased compared with those in the brain of mice in the mock group (**Figures 4D,F**). In the intestine, TNF-α and IL-6 were inhibited in the vaccination group compared with the vehicle group, and TNF-α and IL-6 were increased in the vaccination and vehicle groups compared with the mock group (**Figure 4E**). The antiviral factors IFN-β, IFN-γ, ISG15, Mx1, and OAS1 were significantly upregulated in the intestine of mice in the vaccination group compared with the vehicle group, and the antiviral factors were significantly increased in the vaccination and vehicle groups compared with the mock group (**Figure 4G**).

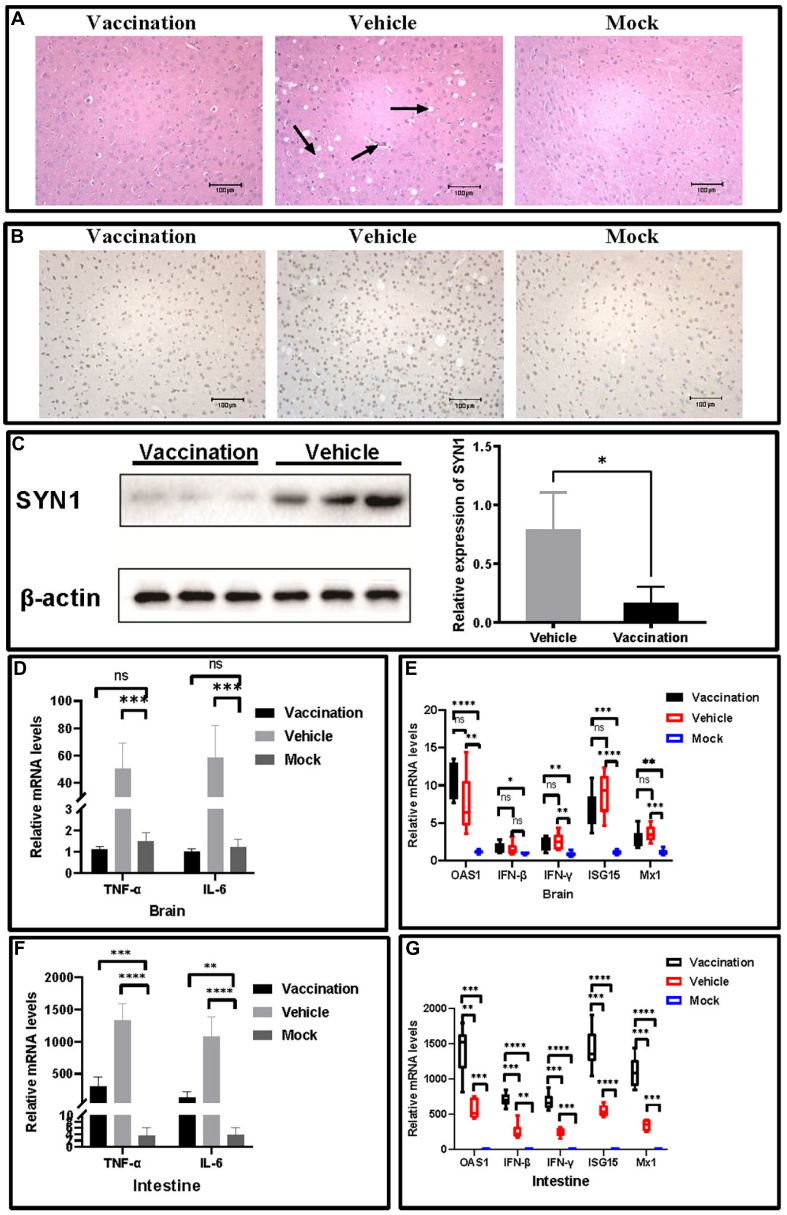


**FIGURE 4 |** The protective effects of pseudorabies virus XJ delgE/gI/TK in mice brain. **(A)** Histopathological observations of mice brain injected with the indicated viral strain or Dulbecco's modified Eagle's medium. The arrows from the left to the right show nuclear cleavage, neuron phagocytosis, and vacuolar neuronal degeneration in the brain, respectively (hematoxylin and eosin staining, × 200 magnification). **(B)** Immunohistochemistry detection of SYN1 in mice. Comparison of the SYN1 expression in mice brain using immunohistochemistry. **(C)** Western blot analysis and relative quantification of the band density of SYN1. **(D)** The fold change of TNF-α and IL-6 in the brain was determined by qRT-PCR. **(E)** The fold change of TNF-α and IL-6 in the intestine was determined by qRT-PCR. **(F)** The fold change of IFN-β, IFN-γ, ISG15, Mx1, and OAS1 in the brain was determined by qRT-PCR. **(G)** The fold change of IFN-β, IFN-γ, ISG15, Mx1, and OAS1 in the intestine was determined by qRT-PCR. Data are presented as mean ± SD ($n = 6$). $^{*}P < 0.05$, $^{**}P < 0.01$, $^{***}P < 0.001$, $^{****}P < 0.0001$.

## DISCUSSION

The PRV variant strains exhibited stronger neurotropism and more serious neuropathological lesions than the PRV classical strains (Luo et al., 2014; Wang et al., 2019b). Many human encephalitis cases were reported (Wang et al., 2019a; Li et al., 2020). The patients started with a high fever, headache, and rapid progression to signs of a central nervous system infection, including altered mental status, seizures, and coma (Yang et al., 2019). Vaccination is still the most efficient way to prevent and control PRV, especially gene-deleted vaccines. The gE target infects second- and third-order neurons of the olfactory and trigeminal routes, and gI affects the anterograde-directed transport of virus in neurons and the spread in non-neuronal cells

(Kratchmarov et al., 2013). TK is involved in the viral replication and neuroinvasiveness of PRV in the central nervous system (Kit et al., 1985). TK deficiency significantly reduced the ability of replication and transmission in nerve cells (Lv et al., 2021). As the classical model animals for PRV research, mice were used in our research. In this study, we constructed a gE/gI/TK-deleted strain and explored the vaccine protection of the central nervous system in mice. The data suggested that PRV XJ delgE/gI/TK was an effective tool strain for investigating neurological damages and a promising vaccine candidate for PRV prevention and control.

It has been reported that inflammation of the central nervous system exacerbates the blood–brain barrier permeability and reduces tight junctional protein expression (McColl et al., 2008). In many nervous system diseases, secondary pathophysiological changes occur in the central nervous system after blood–brain barrier injuries, such as brain edema, elevated intracranial pressure, and internal environment disorder, further aggravating the neurological damage (Laval et al., 2018; Sun et al., 2018; Jiang et al., 2021; Jiao-Yan et al., 2021). Our data showed no blood–brain barrier leakage after the PRV challenge. The blood–brain barrier was not destroyed after the PRV challenge because PRV cannot induce viremia. In addition, the viral loads and inflammation were significantly decreased, and no neurological damages were observed in the vaccination group compared to the vehicle group. Yeh proved that PRV infection increases TNF-α expression, and TNF-α is a key mediator in PRV-induced apoptosis *in vitro* (Yeh et al., 2008), so we speculated that PRV XJ delgE/gI/TK protected the central nervous system from neurological damage by inhibiting inflammation.

Because the gE, gI, and TK deletion PRV strain cannot transport to the central nervous system, the vaccine cannot activate the immunity of the central nervous system by a direct effect with the central nervous system immune cells, including astrocyte, microglial cells, and oligodendrocyte (Pomeranz et al., 2005; Klein et al., 2017). Sun verified that the antiviral factors IFN-β and IFN-γ were upregulated at the early phases of PRV infection and decreased at later periods (Sun et al., 2021). In our research, the reason why ISG15, Mx1, OAS1, IFN-γ, and IFN-β in the brain showed no difference between the vaccination group and the vehicle group might be that the mice were in a later period of infection. In our studies, ISG15, Mx1, OAS1, IFN-γ, and IFN-β in the intestine of the vaccination group were increased compared with the vehicle group. Maybe it is because PRV infection would induce a lot of antiviral factors in the intestine where a variety of immune cells are located, and gE, gI, and TK deletion PRV could induce a higher IFN-β than wild PRV (Lv et al., 2021). Furthermore, the pro-inflammatory factors TNF-α and IL-6 were downregulated in the vaccination group, in the brain and intestine, compared with the vehicle group.

In summary, inflammation was inhibited and intestinal immunity was strongly activated in the vaccination group. Recent studies have demonstrated that gut immune-stimulatory products can influence microglia function to prevent central nervous system damage following a viral infection (Brown et al., 2019). In our study, we found that the PRV XJ has no effect on the intestine, except the intestinal villi height and growth, of the vaccination group compared with the vehicle group (**Supplementary Figure 1**). Therefore, PRV XJ del gE/gI/TK protected the central nervous system from PRV-induced neurological damages by inducing intestinal immunity. We speculate that PRV XJ del gE/gI/TK induced central nervous system immunity through the brain–gut axis, and our laboratory has developed a related research.

## DATA AVAILABILITY STATEMENT

The original contributions presented in the study are included in the article/**Supplementary Material**, further inquiries can be directed to the corresponding author.

## ETHICS STATEMENT

The animal study was reviewed and approved by the Sichuan Agricultural University Ethics Committee.

## AUTHOR CONTRIBUTIONS

LX, J-FW, and LZ contributed to conceptualization. LX and J-FX contributed to methodology. LX and JZ contributed to software and writing—original draft preparation. Z-WX contributed to validation. LX, F-QL, and S-YX contributed to investigation. Y-CZ and Z-WX contributed to resources. LX contributed to data curation and writing—original draft preparation. M-CN contributed to supervision. LZ contributed to project administration and funding acquisition. All authors have read and agreed to the published version of the manuscript.

## FUNDING

This work was supported by the Porcine Major Science and Technology Project of Sichuan Science and Technology Plan (Grant Number 2021ZDZX0010), the R&D Key Research and Development Project of Sichuan Science and Technology Plan (Grant Number 2020YFN0147), the Key R&D Program of Sichuan Province (Grant Number 2018NZ0151), and the Agricultural Industrial Technology System of Sichuan Provincial Department of Agriculture (Grant Number CARS-SVDIP).

## SUPPLEMENTARY MATERIAL

The Supplementary Material for this article can be found online at: https://www.frontiersin.org/articles/10.3389/fmicb.2022.862907/full#supplementary-material

**Supplementary Figure 1 |** Histopathological observations of mice intestine injected with the indicated viral strain or Dulbecco's modified Eagle's medium (hematoxylin and eosin staining, ×200 magnification).

## REFERENCES


An, T.-Q., Peng, J.-M., Tian, Z.-J., Zhao, H.-Y., Li, N., Liu, Y.-M., et al. (2013). Pseudorabies virus variant in Bartha-K61-vaccinated pigs. China, 2012. *Emerg. Infect. Dis.* 19, 1749–1755. doi: 10.3201/eid1911.130177

Brown, D. G., Soto, R., Yandamuri, S., Stone, C., Dickey, L., Gomes-Neto, J. C., et al. (2019). The microbiota protects from viral-induced neurologic damage through microglia-intrinsic TLR signaling. *eLife* 8:e47117. doi: 10.7554/eLife.47117

He, W., Auclert, L. Z., Zhai, X., Wong, G., Zhang, C., Zhu, H., et al. (2019). Interspecies transmission, genetic diversity, and evolutionary dynamics of Pseudorabies Virus. *J. Infect. Dis.* 219, 1705–1715. doi: 10.1093/infdis/jiy731

Jiang, H., Li, H., Cao, Y., Zhang, R., Zhou, L., Zhou, Y., et al. (2021). Effects of cannabinoid (CBD) on blood brain barrier permeability after brain injury in rats. *Brain Res.* 1768:147586. doi: 10.1016/j.brainres.2021.147586

Jiao-Yan, Y., Qing-Qing, L., Xi, L., Mei, Z., Ting, S., Na, H., et al. (2021). Oxymatrine improves blood-brain barrier integrity after cerebral ischemia-reperfusion injury by downregulating CAV1 and MMP9 expression. *Phytomedicine* 84:153505. doi: 10.1016/j.phymed.2021.153505

Kit, S., Kit, M., and Pirtle, E. C. (1985). Attenuated properties of thymidine kinase-negative deletion mutant of pseudorabies virus. *Am. J. Vet. Res.* 46, 1359–1367.

Klein, R. S., Garber, C., and Howard, N. (2017). Infectious immunity in the central nervous system and brain function. *Nat. Immunol.* 18, 132–141.

Kratchmarov, R., Kramer, T., Greco, T. M., Taylor, M. P., Ch'ng, T. H., Cristea, I. M., et al. (2013). Glycoproteins gE and gI are required for efficient KIF1A-dependent anterograde axonal transport of alphaherpesvirus particles in neurons. *J. Virol.* 87, 9431–9440. doi: 10.1128/JVI.01317-13

Laval, K., and Enquist, L. W. (2020). The Neuropathic itch caused by Pseudorabies Virus. *Pathogens* 9:254. doi: 10.3390/pathogens9040254

Laval, K., Vernejoul, J. B., Van Cleemput, J., Koyuncu, O. O., and Enquist, L. W. (2018). Virulent Pseudorabies Virus infection induces a specific and lethal systemic inflammatory response in mice. *J. Virol.* 92:e0161418. doi: 10.1128/jvi.01614-18

Li, X. D., Fu, S. H., Chen, L. Y., Li, F., Deng, J. H., Lu, X. C., et al. (2020). Detection of Pseudorabies Virus antibodies in human encephalitis cases. *Biomed. Environ. Sci.* 33, 444–447. doi: 10.3967/bes2020.059

Luo, Y., Li, N., Cong, X., Wang, C.-H., Du, M., Li, L., et al. (2014). Pathogenicity and genomic characterization of a pseudorabies virus variant isolated from Bartha-K61-vaccinated swine population in China. *Vet. Microbiol.* 174, 107–115. doi: 10.1016/j.vetmic.2014.09.003

Lv, L., Liu, X., Jiang, C., Wang, X., Cao, M., Bai, J., et al. (2021). Pathogenicity and immunogenicity of a gI/gE/TK/UL13-gene-deleted variant pseudorabies virus strain in swine. *Vet. Microbiol.* 258:109104. doi: 10.1016/j.vetmic.2021.109104

McColl, B. W., Rothwell, N. J., and Allan, S. M. (2008). Systemic inflammation alters the kinetics of cerebrovascular tight junction disruption after experimental stroke in mice. *J. Neurosci.* 28, 9451–9462. doi: 10.1523/JNEUROSCI.2674-08.2008

Ou, J., Cai, S., Zheng, F., Lu, G., and Zhang, G. (2020). Human pseudorabies virus infection: a new threat in China. *J. Infect.* 80, 578–606. doi: 10.1016/j.jinf.2019.12.018

Pomeranz, L. E., Reynolds, A. E., and Hengartner, C. J. (2005). Molecular biology of pseudorabies virus: impact on neurovirology and veterinary medicine. *Microbiol. Mol. Biol. Rev.* 69, 462–500. doi: 10.1128/mmbr.69.3.462-500.2005

Sehl, J., Hölper, J. E., Klupp, B. G., Baumbach, C., Teifke, J. P., and Mettenleiter, T. C. (2020). An improved animal model for herpesvirus encephalitis in humans. *PLoS Pathog.* 16:e1008445. doi: 10.1371/journal.ppat.1008445

Sun, H. F., Dong, J., Jiang, C. L., Sun, T., Bai, J., and Jiang, P. (2018). Isolation and pathogenicity of a highly virulent pseudorabies virus in Jangsu province. *Chin. J. Prevent. Vet. Med.* 40, 283–287.

Sun, W., Liu, S., Huang, X., Yuan, R., and Yu, J. (2021). Cytokine storms and pyroptosis are primarily responsible for the rapid death of mice infected with pseudorabies virus. *R. Soc. Open sci.* 8:210296. doi: 10.1098/rsos.210296

Wang, Y., Nian, H., Li, Z., Wang, W., Wang, X., and Cui, Y. (2019a). Human encephalitis complicated with bilateral acute retinal necrosis associated with pseudorabies virus infection: a case report. *Int. J. Infect. Dis.* 89, 51–54. doi: 10.1016/j.ijid.2019.09.019

Wang, Y. L., Jin, Z., Han-Song, Q. I., Qiu, H. J., and Sun, Y. (2019b). Comparison of the pathogenicity of pseudorabies virus variant and classical strains in mice. *Chin. J. Prevent. Vet. Med.* 41, 1199–1203.

Wu, R., Bai, C., Sun, J., Chang, S., and Zhang, X. (2013). Emergence of virulent pseudorabies virus infection in Northern China. *J. Vet. Sci.* 14, 363–365.

Yang, Q.-Y., Sun, Z., Tan, F.-F., Guo, L.-H., Wang, Y.-Z., Wang, J., et al. (2016). Pathogenicity of a currently circulating Chinese variant pseudorabies virus in pigs. *World J. Virol.* 5, 23–30. doi: 10.5501/wjv.v5.i1.23

Yang, X., Guan, H., Li, C., Li, Y., Wang, S., Zhao, X., et al. (2019). Characteristics of human encephalitis caused by pseudorabies virus: a case series study. *Int. J. Infect. Dis.* 87, 92–99. doi: 10.1016/j.ijid.2019.08.007

Yeh, C.-J., Lin, P.-Y., Liao, M.-H., Liu, H.-J., Lee, J.-W., Chiu, S.-J., et al. (2008). TNF-α mediates pseudorabies virus-induced apoptosis *via* the activation of p38 MAPK and JNK/SAPK signaling. *Virology* 381, 55–66. doi: 10.1016/j.virol.2008.08.023

Zhang, L., Zhong, C., Wang, J., Lu, Z., Liu, L., Yang, W., et al. (2015). Pathogenesis of natural and experimental Pseudorabies virus infections in dogs. *Virol. J.* 12:44. doi: 10.1186/s12985-015-0274-8


**Conflict of Interest:** The authors declare that the research was conducted in the absence of any commercial or financial relationships that could be construed as a potential conflict of interest.

**Publisher's Note:** All claims expressed in this article are solely those of the authors and do not necessarily represent those of their affiliated organizations, or those of the publisher, the editors and the reviewers. Any product that may be evaluated in this article, or claim that may be made by its manufacturer, is not guaranteed or endorsed by the publisher.

*Copyright © 2022 Xu, Wei, Zhao, Xu, Lee, Nie, Xu, Zhou and Zhu. This is an open-access article distributed under the terms of the Creative Commons Attribution License (CC BY). The use, distribution or reproduction in other forums is permitted, provided the original author(s) and the copyright owner(s) are credited and that the original publication in this journal is cited, in accordance with accepted academic practice. No use, distribution or reproduction is permitted which does not comply with these terms.*

frontiers | Frontiers in Microbiology

ORIGINAL RESEARCH
published: 12 April 2022
doi: 10.3389/fmicb.2022.864377

# Pathogenicity and Immunogenicity of a Serially Passaged Attenuated Genotype 2c Porcine Epidemic Diarrhea Virus Cultured in Suspended Vero Cells

*Fei-Fei Ge[1], Long-Shan Kang[2], Li-Ping Shen[1], Hai-Xiao Shen[1], De-Quan Yang[1], Xin Li[1], Hou-Bin Ju[1], Hong-jin Zhao[1] and Jian Wang[1]**

[1] Shanghai Animal Disease Control Center, Shanghai, China, [2] College of Life Sciences and Food Engineering, Hebei University of Engineering, Handan, China

OPEN ACCESS

**Edited by:**
*Chunfu Zheng,*
*University of Calgary, Canada*

**Reviewed by:**
*Yan-Dong Tang,*
*Harbin Veterinary Research Institute (CAAS), China*
*Jianfei Chen,*
*Harbin Veterinary Research Institute (CAAS), China*

***Correspondence:**
*Jian Wang*
*jianwhlj@163.com*

**Specialty section:**
*This article was submitted to Virology, a section of the journal Frontiers in Microbiology*

**Received:** *28 January 2022*
**Accepted:** *18 February 2022*
**Published:** *12 April 2022*

**Citation:**
*Ge F-F, Kang L-S, Shen L-P, Shen H-X, Yang D-Q, Li X, Ju H-B, Zhao H-j and Wang J (2022) Pathogenicity and Immunogenicity of a Serially Passaged Attenuated Genotype 2c Porcine Epidemic Diarrhea Virus Cultured in Suspended Vero Cells. Front. Microbiol. 13:864377. doi: 10.3389/fmicb.2022.864377*

In this study, one G2c-subtype strain of porcine epidemic diarrhea virus (PEDV) (SHXX1902 strain) was isolated from clinical samples in suspended Vero cells, which was different from the genotype of the commercial AJ1102 vaccine. As a result, we determined the pathogenicity of different passages' isolates (SHXX1902 strain) and compared the immunogenicity of G2c-subtype strain (SHXX1902 strain) with the commercial AJ1102 vaccine. The viral titer reached $10^7$ 50% tissue culture infectious dose ($TCID_{50}$)/ml, which met the requirement for seed virus replication during vaccine development. Five-day-old piglets were orally infected with viruses from passages P5 and P35 to determine the pathogenicity and immunogenicity of different passages. Pregnant sows were immunized with inactivated SHXX1902-P5 or the commercial AJ1102 vaccine (first immunized with an attenuated vaccine and then boosted with an inactivated vaccine) to study the influence of the culture method on the immunogenicity of the strain. The median pig diarrhea dose ($PDD_{50}$) and the median lethal dose ($LD_{50}$) of the P5 virus were $10^{2.00}$ and $10^{2.84}$ $TCID_{50}$/ml, respectively. All five piglets infected with the SHXX1902-P5 virus shed the virus 24 h after vaccination, whereas only two of the five piglets treated with the SHXX1902-P35 virus shed the virus 48 h after vaccination. The SHXX1902-P35 virus was partially attenuated in the 5-day-old piglets. Inactivated SHXX1902-P5 induced PEDV-specific immunoglobulin G (IgG) antibody responses equivalent to those induced by AJ1102 after infection in sow serum. However, the IgA titer induced by AJ1102 was much higher than that induced by inactivated SHXX1902-P5 since the boost immunization. On days 5 and 7 after farrowing, the IgA titers were similar among the immunized groups. Our study highlights that serial passage can lead to the attenuation of G2c-subtype strain. The immunogenicity of the inactivated strain was similar to the commercial vaccine. Our observation helped conceptualize appropriate study designs for the PEDV vaccine.

**Keywords: G2c-subtype strain, PEDV, pathogenicity, immunogenicity, different passage**

## INTRODUCTION

Porcine epidemic diarrhea virus (PEDV) belongs to the order Nidovirales, family Coronaviridae, and genus Alphacoronavirus. PEDV is now a global pathogen. Mortality due to viral infection varies with age and has approached 100% in 1–3-day-old piglets. Its genome is arranged in the following order: 5′-untranslated region (UTR)-ORF1a/ORF1b-S-ORF3-E-M-N-3′-UTR (Oh et al., 2014). At present, two genotypes of PEDV are recognized. Each of which includes two subgenotypes. The subgenotypes of genogroup 1, which are weakly pathogenic, are classical G1a and recombinant G1b. The subgenotypes of genogroup 2, which are strongly pathogenic, are local epidemic G2a global epidemic or pandemic G2b and G2c (Lee et al., 2010; Lee and Lee, 2014; Oh et al., 2014; Lee, 2015).

There is worldwide porcine epidemic diarrhea (PED), first recorded in Britain and Belgium in 1971 (Wood, 1977). In the 1970s, PED first appeared in the United Kingdom and was caused by the G1a subtype of PEDV. It then spread to Europe and many Asian countries. Researchers developed a vaccine based on this subtype, which is widely used. In the past 30 years, the disease has only been sporadic. Since 2000, in South Korea, the G2a subtype has continued to be prevalent in pigs immunized with an anti-Gla-subtype vaccine. At present, the epidemic area of the G2a subtype is relatively limited and is mainly concentrated in South Korea, Thailand, Japan, and other Asian countries. In 2010, a PED outbreak caused by a G2b-subtype mutant strain was reported in China, which could have been caused by gene deletion, insertion, or point mutation in a virulent Gla-subtype strain. In April 2013, PED caused by a G2b-subtype virus broke out in the United States and spread rapidly to 33 states (Huang et al., 2013). Paarlberg (2014) conducted a loss assessment of this PED outbreak, confirming its damage to the United States pig industry.

The number of live pigs sold at the market decreased by 3%, and the losses to pig farmers and consumers reached US$1 billion (Paarlberg, 2014). At present, variant G2b strains are prevalent throughout the world. In 2014, an epidemic of a G1b-subtype virus was reported in the United States. The new G1b-subtype virus is different from the G2-subtype virus, with deletions and insertions in the S gene (Wang et al., 2014). The G1b subtype may have been produced by the recombination of a classical strain (G1a subtype) and an epidemic strain (G2 subtype) during the process of viral subgenomic transcription (Lee, 2015).

Moreover, reports of the newly discovered G2c strains increased significantly after 2012 in Europe. PEDV strains from different subgroups were also prevalent within the same areas, implying that the coincident "hot spots" in PEDV-endemic areas (e.g., China and South Korea) are critical in determining the sources of some PEDV variations. These hotspot areas are potentially important reservoirs for the evolution of genetic variation in PEDV, arising from recombination between the different PEDV subgroups (Guo et al., 2019).

The vaccination of sows during epidemics or outbreaks of PED is the basic method used to control and eliminate PEDV. Anti-PEDV vaccines include inactivated vaccines, weak viral vaccines, and other vaccines. Piglets can receive protection from the antibodies contained in the colostrum or milk from immunized postnatal females, thereby reducing the incidence of PED. Although PEDV was first detected in European pig populations, researchers did not develop vaccines because the disease was rare. However, in 1980, PEDV was detected in Asian pig populations, which became prevalent in many pig-raising countries. Therefore, weak and inactivated vaccines for G1-subtype strains (CV777 and SM98) were developed and widely used. In 2010, PED caused by a highly pathogenic G2b-subtype PEDV mutant broke out in many provinces in southern China, and the G1a-subtype vaccines did not provide effective immune protection against this mutant.

The difficulties of culturing G2c variant strains of PEDV and the low titers generated exacerbate the urgent need to develop highly effective vaccines against the prevailing PEDV strains. This study generated a serially passaged vaccine candidate (SHXX1902) with the short-term passage of a virulent PEDV isolate in suspended Vero cells. Compared with the parental strain, after passage 5 (P5), the cell-adapted strain showed deletions of 24 nt (equivalent to eight amino acids) and 52 nt (133 amino acids) in ORF1a and ORF3, respectively. Strain SHXX 1902-P5 shared 93.4–100.0% amino acid sequence identity in different regions with SHXX1902-P35 (Ge et al., 2021). Pregnant sows were administered the inactivated SHXX1902-P5 vaccine in two doses at a fortnightly interval before parturition. IgG antibody responses to PEDV were detected in the serum of sows until 2 weeks post farrowing. IgA antibody responses to PEDV were detected in the milk of all the immunized sows with inactivated SHXX1902-P5 vaccine on days 5 and 7 after farrowing. These results demonstrate that intramuscularly injected inactivated PEDV can be used as a vaccine in maternal vaccination strategies to provide durable lactogenic immunity and confer passive protection on litters against PEDV G2c.

## MATERIALS AND METHODS

### Viruses

The isolation and continuous PEDV strain SHXX1902 in Vero cells have been reported previously (Ge et al., 2021). The fifth passage (P5) and 35th passage (P35) of SHXX1902 were used as virulent inocula, and their virulence was compared. Whole-genomic sequence analysis of these strains has been reported previously.

### Growth Kinetics

Vero cell monolayers were infected separately with PEDV P5 or P35 at a multiplicity of infection (MOI) of 0.01, or the cells were mock-infected in six-well plates. The culture supernatants and cell lysates were collected at 12, 24, 36, 48, 60, and 72 h post-infection. After one round of freeze-thawing, the cell culture samples were analyzed in 96-well plates with the Reed–Muench

method to determine the 50% tissue culture infectious dose ($TCID_{50}$/ml).

## Immunofluorescence Assay

Vero cells were infected with PEDV in 24-well plates at an MOI of 0.01. At 12 h post-infection (hpi), the cells were washed three times with phosphate-buffered saline (PBS), fixed with 4% paraformaldehyde at room temperature (RT) for 15 min, and then permeabilized with 0.2% Triton X-100 (Solarbio, Beijing, China) for 15 min. After the cells were washed as described above, they were blocked with 1% bovine serum albumin (Solarbio, Beijing, China) for 30 min at RT. A mouse anti-PEDV-S monoclonal antibody (Veterinary Medical Research and Development, United States) and Alexa-green-conjugated goat anti-mouse antibody were then used as the primary and secondary antibodies, respectively. The cell nuclei were counterstained with 4′,6-diamidino-2-phenylindole (DAPI; Vector Labs, United States) for 5 min at RT in the dark. The cells were washed three times with PBS and observed under a fluorescence microscope.

## Virulence Test of Subcultured Strains

The virulence of strain SHXX1902-P5 was studied in 5-day-old piglets. A virus solution ($10^7$ $TCID_{50}$/ml) was fed orally to the piglets at a 1 ml/piglet dose. Each group (groups 1–5) of five piglets was challenged orally with the 10-fold serially diluted ($10^{-3}$–$10^{-7}$) SHXX1902-P5 virus, whereas the control animals in group 6 were fed cell culture medium. Clinical symptoms, such as vomiting and diarrhea, were checked every day, and fecal swabs of the piglets were collected for PEDV detection. After 5 days, the piglets were killed, and intestinal samples were collected for pathological examination. Histological examinations were performed to determine whether SHXX1902 damaged the intestinal tracts of the infected piglets. Stool samples from the piglets in all groups were collected before infection and after that with 16-in. cotton-tipped swabs and scored for fecal consistency for 5 days after infection: 0 = normal, 1 = pasty, 2 = semiliquid, and 3 = liquid or watery. The median pig diarrhea dose ($PDD_{50}$) and the median lethal dose ($LD_{50}$) of the virus were determined as the reciprocal of the viral dilution at which 50% of the pigs developed watery diarrhea (score 3) or died, respectively, at a given time point, using the Reed–Muench method.

## Comparative Pathogenicity of Strains SHXX1902-P5 and SHXX1902-P35

The piglets were randomly assigned to one of three experimental groups: the SHXX1902-P5-infected group ($n$ = 4), the SHXX1902-P35-infected group ($n$ = 4), and the sham-infected control group ($n$ = 4). The animals were fed commercial milk replacer four times daily. After a 2-day acclimation period, the piglets (5 days old) in the virus-infected groups were orally administered a 1-ml dose of one $10^{5.84}$ $TCID_{50}$/ml virus (equivalent to 1,000 $LD_{50}$, as determined in this study). The sham-infected pigs were administered a cell culture medium as a placebo. The animals were monitored daily for clinical signs of vomiting, diarrhea, and mortality throughout the experiment. Rectal swabs were collected from all the piglets, diluted with PBS to 10% ($w/v$) suspensions, and centrifuged. The clarified supernatants were subjected to real-time PCR with the RT-PCR Detection Kit (Weiboxin Biotechnology, Guangzhou, China) to detect PEDV shedding. The clinical significance score (CSS) was used to measure diarrheal severity with the following scoring criteria, based on visual examination for 7 days post-infection (dpi): 0 = normal and no diarrhea [mean cycle threshold ($Ct$) values of >45]; 1 = mild and fluidic feces; 2 = moderate watery diarrhea; 3 = severe watery and projectile diarrhea (mean $Ct$ values of <20); and 4 = death. Throughout the study, the piglets were necropsied upon death after the challenge, whereas all the piglets that survived the challenge and the control groups were euthanized at 7 dpi for post-mortem examination.

## Pregnant Swine Vaccination Experiments

Vaccination experiments were conducted in six commercial crossbred pregnant sows (Great Yorkshire × Dutch Landrace) with the same parity and expected farrowing date. The animals were allocated randomly to one of three experimental groups: inactivated SHXX1902-P5-vaccinated group 1 ($n$ = 3), group 2, treated with a commercial AJ1102 vaccine ($n$ = 3), and a strict negative control group 3 ($n$ = 1). A multiple-dose PEDV homologous vaccination schedule at bi-weekly intervals, starting before farrowing, was followed in this vaccination study. As the commercial vaccine was immunized according to the instructions, our isolates were not attenuated completely and were inactivated to immunize pigs. The three sows in group 1 were intramuscularly administered twice with a 1-ml dose of SHXX1902-P5 ($10^{4.5}$ $TCID_{50}$/ml) at 35 and 21 days prepartum. The three sows in group 2 were vaccinated with an attenuated vaccine and an inactivated vaccine AJ1102 (Wuhan Keqian Biology Co., Ltd., Wuhan, China). The strict negative control group 3 ($n$ = 1) was used. All the sows were monitored daily for clinical changes and adverse effects following vaccination. Blood samples were collected from the vaccinated sows on days 0, 7, 14, 21, 28, 35, and 49 after the first immunization. Colostrum was collected, and milk was collected on days 3, 5, and 7 after farrowing.

## Reverse Transcriptase-Quantitative Real-Time PCR

Reverse transcriptase-quantitative real-time PCR (RT-qPCR) was performed with the One Step PrimeScript RT-PCR Kit (TaKaRa, Japan). A PEDV isolate with a known infectious titer was serially diluted 10-fold to generate a standard curve for each PCR. The samples' viral concentrations ($TCID_{50}$/mL) were calculated based on the standard curve. The mean $Ct$ values were calculated for the PCR-positive samples, and the mean viral titers were calculated based on all the piglets within each group.

## Histopathology of the Small Intestines

Intestinal tissues and other major organs were grossly examined upon necropsy. Small intestinal tissue specimens (<3 mm thick) collected from each piglet were fixed in 10% formalin for 24 h at RT and embedded in paraffin according to standard laboratory procedures. The fixed samples were sent to Guangzhou Saville for histopathology.

## Porcine Epidemic Diarrhea Virus Enzyme-Linked Immunosorbent Assay

The sera's PEDV-specific immunoglobulin G (IgG) was detected with ID Screen® PEDV Indirect (IDvet, France). According to the supplier's protocol, the PEDV-specific IgA in sera and milk was detected with a PEDV IgA ELISA antibody kit (Anheal Diagnostic, Beijing, China).

## Porcine Epidemic Diarrhea Virus-Neutralizing Antibody Detection

The sera and milk samples were serially diluted. Then, 50 μl of PEDV strain SHXX1902-P5 ($2.0 \times 10^3$ $TCID_{50}$/ml) was added to an equal volume of the sera and milk samples. The mixture was then incubated for 1 h at 37°C and inoculated to a 96-well plate containing confluent Vero cells. After 2 h, the culture plate was washed with PBS three times, and then 100 μl of DMEM containing 2 μg/ml trypsin (Gibco, United States) was added. After 48 h, the neutralization titer was calculated as the reciprocal of the highest dilution of serum that inhibited virus-specific CPE in duplicate wells (Lee et al., 2017).

## Statistical Analysis

All values are expressed as means ± standard deviations (SD) of the means. The statistical significance of all differences was evaluated with Student's *t*-test in GraphPad Prism software version 5.0 (GraphPad Prism Inc., United States).

# RESULTS

## Virus Isolation and *in vitro* Characterization

Porcine epidemic diarrhea virus strains SHXX1902-P5 and SHXX1902-P35 induced cytopathic effects (CPEs) typical of PEDV infection, such as cell fusion, syncytium formation, and Vero cell detachment. The detection of PEDV antigens with immunofluorescence assay (IFA) using an anti-PEDV spike (S)-specific monoclonal antibody confirmed viral propagation. The cytoplasm displayed the distinct staining pattern associated with syncytium formation. Neither CPE nor S-specific monoclonal antibody staining in the mock-infected cells was detected. **Figure 1** shows CPE and corresponding IFA images in cells infected with passage P5 or P35. The SHXX1902-P5 and SHXX1902-P35 strains' titers were determined. SHXX1902-P5 titers ranged from $10^{5.11}$ to $10^{7.01}$ $TCID_{50}$/ml, while SHXX1902-P35 titers ranged from $10^{5.58}$ to $10^{7.09}$ $TCID_{50}$/ml. There was no significant difference between the titers of the two passages ($P > 0.05$).

## Comparative Virulence of Subcultured Strains

Each group (groups 1–5) of five piglets was challenged orally with 10-fold serially diluted ($10^{-3}$–$10^{-7}$) SHXX1902-P5 virus, whereas the control animals in group 6 were administered a cell culture medium. All five piglets in group 1 (infected with viral dilution $10^{-3}$) developed watery diarrhea (score 3) by 3 dpi, which persisted throughout the study. Three, three, and one piglet in groups 2, 3, and 4, respectively, infected with viral dilutions $10^{-4}$–$10^{-6}$, developed moderate-to-watery diarrhea (scores 2–3) by 3 dpi, which persisted throughout the study period (**Table 1**). In contrast, none of the five pigs in group 5 (infected with viral dilution $10^{-7}$) and those in the negative control group remained active and clinically unaffected throughout the 5-day experimental period. By 5 dpi, 100% of the piglets in group 1, 80% of those in group 2, 40% in group 3, and 20% of those in group 4 had died from PEDV-related clinical signs. The $PDD_{50}$ and $LD_{50}$ values for SHXX1902-P5 were determined indirectly and corresponded to theoretical cell culture infectious titers of $10^{2.0}$ and $10^{2.84}$ $TCID_{50}$/ml, respectively.

## Pathogenicity of SHXX1902 Virus in Neonatal Piglets

Animal infection experiments were performed to examine the changes in the *in vivo* viral phenotype associated with the serial *in vitro* passage of strain SHXX1902. The pathogenicity of SHXX1902-P5 and SHXX1902-P35 was characterized in piglets. Twelve piglets were divided into three groups of four animals, each was challenged orally with SHXX1902-P5 (group 1) or SHXX1902-P35 (group 2), and the remaining piglets in the control group received cell culture medium. The clinical signs were recorded daily, and fecal swabs were collected pre- and post-challenge for the duration of the study. During the acclimation period, all the piglets were active, showed no clinical symptoms, and had normal fecal consistency, and their feces contained no PEDV genetic material. After the challenge, none of the negative control piglets developed clinical presentations typical of PEDV throughout the study.

In contrast, the SHXX1902-P5-challenged piglets (group 1) displayed clinical signs, including loss of appetite and diarrheic feces, by 1 dpi and suffered lethal watery diarrhea with vomiting after that. One pig had diarrhea [fecal consistency (FC) score = 2], and the other three pigs had watery diarrhea (FC score = 3) by 1 dpi, which all persisted for 1–7 days. However, no piglets in the SHXX1902-P35-challenged group displayed clinical signs, such as loss of appetite or diarrheic feces, at 1 dpi. Only two of the four SHXX1902-P35-challenged piglets (group 2) displayed clinical signs, including loss of appetite and diarrheic feces, by 2 dpi, or suffered lethal watery diarrhea with vomiting after that (**Figure 2**).

By 1 dpi, all the animals in group 1 were positive for PEDV, as determined with RT-PCR, with mean *Ct* values of 15.78–19.33 (equivalent to $10^{4.07}$–$10^{5.77}$ $TCID_{50}$/ml), and shed significantly smaller amounts of PEDV in their feces with *Ct* values ranging from 20.80 to 22.35 ($10^{4.57}$–$10^{5.14}$ $TCID_{50}$/ml) until 7 dpi (**Figure 3**). No fecal shedding of PEDV was detected in any of the five piglets in group 2 at 1 dpi. PEDV was detected

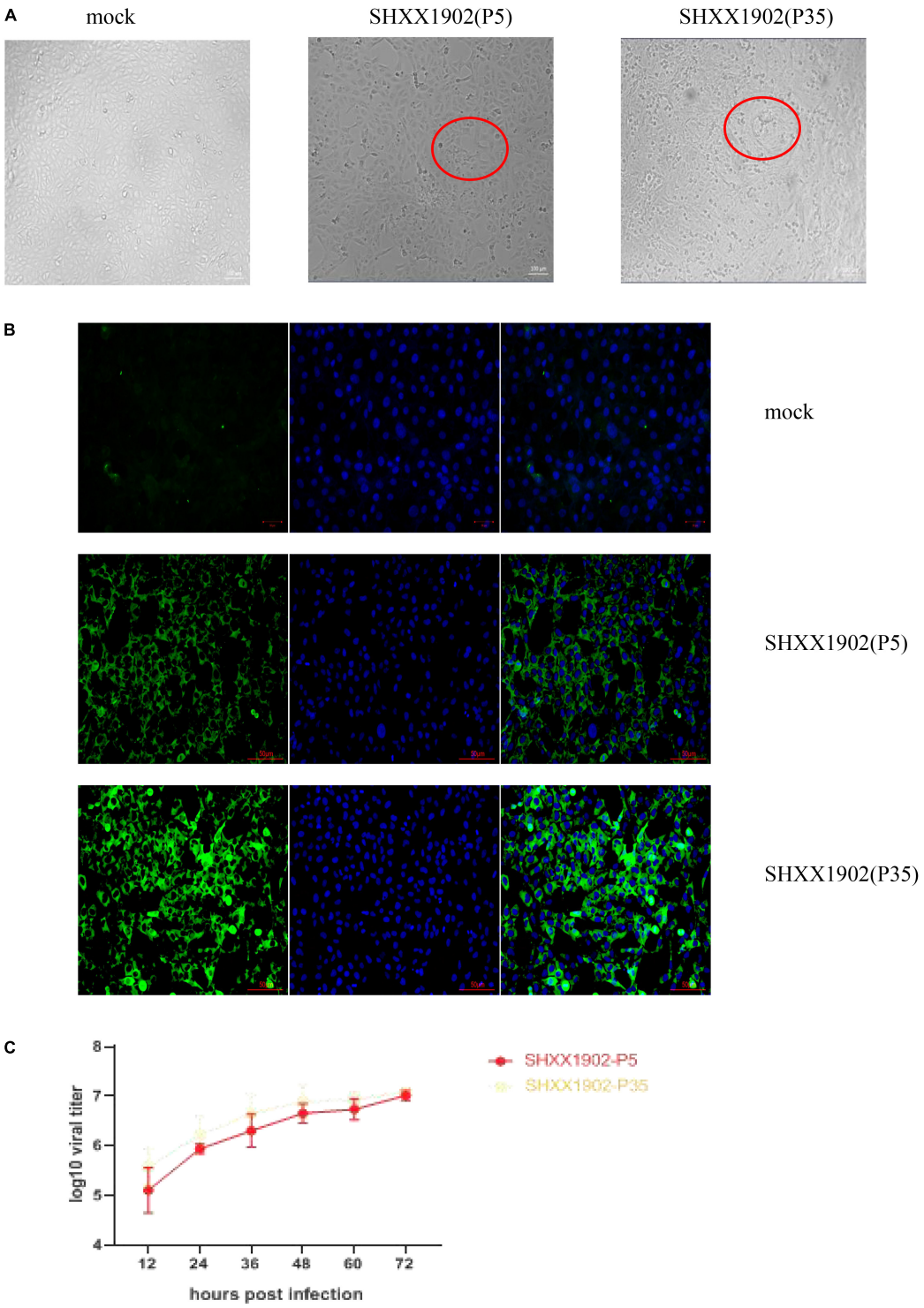


**FIGURE 1 |** Cytopathology and growth properties of PEDV SHXX1902. **(A)** CPE formation in Vero cells infected with strain SHXX1902-P5 or SHXX1902-P35. PEDV-specific CPE was observed daily, and the cells were photographed at 24 hpi using an inverted microscope at a magnification of ×200. The red circle indicates the CPE. **(B)** For immunostaining, infected cells were fixed at 24 hpi and incubated with a monoclonal antibody directed against the S protein and then with Alexa-green-conjugated goat anti-mouse secondary antibody. The cells were then examined under a fluorescence microscope at ×200 magnification. **(C)** One-step growth kinetics of SHXX1902-P5 and SHXX1902-P35. At the indicated time points post-infection, the culture supernatants were harvested from SHXX1902-P5-infected Vero cells, and the viral titers were determined. There was no significant difference between the titers of the two passages ($P > 0.05$). CPE, cytopathic effect; PEDV, porcine epidemic diarrhea virus; DAPI, 4,6-diamidino-2-phenylindole; TCID50, median tissue culture infectious dose.

**TABLE 1 |** Summary of pig groups, group numbers, inocula, and pig diarrhea and death outcomes after inoculation.

| Pig group | Pig numbers | Inoculum dilution* | Calculated inoculum infectious titers (log10 $TCID_{50}$/mL)† | Diarrhea (percent) | Death (percent) |
|---|---|---|---|---|---|
| Group 1 | 5 | $10^{-3}$ | 4 | 5/5 (100) | 5/5 (100) |
| Group 2 | 5 | $10^{-4}$ | 3 | 3/5 (60) | 4/5 (80) |
| Group 3 | 5 | $10^{-5}$ | 2 | 3/5 (60) | 2/5 (40) |
| Group 4 | 5 | $10^{-6}$ | 1 | 1/5 (20) | 1/5 (20) |
| Group 5 | 5 | $10^{-7}$ | 0 | 0/5 (0) | 0/5 (0) |
| Group 6 | 5 | Cell culture media | – | 0/5 (0) | 0/5 (0) |

*Each pig was inoculated orally with 1 mL of inoculum. †Titers were calculated based on the titer of the original viral pool and the fold dilution.*

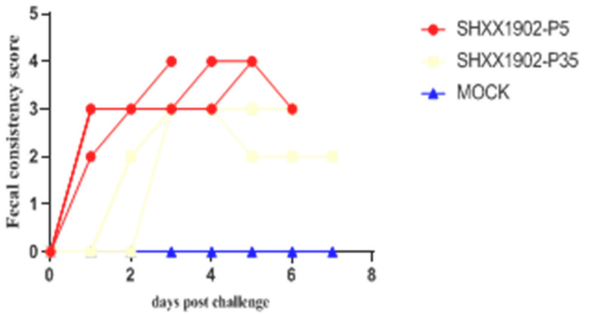


**FIGURE 2 |** Fecal consistency scores in piglets inoculated with PEDV SHXX1902-P5, SHXX1902-P35, or mock inoculated by 7 dpi. {0 = normal and no diarrhea [mean cycle threshold (*Ct*) values of >45]; 1 = mild and fluidic feces; 2 = moderate watery diarrhea; 3 = severe watery and projectile diarrhea [mean *Ct* values of <20]; and 4 = death}.

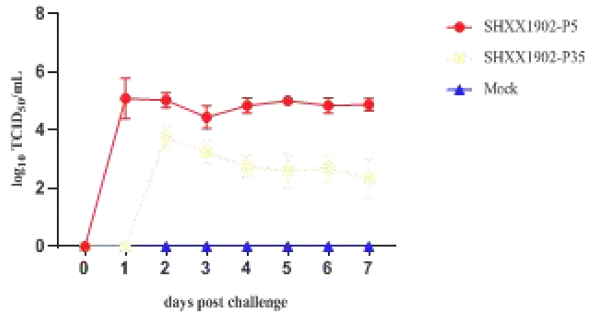


**FIGURE 3 |** Viral shedding in piglets inoculated with PEDV SHXX1902-P5, SHXX1902-P35, or mock inoculated. PEDV titers in rectal swab samples at each time point were determined with RT-qPCR. The viral titers (log10 $TCID_{50}$/ml) are the mean viral titers of all the piglets in each group, and error bars represent SD.

in only three piglets in group 2 at 2 dpi, with mean *Ct* values of 18.09–20.59 ($10^{3.11}$–$10^{4.03}$ $TCID_{50}$/ml), which decreased to the lowest level at 7 dpi. Overall, the quantities of virus in the feces of the group 2 animals were significantly lower than those in group 1, with a wide *Ct* range of 24.46–28.34 ($10^{1.50}$–$10^{3.16}$ $TCID_{50}$/ml) until the termination of the study, indicating the limited viral shedding (an almost 3-log reduction) of strain SHXX1902-P35. The negative control piglets remained active throughout the experimental period, with neither diarrhea nor fecal PEDV shedding.

At 3 dpi, two piglets from the three groups were necropsied. Neither macroscopic nor microscopic intestinal lesions were evident in the negative control piglets. The virulent SHXX1902-P5-infected piglets showed typical macroscopic gross PED-like lesions. Their small intestines were dilated with accumulated yellowish fecal fluid and had thin transparent walls resulting from villous atrophy, whereas their other internal organs appeared normal. In contrast, all the animals infected with SHXX1902-P35 (group 2) displayed markedly visible pathological lesions in their gastrointestinal tracts, albeit with normal bowel wall thickness, similar to that in the negative control group. Altogether, compared with strain SHXX1902-P5, SHXX1902-P35 showed weakened virulence with an attenuated phenotype in highly susceptible piglets under experimental conditions (**Figure 4A**). The microscopic assessment revealed the following: MOCK: The mucosa and submucosa bulged into the intestinal cavity to form more folds (black arrow); the lamina propria bulged into the intestinal cavity to form more intestinal villus structures (blue arrow); the intestinal villi were underdeveloped, differed in height, and were fat or thin, and the mucosal epithelium was complete. Some capillaries in the lamina propria were slightly congested (green arrow), and a small amount of lymphocyte infiltration was seen on top of a small number of intestinal villi (yellow arrow); the glands in the lamina propria were evenly distributed and closely arranged, and Pan's cells at the bottom had disappeared (red arrow). SHXX1902-P5: The lamina propria bulged into the intestinal cavity to form many intestinal villi (blue arrow). The intestinal villi were evenly distributed and long, and the mucosal epithelium was complete. A large number of capillaries in the lamina propria were congested and dilated (green arrow), and more lymphocyte infiltration was seen (yellow arrow); the glands of the lamina propria were loosely arranged, some were irregular in shape (black arrow), and Pan's cells at the bottom had disappeared. SHXX1902-P35: The mucosa and submucosa bulged into the intestinal cavity to form a small number of folds (black arrow), and the lamina propria bulged into the intestinal cavity to form a large number of intestinal villi (blue arrow). The intestinal villi were underdeveloped, differed in height, and were fat or thin, and the mucosal epithelium was complete. Some capillaries of the lamina propria were slightly congested (green arrow); the glands of the lamina propria were evenly distributed and closely arranged, and Pan's cells at the bottom had disappeared

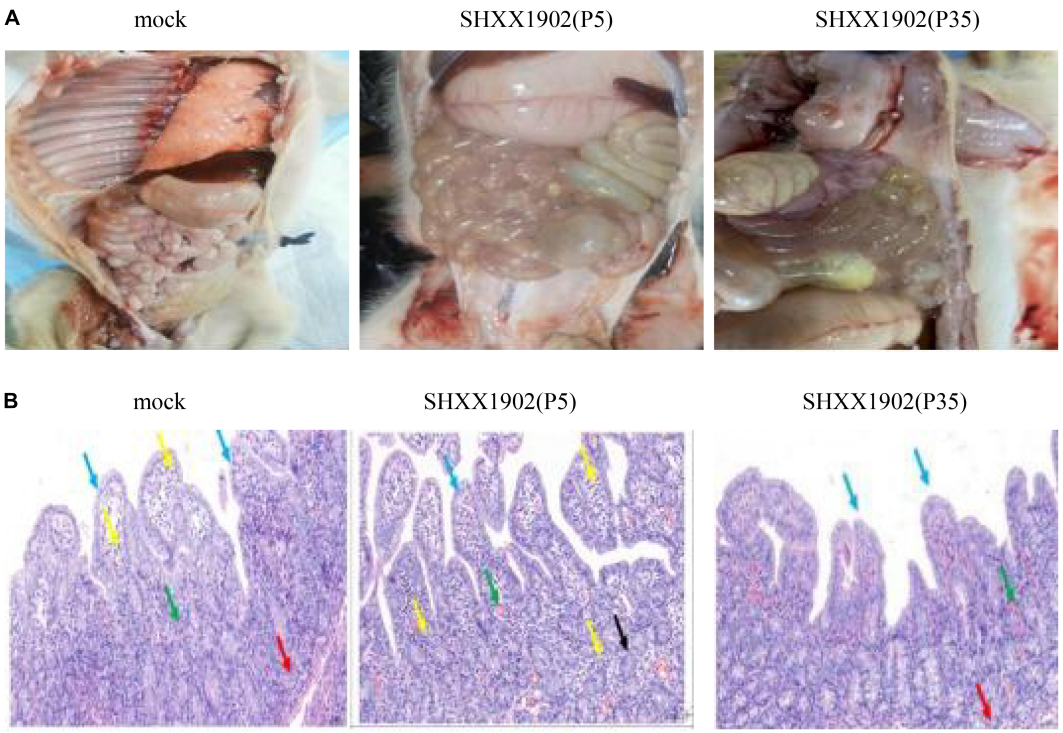


**FIGURE 4 |** Histopathological analysis. **(A)** Comparison of small intestinal lesions in different groups (mock, P5, and P35) at necropsy at 3 dpi. **(B)** Hematoxylin-and-eosin-stained jejunum tissue sections from the different groups at 3 dpi.

(red arrow); no obvious inflammatory cell infiltration was observed (**Figure 4B**).

## Protective Efficacy of the Inactivated SHXX1902-P5 Vaccine

To evaluate the protective efficacy of the inactivated SHXX1902-P5 strain, we used an intramuscular homologous prime-boost vaccination scheme, administered 2 weeks apart before farrowing. At 5 and 2 weeks pre-partum, the three sows in group 1 were primed and boosted with the AJ1102 vaccine, and the three sows in group 2 were orally primed and boosted with the inactivated SHXX1902-P5 strain. None of the sows in the unvaccinated group had any adverse reactions. At farrowing, there were no significant differences in the reproductive performance of the vaccinated and unvaccinated sows.

After the first immunization of sows, the serum IgG levels induced by SHXX1902-P5 and AJ1102 were similar. After the second immunization, the serum IgG titers increased (**Figure 5A**). However, the IgA levels induced by AJ1102 were higher than those induced by SHXX1902-P5 after the second immunization (**Figure 5B**). The IgA levels in the milk from the AJ1102-vaccinated sows were higher than those from the SHXX1902-P5-vaccinated sows on days 1 and 3. However, the IgA levels induced by SHXX1902-P5 and AJ1102 were similar on days 5 and 7 (**Figure 5C**).

The results of PEDV-neutralizing antibody tests showed that the neutralizing antibody levels of the two immunized groups gradually increased until 42 days after the first immunization. The neutralizing antibody titers in serum samples of the two immunized groups were comparable ($P > 0.05$, **Figure 6A**). There were no significant difference in the neutralizing antibody titer in the colostrum and the milk on the 7th day after farrowing between the two immunized groups ($P > 0.05$, **Figure 6B**).

# DISCUSSION

With the pandemic of the PEDV G2b strain ravaging the global swine industry, many novel G2b vaccines have been developed in China. Since 2010, G2c PEDV has spread throughout the world. Many novel G2b vaccines cannot provide sufficient protection against G2c PEDV strains in China on many pig farms. We first isolated the PEDV G2c field strain SHXX1902, which can be efficiently propagated in a Vero cell suspension to address this problem. The G2c isolate SHXX1902-P35 displayed similar growth characteristics to SHXX1902-P5 in terms of its cytopathology, infectious titer, and replication kinetics in Vero cells, as reported previously [9]. With whole-genome analyses, several of the strains circulating in China since 2015 (including XM2-4, CH/HNAY/2015, CH-HB2-2018, and JSCZ1601) have been shown to belong to the same subgroup (G2c) as SHXX1902-P5. However, the S gene of SHXX1902-P5 belongs to subgenotype G2a, whereas the whole genome of SHXX1902-P35 belongs to G2b. It has been reported that most viral mutations occur during extensive passaging of viruses in cell culture, and these

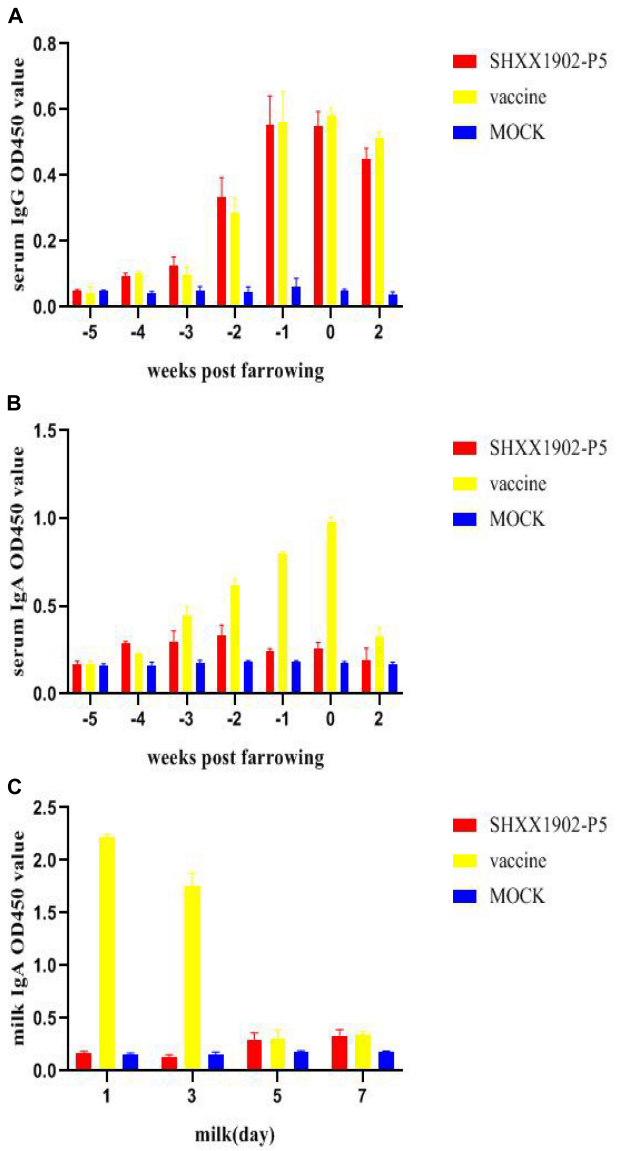


**FIGURE 5 |** Levels of PEDV-specific IgG and IgA antibodies in the serum and IgA antibodies in the milk of sows after immunization with different strains. Levels of PEDV-specific IgG antibodies in the serum **(A)**, IgA antibodies in the serum **(B)**, and IgA antibodies in the milk **(C)** were determined with ELISAs. All data are shown as means ± SD.

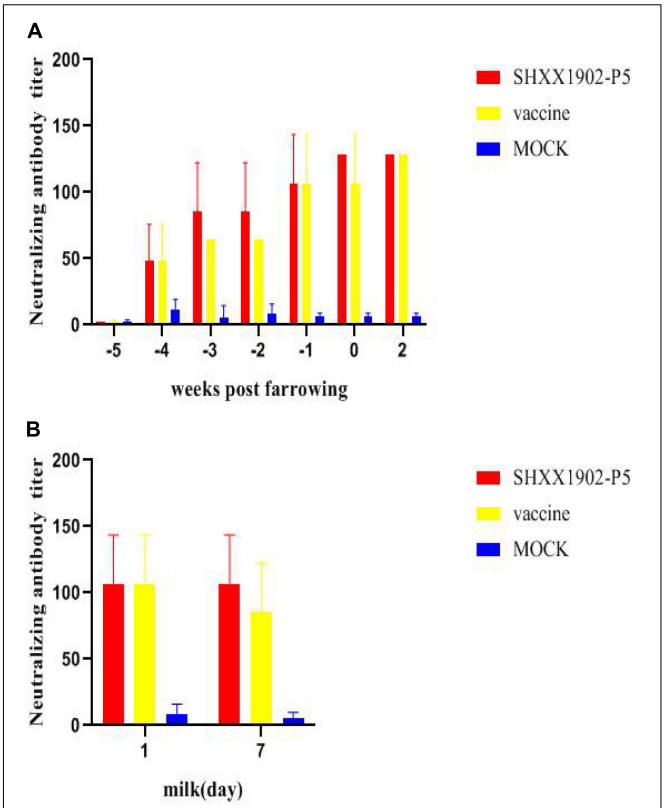


**FIGURE 6 |** Levels of neutralizing antibodies in the serum and the milk of sows after immunization with different strains. Levels of PEDV-specific neutralizing antibodies in the serum **(A)** and PEDV-specific neutralizing antibodies in the milk **(B)** were determined. All data are shown as means ± SD.

mutations have been correlated with viral attenuation. Therefore, we compared the pathogenicity of the two isolates, SHXX1902-P5 and SHXX1902-P35.

Strain SHXX1902-P5 caused earlier viral shedding (at 1 dpi), higher titers of shedding virus, more severe macroscopic and microscopic symptoms, and a higher death rate than strain SHXX1902-P35. However, SHXX1902-P35 still caused mild PEDV syndrome. Therefore, SHXX1902-P35 requires further attenuation before its preparation as an attenuated vaccine. Noticeably, strain SHXX1902-P35 had changed into the G2b subtype. Therefore, to prevent G2c PEDV infection, we selected SHXX1902-P5 and constructed an inactivated vaccine based on the P5 virus.

Paudel et al. (2014) reported that PEDV-negative sows were given one of four vaccine treatments: no vaccination (control group); vaccination with a killed virus, with a killed virus booster (K/K); vaccination with a live virus, with a live virus booster (L/L); and vaccination with a live virus, with a killed virus booster (L/K). All the sows were vaccinated intramuscularly twice, at 5 and 3 weeks before farrowing. The group treated with the K/K strategy had the highest IgG, IgA, and neutralizing antibodies in their sow sera, colostrum, and piglet sera, with the lowest levels in the L/L group. However, in our study, the IgA titer after the L/K treatment was much higher than that in the K/K colostrum and milk on day 3 after farrowing. As the second immunization of AJ1102 was an attenuated vaccine, it can induce mucosal immunity.

In the first reported experimental study of a US PEDV isolate in sows, four sows from a herd naturally infected with a mild SINDEL strain of PEDV were used. As we all know, G2c PEDV is also called the "SINDEL" strain. At about 3 days of age, their piglets were orally challenged with the virulent virus. All the piglets from the PEDV-positive sows survived this challenge, whereas those from the PEDV-naive sows experienced a 33% mortality rate (Goede et al., 2015). That study demonstrated that

the SINDEL strain of PEDV could produce lactogenic immunity and provide the direction of oral vaccine using our isolated strain. Lactogenic immunity is described as the continuous supply of passively acquired immunoglobulins through the ingestion of colostrum and milk. IgG is dominant in colostrum and is transudate from sow serum for piglet protection. SIgA is dominant in milk (Langel et al., 2016). In our study, the IgG titers were similar in the AJ1102- and SHXX1902-P5-vaccinated sows, from the first day after vaccination to 14 days after farrowing. Therefore, our strain is also a promising vaccine candidate against SINDEL strains.

Porcine epidemic diarrhea virus mainly infects the intestines of young piglets, with transient viremia in the serum (Jung et al., 2014). Therefore, mucosal immunity in neonates at birth and throughout the nursing period is important. Suckling piglets *via* colostrum and milk is crucial for their immediate protection against PEDV. It has been reported that the protection level is associated with the antibodies in the milk, but not those in the serum, of the sows (Bohl et al., 1972; Saif et al., 1972; Bohl and Saif, 1975). The injection of an inactivated vaccine or organization of own vaccine induces the non-mucosal immune pathway and does not produce secretory IgA (sIgA). The injection of a live or a purified live virus entails the same problems as the injection of an inactivated vaccine. Oral live vaccines are greatly affected by pepsin, and this effect may vary across strains. The intramuscular injection only improves the single-chain variable fragment (scFv) level in the colostrum and does not induce sIgA. The existence of the blood–milk barrier means that scFv can only neutralize some free viruses in the colostrum stage. In the present study, the IgA titer declined rapidly in the milk immunized with AJ1102 by day 5 after farrowing, which is consistent with the existence of the blood–milk barrier. Bohl and Saif (1975) discovered the gut–mammary–sIgA axis (Langel et al., 2016), explaining why sows naturally infected or orally infected with live TGEV and recovered from the virus had persistently high levels of sIgA antibodies in their milk, which protected their piglets from TGEV infection. Therefore, the induction of the mucosal immune pathway is a promising strategy. However, the neutralizing antibody titer of serum can reach 1:128 after the farrowing day in all immunized sows. The neutralizing antibody titer of colostrum and milk at day 7 was 1:85 or 1:107. As a result, our isolated strain was a promising candidate strain.

## DATA AVAILABILITY STATEMENT

The original contributions presented in the study are included in the article/supplementary material, further inquiries can be directed to the corresponding author.

## ETHICS STATEMENT

The animal study was reviewed and approved by Shanghai Animal Diseases Prevention and Control Center.

## AUTHOR CONTRIBUTIONS

F-FG: conceptualization and writing—original draft preparation. H-XS, D-QY, and XL: methodology. H-BJ, JW, and H-JZ: formal analysis and investigation. F-FG and L-SK: writing—review and editing. All authors contributed to the article and approved the submitted version.

## FUNDING

F-FG was supported by the Natural Science Foundation of Shanghai [No. 2021(04713)]. JW was supported by the 2018 Shanghai Outstanding Agricultural Academic Leaders Plan.

## REFERENCES

Bohl, E. H., Gupta, R. K., Olquin, M. V., and Saif, L. J. (1972). Antibody responses in serum, colostrum, and milk of swine after infection or vaccination with transmissible gastroenteritis virus. *Infect. Immun.* 6, 289–301. doi: 10.1128/iai.6.3.289-301.1972

Bohl, E. H., and Saif, L. J. (1975). Passive immunity in transmissible gastroenteritis of swine: immunoglobulin characteristics of antibodies in milk after inoculating virus by different routes. *Infect. Immun.* 11, 23–32. doi: 10.1128/iai.11.1.23-32.1975

Ge, F. F., Yang, D. Q., Li, X., Ju, H. B., Shen, H. X., Liu, J., et al. (2021). Novel Method for Isolation of Porcine Epidemic Diarrhea Virus with the Use of Suspension Vero Cells and Immunogenicity Analysis. *J. Clin. Microbiol.* 59, e2156–e2120. doi: 10.1128/JCM.02156-20

Goede, D., Murtaugh, M. P., Nerem, J., Yeske, P., Rossow, K., and Morrison, R. (2015). Previous infection of sows with a "mild" strain of porcine epidemic diarrhea virus confers protection against infection with a "severe" strain. *Vet. Microbiol.* 176, 161–164. doi: 10.1016/j.vetmic.2014.12.019

Guo, J., Fang, L., Ye, X., Chen, J., Xu, S., Zhu, X., et al. (2019). Evolutionary and genotypic analyses of global porcine epidemic diarrhea virus strains. *Transbound. Emerg. Dis.* 66, 111–118. doi: 10.1111/tbed.12991

Huang, Y. W., Dickerman, A. W., Piñeyro, P., Li, L., Fang, L., Kiehne, R., et al. (2013). Origin, evolution, and genotyping of emergent porcine epidemic diarrhea virus strains in the United States. *mBio* 4, e737–e713. doi: 10.1128/mBio.00737-13

Jung, K., Wang, Q., Scheuer, K. A., Lu, Z., Zhang, Y., and Saif, L. J. (2014). Pathology of US porcine epidemic diarrhea virus strain PC21A in gnotobiotic pigs. *Emerg. Infect. Dis.* 20, 662–665. doi: 10.3201/eid2004.131685

Langel, S. N., Paim, F. C., Lager, K. M., Vlasova, A. N., and Saif, L. J. (2016). Lactogenic immunity and vaccines for porcine epidemic diarrhea virus (PEDV): historical and current concepts. *Virus Res.* 226, 93–107. doi: 10.1016/j.virusres.2016.05.016

Lee, C. (2015). Porcine epidemic diarrhea virus: an emerging and re-emerging epizootic swine virus. *Virol. J.* 12:193. doi: 10.1186/s12985-016-0465-y

Lee, D. K., Park, C. K., Kim, S. H., and Lee, C. (2010). Heterogeneity in spike protein genes of porcine epidemic diarrhea viruses isolated in Korea. *Virus Res.* 149, 175–182. doi: 10.1016/j.virusres.2010.01.015

Lee, S., and Lee, C. (2014). Outbreak-related porcine epidemic diarrhea virus strains similar to US strains, South Korea, 2013. *Emerg. Infect. Dis.* 20, 1223–1226. doi: 10.3201/eid2007.140294

Lee, S., Son, K. Y., Noh, Y. H., Lee, S. C., Choi, H. W., Yoon, I. J., et al. (2017). Genetic characteristics, pathogenicity, and immunogenicity associated with cell

adaptation of a virulent genotype 2b porcine epidemic diarrhea virus. *Vet. Microbiol.* 207, 248–258. doi: 10.1016/j.vetmic.2017.06.019

Oh, J., Lee, K. W., Choi, H. W., and Lee, C. (2014). Immunogenicity and protective efficacy of recombinant S1 domain of the porcine epidemic diarrhea virus spike protein. *Arch. Virol.* 159, 2977–2987. doi: 10.1007/s00705-014-2163-7

Paarlberg, P. (2014). *Updated Estimated Economic Welfare Impacts of Porcine Epidemic Diarrhea Virus(PEDV). Working Papers*. West Lafayette: Purdue University.

Paudel, S., Park, J. E., Jang, H., Hyun, B. H., Yang, D. G., and Shin, H. J. (2014). Evaluation of antibody response of killed and live vaccines against porcine epidemic diarrhea virus in a field study. *Vet. Q.* 34, 194–200. doi: 10.1080/01652176.2014.973999

Saif, L. J., Bohl, E. H., and Gupta, R. K. (1972). Isolation of porcine immunoglobulins and determination of the immunoglobulin classes of transmissible gastroenteritis viral antibodies. *Infect. Immun.* 6, 600–609. doi: 10.1128/iai.6.4.600-609.1972

Wang, L., Byrum, B., and Zhang, Y. (2014). New variant of porcine epidemic diarrhea virus, United States, 2014. *Emerg. Infect. Dis.* 20, 917–919. doi: 10.3201/eid2005.140195

Wood, E. N. (1977). An apparently new syndrome of porcine epidemic diarrhoea. *Vet. Rec.* 100, 243–244. doi: 10.1136/vr.100.12.243

**Conflict of Interest:** The authors declare that the research was conducted in the absence of any commercial or financial relationships that could be construed as a potential conflict of interest.

**Publisher's Note:** All claims expressed in this article are solely those of the authors and do not necessarily represent those of their affiliated organizations, or those of the publisher, the editors and the reviewers. Any product that may be evaluated in this article, or claim that may be made by its manufacturer, is not guaranteed or endorsed by the publisher.

*Copyright © 2022 Ge, Kang, Shen, Shen, Yang, Li, Ju, Zhao and Wang. This is an open-access article distributed under the terms of the Creative Commons Attribution License (CC BY). The use, distribution or reproduction in other forums is permitted, provided the original author(s) and the copyright owner(s) are credited and that the original publication in this journal is cited, in accordance with accepted academic practice. No use, distribution or reproduction is permitted which does not comply with these terms.*

frontiers | Frontiers in Microbiology

ORIGINAL RESEARCH
published: 26 April 2022
doi: 10.3389/fmicb.2022.845546

# Molecular Evidence of Orthomyxovirus Presence in Colombian Neotropical Bats

*Manuel Uribe*[1,2], *Miguel E. Rodríguez-Posada*[3] *and Gloria C. Ramirez-Nieto*[1]*

[1] *Microbiología y Epidemiologia Research Group, Facultad de Medicina Veterinaria y de Zootecnia, Universidad Nacional de Colombia, Bogotá, Colombia,* [2] *CIBAV Research Group, Veterinary Medicine School, Universidad de Antioquia, Medellín, Colombia,* [3] *Research Center Fundación Reserva Natural La Palmita, Grupo de Investigaciones Territoriales Parael uso y Conservación de la Biodiversidad, Trinidad, Colombia*

The Orthomyxoviridae family includes the genera Influenzavirus, Isavirus, Quaranjavirus, and Thogotovirus. In turn, Influenzavirus can be classified into four types: α, β, γ, and δ (Formerly A, B, C, and D), from which Alphainfluenzavirus (AIV) has the broadest host range, including birds, mammals, reptiles, and amphibians. Additionally, AIV has shown global epidemiological relevance owing to its pandemic potential. The epidemiological relevance of Chiropteran due to its multiple functional characteristics makes them ideal reservoirs for many viral agents. Recently, new influenza-like subtypes have been reported in Neotropical bats, but little is known about the relevance of bats as natural reservoirs of influenza viruses. Therefore, the current study aimed to determine the presence of AIV and new influenza-like subtypes in South American bats. For a better understanding of the drivers and interactions between AIV and bats, we used molecular assays with different gene targets (i.e., M, NP, and PB1) to identify AIV in New World bats. A housekeeping gene (CytB) PCR was used to check for nucleic acid preservation and to demonstrate the bat-origin of the samples. A total of 87 free-living bats belonging to 25 different species of the families Phyllostomidae and Vespertilionidae were collected in Casanare, Colombia. As a result, this study found seven AIV-positive bat species, three of them reported for the first time as AIV prone hosts. Neither of the AIV-like analyzed samples were positive for $H_{17}N_{10}/H_{18}/N_{11}$ subtypes. Although additional information is needed, the presence of a completely new or divergent AIV subtype in neotropical bats cannot be discarded. Collectively, the results presented here expand the epidemiological knowledge and distribution of AIV in neotropical free-ranging bats and emphasize the need to continue studying these viruses to establish the role they could play as a threat to animal and public health.

**Keywords: Orthomyxovirus, Alphainfluenzavirus, bat-virus, influenza, Colombia**

OPEN ACCESS

***Edited by:***
*Douglas Paul Gladue, Plum Island Animal Disease Center, Agricultural Research Service (USDA), United States*

***Reviewed by:***
*Junki Maruyama, University of Texas Medical Branch at Galveston, United States*
*Arun Saravanakumar Annamalai, University of Colorado Denver, United States*

***Correspondence:**
*Gloria C. Ramirez-Nieto*
*gcramirezn@unal.edu.co*

***Specialty section:***
*This article was submitted to Virology, a section of the journal Frontiers in Microbiology*

***Received:*** *29 December 2021*
***Accepted:*** *25 March 2022*
***Published:*** *26 April 2022*

***Citation:***
*Uribe M, Rodríguez-Posada ME and Ramirez-Nieto GC (2022) Molecular Evidence of Orthomyxovirus Presence in Colombian Neotropical Bats. Front. Microbiol. 13:845546. doi: 10.3389/fmicb.2022.845546*

## INTRODUCTION

Orthomyxoviridae is a family of enveloped negative-sense single-stranded RNA (-ssRNA) viruses (Shaw and Palese, 2013) composed of seven genera. The Quaranjavirus and Thogotovirus, both Arboviruses transmitted by ticks, mainly infect wildlife (L'vov et al., 2014; Kosoy et al., 2015; Ballard et al., 2017), Isavirus causes infectious anemia in salmonids (Batts et al., 2017), and

Influenzavirus, the epidemiologically more relevant genus, which includes four types: α, β, γ, and δ (formerly known as A, B, C, and D). These types are determined by specific characteristics of matrix protein 1 (M1) and the nucleoprotein (NP) genes (Palese and Young, 1982; Tobita, 1997; Sanjuan et al., 2009). Within these, Alphainfluenzavirus (AIV) have shown global epidemiological relevance (Messenger et al., 2014) owing to the pandemic potential (Taubenberger and Morens, 2010) and a wide range of susceptible hosts among wild birds and poultry (Causey and Edwards, 2008; Gonzalez-Reiche and Perez, 2012) terrestrial felines, canines, equids (Keawcharoen and Oraveerakul, 2004; Parrish et al., 2015; Zhou et al., 2015; Xie et al., 2016), swine and humans (Rose et al., 2013), as well as marine mammals (Ohishi et al., 2006; Blanc et al., 2009; Ramis et al., 2012; Boyce et al., 2013; Groth et al., 2014), the Amphibia and Reptilia Class (Mancini et al., 2004; Davis and Spackman, 2008; Temple et al., 2015), and bats in which new influenza-*like* subtypes have been reported (Tong et al., 2012, 2013). On the other hand, Beta and Gammainfluenzavirus cause a mild to moderate disease in humans (Taubenberger and Morens, 2008) and they can also infect seals and swine, respectively (Kimura et al., 1997; Osterhaus et al., 2000). Finally, Deltainfluenzavirus, the newest genus, was recently identified in ruminants and swine (Hause et al., 2014; Ferguson et al., 2015; Ng et al., 2015; Quast et al., 2015; Salem et al., 2017).

The order Chiroptera has approximately 1,224 species distributed all over the world (Wilson and Reeder, 2005; Fenton and Simmons, 2015), comprising approximately 25% of mammalian species and, thus, the second most biodiverse order in animal kingdom (Mickleburgh et al., 2002; Burgin et al., 2018). Bats are unique among mammals with remarkable diversity, global distribution, and accumulated flight distances of up to 2,518 km (Fleming and Peggy, 2006; Richter and Cumming, 2008). These characteristics together with unique anatomo-physiological, biological, and etiological features, make them ideal natural reservoirs and key pieces of the eco-epidemiological dynamics of several emergents and reemerging viral infectious diseases linked to human spillovers (Omatsu et al., 2007; Wong and Lau, 2009; Wang et al., 2011; Chan et al., 2013; O'Shea et al., 2014; Brook and Dobson, 2015; Han et al., 2015; Allocati et al., 2016; Plowright et al., 2016). Approximately 61% of human diseases are considered zoonotic and wildlife reservoirs are the source of most human emerging infectious diseases (Taylor et al., 2001; Childs et al., 2007). It is well-known that many viral pathogens have arisen through adaptation and/or cross-species transmission events. Bat-associated viruses database (DBatVir)[1] and other authors report around 30 viral families identified in bat species (**Table 1**) (Chen et al., 2014). Otherwise, global search on bat viruses resulted in the detection and sometimes isolation of over 200 viruses from almost all viral families, thus, suggesting that bats may harbor substantial diversity of viruses rivaling or even surpassing viral diversity found in rodents (Misra, 2020). Despite decades of research into bats and associated pathogens, the bat-virus ecology and molecular biology remain still quite unexplored, with many questions largely unsolved (Letko et al., 2020). There have been several major bat-borne viruses outbreaks such as Hendra, Sosuga, Nipah, Marburg, and Ebola virus diseases, the severe acute respiratory syndrome (SARS-CoV), Middle East respiratory coronavirus (MERS-CoV), and the most recent SARS-CoV-2 virus responsible for the last pandemic, along with the report of two influenza-*like* viruses (Orthomyxoviridae) in South American bats, the $H_{17}N_{10}/H_{18}/N_{11}$ subtypes, which were identified by NGS methodologies in 2012. These two new bats-derived influenza-*like* viruses show different specific structural features affecting sialic acid receptor binding capability making them different from avian or human influenza viruses. To determine whether there is a risk for reassortment, and therefore a major concern about potential influenza pandemics originating from unknown bat origin viruses including orthomyxoviruses, it is necessary to establish the spectrum of viral diversity that exists in the mammalian species of order Chiroptera (Tong et al., 2013; Letko et al., 2020; Irving et al., 2021).

Despite advances to understand the viral dynamics of new influenza-*like* subtypes in bats (Dlugolenski et al., 2013; Aguiar et al., 2016; Ciminski et al., 2017) and characterization of different genomic segments (Garcia-Sastre, 2012; Sun et al., 2013; Zhu et al., 2013; Juozapaitis et al., 2014; Poole et al., 2014; Tefsen et al., 2014; Turkington et al., 2015; Hoffmann et al., 2016; Maruyama et al., 2016), the eco-epidemiology of those viral subtypes remains poorly understood due to sparse reports of influenza-like positive bat species and a lack of studies across Neotropics. Therefore, the present study aims to determine the presence of AIV and influenza-*like* subtypes in Colombian bats through molecular techniques as an approach to contribute to the knowledge of the neotropical distribution of this viral agent.

# MATERIALS AND METHODS

## Studied Areas and Animal Sampling

Different populations of free-ranging bats were investigated in two highly biogeographically divergent regions. The first sampling area was in the south-southwest amazon rainforest biome in the Putumayo department and the second was in the east-southeast floodable savannas of Orinoco Basin (**Figure 1**). The study was conducted from January 2016 to December 2017. A total of 87 wild free-ranging Yangochiroptera bats were captured by mist-netting and manually collected. Thereafter, the bats were morphologically identified and classified into species based on taxonomic keys on external and craniodental morphology by a specialist mastozoologist (**Table 2**). The collected bats were healthy and showed no signs of disease. Next, oropharyngeal, and rectal samples were collected separately by deep swabbing using CLASSIQSwabs™ (Copan) from each bat. Swab samples were preserved in FTA™ classic cards (Whatman™), and RNAlater™ (Invitrogen™), incubated at 4°C overnight, and stored at −80°C until further molecular assays were performed. Additionally, tissue samples were collected.

[1] http://www.mgc.ac.cn/DBatVir/

**TABLE 1 |** Worldwide viral families reported in bat species.

| Viral genome[¥] | | | | | |
|---|---|---|---|---|---|
| **-ssRNA** | **+ssRNA** | **dsDNA** | **ssDNA** | **RT-Virus** | **dsRNA** |
| Arenaviridae[§] | Astroviridae | Adenoviridae | Anelloviridae | Hepadnaviridae | Reoviridae |
| Bornaviridae | Caliciviridae | Asfarviridae[†] | Circoviridae | Retroviridae | Picobirnaviridae[‡] |
| Filoviridae | Coronaviridae | Herpesviridae | Parvoviridae | | |
| Hantaviridae | Flaviviridae | Papillomaviridae | | | |
| Nairoviridae | Hepeviridae | Polyomaviridae | | | |
| Orthomyxoviridae | Picornaviridae | Poxviridae | | | |
| Paramyxoviridae | Togaviridae | | | | |
| Peribunyaviridae | | | | | |
| Phenuiviridae | | | | | |
| Rhabdoviridae | | | | | |

[¥] *Viral classification according to Koonin et al. (2021),* [§] *Cogswell-Hawkinson et al. (2012),* [†] *Hu et al. (2017), and* [‡] *Dacheux et al. (2014). -ssRNA, negative-sense single-stranded RNA; +ssRNA, positive sense-single-stranded RNA; dsDNA, double stranded DNA; ssDNA, single stranded DNA; RT-Virus, reverse transcriptase; dsRNA, double-strand RNA.*

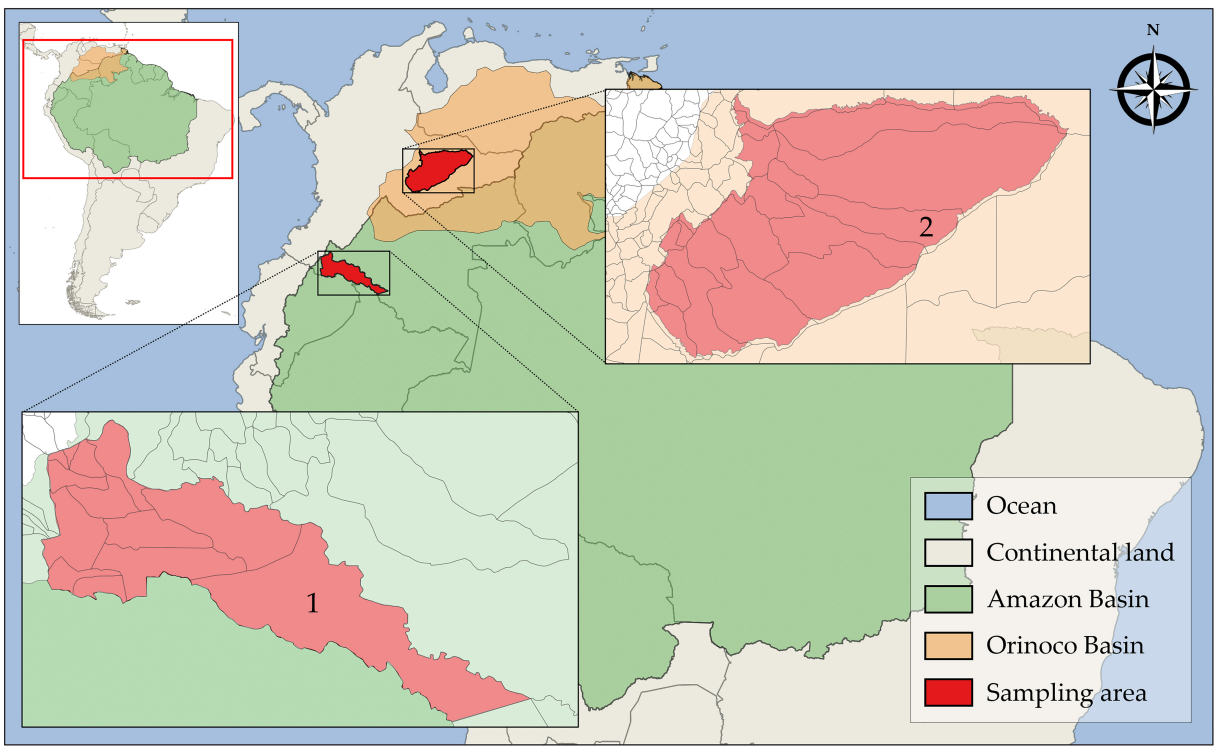


**FIGURE 1 |** Geographic location of sampling areas in the Amazon and Orinoco Basins. (1) Puerto Leguízamo, Putumayo and (2) Trinidad, Casanare.

## Total Nucleic Acid Extraction

Total ribonucleic acid (TRA) from swabs was obtained using the high throughput QIAamp™ Viral RNA Mini Kit (Qiagen™) following the manufacturer's instructions. Previous to the TRA extraction protocol from FTA™ card samples, 6 mm diameter disks were excised and incubated in TE buffer overnight (Sakai et al., 2015) at 4°C (Ndunguru et al., 2005) in absolute darkness. Likewise, RNAlater™ preserved swabs were temperate and gently homogenized by vortex in phosphate-buffered solution previous RNA extraction. All TRA samples were used immediately for molecular assays. High Pure Viral Nucleic Acid Kit (Roche™) was used for tissue total nucleic acid extraction.

## Housekeeping Gene Assay

Small mammal Cytochrome B gene was used as a housekeeping gene. For this purpose, a PCR method with a set of primers designed to amplify a 946 bp highly conserved region of this gene was used. The sequence of universal degenerated

**TABLE 2 |** Complete list of Yangochiroptera bat specimens collected.

| Family | Genus | Species | Diet (food source) | (*n*) |
|---|---|---|---|---|
| Phyllostomidae | *Anoura* | *caudifer* | O | 1 |
| Phyllostomidae | *Artibeus* | *lituratus* | F | 6 |
| Phyllostomidae | *Artibeus* | *planirostris* | F | 2 |
| Phyllostomidae | *Carollia* | *brevicauda* | F/I | 6 |
| Phyllostomidae | *Carollia* | *castanea* | F/I | 1 |
| Phyllostomidae | *Carollia* | *perspicillata* | 0 | 23 |
| Phyllostomidae | *Desmodus* | *rotundus* | H | 1 |
| Vespertilionidae | *Eptesicus* | *chiriquinus* | I | 2 |
| Phyllostomidae | *Gardnerycteris*[§] | *crenulatum* | C/I | 4 |
| Phyllostomidae | *Lonchophylla* | sp. | N | 2 |
| Phyllostomidae | *Lophostoma* | *brasiliense* | O | 2 |
| Phyllostomidae | *Mesophylla* | *macconnelli* | F | 1 |
| Vespertilionidae | *Myotis* | sp. nov. | I | 3 |
| Phyllostomidae | *Phyllostomus* | *discolor* | O | 1 |
| Phyllostomidae | *Phyllostomus* | *hastatus* | O | 1 |
| Phyllostomidae | *Phyllostomus* | *elongatus* | O | 3 |
| Phyllostomidae | *Platyrrhinus* | *brachycephalus* | F | 7 |
| Phyllostomidae | *Platyrrhinus* | *helleri* | F | 1 |
| Phyllostomidae | *Rhinophylla* | *fischerae* | F | 4 |
| Phyllostomidae | *Rhinophylla* | *pumilio* | F/I | 2 |
| Phyllostomidae | *Sturnira* | *tildae* | F | 1 |
| Phyllostomidae | *Sturnira* | *lilium* | F | 7 |
| Phyllostomidae | *Tonatia* | *saurophila* | O | 2 |
| Phyllostomidae | *Trachops* | *cirrhosus* | C/I | 3 |
| Phyllostomidae | *Vampyriscus* | *bidens* | F | 1 |

[§]*Synonym Mimon sp. O, omnivorous; F, frugivorous; I, insectivorous; H, hematophagous; C, carnivorous; N, nectarivore.*

primers was: CytBUnifw 5′-TCATCMTGATGAAAYTTYGG-3′ and CytBUnirev 5′-ACTGGYTGDCCBCCRATTCA-3′, amplification conditions were adapted from Schlegel et al. (2012) and performed in a Labcycler Gradient (SensoQuest™ GmbH).

## Polymerase Chain Reaction Assays for Alphainfluenzavirus Detection

To assess AIV detection in oropharyngeal and rectal swabs, a fluorogenic real-time reverse transcription-polymerase chain reaction (RT-qPCR) targeting a highly conserved region of the M gene was applied. The set of primers and probes used were: IndiForward 5′-GACCRATCCTGTCACCTCTGAC-3′, InfAReverse 5′- AGGGCATTYTGGACAAAKCGTCTA-3′, and InfAProbe 5′-TGCAGTCCTCGCTCACTGGGCACG-3′ (CDC., 2009). The amplification procedure consisted of 30 min at 50°C, followed by 2 min at 95°C, 50 cycles for 15 s at 95°C, and 30 s at 55°C, where fluorescence was collected. Samples were tested by triplicate in a 25 μL final reaction volume. Negative, positive, and non-template controls were included in all tested plates. For quantification of viral load and measure of the Cq threshold, at least two standard template dilutions of known viral concentration from a cloned M segment were included. Unknown viral copy number in samples was calculated from the external curve of known concentration templates analyzed on the same plate.

Additionally, we carry out the detection of influenza-like subtypes by RT-qPCR and endpoint RT-PCR. The RT-qPCR target a 90 bp segment of the nucleoprotein (NP) gene. The reactions were performed using the following specific primers and probes: GTMFluNPFor, GTMFluNPRev, and GTMFluNP probe (Tong, 2015). Thermic amplification conditions were: 30 min at 45°C, followed by 5 min at 94°C, 40 cycles for 15 s at 94°C, and 60 s at 60°C. RT-qPCR assays were performed in a LightCycler™ 480 Instrument II (Roche™) using Super-Script III™ Platinum One-step (Invitrogen™). The TaqMan™ probes were labeled at 5′-end with the 6-carboxyfluorescein reporter and Blackhole Quencher 1 (Biosearch Technologies™) at 3′-end. Based on viral concentration expected in the low cell concentration of cell-free swab samples, an increase of fluorescent signal below the 37 Cq threshold was selected as the cut-off value (Bustin et al., 2009; Bustin and Nolan, 2017). All RT-qPCR AIV results are in agreement with MIQE guidelines (Bustin et al., 2009; Bustin and Nolan, 2017) and RDML data standard[2] (Lefever et al., 2009).

The influenza-like PB1 gene-specific endpoint PCR, designed by Dr. Lucas Matías Ferreri (Department of Population Health, PDRC, UGA, United States) was performed after retrotranscription using Random Hexamer primers (Thermo Scientific™). The following set of PB1-specific primers was used: BatPB1-970For and BatPB1-1260Rev (available upon request). Reactions were performed in a Labcycler Gradient (SensoQuest™ GmbH) using the following amplification conditions: 2 min at 94°C, followed by 40 cycles for 15 s at 94°C, 15 s at 52°C, and 30 s at 72°C, with a final extension step of 30 s at 72°C. High sensibility SuperScript™ III One-Step RT-PCR System with Platinum™ Taq DNA Polymerase (Invitrogen™) was used. The pHW_Bat_NP and the pHW_Bat_PB1 DNA plasmid used as positive control were kindly provided by Dr. Daniel R. Pérez at the Department of Population Health, PDRC, UGA, United States.

# RESULTS

## CytB-Polymerase Chain Reaction as Bat Housekeeping Gene and Preservation Control

A total of 15 liver samples from different bat species of Phyllostomidae and Vespertilionidae bat families analyzed by CytB-PCR showed the expected 946 bp amplicon (**Figure 2**). Therefore, the results of this PCR assay from different bat species confirmed the chiropteran origin of the samples and the suitability of preserved nucleic acids for subsequent molecular assays.

## Alphainfluenzavirus RT-qPCR Assays

A total of 127 swab samples were analyzed by RT-qPCR in triplicates and given as positive when two or more replicates

[2]http://www.rdml.org

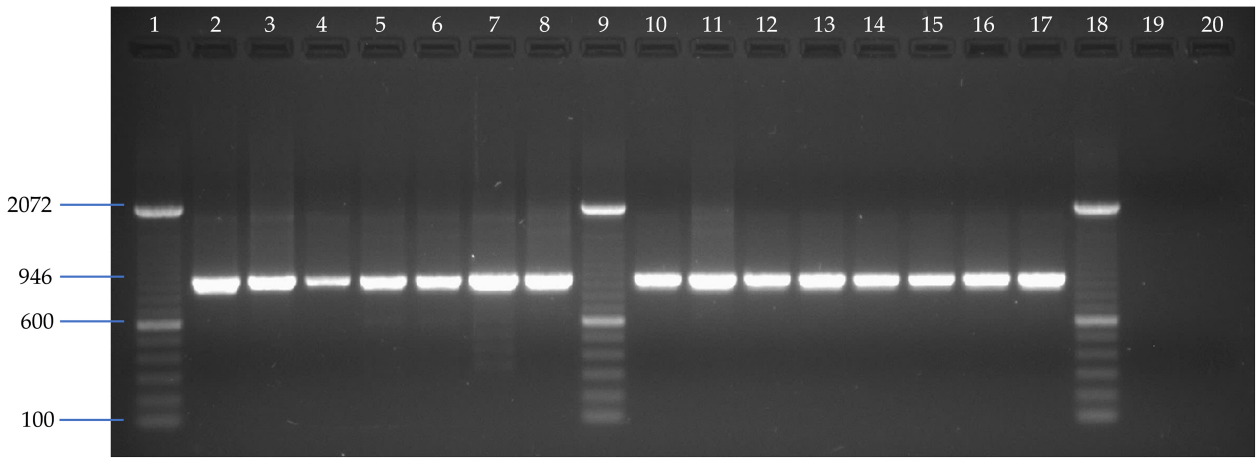


**FIGURE 2 |** Agarose gel electrophoresis of CytB-specific PCR amplified fragments assay. Line 1, 9, and 18: 100 bp DNA ladder (Invitrogen); Line 2: *Vampyriscus bidens*; Line 3: *Anoura caudifer*; Line 4: *Desmodus rotundus*; Line 5: *Carollia brevicauda*; Line 6: *Carollia castanea*; Line 7: *Lonchophylla* sp; Line 8: *Gardnerycteris crenulatum*; Line 10: *Tonatia saurophila*; Line 11: *Sturnira tildae*; Line 12: *Myotis* sp; Line 13: *Trachops cirrhosus*; Line 14: *Platyrrhinus brachycephalus*; Line 15: *Artibeus lituratus*; Line 16: *Eptesicus chiriquinus*; Line 17: *Mesophylla macconnelli*; Line 19 and 20: Negative controls from MDCK cell line and allantoic fluid from chicken embryonated SPF eggs, respectively.

**TABLE 3 |** Alphainfluenzavirus (AIV) positive samples by RT-qPCR assay.

| Species | Copy/reaction | OS | RS | R | F |
|---|---|---|---|---|---|
| *Gardnerycteris crenulatum* | $4{,}51 \times 10^2$ | x | x | x | |
| *Carollia brevicauda* | $1{,}88 \times 10^3$ | | x | | x |
| *Trachops cirrhosus* | $1{,}87 \times 10^3$ | | x | | x |
| *Platyrrhinus brachycephalus* | $1{,}95 \times 10^3$ | | x | | x |
| *Artibeus lituratus* | $1{,}86 \times 10^3$ | x | | | x |
| *Artibeus planirostris* | $6{,}32 \times 10^3$ | x | | | x |
| *Carollia perspicillata* | $4{,}10 \times 10^3$ | | x | | x |
| *Artibeus lituratus* | $6{,}30 \times 10^3$ | x | | | x |
| *Carollia perspicillata* | $6{,}62 \times 10^3$ | x | | | x |
| *Carollia perspicillata* | $5{,}09 \times 10^3$ | x | | | x |

*OS, Oropharyngeal swab; RS, Rectal swab; R, RNAlater-preserved; F, FTA-preserved.*

had a Cq less than or equal to 37 cycles. Quantification of cycle threshold (Cq) ranged from 34.17 to 37. Furthermore, the virus copy number per sample was determined using an eight-point standard curve. As a result, a total of 10 neotropical bat swab samples belonging to 7 different species were found positive for AIV by RT-qPCR assay (**Table 3**). The amount of AIV M gene segment and thus, the number of AIV viral particles by reaction varied from $4{,}51 \times 10^2$ in insectivorous *Gardnerycteris crenulated* from Putumayo to $6{,}62 \times 10^3$ in frugivorous *Carollia perspicillata* from Casanare.

## Alphainfluenzavirus-Like Tested Samples

Neither RT-qPCR targeting nucleoprotein (NP) nor endpoint PCR for the basic polymerase 1 (PB1) gene segments were detected. Therefore, none out of 127 samples tested showed amplification for these genes corresponding to NP and PB1 of the $H_{17}N_{10}$ and $H_{18}N_{11}$ influenza-like virus subtypes.

# DISCUSSION

The results presented here show evidence, for the first time, of the presence of AIV in the Yangochiroptera bat suborder from Colombia, using molecular approaches. Is worth mentioning that three out of the seven positive neotropical bat species had not been reported as AIV prone hosts before (**Figure 3**). Thus, this is not only the first AIV record in Colombian, bats but also the first worldwide report of AIV in these three species, expanding the brief list of naturally susceptible bat species to AIV. Taking advantage of the high diversity of bats in the neotropical region where the country is located, the study allowed us to detect AIV in four unreported bat genera to date: *Carollia* spp., *Gardnerycteris* spp., *Platyrrhinus* spp., and *Trachops* spp. Additionally, neotropical bat species previously reported as seropositive to AIV (Tong et al., 2013) were also found positive for AIV presence by the molecular approaches used in this study (*A. lituratus*, *A. planirostris*, *C. brevicauda*, and *C. perspicillata*). Likewise, AIV presence was detected in two Great fruit-eating bats (*Artibeus lituratus*) and a Flat-faced fruit-eating bat (*Artibeus planirostris*) in this study. In agreement with our results, influenza virus presence has been reported previously in *Artibeus* spp. by serological and molecular methods in different sampling areas and genus species (**Supplementary Table 1**). On the other hand, IgG serological reactivity against recombinant hemagglutinin 17 subtype ($rH_{17}$) has been detected in *A. jamaicensis*, *A. lituratus*, *A. phaeotis,* and *A. obscurus* in Guatemala, and *A. obscurus*, *A. planirostris*, and *A. lituratus* in Peru (Tong et al., 2013). AIV $H_{18}N_{11}$ subtype has also been identified by PCR for the first time in Peruvian *Artibeus planirostris*, and *Artibeus obscurus* in Bolivia (Tong et al., 2013; Liang et al., 2015). The absence of information about AIV and/or influenza-like subtypes in Colombian bats provides more value to the

**FIGURE 3 |** Three new host species for AIV in Phyllostomid bat species: **(A)** *Gardnerycteris crenulatum*, **(B)** *Platyrrhinus brachycephalus*, and **(C,D)** *Trachops cirrhosus*.

findings shown in the present study as there are no reports or surveillance data available on this subject at the time the study was conducted. There is also a lack of indexed information in the Influenza Research Database (IRD) and the Database of Bat-associated virus (DBatVir), where no sequences of any viral family distinct to *Rhabdoviridae*, *Flaviviridae*, and *Togaviridae* have been reported in Colombian bat species (Squires et al., 2012; Chen et al., 2014). Therefore, the results presented here contribute to the knowledge, providing insights on the relevance that different bat species and particularly the *Artibeus* spp, genus could have in the AIV eco-biology and epidemiology of AIV among neotropical chiropterans. It also helps to illuminate the unclear situation of these viral agents in the new world and the distribution of AIV in neotropics.

A detection in bat oropharyngeal swabs, not previously reported, highlights the importance and makes the virological evidence found in the present study another relevant finding, where 60% (6/10) of the positive AIV samples corresponded to oropharyngeal swabs. These results show not only the feasibility of AIV molecular detection in this type of sample but also draw attention to the potential eco-biological consequences that imply, considering the aerosol transmission of influenza viruses (Cáceres et al., 2021) and the relevance and the pivotal role that fruit-eating bats of genus *Artibeus* sp. could have in AIV eco-epidemiology. Even though the behavior of bats and AIV-bat interactions are not fully elucidated, it is valuable to consider that droplets and/or respiratory aerosols are the main transmission routes of AIV (Richard and Fouchier, 2016) and represent a potential risk of infection to naïve hosts, which could favor adaptation events of the cross-species jump. On the other hand, even if non-virological evidence of $H_{17}N_{10}$ and $H_{18}N_{11}$ subtypes were found, it is highly recommended to further study and establish AIV subtypes circulating in neotropical bats. In addition, the absence of $H_{17}N_{10}$/$H_{18}N_{11}$ subtypes molecular detection also opens the possibility that hypothetically divergent lineage of influenza-*like* viruses could be circulating in new unreported hosts and reinforces the enzootic distribution of AIV in neotropical bats (Liang et al., 2015). Molecular approaches like next-generation sequencing would be of major help in clarifying this issue, however, as this was not the purpose of the study, it would be the next step to follow.

Finally, in addition to new worldwide species and sample types reported here for AIV detection, this study allowed to generate of a biobank of molecular grade-preserved samples from various species of Yangochiroptera bats, providing a potential source for molecular identification of diverse infectious agents circulating within bat populations. This is relevant considering that outbreaks, emergence, and the e-emergence of infectious diseases tend to originate from wildlife under anthropic pressure that increases animal/human contact (Uribe-Soto et al., 2020). The results of this study encourage further evaluation of the

role that neotropical bats could play in the epidemiology and dissemination dynamics of AIV in chiropteran populations, emphasizing the biotic and microbiological relevance of this unique flying mammalian order. The study and evaluation of pathogen reservoirs helps to understand and to establish preventive measures to limit the risk of dissemination and emergence of infectious diseases under one health principle. Therefore, studies to detect the plethora of viral agents in South American bats are needed.

## DATA AVAILABILITY STATEMENT

The original contributions presented in the study are included in the article/**Supplementary Material**, further inquiries can be directed to the corresponding author.

## ETHICS STATEMENT

The animal study was reviewed and approved by the Bioethics Committee of the Faculty of Veterinary Medicine and Zootechnies of Universidad Nacional de Colombia through code number CB 119-16.

## AUTHOR CONTRIBUTIONS

MU, GR-N, and MR-P: conceptualization and funding acquisition. MU and MR-P: methodology, visualization, and data curation. MU: software, formal analysis, investigation, and writing—original draft preparation. GR-N and MU: validation and writing—review and editing. MR-P and GR-N: resources. GR-N: supervision and project administration. All authors have read and agreed to the published version of the manuscript.

## FUNDING

This research was funded by the Universidad Nacional de Colombia in collaboration with Fundación Reserva Natural La Palmita. We would like to thank to the CIBAV Research Group and Consolidation Strategy (CODI 2018–2019) of the Universidad de Antioquia.

## SUPPLEMENTARY MATERIAL

The Supplementary Material for this article can be found online at: https://www.frontiersin.org/articles/10.3389/fmicb.2022.845546/full#supplementary-material

## REFERENCES

Aguiar, É, Locher, S., Kolesnikova, L., Bolte, H., and Aydillo, T. (2016). Synthetically derived bat influenza A-like viruses reveal a cell type- but not species-specific tropism. *Proc. Natl. Acad. Sci.* 113, 12797–12802. doi: 10.1073/pnas.1608821113

Allocati, N., Petrucci, A. G., Di Giovanni, P., Masulli, M., Di Ilio, C., and De Laurenzi, V. (2016). Bat-man disease transmission: zoonotic pathogens from wildlife reservoirs to human populations. *Cell Death Discov.* 2:16048. doi: 10.1038/cddiscovery.2016.48

Ballard, J. R., Mickley, R., Gibbs, S. E. J., Dwyer, C., Soos, C., Harms, N. J., et al. (2017). Prevalence and distribution of wellfleet bay virus exposure in the common eider (*Somateria mollissima*). *J. Wildl. Dis.* 53, 81–90. doi: 10.7589/2016-01-019

Batts, W. N., LaPatra, S. E., Katona, R., Leis, E., Ng, T. F. F., Brieuc, M. S. O., et al. (2017). Molecular characterization of a novel orthomyxovirus from rainbow and steelhead trout (*Oncorhynchus mykiss*). *Virus Res.* 230, 38–49. doi: 10.1016/j.virusres.2017.01.005

Blanc, A., Ruschansky, D., Clara, M., Achaval, F., Le Bas, A., and Arbiza, J. (2009). Serologic evidence of influenza A and B viruses in South American fur seals (Arctocephalus australis). *J. Wildl. Dis.* 45, 519–521. doi: 10.7589/0090-3558-45.2.519

Boyce, W. M., Mena, I., Yochem, P. K., Gulland, F., Garcı, A., Moreno, N., et al. (2013). Influenza A (H1N1) pdm09 virus infection in marine mammals in California. *Emerg. Microbes Infect.* 2, 2–3. doi: 10.1038/emi.2013.40

Brook, C. E., and Dobson, A. P. (2015). Bats as "special" reservoirs for emerging zoonotic pathogens. *Trends Microbiol.* 23, 172–180. doi: 10.1016/j.tim.2014.12.004

Burgin, C. J., Colella, J. P., Kahn, P. L., and Upham, N. S. (2018). How many species of mammals are there? *J. Mammal.* 99, 1–14. doi: 10.1093/jmammal/gyx147

Bustin, S. A., Benes, V., Garson, J. A., Hellemans, J., Huggett, J., Kubista, M., et al. (2009). The MIQE guidelines: M inimum I nformation for publication of quantitative real-time PCR experiments SUMMARY:. *Clin. Chem.* 55, 611–622. doi: 10.1373/clinchem.2008.112797

Bustin, S., and Nolan, T. (2017). Talking the talk, but not walking the walk: RT-qPCR as a paradigm for the lack of reproducibility in molecular research. *Eur. J. Clin. Invest.* 47, 756–774. doi: 10.1111/eci.12801

Cáceres, C. J., Rajao, D. S., and Perez, D. R. (2021). Airborne transmission of avian origin H9N2 influenza a viruses in mammals. *Viruses* 13:1919. doi: 10.3390/v13101919

Causey, D., and Edwards, S. V. (2008). Ecology of avian influenza virus in birds. *J. Infect. Dis.* 197 (Suppl. 1), S29–S33. doi: 10.1086/524991

CDC. (2009). *CDC Protocol of Realtime RT-PCR for Influenza A (H1N1)*. Geneva: World Health. Organization.

Chan, J. F.-W., To, K. K.-W., Tse, H., Jin, D.-Y., and Yuen, K.-Y. (2013). Interspecies transmission and emergence of novel viruses: lessons from bats and birds. *Trends Microbiol.* 21, 544–555. doi: 10.1016/j.tim.2013.05.005

Chen, L., Liu, B., Yang, J., and Jin, Q. (2014). DBatVir: the database of bat-associated viruses. *Database* 2014:bau021. doi: 10.1093/database/bau021

Childs, J. E., Mackenzie, J. S., and Richt, J. A. (eds) (2007). *Wildlife and Emerging Zoonotic Diseases: The Biology, Circumstances and Consequences of Cross-Species Transmission*. Heidelberg: Springer. doi: 10.1007/978-3-540-70962-6

Ciminski, K., Thamamongood, T., Zimmer, G., and Schwemmle, M. (2017). Novel insights into bat influenza a viruses. *J. Gen. Virol.* 98, 2393–2400. doi: 10.1099/jgv.0.000927

Cogswell-Hawkinson, A., Bowen, R., James, S., Gardiner, D., Calisher, C. H., Adams, R., et al. (2012). Tacaribe virus causes fatal infection of an ostensible reservoir host, the jamaican fruit bat. *J. Virol.* 86, 5791–5799. doi: 10.1128/JVI.00201-12

Dacheux, L., Cervantes-Gonzalez, M., Guigon, G., Thiberge, J.-M., Vandenbogaert, M., Maufrais, C., et al. (2014). A preliminary study of viral metagenomics of french bat species in contact with humans: identification of new mammalian viruses. *PLoS One* 9:e87194. doi: 10.1371/journal.pone.0087194

Davis, L. M., and Spackman, E. (2008). Do crocodilians get the flu? Looking for influenza a in captive crocodilians. *J. Exp. Zool.* 309A, 571–580. doi: 10.1002/jez.454

Dlugolenski, D., Jones, L., Tompkins, S. M., Crameri, G., Wang, L., and Tripp, A. (2013). Bat cells from *Pteropus alecto* are susceptible to influenza a virus infection and reassortment. *Influenza Other Respi. Viruses* 6, 900–903. doi: 10.1111/irv.12128

Fenton, M., and Simmons, N. (2015). *Bats: A World of Science and Mystery*. Chicago: The University of Chicago Press.

Ferguson, L., Eckard, L., Epperson, W. B., Long, L.-P., Smith, D., Huston, C., et al. (2015). Influenza D virus infection in Mississippi beef cattle. *Virology* 486, 28–34. doi: 10.1016/j.virol.2015.08.030

Fleming, T. H., and Peggy, E. (2006). "Ecology of bat migration," in *Bat Ecology*, eds T. H. Kunz and M. B. Fenton (Chicago: The University of Chicago Press), 156–208.

Garcia-Sastre, A. (2012). The neuraminidase of bat influenza viruses is not a neuraminidase. *Proc. Natl. Acad. Sci.* 109, 18635–18636. doi: 10.1073/pnas.1215857109

Gonzalez-Reiche, A. S., and Perez, D. R. (2012). Where do avian influenza viruses meet in the americas? *Avian Dis.* 56, 1025–1033. doi: 10.1637/10203-041412-Reg.1

Groth, M., Lange, J., Kanrai, P., Pleschka, S., Scholtissek, C., Krumbholz, A., et al. (2014). The genome of an influenza virus from a pilot whale: relation to influenza viruses of gulls and marine mammals. *Infect. Genet. Evol.* 24, 183–186. doi: 10.1016/j.meegid.2014.03.026

Han, H. J., Wen, H. L., Zhou, C. M., Chen, F. F., Luo, L. M., Liu, J. W., et al. (2015). Bats as reservoirs of severe emerging infectious diseases. *Virus Res.* 205, 1–6. doi: 10.1016/j.virusres.2015.05.006

Hause, B. M., Collin, E. A., Liu, R., Huang, B., Sheng, Z., Lu, W., et al. (2014). Characterization of a novel influenza virus in cattle and Swine: proposal for a new genus in the Orthomyxoviridae family. *MBio* 5:e00031–e14. doi: 10.1128/mBio.00031-14

Hoffmann, M., Krüger, N., Zmora, P., Wrensch, F., Herrler, G., and Pöhlmann, S. (2016). The hemagglutinin of bat-associated influenza viruses is activated by TMPRSS2 for pH-dependent entry into bat but not human cells. *PLoS One* 11:e0152134. doi: 10.1371/journal.pone.0152134

Hu, D., Zhu, C., Wang, Y., Ai, L., Yang, L., Ye, F., et al. (2017). Virome analysis for identification of novel mammalian viruses in bats from Southeast China. *Sci. Rep.* 7:10917. doi: 10.1038/s41598-017-11384-w

Irving, A. T., Ahn, M., Goh, G., Anderson, D. E., and Wang, L.-F. (2021). Lessons from the host defences of bats, a unique viral reservoir. *Nature* 589, 363–370. doi: 10.1038/s41586-020-03128-0

Juozapaitis, M., Aguiar Moreira, É, Mena, I., Giese, S., Riegger, D., Pohlmann, A., et al. (2014). An infectious bat-derived chimeric influenza virus harbouring the entry machinery of an influenza a virus. *Nat. Commun* 5:4448. doi: 10.1038/ncomms5448

Keawcharoen, J., and Oraveerakul, K. (2004). Avian influenza H5N1 in tigers and leopards. *Emerg Infect Dis* 10, 2189–2191. doi: 10.3201/eid1012.040759

Kimura, H., Chieko, A., Peng, G., Yasushi, M., Kanetsu, S., Seiji, H., et al. (1997). Virus research. *Virus Res.* 48, 71–79.

Koonin, E. V., Krupovic, M., and Agol, V. I. (2021). The baltimore classification of viruses 50 years later: how does it stand in the light of virus evolution? *Microbiol. Mol. Biol. Rev.* 85. doi: 10.1128/MMBR.00053-21

Kosoy, O. I., Lambert, A. J., Hawkinson, D. J., Pastula, D. M., Goldsmith, C. S., Hunt, D. C., et al. (2015). Novel *Thogotovirus* species associated with febrile illness and death, United States, 2014. *Emerg. Infect. Dis. J.* 21, 760–764. doi: 10.3201/eid2105.150150

L'vov, D. K., Al'khovskii, S. V., Shchelkanov, M. I., Shchetinin, A. M., Deriabin, P. G., Aristova, V. A., et al. (2014). Taxonomic status of the Tyulek virus (TLKV) (Orthomyxoviridae, *Quaranjavirus*, *Quaranfil* group) isolated from the ticks *Argas* vulgaris Filippova, 1961 (*Argasidae*) from the birds burrow nest biotopes in the Kyrgyzstan. *Vopr. Virusol.* 59, 28–32.

Lefever, S., Hellemans, J., Pattyn, F., Przybylski, D. R., and Taylor, C. (2009). RDML: structured language and reporting guidelines for real-time quantitative PCR data. *Nucleic Acids Res.* 37, 2065–2069. doi: 10.1093/nar/gkp056

Letko, M., Seifert, S. N., Olival, K. J., Plowright, R. K., and Munster, V. J. (2020). Bat-borne virus diversity, spillover and emergence. *Nat. Rev. Microbiol.* 18, 461–471. doi: 10.1038/s41579-020-0394-z

Liang, E., Aguirre-Mazzi, E., Hicks, A., Zambrana-Torrelio, C., Navarrete-Macias, I., Rostal, M., et al. (2015). *Influenza A virus (A/dark fruit-eating bat/Bolivia/PBV780-781/2011(H18N11)). Cent. Infect. Immun.* Available online at: http://www.mgc.ac.cn/cgi-bin/DBatVir/main.cgi?func=stat (accessed March 24, 2022).

Mancini, D. A. P., Mendonça, R. M. Z., Cianciarullo, A. M., Kobashi, L. S., Trindade, H. G., Fernandes, W., et al. (2004). Influenza em animais heterotérmicos. *Rev. Soc. Bras. Med. Trop.* 37, 204–209. doi: 10.1590/S0037-86822004000300002

Maruyama, J., Nao, N., Miyamoto, H., Maeda, K., Ogawa, H., Yoshida, R., et al. (2016). Characterization of the glycoproteins of bat-derived in fl uenza viruses. *Virology* 488, 43–50. doi: 10.1016/j.virol.2015.11.002

Messenger, A. M., Barnes, A. N., and Gray, G. C. (2014). Reverse zoonotic disease transmission (Zooanthroponosis): a systematic review of seldom-documented human biological threats to animals. *PLoS One* 9:e89055. doi: 10.1371/journal.pone.0089055

Mickleburgh, S. P., Hutson, A. M., and Racey, P. A. (2002). A review of the global conservation status of bats. *Oryx* 36, 18–34. doi: 10.1017/S0030605302000054

Misra, V. (2020). Bats and viruses. *Lancet Infect. Dis.* 20:1380. doi: 10.1016/S1473-3099(20)30743-X

Ndunguru, J., Taylor, N. J., Yadav, J., Aly, H., Legg, J. P., Aveling, T., et al. (2005). Application of FTA technology for sampling, recovery and molecular characterization of viral pathogens and virus-derived transgenes from plant tissues. *Virol. J.* 2:45. doi: 10.1186/1743-422X-2-45

Ng, T. F. F., Kondov, N. O., Deng, X., Van Eenennaam, A., Neibergs, H. L., and Delwart, E. (2015). A metagenomics and case-control study to identify viruses associated with bovine respiratory disease. *J. Virol* 89, 5340–5349. doi: 10.1128/JVI.00064-15

O'Shea, T. J., Cryan, P. M., Cunningham, A. A., Fooks, A. R., Hayman, D. T. S., Luis, A. D., et al. (2014). Bat flight and zoonotic viruses. *Emerg. Infect. Dis.* 20, 741–745. doi: 10.3201/eid2005.130539

Ohishi, K., Maruyama, T., Ninomiya, A., Kida, H., Zenitani, R., Bando, T., et al. (2006). Serologic investigations if Influenza a virus infection in ceteceans from the Western North Pacific and the Southern Oceans. *Mar. Mammal Sci.* 22, 214–221. doi: 10.1111/j.1748-7692.2006.00016.x

Omatsu, T., Watanabe, S., Akashi, H., and Yoshikawa, Y. (2007). Biological characters of bats in relation to natural reservoir of emerging viruses. *Comp. Immunol. Microbiol. Infect. Dis.* 30, 357–374. doi: 10.1016/j.cimid.2007.05.006

Osterhaus, A. D. M. E., Rimmelzwaan, G. F., and Martina, B. E. E. (2000). Influenza B Virus in Seals. *Science* 288, 1051–1054.

Palese, P., and Young, J. F. (1982). Variation of influenza A, B, and C viruses. *Science* 215, 1468–1474. doi: 10.1126/science.7038875

Parrish, C. R., Murcia, P. R., and Holmes, E. C. (2015). Influenza virus reservoirs and intermediate hosts: dogs, horses, and new possibilities for influenza virus exposure of humans. *J. Virol.* 89, 2990–2994. doi: 10.1128/JVI.03146-14

Plowright, R. K., Peel, A. J., Streicker, D. G., Gilbert, A., McCallum, H., Wood, J., et al. (2016). Transmission or within-host dynamics driving pulses of zoonotic viruses in reservoir-host populations. *PLoS Negl. Trop. Dis.* 10:e0004796. doi: 10.1371/journal.pntd.0004796

Poole, D. S., Yu, S., Cai, Y., Dinis, J. M., Muller, M. A., Jordan, I., et al. (2014). Influenza a virus polymerase is a site for adaptive changes during experimental evolution in bat cells. *J. Virol.* 88, 12572–12585. doi: 10.1128/JVI.01857-14

Quast, M., Sreenivasan, C., Sexton, G., Nedland, H., Singrey, A., Fawcett, L., et al. (2015). Serological evidence for the presence of influenza D virus in small ruminants. *Vet. Microbiol.* 180, 281–285. doi: 10.1016/j.vetmic.2015.09.005

Ramis, A. J., Riel, D., van de Bildt, M. W., and Osterhaus, A. (2012). Influenza A and B virus attachment to respiratory tract in marine mammals. *Emerg. Infect. Dis.* 18, 817–820. doi: 10.3201/eid1805.111828

Richard, M., and Fouchier, R. A. M. (2016). Influenza A virus transmission via respiratory aerosols or droplets as it relates to pandemic potential. *FEMS Microbiol. Rev.* 40, 68–85. doi: 10.1093/femsre/fuv039

Richter, H. V., and Cumming, G. S. (2008). First application of satellite telemetry to track African straw-coloured fruit bat migration. *J. Zool.* 275, 172–176. doi: 10.1111/j.1469-7998.2008.00425.x

Rose, N., Hervé, S., Eveno, E., Barbier, N., Eono, F., Dorenlor, V., et al. (2013). Dynamics of influenza a virus infections in permanently infected pig farms: evidence of recurrent infections, circulation of several swine influenza viruses and reassortment events. *Vet. Res.* 44, 1–14. doi: 10.1186/1297-9716-44-72

Sakai, T., Ishii, A., Segawa, T., Takagi, Y., Kobayashi, Y., and Itou, T. (2015). Establishing conditions for the storage and elution of rabies virus RNA using FTA cards. *J. Vet. Med. Sci.* 77, 461–465. doi: 10.1292/jvms.14-0227

Salem, E., Cook, E. A. J., Lbacha, H. A., Oliva, J., Awoume, F., Muloi, D., et al. (2017). Serologic evidence for influenza C and D virus among ruminants and Camelids, Africa, 1991-2015. *Emerg. Infect. Dis.* 9, 1556–1559. doi: 10.3201/eid2309.170342

Sanjuan, M. A., Green, D. R., Okamura, K., Chung, W., Ruby, J. G., Guo, H., et al. (2009). Endocytosis of influenza viruses. *Microbes Infect* 9, 699–711. doi: 10.1016/j.micinf.2004.05.002.Endocytosis

Schlegel, M., Ali, H. S., Stieger, N., Groschup, M. H., Wolf, R., and Ulrich, R. G. (2012). Molecular identification of small mammal species using novel cytochrome b gene-derived degenerated primers. *Biochem. Genet.* 50, 440–447. doi: 10.1007/s10528-011-9487-8

Shaw, M. L., and Palese, P. (2013). "Orthomyxoviridae," in *Fields Virology*, 6th Edn, eds D. M. Knipe, P. M. Howley, J. I. Cohen, D. E. Griffin, R. A. Lamb, M. A. Martin, et al. (Philadelphia, PA: Lippincott Williams and Wilkins), 1151–1185.

Squires, R. B., Noronha, J., Hunt, V., García-Sastre, A., Macken, C., Baumgarth, N., et al. (2012). Influenza Research Database: an integrated bioinformatics resource for influenza research and surveillance. *Influenza Other Respi. Viruses* 6, 404–416. doi: 10.1111/j.1750-2659.2011.00331.x

Sun, X., Shi, Y., Lu, X., He, J., Gao, F., Yan, J., et al. (2013). Bat-derived influenza hemagglutinin H17 does not bind canonical avian or human receptors and most likely uses a unique entry mechanism. *Cell Rep.* 3, 769–778. doi: 10.1016/j.celrep.2013.01.025

Taubenberger, J. K., and Morens, D. M. (2008). The pathology of influenza virus infections jeffery. *Annu. Rev. Pathol.* 3, 499–522.

Taubenberger, J. K., and Morens, D. M. (2010). Influenza: the once and future pandemic. *Public Health Rep.* 125 (Suppl. 3), 16–26.

Taylor, L. H., Latham, S. M., and Woolhouse, M. E. J. (2001). Risk factors for human disease emergence. *Philos. Trans. R. Soc. London. Ser. B Biol. Sci.* 356, 983–989. doi: 10.1098/rstb.2001.0888

Tefsen, B., Lu, G., Zhu, Y., Haywood, J., Zhao, L., Deng, T., et al. (2014). The N-terminal domain of PA from bat-derived influenza-like virus H17N10 has endonuclease activity. *J. Virol.* 88, 1935–1941. doi: 10.1128/JVI.03270-13

Temple, B. L., Finger, J. W., Jones, C. A., Gabbard, J. D., Jelesijevic, T., Uhl, E. W., et al. (2015). In ovo and in vitro susceptibility of American alligators (*Alligator mississippiensis*) to avian infleunza virus infection. *J. Wildl. Dis.* 51, 187–198. doi: 10.7589/2013-12-321

Tobita, K. (1997). Classification and nomenclature of influenza viruses. *Nihon Rinsho* 55, 2512–2514.

Tong, S. (2015). *Methods Of Detecting Influenza Virus*. Patient no. CDC – US 2015/0133329 A1. 1–33.

Tong, S., Li, Y., Rivailler, P., Conrardy, C., Castillo, D. A., Chen, L.-M., et al. (2012). A distinct lineage of influenza a virus from bats. *Proc. Natl. Acad. Sci. U.S.A.* 109, 4269–4274. doi: 10.1073/pnas.1116200109

Tong, S., Zhu, X., Li, Y., Shi, M., Zhang, J., Bourgeois, M., et al. (2013). New world bats harbor diverse influenza A viruses. *PLoS Pathog.* 9:e1003657. doi: 10.1371/journal.ppat.1003657

Turkington, H. L., Juozapaitis, M., Kerry, P. S., Aydillo, T., Ayllon, J., García-Sastre, A., et al. (2015). Novel bat influenza virus NS1 proteins bind double-stranded RNA and antagonize host innate immunity. *J. Virol.* 89, 10696–10701. doi: 10.1128/JVI.01430-15

Uribe-Soto, M., Gomez, A. P., and Ramirez-Nieto, G. C. (2020). Influenza virus needs an approach as a "one health" problem in Colombia. *Acta biol. Colomb* 26, 421–430. doi: 10.15446/abc.v25n3.79364

Wang, L. F., Walker, P. J., and Poon, L. L. M. (2011). Mass extinctions, biodiversity and mitochondrial function: are bats "special" as reservoirs for emerging viruses? *Curr. Opin. Virol.* 1, 649–657. doi: 10.1016/j.coviro.2011.10.013

Wilson, D. E., and Reeder, D. M. (2005). in *Mammal Species of the World. A Taxonomic and Geographic Reference*, 3rd Edn, eds D. E. Wilson and D. M. Reeder (Baltimore, MD: Johns Hopkins University Press).

Wong, S., and Lau, S. (2009). Bats as a continuing source of emerging infections in humans. *Rev. Med. Virol.* 17, 66–91. doi: 10.1002/rmv

Xie, T., Anderson, B., Daramragchaa, U., Chuluunbaatar, M., and Gray, G. (2016). A review of evidence that equine influenza viruses are zoonotic. *Pathogens* 5:50. doi: 10.3390/pathogens5030050

Zhou, H., He, S. Y., Sun, L., He, H., Ji, F., Sun, Y., et al. (2015). Serological evidence of avian influenza virus and canine influenza virus infections among stray cats in live poultry markets, China. *Vet. Microbiol.* 175, 369–373. doi: 10.1016/j.vetmic.2014.12.018

Zhu, X., Yu, W., McBride, R., Li, Y., Chen, L.-M., Donis, R. O., et al. (2013). Hemagglutinin homologue from H17N10 bat influenza virus exhibits divergent receptor-binding and pH-dependent fusion activities. *Proc. Natl. Acad. Sci. U.S.A.* 110, 1458–1463. doi: 10.1073/pnas.1218509110

**Conflict of Interest:** The authors declare that the research was conducted in the absence of any commercial or financial relationships that could be construed as a potential conflict of interest.

**Publisher's Note:** All claims expressed in this article are solely those of the authors and do not necessarily represent those of their affiliated organizations, or those of the publisher, the editors and the reviewers. Any product that may be evaluated in this article, or claim that may be made by its manufacturer, is not guaranteed or endorsed by the publisher.

*Copyright © 2022 Uribe, Rodríguez-Posada and Ramirez-Nieto. This is an open-access article distributed under the terms of the Creative Commons Attribution License (CC BY). The use, distribution or reproduction in other forums is permitted, provided the original author(s) and the copyright owner(s) are credited and that the original publication in this journal is cited, in accordance with accepted academic practice. No use, distribution or reproduction is permitted which does not comply with these terms.*

frontiers | Frontiers in Microbiology

REVIEW
published: 27 April 2022
doi: 10.3389/fmicb.2022.862270

# Insights Into Persistent HIV-1 Infection and Functional Cure: Novel Capabilities and Strategies

*Tram M. Ta[1†], Sajjaf Malik[1†], Elizabeth M. Anderson[2†], Amber D. Jones[1,3], Jocelyn Perchik[1], Maryann Freylikh[1], Luca Sardo[4], Zackary A. Klase[3,5] and Taisuke Izumi[1*]*

[1] Department of Biological Sciences, Misher College of Arts and Sciences, University of the Sciences in Philadelphia, Philadelphia, PA, United States, [2] Office of the Assistant Secretary for Health, Region 3, U.S. Department of Health and Human Services, Washington, DC, United States, [3] Department of Pharmacology and Physiology, Drexel University College of Medicine, Philadelphia, PA, United States, [4] Department of Infectious Disease and Vaccines, Merck & Co., Inc., Kenilworth, NJ, United States, [5] Center for Neuroimmunology and CNS Therapeutics, Institute of Molecular Medicine and Infectious Diseases, Drexel University of Medicine, Philadelphia, PA, United States

OPEN ACCESS

**Edited by:**
*Chunfu Zheng, University of Calgary, Canada*

**Reviewed by:**
*Shan Cen, Chinese Academy of Medical Sciences and Peking Union Medical College, China*
*Guochun Jiang, University of North Carolina at Chapel Hill, United States*

***Correspondence:**
*Taisuke Izumi*
*tizumi@usciences.edu*

*[†] These authors have contributed equally to this work*

**Specialty section:**
*This article was submitted to Virology, a section of the journal Frontiers in Microbiology*

**Received:** *25 January 2022*
**Accepted:** *21 February 2022*
**Published:** *27 April 2022*

**Citation:**
*Ta TM, Malik S, Anderson EM, Jones AD, Perchik J, Freylikh M, Sardo L, Klase ZA and Izumi T (2022) Insights Into Persistent HIV-1 Infection and Functional Cure: Novel Capabilities and Strategies. Front. Microbiol. 13:862270. doi: 10.3389/fmicb.2022.862270*

Although HIV-1 replication can be efficiently suppressed to undetectable levels in peripheral blood by combination antiretroviral therapy (cART), lifelong medication is still required in people living with HIV (PLWH). Life expectancies have been extended by cART, but age-related comorbidities have increased which are associated with heavy physiological and economic burdens on PLWH. The obstacle to a functional HIV cure can be ascribed to the formation of latent reservoir establishment at the time of acute infection that persists during cART. Recent studies suggest that some HIV reservoirs are established in the early acute stages of HIV infection within multiple immune cells that are gradually shaped by various host and viral mechanisms and may undergo clonal expansion. Early cART initiation has been shown to reduce the reservoir size in HIV-infected individuals. Memory CD4+ T cell subsets are regarded as the predominant cellular compartment of the HIV reservoir, but monocytes and derivative macrophages or dendritic cells also play a role in the persistent virus infection. HIV latency is regulated at multiple molecular levels in transcriptional and post-transcriptional processes. Epigenetic regulation of the proviral promoter can profoundly regulate the viral transcription. In addition, transcriptional elongation, RNA splicing, and nuclear export pathways are also involved in maintaining HIV latency. Although most proviruses contain large internal deletions, some defective proviruses may induce immune activation by expressing viral proteins or producing replication-defective viral-like particles. In this review article, we discuss the state of the art on mechanisms of virus persistence in the periphery and tissue and summarize interdisciplinary approaches toward a functional HIV cure, including novel capabilities and strategies to measure and eliminate the infected reservoirs and induce immune control.

**Keywords: human immunodeficiency virus (HIV), functional HIV cure, HIV latency, HIV persistence, kick-and-kill strategy, Block-and-Lock strategy, defective proviruses, immunotherapy**

## INTRODUCTION

Human Immunodeficiency Virus Type-I (HIV-1) is the infectious agent that causes acquired immunodeficiency syndrome (AIDS) and remains a global concern due to the lack of effective vaccines and curative strategies (No Author, 2006). Despite the ability of combination antiviral therapy (cART) to effectively suppress plasma HIV-1 levels in the majority of people living with HIV (PLWH), HIV-1 persists by the formation of latent reservoirs established very early during the acute phase of HIV infection (Chun et al., 1997; Finzi et al., 1997; Holkmann Olsen et al., 2007; Kousignian et al., 2008; Wong et al., 2019). Furthermore, HIV-infected cells can undergo proliferation and over 50% of latently infected cells observed after prolonged cART are the product of clonal expansion (Ananworanich et al., 2015; Brodin et al., 2016; Yucha et al., 2017; Abrahams et al., 2019; Leite et al., 2019). Upon the cessation of cART, this reservoir can be reactivated and eventually leads to virus rebound in the majority of PLWH (Siliciano et al., 2003). Virus persistence necessitates lifelong cART for the 37.7 million PLWH and is possibly the last unmet challenge toward HIV cure/remission strategies. Persistence depends on multiple factors that are hypothesized to involve complex virus-host interactions. So far, there are two people who have been cured of HIV-1 infection, and one person who is undergoing long-term remission from HIV (Hütter et al., 2009; Allers et al., 2011; Gupta et al., 2019; Peluso et al., 2019). All of them had intercurrent leukemia and underwent a bone marrow transplant from donors who had a homozygous 32 base pair deletion in the CCR5 gene (CCR5-Δ32). Homozygous carriers of Δ32 deletion are largely resistant to HIV-1 infection because the mutation prevents functional expression of CCR5 that is used as a coreceptor for HIV-1 to enter immune cells. This mutation is primarily found in northern Europe because CCR5Δ32 selective pressures were thought to be induced by an intense smallpox epidemic in that region (Klitz et al., 2001; Galvani and Slatkin, 2003). Thus, hematopoietic stem cell transplant is currently the only successful strategy for a cure, but it is high risk and not scalable. Therefore, novel HIV curative strategies are urgently needed. One promising approach to eliminate cells that evade cART is the "kick-and-kill" strategy, where latency reversal agents (LRAs) reactivate the reservoir, allowing for immune cell recognition and elimination of these latently infected cells (Hamer, 2004). In contrast, the "Block-and-Lock" approach aims to induce permanent transcriptional and epigenetic proviral silencing, thereby preventing viral reactivation (Kessing et al., 2017). However, HIV-1 latency is still challenging for functional cure and remission. CRISPR-mediated genome editing is another promising approach to excise and deactivate the integrated HIV-1 DNA (Ebina et al., 2013; Hu et al., 2014). The United States Food and Drug Administration (FDA) recently approved clinical trials with a CRISPR-based strategy for HIV eradication (NCT05144386). Finally, modulation of the immune system has also been considered to address persistent reservoir elimination.

This review article discusses the obstacles to HIV eradication and multiple challenges for a functional cure of persistent HIV-1 infection recently highlighted in our research topic (Sardo et al., 2021).

## HUMAN IMMUNODEFICIENCY VIRUS PERSISTENCE

### Cellular Reservoir

The complexity and heterogeneity of HIV-1 reservoirs are caused by the establishment of latent infection into different cell types (**Figure 1**). HIV-1 primarily infects CD4+ T cells and the differentiation of T cells occurs in a stepwise fashion toward more differentiated cell types. The major cellular reservoirs for HIV-1 during cART reside in the memory CD4+ T cell subsets, especially central memory ($T_{CM}$) subsets (Chomont et al., 2009; Buzon et al., 2014; Soriano-Sarabia et al., 2014; Ait-Ammar et al., 2020). Although having lower levels of integrated HIV-1 DNA due to their relative resistance to HIV-1 infection, the reactivation rate of latent proviruses in naive CD4+ T cells ($T_N$) by LRAs is higher than in memory subsets (Ostrowski et al., 1999; Chomont et al., 2009; Wightman et al., 2010; Josefsson et al., 2013; Soriano-Sarabia et al., 2014). This suggests that the $T_N$ subset might also be an important contributor to viral rebound in PLWH. Latently infected cells can ultimately differentiate into an effector memory subset ($T_{EM}$), an activated phenotype involved in antigen responses (von Stockenstrom et al., 2015). $T_{EM}$ harbors the largest proportion of intact-replication competent provirus (Hiener et al., 2017) and the largest inducible HIV-1 reservoir *in vitro* and *ex vivo* (Kulpa et al., 2019). Gamma delta (γδ) T cells that respond to non-peptide antigens through their distinct T-cell receptors bridge innate and adaptive immunity. The majority of γδ T cells in the blood are comprised of the Vδ2 subset, which also develops a memory phenotype. During HIV-1 infection, Vδ2 T-lymphocytes have been documented to be productively infected and depleted (Ait-Ammar et al., 2020). Vδ2 T cells isolated from HIV-1 infected individuals on prolonged cART contain replication-competent latent HIV-1 proviral DNA (Soriano-Sarabia et al., 2015). Although the memory subset of Vδ2 T cells has not been exclusively studied, peripheral Vδ2 T cells are also suggested to be a potential HIV-1 reservoir and should be targeted in curative approaches. While studies in the cellular reservoir have largely been conducted with the peripheral blood, memory subsets of CD4+ T cells containing HIV-1 sequence in gut-associated lymphoid tissue and lymph nodes (Tissue-resident memory T cells: $T_{RM}$) were observed to contain 2–4 fold higher levels of HIV-1 DNA than the cells isolated from peripheral blood (**Figure 1**; Chun et al., 2008).

Great effort to characterize the persistent reservoir cells has been put into identifying markers that could help determine enriched latently HIV-infected cells (Darcis et al., 2019). Some of the markers, including HLA-DR, CD25, CD32, and CD69, are upregulated in the HIV-infected CD4+ T cells (Darcis et al., 2019). On the other hand, CD2 receptor has been found to be expressed on latently infected resting memory CD4+ T cells in virally suppressed individuals (Iglesias-Ussel et al., 2013). The expression of α4β7 integrin has been shown in a T cell subset that is highly susceptible to HIV-1 infection (Ding et al., 2015).

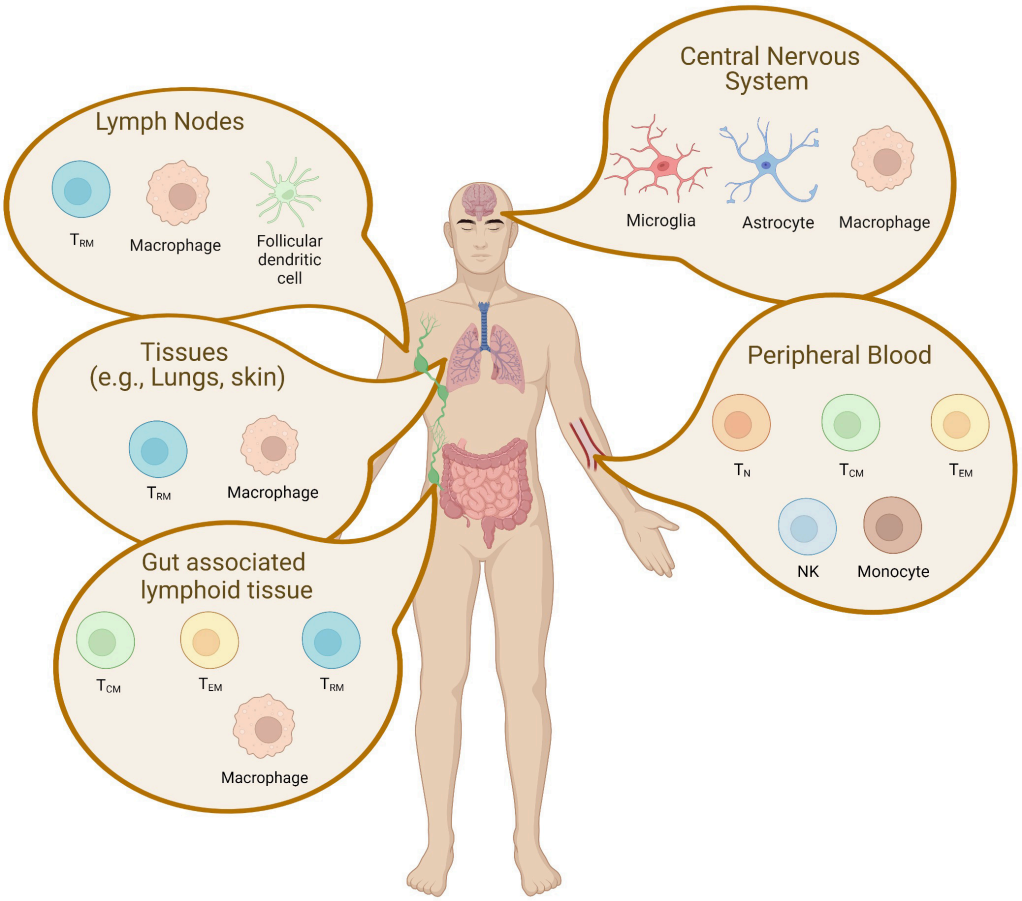


**FIGURE 1 |** Latent cellular reservoir cells in tissue. A schematic representation of latently infected cells in tissues is depicted. The reservoirs are established in unique cell types and are localized across different tissues. CD4+ memory T cell subsets are found in the peripheral blood, the lymphoid tissue, gut-associated lymphoid tissue, and the central nervous system. This figure was created with BioRender.com.

Despite the extensive investigation to characterize latently infected CD4+ T cells, a unique and universal marker of the HIV-1 reservoir cells has not been identified yet.

Although CD4+ T cells are the most studied among cellular reservoirs in the peripheral blood, other targets such as cells of the myeloid lineage contribute to persistence. Myeloid cells are thought to be of great importance for the pathogenesis of HIV-1 in the central nervous system (CNS) (**Figure 1**). As the CNS contains very few CD4+ T cells, CNS reservoirs predominantly include both microglia and perivascular macrophages (Iglesias-Ussel et al., 2013; Ding et al., 2015; Cantero-Pérez et al., 2019; Darcis et al., 2019; Ait-Ammar et al., 2020). Both of these cell types appear to continue to express viral genes despite suppressive cART therapy (Colomer-Lluch et al., 2018; Cantero-Pérez et al., 2019). Like T-cells in the periphery, infected myeloid cells in a tissue can contribute to viral rebound (Gibellini et al., 2008; Ding et al., 2015; Gosselin et al., 2017) and the development of escape mutations (Guihot et al., 2018; Grau-Expósito et al., 2019). Specific to the CNS, these persistently infected myeloid populations are also central drivers of the neuropathologic, behavioral, and cognitive effects collectively known as neuroHIV (Ho et al., 2013; Wightman et al., 2015; Kandathil et al., 2016; Perlman, 2016; Gosselin et al., 2017; Yucha et al., 2017; Darcis et al., 2019; Wong et al., 2019; Zerbato et al., 2019). Myeloid cells have a longer lifespan than lymphocytes and can continue to produce viruses long after initial infection (Perlman, 2016). In addition, myeloid cells are resistant to HIV-induced apoptosis (Morison et al., 2005; Coppé et al., 2010; Perlman, 2016) and myeloid-derived macrophages are resistant against type I IFN inducible innate immunity, and Cytotoxic T-lymphocytes (CTL) mediated immune responses (Cantero-Pérez et al., 2019). This is distinct from infected T cell populations in the periphery (Rangarajan and Weinberg, 2003; Akhtar, 2015) that also become a predominant reservoir.

Laboratory mouse strains play a distinct role in biomedical research due to having many similarities of anatomy and physiology to humans and their ability to be genetically manipulated. However, mice cannot be infected with HIV-1, and thus steps must be taken to modify this usual model organism for use in HIV-1 experimental infections. Humanized mice engrafted with human hematopoietic systems have proven to be versatile experimental models for studying the fundamental

aspects of HIV biology (Monod and Jacob, 1961; Rangarajan and Weinberg, 2003; Morison et al., 2005; Coppé et al., 2010; Bailey et al., 2013; Honeycutt et al., 2017). Both viral DNA and RNA were detected in CD4+ T cells and macrophages in bone marrow, liver, and thymus (BLT) transplanted mice (Honeycutt et al., 2017). The latent reservoir formation in either CD4+ T cells or macrophages was previously demonstrated to be independently developed using T-cell-only or myeloid-only humanized mice (Yucha et al., 2017). This suggests that both cell types are capable of establishing a persistent reservoir. HIV-infected macrophages circulate and infiltrate into various tissue compartments including the brain in human myeloid-only mice, suggesting that myeloid cells may seed deep tissue reservoirs. While most human macrophages have a rapid turnover of approximately 1 day in myeloid-only mice, viral rebound could be observed in the infected mice post ART interruption (Honeycutt et al., 2017), suggesting that specialized long-lived macrophages, such as microglia to persistent in the CNS, may contribute to viral reservoir formation over time. Another *in vivo* model, for instance non-human primates, is needed to further examine the relevance of myeloid-derived cells in HIV-1 reservoir formation.

## Mechanisms of Human Immunodeficiency Virus Type-I Latency

Silent proviruses in infected cells are termed "latent" and are established and maintained, in part, by epigenetic modifications and by transcription factors and signaling molecules that reinforce latency (Van Lint et al., 1996; Triboulet et al., 2007; Sung and Rice, 2009; Mbonye and Karn, 2017). In fact, HIV-1 latency is mediated by both cis- and trans-regulatory mechanisms that prevent transcription factors from accessing the viral promoter region (**Figure 2**; Hakre et al., 2012; Donahue and Wainberg, 2013; Ruelas and Greene, 2013; Van Lint et al., 2013). Chromatin environments are dominantly cis-regulated, while viral and host transcription factors are trans-regulated in latently infected cells (Besnard et al., 2016). Cis-acting mechanisms depend on the chromatin environment at the virus integration site within the host genome (**Figure 2A**; Dahabieh et al., 2015). Cis-regulatory elements work through intracellular interactions between different parts of the same molecule, such as promoters, enhancers, and silencers (Goncalves et al., 2012). These elements are located in the vicinity of the genes they regulate and act as binding sites for transcription factors to regulate transcription rates of nearby genes (Davidson, 2021). DNA methylation, histone methylation, acetylation and crotonylation are commonly found in the viral promoter region as cis-regulatory mechanisms in latently infected cells. On the other hand, trans-regulatory factors cooperate with cis-regulatory elements to suppress viral gene expression (McManus et al., 2010; Goncalves et al., 2012; Wang et al., 2019).

Cellular epigenetic mechanisms to the cis-regulatory proviral regions have been extensively studied in peripheral CD4+ T cells. Clusters of CpG residues termed CG islands around the HIV-1 transcription site may be methylated, which would maintain the HIV-1 promoter in a heterochromatic state to repress HIV-1 transcription (**Figure 2A**; Blazkova et al., 2009; Kauder et al., 2009; Ruelas and Greene, 2013; Weber et al., 2014; Boltz et al., 2021). Histone acetyltransferases (HATs) are recruited to the viral long terminal repeat (LTR) and lead to increasing H3 and H4 lysine acetylation, specifically at H3K9, H3K4, H4K5, H4K8, and H4K16 residues (Benkirane et al., 1998; Hottiger and Nabel, 1998; Marzio et al., 1998; Col et al., 2001; Lusic, 2003). This acetylation leads to the relaxation of chromatin resulting in increased accessibility of transcription factors to the proviral DNA (**Figure 2A**; Mariño-Ramírez et al., 2005). Conversely, histone deacetylases (HDAC), remove acetyl groups from histones to promote chromatin condensation, thereby silencing proviruses (Jiang et al., 2007; Marban et al., 2007; Herbein and Wendling, 2010; Seto and Yoshida, 2014). Thus, HDAC inhibitors have been shown to potently reactivate latent cells *in vitro* (Saayman et al., 2014). In addition, H3 lysine methylations, including H3K4me, H3K36me, and H3K79me, are also involved in HIV DNA transcription and are mediated by histone methyltransferases such as SUV39H1 and EZH2 (du Chéné et al., 2007; Imai et al., 2010; Friedman et al., 2011; Ding et al., 2013; Tchasovnikarova et al., 2015; Li J. et al., 2016). Post-translational modification by lysine crotonylation was found to affect gene expression (Tan et al., 2011; Sabari et al., 2015, 2017). This study showed that histone crotonylation at the LTR through the induction of the enzyme acyl-CoA synthetase short-chain family member 2 (ACSS2) can reactivate latent HIV-1 *in vitro* and *ex vivo* (Jiang et al., 2018). Specifically, ACSS2 induction was found to increase histone crotonylation and acetylation at H3K4 while decreasing histone trimethylation at H3K27.

HIV-1 latency also results from the lack of trans-regulatory factors that enable T cell activation. Although many of these mechanisms are still under investigation, some transcription factors have been found to regulate viral gene expression. The positive transcription elongation factor, P-TEFb, is a critical kinase involved in HIV-1 transcription and is hijacked by the HIV-1 trans-activator, Tat (**Figure 2B**; Burnett et al., 2009). P-TEFb is sequestered by the 7SK small nuclear ribonucleoprotein (snRNP) complex, leading to an initial low expression of Tat (Weinberger et al., 2005). Once Tat is expressed, it associates with P-TEFb at the viral promoter to enhance HIV-1 transcription (Zhu et al., 1997; Yang et al., 2001). P-TEFb consists of CyclinT1 and CDK9 and requires CDK9 phosphorylation to activate the paused RNA Polymerase II (Pol II) (Wei et al., 1998; Ramakrishnan et al., 2009). CDK9 phosphorylation levels are generally lower in the resting CD4+ T cells, which is the dominant compartment of HIV-1 latently infected cells (Budhiraja et al., 2013; Ramakrishnan et al., 2015). A transcription factor, NF-κB, is also involved in the initiation of HIV-1 transcription (Adams et al., 1994; Williams et al., 2006). NF-κB is a host cell master regulator of inflammatory T cells that acts as a transcription factor to initiate HIV transcription in the absence of Tat (West et al., 2001). In resting cells, NF-κB is sequestered in the cytoplasm where it is bound by IκB. The low availability of NF-κB binding at the promoter region causes the change in the chromatin structure surrounding the LTR, leading to the disruption of the recruitment of Poll II and transcriptional

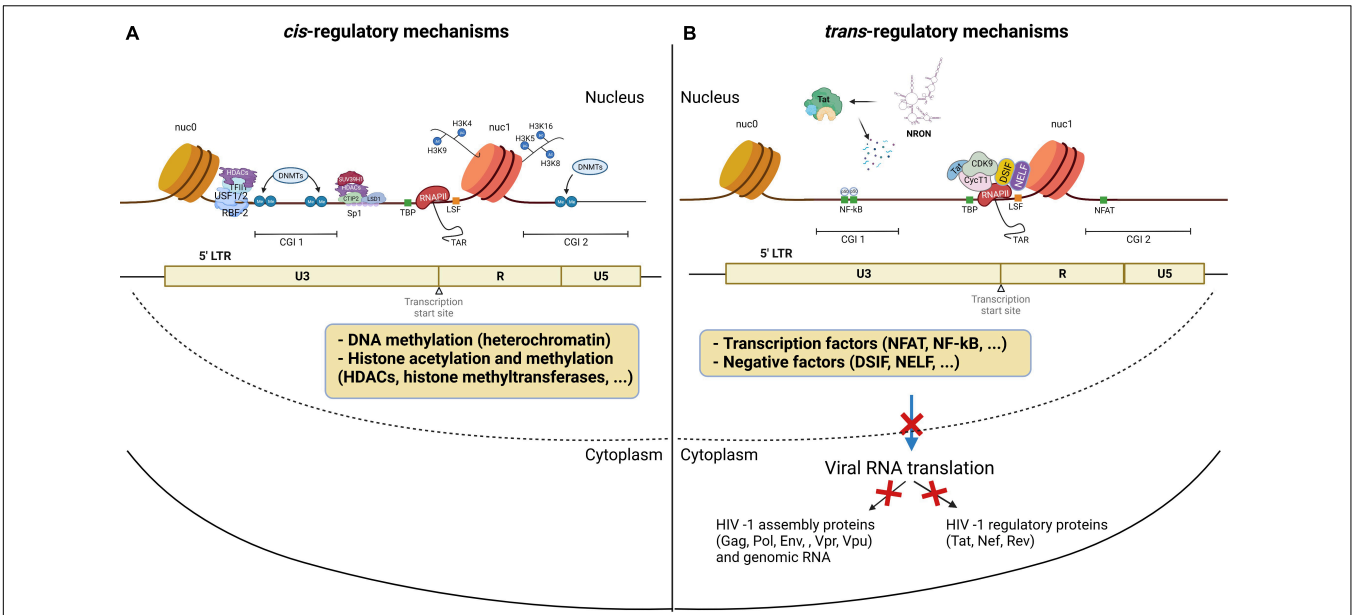


**FIGURE 2 |** HIV-1 latency mechanisms. Latency is established through **(A)** cis-regulation elements, and **(B)** trans-regulation mechanisms predominantly regulate the HIV gene expression in the homeostatically proliferated reservoir cells at the chronic stage. **(A)** DNA methylation of the CG islands around the HIV-1 transcription start site maintains the HIV-1 promoter in a heterochromatic state to provoke HIV-1 transcriptional repression. Histone acetylation induces structural instability and increases access to transcriptional factors accessibility. **(B)** Transcription initiation is blocked by the low availability of NF-κB and phosphorylated NFAT at the promoter region. The binding of p50-p50 homodimers to the NF-κB binding site further inhibits transcription initiation. After initiation, RNA Pol II pauses at the promoter region due to the binding of negative elongation factors NELF and DSIF, leading to blocks in transcription elongation. In addition, P-TEFb is sequestered by the 7SK snRNP complex, causing a low expression level of Tat. The lncRNA called NRON degrades HIV-1 Tat to inhibit the P-TEFb formation. miRNAs targeting CyclinT1 regulate viral production and expression by overexpression in resting cells. This figure was created with BioRender.com.

**TABLE 1 |** HIV latency mechanisms.

| Mechanism of latency | Process | Factor(s) | Reference |
|---|---|---|---|
| Cis-regulation | DNA methylation | Heterochromatin | Blazkova et al., 2009; Kauder et al., 2009; Chávez et al., 2011 |
| | Histone methylation | Histone methyltransferase | Chéné et al., 2007; Imai et al., 2010; Friedman et al., 2011; Boehm et al., 2017; Zhang et al., 2017; Huang et al., 2019 |
| | Histone acetylation | HDACs | Lusic, 2003; Jiang et al., 2007; Marban et al., 2007; Tyagi and Karn, 2007; Li et al., 2018 |
| | Histone crotonylation | ACSS2 | Sabari et al., 2015; Jiang et al., 2018 |
| Trans-regulation | Transcription initiation blocks | Low NFAT,<br>Low NF-κB,<br>Low STAT5,<br>CTIP2,<br>TRIM22,<br>APOBEC3A | Williams et al., 2006; Marban et al., 2007; Della Chiara et al., 2011; Hakre et al., 2012; Turrini et al., 2015; Bosque et al., 2017; Forouzanfar et al., 2019; Taura et al., 2019 |
| | Transcription elongation blocks | NELF,<br>DSIF,<br>Absence of Tat,<br>Low P-TEFb | Yamaguchi et al., 1999; Nguyen et al., 2001; Yang et al., 2001; Weinberger et al., 2005; Burnett et al., 2009; Cherrier et al., 2013; Eilebrecht et al., 2014; Jadlowsky et al., 2014 |
| | Post-transcriptional blocks | Low MATR3,<br>PTB,<br>PSF miRNAs (PCAF,<br>CynclinT1)<br>Long non-coding RNA (NRON) | Triboulet et al., 2007; Kula et al., 2011; Budhiraja et al., 2013; Suzuki et al., 2013; Rice, 2016; Kessing et al., 2017; Sarracino et al., 2018 |

initiation (Adams et al., 1994). Moreover, a mature NF-κB subunit, p50, can homodimerize to further suppress the NF-κB mediated transcription by binding to the HIV-1 promoter region and recruiting HDAC1 (**Figure 2B**; Zhong et al., 2002). Activated cytoplasmic PKC promotes ubiquitination and degradation of IκB to allow for nuclear translocation of NF-κB. The PKC

pathway resulting in the activation of NF-κB is one of the most important pathways in HIV reactivation (reviewed in Colin and Van Lint, 2009; McKernan et al., 2012). PKC agonists, such as prostratin (Gulakowski et al., 1997; Williams et al., 2004), bryostatin-1 (Gutiérrez et al., 2016), and ingenol (Pandeló José et al., 2014), are highly effective in inducing latent HIV-1 expression from the viral reservoir through NK-κB signaling (Jiang and Dandekar, 2015). Therefore, PKC inhibitors have been investigated as promising candidates for HIV-1 eradication. In addition to the canonical NF-κB (cNF-κB) pathway, other NF-κB subpathways, including non-canonical (ncNF-κB) signaling, have been reported to regulate NF-κB responsible elements (Sun and Ley, 2008; Sun, 2017; Wong and Jiang, 2021). While cNF-κB signaling leads to RelA/p50 heterodimer binding to the promoter region (Deng et al., 2018), ncNF-κB signaling cleaves p100 into p52, which forms a transcriptional complex with RelB. Activation of ncNF-κB signaling was recently reported to induce HIV expression in both HIV-infected humanized mice and SIV-infected macaques under suppressive treatment (Hennessy et al., 2013; Nixon et al., 2020), indicating that ncNF-κB signaling is also involved in HIV latency.

Even after transcription initiation, RNA Pol II pauses at the promoter region due to the binding of negative elongation factors such as NELF and DSIF, causing RNA Pol II to terminate prematurely (**Figure 2B**; Yamaguchi et al., 1999). These mechanisms govern the HIV-1 promoter, tangling the LTR and preventing transcription factors from accessing the viral promoter region. Yukl et al. (2018) found that CD4+ T cells from PLWH on cART harbor more blocks to transcriptional elongation, completion, and splicing than transcriptional initiation. This indicates that the repression of HIV-1 transcription and splicing occurs at different stages and is regulated by different mechanisms, overall suggesting that HIV-1 latency is heterogeneous in CD4+ T cells.

Some of the proteins affecting viral transcription have been identified specifically in myeloid cells (Le Douce et al., 2012; Kruize and Kootstra, 2019), and interventions designed to block Tat function have been studied as a means to induce a latent state in macrophages and microglia (Alamer et al., 2020). Epigenetic regulation of HIV transcription does occur in myeloid cells, but studies that have examined changes in epigenetic modifiers at cellular promoters in response to HIV-1 infection in myeloid cells indicate that regulatory mechanisms are distinct from T cells (Wierda et al., 2012; Corley et al., 2016).

Non-coding RNAs (ncRNAs) have also been shown to be involved in gene regulation and mRNA splicing (Ranki et al., 1994), and were found to be involved in HIV-1 latency. Specifically, cellular miRNAs induce RNA silencing and post-transcriptional regulation of gene expression (Bissels et al., 2009). Long non-coding RNAs (lncRNAs) play key roles in RNA splicing and stability (Khalil et al., 2009). miRNAs modulate HIV-1 replication either by directly targeting the HIV-1 mRNA (Hariharan et al., 2005) or host mRNAs that code for transcription factors of HIV-1 (Brass et al., 2008; Zhou et al., 2008; Yeung et al., 2009; Houzet and Jeang, 2011). For instance, miR-17, miR-5p and miR-20a target PCAF (Triboulet et al., 2007), a transcriptional coactivator to interact with Tat and functionally synergize to activate the HIV-1 promoter (Mujtaba et al., 2002), and miR-198, miR-27b, miR-29b, miR-150, miR-223 target CyclinT1 (Sung and Rice, 2009; Chiang et al., 2012; Budhiraja et al., 2013) to regulate viral expression and production. Work by Carpio et al. (2010) and Klase et al. (2007) found that high expression of these miRNAs correlates with less susceptibility to HIV-1 infection in monocytes in comparison to macrophages. A set of mixed miRNAs enriched in monocytes represses the expression of PUR-α, a cofactor of Tat (Shen et al., 2012). The miRNA induced by Tat called miR-217 targets the host protein Sirtuin-1, which deacetylates and inactivates Tat, increasing HIV-1 expression (Zhang et al., 2012). A latency inducible lncRNA represented by NRON is highly expressed in resting CD4+ T cells and is involved in HIV-1 latency by mediating Tat degradation (**Figure 2B**; Li J. et al., 2016). Interestingly, the knockdown of NRON increases HIV-1 replication by enhancing NFAT activity (Imam et al., 2015). In another study, Li et al. reported that a novel lncRNA AK130181 (also named LOC105747689) was highly expressed in latently infected CD4+ T lymphocytes and inhibited HIV-1 transcription in an NF-κB-dependent manner (Li et al., 2020). Considering these latency mechanisms and other regulations for HIV-1 gene expression (**Table 1**), HIV-1 latency appears to be established by both cis- and trans-regulatory elements and in a cell lineage-specific manner.

## Human Immunodeficiency Virus Integration and Clonal Expansion

Integration is a hallmark of retroviruses and a central step in the HIV replication cycle that enables long-term HIV-1 persistence (Anderson and Maldarelli, 2018). HIV-1 integration into the host genome is generally non-specific with slight preferences toward introns of actively transcribed genes and typically exclude promoter regions (Mack et al., 2003; Han et al., 2004; Ikeda et al., 2007). cART successfully halts HIV replication by targeting various steps in the virus replication cycle, however current therapies do not target HIV-1 transcription or result in direct infected cell killing. The cells that harbor latent HIV-1 proviruses can persist for years despite therapy (Finzi et al., 1997; Wong et al., 1997; Siliciano et al., 2003) and undergo clonal expansion (Maldarelli et al., 2014; Wagner et al., 2014). The landscape of HIV-1 infected cells is shaped over time through cytopathic effects, immune responses, and infected cell proliferation (Anderson et al., 2020; Liu et al., 2020). HIV-1 infected cells can undergo clonal expansion through three distinct mechanisms: (1) homeostatic proliferation, (2) in response to the infected cells cognate antigen, or (3) in some cases as the result of the proviral integration site (**Figure 3**; Anderson and Maldarelli, 2018; Liu et al., 2020). Each driver of HIV-1 infected cell division can contribute to sustaining the HIV-1 reservoir despite cART. Homeostatic proliferation promotes HIV-1 persistence by allowing latently infected cells to undergo cell division in the absence of viral reactivation or cellular differentiation (**Figure 3A**; Chomont et al., 2009; Bosque et al., 2011; Musick et al., 2019). This indicates that the homeostatic proliferation of infected cells can sustain and replenish the HIV-1 reservoir while eluding the effects of cART. Antigen-driven

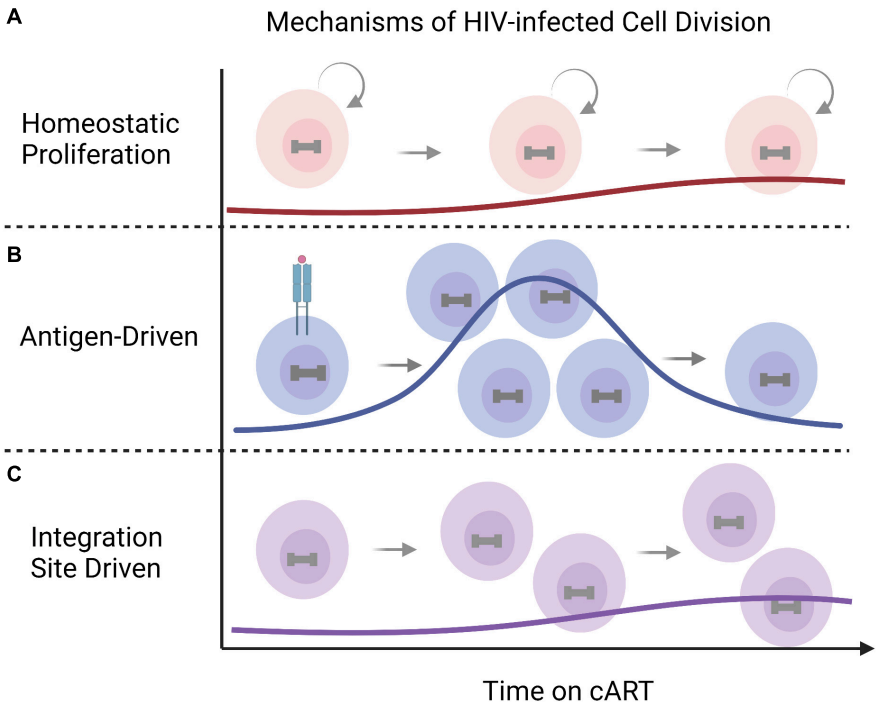


**FIGURE 3 |** Mechanisms of clonal expansion in HIV-1 infected cells. HIV-infected cells undergo cell division overtime to maintain the HIV reservoir despite antiretroviral therapy. The mechanisms of HIV-1 infected clonal expansion include **(A)** normal homeostatic proliferation, **(B)** antigen-driven expansion in response to periodic or persistent cognate antigen exposures, or, in some cases, through **(C)** integration-site driven expansion (for example *BACH2*, *MKL2,* and *STAT5B)*. This figure was created with BioRender.com.

clonal expansion occurs when an HIV-1 infected cell recognizes its cognate antigen (**Figure 3B**; Douek et al., 2002; Mendoza et al., 2020; Simonetti et al., 2021). HIV-1 primarily infects CD4+ T cells, which proliferate in response to antigenic interactions (Douek et al., 2002). The expansion of infected cells driven by antigen interactions is likely reflected in persistent, and/or waxing and waning of clonal populations through chronic and repeat exposures (Wang et al., 2018). Finally, the contribution of integration-site-driven clonal expansion likely plays only a minor role in sustaining the HIV-1 reservoir (**Figure 3C**) (Coffin et al., 2021). Proviral integration into oncogenes, such as *BACH2*, *MKL2,* and *STAT5B,* occurs rarely and is revealed after years of therapy, indicating the integration site itself may provide a selective advantage for long-term persistence (Maldarelli et al., 2014; Wagner et al., 2014; Cohn et al., 2015). All three mechanisms of HIV-1 infected cell proliferation can drive the persistence and expansion of the HIV-1 reservoir cells and pose major obstacles for curative strategies.

Although the majority of integrated proviruses are defective (Ho et al., 2013; Bruner et al., 2016, 2019; Imamichi et al., 2016), cells harboring intact replication-competent proviruses also undergo clonal expansion to sustain the HIV-1 reservoir despite cART (Simonetti et al., 2016; Bui et al., 2017; Lee et al., 2017; Patro et al., 2019). Once cART is stopped, viremia rebounds from this persistent, replication-competent reservoir to near pre-therapy levels within weeks for most individuals (Joos et al., 2008). It has recently been estimated that over 50% of inducible, replication-competent proviruses within the latent reservoir arose as the result of *in vivo* proliferation (Lorenzi et al., 2016; Bui et al., 2017; Hosmane et al., 2017). As this is likely an underestimate, these findings indicate that the proliferation of HIV-1 infected cells harboring replication-competent proviruses is one of the major mechanisms that maintains the reservoir and presents a challenge toward an HIV cure. Future curative strategies may aim to directly target cell-killing of HIV-1 infected cells or to blunt infected cell proliferation.

## Defective Proviruses

Although HIV-1 rebounds from replication-competent reservoir cells harboring intact proviral DNA upon cART cessation, the majority of proviruses are defective with large internal deletions or lethal mutations and clonally expand *in vivo* (Coffin and Hughes, 2021). Defective proviruses account for more than 95% of the total proviruses in the peripheral blood isolated from cART-treated PLWH (Siliciano et al., 2003; Eriksson et al., 2013; Crooks et al., 2015). Defective proviruses were initially thought to have little impact on HIV pathogenesis and disease progression due to their inability to produce infectious virions. However, it has recently been discovered that a fraction of defective proviruses are transcriptionally active (Imamichi et al., 2016) and can contribute to chronic immune activation (Pollack et al., 2017). Novel unspliced forms of viral RNAs transcription from defective proviruses can produce HIV-1 Gag and Pol proteins (Imamichi et al., 2020). These observations indicate that

defective proviruses are capable of producing virus-like particles (VLPs) or viral proteins, which may become constitutive antigens (**Figure 4**). Chronic inflammation and persistent immune activation occurs in most individuals on long-term cART despite successful virus suppression and can induce immunological tolerance that enhances autoreactive antibody production, making it difficult to establish protective humoral immunity (van den Dries et al., 2017). VLPs have previously been employed for immunization purposes and demonstrated that immature morphology enhanced immunogenicity of VLPs and strongly induced IFN-γ secretion and antibody production (Álvarez-Fernández et al., 2012; Gonelli et al., 2019). Approximately 20% of the virions harboring intact protease still remain immature morphology after budding (Sarca et al., 2021), which implies that VLPs generated from defective proviruses might contribute to chronic inflammation in PLWH. In addition, proviruses with defective major splice donors or hypermutations induced by APOBEC3 cytidine deaminase enzymes (Izumi et al., 2008; Fukuda et al., 2019) can produce antigens against CTL and constitutively induce their activation (Shankar et al., 2000; Monajemi et al., 2014; **Figure 4**). It had long been thought that defective proviruses were irrelevant viral DNA sequences. However, defective proviruses capable of transcribing novel unspliced viral RNA can be found in individuals at all stages of virus infection, adding to the complexity of linked chronic immune stimulation in some PLWH.

# CURE STRATEGIES

## Kick-and-Kill Strategy

One of the potential strategies toward HIV-1 eradication has been named "Kick-and-Kill" therapy. This approach is contingent upon the reactivation of latently infected cells in the presence of cART through the use of LRAs, and subsequent elimination of reactivated HIV-1 infected cells by the immune system or other interventions (**Figure 5**). Several pathways related to cis- and trans-regulating factors such as histone deacetylase (HDAC), NF-κB signaling, or PKC activation have been targeted to reactivate latently infected cells (Ait-Ammar et al., 2020). Several classes of LRAs have been described, to date (**Table 2**). Epigenetic modifiers such as histone acetylation/methylation, DNA methylation, or chromatin remodeling affect viral RNA transcription, splicing, or subsequent nuclear export pathway by altering the chromatin structure and DNA accessibility (Darcis et al., 2017; Ait-Ammar et al., 2020). HDAC inhibitors such as vorinostat, panobinostat, and romidepsin have been extensively studied in clinical trials, but the single-use of these inhibitors has not led to the eradication of latently infected cells *in vivo* (Kim et al., 2018). On the other hand, the combination of HIV-1 specific CD8+ cytotoxic T lymphocytes activation upon the usage of vorinostat showed promise to be effective for purging the latent reservoir cells in *ex vivo* experiments (Sengupta and Siliciano, 2018).

PKC agonists may also be a suitable clinical approach for targeting NF-κB signaling in HIV-1 latency reactivation. Bryostatin, targeting NF-κB signaling, has been studied to reactivate latent cells *in vivo*, but unfortunately, no transcriptional enhancement was observed in HIV-1 latently infected cells in clinical settings (French et al., 2020). On the other hand, Derivatives of ingenol have been gaining interest in the reactivation of HIV-1 expression both *in vitro* and *in vivo* through NF-κB signaling (reviewed in Jiang and Dandekar, 2015). Ingenol-3-hexanoate was found to reactivate latent HIV-1 in J-Lat cells at a low concentration, hence lower cellular cytotoxicity (Jiang G. et al., 2014). Ingenol-3-angelate (PEP005), in combination with the P-TEFb agonist, JQ1, can synergistically reactivate latent HIV-1 with 7.5-fold higher effectiveness than PEP005 alone (Jiang et al., 2015). Interestingly, ACSS2-mediated histone crotonylation can also be associated with PEP005 to reactivate latent CD4+ T cells from HIV-infected individuals (Jiang et al., 2018). Ingenol 3,20-dibenzoate was found to activate resting CD4+ T cells from HIV-1 ART-treated aviremic patients and is potentially a marker to measure the reactivation of resting CD4+ T cells from treated PLWH (Spivak et al., 2015).

Recently, a family of IAP inhibitors (IAPi)/the mimetics of second mitochondria-derived activator of caspases (SMACm), such as Debio 1143 and AZD5582, have been proposed as a new class of LRAs *via* the induction of ncNF-κB signaling (Dashti et al., 2020). Debio 1143 was shown to lead to latent HIV reversal through the degradation of BIRC2/cIAP, a ubiquitin ligase that acts as a repressor of the ncNF-κB pathway *in vivo* using ART-suppressive BLT humanized mice or *ex vivo* using resting CD4+ T cells isolated from HIV-infected individuals with cART (Bobardt et al., 2019). AZD5582 was also found to induce SIV-RNA from latency in lymph node tissues of the ART-suppressive SIV-infected rhesus macaques by inhibiting BIRC2/cIAP. While these studies implied a potency of IAPi/SMACm as new LRAs *via* the novel ncNF-κB signaling pathway (Wong and Jiang, 2021), recent research applying AZD5582 failed to reduce reservoir size in the SHIV model (Nixon et al., 2020), indicating that latency reversal efficacy of IAPi/SMACm monotherapy may not be enough (Wong and Jiang, 2021). Furthermore, the induction of ncNF-κB signaling causes cell death in memory CD4+ T cells where latent HIV provirus is enriched (Wong and Jiang, 2021). Therefore, further studies are required to understand the complexity of both cNF-κB and ncNF-κB signaling pathways to create effective LRAs.

Other agonists targeting the innate immune receptors, TLR7 or TLR9, were also used to reactivate HIV-1 latent cells. The combination of HIV-1 Env-specific broadly neutralizing antibodies (bNAb) PGT121 together with the TLR7 agonist, vesatolimod GS-9620, delayed viral rebound following cART cessation in SIV/HIV chimeric virus (SHIV)-infected rhesus macaques that initiated antiretroviral treatment during acute infection (Bruno and Stoughton, 1984; Gutiérrez et al., 2016). However, the use of GS-9620 in phase I clinical trials with HIV-1 infected individuals on cART (NCT02858401) was discontinued due to adverse effects and an underwhelming impact on the plasma HIV-1 RNA and total DNA in CD4+ T cells. In addition, TLR9 agonist MGN1703 showed a moderate latency-reversing effect in HIV-1 infected participants, but a reduction in the reservoir size was not observed (Vibholm et al., 2017, 2019).

Considering that targeting a single mechanism with LRA monotherapy might not be sufficient to reactivate most latent

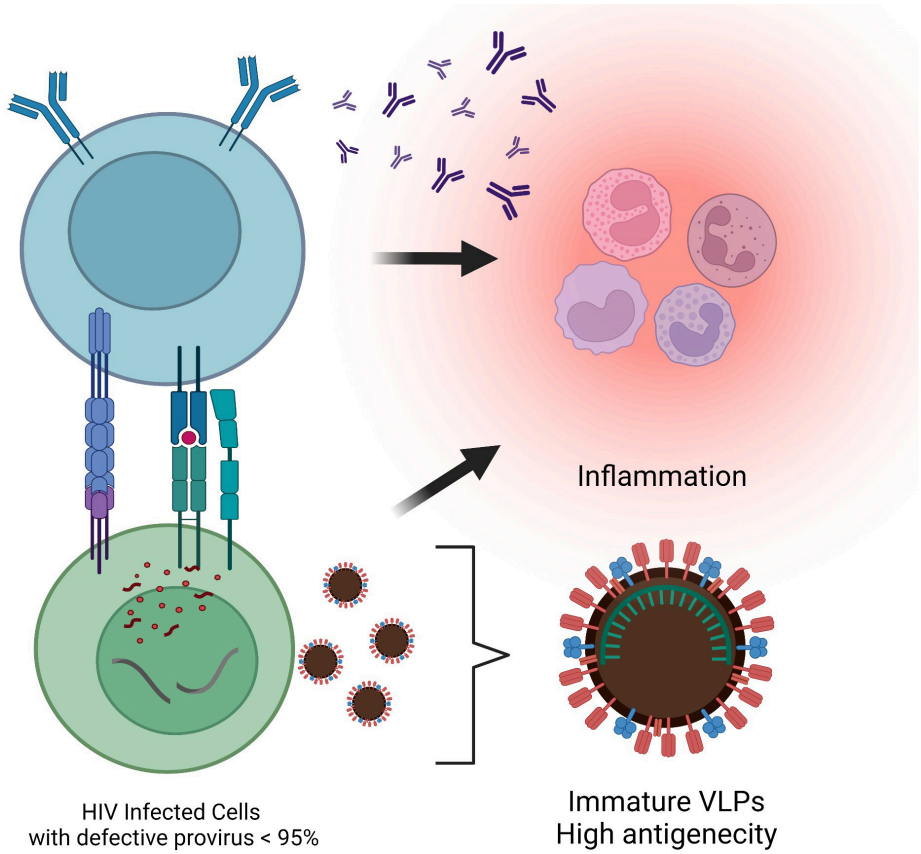


**FIGURE 4 |** Antigenicity of the defective provirus. Most proviruses are defective with large internal deletions or hypermutations. Viral-like particles are released from novel unspliced viral RNAs transcribed from the defective proviruses. In addition, cytotoxic T lymphocytes are activated by the antigens presented by proviruses with defective major splice donors or hypermutations, which results in leading to chronic inflammation in individuals on cART. This figure was created with BioRender.com.

cells, a combination of several different classes of LRAs targeting heterogenous silencing mechanisms may be required (Ait-Ammar et al., 2020). One study participant treated with MGN1703 showed viral control to undetectable levels upon cART cessation along with robust HIV-1 specific effector memory subset of CD8+ T cells and neutralization antibody production (Schleimann et al., 2019). This suggests that adaptive immunity is essential for the kick-and-kill approach. However, LRAs could impair multiple CD8+ T cell functions (Clutton and Jones, 2018). To date, successful reduction of the reservoir size *in vivo* has not been observed with LRA monotherapy, but has been seen using romidepsin and immune checkpoint blockade (ICB) nivolumab targeting PD-1 (Chun et al., 1997; Darcis et al., 2017).

As outlined above, the HIV-1 latent reservoir exists in cellular and tissue compartments and likely has multiple maintenance mechanisms. This may require diverse LRAs targeting a wide variety of latent cells, which poses challenges for therapies. Due to a lack of understanding of the various determinants contributing to the heterogeneity in HIV-1 latency, no LRA has been proved successful in clinical trials. Therefore, there is a need to understand the safety and potency of kick-and-kill strategies to develop effective LRA combination with immunostimulants to treat PLWH (Ait-Ammar et al., 2020).

## Immunomodulation

As we described before, HIV-1 preferentially infects CD4+ T cells and establishes long-term residency within affected individuals (Douek et al., 2002). In the standard progression of HIV-1 without therapy, normal progressors experience a decline in immune function (Boasso et al., 2009). Within the first 6–8 weeks post-exposure to HIV-1, the host experiences a significant decrease in CD4+ T cells, a concomitant increase in viral load, and a corresponding increase in immune activation (Fauci, 1991; Mellors et al., 1996; Coffin et al., 1997; Boasso et al., 2009) and a decrease in immune function. To control the infection, the host mounts an adaptive immune response via CD8+ T cells (Borrow et al., 1994; Koup et al., 1994). Despite these efforts, HIV persists in a small number of cells that can survive for a prolonged time.

Immune activation and inflammation are persistently driven by the ability of HIV-1 to evade detection and elimination by the immune system, the large-scale depletion of CD4+ T cells that regulate the adaptive immune response to infection, and the inability of cART to eliminate latently infected cells (Hazenberg et al., 2000; Gougeon, 2005; Leonard et al., 2008; Dinoso et al., 2009; Chun et al., 2010; Manel and Littman, 2011). During chronic infection, the host immune system must adapt to find new homeostasis which minimizes tissue damage

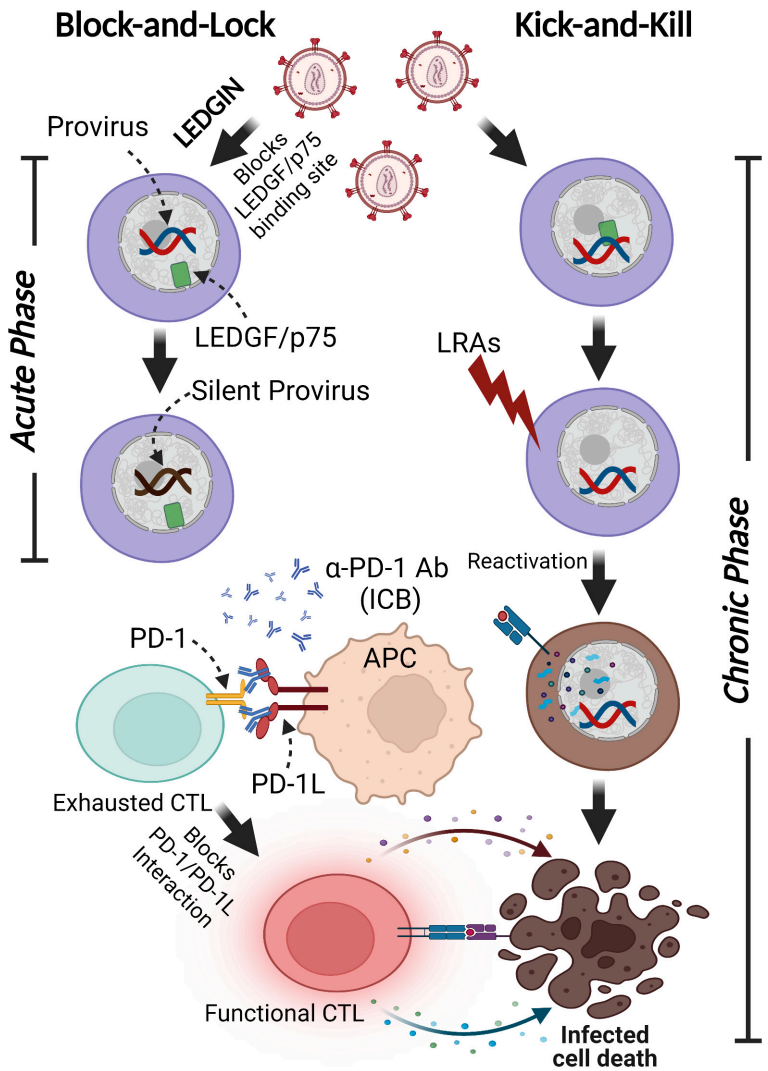


**FIGURE 5 |** Functional cure strategies: Block-and-Lock and Kick-and-Kill approaches. A minor subset of infected cells harbors latent proviruses following infection. LEDGIN-mediated "Block-and-Lock" functional cure aims to permanently silence the provirus to block viral reactivation in the absence of cART. LEDGINs inhibit the LEDGF/p75-Integrase interaction, resulting in the redirection of integration into transcriptionally silent regions. The "Kick-and-Kill" strategy aims to decrease the size of functional HIV-1 reservoirs by reactivating proviral transcription with LRAs, leading to the elimination of infected cells via immune systems stimulated by ICB. This figure was created with BioRender.com.

from persistent inflammation while still maintaining control of infection. To mitigate immunopathology, the immune system has evolved mechanisms to progressively attenuate the immune response during chronic infection. Over time this leads to a state of hypo-responsiveness and eventual immunological tolerance of the virus. T cell exhaustion is one such mechanism in which effector T cells upregulate multiple inhibitory immune checkpoint receptors during chronic infection which results in the hierarchical loss of function (Xiong et al., 2001; Wherry et al., 2003; Saez-Cirion et al., 2007; McLane et al., 2019).

T cell exhaustion has been characterized by the co-expression of multiple inhibitory immune checkpoints such as cytotoxic lymphocyte antigen-4 (CTLA4), programmed cell death-1 (PD-1), T-cell immunoglobulin and mucin-domain-containing 3 (TIM3), T-cell immune receptor with Ig and ITIM domains (TIGIT), and lymphocyte-activation gene 3 (LAG3) on the surface of immune cells (Wherry and Kurachi, 2015). Immune checkpoints receptors, when engaged with their corresponding ligand, negatively regulate T cell activation (Blackburn et al., 2009). T cell exhaustion impacts the ability of CD8+ T cells to suppress viral replication (Mueller et al., 2001; Appay et al., 2002; Wherry et al., 2007; Wherry and Kurachi, 2015).

Recent literature has demonstrated that T cell exhaustion persists despite treatment with cART (Day et al., 2006; Nakanjako et al., 2011; Khoury et al., 2017; de Armas et al., 2019; Macatangay et al., 2020). While cART effectively reduces HIV-1 viral load to undetectable levels and significantly improves life expectancy, it is not a sterilizing cure nor does it fully restore

**TABLE 2 |** LRAs classified based on their various activities.

| LRA Class | Target | Drugs | References |
|---|---|---|---|
| Epigenetic modifiers | HDAC inhibition | HDACis: TSA, trapoxin, SAHA, romidepsin, panobinostat, entinostat, givinostat, valproic acid, MARK-1/11, AR-42, fimepinostat, chidamide | Van Lint et al., 1996; Quivy et al., 2002; Ylisastigui et al., 2004; Archin et al., 2009, 2012; Rasmussen et al., 2013; Wightman et al., 2013; Mates et al., 2015; Søgaard et al., 2015; Banga et al., 2016; Kuai et al., 2018; Yang et al., 2018; Gunst et al., 2019 |
| | Suv39H1, G9a, SMYD2 | HMTis: chaetocin, EPZ-6438, GSK-343, DZNEP, BIX-01294, UNC-0638 | Friedman et al., 2011; Bouchat et al., 2012; Nguyen et al., 2017 |
| | DNMT1, 3a, 3b | DNMTis: 5-AzaC, 5-AzadC | Bouchat et al., 2016 |
| | RUNX1/STAT5 | Benzodiazepines | Klase et al., 2014; Elbezanti et al., 2020; Lin et al., 2021 |
| Benzotriazole derivatives | STAT5 activation | 1-hydroxybenzotriazole (HOBt) | Bosque et al., 2017 |
| Activators of Akt pathway | Upregulation of Akt signaling pathway | Disulfiram | Xing et al., 2011; Doyon et al., 2013; Spivak et al., 2014 |
| Inducers of P-TEFb release | Release of P-TEFb | BETis: JQ1, I-BET, I-BET151, OTX015, UMB-136, MMQO, CPI-203, RVX-208, PFI-1, BI-2536, and BI-6727 HMBA | Contreras et al., 2007; Bartholomeeusen et al., 2012; Lu et al., 2016, 2017; Huang et al., 2017; Abner et al., 2018; Gohda et al., 2018; Liang et al., 2019 |
| SMAC mimetics | Induction of non-canonical NF-κB pathways | SBI-0637142 Birinapant | Pache et al., 2015; Hattori et al., 2018 |
| CCR5 antagonist | NF-κB activation | Maraviroc | López-Huertas et al., 2017; Madrid-Elena et al., 2018 |
| MAPK agonist | Procyanidin trimer C1 | MAP Kinase activation | Cary and Peterlin, 2018 |
| PKC agonists | NF-κB activation | Prostratin Bryostatin-1 Ingenols: Ingenol-B, Ingenol 3,20-dibenzoate (Ingenol-db), ingenol-3-angelate (ingenol mebutate, PEP005) | Kulkosky et al., 2001; DeChristopher et al., 2012; Jiang L. et al., 2014; Spivak et al., 2014, 2015 |
| Tat vaccine | Tat Oyi vaccine Tat-R5M4 protein | Activation of HIV-1 LTR | Geng et al., 2016 |

host immune function (Migueles et al., 2009; Deeks, 2011; Arts and Hazuda, 2012; Wilson and Sereti, 2013; Serrano-Villar et al., 2014; Deeks et al., 2015; Perdomo-Celis et al., 2019). Poor immune reconstitution contributes to comorbidities that arise despite long-term treatment with cART, which necessitates an intervention that can restore an exhausted immune system (Baker et al., 2008). One such approach to rejuvenating exhausted T cells is through the use of immunotherapy in which monoclonal antibodies bind to immune checkpoints receptors, block their inhibitory signaling pathways, and consequently boost the immune response to chronic infection or cancer (Śledzińska et al., 2015). There are several FDA-approved cancer immunotherapies that target CTLA-4, PD-1, and PD-L1, which are now being investigated as potential novel strategies to reinvigorate a dysfunctional immune system exhausted by chronic HIV (Abbar et al., 2020; Sahin et al., 2020). The aspirational goal of such studies is to revitalize the immune system in such a way that PLWH could control the virus immunologically, without the need for intensive cART regimens.

The use of immunotherapy for PLWH was initially evaluated in HIV-1 positive cancer patients and it was determined that it was safe and effective for the treatment of cancer in patients with well-controlled viremia (Uldrick et al., 2017). Additional studies determined that the use of immunotherapy in these patients imposed no adverse effects on both CD4+ T cell count and plasma viral load (Cook and Kim, 2019; Abbar et al., 2020; Sahin et al., 2020), while some studies observed that participants experienced grade 3 or higher adverse events with various types of immunotherapy (Sahin et al., 2020). Guihot et al. (2018) demonstrated that treatment with PD-1 immunotherapy resulted in a dramatic decrease in plasma viral RNA and a concomitant increase in HIV-1 specific CD8+ T cells for a single cancer patient living with HIV (Guihot et al., 2018). The possible dual benefits of using immunotherapy to restore the functionality of exhausted CD8+ T cells, reverse HIV-1 latency through activation of viral transcription in CD4+ T cells (Wherry and Kurachi, 2015; Evans et al., 2018; Fromentin et al., 2019; Van der Sluis et al., 2020), and the favorable results of immunotherapy on HIV-1 positive cancer patients have led investigators to evaluate it for the treatment of virally suppressed otherwise healthy PLWH (Gay et al., 2017; Abbar et al., 2020). These studies concluded that participants were able to maintain viral suppression on immunotherapy, restored anti-HIV activity as demonstrated by a further reduction in plasma viral RNA varied (Gay et al., 2017; Abbar et al., 2020).

Immune checkpoint blockade has been utilized as immunotherapy to treat cells exhausted by chronic infection with cancer but these therapies have also been modestly effective at improving anti-tumor immunity (Pardoll, 2012;

Shayan et al., 2017). One caveat to utilizing ICB for effective immunotherapy is the co-expression of multiple inhibitory receptors on immune cells (Shayan et al., 2017; Zahavi and Weiner, 2019) which might explain their modest impact at further reducing plasma viremia in otherwise healthy PLWH and warrants the use of combinatorial immunotherapy. Combinatorial therapy using ICB might not be sufficient to reverse the effects of exhaustion and restore the functionality of CD8+ T cells as recent studies have identified epigenetic modifications which may also restrict the effectiveness of ICB.

Epigenetic modifications are known to regulate T cell differentiation and are integral to the formation and heritability of various T cell subsets. These T cell subsets permit both the effective control of infection and also regulate effector function (Scharer et al., 2013; Chen et al., 2018; Henning et al., 2018; Zebley et al., 2020). Recent studies have begun to explore the epigenetic landscape of the exhausted CD8+ T cells and have determined that they are an epigenetically distinct subset of cells (Youngblood et al., 2011; Jadhav et al., 2019; Khan et al., 2019; Calle-Fabregat et al., 2020). Scharer et al. evaluated CD8+ T cell response to acute Lymphocytic Choriomeningitis virus infection from naïve and effector T cells and observed genome-wide DNA methylation of CD8+ T cells following T cell activation which permitted the inheritance of effector functions (Scharer et al., 2013). DNA methylation is a contributing epigenetic mechanism that regulates CD8+ T cell exhaustion (Youngblood et al., 2011, 2013; Scharer et al., 2013; Pauken et al., 2016; Ghoneim et al., 2017; Yates et al., 2021) and has been demonstrated to impact CD8 restoration by ICB (Ahn et al., 2016; Pauken et al., 2016; Ghoneim et al., 2017). It was demonstrated that T cell exhaustion can be categorized into two distinct stages which are delineated by *de novo* DNA methylation to the PD-1 promoter (Ghoneim et al., 2017). These epigenetic modifications to CD8+ T cells acquired during the effector phase regulate both the formation and heritability of terminally differentiated exhausted CD8+ T cells which preclude restoration by PD-1 blockade (Ahn et al., 2016; Pauken et al., 2016; Ghoneim et al., 2017). Epigenetic targeted therapy could potentially reverse the repressive epigenetic modifications that enforce CD8+ T cell exhaustion which could lead to a novel strategy in the treatment of HIV.

Chimeric antigen receptor (CAR)-T cell therapy is a kind of adaptive immunotherapy that genetically engineers a patient's T cells to recognize and bind to foreign antigens on the antigen-expressing cells (Maus and Levine, 2016; Hartmann et al., 2017). Patients with hematologic malignancies, such as lymphocytic leukemia, lymphoblastic leukemia, diffuse large B-cell lymphoma, and follicular lymphoma, successfully achieved their treatment plans with CAR-T cell therapy (Porter et al., 2011; Maude et al., 2014; Schuster et al., 2017). Key components of CAR technology are the extracellular single-chain fragment variant derived from the antigen-binding region and the intracellular signaling domains containing CD3ζ, CD28, and 4-1BB (Maher et al., 2002; Imai et al., 2004; Porter et al., 2011; Srivastava and Riddell, 2015). Therefore, CAR can be designed to recognize specific antigens and subsequently induce activation of the immune response against target antigens. CD8+ T cells are collected from HIV-infected individuals and inserted with CAR genes *in vitro*, whose anti-HIV efficacy was verified, and then autologous HIV-specific CAR-T cells were transplanted into the patients (Qi et al., 2020). Recently, broadly neutralizing antibodies (bNAbs) targeting HIV-1 envelope glycoprotein have been used to construct anti-HIV specific CAR-T cells (Kwong et al., 2013; Ali et al., 2016). Hale et al. showed that CARs engineered with four types of bNAbs (PGT-128, PGT-145, VRC07-523, and 10E8) effectively activate and kill HIV-infected cells. Moreover, the integration of an HIV-1 CAR gene expression cassette into the CCR5 locus *via* homology-directed repair leads to the suppression of replicating of the virus (Hale et al., 2017). Currently, there are two ongoing clinical trials of CAR-T cell therapy in PLWH under cART (NCT03240328 and NCT03617198) to evaluate CD4-CAR T cells with CCR5 disruption for HIV resistance. Although there are obstacles in CAR-T cell therapy development, such as cell expansion *in vivo*, off-target effects, and severe cytokine storm (reviewed in Qi et al., 2020), it is worth exploring the potential of CAR-engineered T-cell therapy for an HIV cure.

Although current cART is very effective in targeting HIV pathogenesis, the pervasive nature of this disease requires the continued development of new ways to target viral replication and improve immune function. A focus on understanding the mechanisms of HIV-1 suppression by those with the innate ability to control the virus (Clerici et al., 1992; Kelker et al., 1992; Cao et al., 1995; Huang et al., 1995; Pinto et al., 1995; Rowland-Jones et al., 1995; Fowke et al., 1996; Lefrère et al., 1999; Shacklett, 2006; Dyer et al., 2008; Pereyra et al., 2008; Gonzalo-Gil et al., 2017; Pernas et al., 2018; Lopez-Galindez et al., 2019; Nguyen et al., 2019; Macatangay et al., 2020) has the potential to identify novel ways to improve host immune function, give insight into immune mechanisms that are common to both chronic infection and cancer, and rapidly treat PLWH with FDA approved therapies. As cells harboring reactivated proviruses by LRAs would then be required to be eliminated by CTL, the combination therapy with LRAs and ICBs/CAR-T could achieve a functional HIV-1 cure for chronic HIV infection (**Figure 5**).

## Block-and-Lock Strategy

The inability of the immune system to eradicate latently infected cells, due to the lack of viral protein expression, permits the long-term persistence of HIV-1 infected cells. In contrast to the "Kick-and-Kill" strategy, the "Block-and-Lock" approach aims to promote permanent provirus silencing even after cART cessation. This strategy ultimately seeks to affect both pre-integration and post-integration stages. HIV-1 DNA is preferentially integrated into transcriptionally active sites located near the nuclear pore, where chromatin is decondensed (Demeulemeester et al., 2015). Integration into a transcriptionally inactive site promotes proviral silencing. Lens epithelium-derived growth factor (LEDGF/p75) is a chromatin-binding host protein that supports HIV-1 DNA integration through interactions with the HIV-1 integrase protein (Vranckx et al., 2016). Treatment with a LEDGF inhibitor, LEDGINs, can dramatically redirect HIV-1 DNA integration sites to regions that are resistant to reactivation, potentially leading to a deeply silenced reservoir

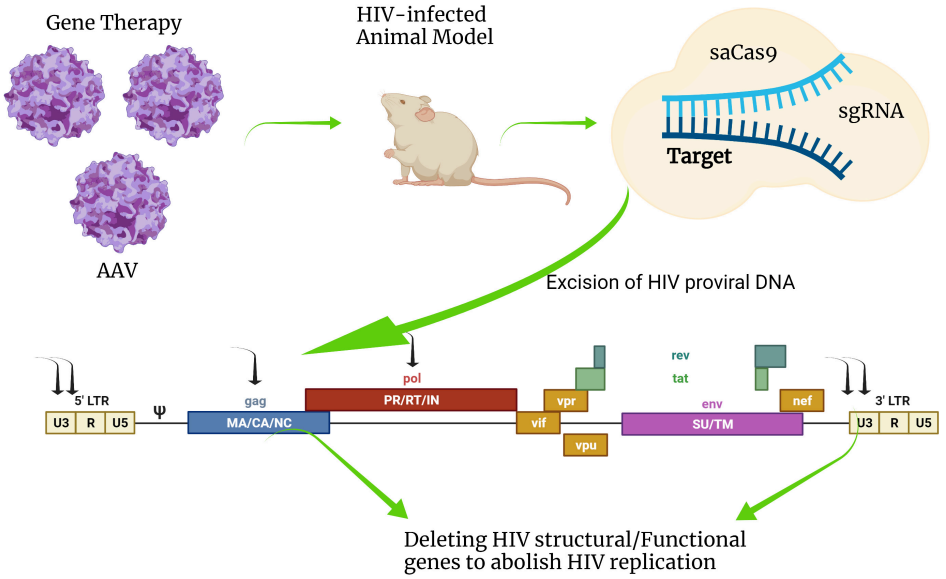


**FIGURE 6 |** Schematic diagram of HIV-1 provirus DNA deactivation by CRISPR/Cas9 genome editing technology. Cas9 nuclease combined with gRNAs targeting multiple sites in HIV-1 DNA sequences such as 5′-LTR, 3′-LTR, gag, or pol can deactivate integrated viral DNA. Cas9 can be efficiently delivered by an adeno-associated virus vector (AAV) system *in vivo*. This figure was created with BioRender.com.

even after cART cessation (**Figure 5**; Christ et al., 2012; Kessl et al., 2012; Vranckx et al., 2016). LEDGIN treatment in the case of successful viral integration retargets the transcriptional factors out of active genes, which results in a prolonged latent state. This can lead to the inability of LRAs to reactivate silenced integrated proviruses (Gao et al., 2020). Therefore, LEDGINs might only help to reduce HIV-1 reservoir susceptibility to reactivation early after infection, prior to integration and the seeding of the reservoir.

A post-integration Block-and-Lock strategy aims to permanently suppress HIV-1 transcription to prevent viral reactivation even after successful proviral DNA integration. Post-integration silencing methods target the trans-regulation mechanisms to suppress viral gene expression by inhibiting viral and host transcription factors such as HIV-1 Tat, P-TEFb, and NF-κB. Tat is required for the stimulation of HIV-1 transcriptional elongation by binding an RNA element in the LTR and recruiting several transcription-activating proteins (Roy et al., 1990; Zhu et al., 1997). Didehydro-cortistatin A (dCA), the equipotent analog of cortistatin A, inhibits Tat-mediated transactivation through the interaction with the TAR domain of Tat (Li et al., 2019; Mediouni et al., 2019). Prior studies demonstrated that CDK9 inhibitors block viral transcription by disrupting P-TEFb formation (Pisell et al., 2001; Rice, 2016). In addition, activation of CDK2 that inhibits HIV-1 transcription and activation of the HIV-1 provirus through Tat phosphorylation was also targeted for the "Block-and-Lock" Strategy (Ammosova et al., 2006). Bisacetamide-induced protein (HEXIM-1) and 7SK small nuclear RNA interact and retain P-TEFb away from HIV-1 LTR (Yang et al., 2001; Yik et al., 2003). Bromodomain-containing protein 4 (BRD4) that competes with Tat for the P-TEFb interaction domain to further prevent HIV transcription is another target for permanent silencing (Jang et al., 2005; Bisgrove et al., 2007).

NF-κB is predominantly sequestered in the cytoplasm by IκB and cannot activate HIV-1 transcription in resting latently infected cells (Baeuerle and Henkel, 1994; Baldwin, 1996). Inhibition of NF-κB signaling is also considered as a Block-and-Lock strategy. Latent HIV proviruses were less reactivated by curaxin, a drug also used in immuno-oncology that inhibits NF-κB mediated transcription (Orphanides et al., 1998; Gasparian et al., 2011). This led to the hypothesis that curaxin could induce HIV latency via strengthening NF-κB inhibition.

Tat and NF-κB are required for HIV-1 gene expression, therefore inhibition of these critical components can lead to a post-integration "Block-and-Lock" strategy. The post-integration approach may necessitate PLWH to undergo life-long treatment to permanently suppress viral expression and frequently monitor viremia levels. Therefore, the combination of both methods, "Block-and-Kick-and-Kill" would lead to the functional cure for HIV-1 infection by reducing the reservoir size during acute infection through the redirection of HIV-1 DNA integration sites while subsequently reactivating the residual latently infected cells that are not deeply silenced, and eventually eliminate the reactivated cells by HIV-1 specific immune cells (**Figure 5**).

## Genome Editing Strategy

Genome editing technologies, such as the transcription activator-like nucleases (TALENs), zinc finger nucleases (ZFNs), and clustered regularly interspaced short palindromic repeat (CRISPR)-associated nuclease 9 (Cas9) have been proposed for novel approaches toward cure strategies. The use of Cas9 has recently been investigated with the advantages of precise insertion, deletion, and replacement of target double-strand

DNA (dsDNA) (White et al., 2017). Cas9 has quickly become the preferred genome-editing platform for interrogating endogenous gene function *in vivo*. It was originally found in a bacterial adaptive immune defense system to play a vital role against DNA viruses or plasmids. Cas9 ribonucleoprotein complex consists of two components using endonuclease enzymes with a short-guide RNA (gRNA). Cas9 proteins are a specific class of enzymes that break the target dsDNA identified by gRNA, which is engineered with a particular sequence that guides the Cas9 protein to the target DNA sequence. Cas9 unwinds foreign DNA at sites complementary to the 20 base pair spacer region of the gRNA. If the DNA substrate is complementary to the gRNA, the Cas9 cleaves the invading DNA leading to gene inactivation. According to these unique features of Cas9 enzymatic activity, this system has been used as a genetic engineering technique to modify the genomes of living organisms.

Two people who had been living with HIV have been cured so far, the famous first case of the *Berlin patient* (Hütter et al., 2009; Allers et al., 2011), the second *London Patient* (Gupta et al., 2019), and a third individual, known as the *Dusseldorf Patient*, who is currently experiencing long-term remission (Peluso et al., 2019). These three individuals received a bone marrow transplant from matched donors with a homozygous 32 base pair deletion in the CCR5 gene (CCR5-Δ32) as part of their leukemia treatment. It has been documented that homozygous carriers of Δ32 mutation are largely resistant to R5 tropic HIV-1 infection that is exclusively detected in the transmitted founder viruses during the acute infection because the mutation prevents functional expression of CCR5, a coreceptor used by HIV-1 to enter immune cells (Cocchi et al., 1995; Samson et al., 1996; Biti et al., 1997). In addition, CCR5 gene editing of CD4+ T cells mediated by ZFN has been conducted clinically in HIV-1 infected individuals and was demonstrated to be safe (NCT00842634) (Tebas et al., 2014). Long-term CCR5 disruption in hematopoietic stem cells (HSCs) by the CRISPR/Cas9 system was achieved in a mouse model in 2017 to confer HIV-1 resistance *in vivo* (Xu et al., 2017). Although the other HIV-1 coreceptor, CXCR4, has also been targeted by Cas9, CXCR4 modified cells showed resistance against HIV-1 infection (Schumann et al., 2015). However, possible adverse side effects after CXCR4 disruption are of great concern as CXCR4 plays a vital role in hematopoietic cell development and thymic differentiation (Samson et al., 1996; Dar et al., 2006). To overcome these challenges, a combination of the Cas9 genome editing system and piggyBac transposase tools enabled the introduction of a point mutation, P191A, in the CXCR4 gene that specifically prohibits HIV-1 infection without disrupting CXCR4 receptor function (Liu et al., 2018). Although it should be noted that the virus rebound had not been observed in spite of the CXCR4-tropic virus existence in the Berlin patient, another case has been reported in a patient with allogeneic transplantation from a CCR5Δ32 donor, where a CXCR4-tropic virus rebounded after cART cessation (Kordelas et al., 2014). In addition, it has also been shown that HIV-1 can infect macrophages in a coreceptor-independent manner, leading to endocytosis of the virus (Gobeil et al., 2012). Therefore, targeting HIV-1 coreceptors by gene editing machinery should be considered carefully for HIV cure strategy.

Cas9 could directly eliminate integrated proviral DNA *in vitro* by targeting the conserved sequence of the HIV-1 LTR U3 region in a latently infected T cell line, a monocytic cell line, and a microglial cell line (Hu et al., 2014). Recently, the excision of proviruses from latent reservoir cells was demonstrated *in vivo* in humanized mice by combining a provirus targeting genome editing tool with long-acting slow-effective antiviral therapy (Dash et al., 2019; **Figure 6**). Looking ahead to the future of CRISPR/Cas9 HIV treatment options, the U.S. Food and Drug Administration (FDA) has recently approved to begin trials testing EBT-101, an *in vivo* CRISPR/Cas9 gene therapy designed to excise HIV-1 proviral DNA. This is the first time the FDA has given investigational new drug (IND) approval to a CRISPR-based therapy for HIV treatment. Trials will evaluate the safety, tolerability, and efficacy of EBT-101 in healthy individuals living with HIV (NCT05144386).

Although many classes of viral vectors exist, the adeno-associated virus vector (AAV) has largely been used for delivering genome-editing machinery *in vivo* (Yin et al., 2017), and in clinical trials (NCT05144386). AAV is thought to be one of the most suitable viral vectors for gene therapy applications and gene transfer *in vivo*. AAV was approved for a number of human clinical trials in gene augmentation therapies due to its favorable safety profile. One major advantage of using AAV is a very mild immune response and toxicity elicited by AAV in animal models. However, AAV has some disadvantages, such as small cargo capacity, prolonged time for large-scale production, and relatively high cost. AAV has a substantial limitation in small viral genome packing capacity that is generally considered to be less than 5 kb, which is not suitable for large transgenes and is only available for Cas9 derived from smaller orthologs such as *Staphylococcus aureus (SaCas9)* or *Campylobacter jejuni* (CjCas9). The gRNA for Cas9 also requires a specific protospacer adjacent motif (PAM) that varies depending on the bacterial species. The most common Cas9 derived from *Staphylococcus pyogenes* (SpCas9) recognizes NGG directly downstream of the target sequence in the genomic DNA, while the PAM sequence of SaCas9 for optical target requires NNGRRT, limiting the design of specific gRNA target site. The length of the SpCas9 encoding gene is oversized to be packaged in AAV. The AAV-CRISPR system holds the potential to develop therapeutic options, but on the other hand, the development of a novel *in vivo* Cas9 delivery platform is urgently required to increase its flexibility.

# HUMAN IMMUNODEFICIENCY VIRUS TYPE-I RESERVOIR DETECTION

## Analytic Treatment Interruption

Accurately measuring the latent HIV reservoir is critical to assessing the effectiveness of curative strategies aimed at HIV remission. To date, the only way to definitively evaluate the effectiveness of curative strategies is with an analytic treatment interruption (ATI) in which the individual stops taking cART (Harari et al., 2012). The time that it takes for the viral rebound to occur after treatment cessation can be used to evaluate reservoir reduction. Theoretically, since viral rebound reflects the release of the virus from a stable reservoir, the smaller the size of the

reservoir, the longer it takes for the viral rebound to occur (Hill et al., 2016; Li J. Z. et al., 2016). In the hopes to manage adverse effects associated with long-term use of cART, a clinical trial was performed in which HIV-infected individuals were randomly assigned to undergo either continuous suppressive cART or CD4+ count-guided episodic use of cART (NCT00027352) (El-Sadr et al., 2006). This study found that participants who undergo episodic treatment interruptions have significantly higher rates of opportunistic diseases or death from any cause when compared to participants on continuous cART. Moreover, the selection of drug-resistant mutations can occur during repeated treatment interruptions (Martinez-Picado et al., 2002), and rebounding viruses display increased IFNα2 and IFNβ resistance (Gondim et al., 2021). However, in some cases, individuals with high CD4 counts (>500 cells/ul) can safely undergo short CD4+ T cell count guided treatment interruptions without increased risk of morbidity or mortality and without developing drug resistance (Maggiolo et al., 2009; Routy et al., 2012; Ananworanich et al., 2015). While treatment interruption may provide evidence of complete viral eradication, individuals will most likely require long-term monitoring as unpredictable stochastic events can lead to viral rebound months to years later if the latent reservoir is not completely eradicated but only greatly reduced. Furthermore, the individual variability in time to rebound makes it hard to assess the magnitude of reservoir reduction as a result of eradication efforts.

## Quantitative Viral Outgrowth Assay

Currently, there is no accurate way to measure the latent reservoir *in vivo*. The quantitative viral outgrowth assay (QVOA) has been regarded as the "gold standard" for measuring the replication-competent latent reservoir size *ex vivo* (Finzi et al., 1997; Siliciano et al., 2003). QVOA measures the frequency of resting CD4+ T cells that produce infectious viruses after a single round of maximum global T cell activation. To this end, a large volume of resting CD4+ T cells are isolated from HIV-infected individuals and stimulated with the mitogen phytohemagglutinin (PHA) in the presence of uninfected γ-irradiated allogeneic PBMCs. Then the donor cells are co-cultured with either CD4+ T cells from a healthy donor or a cell line for 2–3 weeks before the infectious virus is measured in the culture supernatant by HIV-1 P24 ELISA (Finzi et al., 1997; Stuelke et al., 2020) or using a quantitative RT-PCR assay (Laird et al., 2013). However, some replication-competent viruses are induced only after multiple rounds of stimulation, indicating that standard QVOA may underestimate the size of the inducible latent reservoir (Abrahams et al., 2019). Furthermore, traditional QVOA is labor intensive and requires large amounts of sample. These limitations have led to the development of other approaches to estimate the size of the latent reservoir.

## PCR-Based Methods to Detect Human Immunodeficiency Virus Type-I Proviruses

Standard PCR-based techniques to quantify total HIV DNA are the easiest way to measure HIV-infected cells in PLWH. Total HIV DNA measurements inherently overestimate the size of the HIV reservoir since the majority of proviruses are defective or deleted (Bruner et al., 2016). However, total HIV DNA remains an important biomarker for viral persistence (Avettand-Fènoël et al., 2016), and levels of this marker are associated with viral rebound upon treatment cessation (Yerly et al., 2004; Williams et al., 2014). Recent approaches using droplet digital PCR (ddPCR) employ absolute quantification, which is more accurate than traditional quantitative PCR (qPCR) methods (Strain et al., 2013). Multiplexed ddPCR based assays have been used to track the fraction of deleted proviruses during cART (Anderson and Maldarelli, 2018; Anderson et al., 2020). Still, total HIV DNA measurements are at least two orders of magnitude higher than latent reservoir size measurements by QVOA (Eriksson et al., 2013). Total HIV DNA measurements may be further confounded by unintegrated HIV in either linear or 2-LTR circle forms, as these methods cannot distinguish integrated HIV DNA from non-integrated forms. Efforts to quantify only integrated HIV DNA utilize *Alu*-PCR (O'Doherty et al., 2002; Brady et al., 2013; De Spiegelaere et al., 2014). *Alu-gag*-PCR employs an outer forward primer that binds *Alu,* a repetitive element that is abundant in the human genome, and a reverse primer that is complementary to HIV *gag* DNA. This method will only amplify HIV proviruses integrated into the host genome and contain the primer target region of *gag* (O'Doherty et al., 2002; Liszewski et al., 2009). *Alu-gag*-PCR gives latent reservoir size estimates that are lower than total HIV DNA measurements but are still orders of magnitude higher than QVOA due to the inability of these assays to distinguish between replication-competent and defective proviruses (Eriksson et al., 2013).

Multiple methods have been developed to assess the proportion of intact versus obviously defective or deleted proviruses. Sequencing approaches such as matched integration site and proviral sequencing (MIP-seq) (Einkauf et al., 2019) and multiple-displacement amplification single genome sequencing (MDA-SGS) (Patro et al., 2019) can link full-length proviral sequences with their respective integration sites to infer replication competence as well as clonality. While these assays will provide great insights into the proviral landscape, the costs and labor required may hinder their use in large-scale studies. The intact proviral DNA assay (IPDA) is a high throughput ddPCR assay designed with two sets of primers located in conserved and frequently deleted regions of the viral genome (Bruner et al., 2019). IPDA offers a robust tool to estimate the number of intact proviruses and has been utilized as a surrogate for the latent reservoir (Simonetti et al., 2020). However, PCR failure as a result of primer mismatch due to HIV-1 diversity (Kinloch et al., 2021) and the inability to exclude proviruses that are defective or deleted in other regions (Gaebler et al., 2021) may preclude proper latent reservoir size measurements by IPDA. Other ddPCR strategies that utilize more target regions can further exclude defective proviruses. For example, a triplex digital PCR method (van Snippenberg et al., 2021) and a five-region approach that combines two triplex ddPCR assays (Levy et al., 2021) have been developed to help overcome the mischaracterization of intact proviruses while still utilizing a high throughput and relatively inexpensive digital PCR platform. The

recently developed quadruplex PCR with four probes (Q4PCR) assay combines a four-probe qPCR strategy with near full-length sequencing to distinguish between intact and defective proviruses (Gaebler et al., 2019; Cho et al., 2022). In this assay, individual HIV genomes are amplified to near full length and are screened for the presence of 4 HIV targets with qPCR. Wells that are positive for at least two targets are then selected to undergo full-length proviral sequencing (Gaebler et al., 2019). Q4PCR is a lower-throughput assay compared to IPDA but allows for confirmation of proviral intactness. When compared head-to-head, IPDA and Q4PCR measurements correlated with one another but levels of intact proviruses measured with IPDA were approximately 19-fold higher than Q4PCR measurements (Gaebler et al., 2021). These differences in reservoir size estimates are likely from a combination of an overestimation by IPDA due to its inability to exclude defects in other regions of the provirus, and an underestimation by Q4PCR, due to inefficiencies from long-distance PCR. The actual number of intact proviruses may lie in between the measurements from IPDA and Q4PCR. Moreover, not all intact proviruses are replication-competent and ultimately give rise to rebound viremia. The chromatin environment at the proviral integration site as well as defects in transcription and/or translation of the provirus govern its ability to give rise to the infectious virus (Einkauf et al., 2022).

## Quantifying Functional Human Immunodeficiency Virus Type-I Proviruses

Strategies to more accurately estimate latent reservoir size aim to quantify replication-competent proviruses. The Tat/rev Induced Limiting Dilution Assay (TILDA) measures the frequency of cells harboring viral genomes that produce *tat/rev* multiply spliced HIV RNA (msRNA) upon maximum activation of CD4+ T cells (Procopio et al., 2015). The *tat/rev* msRNA is essential to produce infectious viruses (Pasternak et al., 2008). Many deleted proviruses lack *tat* and *rev* genes (Abrahams et al., 2019), and cells that contain *tat/rev* msRNA likely harbor a replication-competent infectious provirus. However, TILDA may still overestimate the actual size of the HIV reservoir since integrated proviruses that produce msRNA are not guaranteed to be infectious (Procopio et al., 2015). Recent advances in the development of next-generation *in situ* hybridization (ISH) technologies allow the detection of native viral DNA and RNA markers in histological specimens with greater sensitivity and faster workflow than traditional ISH (Deleage et al., 2016, 2018). These methods, namely DNAScope and RNAScope, can be leveraged to quantify the number of HIV-DNA and RNA-positive cells per gram of tissue (Estes et al., 2017). Uniquely among the methods described in this section, which are based on bulk sampling, tissue imaging approaches bypass the requirement of tissue homogenization and can provide spatial localization of the viral reservoir in tissue compartments. In addition, these allow multiplexing the detection of viral and host biomarkers to phenotype latently and actively infected cells and characterizing the complex heterogeneity of microenvironments that sustain virus persistence. However, these imaging-based approaches remain limited by the scarce accessibility of tissue specimens from clinical trials as opposed to blood and by the two-dimensional analysis of a few representative sections, which is based on the assumption that observations made can be inferred to the entire organ. In this regard, it is encouraging to see the emergence of total body positron emission tomography (PET) scanning (Santangelo et al., 2015; Henrich et al., 2019; Taylor et al., 2021) and whole organ imaging with novel tissue clearing technologies coupled with light-sheet microscopy (Tomer et al., 2014), which may represent new frontiers to detect viral reservoirs and broaden our understanding of virus persistence in tissue. Other approaches to identifying replication-competent reservoirs measure translation competent proviruses (Baxter et al., 2016). A flow-based RNA FISH assay simultaneously measures HIV RNA as well as Gag proteins upon phorbol 12-myristate 13-acetate (PMA) stimulation to identify single cells that are double positive for both cell-associated unspliced HIV *gag* RNA and its translation product Gag protein ($HIV^{RNA+/Gag+}$). $HIV^{RNA+/Gag+}$ cells likely give rise to the infectious virus, enabling this assay to more accurately estimate the latent reservoir size compared to assays that viral RNA transcripts alone (Baxter et al., 2016). The advancement of digital enzyme-linked immunosorbent assay with a single molecule array (Simoa) has enabled the detection of cell-associated HIV gag p24 protein from both peripheral and tissue compartments with sensitivity higher than traditional ELISA (Passaes et al., 2017; Wu et al., 2017, 2021; Stuelke et al., 2020). These assays can be used to quantify steady-state and inducible reservoirs with the advantage of focusing on viruses capable of translating and processing Gag antigens that are relevant for infected cells clearance (Abdel-Mohsen et al., 2020). These further characterize reservoirs independently from their genetic intactness as defective proviruses can produce viral antigens and contribute to chronic immune system stimulation (Imamichi et al., 2020). Overall, rapid and accurate measurements of the true latent reservoir are needed to assess the effectiveness of curative strategies. For now, a combination of the described assays can be used to estimate the size of the latent reservoir, and the true size likely lies somewhere in between QVOA estimates and translation competent measurements.

## SUMMARY

Once HIV infection is established, cART cannot eradicate the integrated proviruses due to latency establishment in multiple mechanisms (**Table 1**). HIV-1 gene transcription and subsequent translation are highly controlled by cis- and trans-regulatory elements and form distinct phenotypes of latent cells (**Figure 2**). HIV-1 reservoirs are generated in the early acute phase of virus infection with long-lasting treatment-resistant cells that can undergo clonal expansion during cART. Various strategies have been proposed to perturb the latent reservoir. The "Block-and-Lock" strategy aims to permanently silence the latent reservoir using latency-promoting agents such as LEDGINs. LEDGINSs can alter HIV-1 DNA integration sites to deeply silenced regions that are inefficient for reactivation even after cART cessation (**Figure 5**). While this treatment could be an approach to silence virus expression once and for all, it is not designed to have a

profound effect on eradication after reservoir formation. Thus, the "Block-and-Lock" strategy could be effective when used during acute viral infection. The "Kick-and-Kill" strategy is designed to induce the expression of viral antigens by reactivation of latent cells (**Figure 5**). LRAs target both cis- and trans-mechanisms of the suppressive viral promoter to reactivate the latent cells, leading to the subsequent elimination by immune cells. Since individual LRA studies to date have ineffectively reduced reservoir size in clinical trials, several LRAs with distinct mechanisms of action may be needed to address the heterogeneity in latency.

While CD4+ T cells have been regarded as major cellular reservoir compartment, tissue localized long-lived myeloid cells may also have an essential role in HIV reservoir formation (**Figure 1**). The memory subsets of latently infected CD4+ T cells containing replication-competent proviral DNA are frequently detected in lymphoid tissue. In addition to the memory T cell subsets in peripheral blood and lymphoid tissue, macrophagic and astrocytic myeloid cells in the CNS pose a unique challenge for virus elimination (**Figure 1**).

During chronic infection, the immune system is in a state of non-reactivity to HIV-1 antigen caused by constant stimulation by viral antigens presentation or viral-like particles (VLPs) produced by defective proviruses that have large internal deletions or hypermutations (**Figure 4**).

The immune checkpoint blockade (ICB), which could either activate or inactivate specific immune cells could be useful to purge reactivated cells. The combination of LRAs with ICB has been demonstrated to effectively reduce the reservoir size *in vivo*, indicating that combinatorial approaches, in which LRAs are used to obtain a more effective shock and ICBs restore HIV-1 specific immune cells to eliminate reactivated reservoirs (**Figure 5**).

The Food and Drug Administration recently approved a human trial for HIV cure with CRISPR/Cas9 genome editing technology (**Figure 6**). While the adeno-associated viral vector (AAV) delivery system has several limitations, AAV is a valid option for *in vivo* Cas9 delivery to deactivate proviruses in tissue-localized reservoir cells in mice models. Cas9 targeting HIV-1 proviral DNA could potentially deactivate intact reservoir cells after the Kick-and-Kill therapy. Taken together, combining appropriate therapies at the stages of HIV acute and chronic infection, could contribute to new cases of cure without resorting to risky and unscalable bone marrow or stem cell transplantation.

## AUTHOR CONTRIBUTIONS

TT, SM, EA, JP, MF, and TI draw figures. EA, LS, ZK, and TI designed the project. ZK and TI contributed to financial assistance. All authors listed wrote the manuscript and contributed to the article and approved the submitted version.

## FUNDING

This project was supported in part by start-up from the University of the Sciences in Philadelphia to TI and from NIDA/NIH (DP2DA044550-01) and PA Department of Health CURE (4100088542) to ZK.

## REFERENCES

Abbar, B., Baron, M., Katlama, C., Marcelin, A.-G., Veyri, M., Autran, B., et al. (2020). Immune checkpoint inhibitors in people living with HIV: what about anti-HIV effects? *AIDS* 34, 167–175. doi: 10.1097/QAD.0000000000002397

Abdel-Mohsen, M., Richman, D., Siliciano, R. F., Nussenzweig, M. C., Howell, B., Martinez-Picado, J., et al. (2020). Recommendations for measuring HIV reservoir size in cure-directed clinical trials. *Nat. Med.* 26, 1339–1350. doi: 10.1038/s41591-020-1022-1

Abner, E., Stoszko, M., Zeng, L., Chen, H.-C., Izquierdo-Bouldstridge, A., Konuma, T., et al. (2018). A New Quinoline BRD4 Inhibitor Targets a Distinct Latent HIV-1 Reservoir for Reactivation from Other "Shock" Drugs. *J. Virol.* 2018:17. doi: 10.1128/JVI.02056-17

Abrahams, M.-R., Joseph, S. B., Garrett, N., Tyers, L., Moeser, M., Archin, N., et al. (2019). The replication-competent HIV-1 latent reservoir is primarily established near the time of therapy initiation. *Sci. Transl. Med.* 11:eaaw5589. doi: 10.1126/scitranslmed.aaw5589

Adams, M., Sharmeen, L., Kimpton, J., Romeo, J. M., Garcia, J. V., Peterlin, B. M., et al. (1994). Cellular latency in human immunodeficiency virus-infected individuals with high CD4 levels can be detected by the presence of promoter-proximal transcripts. *Proc. Natl. Acad. Sci.* 91, 3862–3866. doi: 10.1073/pnas.91.9.3862

Ahn, E., Youngblood, B., Lee, J., Lee, J., Sarkar, S., and Ahmed, R. (2016). Demethylation of the PD-1 Promoter Is Imprinted during the Effector Phase of CD8 T Cell Exhaustion. *J. Virol.* 90, 8934–8946. doi: 10.1128/JVI.00798-16

Ait-Ammar, A., Kula, A., Darcis, G., Verdikt, R., De Wit, S., Gautier, V., et al. (2020). Current Status of Latency Reversing Agents Facing the Heterogeneity of HIV-1 Cellular and Tissue Reservoirs. *Front. Microbiol.* 10:3060. doi: 10.3389/fmicb.2019.03060

Akhtar, A. (2015). The Flaws and Human Harms of Animal Experimentation. *Camb. Q. Healthc. Ethics* 24, 407–419. doi: 10.1017/S0963180115000079

Alamer, E., Zhong, C., Liu, Z., Niu, Q., Long, F., Guo, L., et al. (2020). Epigenetic Suppression of HIV in Myeloid Cells by the BRD4-Selective Small Molecule Modulator ZL0580. *J. Virol.* 94:19. doi: 10.1128/JVI.01880-19

Ali, A., Kitchen, S. G., Chen, I. S. Y., Ng, H. L., Zack, J. A., and Yang, O. O. (2016). HIV-1-Specific Chimeric Antigen Receptors Based on Broadly Neutralizing Antibodies. *J. Virol.* 90, 6999–7006. doi: 10.1128/JVI.00805-16

Allers, K., Hütter, G., Hofmann, J., Loddenkemper, C., Rieger, K., Thiel, E., et al. (2011). Evidence for the cure of HIV infection by CCR5Δ32/Δ32 stem cell transplantation. *Blood* 117, 2791–2799. doi: 10.1182/blood-2010-09-309591

Álvarez-Fernández, C., Crespo Guardo, A., García-Pérez, J., García, F., Blanco, J., Escribà-García, L., et al. (2012). Generation and characterization of a defective HIV-1 Virus as an immunogen for a therapeutic vaccine. *PLoS One* 7:e48848. doi: 10.1371/journal.pone.0048848

Ammosova, T., Berro, R., Jerebtsova, M., Jackson, A., Charles, S., Klase, Z., et al. (2006). Phosphorylation of HIV-1 Tat by CDK2 in HIV-1 transcription. *Retrovirology* 3:78. doi: 10.1186/1742-4690-3-78

Ananworanich, J., Chomont, N., Fletcher, J. L. K., Pinyakorn, S., Schuetz, A., Sereti, I., et al. (2015). Markers of HIV reservoir size and immune activation after treatment in acute HIV infection with and without raltegravir and maraviroc intensification. *J. Virus Eradicat.* 1, 116–122. doi: 10.1016/S2055-6640(20)30482-9

Anderson, E. M., and Maldarelli, F. (2018). The role of integration and clonal expansion in HIV infection: live long and prosper. *Retrovirology* 15:71. doi: 10.1186/s12977-018-0448-8

Anderson, E. M., Simonetti, F. R., Gorelick, R. J., Hill, S., Gouzoulis, M. A., Bell, J., et al. (2020). Dynamic Shifts in the HIV Proviral Landscape During Long Term Combination Antiretroviral Therapy: Implications for Persistence and Control of HIV Infections. *Viruses* 12:E136. doi: 10.3390/v12020136

Appay, V., Papagno, L., Spina, C. A., Hansasuta, P., King, A., Jones, L., et al. (2002). Dynamics of T Cell Responses in HIV Infection. *J. Immunol.* 168, 3660–3666. doi: 10.4049/jimmunol.168.7.3660

Archin, N. M., Keedy, K. S., Espeseth, A., Dang, H., Hazuda, D. J., and Margolis, D. M. (2009). Expression of latent human immunodeficiency type 1 is induced by novel and selective histone deacetylase inhibitors. *AIDS* 23, 1799–1806. doi: 10.1097/QAD.0b013e32832ec1dc

Archin, N. M., Liberty, A. L., Kashuba, A. D., Choudhary, S. K., Kuruc, J. D., Crooks, A. M., et al. (2012). Administration of vorinostat disrupts HIV-1 latency in patients on antiretroviral therapy. *Nature* 487, 482–485. doi: 10.1038/nature11286

Arts, E. J., and Hazuda, D. J. (2012). HIV-1 Antiretroviral Drug Therapy. *Cold Spring Harb. Perspect. Med.* 2, a007161–a007161. doi: 10.1101/cshperspect.a007161

Avettand-Fènoël, V., Hocqueloux, L., Ghosn, J., Cheret, A., Frange, P., Melard, A., et al. (2016). Total HIV-1 DNA, a Marker of Viral Reservoir Dynamics with Clinical Implications. *Clin. Microbiol. Rev.* 29, 859–880. doi: 10.1128/CMR.00015-16

Baeuerle, P. A., and Henkel, T. (1994). Function and activation of NF-kappa B in the immune system. *Annu. Rev. Immunol.* 12, 141–179. doi: 10.1146/annurev.iy.12.040194.001041

Bailey, M., Christoforidou, Z., and Lewis, M. C. (2013). The evolutionary basis for differences between the immune systems of man, mouse, pig and ruminants. *Vet. Immunol. Immunopathol.* 152, 13–19. doi: 10.1016/j.vetimm.2012.09.022

Baker, J. V., Peng, G., Rapkin, J., Abrams, D. I., Silverberg, M. J., MacArthur, R. D., et al. (2008). CD4+ count and risk of non-AIDS diseases following initial treatment for HIV infection. *AIDS* 22, 841–848. doi: 10.1097/QAD.0b013e3282f7cb76

Baldwin, A. S. (1996). THE NF-κB AND IκB PROTEINS: New Discoveries and Insights. *Annu. Rev. Immunol.* 14, 649–681. doi: 10.1146/annurev.immunol.14.1.649

Banga, R., Procopio, F. A., Noto, A., Pollakis, G., Cavassini, M., Ohmiti, K., et al. (2016). PD-1+ and follicular helper T cells are responsible for persistent HIV-1 transcription in treated aviremic individuals. *Nat. Med.* 22, 754–761. doi: 10.1038/nm.4113

Bartholomeeusen, K., Xiang, Y., Fujinaga, K., and Peterlin, B. M. (2012). Bromodomain and extra-terminal (BET) bromodomain inhibition activate transcription *via* transient release of positive transcription elongation factor b (P-TEFb) from 7SK small nuclear ribonucleoprotein. *J. Biol. Chem.* 287, 36609–36616. doi: 10.1074/jbc.M112.410746

Baxter, A. E., Niessl, J., Fromentin, R., Richard, J., Porichis, F., Charlebois, R., et al. (2016). Single-Cell Characterization of Viral Translation-Competent Reservoirs in HIV-Infected Individuals. *Cell Host Microbe* 20, 368–380. doi: 10.1016/j.chom.2016.07.015

Benkirane, M., Chun, R. F., Xiao, H., Ogryzko, V. V., Howard, B. H., Nakatani, Y., et al. (1998). Activation of integrated provirus requires histone acetyltransferase. p300 and P/CAF are coactivators for HIV-1 Tat. *J. Biol. Chem.* 273, 24898–24905. doi: 10.1074/jbc.273.38.24898

Besnard, E., Hakre, S., Kampmann, M., Lim, H. W., Hosmane, N. N., Martin, A., et al. (2016). The mTOR Complex Controls HIV Latency. *Cell Host Microbe* 20, 785–797. doi: 10.1016/j.chom.2016.11.001

Bisgrove, D. A., Mahmoudi, T., Henklein, P., and Verdin, E. (2007). Conserved P-TEFb-interacting domain of BRD4 inhibits HIV transcription. *PNAS* 104, 13690–13695. doi: 10.1073/pnas.0705053104

Bissels, U., Wild, S., Tomiuk, S., Holste, A., Hafner, M., Tuschl, T., et al. (2009). Absolute quantification of microRNAs by using a universal reference. *RNA* 15, 2375–2384. doi: 10.1261/rna.1754109

Biti, R., Ffrench, R., Young, J., Bennetts, B., Stewart, G., and Liang, T. (1997). HIV-1 infection in an individual homozygous for the CCR5 deletion allele. *Nat. Med.* 3, 252–253. doi: 10.1038/nm0397-252

Blackburn, S. D., Shin, H., Haining, W. N., Zou, T., Workman, C. J., Polley, A., et al. (2009). Coregulation of CD8+ T cell exhaustion by multiple inhibitory receptors during chronic viral infection. *Nat. Immunol.* 10, 29–37. doi: 10.1038/ni.1679

Blazkova, J., Trejbalova, K., Gondois-Rey, F., Halfon, P., Philibert, P., Guiguen, A., et al. (2009). CpG Methylation Controls Reactivation of HIV from Latency. *PLoS Pathog.* 5:e1000554. doi: 10.1371/journal.ppat.1000554

Boasso, A., Shearer, G. M., and Chougnet, C. (2009). Immune dysregulation in human immunodeficiency virus infection: know it, fix it, prevent it? *J. Internal Med.* 265, 78–96. doi: 10.1111/j.1365-2796.2008.02043.x

Bobardt, M., Kuo, J., Chatterji, U., Chanda, S., Little, S. J., Wiedemann, N., et al. (2019). The inhibitor apoptosis protein antagonist Debio 1143 Is an attractive HIV-1 latency reversal candidate. *PLoS One* 14:e0211746. doi: 10.1371/journal.pone.0211746

Boehm, D., Jeng, M., Camus, G., Gramatica, A., Schwarzer, R., Johnson, J. R., et al. (2017). SMYD2-Mediated Histone Methylation Contributes to HIV-1 Latency. *Cell Host Microbe* 21, 569.e–579.e. doi: 10.1016/j.chom.2017.04.011

Boltz, V. F., Ceriani, C., Rausch, J. W., Shao, W., Bale, M. J., Keele, B. F., et al. (2021). CpG Methylation Profiles of HIV-1 Proviral DNA in Individuals on ART. *Viruses* 13:799. doi: 10.3390/v13050799

Borrow, P., Lewicki, H., Hahn, B. H., Shaw, G. M., and Oldstone, M. B. (1994). Virus-specific CD8+ cytotoxic T-lymphocyte activity associated with control of viremia in primary human immunodeficiency virus type 1 infection. *J. Virol.* 68, 6103–6110. doi: 10.1128/jvi.68.9.6103-6110.1994

Bosque, A., Famiglietti, M., Weyrich, A. S., Goulston, C., and Planelles, V. (2011). Homeostatic proliferation fails to efficiently reactivate HIV-1 latently infected central memory CD4+ T cells. *PLoS Pathog.* 7:e1002288. doi: 10.1371/journal.ppat.1002288

Bosque, A., Nilson, K. A., Macedo, A. B., Spivak, A. M., Archin, N. M., Van Wagoner, R. M., et al. (2017). Benzotriazoles Reactivate Latent HIV-1 through Inactivation of STAT5 SUMOylation. *Cell Rep.* 18, 1324–1334. doi: 10.1016/j.celrep.2017.01.022

Bouchat, S., Delacourt, N., Kula, A., Darcis, G., Van Driessche, B., Corazza, F., et al. (2016). Sequential treatment with 5-aza-2'-deoxycytidine and deacetylase inhibitors reactivates HIV-1. *EMBO Mol. Med.* 8, 117–138. doi: 10.15252/emmm.201505557

Bouchat, S., Gatot, J.-S., Kabeya, K., Cardona, C., Colin, L., Herbein, G., et al. (2012). Histone methyltransferase inhibitors induce HIV-1 recovery in resting CD4+ T cells from HIV-1-infected HAART-treated patients. *AIDS* 26, 1473–1482. doi: 10.1097/QAD.0b013e32835535f5

Brady, T., Kelly, B. J., Male, F., Roth, S., Bailey, A., Malani, N., et al. (2013). Quantitation of HIV DNA integration: Effects of differential integration site distributions on Alu-PCR assays. *J. Virol. Methods* 189, 53–57. doi: 10.1016/j.jviromet.2013.01.004

Brass, A. L., Dykxhoorn, D. M., Benita, Y., Yan, N., Engelman, A., Xavier, R. J., et al. (2008). Identification of host proteins required for HIV infection through a functional genomic screen. *Science* 319, 921–926. doi: 10.1126/science.1152725

Brodin, J., Zanini, F., Thebo, L., Lanz, C., Bratt, G., Neher, R. A., et al. (2016). Establishment and stability of the latent HIV-1 DNA reservoir. *eLife* 5:e18889. doi: 10.7554/eLife.18889

Bruner, K. M., Murray, A. J., Pollack, R. A., Soliman, M. G., Laskey, S. B., Capoferri, A. A., et al. (2016). Defective proviruses rapidly accumulate during acute HIV-1 infection. *Nat. Med.* 22, 1043–1049. doi: 10.1038/nm.4156

Bruner, K. M., Wang, Z., Simonetti, F. R., Bender, A. M., Kwon, K. J., Sengupta, S., et al. (2019). A quantitative approach for measuring the reservoir of latent HIV-1 proviruses. *Nature* 566, 120–125. doi: 10.1038/s41586-019-0898-8

Bruno, J., and Stoughton, A. M. (1984). Computer-aided communication device for a child with cerebral palsy. *Arch. Phys. Med. Rehabil.* 65, 603–605.

Budhiraja, S., Famiglietti, M., Bosque, A., Planelles, V., and Rice, A. P. (2013). Cyclin T1 and CDK9 T-Loop Phosphorylation Are Downregulated during Establishment of HIV-1 Latency in Primary Resting Memory CD4 $^{+}$ T Cells. *J. Virol.* 87, 1211–1220. doi: 10.1128/JVI.02413-12

Bui, J. K., Sobolewski, M. D., Keele, B. F., Spindler, J., Musick, A., Wiegand, A., et al. (2017). Proviruses with identical sequences comprise a large fraction of the replication-competent HIV reservoir. *PLoS Pathog.* 13:e1006283. doi: 10.1371/journal.ppat.1006283

Burnett, J. C., Miller-Jensen, K., Shah, P. S., Arkin, A. P., and Schaffer, D. V. (2009). Control of Stochastic Gene Expression by Host Factors at the HIV Promoter. *PLoS Pathog.* 5:e1000260. doi: 10.1371/journal.ppat.1000260

Buzon, M. J., Sun, H., Li, C., Shaw, A., Seiss, K., Ouyang, Z., et al. (2014). HIV-1 persistence in CD4+ T cells with stem cell–like properties. *Nat. Med.* 20, 139–142. doi: 10.1038/nm.3445

Calle-Fabregat, C., de la Morante-Palacios, O., and Ballestar, E. (2020). Understanding the Relevance of DNA Methylation Changes in Immune Differentiation and Disease. *Genes* 11:110. doi: 10.3390/genes11010110

Cantero-Pérez, J., Grau-Expósito, J., Serra-Peinado, C., Rosero, D. A., Luque-Ballesteros, L., Astorga-Gamaza, A., et al. (2019). Resident memory T cells are a cellular reservoir for HIV in the cervical mucosa. *Nat. Commun.* 10:4739. doi: 10.1038/s41467-019-12732-2

Cao, Y., Qin, L., Zhang, L., Safrit, J., and Ho, D. D. (1995). Virologic and Immunologic Characterization of Long-Term Survivors of Human Immunodeficiency Virus Type 1 Infection. *N. Engl. J. Med.* 332, 201–208. doi: 10.1056/NEJM199501263320401

Carpio, L., Klase, Z., Coley, W., Guendel, I., Choi, S., Van Duyne, R., et al. (2010). microRNA machinery is an integral component of drug-induced transcription inhibition in HIV-1 infection. *J. RNAi Gene Silencing* 6, 386–400.

Cary, D. C., and Peterlin, B. M. (2018). Natural Products and HIV/AIDS. *AIDS Res. Hum. Retrovir.* 34, 31–38. doi: 10.1089/aid.2017.0232

Chávez, L., Kauder, S., and Verdin, E. (2011). *In vivo*, *in vitro*, and in silico analysis of methylation of the HIV-1 provirus. *Methods* 53, 47–53. doi: 10.1016/j.ymeth.2010.05.009

Chen, Y., Zander, R., Khatun, A., Schauder, D. M., and Cui, W. (2018). Transcriptional and Epigenetic Regulation of Effector and Memory CD8 T Cell Differentiation. *Front. Immunol.* 9:2826. doi: 10.3389/fimmu.2018.02826

Chéné, I., du, Basyuk, E., Lin, Y.-L., Triboulet, R., Knezevich, A., et al. (2007). Suv39H1 and HP1γ are responsible for chromatin-mediated HIV-1 transcriptional silencing and post-integration latency. *EMBO J.* 26, 424–435. doi: 10.1038/sj.emboj.7601517

Cherrier, T., Le Douce, V., Eilebrecht, S., Riclet, R., Marban, C., Dequiedt, F., et al. (2013). CTIP2 is a negative regulator of P-TEFb. *Proc. Natl. Acad. Sci.* 110, 12655–12660. doi: 10.1073/pnas.1220136110

Chiang, K., Sung, T.-L., and Rice, A. P. (2012). Regulation of cyclin T1 and HIV-1 Replication by microRNAs in resting CD4+ T lymphocytes. *J. Virol.* 86, 3244–3252. doi: 10.1128/JVI.05065-11

Cho, A., Gaebler, C., Olveira, T., Ramos, V., Saad, M., Lorenzi, J. C. C., et al. (2022). Longitudinal clonal dynamics of HIV-1 latent reservoirs measured by combination quadruplex polymerase chain reaction and sequencing. *PNAS* 2022:119. doi: 10.1073/pnas.2117630119

Chomont, N., El-Far, M., Ancuta, P., Trautmann, L., Procopio, F. A., Yassine-Diab, B., et al. (2009). HIV reservoir size and persistence are driven by T cell survival and homeostatic proliferation. *Nat. Med.* 15, 893–900. doi: 10.1038/nm.1972

Christ, F., Shaw, S., Demeulemeester, J., Desimmie, B. A., Marchand, A., Butler, S., et al. (2012). Small-molecule inhibitors of the LEDGF/p75 binding site of integrase block HIV replication and modulate integrase multimerization. *Antimicrob. Agents Chemother.* 56, 4365–4374. doi: 10.1128/AAC.00717-12

Chun, T., Nickle, D. C., Justement, J. S., Meyers, J. H., Roby, G., Hallahan, C. W., et al. (2008). Persistence of HIV in Gut-Associated Lymphoid Tissue despite Long-Term Antiretroviral Therapy. *J. Infect. Dis.* 197, 714–720. doi: 10.1086/527324

Chun, T.-W., Justement, J. S., Murray, D., Hallahan, C. W., Maenza, J., Collier, A. C., et al. (2010). Rebound of plasma viremia following cessation of antiretroviral therapy despite profoundly low levels of HIV reservoir: implications for eradication. *AIDS* 24, 2803–2808. doi: 10.1097/QAD.0b013e328340a239

Chun, T.-W., Stuyver, L., Mizell, S. B., Ehler, L. A., Mican, J. A. M., Baseler, M., et al. (1997). Presence of an inducible HIV-1 latent reservoir during highly active antiretroviral therapy. *Proc. Natl. Acad. Sci.* 94, 13193–13197. doi: 10.1073/pnas.94.24.13193

Clerici, M., Giorgi, J. V., Chou, C.-C., Gudeman, V. K., Zack, J. A., Gupta, P., et al. (1992). Cell-Mediated Immune Response to Human Immunodeficiency Virus (HIV) Type 1 in Seronegative Homosexual Men with Recent Sexual Exposure to HIV-1. *J. Infect. Dis.* 165, 1012–1019. doi: 10.1093/infdis/165.6.1012

Clutton, G. T., and Jones, R. B. (2018). Diverse Impacts of HIV Latency-Reversing Agents on CD8+ T-Cell Function: Implications for HIV Cure. *Front. Immunol.* 9:1452. doi: 10.3389/fimmu.2018.01452

Cocchi, F., DeVico, A. L., Garzino-Demo, A., Arya, S. K., Gallo, R. C., and Lusso, P. (1995). Identification of RANTES, MIP-1α, and MIP-1β as the Major HIV-Suppressive Factors Produced by CD8 $^+$ T Cells. *Science* 270, 1811–1815. doi: 10.1126/science.270.5243.1811

Coffin, J. M., and Hughes, S. H. (2021). Clonal Expansion of Infected CD4+ T Cells in People Living with HIV. *Viruses* 13:2078. doi: 10.3390/v13102078

Coffin, J. M., Bale, M. J., Wells, D., Guo, S., Luke, B., Zerbato, J. M., et al. (2021). Integration in oncogenes plays only a minor role in determining the *in vivo* distribution of HIV integration sites before or during suppressive antiretroviral therapy. *PLoS Pathog.* 17:e1009141. doi: 10.1371/journal.ppat.1009141

Coffin, J. M., Hughes, S. H., and Varmus, H. (eds) (1997). *Retroviruses*. Plainview, NY: Cold Spring Harbor Laboratory Press.

Cohn, L. B., Silva, I. T., Oliveira, T. Y., Rosales, R. A., Parrish, E. H., Learn, G. H., et al. (2015). HIV-1 integration landscape during latent and active infection. *Cell* 160, 420–432. doi: 10.1016/j.cell.2015.01.020

Col, E., Caron, C., Seigneurin-Berny, D., Gracia, J., Favier, A., and Khochbin, S. (2001). The histone acetyltransferase, hGCN5, interacts with and acetylates the HIV transactivator. *Tat. J. Biol. Chem.* 276, 28179–28184. doi: 10.1074/jbc.M101385200

Colin, L., and Van Lint, C. (2009). Molecular control of HIV-1 postintegration latency: implications for the development of new therapeutic strategies. *Retrovirology* 6:111. doi: 10.1186/1742-4690-6-111

Colomer-Lluch, M., Ruiz, A., Moris, A., and Prado, J. G. (2018). Restriction Factors: From Intrinsic Viral Restriction to Shaping Cellular Immunity Against HIV-1. *Front. Immunol.* 9:2876. doi: 10.3389/fimmu.2018.02876

Contreras, X., Barboric, M., Lenasi, T., and Peterlin, B. M. (2007). HMBA releases P-TEFb from HEXIM1 and 7SK snRNA *via* PI3K/Akt and activates HIV transcription. *PLoS Pathog.* 3:1459–1469. doi: 10.1371/journal.ppat.0030146

Cook, M. R., and Kim, C. (2019). Safety and Efficacy of Immune Checkpoint Inhibitor Therapy in Patients With HIV Infection and Advanced-Stage Cancer: A Systematic Review. *JAMA Oncol.* 5:1049. doi: 10.1001/jamaoncol.2018.6737

Coppé, J.-P., Patil, C. K., Rodier, F., Krtolica, A., Beauséjour, C. M., Parrinello, S., et al. (2010). A Human-Like Senescence-Associated Secretory Phenotype Is Conserved in Mouse Cells Dependent on Physiological Oxygen. *PLoS One* 5:e9188. doi: 10.1371/journal.pone.0009188

Corley, M. J., Dye, C., D'Antoni, M. L., Byron, M. M., Yo, K. L.-A., Lum-Jones, A., et al. (2016). Comparative DNA Methylation Profiling Reveals an Immunoepigenetic Signature of HIV-related Cognitive Impairment. *Sci. Rep.* 6:33310. doi: 10.1038/srep33310

Crooks, A. M., Bateson, R., Cope, A. B., Dahl, N. P., Griggs, M. K., Kuruc, J. D., et al. (2015). Precise Quantitation of the Latent HIV-1 Reservoir: Implications for Eradication Strategies. *J. Infect. Dis.* 212, 1361–1365. doi: 10.1093/infdis/jiv218

Dahabieh, M., Battivelli, E., and Verdin, E. (2015). Understanding HIV Latency: The Road to an HIV Cure. *Annu. Rev. Med.* 66, 407–421. doi: 10.1146/annurev-med-092112-152941

Dar, A., Kollet, O., and Lapidot, T. (2006). Mutual, reciprocal SDF-1/CXCR4 interactions between hematopoietic and bone marrow stromal cells regulate human stem cell migration and development in NOD/SCID chimeric mice. *Exp. Hematol.* 34, 967–975. doi: 10.1016/j.exphem.2006.04.002

Darcis, G., Berkhout, B., and Pasternak, A. O. (2019). The Quest for Cellular Markers of HIV Reservoirs: Any Color You Like. *Front. Immunol.* 10:2251. doi: 10.3389/fimmu.2019.02251

Darcis, G., Bouchat, S., Kula, A., Van Driessche, B., Delacourt, N., Vanhulle, C., et al. (2017). Reactivation capacity by latency-reversing agents *ex vivo* correlates with the size of the HIV-1 reservoir. *AIDS* 31, 181–189. doi: 10.1097/QAD.0000000000001290

Dash, P. K., Kaminski, R., Bella, R., Su, H., Mathews, S., Ahooyi, T. M., et al. (2019). Sequential LASER ART and CRISPR Treatments Eliminate HIV-1 in a Subset of Infected Humanized Mice. *Nat. Commun.* 10:2753. doi: 10.1038/s41467-019-10366-y

Dashti, A., Waller, C., Mavigner, M., Schoof, N., Bar, K. J., Shaw, G. M., et al. (2020). SMAC Mimetic Plus Triple-Combination Bispecific HIVxCD3 Retargeting Molecules in SHIV.C.CH505-Infected, Antiretroviral Therapy-Suppressed Rhesus Macaques. *J. Virol.* 94, e793–e720. doi: 10.1128/JVI.00793-20

Davidson, E. (2021). *The Regulatory Genome*, 1st Edn. Available online at: https://www.elsevier.com/books/the-regulatory-genome/davidson/978-0-12-088563-3 (accessed December 20, 2021)

Day, C. L., Kaufmann, D. E., Kiepiela, P., Brown, J. A., Moodley, E. S., Reddy, S., et al. (2006). PD-1 expression on HIV-specific T cells is associated with T-cell exhaustion and disease progression. *Nature* 443, 350–354. doi: 10.1038/nature05115

de Armas, L. R., Pallikkuth, S., Rinaldi, S., Pahwa, R., and Pahwa, S. (2019). Implications of Immune Checkpoint Expression During Aging in HIV-Infected People on Antiretroviral Therapy. *AIDS Res. Hum. Retrovir.* 35, 1112–1122. doi: 10.1089/aid.2019.0135

De Spiegelaere, W., Malatinkova, E., Lynch, L., Van Nieuwerburgh, F., Messiaen, P., O'Doherty, U., et al. (2014). Quantification of integrated HIV DNA by repetitive-sampling Alu-HIV PCR on the basis of poisson statistics. *Clin. Chem.* 60, 886–895. doi: 10.1373/clinchem.2013.219378

DeChristopher, B. A., Loy, B. A., Marsden, M. D., Schrier, A. J., Zack, J. A., and Wender, P. A. (2012). Designed, synthetically accessible bryostatin analogues potently induce activation of latent HIV reservoirs in vitro. *Nat. Chem.* 4, 705–710. doi: 10.1038/nchem.1395

Deeks, S. G. (2011). HIV Infection, Inflammation, Immunosenescence, and Aging. *Annu. Rev. Med.* 62, 141–155. doi: 10.1146/annurev-med-042909-093756

Deeks, S. G., Overbaugh, J., Phillips, A., and Buchbinder, S. (2015). HIV infection. *Nat. Rev. Dis. Primers* 1:15035. doi: 10.1038/nrdp.2015.35

Deleage, C., Chan, C. N., Busman-Sahay, K., and Estes, J. D. (2018). Next-generation in situ hybridization approaches to define and quantify HIV and SIV reservoirs in tissue microenvironments. *Retrovirology* 15:4. doi: 10.1186/s12977-017-0387-9

Deleage, C., Wietgrefe, S. W., Del Prete, G., Morcock, D. R., Hao, X. P., Piatak, M., et al. (2016). Defining HIV and SIV Reservoirs in Lymphoid Tissues. *Pathog. Immun.* 1, 68–106. doi: 10.20411/pai.v1i1.100

Della Chiara, G., Crotti, A., Liboi, E., Giacca, M., Poli, G., and Lusic, M. (2011). Negative Regulation of HIV-1 Transcription by a Heterodimeric NF-κB1/p50 and C-Terminally Truncated STAT5 Complex. *J. Mol. Biol.* 410, 933–943. doi: 10.1016/j.jmb.2011.03.044

Demeulemeester, J., De Rijck, J., Gijsbers, R., and Debyser, Z. (2015). Retroviral integration: Site matters: Mechanisms and consequences of retroviral integration site selection. *Bioessays* 37, 1202–1214. doi: 10.1002/bies.201500051

Deng, L., Zeng, Q., Wang, M., Cheng, A., Jia, R., Chen, S., et al. (2018). Suppression of NF-κB Activity: A Viral Immune Evasion Mechanism. *Viruses* 10:E409. doi: 10.3390/v10080409

Ding, D., Qu, X., Li, L., Zhou, X., Liu, S., Lin, S., et al. (2013). Involvement of histone methyltransferase GLP in HIV-1 latency through catalysis of H3K9 dimethylation. *Virology* 440, 182–189. doi: 10.1016/j.virol.2013.02.022

Ding, J., Tasker, C., Lespinasse, P., Dai, J., Fitzgerald-Bocarsly, P., Lu, W., et al. (2015). Integrin α4β7 Expression Increases HIV Susceptibility in Activated Cervical CD4+ T Cells by an HIV Attachment-Independent Mechanism. *JAIDS* 69, 509–518. doi: 10.1097/QAI.0000000000000676

Dinoso, J. B., Kim, S. Y., Wiegand, A. M., Palmer, S. E., Gange, S. J., Cranmer, L., et al. (2009). Treatment intensification does not reduce residual HIV-1 viremia in patients on highly active antiretroviral therapy. *Proc. Natl. Acad. Sci. U S A.* 106, 9403–9408. doi: 10.1073/pnas.0903107106

Donahue, D. A., and Wainberg, M. A. (2013). Cellular and molecular mechanisms involved in the establishment of HIV-1 latency. *Retrovirology* 10:11. doi: 10.1186/1742-4690-10-11

Douek, D. C., Brenchley, J. M., Betts, M. R., Ambrozak, D. R., Hill, B. J., Okamoto, Y., et al. (2002). HIV preferentially infects HIV-specific CD4+ T cells. *Nature* 417, 95–98. doi: 10.1038/417095a

Doyon, A., Kracht, D., Bayazit, A. K., Deveci, M., Duzova, A., Krmar, R. T., et al. (2013). Carotid Artery Intima-Media Thickness and Distensibility in Children and Adolescents: Reference Values and Role of Body Dimensions. *Hypertension* 62, 550–556. doi: 10.1161/HYPERTENSIONAHA.113.01297

du Chéné, I., Basyuk, E., Lin, Y.-L., Triboulet, R., Knezevich, A., Chable-Bessia, C., et al. (2007). Suv39H1 and HP1gamma are responsible for chromatin-mediated HIV-1 transcriptional silencing and post-integration latency. *EMBO J.* 26, 424–435.

Dyer, W. B., Zaunders, J. J., Yuan, F. F., Wang, B., Learmont, J. C., Geczy, A. F., et al. (2008). Mechanisms of HIV non-progression; robust and sustained CD4+ T-cell proliferative responses to p24 antigen correlate with control of viraemia and lack of disease progression after long-term transfusion-acquired HIV-1 infection. *Retrovirology* 5:112. doi: 10.1186/1742-4690-5-112

Ebina, H., Misawa, N., Kanemura, Y., and Koyanagi, Y. (2013). Harnessing the CRISPR/Cas9 system to disrupt latent HIV-1 provirus. *Sci. Rep.* 3:2510. doi: 10.1038/srep02510

Eilebrecht, S., Le Douce, V., Riclet, R., Targat, B., Hallay, H., Van Driessche, B., et al. (2014). HMGA1 recruits CTIP2-repressed P-TEFb to the HIV-1 and cellular target promoters. *Nucleic Acids Res.* 42, 4962–4971. doi: 10.1093/nar/gku168

Einkauf, K. B., Lee, G. Q., Gao, C., Sharaf, R., Sun, X., Hua, S., et al. (2019). Intact HIV-1 proviruses accumulate at distinct chromosomal positions during prolonged antiretroviral therapy. *J. Clin. Invest.* 129, 988–998. doi: 10.1172/JCI124291

Einkauf, K. B., Osborn, M. R., Gao, C., Sun, W., Sun, X., Lian, X., et al. (2022). Parallel analysis of transcription, integration, and sequence of single HIV-1 proviruses. *Cell* 185, 266.e–282.e. doi: 10.1016/j.cell.2021.12.011

Elbezanti, W., Lin, A., Schirling, A., Jackson, A., Marshall, M., Duyne, R. V., et al. (2020). Benzodiazepines Drive Alteration of Chromatin at the Integrated HIV-1 LTR. *Viruses* 12:E191. doi: 10.3390/v12020191

El-Sadr, W. M., Lundgren, J. D., Neaton, J. D., Gordin, F., Abrams, D., Arduino, R. C., et al. (2006). CD4+ Count–Guided Interruption of Antiretroviral Treatment. *N. Engl. J. Med.* 355, 2283–2296. doi: 10.1056/NEJMoa062360

Eriksson, S., Graf, E. H., Dahl, V., Strain, M. C., Yukl, S. A., Lysenko, E. S., et al. (2013). Comparative Analysis of Measures of Viral Reservoirs in HIV-1 Eradication Studies. *PLoS Pathog.* 9:e1003174. doi: 10.1371/journal.ppat.1003174

Estes, J. D., Kityo, C., Ssali, F., Swainson, L., Makamdop, K. N., Del Prete, G. Q., et al. (2017). Defining total-body AIDS-virus burden with implications for curative strategies. *Nat. Med.* 23, 1271–1276. doi: 10.1038/nm.4411

Evans, V. A., van der Sluis, R. M., Solomon, A., Dantanarayana, A., McNeil, C., Garsia, R., et al. (2018). Programmed cell death-1 contributes to the establishment and maintenance of HIV-1 latency. *AIDS* 32, 1491–1497. doi: 10.1097/QAD.0000000000001849

Fauci, A. S. (1991). Immunopathogenic Mechanisms in Human Immunodeficiency Virus (HIV) Infection. *Ann. Intern. Med.* 114:678. doi: 10.7326/0003-4819-114-8-678

Finzi, D., Hermankova, M., Pierson, T., Carruth, L. M., Buck, C., Chaisson, R. E., et al. (1997). Identification of a Reservoir for HIV-1 in Patients on Highly Active Antiretroviral Therapy. *Science* 278, 1295–1300. doi: 10.1126/science.278.5341.1295

Forouzanfar, F., Ali, S., Wallet, C., De Rovere, M., Ducloy, C., El Mekdad, H., et al. (2019). HIV-1 Vpr mediates the depletion of the cellular repressor CTIP2 to counteract viral gene silencing. *Sci. Rep.* 9:13154. doi: 10.1038/s41598-019-48689-x

Fowke, K. R., Nagelkerke, N. J., Kimani, J., Simonsen, J. N., Anzala, A. O., Bwayo, J. J., et al. (1996). Resistance to HIV-1 infection among persistently seronegative prostitutes in Nairobi, Kenya. *Lancet* 348, 1347–1351. doi: 10.1016/S0140-6736(95)12269-2

French, A. J., Natesampillai, S., Krogman, A., Correia, C., Peterson, K. L., Alto, A., et al. (2020). Reactivating latent HIV with PKC agonists induces resistance to apoptosis and is associated with phosphorylation and activation of BCL2. *PLoS Pathog.* 16:e1008906. doi: 10.1371/journal.ppat.1008906

Friedman, J., Cho, W.-K., Chu, C. K., Keedy, K. S., Archin, N. M., Margolis, D. M., et al. (2011). Epigenetic silencing of HIV-1 by the histone H3 lysine 27 methyltransferase enhancer of Zeste 2. *J. Virol.* 85, 9078–9089. doi: 10.1128/JVI.00836-11

Fromentin, R., DaFonseca, S., Costiniuk, C. T., El-Far, M., Procopio, F. A., Hecht, F. M., et al. (2019). PD-1 blockade potentiates HIV latency reversal *ex vivo* in CD4+ T cells from ART-suppressed individuals. *Nat. Commun.* 10:814. doi: 10.1038/s41467-019-08798-7

Fukuda, H., Li, S., Sardo, L., Smith, J. L., Yamashita, K., Sarca, A. D., et al. (2019). Structural Determinants of the APOBEC3G N-Terminal Domain for HIV-1 RNA Association. *Front. Cell. Infect. Microbiol.* 9:129. doi: 10.3389/fcimb.2019.00129

Gaebler, C., Cetrulo Lorenzi, J. C., Oliveira, T., Nogueira, L., Ramos, V., Lu, C.-L., et al. (2019). Combination of quadruplex qPCR and next-generation sequencing for qualitative and quantitative analysis of the HIV-1 latent reservoir. *J. Exp. Med.* 216:20190896. doi: 10.1084/jem.20190896

Gaebler, C., Falcinelli, S. D., Stoffel, E., Read, J., Murtagh, R., Oliveira, T. Y., et al. (2021). Sequence Evaluation and Comparative Analysis of Novel Assays for Intact Proviral HIV-1 DNA. *J. Virol.* 95, e1986–e1920. doi: 10.1128/JVI.01986-20

Galvani, A. P., and Slatkin, M. (2003). Evaluating plague and smallpox as historical selective pressures for the CCR5- 32 HIV-resistance allele. *Proc. Natl. Acad. Sci.* 100, 15276–15279. doi: 10.1073/pnas.2435085100

Gao, R., Bao, J., Yan, H., Xie, L., Qin, W., Ning, H., et al. (2020). Competition between PAF1 and MLL1/COMPASS confers the opposing function of LEDGF/p75 in HIV latency and proviral reactivation. *Sci. Adv.* 6:eaaz8411. doi: 10.1126/sciadv.aaz8411

Gasparian, A. V., Burkhart, C. A., Purmal, A. A., Brodsky, L., Pal, M., Saranadasa, M., et al. (2011). Curaxins: Anticancer Compounds That Simultaneously Suppress NF-κB and Activate p53 by Targeting FACT. *Sci. Translat. Med.* 2011:3002530. doi: 10.1126/scitranslmed.3002530

Gay, C. L., Bosch, R. J., Ritz, J., Hataye, J. M., Aga, E., Tressler, R. L., et al. (2017). Clinical Trial of the Anti-PD-L1 Antibody BMS-936559 in HIV-1 Infected Participants on Suppressive Antiretroviral Therapy. *J. Infect. Dis.* 215, 1725–1733. doi: 10.1093/infdis/jix191

Geng, Y., Mosyak, L., Kurinov, I., Zuo, H., Sturchler, E., Cheng, T. C., et al. (2016). Structural mechanism of ligand activation in human calcium-sensing receptor. *eLife* 5:e13662. doi: 10.7554/eLife.13662

Ghoneim, H. E., Fan, Y., Moustaki, A., Abdelsamed, H. A., Dash, P., Dogra, P., et al. (2017). De Novo Epigenetic Programs Inhibit PD-1 Blockade-Mediated T Cell Rejuvenation. *Cell* 170, 142.e–157.e. doi: 10.1016/j.cell.2017.06.007

Gibellini, D., Borderi, M., De Crignis, E., Cicola, R., Cimatti, L., Vitone, F., et al. (2008). HIV-1 DNA load analysis in peripheral blood lymphocytes and monocytes from naïve and HAART-treated individuals. *J. Infect.* 56, 219–225. doi: 10.1016/j.jinf.2008.01.001

Gobeil, L.-A., Lodge, R., and Tremblay, M. J. (2012). Differential HIV-1 endocytosis and susceptibility to virus infection in human macrophages correlate with cell activation status. *J. Virol.* 86, 10399–10407. doi: 10.1128/JVI.01051-12

Gohda, J., Suzuki, K., Liu, K., Xie, X., Takeuchi, H., Inoue, J., et al. (2018). BI-2536 and BI-6727, dual Polo-like kinase/bromodomain inhibitors, effectively reactivate latent HIV-1. *Sci. Rep.* 8:3521. doi: 10.1038/s41598-018-21942-5

Goncalves, A., Leigh-Brown, S., Thybert, D., Stefflova, K., Turro, E., Flicek, P., et al. (2012). Extensive compensatory cis-trans regulation in the evolution of mouse gene expression. *Genome Res.* 22, 2376–2384. doi: 10.1101/gr.142281.112

Gondim, M. V. P., Sherrill-Mix, S., Bibollet-Ruche, F., Russell, R. M., Trimboli, S., Smith, A. G., et al. (2021). Heightened resistance to host type 1 interferons characterizes HIV-1 at transmission and after antiretroviral therapy interruption. *Sci. Transl. Med.* 13:eabd8179. doi: 10.1126/scitranslmed.abd8179

Gonelli, C. A., Khoury, G., Center, R. J., and Purcell, D. F. J. (2019). HIV-1-Based Virus-like Particles that Morphologically Resemble Mature, Infectious HIV-1 Virions. *Viruses* 11:507. doi: 10.3390/v11060507

Gonzalo-Gil, E., Ikediobi, U., and Sutton, R. E. (2017). Mechanisms of Virologic Control and Clinical Characteristics of HIV+ Elite/Viremic Controllers. *Yale J. Biol. Med.* 90, 245–259.

Gosselin, A., Wiche Salinas, T. R., Planas, D., Wacleche, V. S., Zhang, Y., Fromentin, R., et al. (2017). HIV persists in CCR6+CD4+ T cells from colon and blood during antiretroviral therapy. *AIDS* 31, 35–48. doi: 10.1097/QAD.0000000000001309

Gougeon, M.-L. (2005). To kill or be killed: how HIV exhausts the immune system. *Cell Death Differ.* 12(Suppl. 1), 845–854. doi: 10.1038/sj.cdd.4401616

Grau-Expósito, J., Luque-Ballesteros, L., Navarro, J., Curran, A., Burgos, J., Ribera, E., et al. (2019). Latency reversal agents affect differently the latent reservoir present in distinct CD4+ T subpopulations. *PLoS Pathog.* 15:e1007991. doi: 10.1371/journal.ppat.1007991

Guihot, A., Marcelin, A.-G., Massiani, M.-A., Samri, A., Soulié, C., Autran, B., et al. (2018). Drastic decrease of the HIV reservoir in a patient treated with nivolumab for lung cancer. *Ann. Oncol.* 29, 517–518. doi: 10.1093/annonc/mdx696

Gulakowski, R. J., McMahon, J. B., Buckheit, R. W., Gustafson, K. R., and Boyd, M. R. (1997). Antireplicative and anticytopathic activities of prostratin, a non-tumor-promoting phorbol ester, against human immunodeficiency virus (HIV). *Antiviral Res.* 33, 87–97. doi: 10.1016/s0166-3542(96)01004-2

Gunst, M., Jarman, K., Yarwood, V., Rokadiya, S., Capsaskis, L., Orcutt, M., et al. (2019). Healthcare access for refugees in Greece: Challenges and opportunities. *Health Policy* 123, 818–824. doi: 10.1016/j.healthpol.2019.06.003

Gupta, R. K., Abdul-Jawad, S., McCoy, L. E., Mok, H. P., Peppa, D., Salgado, M., et al. (2019). HIV-1 remission following CCR5Δ32/Δ32 haematopoietic stem-cell transplantation. *Nature* 568, 244–248. doi: 10.1038/s41586-019-1027-4

Gutiérrez, C., Serrano-Villar, S., Madrid-Elena, N., Pérez-Elías, M. J., Martín, M. E., Barbas, C., et al. (2016). Bryostatin-1 for latent virus reactivation in HIV-infected patients on antiretroviral therapy. *AIDS* 30, 1385–1392. doi: 10.1097/QAD.0000000000001064

Hakre, S., Chavez, L., Shirakawa, K., and Verdin, E. (2012). HIV latency: experimental systems and molecular models. *FEMS Microbiol. Rev.* 36, 706–716. doi: 10.1111/j.1574-6976.2012.00335.x

Hale, M., Mesojednik, T., Romano Ibarra, G. S., Sahni, J., Bernard, A., Sommer, K., et al. (2017). Engineering HIV-Resistant, Anti-HIV Chimeric Antigen Receptor T Cells. *Mol. Ther.* 25, 570–579. doi: 10.1016/j.ymthe.2016.12.023

Hamer, D. (2004). Can HIV be Cured? Mechanisms of HIV Persistence and Strategies to Combat It. *CHR* 2, 99–111. doi: 10.2174/1570162043484915

Han, Y., Lassen, K., Monie, D., Sedaghat, A. R., Shimoji, S., Liu, X., et al. (2004). Resting CD4+ T cells from human immunodeficiency virus type 1 (HIV-1)-infected individuals carry integrated HIV-1 genomes within actively transcribed host genes. *J. Virol.* 78, 6122–6133. doi: 10.1128/JVI.78.12.6122-6133.2004

Harari, A., Rozot, V., Cavassini, M., Bellutti Enders, F., Viganò, S., Castro, E., et al. (2012). NYVAC immunization induces polyfunctional HIV-specific T-cell responses in chronically-infected, ART-treated HIV patients. *Eur. J. Immunol.* 42:201242696. doi: 10.1002/eji.201242696

Hariharan, M., Scaria, V., Pillai, B., and Brahmachari, S. K. (2005). Targets for human encoded microRNAs in HIV genes. *Biochem. Biophys. Res. Commun.* 337, 1214–1218. doi: 10.1016/j.bbrc.2005.09.183

Hartmann, J., Schüßler-Lenz, M., Bondanza, A., and Buchholz, C. J. (2017). Clinical development of CAR T cells-challenges and opportunities in translating innovative treatment concepts. *EMBO Mol. Med.* 9, 1183–1197. doi: 10.15252/emmm.201607485

Hattori, S., Matsuda, K., Tsuchiya, K., Gatanaga, H., Oka, S., Yoshimura, K., et al. (2018). Combination of a Latency-Reversing Agent With a Smac Mimetic Minimizes Secondary HIV-1 Infection in vitro. *Front. Microbiol.* 9:2022. doi: 10.3389/fmicb.2018.02022

Hazenberg, M. D., Hamann, D., Schuitemaker, H., and Miedema, F. (2000). T cell depletion in HIV-1 infection: how CD4+ T cells go out of stock. *Nat. Immunol.* 1, 285–289. doi: 10.1038/79724

Hennessy, E. J., Adam, A., Aquila, B. M., Castriotta, L. M., Cook, D., Hattersley, M., et al. (2013). Discovery of a novel class of dimeric Smac mimetics as potent IAP antagonists resulting in a clinical candidate for the treatment of cancer (AZD5582). *J. Med. Chem.* 56, 9897–9919. doi: 10.1021/jm401075x

Henning, A. N., Roychoudhuri, R., and Restifo, N. P. (2018). Epigenetic control of CD8+ T cell differentiation. *Nat. Rev. Immunol.* 18, 340–356. doi: 10.1038/nri.2017.146

Henrich, T. J., Hsue, P. Y., and VanBrocklin, H. (2019). Seeing Is Believing: Nuclear Imaging of HIV Persistence. *Front. Immunol.* 10:2077. doi: 10.3389/fimmu.2019.02077

Herbein, G., and Wendling, D. (2010). Histone deacetylases in viral infections. *Clin. Epigenet.* 1, 13–24. doi: 10.1007/s13148-010-0003-5

Hiener, B., Horsburgh, B. A., Eden, J.-S., Barton, K., Schlub, T. E., Lee, E., et al. (2017). Identification of Genetically Intact HIV-1 Proviruses in Specific CD4+ T Cells from Effectively Treated Participants. *Cell Rep.* 21, 813–822. doi: 10.1016/j.celrep.2017.09.081

Hill, A. L., Rosenbloom, D. I. S., Goldstein, E., Hanhauser, E., Kuritzkes, D. R., Siliciano, R. F., et al. (2016). Real-Time Predictions of Reservoir Size and Rebound Time during Antiretroviral Therapy Interruption Trials for HIV. *PLoS Pathog.* 12:e1005535. doi: 10.1371/journal.ppat.1005535

Ho, Y.-C., Shan, L., Hosmane, N. N., Wang, J., Laskey, S. B., Rosenbloom, D. I. S., et al. (2013). Replication-Competent Noninduced Proviruses in the Latent Reservoir Increase Barrier to HIV-1 Cure. *Cell* 155, 540–551. doi: 10.1016/j.cell.2013.09.020

Holkmann Olsen, C., Mocroft, A., Kirk, O., Vella, S., Blaxhult, A., Clumeck, N., et al. (2007). Interruption of combination antiretroviral therapy and risk of clinical disease progression to AIDS or death. *HIV Med.* 8, 96–104. doi: 10.1111/j.1468-1293.2007.00436.x

Honeycutt, J. B., Thayer, W. O., Baker, C. E., Ribeiro, R. M., Lada, S. M., Cao, Y., et al. (2017). HIV persistence in tissue macrophages of humanized myeloid-only mice during antiretroviral therapy. *Nat. Med.* 23, 638–643. doi: 10.1038/nm.4319

Hosmane, N. N., Kwon, K. J., Bruner, K. M., Capoferri, A. A., Beg, S., Rosenbloom, D. I. S., et al. (2017). Proliferation of latently infected CD4+ T cells carrying replication-competent HIV-1: Potential role in latent reservoir dynamics. *J. Exp. Med.* 214, 959–972. doi: 10.1084/jem.20170193

Hottiger, M. O., and Nabel, G. J. (1998). Interaction of human immunodeficiency virus type 1 Tat with the transcriptional coactivators p300 and CREB binding protein. *J. Virol.* 72, 8252–8256. doi: 10.1128/JVI.72.10.8252-8256.1998

Houzet, L., and Jeang, K.-T. (2011). Genome-wide screening using RNA interference to study host factors in viral replication and pathogenesis. *Exp. Biol. Med.* 236, 962–967. doi: 10.1258/ebm.2010.010272

Hu, W., Kaminski, R., Yang, F., Zhang, Y., Cosentino, L., Li, F., et al. (2014). RNA-directed gene editing specifically eradicates latent and prevents new HIV-1 infection. *Proc. Natl. Acad. Sci.* 111, 11461–11466. doi: 10.1073/pnas.1405186111

Huang, H., Kong, W., Jean, M., Fiches, G., Zhou, D., Hayashi, T., et al. (2019). A CRISPR/Cas9 screen identifies the histone demethylase MINA53 as a novel HIV-1 latency-promoting gene (LPG). *Nucleic Acids Res.* 47, 7333–7347. doi: 10.1093/nar/gkz493

Huang, H., Liu, S., Jean, M., Simpson, S., Huang, H., Merkley, M., et al. (2017). A Novel Bromodomain Inhibitor Reverses HIV-1 Latency through Specific Binding with BRD4 to Promote Tat and P-TEFb Association. *Front. Microbiol.* 8:1035. doi: 10.3389/fmicb.2017.01035

Huang, Y., Zhang, L., and Ho, D. D. (1995). Characterization of nef sequences in long-term survivors of human immunodeficiency virus type 1 infection. *J. Virol.* 1995:1995. doi: 10.1128/jvi.69.1.93-100.1995

Hütter, G., Nowak, D., Mossner, M., Ganepola, S., Müssig, A., Allers, K., et al. (2009). Long-term control of HIV by CCR5 Delta32/Delta32 stem-cell transplantation. *N. Engl. J. Med.* 360, 692–698. doi: 10.1056/NEJMoa0802905

Iglesias-Ussel, M., Vandergeeten, C., Marchionni, L., Chomont, N., and Romerio, F. (2013). High levels of CD2 expression identify HIV-1 latently infected resting memory CD4+ T cells in virally suppressed subjects. *J. Virol.* 87, 9148–9158. doi: 10.1128/JVI.01297-13

Ikeda, T., Shibata, J., Yoshimura, K., Koito, A., and Matsushita, S. (2007). Recurrent HIV-1 integration at the BACH2 locus in resting CD4+ T cell populations during effective highly active antiretroviral therapy. *J. Infect. Dis.* 195, 716–725. doi: 10.1086/510915

Imai, C., Mihara, K., Andreansky, M., Nicholson, I. C., Pui, C.-H., Geiger, T. L., et al. (2004). Chimeric receptors with 4-1BB signaling capacity provoke potent cytotoxicity against acute lymphoblastic leukemia. *Leukemia* 18, 676–684. doi: 10.1038/sj.leu.2403302

Imai, K., Togami, H., and Okamoto, T. (2010). Involvement of histone H3 lysine 9 (H3K9) methyltransferase G9a in the maintenance of HIV-1 latency and its reactivation by BIX01294. *J. Biol. Chem.* 285, 16538–16545. doi: 10.1074/jbc.M110.103531

Imam, H., Bano, A. S., Patel, P., Holla, P., and Jameel, S. (2015). The lncRNA NRON modulates HIV-1 replication in a NFAT-dependent manner and is differentially regulated by early and late viral proteins. *Sci. Rep.* 5:8639. doi: 10.1038/srep08639

Imamichi, H., Dewar, R. L., Adelsberger, J. W., Rehm, C. A., O'Doherty, U., Paxinos, E. E., et al. (2016). Defective HIV-1 proviruses produce novel protein-coding RNA species in HIV-infected patients on combination antiretroviral therapy. *PNAS* 113, 8783–8788. doi: 10.1073/pnas.1609057113

Imamichi, H., Smith, M., Adelsberger, J. W., Izumi, T., Scrimieri, F., Sherman, B. T., et al. (2020). Defective HIV-1 proviruses produce viral proteins. *PNAS* 117, 3704–3710. doi: 10.1073/pnas.1917876117

Izumi, T., Shirakawa, K., and Takaori-Kondo, A. (2008). Cytidine deaminases as a weapon against retroviruses and a new target for antiviral therapy. *Mini Rev. Med. Chem.* 8, 231–238. doi: 10.2174/138955708783744047

Jadhav, R. R., Im, S. J., Hu, B., Hashimoto, M., Li, P., Lin, J.-X., et al. (2019). Epigenetic signature of PD-1+ TCF1+ CD8 T cells that act as resource cells during chronic viral infection and respond to PD-1 blockade. *Proc. Natl. Acad. Sci. U S A.* 116, 14113–14118. doi: 10.1073/pnas.1903520116

Jadlowsky, J. K., Wong, J. Y., Graham, A. C., Dobrowolski, C., Devor, R. L., Adams, M. D., et al. (2014). Negative Elongation Factor Is Required for the Maintenance of Proviral Latency but Does Not Induce Promoter-Proximal Pausing of RNA Polymerase II on the HIV Long Terminal Repeat. *Mol. Cell. Biol.* 34, 1911–1928. doi: 10.1128/MCB.01013-13

Jang, M. K., Mochizuki, K., Zhou, M., Jeong, H.-S., Brady, J. N., and Ozato, K. (2005). The bromodomain protein Brd4 is a positive regulatory component of P-TEFb and stimulates RNA polymerase II-dependent transcription. *Mol. Cell* 19, 523–534. doi: 10.1016/j.molcel.2005.06.027

Jiang, G., and Dandekar, S. (2015). Targeting NF-κB Signaling with Protein Kinase C Agonists As an Emerging Strategy for Combating HIV Latency. *AIDS Res. Hum. Retroviruses* 31, 4–12. doi: 10.1089/aid.2014.0199

Jiang, G., Espeseth, A., Hazuda, D. J., and Margolis, D. M. (2007). c-Myc and Sp1 Contribute to Proviral Latency by Recruiting Histone Deacetylase 1 to the Human Immunodeficiency Virus Type 1 Promoter. *J. Virol.* 81, 10914–10923. doi: 10.1128/JVI.01208-07

Jiang, G., Mendes, E. A., Kaiser, P., Sankaran-Walters, S., Tang, Y., Weber, M. G., et al. (2014). Reactivation of HIV latency by a newly modified Ingenol derivative *via* protein kinase Cδ–NF-κB signaling. *AIDS* 28, 1555–1566. doi: 10.1097/QAD.0000000000000289

Jiang, G., Mendes, E. A., Kaiser, P., Wong, D. P., Tang, Y., Cai, I., et al. (2015). Synergistic Reactivation of Latent HIV Expression by Ingenol-3-Angelate, PEP005, Targeted NF-kB Signaling in Combination with JQ1 Induced p-TEFb Activation. *PLoS Pathog.* 11:e1005066. doi: 10.1371/journal.ppat.1005066

Jiang, G., Nguyen, D., Archin, N. M., Yukl, S. A., Méndez-Lagares, G., Tang, Y., et al. (2018). HIV latency is reversed by ACSS2-driven histone crotonylation. *J. Clin. Invest.* 128, 1190–1198. doi: 10.1172/JCI98071

Jiang, L., Yang, K.-H., Chen, Y., Guan, Q.-L., Zhao, P., Tian, J.-H., et al. (2014). Systematic review and meta-analysis of the effectiveness and safety of extended lymphadenectomy in patients with resectable gastric cancer. *Br. J. Surg.* 101, 595–604. doi: 10.1002/bjs.9497

Joos, B., Fischer, M., Kuster, H., Pillai, S. K., Wong, J. K., Böni, J., et al. (2008). HIV rebounds from latently infected cells, rather than from continuing low-level replication. *Proc. Natl. Acad. Sci. U S A.* 105, 16725–16730. doi: 10.1073/pnas.0804192105

Josefsson, L., Stockenstrom, S., von, Faria, N. R., Sinclair, E., Bacchetti, P., et al. (2013). The HIV-1 reservoir in eight patients on long-term suppressive antiretroviral therapy is stable with few genetic changes over time. *PNAS* 2013:1308313110. doi: 10.1073/pnas.1308313110

Kandathil, A. J., Sugawara, S., and Balagopal, A. (2016). Are T cells the only HIV-1 reservoir? *Retrovirology* 13:86. doi: 10.1186/s12977-016-0323-4

Kauder, S. E., Bosque, A., Lindqvist, A., Planelles, V., and Verdin, E. (2009). Epigenetic regulation of HIV-1 latency by cytosine methylation. *PLoS Pathog.* 5:e1000495. doi: 10.1371/journal.ppat.1000495

Kelker, H. C., Seidlin, M., Vogler, M., and Valentine, F. T. (1992). Lymphocytes from Some Long-Term Seronegative Heterosexual Partners of HIV-Infected Individuals Proliferate in Response to HIV Antigens. *AIDS Res. Hum. Retroviruses* 8, 1355–1359. doi: 10.1089/aid.1992.8.1355

Kessing, C. F., Nixon, C. C., Li, C., Tsai, P., Takata, H., Mousseau, G., et al. (2017). *In Vivo* Suppression of HIV Rebound by Didehydro-Cortistatin A, a "Block-and-Lock" Strategy for HIV-1 Treatment. *Cell Rep.* 21, 600–611. doi: 10.1016/j.celrep.2017.09.080

Kessl, J. J., Jena, N., Koh, Y., Taskent-Sezgin, H., Slaughter, A., Feng, L., et al. (2012). Multimode, cooperative mechanism of action of allosteric HIV-1 integrase inhibitors. *J. Biol. Chem.* 287, 16801–16811. doi: 10.1074/jbc.M112.354373

Khalil, A. M., Guttman, M., Huarte, M., Garber, M., Raj, A., Rivea Morales, D., et al. (2009). Many human large intergenic noncoding RNAs associate with chromatin-modifying complexes and affect gene expression. *PNAS* 106, 11667–11672. doi: 10.1073/pnas.0904715106

Khan, O., Giles, J. R., McDonald, S., Manne, S., Ngiow, S. F., Patel, K. P., et al. (2019). TOX transcriptionally and epigenetically programs CD8+ T cell exhaustion. *Nature* 571, 211–218. doi: 10.1038/s41586-019-1325-x

Khoury, A. L., Morey, M. C., Wong, T. C., McNeil, D. L., Humphries, B., Frankey, K., et al. (2017). Diminished physical function in older HIV-infected adults in the Southeastern U.S. despite successful antiretroviral therapy. *PLoS One* 12:e0179874. doi: 10.1371/journal.pone.0179874

Kim, Y., Anderson, J. L., and Lewin, S. R. (2018). Getting the "Kill" into "Shock and Kill": Strategies to Eliminate Latent HIV. *Cell Host Microbe* 23, 14–26. doi: 10.1016/j.chom.2017.12.004

Kinloch, N. N., Ren, Y., Conce Alberto, W. D., Dong, W., Khadka, P., Huang, S. H., et al. (2021). HIV-1 diversity considerations in the application of the Intact

Proviral DNA Assay (IPDA). *Nat. Commun.* 12:165. doi: 10.1038/s41467-020-20442-3

Klase, Z., Kale, P., Winograd, R., Gupta, M. V., Heydarian, M., Berro, R., et al. (2007). HIV-1 TAR element is processed by Dicer to yield a viral micro-RNA involved in chromatin remodeling of the viral LTR. *BMC Mol. Biol.* 8:63. doi: 10.1186/1471-2199-8-63

Klase, Z., Yedavalli, V. S. R. K., Houzet, L., Perkins, M., Maldarelli, F., Brenchley, J., et al. (2014). Activation of HIV-1 from Latent Infection *via* Synergy of RUNX1 Inhibitor Ro5-3335 and SAHA. *PLoS Pathog.* 10:e1003997. doi: 10.1371/journal.ppat.1003997

Klitz, W., Brautbar, C., Schito, A. M., Barcellos, L. F., and Oksenberg, J. R. (2001). Evolution of the CCR5 δ32 mutation based on haplotype variation in Jewish and Northern European population samples. *Hum. Immunol.* 62, 530–538. doi: 10.1016/S0198-8859(01)00239-7

Kordelas, L., Verheyen, J., and Esser, S. (2014). Shift of HIV Tropism in Stem-Cell Transplantation with CCR5 Delta32 Mutation. *N. Engl. J. Med.* 371, 880–882. doi: 10.1056/NEJMc1405805

Koup, R. A., Safrit, J. T., Cao, Y., Andrews, C. A., McLeod, G., Borkowsky, W., et al. (1994). Temporal association of cellular immune responses with the initial control of viremia in primary human immunodeficiency virus type 1 syndrome. *J. Virol.* 68, 4650–4655. doi: 10.1128/JVI.68.7.4650-4655.1994

Kousignian, I., Abgrall, S., Grabar, S., Mahamat, A., Teicher, E., Rouveix, E., et al. (2008). Maintaining Antiretroviral Therapy Reduces the Risk of AIDS-Defining Events in Patients with Uncontrolled Viral Replication and Profound Immunodeficiency. *Clin. Infect. Dis.* 46, 296–304. doi: 10.1086/524753

Kruize, Z., and Kootstra, N. A. (2019). The Role of Macrophages in HIV-1 Persistence and Pathogenesis. *Front. Microbiol.* 10:2828. doi: 10.3389/fmicb.2019.02828

Kuai, Q., Lu, X., Qiao, Z., Wang, R., Wang, Y., Ye, S., et al. (2018). Histone deacetylase inhibitor chidamide promotes reactivation of latent human immunodeficiency virus by introducing histone acetylation. *J. Med. Virol.* 90, 1478–1485. doi: 10.1002/jmv.25207

Kula, A., Guerra, J., Knezevich, A., Kleva, D., Myers, M. P., and Marcello, A. (2011). Characterization of the HIV-1 RNA associated proteome identifies Matrin 3 as a nuclear cofactor of Rev function. *Retrovirology* 8:60. doi: 10.1186/1742-4690-8-60

Kulkosky, J., Culnan, D. M., Roman, J., Dornadula, G., Schnell, M., Boyd, M. R., et al. (2001). Prostratin: activation of latent HIV-1 expression suggests a potential inductive adjuvant therapy for HAART. *Blood* 98, 3006–3015. doi: 10.1182/blood.V98.10.3006

Kulpa, D. A., Talla, A., Brehm, J. H., Ribeiro, S. P., Yuan, S., Bebin-Blackwell, A.-G., et al. (2019). Differentiation into an Effector Memory Phenotype Potentiates HIV-1 Latency Reversal in CD4+ T Cells. *J. Virol.* 93, e969–e919. doi: 10.1128/JVI.00969-19

Kwong, P. D., Mascola, J. R., and Nabel, G. J. (2013). Broadly neutralizing antibodies and the search for an HIV-1 vaccine: the end of the beginning. *Nat. Rev. Immunol.* 13, 693–701. doi: 10.1038/nri3516

Laird, G. M., Eisele, E. E., Rabi, S. A., Lai, J., Chioma, S., Blankson, J. N., et al. (2013). Rapid quantification of the latent reservoir for HIV-1 using a viral outgrowth assay. *PLoS Pathog.* 9:e1003398. doi: 10.1371/journal.ppat.1003398

Le Douce, V., Colin, L., Redel, L., Cherrier, T., Herbein, G., Aunis, D., et al. (2012). LSD1 cooperates with CTIP2 to promote HIV-1 transcriptional silencing. *Nucleic Acids Res.* 40, 1904–1915. doi: 10.1093/nar/gkr857

Lee, G. Q., Orlova-Fink, N., Einkauf, K., Chowdhury, F. Z., Sun, X., Harrington, S., et al. (2017). Clonal expansion of genome-intact HIV-1 in functionally polarized Th1 CD4+ T cells. *J. Clin. Invest.* 127, 2689–2696. doi: 10.1172/JCI93289

Lefrère, J., Mariotti, M., Morand-Joubert, L., Thauvin, M., and Roudot-Thoraval, F. (1999). Plasma Human Immunodeficiency Virus RNA Below 40 Copies/mL Is Rarein Untreated Persons Even in the First Years of Infection. *J. Infect. Dis.* 180, 526–529. doi: 10.1086/314906

Leite, T. F., Delatorre, E., Côrtes, F. H., Ferreira, A. C. G., Cardoso, S. W., Grinsztejn, B., et al. (2019). Reduction of HIV-1 Reservoir Size and Diversity After 1 Year of cART Among Brazilian Individuals Starting Treatment During Early Stages of Acute Infection. *Front. Microbiol.* 10:145. doi: 10.3389/fmicb.2019.00145

Leonard, J. N., Shah, P. S., Burnett, J. C., and Schaffer, D. V. (2008). HIV Evades RNA Interference Directed at TAR by an Indirect Compensatory Mechanism. *Cell Host Microbe* 4, 484–494. doi: 10.1016/j.chom.2008.09.008

Levy, C. N., Hughes, S. M., Roychoudhury, P., Reeves, D. B., Amstuz, C., Zhu, H., et al. (2021). A highly multiplexed droplet digital PCR assay to measure the intact HIV-1 proviral reservoir. *Cell Rep. Med.* 2:100243. doi: 10.1016/j.xcrm.2021.100243

Li, C., Mousseau, G., and Valente, S. (2019). Tat inhibition by didehydro-Cortistatin A promotes heterochromatin formation at the HIV-1 long terminal repeat. *Epigenetics Chromatin* 12:23. doi: 10.1186/s13072-019-0267-8

Li, H., Chi, X., Li, R., Ouyang, J., and Chen, Y. (2020). A Novel lncRNA, AK130181, Contributes to HIV-1 Latency by Regulating Viral Promoter-Driven Gene Expression in Primary CD4+ T Cells. *Mol. Ther. Nucleic Acids* 20, 754–763. doi: 10.1016/j.omtn.2020.04.011

Li, J., Chen, C., Ma, X., Geng, G., Liu, B., Zhang, Y., et al. (2016). Long noncoding RNA NRON contributes to HIV-1 latency by specifically inducing tat protein degradation. *Nat. Commun.* 7:11730. doi: 10.1038/ncomms11730

Li, J. Z., Etemad, B., Ahmed, H., Aga, E., Bosch, R. J., Mellors, J. W., et al. (2016). The size of the expressed HIV reservoir predicts timing of viral rebound after treatment interruption. *AIDS* 30, 343–353. doi: 10.1097/QAD.0000000000000953

Li, Z., Mbonye, U., Feng, Z., Wang, X., Gao, X., Karn, J., et al. (2018). The KAT5-Acetyl-Histone4-Brd4 axis silences HIV-1 transcription and promotes viral latency. *PLoS Pathog.* 14:e1007012. doi: 10.1371/journal.ppat.1007012

Liang, T., Zhang, X., Lai, F., Lin, J., Zhou, C., Xu, X., et al. (2019). A novel bromodomain inhibitor, CPI-203, serves as an HIV-1 latency-reversing agent by activating positive transcription elongation factor b. *Biochem. Pharmacol.* 164, 237–251. doi: 10.1016/j.bcp.2019.04.005

Lin, J. E., Asfour, A., Sewell, T. B., Hooe, B., Pryce, P., Earley, C., et al. (2021). Neurological issues in children with COVID-19. *Neurosci. Lett.* 743:135567. doi: 10.1016/j.neulet.2020.135567

Liszewski, M. K., Yu, J. J., and O'Doherty, U. (2009). Detecting HIV-1 integration by repetitive-sampling Alu-gag PCR. *Methods* 47, 254–260. doi: 10.1016/j.ymeth.2009.01.002

Liu, L., Shawki, D., Voulgarakis, A., Kasoar, M., Samset, B. H., Myhre, G., et al. (2018). A PDRMIP Multimodel Study on the Impacts of Regional Aerosol Forcings on Global and Regional Precipitation. *J. Clim.* 31, 4429–4447. doi: 10.1175/JCLI-D-17-0439.1

Liu, R., Simonetti, F. R., and Ho, Y.-C. (2020). The forces driving clonal expansion of the HIV-1 latent reservoir. *Virol. J.* 17:4. doi: 10.1186/s12985-019-1276-8

Lopez-Galindez, C., Pernas, M., Casado, C., Olivares, I., and Lorenzo-Redondo, R. (2019). Elite controllers and lessons learned for HIV-1 cure. *Curr. Opin. Virol.* 38, 31–36. doi: 10.1016/j.coviro.2019.05.010

López-Huertas, M. R., Jiménez-Tormo, L., Madrid-Elena, N., Gutiérrez, C., Rodríguez-Mora, S., Coiras, M., et al. (2017). The CCR5-antagonist Maraviroc reverses HIV-1 latency in vitro alone or in combination with the PKC-agonist Bryostatin-1. *Sci. Rep.* 7:2385. doi: 10.1038/s41598-017-02634-y

Lorenzi, J. C. C., Cohen, Y. Z., Cohn, L. B., Kreider, E. F., Barton, J. P., Learn, G. H., et al. (2016). Paired quantitative and qualitative assessment of the replication-competent HIV-1 reservoir and comparison with integrated proviral DNA. *Proc. Natl. Acad. Sci. U S A.* 113, E7908–E7916. doi: 10.1073/pnas.1617789113

Lu, P., Shen, Y., Yang, H., Wang, Y., Jiang, Z., Yang, X., et al. (2017). BET inhibitors RVX-208 and PFI-1 reactivate HIV-1 from latency. *Sci. Rep.* 7:16646. doi: 10.1038/s41598-017-16816-1

Lu, Z., Zhang, Q. C., Lee, B., Flynn, R. A., Smith, M. A., Robinson, J. T., et al. (2016). RNA Duplex Map in Living Cells Reveals Higher-Order Transcriptome Structure. *Cell* 165, 1267–1279. doi: 10.1016/j.cell.2016.04.028

Lusic, M. (2003). Regulation of HIV-1 gene expression by histone acetylation and factor recruitment at the LTR promoter. *EMBO J.* 22, 6550–6561. doi: 10.1093/emboj/cdg631

Macatangay, B. J. C., Gandhi, R. T., Jones, R. B., Mcmahon, D. K., Lalama, C. M., Bosch, R. J., et al. (2020). T cells with high PD-1 expression are associated with lower HIV-specific immune responses despite long-term antiretroviral therapy. *AIDS* 34, 15–24. doi: 10.1097/QAD.0000000000002406

Mack, K. D., Jin, X., Yu, S., Wei, R., Kapp, L., Green, C., et al. (2003). HIV insertions within and proximal to host cell genes are a common finding in tissues containing high levels of HIV DNA and macrophage-associated p24 antigen expression. *J. Acquir. Immune Defic. Syndr.* 33, 308–320. doi: 10.1097/00126334-200307010-00004

Madrid-Elena, N., García-Bermejo, M. L., Serrano-Villar, S., Díaz-de Santiago, A., Sastre, B., Gutiérrez, C., et al. (2018). Maraviroc Is Associated with Latent

HIV-1 Reactivation through NF-κB Activation in Resting CD4 $^{+}$ T Cells from HIV-Infected Individuals on Suppressive Antiretroviral Therapy. *J. Virol.* 92:17. doi: 10.1128/JVI.01931-17

Maggiolo, F., Airoldi, M., Callegaro, A., Martinelli, C., Dolara, A., Bini, T., et al. (2009). CD4 cell-guided scheduled treatment interruptions in HIV-infected patients with sustained immunologic response to HAART. *AIDS* 23, 799–807. doi: 10.1097/QAD.0b013e328321b75e

Maher, J., Brentjens, R. J., Gunset, G., Rivière, I., and Sadelain, M. (2002). Human T-lymphocyte cytotoxicity and proliferation directed by a single chimeric TCRζ /CD28 receptor. *Nat. Biotechnol.* 20, 70–75. doi: 10.1038/nbt0102-70

Maldarelli, F., Wu, X., Su, L., Simonetti, F. R., Shao, W., Hill, S., et al. (2014). HIV latency. Specific HIV integration sites are linked to clonal expansion and persistence of infected cells. *Science* 345, 179–183. doi: 10.1126/science.1254194

Manel, N., and Littman, D. R. (2011). Hiding in Plain Sight: How HIV Evades Innate Immune Responses. *Cell* 147, 271–274. doi: 10.1016/j.cell.2011.09.010

Marban, C., Suzanne, S., Dequiedt, F., de Walque, S., Redel, L., Van Lint, C., et al. (2007). Recruitment of chromatin-modifying enzymes by CTIP2 promotes HIV-1 transcriptional silencing. *EMBO J.* 26, 412–423. doi: 10.1038/sj.emboj.7601516

Mariño-Ramírez, L., Kann, M. G., Shoemaker, B. A., and Landsman, D. (2005). Histone structure and nucleosome stability. *Expert Rev. Proteom.* 2, 719–729. doi: 10.1586/14789450.2.5.719

Martinez-Picado, J., Morales-Lopetegi, K., Wrin, T., Prado, J. G., Frost, S. D. W., Petropoulos, C. J., et al. (2002). Selection of drug-resistant HIV-1 mutants in response to repeated structured treatment interruptions. *AIDS* 16, 895–899. doi: 10.1097/00002030-200204120-00009

Marzio, G., Tyagi, M., Gutierrez, M. I., and Giacca, M. (1998). HIV-1 Tat transactivator recruits p300 and CREB-binding protein histone acetyltransferases to the viral promoter. *PNAS* 95, 13519–13524. doi: 10.1073/pnas.95.23.13519

Mates, J. M., de Silva, S., Lustberg, M., Van Deusen, K., Baiocchi, R. A., Wu, L., et al. (2015). A Novel Histone Deacetylase Inhibitor, AR-42, Reactivates HIV-1 from Chronically and Latently Infected CD4+ T-cells. *Retrovirology* 7, 1–5. doi: 10.4137/RRT.S31632

Maude, S. L., Frey, N., Shaw, P. A., Aplenc, R., Barrett, D. M., Bunin, N. J., et al. (2014). Chimeric antigen receptor T cells for sustained remissions in leukemia. *N. Engl. J. Med.* 371, 1507–1517. doi: 10.1056/NEJMoa1407222

Maus, M. V., and Levine, B. L. (2016). Chimeric Antigen Receptor T-Cell Therapy for the Community Oncologist. *Oncologist* 21, 608–617. doi: 10.1634/theoncologist.2015-0421

Mbonye, U., and Karn, J. (2017). The Molecular Basis for Human Immunodeficiency Virus Latency. *Annu. Rev. Virol.* 4, 261–285. doi: 10.1146/annurev-virology-101416-041646

McKernan, L. N., Momjian, D., and Kulkosky, J. (2012). Protein Kinase C: One Pathway towards the Eradication of Latent HIV-1 Reservoirs. *Adv. Virol.* 2012:e805347. doi: 10.1155/2012/805347

McLane, L. M., Abdel-Hakeem, M. S., and Wherry, E. J. (2019). CD8 T Cell Exhaustion During Chronic Viral Infection and Cancer. *Annu. Rev. Immunol.* 37, 457–495. doi: 10.1146/annurev-immunol-041015-055318

McManus, C. J., Coolon, J. D., Duff, M. O., Eipper-Mains, J., Graveley, B. R., and Wittkopp, P. J. (2010). Regulatory divergence in Drosophila revealed by mRNA-seq. *Genome Res.* 20, 816–825. doi: 10.1101/gr.102491.109

Mediouni, S., Chinthalapudi, K., Ekka, M. K., Usui, I., Jablonski, J. A., Clementz, M. A., et al. (2019). Didehydro-Cortistatin A Inhibits HIV-1 by Specifically Binding to the Unstructured Basic Region of Tat. *mBio* 2019:18. doi: 10.1128/mBio.02662-18

Mellors, J. W., Rinaldo, C. R., Gupta, P., White, R. M., Todd, J. A., and Kingsley, L. A. (1996). Prognosis in HIV-1 Infection Predicted by the Quantity of Virus in Plasma. *Science* 272, 1167–1170. doi: 10.1126/science.272.5265.1167

Mendoza, P., Jackson, J. R., Oliveira, T. Y., Gaebler, C., Ramos, V., Caskey, M., et al. (2020). Antigen-responsive CD4+ T cell clones contribute to the HIV-1 latent reservoir. *J. Exp. Med.* 217:e20200051. doi: 10.1084/jem.20200051

Migueles, S. A., Weeks, K. A., Nou, E., Berkley, A. M., Rood, J. E., Osborne, C. M., et al. (2009). Defective Human Immunodeficiency Virus-Specific CD8 $^{+}$ T-Cell Polyfunctionality, Proliferation, and Cytotoxicity Are Not Restored by Antiretroviral Therapy. *J. Virol.* 83, 11876–11889. doi: 10.1128/JVI.01153-09

Monajemi, M., Woodworth, C. F., Zipperlen, K., Gallant, M., Grant, M. D., and Larijani, M. (2014). Positioning of APOBEC3G/F Mutational Hotspots in the Human Immunodeficiency Virus Genome Favors Reduced Recognition by CD8+ T Cells. *PLoS One* 9:e93428. doi: 10.1371/journal.pone.0093428

Monod, J., and Jacob, F. (1961). General Conclusions: Teleonomic Mechanisms in Cellular Metabolism, Growth, and Differentiation. *Cold Spring Harb. Symposia Quantit. Biol.* 26, 389–401. doi: 10.1101/SQB.1961.026.01.048

Morison, I. M., Ramsay, J. P., and Spencer, H. G. (2005). A census of mammalian imprinting. *Trends Genet.* 21, 457–465. doi: 10.1016/j.tig.2005.06.008

Mueller, Y. M., De Rosa, S. C., Hutton, J. A., Witek, J., Roederer, M., Altman, J. D., et al. (2001). Increased CD95/Fas-Induced Apoptosis of HIV-Specific CD8+ T Cells. *Immunity* 15, 871–882. doi: 10.1016/S1074-7613(01)00246-1

Mujtaba, S., He, Y., Zeng, L., Farooq, A., Carlson, J. E., Ott, M., et al. (2002). Structural basis of lysine-acetylated HIV-1 Tat recognition by PCAF bromodomain. *Mol. Cell* 9, 575–586. doi: 10.1016/s1097-2765(02)00483-5

Musick, A., Spindler, J., Boritz, E., Pérez, L., Crespo-Vélez, D., Patro, S. C., et al. (2019). HIV Infected T Cells Can Proliferate *in vivo* Without Inducing Expression of the Integrated Provirus. *Front. Microbiol.* 10:2204. doi: 10.3389/fmicb.2019.02204

Nakanjako, D., Ssewanyana, I., Mayanja-Kizza, H., Kiragga, A., Colebunders, R., Manabe, Y. C., et al. (2011). High T-cell immune activation and immune exhaustion among individuals with suboptimal CD4 recovery after 4 years of antiretroviral therapy in an African cohort. *BMC Infect. Dis.* 11:43. doi: 10.1186/1471-2334-11-43

Nguyen, S., Deleage, C., Darko, S., Ransier, A., Truong, D. P., Agarwal, D., et al. (2019). Elite control of HIV is associated with distinct functional and transcriptional signatures in lymphoid tissue CD8 $^{+}$ T cells. *Sci. Transl. Med.* 11:eaax4077. doi: 10.1126/scitranslmed.aax4077

Nguyen, T., Tagett, R., Diaz, D., and Draghici, S. (2017). A novel approach for data integration and disease subtyping. *Genome Res.* 27, 2025–2039. doi: 10.1101/gr.215129.116

Nguyen, V. T., Kiss, T., Michels, A. A., and Bensaude, O. (2001). 7SK small nuclear RNA binds to and inhibits the activity of CDK9/cyclin T complexes. *Nature* 414, 322–325. doi: 10.1038/35104581

Nixon, C. C., Mavigner, M., Sampey, G. C., Brooks, A. D., Spagnuolo, R. A., Irlbeck, D. M., et al. (2020). Systemic HIV and SIV latency reversal *via* non-canonical NF-κB signalling *in vivo*. *Nature* 578, 160–165. doi: 10.1038/s41586-020-1951-3

No Author (2006). HHS-CDC News: The Global HIV/AIDS Pandemic, 2006. *Ann. Pharmacother.* 40, 1708–1708. doi: 10.1345/aph.1N117

O'Doherty, U., Swiggard, W., Jeyakumar, D., McGain, D., and Malim, M. (2002). A Sensitive, Quantitative Assay for Human Immunodeficiency Virus Type 1 Integration. *J. Virol.* 76, 10942–10950. doi: 10.1128/JVI.76.21.10942-10950.2002

Orphanides, G., LeRoy, G., Chang, C. H., Luse, D. S., and Reinberg, D. (1998). FACT, a factor that facilitates transcript elongation through nucleosomes. *Cell* 92, 105–116. doi: 10.1016/s0092-8674(00)80903-4

Ostrowski, M. A., Chun, T. W., Justement, S. J., Motola, I., Spinelli, M. A., Adelsberger, J., et al. (1999). Both memory and CD45RA+/CD62L+ naive CD4(+) T cells are infected in human immunodeficiency virus type 1-infected individuals. *J. Virol.* 73, 6430–6435. doi: 10.1128/JVI.73.8.6430-6435.1999

Pache, L., Dutra, M. S., Spivak, A. M., Marlett, J. M., Murry, J. P., Hwang, Y., et al. (2015). BIRC2/cIAP1 Is a Negative Regulator of HIV-1 Transcription and Can Be Targeted by Smac Mimetics to Promote Reversal of Viral Latency. *Cell Host Microbe* 18, 345–353. doi: 10.1016/j.chom.2015.08.009

Pandeló José, D., Bartholomeeusen, K., da Cunha, R. D., Abreu, C. M., Glinski, J., da Costa, T. B. F., et al. (2014). Reactivation of latent HIV-1 by new semi-synthetic ingenol esters. *Virology* 462–463, 328–339. doi: 10.1016/j.virol.2014.05.033

Pardoll, D. M. (2012). The blockade of immune checkpoints in cancer immunotherapy. *Nat. Rev. Cancer* 12, 252–264. doi: 10.1038/nrc3239

Passaes, C. P. B., Bruel, T., Decalf, J., David, A., Angin, M., Monceaux, V., et al. (2017). Ultrasensitive HIV-1 p24 Assay Detects Single Infected Cells and Differences in Reservoir Induction by Latency Reversal Agents. *J. Virol.* 91:16. doi: 10.1128/jvi.02296-16

Pasternak, A. O., Adema, K. W., Bakker, M., Jurriaans, S., Berkhout, B., Cornelissen, M., et al. (2008). Highly sensitive methods based on seminested real-time reverse transcription-PCR for quantitation of human immunodeficiency virus type 1 unspliced and multiply spliced RNA and proviral DNA. *J. Clin. Microbiol.* 46, 2206–2211. doi: 10.1128/JCM.00055-08

Patro, S. C., Brandt, L. D., Bale, M. J., Halvas, E. K., Joseph, K. W., Shao, W., et al. (2019). Combined HIV-1 sequence and integration site analysis informs viral dynamics and allows reconstruction of replicating viral ancestors. *Proc. Natl. Acad. Sci. U S A.* 116, 25891–25899. doi: 10.1073/pnas.1910334116

Pauken, K. E., Sammons, M. A., Odorizzi, P. M., Manne, S., Godec, J., Khan, O., et al. (2016). Epigenetic stability of exhausted T cells limits durability of reinvigoration by PD-1 blockade. *Science* 354, 1160–1165. doi: 10.1126/science.aaf2807

Peluso, M. J., Deeks, S. G., and McCune, J. M. (2019). HIV "cure": A shot in the arm? *EBioMed.* 42, 3–5. doi: 10.1016/j.ebiom.2019.04.011

Perdomo-Celis, F., Velilla, P. A., Taborda, N. A., and Rugeles, M. T. (2019). An altered cytotoxic program of CD8+ T-cells in HIV-infected patients despite HAART-induced viral suppression. *PLoS One* 14:e0210540. doi: 10.1371/journal.pone.0210540

Pereyra, F., Addo, M. M., Kaufmann, D. E., Liu, Y., Miura, T., Rathod, A., et al. (2008). Genetic and Immunologic Heterogeneity among Persons Who Control HIV Infection in the Absence of Therapy. *J. Infect. Dis.* 197, 563–571. doi: 10.1086/526786

Perlman, R. L. (2016). Mouse Models of Human Disease: An Evolutionary Perspective. *EMPH* 2016:eow014. doi: 10.1093/emph/eow014

Pernas, M., Tarancón-Diez, L., Rodríguez-Gallego, E., Gómez, J., Prado, J. G., Casado, C., et al. (2018). Factors Leading to the Loss of Natural Elite Control of HIV-1 Infection. *J. Virol.* 92:17. doi: 10.1128/JVI.01805-17

Pinto, L. A., Sullivan, J., Berzofsky, J. A., Clerici, M., Kessler, H. A., Landay, A. L., et al. (1995). ENV-specific cytotoxic T lymphocyte responses in HIV seronegative health care workers occupationally exposed to HIV-contaminated body fluids. *J. Clin. Invest.* 96, 867–876. doi: 10.1172/JCI118133

Pisell, T. L., Ho, O., Lee, G., and Butera, S. T. (2001). Spectrum of cdk-9 inhibitor activity against HIV-1 replication among various models of chronic and latent infection. *Antivir. Chem. Chemother.* 12(Suppl. 1), 33–41.

Pollack, R. A., Jones, R. B., Pertea, M., Bruner, K. M., Martin, A. R., Thomas, A. S., et al. (2017). Defective HIV-1 Proviruses Are Expressed and Can Be Recognized by Cytotoxic T Lymphocytes, which Shape the Proviral Landscape. *Cell Host Microbe* 21, 494.e–506.e. doi: 10.1016/j.chom.2017.03.008

Porter, D. L., Levine, B. L., Kalos, M., Bagg, A., and June, C. H. (2011). Chimeric antigen receptor-modified T cells in chronic lymphoid leukemia. *N. Engl. J. Med.* 365, 725–733. doi: 10.1056/NEJMoa1103849

Procopio, F. A., Fromentin, R., Kulpa, D. A., Brehm, J. H., Bebin, A.-G., Strain, M. C., et al. (2015). A Novel Assay to Measure the Magnitude of the Inducible Viral Reservoir in HIV-infected Individuals. *EBioMedicine* 2, 874–883. doi: 10.1016/j.ebiom.2015.06.019

Qi, J., Ding, C., Jiang, X., and Gao, Y. (2020). Advances in Developing CAR T-Cell Therapy for HIV Cure. *Front. Immunol.* 11:361. doi: 10.3389/fimmu.2020.00361

Quivy, V., Adam, E., Collette, Y., Demonte, D., Chariot, A., Vanhulle, C., et al. (2002). Synergistic Activation of Human Immunodeficiency Virus Type 1 Promoter Activity by NF-κB and Inhibitors of Deacetylases: Potential Perspectives for the Development of Therapeutic Strategies. *J. Virol.* 2002:2002. doi: 10.1128/JVI.76.21.11091-11103.2002

Ramakrishnan, R., Dow, E. C., and Rice, A. P. (2009). Characterization of Cdk9 T-loop phosphorylation in resting and activated CD4 $^{+}$ T lymphocytes. *J. Leukocyte Biol.* 86, 1345–1350. doi: 10.1189/jlb.0509309

Ramakrishnan, R., Liu, H., and Rice, A. P. (2015). Short Communication: SAHA (Vorinostat) Induces CDK9 Thr-186 (T-Loop) Phosphorylation in Resting CD4 $^{+}$ T Cells: Implications for Reactivation of Latent HIV. *AIDS Res. Hum. Retroviruses* 31, 137–141. doi: 10.1089/aid.2013.0288

Rangarajan, A., and Weinberg, R. A. (2003). Comparative biology of mouse versus human cells: modelling human cancer in mice. *Nat. Rev. Cancer* 3, 952–959. doi: 10.1038/nrc1235

Ranki, A., Lagerstedt, A., Ovod, V., Aavik, E., and Krohn, K. J. E. (1994). Expression kinetics and subcellular localization of HIV-1 regulatory proteins Nef, Tat and Rev in acutely and chronically infected lymphoid cell lines. *Arch. Virol.* 139, 365–378. doi: 10.1007/BF01310798

Rasmussen, T. A., Søgaard, O. S., Brinkmann, C., Wightman, F., Lewin, S. R., Melchjorsen, J., et al. (2013). Comparison of HDAC inhibitors in clinical development. *Hum. Vacc. Immunotherap.* 9, 993–1001. doi: 10.4161/hv.23800

Rice, A. P. (2016). Cyclin-dependent kinases as therapeutic targets for HIV-1 infection. *Expert Opin. Ther. Targets* 20, 1453–1461. doi: 10.1080/14728222.2016.1254619

Routy, J.-P., Boulassel, M., Nicolette, C. A., and Jacobson, J. M. (2012). Assessing risk of a short-term antiretroviral therapy discontinuation as a read-out of viral control in immune-based therapy. *J. Med. Virol.* 84, 885–889. doi: 10.1002/jmv.23297

Rowland-Jones, S., Sutton, J., Ariyoshi, K., Dong, T., Gotch, F., McAdam, S., et al. (1995). HIV-specific cytotoxic T-cells in HIV-exposed but uninfected Gambian women. *Nat. Med.* 1, 59–64. doi: 10.1038/nm0195-59

Roy, S., Delling, U., Chen, C. H., Rosen, C. A., and Sonenberg, N. (1990). A bulge structure in HIV-1 TAR RNA is required for Tat binding and Tat-mediated trans-activation. *Genes Dev.* 4, 1365–1373. doi: 10.1101/gad.4.8.1365

Ruelas, D. S., and Greene, W. C. (2013). An Integrated Overview of HIV-1 Latency. *Cell* 155, 519–529. doi: 10.1016/j.cell.2013.09.044

Saayman, S., Ackley, A., Turner, A.-M. W., Famiglietti, M., Bosque, A., Clemson, M., et al. (2014). An HIV-Encoded Antisense Long Noncoding RNA Epigenetically Regulates Viral Transcription. *Mol. Ther.* 22, 1164–1175. doi: 10.1038/mt.2014.29

Sabari, B. R., Tang, Z., Huang, H., Yong-Gonzalez, V., Molina, H., Kong, H. E., et al. (2015). Intracellular Crotonyl-CoA Stimulates Transcription through p300-Catalyzed Histone Crotonylation. *Mol. Cell* 58, 203–215. doi: 10.1016/j.molcel.2015.02.029

Sabari, B. R., Zhang, D., Allis, C. D., and Zhao, Y. (2017). Metabolic regulation of gene expression through histone acylations. *Nat. Rev. Mol. Cell Biol.* 18, 90–101. doi: 10.1038/nrm.2016.140

Saez-Cirion, A., Lacabaratz, C., Lambotte, O., Versmisse, P., Urrutia, A., Boufassa, F., et al. (2007). HIV controllers exhibit potent CD8 T cell capacity to suppress HIV infection *ex vivo* and peculiar cytotoxic T lymphocyte activation phenotype. *Proc. Natl. Acad. Sci.* 104, 6776–6781. doi: 10.1073/pnas.0611244104

Sahin, I. H., Kane, S. R., Brutcher, E., Guadagno, J., Smith, K. E., Wu, C., et al. (2020). Safety and Efficacy of Immune Checkpoint Inhibitors in Patients With Cancer Living With HIV: A Perspective on Recent Progress and Future Needs. *JCO Oncol. Pract.* 16, 319–325. doi: 10.1200/JOP.19.00754

Samson, M., Libert, F., Doranz, B. J., Rucker, J., Liesnard, C., Farber, C.-M., et al. (1996). Resistance to HIV-1 infection in Caucasian individuals bearing mutant alleles of the CCR-5 chemokine receptor gene. *Nature* 382, 722–725. doi: 10.1038/382722a0

Santangelo, P. J., Rogers, K. A., Zurla, C., Blanchard, E. L., Gumber, S., Strait, K., et al. (2015). Whole-body immunoPET reveals active SIV dynamics in viremic and antiretroviral therapy-treated macaques. *Nat. Methods* 12, 427–432. doi: 10.1038/nmeth.3320

Sarca, A. D., Sardo, L., Fukuda, H., Matsui, H., Shirakawa, K., Horikawa, K., et al. (2021). FRET-Based Detection and Quantification of HIV-1 Virion Maturation. *Front. Microbiol.* 12:647452. doi: 10.3389/fmicb.2021.647452

Sardo, L., Parolin, C., Yoshida, T., Garzino-Demo, A., and Izumi, T. (2021). Editorial: Novel Insights Into a Functional HIV Cure. *Front. Microbiol.* 12:3705. doi: 10.3389/fmicb.2021.797570

Sarracino, A., Gharu, L., Kula, A., Pasternak, A. O., Avettand-Fenoel, V., Rouzioux, C., et al. (2018). Posttranscriptional Regulation of HIV-1 Gene Expression during Replication and Reactivation from Latency by Nuclear Matrix Protein MATR3. *mBio* 9:18. doi: 10.1128/mBio.02158-18

Scharer, C. D., Barwick, B. G., Youngblood, B. A., Ahmed, R., and Boss, J. M. (2013). Global DNA Methylation Remodeling Accompanies CD8 T Cell Effector Function. *JI* 191, 3419–3429. doi: 10.4049/jimmunol.1301395

Schleimann, M. H., Kobberø, M.-L., Vibholm, L. K., Kjær, K., Giron, L. B., Busman-Sahay, K., et al. (2019). TLR9 agonist MGN1703 enhances B cell differentiation and function in lymph nodes. *EBioMedicine* 45, 328–340. doi: 10.1016/j.ebiom.2019.07.005

Schumann, K., Lin, S., Boyer, E., Simeonov, D. R., Subramaniam, M., Gate, R. E., et al. (2015). Generation of knock-in primary human T cells using Cas9 ribonucleoproteins. *Proc. Natl. Acad. Sci. U S A.* 112, 10437–10442. doi: 10.1073/pnas.1512503112

Schuster, S. J., Svoboda, J., Chong, E. A., Nasta, S. D., Mato, A. R., Anak, Ö, et al. (2017). Chimeric Antigen Receptor T Cells in Refractory B-Cell Lymphomas. *N. Engl. J. Med.* 377, 2545–2554. doi: 10.1056/NEJMoa1708566

Sengupta, S., and Siliciano, R. F. (2018). Targeting the Latent Reservoir for HIV-1. *Immunity* 48, 872–895. doi: 10.1016/j.immuni.2018.04.030

Serrano-Villar, S., Sainz, T., Lee, S. A., Hunt, P. W., Sinclair, E., Shacklett, B. L., et al. (2014). HIV-Infected Individuals with Low CD4/CD8 Ratio despite Effective Antiretroviral Therapy Exhibit Altered T Cell Subsets, Heightened CD8+ T Cell Activation, and Increased Risk of Non-AIDS Morbidity and Mortality. *PLoS Pathog.* 10:e1004078. doi: 10.1371/journal.ppat.1004078

Seto, E., and Yoshida, M. (2014). Erasers of Histone Acetylation: The Histone Deacetylase Enzymes. *Cold Spring Harb. Perspect. Biol.* 6:a018713. doi: 10.1101/cshperspect.a018713

Shacklett, B. L. (2006). Understanding the "lucky few": The conundrum of HIV-exposed, seronegative individuals. *Curr. HIV/AIDS Rep.* 3, 26–31. doi: 10.1007/s11904-006-0005-2

Shankar, P., Russo, M., Harnisch, B., Patterson, M., Skolnik, P., and Lieberman, J. (2000). Impaired function of circulating HIV-specific CD8(+) T cells in chronic human immunodeficiency virus infection. *Blood* 96, 3094–3101.

Shayan, G., Srivastava, R., Li, J., Schmitt, N., Kane, L. P., and Ferris, R. L. (2017). Adaptive resistance to anti-PD1 therapy by Tim-3 upregulation is mediated by the PI3K-Akt pathway in head and neck cancer. *OncoImmunology* 6:e1261779. doi: 10.1080/2162402X.2016.1261779

Shen, C.-J., Jia, Y.-H., Tian, R.-R., Ding, M., Zhang, C., and Wang, J.-H. (2012). Translation of Pur-α is targeted by cellular miRNAs to modulate the differentiation-dependent susceptibility of monocytes to HIV-1 infection. *FASEB J.* 26, 4755–4764. doi: 10.1096/fj.12-209023

Siliciano, J. D., Kajdas, J., Finzi, D., Quinn, T. C., Chadwick, K., Margolick, J. B., et al. (2003). Long-term follow-up studies confirm the stability of the latent reservoir for HIV-1 in resting CD4+ T cells. *Nat. Med.* 9, 727–728. doi: 10.1038/nm880

Simonetti, F. R., Sobolewski, M. D., Fyne, E., Shao, W., Spindler, J., Hattori, J., et al. (2016). Clonally expanded CD4+ T cells can produce infectious HIV-1 *in vivo*. *Proc. Natl. Acad. Sci. U S A.* 113, 1883–1888. doi: 10.1073/pnas.1522675113

Simonetti, F. R., White, J. A., Tumiotto, C., Ritter, K. D., Cai, M., Gandhi, R. T., et al. (2020). Intact proviral DNA assay analysis of large cohorts of people with HIV provides a benchmark for the frequency and composition of persistent proviral DNA. *Proc. Natl. Acad. Sci. U S A.* 117, 18692–18700. doi: 10.1073/pnas.2006816117

Simonetti, F. R., Zhang, H., Soroosh, G. P., Duan, J., Rhodehouse, K., Hill, A. L., et al. (2021). Antigen-driven clonal selection shapes the persistence of HIV-1-infected CD4+ T cells *in vivo*. *J. Clin. Invest.* 131:145254. doi: 10.1172/JCI145254

Śledzińska, A., Menger, L., Bergerhoff, K., Peggs, K. S., and Quezada, S. A. (2015). Negative immune checkpoints on T lymphocytes and their relevance to cancer immunotherapy. *Mol. Oncol.* 9, 1936–1965. doi: 10.1016/j.molonc.2015.10.008

Søgaard, O. S., Graversen, M. E., Leth, S., Olesen, R., Brinkmann, C. R., Nissen, S. K., et al. (2015). The Depsipeptide Romidepsin Reverses HIV-1 Latency *In Vivo*. *PLoS Pathog.* 11:e1005142. doi: 10.1371/journal.ppat.1005142

Soriano-Sarabia, N., Archin, N. M., Bateson, R., Dahl, N. P., Crooks, A. M., Kuruc, J. D., et al. (2015). Peripheral Vγ9Vδ2 T Cells Are a Novel Reservoir of Latent HIV Infection. *PLoS Pathog.* 11:e1005201. doi: 10.1371/journal.ppat.1005201

Soriano-Sarabia, N., Bateson, R. E., Dahl, N. P., Crooks, A. M., Kuruc, J. D., Margolis, D. M., et al. (2014). Quantitation of Replication-Competent HIV-1 in Populations of Resting CD4 $^{+}$ T Cells. *J. Virol.* 88, 14070–14077. doi: 10.1128/JVI.01900-14

Spivak, A. M., Andrade, A., Eisele, E., Hoh, R., Bacchetti, P., Bumpus, N. N., et al. (2014). A pilot study assessing the safety and latency-reversing activity of disulfiram in HIV-1-infected adults on antiretroviral therapy. *Clin. Infect. Dis.* 58, 883–890. doi: 10.1093/cid/cit813

Spivak, A. M., Bosque, A., Balch, A. H., Smyth, D., Martins, L., and Planelles, V. (2015). *Ex Vivo* Bioactivity and HIV-1 Latency Reversal by Ingenol Dibenzoate and Panobinostat in Resting CD4+ T Cells from Aviremic Patients. *Antimicrob. Agents Chemother.* 2015:15. doi: 10.1128/AAC.01077-15

Srivastava, S., and Riddell, S. R. (2015). Engineering CAR-T cells: Design concepts. *Trends Immunol.* 36, 494–502. doi: 10.1016/j.it.2015.06.004

Strain, M. C., Lada, S. M., Luong, T., Rought, S. E., Gianella, S., Terry, V. H., et al. (2013). Highly precise measurement of HIV DNA by droplet digital PCR. *PLoS One* 8:e55943. doi: 10.1371/journal.pone.0055943

Stuelke, E. L., James, K. S., Kirchherr, J. L., Allard, B., Baker, C., Kuruc, J. D., et al. (2020). Measuring the Inducible, Replication-Competent HIV Reservoir Using an Ultra-Sensitive p24 Readout, the Digital ELISA Viral Outgrowth Assay. *Front. Immunol.* 11:1971. doi: 10.3389/fimmu.2020.01971

Sun, S.-C. (2017). The non-canonical NF-κB pathway in immunity and inflammation. *Nat. Rev. Immunol.* 17, 545–558. doi: 10.1038/nri.2017.52

Sun, S.-C., and Ley, S. C. (2008). New insights into NF-κB regulation and function. *Trends Immunol.* 29, 469–478. doi: 10.1016/j.it.2008.07.003

Sung, T.-L., and Rice, A. P. (2009). miR-198 Inhibits HIV-1 Gene Expression and Replication in Monocytes and Its Mechanism of Action Appears To Involve Repression of Cyclin T1. *PLoS Pathog.* 5:e1000263. doi: 10.1371/journal.ppat.1000263

Suzuki, K., Hattori, S., Marks, K., Ahlenstiel, C., Maeda, Y., Ishida, T., et al. (2013). Promoter Targeting shRNA Suppresses HIV-1 Infection *In vivo* Through Transcriptional Gene Silencing. *Mol. Therapy Nucleic Acids* 2, e137. doi: 10.1038/mtna.2013.64

Tan, M., Luo, H., Lee, S., Jin, F., Yang, J. S., Montellier, E., et al. (2011). Identification of 67 Histone Marks and Histone Lysine Crotonylation as a New Type of Histone Modification. *Cell* 146, 1016–1028. doi: 10.1016/j.cell.2011.08.008

Taura, M., Song, E., Ho, Y.-C., and Iwasaki, A. (2019). Apobec3A maintains HIV-1 latency through recruitment of epigenetic silencing machinery to the long terminal repeat. *Proc. Natl. Acad. Sci. U S A.* 116, 2282–2289. doi: 10.1073/pnas.1819386116

Taylor, R. A., Xiao, S., Carias, A. M., McRaven, M. D., Thakkar, D. N., Araínga, M., et al. (2021). PET/CT targeted tissue sampling reveals virus specific dIgA can alter the distribution and localization of HIV after rectal exposure. *PLoS Pathog.* 17:e1009632. doi: 10.1371/journal.ppat.1009632

Tchasovnikarova, I. A., Timms, R. T., Matheson, N. J., Wals, K., Antrobus, R., Göttgens, B., et al. (2015). Epigenetic silencing by the HUSH complex mediates position-effect variegation in human cells. *Science* 348, 1481–1485. doi: 10.1126/science.aaa7227

Tebas, P., Stein, D., Tang, W. W., Frank, I., Wang, S. Q., Lee, G., et al. (2014). Gene Editing of CCR5 in Autologous CD4 T Cells of Persons Infected with HIV. *N. Engl. J. Med.* 370, 901–910. doi: 10.1056/NEJMoa1300662

Tomer, R., Ye, L., Hsueh, B., and Deisseroth, K. (2014). Advanced CLARITY for rapid and high-resolution imaging of intact tissues. *Nat. Protoc.* 9, 1682–1697. doi: 10.1038/nprot.2014.123

Triboulet, R., Mari, B., Lin, Y.-L., Chable-Bessia, C., Bennasser, Y., Lebrigand, K., et al. (2007). Suppression of MicroRNA-Silencing Pathway by HIV-1 During Virus Replication. *Science* 315, 1579–1582. doi: 10.1126/science.1136319

Turrini, F., Marelli, S., Kajaste-Rudnitski, A., Lusic, M., Van Lint, C., Das, A. T., et al. (2015). HIV-1 transcriptional silencing caused by TRIM22 inhibition of Sp1 binding to the viral promoter. *Retrovirology* 12:104. doi: 10.1186/s12977-015-0230-0

Tyagi, M., and Karn, J. (2007). CBF-1 promotes transcriptional silencing during the establishment of HIV-1 latency. *EMBO J.* 26, 4985–4995. doi: 10.1038/sj.emboj.7601928

Uldrick, T. S., Ison, G., Rudek, M. A., Noy, A., Schwartz, K., Bruinooge, S., et al. (2017). Modernizing Clinical Trial Eligibility Criteria: Recommendations of the American Society of Clinical Oncology-Friends of Cancer Research HIV Working Group. *J. Clin. Oncol.* 35, 3774–3780. doi: 10.1200/JCO.2017.73.7338

van den Dries, L., Claassen, M. A. A., Groothuismink, Z. M. A., van Gorp, E., and Boonstra, A. (2017). Immune activation in prolonged cART-suppressed HIV patients is comparable to that of healthy controls. *Virology* 509, 133–139. doi: 10.1016/j.virol.2017.06.014

Van der Sluis, R. M., Kumar, N. A., Pascoe, R. D., Zerbato, J. M., Evans, V. A., Dantanarayana, A. I., et al. (2020). Combination Immune Checkpoint Blockade to Reverse HIV Latency. *JI* 204, 1242–1254. doi: 10.4049/jimmunol.1901191

Van Lint, C., Bouchat, S., and Marcello, A. (2013). HIV-1 transcription and latency: an update. *Retrovirology* 10:67. doi: 10.1186/1742-4690-10-67

Van Lint, C., Emiliani, S., Ott, M., and Verdin, E. (1996). Transcriptional activation and chromatin remodeling of the HIV-1 promoter in response to histone acetylation. *EMBO J.* 15, 1112–1120. doi: 10.1002/j.1460-2075.1996.tb00449.x

van Snippenberg, W., Gleerup, D., Rutsaert, S., Vandekerckhove, L., De Spiegelaere, W., and Trypsteen, W. (2021). Triplex digital PCR assays for the quantification of intact proviral HIV-1 DNA. *Methods* 2021:S1046202321001328. doi: 10.1016/j.ymeth.2021.05.006

Vibholm, L. K., Konrad, C. V., Schleimann, M. H., Frattari, G., Winckelmann, A., Klastrup, V., et al. (2019). Effects of 24-week Toll-like receptor 9 agonist treatment in HIV type 1+ individuals. *AIDS* 33, 1315–1325. doi: 10.1097/QAD.0000000000002213

Vibholm, L., Schleimann, M. H., Højen, J. F., Benfield, T., Offersen, R., Rasmussen, K., et al. (2017). Short-Course Toll-Like Receptor 9 Agonist Treatment Impacts Innate Immunity and Plasma Viremia in Individuals With Human Immunodeficiency Virus Infection. *Clin. Infect. Dis.* 64, 1686–1695. doi: 10.1093/cid/cix201

von Stockenstrom, S., Odevall, L., Lee, E., Sinclair, E., Bacchetti, P., Killian, M., et al. (2015). Longitudinal Genetic Characterization Reveals That Cell Proliferation Maintains a Persistent HIV Type 1 DNA Pool During Effective HIV Therapy. *J. Infect. Dis.* 212, 596–607. doi: 10.1093/infdis/jiv092

Vranckx, L. S., Demeulemeester, J., Saleh, S., Boll, A., Vansant, G., Schrijvers, R., et al. (2016). LEDGIN-mediated Inhibition of Integrase-LEDGF/p75 Interaction Reduces Reactivation of Residual Latent HIV. *EBioMedicine* 8, 248–264. doi: 10.1016/j.ebiom.2016.04.039

Wagner, T. A., McLaughlin, S., Garg, K., Cheung, C. Y. K., Larsen, B. B., Styrchak, S., et al. (2014). HIV latency. Proliferation of cells with HIV integrated into cancer genes contributes to persistent infection. *Science* 345, 570–573. doi: 10.1126/science.1256304

Wang, Q., Jia, Y., Wang, Y., Jiang, Z., Zhou, X., Zhang, Z., et al. (2019). Evolution of cis- and trans-regulatory divergence in the chicken genome between two contrasting breeds analyzed using three tissue types at one-day-old. *BMC Genomics* 20:933. doi: 10.1186/s12864-019-6342-5

Wang, Z., Gurule, E. E., Brennan, T. P., Gerold, J. M., Kwon, K. J., Hosmane, N. N., et al. (2018). Expanded cellular clones carrying replication-competent HIV-1 persist, wax, and wane. *Proc. Natl. Acad. Sci. U S A.* 115, E2575–E2584. doi: 10.1073/pnas.1720665115

Weber, S., Weiser, B., Kemal, K. S., Burger, H., Ramirez, C. M., Korn, K., et al. (2014). Epigenetic analysis of HIV-1 proviral genomes from infected individuals: Predominance of unmethylated CpG's. *Virology* 449, 181–189. doi: 10.1016/j.virol.2013.11.013

Wei, P., Garber, M. E., Fang, S.-M., Fischer, W. H., and Jones, K. A. (1998). A Novel CDK9-Associated C-Type Cyclin Interacts Directly with HIV-1 Tat and Mediates Its High-Affinity, Loop-Specific Binding to TAR RNA. *Cell* 92, 451–462. doi: 10.1016/S0092-8674(00)80939-3

Weinberger, L. S., Burnett, J. C., Toettcher, J. E., Arkin, A. P., and Schaffer, D. V. (2005). Stochastic Gene Expression in a Lentiviral Positive-Feedback Loop: HIV-1 Tat Fluctuations Drive Phenotypic Diversity. *Cell* 122, 169–182. doi: 10.1016/j.cell.2005.06.006

West, M. J., Lowe, A. D., and Karn, J. (2001). Activation of Human Immunodeficiency Virus Transcription in T Cells Revisited: NF-κB p65 Stimulates Transcriptional Elongation. *J. Virol.* 2001:2001. doi: 10.1128/JVI.75.18.8524-8537.2001

Wherry, E. J., and Kurachi, M. (2015). Molecular and cellular insights into T cell exhaustion. *Nat. Rev. Immunol.* 15, 486–499. doi: 10.1038/nri3862

Wherry, E. J., Blattman, J. N., Murali-Krishna, K., van der Most, R., and Ahmed, R. (2003). Viral Persistence Alters CD8 T-Cell Immunodominance and Tissue Distribution and Results in Distinct Stages of Functional Impairment. *J. Virol.* 77, 4911–4927. doi: 10.1128/JVI.77.8.4911-4927.2003

Wherry, E. J., Ha, S.-J., Kaech, S. M., Haining, W. N., Sarkar, S., Kalia, V., et al. (2007). Molecular Signature of CD8+ T Cell Exhaustion during Chronic Viral Infection. *Immunity* 27, 670–684. doi: 10.1016/j.immuni.2007.09.006

White, M. K., Kaminski, R., Young, W., Roehm, P. C., and Khalili, K. (2017). CRISPR Editing Technology in Biological and Biomedical Investigation. *J. Cell. Biochem.* 118, 3586–3594. doi: 10.1002/jcb.26099

Wierda, R. J., Kuipers, H. F., van Eggermond, M. C. J. A., Benard, A., van Leeuwen, J. C., Carluccio, S., et al. (2012). Epigenetic control of CCR5 transcript levels in immune cells and modulation by small molecules inhibitors. *J. Cell. Mol. Med.* 16, 1866–1877. doi: 10.1111/j.1582-4934.2011.01482.x

Wightman, F., Lu, H. K., Solomon, A. E., Saleh, S., Harman, A. N., Cunningham, A. L., et al. (2013). Entinostat is a histone deacetylase inhibitor selective for class 1 histone deacetylases and activates HIV production from latently infected primary T cells. *AIDS* 27, 2853–2862. doi: 10.1097/QAD.0000000000000067

Wightman, F., Solomon, A., Khoury, G., Green, J. A., Gray, L., Gorry, P. R., et al. (2010). Both CD31 $^{+}$ and CD31 $^{-}$ Naive CD4 $^{+}$ T Cells Are Persistent HIV Type 1–Infected Reservoirs in Individuals Receiving Antiretroviral Therapy. *J. Infect. Dis.* 202, 1738–1748. doi: 10.1086/656721

Wightman, F., Solomon, A., Kumar, S. S., Urriola, N., Gallagher, K., Hiener, B., et al. (2015). Effect of ipilimumab on the HIV reservoir in an HIV-infected individual with metastatic melanoma. *AIDS* 29, 504–506. doi: 10.1097/QAD.0000000000000562

Williams, J. P., Hurst, J., Stöhr, W., Robinson, N., Brown, H., Fisher, M., et al. (2014). HIV-1 DNA predicts disease progression and post-treatment virological control. *eLife* 3:e03821. doi: 10.7554/eLife.03821

Williams, S. A., Chen, L.-F., Kwon, H., Fenard, D., Bisgrove, D., Verdin, E., et al. (2004). Prostratin antagonizes HIV latency by activating NF-kappaB. *J. Biol. Chem.* 279, 42008–42017. doi: 10.1074/jbc.M402124200

Williams, S. A., Chen, L.-F., Kwon, H., Ruiz-Jarabo, C. M., Verdin, E., and Greene, W. C. (2006). NF-κB p50 promotes HIV latency through HDAC recruitment and repression of transcriptional initiation. *EMBO J.* 25, 139–149. doi: 10.1038/sj.emboj.7600900

Wilson, E. M. P., and Sereti, I. (2013). Immune restoration after antiretroviral therapy: the pitfalls of hasty or incomplete repairs. *Immunol. Rev.* 254, 343–354. doi: 10.1111/imr.12064

Wong, J. K., Hezareh, M., Günthard, H. F., Havlir, D. V., Ignacio, C. C., Spina, C. A., et al. (1997). Recovery of replication-competent HIV despite prolonged suppression of plasma viremia. *Science* 278, 1291–1295. doi: 10.1126/science.278.5341.1291

Wong, L. M., and Jiang, G. (2021). NF-κB sub-pathways and HIV cure: A revisit. *EBioMedicine* 63:103159. doi: 10.1016/j.ebiom.2020.103159

Wong, M. E., Jaworowski, A., and Hearps, A. C. (2019). The HIV Reservoir in Monocytes and Macrophages. *Front. Immunol.* 10:1435. doi: 10.3389/fimmu.2019.01435

Wu, G., Cheney, C., Huang, Q., Hazuda, D. J., Howell, B. J., and Zuck, P. (2021). Improved Detection of HIV Gag p24 Protein Using a Combined Immunoprecipitation and Digital ELISA Method. *Front. Microbiol.* 12:636703. doi: 10.3389/fmicb.2021.636703

Wu, G., Swanson, M., Talla, A., Graham, D., Strizki, J., Gorman, D., et al. (2017). HDAC inhibition induces HIV-1 protein and enables immune-based clearance following latency reversal. *JCI Insight* 2:92901. doi: 10.1172/jci.insight.92901

Xing, S., Bullen, C. K., Shroff, N. S., Shan, L., Yang, H.-C., Manucci, J. L., et al. (2011). Disulfiram reactivates latent HIV-1 in a Bcl-2-transduced primary CD4+ T cell model without inducing global T cell activation. *J. Virol.* 85, 6060–6064. doi: 10.1128/JVI.02033-10

Xiong, Y., Luscher, M. A., Altman, J. D., Hulsey, M., Robinson, H. L., Ostrowski, M., et al. (2001). Simian Immunodeficiency Virus (SIV) Infection of a Rhesus Macaque Induces SIV-Specific CD8 $^{+}$ T Cells with a Defect in Effector Function That Is Reversible on Extended Interleukin-2 Incubation. *J. Virol.* 75, 3028–3033. doi: 10.1128/JVI.75.6.3028-3033.2001

Xu, L., Yang, H., Gao, Y., Chen, Z., Xie, L., Liu, Y., et al. (2017). CRISPR/Cas9-Mediated CCR5 Ablation in Human Hematopoietic Stem/Progenitor Cells Confers HIV-1 Resistance *In Vivo*. *Mol. Therapy* 25, 1782–1789. doi: 10.1016/j.ymthe.2017.04.027

Yamaguchi, Y., Takagi, T., Wada, T., Yano, K., Furuya, A., Sugimoto, S., et al. (1999). NELF, a Multisubunit Complex Containing RD, Cooperates with DSIF to Repress RNA Polymerase II Elongation. *Cell* 97, 41–51. doi: 10.1016/S0092-8674(00)80713-8

Yang, C., Dove, M. T., Brazhkin, V. V., and Trachenko, K. (2018). Yang et al. Reply. *Phys. Rev. Lett.* 120:219602. doi: 10.1103/PhysRevLett.120.219602

Yang, Z., Zhu, Q., Luo, K., and Zhou, Q. (2001). The 7SK small nuclear RNA inhibits the CDK9/cyclin T1 kinase to control transcription. *Nature* 414, 317–322. doi: 10.1038/35104575

Yates, K. B., Tonnerre, P., Martin, G. E., Gerdemann, U., Al Abosy, R., Comstock, D. E., et al. (2021). Epigenetic scars of CD8+ T cell exhaustion persist after cure of chronic infection in humans. *Nat. Immunol.* 22, 1020–1029. doi: 10.1038/s41590-021-00979-1

Yerly, S., Günthard, H. F., Fagard, C., Joos, B., Perneger, T. V., Hirschel, B., et al. (2004). Proviral HIV-DNA predicts viral rebound and viral setpoint after structured treatment interruptions. *AIDS* 18, 1951–1953. doi: 10.1097/00002030-200409240-00011

Yeung, M. L., Houzet, L., Yedavalli, V. S. R. K., and Jeang, K.-T. (2009). A genome-wide short hairpin RNA screening of jurkat T-cells for human proteins contributing to productive HIV-1 replication. *J. Biol. Chem.* 284, 19463–19473. doi: 10.1074/jbc.M109.010033

Yik, J. H. N., Chen, R., Nishimura, R., Jennings, J. L., Link, A. J., and Zhou, Q. (2003). Inhibition of P-TEFb (CDK9/Cyclin T) kinase and RNA polymerase II

transcription by the coordinated actions of HEXIM1 and 7SK snRNA. *Mol. Cell* 12, 971–982. doi: 10.1016/s1097-2765(03)00388-5

Yin, C., Zhang, T., Qu, X., Zhang, Y., Putatunda, R., Xiao, X., et al. (2017). *In Vivo* Excision of HIV-1 Provirus by saCas9 and Multiplex Single-Guide RNAs in Animal Models. *Mol. Therapy* 25, 1168–1186. doi: 10.1016/j.ymthe.2017.03.012

Ylisastigui, L., Archin, N. M., Lehrman, G., Bosch, R. J., and Margolis, D. M. (2004). Coaxing HIV-1 from resting CD4 T cells: histone deacetylase inhibition allows latent viral expression. *AIDS* 18, 1101–1108. doi: 10.1097/00002030-200405210-00003

Youngblood, B., Noto, A., Porichis, F., Akondy, R. S., Ndhlovu, Z. M., Austin, J. W., et al. (2013). Cutting edge: Prolonged exposure to HIV reinforces a poised epigenetic program for PD-1 expression in virus-specific CD8 T cells. *J. Immunol.* 191, 540–544. doi: 10.4049/jimmunol.1203161

Youngblood, B., Oestreich, K. J., Ha, S.-J., Duraiswamy, J., Akondy, R. S., West, E. E., et al. (2011). Chronic Virus Infection Enforces Demethylation of the Locus that Encodes PD-1 in Antigen-Specific CD8+ T Cells. *Immunity* 35, 400–412. doi: 10.1016/j.immuni.2011.06.015

Yucha, R. W., Hobbs, K. S., Hanhauser, E., Hogan, L. E., Nieves, W., Ozen, M. O., et al. (2017). High-throughput Characterization of HIV-1 Reservoir Reactivation Using a Single-Cell-in-Droplet PCR Assay. *EBioMedicine* 20, 217–229. doi: 10.1016/j.ebiom.2017.05.006

Yukl, S. A., Kaiser, P., Kim, P., Telwatte, S., Joshi, S. K., Vu, M., et al. (2018). HIV latency in isolated patient CD4 $^{+}$ T cells may be due to blocks in HIV transcriptional elongation, completion, and splicing. *Sci. Transl. Med.* 10:eaa9927. doi: 10.1126/scitranslmed.aap9927

Zahavi, D. J., and Weiner, L. M. (2019). Targeting Multiple Receptors to Increase Checkpoint Blockade Efficacy. *Int. J. Mol. Sci.* 20:E158. doi: 10.3390/ijms20010158

Zebley, C. C., Gottschalk, S., and Youngblood, B. (2020). Rewriting History: Epigenetic Reprogramming of CD8+ T Cell Differentiation to Enhance Immunotherapy. *Trends Immunol.* 41, 665–675. doi: 10.1016/j.it.2020.06.008

Zerbato, J. M., McMahon, D. K., Sobolewski, M. D., Mellors, J. W., and Sluis-Cremer, N. (2019). Naive CD4+ T Cells Harbor a Large Inducible Reservoir of Latent, Replication-competent Human Immunodeficiency Virus Type 1. *Clin. Infect. Dis.* 69, 1919–1925. doi: 10.1093/cid/ciz108

Zhang, H.-S., Wu, T.-C., Sang, W.-W., and Ruan, Z. (2012). MiR-217 is involved in Tat-induced HIV-1 long terminal repeat (LTR) transactivation by down-regulation of SIRT1. *Biochim. Biophys. Acta* 1823, 1017–1023. doi: 10.1016/j.bbamcr.2012.02.014

Zhang, Z., Nikolai, B. C., Gates, L. A., Jung, S. Y., Siwak, E. B., He, B., et al. (2017). Crosstalk between histone modifications indicates that inhibition of arginine methyltransferase CARM1 activity reverses HIV latency. *Nucleic Acids Res.* 45, 9348–9360. doi: 10.1093/nar/gkx550

Zhong, H., May, M. J., Jimi, E., and Ghosh, S. (2002). The Phosphorylation Status of Nuclear NF-KB Determines Its Association with CBP/p300 or HDAC-1. *Mol. Cell* 9, 625–636. doi: 10.1016/S1097-2765(02)00477-X

Zhou, H., Xu, M., Huang, Q., Gates, A. T., Zhang, X. D., Castle, J. C., et al. (2008). Genome-scale RNAi screen for host factors required for HIV replication. *Cell Host Microbe* 4, 495–504. doi: 10.1016/j.chom.2008.10.004

Zhu, Y., Pe'ery, T., Peng, J., Ramanathan, Y., Marshall, N., Marshall, T., et al. (1997). Transcription elongation factor P-TEFb is required for HIV-1 Tat transactivation in vitro. *Genes Dev.* 11, 2622–2632. doi: 10.1101/gad.11.20.2622

**Author Disclaimer:** The findings of this article are those of the authors. They do not necessarily reflect the views of the Office of the Assistant Secretary for Health or the U.S. Department of Health and Human Services.

**Conflict of Interest:** LS is employed by Merck Sharp & Dohme Corp., a subsidiary of Merck & Co., Inc., Kenilworth, NJ, United States.

The remaining authors declare that the research was conducted in the absence of any commercial or financial relationships that could be construed as a potential conflict of interest.

**Publisher's Note:** All claims expressed in this article are solely those of the authors and do not necessarily represent those of their affiliated organizations, or those of the publisher, the editors and the reviewers. Any product that may be evaluated in this article, or claim that may be made by its manufacturer, is not guaranteed or endorsed by the publisher.

*Copyright © 2022 Ta, Malik, Anderson, Jones, Perchik, Freylikh, Sardo, Klase and Izumi. This is an open-access article distributed under the terms of the Creative Commons Attribution License (CC BY). The use, distribution or reproduction in other forums is permitted, provided the original author(s) and the copyright owner(s) are credited and that the original publication in this journal is cited, in accordance with accepted academic practice. No use, distribution or reproduction is permitted which does not comply with these terms.*

# Frontiers in Microbiology

**Explores the habitable world and the potential of microbial life**

The largest and most cited microbiology journal which advances our understanding of the role microbes play in addressing global challenges such as healthcare, food security, and climate change.

---

## Discover the latest Research Topics

See more →

**Frontiers**

Avenue du Tribunal-Fédéral 34
1005 Lausanne, Switzerland
frontiersin.org

**Contact us**

+41 (0)21 510 17 00
frontiersin.org/about/contact